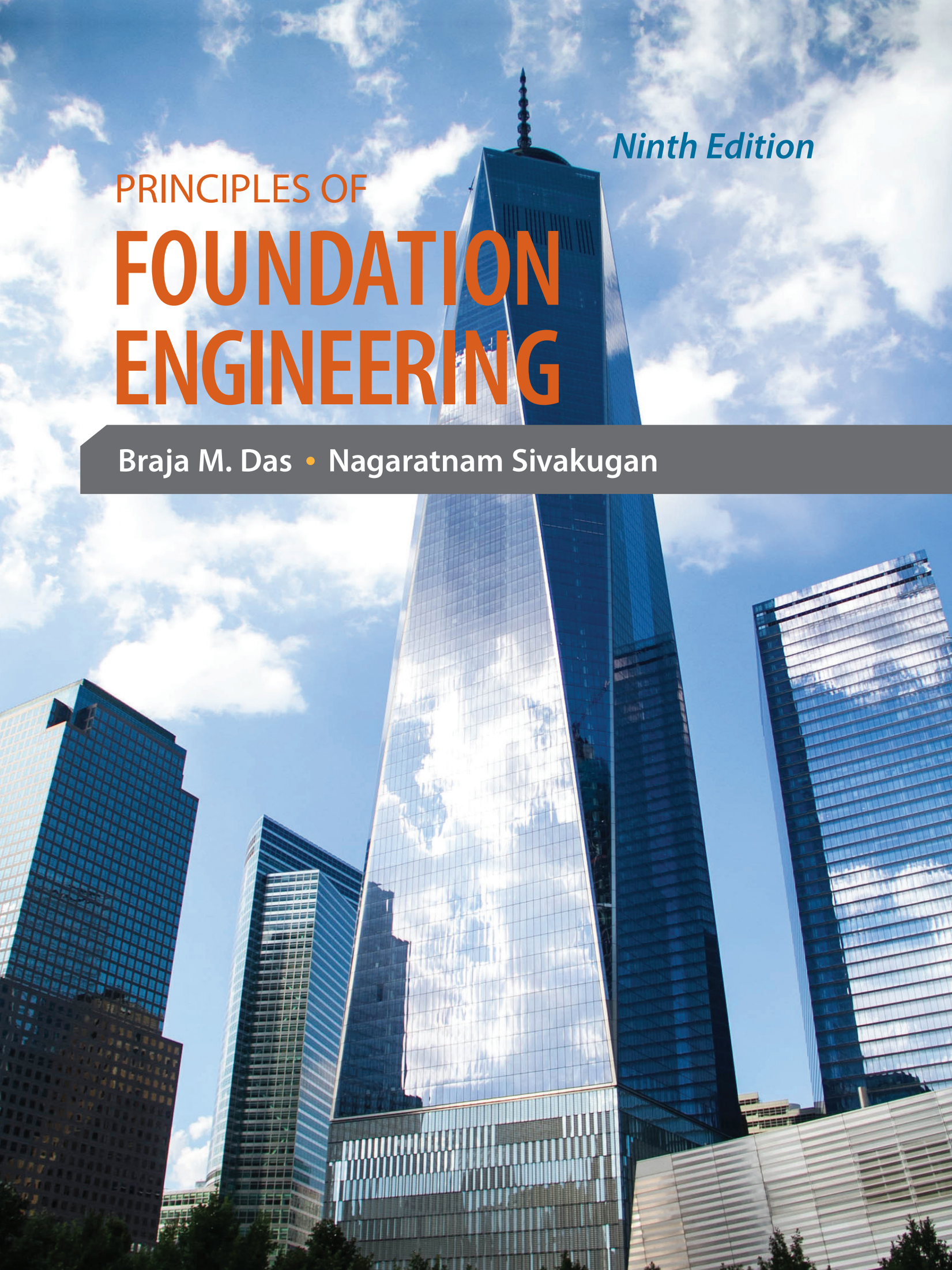


Ninth Edition

PRINCIPLES OF FOUNDATION ENGINEERING

Braja M. Das • Nagaratnam Sivakugan

CONVERSION FACTORS FROM SI TO ENGLISH UNITS

Length:	1 m	= 3.281 ft
	1 cm	= 3.281×10^{-2} ft
	1 mm	= 3.281×10^{-3} ft
	1 m	= 39.37 in.
	1 cm	= 0.3937 in.
	1 mm	= 0.03937 in.
Area:	1 m^2	= 10.764 ft^2
	1 cm^2	= 10.764×10^{-4} ft^2
	1 mm^2	= 10.764×10^{-6} ft^2
	1 m^2	= 1550 in^2
	1 cm^2	= 0.155 in^2
	1 mm^2	= 0.155×10^{-2} in^2
Volume:	1 m^3	= 35.32 ft^3
	1 cm^3	= 35.32×10^{-4} ft^3
	1 m^3	= 61,023.4 in^3
	1 cm^3	= 0.061023 in^3
Force:	1 N	= 0.2248 lb
	1 kN	= 224.8 lb
	1 kgf	= 2.2046 lb
	1 kN	= 0.2248 kip
	1 kN	= 0.1124 U.S. ton
	1 metric ton	= 2204.6 lb
	1 N/m	= 0.0685 lb/ft
Stress:	1 N/m^2	= 20.885×10^{-3} lb/ft^2
	1 kN/m^2	= 20.885 lb/ft^2
	1 kN/m^2	= 0.01044 U.S. ton/ft^2
	1 kN/m^2	= 20.885×10^{-3} kip/ft^2
	1 kN/m^2	= 0.145 lb/in^2
Unit weight:	1 kN/m^3	= 6.361 lb/ft^3
	1 kN/m^3	= 0.003682 lb/in^3
Moment:	1 N·m	= 0.7375 lb-ft
	1 N·m	= 8.851 lb-in.
Energy:	1 J	= 0.7375 ft-lb
Moment of inertia:	1 mm^4	= 2.402×10^{-6} in^4
	1 m^4	= 2.402×10^{6} in^4
Section modulus:	1 mm^3	= 6.102×10^{-5} in^3
	1 m^3	= 6.102×10^{4} in^3
Hydraulic conductivity:	1 m/min	= 3.281 ft/min
	1 cm/min	= 0.03281 ft/min
	1 mm/min	= 0.003281 ft/min
	1 m/sec	= 3.281 ft/sec
	1 mm/sec	= 0.03281 ft/sec
	1 m/min	= 39.37 in./min
	1 cm/sec	= 0.3937 in./sec
	1 mm/sec	= 0.03937 in./sec
Coefficient of consolidation:	1 cm^2/sec	= 0.155 in^2/sec
	1 m^2/yr	= 4.915×10^{-5} in^2/sec
	1 cm^2/sec	= 1.0764×10^{-3} ft^2/sec

CONVERSION FACTORS FROM ENGLISH TO SI UNITS

Length:	1 ft	= 0.3048 m
	1 ft	= 30.48 cm
	1 ft	= 304.8 mm
	1 in.	= 0.0254 m
	1 in.	= 2.54 cm
	1 in.	= 25.4 mm
Area:	1 ft^2	= 929.03×10^{-4} m^2
	1 ft^2	= 929.03 cm^2
	1 ft^2	= 929.03×10^2 mm^2
	1 in^2	= 6.452×10^{-4} m^2
	1 in^2	= 6.452 cm^2
	1 in^2	= 645.16 mm^2
Volume:	1 ft^3	= 28.317×10^{-3} m^3
	1 ft^3	= 28.317×10^3 cm^3
	1 in^3	= 16.387×10^{-6} m^3
	1 in^3	= 16.387 cm^3
Force:	1 lb	= 4.448 N
	1 lb	= 4.448×10^{-3} kN
	1 lb	= 0.4536 kgf
	1 kip	= 4.448 kN
	1 U.S. ton	= 8.896 kN
	1 lb	= 0.4536×10^{-3} metric ton
	1 lb/ft	= 14.593 N/m

Stress:	1 lb/ft^2	= 47.88 N/m^2
	1 lb/ft^2	= 0.04788 kN/m^2
	1 U.S. ton/ft^2	= 95.76 kN/m^2
	1 kip/ft^2	= 47.88 kN/m^2
	1 lb/in^2	= 6.895 kN/m^2
Unit weight:	1 lb/ft^3	= 0.1572 kN/m^3
	1 lb/in^3	= 271.43 kN/m^3
Moment:	1 lb-ft	= 1.3558 N·m
	1 lb-in.	= 0.11298 N·m
Energy:	1 ft-lb	= 1.3558 J
Moment of inertia:	1 in^4	= 0.4162×10^6 mm^4
	1 in^4	= 0.4162×10^{-6} m^4
Section modulus:	1 in^3	= 0.16387×10^5 mm^3
	1 in^3	= 0.16387×10^{-4} m^3
Hydraulic conductivity:	1 ft/min	= 0.3048 m/min
	1 ft/min	= 30.48 cm/min
	1 ft/min	= 304.8 mm/min
	1 ft/sec	= 0.3048 m/sec
	1 ft/sec	= 304.8 mm/sec
	1 in./min	= 0.0254 m/min
	1 in./sec	= 2.54 cm/sec
	1 in./sec	= 25.4 mm/sec
Coefficient of consolidation:	1 in^2/sec	= 6.452 cm^2/sec
	1 in^2/sec	= 20.346×10^3 m^2/yr
	1 ft^2/sec	= 929.03 cm^2/sec

9E

Principles of Foundation Engineering



Braja M. Das
Dean Emeritus, California State University
Sacramento, California, USA

Nagaratnam Sivakugan
Associate Professor, College of Science & Engineering
James Cook University, Queensland, Australia

CENGAGE

Australia • Brazil • Mexico • Singapore • United Kingdom • United States



Principles of Foundation Engineering,
Ninth Edition
Braja M. Das, Nagaratnam Sivakugan

Product Director, Global Engineering: Timothy L. Anderson

Associate Media Content Developer: Angie Rubino

Product Assistant: Alexander Sham

Marketing Manager: Kristin Stine

Senior Content Project Manager: Michael Lepera

Manufacturing Planner: Doug Wilke

IP Analyst: Christine Myaskovsky

IP Project Manager: Sarah Shainwald

Text and Image Permissions Researcher: Kristiina Paul

Production Service: RPK Editorial Services, Inc.

Compositor: MPS Limited

Senior Art Director: Michelle Kunkler

Text Designer: Terri Wright

Cover Designer: Imbue Design/Kim Torbeck

Cover Image: Spinel/Shutterstock.com

© 2019, 2016 Cengage Learning, Inc.

Unless otherwise noted, all content is © Cengage

ALL RIGHTS RESERVED. No part of this work covered by the copyright herein may be reproduced or distributed in any form or by any means, except as permitted by U.S. copyright law, without the prior written permission of the copyright owner.

For product information and technology assistance, contact us at **Cengage Customer & Sales Support, 1-800-354-9706**.

For permission to use material from this text or product, submit all requests online at **www.cengage.com/permissions**. Further permissions questions can be emailed to **permissionrequest@cengage.com**.

Library of Congress Control Number: 2017948538

Student Edition:
ISBN: 978-1-337-70502-8

Loose-leaf Edition:
ISBN: 978-1-337-70529-5

Cengage
20 Channel Center Street
Boston, MA 02210
USA

Cengage is a leading provider of customized learning solutions with employees residing in nearly 40 different countries and sales in more than 125 countries around the world. Find your local representative at **www.cengage.com**.

Cengage products are represented in Canada by Nelson Education Ltd.

To learn more about Cengage platforms and services, visit **www.cengage.com**.

To register or access your online learning solution or purchase materials for your course, visit **www.cengagebrain.com**.

Printed in the United States of America
Print Number: 01 Print Year: 2017

To Janice, Rohini, Joe, Valerie,
and Elizabeth.

Contents

Preface xv
About the Authors xxi


Firma V/shutterstock.com

1 Introduction 1

1.1 Geotechnical Engineering 2
1.2 Foundation Engineering 2
1.3 Soil Exploration 2
1.4 Ground Improvement 3
1.5 Solution Methods 4
1.6 Numerical Modeling 4
1.7 Empiricism 5
1.8 Literature 5
REFERENCES 6

Part 1 Geotechnical Properties and Soil Exploration 7


EcoPrint/Shutterstock.com

2 Geotechnical Properties of Soil 8

2.1 Introduction 9
2.2 Grain-Size Distribution 9
2.3 Size Limits for Soil 12
2.4 Weight–Volume Relationships 12
2.5 Relative Density 16
2.6 Atterberg Limits 18
2.7 Liquidity Index 19
2.8 Activity 19
2.9 Soil Classification Systems 20
2.10 Hydraulic Conductivity of Soil 27
2.11 Steady-State Seepage 32
2.12 Effective Stress 33
2.13 Consolidation 36
2.14 Calculation of Primary Consolidation Settlement 41
2.15 Time Rate of Consolidation 42
2.16 Range of Coefficient of Consolidation, c_v 48
2.17 Degree of Consolidation Under Ramp Loading 49
2.18 Shear Strength 51
2.19 Unconfined Compression Test 56
2.20 Comments on Friction Angle, ϕ' 57
2.21 Correlations for Undrained Shear Strength, c_u 60
2.22 Selection of Shear Strength Parameters 60
2.23 Sensitivity 61

2.24 Summary 62
PROBLEMS 62
REFERENCES 65


Brendan Howard/Shutterstock.com

3 Natural Soil Deposits and Subsoil Exploration 67
3.1 Introduction 68

Natural Soil Deposits 68
3.2 Soil Origin 68
3.3 Residual Soil 69
3.4 Gravity-Transported Soil 70
3.5 Alluvial Deposits 71
3.6 Lacustrine Deposits 73
3.7 Glacial Deposits 74
3.8 Aeolian Soil Deposits 75
3.9 Organic Soil 76
3.10 Some Local Terms for Soil 76

Subsurface Exploration 77
3.11 Purpose of Subsurface Exploration 77
3.12 Subsurface Exploration Program 77
3.13 Exploratory Borings in the Field 80
3.14 Procedures for Sampling Soil 83
3.15 Split-Spoon Sampling and Standard Penetration Test 83
3.16 Sampling with a Scraper Bucket 92
3.17 Sampling with a Thin-Walled Tube 93
3.18 Sampling with a Piston Sampler 93
3.19 Observation of Water Tables 95
3.20 Vane Shear Test 96
3.21 Cone Penetration Test 100
3.22 Pressuremeter Test (PMT) 108
3.23 Dilatometer Test 111
3.24 Iowa Borehole Shear Test 114
3.25 K_0 Stepped-Blade Test 116
3.26 Coring of Rocks 117
3.27 Preparation of Boring Logs 120
3.28 Geophysical Exploration 121
3.29 Subsoil Exploration Report 127
3.30 Summary 128
PROBLEMS 129
REFERENCES 131


Skinfaxi/Shutterstock.com

4 Instrumentation and Monitoring in Geotechnical Engineering 134
4.1 Introduction 135
4.2 Need for Instrumentation 135
4.3 Geotechnical Measurements 136
4.4 Geotechnical Instruments 137
4.5 Planning an Instrumentation Program 142
4.6 Typical Instrumentation Projects 143
4.7 Summary 143
REFERENCES 143

Part 2 Soil Improvement 145


Nicolae Cucurudza/Shutterstock.com

5 Soil Improvement and Ground Modification 146

5.1 Introduction 147
5.2 General Principles of Compaction 147
5.3 Empirical Relationships for Compaction 150
5.4 Field Compaction 154
5.5 Compaction Control for Clay Hydraulic Barriers 156
5.6 Vibroflotation 160
5.7 Blasting 164
5.8 Precompression 165
5.9 Sand Drains 170
5.10 Prefabricated Vertical Drains 179
5.11 Lime Stabilization 184
5.12 Cement Stabilization 187
5.13 Fly-Ash Stabilization 189
5.14 Stone Columns 189
5.15 Sand Compaction Piles 194
5.16 Dynamic Compaction 195
5.17 Jet Grouting 198
5.18 Deep Mixing 199
5.19 Summary 201

PROBLEMS 201
REFERENCES 202

Part 3 Foundation Analysis 205


stockthrone.com/Shutterstock.com

6 Shallow Foundations: Ultimate Bearing Capacity 206

6.1 Introduction 207
6.2 General Concept 208
6.3 Terzaghi's Bearing Capacity Theory 212
6.4 Factor of Safety 216
6.5 Modification of Bearing Capacity Equations for Water Table 217
6.6 The General Bearing Capacity Equation 218
6.7 Other Solutions for Bearing Capacity, Shape, and Depth Factors 225
6.8 Case Studies on Ultimate Bearing Capacity 227
6.9 Effect of Soil Compressibility 231
6.10 Eccentrically Loaded Foundations 235
6.11 Ultimate Bearing Capacity Under Eccentric Loading—One-Way Eccentricity 236
6.12 Bearing Capacity—Two-Way Eccentricity 242
6.13 A Simple Approach for Bearing Capacity with Two-Way Eccentricity 249
6.14 Bearing Capacity of a Continuous Foundation Subjected to Eccentrically Inclined Loading 251
6.15 Plane-Strain Correction of Friction Angle 254

6.16 Summary 254
PROBLEMS 254
REFERENCES 256


PHATR/Shutterstock.com

7 Ultimate Bearing Capacity of Shallow Foundations: Special Cases 258

7.1 Introduction 259
7.2 Foundation Supported by a Soil with a Rigid Base at Shallow Depth 259
7.3 Foundations on Layered Clay 266
7.4 Bearing Capacity of Layered Soil: Stronger Soil Underlain by Weaker Soil ($c' - \phi'$ soil) 268
7.5 Bearing Capacity of Layered Soil: Weaker Soil Underlain by Stronger Soil 275
7.6 Continuous Foundation on Weak Clay with a Granular Trench 278
7.7 Closely Spaced Foundations—Effect on Ultimate Bearing Capacity 280
7.8 Bearing Capacity of Foundations on Top of a Slope 282
7.9 Bearing Capacity of Foundations on a Slope 285
7.10 Seismic Bearing Capacity and Settlement in Granular Soil 286
7.11 Foundations on Rock 289
7.12 Ultimate Bearing Capacity of Wedge-Shaped Foundations 291
7.13 Uplift Capacity of Foundations 293
7.14 Summary 298
PROBLEMS 299
REFERENCES 300


Bertold Werkmann/Shutterstock.com

8 Vertical Stress Increase in Soil 302

8.1 Introduction 303
8.2 Stress Due to a Concentrated Load 303
8.3 Stress Due to a Circularly Loaded Area 304
8.4 Stress Due to a Line Load 305
8.5 Stress Below a Vertical Strip Load of Finite Width and Infinite Length 306
8.6 Stress Below a Horizontal Strip Load of Finite Width and Infinite Length 310
8.7 Stress Below a Rectangular Area 312
8.8 Stress Isobars 317
8.9 Average Vertical Stress Increase Due to a Rectangularly Loaded Area 318
8.10 Average Vertical Stress Increase Below the Center of a Circularly Loaded Area 323
8.11 Stress Increase Under an Embankment 325
8.12 Westergaard's Solution for Vertical Stress Due to a Point Load 328
8.13 Stress Distribution for Westergaard Material 330

8.14 Summary 333
PROBLEMS 333
REFERENCES 335


Rachata Kietsirikul/Shutterstock.com

9 Settlement of Shallow Foundations 336

9.1 Introduction 337
9.2 Elastic Settlement of Shallow Foundation on Saturated Clay ($\mu_s = 0.5$) 337

Elastic Settlement in Granular Soil 339

9.3 Settlement Based on the Theory of Elasticity 339
9.4 Improved Equation for Elastic Settlement 350
9.5 Settlement of Sandy Soil: Use of Strain Influence Factor 354
9.6 Settlement of Foundation on Sand Based on Standard Penetration Resistance 361
9.7 Settlement Considering Soil Stiffness Variation with Stress Level 366
9.8 Settlement Based on Pressuremeter Test (PMT) 370
9.9 Settlement Estimation Using the $L_1 - L_2$ Method 375
9.10 Effect of the Rise of Water Table on Elastic Settlement 378

Consolidation Settlement 380

9.11 Primary Consolidation Settlement Relationships 380
9.12 Three-Dimensional Effect on Primary Consolidation Settlement 382
9.13 Settlement Due to Secondary Consolidation 386
9.14 Field Load Test 388
9.15 Presumptive Bearing Capacity 389
9.16 Tolerable Settlement of Buildings 390
9.17 Summary 392
PROBLEMS 392
REFERENCES 394


Kekyalyaynen/Shutterstock.com

10 Mat Foundations 396

10.1 Introduction 397
10.2 Combined Footings 397
10.3 Common Types of Mat Foundations 401
10.4 Bearing Capacity of Mat Foundations 403
10.5 Differential Settlement of Mats 406
10.6 Field Settlement Observations for Mat Foundations 407
10.7 Compensated Foundation 407
10.8 Structural Design of Mat Foundations 411
10.9 Summary 424
PROBLEMS 425
REFERENCES 425


Oliver Foerstner/Shutterstock.com

11 Load and Resistance Factor Design (LRFD) 427

11.1 Introduction 428
11.2 Design Philosophy 429

11.3 Allowable Stress Design (ASD) 431
11.4 Limit State Design (LSD) and Partial Safety Factors 432
11.5 Load and Resistance Factor Design (LRFD) 433
11.6 Summary 436
PROBLEMS 436
REFERENCES 437


DESIGNFACTS/Shutterstock.com

12 Pile Foundations 438
12.1 Introduction 439
12.2 Pile Materials 440
12.3 Continuous Flight Auger (CFA) Piles 450
12.4 Point Bearing and Friction Piles 451
12.5 Installation of Piles 452
12.6 Pile Driving 453
12.7 Load Transfer Mechanism 458
12.8 Equations for Estimating Pile Capacity 461
12.9 Meyerhof's Method for Estimating Q_p 463
12.10 Vesic's Method for Estimating Q_p 466
12.11 Coyle and Castello's Method for Estimating Q_p in Sand 469
12.12 Correlations for Calculating Q_p with SPT and CPT Results in Granular Soil 473
12.13 Frictional Resistance (Q_s) in Sand 474
12.14 Frictional (Skin) Resistance in Clay 480
12.15 Ultimate Capacity of Continuous Flight Auger Pile 485
12.16 Point Bearing Capacity of Piles Resting on Rock 487
12.17 Pile Load Tests 493
12.18 Elastic Settlement of Piles 497
12.19 Laterally Loaded Piles 502
12.20 Pile-Driving Formulas 514
12.21 Pile Capacity for Vibration-Driven Piles 520
12.22 Wave Equation Analysis 521
12.23 Negative Skin Friction 524

Group Piles 528
12.24 Group Efficiency 528
12.25 Ultimate Capacity of Group Piles in Saturated Clay 531
12.26 Elastic Settlement of Group Piles 534
12.27 Consolidation Settlement of Group Piles 536
12.28 Piles in Rock 538
12.29 Summary 539
PROBLEMS 539
REFERENCES 543


CHAIYA/Shutterstock.com

13 Drilled-Shaft Foundations 546
13.1 Introduction 547
13.2 Types of Drilled Shafts 547
13.3 Construction Procedures 548
13.4 Other Design Considerations 554

13.5 Load Transfer Mechanism 555
13.6 Estimation of Load-Bearing Capacity 556
13.7 Load-Bearing Capacity in Granular Soil 558
13.8 Load-Bearing Capacity in Granular Soil Based on Settlement 561
13.9 Load-Bearing Capacity in Clay 568
13.10 Load-Bearing Capacity in Clay Based on Settlement 570
13.11 Settlement of Drilled Shafts at Working Load 575
13.12 Lateral Load-Carrying Capacity—Characteristic Load and Moment Method 576
13.13 Drilled Shafts Extending into Rock 583
13.14 Summary 588
PROBLEMS 589
REFERENCES 590


1Roman Makedonsky/Shutterstock.com

14 Piled Rafts: An Overview 592
14.1 Introduction 593
14.2 Load-Settlement Plots of Unpiled and Piled Rafts Under Different Design Conditions 594
14.3 Poulos–Davis–Randolph Simplified Design Method 595
14.4 Case Study: Burj Khalifa Tower in Dubai 600
14.5 Summary 602
PROBLEMS 602
REFERENCES 602


CHAIYA/Shutterstock.com

15 Foundations on Difficult Soil 603
15.1 Introduction 604
Collapsible Soil 604
15.2 Definition and Types of Collapsible Soil 604
15.3 Physical Parameters for Identification 606
15.4 Procedure for Calculating Collapse Settlement 608
15.5 Foundations in Soil Not Susceptible to Wetting 609
15.6 Foundations in Soil Susceptible to Wetting 611
Expansive Soil 612
15.7 General Nature of Expansive Soil 612
15.8 Unrestrained Swell Test 615
15.9 Swelling Pressure Test 617
15.10 Classification of Expansive Soil on the Basis of Index Tests 621
15.11 Foundation Considerations for Expansive Soil 624
15.12 Construction on Expansive Soil 626
Sanitary Landfills 630
15.13 General Nature of Sanitary Landfills 630
15.14 Settlement of Sanitary Landfills 631
15.15 Summary 633
PROBLEMS 633
REFERENCES 634

Part 4 Lateral Earth Pressure and Earth Retaining Structures 637


Operation Shooting/Shutterstock.com

16 Lateral Earth Pressure 638

16.1 Introduction 639
16.2 Lateral Earth Pressure at Rest 640

Active Pressure 644

16.3 Rankine Active Earth Pressure 644
16.4 A Generalized Case for Rankine Active Pressure—Granular Backfill 649
16.5 Generalized Case for Rankine Seismic Active Earth Pressure—Granular Backfill 653
16.6 Rankine Active Pressure with Vertical Wall Backface and Inclined $c' - \phi'$ Soil Backfill 655
16.7 Coulomb's Active Earth Pressure 658
16.8 Lateral Earth Pressure Due to Surcharge 665
16.9 Active Earth Pressure for Earthquake Conditions—Granular Backfill 668
16.10 Active Earth Pressure for Earthquake Condition (Vertical Backface of Wall and $c' - \phi'$ Backfill) 672

Passive Pressure 676

16.11 Rankine Passive Earth Pressure 676
16.12 Rankine Passive Earth Pressure—Vertical Backface and Inclined Backfill 679
16.13 Coulomb's Passive Earth Pressure 681
16.14 Comments on the Failure Surface Assumption for Coulomb's Pressure Calculations 683
16.15 Caquot and Kerisel Solution for Passive Earth Pressure (Granular Backfill) 684
16.16 Solution for Passive Earth Pressure by the Lower Bound Theorem of Plasticity (Granular Backfill) 686
16.17 Passive Force on Walls with Earthquake Forces 688
16.18 Summary 691

PROBLEMS 691
REFERENCES 693


Jarous/Shutterstock.com

17 Retaining Walls 694

17.1 Introduction 695

Gravity and Cantilever Walls 697

17.2 Proportioning Retaining Walls 697
17.3 Application of Lateral Earth Pressure Theories to Design 698
17.4 Stability of Retaining Walls 699
17.5 Check for Overturning 701
17.6 Check for Sliding Along the Base 703
17.7 Check for Bearing Capacity Failure 706
17.8 Construction Joints and Drainage from Backfill 714

17.9 Comments on Design of Retaining Walls and a Case Study 717
17.10 Gravity Retaining-Wall Design for Earthquake Conditions 720

Mechanically Stabilized Retaining Walls 722

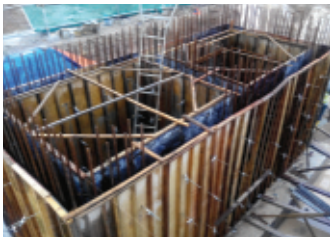
17.11 Soil Reinforcement 723
17.12 Considerations in Soil Reinforcement 723
17.13 General Design Considerations 727
17.14 Retaining Walls with Metallic Strip Reinforcement 728
17.15 Step-by-Step-Design Procedure Using Metallic Strip Reinforcement 734
17.16 Retaining Walls with Geotextile Reinforcement 738
17.17 Retaining Walls with Geogrid Reinforcement—General 744
17.18 Design Procedure for Geogrid-Reinforced Retaining Wall 746
17.19 Summary 748
PROBLEMS 749
REFERENCES 750


Aisyaqilumaranas/Shutterstock.com

18 Sheet-Pile Walls 752

18.1 Introduction 753
18.2 Construction Methods 756
18.3 Cantilever Sheet-Pile Walls 757
18.4 Cantilever Sheet Piling Penetrating Sandy Soil 758
18.5 Special Cases for Cantilever Walls Penetrating a Sandy Soil 764
18.6 Cantilever Sheet Piling Penetrating Clay 767
18.7 Special Cases for Cantilever Walls Penetrating Clay 772
18.8 Cantilever Sheet Piles Penetrating Sandy Soil—A Simplified Approach 775
18.9 Anchored Sheet-Pile Walls 779
18.10 Free Earth Support Method for Penetration of Sandy Soil—A Simplified Approach 780
18.11 Free Earth Support Method for Penetration of Sandy Soil—Net Lateral Pressure Method 782
18.12 Design Charts for Free Earth Support Method (Penetration into Sandy Soil) 785
18.13 Moment Reduction for Anchored Sheet-Pile Walls Penetrating into Sand 789
18.14 Computational Pressure Diagram Method for Penetration into Sandy Soil 792
18.15 Field Observations for Anchor Sheet-Pile Walls 795
18.16 Free Earth Support Method for Penetration of Clay 797
18.17 Anchors 802
18.18 Holding Capacity of Deadman Anchors 804
18.19 Holding Capacity of Anchor Plates in Sand 804
18.20 Holding Capacity of Anchor Plates in Clay ($\phi = 0$ Condition) 811

18.21 Ultimate Resistance of Tiebacks 811
18.22 Summary 812
PROBLEMS 812
REFERENCES 813


Aisyaqilumaranas/Shutterstock.com

19 Braced Cuts 814
19.1 Introduction 815
19.2 Braced-Cut Analysis Based on General Wedge Theory 817
19.3 Pressure Envelope for Braced-Cut Design 820
19.4 Pressure Envelope for Cuts in Layered Soil 822
19.5 Design of Various Components of a Braced Cut 823
19.6 Case Studies of Braced Cuts 831
19.7 Bottom Heave of a Cut in Clay 835
19.8 Stability of the Bottom of a Cut in Sand 839
19.9 Lateral Yielding of Sheet Piles and Ground Settlement 843
19.10 Summary 845
PROBLEMS 845
REFERENCES 846

Answers to Problems 847

Index 851

Preface

Soil mechanics and foundation engineering have developed rapidly during the last seventy years. Intensive research and observation in the field and the laboratory have refined and improved the science of foundation design. Originally published in the fall of 1983, *Principles of Foundation Engineering* is now in the ninth edition. It is intended primarily for use by undergraduate civil engineering students. The use of this text throughout the world has increased greatly over the years. It has also been translated into several languages. New and improved materials that have been published in various geotechnical engineering journals and conference proceedings, consistent with the level of understanding of the intended users, have been incorporated into each edition of the text.

NEW TO THIS EDITION

Based on the increased developments in the field of geotechnical engineering, the authors have added three new chapters to this edition. The ninth edition of *Principles of Foundation Engineering* contains a total of 19 chapters. Listed here is a summary of the major revisions from the eighth edition and new additions to this edition.

- Numerous new photographs in full color have been included in various chapters as needed.
- The **Introduction** Chapter (Chapter 1) has been entirely revised and expanded with sections on geotechnical engineering, foundation engineering, soil exploration, ground improvement, solution methods, numerical modeling, empiricism, and literature.
- Chapter 2 on **Geotechnical Properties of Soil** includes new sections on the range of coefficient of consolidation and selection of shear strength parameters for design. All of the end-of-chapter problems are new.
- Chapter 3 on **Natural Soil Deposits and Subsoil Exploration** has an improved figure on soil behavior type chart based on cone penetration test. Approximately half of the end-of-chapter problems are new.
- Chapter 4 on **Instrumentation and Monitoring in Geotechnical Engineering** is a new chapter that describes the use of instruments in geotechnical projects, such as piezometer, earth pressure cell, load cell, inclinometer, settlement plate, strain gauge, and others.
- **Soil Improvement** (Chapter 5) has some details on typical compaction requirements as well as improved figures in the section of precompression. About half of the problems at the end of the chapter are new.
- Chapter 6 on **Shallow Foundations: Ultimate Bearing Capacity** has new sections on a simple approach for bearing capacity with two-way eccentricities, and plane strain correction of friction angle.
- Chapter 7 on **Ultimate Bearing Capacity on Shallow Foundation: Special Cases** has a section on ultimate bearing capacity of a wedge-shaped foundation. About half of the end-of-chapter problems are new.
- Chapter 8 on **Vertical Stress Increase in Soil** has a new section on stress below a horizontal strip load of finite width and infinite length. The majority of the end-of-chapter problems are new.

- In Chapter 9 on **Settlement of Shallow Foundations**, Section 9.3 on settlement based on the theory of elasticity has been thoroughly revised with the addition of the results of the studies of Poulos and Davis (1974) and Giroud (1968). In Section 9.6, which discusses the topic of settlement of foundation on sand based on standard penetration resistance, Terzaghi and Peck's method (1967) has been added. Elastic settlement considering soil stiffness variation with stress level is given in a new section (Section 9.7). Other additions include settlement estimation using the $L_1 - L_2$ method (Section 9.9) (Akbas and Kulhawy, 2009) and Shahriar et al.'s (2014) method to estimate elastic settlement in granular soil due to the rise of ground water table (Section 9.10). The section on tolerable settlement of buildings has been fully revised. More than half of the end-of-chapter problems are new.
- In Chapter 10 on **Mat Foundations**, the reinforcement design portion for the mats was removed to concentrate more on the geotechnical portion. All end-of-chapter problems are new.
- Chapter 11 on **Load and Resistance Factor Design (LRFD)** is a new chapter. It provides the design philosophies of the allowable stress design (ASD) and load and resistance factor design in a simple way.
- Chapter 12 on **Pile Foundations** has a new section defining point bearing and friction piles (Section 12.5). Section 12.5 on installation of piles has been thoroughly revised. Factor of safety for axially loaded piles suggested by USACE (1991) has been incorporated in Section 12.8 on equations for estimating pile capacity. The analysis by Poulos and Davis (1974) for estimation of elastic settlement of piles has been included in Section 9.17. About half of the end-of-chapter problems are new.
- In Chapter 13 on **Drilled Shaft Foundations**, several figures have been improved to aid in better interpolation for solving problems. More than half of the end-of-chapter problems are new.
- Chapter 14 on **Piled Rafts—An Overview** is a new chapter. It describes optimizations of the advantages of pile foundations and raft foundations for construction of very tall buildings.
- In Chapter 15 on **Foundations on Difficult Soil**, all but two of end-of-chapter problems are new.
- Chapter 16 on **Lateral Earth Pressure** has two new sections on (a) generalized case for Rankine seismic active pressure—granular backfill (Section 16.5), and (b) solution for passive earth pressure by lower bound theorem of plasticity (Section 16.15). The section on passive force on walls with earthquake forces (Section 16.7) has been expanded. All end-of-chapter problems are new.
- In Chapter 17 on **Retaining Walls**, a new section (Section 17.10) on gravity retaining wall design for earthquake conditions has been added. Discussion on the properties of geotextile has been expanded along with some new geotextile photographs. More than half of the end-of-chapter problems are new.
- Chapter 18 on **Sheet-Pile Walls** has three new sections added: (a) cantilever sheet piles penetrating sandy soil—a simplified approach (Section 18.8); (b) free earth support method for penetration of sandy soil—a simplified approach (Section 18.10); and (c) holding capacity of deadman anchors (Section 18.18). All end-of-chapter problems are new.
- In Chapter 19 on **Braced Cuts**, all end-of-chapter problems are new.
- Each chapter now includes a **Summary** section. New and revised example problems are presented in various chapters as needed.

INSTRUCTOR RESOURCES

A detailed **Instructor's Solutions Manual** containing solutions to all end-of-chapter problems, an **image bank** with figures and tables in the book, and **Lecture Note PowerPoint Slides** are available via a secure, password-protected Instructor Resource Center at https://login.cengage.com.

Principles of Foundation Engineering is also available through **MindTap**, Cengage's digital course platform. See the following section for more details about this format.

Custom Options for *Principles of Foundation Engineering*

Would you prefer to easily create your own personalized text, choosing the elements that best serve your course's unique learning objectives?

Cengage's Compose platform provides the full range of Cengage content, allowing you to create exactly the textbook you need. The Compose website lets you quickly review materials to select everything you need for your text. You can even seamlessly add your own materials, like exercises, notes, and handouts! Easily assemble a new print or eBook and then preview it on our site.

Cengage offers the easiest and fastest way to create custom learning materials that are as unique as your course is. To learn more about customizing your book with Compose, visit compose.cengage.com, or contact your Cengage Learning Consultant.

ACKNOWLEDGMENTS

- We are deeply grateful to Janice Das for her assistance in completing the revision. She has been the driving force behind this textbook since the preparation of the first edition.
- Special thanks are due to Rohini Sivakugan for her help during the preparation of the manuscript for this edition.
- It is fitting to thank Rose P. Kernan of RPK Editorial Services. She has been instrumental in shaping the style and overseeing the production of this edition of *Principles of Foundation Engineering* as well as several previous editions.
- We also wish to thank the Global Engineering team at Cengage who worked in the development of this edition. Especially, we would like to extend our thanks to Timothy Anderson, Product Director; Angie Rubino, Associate Content Developer; Kristin Stine, Marketing Manager; and Alexander Sham, Product Assistant.

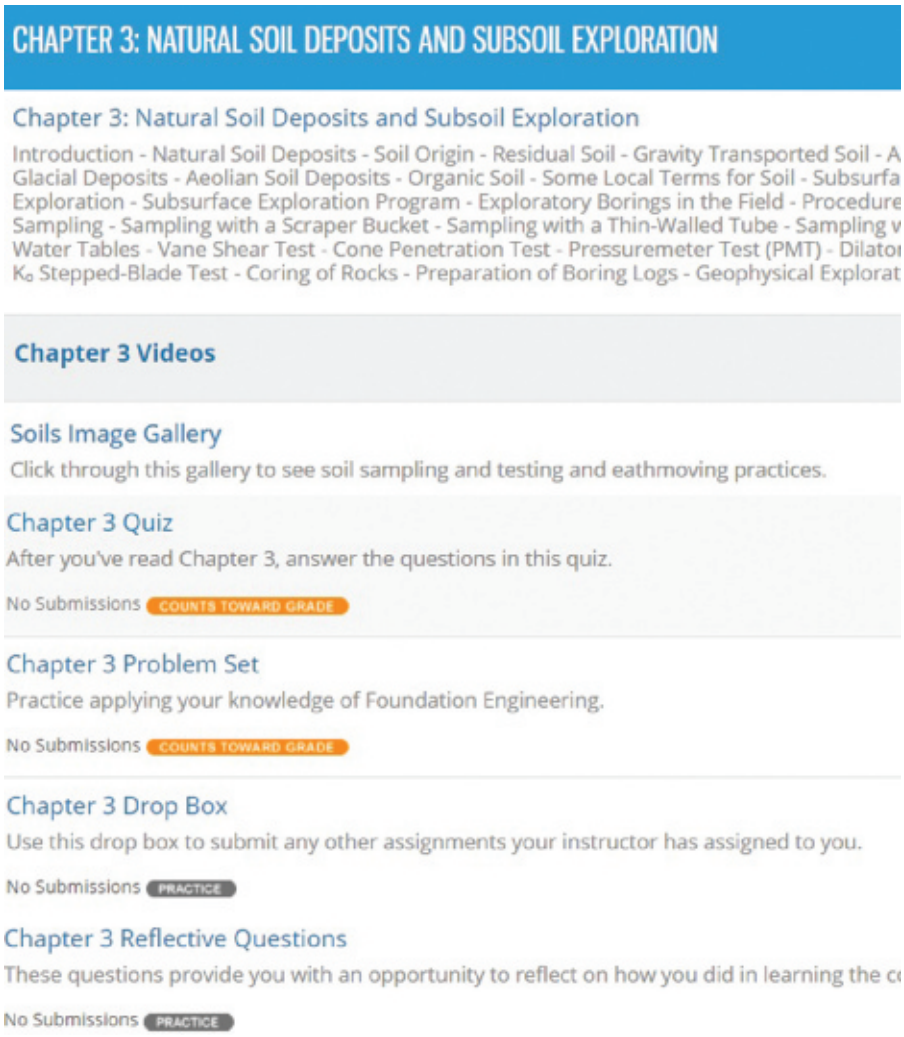
Braja M. Das

Nagaratnam Sivakugan

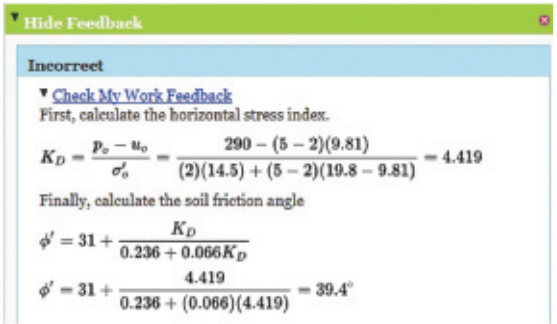
MindTap Online Course



Principles of Foundation Engineering, Ninth Edition is also available with **MindTap**, Cengage's digital learning experience. The textbook's carefully-crafted pedagogy and exercises are made even more effective by an interactive, customizable eBook accompanied by automatically graded assessments and a full suite of study tools.



MindTap gives you complete control of your course—to provide engaging content, to challenge every individual, and to prepare students for professional practice. Adopting MindTap cuts your prep time and lets you teach more effectively with videos, assessments, algorithmically generated problem sets, and



more. Built-in metrics provide insight into engagement, identify topics needing extra instruction, and let you instantly communicate with your students. Finally, every MindTap adoption includes support from our dedicated, personalized team. We'll help you set up your course, tailor it to your specifications, and stand by to offer support to you and your students whenever you need us.

How Does MindTap Benefit Instructors?

- Customize and personalize your course by integrating your own content into the **MindTap Reader** (like lecture notes, audio and video recordings, or problem sets to download) or pull from sources such as RSS feeds, YouTube videos, websites, and more.
- Save grading time by leveraging MindTap's **automatically graded assignments and quizzes**, including **algorithmically generated problem sets.** These problems include immediate, specific feedback, so students know exactly where they need more practice.



- The **Message Center** helps you to quickly and easily contact students directly from MindTap. Messages are communicated immediately by email, social media, or even text message.
- **StudyHub** is an all-in-one studying destination that allows you to deliver important information and empowers your students to personalize their experience. Instructors can choose to annotate the text with **notes** and **highlights**, share content from the MindTap Reader, and create custom **flashcards** to help their students focus and succeed.
- The **Progress App** lets you know exactly how your students are doing (and where they are struggling) with live analytics. You can see overall class engagement levels and drill down into individual student performance, enabling you to identify topics needing extra instruction and instantly communicate with struggling students to speed progress.

How Does MindTap Benefit Your Students?

- The **MindTap Mobile App** includes the entire eBook accompanied by flashcards, quizzes, and course alerts to help students understand core concepts, achieve better grades, and prepare for their future courses.
- **Flashcards** are prepopulated to provide a jump start on studying, and students and instructors can also create customized cards as they move through the course.



- The **Progress App** allows students to monitor their individual grades, as well as their level compared to the class average. This not only helps them stay on track in the course but also motivates them to do more, and ultimately to do better.
- The **StudyHub** is a single-destination studying tool that empowers students to personalize their experience. They can quickly and easily access all notes and highlights marked in the MindTap Reader, locate bookmarked pages, review notes and Flashcards shared by their instructor, and create custom study guides.
- The **MindTap Reader** includes the abilities to have the content read aloud, to print from the digital textbook, and to take notes and highlights directly in the text while also capturing them within the linked **StudyHub App**.

For more information about MindTap for Engineering, or to schedule a demonstration, please call (800) 354-9706 or email higheredcs@cengage.com. For instructors outside the United States, please visit http://www.cengage.com /contact/ to locate your regional office.

About the Authors

Dr. Braja Das is Dean Emeritus of the College of Engineering and Computer Science at California State University, Sacramento. He received his B.Sc. degree with honors in Physics and B.Sc. degree in Civil Engineering from Utkal University, India; his M.S. in Civil Engineering from the University of Iowa, Iowa City; and his Ph.D. in Geotechnical Engineering from the University of Wisconsin at Madison. He is the author of a number of geotechnical engineering texts and reference books and more than 300 technical papers. His primary areas of research include shallow foundations, earth anchors, and geosynthetics.

Dr. Das is a Fellow and Life Member of the American Society of Civil Engineers, a Life Member of the American Society for Engineering Education, and an Emeritus Member of the Stabilization of Geomaterials and Recycled Materials Committee of the Transportation Research Board of the National Research Council (Washington DC). He has previously served as a member on the editorial board of the Journal of Geotechnical Engineering of ASCE, a member of the editorial board of Lowland Technology International Journal (Japan), as associate editor of the International Journal of Offshore and Polar Engineering (ISOPE), and as co-editor of the Journal of Geotechnical and Geological Engineering (Springer, The Netherlands). Presently he is the editor-in-chief of the International Journal of Geotechnical Engineering (Taylor & Francis, U.K.). He has received numerous awards for teaching excellence, including the AMOCO Foundation Award, the AT&T Award for Teaching Excellence from the American Society for Engineering Education, the Ralph Teetor Award from the Society of Automotive Engineers, and the Distinguished Achievement Award for Teaching Excellence from the University of Texas at El Paso.

Dr. Das is widely recognized in his field and has been invited as a keynote speaker to multiple conferences worldwide. His prolific career has taken him to Australia, Mexico, the Dominican Republic, Costa Rica, El Salvador, Peru, Colombia, Ecuador, India, Korea, Bolivia, Venezuela, Turkey, the Turkish Republic of North Cyprus, United Arab Emirates, Tunisia, and the United Kingdom. He has also been named as the first Eulalio Juárez Badillo Lecturer by the Mexican Society of Geotechnical Engineers. The Soil-Structure Interaction Group of Egypt established an honor lecture series that takes place once every two years in Egypt. The first lecture was delivered during the Geo-Middle-East Conference in July 2017.

Dr. Nagaratnam Sivakugan received his Bachelor's degree in Civil Engineering from the University of Peradeniya, Sri Lanka, with First Class Honors. He earned his MSCE and Ph.D. from Purdue University, West Lafayette, USA Dr. Sivakugan's writings include eight books, 140 refereed international journal papers, 100 refereed international conference papers, and more than 100 consulting reports. As a registered professional engineer of Queensland and a chartered professional engineer, Dr. Sivakugan does substantial consulting work for the geotechnical and mining industry in Australia and overseas, including the World Bank. He is a Fellow of the American Society of Civil Engineers and Engineers Australia. He has supervised 14 Ph.D. students to completion at James Cook University, Queensland, Australia, where he was the Head of Civil Engineering from 2003 to 2014. He is an Associate Editor for three international journals and serves on the editorial boards of the Canadian Geotechnical Journal and the Indian Geotechnical Journal.

1

Introduction



Firma V/shutterstock.com

1.1 Geotechnical Engineering 2
1.2 Foundation Engineering 2
1.3 Soil Exploration 2
1.4 Ground Improvement 3
1.5 Solution Methods 4
1.6 Numerical Modeling 4
1.7 Empiricism 5
1.8 Literature 5
REFERENCES 6

1.1 Geotechnical Engineering

Geotechnical engineering, also known as *geomechanics*, is an emerging area in civil engineering. It deals with soil mechanics, with some emphasis on rock mechanics, where we apply engineering principles, such as the theory of elasticity, Mohr's circle, and continuum mechanics, to develop simple solutions that can be applied to geotechnical and foundation engineering problems. When dealing with problems related to *geomaterials*, which include soil, aggregates, and rocks, some knowledge of geology is always an advantage.

A thorough understanding of the geotechnical engineering fundamentals is a prerequisite for studying foundation engineering. These include phase relations, soil classification, compaction, permeability, seepage, consolidation, shear strength, slope stability, and soil exploration. These areas are covered in *Principles of Geotechnical Engineering* (9th Edition) in good detail. The main points are discussed very briefly in Chapters 2 and 3 in Part 1 of this text.

A new chapter on *geotechnical instrumentation* is included in this edition as Chapter 4 in Part 1. When projects become complex or the design or construction methods are nonstandard, it is often advisable to use instruments and measure the loads, stresses, deformations, and strains at critical locations and monitor them over a certain period to ensure the performance of the structure is satisfactory. This new chapter gives an overview of the major instruments used in geotechnical engineering.

1.2 Foundation Engineering

Every civil engineering project has some geotechnical or foundation engineering component. This includes all earth and earth-supported structures, namely, *foundations* and *earth-retaining structures*, the two broad categories discussed in this book. The related chapters are bundled into Parts 3 and 4, respectively. Under foundations (Part 3), shallow foundations and deep foundations are discussed. In this edition, a new chapter is introduced on the *load and resistance factor design* (LRFD) method, which is quite different compared to the traditional *allowable stress design* (ASD) method that has been used by geotechnical engineers for decades. The LRFD was initially brought into practice by the American Concrete Institute (ACI) in the 1960s. It is widely used in structural engineering and is becoming popular in foundation engineering applications such as footings, piles, and retaining walls. The main difference between LRFD and ASD is the way the safety factor is applied.

A new introductory chapter on piled-raft foundations is included in this edition (Chapter 14). Piled rafts exploit the advantages of piles and rafts, two different types of foundations. For tall buildings, they appear to give economical solutions compared to those given by rafts or piles alone.

Retaining walls, sheet piles, and braced cuts are covered under earth-retaining structures in Part 4.

1.3 Soil Exploration

All geotechnical designs require knowledge of the soil and rock properties in the vicinity of the structure. These are determined through a *soil exploration* (also known as *site investigation*) program that consists of (a) *in situ* tests, (b) sampling at the



FIGURE 1.1 Soil exploration program (Courtesy of N. Sivakugan, James Cook University, Australia)

site, and (c) laboratory tests on the samples taken from the site. Based on the soil exploration data, a simplified soil profile can be developed, which can be the basis for geotechnical designs. Figure 1.1 shows drilling in progress as part of a subsoil investigation.

The heterogeneous nature of the ground conditions and the spatial variability in the soil properties make it difficult to assign the design parameters to a simplified soil model. Every borehole and its associated tests can cost thousands of dollars to the client, and it is often the case that our wish list is longer than what the budget permits. Therefore, it is prudent to plan the soil exploration program to extract the maximum possible data from the ground that is relevant to the project at a reasonable cost.

Due to budgetary constraints, it is sometimes necessary to strike a balance between laboratory and *in situ* tests. The same parameters can be determined by laboratory or *in situ* tests. Some good geotechnical judgment is required here to select the right tests. Laboratory and *in situ* tests must complement each other. One should never be chosen at the expense of the other. They have their own advantages and disadvantages.

1.4 Ground Improvement

When designing a beam or a bridge, an engineer has the luxury of specifying the strength of concrete. The same thing applies to most engineering materials. When it comes to soil, the situation is different. Once the site is identified, one has to design the structure to suit the soil conditions. Any attempt to replace the soil with a better-performing soil can be an expensive option. However, the existing ground can be improved through one of the many ground improvement techniques.

Very often, the soil conditions at a site do not meet the design requirements in their present form. The soil may be too weak, undergo excessive deformations, and/or lead to possible failure. Even if the soil at the surface is suitable, the subsoil conditions may be unfavorable. Designing the structure or facility to suit the existing soil conditions is not necessarily the best option. Instead, improving the ground and looking for more economical alternatives can save millions of dollars.

Compaction is a simple and inexpensive ground improvement technique that works on all types of soil. Figure 1.2 shows some soil compaction in progress for a highway construction project. The other ground improvement techniques include



FIGURE 1.2 Soil compaction for a highway construction project (Courtesy of N. Sivakugan, James Cook University, Australia)

vibroflotation, dynamic compaction, blasting, preloading, vertical drains, lime/cement stabilization, stone columns, jet grouting, and deep mixing. They are discussed briefly in Chapter 5 (Part 2).

1.5 Solution Methods

In geotechnical or foundation engineering, there are three ways of solving a problem. They are:

- analytical methods
- physical modeling
- numerical modeling

For simple problems, similar to those discussed in textbooks, it is possible to apply the geotechnical engineering principles and the closed form solutions available in the literature. This applies to situations where the soil conditions are relatively uniform and the boundary conditions are well defined. In some instances, it is also possible to build a small scale model that can be tested in the laboratory to investigate the different scenarios. This is known as physical modeling. In larger projects, where the soil conditions and the boundary conditions are complex, it is difficult to apply the geotechnical theories and arrive at closed form solutions. Here, numerical modeling becomes a valuable tool. Once the model is developed, it can be used to carry out a thorough sensitivity analysis, exploring the effects of different parameters on the performance of the structure.

1.6 Numerical Modeling

Soil is a *particulate* medium. For simplicity it is treated as a *continuum*, which is assumed to follow one of the many *constitutive models* such as Mohr–Coulomb, linear elastic, nonlinear elastic, Cam Clay, or Drucker–Prager. These constitutive models

define how the soil behaves. The *boundary conditions* define the loadings and displacements at the boundaries of the region of interest.

In large projects, the boundary conditions can be so complex that it is not possible to carry out the traditional analysis using the simplified theories, equations, and design charts covered in textbooks. This situation is even made more complex by the soil variability. Under these circumstances, *numerical modeling* can be very useful. Numerical modeling can be carried out on foundations, retaining walls, dams, and other earth-supported structures. This can model the *soil-structure interaction* very effectively.

Finite element analysis and *finite difference* analysis are two different numerical modeling techniques. Here, the problem domain is divided into a *mesh*, consisting of thousands of *elements* and *nodes*. Boundary conditions and appropriate constitutive models are specified to the problem domain, and equations are developed for the nodes/elements. By solving these equations, the variables at the nodes/elements are determined.

There are people who write their own finite element program to solve a specific geotechnical problem. For novices, there are off-the-shelf programs that can be used for such purposes. *PLAXIS* (http://www.plaxis.nl) is a very popular finite element program that is widely used by professional engineers. *FLAC* (http://www.itasca.com) is a powerful finite difference program used in geotechnical and mining engineering. There are also other numerical modeling software programs tailored for geotechnical applications, such as those developed by GEO-SLOPE International Ltd. (http://www.geo-slope.com), Soil Vision Systems Ltd. (http://www.soilvision.com), and GGU-Software (http://www.ggu-software.com). In addition, some of the more powerful software packages developed for structural, material, and concrete engineering also have the ability to model geotechnical problems. *Abaqus*® and *Ansys*® are two such finite element packages that are widely used in universities for teaching and research.

1.7 Empiricism

Experience, intuition, and judgment play a major role in geotechnical engineering. In addition to what has been developed through rational theories in soil and rock mechanics, there are many lessons learned through decades of experience, which help in fine-tuning these theoretical developments that may have been oversimplified. Empiricism is knowledge developed through experience, intuition, and judgment, often backed by reliable data.

There are literally hundreds of empirical correlations in the form of equations or charts that can be used in deriving soil properties. They were developed from large databases and are very valuable in the preliminary design stages, when limited soil data are available. These are derived based on laboratory or field data, past experience, and good judgment.

Geotechnical data, whether from the field or laboratory, can be quite expensive. We often have access to very limited field data [e.g., Standard Penetration Test (SPT)] from a limited number of boreholes, along with some laboratory test data on samples obtained from these boreholes and/or trial pits. We use the empirical correlations sensibly to complement the site investigation program and, hence, extract the maximum possible information from the limited laboratory and field data.

1.8 Literature

There are times when one is expected to go beyond what is covered in textbooks. When you are carrying out research on a new topic or trying to learn more about something covered only briefly in the textbook, a thorough literature review is

necessary. A Web search can be a good start in locating some literature. There are also specialized geotechnical journals and conference proceedings that discuss the latest developments.

The U.S. Army, Navy, and Air Force do excellent engineering work and invest significantly in research and development. Their design guides, empirical equations, and charts are well proven and tested. They are generally conservative, which is desirable in engineering practice. Most of these manuals are available for free download. They (e.g., NAVFAC 7.1) are valuable additions to your professional libraries. The *Canadian Foundation Engineering Manual* (Canadian Geotechnical Society 2006), Kulhawy and Mayne (1990), and Ameratunga et al. (2016) have collated and critically reviewed the empirical correlations relating the soil and rock properties derived from laboratory and *in situ* tests.

REFERENCES

Ameratunga, J., Sivakugan, N., and Das, B. M. (2016). *Correlations of Soil and Rock Properties in Geotechnical Engineering*, Springer, New Delhi, India.

Canadian Geotechnical Society (2006). *Canadian Foundation Engineering Manual*, 4th ed., BiTech Publisher Ltd., British Columbia, Canada.

Kulhawy, F. H. and Mayne, P. W. (1990). *Manual on Estimating Soil Properties for Foundation Design*, Final Report 1493-6, ET-6800, Electric Power Research Institute (EPRI), Palo Alto, CA.

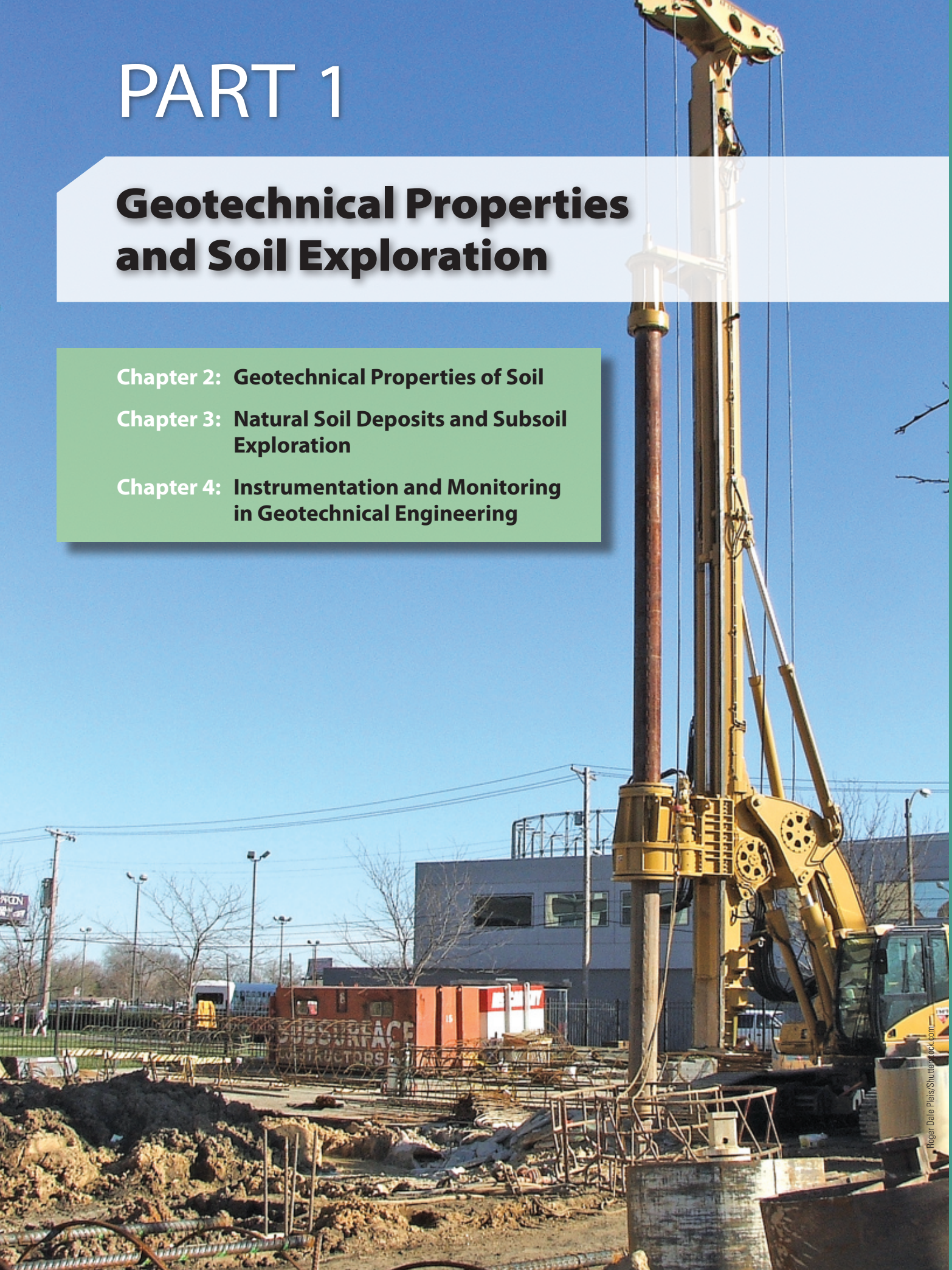
PART 1

Geotechnical Properties and Soil Exploration

Chapter 2: Geotechnical Properties of Soil

Chapter 3: Natural Soil Deposits and Subsoil Exploration

Chapter 4: Instrumentation and Monitoring in Geotechnical Engineering



Roger Dale Pleis/Shutterstock.com

2

Geotechnical Properties of Soil



EcoPrint/Shutterstock.com

2.1 Introduction 9
2.2 Grain-Size Distribution 9
2.3 Size Limits for Soils 12
2.4 Weight–Volume Relationships 12
2.5 Relative Density 16
2.6 Atterberg Limits 18
2.7 Liquidity Index 19
2.8 Activity 19
2.9 Soil Classification Systems 20
2.10 Hydraulic Conductivity of Soil 27
2.11 Steady-State Seepage 32
2.12 Effective Stress 33
2.13 Consolidation 36
2.14 Calculation of Primary Consolidation Settlement 41
2.15 Time Rate of Consolidation 42
2.16 Range of Coefficient of Consolidation, c_v 48
2.17 Degree of Consolidation Under Ramp Loading 49
2.18 Shear Strength 51
2.19 Unconfined Compression Test 56
2.20 Comments on Friction Angle, ϕ' 57
2.21 Correlations for Undrained Shear Strength, c_u 60
2.22 Selection of Shear Strength Parameters 60
2.23 Sensitivity 61
2.24 Summary 62
PROBLEMS 62
REFERENCES 65

2.1 Introduction

The design of foundations of structures such as buildings, bridges, and dams generally requires a knowledge of such factors as (a) the load that will be transmitted by the superstructure to the foundation system, (b) the requirements of the local building code, (c) the behavior and stress-related deformability of soil that will support the foundation system, and (d) the geological conditions of the soil under consideration. To a foundation engineer, the last two factors are extremely important because they concern soil mechanics.

The geotechnical properties of a soil—such as its grain-size distribution, plasticity, compressibility, and shear strength—can be assessed by proper laboratory testing. In addition, recently emphasis has been placed on the *in situ* determination of strength and deformation properties of soil, because this process avoids disturbing samples during field exploration. However, under certain circumstances, not all of the needed parameters can be or are determined, because of economic or other reasons. In such cases, the engineer must make certain assumptions regarding the properties of the soil. To assess the accuracy of soil parameters—whether they were determined in the laboratory and the field or whether they were assumed—the engineer must have a good grasp of the basic principles of soil mechanics. At the same time, he or she must realize that the natural soil deposits on which foundations are constructed are not homogeneous in most cases. Thus, the engineer must have a thorough understanding of the geology of the area—that is, the origin and nature of soil stratification and also the groundwater conditions. Foundation engineering is a clever combination of soil mechanics, engineering geology, and proper judgment derived from past experience. To a certain extent, it may be called an art.

This chapter serves primarily as a review of the basic geotechnical properties of soil. It includes topics such as grain-size distribution, plasticity, soil classification, hydraulic conductivity, effective stress, consolidation, and shear strength parameters. It is assumed that you have already been exposed to these concepts in a basic soil mechanics course.

2.2 Grain-Size Distribution

Grain-size distribution is knowing what grain sizes are present within the soil in what percentage. The geotechnical characteristics of a coarse-grained soil are very much influenced by the grain size distribution. It is not so in the case of fine-grained soil, where the plasticity determines the geotechnical engineering behavior. Soil often contain both coarse and fine grains, and it is necessary to determine the grain-size distribution to classify them and to better understand their engineering properties. The grain-size distribution of *coarse-grained* soil is generally determined by means of *sieve analysis*. For a *fine-grained* soil, the grain-size distribution can be obtained by means of *hydrometer analysis*. The fundamental features of these analyses are presented in this section. For detailed descriptions, see any soil mechanics laboratory manual (e.g., Das, 2016). These days, a laser sizer is used for quick and precise determination of the grain-size distribution of soil where the grains are less than about 1 mm in size.

TABLE 2.1 U.S. Standard Sieve Sizes

Sieve No.	Opening (mm)
4	4.750
6	3.350
8	2.360
10	2.000
16	1.180
20	0.850
30	0.600
40	0.425
50	0.300
60	0.250
80	0.180
100	0.150
140	0.106
170	0.088
200	0.075
270	0.053

SIEVE ANALYSIS

A sieve analysis is conducted by taking a measured amount of dry, well-pulverized soil and passing it through a stack of progressively finer sieves with a pan at the bottom. The amount of soil retained on each sieve is measured, and the cumulative percentage of soil passing through each is determined. This percentage is generally referred to as *percent finer*. Table 2.1 contains a list of U.S. sieve numbers and the corresponding size of their openings. These sieves are commonly used for the analysis of soil for classification purposes.

The percent finer for each sieve, determined by a sieve analysis, is plotted on *semilogarithmic graph paper*, as shown in Figure 2.1. Since the grain diameter, D, can vary over a wide range, it is plotted on the *logarithmic scale*, and the percent finer is plotted on the *arithmetic scale*.

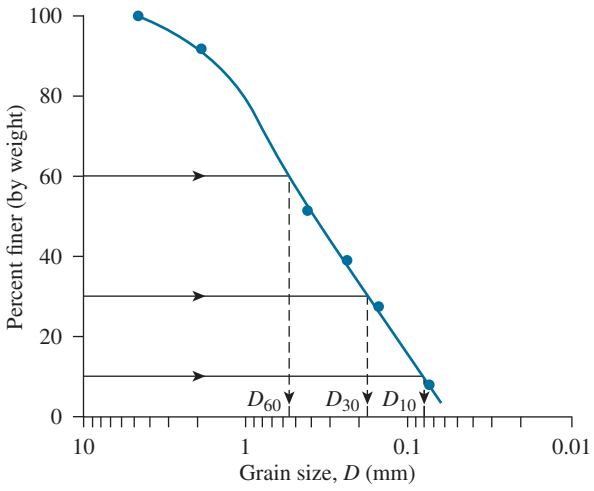


FIGURE 2.1

Two parameters can be determined from the grain-size distribution curves of coarse-grained soil: (1) the *uniformity coefficient* (C_u) and (2) the *coefficient of gradation*, or *coefficient of curvature* (C_c). These coefficients are

$$C_u = \frac{D_{60}}{D_{10}} \tag{2.1}$$

and

$$C_c = \frac{D_{30}^2}{(D_{60})(D_{10})} \tag{2.2}$$

where D_{10}, D_{30}, and D_{60} are the diameters corresponding to percents finer than 10, 30, and 60%, respectively (see Figure 2.1). D_{10} of a granular soil is known as the *effective grain size*, which is a measure of the permeability characteristics of the soil.

For the grain-size distribution curve shown in Figure 2.1, $D_{10} = 0.08$ mm, $D_{30} = 0.17$ mm, and $D_{60} = 0.57$ mm. Thus, the values of C_u and C_c are

$$C_u = \frac{0.57}{0.08} = 7.13$$

and

$$C_c = \frac{0.17^2}{(0.57)(0.08)} = 0.63$$

Parameters C_u and C_c are used in the *Unified Soil Classification System*, which is described later in the chapter.

HYDROMETER ANALYSIS

Hydrometer analysis is based on the principle of sedimentation of soil particles in water. This test involves the use of 50 grams of dry, pulverized soil. A *deflocculating agent* is always added to the soil. The most common deflocculating agent used for hydrometer analysis is 125 cc of 4% solution of sodium hexametaphosphate. The soil is allowed to soak for at least 16 hours in the deflocculating agent. After the soaking period, distilled water is added, and the soil–deflocculating agent mixture is thoroughly agitated. The sample is then transferred to a 1000 ml measuring cylinder. More distilled water is added to the cylinder to fill it to the 1000 ml mark, and then the mixture is again thoroughly agitated. A hydrometer is placed in the cylinder to measure the specific gravity of the soil–water suspension in the vicinity of the instrument's bulb (Figure 2.2), usually over a 24-hour period. Hydrometers are calibrated to show the amount of soil that is still in suspension at any given time t. The largest diameter of the soil particles still in suspension at time t can be determined by Stokes' law,

$$D = \sqrt{\frac{18\eta}{(G_s - 1)\gamma_w}}\sqrt{\frac{L}{t}} \tag{2.3}$$

where

D = diameter of the soil particle

G_s = specific gravity of soil solids

η = dynamic viscosity of water

γ_w = unit weight of water

L = effective length (i.e., length measured from the water surface in the cylinder to the center of gravity of the hydrometer; see Figure 2.2)

t = time

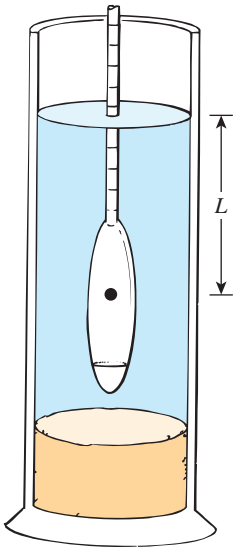


FIGURE 2.2 Hydrometer analysis

Soil particles having diameters larger than those calculated by Eq. (2.3) would have settled beyond the zone of measurement. In this manner, with hydrometer readings taken at various times, the soil *percent finer* than a given diameter D can be calculated and a grain-size distribution plot prepared. The sieve and hydrometer techniques may be combined for a soil having both coarse-grained and fine-grained soil constituents. Here, the soil fraction passing the No. 200 (0.075 mm) sieve is tested in the hydrometer.

2.3 Size Limits for Soil

Several organizations have attempted to develop the size limits for *gravel, sand, silt*, and *clay* on the basis of the grain sizes present in soil. Table 2.2 presents the size limits recommended by the American Association of State Highway and Transportation Officials (AASHTO) and the Unified Soil Classification System (Corps of Engineers, Department of the Army, and Bureau of Reclamation). The table shows that soil particles smaller than 0.002 mm have been classified as *clay*. However, clays by nature are cohesive and can be rolled into a thread when moist. This property is caused by the presence of *clay minerals* such as *kaolinite, illite*, and *montmorillonite*. In contrast, some minerals, such as *quartz* and *feldspar*, may be present in a soil in particle sizes as small as clay minerals, but these particles will not have the cohesive property of clay minerals. Hence, they are called *clay-size particles*, not *clay particles*.

2.4 Weight–Volume Relationships

In nature, soil are three-phase systems consisting of solid soil particles, water, and air (or gas). To develop the *weight–volume relationships* for a soil, the three phases can be separated as shown in Figure 2.3a. Based on this separation, the volume relationships can then be defined.

The *void ratio, e*, is the ratio of the volume of voids to the volume of soil solids in a given soil mass, or

$$e = \frac{V_v}{V_s} \tag{2.4}$$

where

V_v = volume of voids

V_s = volume of soil solids

TABLE 2.2 Soil-Separate Size Limits

Classification system	Grain size (mm)
USCS	Gravel: 75 mm to 4.75 mm
	Sand: 4.75 mm to 0.075 mm
	Silt and clay (fines): <0.075 mm
AASHTO	Gravel: 75 mm to 2 mm
	Sand: 2 mm to 0.05 mm
	Silt: 0.05 mm to 0.002 mm
	Clay: <0.002 mm

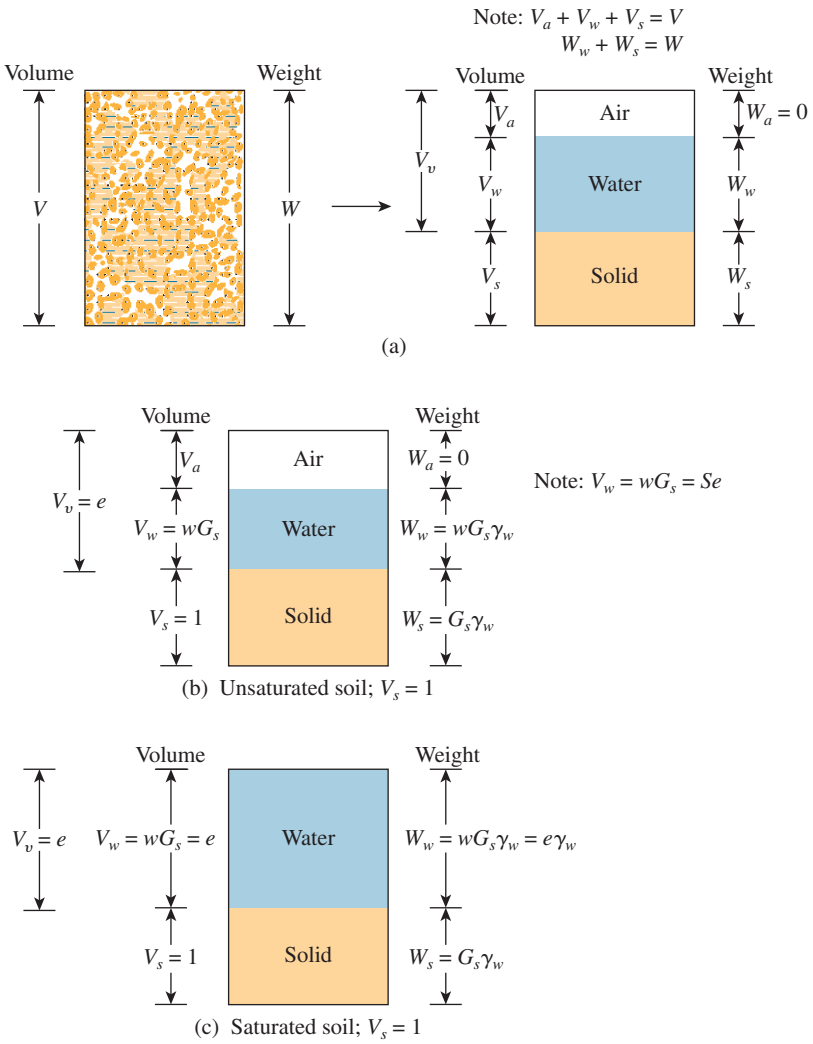


FIGURE 2.3 Weight–volume relationships

The *porosity, n*, is the ratio of the volume of voids to the volume of the soil specimen, or

$$n = \frac{V_v}{V} \tag{2.5}$$

where

V = total volume of soil

Moreover,

$$n = \frac{V_v}{V} = \frac{V_v}{V_s + V_v} = \frac{\dfrac{V_v}{V_s}}{\dfrac{V_s}{V_s} + \dfrac{V_v}{V_s}} = \frac{e}{1 + e} \tag{2.6}$$

The *degree of saturation, S*, is the ratio of the volume of water in the void spaces to the volume of voids, generally expressed as a percentage, or

$$S(\%) = \frac{V_w}{V_v} \times 100 \tag{2.7}$$

where

V_w = volume of water

Note that, for saturated soil, the degree of saturation is 100%.

The weight relationships are *moisture content, moist unit weight, dry unit weight*, and *saturated unit weight*, often defined as follows:

$$\text{Moisture content} = w(\%) = \frac{W_w}{W_s} \times 100 \tag{2.8}$$

where

W_s = weight of the soil solids

W_w = weight of water

$$\text{Moist unit weight} = \gamma = \frac{W}{V} \tag{2.9}$$

where

W = total weight of the soil specimen = $W_s + W_w$

The weight of air, W_a, in the soil mass is assumed to be negligible.

$$\text{Dry unit weight} = \gamma_d = \frac{W_s}{V} \tag{2.10}$$

When a soil mass is completely saturated (i.e., all the void volume is occupied by water), the moist unit weight of a soil [Eq. (2.9)] becomes equal to the *saturated unit weight* (γ_{sat}). So $\gamma = \gamma_{sat}$ if $V_v = V_w$.

More useful relations can now be developed by considering a representative soil specimen in which the volume of soil solids is equal to *unity*, as shown in Figure 2.3b. Note that if $V_s = 1$, then, from Eq. (2.4), $V_v = e$, and the weight of the soil solids is

$$W_s = G_s \gamma_w$$

where

G_s = specific gravity of soil solids

γ_w = unit weight of water (9.81 kN/m^3, or 62.4 lb/ft^3)

Also, from Eq. (2.8), the weight of water $W_w = wW_s$. Thus, for the soil specimen under consideration, $W_w = wW_s = wG_s\gamma_w$. Now, for the general relation for moist unit weight given in Eq. (2.9),

$$\gamma = \frac{W}{V} = \frac{W_s + W_w}{V_s + V_v} = \frac{G_s\gamma_w(1 + w)}{1 + e} \tag{2.11}$$

Similarly, the dry unit weight [Eq. (2.10)] is

$$\gamma_d = \frac{W_s}{V} = \frac{W_s}{V_s + V_v} = \frac{G_s\gamma_w}{1 + e} \tag{2.12}$$

From Eqs. (2.11) and (2.12), note that

$$\gamma_d = \frac{\gamma}{1 + w} \tag{2.13}$$

According to Eq. (2.7), degree of saturation is

$$S = \frac{V_w}{V_v}$$

Now, referring to Figure 2.3b,

$$V_w = wG_s$$

and

$$V_v = e$$

Thus,

$$S = \frac{V_w}{V_v} = \frac{wG_s}{e} \tag{2.14}$$

For a saturated soil, $S = 1$. So

$$e = wG_s \tag{2.15}$$

The saturated unit weight of soil then becomes

$$\gamma_{\text{sat}} = \frac{W_s + W_w}{V_s + V_v} = \frac{G_s\gamma_w + e\,\gamma_w}{1 + e} \tag{2.16}$$

In SI units, newton (N) or kilonewton (kN) is weight and is a derived unit, and g or kg is mass. The relationships given in Eqs. (2.11), (2.12), and (2.16) can be expressed as moist, dry, and saturated densities as follows:

$$\rho = \frac{G_s\rho_w(1 + w)}{1 + e} \tag{2.17}$$

$$\rho_d = \frac{G_s\rho_w}{1 + e} \tag{2.18}$$

$$\rho_{\text{sat}} = \frac{\rho_w(G_s + e)}{1 + e} \tag{2.19}$$

where ρ, ρ_d, ρ_{sat} = moist density, dry density, and saturated density, respectively
ρ_w = density of water (= 1000 kg/m^3 or 1 g/cm^3)

Relationships similar to Eqs. (2.11), (2.12), and (2.16) in terms of porosity can also be obtained by considering a representative soil specimen with a unit volume. These relationships are

$$\gamma = G_s\gamma_w(1 - n)(1 + w) \tag{2.20}$$

$$\gamma_d = (1 - n)G_s\gamma_w \tag{2.21}$$

and

$$\gamma_{\text{sat}} = [(1 - n)G_s + n]\gamma_w \tag{2.22}$$

Table 2.3 gives a summary of various forms of relationships that can be obtained for γ, γ_d, and γ_{sat}.

Except for peat and highly organic soil, the general range of the values of specific gravity of soil solids (G_s) found in nature is rather small. Table 2.4 gives some representative values. For practical purposes, a reasonable value can be assumed in lieu of running a test.

TABLE 2.3 Relationships for γ, γ_d, and γ_{sat}

Unit weight relationship	Dry unit weight	Saturated unit weight
$\gamma = \dfrac{(1+w)G_s\gamma_w}{1+e}$	$\gamma_d = \dfrac{\gamma}{1+w}$	$\gamma_{sat} = \dfrac{(G_s+e)\gamma_w}{1+e}$
$\gamma = \dfrac{(G_s+Se)\gamma_w}{1+e}$	$\gamma_d = \dfrac{G_s\gamma_w}{1+e}$	$\gamma_{sat} = [(1-n)G_s+n]\gamma_w$
$\gamma = \dfrac{(1+w)G_s\gamma_w}{1+\dfrac{wG_s}{S}}$	$\gamma_d = G_s\gamma_w(1-n)$	$\gamma_{sat} = \left(\dfrac{1+w}{1+wG_s}\right)G_s\gamma_w$
$\gamma = G_s\gamma_w(1-n)(1+w)$	$\gamma_d = \dfrac{G_s}{1+\dfrac{wG_s}{S}}\gamma_w$	$\gamma_{sat} = \left(\dfrac{e}{w}\right)\left(\dfrac{1+w}{1+e}\right)\gamma_w$
	$\gamma_d = \dfrac{eS\gamma_w}{(1+e)w}$	$\gamma_{sat} = \gamma_d + n\gamma_w$
	$\gamma_d = \gamma_{sat} - n\gamma_w$	$\gamma_{sat} = \gamma_d + \left(\dfrac{e}{1+e}\right)\gamma_w$
	$\gamma_d = \gamma_{sat} - \left(\dfrac{e}{1+e}\right)\gamma_w$	

TABLE 2.4 Specific Gravities of Some Soil

Type of soil	G_s
Quartz sand	2.64–2.66
Silt	2.67–2.73
Clay	2.70–2.90
Chalk	2.60–2.75
Loess	2.65–2.73
Peat	1.30–1.90
Mine tailings	2.80–4.50

2.5 Relative Density

In *granular soil*, the degree of compaction in the field can be measured according to the *relative density*, defined as

$$D_r(\%) = \frac{e_{max} - e}{e_{max} - e_{min}} \times 100 \tag{2.23}$$

where

e_{max} = void ratio of the soil in the loosest state

e_{min} = void ratio in the densest state

e = *in situ* void ratio

Relative density is also known as the *density index*, denoted by I_D. From Eq. (2.12), the relative density can also be expressed in terms of dry unit weight as

$$D_r(\%) = \left\{\frac{\gamma_d - \gamma_{d(min)}}{\gamma_{d(max)} - \gamma_{d(min)}}\right\}\frac{\gamma_{d(max)}}{\gamma_d} \times 100 \tag{2.24}$$

TABLE 2.5 Denseness of a Granular Soil

Relative density, D_r(%)	Description
0–15	Very loose
15–35	Loose
35–65	Medium
65–85	Dense
85–100	Very dense

where

γ_d = *in situ* dry unit weight

$\gamma_{d(\max)}$ = dry unit weight in the *densest* state; that is, when the void ratio is $e_{\min}$

$\gamma_{d(\min)}$ = dry unit weight in the *loosest* state; that is, when the void ratio is $e_{\max}$

The denseness of a granular soil is sometimes related to the soil's relative density. Table 2.5 gives a general correlation of the denseness and D_r. For naturally occurring sands, the magnitudes of $e_{\max}$ and $e_{\min}$ [Eq. (2.23)] may differ widely. The main reasons for such wide range are the uniformity coefficient, C_u, and the roundness of the particles.

Cubrinovski and Ishihara (2002) studied the variation of $e_{\max}$ and $e_{\min}$ for a very large number of soil. Based on the best-fit linear regression lines, they provided the following relationships.

- Clean sand (F_c = 0 to 5%)

$$e_{\max} = 0.072 + 1.53e_{\min} \tag{2.25}$$

- Sand with fines ($5 < F_c \leq 15\%$)

$$e_{\max} = 0.25 + 1.37e_{\min} \tag{2.26}$$

- Sand with fines and clay ($15 < P_c \leq 30\%$; F_c = 5 to 20%)

$$e_{\max} = 0.44 + 1.21e_{\min} \tag{2.27}$$

- Silty soil ($30 < F_c \leq 70\%$; P_c = 5 to 20%)

$$e_{\max} = 0.44 + 1.32e_{\min} \tag{2.28}$$

where

F_c = fine fraction for which grain size is smaller than 0.075 mm

P_c = clay-size fraction (< 0.005 mm)

Cubrinovski and Ishihara (1999, 2002) also provided the correlation

$$e_{\max} - e_{\min} = 0.23 + \frac{0.06}{D_{50}\,(\text{mm})} \tag{2.29}$$

where D_{50} = median grain size (sieve size through which 50% of soil passes).

EXAMPLE 2.1

A saturated soil below the water table has unit weight of 20.5 kN/m^3 and moisture content of 26.5%. Assuming G_s of 2.70, find the void ratio of the soil.

SOLUTION

The soil below the water table is saturated, and hence γ_{sat} = 20.5 kN/m^3. From Eq. (2.16),

$$20.5 = \frac{(2.70 + e) \times 9.81}{1 + e}$$

$$e = \mathbf{0.560}$$

EXAMPLE 2.2

A 75 mm diameter and 150 mm high clay specimen has a mass of 1392.5 g. When it is dried, the mass becomes 1196.5 g. Find the degree of saturation in the specimen, assuming the specific gravity of the soil grains is 2.70.

SOLUTION

Volume of the specimen $V = \frac{\pi}{4} \times 7.5^2 \times 15 = 662.7 \text{ cm}^3$

Mass of the specimen $W = 1392.5$ g

Dry mass of the specimen $W_s = 1196.5$ g

$$w = \frac{1392.5 - 1196.5}{1196.5} \times 100 = 16.4\% \text{ and } \rho_d = \frac{1196.5}{662.7} = 1.806 \text{ g/cm}^3$$

From Eq. (2.18), $\rho_d = \frac{G_s \rho_w}{1 + e}$.

$$e = \frac{G_s \rho_w}{\rho_d} - 1 = \frac{2.70 \times 1.0}{1.806} - 1 = 0.495$$

From Eq. (2.14),

$$S = \frac{w G_s}{e} = \frac{0.164 \times 2.70}{0.495} = 0.895 \text{ or } \mathbf{89.5\%}$$

EXAMPLE 2.3

The maximum and minimum unit weights of a granular soil are 117.1 lb/ft^3 and 91.0 lb/ft^3, respectively. $G_s = 2.65$. What would be the relative density of the same sand compacted to a void ratio of 0.625?

SOLUTION

From Eq. (2.12),

$$e_{\min} = \frac{2.65 \times 62.4}{117.1} - 1 = 0.412$$

$$e_{\max} = \frac{2.65 \times 62.4}{91.0} - 1 = 0.817$$

From Eq. (2.23),

$$D_r = \frac{0.817 - 0.625}{0.817 - 0.412} = \mathbf{0.474 \text{ or } 47.4\%}$$

2.6 Atterberg Limits

When a clayey soil is mixed with an excessive amount of water, it may flow like a *semiliquid.* If the soil is gradually dried, it will behave like a *plastic, semisolid*, or *solid* material, depending on its moisture content. The moisture content, in percent, at which the soil changes from a semiliquid to a plastic state is defined as the *liquid limit* (LL). Similarly, the moisture content, in percent, at which the soil changes from a plastic to a semisolid state and from a semisolid to a solid state is defined as the *plastic limit* (PL) and the *shrinkage limit* (SL), respectively. These limits are referred to as *Atterberg limits* (Figure 2.4):

- The *liquid limit* of a soil is determined by Casagrande's liquid device (ASTM Test Designation D-4318) and is defined as the moisture content at which a groove closure of 12.7 mm (1/2 in.) occurs at 25 blows.

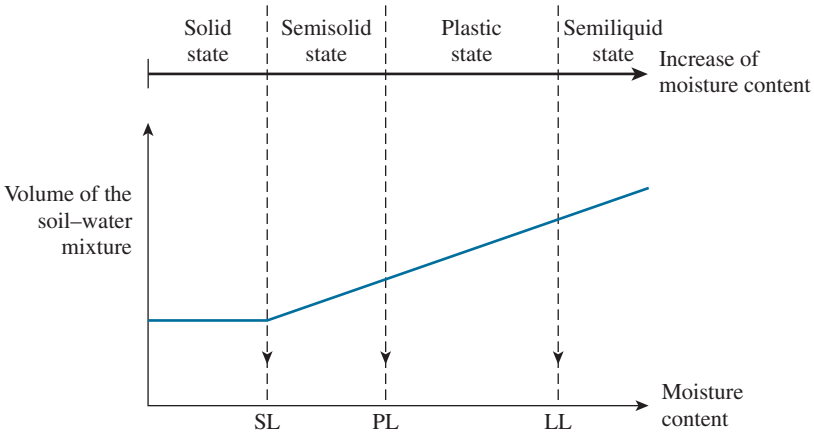


FIGURE 2.4 Definition of Atterberg limits

- The *plastic limit* is defined as the moisture content at which the soil crumbles when rolled into a thread of 3.18 mm (1/8 in.) in diameter (ASTM Test Designation D-4318).
- The *shrinkage limit* is defined as the moisture content at which the soil does not undergo any further change in volume with loss of moisture (ASTM Test Designation D-4943).

The difference between the liquid limit and the plastic limit of a soil is defined as the *plasticity index* (PI), or

$$\text{PI} = \text{LL} - \text{PL} \tag{2.30}$$

2.7 Liquidity Index

The relative consistency of a cohesive soil in the natural state can be defined by a ratio called the *liquidity index*, which is given by

$$\text{LI} = \frac{w - \text{PL}}{\text{LL} - \text{PL}} \tag{2.31}$$

where w = *in situ* moisture content of soil.

In bore logs, the natural moisture content is sometimes shown with respect to PL and LL, indicating how close the natural moisture content is to the LL or PL.

The *in situ* moisture content for a sensitive clay may be greater than the liquid limit. In this case,

$$\text{LI} > 1$$

These soil, when remolded, can be transformed into a viscous form to flow like a liquid.

Soil deposits that are heavily overconsolidated may have a natural moisture content less than the plastic limit. In this case,

$$\text{LI} < 0$$

2.8 Activity

Because the plasticity of soil is caused by the adsorbed water that surrounds the clay particles, we can expect that the type of clay minerals and their proportional amounts in a soil will affect the liquid and plastic limits. Skempton (1953) observed that the plasticity index of a soil derived from a specific clay mineral increases linearly with the

TABLE 2.6 Typical Values of Liquid Limit, Plastic Limit, and Activity of Some Clay Minerals

Mineral	Liquid limit, LL	Plastic limit, PL	Activity, *A*
Kaolinite	35–100	20–40	0.3–0.5
Illite	60–120	35–60	0.5–1.2
Montmorillonite	100–900	50–100	1.5–7.0
Halloysite (hydrated)	50–70	40–60	0.1–0.2
Halloysite (dehydrated)	40–55	30–45	0.4–0.6
Attapulgite	150–250	100–125	0.4–1.3
Allophane	200–250	120–150	0.4–1.3

percentage of clay-size fraction (% finer than 2 μm by weight) present. The correlations of PI with the clay-size fractions for different clays plot separate lines. This difference is due to the diverse plasticity characteristics of the various types of clay minerals. On the basis of these results, Skempton defined a quantity called *activity*, which is the slope of the line correlating PI and % finer than 2 μm. This activity may be expressed as

$$A = \frac{\text{PI}}{(\%\text{ of clay-size fraction, by weight})} \tag{2.32}$$

Activity is used as an index for identifying the swelling potential of clay soil. Activity exceeding 1.0 suggests that the clay has high swelling potentital. Typical values of liquid limit, plastic limit, and activity for various clay minerals are given in Table 2.6.

2.9 Soil Classification Systems

Soil classification systems divide soil into groups and subgroups based on common engineering properties such as the *grain-size distribution, liquid limit*, and *plastic limit*. The two major classification systems presently in use are (1) the *American Association of State Highway and Transportation Officials* (AASHTO) *System* and (2) the *Unified Soil Classification System* (also ASTM). The AASHTO system is used mainly for the classification of highway subgrades. It is not used in foundation construction.

AASHTO SYSTEM

The AASHTO Soil Classification System was originally proposed by the Highway Research Board's Committee on Classification of Materials for Subgrades and Granular Type Roads (1945). According to the present form of this system, soil can be classified according to eight major groups, A-1 through A-8, based on their grain-size distribution, liquid limit, and plasticity indices. Soil listed in groups A-1, A-2, and A-3 are coarse-grained materials, and those in groups A-4, A-5, A-6, and A-7 are fine-grained materials. Peat, muck, and other highly organic soil are classified under A-8. They are identified by visual inspection.

The AASHTO classification system (for soil A-1 through A-7) is presented in Table 2.7. Note that group A-7 includes two types of soil. For the A-7-5 type, the plasticity index of the soil is less than or equal to the liquid limit minus 30. For the A-7-6 type, the plasticity index is greater than the liquid limit minus 30.

For qualitative evaluation of the desirability of a soil as a highway subgrade material, a number referred to as the *group index* has also been developed. The higher the value of the group index for a given soil, the weaker will be the soil's performance as a subgrade. A group index of 20 or more indicates a very poor subgrade material. The formula for the group index is

$$\text{GI} = (F_{200} - 35)[0.2 + 0.005(\text{LL} - 40)] + 0.01(F_{200} - 15)(\text{PI} - 10) \tag{2.33}$$

TABLE 2.7 AASHTO Soil Classification System

General classification	Granular materials (35% or less of total sample passing No. 200 sieve)						
	A-1			A-2			
Group classification	A-1-a	A-1-b	A-3	A-2-4	A-2-5	A-2-6	A-2-7
Sieve analysis (% passing)							
No. 10 sieve	50 max						
No. 40 sieve	30 max	50 max	51 min				
No. 200 sieve	15 max	25 max	10 max	35 max	35 max	35 max	35 max
For fraction passing No. 40 sieve							
Liquid limit (LL)				40 max	41 min	40 max	41 min
Plasticity index (PI)	6 max		Nonplastic	10 max	10 max	11 min	11 min
Usual type of material	Stone fragments, gravel, and sand		Fine sand	Silty or clayey gravel and sand			
Subgrade rating	Excellent to good						

General classification	Silt–clay materials (More than 35% of total sample passing No. 200 sieve)			
Group classification	A-4	A-5	A-6	A-7
				A-7-5[a] A-7-6[b]
Sieve analysis (% passing)				
No. 10 sieve				
No. 40 sieve				
No. 200 sieve	36 min	36 min	36 min	36 min
For fraction passing No. 40 sieve				
Liquid limit (LL)	40 max	41 min	40 max	41 min
Plasticity index (PI)	10 max	10 max	11 min	11 min
Usual types of material	Mostly silty soil		Mostly clayey soil	
Subgrade rating	Fair to poor			

[a]If PI $\leq$ LL $-$ 30, the classification is A-7-5.

[b]If PI $>$ LL $-$ 30, the classification is A-7-6.

where

F_{200} = percent passing No. 200 sieve, expressed as a whole number

LL = liquid limit

PI = plasticity index

When calculating the group index for a soil belonging to group A-2-6 or A-2-7, use only the partial group-index equation relating to the plasticity index:

$$\text{GI} = 0.01(F_{200} - 15)(\text{PI} - 10) \tag{2.34}$$

The group index is rounded to the nearest whole number and written next to the soil group in parentheses; for example, we have

$$\underbrace{\text{A-4}}_{\text{Soil group}} \qquad \underbrace{(5)}_{\text{Group index}}$$

TABLE 2.8 USCS Symbols

	Soil group (*X*)	Descriptor (*Y*)
Coarse-grained soil:	Gravel (G) Sand (S)	Well graded (W) Poorly graded (P) Silty (M) Clayey (C)
Fine-grained soil:	Silt (M) Clay (C) Organic silts and clays (O)	Low plasticity (L) High plasticity (H)
Others:	Peat and highly organic soil (Pt)	—

The group index for soil which fall in groups A-1-a, A-1-b, A-3, A-2-4, and A-2-5 is always zero.

UNIFIED SOIL CLASSIFICATION SYSTEM

The Unified Soil Classification System (USCS) was originally proposed by A. Casagrande in 1942 and was later revised and adopted by the United States Bureau of Reclamation and the U.S. Army Corps of Engineers. The system is currently used in practically all geotechnical work worldwide.

The USCS symbol generally consists of two letters *XY*, where *X* defines the major soil group and *Y* describes the characteristics of the soil group (Table 2.8). Possible symbols for coarse-grained soil are GW, GP, GM, GC, SW, SP, SM, and SC. The fine-grained soil include ML, MH, CL, CH, OL, and OH.

While coarse-grained soil are classified on the basis of the grain-size distribution, the fines are classified based on plasticity, using Casagrande's plasticity chart shown in Figure 2.5. Here, the A-line separates the clays and silts, and the U-line sets the upper limit for any fine-grained soil. All fine-grained soil must plot below the U-line.

The plasticity chart (Figure 2.5) and Table 2.9 show the procedure for determining the group symbols for various types of soil. When the fine content is in the range of 5–12%, it is advisable to use dual symbols describing both the coarse- and the fine-grained soil (see Figure 2.6). Peat and highly organic soil are assigned a symbol Pt. Fine-grained soil that lie within the hatched area in Figure 2.5 are silty clays with symbol CL-ML. Figures 2.6, 2.7, and 2.8 give flowcharts for obtaining the group names for coarse-grained soil, inorganic fine-grained soil, and organic fine-grained soil, respectively.

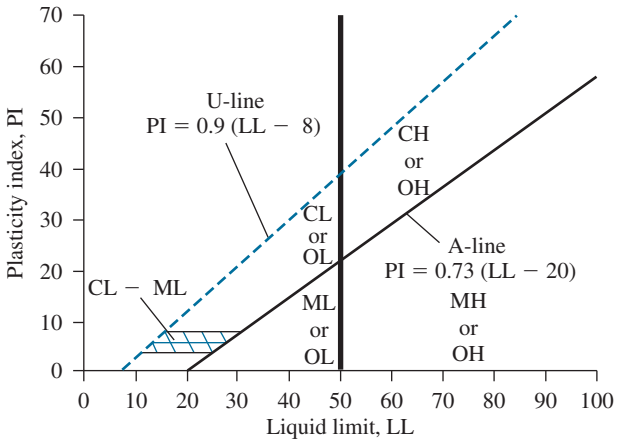


FIGURE 2.5 Plasticity chart

TABLE 2.9 Unified Soil Classification Chart (after ASTM, 2011) (Based on ASTM D2487-10: Standard Practice for Classification of Soil for Engineering Purposes (Unified Soil Classification))

Criteria for assigning group symbols and group names using laboratory tests[a]				Soil classification	
				Group symbol	Group name[b]
Coarse-grained soil More than 50% retained on No. 200 sieve	Gravels More than 50% of coarse fraction retained on No. 4 sieve	Clean Gravels Less than 5% fines[c]	$C_u \geq 4$ and $1 \leq C_c \leq 3$[e]	GW	Well-graded gravel[f]
			$C_u < 4$ and/or $1 > C_c > 3$[e]	GP	Poorly graded gravel[f]
		Gravels with Fines More than 12% fines[c]	Fines classify as ML or MH	GM	Silty gravel[f,g,h]
			Fines classify as CL or CH	GC	Clayey gravel[f,g,h]
	Sands 50% or more of coarse fraction passes No. 4 sieve	Clean Sands Less than 5% fines[d]	$C_u \geq 6$ and $1 \leq C_c \leq 3$[e]	SW	Well-graded sand[i]
			$C_u < 6$ and/or $1 > C_c > 3$[e]	SP	Poorly graded sand[i]
		Sand with Fines More than 12% fines[d]	Fines classify as ML or MH	SM	Silty sand[g,h,i]
			Fines classify as CL or CH	SC	Clayey sand[g,h,i]
Fine-grained soil 50% or more passes the No. 200 sieve	Silts and Clays Liquid limit less than 50	Inorganic	PI > 7 and plots on or above "A" line[j]	CL	Lean clay[k,l,m]
			PI < 4 or plots below "A" line[j]	ML	Silt[k,l,m]
		Organic	$\frac{\text{Liquid limit—oven dried}}{\text{Liquid limit—not dried}} < 0.75$	OL	Organic clay[k,l,m,n] / Organic silt[k,l,m,o]
	Silts and Clays Liquid limit 50 or more	Inorganic	PI plots on or above "A" line	CH	Fat clay[k,l,m]
			PI plots below "A" line	MH	Elastic silt[k,l,m]
		Organic	$\frac{\text{Liquid limit—oven dried}}{\text{Liquid limit—not dried}} < 0.75$	OH	Organic clay[k,l,m,p] / Organic silt[k,l,m,q]
Highly organic soil	Primarily organic matter, dark in color, and organic odor			PT	Peat

[a]Based on the material passing the 75-mm. (3-in.) sieve.

[b]If field sample contained cobbles or boulders, or both, add "with cobbles or boulders, or both" to group name.

[c]Gravels with 5 to 12% fines require dual symbols: GW-GM well-graded gravel with silt; GW-GC well-graded gravel with clay; GP-GM poorly graded gravel with silt; GP-GC poorly graded gravel with clay.

[d]Sands with 5 to 12% fines require dual symbols: SW-SM well-graded sand with silt; SW-SC well-graded sand with clay; SP-SM poorly graded sand with silt; SP-SC poorly graded sand with clay.

[e]$C_u = D_{60}/D_{10}$ $C_c = \dfrac{(D_{30})^2}{D_{10} \times D_{60}}$

[f]If soil contains ≥15% sand, add "with sand" to group name.

[g]If fines classify as CL-ML, use dual symbol GC-GM or SC-SM.

[h]If fines are organic, add "with organic fines" to group name.

[i]If soil contains ≥15% gravel, add "with gravel" to group name.

[j]If Atterberg limits plot in hatched area, soil is a CL-ML, silty clay.

[k]If soil contains 15 to 29% plus No. 200, add "with sand" or "with gravel," whichever is predominant.

[l]If soil contains ≥30% plus No. 200, predominantly sand, add "sandy" to group name.

[m]If soil contains ≥30% plus No. 200, predominantly gravel, add "gravelly" to group name.

[n]PI ≥ 4 and plots on or above A-line.

[o]PI < 4 or plots below A-line.

[p]PI plots on or above A-line.

[q]PI plots below A-line.

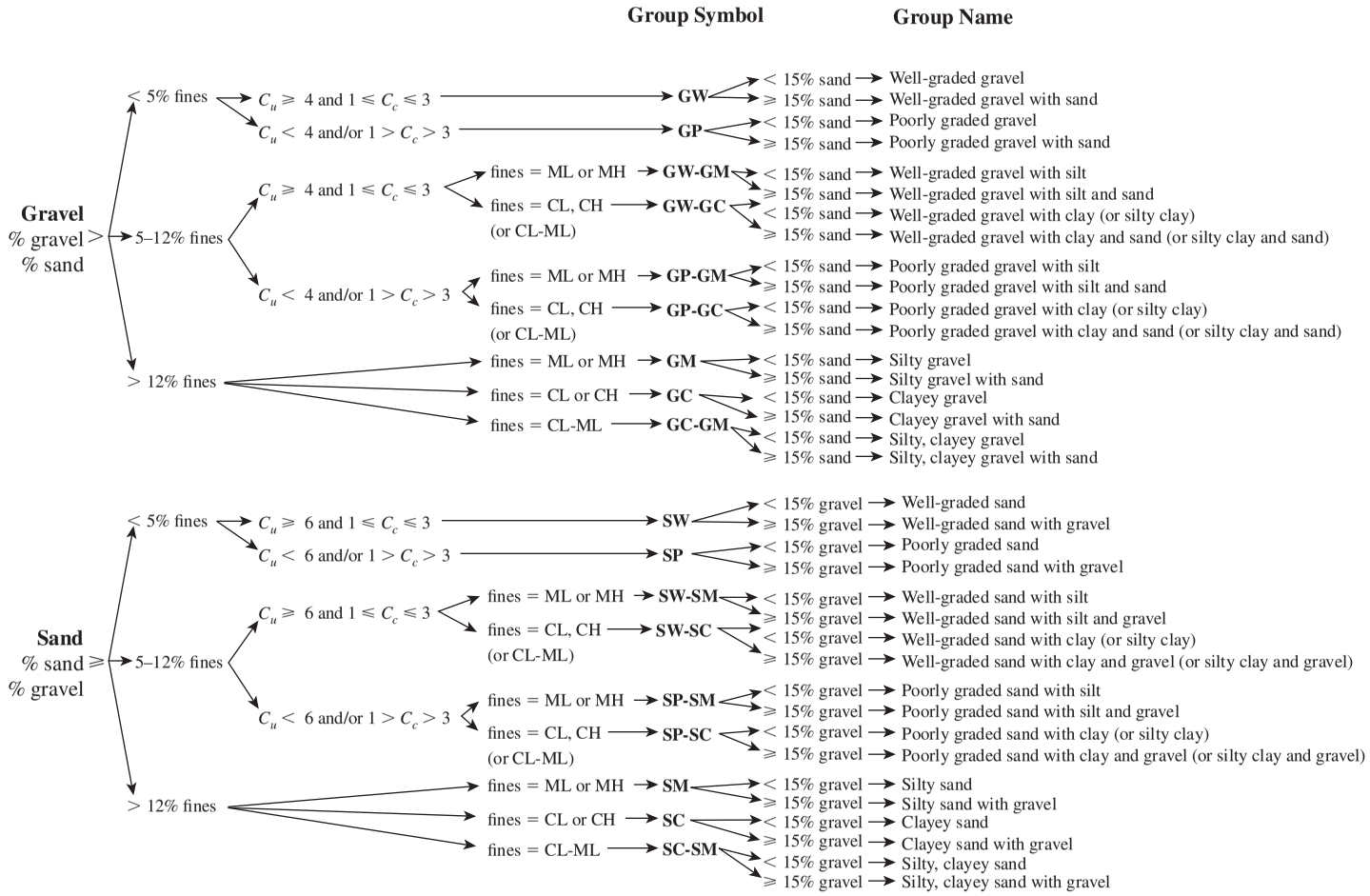


FIGURE 2.6 Flowchart for classifying coarse-grained soil (more than 50% retained on No. 200 Sieve) (After ASTM, 2011) (Based on ASTM D2487-10: Standard Practice for Classification of Soil for Engineering Purposes (Unified Soil Classification))

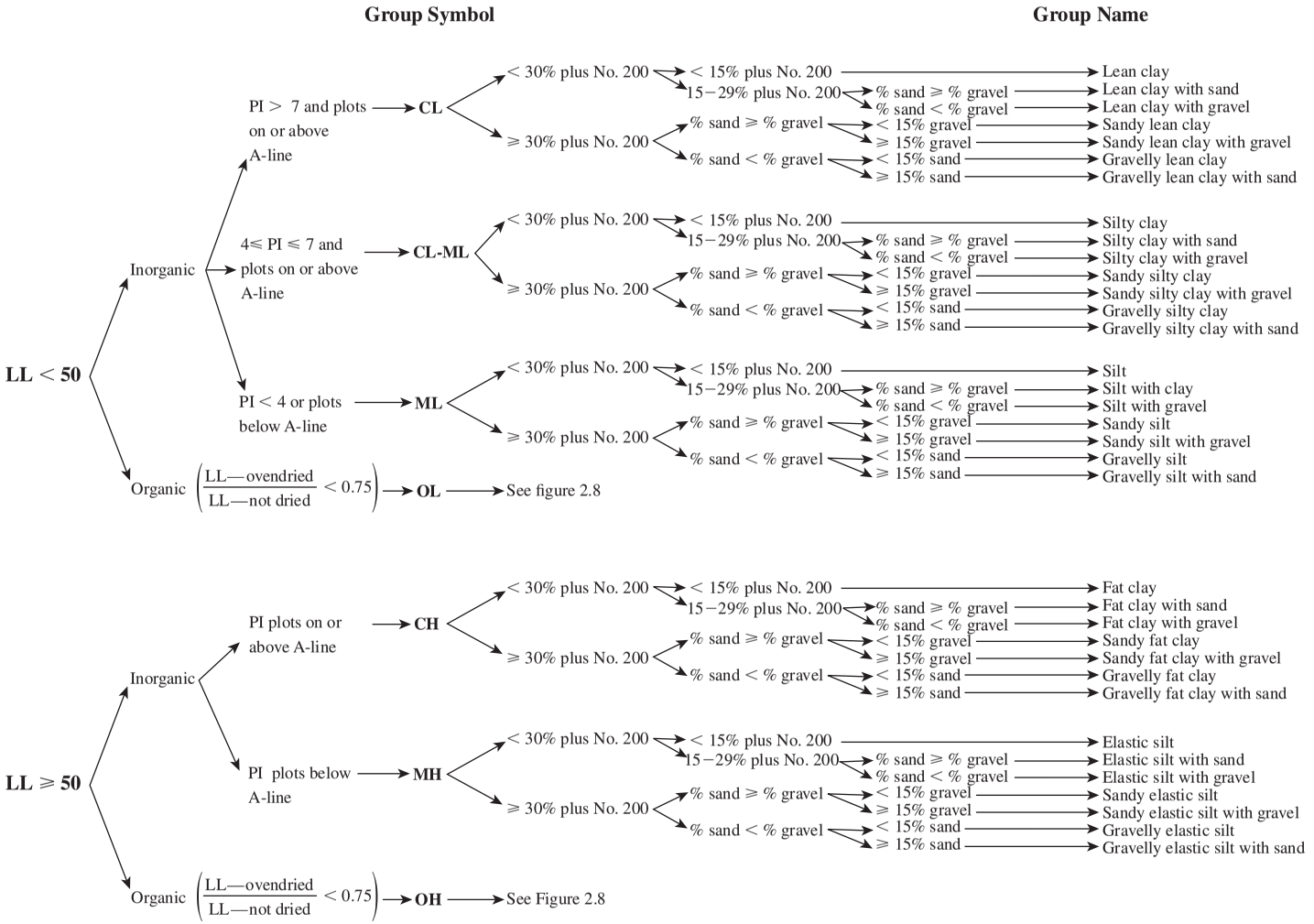


FIGURE 2.7 Flowchart for classifying fine-grained soil (50% or more passes No. 200 Sieve) (After ASTM, 2011) (Based on ASTM D2487-10: Standard Practice for Classification of Soil for Engineering Purposes (Unified Soil Classification))

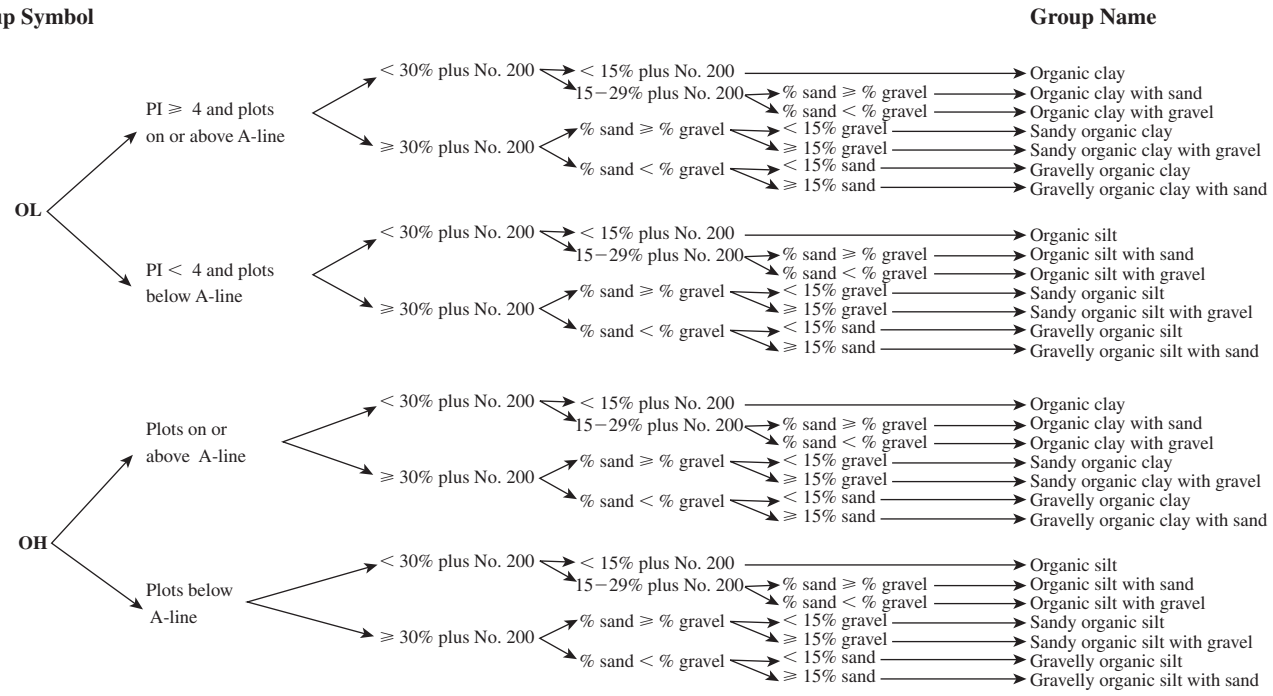


FIGURE 2.8 Flowchart for classifying organic fine-grained soil (50% or more passes No. 200 Sieve) (After ASTM, 2011) (Based on ASTM D2487-10: Standard Practice for Classification of Soil for Engineering Purposes (Unified Soil Classification))

EXAMPLE 2.4

Classify the following soil by the AASHTO classification system.

Percent passing No. 4 sieve = 82
Percent passing No. 10 sieve = 71
Percent passing No. 40 sieve = 64
Percent passing No. 200 sieve = 41
Liquid limit = 31
Plasticity index = 12

SOLUTION

Refer to Table 2.7. More than 35% passes through a No. 200 sieve, so it is a silt–clay material. It could be A-4, A-5, A-6, or A-7. Because LL = 31 (that is, less than 40) and PI = 12 (that is, greater than 11), this soil falls in group A-6. From Eq. (2.33),

$$GI = (F_{200} - 35)[0.02 + 0.005(LL - 40)] + 0.01\,(F_{200} - 15)(PI - 10)$$

So

$$GI = (41 - 35)[0.02 + 0.005(31 - 40)] + 0.01(41 - 15)(12 - 10)$$
$$= 0.37 \approx 0$$

Thus, the soil is **A-6(0)**.

■

EXAMPLE 2.5

Classify the following soil by the AASHTO classification system.

Percent passing No. 4 sieve = 92
Percent passing No. 10 sieve = 87

Percent passing No. 40 sieve = 65
Percent passing No. 200 sieve = 30
Liquid limit = 22
Plasticity index = 8

SOLUTION

Table 2.7 shows that it is a granular material because less than 35% is passing a No. 200 sieve. With LL = 22 (that is, less than 40) and PI = 8 (that is, less than 10), the soil falls in group A-2-4. From Eq. (2.34),

$$\begin{aligned} \text{GI} &= 0.01(F_{200} - 15)(\text{PI} - 10) = 0.01(30 - 15)(8 - 10) \\ &= -0.3 \approx 0 \end{aligned}$$

The soil is **A-2-4(0)**.

EXAMPLE 2.6

Classify the following soil by the Unified Soil Classification System.

Percent passing No. 4 sieve = 82
Percent passing No. 10 sieve = 71
Percent passing No. 40 sieve = 64
Percent passing No. 200 sieve = 41
Liquid limit = 31
Plasticity index = 12

SOLUTION

We are given that $F_{200} = 41$, LL = 31, and PI = 12. Since 59% of the sample is retained on a No. 200 sieve, the soil is a coarse-grained material. The percentage passing a No. 4 sieve is 82, so 18% is retained on No. 4 sieve (gravel fraction). The coarse fraction passing a No. 4 sieve (sand fraction) is 59 − 18 = 41% (which is more than 50% of the total coarse fraction). Hence, the specimen is a sandy soil.

Now, using Table 2.9 and Figure 2.5, we identify the group symbol of the soil as **SC.**

From Figure 2.6, since the gravel fraction is greater than 15%, the group name is **clayey sand with gravel.**

2.10 Hydraulic Conductivity of Soil

The void spaces, or pores, between soil grains allow water to flow through them. In soil mechanics and foundation engineering, you must know how much water is flowing through a soil per unit time. This knowledge is required to design earth dams, determine the quantity of seepage under hydraulic structures, and dewater foundations before and during their construction. Darcy (1856) proposed the following equation (Figure 2.9) for calculating the velocity of flow of water through a soil assuming laminar flow:

$$v = ki \tag{2.35}$$

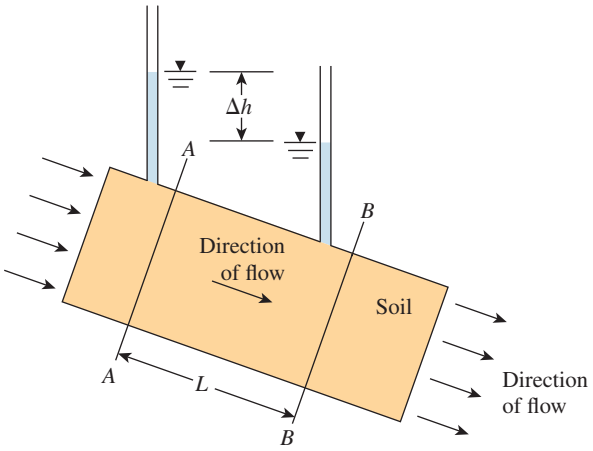


FIGURE 2.9 Definition of Darcy's law

In this equation,

v = Darcy velocity

k = hydraulic conductivity of soil

i = hydraulic gradient

The hydraulic gradient is defined as

$$i = \frac{\Delta h}{L} \tag{2.36}$$

where

Δh = piezometric or total head difference between the sections at *AA* and *BB*

L = distance between the sections at *AA* and *BB*

(*Note:* Sections *AA* and *BB* are perpendicular to the direction of flow.)

Hydraulic gradient is the total head loss per unit length along the flow path. It is a dimensionless quantity. The *hydraulic conductivity*, also known as the *permeability*, has unit of velocity and is commonly expressed in cm/s or m/s.

Darcy's law [Eq. (2.35)] is valid for a wide range of soil. However, with materials like clean gravel and open-graded rockfills, the law breaks down because of the turbulent nature of flow through them.

The value of the hydraulic conductivity of soil varies greatly. In the laboratory, it can be determined by means of *constant-head* or *falling-head* permeability tests. The constant-head test is more suitable for granular soil. The falling-head test is more suitable for fine-grained soil. Table 2.10 provides the general range for the values of k for various soil.

TABLE 2.10 Range of the Hydraulic Conductivity for Various Soil

Type of soil	Hydraulic conductivity, k (cm/s)
Medium to coarse gravel	Greater than 10^{-1}
Coarse to fine sand	10^{-1} to 10^{-3}
Fine sand, silty sand	10^{-3} to 10^{-5}
Silt, clayey silt, silty clay	10^{-4} to 10^{-6}
Clays	10^{-7} or less

HYDRAULIC CONDUCTIVITY OF GRANULAR SOIL

In granular soil, the value of hydraulic conductivity depends primarily on the void ratio. In the past, several equations have been proposed to relate the value of k to the void ratio in granular soil. However the authors recommend the following equation for use (also see Carrier, 2003):

$$k \propto \frac{e^3}{1+e} \tag{2.37}$$

where

k = hydraulic conductivity

e = void ratio

Chapuis (2004) proposed an empirical relationship for k in conjunction with Eq. (2.37) as

$$k(\text{cm/s}) = 2.4622\left[D_{10}^2\frac{e^3}{(1+e)}\right]^{0.7825} \tag{2.38}$$

where D_{10} = effective grain size (mm).

The preceding equation is valid for natural, uniform sand and gravel to predict k that is in the range of 10^{-1} to 10^{-3} cm/s. This can be extended to natural silty sands without plasticity. It is not valid for crushed materials or silty soil with some plasticity.

Based on laboratory experimental results, Amer and Awad (1974) proposed the following relationship for k in granular soil:

$$k = 3.5 \times 10^{-4}\left(\frac{e^3}{1+e}\right)C_u^{0.6}D_{10}^{2.32}\left(\frac{\rho_w}{\eta}\right) \tag{2.39}$$

where

k is in cm/s

C_u = uniformity coefficient

D_{10} = effective grain size (mm)

ρ_w = density of water (g/cm^3)

η = dynamic viscosity of water (g · s/cm^2)

At 20°C, $\rho_w = 1$ g/cm^3 and $\eta \approx 0.1 \times 10^{-4}$ g · s/cm^2. So

$$k = 3.5 \times 10^{-4}\left(\frac{e^3}{1+e}\right)C_u^{0.6}D_{10}^{2.32}\left(\frac{1}{0.1 \times 10^{-4}}\right)$$

or

$$k\ (\text{cm/s}) = 35\left(\frac{e^3}{1+e}\right)C_u^{0.6}D_{10}^{2.32} \tag{2.40}$$

On the basis of laboratory experiments, the U.S. Department of Navy (1986) provided an empirical correlation between k and D_{10} (mm) for granular soil with the uniformity coefficient varying between 2 and 12 and $D_{10}/D_5 < 1.4$. This correlation is shown in Figure 2.10.

HYDRAULIC CONDUCTIVITY OF COHESIVE SOIL

According to their experimental observations, Samarasinghe et al. (1982) suggested that the hydraulic conductivity of normally consolidated clays could be given by the equation

$$k = C\frac{e^n}{1+e} \tag{2.41}$$

where C and n are constants to be determined experimentally.

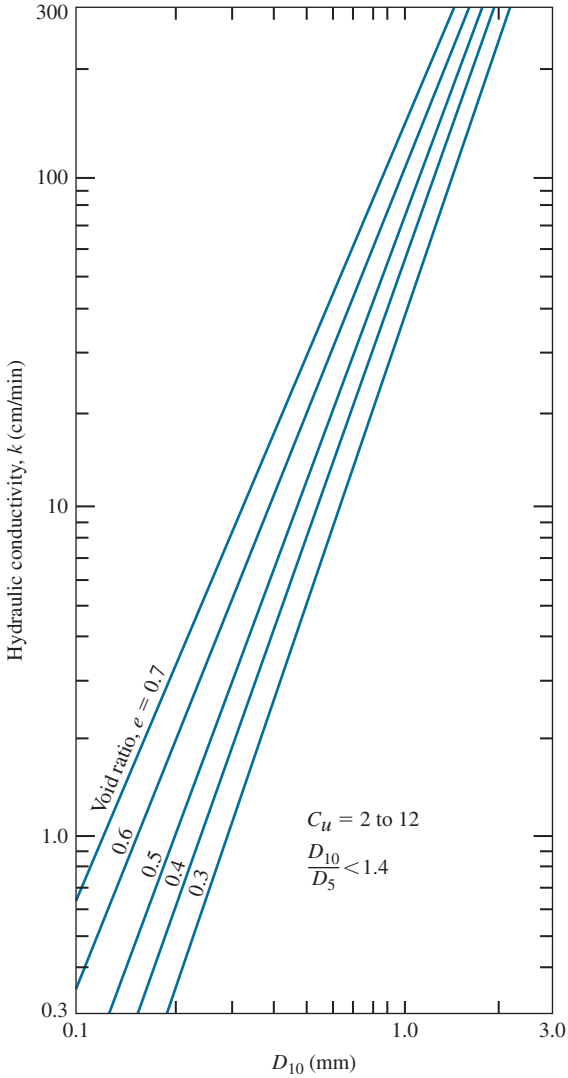


FIGURE 2.10 Hydraulic conductivity of granular soil (Redrawn from U.S. Department of Navy, 1986)

TABLE 2.11 Empirical Relationships for Estimating Hydraulic Conductivity in Clayey Soil

Type of soil	Source	Relationship[a]
Clay	Mesri and Olson (1971)	$\log k = A' \log e + B'$
	Taylor (1948)	$\log k = \log k_0 - \frac{e_0 - e}{C_k}$
		$C_k \approx 0.5 e_0$

[a] k_0 = *in situ* hydraulic conductivity at void ratio e_0
k = hydraulic conductivity at void ratio e
C_k = hydraulic conductivity change index

Some other empirical relationships for estimating the hydraulic conductivity in clayey soil are given in Table 2.11. One should keep in mind, however, that any empirical relationship of this type is for estimation only, because the magnitude of k is a highly variable parameter and depends on several factors.

EXAMPLE 2.7

For a normally consolidated clay soil, the following values are given.

Void ratio	k (cm/s)
1.1	0.302×10^{-7}
0.9	0.12×10^{-7}

Estimate the hydraulic conductivity of the clay at a void ratio of 0.75. Use Eq. (2.41).

SOLUTION

From Eq. (2.41), we have

$$k = C\left(\frac{e^n}{1+e}\right)$$

$$\frac{k_1}{k_2} = \frac{\left(\frac{e_1^n}{1+e_1}\right)}{\left(\frac{e_2^n}{1+e_2}\right)}$$

(*Note*: k_1 and k_2 are hydraulic conductivities at void ratios e_1 and e_2, respectively.)

$$\frac{0.302 \times 10^{-7}}{0.12 \times 10^{-7}} = \frac{\frac{(1.1)^n}{1+1.1}}{\frac{(0.9)^n}{1+0.9}}$$

$$2.517 = \left(\frac{1.9}{2.1}\right)\left(\frac{1.1}{0.9}\right)^n$$

$$2.782 = (1.222)^n$$

$$n = \frac{\log(2.782)}{\log(1.222)} = \frac{0.444}{0.087} = 5.1$$

so

$$k = C\left(\frac{e^{5.1}}{1+e}\right)$$

To find C, we perform the calculation:

$$0.302 \times 10^{-7} = C\left[\frac{(1.1)^{5.1}}{1+1.1}\right] = \left(\frac{1.626}{2.1}\right)C$$

$$C = \frac{(0.302 \times 10^{-7})(2.1)}{1.626} = 0.39 \times 10^{-7}$$

Hence,

$$k = (0.39 \times 10^{-7}\text{cm/s})\left(\frac{e^n}{1+e}\right)$$

At a void ratio of 0.75, we have

$$k = (0.39 \times 10^{-7})\left(\frac{0.75^{5.1}}{1+0.75}\right) = \mathbf{0.514 \times 10^{-8}\ cm/s}$$

2.11 Steady-State Seepage

For most cases of seepage under hydraulic structures, the flow path changes direction and is not uniform over the entire area. In such cases, one of the ways of determining the rate of seepage is by a graphical construction referred to as the *flow net*, a concept based on Laplace's theory of continuity. According to this theory, for a steady flow condition, the flow at any point A (Figure 2.11) can be represented by the equation

$$k_x\frac{\partial^2 h}{\partial x^2} + k_y\frac{\partial^2 h}{\partial y^2} + k_z\frac{\partial^2 h}{\partial z^2} = 0 \tag{2.42}$$

where

k_x, k_y, k_z = hydraulic conductivity of the soil in the x, y, and z directions, respectively
h = total head at point A (i.e., the head of water that a piezometer placed at A would show with the *downstream water level* as *datum*, as shown in Figure 2.11)

For a two-dimensional flow condition, as shown in Figure 2.11 with no flow in the y direction,

$$\frac{\partial^2 h}{\partial^2 y} = 0$$

so Eq. (2.42) takes the form

$$k_x\frac{\partial^2 h}{\partial x^2} + k_z\frac{\partial^2 h}{\partial z^2} = 0 \tag{2.43}$$

If the soil is isotropic with respect to hydraulic conductivity, $k_x = k_z = k$, and

$$\frac{\partial^2 h}{\partial x^2} + \frac{\partial^2 h}{\partial z^2} = 0 \tag{2.44}$$

Equation (2.44), which is referred to as Laplace's equation and is valid for confined flow, represents two orthogonal sets of curves known as *flow lines* and *equipotential lines*. A flow net is a combination of numerous equipotential lines and flow lines. A flow line is a path that a water particle would follow in traveling from the upstream side

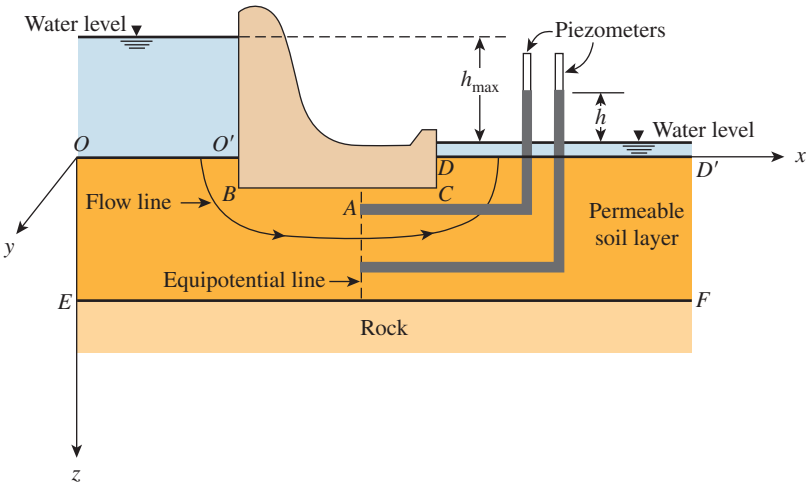


FIGURE 2.11 Steady-state seepage

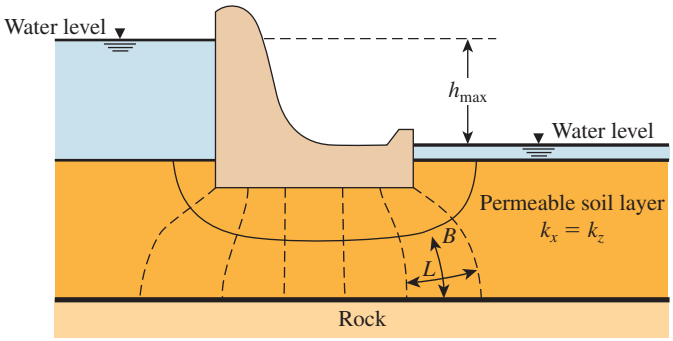


FIGURE 2.12 Flow net

to the downstream side. An equipotential is the locus of points having the same total head, where the water would rise to the same level in piezometers (see Figure 2.11). Along a flow line, the total head decreases steadily from upstream to downstream in overcoming the resistance to the flow provided by the soil.

In drawing a flow net, you need to establish the *boundary conditions*. For example, in Figure 2.11, the ground surfaces on the upstream (OO') and downstream (DD') sides are equipotential lines. The base of the dam below the ground surface, $O'BCD$, is a flow line. The top of the rock surface, EF, is also a flow line. Once the boundary conditions are established, a number of flow lines and equipotential lines are drawn by trial and error so that all the flow elements in the net have the same length-to-width ratio (L/B). In most cases, L/B is held to unity, that is, the flow elements are drawn as curvilinear "squares." This method is illustrated by the flow net shown in Figure 2.12. Note that all flow lines must intersect all equipotential lines at *right angles*.

Once the flow net is drawn, the seepage (in unit time per unit length of the structure) can be calculated as

$$q = kh_{max}\frac{N_f}{N_d}n \tag{2.45}$$

where

N_f = number of flow channels

N_d = number of drops

n = width-to-length ratio of the flow elements in the flow net (B/L)

h_{max} = difference in water level between the upstream and downstream sides

The space between two consecutive flow lines is defined as a *flow channel*, and the space between two consecutive equipotential lines is called a *drop*. In Figure 2.12, $N_f = 2$, $N_d = 7$, and $n = 1$. When square elements are drawn in a flow net,

$$q = kh_{max}\frac{N_f}{N_d} \tag{2.46}$$

2.12 Effective Stress

The normal stress acting on a point within a saturated soil mass is shared by the soil grains and the water. The component carried by the soil grains is the effective stress, and the remainder carried by the pore water is called the pore water pressure.

The *total* stress at a given point in a soil mass can be expressed as

$$\sigma = \sigma' + u \tag{2.47}$$

where

σ = total stress

σ' = effective stress

u = pore water pressure

The effective stress, σ', is the vertical component of forces at solid-to-solid contact points over a unit cross-sectional area. Referring to Figure 2.13a, at point A

$$\sigma = \gamma h_1 + \gamma_{sat} h_2$$
$$u = h_2 \gamma_w$$

where

γ_w = unit weight of water

γ_{sat} = saturated unit weight of soil

So

$$\begin{aligned}\sigma' &= (\gamma h_1 + \gamma_{sat} h_2) - (h_2 \gamma_w) \\ &= \gamma h_1 + h_2(\gamma_{sat} - \gamma_w) \\ &= \gamma h_1 + \gamma' h_2\end{aligned} \tag{2.48}$$

where γ' = effective or submerged unit weight of soil.

For the problem in Figure 2.13a, there was *no seepage of water* in the soil. Figure 2.13b shows a simple condition in a soil profile in which there is upward seepage. For this case, at point A,

$$\sigma = h_1 \gamma_w + h_2 \gamma_{sat}$$

and

$$u = (h_1 + h_2 + h)\gamma_w$$

Thus, from Eq. (2.47),

$$\begin{aligned}\sigma' = \sigma - u &= (h_1 \gamma_w + h_2 \gamma_{sat}) - (h_1 + h_2 + h)\gamma_w \\ &= h_2(\gamma_{sat} - \gamma_w) - h\gamma_w = h_2 \gamma' - h\gamma_w\end{aligned}$$

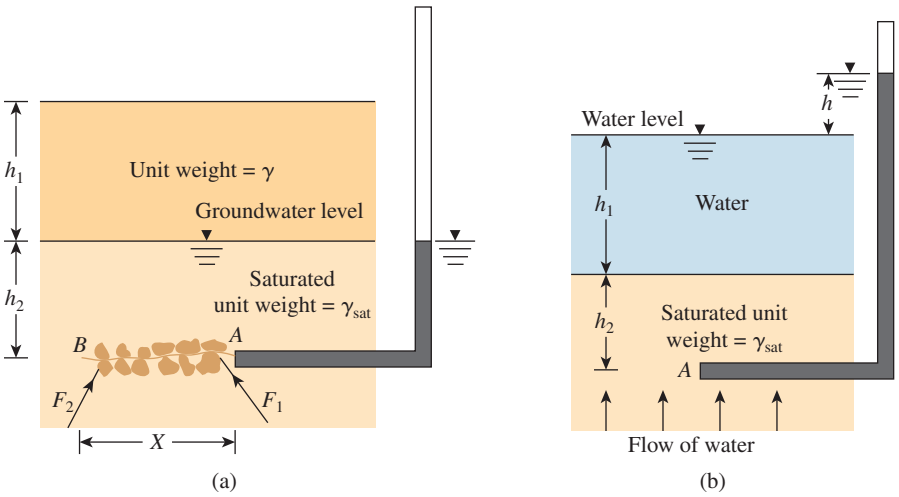


FIGURE 2.13 Calculation of effective stress: (a) static condition; (b) upward flow

or

$$\sigma' = h_2\left(\gamma' - \frac{h}{h_2}\gamma_w\right) = h_2(\gamma' - i\gamma_w) \tag{2.49}$$

Note in Eq. (2.49) that h/h_2 is the hydraulic gradient i. If the hydraulic gradient is very high, so that $\gamma' - i\gamma_w$ becomes zero, *the effective stress will become zero*. In other words, there is no contact stress between the soil particles, and the soil will break up. This situation is referred to as the *quick condition*, or *failure by heave*. So, for heave,

$$i = i_{cr} = \frac{\gamma'}{\gamma_w} = \frac{G_s - 1}{1 + e} \tag{2.50}$$

where i_{cr} = critical hydraulic gradient.

For most sandy soil, i_{cr} ranges from 0.9 to 1.1, with an average of about unity.

EXAMPLE 2.8

Figure 2.14a shows the soil profile for the top 9 m at a site, where the water table is at a depth of 5 m below the ground level. The top 3 m consists of dry silty gravel with a unit weight of 17.9 kN/m^3. The next 6 m consists of sand where the unit weights above and below the water table are 17.0 kN/m^3 and 19.5 kN/m^3, respectively. Plot the variations of the total stress, effective stress, and pore water pressure with depth for the soil profile.

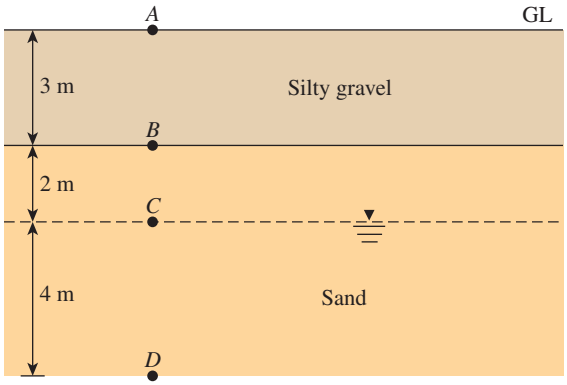


FIGURE 2.14a

SOLUTION

Let's select four points A (at the ground level), B (silty gravel–sand interface), C (water table), and D (bottom of sand) and compute the values at these points.

Point	Depth below GL (m)	Total stress σ (kN/m^2)	Pore water pressure u (kN/m^2)	Eff. stress σ' (kN/m^2)
A	0	0	0	0
B	3	$3 \times 17.9 = 53.7$	0	53.7
C	5	$3 \times 17.9 + 2 \times 17.0 = 87.7$	0	87.7
D	9	$3 \times 17.9 + 2 \times 17.0 + 4 \times 19.5 = 165.7$	$4 \times 9.81 = 39.2$	126.5

The values of σ, u, and σ' are plotted against depth in Figure 2.14b. While the unit weights remain the same, the stresses increase linearly with depth. The break in the gradient occurs only when the unit weight changes.

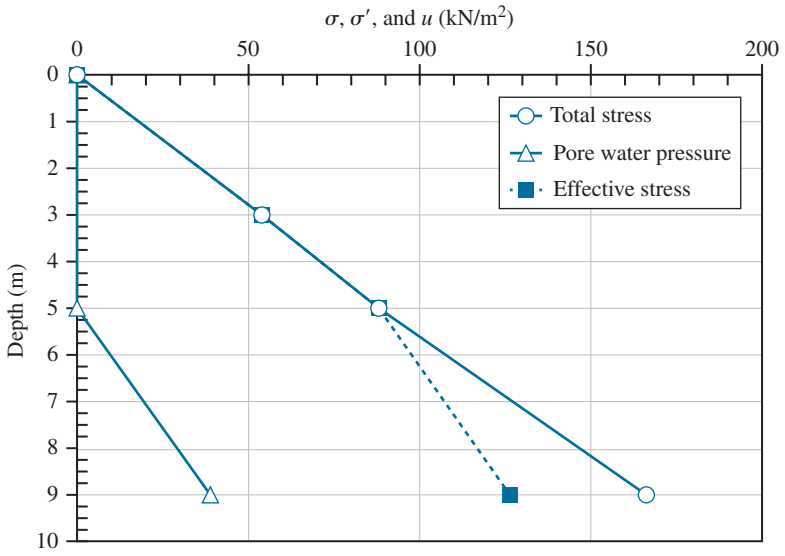


FIGURE 2.14b

2.13 Consolidation

In the field, when the total stress on a saturated clay layer is increased—for example, by the construction of a foundation—the pore water pressure in the clay will increase. Because the hydraulic conductivity of clays is very small, some time will be required for the excess pore water pressure to dissipate and the increase in stress to be transferred to the soil skeleton. According to Figure 2.15, if $\Delta\sigma$ is a surcharge at the ground surface over a very large area, the increase in total stress at any depth of the clay layer will be equal to $\Delta\sigma$.

However, at time $t = 0$ (i.e., immediately after the stress is applied), the excess pore water pressure at any depth Δu will equal $\Delta\sigma$, or

$$\Delta u = \Delta h_i \gamma_w = \Delta\sigma \text{ (at time } t = 0)$$

Hence, the increase in effective stress at time $t = 0$ will be

$$\Delta\sigma' = \Delta\sigma - \Delta u = 0$$

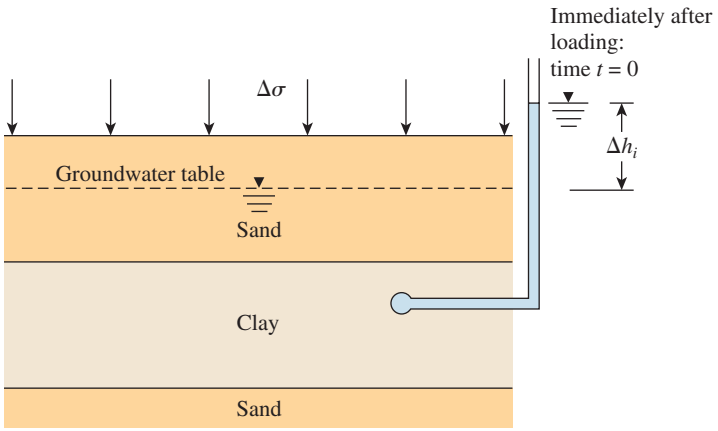


FIGURE 2.15 Principles of consolidation

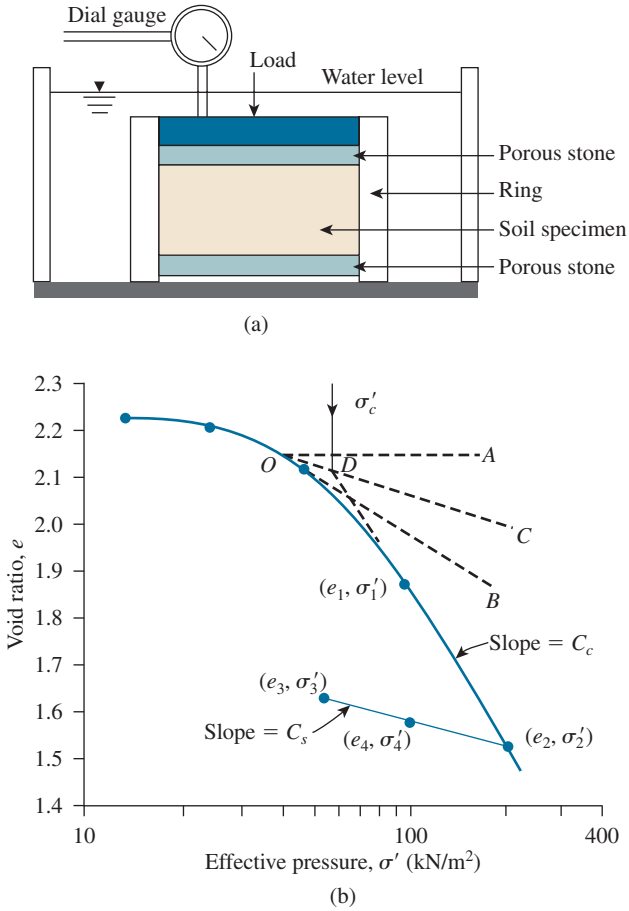


FIGURE 2.16 (a) Schematic diagram of consolidation test arrangement; (b) e–log σ' curve for a soft clay from East St. Louis, Illinois (*Note:* At the end of consolidation, $\sigma = \sigma'$)

Theoretically, at time $t = \infty$, when all the excess pore water pressure in the clay layer has dissipated as a result of drainage into the sand layers,

$$\Delta u = 0 \quad (\text{at time } t = \infty)$$

Then the increase in effective stress in the clay layer is

$$\Delta\sigma' = \Delta\sigma - \Delta u = \Delta\sigma - 0 = \Delta\sigma$$

This gradual increase in the effective stress in the clay layer will cause settlement over a period of time and is referred to as *consolidation*.

Laboratory tests on undisturbed saturated clay specimens can be conducted (ASTM Test Designation D-2435) to determine the consolidation settlement caused by various incremental loadings. The test specimens are usually 63.5 mm (2.5 in.) in diameter and 25.4 mm (1 in.) in height. Specimens are placed inside a ring, with one porous stone at the top and one at the bottom of the specimen (Figure 2.16a). A load on the specimen is then applied so that the total vertical stress is equal to σ. Settlement readings for the specimen are taken periodically for 24 hours. After that, the load on the specimen is doubled and more settlement readings are taken. At all times during the test, the specimen is kept under water. The procedure is continued until the desired limit of stress on the clay specimen is reached.

Based on the laboratory tests, a graph can be plotted showing the variation of the void ratio e at the *end* of consolidation against the corresponding vertical effective stress σ'. (On a semilogarithmic graph, e is plotted on the arithmetic scale and σ' on

the log scale.) The nature of the variation of e against log σ' for a clay specimen is shown in Figure 2.16b. After the desired consolidation pressure has been reached, the specimen gradually can be unloaded, which will result in the swelling of the specimen. The figure also shows the variation of the void ratio during the unloading period.

From the e–log σ' curve shown in Figure 2.16b, three parameters necessary for calculating settlement in the field can be determined. They are preconsolidation pressure (σ'_c), compression index (C_c), and the swelling index (C_s). The following are more detailed descriptions for each of the parameters.

PRECONSOLIDATION PRESSURE

The *preconsolidation pressure*, σ'_c, is the *maximum past effective overburden pressure* to which the soil specimen has been subjected. It can be determined by using a simple graphical procedure proposed by Casagrande (1936). The procedure involves five steps (see Figure 2.16b):

a. Determine the point O on the e–log σ' curve that has the sharpest curvature (i.e., the smallest radius of curvature).
b. Draw a horizontal line OA.
c. Draw a line OB that is tangent to the e–log σ' curve at O.
d. Draw a line OC that bisects the angle AOB.
e. Produce the straight-line portion of the e–log σ' curve backward to intersect OC. This is point D. The pressure that corresponds to point D is the preconsolidation pressure σ'_c.

Natural soil deposits can be *normally consolidated* or *overconsolidated* (or *preconsolidated*). If the present effective overburden pressure $\sigma' = \sigma'_o$ is equal to the preconsolidated pressure σ'_c, the soil is *normally consolidated*. However, if $\sigma'_o < \sigma'_c$, the soil is *overconsolidated*.

Stas and Kulhawy (1984) correlated the preconsolidation pressure with liquidity index in the following form:

$$\frac{\sigma'_c}{p_a} = 10^{(1.11-1.62\,\mathrm{LI})} \tag{2.51}$$

where

p_a = atmospheric pressure (≈2000 lb/ft^2 or 100 kN/m^2)

LI = liquidity index

A similar correlation has also been provided by Kulhawy and Mayne (1990), which is based on the work of Wood (1983) as

$$\sigma'_c = \sigma'_o \left\{ 10^{\left[1-2.5\mathrm{LI}-1.25\log\left(\frac{\sigma'_o}{p_a}\right)\right]} \right\} \tag{2.52}$$

where σ'_o = *in situ* effective overburden pressure.

The ratio of preconsolidation pressure σ'_c to the effective *in situ* overburden pressure σ'_o is defined as the *overconsolidation ratio* (OCR). For normally consolidated clays, the OCR is unity.

COMPRESSION INDEX

The *compression index*, C_c, is the slope of the straight-line portion (the latter part) of the loading curve, or

$$C_c = \frac{e_1 - e_2}{\log \sigma'_2 - \log \sigma'_1} = \frac{e_1 - e_2}{\log\left(\frac{\sigma'_2}{\sigma'_1}\right)} \tag{2.53}$$

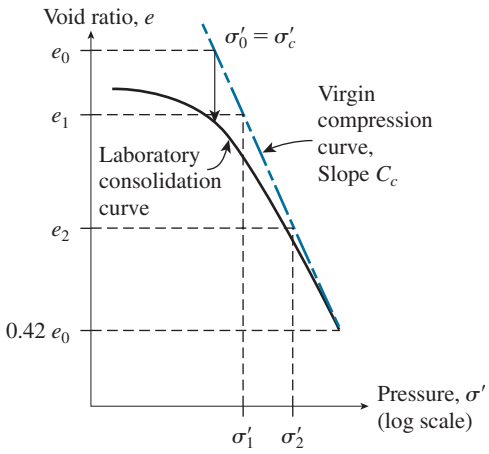


FIGURE 2.17 Construction of virgin compression curve for normally consolidated clay

where e_1 and e_2 are the void ratios at the end of consolidation under effective stresses σ'_1 and σ'_2, respectively.

The *compression index*, as determined from the laboratory e–log σ' curve, will be somewhat different from that encountered in the field. The primary reason is that the soil remolds itself to some degree during the field exploration. The nature of variation of the e–log σ' curve in the field for a normally consolidated clay is shown in Figure 2.17. The curve, generally referred to as the *virgin compression curve*, approximately intersects the laboratory curve at a void ratio of $0.42e_o$ (Terzaghi and Peck, 1967). Note that e_o is the void ratio of the clay in the field. Knowing the values of e_o and σ'_c, you can easily construct the virgin curve and calculate its compression index by using Eq. (2.53).

The value of C_c can vary widely, depending on the soil. Skempton (1944) gave an empirical correlation for the compression index in which

$$C_c = 0.009(\text{LL} - 10) \tag{2.54}$$

where LL = liquid limit.

Besides Skempton, several other investigators also have proposed correlations for the compression index. Some of those are given here:

Rendon-Herrero (1983):

$$C_c = 0.141G_s^{1.2}\left(\frac{1 + e_o}{G_s}\right)^{2.38} \tag{2.55}$$

Nagaraj and Murty (1985):

$$C_c = 0.2343\left[\frac{\text{LL}(\%)}{100}\right]G_s \tag{2.56}$$

Park and Koumoto (2004):

$$C_c = \frac{n_o}{371.747 - 4.275n_o} \tag{2.57}$$

where n_o = *in situ* porosity of soil (%).

Wroth and Wood (1978):

$$C_c = 0.5G_s\left(\frac{\text{PI}(\%)}{100}\right) \tag{2.58}$$

If a typical value of $G_s = 2.7$ is used in Eq. (2.58), we obtain (Kulhawy and Mayne, 1990)

$$C_c = \frac{\text{PI}(\%)}{74} \tag{2.59}$$

SWELLING INDEX

The *swelling index,* C_s, is the slope of the unloading portion of the e–log σ' curve. In Figure 2.16b, it is defined as

$$C_s = \frac{e_3 - e_4}{\log\left(\frac{\sigma'_4}{\sigma'_3}\right)} \tag{2.60}$$

In most cases, the value of the swelling index is $\frac{1}{5}$ to $\frac{1}{10}$ of the compression index. Following are some representative values of C_s/C_c for natural soil deposits:

Description of soil	C_s/C_c
Boston Blue clay	0.24–0.33
Chicago clay	0.15–0.3
New Orleans clay	0.15–0.28
St. Lawrence clay	0.05–0.1

The swelling index is also referred to as the *recompression index* and is denoted by C_r.

The determination of the swelling index is important in the estimation of consolidation settlement of *overconsolidated clays.* In the field, depending on the pressure increase, an overconsolidated clay will follow an e–log σ' path *abc*, as shown in Figure 2.18. Note that point *a*, with coordinates σ'_o and e_o, corresponds to the field conditions before any increase in pressure. Point *b* corresponds to the preconsolidation pressure (σ'_c) of the clay. Line *ab* is approximately parallel to the laboratory unloading curve *cd* (Schmertmann, 1953). Hence, if you know e_o, σ'_o, σ'_c, C_c, and C_s, you can easily construct the field consolidation curve.

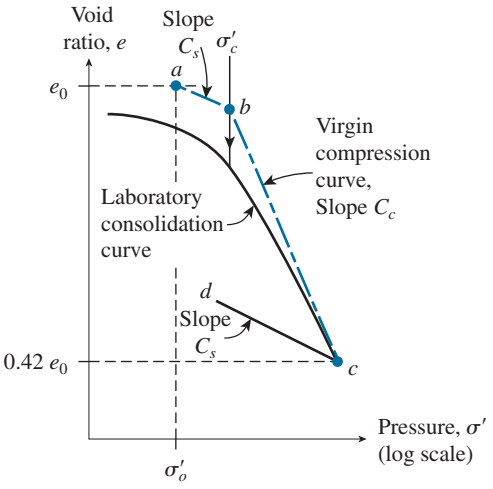


FIGURE 2.18 Construction of field consolidation curve for overconsolidated clay

Using the modified Cam clay model and Eq. (2.58), Kulhawy and Mayne (1990) have shown that

$$C_s = \frac{\text{PI}(\%)}{370} \tag{2.61}$$

Comparing Eqs. (2.59) and (2.61), we obtain

$$C_s \approx \frac{1}{5} C_c \tag{2.62}$$

2.14 Calculation of Primary Consolidation Settlement

The one-dimensional primary consolidation settlement (caused by an additional load) of a clay layer (Figure 2.19) having a thickness H_c may be calculated as

$$S_c = \frac{\Delta e}{1 + e_o} H_c \tag{2.63}$$

where

S_c = primary consolidation settlement

Δe = total change of void ratio caused by the additional load application

e_o = void ratio of the clay before the application of load

For normally consolidated clay (that is, $\sigma'_o = \sigma'_c$)

$$\Delta e = C_c \log \frac{\sigma'_o + \Delta\sigma'}{\sigma'_o} \tag{2.64}$$

where

σ'_o = average effective vertical stress on the clay layer

$\Delta\sigma'$ = $\Delta\sigma$ (that is, added pressure)

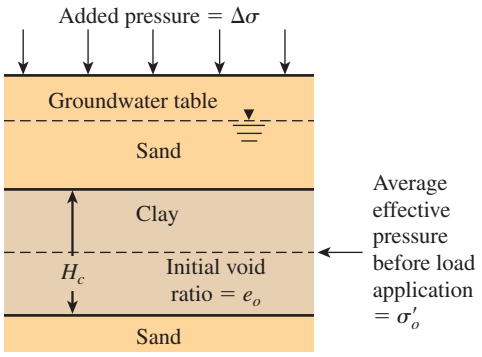


FIGURE 2.19 One-dimensional settlement calculation

Now, combining Eqs. (2.63) and (2.64) yields

$$S_c = \frac{C_c H_c}{1 + e_o} \log \frac{\sigma'_o + \Delta\sigma'}{\sigma'_o} \tag{2.65}$$

For overconsolidated clay with $\sigma'_o + \Delta\sigma' \le \sigma'_c$,

$$\Delta e = C_s \log \frac{\sigma'_o + \Delta\sigma'}{\sigma'_o} \tag{2.66}$$

Combining Eqs. (2.63) and (2.66) gives

$$S_c = \frac{C_s H_c}{1 + e_o} \log \frac{\sigma'_o + \Delta\sigma'}{\sigma'_o} \tag{2.67}$$

For overconsolidated clay, if $\sigma'_c < \sigma'_o + \Delta\sigma'$, then

$$\Delta e = \Delta e_1 + \Delta e_2 = C_s \log \frac{\sigma'_c}{\sigma'_o} + C_c \log \frac{\sigma'_o + \Delta\sigma'}{\sigma'_c} \tag{2.68}$$

Now, combining Eqs. (2.63) and (2.68) yields

$$S_c = \frac{C_s H_c}{1 + e_o} \log \frac{\sigma'_c}{\sigma'_o} + \frac{C_c H_c}{1 + e_o} \log \frac{\sigma'_o + \Delta\sigma'}{\sigma'_c} \tag{2.69}$$

2.15 Time Rate of Consolidation

During the consolidation process, the applied load that was initially carried by the water is gradually transferred to the soil skeleton. In Section 2.13 (see Figure 2.15), we showed that consolidation is the result of the gradual dissipation of the excess pore water pressure from a clay layer. The dissipation of pore water pressure, in turn, increases the effective stress, which induces settlement. Hence, to estimate the degree of consolidation of a clay layer at some time t after the load is applied, you need to know the rate of dissipation of the excess pore water pressure.

Figure 2.20 shows a clay layer of thickness H_c that has highly permeable sand layers at its top and bottom. Here, the excess pore water pressure at any point A at any time t after the load is applied is $\Delta u = (\Delta h)\gamma_w$. For a vertical drainage condition

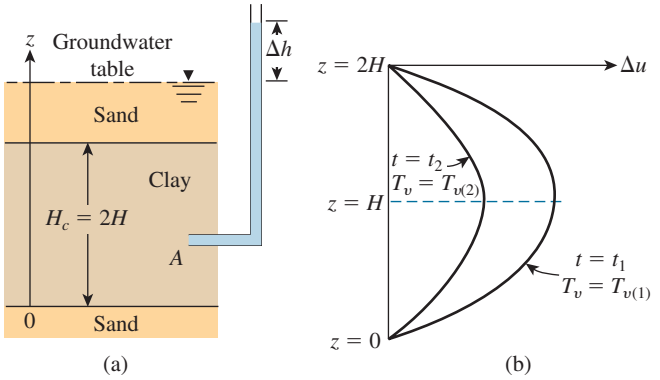


FIGURE 2.20 (a) Derivation of Eq. (2.72); (b) variation of Δu with time and depth

(that is, in the direction of z only) from the clay layer, Terzaghi derived the differential equation

$$\frac{\partial(\Delta u)}{\partial t} = c_v \frac{\partial^2(\Delta u)}{\partial z^2} \tag{2.70}$$

where c_v = coefficient of consolidation, defined by

$$c_v = \frac{k}{m_v \gamma_w} = \frac{k}{\dfrac{\Delta e}{\Delta \sigma'(1 + e_{av})}\gamma_w} \tag{2.71}$$

in which

k = hydraulic conductivity of the clay

γ_w = unit weight of water

Δe = total change of void ratio caused by an effective stress increase of $\Delta \sigma'$

e_{av} = average void ratio during consolidation

m_v = volume coefficient of compressibility $= \dfrac{a_v}{1 + e_{av}} = \Delta e/[\Delta \sigma'(1 + e_{av})]$

$a_v = \dfrac{\Delta e}{\Delta \sigma'}$

Equation (2.70) can be solved to obtain Δu as a function of time t with the following boundary conditions:

1. Because highly permeable sand layers are located at $z = 0$ and $z = H_c$, the excess pore water pressure developed in the clay at those points will be immediately dissipated. Hence,

   $$\Delta u = 0 \quad \text{at} \quad z = 0$$

   and

   $$\Delta u = 0 \quad \text{at} \quad z = H_c = 2H$$

   where H = length of maximum drainage path (due to two-way drainage condition—that is, at the top and bottom of the clay).
2. At time $t = 0$, $\Delta u = \Delta u_0$ = initial excess pore water pressure after the load is applied. With the preceding boundary conditions, Eq. (2.70) yields

   $$\Delta u = \sum_{m=0}^{m=\infty} \left[\frac{2(\Delta u_0)}{M} \sin\left(\frac{Mz}{H}\right)\right] e^{-M^2 T_v} \tag{2.72}$$

   where

   $M = [(2m + 1)\pi]/2$

   m = an integer = 1, 2, ...

   T_v = nondimensional time factor $= (c_v t)/H^2$ (2.73)

The value of Δu for various depths (i.e., $z = 0$ to $z = 2H$) at any given time t (and thus T_v) can be calculated from Eq. (2.72). The nature of this variation of Δu is shown in Figures 2.21a and b. Figure 2.21c shows the variation of $\Delta u/\Delta u_0$ with T_v and H/H_c using Eqs. (2.72) and (2.73).

The *average degree of consolidation* of the clay layer can be defined as

$$U = \frac{S_{c(t)}}{S_{c(\max)}} \tag{2.74}$$

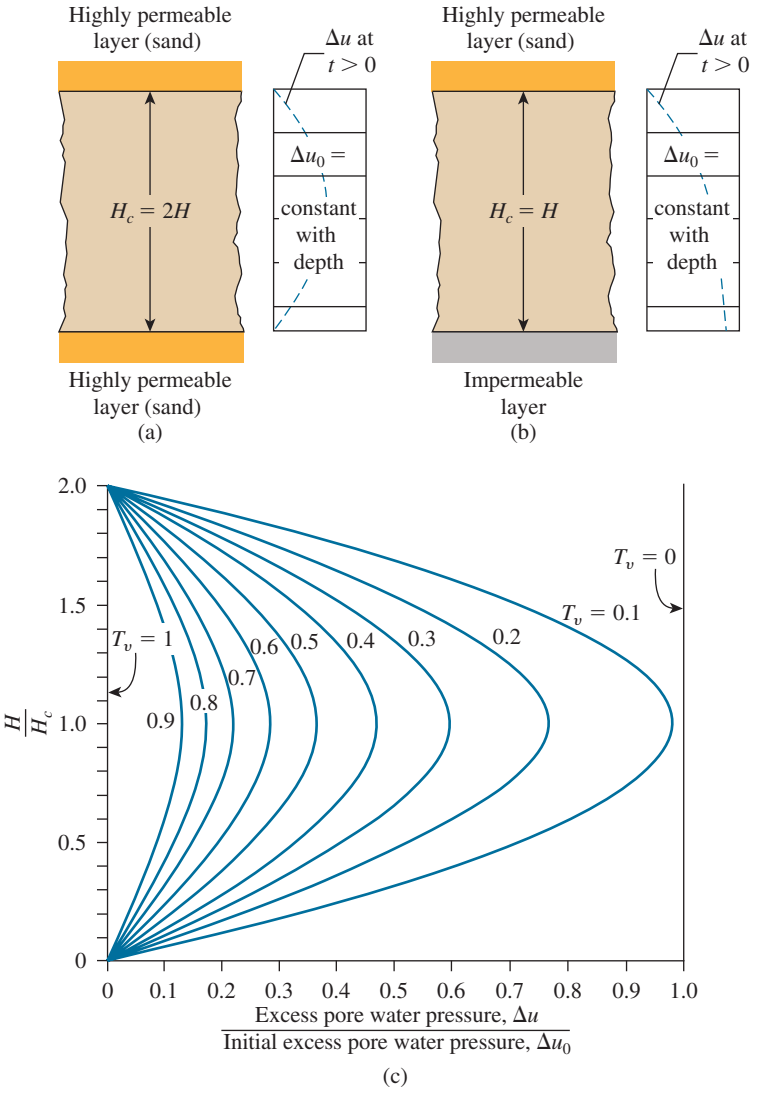


FIGURE 2.21 Drainage condition for consolidation: (a) two-way drainage; (b) one-way drainage; (c) plot of $\Delta u/\Delta u_0$ with T_v and H/H_c

where

$S_{c(t)}$ = settlement of a clay layer at time t after the load is applied

$S_{c(\max)}$ = maximum consolidation settlement that the clay will undergo under a given loading, determined by Eqs. (2.65), (2.67), and (2.69)

If the initial pore water pressure (Δu_0) distribution is constant with depth, as shown in Figures 2.21a and b the average degree of consolidation also can be expressed as

$$U = \frac{S_{c(t)}}{S_{c(\max)}} = \frac{\int_0^{2H} (\Delta u_0)\,dz - \int_0^{2H} (\Delta u)\,dz}{\int_0^{2H} (\Delta u_0)\,dz} \tag{2.75}$$

or

$$U = \frac{(\Delta u_0)2H - \int_0^{2H} (\Delta u)\,dz}{(\Delta u_0)2H} = 1 - \frac{\int_0^{2H} (\Delta u)\,dz}{2H(\Delta u_0)} \tag{2.76}$$

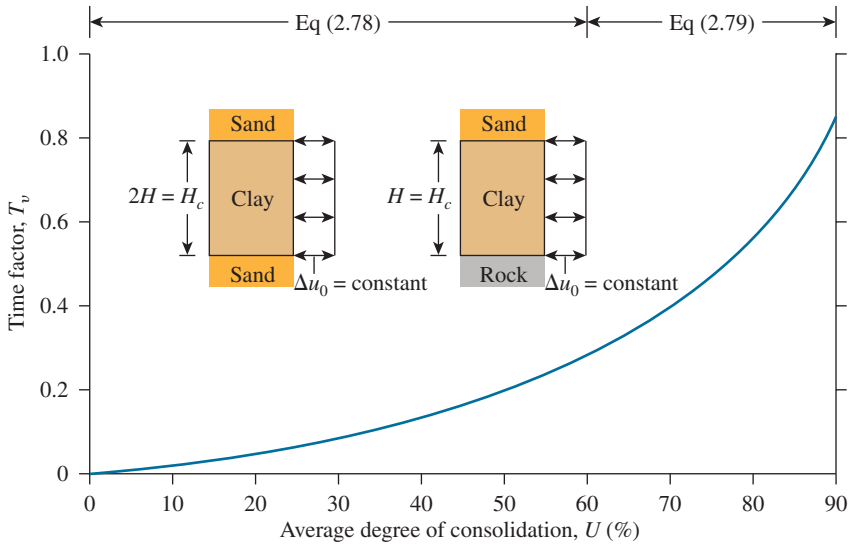


FIGURE 2.22 Plot of time factor against average degree of consolidation (Δu_0 = constant)

Now, combining Eqs. (2.72) and (2.76), we obtain

$$U = \frac{S_{c(t)}}{S_{c(\max)}} = 1 - \sum_{m=0}^{m=\infty} \left(\frac{2}{M^2}\right) e^{-M^2 T_v} \tag{2.77}$$

The variation of U with T_v can be calculated from Eq. (2.77) and is plotted in Figure 2.22. Note that Eq. (2.77) and thus Figure 2.22 are also valid when an impermeable layer is located at the bottom of the clay layer (Figure 2.21). In that case, the dissipation of excess pore water pressure can take place in one direction only. The length of the *maximum drainage path* is then equal to $H = H_c$.

The variation of T_v with U shown in Figure 2.22 can also be approximated by

$$T_v = \frac{\pi}{4}\left(\frac{U\%}{100}\right)^2 \quad (\text{for } U = 0 \text{ to } 60\%) \tag{2.78}$$

and

$$T_v = 1.781 - 0.933 \log (100 - U\%) \quad (\text{for } U > 60\%) \tag{2.79}$$

Table 2.12 gives the variation of T_v with U on the basis of Eqs. (2.78) and (2.79).

Sivaram and Swamee (1977) gave the following equation for U varying from 0 to 100%:

$$\frac{U\%}{100} = \frac{(4T_v/\pi)^{0.5}}{[1 + (4T_v/\pi)^{2.8}]^{0.179}} \tag{2.80}$$

or

$$T_v = \frac{(\pi/4)(U\%/100)^2}{[1 - (U\%/100)^{5.6}]^{0.357}} \tag{2.81}$$

Equations (2.80) and (2.81) give an error in T_v of less than 1% for $0\% < U < 90\%$ and less than 3% for $90\% < U < 100\%$.

TABLE 2.12 Variation of T_v with U

U (%)	T_v	U (%)	T_v	U (%)	T_v	U (%)	T_v
0	0	26	0.0531	52	0.212	78	0.529
1	0.00008	27	0.0572	53	0.221	79	0.547
2	0.0003	28	0.0615	54	0.230	80	0.567
3	0.00071	29	0.0660	55	0.239	81	0.588
4	0.00126	30	0.0707	56	0.248	82	0.610
5	0.00196	31	0.0754	57	0.257	83	0.633
6	0.00283	32	0.0803	58	0.267	84	0.658
7	0.00385	33	0.0855	59	0.276	85	0.684
8	0.00502	34	0.0907	60	0.286	86	0.712
9	0.00636	35	0.0962	61	0.297	87	0.742
10	0.00785	36	0.102	62	0.307	88	0.774
11	0.0095	37	0.107	63	0.318	89	0.809
12	0.0113	38	0.113	64	0.329	90	0.848
13	0.0133	39	0.119	65	0.304	91	0.891
14	0.0154	40	0.126	66	0.352	92	0.938
15	0.0177	41	0.132	67	0.364	93	0.993
16	0.0201	42	0.138	68	0.377	94	1.055
17	0.0227	43	0.145	69	0.390	95	1.129
18	0.0254	44	0.152	70	0.403	96	1.219
19	0.0283	45	0.159	71	0.417	97	1.336
20	0.0314	46	0.166	72	0.431	98	1.500
21	0.0346	47	0.173	73	0.446	99	1.781
22	0.0380	48	0.181	74	0.461	100	∞
23	0.0415	49	0.188	75	0.477		
24	0.0452	50	0.197	76	0.493		
25	0.0491	51	0.204	77	0.511		

EXAMPLE 2.9

A laboratory consolidation test on a normally consolidated clay showed the following results:

Stress, $\Delta\sigma'$ (kN/m^2)	Void ratio at the end of consolidation, e
140	0.92
212	0.86

The specimen tested was 25.4 mm in thickness and drained on both sides. The time required for the specimen to reach 50% consolidation was 4.5 min.

A similar clay layer in the field, 2.8 m thick and drained on both sides, is subjected to a similar increase in average effective pressure (i.e., $\sigma'_0 = 140$ kN/m^2 and $\sigma'_0 + \Delta\sigma' = 212$ kN/m^2). Determine the following.

a. The expected maximum primary consolidation settlement in the field.
b. The length of time required for the total settlement in the field to reach 40 mm. (Assume a uniform initial increase in excess pore water pressure with depth.)

SOLUTION

Part a

For normally consolidated clay [Eq. (2.53)],

$$C_c = \frac{e_1 - e_2}{\log\left(\frac{\sigma_2'}{\sigma_1'}\right)} = \frac{0.92 - 0.86}{\log\left(\frac{212}{140}\right)} = 0.333$$

From Eq. (2.65),

$$S_c = \frac{C_c H_c}{1 + e_0} \log \frac{\sigma_0' + \Delta\sigma'}{\sigma_0'} = \frac{(0.333)(2.8)}{1 + 0.92} \log \frac{212}{140} = 0.0875 \text{ m} = \mathbf{87.5 \text{ mm}}$$

Part b

From Eq. (2.74), the average degree of consolidation is

$$U = \frac{S_{c(t)}}{S_{c(\max)}} = \frac{40}{87.5}(100) = 45.7\%$$

The coefficient of consolidation, c_v, can be calculated from the laboratory test. From Eq. (2.73),

$$T_v = \frac{c_v t}{H^2}$$

For 50% consolidation (Figure 2.22), $T_v = 0.197$, $t = 4.5$ min, and $H = H_c/2 = 12.7$ mm, so

$$c_v = T_{50}\frac{H^2}{t} = \frac{(0.197)(12.7)^2}{4.5} = 7.061 \text{ mm}^2/\text{min}$$

Again, for field consolidation, $U = 45.7\%$. From Eq. (2.78),

$$T_v = \frac{\pi}{4}\left(\frac{U\%}{100}\right)^2 = \frac{\pi}{4}\left(\frac{45.7}{100}\right)^2 = 0.164$$

But

$$T_v = \frac{c_v t}{H^2}$$

or

$$t = \frac{T_v H^2}{c_v} = \frac{0.164\left(\frac{2.8 \times 1000}{2}\right)^2}{7.061} = 45{,}523 \text{ min} = \mathbf{31.6 \text{ days}}$$

EXAMPLE 2.10

A laboratory consolidation test on a soil specimen (drained on both sides) determined the following results:

Thickness of the clay specimen = 25 mm

$\sigma_1' = 50$ kN/m^2 $\quad e_1 = 0.92$
$\sigma_2' = 120$ kN/m^2 $\quad e_2 = 0.78$

Time for 50% consolidation = 2.5 min

Determine the hydraulic conductivity, k, of the clay for the loading range.

SOLUTION

$$m_v = \frac{a_v}{1 + e_{av}} = \frac{(\Delta e/\Delta\sigma')}{1 + e_{av}}$$

$$= \frac{\dfrac{0.92 - 0.78}{120 - 50}}{1 + \dfrac{0.92 + 0.78}{2}} = 0.00108 \text{ m}^2/\text{kN}$$

$$c_v = \frac{T_{50}H^2}{t_{50}}$$

From Table 2.11 for $U = 50\%$, the value of $T_v = 0.197$, so

$$c_v = \frac{(0.197)\left(\dfrac{0.025\text{ m}}{2}\right)^2}{2.5\text{ min}} = 1.23 \times 10^{-5}\text{ m}^2/\text{min}$$

$$k = c_v m_v \gamma_w = (1.23 \times 10^{-5})(0.00108)(9.81)$$

$$= \mathbf{1.303 \times 10^{-7}\ m/min}$$

2.16 Range of Coefficient of Consolidation, c_v

Figure 2.23, proposed by the U.S. Navy (1986), can be used as a guide for checking c_v values determined in the laboratory. It can be seen that the c_v values for overconsolidated clays are significantly greater than those of normally consolidated clays. Therefore, overconsolidated clays consolidate faster than normally consolidated clays. The value of c_v can vary from less than 1 m^2/year for low permeability clays to more than 100 m^2/year for overconsolidated sandy clays of high permeability.

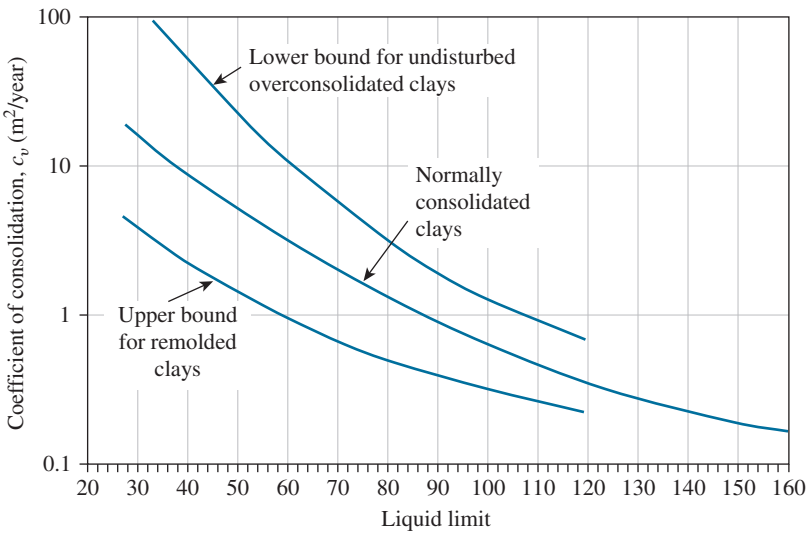


FIGURE 2.23 Approximate correlations for c_v with liquid limit (Adapted from U.S. Navy 1986)

2.17 Degree of Consolidation Under Ramp Loading

The relationships derived for the average degree of consolidation in Section 2.15 assume that the surcharge load per unit area ($\Delta\sigma$) is applied instantly at time $t = 0$. However, in most practical situations, $\Delta\sigma$ increases gradually with time to a maximum value and remains constant thereafter. Figure 2.24 shows $\Delta\sigma$ increasing linearly with time (t) up to a maximum at time t_c (a condition called ramp loading). For $t \geq t_c$, the magnitude of $\Delta\sigma$ remains constant. Olson (1977) considered this phenomenon and presented the average degree of consolidation, U, in the following form:

For $T_v \leq T_c$,

$$U = \frac{T_v}{T_c}\left\{1 - \frac{2}{T_v}\sum_{m=0}^{m=\infty}\frac{1}{M^4}[1 - \exp(-M^2T_v)]\right\} \tag{2.82}$$

and for $T_v \geq T_c$,

$$U = 1 - \frac{2}{T_c}\sum_{m=0}^{m=\infty}\frac{1}{M^4}[\exp(M^2T_c) - 1]\exp(-M^2T_c) \tag{2.83}$$

where m, M, and T_v have the same definition as in Eq. (2.72) and where

$$T_c = \frac{c_v\, t_c}{H^2} \tag{2.84}$$

Figure 2.25 shows the variation of U with T_v for various values of T_c, based on the solution given by Eqs. (2.82) and (2.83).

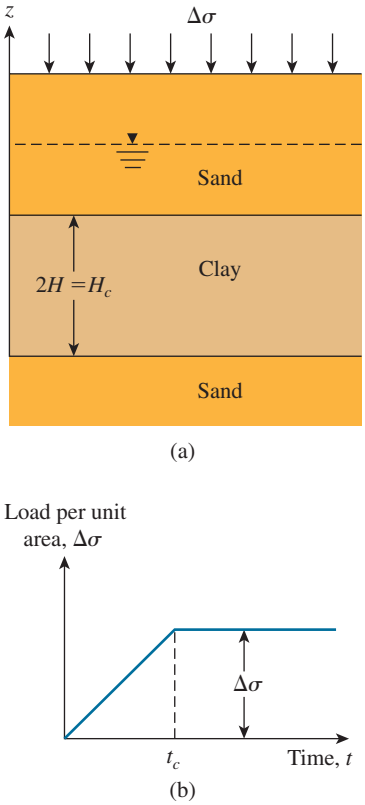


FIGURE 2.24 One-dimensional consolidation due to single ramp loading

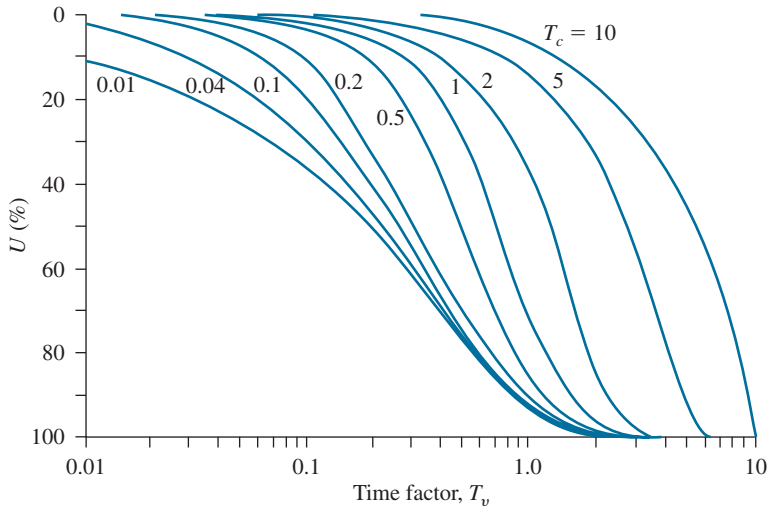


FIGURE 2.25 Olson's ramp-loading solution: plot of U versus T_v (Eqs. 2.82 and 2.83)

EXAMPLE 2.11

In Example 2.9, Part (b), if the increase in $\Delta\sigma$ would have been in the manner shown in Figure 2.26, calculate the settlement of the clay layer at time $t = 31.6$ days after the beginning of the surcharge.

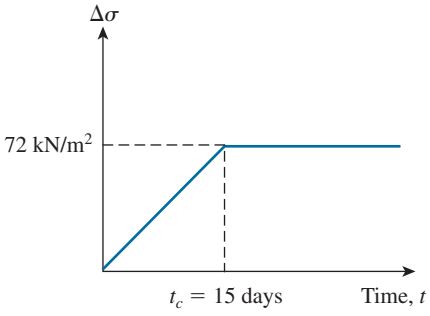


FIGURE 2.26 Ramp loading

SOLUTION

From Part (b) of Example 2.9, $c_v = 7.061$ mm^2/min. From Eq. (2.84),

$$T_c = \frac{c_v t_c}{H^2} = \frac{(7.061 \text{ mm}^2/\text{min})\,(15 \times 24 \times 60 \text{ min})}{\left(\frac{2.8}{2} \times 1000 \text{ mm}\right)^2} = 0.0778$$

Also,

$$T_v = \frac{c_v t}{H^2} = \frac{(7.061 \text{ mm}^2/\text{min})\,(31.6 \times 24 \times 60 \text{ min})}{\left(\frac{2.8}{2} \times 1000 \text{ mm}\right)^2} = 0.164$$

From Figure 2.25, for $T_v = 0.164$ and $T_c = 0.0778$, the value of U is about 36%. Thus,

$$S_{c(t=31.6 \text{ days})} = S_{c(\max)}(0.36) = (87.5)\,(0.36) = \mathbf{31.5 \text{ mm}}$$

■

2.18 Shear Strength

The shear strength of a soil, defined in terms of effective stress, is

$$s = c' + \sigma' \tan \phi' \tag{2.85}$$

where

σ' = effective normal stress on plane of shearing

c' = cohesion, or apparent cohesion

ϕ' = effective stress angle of friction

Equation (2.85) is referred to as the *Mohr–Coulomb failure criterion*. The value of c' for sands and normally consolidated clays is equal to zero. For overconsolidated clays, $c' > 0$.

For most day-to-day work, the shear strength parameters of a soil (i.e., c' and ϕ') are determined by two standard laboratory tests: the *direct shear test* and the *triaxial test.*

DIRECT SHEAR TEST

Dry sand can be conveniently tested by direct shear tests. The sand is placed in a shear box that is split into two halves (Figure 2.27a). First a normal load is applied to the specimen. Then a shear force is applied to the top half of the shear box to cause failure in the sand. The normal and shear stresses at failure are

$$\sigma' = \frac{N}{A}$$

and

$$s = \frac{R}{A}$$

where A = area of the failure plane in soil—that is, the cross-sectional area of the shear box.

Several tests of this type can be conducted by varying the normal load. The angle of friction of the sand can be determined by plotting a graph of s against σ' ($= \sigma$ for dry sand), as shown in Figure 2.27b, or

$$\phi' = \tan^{-1}\left(\frac{s}{\sigma'}\right) \tag{2.86}$$

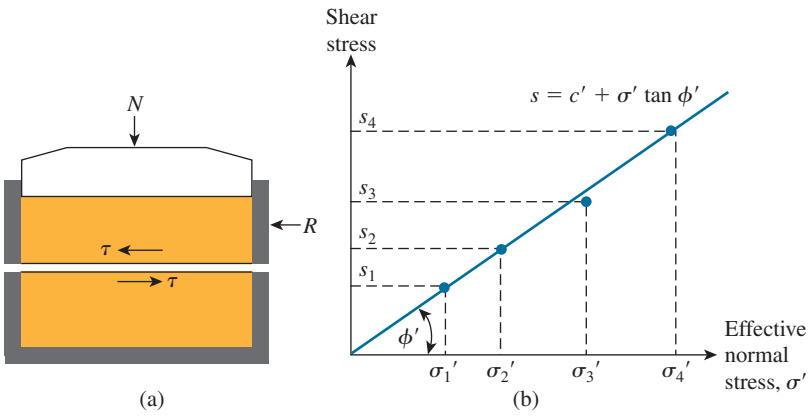


FIGURE 2.27 Direct shear test in sand: (a) schematic diagram of test equipment; (b) plot of test results to obtain the friction angle ϕ'

TABLE 2.13 Relationship Between Relative Density and Angle of Friction of Cohesionless Soil

State of packing	Relative density (%)	Angle of friction, ϕ' (deg.)
Very loose	<15	<28
Loose	15–35	28–30
Compact or medium	35–65	30–36
Dense	65–85	36–41
Very dense	>85	>41

For sands, the angle of friction usually ranges from 26° to 45°, increasing with the relative density of compaction. A general range of the friction angle, ϕ', for sands is given in Table 2.13.

In 1970, Brinch Hansen (see Hansbo, 1975, and Thinh, 2001) gave the following correlation for ϕ' of granular soil:

$$\phi' \text{ (deg)} = 26° + 10D_r + 0.4C_u + 1.6 \log (D_{50}) \tag{2.87}$$

where

D_r = relative density (fraction)

C_u = uniformity coefficient

D_{50} = median grain size, in mm (i.e., the diameter through which 50% of the soil passes)

Teferra (1975) suggested the following empirical correlation based on a large database.

$$\phi'(\text{deg}) = \tan^{-1}\left(\frac{1}{ae+b}\right) \tag{2.88}$$

where

e = void ratio

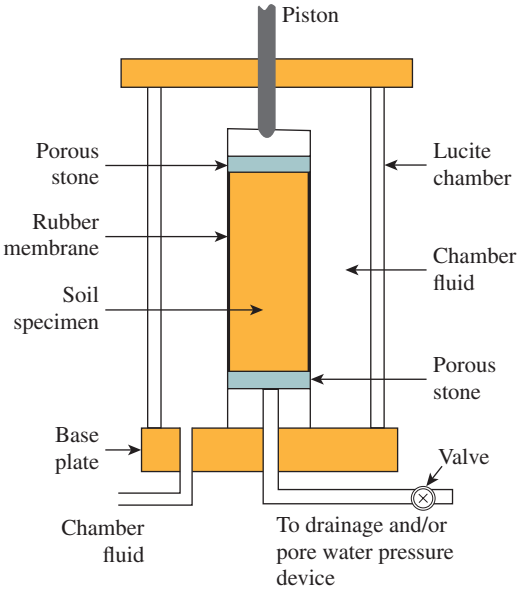
$$a = 2.101 + 0.097\left(\frac{D_{85}}{D_{15}}\right) \tag{2.89}$$

$$b = 0.845 - 0.398a \tag{2.90}$$

D_{85} and D_{15} = diameters through which, respectively, 85% and 15% of soil passes. Thinh (2001) suggested that Eq. (2.88) provides a better correlation for ϕ' compared to Eq. (2.87).

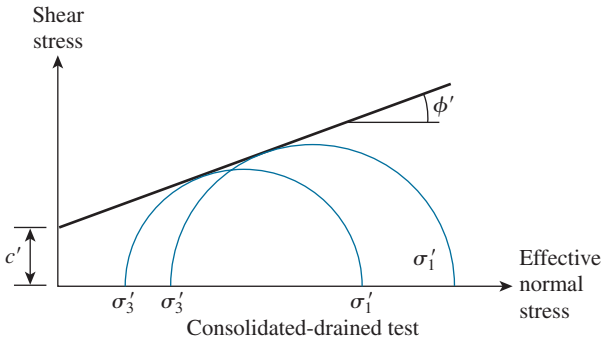
TRIAXIAL TESTS

Triaxial compression tests can be conducted on sands and clays. Figure 2.28a shows a schematic diagram of the triaxial test arrangement. Essentially, the test consists of placing a soil specimen confined by a rubber membrane into a lucite chamber and then applying an all-around confining pressure (σ_3) to the specimen by means of the chamber fluid (generally, water or glycerin). An added stress ($\Delta\sigma$) can also be applied to the specimen in the axial direction to cause failure ($\Delta\sigma = \Delta\sigma_f$ at failure). Drainage from the specimen can be allowed or stopped, depending on the



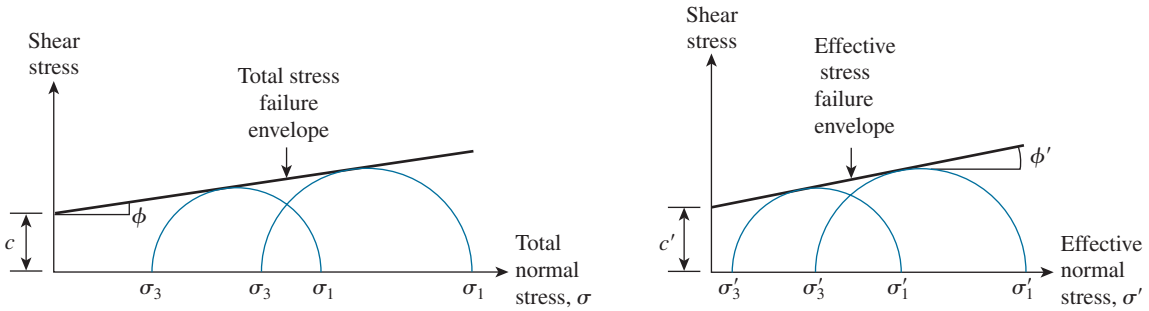
Schematic diagram of triaxial test equipment

(a)



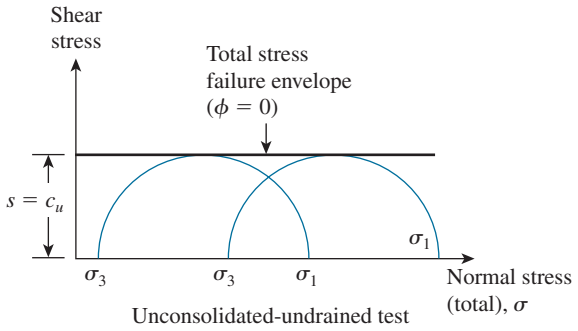
Consolidated-drained test

(b)



Consolidated-undrained test

(c)



Unconsolidated-undrained test

(d)

FIGURE 2.28 Triaxial test: (a) triaxial test equipment; (b) consolidated-drained test; (c) consolidated-undrained test; (d) unconsolidated-undrained test

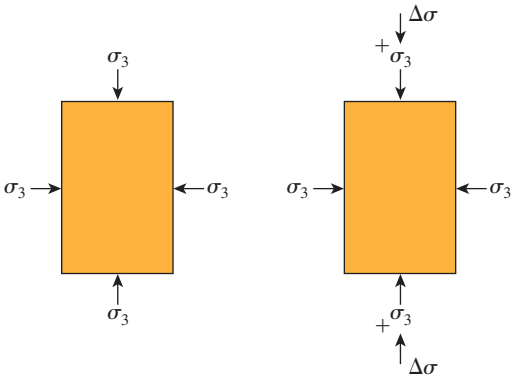


FIGURE 2.29 Sequence of stress application in triaxial test

condition being tested. For clays, three main types of tests can be conducted with triaxial equipment (see Figure 2.29):

1. Consolidtated-Drained Test (CD test)
2. Consolidated-Undrained Test (CU test)
3. Unconsolidated-Undrained Test (UU test)

a. *Consolidated-Drained Tests:*

Step 1. Apply chamber pressure σ_3. Allow complete drainage, so that the pore water pressure ($u = u_0$) developed is zero.

Step 2. Apply a deviator stress $\Delta\sigma$ slowly. Allow drainage, so that the pore water pressure ($u = u_d$) developed through the application of $\Delta\sigma$ is zero. At failure, $\Delta\sigma = \Delta\sigma_f$; the total pore water pressure $u_f = u_0 + u_d = 0$.

So for *consolidated-drained tests,* at failure,

Major principal effective stress $= \sigma_3 + \Delta\sigma_f = \sigma_1 = \sigma_1'$
Minor principal effective stress $= \sigma_3 = \sigma_3'$

Changing σ_3 allows several tests of this type to be conducted on various clay specimens. The shear strength parameters (c' and ϕ') can now be determined by plotting Mohr's circle at failure, as shown in Figure 2.28b, and drawing a common tangent to the Mohr's circles. This is the *Mohr–Coulomb failure envelope.* (*Note:* For normally consolidated clay, $c' \approx 0$.) At failure, σ_1 and σ_3 are related by

$$\sigma_1' = \sigma_3' \tan^2\left(45 + \frac{\phi'}{2}\right) + 2c' \tan\left(45 + \frac{\phi'}{2}\right) \tag{2.91}$$

b. *Consolidated-Undrained Tests:*

Step 1. Apply chamber pressure σ_3. Allow complete drainage, so that the pore water pressure ($u = u_0$) developed is zero.

Step 2. Apply a deviator stress $\Delta\sigma$. Do not allow drainage, so that the pore water pressure $u = u_d \neq 0$. At failure, $\Delta\sigma = \Delta\sigma_f$; the pore water pressure $u_f = u_0 + u_d = 0 + u_{d(f)}$.

Hence, at failure,

Major principal total stress $= \sigma_3 + \Delta\sigma_f = \sigma_1$

Minor principal total stress $= \sigma_3$

Major principal effective stress $= (\sigma_3 + \Delta\sigma_f) - u_f = \sigma_1'$

Minor principal effective stress $= \sigma_3 - u_f = \sigma_3'$

Changing σ_3 permits multiple tests of this type to be conducted on several soil specimens. The total stress Mohr's circles at failure can now be plotted, as shown in Figure 2.28c, and then a common tangent can be drawn to define the *failure envelope.* This *total stress failure envelope* is defined by the equation

$$s = c + \sigma \tan \phi \tag{2.92}$$

where c and ϕ are the *consolidated-undrained cohesion* and *angle of friction*, respectively. (*Note:* $c \approx 0$ for normally consolidated clays.)

Similarly, effective stress Mohr's circles at failure can be drawn to determine the *effective stress failure envelope* (Figure 2.28c), which satisfies the relation expressed in Eq. (2.85).

c. *Unconsolidated-Undrained Tests:*

Step 1. Apply chamber pressure σ_3. Do not allow drainage, so that the pore water pressure ($u = u_0$) developed through the application of σ_3 is not zero.

Step 2. Apply a deviator stress $\Delta\sigma$. Do not allow drainage ($u = u_d \neq 0$). At failure, $\Delta\sigma = \Delta\sigma_f$; the pore water pressure $u_f = u_0 + u_{d(f)}$.

For *unconsolidated-undrained* triaxial tests,

Major principal total stress $= \sigma_3 + \Delta\sigma_f = \sigma_1$
Minor principal total stress $= \sigma_3$

The total stress Mohr's circle at failure can now be drawn, as shown in Figure 2.28d. For saturated clays, the value of $\sigma_1 - \sigma_3 = \Delta\sigma_f$ is a constant, irrespective of the chamber confining pressure σ_3 (also shown in Figure 2.28d). The tangent to these Mohr's circles will be a horizontal line, called the $\phi = 0$ condition. The shear strength for this condition is

$$s = c_u = \frac{\Delta\sigma_f}{2} \tag{2.93}$$

where c_u = undrained cohesion (or undrained shear strength).

The pore pressure developed in the soil specimen during the unconsolidated-undrained triaxial test is

$$u = u_0 + u_d \tag{2.94}$$

The pore pressure u_0 is the contribution of the hydrostatic chamber pressure σ_3. Hence,

$$u_0 = B\sigma_3 \tag{2.95}$$

where B = Skempton's pore pressure parameter.

Similarly, the pore parameter u_d is the result of the added axial stress $\Delta\sigma$, so

$$u_d = A\Delta\sigma \tag{2.96}$$

where A = Skempton's pore pressure parameter.

However,

$$\Delta\sigma = \sigma_1 - \sigma_3 \tag{2.97}$$

Combining Eqs. (2.94), (2.95), (2.96), and (2.97) gives

$$u = u_0 + u_d = B\sigma_3 + A(\sigma_1 - \sigma_3) \tag{2.98}$$

The pore water pressure parameter B in soft saturated soil is approximately 1, so

$$u = \sigma_3 + A(\sigma_1 - \sigma_3) \tag{2.99}$$

The value of the pore water pressure parameter A at failure (A_f) will vary with the type of soil. Following is a general range of the values of A at failure for various types of clayey soil encountered in nature:

Type of soil	A at failure (A_f)
Sandy clays	0.5–0.7
Normally consolidated clays	0.5–1
Overconsolidated clays	−0.5–0

2.19 Unconfined Compression Test

The *unconfined compression test* (Figure 2.30a) is a special type of unconsolidated-undrained triaxial test in which the confining pressure $\sigma_3 = 0$, as shown in Figure 2.30b. In this test, an axial stress $\Delta\sigma$ is applied to the specimen to cause failure

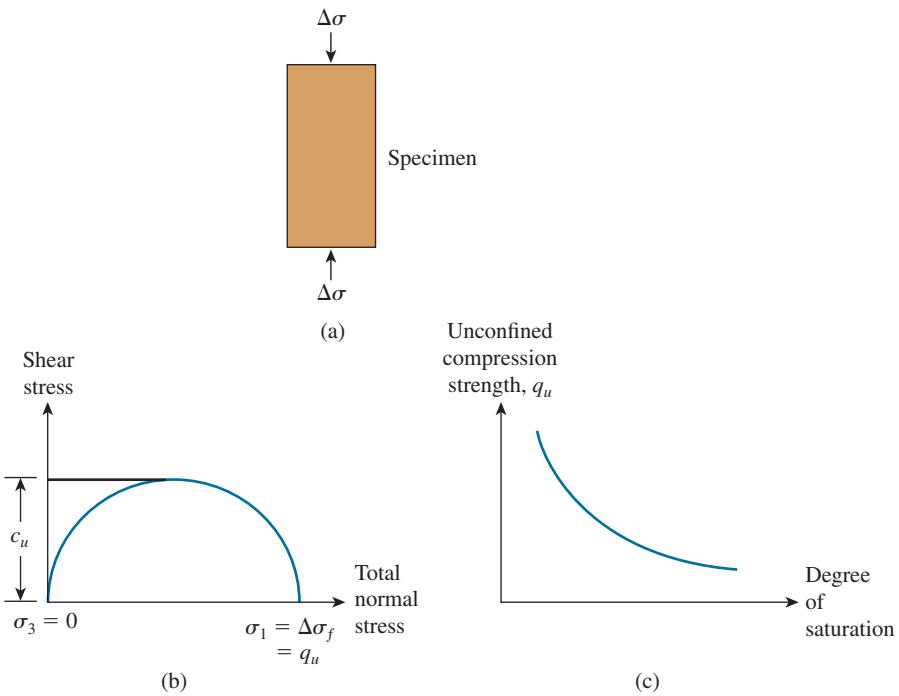


FIGURE 2.30 Unconfined compression test: (a) soil specimen; (b) Mohr's circle for the test; (c) variation of q_u with the degree of saturation

TABLE 2.14 Consistency Terms for Clays Based on Unconfined Compressive Strength

Consistency	q_u (kN/m^2)	q_u (lb/ft^2)
Very soft	0–25	0–500
Soft	25–50	500–1000
Medium	50–100	1000–2000
Stiff	100–200	2000–4000
Very stiff	200–400	4000–8000
Hard	> 400	> 8000

(i.e., $\Delta\sigma = \Delta\sigma_f$). The corresponding Mohr's circle is shown in Figure 2.30b. Note that, for this case,

Major principal total stress $= \Delta\sigma_f = q_u$
Minor principal total stress $= 0$

The axial stress at failure, $\Delta\sigma_f = q_u$, is generally referred to as the *unconfined compression strength*. The shear strength of saturated clays under this condition ($\phi = 0$), from Eq. (2.85), is

$$s = c_u = \frac{q_u}{2} \tag{2.100}$$

The unconfined compression strength can be used as an indicator of the consistency of clays. A quick estimate of the unconfined compressive strength q_u of a saturated clay can be made using a pocket penetrometer.

Unconfined compression tests are sometimes conducted on unsaturated soil. With the void ratio of a soil specimen remaining constant, the unconfined compression strength rapidly decreases with the degree of saturation (Figure 2.30c). The consistency of a clay is defined based on the unconfined compressive strength, as shown in Table 2.14.

2.20 Comments on Friction Angle, ϕ'

EFFECTIVE STRESS FRICTION ANGLE OF GRANULAR SOIL

In general, the direct shear test yields a higher angle of friction compared with that obtained by the triaxial test. Also, note that the failure envelope for a given soil is actually curved. The Mohr–Coulomb failure criterion defined by Eq. (2.85) is only an approximation. Because of the curved nature of the failure envelope, a soil tested at higher normal stress will yield a lower value of ϕ'. An example of this relationship is shown in Figure 2.31, which is a plot of ϕ' versus the void ratio e for Chattachoochee River sand near Atlanta, Georgia (Vesic, 1963). The friction angles shown were obtained from triaxial tests. Note that, for a given value of e, the magnitude of ϕ' is about 4° to 5° smaller when the confining pressure σ_3' is greater than about 70 kN/m^2 (10 lb/in.^{2}), compared with that when $\sigma_3' < 70$ kN/m^2 ($\approx$ 10 lb/in.^{2}).

EFFECTIVE STRESS FRICTION ANGLE OF COHESIVE SOIL

Figure 2.32 shows the variation of effective stress friction angle, ϕ', for several normally consolidated clays (Bjerrum and Simons, 1960; Kenney, 1959). It can be seen

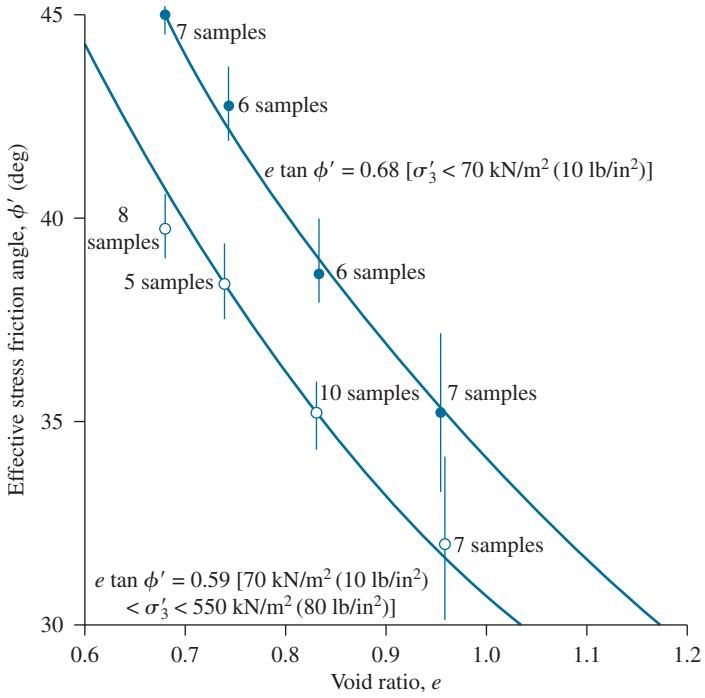


FIGURE 2.31 Variation of friction angle ϕ' with void ratio for Chattachoochee River sand (After Vesic, 1963) (Based on Vesic, A. B. Bearing Capacity of Deep Foundations in Sand. In *Highway Research Record 39*, Highway Research Board. National Research Council, Washington, DC, 1963, Figure 11, p. 123)

from the figure that, in general, the friction angle ϕ' decreases with the increase in plasticity index. The value of ϕ' generally decreases from about 37 to 38° with a plasticity index of about 10 to about 25° or less with a plasticity index of about 100. The consolidated undrained friction angle (ϕ) of normally consolidated saturated clays generally ranges from 5 to 20°.

The consolidated drained triaxial test was described in Section 2.18. Figure 2.33 shows a schematic diagram of a plot of $\Delta\sigma$ versus axial strain in a drained triaxial test

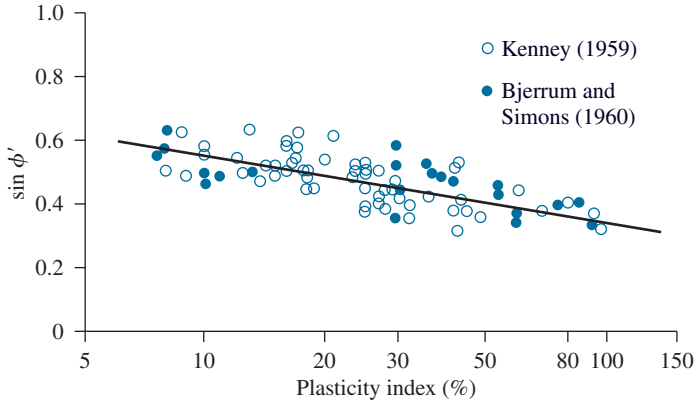


FIGURE 2.32 Variation of sin ϕ' with plasticity index (PI) for several normally consolidated clays

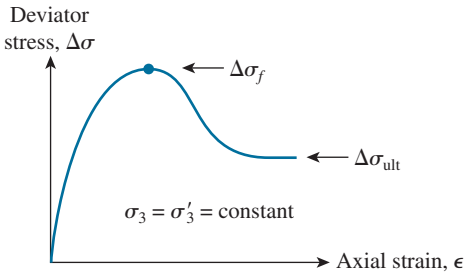


FIGURE 2.33 Plot of deviator stress versus axial strain–drained triaxial test

for a clay. At failure, for this test, $\Delta\sigma = \Delta\sigma_f$. However, at large axial strain (i.e., the ultimate strength condition), we have the following relationships:

Major principal stress: $\sigma'_{1(\text{ult})} = \sigma_3 + \Delta\sigma_{\text{ult}}$
Minor principal stress: $\sigma'_{3(\text{ult})} = \sigma_3$

At failure (i.e., peak strength), the relationship between σ'_1 and σ'_3 is given by Eq. (2.91). However, for ultimate strength, it can be shown that

$$\sigma'_{1(\text{ult})} = \sigma'_3 \tan^2\left(45 + \frac{\phi'_r}{2}\right) \tag{2.101}$$

where ϕ'_r = residual effective stress friction angle.

Figure 2.34 shows the general nature of the failure envelopes at peak strength and ultimate strength (or *residual strength*). The residual shear strength of clays is important in the evaluation of the long-term stability of new and existing slopes and the design of remedial measures. The effective stress residual friction angles ϕ'_r of clays may be substantially smaller than the effective stress peak friction angle $\phi' = \phi'_{\text{peak}}$. Past research has shown that the clay fraction (i.e., the percent finer than 2 microns) present in a given soil, CF, and the clay mineralogy are the two primary factors that control ϕ'_r. The following is a summary of the effects of CF on ϕ'_r.

1. If CF is less than about 15%, then ϕ'_r is greater than about 25°.
2. For CF > about 50%, ϕ'_r is entirely governed by the sliding of clay minerals and may be in the range of about 10 to 15°.
3. For kaolinite, illite, and montmorillonite, ϕ'_r is about 15°, 10°, and 5°, respectively.

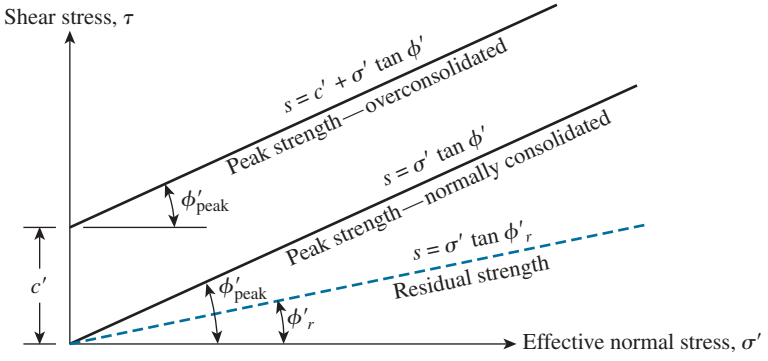


FIGURE 2.34 Peak- and residual-strength envelopes for clay

TABLE 2.15 Variation of Residual Friction Angle for Some Clays (Based on Skempton, 1964)

Soil	Clay-size fraction (%)	Residual friction angle, ϕ_r' (deg)
Selset	17.7	29.8
Wiener Tegel	22.8	25.1
Jackfield	35.4	19.1
Oxford clay	41.9	16.3
Jari	46.5	18.6
London clay	54.9	16.3
Walton's Wood	67	13.2
Weser-Elbe	63.2	9.3
Little Beit	77.2	11.2
Biotite	100	7.5

Skempton (1964) provided the results of the variation of the residual angle of friction, ϕ_r', of a number of clayey soil with the clay-size fraction ($\leq 2\ \mu$m) present. A summary of these results is shown in Table 2.15.

2.21 Correlations for Undrained Shear Strength, c_u

Several empirical relationships can be observed between c_u and the effective overburden pressure (σ_0') in the field. Some of these relationships are summarized in Table 2.16.

2.22 Selection of Shear Strength Parameters

We have come across different forms of shear strength parameters that define the Mohr–Coulomb failure envelope. They are:

- c' and ϕ' (drained shear strength parameters)
- c_u and $\phi = 0$ (undrained shear strength parameters)
- c'_{peak} and ϕ'_{peak} (peak shear strength parameters)
- c_r' and ϕ_r' (residual shear strength parameters)

The trickiest part of geotechnical engineering is to understand the difference between these and use them appropriately in the design. A simple rule is to use effective strength parameters in any effective stress analysis and total stress parameters (c_u and $\phi = 0$) in all total stress analyses.

When analyzing a geotechnical problem such as foundation or embankment in terms of effective stresses, it is necessary to use the effective stress shear strength parameters $c'$and ϕ'. These parameters can be determined from either a consolidated drained or a consolidated undrained triaxial test. When the soil is fully drained or when the pore water pressures are known, it is possible to separate the effective stresses and pore water pressures and, hence, carry out the analysis in terms of effective stresses.

TABLE 2.16 Empirical Equations Related to c_u

Reference	Relationship	Remarks
Skempton (1957)	$\frac{c_{u(\text{VST})}}{\sigma'_o} = 0.11 + 0.00037\ (\text{PI})$ PI = plasticity index (%) $c_{u(\text{VST})}$ = undrained shear strength from vane shear test	For normally consolidated clay
Chandler (1988)	$\frac{c_{u(\text{VST})}}{\sigma'_c} = 0.11 + 0.0037\ (\text{PI})$ σ'_c = preconsolidation pressure	Can be used in overconsolidated soil; accuracy ±25%; not valid for sensitive and fissured clays
Jamiolkowski et al. (1985)	$\frac{c_u}{\sigma'_c} = 0.23 \pm 0.04$	For lightly overconsolidated clays
Mesri (1989)	$\frac{c_u}{\sigma'_o} = 0.22$	
Bjerrum and Simons (1960)	$\frac{c_u}{\sigma'_o} = 0.45\left(\frac{\text{PI}\%}{100}\right)^{0.5}$ for PI > 50%	Normally consolidated clay
	$\frac{c_u}{\sigma'_o} = 0.118\ (\text{LI})^{0.15}$ for LI = liquidity index > 0.5	Normally consolidated clay
Ladd et al. (1977)	$\frac{\left(\frac{c_u}{\sigma'_o}\right)_{\text{overconsolidated}}}{\left(\frac{c_u}{\sigma'_o}\right)_{\text{normally consolidated}}} = \text{OCR}^{0.8}$ OCR = overconsolidation ratio = σ'_c/σ'_o	

When analyzing the long-term stability of a foundation or an embankment or when it is known that the loading is very slow, it can be assumed that the soil has fully drained, and an effective stress analysis can be carried out using c' and ϕ'. Granular soil are always drained due to their high permeability and should be analyzed using effective stresses.

In situations where the soil is undrained (e.g., short-term stability of a footing in clay), we do not bother separating the effective stresses and pore water pressure and carry out the analysis in terms of total stresses. Here, we use *undrained shear strength* $c_u(\phi = 0)$ and carry out the analysis in terms of total stresses.

The direct shear test can be carried out as drained (i.e., very slow loading with no pore water pressure development) or undrained (i.e., quick loading with no drainage) to determine c' and ϕ', or c_u.

In most geotechnical problems, the strains are small and it is suggested to use the peak cohesion (c') and friction angle (ϕ'). Only when analyzing situations where strains are known to be large (e.g., landslides) is it recommended to use residual shear strength parameters c'_r and ϕ'_r. At the residual state, the soil fabric is destroyed, and hence $c'_r = 0$ (see Figure 2.34).

2.23 Sensitivity

For many naturally deposited clay soil, the unconfined compression strength is much less when the soil are tested after remolding without any change in the moisture content. This property of clay soil is called *sensitivity*. The degree of sensitivity is

the ratio of the unconfined compression strength in an undisturbed state to that in a remolded state, or

$$S_t = \frac{q_{u(\text{undisturbed})}}{q_{u(\text{remolded})}} \tag{2.102}$$

The sensitivity ratio of most clays ranges from about 1 to 8; however, highly flocculent marine clay deposits may have sensitivity ratios ranging from about 10 to 80. Some clays turn to viscous liquids upon remolding, and these clays are referred to as "quick" clays. The loss of strength of clay soil from remolding is caused primarily by the destruction of the clay particle structure that was developed during the original process of sedimentation.

2.24 Summary

Phase relations are useful in computing the masses and volumes of the different phases in the soil and in determining the moisture content, void ratio, degree of saturation, and unit weights. Two major soil classification systems used in geotechnical engineering are USCS (Unified Soil Classification System) and AASHTO (American Association of State Highway and Transportation Officials). While AASHTO is widely used for roadwork, USCS is used in all other geotechnical applications. Coarse-grained soil are classified based on their grain-size distributions. Fine-grained soil are classified based on the Atterberg limits.

Hydraulic conductivity, also known as permeability, is an important parameter in seepage-related problems, including dewatering. It can be determined through a constant head or falling head permeability test in the laboratory or estimated using empirical correlations.

Consolidation is a time-dependent process where the water within the void spaces of a saturated clay is squeezed out by external loads. The parameters required for consolidation settlement calculations are determined through oedometer tests on undisturbed clay specimens. The final consolidation settlement S_c is influenced by the preconsolidation pressure, compression index, swelling index, initial void ratio, initial effective overburden stress, applied loads, and the layer thickness. How fast the consolidation occurs depends on whether the clay is singly or doubly drained and on the coefficient of consolidation.

Soil fail in shear and follow the Mohr–Coulomb failure criterion. The failure envelope is defined by the two parameters cohesion c and friction angle ϕ, which can be defined in terms of total or effective stresses and determined by triaxial or direct shear tests.

PROBLEMS

2.1 A large piece of dry rock has a mass of 2450 kg and volume of 0.925 m^3. The specific gravity of the rock mineral is 2.80. Determine the porosity of the rock.

2.2 The bulk density of a compacted soil specimen ($G_s = 2.70$) and its water content are 2060 kg/m^3 and 15.3%, respectively. If the specimen is soaked in a bucket of water for several days until it is fully saturated, what should the saturated density be?

2.3 The top 500 mm of a site consists of a clayey sand with void ratio of 0.90 and water content of 20.0%. The specific gravity of the soil grains is 2.68. When the ground is compacted at the same water content, there is 45 mm reduction in the thickness of this layer. Determine the new void ratio and the moist unit weight of the soil.

2.4 The soil at a borrow area is at moisture content of 8.5% and unit weight of 17.5 kN/m^3. This soil is used in the

construction of a compacted road base where the dry unit weight is 19.5 kN/m^3 and the moisture content is 14.0%. If the finished volume of the road base is 120,000 m^3, what would be the volume of the soil removed from the borrow pit? How much water would be added to the soil from the borrow pit?

2.5 A granular soil with $G_s = 2.65$, $e_{max} = 0.870$, and $e_{min} = 0.515$ is compacted to a moist unit weight of 110.4 lb/ft^3 at moisture content of 10.5%. What is the relative density of this compacted sand?

2.6 In AASHTO, which group are the following soil likely to fall into?

a. A well-graded gravel with approximately 10% fines
b. A well-graded sand with approximately 10% fines
c. A uniform fine sand
d. A high plastic clay

2.7 Figure P2.7 shows the grain-size distribution of four soil A, B, C, and D. The plastic limit and liquid limit of the fines are as follows.

Soil	LL	PL
A	58	34
B	42	22
C	—	—
D	75	31

Describe the four soil and give their USCS symbols.

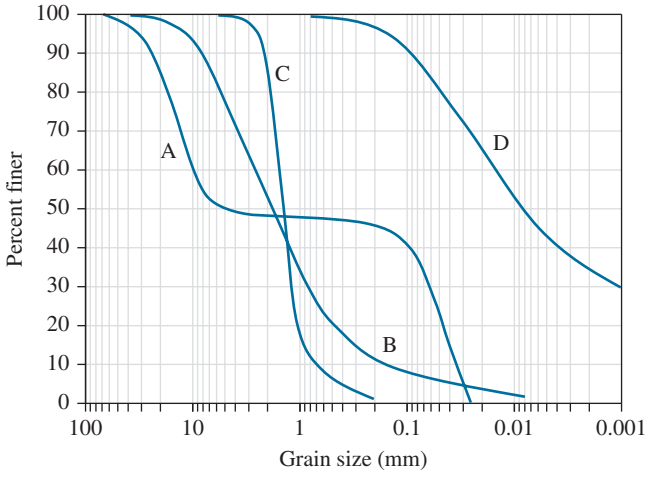


FIGURE P2.7

2.8 A 500 m long levee made of compacted clay impounds water in a reservoir as shown in Figure P2.8. There is a 1 m thick (measured in the direction perpendicular to the seam) sand seam continuing along the entire length of the levee, at 10° inclination to the horizontal, which connects the reservoir and the ditch. The hydraulic conductivity of the sand is 2.6×10^{-3} cm/s. Determine the volume of water that flows into the ditch every day.

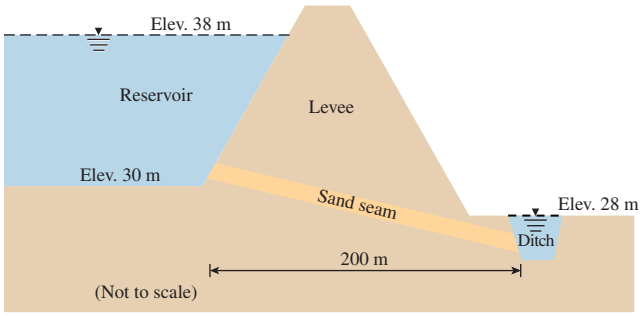


FIGURE P2.8

2.9 Seepage takes place around a retaining wall shown in Figure P2.9. The hydraulic conductivity of the sand is 1.5×10^{-3} cm/s. The retaining wall is 50 m long. Determine the quantity of seepage across the entire wall per day.

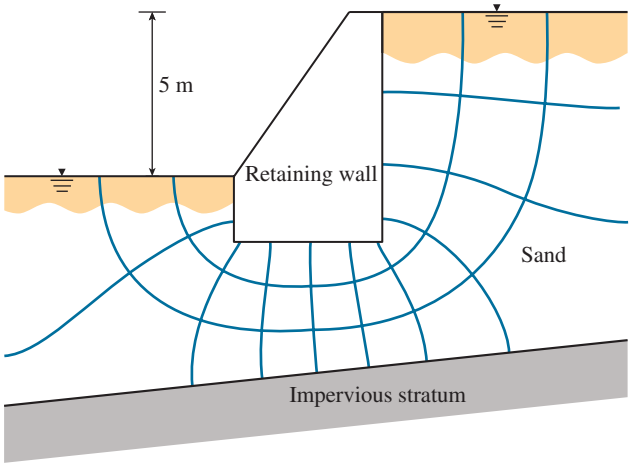


FIGURE P2.9

2.10 The soil profile at a site consists of 10 m of gravelly sand underlain by a soft clay layer. The water table lies 1 m below the ground level. The moist and saturated unit weights of the gravelly sand are 17.0 kN/m^3 and 20.0 kN/m^3, respectively. Due to some ongoing construction work, it is proposed to lower the water table to 3 m below the ground level. What will be the change in the effective stress on top of the soft clay layer?

2.11 The depth of water in a lake is 4 m. The soil at the bottom of the lake consists of sandy clay. The water content of the soil was determined to be 25.0%. The specific gravity of the soil grains is 2.70. Determine the void ratio and the unit weight of the soil. What would be the total stress, effective stress, and pore water pressure at the 5 m depth into the bottom of the lake?

2.12 In a normally consolidated clay specimen, the following data are given from the laboratory consolidation test.

$e_1 = 1.10$ $\quad \sigma'_1 = 65.0$ kN/m^2
$e_2 = 0.85$ $\quad \sigma'_2 = 240.0$ kN/m^2

a. Find the compression index C_c.
b. What will be the void ratio when the next pressure increment raises the pressure to 460.0 kN/m^2?

2.13 The soil profile at a site is shown in Figure P2.13. The moist and saturated unit weights of the sand are 17.0 kN/m^3 and 20.0 kN/m^3, respectively. A soil specimen was taken from the middle of the clay layer and subjected to a consolidation test, and the following properties are reported:

Natural water content of the clay = 22.5%
Specific gravity of the soil grains = 2.72
Preconsolidation pressure = 110.0 kN/m^2
Compression index = 0.52
Swelling index = 0.06

a. Is the clay normally consolidated or overconsolidated?
b. If a 2 m high compacted fill with a unit weight of 20.0 kN/m^3 is placed on the ground, what would be the final consolidation settlement?

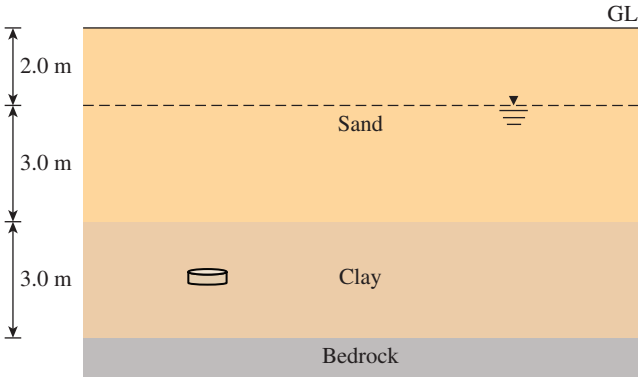


FIGURE P2.13

2.14 A clay layer with two-way drainage reached 75% consolidation in t years. How long would it take for the same clay to consolidate 75% if it has one-way drainage?

2.15 The soil profile at a site consists of 2 m of sand at the ground level, underlain by 6 m of clay, followed by a very stiff clay stratum that can be assumed to be impervious and incompressible. The water table is at 1.5 m below the ground level. The moist and saturated unit weights of the sand are 17.0 kN/m^3 and 18.5 kN/m^3, respectively. The clay has an initial void ratio of 0.810, saturated unit weight of 19.0 kN/m^3, and coefficient of consolidation of 0.0014 cm^2/s.

a. When the ground is surcharged with 3 m high compacted fill with moist unit weight of 19.0 kN/m^3, the settlement was 160 mm in the first year. What would be the consolidation settlement in the first two years?
b. If the clay is normally consolidated, what is the compression index of the clay?

2.16 The soil profile at a site consists of a 2.0 m thick sand layer at the top, underlain by a 3.0 m thick clay layer. The water table lies at a depth of 1.0 m below the ground level. The bulk and saturated unit weights of the sand are 16.0 kN/m^3 and 19.0 kN/m^3, respectively. The properties of the clay are: water content = 45.0%, specific gravity of the soil grains = 2.70, compression index = 0.65, swelling index = 0.08, and overconsolidation ratio = 1.5.

a. The ground level is raised by placing a 1.5 m high compacted fill with unit weight of 20.0 kN/m^3. What is the consolidation settlement?
b. When the consolidation due to the fill is completed, it is proposed to construct a warehouse imposing a uniform pressure of 40.0 kN/m^2. What would be the consolidation settlement due to the construction of the warehouse?

2.17 A direct shear test is conducted on a 60 mm × 60 mm overconsolidated clay specimen. The loading was very slow, ensuring that there is no pore water pressure development within the specimen (i.e., drained loading). The following data were recorded.

Normal load (N)	Shear load (N)	σ (kN/m^2)	s (kN/m^2)
178	102	49.4	28.3
362	174	100.6	48.3
537	256	149.2	71.1
719	332	199.7	92.2

Determine the shear strength parameters c' and ϕ'.

2.18 A consolidated-drained triaxial test is carried out on a sand specimen that is subjected to 100 kN/m^2 confining pressure. The vertical deviator stress was increased slowly such that there is no build-up of pore water pressure within the specimen. The specimen failed when the additional axial stress $\Delta\sigma$ reached 260 kN/m^2.

a. Find the friction angle of the sand.
b. Another identical sand specimen is subjected to 200 kN/m^2 confining pressure. What would be the deviator stress at failure?

2.19 A consolidated-drained triaxial test was carried out on a normally consolidated clay specimen, and the following results were recorded: σ'_3 = 150 kN/m^2 and $\Delta\sigma_f$ = 260 kN/m^2. An identical specimen from the same clay was subjected to a consolidated-undrained test with a confining pressure of 150 kN/m^2, and the additional axial stress at failure was 115 kN/m^2.

a. What is the pore water pressure at failure in this second specimen?
b. What is Skempton's pore pressure parameter A at failure?

2.20 The specimens obtained from a clay layer at a site gave the following shear strength parameters from a consolidated-drained triaxial test: c' = 10 kN/m^2 and ϕ' = 26°. A consolidated-undrained triaxial test is carried out on this soil, where a specimen is consolidated under confining pressure of 100 kN/m^2 and loaded under undrained conditions. The specimen failed under an additional axial stress of 107.0 kN/m^2. What is the pore water pressure within the specimen?

2.21 The data from a series of consolidated-undrained triaxial tests are summarized below. Draw the three Mohr circles, plot the failure envelope in terms of effective stresses, and find c' and ϕ'.

Sample number	Cell pressure (kN/m^2)	Additional axial stress at failure (kN/m^2)	Pore water pressure at failure (kN/m^2)
1	100	88.2	57.4
2	200	138.5	123.7
3	300	232.1	208.8

2.22 Steel plates with mass of 1500 g each were stacked on top of a 75 mm diameter and 150 mm high clay specimen, as shown in Figure P2.22. If the undrained shear strength of the specimen is 45.0 kN/m^2, how many plates can be stacked before the specimen fails? What is the consistency term for this clay?

2.23 Estimate the friction angle of the soil C in Problem 2.7 (see Figure P2.7) at 80% relative density and void ratio of 0.61 using the empirical correlations given by
a. Eq. (2.87)
b. Eq. (2.88)

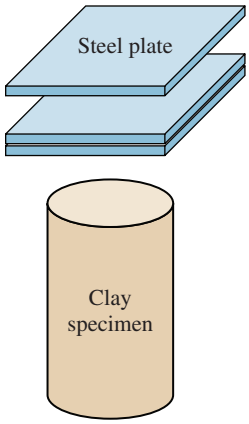


FIGURE P2.22

REFERENCES

Amer, A. M. and Awad, A. A. (1974). "Permeability of Cohesionless Soil," *Journal of the Geotechnical Engineering Division*, American Society of Civil Engineers, Vol. 100, No. GT12, pp. 1309–1316.

American Society for Testing and Materials (2011). *Annual Book of ASTM Standards*, Vol. 04.08, West Conshohocken, PA.

Bjerrum, L. and Simons, N. E. (1960). "Comparison of Shear Strength Characteristics of Normally Consolidated Clay," *Proceedings, Research Conference on Shear Strength of Cohesive Soil*, ASCE, pp. 711–726.

Carrier III, W. D. (2003). "Goodbye, Hazen; Hello, Kozeny-Carman," *Journal of Geotechnical and Geoenvironmental Engineering*, ASCE, Vol. 129, No. 11, pp. 1054–1056.

Casagrande, A. (1936). "Determination of the Preconsolidation Load and Its Practical Significance," *Proceedings, First International Conference on Soil Mechanics and Foundation Engineering*, Cambridge, MA, Vol. 3, pp. 60–64.

Chandler, R. J. (1988). "The *in situ* Measurement of the Undrained Shear Strength of Clays Using the Field Vane," *STP 1014, Vane Shear Strength Testing in Soil: Field and Laboratory Studies*, American Society for Testing and Materials, pp. 13–44.

Chapuis, R. P. (2004). "Predicting the Saturated Hydraulic Conductivity of Sand and Gravel Using Effective Diameter and Void Ratio," *Canadian Geotechnical Journal*, Vol. 41, No. 5, pp. 787–795.

Cubrinovski, M. and Ishihara, K. (1999). "Empirical Correlation Between SPT N-Value and Relative Density for Sandy Soil," *Soil and Foundations*. Vol. 39, No. 5, pp. 61–71.

Cubrinovski, M. and Ishihara, K. (2002). "Maximum and Minimum Void Ratio Characteristics of Sands," *Soil and Foundations*. Vol. 42, No. 6, pp. 65–78.

Darcy, H. (1856). *Les Fontaines Publiques de la Ville de Dijon*, Paris.

Das, B. M. (2016). *Soil Mechanics Laboratory Manual*, 9th ed., Oxford University Press, New York.

Hansbo, S. (1975). *Jordmateriallära*: 211, Stockholm, Awe/Gebers.

Highway Research Board (1945). *Report of the Committee on Classification of Materials for Subgrades and Granular Type Roads*, Vol. 25, pp. 375–388.

Jamilkowski, M., Ladd, C. C., Germaine, J. T., and Lancellotta, R. (1985). "New Developments in Field and Laboratory Testing of Soil," *Proceedings, XI International Conference on Soil Mechanics and Foundations Engineering*, San Francisco, Vol. 1, pp. 57–153.

Kenney, T. C. (1959). "Discussion," *Journal of the Soil Mechanics and Foundations Division*, American Society of Civil Engineers, Vol. 85, No. SM3, pp. 67–69.

Kulhawy, F. H. and Mayne, P. W. (1990). *Manual of Estimating Soil Properties for Foundation Design*, Electric Power Research Institute, Palo Alto, CA.

Ladd, C. C., Foote, R., Ishihara, K., Schlosser, F., and Poulos, H. G. (1977). "Stress Deformation and Strength Characteristics," *Proceedings*, *Ninth International Conference on Soil Mechanics and Foundation Engineering*, Tokyo, Vol. 2, pp. 421–494.

Mesri, G. (1989). "A Re-evaluation of $s_{u(\text{mob})} \approx 0.22\sigma_p$ Using Laboratory Shear Tests," *Canadian Geotechnical Journal*, Vol. 26, No. 1, pp. 162–164.

Mesri, G. and Olson, R. E. (1971). "Mechanism Controlling the Permeability of Clays," *Clay and Clay Minerals*, Vol. 19, pp. 151–158.

Olson, R. E. (1977). "Consolidation Under Time-Dependent Loading," *Journal of Geotechnical Engineering*, ASCE, Vol. 103, No. GT1, pp. 55–60.

Park, J. H. and Koumoto, T. (2004). "New Compression Index Equation," *Journal of Geotechnical and Geoenvironmental Engineering*, ASCE, Vol. 130, No. 2, pp. 223–226.

Rendon-Herrero, O. (1980). "Universal Compression Index Equation," *Journal of the Geotechnical Engineering Division*, American Society of Civil Engineers, Vol. 106, No. GT11, pp. 1178–1200.

Samarasinghe, A. M., Huang, Y. H., and Drnevich, V. P. (1982). "Permeability and Consolidation of Normally Consolidated Soil," *Journal of the Geotechnical Engineering Division*, ASCE, Vol. 108, No. GT6, pp. 835–850.

Schmertmann, J. H. (1953). "Undisturbed Consolidation Behavior of Clay," *Transactions*, American Society of Civil Engineers, Vol. 120, p. 1201.

Sivaram, B. and Swamee, A. (1977), "A Computational Method for Consolidation Coefficient," *Soil and Foundations*, Vol. 17, No. 2, pp. 48–52.

Skempton, A. W. (1944). "Notes on the Compressibility of Clays," *Quarterly Journal of Geological Society*, London, Vol. C, pp. 119–135.

Skempton, A. W. (1953). "The Colloidal Activity of Clays," *Proceedings, 3rd International Conference on Soil Mechanics and Foundation Engineering*, London, Vol. 1, pp. 57–61.

Skempton, A. W. (1957). "The Planning and Design of New Hong Kong Airport," *Proceedings, The Institute of Civil Engineers*, London, Vol. 7, pp. 305–307.

Skempton, A. W. (1964). "Long-Term Stability of Clay Slopes," *Geotechnique*, Vol. 14, p. 77.

Skempton, A. W. (1985). "Residual Strength of Clays in Landslides, Folded Strata, and the Laboratory," *Geotechnique*, Vol. 35, No. 1, pp. 3–18.

Stas, C. V. and Kulhawy, F. H. (1984). "Critical Evaluation of Design Methods for Foundations Under Axial Uplift and Compression Loading," *REPORT EL-3771*, Electric Power Research Institute, Palo Alto, CA.

Taylor, D. W. (1948). *Fundamentals of Soil Mechanics*, John Wiley & Sons, New York.

Teferra, A. (1975). *Beziehungen zwischen Reibungswinkel, Lagerungsdichte und Sonderwiderständen nichtbindiger Böden mit verschiedener Kornverteilung.* Ph.D. Thesis, Technical University of Aachen Germany.

Terzaghi, K. and Peck, R. B. (1967). *Soil Mechanics in Engineering Practice*, John Wiley & Sons, New York.

Thinh, K. D. (2001). "How Reliable is Your Angle of Internal Friction?" *Proceedings, XV International Conference on Soil Mechanics and Geotechnical Engineering*, Istanbul, Turkey, Vol. 1, pp. 73–76.

U.S. Department of Navy (1986). "Soil Mechanics Design Manual 7.01," U.S. Government Printing Office, Washington, DC.

Vesic, A. S. (1963). "Bearing Capacity of Deep Foundations in Sand," *Highway Research Record No. 39*, National Academy of Sciences, Washington DC, pp. 112–154.

Wood, D. M. (1983). "Index Properties and Critical State Soil Mechanics," *Proceedings, Symposium on Recent Developments in Laboratory and Field Tests and Analysis of Geotechnical Problems*, Bangkok, p. 309.

Wroth, C. P. and Wood, D. M. (1978). "The Correlation of Index Properties with Some Basic Engineering Properties of Soil," *Canadian Geotechnical Journal*, Vol. 15, No. 2, pp. 137–145.

3

Natural Soil Deposits and Subsoil Exploration



Brendan Howard/Shutterstock.com

3.1 Introduction 68
3.2 Soil Origin 68
3.3 Residual Soil 69
3.4 Gravity-Transported Soil 70
3.5 Alluvial Deposits 71
3.6 Lacustrine Deposits 73
3.7 Glacial Deposits 74
3.8 Aeolian Soil Deposits 75
3.9 Organic Soil 76
3.10 Some Local Terms for Soil 76
3.11 Purpose of Subsurface Exploration 77
3.12 Subsurface Exploration Program 77
3.13 Exploratory Borings in the Field 80
3.14 Procedures for Sampling Soil 83
3.15 Split-Spoon Sampling and Standard Penetration Test 83
3.16 Sampling with a Scraper Bucket 92
3.17 Sampling with a Thin-Walled Tube 93
3.18 Sampling with a Piston Sampler 93
3.19 Observation of Water Tables 95
3.20 Vane Shear Test 96
3.21 Cone Penetration Test 100
3.22 Pressuremeter Test (PMT) 108
3.23 Dilatometer Test 111
3.24 Iowa Borehole Shear Test 114
3.25 K_0 Stepped-Blade Test 116
3.26 Coring of Rocks 117
3.27 Preparation of Boring Logs 120
3.28 Geophysical Exploration 121
3.29 Subsoil Exploration Report 127
3.30 Summary 128
PROBLEMS 129
REFERENCES 131

3.1 Introduction

The design and construction of a foundation, retaining wall, or an embankment require a thorough understanding of the subsoil at the site. The soil profile showing the different soil present, their geotechnical properties, and the groundwater table location are some of the data generally required. The nonhomogeneous nature of the soil makes it difficult to characterize the subsoil within a limited budget. Soil mechanics theories involve idealized conditions, so the application of the theories to foundation engineering problems involves a judicious evaluation of site conditions and soil parameters. It also requires some knowledge of the geological process by which the soil deposit at the site was formed, supplemented by subsurface exploration. Good professional judgment constitutes an essential part of geotechnical engineering—and it comes only with practice.

This chapter is divided into two parts. The first is a general overview of natural soil deposits generally encountered, and the second describes the general principles of subsoil exploration, the different sampling methods and *in situ* tests, and interpretation of the *in situ* tests.

Natural Soil Deposits

3.2 Soil Origin

Most of the soil that cover the earth are formed by the weathering of various rocks. There are two general types of weathering: (1) mechanical weathering and (2) chemical weathering.

Mechanical weathering is a process by which rocks are broken down into smaller and smaller pieces by physical forces without any change in the chemical composition. Changes in temperature result in *expansion and contraction of rock* due to gain and loss of heat. Continuous expansion and contraction will result in the development of cracks in rocks. Flakes and large fragments of rocks are split. *Frost action* is another source of mechanical weathering of rocks. Water can enter the pores, cracks, and other openings in the rock. When the temperature drops, the water freezes, thereby increasing its volume by about 9%. This results in an outward pressure from inside the rock. Continuous freezing and thawing will result in the breakup of a rock mass. *Exfoliation* is another mechanical weathering process by which rock plates are peeled off from large rocks by physical forces. Mechanical weathering of rocks also takes place due to the action of *running water, glaciers, wind, ocean waves*, and so forth.

Chemical weathering is a process of decomposition or mineral alteration in which the original minerals are changed into something entirely different. For example, the common minerals in igneous rocks are quartz, feldspars, and ferromagnesian minerals. The decomposed products of these minerals due to chemical weathering are listed in Table 3.1.

Most rock weathering is a combination of mechanical and chemical weathering. Soil produced by the weathering of rocks can be transported by physical processes to other places. The resulting soil deposits are called *transported soil.* In contrast, some

TABLE 3.1 Some Decomposed Products of Minerals in Igneous Rock

Mineral	Decomposed product
Quartz	Quartz (sand grains)
Potassium feldspar ($KAlSi_3O_8$) and sodium feldspar ($NaAlSi_3O_8$)	Kaolinite (clay) Bauxite Illite (clay) Silica
Calcium feldspar ($CaAl_2Si_2O_8$)	Silica Calcite
Biotite	Clay Limonite Hematite Silica Calcite
Olivine $(Mg, Fe)_2SiO_4$	Limonite Serpentine Hematite Silica

soil stay where they were formed and cover the rock surface from which they derive. These soil are referred to as *residual soil.*

Transported soil can be subdivided into five major categories based on the *transporting agent*:

1. *Gravity-transported* (colluvial) soil
2. *Lacustrine* (lake) soil deposited in lakes
3. *Alluvial* or *fluvial* soil deposited by running water
4. *Glacial* soil deposited by glaciers
5. *Aeolian* soil deposited by the wind

In addition to transported and residual soil, there are *peats* and *organic soil*, which derive from the decomposition of organic materials.

About 90–95% of the earth's crust by volume is made of igneous and metamorphic rocks, with only 5–10% of sedimentary rocks. However, 80% of the rocks at the surface are sedimentary rocks.

3.3 Residual Soil

Residual soil are found in areas where the rate of weathering is more than the rate at which the weathered materials are carried away by transporting agents. The rate of weathering is higher in warm and humid regions compared to cooler and drier regions and, depending on the climatic conditions, the effect of weathering may vary widely.

Residual soil deposits are common in the tropics, on islands such as the Hawaiian Islands, and in the southeastern United States. The nature of a residual soil deposit will generally depend on the parent rock. When hard rocks such as granite and gneiss undergo weathering, most of the materials are likely to remain in place. These soil deposits generally have a top layer of clayey or silty clay material, below which are silty or sandy soil layers. These layers in turn are generally underlain by a partially weathered rock and then sound bedrock. The depth of the sound bedrock may vary

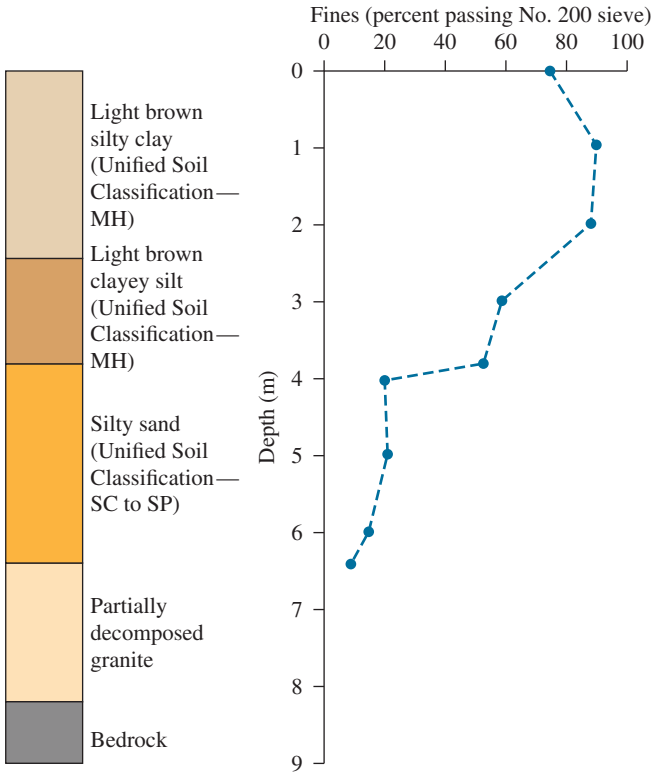


FIGURE 3.1 Boring log for a residual soil derived from granite

widely, even within a distance of a few meters. Figure 3.1 shows the boring log of a residual soil deposit derived from the weathering of granite.

In contrast to hard rocks, there are some rocks formed by chemical weathering, such as limestone, that are chiefly made up of calcite ($CaCO_3$) minerals. Chalk and dolomite have large concentrations of dolomite minerals [$Ca\ Mg(CO_3)_2$]. These rocks have large amounts of soluble materials, some of which are removed by groundwater, leaving behind the insoluble fraction of the rock and forming sinkholes. Residual soil that derive from chemical rocks do not possess a gradual transition zone to the bedrock, as seen in Figure 3.1. The residual soil derived from the weathering of limestone-like rocks are mostly red in color. Although uniform in kind, the depth of weathering may vary greatly. The residual soil immediately above the bedrock may be normally consolidated. Large foundations with heavy loads may be susceptible to large consolidation settlements on these soil.

3.4 Gravity-Transported Soil

Residual soil on a natural slope can move downward. Cruden and Varnes (1996) proposed a velocity scale for soil movement on a slope, which is summarized in Table 3.2. When residual soil move down a natural slope very slowly, the process is usually referred to as *creep*. When the downward movement of soil is sudden and rapid, it is called a *landslide*. The deposits formed by down-slope creep and landslides are *colluvium*.

Colluvium is a heterogeneous mixture of soil and rock fragments ranging from clay-sized particles to rocks having diameters of one meter or more. *Mudflows* are one type of gravity-transported soil. Flows are downward movements of earth that resemble a viscous fluid (Figure 3.2) and come to rest in a more dense condition.

TABLE 3.2 Velocity Scale for Soil Movement on a Slope

Description	Velocity (mm/s)
Very slow	5×10^{-5} to 5×10^{-7}
Slow	5×10^{-3} to 5×10^{-5}
Moderate	5×10^{-1} to 5×10^{-3}
Rapid	5×10^{1} to 5×10^{-1}

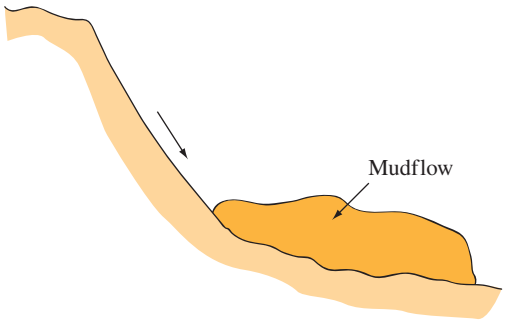


FIGURE 3.2 Mudflow

The soil deposits derived from past mudflows are highly heterogeneous in composition.

3.5 Alluvial Deposits

Alluvial soil deposits derive from the action of streams and rivers and can be divided into two major categories: (1) *braided-stream deposits* and (2) deposits caused by the *meandering belt of streams.*

DEPOSITS FROM BRAIDED STREAMS

Braided streams are high-gradient, rapidly flowing streams that are highly erosive and carry large amounts of sediment. Because of the high bed load, a minor change in the velocity of flow will cause sediments to deposit. By this process, these streams may build up a complex tangle of converging and diverging channels separated by sandbars and islands.

The deposits formed from braided streams are highly irregular in stratification and have a wide range of grain sizes. Figure 3.3 shows a cross section of such a deposit. These deposits share several characteristics:

1. The grain sizes usually range from gravel to silt. Clay-sized particles are generally *not* found in deposits from braided streams.
2. Although grain size varies widely, the soil in a given pocket or lens is rather uniform.
3. At any given depth, the void ratio and unit weight may vary over a wide range within a lateral distance of only a few meters. This variation can be observed during soil exploration for the construction of a foundation for a structure. The standard penetration resistance at a given depth obtained from various boreholes will be highly irregular and variable.

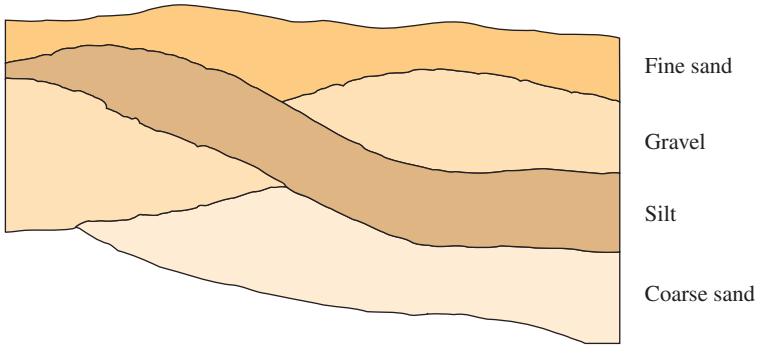


FIGURE 3.3 Cross section of a braided-stream deposit

Alluvial deposits are present in several parts of the western United States, such as Southern California, Utah, and the basin and range sections of Nevada. Also, a large amount of sediment originally derived from the Rocky Mountain range was carried eastward to form the alluvial deposits of the Great Plains. On a smaller scale, this type of natural soil deposit, left by braided streams, can be encountered locally.

MEANDER BELT DEPOSITS

The term *meander* is derived from the Greek word *maiandros*, after the Maiandros (now Menderes) River in Asia, famous for its winding course. Mature streams in a valley curve back and forth. The valley floor in which a river meanders is referred to as the *meander belt.* In a meandering river, the soil from the bank is continually eroded from the points where it is concave in shape and is deposited at points where the bank is convex in shape, as shown in Figure 3.4. These deposits are called *point bar deposits*, and they usually consist of sand and silt-size particles. Sometimes, during the process of erosion and deposition, the river abandons a meander and cuts

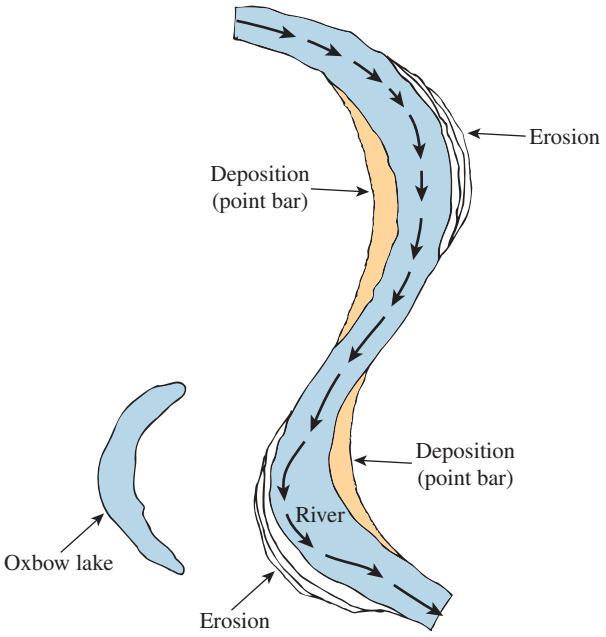


FIGURE 3.4 Formation of point bar deposits and oxbow lake in a meandering stream

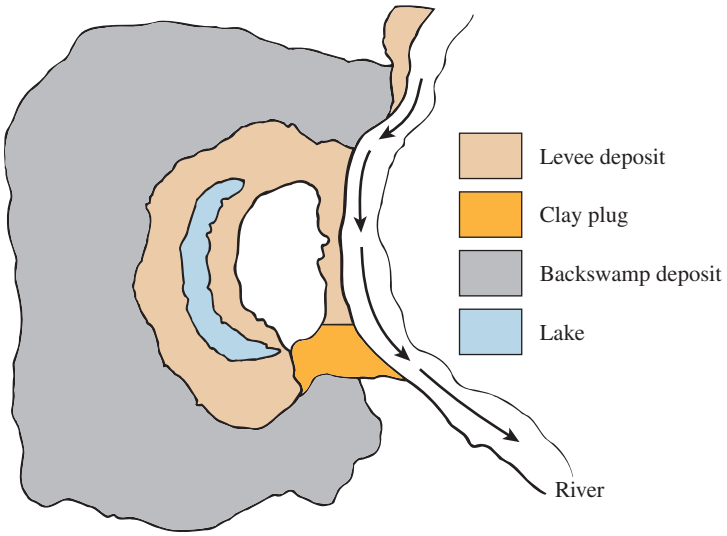


FIGURE 3.5 Levee and backswamp deposit

TABLE 3.3 Properties of Deposits Within the Mississippi Alluvial Valley

Environment	Soil texture	Natural water content (%)	Liquid limit	Plasticity index
Natural levee	Clay (CL)	25–35	35–45	15–25
	Silt (ML)	15–35	NP–35	NP–5
Point bar	Silt (ML) and silty sand (SM)	25–45	30–55	10–25
Abandoned channel	Clay (CL, CH)	30–95	30–100	10–65
Backswamps	Clay (CH)	25–70	40–115	25–100
Swamp	Organic clay (OH)	100–265	135–300	100–165

(*Note:* NP—Nonplastic)

a shorter path. The abandoned meander, when filled with water, is called an *oxbow lake.* (See Figure 3.4.)

During floods, rivers overflow low-lying areas. The sand and silt-size particles carried by the river are deposited along the banks to form ridges known as *natural levees* (Figure 3.5). Finer soil particles consisting of silts and clays are carried by the water farther onto the floodplains. These particles settle at different rates to form what is referred to as *backswamp deposits* (Figure 3.5), which are often highly plastic clays.

Table 3.3 gives some properties of soil deposits found in natural levees, point bars, abandoned channels, backswamps, and swamps within the alluvial Mississippi Valley (Kolb and Shockley, 1959).

3.6 Lacustrine Deposits

Water from rivers and springs flows into lakes. In arid regions, streams carry large amounts of suspended solids. Where the stream enters the lake, granular particles are deposited in the area and form a delta. Some coarser particles and the finer particles (that is, silt and clay) that are carried into the lake are deposited onto the lake bottom in

alternate layers of coarse-grained and fine-grained particles. The deltas formed in humid regions usually have finer-grained soil deposits compared to those in arid regions.

Varved clays are alternate layers of silt and silty clay with layer thicknesses rarely exceeding about 13 mm (½ in.). The silt and silty clay that constitute the layers were carried into freshwater lakes by meltwater at the end of the Ice Age. The hydraulic conductivity of varved clays exhibits a high degree of anisotropy.

3.7 Glacial Deposits

During the Pleistocene Ice Age, glaciers covered large areas of the earth. The glaciers advanced and retreated with time. During their advance, the glaciers carried large amounts of sand, silt, clay, gravel, and boulders. *Drift* is a general term usually applied to the deposits laid down by glaciers. The drifts can be broadly divided into two major categories: (a) unstratified drifts and (b) stratified drifts. A brief description of each category follows.

UNSTRATIFIED DRIFTS

The *unstratified drifts* laid down by melting glaciers are referred to as *till*. The physical characteristics of till may vary from glacier to glacier. Till is called *clay till* because of the presence of large amount of clay-sized particles. In some areas, tills constitute large amounts of boulders and are referred to as *boulder till*. The range of grain sizes in a given till varies greatly. The amount of clay-sized fractions present and the plasticity indices of tills also vary widely. During the field exploration program, erratic values of standard penetration resistance (Section 3.13) also may be expected.

The land forms that developed from the till deposits are called *moraines*. A *terminal moraine* (Figure 3.6) is a ridge of till that marks the maximum limit of a glacier's advance. *Recessional moraines* are ridges of till developed behind the terminal moraine at varying distances apart. They are the result of temporary stabilization of the glacier during the recessional period. The till deposited by the glacier between the moraines is referred to as *ground moraine* (Figure 3.6). Ground moraines constitute large areas of the central United States and are called *till plains*.

STRATIFIED DRIFTS

The sand, silt, and gravel that are carried by the melting water from the front of a glacier are called *outwash*. The melted water sorts out the particles by the grain size and forms stratified deposits. In a pattern similar to that of braided-stream deposits, the melted water also deposits the outwash, forming *outwash plains* (Figure 3.6), also called *glaciofluvial deposits*.

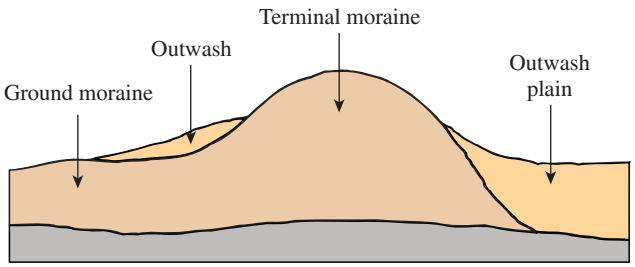


FIGURE 3.6 Terminal moraine, ground moraine, and outwash plain

3.8 Aeolian Soil Deposits

Wind is also a major transporting agent leading to the formation of soil deposits. When large areas of sand lie exposed, wind can blow the sand away and redeposit it elsewhere. Deposits of windblown sand generally take the shape of *dunes* (Figure 3.7). As dunes are formed, the sand is blown over the crest by the wind. Beyond the crest, the sand particles roll down the slope. The process tends to form a *compact sand deposit* on the *windward side* and a rather *loose deposit* on the *leeward side* of the dune.

Dunes exist along the southern and eastern shores of Lake Michigan, the Atlantic Coast, the southern coast of California, and at various places along the coasts of Oregon and Washington. Sand dunes can also be found in the alluvial and rocky plains of the western United States. Following are some of the typical properties of *dune sand:*

1. The grain-size distribution of the sand at any particular location is surprisingly uniform. This uniformity can be attributed to the sorting action of the wind.
2. The general grain size decreases with distance from the source, because the wind carries the small particles farther than the large ones.
3. The relative density of sand deposited on the windward side of dunes may be as high as 50 to 65%, decreasing to about 0 to 15% on the leeward side.

Figure 3.8 shows some sand dunes in the Sahara desert in Egypt.

Loess is an aeolian deposit consisting of silt and silt-sized particles. The grain-size distribution of loess is rather uniform. The cohesion of loess is generally derived

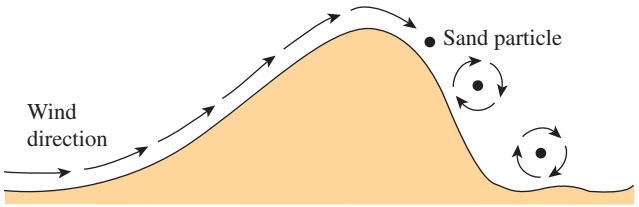


FIGURE 3.7 Sand dune



FIGURE 3.8 Sand dunes in the Sahara desert in Egypt (Courtesy of Janice Das)

from a clay coating over the silt-sized particles, which contributes to a stable soil structure in an unsaturated state. The cohesion may also be the result of the precipitation of chemicals leached by rainwater. Loess is a *collapsing* soil, because when the soil becomes saturated, it loses its binding strength between particles. Special precautions need to be taken for the construction of foundations over loessial deposits. There are extensive deposits of loess in the United States, mostly in the midwestern states of Iowa, Missouri, Illinois, and Nebraska and for some distance along the Mississippi River in Tennessee and Mississippi.

Volcanic ash (with grain sizes between 0.25 to 4 mm) and volcanic dust (with grain sizes less than 0.25 mm) may be classified as wind-transported soil. Volcanic ash is a lightweight sand or sandy gravel. Decomposition of volcanic ash results in highly plastic and compressible clays.

3.9 Organic Soil

Organic soil are usually found in low-lying areas where the water table is near or above the ground surface. The presence of a high water table helps in the growth of aquatic plants that, when decomposed, form organic soil. This type of soil deposit is usually encountered in coastal areas and in glaciated regions. Organic soil show the following characteristics:

1. Their natural moisture content may range from 200 to 300%.
2. They are highly compressible.
3. Laboratory tests have shown that, under loads, a large amount of settlement is derived from secondary consolidation.

3.10 Some Local Terms for Soil

Soil are sometimes referred to by local terms. The following are a few of these terms with a brief description of each.

1. *Caliche*: a Spanish word derived from the Latin word *calx*, meaning *lime*. It is mostly found in the desert southwest of the United States. It is a mixture of sand, silt, and gravel bonded together by *calcareous deposits*. The calcareous deposits are brought to the surface by a net upward migration of water. The water evaporates in the high local temperature. Because of the sparse rainfall, the carbonates are not washed out of the top layer of soil.
2. *Gumbo*: a highly plastic, clayey soil.
3. *Adobe*: a highly plastic, clayey soil found in the southwestern United States.
4. *Terra rossa*: residual soil deposits that are red in color and derive from limestone and dolomite.
5. *Muck*: organic soil with a very high moisture content.
6. *Muskeg*: organic soil deposit.
7. *Saprolite*: residual soil deposit derived from mostly insoluble rock.
8. *Loam*: a mixture of soil grains of various sizes, such as sand, silt, and clay.
9. *Laterite*: characterized by the accumulation of iron oxide (Fe_2O_3) and aluminum oxide (Al_2O_3) near the surface and the leaching of silica. Lateritic soil in Central America contain about 80 to 90% of clay and silt-size particles. In the United States, lateritic soil can be found in the southeastern states, such as Alabama, Georgia, and the Carolinas.

Subsurface Exploration

3.11 Purpose of Subsurface Exploration

The process of identifying the layers of deposits that underlie a proposed structure and their physical characteristics is generally referred to as *subsurface exploration.* The purpose of subsurface exploration is to obtain information that will aid the geotechnical engineer in

1. Selecting the type and depth of foundation suitable for a given structure.
2. Evaluating the load-bearing capacity of the foundation.
3. Estimating the probable settlement of a structure.
4. Determining potential foundation problems (e.g., expansive soil, collapsible soil, sanitary landfill, and so on).
5. Determining the location of the water table.
6. Predicting the lateral earth pressure for structures such as retaining walls, sheet pile bulkheads, and braced cuts.
7. Establishing construction methods for changing subsoil conditions.

Subsurface exploration may also be necessary when additions and alterations to existing structures are contemplated.

3.12 Subsurface Exploration Program

Subsurface exploration comprises several steps, including the collection of preliminary information, reconnaissance, and site investigation.

COLLECTION OF PRELIMINARY INFORMATION

This step involves obtaining information regarding the type of structure to be built and its general use. For the construction of buildings, the approximate column loads and their spacing and the local building-code and basement requirements should be known. The construction of bridges requires determining the lengths of their spans and the loading on piers and abutments.

A general idea of the topography and the type of soil to be encountered near and around the proposed site can be obtained from the following sources:

1. Google Maps.
2. United States Geological Survey maps.
3. State government geological survey maps.
4. United States Department of Agriculture's Soil Conservation Service county soil reports.
5. Agronomy maps published by the agriculture departments of various states.
6. Hydrological information published by the United States Corps of Engineers, including records of stream flow, information on high flood levels, tidal records, and so on.
7. Highway department soil manuals published by several states.

The information collected from these sources can be extremely helpful in planning a site investigation. In some cases, substantial savings may be realized by anticipating problems that may be encountered later in the exploration program.

RECONNAISSANCE

The engineer should always make a visual inspection of the site to obtain information about

1. The general topography of the site, the possible existence of drainage ditches, abandoned dumps of debris, and other materials present at the site. Also, evidence of creep of slopes and deep, wide shrinkage cracks at regularly spaced intervals may be indicative of expansive soil.
2. Soil stratification from deep cuts, such as those made for the construction of nearby highways and railroads.
3. The type of vegetation at the site, which may indicate the nature of the soil. For example, a mesquite cover in central Texas may indicate the existence of expansive clays that can cause foundation problems.
4. High-water marks on nearby buildings and bridge abutments.
5. Groundwater levels, which can be determined by checking nearby wells.
6. The types of construction nearby and the existence of any cracks in walls or other problems.
7. Rock outcrops.

The nature of the stratification and physical properties of the soil nearby also can be obtained from any available soil-exploration reports on existing structures.

SITE INVESTIGATION

The site investigation phase of the exploration program consists of planning, making test boreholes, and collecting soil samples at desired intervals for subsequent observation and laboratory tests. The approximate required minimum depth of the borings should be predetermined. The depth can be changed during the drilling operation, depending on the subsoil encountered. To determine the approximate minimum depth of boring, engineers may use the rules established by the American Society of Civil Engineers (1972):

1. Determine the net increase in the effective stress, $\Delta\sigma'$, under a foundation with depth as shown in Figure 3.9. (The general equations for estimating increases in stress are given in Chapter 8.)
2. Estimate the variation of the vertical effective overburden stress, σ'_o, with depth.
3. Determine the depth, $D = D_1$, at which the effective stress increase $\Delta\sigma'$ is equal to $\left(\frac{1}{10}\right)q$ (q = estimated net stress on the foundation).
4. Determine the depth, $D = D_2$, at which $\Delta\sigma'/\sigma'_o = 0.05$.
5. Choose the smaller of the two depths, D_1 and D_2, just determined as the approximate minimum depth of boring required, unless bedrock is encountered.

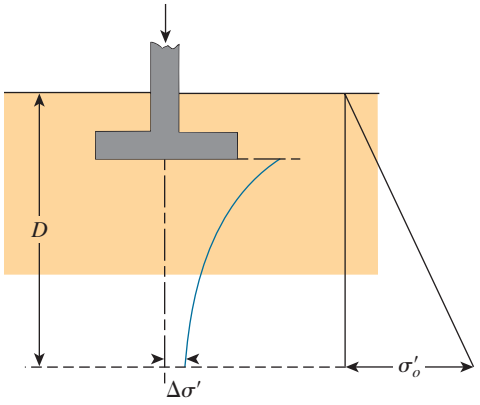


FIGURE 3.9 Determination of the minimum depth of boring

If the preceding rules are used, the depths of boring for a building with a width of 30 m (100 ft) will be approximately the following, according to Sowers and Sowers (1970):

No. of stories	Boring depth	
1	3.5 m	(11 ft)
2	6 m	(20 ft)
3	10 m	(33 ft)
4	16 m	(53 ft)
5	24 m	(79 ft)

To determine the boring depth for hospitals and office buildings, Sowers and Sowers (1970) also used the following rules.

- For light steel or narrow concrete buildings,

$$\frac{D_b}{S^{0.7}} = a \tag{3.1}$$

where

D_b = depth of boring

S = number of stories

$$a = \begin{cases} \approx 3 \text{ if } D_b \text{ is in meters} \\ \approx 10 \text{ if } D_b \text{ is in feet} \end{cases}$$

- For heavy steel or wide concrete buildings,

$$\frac{D_b}{S^{0.7}} = b \tag{3.2}$$

where

$$b = \begin{cases} \approx 6 \text{ if } D_b \text{ is in meters} \\ \approx 20 \text{ if } D_b \text{ is in feet} \end{cases}$$

When deep excavations are anticipated, the depth of boring should be at least 1.5 times the depth of excavation.

Sometimes, subsoil conditions require that the foundation load be transmitted to bedrock. The minimum depth of core boring into the bedrock is about 3 m (10 ft). If the bedrock is irregular or weathered, the core borings may have to be deeper.

There are no hard-and-fast rules for borehole spacing. Table 3.4 gives some general guidelines. Spacing can be increased or decreased, depending on the condition

TABLE 3.4 Approximate Spacing of Boreholes

Type of project	Spacing (m)	Spacing (ft)
Multistory building	10–30	30–100
One-story industrial plants	20–60	60–200
Highways	250–500	800–1600
Residential subdivision	250–500	800–1600
Dams and dikes	40–80	130–260

of the subsoil. If various soil strata are more or less uniform and predictable, fewer boreholes are needed than in nonhomogeneous soil strata.

The engineer should also take into account the ultimate cost of the structure when making decisions regarding the extent of field exploration. The exploration cost generally should be 0.1 to 0.5% of the cost of the structure. Soil borings can be made by several methods, including auger boring, wash boring, percussion drilling, and rotary drilling.

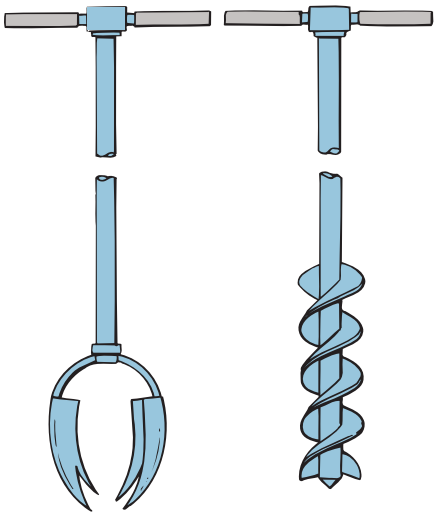
Trial pits are useful in supplementing the information derived from boreholes. Trial pits up to 4 m in depth can be made using backhoes. They are inexpensive when compared to boreholes and give a clear picture of the soil conditions, but are limited in depth. Boreholes are necessary for exploring soil and taking samples at greater depths.

3.13 Exploratory Borings in the Field

Auger boring is the simplest method of making exploratory boreholes. Figure 3.10 shows two types of hand auger the *posthole auger* and the *helical auger.* Hand augers cannot be used for advancing holes to depths exceeding 3 to 5 m (10 to 16 ft). However, they can be used for soil exploration work on some highways and small structures. *Portable power-driven helical augers* (76 mm to 305 mm in diameter) are available for making deeper boreholes. The soil samples obtained from such borings are highly disturbed and can be used for soil indentification and classification. In some noncohesive soil or soil having low cohesion, the walls of the boreholes will not stand unsupported. In such circumstances, a metal pipe is used as a *casing* to prevent the soil from caving in.

When power is available, *continuous-flight augers* are probably the most common method used for advancing a borehole. The power for drilling is delivered by truck- or tractor-mounted drilling rigs. Boreholes up to about 60 to 70 m (200 to 230 ft) can easily be made by this method. Continuous-flight augers are available in sections of about 1 to 2 m (3 to 6 ft) with either a solid or hollow stem. Some of the commonly used solid-stem augers have outside diameters of 66.68 mm ($2\frac{5}{8}$ in.), 82.55 mm ($3\frac{1}{4}$ in.), 101.6 mm (4 in.), and 114.3 mm ($4\frac{1}{2}$ in.). Common commercially available hollow-stem augers have dimensions of 63.5 mm ID and 158.75 mm OD (2.5 in. × 6.25 in.), 69.85 mm ID and 177.8 OD (2.75 in. × 7 in.), 76.2 mm ID and 203.2 OD (3 in. × 8 in.), and 82.55 mm ID and 28.6 mm OD (3.25 in. × 9 in.).

The tip of the auger is attached to a cutter head, which is sometimes made of materials with high hardness such as tungsten or carbide (Figure 3.11). During the drilling operation (Figure 3.12), section after section of auger can be added and the hole extended downward. The flights of the augers bring the loose soil from the bottom



(a) (b)

FIGURE 3.10 Hand tools: (a) posthole auger; (b) helical auger

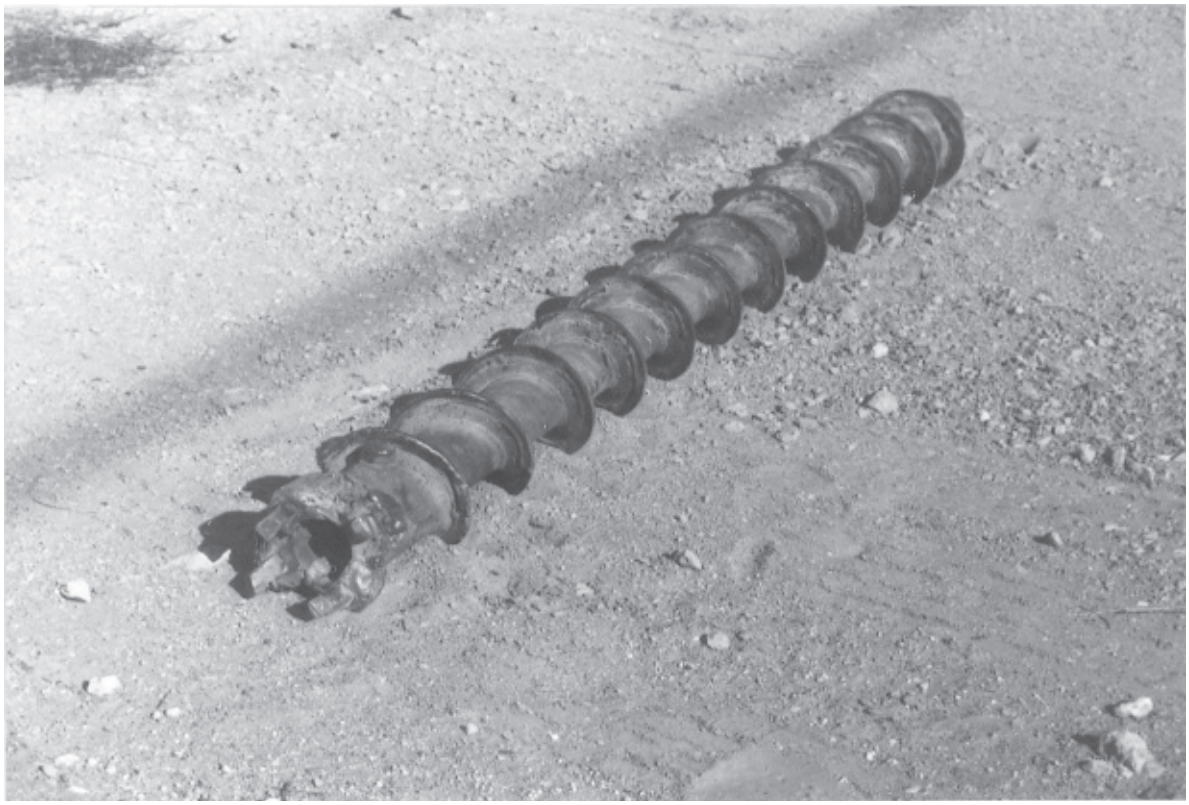


FIGURE 3.11 Carbide-tipped cutting head on auger flight (Courtesy of Braja M. Das, Henderson, Nevada)



FIGURE 3.12 Drilling with continuous-flight augers (Danny R. Anderson, PE of Professional Service Industries, Inc., El Paso, Texas)

of the hole to the surface. The driller can detect changes in the type of soil by noting changes in the speed and sound of drilling. When solid-stem augers are used, the auger must be withdrawn at regular intervals to obtain soil samples and also to conduct other operations such as standard penetration tests. Hollow-stem augers have a distinct advantage over solid-stem augers in that they do not have to be removed frequently for sampling or other tests. As shown schematically in Figure 3.13, the outside of the hollow-stem auger acts as a casing.

The hollow-stem auger system includes the following components:

Outer component:	(a) hollow auger sections, (b) hollow auger cap, and (c) drive cap
Inner component:	(a) pilot assembly, (b) center rod column, and (c) rod-to-cap adapter

The auger head contains replaceable carbide teeth. During drilling, if soil samples are to be collected at a certain depth, the pilot assembly and the center rod are removed. The soil sampler is then inserted through the hollow stem of the auger column.

Wash boring is another method of advancing boreholes. In this method, a casing about 2 to 3 m (6 to 10 ft) long is driven into the ground. The soil inside the casing is then removed by means of a chopping bit attached to a drilling rod. Water is forced through the drilling rod and exits at a very high velocity through the holes at the bottom of the chopping bit (Figure 3.14). The water and the chopped soil particles rise in the drill hole and overflow at the top of the casing through a T connection. The washwater is collected in a container. The casing can be extended with additional pieces as the borehole progresses; however, that is not required if the borehole will stay open and not cave in. Wash borings are rarely used now in the United States and other developed countries.

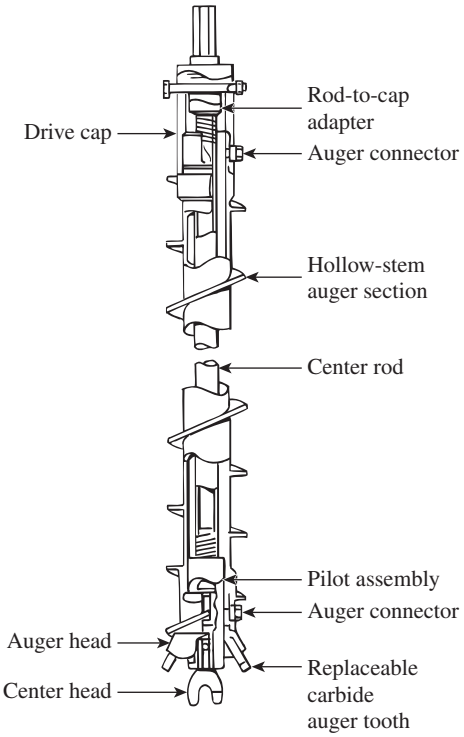


FIGURE 3.13 Hollow-stem auger components (After ASTM, 2001) (Based on ASTM D4700-91: Standard Guide for Soil Sampling from the Vadose Zone)

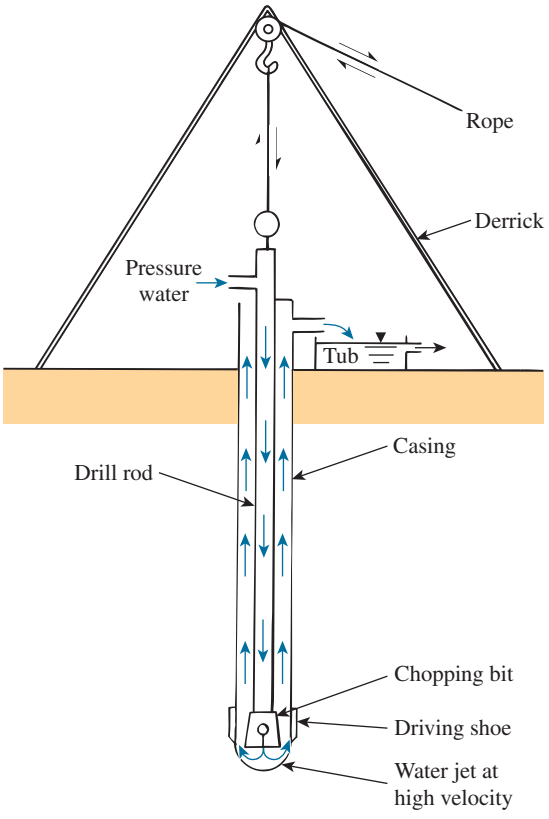


FIGURE 3.14 Wash boring

Rotary drilling is a procedure by which rapidly rotating drilling bits attached to the bottom of drilling rods cut and grind the soil and advance the borehole. There are several types of drilling bit. Rotary drilling can be used in sand, clay, and rocks (unless they are badly fissured). Water or *drilling mud* is forced down the drilling rods to the bits, and the return flow forces the cuttings to the surface. Boreholes with diameters of 50 to 203 mm (2 to 8 in.) can easily be made by this technique. The drilling mud is a slurry of water and bentonite. Generally, it is used when the soil that is encountered is likely to cave in. When soil samples are needed, the drilling rod is raised and the drilling bit is replaced by a sampler. For environmental drilling applications, rotary drilling with air is becoming more common.

Percussion drilling is an alternative method of advancing a borehole, particularly through hard soil and rock. A heavy drilling bit is raised and lowered to chop the hard soil. The chopped soil particles are brought up by the circulation of water. Percussion drilling may require casing.

3.14 Procedures for Sampling Soil

Two types of soil samples can be obtained during subsurface exploration: *disturbed* and *undisturbed.* Disturbed, but representative, samples can generally be used for the following types of laboratory test:

1. Grain-size analysis
2. Determination of liquid and plastic limits
3. Specific gravity of soil solids
4. Determination of organic content
5. Classification of soil

Disturbed soil samples, however, cannot be used for consolidation, hydraulic conductivity, or shear strength tests. Undisturbed soil samples must be obtained for these types of laboratory tests. Sections 3.15 through 3.18 describe some procedures for obtaining soil samples during field exploration.

3.15 Split-Spoon Sampling and Standard Penetration Test

Split-spoon sampling is part of a *standard penetration test* (SPT), one of the most popular *in situ* tests carried out worldwide. The test was developed in the United States in the 1920s. Split-spoon samplers can be used in the field to obtain soil samples that are generally disturbed, but still representative. A section of a *standard split-spoon sampler* is shown in Figure 3.15a. The tool consists of a steel driving shoe, a steel tube that is split longitudinally in half, and a coupling at the top. The coupling connects the sampler to the drill rod. The standard split tube has an inside diameter of 34.93 mm ($1\frac{3}{8}$ in.) and an outside diameter of 50.8 mm (2 in.); however, samplers having inside and outside diameters up to 63.5 mm ($2\frac{1}{2}$ in.) and 76.2 mm (3 in.), respectively, are also available. When a borehole is extended to a predetermined depth, the drill tools are removed, and the sampler is lowered to the bottom of the hole. The sampler is driven into the soil by hammer blows to the top of the drill rod. The standard weight of the hammer is 622.72 N (140 lb), and for each blow, the hammer drops a distance of 0.762 m (30 in.). The number of blows required for a spoon penetration of three consecutive 152.4 mm (6 in.) intervals is recorded. The number of blows required for the last two intervals is added to give the *standard penetration number* or *blow count, N*, at that depth. This number is generally referred to as the *N value* (American Society for Testing and Materials, 2016, Designation D-1586-11).

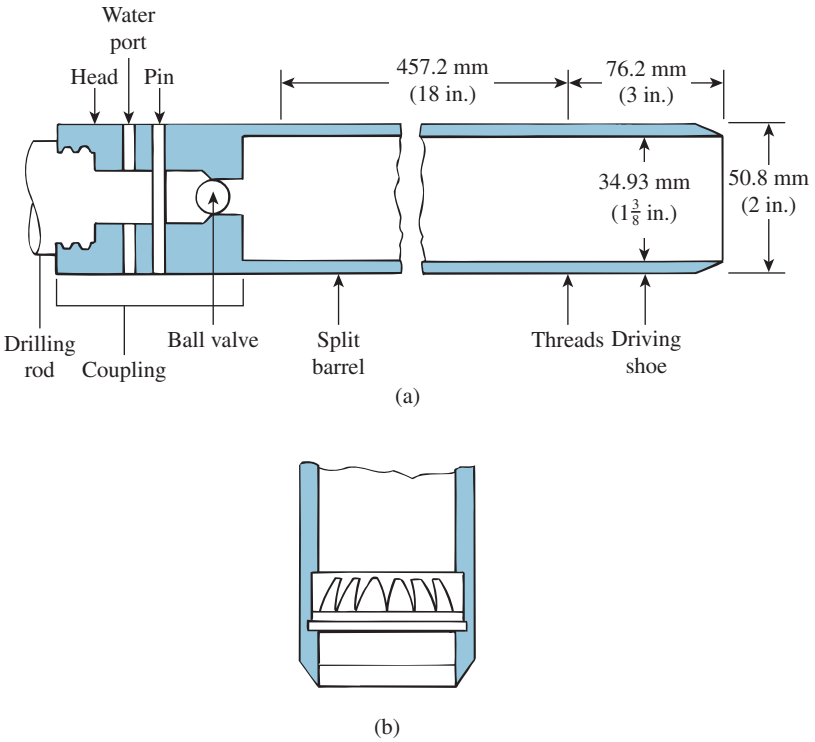


FIGURE 3.15 (a) Standard split-spoon sampler; (b) spring core catcher

The sampler is then withdrawn, and the shoe and coupling are removed. Finally, the soil sample recovered from the tube is placed in a glass bottle and transported to the laboratory. This field test is called the standard penetration test (SPT). Figures 3.16a and b show a split-spoon sampler unassembled before and after sampling.

The degree of disturbance for a soil sample is usually expressed as

$$A_R(\%) = \frac{D_o^2 - D_i^2}{D_i^2}(100) \tag{3.3}$$



(a) (b)

FIGURE 3.16 (a) Unassembled split-spoon sampler; (b) after sampling (Courtesy of Professional Service Industries, Inc. (PSI), Waukesha, Wisconsin)

where

A_R = area ratio (ratio of disturbed area to total area of soil)

D_o = outside diameter of the sampling tube

D_i = inside diameter of the sampling tube

When the area ratio is 10% or less, the sample generally is considered to be undisturbed. For a standard split-spoon sampler,

$$A_R(\%) = \frac{(50.8)^2 - (34.93)^2}{(34.93)^2}(100) = 111.5\%$$

Hence, these samples are highly disturbed. Split-spoon samples generally are taken at intervals of about 1.5 m (5 ft). When the material encountered in the field is sand (in particular, fine sand below the water table), recovery of the sample by a split-spoon sampler may be difficult. In that case, a device such as a *spring core catcher* may have to be placed inside the split spoon (Figure 3.15b).

At this juncture, it is important to point out that several factors contribute to the variation of the standard penetration number N at a given depth for similar soil profiles. Among these factors are the SPT hammer efficiency, borehole diameter, sampling method, and rod length (Seed et al., 1985; Skempton, 1986). The SPT hammer energy efficiency can be expressed as

$$E_r(\%) = \frac{\text{actual hammer energy to the sampler}}{\text{input energy}} \times 100 \tag{3.4}$$

$$\text{Theoretical input energy} = Wh \tag{3.5}$$

where

W = weight of the hammer $\approx$ 0.623 kN (140 lb)

h = height of drop $\approx$ 0.76 mm (30 in.)

So,

$$Wh = (0.623)(0.76) = 0.474\ \text{kN}\cdot\text{m}\ (4200\ \text{in.}\cdot\text{lb})$$

In the field, the magnitude of E_r can vary from 30 to 90%. The standard practice now in the United States is to express the N-value to an average energy ratio of 60% ($\approx N_{60}$). In addition, the borehole diameter, rod length (i.e., borehole depth), and whether a liner is used within the sampler can contribute to the energy loss and hence influence the N-value. Therefore, the N-value corrected to account for these factors can be written as

$$N_{60} = \frac{N\eta_H\eta_B\eta_S\eta_R}{60} \tag{3.6}$$

where

N_{60} = standard penetration number, corrected for field conditions

N = measured penetration number

η_H = hammer efficiency (%)

η_B = correction for borehole diameter

η_S = sampler correction

η_R = correction for rod length

Variations of η_H, η_B, η_S, and η_R, based on recommendations by Seed et al. (1985) and Skempton (1986) are summarized in Table 3.5.

TABLE 3.5 Variations of η_H, η_B, η_S, and η_R [Eq. (3.6)]

1. Variation of η_H

Country	Hammer type	Hammer release	η_H (%)
Japan	Donut	Free fall	78
	Donut	Rope and pulley	67
United States	Safety	Rope and pulley	60
	Donut	Rope and pulley	45
Argentina	Donut	Rope and pulley	45
China	Donut	Free fall	60
	Donut	Rope and pulley	50

2. Variation of η_B

Diameter		
mm	in.	η_B
60–120	2.4–4.7	1
150	6	1.05
200	8	1.15

3. Variation of η_S

Variable	η_S
Standard sampler	1.0
With liner for dense sand and clay	0.8
With liner for loose sand	0.9

4. Variation of η_R

Rod length		
m	ft	η_R
>10	>30	1.0
6–10	20–30	0.95
4–6	12–20	0.85
0–4	0–12	0.75

CORRELATIONS FOR N_{60} IN COHESIVE SOIL

The standard penetration test works very well in granular soil. Due to the pore water pressures developed while driving the sampler through clays, the effective stresses are changed, which can influence the *N*-values. As a result, the standard penetration test and the *N*-values are not reliable in clays. Nevertheless, when N_{60} for clays is available, the consistency, undrained shear strength, preconsolidation pressure, and the overconsolidation ratio (OCR) of the clay can be estimated using empirical correlations. Szechy and Vargi (1978) calculated the *consistency index* (CI) as

$$\text{CI} = \frac{\text{LL} - w}{\text{LL} - \text{PL}} \tag{3.7}$$

where

w = natural moisture content (%)

LL = liquid limit

PL = plastic limit

The approximate correlation among CI, N_{60}, and the unconfined compression strength (q_u) is given in Table 3.6.

TABLE 3.6 Approximate Correlation Among CI, N_{60}, and q_u

Standard penetration number, N_{60}	Consistency	CI	Unconfined compression strength, q_u (kN/m^2)	Unconfined compression strength, q_u (lb/ft^2)
<2	Very soft	<0.5	<25	500
2–8	Soft to medium	0.5–0.75	25–100	500–2100
8–15	Stiff	0.75–1.0	100–200	2100–4200
15–30	Very stiff	1.0–1.5	200–400	4200–8400
>30	Hard	>1.5	>400	8400

Hara et al. (1974) also suggested the following correlation between the undrained shear strength of clay (c_u) and N_{60} for clays from Japan with OCR = 1–3.

$$\frac{c_u}{p_a} = 0.29N_{78}^{0.72} \tag{3.8a}$$

where p_a = atmospheric pressure (≈ 100 kN/m^2; ≈ 2000 lb/in^2). Since $N_{78} = 0.77N_{60}$, in terms of N_{60}, Eq. (3.8a) becomes

$$\frac{c_u}{p_a} = 0.24N_{60}^{0.72} \tag{3.8b}$$

The overconsolidation ratio, OCR, of a natural clay deposit can also be correlated with the standard penetration number. On the basis of the regression analysis of 110 data points, Mayne and Kemper (1988) obtained the relationship

$$\text{OCR} = 0.193\left(\frac{N_{60}}{\sigma'_o}\right)^{0.689} \tag{3.9}$$

where σ'_o = effective vertical stress in MN/m^2.

It is important to point out that any correlation among c_u, OCR, and N_{60} is only approximate.

Using the field test results of Mayne and Kemper (1988) and others (112 data points), Kulhawy and Mayne (1990) suggested the approximate correlation

$$\text{OCR} = 0.58\frac{N_{60}p_a}{\sigma'_o} \tag{3.10}$$

Kulhawy and Mayne (1990) have also provided an approximate correlation for the preconsolidation pressure (σ'_c) of clay as

$$\sigma'_c = 0.47N_{60}p_a \tag{3.11}$$

CORRECTION FOR N_{60} IN GRANULAR SOIL

In granular soil, the value of N_{60} is affected by the effective overburden pressure, σ'_o. For that reason, the value of N_{60} obtained from field exploration under different effective overburden pressures should be changed to correspond to a standard value of σ'_o. That is,

$$(N_1)_{60} = C_N N_{60} \tag{3.12}$$

where

$(N_1)_{60}$ = value of N_{60} corrected to a standard value of $\sigma'_a = p_a \approx [100$ kN/m^2 (2000 lb/ft^2)]

C_N = correction factor

N_{60} = value of N obtained from field exploration [Eq. (3.6)]

In the past, a number of empirical relations were proposed for C_N. Some of the relationships are given next. The most commonly cited relationships are those of Liao and Whitman (1986) and Skempton (1986).

In the following relationships for C_N, note that σ'_o is the effective overburden pressure and p_a = atmospheric pressure ($\approx$ 100 kN/m^2, or $\approx$ 2000 lb/ft^2):

Liao and Whitman's relationship (1986):

$$C_N = \left[\frac{1}{\left(\frac{\sigma'_o}{p_a}\right)}\right]^{0.5} \tag{3.13}$$

Skempton's relationship (1986):

$$C_N = \frac{2}{1 + \left(\frac{\sigma'_o}{p_a}\right)} \quad \text{(for normally consolidated fine sand)} \tag{3.14}$$

$$C_N = \frac{3}{2 + \left(\frac{\sigma'_o}{p_a}\right)} \quad \text{(for normally consolidated coarse sand)} \tag{3.15}$$

$$C_N = \frac{1.7}{0.7 + \left(\frac{\sigma'_o}{p_a}\right)} \quad \text{(for overconsolidated sand)} \tag{3.16}$$

Seed et al.'s relationship (1975):

$$C_N = 1 - 1.25 \log\left(\frac{\sigma'_o}{p_a}\right) \tag{3.17}$$

Peck et al.'s relationship (1974):

$$C_N = 0.77 \log\left[\frac{20}{\left(\frac{\sigma'_o}{p_a}\right)}\right] \left(\text{for } \frac{\sigma'_o}{p_a} \geq 0.25\right) \tag{3.18}$$

Bazaraa (1967):

$$C_N = \frac{4}{1 + 4\left(\frac{\sigma'_o}{p_a}\right)} \left(\text{for } \frac{\sigma'_o}{p_a} \leq 0.75\right) \tag{3.19}$$

$$C_N = \frac{4}{3.25 + \left(\frac{\sigma'_o}{p_a}\right)} \left(\text{for } \frac{\sigma'_o}{p_a} > 0.75\right) \tag{3.20}$$

Table 3.7 shows the comparison of C_N derived using various relationships cited above. It can be seen that the magnitude of the correction factor estimated by using

TABLE 3.7 Variation of C_N

	C_N						
$\frac{\sigma'_o}{p_a}$	Eq. (3.13)	Eq. (3.14)	Eq. (3.15)	Eq. (3.16)	Eq. (3.17)	Eq. (3.18)	Eqs. (3.19) and (3.20)
0.25	2.00	1.60	1.33	1.78	1.75	1.47	2.00
0.50	1.41	1.33	1.20	1.17	1.38	1.23	1.33
0.75	1.15	1.14	1.09	1.17	1.15	1.10	1.00
1.00	1.00	1.00	1.00	1.00	1.00	1.00	0.94
1.50	0.82	0.80	0.86	0.77	0.78	0.87	0.84
2.00	0.71	0.67	0.75	0.63	0.62	0.77	0.76
3.00	0.58	0.50	0.60	0.46	0.40	0.63	0.65
4.00	0.50	0.40	0.60	0.36	0.25	0.54	0.55

any one of the relationships is approximately the same, considering the uncertainties involved in conducting the standard penetration tests. Hence, Eq. (3.13) may be used for all calculations.

EXAMPLE 3.1

A standard penetration test is carried out in sand where the efficiency of the hammer $\eta_H = 70\%$. If the measured N-value at 30 ft depth is 24, find N_{60} and $(N_1)_{60}$. The unit weight of the sand is 115.0 lb/ft^3. Assume $\eta_B = \eta_S = \eta_R = 1$.

SOLUTION

From Eq. (3.6),

$$N_{60} = \frac{(N)(\eta_H)(1)(1)(1)}{60} = \frac{(24)(70)}{60} = 28$$

From Eq. (3.13),

$$C_N = \left[\frac{1}{\sigma'_o/p_a}\right]^{0.5} = \left[\frac{1}{(30 \times 115)/2000}\right]^{0.5} = 0.76$$

From Eq. (3.12),

$$(N_1)_{60} = C_N N_{60} = 0.76 \times 28 \approx \mathbf{21}$$

■

CORRELATION BETWEEN N_{60} AND RELATIVE DENSITY OF GRANULAR SOIL

Kulhawy and Mayne (1990) modified an empirical relationship for relative density that was given by Marcuson and Bieganousky (1977), which can be expressed as

$$D_r(\%) = 12.2 + 0.75\left[222N_{60} + 2311 - 711\text{OCR} - 779\left(\frac{\sigma'_o}{p_a}\right) - 50C_u^2\right]^{0.5} \tag{3.21}$$

where

D_r = relative density

σ'_o = effective overburden pressure

C_u = uniformity coefficient of sand

$$\text{OCR} = \frac{\text{preconsolidation pressure}, \sigma'_c}{\text{effective overburden pressure}, \sigma'_o}$$

p_a = atmospheric pressure

Meyerhof (1957) developed a correlation between D_r and N_{60} as

$$N_{60} = \left[17 + 24\left(\frac{\sigma'_o}{p_a}\right)\right]D_r^2$$

or

$$D_r = \left\{\frac{N_{60}}{\left[17 + 24\left(\frac{\sigma'_o}{p_a}\right)\right]}\right\}^{0.5} \tag{3.22}$$

Equation (3.22) provides a reasonable estimate only for clean, medium-fine sand.

Cubrinovski and Ishihara (1999) also proposed a correlation between N_{60} and the relative density of sand (D_r) that can be expressed as

$$D_r(\%) = \left[\frac{N_{60}\left(0.23 + \dfrac{0.06}{D_{50}}\right)^{1.7}}{9}\left(\frac{1}{\dfrac{\sigma'_o}{p_a}}\right)\right]^{0.5}(100) \tag{3.23}$$

where

p_a = atmospheric pressure ($\approx$ 100 kN/m^2, or $\approx$ 2000 lb/ft^2)

D_{50} = sieve size through which 50% of the soil will pass (mm)

Kulhawy and Mayne (1990) correlated the corrected standard penetration number and the relative density of sand in the form

$$D_r(\%) = \left[\frac{(N_1)_{60}}{C_p C_A C_{OCR}}\right]^{0.5}(100) \tag{3.24}$$

where

$$C_P = \text{grain-size correlations factor} = 60 + 25 \log D_{50} \tag{3.25}$$

$$C_A = \text{correlation factor for aging} = 1.2 + 0.05 \log\left(\frac{t}{100}\right) \tag{3.26}$$

$$C_{OCR} = \text{correlation factor for overconsolidation} = \text{OCR}^{0.18} \tag{3.27}$$

D_{50} = diameter through which 50% soil will pass through (mm)

t = age of soil since deposition (years)

OCR = overconsolidation ratio

It is difficult to estimate the geologic age of a granular soil deposit. In the absence of any reliable data, it can be assumed to be 1000–5000 years with negligible error in the estimate of D_r.

Skempton (1986) suggested that, for sands with a relative density greater than 35%,

$$\frac{(N_1)_{60}}{D_r^2} \approx 60 \tag{3.28}$$

where $(N_1)_{60}$ should be multiplied by 0.92 for coarse sands and 1.08 for fine sands.

It can be seen from all the correlations relating D_r with N-value that the effective overburden pressure has to come into the picture. The correlations for D_r are either in terms of N_{60} and σ'_o or in terms of $(N_1)_{60}$, which includes the effective overburden pressure. This also applies to the friction angle correlations discussed in the following section.

CORRELATION BETWEEN ANGLE OF FRICTION AND STANDARD PENETRATION NUMBER

The peak friction angle, ϕ', of granular soil has also been correlated with N_{60} or $(N_1)_{60}$ by several investigators. Some of these correlations are as follows:

1. Peck et al. (1974) give a correlation between $(N_1)_{60}$ and ϕ' in a graphical form, which can be approximated as (Wolff, 1989)

$$\phi'(\text{deg}) = 27.1 + 0.3(N_1)_{60} - 0.00054[(N_1)_{60}]^2 \tag{3.29}$$

2. Schmertmann (1975) provided the correlation among N_{60}, σ'_o, and ϕ'. Mathematically, the correlation can be approximated as (Kulhawy and Mayne, 1990)

$$\phi' = \tan^{-1}\left[\frac{N_{60}}{12.2 + 20.3\left(\frac{\sigma'_o}{p_a}\right)}\right]^{0.34} \tag{3.30}$$

where

N_{60} = field standard penetration number

σ'_o = effective overburden pressure

p_a = atmospheric pressure in the same unit as σ'_o

ϕ' = soil friction angle

3. Hatanaka and Uchida (1996) provided a simple correlation between ϕ' and $(N_1)_{78}$ that can be expressed as

$$\phi' = \sqrt{20(N_1)_{78}} + 20 \tag{3.31a}$$

In terms of $(N_1)_{60}$, Eq. (3.31a) becomes

$$\phi' = \sqrt{15.4(N_1)_{60}} + 20 \tag{3.31b}$$

The following qualifications should be noted when standard penetration resistance values are used in the preceding correlations to estimate soil parameters:

1. The equations are approximate.
2. Because the soil is not homogeneous, the values of N_{60} obtained from a given borehole vary widely.
3. In soil deposits that contain large boulders and gravel, standard penetration numbers may be erratic and unreliable.

Although approximate, with correct interpretation the standard penetration test provides a good evaluation of soil properties. The primary sources of error in standard penetration tests are inadequate cleaning of the borehole, careless measurement of the blow count, eccentric hammer strikes on the drill rod, and inadequate maintenance of water head in the borehole. Figure 3.17 shows approximate borderline values for D_r, N_{60}, $(N_1)_{60}$, ϕ', and $\frac{(N_1)_{60}}{D_r^2}$.

CORRELATION BETWEEN MODULUS OF ELASTICITY AND STANDARD PENETRATION NUMBER

The modulus of elasticity of granular soil (E_s) is an important parameter in estimating the elastic settlement of foundations. A first-order estimation for E_s was given by Kulhawy and Mayne (1990) as

$$\frac{E_s}{p_a} = \alpha N_{60} \tag{3.32}$$

where

p_a = atmospheric pressure (same unit as E_s)

$$\alpha = \begin{cases} 5 \text{ for sands with fines} \\ 10 \text{ for clean normally consolidated sand} \\ 15 \text{ for clean overconsolidated sand} \end{cases}$$

	*Very loose	Loose	Medium dense	Dense	Very dense	
#D_r (%)	0	15	35	65	85	100
*N_{60}		4	10	30	50	
##$(N_1)_{60}$		3	8	25	42	
**ϕ'(deg)		28	30	36	41	
##$(N_1)_{60}/D_r^2$			65	59	58	

*Terzaghi & Peck (1948); #Gibb & Holtz (1957); ##Skempton (1986); **Peck et al. (1974)

FIGURE 3.17 Approximate borderline values for D_r, N_{60}, $(N_1)_{60}$, and $\dfrac{(N_1)_{60}}{D_r^2}$ (After Sivakugan and Das, 2010. With permission from J. Ross Publishing Co., Fort Lauderdale, FL)

EXAMPLE 3.2

In a sand with unit weight of 113.0 lb/ft^3, a standard penetration test is carried out. The N_{60} values are as follows:

Depth (ft)	10	15	20	25	30
N_{60}	16	20	22	24	26

Determine the friction angles at these depths using Peck et al. (1974), Schmertmann (1975), and Hatanaka and Uchida (1996) correlations.

SOLUTION

					Friction angle (degrees)		
Depth (ft)	σ'_o (lb/ft^2)	N_{60}	C_N (Liao & Whitman)	$(N_1)_{60}$	**Peck et al.**	**Schmertmann**	**Hatanaka & Uchida**
10	1130	16	1.330	21.3	33.2	41.2	38.1
15	1695	20	1.086	21.7	33.4	41.3	38.3
20	2260	22	0.941	20.7	33.1	40.5	37.9
25	2825	24	0.841	20.2	32.9	39.8	37.6
30	3390	26	0.768	20.0	32.9	39.4	37.5

3.16 Sampling with a Scraper Bucket

When the soil deposits are sand mixed with pebbles, obtaining samples by split spoon with a spring core catcher may not be possible because the pebbles may prevent the springs from closing. In such cases, a scraper bucket may be used to obtain disturbed representative samples (Figure 3.18). The scraper bucket has a driving point and can be attached to a drilling rod. The sampler is driven down into the soil and rotated, and the scrapings from the side fall into the bucket.

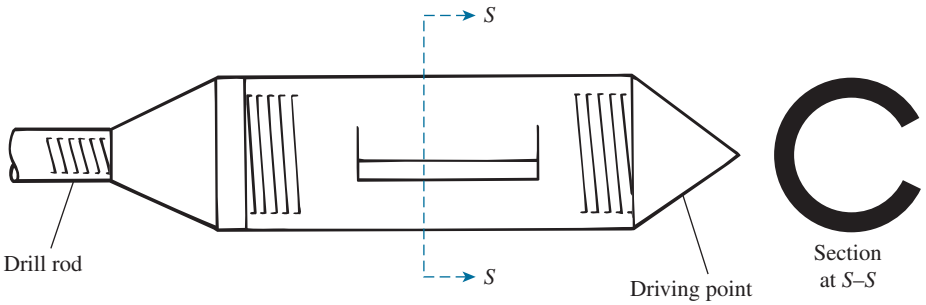


FIGURE 3.18 Scraper bucket

3.17 Sampling with a Thin-Walled Tube

Thin-walled tubes are sometimes referred to as *Shelby tubes*. They are made of seamless steel and are frequently used to obtain undisturbed samples from clayey soil. The most common thin-walled tube samplers have outside diameters of 50.8 mm (2 in.) and 76.2 mm (3 in.). The bottom end of the tube is sharpened. The tubes can be attached to drill rods (Figure 3.19). The drill rod with the sampler attached is lowered to the bottom of the borehole, and the sampler is pushed into the soil. The soil sample inside the tube is then pulled out. The two ends are sealed, and the sampler is sent to the laboratory for testing. Figure 3.20 shows the sequence of sampling with a thin-walled tube in the field.

Samples obtained in this manner may be used for consolidation or shear tests. A thin-walled tube with a 50.8 mm (2 in.) outside diameter has an inside diameter of about 47.63 mm ($1\frac{7}{8}$ in.). The area ratio is

$$A_R(\%) = \frac{D_o^2 - D_i^2}{D_i^2}(100) = \frac{(50.8)^2 - (47.63)^2}{(47.63)^2}(100) = 13.75\%$$

Increasing the diameters of samples increases the cost of obtaining them.

3.18 Sampling with a Piston Sampler

When undisturbed soil samples are very soft or larger than 76.2 mm (3 in.) in diameter, they tend to fall out of the sampler. Piston samplers are particularly useful under such conditions. There are several types of piston sampler; however, the sampler proposed by Osterberg (1952) is the most useful (see Figures 3.21a and 3.21b). It consists of a thin-walled tube with a piston. Initially, the piston closes the end

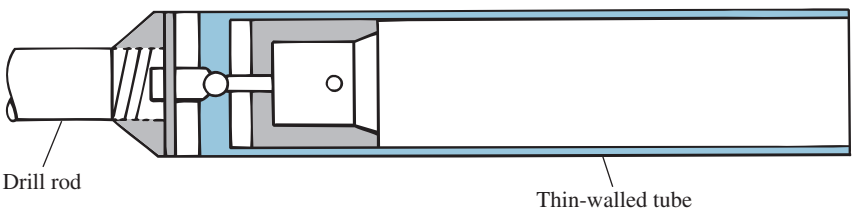


FIGURE 3.19 Thin-walled tube



(a)



(b)



(c)

FIGURE 3.20 Sampling with a thin-walled tube: (a) tube being attached to drill rod; (b) tube sampler pushed into soil; (c) recovery of soil sample (Courtesy of Khaled Sobhan, Florida Atlantic University, Boca Raton, FL)

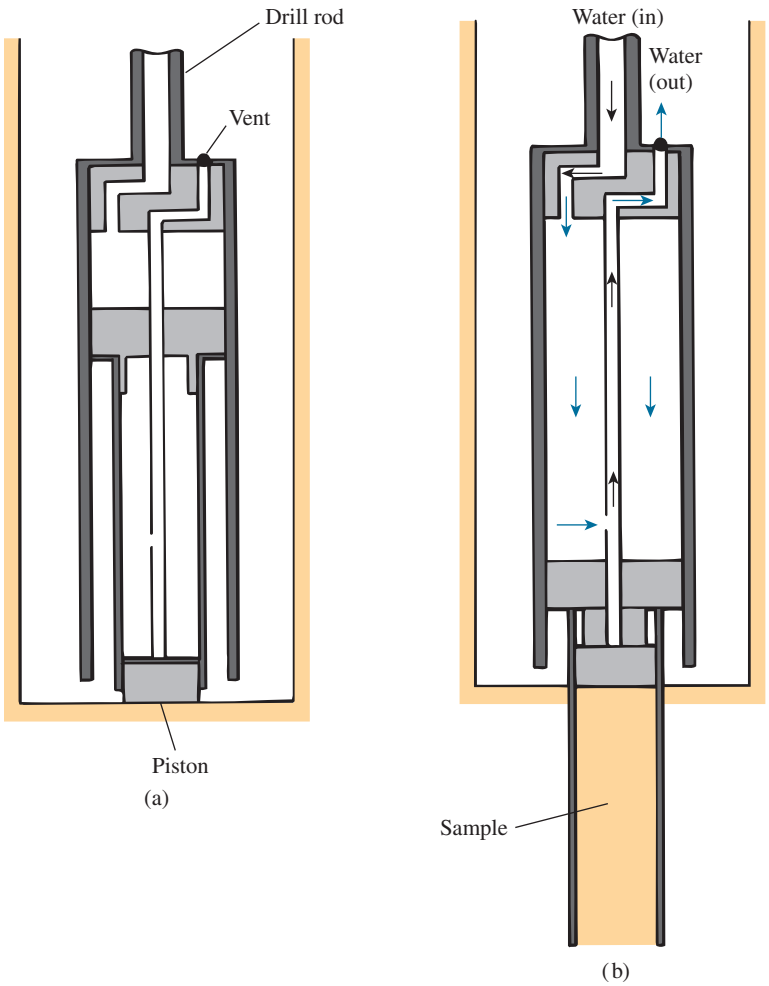


FIGURE 3.21 Piston sampler: (a) sampler at the bottom of borehole; (b) tube pushed into the soil hydraulically

of the tube. The sampler is lowered to the bottom of the borehole (Figure 3.21a), and the tube is pushed into the soil hydraulically, past the piston. Then the pressure is released through a hole in the piston rod (Figure 3.21b). To a large extent, the presence of the piston prevents distortion in the sample by not letting the soil squeeze into the sampling tube very fast and by not admitting excess soil. Consequently, samples obtained in this manner are less disturbed than those obtained by Shelby tubes.

3.19 Observation of Water Tables

The presence of a water table near a foundation significantly affects the foundation's load-bearing capacity and settlement, among other things. The water level will change seasonally and sometimes daily in coastal areas. In many cases, establishing the highest and lowest possible levels of water during the life of a project may become necessary.

If water is encountered in a borehole during a field exploration, that fact should be recorded. In soil with high hydraulic conductivity, the level of water in a borehole will stabilize about 24 hours after completion of the boring. The depth of the water table can then be recorded by lowering a chain or tape into the borehole. There are

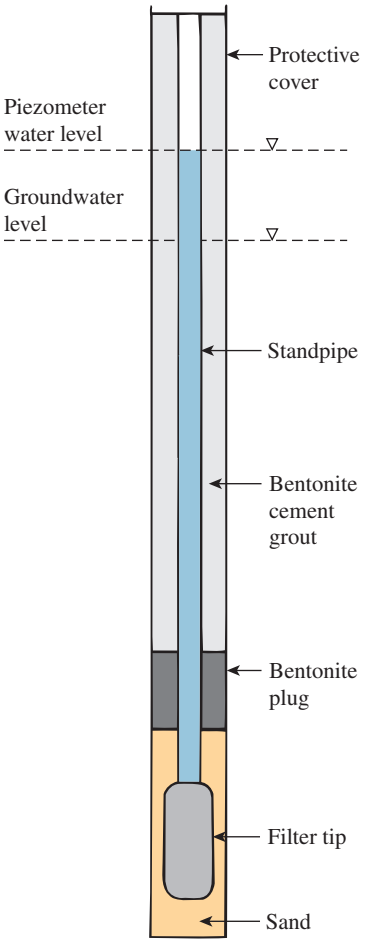


FIGURE 3.22 Casagrande-type piezometer (Courtesy of N. Sivakugan, James Cook University, Australia)

water-level sensors that can be lowered into the borehole to measure the water level, with an electric buzzer or light to indicate contact with water, are accurate within 1 mm.

In highly impermeable layers, the water level in a borehole may not stabilize for several weeks. In such cases, if accurate water-level measurements are required, a *piezometer* can be used. A piezometer basically consists of a porous stone or a perforated pipe with a plastic standpipe attached to it. Figure 3.22 shows the general placement of a piezometer in a borehole. This procedure will allow periodic checking until the water level stabilizes.

3.20 Vane Shear Test

The *vane shear test* (ASTM D-2573) may be used during the drilling operation to determine the *in situ* undrained shear strength (c_u) of clay soil—particularly soft clays. The vane shear apparatus consists of four blades on the end of a rod, as shown in Figure 3.23. The height, H, of the vane is twice the diameter, D. The vane can be either rectangular or tapered (see Figure 3.23). The dimensions of vanes used in the field are given in Table 3.8. The vanes of the apparatus are pushed into the soil at the bottom of a borehole without disturbing the soil appreciably. Torque is applied at the top of the rod to rotate the vanes at a standard rate of 0.1°/s. This rotation will induce failure in a soil of cylindrical shape surrounding the vanes. The maximum torque, T, applied to cause failure is measured. Note that

$$T = f(c_u, H, \text{and } D) \tag{3.33}$$

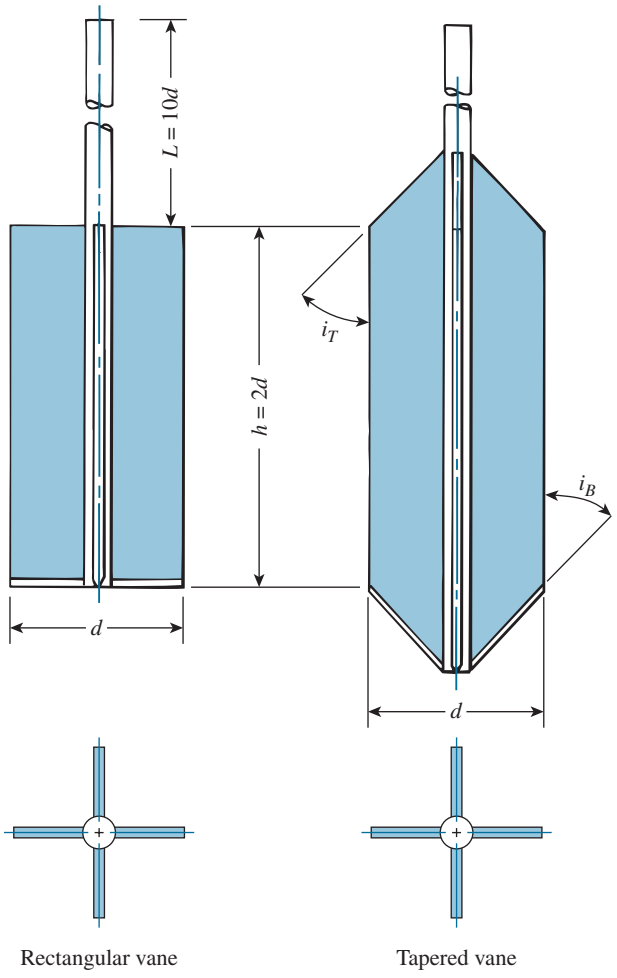


FIGURE 3.23 Geometry of field vane (After ASTM, 2014) (Based on *Annual Book of ASTM Standards, Vol. 04.08*)

or

$$c_u = \frac{T}{K} \tag{3.34}$$

According to ASTM (2014), for rectangular vanes,

$$K = \frac{\pi d^2}{2}\left(h + \frac{d}{3}\right) \tag{3.35}$$

TABLE 3.8 ASTM Recommended Dimensions of Field Vanes[a] (Based on *Annual Book of ASTM Standards, Vol. 04.08*)

Casing size	Diameter, *d* mm (in.)	Height, *h* mm (in.)	Thickness of blade mm (in.)	Diameter of rod mm (in.)
AX	38.1 ($1\frac{1}{2}$)	76.2 (3)	1.6 ($\frac{1}{16}$)	12.7 ($\frac{1}{2}$)
BX	50.8 (2)	101.6 (4)	1.6 ($\frac{1}{16}$)	12.7 ($\frac{1}{2}$)
NX	63.5 ($2\frac{1}{2}$)	127.0 (5)	3.2 ($\frac{1}{8}$)	12.7 ($\frac{1}{2}$)
101.6 mm (4 in.)[b]	92.1 ($3\frac{5}{8}$)	184.1 ($7\frac{1}{4}$)	3.2 ($\frac{1}{8}$)	12.7 ($\frac{1}{2}$)

[a]The selection of a vane size is directly related to the consistency of the soil being tested; that is, the softer the soil, the larger the vane diameter should be.

[b]Inside diameter.

If $h/d = 2$,

$$K = \frac{7\pi d^3}{6} \tag{3.36}$$

Thus,

$$c_u = \frac{6T}{7\pi d^3} \tag{3.37}$$

For tapered vanes,

$$K = \frac{\pi d^2}{12}\left(\frac{d}{\cos i_T} + \frac{d}{\cos i_B} + 6h\right) \tag{3.38}$$

The angles i_T and i_B are defined in Figure 3.23.

Field vane shear tests are moderately rapid and economical and are used extensively in field soil-exploration programs. The test gives good results in soft and medium-stiff clays and gives excellent results in determining the properties of sensitive clays.

Field vane shear tests are commonly used to measure both peak and residual undrained shear strengh by noting the torque required to overcome the maximum resistance and later the torque required to rotate the vane 5–10 revolutions within the clay.

Sources of significant error in the field vane shear test are poor calibration of torque measurement and damaged vanes. Other errors may be introduced if the rate of rotation of the vane is not properly controlled.

For actual design purposes, the undrained shear strength values obtained from field vane shear tests [$c_{u(\text{VST})}$] are too high, and it is recommended that they be corrected according to the equation

$$c_{u(\text{corrected})} = \lambda c_{u(\text{VST})} \tag{3.39}$$

where λ = correction factor.

Several correlations have been given previously for the correction factor λ. The most commonly used correlation for λ is that given by Bjerrum (1972), which can be expressed as

$$\lambda = 1.7 - 0.54 \log [\text{PI}(\%)] \tag{3.40a}$$

Morris and Williams (1994) provided the following correlations:

$$\lambda = 1.18e^{-0.08(\text{PI})} + 0.57 \text{ (for PI} > 5) \tag{3.40b}$$

$$\lambda = 7.01e^{-0.08(\text{LL})} + 0.57 \text{ (where LL is in \%)} \tag{3.40c}$$

The field vane shear strength can be correlated with the preconsolidation pressure and the overconsolidation ratio of the clay. Using 343 data points, Mayne and Mitchell (1988) derived the following empirical relationship for estimating the preconsolidation pressure of a natural clay deposit:

$$\sigma_c' = 7.04[c_{u(\text{field})}]^{0.83} \tag{3.41}$$

Here,

σ_c' = preconsolidation pressure (kN/m^2)

$c_{u(\text{field})}$ = field vane shear strength (kN/m^2)

The overconsolidation ratio, OCR, also can be correlated to $c_{u(\text{field})}$ according to the equation

$$\text{OCR} = \beta\frac{c_{u(\text{field})}}{\sigma_o'} \tag{3.42}$$

where σ_o' = effective overburden pressure.

The magnitudes of β developed by various investigators are given below.

- Mayne and Mitchell (1988):

$$\beta = 22[\text{PI}(\%)]^{-0.48} \tag{3.43}$$

- Hansbo (1957):

$$\beta = \frac{222}{w(\%)} \tag{3.44}$$

- Larsson (1980):

$$\beta = \frac{1}{0.08 + 0.0055(\text{PI})} \tag{3.45}$$

EXAMPLE 3.3

Refer to Figure 3.23. Vane shear tests (tapered vane) were conducted in the clay layer. The vane dimensions were 63.5 mm (d) × 127 m (h), and $i_T = i_B = 458$. For a test at a certain depth in the clay, the torque required to cause failure was 20 N · m. For the clay, liquid limit was 50 and plastic limit was 18. Estimate the undrained cohesion of the clay for use in the design by using each equation:

a. Bjerrum's λ relationship [Eq. (3.40a)]
b. Morris and Williams' λ and PI relationship [Eq. (3.40b)]
c. Morris and Williams' λ and LL relationship [Eq. (3.40c)]
d. Estimate the preconsolidation pressure of clay, σ_c'.

SOLUTION

Part a

Given: $h/d = 127/63.5 = 2$
From Eq. (3.38),

$$\begin{aligned} K &= \frac{\pi d^2}{12}\left(\frac{d}{\cos i_T} + \frac{d}{\cos i_B} + 6h\right) \\ &= \frac{\pi(0.0635)^2}{12}\left[\frac{0.0635}{\cos 45} + \frac{0.0635}{\cos 45} + 6(0.127)\right] \\ &= (0.001056)(0.0898 + 0.0898 + 0.762) \\ &= 0.000994 \end{aligned}$$

From Eq. (3.34),

$$\begin{aligned} c_{u(\text{VST})} &= \frac{T}{K} = \frac{20}{0.000994} \\ &= 20{,}121 \text{ N/m}^2 \approx 20.12 \text{ kN/m}^2 \end{aligned}$$

From Eqs. (3.40a) and (3.39),

$$\begin{aligned} c_{u(\text{corrected})} &= [1.7 - 0.54 \log (\text{PI}\%)]c_{u(\text{VST})} \\ &= [1.7 - 0.54 \log(50 - 18)](20.12) \\ &= \mathbf{17.85 \text{ kN/m}^2} \end{aligned}$$

Part b

From Eqs. (3.40b) and (3.39),

$$\begin{aligned} c_{u(\text{corrected})} &= [1.18e^{-0.08(\text{PI})} + 0.57]c_{u(\text{VST})} \\ &= [1.18e^{-0.08(50-18)} + 0.57](20.12) \\ &= \mathbf{13.3 \text{ kN/m}^2} \end{aligned}$$

Part c

From Eqs. (3.40c) and (3.39),

$$c_{u(\text{corrected})} = [7.01e^{-0.08(\text{LL})} + 0.57]c_{u(\text{VST})}$$
$$= [7.01e^{-0.08(50)} + 0.57](20.12)$$
$$= \mathbf{14.05\ kN/m^2}$$

Part d

From Eq. (3.41),

$$\sigma_c' = 7.04[c_{u(\text{VST})}]^{0.83} = 7.04(20.12)^{0.83} = \mathbf{85\ kN/m^2}$$

3.21 Cone Penetration Test

The *cone penetration test* (CPT), originally known as the Dutch cone penetration test, is a versatile *in situ* test that can be carried out in most soil conditions to determine the soil profile and various soil parameters. The interpretation of the test is more rational than that of the standard penetration test. SPT and CPT are used in more than 90% of soil exploration programs worldwide.

The original Dutch cone developed in Holland in 1932 was a 60° *mechanical cone* with a 35 mm outside diameter, with approximately 10 cm^2 (1.55 in^2) projected area. The cone is pushed into the ground, and the resistance at the cone, known as *cone resistance* (q_c), and the sleeve friction (f_s) are measured separately. The measurements are recorded at larger intervals in the order of 200 mm (8 in.). The mechanical cones (Figure 3.24) are labor intensive and are limited in accuracy.

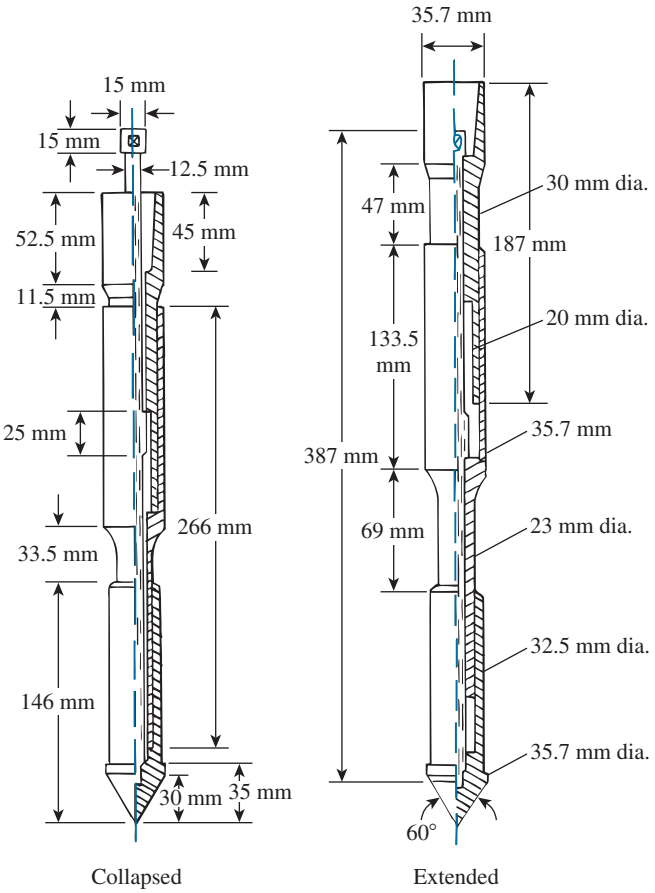
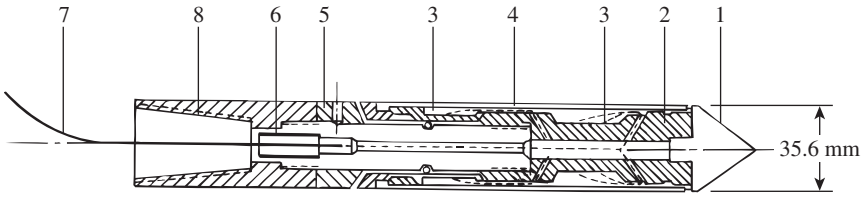


FIGURE 3.24 Mechanical friction-cone penetrometer (After ASTM, 2001) (Based on *Annual Book of ASTM Standards, Vol. 04.08*)



1 Conical point (10 cm^2)
2 Load cell
3 Strain gauges
4 Friction sleeve (150 cm^2)
5 Adjustment ring
6 Waterproof bushing
7 Cable
8 Connection with rods

FIGURE 3.25 Electric friction-cone penetrometer (After ASTM, 2001) (Based on *Annual Book of ASTM Standards, Vol. 04.08*)

Fugro developed the first electric cone in 1965 as an improvement of the mechanical cone. In the electric cone (Figures 3.25 and 3.26), the measurements are made using strain gauges and transducers, generally for every 20 mm (0.8 in.), thereby almost giving continuous measurements with depth. The modern cones, which are also able to measure pore water pressure, are known as *piezocones* (CPTu). The standard cone of 10 cm^2 has a friction sleeve area of 150 cm^2 (23.3 in^2). The 133.7 mm (5.3 in.) long frictional sleeve has an outer diameter of 35.7 mm (1.4 in.). Piezocones are the modern electric friction cones. With the addition of sensors such as geophones, seismic cone penetration tests (SCPTs) can now also measure shear wave velocity v_s and hence the shear modulus G.

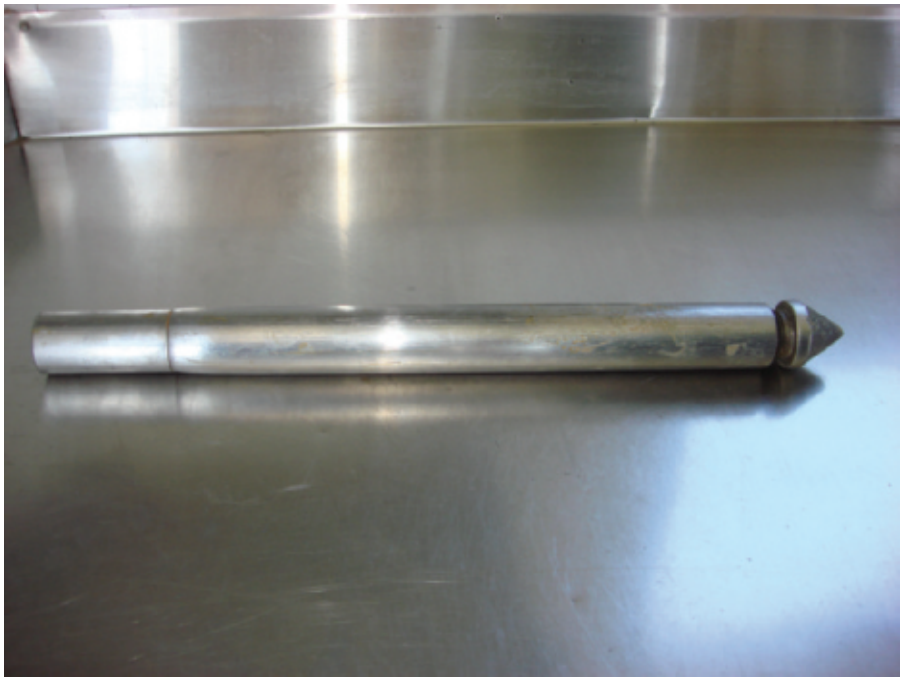


FIGURE 3.26 Photograph of an electric friction-cone penetrometer (Courtesy of Sanjeev Kumar, Southern Illinois University, Carbondale, IL)



(a)



(b)



(c)

FIGURE 3.27 Cone penetration test in field: (a) mounted CPT rig; (b) cone penetrometer being set in proper location; (c) test in progress (Courtesy of Sanjeev Kumar, Southern Illinois University, Carbondale, IL)

Figure 3.27 shows the sequence of a cone penetration test in the field. A truck-mounted CPT rig is shown in Figure 3.27a. A hydraulic ram located inside the truck pushes the cone into the ground. Figure 3.27b shows the cone penetrometer in the truck being put in the proper location. Figure 3.27c shows the progress of the CPT. Figure 3.28 shows the results of a penetrometer test in a soil profile in which friction measurement was done via an electric friction-cone penetrometer.

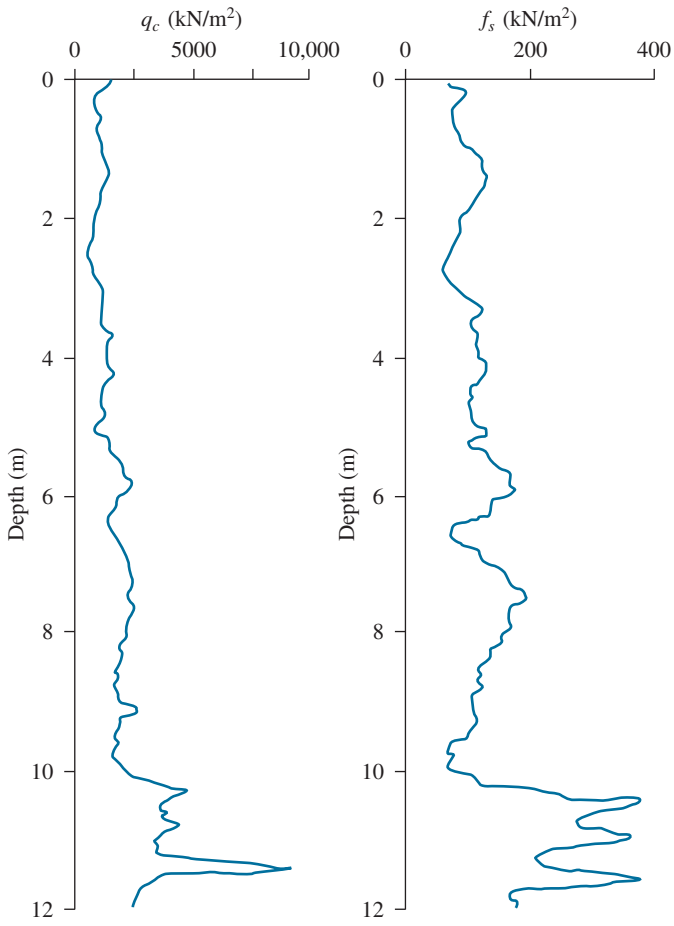


FIGURE 3.28 Cone penetrometer test with friction measurement

The *friction ratio* (F_r) is defined as

$$F_r(\%) = \frac{\text{sleeve friction}, f_s}{\text{cone resistance}, q_c} \times 100 \tag{3.46}$$

It varies in the range of 0–10%, with the lower end of the range for granular soil and the upper end for cohesive soil.

In a recent study on several soil in Greece, Anagnostopoulos et al. (2003) expressed F_r as

$$F_r(\%) = 1.45 - 1.36 \log D_{50} \text{ (electric cone)} \tag{3.47}$$

and

$$F_r(\%) = 0.7811 - 1.611 \log D_{50} \text{ (mechanical cone)} \tag{3.48}$$

where D_{50} = size through which 50% of soil will pass through (mm).

The D_{50} for soil based on which Eqs. (3.47) and (3.48) have been developed ranged from 0.001 mm to about 10 mm.

As in the case of standard penetration tests, several correlations have been developed between q_c and other soil properties. Some of these correlations are presented next.

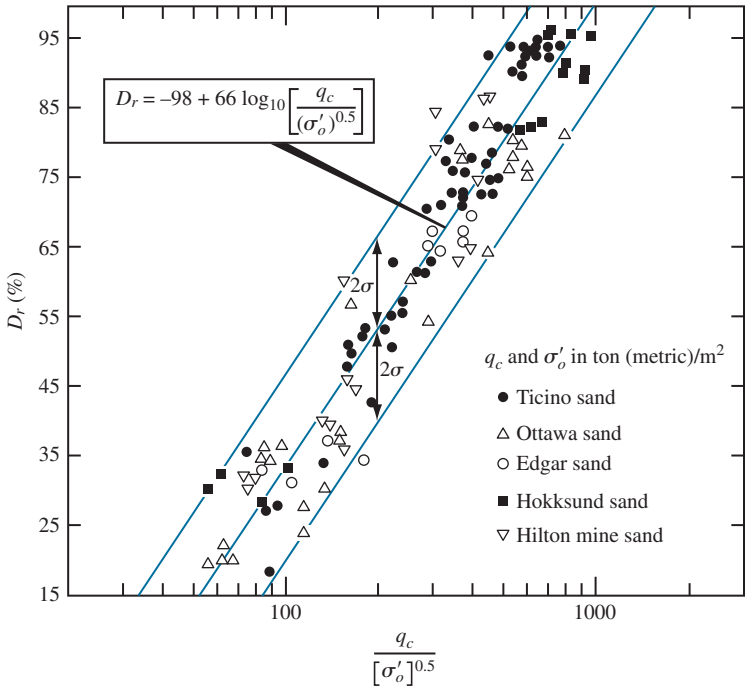


FIGURE 3.29 Relationship between D_r and q_c (Based on Lancellotta, 1983, and Jamiolski et al., 1985)

CORRELATION BETWEEN RELATIVE DENSITY (D_r) AND q_c FOR SAND

Lancellotta (1983) and Jamiolkowski et al. (1985) showed that the relative density of *normally consolidated sand,* D_r, and q_c can be correlated according to the following formula (Figure 3.29):

$$D_r(\%) = A + B \log_{10}\left(\frac{q_c}{\sqrt{\sigma'_o}}\right) \tag{3.49}$$

The preceding relationship can be rewritten as (Kulhawy and Mayne, 1990)

$$D_r(\%) = 68\left[\log\left(\frac{q_c}{\sqrt{p_a \cdot \sigma'_o}}\right) - 1\right] \tag{3.50}$$

where

p_a = atmospheric pressure (≈ 100 kN/m^2 or 2000 lb/ft^2)

σ'_o = vertical effective stress

Kulhawy and Mayne (1990) proposed the following relationship to correlate D_r, q_c, and the vertical effective stress σ'_o:

$$D_r = \sqrt{\left[\frac{1}{305 Q_c \text{OCR}^{1.8}}\right]\left[\frac{\frac{q_c}{p_a}}{\left(\frac{\sigma'_o}{p_a}\right)^{0.5}}\right]} \tag{3.51}$$

In this equation,

OCR = overconsolidation ratio

p_a = atmospheric pressure

Q_c = compressibility factor

The recommended values of Q_c are as follows:

Highly compressible sand = 0.91

Moderately compressible sand = 1.0

Low compressible sand = 1.09

CORRELATION BETWEEN q_c AND DRAINED FRICTION ANGLE (ϕ') FOR SAND

On the basis of experimental results, Robertson and Campanella (1983) suggested the variation of D_r, σ'_o, and ϕ' for normally consolidated quartz sand. This relationship can be expressed as (Kulhawy and Mayne, 1990)

$$\phi' = \tan^{-1}\left[0.1 + 0.38 \log\left(\frac{q_c}{\sigma'_o}\right)\right] \tag{3.52}$$

Based on the cone penetration tests on the soil in the Venice Lagoon (Italy), Ricceri et al. (2002) proposed a similar relationship for soil with classifications of ML and SP-SM as

$$\phi' = \tan^{-1}\left[0.38 + 0.27 \log\left(\frac{q_c}{\sigma'_o}\right)\right] \tag{3.53}$$

Lee et al. (2004) developed a correlation among ϕ', q_c, and the horizontal effective stress (σ'_h) in the form

$$\phi' = 15.575\left(\frac{q_c}{\sigma'_h}\right)^{0.1714} \tag{3.54}$$

CORRELATION BETWEEN q_c AND N_{60}

For granular soil, several correlations have been proposed to correlate q_c and N_{60} (N_{60} = standard penetration resistance) against the mean grain size (D_{50} in mm). These correlations are of the form

$$\frac{\left(\frac{q_c}{p_a}\right)}{N_{60}} = cD_{50}^{a} \tag{3.55}$$

Table 3.9 shows the values of c and a as developed from various studies.

CORRELATIONS OF SOIL TYPES

The soil at a specific depth can be identified from the combination of q_c and f_s values. Robertson et al. (1986) proposed the first soil behavior type chart, which was later updated by Robertson (2010). From this chart, shown in Figure 3.30, it is possible to identify the soil type based on the q_c and F_r values. The values of $(q_c/p_a)/N_{60}$ are shown in parentheses.

TABLE 3.9 Values of c and a [Eq. (3.55)]

Investigator		c	a
Burland and Burbidge (1985)	Upper limit	15.49	0.33
	Lower limit	4.9	0.32
Robertson and Campanella (1983)	Upper limit	10	0.26
	Lower limit	5.75	0.31
Kulhawy and Mayne (1990)		5.44	0.26
Anagnostopoulos et al. (2003)		7.64	0.26

CORRELATIONS FOR UNDRAINED SHEAR STRENGTH (c_u), PRECONSOLIDATION PRESSURE (σ_c'), AND OVERCONSOLIDATION RATIO (OCR) FOR CLAYS

The undrained shear strength, c_u, can be expressed as

$$c_u = \frac{q_c - \sigma_o}{N_k} \tag{3.56}$$

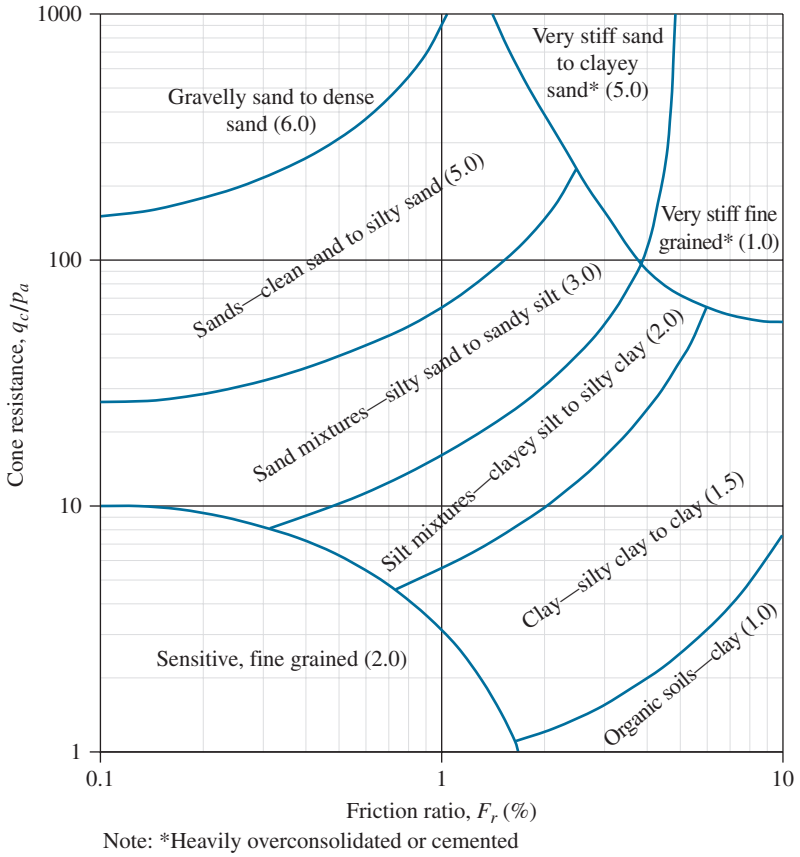


FIGURE 3.30 Soil behavior type chart (Based on Robertson et al., 1986 and Robertson, 2010)

where

σ_o = total vertical stress

N_k = bearing capacity factor

The bearing capacity factor, N_k, may vary from 11 to 19 for normally consolidated clays and may approach 25 for overconsolidated clay. According to Mayne and Kemper (1988),

$$N_k = 15 \text{ (for electric cone)}$$

and

$$N_k = 20 \text{ (for mechanical cone)}$$

Based on tests in Greece, Anagnostopoulos et al. (2003) determined

$$N_k = 17.2 \text{ (for electric cone)}$$

and

$$N_k = 18.9 \text{ (for mechanical cone)}$$

These field tests also showed that

$$c_u = \frac{f_s}{1.26} \text{ (for mechanical cones)} \tag{3.57}$$

and

$$c_u = f_s \text{ (for electrical cones)} \tag{3.58}$$

Mayne and Kemper (1988) provided correlations for preconsolidation pressure (σ'_c) and overconsolidation ratio (OCR) as

$$\underset{\text{MN/m}^2}{\sigma'_c} = 0.243 \underbrace{(q_c)^{0.96}}_{\text{MN/m}^2} \tag{3.59}$$

and

$$\text{OCR} = 0.37\left(\frac{q_c - \sigma_o}{\sigma'_o}\right)^{1.01} \tag{3.60}$$

where σ_o and σ'_o = total and effective stress, respectively.

EXAMPLE 3.4

At a depth of 12.5 m in a *moderately compressible sand deposit*, a cone penetration test showed $q_c = 20$ MN/m^2. For the sand given, $\gamma = 16$ kN/m^3 and OCR = 2. Estimate the relative density of the sand. Use Eq. (3.51).

SOLUTION

Vertical effective stress $\sigma'_o = (12.5)(16) = 200$ kN/m^2.

Q_c (moderately compressible sand) ≈ 1.

From Eq. (3.51),

$$D_r = \sqrt{\frac{1}{305(\text{OCR})^{1.8}}\left[\frac{\left(\frac{q_c}{p_a}\right)}{\left(\frac{\sigma'_o}{p_a}\right)^{0.5}}\right]}$$

$$= \sqrt{\frac{1}{(305)(2)^{1.8}}\left[\frac{\left(\frac{20{,}000\ \text{kN/m}^2}{100\ \text{kN/m}^2}\right)}{\left(\frac{200\ \text{kN/m}^2}{100\ \text{kN/m}^2}\right)^{0.5}}\right]}$$

$$= \sqrt{(0.00094)(141.41)} = 0.365$$

Hence,

$$D_r = \mathbf{36.5\%}$$

3.22 Pressuremeter Test (PMT)

The pressuremeter test is an *in situ* test conducted in a borehole. It was originally developed by Menard (1956) to measure the strength and deformability of soil. It has also been adopted by ASTM as Test Designation 4719. The Menard-type PMT consists essentially of a probe with three cells. The top and bottom ones are *guard cells*, and the middle one is the *measuring cell*, as shown schematically in Figure 3.31a. The test is conducted in a prebored hole with a diameter that is between 1.03 and 1.2 times the nominal diameter of the probe. The probe that is most commonly used has a diameter of 58 mm and a length of 420 mm. The probe cells can be expanded by either liquid or gas. The guard cells are expanded to reduce the end-condition effect on the measuring cell, which has a volume (V_o) of 535 cm^3. Following are the dimensions for the probe diameter and the diameter of the borehole, as recommended by ASTM:

Probe diameter (mm)	Borehole diameter	
	Nominal (mm)	Maximum (mm)
44	45	53
58	60	70
74	76	89

In order to conduct a test, the measuring cell volume, V_o, is measured and the probe is inserted into the borehole. Pressure is applied in increments and the new volume of the cell is measured. The process is continued until the soil fails or until the pressure limit of the device is reached. The soil is considered to have failed when the total volume of the expanded cavity (V) is about twice the volume of the original cavity. Upon completion of the test, the probe is deflated and advanced for testing at another depth.

The results of the pressuremeter test are expressed in the graphical form of pressure versus volume, as shown in Figure 3.31b. In the figure, Zone I represents the reloading portion during which the soil around the borehole is pushed back

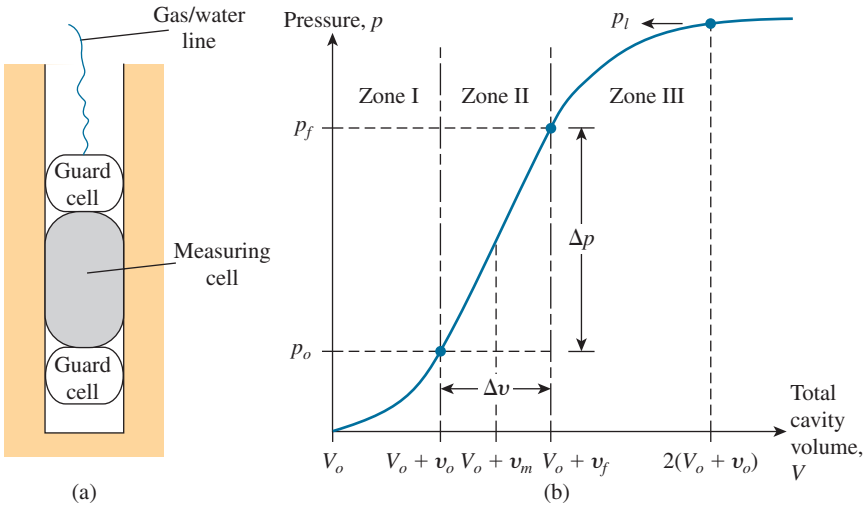


FIGURE 3.31 (a) Pressuremeter; (b) plot of pressure versus total cavity volume

into the initial state (i.e., the state it was in before drilling). The pressure p_o represents the *in situ* total horizontal stress. Zone II represents a pseudoelastic zone in which the cell volume versus cell pressure is practically linear. The pressure p_f represents the creep, or yield, pressure. The zone marked III is the plastic zone. The pressure p_l represents the limit pressure. Figure 3.32 shows a pressuremeter test in the field.

The pressuremeter modulus, E_p, of the soil is determined with the use of the theory of expansion of an infinitely thick cylinder. Thus,

$$E_p = 2(1 + \mu_s)(V_o + v_m)\left(\frac{\Delta p}{\Delta v}\right) \tag{3.61}$$

where

$$v_m = \frac{v_o + v_f}{2}$$

$$\Delta p = p_f - p_o$$

$$\Delta v = v_f - v_o$$

μ_s = Poisson's ratio (which may be assumed to be 0.33)

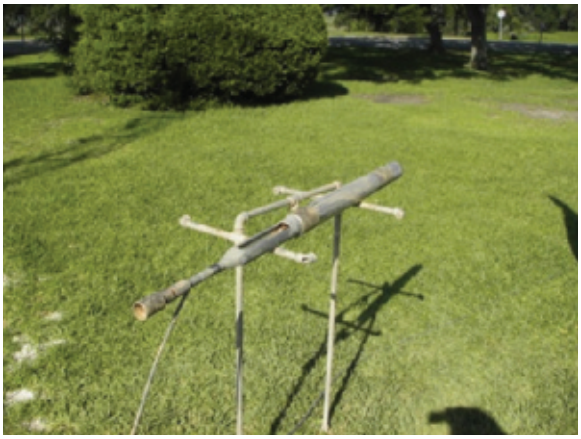
The limit pressure p_l is usually obtained by extrapolation and not by direct measurement.

In order to overcome the difficulty of preparing the borehole to the proper size, self-boring pressuremeters (SBPMTs) have also been developed. Detailed information on SBPMTs can be found in the work of Baguelin et al. (1978).

Correlations between various soil parameters and the results obtained from the pressuremeter tests have been developed by various investigators. Kulhawy and Mayne (1990) proposed that, for clays,

$$\sigma_c' = 0.45 p_l \tag{3.62}$$

where σ_c' = preconsolidation pressure.



(a)



(c)



(b)



(d)

FIGURE 3.32 Pressuremeter test in the field: (a) the pressuremeter probe; (b) drilling the bore hole by wet rotary method; (c) pressuremeter control unit with probe in the background; (d) getting ready to insert the pressuremeter probe into the borehole (Courtesy of Jean-Louis Briaud, Texas A&M University, College Station, TX)

On the basis of the cavity expansion theory, Baguelin et al. (1978) proposed that

$$c_u = \frac{(p_l - p_o)}{N_p} \tag{3.63}$$

where

c_u = undrained shear strength of a clay

$$N_p = 1 + \ln\left(\frac{E_p}{3c_u}\right)$$

Typical values of N_p vary between 5 and 12, with an average of about 8.5. Ohya et al. (1982) (see also Kulhawy and Mayne, 1990) correlated E_p with field standard penetration numbers (N_{60}) for sand and clay as follows:

$$\text{Clay: } E_p(\text{kN/m}^2) = 1930\, N_{60}^{0.63} \tag{3.64}$$

$$\text{Sand: } E_p(\text{kN/m}^2) = 908\, N_{60}^{0.66} \tag{3.65}$$

3.23 Dilatometer Test

The flat-plate dilatometer test (DMT) accessories (Marchetti, 1980; Schmertmann, 1986) essentially consists of a flat plate measuring 220 mm (length) × 95 mm (width) × 14 mm (thickness) (8.66 in. × 3.74 in. × 0.55 in.). A thin, flat, circular, expandable steel membrane having a diameter of 60 mm (2.36 in.) is located flush at the center on one side of the plate (Figure 3.33a). Figure 3.34 shows two flat-plate dilatometers with other instruments for conducting a test in the field. The dilatometer probe is inserted into the ground with a cone penetrometer testing rig (Figure 3.33b). Gas and electric lines extend from the surface control box, through the penetrometer rod, and into the blade. At the required depth, high-pressure nitrogen gas is used to inflate the membrane. Two pressure readings are taken:

1. The pressure A required to "lift off" the membrane.
2. The pressure B at which the membrane expands 1.1 mm (0.4 in.) into the surrounding soil.

The A and B readings are corrected as follows (Schmertmann, 1986):

$$\text{Contact stress, } p_o = 1.05(A + \Delta A - Z_m) - 0.05(B - \Delta B - Z_m) \tag{3.66}$$

$$\text{Expansion stress, } p_1 = B - Z_m - \Delta B \tag{3.67}$$

where

ΔA = vacuum pressure required to keep the membrane in contact with its seating

ΔB = air pressure required inside the membrane to deflect it outward to a center expansion of 1.1 mm

Z_m = gauge pressure deviation from zero when vented to atmospheric pressure

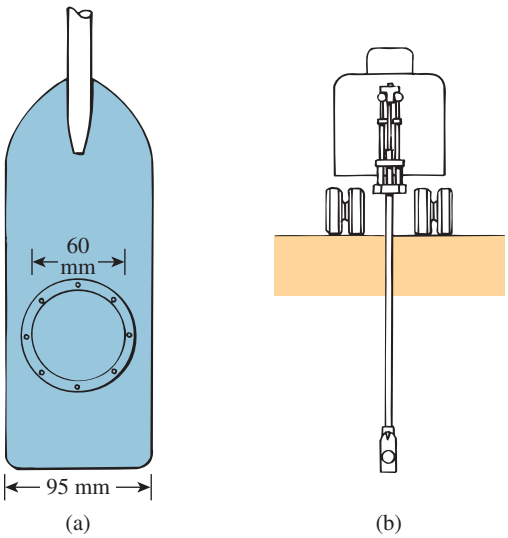


FIGURE 3.33 (a) Schematic diagram of a flat-plate dilatometer; (b) dilatometer probe inserted into ground

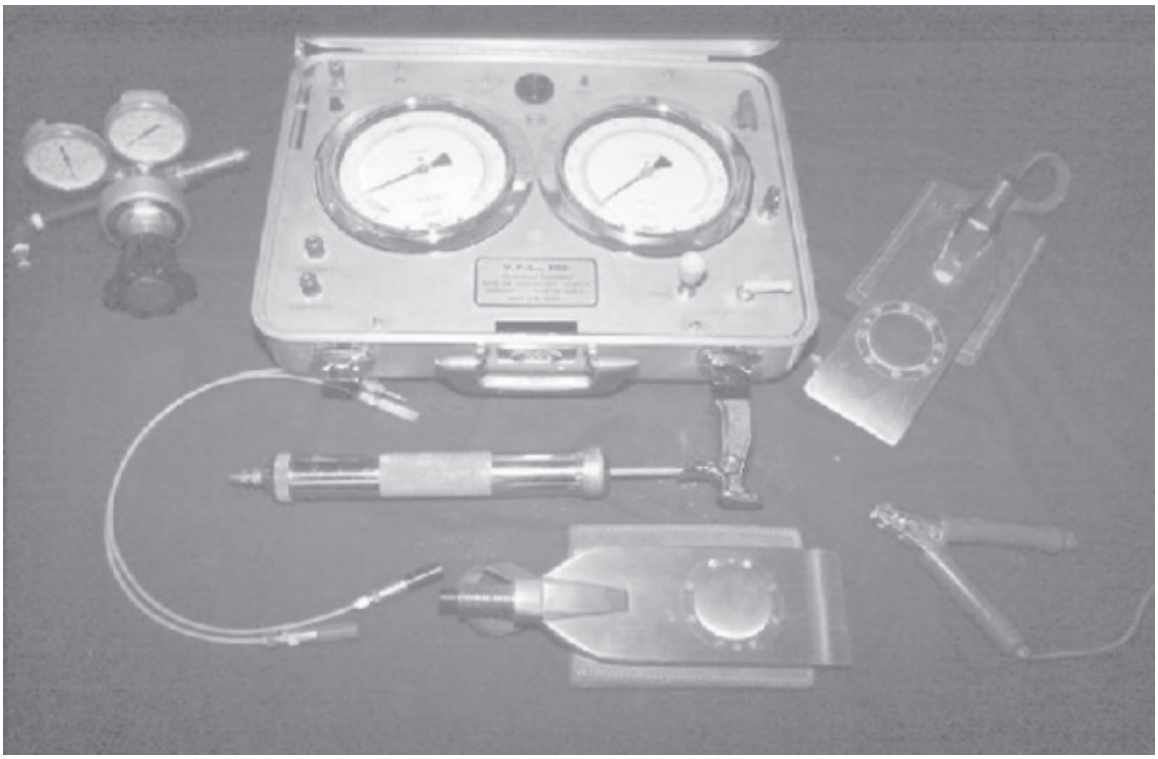


FIGURE 3.34 Dilatometer and other accessories (Courtesy of N. Sivakugan, James Cook University, Australia)

The test is normally conducted at depths 200 to 300 mm apart. The result of a given test is used to determine three parameters:

1. Material index, $I_D = \dfrac{p_1 - p_o}{p_o - u_o}$
2. Horizontal stress index, $K_D = \dfrac{p_o - u_o}{\sigma'_o}$
3. Dilatometer modulus, $E_D(\text{kN/m}^2) = 34.7\ [p_1(\text{kN/m}^2) - p_o\ (\text{kN/m}^2)]$

where

u_o = pore water pressure

σ'_o = *in situ* vertical effective stress

Figure 3.35 shows the results of a dilatometer test conducted in Bangkok soft clay and reported by Shibuya and Hanh (2001). Based on his initial tests, Marchetti (1980) provided the following correlations:

$$K_o = \left(\frac{K_D}{1.5}\right)^{0.47} - 0.6 \tag{3.68}$$

$$\text{OCR} = (0.5K_D)^{1.56} \tag{3.69}$$

$$\frac{c_u}{\sigma'_o} = 0.22 \qquad \text{(for normally consolidated clay)} \tag{3.70}$$

$$\left(\frac{c_u}{\sigma'_o}\right)_{\text{OC}} = \left(\frac{c_u}{\sigma'_o}\right)_{\text{NC}} (0.5K_D)^{1.25} \tag{3.71}$$

$$E_s = (1 - \mu_s^2)E_D \tag{3.72}$$

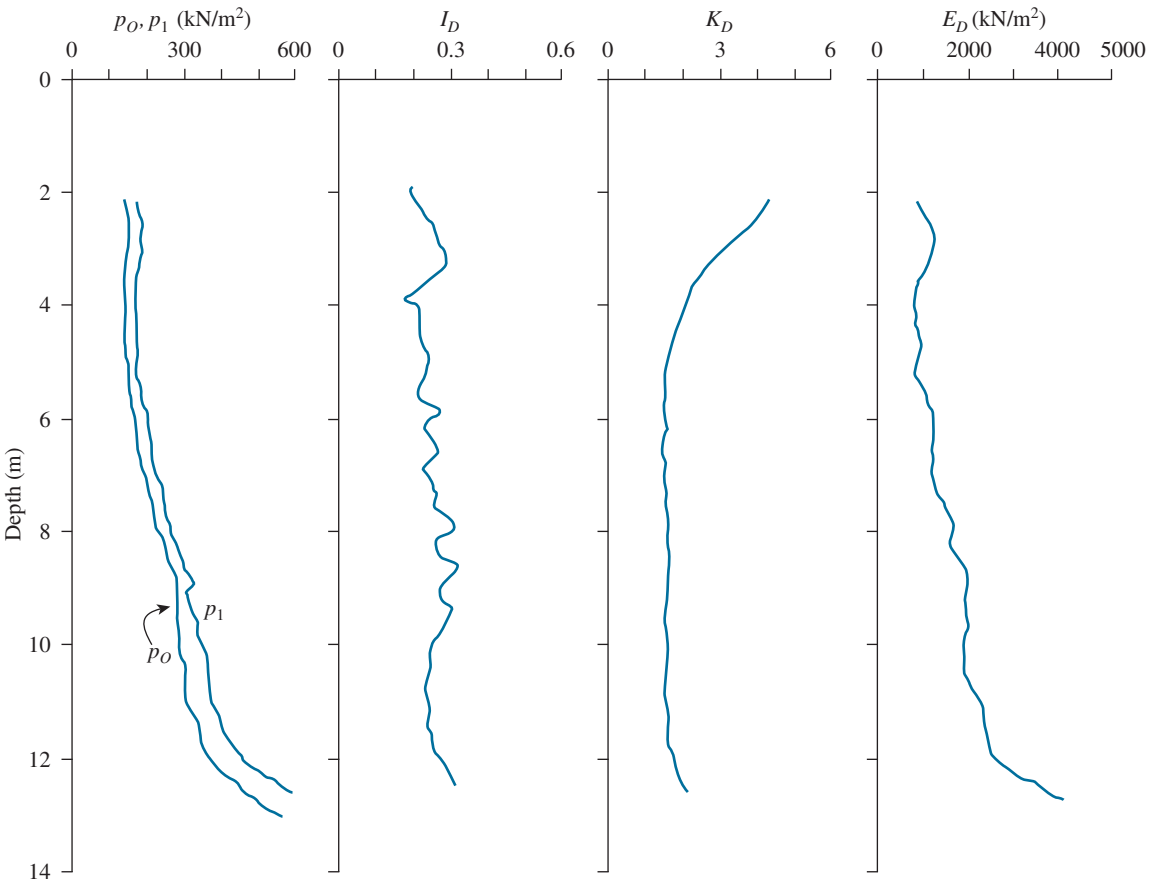


FIGURE 3.35 A dilatometer test result conducted on soft Bangkok clay (Based on Lancellotta, 1983, and Jamiolski et al., 1985)

where

K_o = coefficient of at-rest earth pressure

OCR = overconsolidation ratio

OC = overconsolidated soil

NC = normally consolidated soil

E_s = modulus of elasticity

Other relevant correlations using the results of dilatometer tests are as follows:

- For undrained cohesion in clay (Kamei and Iwasaki, 1995):

$$c_u = 0.35\sigma'_o\,(0.47K_D)^{1.14} \tag{3.73}$$

- For soil friction angle (ML and SP-SM soil) (Ricceri et al., 2002):

$$\phi' = 31 + \frac{K_D}{0.236 + 0.066K_D} \tag{3.74a}$$

$$\phi'_{\text{ult}} = 28 + 14.6 \log K_D - 2.1(\log K_D)^2 \tag{3.74b}$$

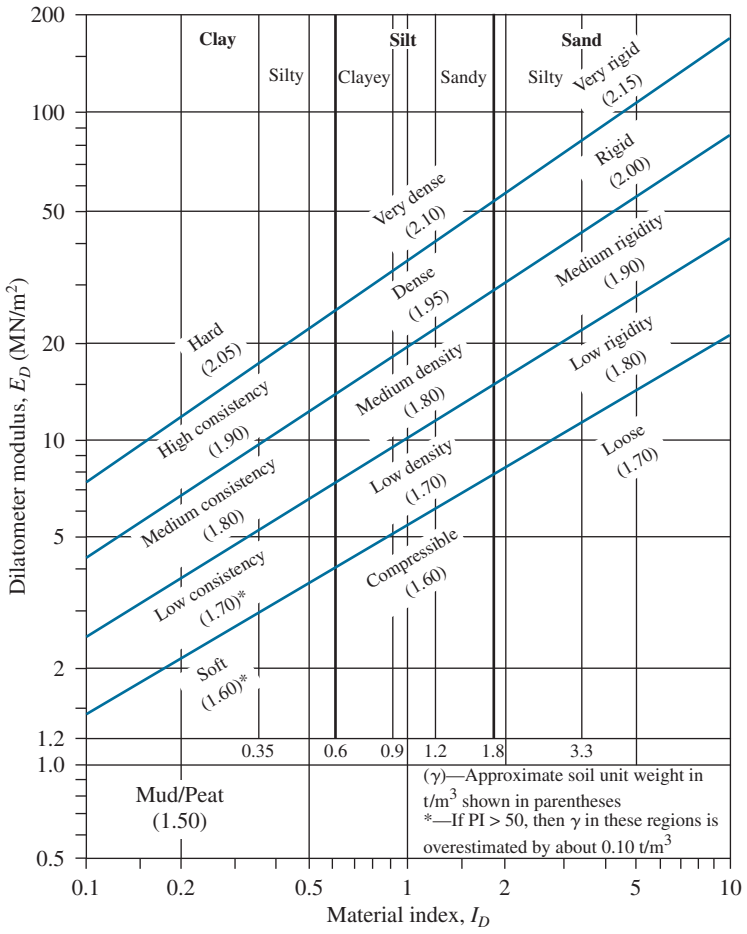


FIGURE 3.36 Chart for determination of soil description and unit weight (After Schmertmann, 1986) (*Note:* 1 t/m^3 = 9.81 kN/m^3) (Based on Schmertmann, J. H. (1986). "Suggested method for performing that flat dilatometer test," *Geotechnical Testing Journal*, ASTM, Vol. 9, No. 2, pp. 93–101, Fig. 2)

Schmertmann (1986) also provided a correlation between the material index (I_D) and the dilatometer modulus (E_D) for a determination of the nature of the soil and its unit weight (γ). This relationship is shown in Figure 3.36.

3.24 Iowa Borehole Shear Test

The Iowa borehole shear test is a simple device to determine the shear strength parameters of soil at a given depth during subsoil exploration. The shear device consists of two grooved plates that are pushed into the borehole (Figure 3.37). A controlled normal force (N) can be applied to each of the grooved plates. Shear failure in soil close to the plates is induced by applying a vertical force S, after allowing the soil to consolidate under the normal stress (5 minutes in sand and 10 to 20 minutes in clay). The effective normal stress (σ') on the wall of the borehole can be given as

$$\sigma' = \frac{N}{A} \tag{3.75}$$

where A = area of each plate in contact with the soil.

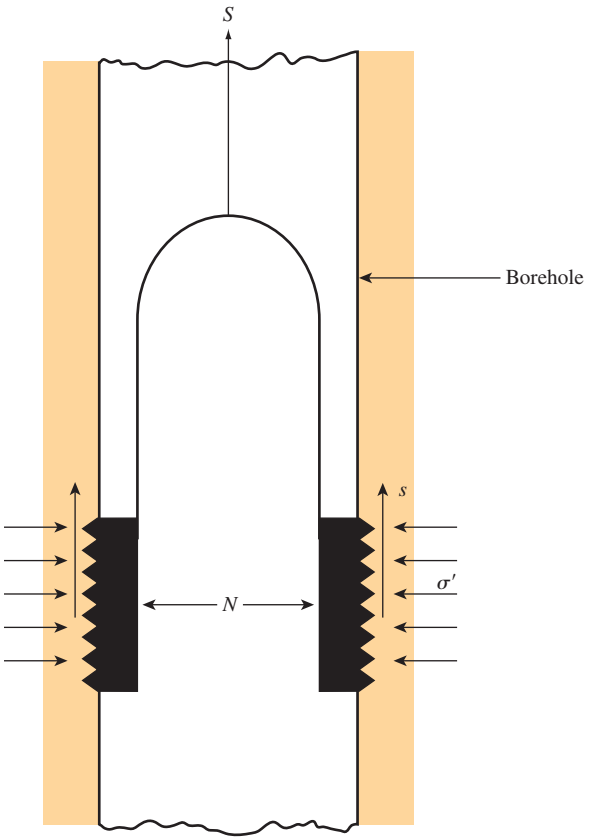


FIGURE 3.37 Iowa borehole shear test

Similarly, the shear stress at failure (s) is

$$s = \frac{S}{2A} \tag{3.76}$$

The test could be repeated with a number of increasing normal forces (N) without removing the shearing device. The results can be plotted in graphic form (Figure 3.38) to obtain the shear strength parameters (that is, cohesion c' and angle of friction ϕ') of the soil. The shear strength parameters obtained in this manner are likely to represent those of a consolidated drained test.

Figure 3.39 shows a shear head and a hand pump.

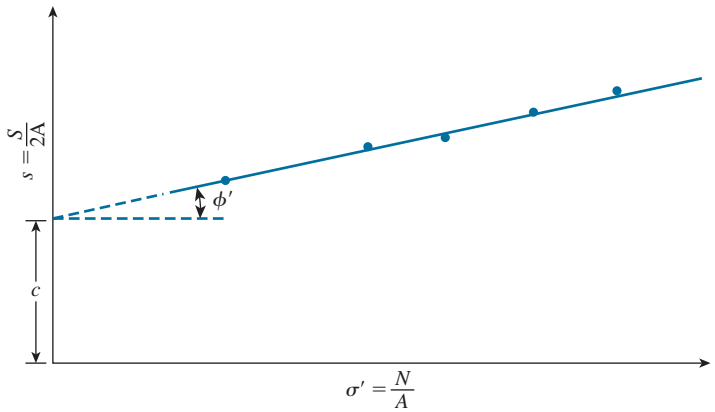


FIGURE 3.38 Variation of s with σ' from Iowa borehole shear test



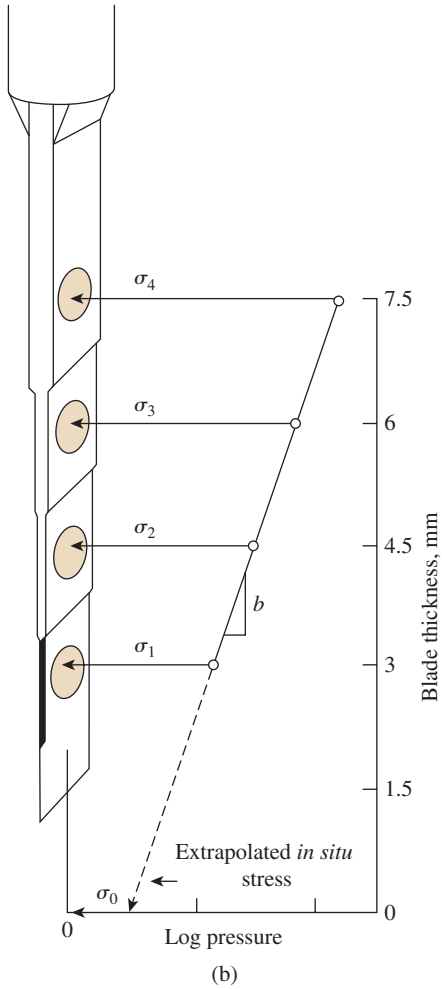
FIGURE 3.39 Shear head and hand pump (Courtesy of R. L. Handy, Iowa State University, Ames, IA)

3.25 K_0 Stepped-Blade Test

In the 1970s, the K_0 stepped-blade test for measuring lateral *in situ* stress (and hence K_0 as the at-rest earth pressure coefficient) was developed by Dr. Richard L. Handy at Iowa State University. Figure 3.40a shows a K_0 stepped-blade test in progress. The long blade consists of four steps, 100 mm apart, ranging from 3 mm thin to 7.5 mm thick from its bottom to its top (Figure 3.40b). Even the thickest step is thinner than



(a)



(b)

FIGURE 3.40 K_0 stepped-blade test: (a) Test in progress in the field; (b) Schematic diagram of the blade (Courtesy of R. L. Handy, Iowa State University, Ames, IA)

the dilatometer; therefore, the soil disturbance is relatively less. Each step carries a pneumatic pressure cell flush with the flat surface that comes in contact with the soil when pushed into it.

The test is conducted in a borehole where the first blade is pushed into the soil at the bottom of the hole and the stress in the bottom step, σ_1, is measured. The second blade is pushed into the soil and the stress in the bottom two steps (σ_1 and σ_2) is measured. This is repeated until all of the steps are in the soil, giving 14 ($= 1+2+3+4+4$) stress measurements. The fifth step has the same thickness as the fourth but with no pressure cell (see Figure 3.40b). As shown in Figure 3.40b, the logarithm of stress is plotted against the blade thickness. The stress corresponding to zero blade thickness, σ_0, is extrapolated from the figure and is taken as the *total in situ* horizontal stress from which K_0 can be computed once the pore water pressure is known from the ground-water table depth. The pressure should increase with blade thickness. Any data that do not show an increase in stress with an increase in step thickness must be discarded, and only the remaining data should be used in estimating the *in situ* horizontal stress.

3.26 Coring of Rocks

When a rock layer is encountered during a drilling operation, rock coring may be necessary. To core rocks, a *core barrel* is attached to a drilling rod. A *coring bit* is attached to the bottom of the barrel (Figure 3.41). The cutting elements may be diamond, tungsten, carbide, and so on. Table 3.10 summarizes the various types of core barrels and their sizes, as well as the compatible drill rods commonly used for

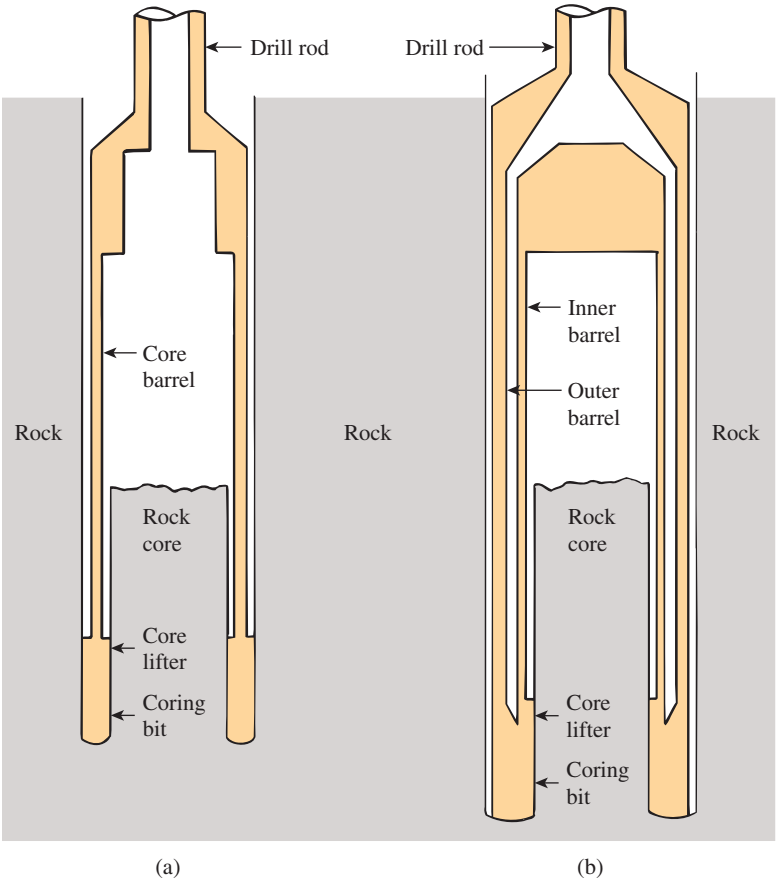


FIGURE 3.41 Rock coring: (a) single-tube core barrel; (b) double-tube core barrel

TABLE 3.10 Standard Size and Designation of Casing, Core Barrel, and Compatible Drill Rod

Casing and core barrel designation	Outside diameter of core barrel bit		Drill rod designation	Outside diameter of drill rod		Diameter of borehole		Diameter of core sample	
	(mm)	(in.)		(mm)	(in.)	(mm)	(in.)	(mm)	(in.)
EX	36.51	$1\frac{7}{16}$	E	33.34	$1\frac{5}{16}$	38.1	$1\frac{1}{2}$	22.23	$\frac{7}{8}$
AX	47.63	$1\frac{7}{8}$	A	41.28	$1\frac{5}{8}$	50.8	2	28.58	$1\frac{1}{8}$
BX	58.74	$2\frac{5}{16}$	B	47.63	$1\frac{7}{8}$	63.5	$2\frac{1}{2}$	41.28	$1\frac{5}{8}$
NX	74.61	$2\frac{15}{16}$	N	60.33	$2\frac{3}{8}$	76.2	3	53.98	$2\frac{1}{8}$

exploring foundations. The coring is advanced by rotary drilling. Water is circulated through the drilling rod during coring, and the cutting is washed out.

Two types of core barrel are available: the *single-tube core barrel* (Figure 3.41a) and the *double-tube core barrel* (Figure 3.41b). Rock cores obtained by single-tube core barrels can be highly disturbed and fractured because of torsion. Rock cores smaller than the BX size tend to fracture during the coring process. Figure 3.42 shows a diamond coring bit. Figure 3.43 shows the end and side views of a diamond coring bit attached to a double-tube core barrel.

When the core samples are recovered, the depth of recovery should be properly recorded for further evaluation in the laboratory. Based on the length of the rock core recovered from each run, the following quantities may be calculated for a general evaluation of the rock quality encountered:

$$\text{Recovery ratio} = \frac{\text{length of core recovered}}{\text{theoretical length of rock cored}} \tag{3.77}$$

$$\text{Rock quality designation (RQD)} = \frac{\Sigma \text{ length of recovered pieces equal to or larger than 101.6 mm (4 in.)}}{\text{theoretical length of rock cored}} \tag{3.78}$$

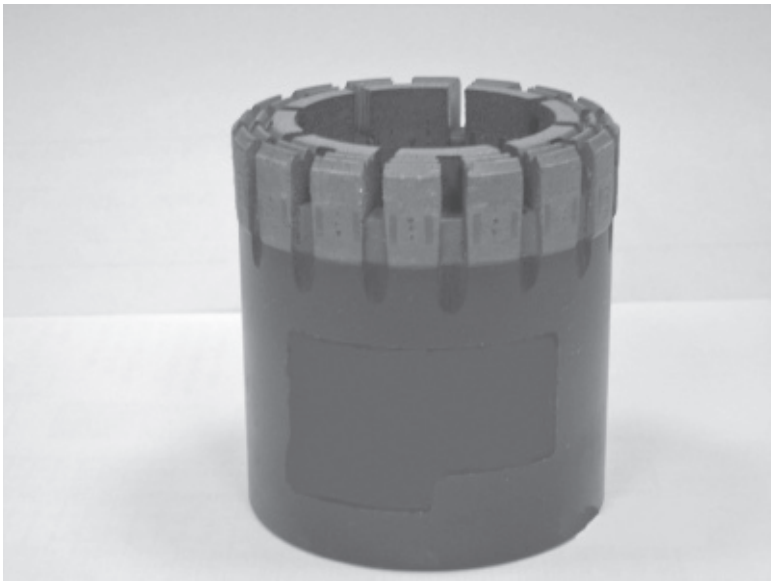


FIGURE 3.42 Diamond coring bit (Courtesy of Braja M. Das, Henderson, NV)



(a)



(b)

FIGURE 3.43 Diamond coring bit attached to a double-tube core barrel: (a) end view; (b) side view (Courtesy of Professional Service Industries, Inc. (PSI), Waukesha, WI)

A recovery ratio of unity indicates the presence of intact rock; for highly fractured rocks, the recovery ratio may be 0.5 or smaller. Table 3.11 presents the general relationship (Deere, 1963) between the RQD and the *in situ* rock quality.

TABLE 3.11 Relation Between *in situ* Rock Quality and RQD

RQD	Rock quality
0–0.25	Very poor
0.25–0.5	Poor
0.5–0.75	Fair
0.75–0.9	Good
0.9–1	Excellent

3.27 Preparation of Boring Logs

The detailed information gathered from each borehole is presented in a graphical form called the *boring log*. As a borehole is advanced downward, the driller generally should record the following information in a standard log:

1. Name and address of the drilling company
2. Driller's name
3. Job description and number
4. Number, type, and location of boring
5. Date of boring
6. Subsurface stratification, which can be obtained by visual observation of the soil brought out by auger, split-spoon sampler, and thin-walled Shelby tube sampler
7. Elevation of water table and date observed, use of casing and mud losses, and so on
8. Standard penetration resistance and the depth of SPT
9. Number, type, and depth of soil sample collected
10. In case of rock coring, type of core barrel used and, for each run, the actual length of coring, length of core recovery, and RQD

This information should never be left to memory, because doing so often results in erroneous boring logs.

After completion of the necessary laboratory tests, the geotechnical engineer prepares a finished log that includes notes from the driller's field log and the results of tests conducted in the laboratory. Figure 3.44 shows a typical boring log. These

Boring Log

Name of the Project: Two-story apartment building

Location: Johnson & Olive St. Date of Boring: March 2, 2015

Boring No.: 3 Type of Boring: Hollow-stem auger Ground Elevation: 60.8 m

Soil description	Depth (m)	Soil sample type and number	N_{60}	w_n (%)	Comments
Light brown clay (fill)					
Silty sand (SM)	1–2	SS-1	9	8.2	
°G.W.T. 3.5 m	3	SS-2	12	17.6	LL = 38 PI = 11
Light gray clayey silt (ML)	4–5	ST-1		20.4	LL = 36 q_u = 112 kN/m^2
	6	SS-3	11	20.6	
Sand with some gravel (SP)	7				
End of boring @ 8 m	8	SS-4	27	9	

N_{60} = standard penetration number
w_n = natural moisture content
LL = liquid limit; PI = plasticity index
q_u = unconfined compression strength
SS = split-spoon sample; ST = Shelby tube sample

Groundwater table observed after one week of drilling

FIGURE 3.44 A typical boring log

logs have to be attached to the final soil exploration report submitted to the client. The figure also lists the classifications of the soil in the left-hand column, along with the description of each soil (based on the Unified Soil Classification System).

3.28 Geophysical Exploration

Several types of geophysical exploration techniques permit a rapid evaluation of subsoil characteristics. These methods also allow rapid coverage of large areas and are less expensive than conventional exploration by drilling. However, in many cases, definitive interpretation of the results is difficult. For that reason, such techniques should be used for preliminary work only. Here, we discuss three types of geophysical exploration techniques: the seismic refraction survey, cross-hole seismic survey, and resistivity survey.

SEISMIC REFRACTION SURVEY

Seismic refraction surveys are useful in obtaining preliminary information about the thickness of the layering of various soil and the depth to rock or hard soil at a site. Refraction surveys are conducted by impacting the surface, such as at point *A* in Figure 3.45a, and observing the first arrival of the disturbance (stress waves) at several other points (e.g., *B, C, D*, . . .). The impact can be created by a hammer blow or by a small explosive charge. The first arrival of disturbance waves at various points can be recorded by geophones.

The impact on the ground surface creates two types of *stress waves: P waves* (*plane waves* or *compression waves*) and *S waves* (or *shear waves*). *P* waves travel faster than *S* waves; hence, the first arrival of disturbance waves will be related

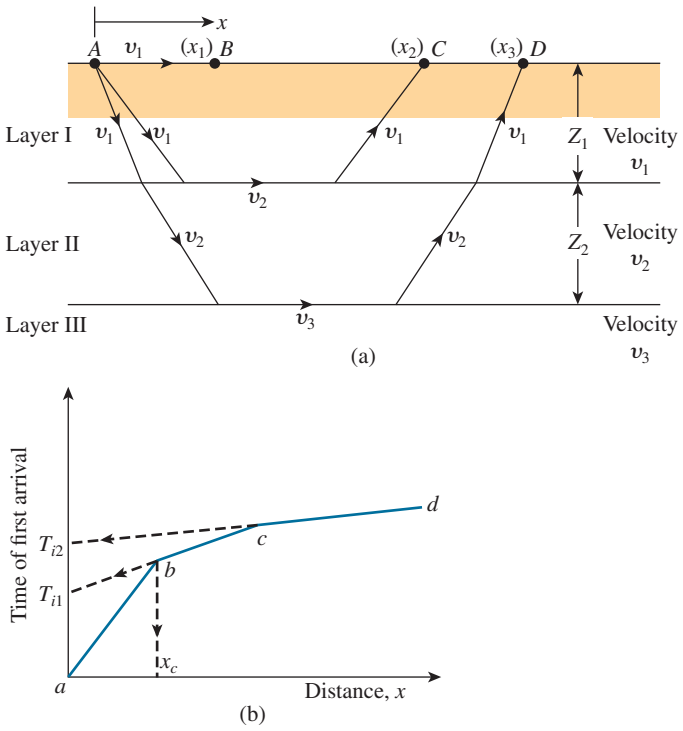


FIGURE 3.45 Seismic refraction survey

to the velocities of the *P* waves in various layers. The velocity of *P* waves in a medium is

$$v = \sqrt{\frac{E_s}{\left(\frac{\gamma}{g}\right)} \frac{(1 - \mu_s)}{(1 - 2\mu_s)(1 + \mu_s)}} \tag{3.79}$$

where

E_s = modulus of elasticity of the medium

γ = unit weight of the medium

g = acceleration due to gravity

μ_s = Poisson's ratio

To determine the velocity v of *P* waves in various layers and the thicknesses of those layers, we use the following procedure:

Step 1. Obtain the times of first arrival, $t_1, t_2, t_3, \ldots$, at various distances $x_1, x_2, x_3, \ldots$ from the point of impact.

Step 2. Plot a graph of time t against distance x. The graph will look like the one shown in Figure 3.45b.

Step 3. Determine the slopes of the lines *ab, bc, cd*, . . . :

$$\text{Slope of } ab = \frac{1}{v_1}$$

$$\text{Slope of } bc = \frac{1}{v_2}$$

$$\text{Slope of } cd = \frac{1}{v_3}$$

Here, $v_1, v_2, v_3, \ldots$ are the *P*-wave velocities in layers I, II, III, . . . , respectively (Figure 3.45a).

Step 4. Determine the thickness of the top layer:

$$Z_1 = \frac{1}{2}\sqrt{\frac{v_2 - v_1}{v_2 + v_1}}\, x_c \tag{3.80}$$

The value of x_c can be obtained from the plot, as shown in Figure 3.45b.

Step 5. Determine the thickness of the second layer:

$$Z_2 = \frac{1}{2}\left[T_{i2} - 2Z_1\frac{\sqrt{v_3^2 - v_1^2}}{v_3 v_1}\right]\frac{v_3 v_2}{\sqrt{v_3^2 - v_2^2}} \tag{3.81}$$

Here, T_{i2} is the time intercept of the line *cd* in Figure 3.45b, extended backward.

(For detailed derivatives of these equations and other related information, see Dobrin, 1960, and Das, 1992.)

The velocities of *P* waves in various layers indicate the types of soil or rock that are present below the ground surface. The range of the *P*-wave velocity that is generally encountered in different types of soil and rock at shallow depths is given in Table 3.12.

TABLE 3.12 Range of *P*-Wave Velocity in Various Soil and Rocks

Type of soil or rock	*P*-wave velocity	
	m/s	ft/s
Soil		
Sand, dry silt, and fine-grained topsoil	200–1000	650–3300
Alluvium	500–2000	1650–6600
Compacted clays, clayey gravel, and dense clayey sand	1000–2500	3300–8200
Loess	250–750	800–2450
Rock		
Slate and shale	2500–5000	8200–16,400
Sandstone	1500–5000	4900–16,400
Granite	4000–6000	13,100–19,700
Sound limestone	5000–10,000	16,400–32,800

In analyzing the results of a refraction survey, two limitations need to be kept in mind:

1. The basic equations for the survey—that is, Eqs. (3.80) and (3.81)—are based on the assumption that the *P*-wave velocity $v_1 < v_2 < v_3 < \ldots$.
2. When a soil is saturated below the water table, the *P*-wave velocity may be deceptive. *P* waves can travel with a velocity of about 1500 m/s (5000 ft/s) through water. For dry, loose soil, the velocity may be well below 1500 m/s. However, in a saturated condition, the waves will travel through water that is present in the void spaces with a velocity of about 1500 m/s. If the presence of groundwater has not been detected, the *P*-wave velocity may be erroneously interpreted to indicate a stronger material (e.g., sandstone) than is actually present *in situ.* In general, geophysical interpretations should always be verified by the results obtained from borings.

EXAMPLE 3.5

The results of a refraction survey at a site are given in the following table:

Distance of geophone from the source of disturbance (m)	Time of first arrival ($s \times 10^3$)
2.5	11.2
5	23.3
7.5	33.5
10	42.4
15	50.9
20	57.2
25	64.4
30	68.6
35	71.1
40	72.1
50	75.5

Determine the *P*-wave velocities and the thickness of the material encountered.

SOLUTION

Velocity

In Figure 3.46, the times of first arrival of the *P* waves are plotted against the distance of the geophone from the source of disturbance. The plot has three straight-line segments. The velocity of the top three layers can now be calculated as:

$$\text{Slope of segment } 0a = \frac{1}{v_1} = \frac{\text{time}}{\text{distance}} = \frac{23 \times 10^{-3}}{5.25}$$

or

$$v_1 = \frac{5.25 \times 10^3}{23} = \mathbf{228\ m/s\ (top\ layer)}$$

$$\text{Slope of segment } ab = \frac{1}{v_2} = \frac{13.5 \times 10^{-3}}{11}$$

or

$$v_2 = \frac{11 \times 10^3}{13.5} = \mathbf{814.8\ m/s\ (middle\ layer)}$$

$$\text{Slope of segment } bc = \frac{1}{v_3} = \frac{3.5 \times 10^{-3}}{14.75}$$

or

$$v_3 = \mathbf{4214\ m/s\ (third\ layer)}$$

Comparing the velocities obtained here with those given in Table 3.12 indicates that the third layer is a *rock layer.*

Thickness of Layers

From Figure 3.46, $x_c = 10.5$ m, so

$$Z_1 = \frac{1}{2}\sqrt{\frac{v_2 - v_1}{v_2 + v_1}}x_c$$

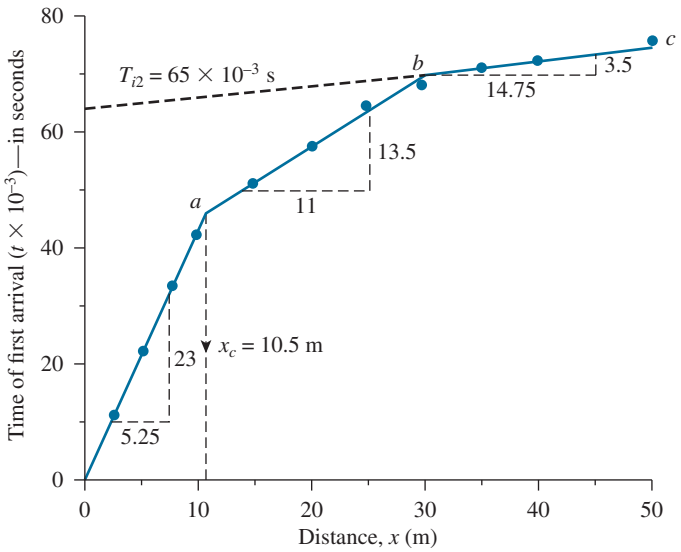


FIGURE 3.46 Plot of first arrival time of *P* wave versus distance of geophone from source of disturbance

Thus,

$$Z_1 = \frac{1}{2}\sqrt{\frac{814.8 - 228}{814.8 + 228}} \times 10.5 = \mathbf{3.94\ m}$$

Again, from Eq. (3.81),

$$Z_2 = \frac{1}{2}\left[T_{i2} - \frac{2Z_1\sqrt{v_3^2 - v_1^2}}{(v_3 v_1)}\right]\frac{(v_3)(v_2)}{\sqrt{v_3^2 - v_2^2}}$$

The value of T_{i2} (from Figure 3.46) is 65×10^{-3} s. Hence,

$$Z_2 = \frac{1}{2}\left[65 \times 10^{-3} - \frac{2(3.94)\sqrt{(4214)^2 - (228)^2}}{(4214)(228)}\right]\frac{(4214)(814.8)}{\sqrt{(4214)^2 - (814.8)^2}}$$

$$= \frac{1}{2}(0.065 - 0.0345)830.47 = \mathbf{12.66\ m}$$

Thus, the rock layer lies at a depth of $Z_1 + Z_2 = 3.94 + 12.66 = \mathbf{16.60\ m}$ from the surface of the ground.

CROSS-HOLE SEISMIC SURVEY

The velocity of shear waves created as the result of an impact to a given layer of soil can be effectively determined by the *cross-hole seismic survey* (Stokoe and Woods, 1972). The principle of this technique is illustrated in Figure 3.47, which shows two holes drilled into the ground a distance L apart. A vertical impulse is created at the bottom of one borehole by means of an impulse rod. The shear waves thus generated are recorded by a vertically sensitive transducer. The velocity of shear waves can be calculated as

$$v_s = \frac{L}{t} \tag{3.82}$$

where t = travel time of the waves.

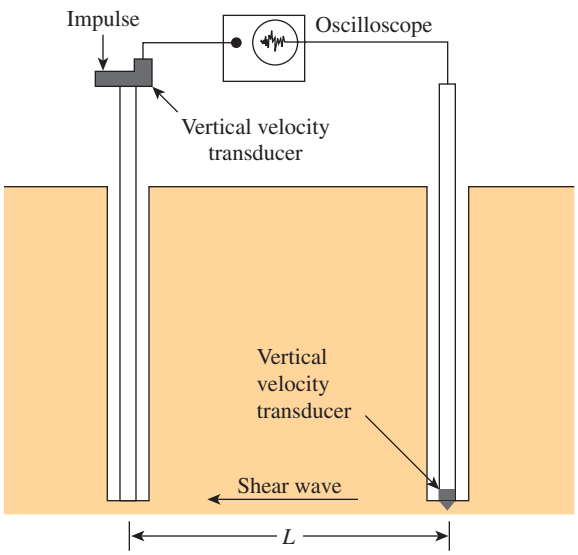


FIGURE 3.47 Cross-hole method of seismic survey

The shear modulus G_s of the soil at the depth at which the test is taken can be determined from the relation

$$v_s = \sqrt{\frac{G_s}{(\gamma/g)}}$$

or

$$G_s = \frac{v_s^2 \gamma}{g} \tag{3.83}$$

where

v_s = velocity of shear waves

γ = unit weight of soil

g = acceleration due to gravity

The shear modulus is useful in the design of foundations to support vibrating machinery and the like.

RESISTIVITY SURVEY

Another geophysical method for subsoil exploration is the *electrical resistivity survey.* The electrical resistivity of any conducting material having a length L and an area of cross section A can be defined as

$$\rho = \frac{RA}{L} \tag{3.84}$$

where R = electrical resistance.

The unit of resistivity is *ohm-centimeter* or *ohm-meter.* The resistivity of various soil depends primarily on their moisture content and also on the concentration of dissolved ions in them. Saturated clays have a very low resistivity; dry soil and rocks have a high resistivity. The range of resistivity generally encountered in various soil and rocks is given in Table 3.13.

The most common procedure for measuring the electrical resistivity of a soil profile makes use of four electrodes driven into the ground and spaced equally along a straight line. The procedure is generally referred to as the *Wenner method* (Figure 3.48a). The two outside electrodes are used to send an electrical current I (usually a dc current with nonpolarizing potential electrodes) into the ground. The current is typically in the range of 50 to 100 mA. The voltage drop, V, is measured between the two inside electrodes. If the soil profile is homogeneous, its electrical resistivity is

$$\rho = \frac{2\pi dV}{I} \tag{3.85}$$

In most cases, the soil profile may consist of various layers with different resistivities, and Eq. (3.85) will yield the *apparent resistivity.* To obtain the *actual*

TABLE 3.13 Representative Values of Resistivity

Material	Resistivity (ohm · m)
Sand	500–1500
Clays, saturated silt	0–100
Clayey sand	200–500
Gravel	1500–4000
Weathered rock	1500–2500
Sound rock	>5000

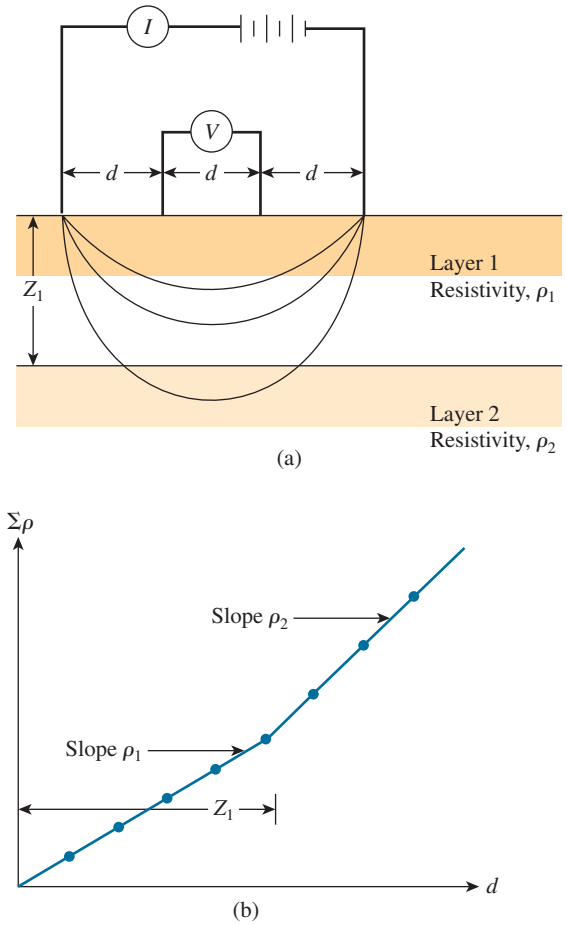


FIGURE 3.48 Electrical resistivity survey: (a) Wenner method; (b) empirical method for determining resistivity and thickness of each layer

resistivity of various layers and their thicknesses, one may use an empirical method that involves conducting tests at various electrode spacings (i.e., d is changed). The sum of the apparent resistivities, $\Sigma\rho$, is plotted against the spacing d, as shown in Figure 3.48b. The plot thus obtained has relatively straight segments, the slopes of which give the resistivity of individual layers. The thicknesses of various layers can be estimated as shown in Figure 3.48b.

The resistivity survey is particularly useful in locating gravel deposits within a fine-grained soil. Some recent geophysical methods include *ground penetrating radar* (GPR), *spectral analysis of surface waves* (SASW), and *multichannel analysis of surface waves* (MASW). The geophysical methods in general are very effective in covering a large terrain. In addition to determining the soil profile, these methods can also be used to determine the shear wave velocity, an important property in dynamic problems in soil.

3.29 Subsoil Exploration Report

At the end of all soil exploration programs, the soil and rock specimens collected in the field are subject to visual observation and appropriate laboratory testing. (The basic soil tests were described in Chapter 2.) After all the required information has been compiled, a soil exploration report is prepared for use by the design office and for reference during future construction work. Although the details and sequence of information in such reports may vary to some degree, depending on the structure

under consideration and the person compiling the report, each report should include the following items:

1. A description of the scope of the investigation
2. A description of the proposed structure for which the subsoil exploration has been conducted
3. A description of the location of the site, including any structures nearby, drainage conditions, the nature of vegetation on the site and surrounding it, and any other features unique to the site
4. A description of the geological setting of the site
5. Details of the field exploration—that is, number of borings, depths of borings, types of borings involved, and so on
6. A general description of the subsoil conditions, as determined from soil specimens and from related laboratory tests, standard penetration resistance and cone penetration resistance, and so on
7. A description of the water-table conditions
8. Recommendations regarding the foundation, including the type of foundation recommended, the allowable bearing pressure, and any special construction procedure that may be needed; alternative foundation design procedures should also be discussed in this portion of the report
9. Conclusions and limitations of the investigations

The following graphical presentations should be attached to the report:

1. A site location map
2. A plan view of the location of the borings with respect to the proposed structures and those nearby
3. Boring logs
4. Laboratory test results
5. Other special graphical presentations

The exploration reports should be well planned and documented, as they will help in answering questions and solving foundation problems that may arise later during design and construction.

3.30 Summary

Subsoil exploration is an integral part of all geotechnical engineering projects. It is carried out during the very early stages of the projects in an attempt to adequately define the soil conditions and the design parameters of the different soil layers. The soil exploration includes *in situ* tests, sample collection, and tests in the laboratory. There is a substantial cost associated with the soil exploration program, and budgetary constraints often restrict the extent of the site investigation.

In situ tests generally involve inserting a probe into the ground and measuring the resistance to penetration, which is related to the strength and stiffness of the soil. The standard penetration test and cone penetration test are the two major *in situ* tests commonly carried out in geotechnical engineering projects. In soft clays, the vane shear test is very effective in determining the undrained shear strength. The pressuremeter test and dilatometer test are two specialized tests that are becoming popular.

Geophysical methods can also be used for soil exploration, as well as for determining the soil profile and shear wave velocities. They are effective in covering large areas. They can be complemented by traditional *in situ* tests, such as SPT or CPT.

PROBLEMS

3.1 A Shelby tube has outside diameter of 3.0 in. and wall thickness of 0.065 in. What is the area ratio of the tube?

3.2 A thin-walled sampling tube must be fabricated to obtain good-quality undisturbed clay samples of 75 mm diameter. What is the maximum possible wall thickness?

3.3 A soil profile is shown in Figure P3.3 along with the standard penetration numbers in the clay layer. Use Eqs. (3.8b) and (3.9) to determine the variation of c_u and OCR with depth. What is the average value of c_u and OCR?

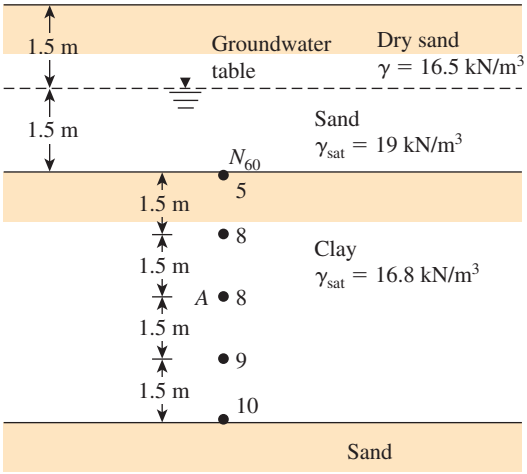


FIGURE P3.3

3.4 Refer to Figure P3.3. Use Eqs. (3.10) and (3.11) to determine the variation of OCR and preconsolidation pressure σ_c'.

3.5 Following is the variation of the field standard penetration number (N_{60}) in a sand deposit:

Depth (m)	N_{60}
1.5	6
3	8
4.5	9
6	8
7.9	13
9	14

The groundwater table is located at a depth of 6 m. Given: the dry unit weight of sand from 0 to a depth of 6 m is 18 kN/m^3, and the saturated unit weight of sand for depth 6 to 12 m is 20.2 kN/m^3. Use the relationship given in Eq. (3.13) to calculate the corrected penetration numbers.

3.6 Redo Problem 3.5 using Eq. (3.14).

3.7 For the soil profile described in Problem 3.5, estimate an average peak soil friction angle. Use Eq. (3.31b).

3.8 Repeat Problem 3.7 using Eq. (3.30).

3.9 Repeat Problem 3.7 using Eq. (3.29). Use $(N_1)_{60}$ from Problem 3.5.

3.10 Refer to Problem 3.5. Using Eq. (3.22), determine the average relative density of the sand.

3.11 Refer to Problem 3.5. Using Eq. (3.28), determine the average relative density of the sand. Assume it is a fine sand. Use Eq. (3.13) to obtain $(N_1)_{60}$.

3.12 Standard penetration tests were carried out in normally consolidated fine sands at different locations. The following data were collected, with average unit weights assumed for the entire depth. Determine the $(N_1)_{60}$ values using the correction factors proposed by (a) Liao and Whitman (1986) and (b) Skempton (1986).

Depth (m)	Average unit weight (kN/m^3)	N_{60}
3.5	18.0	12
8.8	18.0	8
12.4	18.5	15
18.5	18.5	19
23.6	19.0	21
16.9	19.0	26

3.13 A standard penetration test was carried out in a normally consolidated sand at 25 ft depth where the N_{60} was determined to be 28. The unit weight of the sand is 110 lb/ft^3, and the grain-size distribution suggests that $D_{50} = 1.2$ mm and $C_u = 3.2$. The age of the soil since deposition is approximately 5000 years. Determine the relative density using the different correlations discussed in Section 3.15 [i.e., Eqs. (3.21), (3.22), (3.23), (3.24), and (3.28)].

3.14 Standard penetration tests were carried out in sands where the N_{60} values at certain depths are reported as follows. The unit weight of the sand is 18.5 kN/m^3. The water table is well below the test depths.

Depth (m)	2.0	3.5	5.0	6.5	8.0
N_{60}	17	23	26	28	29

Use Eq. (3.13) for C_N. Determine the friction angle ϕ' using Eqs. (3.29), (3.30), and (3.31b).

3.15 In a site consisting of normally consolidated clean sands, the water table is at 10 ft depth. The average unit weight of the sand above and below the water table is 111.5 lb/ft^3 and 125.0 lb/ft^3, respectively. At a 25 ft depth, N_{60} was reported as 26. Determine the following:

- **a.** $(N_1)_{60}$ using Liao and Whitman's (1986) equation for C_N [Eq. (3.13)]
- **b.** D_r using Skempton's (1986) correlation [Eq. (3.28)]
- **c.** Friction angle using Schmertmann's (1975) correlation [Eq. (3.30)]
- **d.** Modulus of elasticity using Kulhawy and Mayne's (1990) correlation [Eq. (3.32)]

3.16 Refer to Figure P3.3. Vane shear tests were conducted in the clay layer. The vane (tapered) dimensions were 63.5 mm (d) × 127 mm (h), $i_B = i_T = 45°$ (see Figure 3.23). For the

test at A, the torque required to cause failure was 51 N · m. For the clay, given: liquid limit = 46 and plastic limit = 21. Estimate the undrained cohesion of the clay for use in the design by using Bjerrum's λ relationship [Eq. (3.40a)].

3.17 Refer to Problem 3.16. Estimate the overconsolidation ratio of the clay. Use Eqs. (3.42) and (3.43).

3.18 **a.** A vane shear test was conducted in a saturated clay. The height and diameter of the rectangular vane were 4 in. and 2 in., respectively. During the test, the maximum torque applied was 230 lb · in. Determine the undrained shear strength of the clay.

b. The clay soil described in part (a) has a liquid limit of 58 and a plastic limit of 29. What would be the corrected undrained shear strength of the clay for design purposes? Use Bjerrum's relationship for λ [Eq. (3.40a)].

3.19 Refer to Problem 3.18. Determine the overconsolidation ratio for the clay. Use Eqs. (3.42) and (3.45). Use $\sigma'_o = 1340$ lb/ft^2.

3.20 A vane shear test was conducted in a saturated soft clay, using a 100 mm × 200 mm vane. When the vane was rotated at the standard rate of 0.1°/s, the torque measured in the torque meter increased to 60 N · m, and with further rotation reduced to 35 N · m. Determine the peak and residual undrained shear strengths of the clay.

3.21 By considering the failure surfaces in a vane shear test, show from the first principles that, for a rectangular vane,

$$K = \frac{\pi d^2}{2}\left(h + \frac{d}{3}\right)$$

3.22 A cone penetration test was carried out in normally consolidated sand, for which the results are summarized below:

Depth (m)	Cone resistance, q_c (MN/m^2)
2.0	3.12
3.5	4.25
5.0	5.14
6.5	9.23
8.0	12.2

The average unit weight of the sand is 16.5 kN/m^3. Determine the friction angle at each depth using Eq. (3.52).

3.23 For the data given in Problem 3.22, determine the relative density at each depth using Eq. (3.51). Assume moderately compressible sand and hence $Q_c = 1$.

3.24 For the data given in Problem 3.22, if $D_{50} = 0.8$ mm, find the N_{60} values at each depth. Use Eq. (3.55) with Kulhawy and Mayne values for a and c.

3.25 In a site consisting entirely of clays, an electric friction cone penetrometer measures the cone resistance q_c at a depth of 8.0 m as 0.75 MN/m^2. The water table is at 3.0 m below the ground level. The unit weights of the clay above and below the water table are 16.5 kN/m^3 and 19.0 kN/m^3, respectively. Estimate the undrained shear strength, preconsolidation pressure, and overconsolidation ratio at this depth.

3.26 A piezocone test was carried out at a site, and the following readings were recorded for the cone resistance q_c and sleeve friction f_s. Determine the soil present at these depths.

Depth (m)	Cone resistance, q_c (MN/m^2)	Sleeve friction, f_s (kN/m^2)
5	0.21	12.5
10	1.05	40.5
15	3.23	75.2
20	9.66	60.7
25	12.50	62.5

3.27 In a pressuremeter test in a soft saturated clay, the measuring cell volume $V_o = 535$ cm^3, $p_o = 42.4$ kN/m^2, $p_f = 326.5$ kN/m^2, $v_o = 46$ cm^3, and $v_f = 180$ cm^3. Assuming Poisson's ratio (μ_s) to be 0.5 and using Figure 3.31, calculate the pressuremeter modulus (E_p).

3.28 A dilatometer test was conducted in a clay deposit. The groundwater table was located at a depth of 3 m below the surface. At a depth of 8 m below the surface, the contact pressure (p_o) was 280 kN/m^2 and the expansion stress (p_1) was 350 kN/m^2. Determine the following:

a. Coefficient of at-rest earth pressure, K_o

b. Overconsolidation ratio, OCR

c. Modulus of elasticity, E_s

Assume σ'_o at a depth of 8 m to be 95 kN/m^2 and $\mu_s = 0.35$.

3.29 A dilatometer test was conducted in a sand deposit at a depth of 6 m. The groundwater table was located at a depth of 2 m below the ground surface. Given, for the sand: $\gamma_d = 14.5$ kN/m^3 and $\gamma_{sat} = 19.8$ kN/m^3. The contact stress during the test was 260 kN/m^2. Estimate the soil friction angle, ϕ'.

3.30 The P-wave velocity in a soil is 105 m/s. Assuming Poisson's ratio to be 0.32, calculate the modulus of elasticity of the soil. Assume that the unit weight of soil is 18 kN/m^3.

3.31 The results of a refraction survey (Figure 3.45a) at a site are given in the following table. Determine the thickness and the P-wave velocity of the materials encountered.

Distance from the source of disturbance (m)	Time of first arrival of P waves (s × 10^3)
2.5	5.08
5.0	10.16
7.5	15.24
10.0	17.01
15.0	20.02
20.0	24.2
25.0	27.1
30.0	28.0
40.0	31.1
50.0	33.9

REFERENCES

American Society for Testing and Materials (2001). *Annual Book of ASTM Standards*, Vol. 04.08, West Conshohocken, PA.

American Society for Testing and Materials (2016). *Annual Book of ASTM Standards*, Vol. 04.08, West Conshohocken, PA.

American Society of Civil Engineers (1972). "Subsurface Investigation for Design and Construction of Foundations of Buildings," *Journal of the Soil Mechanics and Foundations Division*, American Society of Civil Engineers, Vol. 98, No. SM5, pp. 481–490.

Anagnostopoulos, A., Koukis, G., Sabatakakis, N., and Tsiambaos, G. (2003). "Empirical Correlations of Soil Parameters Based on Cone Penetration Tests (CPT) for Greek Soil," *Geotechnical and Geological Engineering*, Vol. 21, No. 4, pp. 377–387.

Baguelin, F., Jézéquel, J. F., and Shields, D. H. (1978). *The Pressuremeter and Foundation Engineering*, Trans Tech Publications, Clausthal, Germany.

Baldi, G., Bellotti, R., Ghionna, V., and Jamiolkowski, M. (1982). "Design Parameters for Sands from CPT," *Proceedings, Second European Symposium on Penetration Testing*, Amsterdam, Vol. 2, pp. 425–438.

Bazaraa, A. (1967). *Use of the Standard Penetration Test for Estimating Settlements of Shallow Foundations on Sand*, Ph.D. Dissertation, Civil Engineering Department, University of Illinois, Champaign-Urbana, Illinois.

Bjerrum, L. (1972). "Embankments on Soft Ground," *Proceedings of the Specialty Conference*, American Society of Civil Engineers, Vol. 2, pp. 1–54.

Burland, J. B. and Burbidge, M. C. (1985). "Settlement of Foundations on Sand and Gravel," *Proceedings*, *Institute of Civil Engineers*, Part I, Vol. 7, pp. 1325–1381.

Cruden, D. M. and Varnes, D. J. (1996). "Landslide Types and Processes," *Special Report 247*, Transportation Research Board, pp. 36–75.

Cubrinovski, M. and Ishihara, K. (1999). "Empirical Correlations between SPT *N*-Values and Relative Density for Sandy Soil," *Soil and Foundations*, Vol. 39, No. 5, pp. 61–92.

Das, B. M. and Luo, Z. (2017). *Principles of Soil Dynamics*, 3rd ed., Cengage, Boston.

Deere, D. U. (1963). "Technical Description of Rock Cores for Engineering Purposes," *Felsmechanik und Ingenieurgeologie*, Vol. 1, No. 1, pp. 16–22.

Dobrin, M. B. (1960). *Introduction to Geophysical Prospecting*, McGraw-Hill, New York.

Hansbo, S. (1957). *A New Approach to the Determination of the Shear Strength of Clay by the Fall Cone Test*, Swedish Geotechnical Institute, Report No. 114.

Hara, A., Ohta, T., Niwa, M., Tanaka, S., and Banno, T. (1974). "Shear Modulus and Shear Strength of Cohesive Soil," *Soil and Foundations*, Vol. 14, No. 3, pp. 1–12.

Hatanaka, M. and Uchida, A. (1996). "Empirical Correlation between Penetration Resistance and Internal Friction Angle of Sandy Soil," *Soil and Foundations*, Vol. 36, No. 4, pp. 1–10.

Jamiolkowski, M., Ladd, C. C., Germaine, J. T., and Lancellotta, R. (1985). "New Developments in Field and Laboratory Testing of Soil," *Proceedings, 11th International Conference on Soil Mechanics and Foundation Engineering*, Vol. 1, pp. 57–153.

Kamei, T. and Iwasaki, K. (1995). "Evaluation of Undrained Shear Strength of Cohesive Soil Using a Flat Dilatometer," *Soil and Foundations*, Vol. 35, No. 2, pp. 111–116.

Kolb, C. R. and Shockley, W. G. (1959). "Mississippi Valley Geology: Its Engineering Significance" *Proceedings*, *American Society of Civil Engineers*, Vol. 124, pp. 633–656.

Kulhawy, F. H. and Mayne, P. W. (1990). *Manual on Estimating Soil Properties for Foundation Design*, Electric Power Research Institute, Palo Alto, CA.

Lancellotta, R. (1983). *Analisi di Affidabilità in Ingegneria Geotecnica*, Atti Istituto Scienza Construzioni, No. 625, Politecnico di Torino.

Larsson, R. (1980). "Undrained Shear Strength in Stability Calculation of Embankments and Foundations on Clay," *Canadian Geotechnical Journal*, Vol. 17, pp. 591–602.

Lee, J., Salgado, R., and Carraro, A. H. (2004). "Stiffness Degradation and Shear Strength of Silty Sand," *Canadian Geotechnical Journal*, Vol. 41, No. 5, pp. 831–843.

Liao, S. S. C. and Whitman, R. V. (1986). "Overburden Correction Factors for SPT in Sand," *Journal of Geotechnical Engineering*, American Society of Civil Engineers, Vol. 112, No. 3, pp. 373–377.

Marchetti, S. (1980). "*In Situ* Test by Flat Dilatometer," *Journal of Geotechnical Engineering Division*, ASCE, Vol. 106, GT3, pp. 299–321.

Marcuson, W. F. III, and Bieganousky, W. A. (1977). "SPT and Relative Density in Coarse Sands," *Journal of Geotechnical Engineering Division*, American Society of Civil Engineers, Vol. 103, No. 11, pp. 1295–1309.

Mayne, P. W. and Kemper, J. B. (1988). "Profiling OCR in Stiff Clays by CPT and SPT," *Geotechnical Testing Journal*, ASTM, Vol. 11, No. 2, pp. 139–147.

Mayne, P. W. and Mitchell, J. K. (1988). "Profiling of Overconsolidation Ratio in Clays by Field Vane," *Canadian Geotechnical Journal*, Vol. 25, No. 1, pp. 150–158.

Menard, L. (1956). *An Apparatus for Measuring the Strength of Soil in Place*, Master's thesis, University of Illinois, Champaign-Urbana, IL.

Meyerhof, G. G. (1957). "Discussion on Research on Determining the Density of Sands by Spoon Penetration Testing," *Proceedings*, *Fourth International Conference on Soil Mechanics and Foundation Engineering*, Vol. 3, p. 110.

Morris, P. M. and Williams, D. T. (1994). "Effective Stress Vane Shear Strength Correction Factor Correlations," *Canadian Geotechnical Journal*, Vol. 31, No. 3, pp. 335–342.

Ohya, S., Imai, T., and Matsubara, M. (1982). "Relationships between *N* Value by SPT and LLT Pressuremeter Results," *Proceedings, 2nd European Symposium on Penetration Testing*, Vol. 1, Amsterdam, pp. 125–130.

Osterberg, J. O. (1952). "New Piston-Type Soil Sampler," *Engineering News-Record*, April 24.

Peck, R. B., Hanson, W. E., and Thornburn, T. H. (1974). *Foundation Engineering*, 2nd ed., John Wiley & Sons, New York.

Ricceri, G., Simonini, P., and Cola, S. (2002). "Applicability of Piezocone and Dilatometer to Characterize the Soil of the Venice Lagoon" *Geotechnical and Geological Engineering*, Vol. 20, No. 2, pp. 89–121.

Robertson, P. K. (2010). "Soil Behavior Type from the CPT: An Update," *2nd International Symposium on Cone Penetration Testing*, CPT '10, Huntington Beach, CA.

Robertson, P. K. and Campanella, R. G. (1983). "Interpretation of Cone Penetration Tests. Part I: Sand," *Canadian Geotechnical Journal*, Vol. 20, No. 4, pp. 718–733.

Robertson, P. K., Campanella, R. G., Gillespie, D., and Greig, J. (1986). "Use of Piezometer Cone Data," *Use of* In Situ *Tests in Geotechnical Engineering*, Geotechnical Special Publication, No. 6, ASCE, pp. 1263–1280.

Schmertmann, J. H. (1975). "Measurement of *In Situ* Shear Strength," *Proceedings, Specialty Conference on* In Situ *Measurement of Soil Properties*, ASCE, Vol. 2, pp. 57–138.

Schmertmann, J. H. (1986). "Suggested Method for Performing the Flat Dilatometer Test," *Geotechnical Testing Journal*, ASTM, Vol. 9, No. 2, pp. 93–101.

Seed, H. B., Arango, I., and Chan, C. K. (1975). *Evaluation of Soil Liquefaction Potential during Earthquakes*, Report No. EERC 75-28, Earthquake Engineering Research Center, University of California, Berkeley.

Seed, H. B., Tokimatsu, K., Harder, L. F., and Chung, R. M. (1985). "Influence of SPT Procedures in Soil Liquefaction Resistance Evaluations," *Journal of Geotechnical Engineering*, ASCE, Vol. 111, No. 12, pp. 1425–1445.

Shibuya, S. and Hanh, L. T. (2001). "Estimating Undrained Shear Strength of Soft Clay Ground Improved by Pre-Loading with PVD—Case History in Bangkok," *Soil and Foundations*, Vol. 41, No. 4, pp. 95–101.

Sivakugan, N. and Das, B. (2010). *Geotechnical Engineering—A Practical Problem Solving Approach*, J. Ross Publishing Co., Fort Lauderdale, FL.

Skempton, A. W. (1986). "Standard Penetration Test Procedures and the Effect in Sands of Overburden Pressure, Relative Density, Particle Size, Aging and Overconsolidation," *Geotechnique*, Vol. 36, No. 3, pp. 425–447.

Sowers, G. B. and Sowers, G. F. (1970). *Introductory Soil Mechanics and Foundations*, 3rd ed., Macmillan, New York.

Stokoe, K. H. and Woods, R. D. (1972). "*In Situ* Shear Wave Velocity by Cross-Hole Method," *Journal of Soil Mechanics and Foundations Division*, American Society of Civil Engineers, Vol. 98, No. SM5, pp. 443–460.

Szechy, K. and Varga, L. (1978). *Foundation Engineering—Soil Exploration and Spread Foundation*, Akademiai Kiado, Budapest, Hungary.

Wolff, T. F. (1989). "Pile Capacity Prediction Using Parameter Functions," in *Predicted and Observed Axial Behavior of Piles*, *Results of a Pile Prediction Symposium*, sponsored by the Geotechnical Engineering Division, ASCE, Evanston, IL, June, 1989, ASCE Geotechnical Special Publication No. 23, pp. 96–106.

4

Instrumentation and Monitoring in Geotechnical Engineering



Skinfaxi/Shutterstock.com

4.1 Introduction 135
4.2 Need for Instrumentation 135
4.3 Geotechnical Measurements 136
4.4 Geotechnical Instruments 137
4.5 Planning an Instrumentation Program 142
4.6 Typical Instrumentation Projects 143
4.7 Summary 143
REFERENCES 143

4.1 Introduction

A typical geotechnical engineering project may include one or more of the following: earthworks, excavation, ground improvement, foundations, retaining walls, sheet piles, braced excavations, embankments, dams, tunneling, and bridge abutments. The geotechnical design and analysis are generally based on a simplified soil profile and a site model. The soil mechanics principles that we often apply assume isotropy, homogeneity, and specific constitutive relations (e.g., Mohr–Coulomb linear elastic, rigid-plastic). In actual field conditions, these assumptions may not be true. These are approximations or assumptions that enable us to arrive at reasonable solutions within a realistic time frame. Uncertainties arise due to geotechnical parameters derived from limited site investigation data and design loads estimated from different load combinations. Adequate factor of safety is in place to guard against these unknowns, but there is no better way to minimize risk than to instrument the structure and monitor its performance for as long as necessary to ensure safety.

While the measurements taken during the site investigation program are *one-off* at a specific location, the measurements taken in the instrumentation program are *ongoing* and may continue for a long period. Although instruments are used in both programs, they vary greatly and are used for different purposes. While the site investigations are normally carried out prior to the design stage, the geotechnical instrumentation can be carried out during the design stage, construction stage, or while the structure is in service.

4.2 Need for Instrumentation

Geotechnical instrumentation is about using the different instruments to monitor the performance of an earth or earth-supported structure. Some of the reasons for instrumenting a structure are as follows:

a. Design verification
It is always a good practice to monitor the construction and performance of a structure irrespective of the confidence we have in the data or design method. When the design method is relatively new or the assumptions are questionable, instruments and monitoring become more important. Examples include a pile load test to verify its load-carrying capacity and settlement records to assess if an embankment underlain by a compressible soil layer settles as predicted.

b. Construction control
The construction sequence planned during the early stages of the project may be revised during the later stages depending on the data from instrumentation. Instruments can be used to monitor the effects of construction methods and hence to control the rate of construction and to ensure there is no risk of failure or adverse effects. An example is a deep excavation adjacent to a building that has been instrumented.

c. Verification of long-term performance
The in-service performance of a structure (e.g., drainage behind a retaining wall, load on a tieback) may require monitoring using the appropriate instruments.

d. Safety
Instrumentation can warn of impending failures. It can be very effective as an early warning system in areas prone to landslides, earthquakes, and tsunamis.

e. Quality assurance
Instrumentation can assure that the work is carried out per the specifications and can serve as a useful tool in quality assurance.

f. Legal protection
In legal disputes that arise in projects (e.g., blast vibration in nearby buildings), data recorded via instrumentation can provide strong evidence.

g. Advancing the state of the art
Geotechnical instrumentation has an important role to play in research and development and in advancing the state of the art. When developing new construction methods or new theories, a good instrumentation exercise can go a long way toward validating these theories and methods.

4.3 Geotechnical Measurements

Table 4.1 summarizes the instruments used to measure various parameters. The factors to consider in selecting the instruments include the following:

- Range: The highest and lowest possible readings from the instrument
- Resolution: The smallest change that can be displayed in the readout device
- Accuracy: A measure of how close the average reading is to the actual value
- Precision: A measure of repeatability or reproducibility

Dunnicliff (1993) distinguishes between accuracy and precision as shown in Figure 4.1, where the bull's-eye represents the true value. In Figure 4.1a, the measurements are

TABLE 4.1 Instrumentation Devices

Parameter	Instrument
Pore water pressure	Piezometer
Earth pressure	Earth pressure cell
Load	Load cell, proving ring
Strain	Strain gauge
Deformation	Dial gauge, LVDT, inclinometer, extensometer, settlement plate
Vibration	Seismograph, geophone
Temperature	Thermometer, thermocouple, thermistor

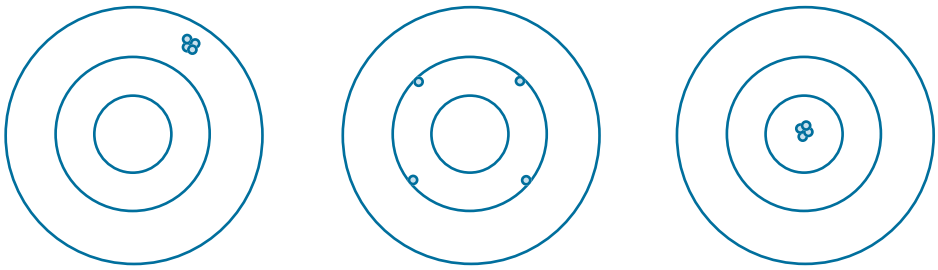


FIGURE 4.1 Accuracy and precision: (a) precise but not accurate; (b) not precise but accurate; and (c) precise and accurate (Based on Dunnicliff, 1993)

about the same and hence precise, but they are far from the true value and thus inaccurate. In Figure 4.1b, the measurements vary, but the average is close to the true value. Here, a large number of readings will ensure that the average is accurate. In Figure 4.1c, the measurements are about the same, and they are close to the true value. The cost of an instrument increases with higher resolution, accuracy, and precision.

4.4 Geotechnical Instruments

Some of the most common geotechnical instruments are discussed in this section.

a. Piezometer
Pore water pressure measurements are necessary to establish the initial ground conditions and also to monitor excess pore water pressures developed during construction activities, such as placement of fill or pile driving. Applications include

- Groundwater table and fluctuations
- Preloading of clay layers
- Slope stability investigations
- Land reclamation
- Embankment construction
- Dynamic compaction
- Pressures behind retaining walls and diaphragm walls
- Detection of the rate and direction of movement of a contamination plume

A *standpipe piezometer*, also known as a *Casagrande piezometer*, is a simple device wherein the water rises in a standpipe (Figure 4.2a) and the water level is monitored. A *water level indicator*, also known as a *dip meter* (Figure 4.2b), is used for measuring the water level within the riser pipe. The disadvantages of this device include the slow response time in low-permeability soil and the inability to log data and to access the instrument remotely, thus requiring manual operation. There are other



(a) (b) (c)

FIGURE 4.2 (a) Standpipe piezometer; (b) water level indicator; and (c) a vibrating wire piezometer for measuring pore water pressure (Courtesy of N. Sivakugan, James Cook University, Australia)



FIGURE 4.3 Earth pressure cells (Courtesy of N. Sivakugan, James Cook University, Australia)

types of more versatile piezometers, such as *vibrating wire* (Figure 4.2c), *pneumatic, hydraulic*, and *strain gauge piezometers*. They can be installed in boreholes or buried in the ground. Of these various types, vibrating wire piezometers are the most common. They have negligible time lag and are very sensitive.

b. Earth pressure cell
Earth pressure cells, also called total earth pressure cells (TPCs), measure the *total* earth pressures at the locations where they are installed. They are used in embankments, retaining walls, and buried structures. They can be used within the soil (e.g., beneath an embankment) or on the surface of structures such as retaining walls, piles, or culverts. An array of earth pressure cells can be used to determine the pressure distribution within the soil. Earth pressure cells are used mainly to verify the earth pressures computed in the structural design phase. Figure 4.3 shows hydraulic earth pressure cells that employ vibrating wire pressure transducers. The typical diameter of an earth pressure cell is about 200–300 mm. Smaller cells are difficult to place and can give erroneous readings.

c. Load cell
Load cells come in various shapes and are used for proof load testing and for measuring the service loads in rock bolts, ground anchors, tiebacks, struts, and piles. The proof load test generally involves applying a load using a hydraulic jack, which is increased gradually to the desired load, at which time the strain or displacement is measured. Load cells are also commonly used in pile load tests. Figure 4.4 shows a load cell placed between the pile head and the applied load to monitor the load during the pile load test. Also shown in the figure are LVDTs (linear variable differential transformers) at the corners of the square pile head; these are used to monitor settlement of the pile head.

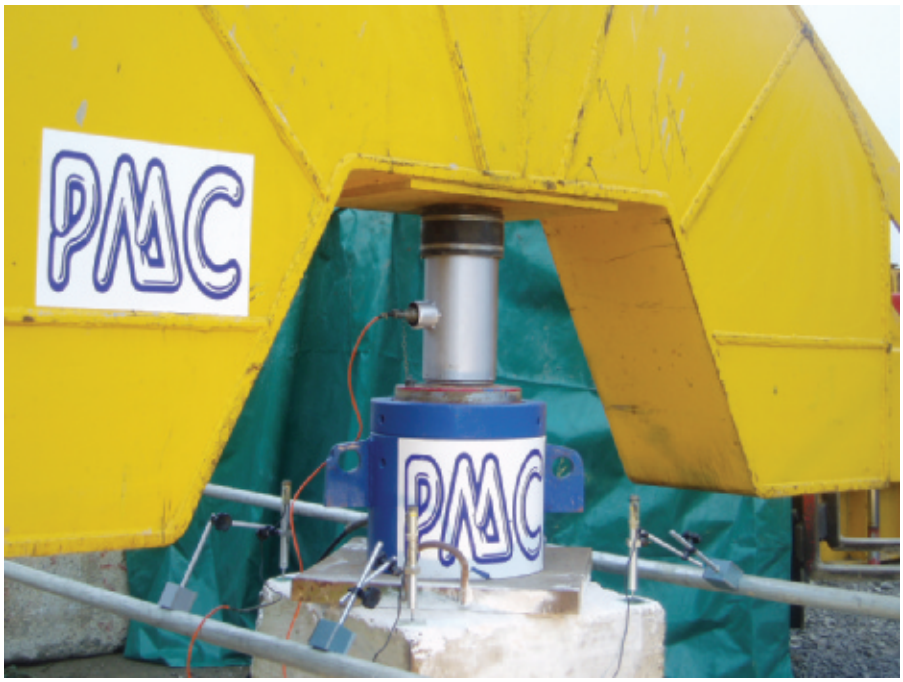


FIGURE 4.4 Load cell and LVDTs used in a pile load test to measure load and settlement (Courtesy of N. Sivakugan, James Cook University, Australia)

d. Inclinometer

Inclinometers are used to detect lateral or vertical deformations by installing the casing vertically or horizontally, respectively, and to send a probe through the casing that can detect the deflections perpendicular to the axis of the casing. Figure 4.5 shows an inclinometer casing, the probe, and the cable attached to the probe. A piezometer can be attached to the outside wall of the inclinometer casing when installed in the ground. A series of vertical inclinometers can capture the lateral deformations taking place during landslides at a site. A horizontal inclinometer can capture the settlement profile beneath an embankment.

Inclinometers are used for monitoring long-term deformations and can detect potential failures and provide early warning. They can be installed in slopes and embankments, near sheet pile or diaphragm walls, or in the vicinity of tunnelling work. The grooves in the inclinometer casing ensure proper alignment of the probe during the travel within the casing.

e. Settlement plate

A *settlement plate* is a simple device wherein a vertical stem is attached to a horizontal plate that is embedded at the location where the settlement is measured. The settlement is monitored by measuring the elevation of the top of the stem using surveying equipment. It is necessary to have a reliable survey benchmark that can be used as the datum during the monitoring period. Figure 4.6 shows a settlement plate monitoring the ongoing settlement of a clay layer underneath.

f. Strain gauge

Strain gauges are used for measuring strains. They are inexpensive and are bought in packs. They are used for measuring strains on tieback anchors, sheet pile or diaphragm walls, and retaining walls. They are also used for measuring strain along the length of a pile.

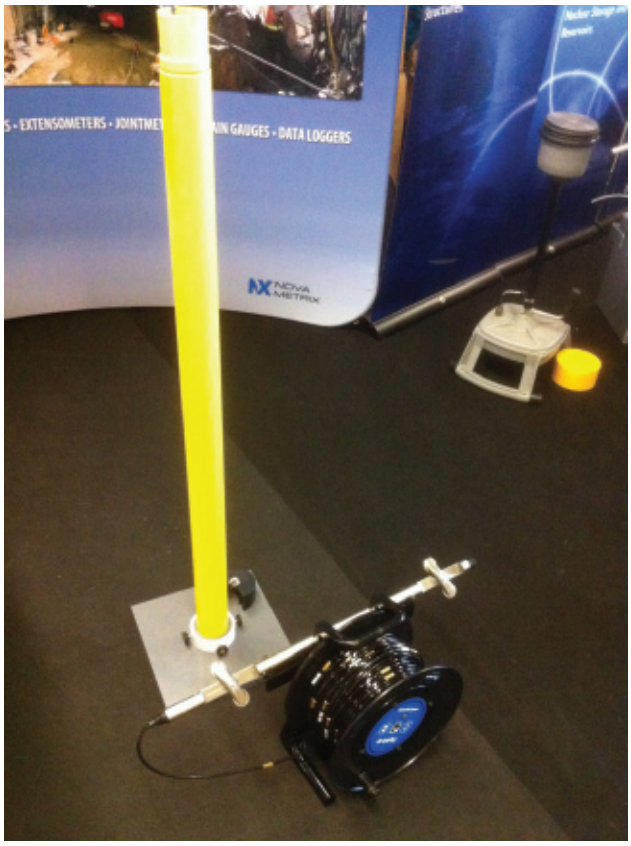


FIGURE 4.5 Inclinometer with casing, probe, and cable (Courtesy of N. Sivakugan, James Cook University, Australia)



FIGURE 4.6 Settlement plate to monitor the consolidation settlement of an underlying clay layer (Courtesy of N. Sivakugan, James Cook University, Australia)

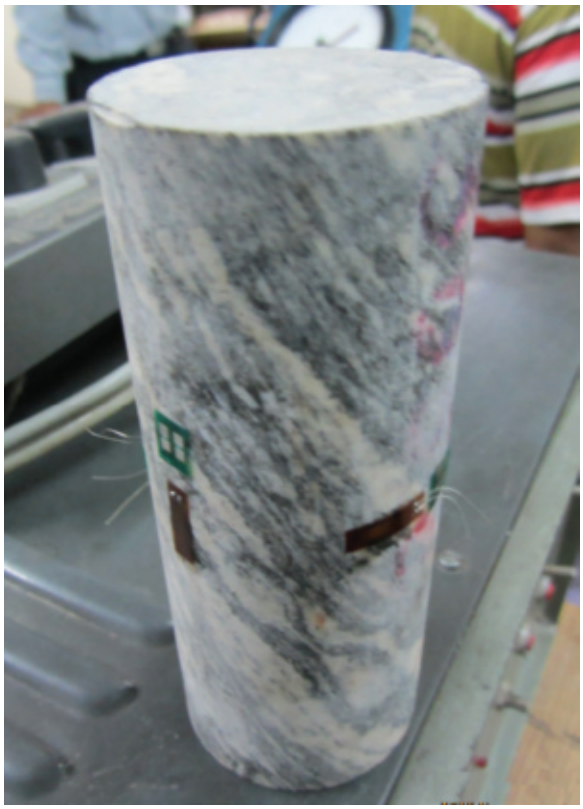
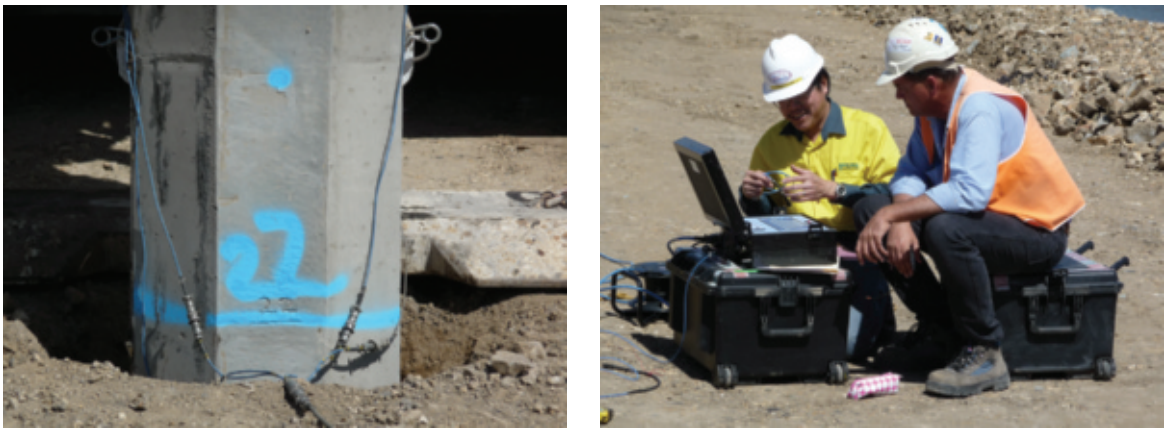


FIGURE 4.7 Strain gauges used in a uniaxial compression test on a rock specimen (Courtesy of N. Sivakugan, James Cook University, Australia)

Figure 4.7 shows strain gauges mounted on a rock specimen for measuring the longitudinal and diametrical strains. In some applications, strains can be translated into loads using elastic theories.

g. Others

Figure 4.8 shows the instrumentation in a pile driving exercise where the monitoring is carried out using a *pile driving analyzer* (PDA). Nowadays, it is common to see real-time monitoring and Web-based monitoring from remote sites,



(a) (b)

FIGURE 4.8 (a) Instrumented pile; (b) pile driving analyzer (Courtesy of N. Sivakugan, James Cook University, Australia)

some using handheld devices such as smart phones. For example, a pile driving monitoring exercise occurring in Texas can be monitored from New York.

Tilt meters are used to monitor changes in inclination or rotation. They are used for monitoring tilting of retaining walls, bridge abutments, and rock slopes. *Extensometers* are used for detecting the change in distance between two points. Nowadays, Web cams are used for the continuous monitoring of risk-prone areas so that potential problems can be detected and remedial action taken if necessary.

4.5 Planning an Instrumentation Program

The factors to consider and the key steps in planning a geotechnical instrumentation program are as follows:

a. *Site conditions*
A good understanding of the ground conditions, including the geology and the expected mechanisms that control the behavior of the proposed structure, provides a better appreciation of the expected problems. This, in turn, facilitates the instrument selection.

b. *Purpose of instrumentation*
The client will usually define the purpose of the instrumentation program. Instrumentation can be required during the design, construction, or operational phases of the project. It can be used for construction control, as evidence against legal disputes, or for one of the many reasons given in Section 4.2.

c. *Identification of the variables to monitor*
Depending on the nature of the project, there are critical parameters that have to be measured at certain locations. There may be complementary parameters that can be obtained at a slight additional cost with significant benefit in correlating with other measurements.

d. *Prediction of behavior*
The geotechnical engineer planning the instrumentation exercise should know what to expect. From basic preliminary calculations to more sophisticated numerical analyses, the engineer can use models to gain a good understanding of the structure's expected performance. This would inform the engineer of the approximate maximum values that must be measured.

e. *Remedial action planning*
Possible remedial measures must be in place for potential problems that may be disclosed during monitoring.

f. *Selection of instruments*
Instruments must be selected based on the following factors: environmental conditions, instrument performance (e.g., precision, accuracy, resolution, and range), data acquisition, instrument life, and cost. The instrument must be robust, reliable, and capable of functioning throughout the required period in the installed environment; the instrument must respond precisely to changes in the parameters being measured.

g. *Planning of instrument layout*
Instruments must be placed in a way that maximizes their effectiveness.

h. *Procurement of instruments*
During procurement, instrument specifications, calibration, and pricing must be considered carefully. There are several instrument manufacturers in the market with competing products.

i. *Installation of instruments*
Installation requires training staff to use the instruments, scheduling the installation, and coordinating the plans with the contractor.

j. *Monitoring*
Monitoring requires careful data analysis, interpretation, and reporting.

4.6 Typical Instrumentation Projects

Peck (1969) discussed the value of the observational (learn-as-you-go) method where the engineer modifies the design and construction as the construction progresses and more data become available. Following is a list of some typical situations where a geotechnical instrumentation program is required.

- Monitoring settlements and pore pressures beneath an embankment on soft clay
- Monitoring loads and settlements of a drilled shaft
- Monitoring the loads and deflections on the tiebacks on retaining walls
- Monitoring deformations at excavations near buildings
- Monitoring noise levels and vibrations during blasting near buildings or residential areas
- Monitoring deflections of sheet piles
- Monitoring ground movements during tunnelling

4.7 Summary

As projects become increasingly complex and as clients present rigid constraints and stringent requirements, there is increasing demand for geotechnical instrumentation. Geotechnical instrumentation can be carried out in the design, construction, or operational phases of the project to monitor certain parameters such as loads, deflections, pressures, or strains continuously over a certain period. A meticulous planning of the instrumentation program is required to ensure it is carried out successfully.

REFERENCES

DUNNICLIFF, J. (1993). *Geotechnical Instrumentation for Monitoring Field Performance*, Wiley-Interscience, New York.

PECK, R. B. (1969). "Advantages and Limitations of the Observational Method in Applied Soil Mechanics," 9th Rankine Lecture, *Geotechnique*, 19(2), 171–187.

PART 2

Soil Improvement

Chapter 5: Soil Improvement and Ground Modification



Richard Thornton/Shutterstock.com

5

Soil Improvement and Ground Modification



Nicolae Cucurudza/Shutterstock.com

5.1 Introduction 147
5.2 General Principles of Compaction 147
5.3 Empirical Relationships for Compaction 150
5.4 Field Compaction 154
5.5 Compaction Control for Clay Hydraulic Barriers 156
5.6 Vibroflotation 160
5.7 Blasting 164
5.8 Precompression 165
5.9 Sand Drains 170
5.10 Prefabricated Vertical Drains 179
5.11 Lime Stabilization 184
5.12 Cement Stabilization 187
5.13 Fly-Ash Stabilization 189
5.14 Stone Columns 189
5.15 Sand Compaction Piles 194
5.16 Dynamic Compaction 195
5.17 Jet Grouting 198
5.18 Deep Mixing 199
5.19 Summary 201

PROBLEMS 201
REFERENCES 202

5.1 Introduction

The natural ground conditions at the site may not always be totally suitable for supporting the proposed structures, such as buildings, bridges, highways, and dams. One or more of the subsoil layers can be problematic and require some improvement. Near the surface, it is possible to replace problematic soil with better-performing ones. An alternative is to modify these soil through a ground improvement technique, such as compaction. When these soil are present at large depths, soil replacement or compaction may not be possible. Other techniques, such as vibroflotation, vertical drains, stabilization using additives, deep mixing, and stone columns, can be used for such situations.

The common problems that are associated with poor ground conditions and that necessitate some form of soil improvement are as follows:

1. Low shear strength
2. Low stiffness
3. High permeability
4. High swell–shrink potential

Loose granular soil or soft clays have low shear strength and low stiffness. Low shear strength can lead to shear failure in the surrounding soil, and low stiffness can result in large deformations or settlements. While there are several ground improvement techniques, they have their limitations. Not all techniques will work well in all soil conditions.

This chapter discusses some of the general principles of soil improvement, such as compaction, vibroflotation, precompression, sand drains, wick drains, stabilization by admixtures, jet grouting, and deep mixing, as well as the use of stone columns and sand compaction piles in weak clay to construct foundations.

5.2 General Principles of Compaction

Compaction is the oldest and simplest ground improvement technique. The soil is densified by applying external pressure using rollers. Water is added to act as a lubricant between the soil grains and enhance the compaction process. The moisture content at which the *maximum dry unit weight* [$\gamma_{d(\max)}$] is achieved is referred to as the *optimum moisture content* (w_{opt}). Good geotechnical properties are achieved when the soil is compacted near w_{opt}. These values are determined through laboratory compaction tests, where the soil is compacted in layers within a cylindrical mold to a specific compaction energy. By plotting the dry unit weight against moisture content, the optimum moisture content and maximum dry unit weight are determined.

The standard Proctor (ASTM D-698) and modified Proctor (ASTM D-1557) are two common test procedures that apply different levels of compaction energy. The specifications for the two tests are given in Tables 5.1 and 5.2, where method C with a larger mold is suggested for soil containing larger aggregates.

TABLE 5.1 Specifications for Standard Proctor Test (Based on ASTM Designation 698)

Item	Method A	Method B	Method C
Diameter of mold	101.6 mm (4 in.)	101.6 mm (4 in.)	152.4 mm (6 in.)
Volume of mold	944 cm^3 $\left(\frac{1}{30}\ ft^3\right)$	944 cm^3 $\left(\frac{1}{30}\ ft^3\right)$	2124 cm^3 (0.075 ft^3)
Mass (weight) of hammer	2.5 kg (5.5 lb)	2.5 kg (5.5 lb)	2.5 kg (5.5 lb)
Height of hammer drop	304.8 mm (12 in.)	304.8 mm (12 in.)	304.8 mm (12 in.)
Number of hammer blows per layer of soil	25	25	56
Number of layers of compaction	3	3	3
Energy of compaction	600 $kN \cdot m/m^3$ (12,400 $ft \cdot lb/ft^3$)	600 $kN \cdot m/m^3$ (12,400 $ft \cdot lb/ft^3$)	600 $kN \cdot m/m^3$ (12,400 $ft \cdot lb/ft^3$)
Soil to be used	Portion passing No. 4 (4.75-mm) sieve. May be used if 20% *or less* by weight of material is retained on No. 4 sieve.	Portion passing $\frac{3}{8}$-in. (9.5-mm) sieve. May be used if soil retained on No. 4 sieve *is more than* 20% and 20% *or less* by weight is retained on 9.5-mm $\left(\frac{3}{8}\text{-in.}\right)$ sieve.	Portion passing $\frac{3}{4}$-in. (19.0-mm) sieve. May be used if *more than* 20% by weight of material is retained on 9.5 mm $\left(\frac{3}{8}\text{-in.}\right)$ sieve and *less than* 30% by weight is retained on 19.00-mm $\left(\frac{3}{4}\text{-in.}\right)$ sieve.

TABLE 5.2 Specifications for Modified Proctor Test (Based on ASTM Designation 1557)

Item	Method A	Method B	Method C
Diameter of mold	101.6 mm (4 in.)	101.6 mm (4 in.)	152.4 mm (6 in.)
Volume of mold	944 cm^3 $\left(\frac{1}{30}\ ft^3\right)$	944 cm^3 $\left(\frac{1}{30}\ ft^3\right)$	2124 cm^3 (0.075 ft^3)
Mass (weight) of hammer	4.54 kg (10 lb)	4.54 kg (10 lb)	4.54 kg (10 lb)
Height of hammer drop	457.2 mm (18 in.)	457.2 mm (18 in.)	457.2 mm (18 in.)
Number of hammer blows per layer of soil	25	25	56
Number of layers of compaction	5	5	5
Energy of compaction	2700 $kN \cdot m/m^3$ (56,000 $ft \cdot lb/ft^3$)	2700 $kN \cdot m/m^3$ (56,000 $ft \cdot lb/ft^3$)	2700 $kN \cdot m/m^3$ (56,000 $ft \cdot lb/ft^3$)
Soil to be used	Portion passing No. 4 (4.75-mm) sieve. May be used if 20% *or less* by weight of material is retained on No. 4 sieve.	Portion passing 9.5-mm $\left(\frac{3}{8}\text{-in.}\right)$ sieve. May be used if soil retained on No. 4 sieve *is more than* 20% and 20% *or less* by weight is retained on 9.5-mm $\left(\frac{3}{8}\text{-in.}\right)$ sieve.	Portion passing 19.0-mm $\left(\frac{3}{4}\text{-in.}\right)$ sieve. May be used if *more than* 20% by weight of material is retained on 9.5-mm $\left(\frac{3}{8}\text{-in.}\right)$ sieve and *less than* 30% by weight is retained on 19-mm $\left(\frac{3}{4}\text{-in.}\right)$sieve.

Figure 5.1 shows a plot of γ_d against w (%) for a clayey silt obtained from standard and modified Proctor tests (method A). The following conclusions may be drawn:

1. The maximum dry unit weight and the optimum moisture content depend on the degree of compaction.

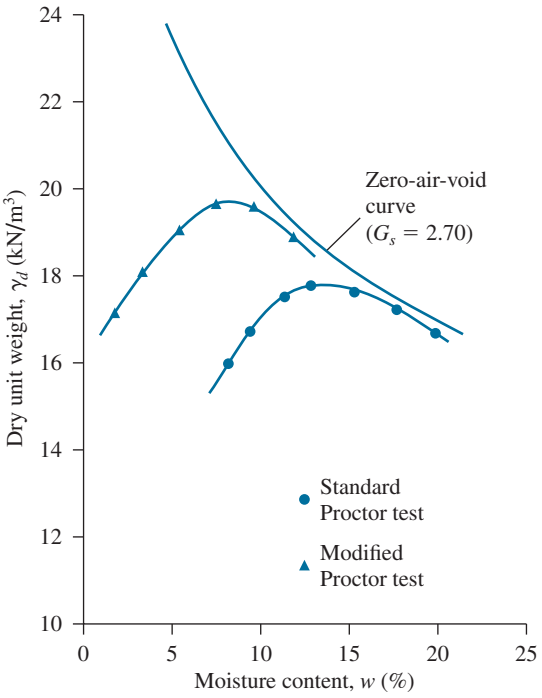


FIGURE 5.1 Standard and modified Proctor compaction curves for a clayey silt (method A)

2. The higher the energy of compaction, the higher the maximum dry unit weight.
3. The higher the energy of compaction, the lower the optimum moisture content.
4. No portion of the compaction curve can lie to the right of the zero-air-void line. The zero-air-void dry unit weight, γ_{zav}, at a given moisture content is the theoretical maximum value of γ_d, which means that all the void spaces of the compacted soil are filled with water, or

$$\gamma_{zav} = \frac{\gamma_w}{\frac{1}{G_s} + w} \tag{5.1}$$

where

γ_w = unit weight of water

G_s = specific gravity of the soil solids

w = moisture content of the soil

5. The maximum dry unit weight of compaction and the corresponding optimum moisture content will vary from soil to soil.

Using the results of laboratory compaction (γ_d versus w), specifications may be written for the compaction of a given soil in the field. In most cases, the contractor is required to achieve a relative compaction of 90% or more on the basis of a specific laboratory test (either the standard or the modified Proctor compaction test). These days, the modified Proctor compactive effort is specified more commonly, and some typical requirements, as suggested by the U.S. Navy (1982) and Hausmann (1990), are summarized in Table 5.3. The relative compaction is defined as

$$\text{RC} = \frac{\gamma_{d(\text{field})}}{\gamma_{d(\text{max})}} \tag{5.2}$$

TABLE 5.3 Typical Compaction Requirements [Based on U.S. Navy (1982) and Hausmann (1990)]

Fill used for	% of $\gamma_{d(\max)}$ from modified Proctor	Moisture content range about optimum (%)
Roads:	90–105*	−2 to +2
Depth of 0–0.5 m (0–1.6 ft)	90–95*	−2 to +2
Depth > 0.5 m (1.6 ft)		
Small earth dam	90–95	−1 to +3
Large earth dam	95	−1 to +2
Railway embankment	95	−2 to +2
Foundation for structure	95	−2 to +2
Backfill behind walls/trenches	90	−2 to +2
Canal linings of clays	90	−2 to +2
Drainage blanket or filter	90	Thoroughly wet

*Depending on soil type, traffic, and function of the layer

Chapter 2 introduced the concept of relative density (for the compaction of granular soil), defined as

$$D_r = \left[\frac{\gamma_d - \gamma_{d(\min)}}{\gamma_{d(\max)} - \gamma_{d(\min)}}\right]\frac{\gamma_{d(\max)}}{\gamma_d}$$

where

γ_d = dry unit weight of compaction in the field

$\gamma_{d(\max)}$ = maximum dry unit weight of compaction as determined in the laboratory

$\gamma_{d(\min)}$ = minimum dry unit weight of compaction as determined in the laboratory

For granular soil in the field, the degree of compaction obtained is often measured in terms of relative density. Comparing the expressions for relative density and relative compaction reveals that

$$\text{RC} = \frac{A}{1 - D_r(1 - A)} \tag{5.3}$$

where $A = \dfrac{\gamma_{d(\min)}}{\gamma_{d(\max)}}$. Here it is assumed that $\gamma_{d(\max)}$ determined from the compaction test (ASTM D-698 or D-1557) is the same as that determined in defining the densest state corresponding to $e_{\min}$ (ASTM D-4253). Because the procedures are different, the two values for $\gamma_{d(\max)}$ can be slightly different.

5.3 Empirical Relationships for Compaction

Good geotechnical engineers or soil technicians can estimate the optimum moisture content simply by feeling the moist soil between their fingers. In clays, the optimum moisture content from a standard Proctor compaction test is 2–4% less than the plastic limit, with high plastic clays falling in the lower end of the range. In sands, the optimum moisture content is approximately the lowest moisture content at which

a drop of water can be squeezed out. Fine-grained soil compacted by a standard Proctor compaction effort are near 80–85% degrees of saturation at the optimum moisture content. When they are compacted wet of optimum, the degree of saturation is in the range 90–95%. The differences in the optimum water content and maximum dry density between the standard and modified Proctor compaction tests are more pronounced for clays than sands. The maximum dry density under a standard Proctor compactive effort can be about 85–97% of the modified Proctor compactive effort. The optimum water content under the modified Proctor compactive effort can be 2–5% lower than that of the standard Proctor compactive effort (Hausmann 1990).

Omar et al. (2003) presented the results of modified Proctor compaction tests on 311 soil samples. Of these samples, 45 were gravelly soil (GP, GP-GM, GW, GW-GM, and GM), 264 were sandy soil (SP, SP-SM, SW-SM, SW, SC-SM, SC, and SM), and two were clay with low plasticity (CL). All compaction tests were conducted using ASTM 1557 method C to avoid over-size correction. Based on the tests, the following correlations were developed.

$$\rho_{d(\max)}(\text{kg/m}^3) = [4{,}804{,}574G_S - 195.55(\text{LL})^2 + 156.971(\text{R\#4})^{0.5} - 9{,}527{,}830]^{0.5} \tag{5.4}$$

$$\ln(w_{\text{opt}}) = 1.195 \times 10^{-4}(\text{LL})^2 - 1.964G_s - 6.617 \times 10^{-5}(\text{R\#4}) + 7.651 \tag{5.5}$$

where

$\rho_{d(\max)}$ = maximum dry density

w_{opt} = optimum moisture content

G_s = specific gravity of soil solids

LL = liquid limit, in percent

R#4 = percent retained on No. 4 sieve (4.75 mm opening)

Equations (5.4) and (5.5) contain the term liquid limit. This is because the soil that were considered included silty and clayey sands.

For granular soil with less than 12% fines (i.e., finer than No. 200 sieve), relative density may be a better indicator for end product compaction specification in the field. Based on laboratory compaction tests on 55 clean sands (less than 5% finer than No. 200 sieve), Patra et al. (2010) provided the following relationships:

$$D_r = AD_{50}^{-B} \tag{5.6}$$

$$A = 0.216 \ln E - 0.850 \tag{5.7}$$

$$B = -0.03 \ln E + 0.306 \tag{5.8}$$

where D_r = maximum relative density of compaction achieved with compaction energy E (kN·m/m^3)

D_{50} = median grain size (mm)

Gurtug and Sridharan (2004) proposed correlations for optimum moisture content and maximum dry unit weight with the plastic limit (PL) of cohesive soil. These correlations can be expressed as

$$w_{\text{opt}}(\%) = [1.95 - 0.38(\log E)](\text{PL}) \tag{5.9}$$

$$\gamma_{d(\max)}(\text{kN/m}^3) = 22.68e^{-0.0183w_{\text{opt}}(\%)} \tag{5.10}$$

where PL = plastic limit (%)

E = compaction energy (kN·m/m^3)

For the modified Proctor test, $E = 2700\ \text{kN}\cdot\text{m/m}^3$. Hence,

$$w_{\text{opt}}(\%) \approx 0.65\,(\text{PL})$$

and

$$\gamma_{d(\text{max})}(\text{kN/m}^3) = 22.68e^{-0.012(\text{PL})}$$

Osman et al. (2008) analyzed a number of laboratory compaction-test results on fine-grained (cohesive) soil. Based on this study, the following correlations were developed:

$$w_{\text{opt}}(\%) = (1.99 - 0.165 \ln E)(\text{PI}) \tag{5.11}$$

and

$$\gamma_{d(\text{max})} = L - Mw_{\text{opt}} \tag{5.12}$$

where

$$L = 14.34 + 1.195 \ln E \tag{5.13}$$

$$M = -0.19 + 0.073 \ln E \tag{5.14}$$

w_{opt} = optimum moisture content (%)

PI = plasticity index (%)

$\gamma_{d(\text{max})}$ = maximum dry unit weight (kN/m^3)

E = compaction energy ($\text{kN}\cdot\text{m/m}^3$)

Matteo et al. (2009) analyzed the results of 71 fine-grained soil and provided the following correlations for optimum moisture content (w_{opt}) and maximum dry unit weight [$\gamma_{d(\text{max})}$] for the modified Proctor test ($E = 2700\ \text{kN}\cdot\text{m/m}^3$):

$$w_{\text{opt}}(\%) = -0.86(\text{LL}) + 3.04\left(\frac{\text{LL}}{G_s}\right) + 2.2 \tag{5.15}$$

and

$$\gamma_{d(\text{max})}(\text{kN/m}^3) = 40.316\,(w_{\text{opt}}^{-0.295})(\text{PI}^{0.032}) - 2.4 \tag{5.16}$$

where LL = liquid limit (%)

PI = plasticity index (%)

G_s = specific gravity of soil solids

EXAMPLE 5.1

For a granular soil, the following are given:

- $G_s = 2.6$
- Liquid limit on the fraction passing No. 40 sieve = 20
- Percent retained on No. 4 sieve = 20

Using Eqs. (5.4) and (5.5), estimate the maximum dry density of compaction and the optimum moisture content based on the modified Proctor test.

SOLUTION

From Eq. (5.4),

$$\begin{aligned}\rho_{d(\text{max})}(\text{kg/m}^3) &= [4{,}804{,}574G_s - 195.55(\text{LL})^2 + 156{,}971(R\#4)^{0.5} - 9{,}527{,}830]^{0.5} \\ &= [4{,}804{,}574(2.6) - 195.55(20)^2 + 156{,}971(20)^{0.5} - 9{,}527{,}830]^{0.5} \\ &= \mathbf{1894\ kg/m^3}\end{aligned}$$

From Eq. (5.5),

$$\begin{aligned}\text{In}\,(w_{\text{opt}}) &= 1.195 \times 10^{-4}(\text{LL})^2 - 1.964G_s - 6.617 \times 10^{-5}(R\#4) + 7651\\ &= 1.195 \times 10^{-4}(20)^2 - 1.964(2.6) - 6.617 \times 10^{-5}(20) + 7651\\ &= 2.591\\ w_{\text{opt}} &= \mathbf{13.35\%}\end{aligned}$$

EXAMPLE 5.2

For a sand with 4% finer than No. 200 sieve, estimate the maximum relative density of compaction that may be obtained from a modified Proctor test. Given $D_{50} = 1.4$ mm.

SOLUTION

For modified Proctor test, $E = 2700\ \text{kN}\cdot\text{m/m}^3$.

From Eq. (5.7),

$$A = 0.216 \ln E - 0.850 = (0.216)(\ln 2700) - 0.850 = 0.857$$

From Eq. (5.8),

$$B = -0.03 \ln E + 0.306 = -(0.03)(\ln 2700) + 0.306 = 0.069$$

From Eq. (5.6),

$$D_r = AD_{50}^{-B} = (0.857)(1.4)^{-0.069} = 0.837 = \mathbf{83.7\%}$$

EXAMPLE 5.3

For a silty clay soil given LL = 43 and PL = 18. Estimate the maximum dry unit weight of compaction that can be achieved by conducting a modified Proctor test. Use Eq. (5.12).

SOLUTION

For modified Proctor test, $E = 2700\ \text{kN}\cdot\text{m/m}^3$. From Eqs. (5.13) and (5.14),

$$L = 14.34 + 1.195 \ln E = 14.34 + 1.195 \ln (2700) = 23.78$$
$$M = -0.19 + 0.073 \ln E = -0.19 + 0.073 \ln (2700) = 0.387$$

From Eq. (5.11),

$$\begin{aligned}w_{\text{opt}}(\%) &= (1.99 - 0.165 \ln E)(\text{PI})\\ &= [1.99 - 0.165 \ln(2700)](43 - 18)\\ &= 17.16\%\end{aligned}$$

From Eq. (5.12),

$$\gamma_{d(\max)} = L - Mw_{\text{opt}} = 23.78 - (0.387)(17.16) = \mathbf{17.14\ kN/m^3}$$

5.4 Field Compaction

Ordinary compaction in the field is done by rollers. Of the several types of rollers used, the most common are

1. Smooth-wheel rollers (or smooth drum rollers)
2. Pneumatic rubber-tired rollers
3. Sheepsfoot rollers
4. Vibratory rollers

Figure 5.2 shows a *smooth-wheel roller* that can also create vertical vibration during compaction. Smooth-wheel rollers are suitable for proof-rolling subgrades and for finishing the construction of fills with sandy or clayey soil. They provide 100% coverage under the wheels, and the contact pressure can be as high as 300 to 400 kN/m^2 (≈45 to 60 lb/in^2). However, they do not produce a uniform unit weight of compaction when used on thick layers.

Pneumatic rubber-tired rollers (Figure 5.3) are better in many respects than smooth-wheel rollers. Pneumatic rollers, which may weigh as much as 2000 kN (450 kip), consist of a heavily loaded wagon with several rows of tires. The tires are closely spaced—four to six in a row. The contact pressure under the tires may range up to 600 to 700 kN/m^2 (≈85 to 100 lb/in^2), and they give about 70 to 80% coverage. Pneumatic rollers, which can be used for sandy and clayey soil compaction, produce a combination of pressure and kneading action.

Sheepsfoot rollers (Figure 5.4) consist basically of drums with large numbers of projections. The area of each of the projections may be 25 to 90 cm^2 (4 to 14 in^2). These rollers are *most effective in compacting cohesive soil*. The contact pressure under the projections may range from 1500 to 7500 kN/m^2 (≈215 to 1100 lb/in^2). During compaction in the field, the initial passes compact the lower portion of a lift. Later, the middle and top of the lift are compacted.

Vibratory rollers are efficient in compacting granular soil. Vibrators can be attached to smooth-wheel, pneumatic rubber-tired, or sheepsfoot rollers to send vibrations into



FIGURE 5.2 Vibratory smooth-wheel rollers (Dmitry Kalinovsky/Shutterstock.com)



FIGURE 5.3 Pneumatic rubber-tired roller (Vadim Ratnikov/Shutterstock.com)



FIGURE 5.4 Vibratory sheepsfoot roller (Artit Thongchuea/Shutterstock.com)

the soil being compacted. Figures 5.2 and 5.4 show vibratory smooth-wheel rollers and a vibratory sheepsfoot roller, respectively.

In general, compaction in the field depends on several factors, such as the type of compactor, type of soil, moisture content, lift thickness, towing speed of the compactor, and number of passes the roller makes.

Figure 5.5 shows the variation of the unit weight of compaction with depth for a poorly graded dune sand compacted by a vibratory drum roller. Vibration was produced by mounting an eccentric weight on a single rotating shaft within the drum cylinder. The weight of the roller used for this compaction was 55.7 kN (12.5 kip), and the drum diameter was 1.19 m (3.9 ft). The lifts were kept at 2.44 m (8 ft). Note that, at any depth, the dry unit weight of compaction increases

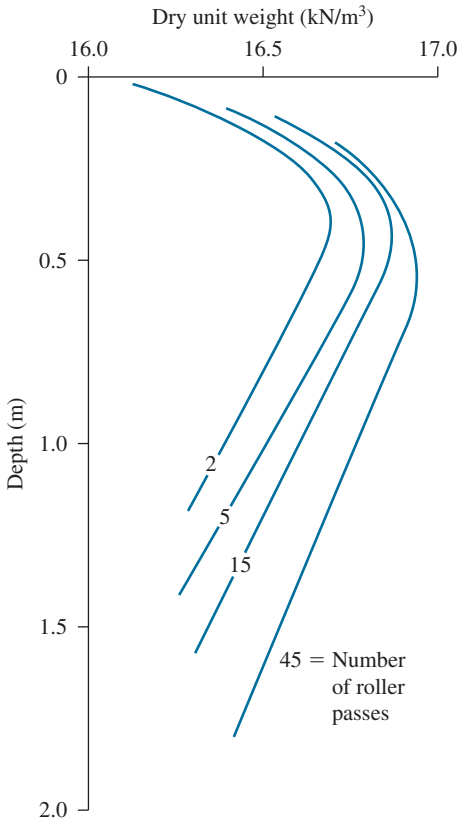


FIGURE 5.5 Vibratory compaction of a sand: Variation of dry unit weight with depth and number of roller passes; lift thickness = 2.44 m (Based on D'Appolonia, D. J., Whitman, R. V. and D'Appolonia, E. (1969). "Sand Compaction with Vibratory Rollers," *Journal of the Soil Mechanics and Foundations Division*, American Society of Civil Engineers, Vol. 95, N. SM1, pp. 263–284.)

with the number of passes the roller makes. However, the rate of increase in unit weight gradually decreases after about 15 passes. Note also the variation of dry unit weight with depth by the number of roller passes. The dry unit weight and hence the relative density, D_r, reach maximum values at a depth of about 0.5 m (≈1.6 ft) and then gradually decrease as the depth increases. The reason is the lack of confining pressure toward the surface. Once the relation between depth and relative density (or dry unit weight) for a soil for a given number of passes is determined, for satisfactory compaction based on a given specification, the approximate thickness of each lift can be easily estimated.

Hand-held vibrating plates can be used for effective compaction of granular soil over a limited area. Vibrating plates are also gang-mounted on machines. These can be used in less restricted areas.

5.5 Compaction Control for Clay Hydraulic Barriers

Compacted clays are commonly used as hydraulic barriers in cores of earth dams, liners and covers of landfills, and liners of surface impoundments. Since the primary purpose of a barrier is to minimize flow, the hydraulic conductivity, k, is the controlling factor. In many cases, it is desired that the hydraulic conductivity be less than 10^{-7}cm/s. This can be achieved by controlling the minimum degree of saturation during compaction, a relation that can be explained by referring to the compaction characteristics of three soil described in Table 5.4 (Othman and Luettich, 1994).

TABLE 5.4 Characteristics of Soil Reported in Figures 5.6, 5.7, and 5.8

Soil	Classification	Liquid limit	Plasticity index	Percent finer than No. 200 sieve (0.075 mm)
Wisconsin A	CL	34	16	85
Wisconsin B	CL	42	19	99
Wisconsin C	CH	84	60	71

Figures 5.6, 5.7, and 5.8 show the standard and modified Proctor test results and the hydraulic conductivities of compacted specimens. Note that the solid symbols represent specimens with hydraulic conductivities of 10^{-7} cm/s or less. As can be seen from these figures, the data points plot generally parallel to the

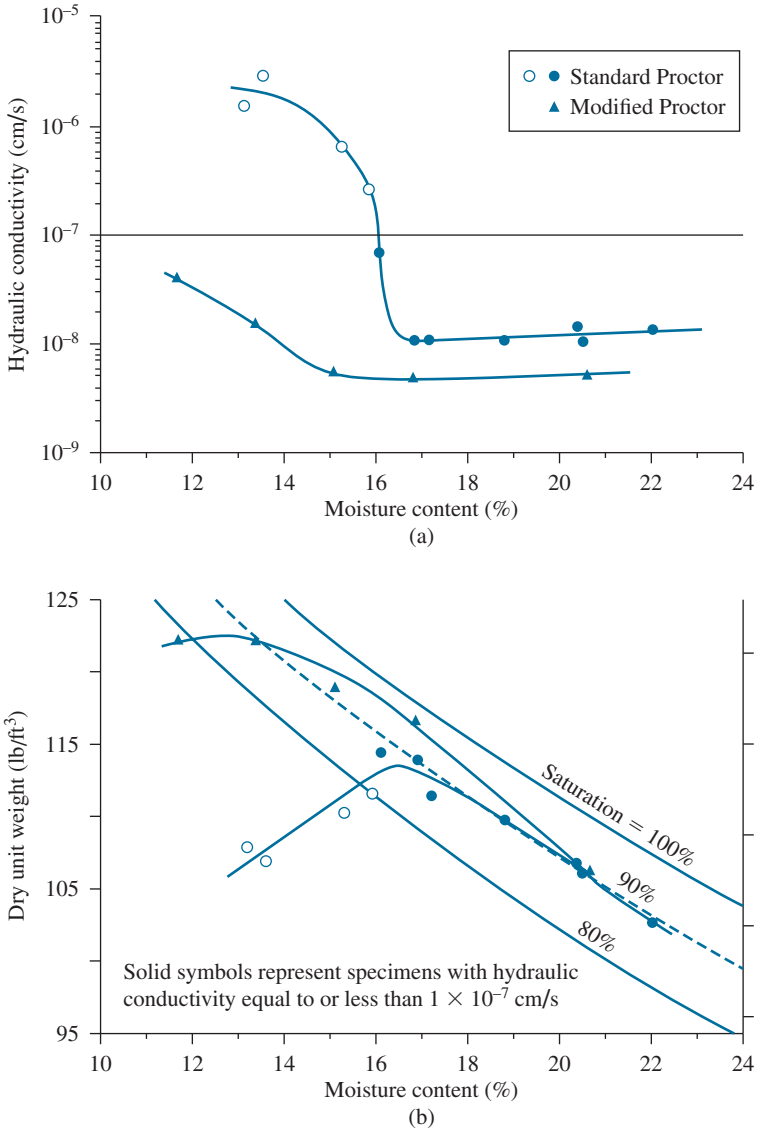


FIGURE 5.6 Standard and modified Proctor test results and hydraulic conductivity of Wisconsin A soil (Based on Othman, M. A., and S. M. Luettich, "Compaction Control Criteria for Clay Hydraulic Barriers," *Transportation Research Record 1462*, Transportation Research Board, National Research Council, Washington, D.C., 1994)

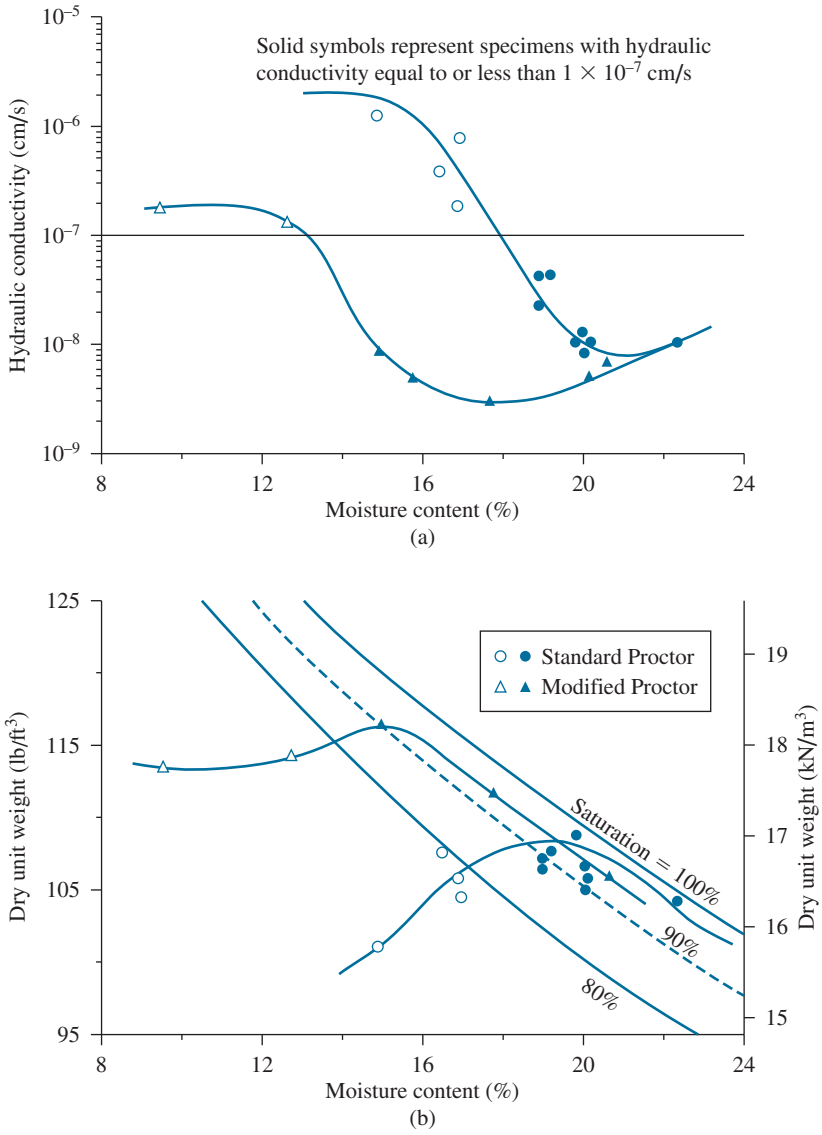


FIGURE 5.7 Standard and modified Proctor test results and hydraulic conductivity of Wisconsin B soil (Based on Othman, M. A., and S. M. Luettich, "Compaction Control Criteria for Clay Hydraulic Barriers," *Transportation Research Record 1462*, Transportation Research Board, National Research Council, Washington, D.C., 1994)

line of full saturation. Figure 5.9 shows the effect of the degree of saturation during compaction on the hydraulic conductivity of the three soil. It is evident from the figure that, if it is desired that the maximum hydraulic conductivity be 10^{-7} cm/s, then all soil should be compacted at a minimum degree of saturation of 88%.

In field compaction at a given site, soil of various composition may be encountered. Small changes in the content of fines will change the magnitude of hydraulic conductivity. Hence, considering the various soil likely to be encountered at a given site, the procedure just described aids in developing a minimum-degree-of-saturation criterion for compaction to construct hydraulic barriers.

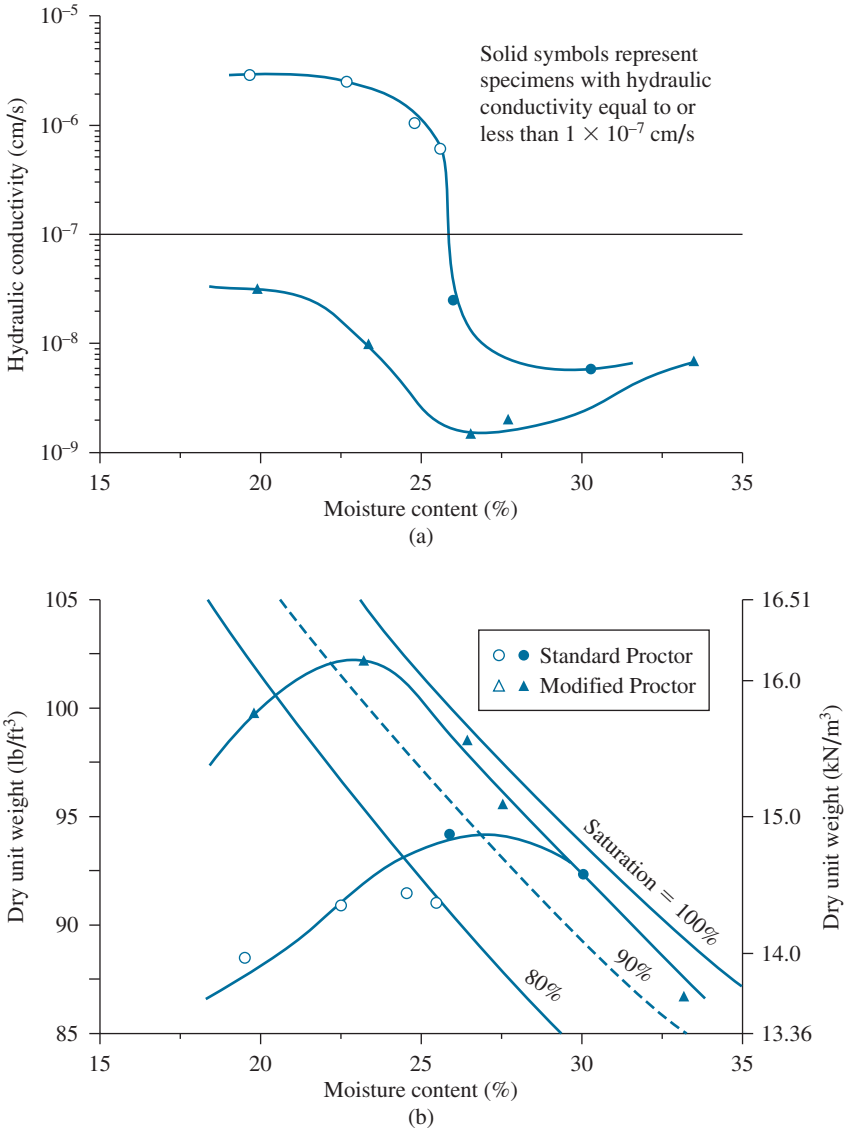


FIGURE 5.8 Standard and modified Proctor test results and hydraulic conductivity of Wisconsin C soil (Based on Othman, M. A., and S. M. Luettich, "Compaction Control Criteria for Clay Hydraulic Barriers," *Transportation Research Record 1462*, Transportation Research Board, National Research Council, Washington, D.C., 1994)

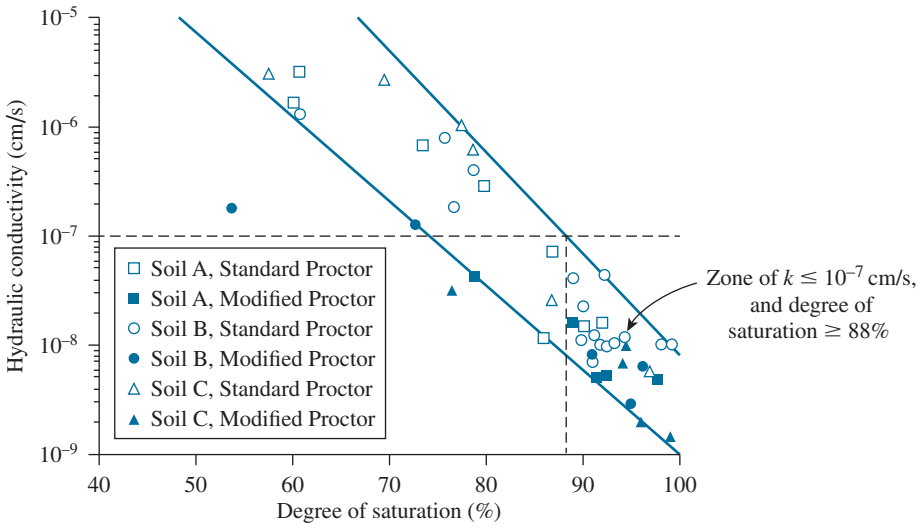


FIGURE 5.9 Effect of degree of saturation on hydraulic conductivity of Wisconsin A, B, and C soil (After Othman and Luettich, 1994) (Based on Othman, M. A., and S. M. Luettich, "Compaction Control Criteria for Clay Hydraulic Barriers," *Transportation Research Record 1462*, Transportation Research Board, National Research Council, Washington, D.C., 1994)

5.6 Vibroflotation

Vibroflotation is a technique developed in Germany in the 1930s for *in situ* densification of thick layers of loose granular soil deposits. Vibroflotation was first used in the United States about 10 years later. The process involves the use of a *vibroflot* (called the *vibrating unit*), as shown in Figure 5.10. The device is about 2 m (6 ft) in length. This vibrating unit has an eccentric weight inside it and can develop a centrifugal force. The weight enables the unit to vibrate horizontally. Openings at the bottom and top of the unit are for water jets. The vibrating unit is attached to a follow-up pipe. The figure shows the vibroflotation equipment necessary for compaction in the field.

The entire compaction process can be divided into four steps (see Figure 5.11):

Step 1. The jet at the bottom of the vibroflot is turned on, and the vibroflot is lowered into the ground.

Step 2. The water jet creates a quick condition in the soil, which allows the vibrating unit to sink.

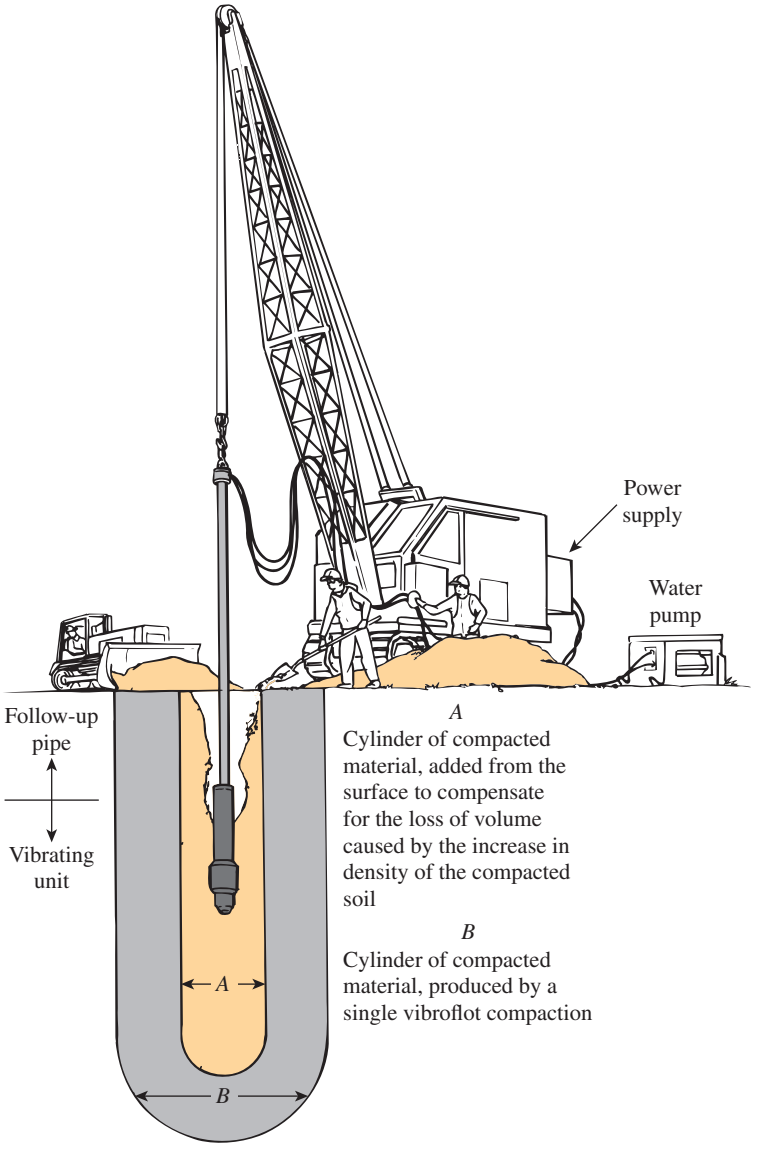


FIGURE 5.10 Vibroflotation unit (Based on Brown, 1977)

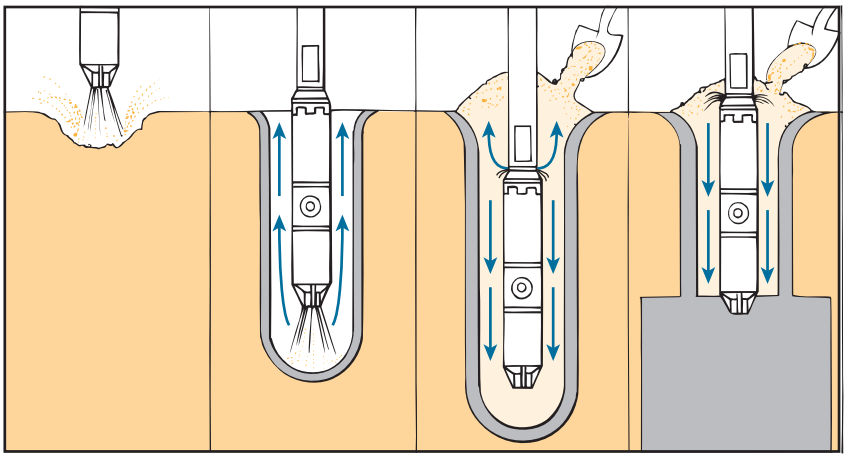


FIGURE 5.11 Compaction by the vibroflotation process (Based on Brown, 1977)

Step 3. Granular material is poured into the top of the hole. The water from the lower jet is transferred to the jet at the top of the vibrating unit. This water carries the granular material down the hole.

Step 4. The vibrating unit is gradually raised in about 0.3 m (1 ft) lifts and is held vibrating for about 30 seconds at a time. This process compacts the soil to the desired unit weight.

Table 5.5 gives the details of various types of vibroflot units used in the United States. The 30 HP electric units have been used since the latter part of the 1940s. The 100 HP units were introduced in the early 1970s. The zone of compaction around a single probe will vary according to the type of vibroflot used. The cylindrical zone of compaction will have a radius of about 2 m (6 ft) for a 30 HP unit and about 3 m (10 ft) for a 100 HP unit. Compaction by vibroflotation involves various probe spacings, depending on the zone of compaction (see Figure 5.12). Mitchell (1970) and Brown (1977) reported several successful cases of foundation design that used vibroflotation.

The success of densification of *in situ* soil depends on several factors, the most important of which are the grain-size distribution of the soil and the nature of the backfill used to fill the holes during the withdrawal period of the vibroflot. The range of the grain-size distribution of *in situ* soil marked Zone 1 in Figure 5.13 is most suitable for compaction by vibroflotation. Soil that contain excessive amounts of fine sand and silt-size particles are difficult to compact; for such soil, considerable effort is needed to reach the proper relative density of compaction. Zone 2 in Figure 5.13 is the approximate lower limit of grain-size distribution for compaction by vibroflotation. Soil deposits whose grain-size distribution falls into Zone 3 contain appreciable amounts of gravel. For these soil, the rate of probe penetration may be rather slow, so compaction by vibroflotation might prove to be uneconomical in the long run.

The grain-size distribution of the backfill material is one of the factors that controls the rate of densification. Brown (1977) defined a quantity called the *suitability number* for rating a backfill material. The suitability number is given by the formula

$$S_N = 1.7\sqrt{\frac{3}{(D_{50})^2} + \frac{1}{(D_{20})^2} + \frac{1}{(D_{10})^2}} \tag{5.17}$$

TABLE 5.5 Types of Vibrating Units[a]

	100 HP electric and hydraulic motors	30 HP electric motors
	(a) Vibrating tip	
Length	2.1 m (7 ft)	1.86 m (6.11 ft)
Diameter	406 mm (16 in.)	381 mm (15 in.)
Weight	18 kN (4000 lb)	18 kN (4000 lb)
Maximum movement when free	12.5 mm (0.49 in.)	7.6 mm (0.3 in.)
Centrifugal force	160 kN (18 ton)	90 kN (10 ton)
	(b) Eccentric	
Weight	1.16 kN (260 lb)	0.76 kN (170 lb)
Offset	38 mm (1.5 in.)	32 mm (1.25 in.)
Length	610 mm (24 in.)	387 mm (15.3 in.)
Speed	1800 rpm	1800 rpm
	(c) Pump	
Operating flow rate	0–1.6 m^3/min (0–400 gal/min)	0–0.6 m^3/min (0–150 gal/min)
Pressure	690–1035 kN/m^2 (100–150 $lb/in.^2$)	690–1035 kN/m^2 (100–150 lb/in^2)
	(d) Lower follow-up pipe and extensions	
Diameter	305 mm (12 in.)	305 mm (12 in.)
Weight	3.65 kN/m (250 lb/ft)	3.65 kN/m (250 lb/ft)

[a]Based on data from Brown, E. E. (1977), "Vibroflotation Compaction of Cohensionless Soils," *Journal of the Geotechnical Engineering Divison,* Vol. 103, No. GT12.

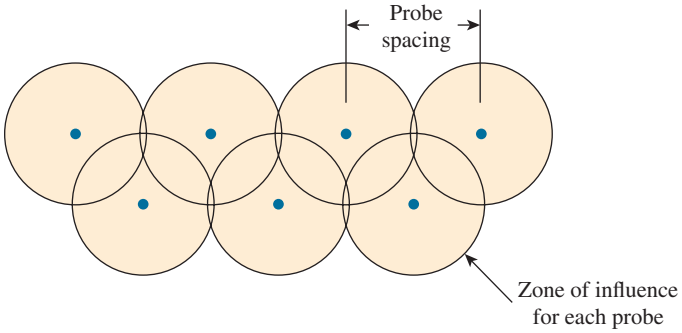


FIGURE 5.12 Nature of probe spacing for vibroflotation

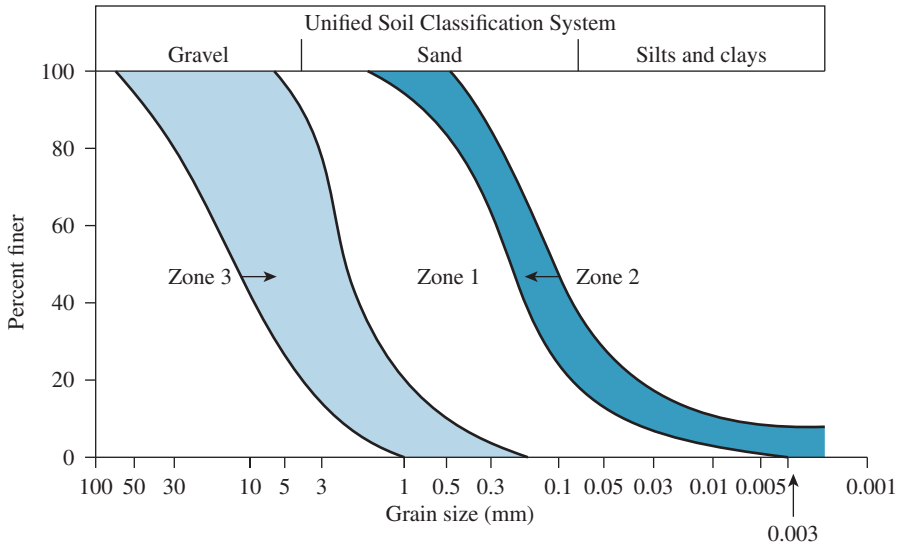


FIGURE 5.13 Effective range of grain-size distribution of soil for vibroflotation

where D_{50}, D_{20}, and D_{10} are the diameters (in mm) through which 50%, 20%, and 10%, respectively, of the material is passing. The smaller the value of S_N, the more desirable is the backfill material. A backfill rating system proposed by Brown (1977) is given in Table 5.6.

An excellent case study that evaluated the benefits of vibroflotation was presented by Basore and Boitano (1969). Densification of granular subsoil was necessary for the construction of a three-story office building at the Treasure Island Naval Station in San Francisco, California. The top 9 m (≈30 ft) of soil at the site was loose to medium-dense sand fill that had to be compacted. Figure 5.14a shows the nature of the layout of the vibroflotation points. Sixteen compaction points were arranged in groups of four, with 1.22 m (4 ft), 1.52 m (5 ft), 1.83 m (6 ft), and 2.44 m (8 ft) spacing. Prior to compaction, standard penetration tests were conducted at the centers of groups of three compaction points. After the completion of compaction by vibroflotation, the variation of the standard penetration resistance with depth was determined at the same points.

Figure 5.14b shows the variation of standard penetration resistance, N_{60}, with depth before and after compaction for vibroflotation point spacings $S' = 1.22$ m (4 ft) and 2.44 m (8 ft). From this figure, the following general conclusions can be drawn:

- For any given S', the magnitude of N_{60} after compaction decreases with an increase in depth.
- An increase in N_{60} indicates an increase in the relative density of sand.
- The degree of compaction decreases with the increase in S'. At $S' = 1.22$ m (4 ft), the degree of compaction at any depth is the largest. However, at $S' = 2.44$ m (8 ft), the vibroflotation had practically no effect in compacting soil.

TABLE 5.6 Backfill Rating System for Vibroflotation

Range of S_N	Rating as backfill
0–10	Excellent
10–20	Good
20–30	Fair
30–50	Poor
>50	Unsuitable

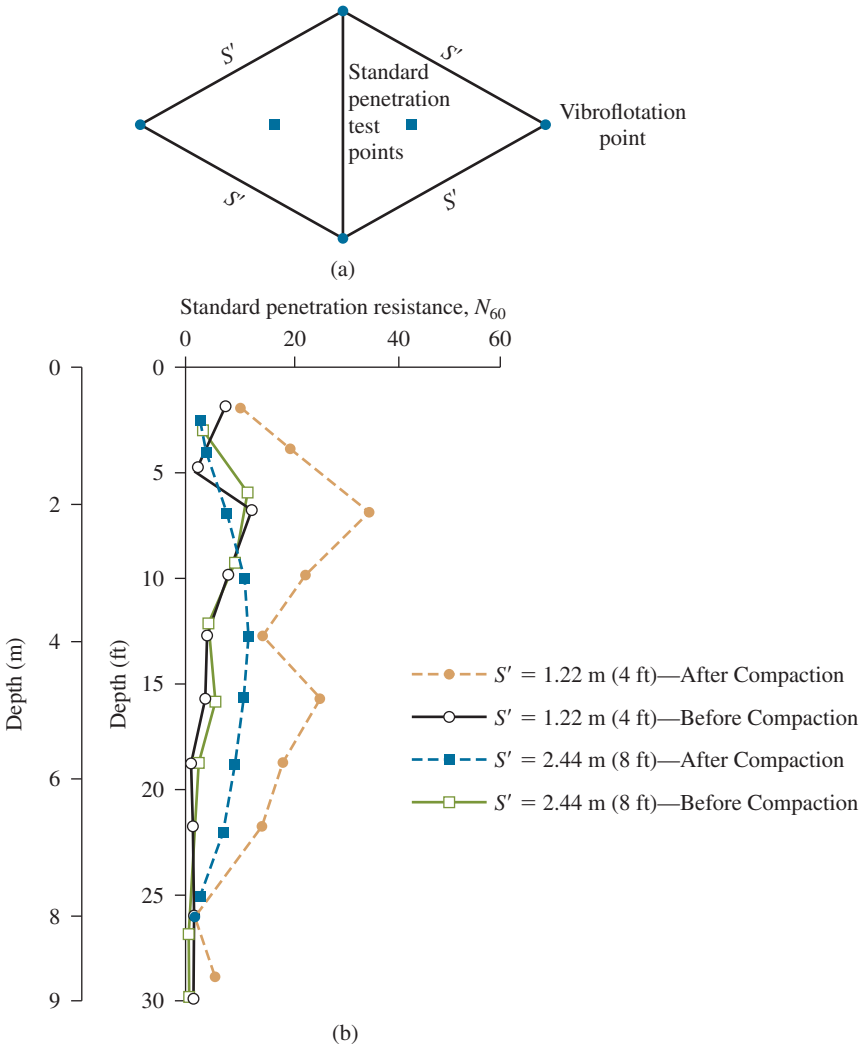


FIGURE 5.14 (a) Layout of vibroflotation compaction points; (b) variation of standard penetration resistance (N_{60}) before and after compaction (Based on Basore, C. E. and Boitano, J. D. (1969). "Sand Densification by Piles and Vibrofloation," *Journal of Soil Mechanics and Foundation Engineering Division*, American Society of Civil Engineers, Vol. 95, No. 6, pp. 1301–1323, Figure 16.)

During the past 50 years, the vibroflotation technique has been used successfully on large projects to compact granular subsoils, thereby controlling structural settlement.

5.7 Blasting

Blasting is a technique that has been used successfully in many projects (Mitchell, 1970) for the densification of granular soil. The general soil grain sizes suitable for compaction by blasting are the same as those for compaction by vibroflotation. The process involves the detonation of explosive charges such as 60% dynamite at a certain depth below the ground surface in saturated soil. The lateral spacing of the charges varies from about 3 to 9 m (10 to 30 ft). Three to five successful detonations

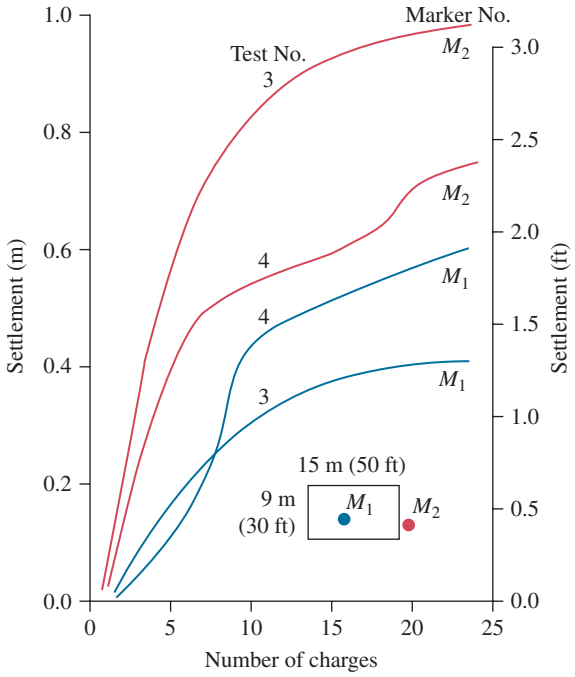


FIGURE 5.15 Ground settlement as a function of number of explosive charges

are usually necessary to achieve the desired compaction. Compaction (up to a relative density of about 80%) up to a depth of about 18 m (60 ft) over a large area can easily be achieved by using this process. Usually, the explosive charges are placed at a depth of about two-thirds of the thickness of the soil layer desired to be compacted. The sphere of influence of compaction by a 60% dynamite charge can be given as follows (Mitchell, 1970):

$$r = \sqrt{\frac{W_{EX}}{C}} \tag{5.18}$$

where r = sphere of influence

W_{EX} = weight of explosive (60% dynamite)

C = 0.0122 when W_{EX} is in kg and r is in m

= 0.0025 when W_{EX} is in lb and r is in ft

Figure 5.15 shows the test results of soil densification by blasting in an area measuring 15 m by 9 m (50 ft by 30 ft) (Mitchell, 1970). For these tests, twenty 2.09 kg (4.6 lb) charges of Gelamite No. 1 (Hercules Powder Company, Wilmington, Delaware) were used.

5.8 Precompression

When highly compressible, normally consolidated clayey soil layers lie at a limited depth and large consolidation settlements are expected as the result of the construction of large buildings, highway embankments, or earth dams, precompression of soil may be used to minimize postconstruction settlement. The principles of precompression are best explained by reference to Figure 5.16. Here, the proposed

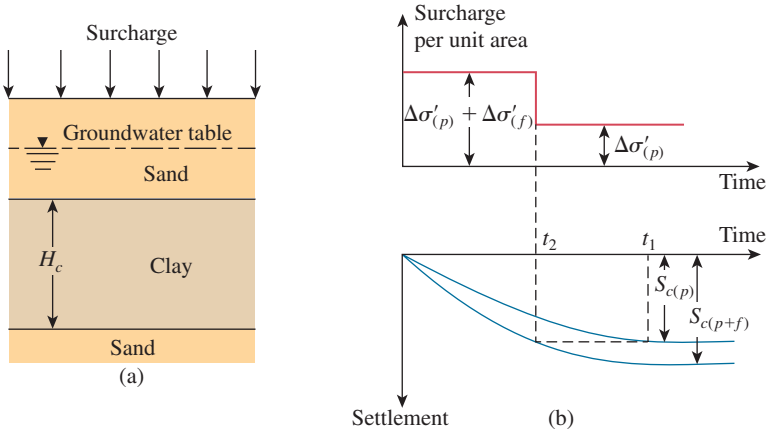


FIGURE 5.16 Principles of precompression

structural load per unit area is $\Delta\sigma'_{(p)}$, and the thickness of the clay layer undergoing consolidation is H_c. The maximum primary consolidation settlement caused by the structural load is then

$$S_{c(p)} = \frac{C_c H_c}{1 + e_o} \log \frac{\sigma'_o + \Delta\sigma'_{(p)}}{\sigma'_o} \tag{5.19}$$

The settlement–time relationship under the structural load will be like that shown in Figure 5.16b. However, if a surcharge of $\Delta\sigma'_{(p)} + \Delta\sigma'_{(f)}$ is placed on the ground, the primary consolidation settlement will be

$$S_{c(p+f)} = \frac{C_c H_c}{1 + e_o} \log \frac{\sigma'_o + [\Delta\sigma'_{(p)} + \Delta\sigma'_{(f)}]}{\sigma'_o} \tag{5.20}$$

The settlement–time relationship under a surcharge of $\Delta\sigma'_{(p)} + \Delta\sigma'_{(f)}$ is also shown in Figure 5.16b. Note that a total settlement of $S_{c(p)}$ would occur at time t_2, which is much shorter than t_1. So, if a temporary total surcharge of $\Delta\sigma'_{(p)} + \Delta\sigma'_{(f)}$ is applied on the ground surface for time t_2, the settlement will equal $S_{c(p)}$. At that time, if the total surcharge is removed and a structure with a permanent load per unit area of $\Delta\sigma'_{(p)}$ is built, no appreciable settlement will occur. The procedure just described is called *precompression*. The total surcharge $\Delta\sigma'_{(p)} + \Delta\sigma'_{(f)}$ can be applied by means of temporary fills.

DERIVATION OF EQUATIONS FOR OBTAINING $\Delta\sigma'_{(f)}$ AND t_2

Figure 5.16b shows that, under a surcharge of $\Delta\sigma'_{(p)} + \Delta\sigma'_{(f)}$, the degree of consolidation at time t_2 after the application of the load is

$$U = \frac{S_{c(p)}}{S_{c(p+f)}} \tag{5.21}$$

Substitution of Eqs. (5.19) and (5.20) into Eq. (5.21) yields

$$U = \frac{\log\left[\dfrac{\sigma'_o + \Delta\sigma'_{(p)}}{\sigma'_o}\right]}{\log\left[\dfrac{\sigma'_o + \Delta\sigma'_{(p)} + \Delta\sigma'_{(f)}}{\sigma'_o}\right]} = \frac{\log\left[1 + \dfrac{\Delta\sigma'_{(p)}}{\sigma'_o}\right]}{\log\left\{1 + \dfrac{\Delta\sigma'_{(p)}}{\sigma'_o}\left[1 + \dfrac{\Delta\sigma'_{(f)}}{\Delta\sigma'_{(p)}}\right]\right\}} \tag{5.22}$$

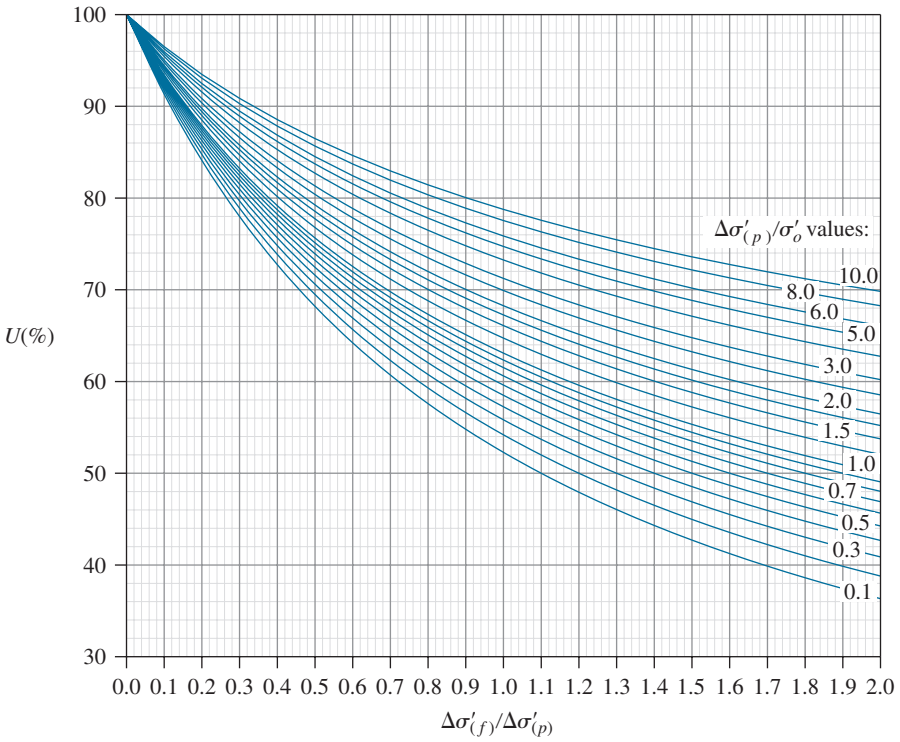


FIGURE 5.17 Plot of U against $\Delta\sigma'_{(f)}/\Delta\sigma'_{(p)}$ for various values of $\Delta\sigma'_{(p)}/\sigma'_o$—Eq. (5.22)

Figure 5.17 gives magnitudes of U for various combinations of $\Delta\sigma'_{(p)}/\sigma'_o$ and $\Delta\sigma'_{(f)}/\Delta\sigma'_{(p)}$. The degree of consolidation referred to in Eq. (5.22) is actually the average degree of consolidation at time t_2, as shown in Figure 5.17. However, if the average degree of consolidation is used to determine t_2, some construction problems might occur. The reason is that, after the removal of the surcharge and placement of the structural load, the portion of clay close to the drainage surface will continue to swell, and the soil close to the midplane will continue to settle (see Figure 5.18). In some cases, net continuous settlement might result. A conservative approach may solve the problem; that is, assume that U in Eq. (5.22) is the midplane degree of consolidation, which is smaller (Johnson, 1970a). By underestimating U, we conservatively overestimate the required preload $\Delta\sigma'_{(f)}$. Now, from Eq. (2.77),

$$U = 1 - \sum_{m=0}^{m=\infty}\left(\frac{2}{M^2}\right)e^{-M^2T_v} \tag{2.77}$$

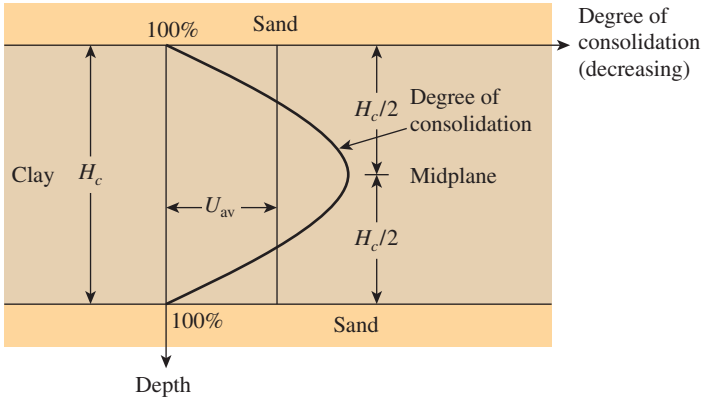
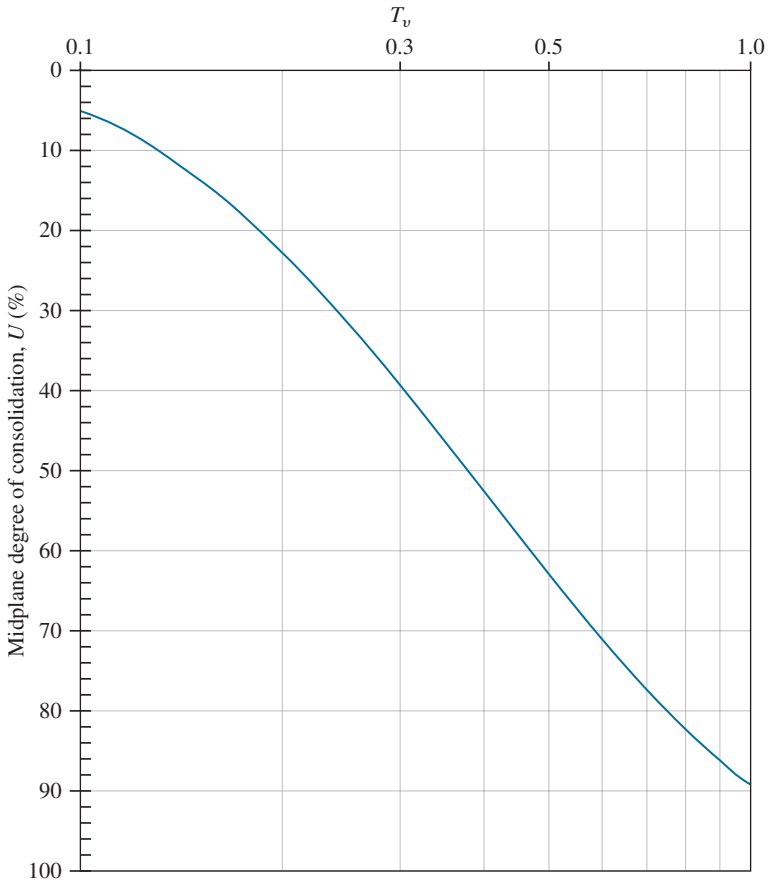


FIGURE 5.18



T_v	U (%)
0.05	0.31
0.10	5.07
0.15	13.58
0.20	22.77
0.25	31.46
0.30	39.32
0.40	52.55
0.50	62.92
0.60	71.03
0.70	77.36
0.80	82.31
0.90	86.18
1.00	89.2
1.50	96.86

FIGURE 5.19 Plot of midplane degree of consolidation against T_v

where

T_v = time factor = $c_v t_2/H^2$

c_v = coefficient of consolidation

t_2 = time

H = maximum drainage path (=$H_c/2$ for two-way drainage and H_c for one-way drainage)

The variation of U (the midplane degree of consolidation) with T_v is given in Figure 5.19.

PROCEDURE FOR OBTAINING PRECOMPRESSION PARAMETERS

Two problems may be encountered by engineers during precompression work in the field:

1. The value of $\Delta\sigma'_{(f)}$ is known, but t_2 must be obtained. In such a case, obtain σ'_o, $\Delta\sigma_{(p)}$, and solve for U, using Eq. (5.22) or Figure 5.17. For this value of U, obtain T_v from Figure 5.19. Then

$$t_2 = \frac{T_v H^2}{c_v} \tag{5.23}$$

2. For a specified value of t_2, $\Delta\sigma'_{(f)}$ must be obtained. In such a case, calculate T_v. Then use Figure 5.19 to obtain the midplane degree of consolidation, U. With the estimated value of U, go to Figure 5.17 to get the required value of $\Delta\sigma'_{(f)}/\Delta\sigma'_{(p)}$, and then calculate $\Delta\sigma'_{(f)}$.

Several case histories on the successful use of precompression techniques for improving foundation soil are available in the literature (for example, Johnson, 1970a).

EXAMPLE 5.4

Examine Figure 5.16. During the construction of a highway bridge, the average permanent load on the clay layer is expected to increase by about 115 kN/m^2. The average effective overburden pressure at the middle of the clay layer is 210 kN/m^2. Here, $H_c = 6$ m, $C_c = 0.28$, $e_o = 0.9$, and $c_v = 0.36$ m^2/mo. The clay is normally consolidated. Determine

(a) The total primary consolidation settlement of the bridge without precompression

(b) The surcharge, $\Delta\sigma'_{(f)}$, needed to eliminate the entire primary consolidation settlement in nine months by precompression.

SOLUTION

Part a

The total primary consolidation settlement may be calculated from Eq. (5.19):

$$S_{c(p)} = \frac{C_c H_c}{1 + e_o} \log\left[\frac{\sigma'_o + \Delta\sigma'_{(p)}}{\sigma'_o}\right] = \frac{(0.28)(6)}{1 + 0.9} \log\left[\frac{210 + 115}{210}\right]$$
$$= 0.1677 \text{ m} = \mathbf{167.7 \text{ mm}}$$

Part b

We have

$$T_v = \frac{c_v t_2}{H^2}$$
$$c_v = 0.36 \text{ m}^2/\text{mo.}$$
$$H = 3 \text{ m (two-way drainage)}$$
$$t_2 = 9 \text{ mo.}$$

Hence,

$$T_v = \frac{(0.36)(9)}{3^2} = 0.36$$

According to Figure 5.19, for $T_v = 0.36$, the value of U is 47%. Now,

$$\Delta\sigma'_{(p)} = 115 \text{ kN/m}^2$$

and

$$\sigma'_o = 210 \text{ kN/m}^2$$

so

$$\frac{\Delta\sigma'_{(p)}}{\sigma'_o} = \frac{115}{210} = 0.548$$

According to Figure 5.17, for $U = 47\%$ and $\Delta\sigma'_{(p)}/\sigma'_o = 0.548$, $\Delta\sigma'_{(f)}/\Delta\sigma'_{(p)} \approx 1.8$; thus,

$$\Delta\sigma'_{(f)} = (1.8)(115) = \mathbf{207 \text{ kN/m}^2}$$

Note: The total surcharge to be applied during the 9 months would be

$$\Delta\sigma'_{(p)} + \Delta\sigma'_{(f)} = 115 + 207 = 322 \text{ kN/m}^2$$

5.9 Sand Drains

The use of sand drains is another way to accelerate the consolidation settlement of soft, normally consolidated clay layers and achieve precompression before the construction of a desired foundation, thus reducing the postconstruction settlement. Sand drains are constructed by drilling holes through the clay layer(s) in the field at regular intervals. The holes are then backfilled with sand. This can be achieved by several means, such as (a) rotary drilling and then backfilling with sand; (b) drilling by continuous-flight auger with a hollow stem and backfilling with sand (through the hollow steam); and (c) driving hollow steel piles. The soil inside the pile is then jetted out, after which backfilling with sand is done. Figure 5.20 shows a schematic diagram of sand drains. After backfilling the drill holes with sand, a surcharge is applied at the ground surface. The surcharge will increase the pore water pressure in the clay. The excess pore water pressure in the clay will be dissipated by drainage—both vertically and radially to the sand drains—thereby accelerating settlement of the clay layer. In Figure 5.20a, note that the radius of the sand drains is r_w. Figure 5.20b shows the plan of the layout of the sand drains. The effective zone from which the radial drainage will be directed toward a given sand drain is approximately cylindrical, with a diameter of d_e.

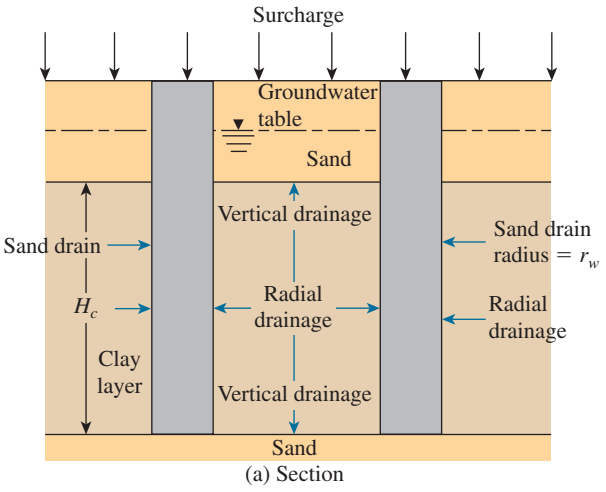


FIGURE 5.20 Sand drains

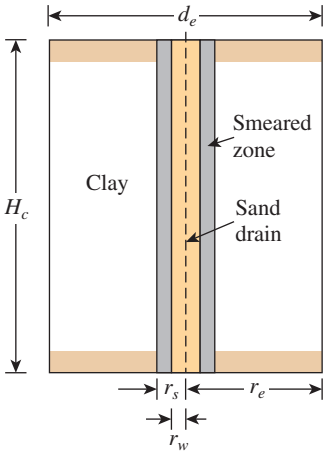


FIGURE 5.21 Schematic diagram of a sand drain

To determine the surcharge that needs to be applied at the ground surface and the length of time that it has to be maintained, see Figure 5.16 and use the corresponding equation, Eq. (5.22):

$$U_{v,r} = \frac{\log\left[1 + \dfrac{\Delta\sigma'_{(p)}}{\sigma'_o}\right]}{\log\left\{1 + \dfrac{\Delta\sigma'_{(p)}}{\sigma'_o}\left[1 + \dfrac{\Delta\sigma'_{(f)}}{\Delta\sigma'_{(p)}}\right]\right\}} \tag{5.24}$$

The notations $\Delta\sigma'_{(p)}$, σ'_o, and $\Delta\sigma'_{(f)}$ are the same as those in Eq. (5.22); however, the left-hand side of Eq. (5.24) is the *average degree* of consolidation instead of the degree of consolidation at midplane. Both *radial* and *vertical* drainage contribute to the average degree of consolidation. If $U_{v,r}$ can be determined for any time t_2 (see Figure 5.16b), the total surcharge $\Delta\sigma'_{(f)} + \Delta\sigma'_{(p)}$ may be obtained easily from Figure 5.17. The procedure for determining the average degree of consolidation ($U_{v,r}$) follows:

For a given surcharge and duration, t_2, the average degree of consolidation due to drainage in the vertical and radial directions is

$$U_{v,r} = 1 - (1 - U_r)(1 - U_v) \tag{5.25}$$

where

U_r = average degree of consolidation with radial drainage only

U_v = average degree of consolidation with vertical drainage only

The successful use of sand drains has been described in detail by Johnson (1970b). As with precompression, constant field settlement observations may be necessary during the period the surcharge is applied.

AVERAGE DEGREE OF CONSOLIDATION DUE TO RADIAL DRAINAGE ONLY

Figure 5.21 shows a schematic diagram of a sand drain. In the figure, r_w is the radius of the sand drain, and $r_e = d_e/2$ is the radius of the effective zone of drainage. It is also important to realize that, during the installation of sand drains, a certain zone of clay surrounding them is smeared, thereby changing the hydraulic conductivity of the clay. In the figure, r_s is the radial distance from the center of the sand drain to the farthest point of the smeared zone. Now, for the average-degree-of-consolidation relationship, we will use the *theory of equal strain*. Two cases may arise that relate to the nature of the application of surcharge, and they are shown in Figure 5.22. (See the notations shown in Figure 5.16.) Either (a) the entire surcharge is applied instantaneously

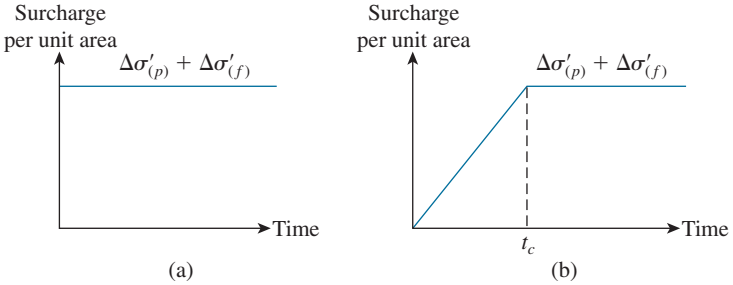


FIGURE 5.22 Nature of application of surcharge

(see Figure 5.22a), or (b) the surcharge is applied in the form of a ramp load (see Figure 5.22b). When the entire surcharge is applied instantaneously (Barron, 1948),

$$U_r = 1 - \exp\left(\frac{-8T_r}{m}\right) \tag{5.26}$$

where

$$m = \frac{n^2}{n^2 - S^2}\ln\left(\frac{n}{S}\right) - \frac{3}{4} + \frac{S^2}{4n^2} + \frac{k_h}{k_s}\left(\frac{n^2 - S^2}{n^2}\right)\ln S \tag{5.27}$$

in which

$$n = \frac{d_e}{2r_w} = \frac{r_e}{r_w} \tag{5.28}$$

$$S = \frac{r_s}{r_w} \tag{5.29}$$

and

k_h = hydraulic conductivity of clay in the horizontal direction in the unsmeared zone

k_s = horizontal hydraulic conductivity in the smeared zone

T_r = nondimensional time factor for radial drainage only $= \dfrac{c_{\text{vr}}t_2}{d_e^2}$ (5.30)

c_{vr} = coefficient of consolidation for radial drainage

$$= \frac{k_h}{\left[\dfrac{\Delta e}{\Delta\sigma'(1 + e_{\text{av}})}\right]\gamma_w} \tag{5.31}$$

For a *no-smear case*, $r_s = r_w$ and $k_h = k_s$, so $S = 1$ and Eq. (5.27) becomes

$$m = \left(\frac{n^2}{n^2 - 1}\right)\ln(n) - \frac{3n^2 - 1}{4n^2} \tag{5.32}$$

Table 5.7 gives the values of U_r for various values of T_r and n.

If the surcharge is applied in the form of a *ramp* and *there is no smear*, then (Olson, 1977)

$$U_r = \frac{T_r - \dfrac{1}{A}[1 - \exp(-AT_r)]}{T_{\text{rc}}} \quad (\text{for } T_r \le T_{\text{rc}}) \tag{5.33}$$

and

$$U_r = 1 - \frac{1}{AT_{\text{rc}}}[\exp(AT_{\text{rc}}) - 1]\exp(-AT_{\text{rc}}) \quad (\text{for } T_r \ge T_{\text{rc}}) \tag{5.34}$$

where

$$T_{\text{rc}} = \frac{c_{\text{vr}}t_c}{d_e^2} \text{ (see Figure 5.22b for the definition of } t_c) \tag{5.35}$$

and

$$A = \frac{2}{m} \tag{5.36}$$

TABLE 5.7 Variation of U_r for Various Values of T_r and n, No-Smear Case [Eqs. (5.26) and (5.32)]

Degree of consolidation U_r (%)	Time factor T_r for value of n ($= r_e/r_w$)				
	5	10	15	20	25
0	0	0	0	0	0
1	0.0012	0.0020	0.0025	0.0028	0.0031
2	0.0024	0.0040	0.0050	0.0057	0.0063
3	0.0036	0.0060	0.0075	0.0086	0.0094
4	0.0048	0.0081	0.0101	0.0115	0.0126
5	0.0060	0.0101	0.0126	0.0145	0.0159
6	0.0072	0.0122	0.0153	0.0174	0.0191
7	0.0085	0.0143	0.0179	0.0205	0.0225
8	0.0098	0.0165	0.0206	0.0235	0.0258
9	0.0110	0.0186	0.0232	0.0266	0.0292
10	0.0123	0.0208	0.0260	0.0297	0.0326
11	0.0136	0.0230	0.0287	0.0328	0.0360
12	0.0150	0.0252	0.0315	0.0360	0.0395
13	0.0163	0.0275	0.0343	0.0392	0.0431
14	0.0177	0.0298	0.0372	0.0425	0.0467
15	0.0190	0.0321	0.0401	0.0458	0.0503
16	0.0204	0.0344	0.0430	0.0491	0.0539
17	0.0218	0.0368	0.0459	0.0525	0.0576
18	0.0232	0.0392	0.0489	0.0559	0.0614
19	0.0247	0.0416	0.0519	0.0594	0.0652
20	0.0261	0.0440	0.0550	0.0629	0.0690
21	0.0276	0.0465	0.0581	0.0664	0.0729
22	0.0291	0.0490	0.0612	0.0700	0.0769
23	0.0306	0.0516	0.0644	0.0736	0.0808
24	0.0321	0.0541	0.0676	0.0773	0.0849
25	0.0337	0.0568	0.0709	0.0811	0.0890
26	0.0353	0.0594	0.0742	0.0848	0.0931
27	0.0368	0.0621	0.0776	0.0887	0.0973
28	0.0385	0.0648	0.0810	0.0926	0.1016
29	0.0401	0.0676	0.0844	0.0965	0.1059
30	0.0418	0.0704	0.0879	0.1005	0.1103
31	0.0434	0.0732	0.0914	0.1045	0.1148
32	0.0452	0.0761	0.0950	0.1087	0.1193
33	0.0469	0.0790	0.0987	0.1128	0.1239
34	0.0486	0.0820	0.1024	0.1171	0.1285
35	0.0504	0.0850	0.1062	0.1214	0.1332
36	0.0522	0.0881	0.1100	0.1257	0.1380
37	0.0541	0.0912	0.1139	0.1302	0.1429

TABLE 5.7 Variation of U_r for Various Values of T_r and n, No-Smear Case [Eqs. (5.26) and (5.32)] (*Continued*)

Degree of consolidation U_r (%)	Time factor T_r for value of n ($= r_e/r_w$)				
	5	10	15	20	25
38	0.0560	0.0943	0.1178	0.1347	0.1479
39	0.0579	0.0975	0.1218	0.1393	0.1529
40	0.0598	0.1008	0.1259	0.1439	0.1580
41	0.0618	0.1041	0.1300	0.1487	0.1632
42	0.0638	0.1075	0.1342	0.1535	0.1685
43	0.0658	0.1109	0.1385	0.1584	0.1739
44	0.0679	0.1144	0.1429	0.1634	0.1793
45	0.0700	0.1180	0.1473	0.1684	0.1849
46	0.0721	0.1216	0.1518	0.1736	0.1906
47	0.0743	0.1253	0.1564	0.1789	0.1964
48	0.0766	0.1290	0.1611	0.1842	0.2023
49	0.0788	0.1329	0.1659	0.1897	0.2083
50	0.0811	0.1368	0.1708	0.1953	0.2144
51	0.0835	0.1407	0.1758	0.2020	0.2206
52	0.0859	0.1448	0.1809	0.2068	0.2270
53	0.0884	0.1490	0.1860	0.2127	0.2335
54	0.0909	0.1532	0.1913	0.2188	0.2402
55	0.0935	0.1575	0.1968	0.2250	0.2470
56	0.0961	0.1620	0.2023	0.2313	0.2539
57	0.0988	0.1665	0.2080	0.2378	0.2610
58	0.1016	0.1712	0.2138	0.2444	0.2683
59	0.1044	0.1759	0.2197	0.2512	0.2758
60	0.1073	0.1808	0.2258	0.2582	0.2834
61	0.1102	0.1858	0.2320	0.2653	0.2912
62	0.1133	0.1909	0.2384	0.2726	0.2993
63	0.1164	0.1962	0.2450	0.2801	0.3075
64	0.1196	0.2016	0.2517	0.2878	0.3160
65	0.1229	0.2071	0.2587	0.2958	0.3247
66	0.1263	0.2128	0.2658	0.3039	0.3337
67	0.1298	0.2187	0.2732	0.3124	0.3429
68	0.1334	0.2248	0.2808	0.3210	0.3524
69	0.1371	0.2311	0.2886	0.3300	0.3623
70	0.1409	0.2375	0.2967	0.3392	0.3724
71	0.1449	0.2442	0.3050	0.3488	0.3829
72	0.1490	0.2512	0.3134	0.3586	0.3937
73	0.1533	0.2583	0.3226	0.3689	0.4050
74	0.1577	0.2658	0.3319	0.3795	0.4167
75	0.1623	0.2735	0.3416	0.3906	0.4288

TABLE 5.7 Variation of U_r for Various Values of T_r and n, No-Smear Case [Eqs. (5.26) and (5.32)] (*Continued*)

Degree of consolidation U_r (%)	Time factor T_r for value of n ($= r_e/r_w$)				
	5	10	15	20	25
76	0.1671	0.2816	0.3517	0.4021	0.4414
77	0.1720	0.2900	0.3621	0.4141	0.4546
78	0.1773	0.2988	0.3731	0.4266	0.4683
79	0.1827	0.3079	0.3846	0.4397	0.4827
80	0.1884	0.3175	0.3966	0.4534	0.4978
81	0.1944	0.3277	0.4090	0.4679	0.5137
82	0.2007	0.3383	0.4225	0.4831	0.5304
83	0.2074	0.3496	0.4366	0.4992	0.5481
84	0.2146	0.3616	0.4516	0.5163	0.5668
85	0.2221	0.3743	0.4675	0.5345	0.5868
86	0.2302	0.3879	0.4845	0.5539	0.6081
87	0.2388	0.4025	0.5027	0.5748	0.6311
88	0.2482	0.4183	0.5225	0.5974	0.6558
89	0.2584	0.4355	0.5439	0.6219	0.6827
90	0.2696	0.4543	0.5674	0.6487	0.7122
91	0.2819	0.4751	0.5933	0.6784	0.7448
92	0.2957	0.4983	0.6224	0.7116	0.7812
93	0.3113	0.5247	0.6553	0.7492	0.8225
94	0.3293	0.5551	0.6932	0.7927	0.8702
95	0.3507	0.5910	0.7382	0.8440	0.9266
96	0.3768	0.6351	0.7932	0.9069	0.9956
97	0.4105	0.6918	0.8640	0.9879	1.0846
98	0.4580	0.7718	0.9640	1.1022	1.2100
99	0.5391	0.9086	1.1347	1.2974	1.4244

AVERAGE DEGREE OF CONSOLIDATION DUE TO VERTICAL DRAINAGE ONLY

Using Figure 5.22a, for instantaneous application of a surcharge, we may obtain the average degree of consolidation due to vertical drainage only from Eqs. (2.78) and (2.79). We have

$$T_v = \frac{\pi}{4}\left[\frac{U_v(\%)}{100}\right]^2 \quad (\text{for } U_v = 0 \text{ to } 60\%) \qquad \text{[Eq. (2.78)]}$$

and

$$T_v = 1.781 - 0.933 \log [100 - U_v(\%)] \quad (\text{for } U_v > 60\%) \qquad \text{[Eq. (2.79)]}$$

where U_v = average degree of consolidation due to vertical drainage only, and

$$T_v = \frac{c_v t_2}{H^2} \qquad \text{[Eq. (2.73)]}$$

where c_v = coefficient of consolidation for vertical drainage.

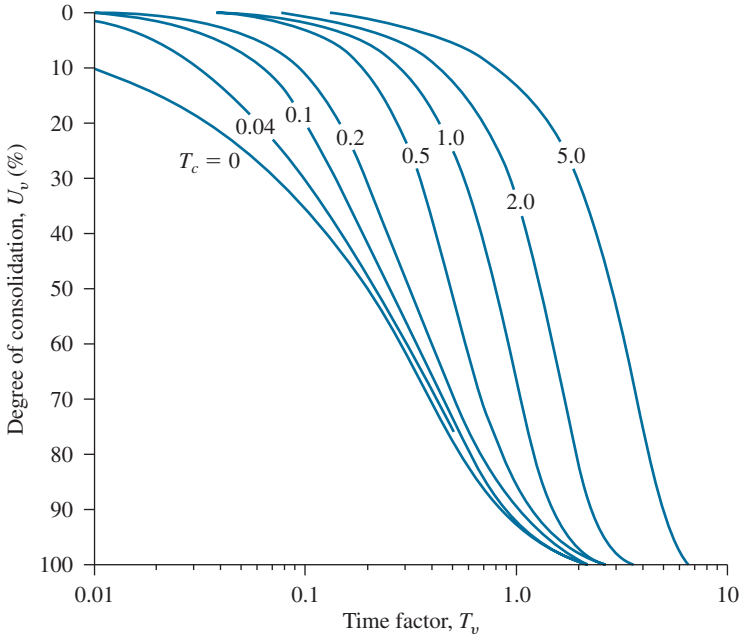


FIGURE 5.23 Variation of U_v with T_v and T_c [Eqs. (5.37) and (5.38)]

For the case of ramp loading, as shown in Figure 5.22b, the variation of U_v with T_v can be expressed as (Olson, 1977):

For $T_v \leq T_c$:

$$U_v = \frac{T_v}{T_c}\left\{1 - \frac{2}{T_v}\Sigma\frac{1}{M^4}[1 - \exp(-M^2T_v)]\right\} \tag{5.37}$$

For $T_v \geq T_c$:

$$U_v = 1 - \frac{2}{T_c}\Sigma\frac{1}{M^4}[\exp(M^2T_c) - 1]\exp(-M^2T_v) \tag{5.38}$$

where

$$M = \frac{\pi}{2}(2m' + 1)$$
$$m' = 0, 1, 2, \ldots$$

$$T_c = \frac{c_v t_c}{H^2} \tag{5.39}$$

where H = length of maximum vertical drainage path. Figure 5.23 shows the variation of U_v (%) with T_c and T_v.

EXAMPLE 5.5

Redo Example 5.4, with the addition of some sand drains. Assume that $r_w = 0.1$ m, $d_e = 3$ m, $c_v = c_{vr}$, and the surcharge is applied instantaneously. (See Figure 5.22a.) Also assume that this is a no-smear case.

SOLUTION

Part a

The total primary consolidation settlement will be 167.7 mm, as before.

Part b

From Example 5.4, $T_v = 0.36$. Using Eq. (2.78), we obtain

$$T_v = \frac{\pi}{4}\left[\frac{U_v(\%)}{100}\right]^2$$

or

$$U_v = \sqrt{\frac{4T_v}{\pi}} \times 100 = \sqrt{\frac{(4)(0.36)}{\pi}} \times 100 = 67.7\%$$

Also,

$$n = \frac{d_e}{2r_w} = \frac{3}{2 \times 0.1} = 15$$

Again,

$$T_r = \frac{c_{vr} t_2}{d_e^2} = \frac{(0.36)(9)}{(3)^2} = 0.36$$

From Table 5.7 for $n = 15$ and $T_r = 0.36$, the value of U_r is about 77%. Hence,

$$\begin{aligned} U_{v,r} &= 1 - (1 - U_v)(1 - U_r) = 1 - (1 - 0.67)(1 - 0.77) \\ &= 0.924 = 92.4\% \end{aligned}$$

Now, from Figure 5.17, for $\Delta\sigma'_p/\sigma'_o = 0.548$ and $U_{v,r} = 92.4\%$, the value of $\Delta\sigma'_f/\Delta\sigma'_p \approx 0.12$. Hence,

$$\Delta\sigma'_{(f)} = (115)(0.12) = \mathbf{13.8\ kN/m^2}$$

Note: The total surcharge to be applied during the 9 months would be

$$\Delta\sigma'_{(p)} + \Delta\sigma'_{(f)} = 115 + 13.8 = 128.8\ \text{kN/m}^2$$

The provision of sand drains reduces the required surcharge significantly.

■

EXAMPLE 5.6

Suppose that, for the sand drain project of Figure 5.21, the clay is normally consolidated. We are given the following data:

Clay:

$H_c = 15$ ft (two-way drainage)

$C_c = 0.31$

$e_o = 1.1$

Effective overburden pressure at the middle of the clay layer

$= 1000\ \text{lb/ft}^2$

$c_v = 0.115\ \text{ft}^2\text{/day}$

Sand drain:

$r_w = 0.3$ ft

$d_e = 6$ ft

$c_v = c_{vr}$

A surcharge is applied as shown in Figure 5.24. Assume this to be a no-smear case. Calculate the degree of consolidation 30 days after the surcharge is first applied. Also, determine the consolidation settlement at that time due to the surcharge.

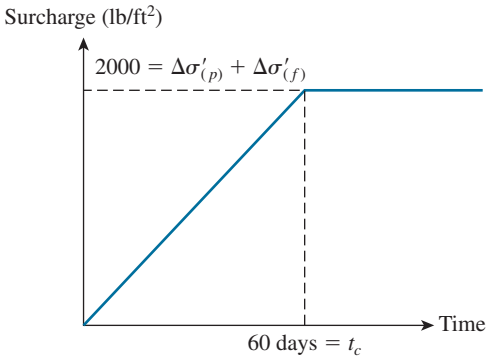


FIGURE 5.24 Ramp load for a sand drain project

SOLUTION

From Eq. (5.39),

$$T_c = \frac{c_v t_c}{H^2} = \frac{(0.115 \text{ ft}^2/\text{day})(60)}{\left(\frac{15}{2}\right)^2} = 0.123$$

and

$$T_v = \frac{c_v t_2}{H^2} = \frac{(0.115)(30)}{\left(\frac{15}{2}\right)^2} = 0.061$$

Using Figure 5.23 for $T_c = 0.123$ and $T_v = 0.061$, we have $U_v \approx 9\%$. For the sand drain,

$$n = \frac{d_e}{2r_w} = \frac{6}{(2)(0.3)} = 10$$

From Eq. (5.35),

$$T_{\text{rc}} = \frac{c_{\text{vr}} t_c}{d_e^2} = \frac{(0.115)(60)}{(6)^2} = 0.192$$

and

$$T_r = \frac{c_{\text{vr}} t_2}{d_e^2} = \frac{(0.115)(30)}{(6)^2} = 0.096$$

Again, from Eq. (5.33),

$$U_r = \frac{T_r - \frac{1}{A}[1 - \exp(-AT_r)]}{T_{\text{rc}}}$$

Also, for the no-smear case,

$$m = \frac{n^2}{n^2 - 1}\ln(n) - \frac{3n^2 - 1}{4n^2} = \frac{10^2}{10^2 - 1}\ln(10) - \frac{3(10)^2 - 1}{4(10)^2} = 1.578$$

and

$$A = \frac{2}{m} = \frac{2}{1.578} = 1.267$$

so

$$U_r = \frac{0.096 - \frac{1}{1.267}[1 - \exp(-1.267 \times 0.096)]}{0.192} = 0.03 = 3\%$$

From Eq. (5.25),

$$U_{v,r} = 1 - (1 - U_r)(1 - U_v) = 1 - (1 - 0.03)(1 - 0.09) = 0.117 = \mathbf{11.7\%}$$

The total primary settlement is thus

$$S_{c(p)} = \frac{C_c H_c}{1 + e_o} \log \left[\frac{\sigma'_o + \Delta\sigma'_{(p)} + \Delta\sigma'_f}{\sigma'_o} \right]$$

$$= \frac{(0.31)(15)}{1 + 1.1} \log \left(\frac{1000 + 2000}{1000} \right) = 1.056 \text{ ft}$$

and the settlement after 30 days is

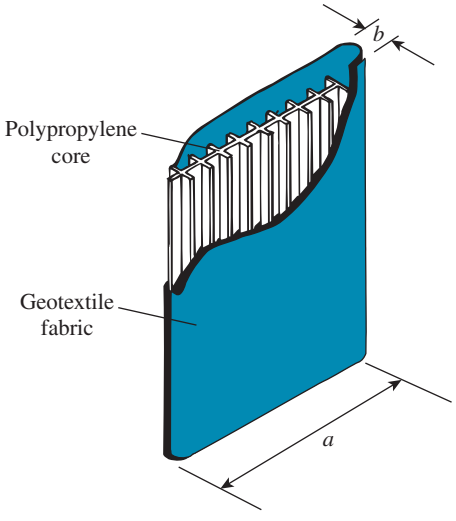
$$S_{c(p)} U_{v,r} = (1.056)(0.117)(12) = \mathbf{1.48 \text{ in}}.$$

5.10 Prefabricated Vertical Drains

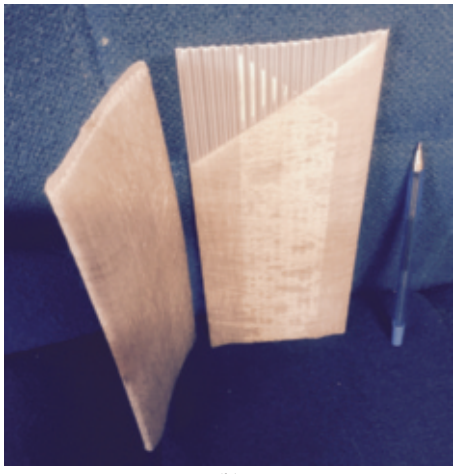
Prefabricated vertical drains (PVDs), also referred to as *wick* or *strip drains*, were originally developed as a substitute for the commonly used sand drain. With advances in materials science, these drains began to be manufactured from synthetic polymers such as polypropylene and high-density polyethylene. PVDs are normally manufactured with a corrugated or channeled synthetic core enclosed by a geotextile filter, as shown in Figure 5.25. Installation rates reported in the literature are on the order of 0.1 to 0.3 m/s (4 to 12 in./s), excluding equipment mobilization and setup time. PVDs have been used extensively in the past for expedient consolidation of low-permeability soil under surface surcharge. The main advantage of PVDs over sand drains is that they do not require drilling; thus, installation is much faster. Figures 5.26a and b are photographs of the installation of PVDs in the field.

DESIGN OF PVDs

The relationships for the average degree of consolidation due to radial drainage into sand drains are given in Eqs. (5.26) through (5.31) for equal-strain cases. Yeung (1997) used these relationships to develop design curves for PVDs. The theoretical developments used by Yeung are given next.



(a)



(b)

FIGURE 5.25 Prefabricated vertical drain (PVD): (a) schematic diagram; (b) a photograph (Courtesy of N. Sivakugan, James Cook University, Australia)



(a)



(b)

FIGURE 5.26 Installation of PVDs in the field [*Note:* (b) is a closeup view of (a)] (Courtesy of E. C. Shin, University of Incheon, Korea)

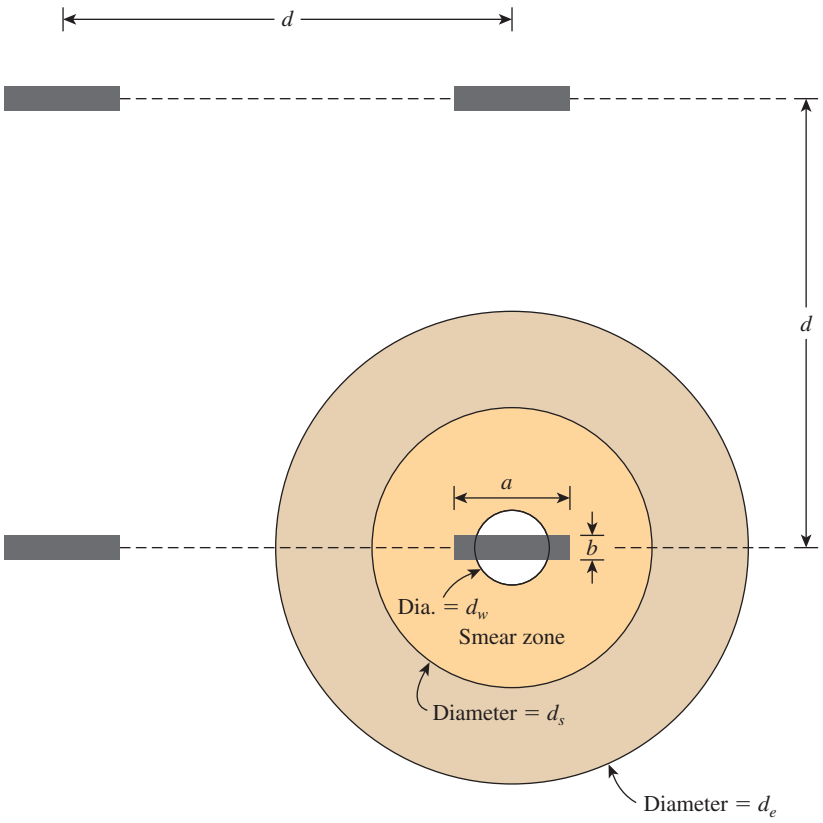


FIGURE 5.27 Square-grid pattern layout of prefabricated vertical drains

Figure 5.27 shows the layout of a square-grid pattern of prefabricated vertical drains. (See also Figure 5.25a for the definition of a and b.) The equivalent diameter of a PVD can be given as

$$d_w = \frac{2(a + b)}{\pi} \tag{5.40}$$

Now, Eq. (5.26) can be rewritten as

$$U_r = 1 - \exp\left(-\frac{8c_{vr}t}{d_w^2}\frac{d_w^2}{d_e^2 m}\right) = 1 - \exp\left(-\frac{8T_r'}{\alpha'}\right) \tag{5.41}$$

where d_e = diameter of the effective zone of drainage = $2r_e$. Also,

$$T_r' = \frac{C_{vr}t}{d_w^2} \tag{5.42}$$

$$\alpha' = n^2 m = \frac{n^4}{n^2 - S^2}\ln\left(\frac{n}{S}\right) - \left(\frac{3n^2 - S^2}{4}\right) + \frac{k_h}{k_s}(n^2 - S^2)\ln S \tag{5.43}$$

and

$$n = \frac{d_e}{d_w} \tag{5.44}$$

From Eq. (5.41),

$$T_r' = -\frac{\alpha'}{8}\ln(1 - U_r)$$

or

$$(T_r')_1 = \frac{T_r'}{\alpha'} = -\frac{\ln (1 - U_r)}{8} \tag{5.45}$$

Table 5.8 gives the variation of $(T_r')_1$ with U_r. Also, Figure 5.28 shows plots of α' versus n for $k_h/k_s = 5$ and 10 and $S = 2$ and 3.

Following is a step-by-step procedure for the design of prefabricated vertical drains:

Step 1. Determine the time t_2 available for the consolidation process and the $U_{v,r}$ required therefore [Eq. (5.24)]

Step 2. Determine U_r at time t_2 due to vertical drainage. From Eq. (5.25),

$$U_r = 1 - \frac{1 - U_{v,r}}{1 - U_v} \tag{5.46}$$

Step 3. For the PVD that is to be used, calculate d_w from Eq. (5.40).

Step 4. Determine $(T_r')_1$ from Eqs. (5.45) and (5.46).

Step 5. Determine T_r' from Eq. (5.42).

Step 6. Determine

$$\alpha' = \frac{T_r'}{(T_r')_1}$$

TABLE 5.8 **Variation of $(T_r')_1$ with U_r [Eq. (5.45)]**

U_r (%)	$(T_r')_1$
0	0
5	0.006
10	0.013
15	0.020
20	0.028
25	0.036
30	0.045
35	0.054
40	0.064
45	0.075
50	0.087
55	0.100
60	0.115
65	0.131
70	0.150
75	0.173
80	0.201
85	0.237
90	0.288
95	0.374

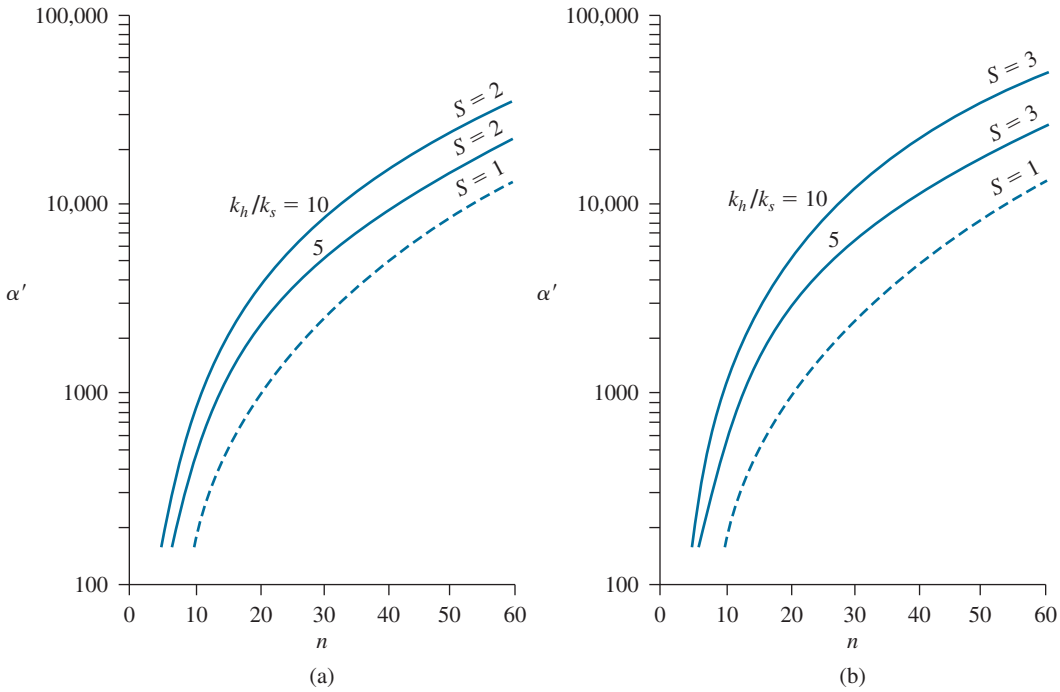


FIGURE 5.28 Plot of α' versus n: (a) $S = 2$; (b) $S = 3$ [Eq. (5.43)]

Step 7. Using Figure 5.28 and α' determined from Step 6, determine n.

Step 8. From Eq. (5.44),

$$d_e = n \quad d_w$$
$$\uparrow \quad \uparrow$$
$$\text{Step 7} \quad \text{Step 3}$$

Step 9. Choose the drain spacing:

$$d = \frac{d_e}{1.05} \qquad \text{(for triangular pattern)}$$

$$d = \frac{d_e}{1.128} \qquad \text{(for square pattern)}$$

A CASE HISTORY

The installation of PVDs combined with preloading is an efficient way to gain strength in soft clays for construction of foundations. An example of a field study can be found in the work of Shibuya and Hanh (2001), which describes a full-scale test embankment 40 m × 40 m in plan constructed over a soft clay layer located at Nong Ngu Hao, Thailand. PVDs were installed in the soft clay layer in a triangular pattern (Figure 5.29a). Figure 5.29b shows the pattern of preloading at the site, along with the settlement-time plot at the ground surface below the center of the test embankment. Maximum settlement was reached after about four months. The variation of the undrained shear strength (c_u) with depth in the soft clay layer before and after the soil improvement is shown in Figure 5.29c. The variation of c_u with depth is based on field vane shear tests. The undrained shear strength increases by about 50 to 100% at various depths.

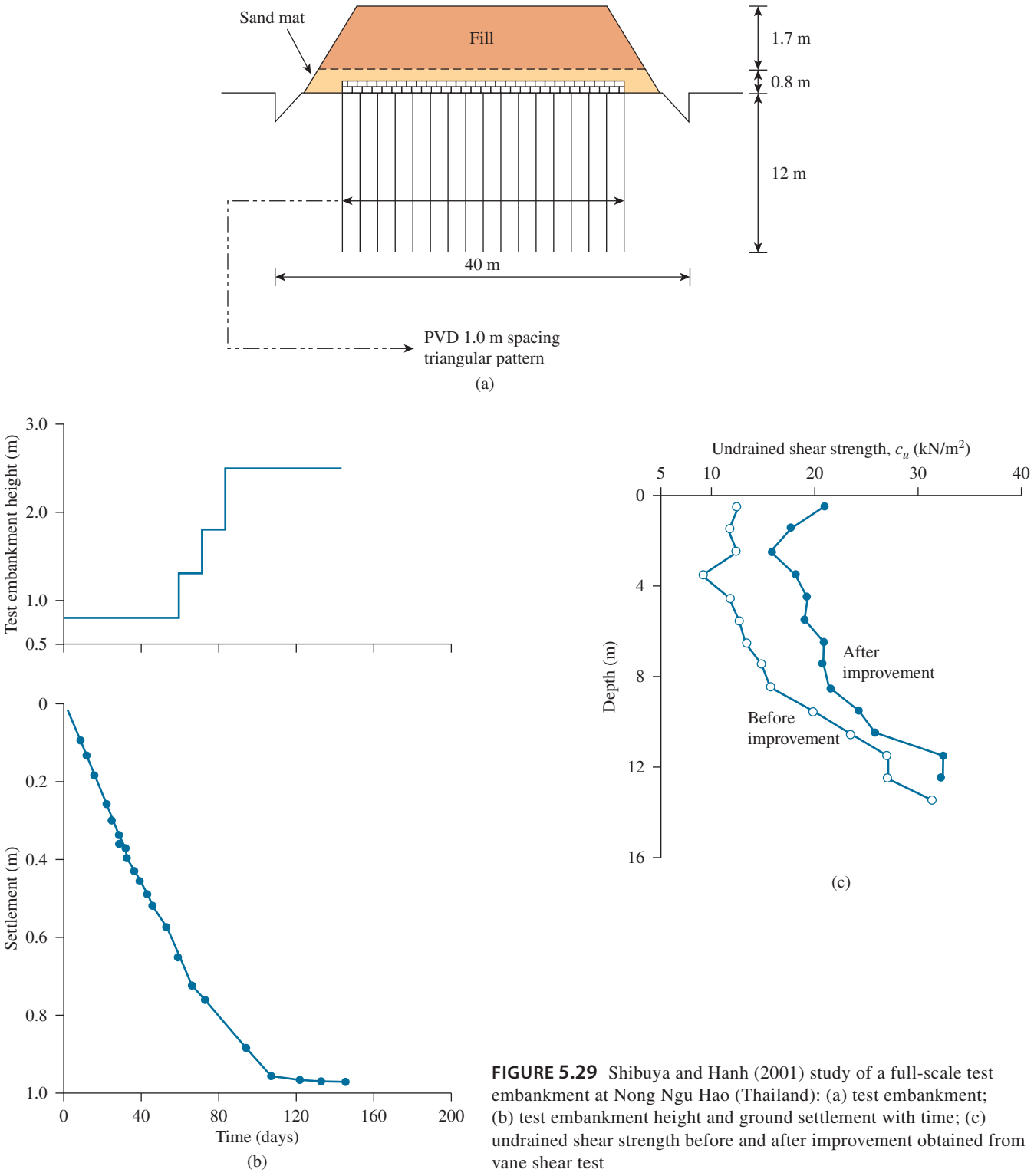


FIGURE 5.29 Shibuya and Hanh (2001) study of a full-scale test embankment at Nong Ngu Hao (Thailand): (a) test embankment; (b) test embankment height and ground settlement with time; (c) undrained shear strength before and after improvement obtained from vane shear test

5.11 Lime Stabilization

As mentioned in Section 5.1, admixtures are occasionally used to stabilize soil in the field—particularly fine-grained soil. The most common admixtures are lime, cement, and lime–fly ash. The main purposes of stabilizing the soil are to

(a) modify the soil, (b) expedite construction, and (c) improve the strength and durability of the soil.

The types of *lime* commonly used to stabilize fine-grained soil are hydrated high-calcium lime [$Ca(OH)_2$], calcitic quicklime (CaO), monohydrated dolomitic lime [$Ca(OH)_2 \cdot MgO$], and dolomitic quicklime ($CaO \cdot MgO$). The quantity of lime used to stabilize most soil usually is in the range from 5 to 10%. When lime is added to clayey soil, two *pozzolanic* chemical reactions occur: *cation exchange* and *flocculation–agglomeration*. In the cation exchange and flocculation–agglomeration reactions, the *monovalent* cations generally associated with clays are replaced by the *divalent* calcium ions. The cations can be arranged in a series based on their affinity for exchange:

$$Al^{3+} > Ca^{2+} > Mg^{2+} > NH_4^+ > K^+ > Na^+ > Li^+$$

Any cation can replace the ions to its right. For example, calcium ions can replace potassium and sodium ions from a clay. Flocculation–agglomeration produces a change in the texture of clay soil. The clay particles tend to clump together to form larger particles, thereby (a) decreasing the liquid limit, (b) increasing the plastic limit, (c) decreasing the plasticity index, (d) increasing the shrinkage limit, (e) increasing the workability, and (f) improving the strength and deformation properties of a soil. Some examples in which lime influences the plasticity of clayey soil are given in Table 5.9.

Pozzolanic reaction between soil and lime involves a reaction between lime and the silica and alumina of the soil to form cementing material. One such reaction is

$$Ca(OH)_2 + SiO_2 \rightarrow \underset{\substack{\uparrow \\ \text{Clay silica}}}{CSH}$$

where

$C = CaO$

$S = SiO_2$

$H = H_2O$

The pozzolanic reaction may continue for a long time.

The first 2 to 3% of lime (on the dry-weight basis) substantially influences the workability and the property (such as plasticity) of the soil. The addition of lime to clayey soil also affects their compaction characteristics.

PROPERTIES OF CURED LIME-STABILIZED SOIL

The unconfined compression strength (q_u) of fine-grained soil compacted at optimum moisture content may range from 170 kN/m^2 to 2100 kN/m^2 (25 lb/in^2 to 300 lb/in^2), depending upon the nature of the soil. With about 3 to 5% addition of lime and a curing period of 28 days, the unconfined compression strength may increase by 700 kN/m^2 (100 lb/in^2) or more.

TABLE 5.9 Influence of Lime on Plasticity of Clay (Based on data from Thompson, 1967)

Soil	AASHTO Classification	0% Lime		5% Lime	
		Liquid limit	Plasticity index	Liquid limit	Plasticity index
Bryce B	A-7-6(18)	53	29	NP	NP
Cowden B	A-7-6(19)	54	33	NP	NP
Drummer B	A-7-6(19)	54	31	NP	NP
Huey B	A-7-6(17)	46	29	NP	NP

Note: NP—Nonplastic

The tensile strength (σ_T) of cured fine-grained soil also increases with lime stabilization. Tullock et al. (1970) gave the following relationship between σ_T and q_u:

SI Units

$$\sigma_T\,(\text{kN/m}^2) = 47.54 + 50.6q_u\,(\text{MN/m}^2) \tag{5.47a}$$

English Units

$$\sigma_T\,(\text{lb/in}^2) = 6.89 + 50.6q_u\,(\text{kip/in}^2) \tag{5.47b}$$

where σ_T is the indirect tensile strength.

Thompson (1966) provided the following relationship to estimate the modulus of elasticity (E_s) of lime-stabilized soil:

SI Units

$$E_s(\text{MN/m}^2) = 68.86 + 0.124q_u\,(\text{kN/m}^2) \tag{5.48a}$$

English Units

$$E_s\,(\text{kip/in}^2) = 9.98 + 0.124q_u\,(\text{lb/in}^2) \tag{5.48b}$$

Poisson's ratio (μ_s) of cured, stabilized soil with about 5% lime varies between 0.08 to 0.12 (with an average of 0.11) at a stress level of 25% or less of the ultimate compressive strength. It increases to about 0.27 to 0.37 (with an average of 0.31) at a stress level greater than 50 to 75% of the ultimate compression strength (Transportation Research Board, 1987).

LIME STABILIZATION IN THE FIELD

Lime stabilization in the field can be done in three ways:

1. The *in situ* material or the borrowed material can be mixed with the proper amount of lime at the site and then compacted after the addition of moisture.
2. The soil can be mixed with the proper amount of lime and water at a plant and then hauled back to the site for compaction.
3. Lime slurry can be pressure injected into the soil to a depth of 4 to 5 m (12 to 16 ft). Figure 5.30 shows a vehicle used for pressure injection of lime slurry.

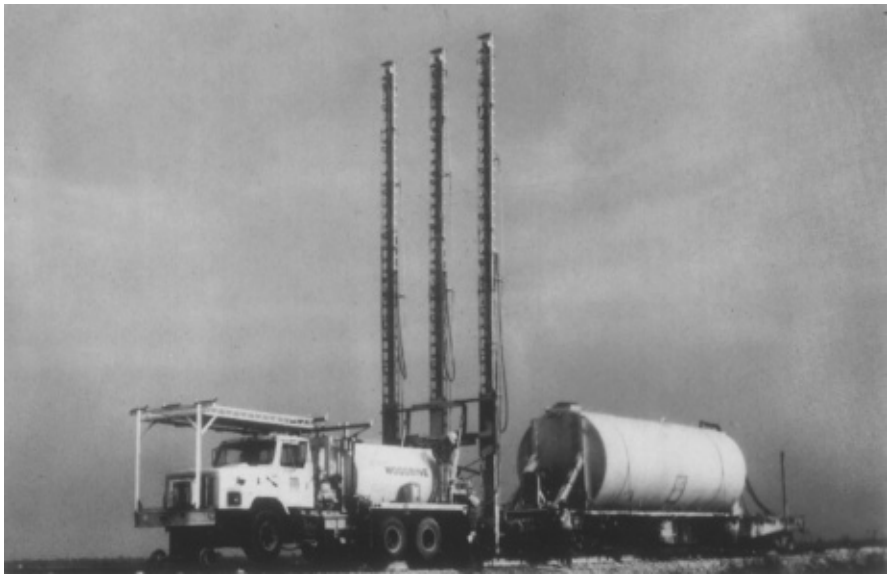


FIGURE 5.30 Equipment for pressure injection of lime slurry (Courtesy of Hayward Baker Inc., Odenton, Maryland)

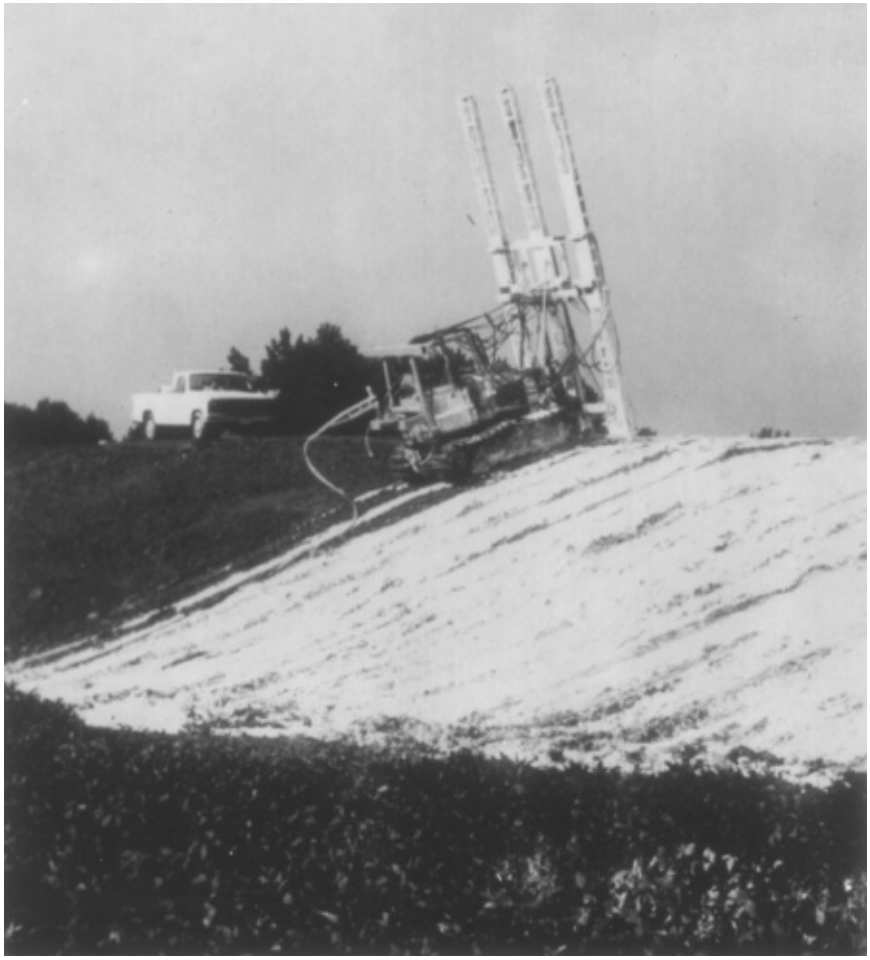


FIGURE 5.31 Pressure injection of lime slurry (Courtesy of Hayward Baker Inc., Odenton, Maryland)

The slurry-injection mechanical unit is mounted to the injection vehicle. A common injection unit is a hydraulic-lift mast with crossbeams that contain the injection rods. The rods are pushed into the ground by the action of the lift mast beams. The slurry is generally mixed in a batching tank about 3 m (10 ft) in diameter and 12 m (36 ft) long and is pumped at high pressure to the injection rods. Figure 5.31 shows the lime slurry pressure-injection process. The ratio typically specified for the preparation of lime slurry is 1.13 kg (2.5 lb) of dry lime to a gallon of water.

Because the addition of hydrated lime to soft clayey soil immediately increases the plastic limit, thus changing the soil from plastic to solid and making it appear to "dry up," limited amounts of the lime can be thrown on muddy and troublesome construction sites. This action improves trafficability and may save money and time. Quicklimes have also been successfully used in drill holes having diameters of 100 to 150 mm (4 to 6 in.) for stabilization of subgrades and slopes. For this type of work, holes are drilled in a grid pattern and then filled with quicklime.

5.12 Cement Stabilization

Cement is being increasingly used as a stabilizing material for soil, particularly in the construction of highways and earth dams. The first controlled soil–cement construction in the United States was carried out near Johnsonville, South Carolina, in 1935. Cement

TABLE 5.10 Cement Requirement by Volume for Effective Stabilization of Various Soil[a]

Soil type		Percent cement by volume
AASHTO classification	Unified classification	
A-2 and A-3	GP, SP, and SW	6–10
A-4 and A-5	CL, ML, and MH	8–12
A-6 and A-7	CL, CH	10–14

[a]Based on data from Mitchell, J. K. and Freitag, D. R. (1959). "A Review and Evaluation of Soil-Cement Pavements," *Journal of the Soil Mechanics and Foundations Division,* American Society of Civil Engineers, Vol. 85, No. SM6, pp. 49–73.

can be used to stabilize sandy and clayey soil. As in the case of lime, cement helps decrease the liquid limit and increase the plasticity index and workability of clayey soil. Cement stabilization is effective for clayey soil when the liquid limit is less than 45 to 50 and the plasticity index is less than about 25. The optimum requirements of cement by volume for effective stabilization of various types of soil are given in Table 5.10.

Like lime, cement helps increase the strength of soil, and strength increases with curing time. Table 5.11 presents some typical values of the unconfined compressive strength of various types of untreated soil and of soil–cement mixtures made with approximately 10% cement by weight.

Granular soil and clayey soil with low plasticity obviously are most suitable for cement stabilization. Calcium clays are more easily stabilized by the addition of cement, whereas sodium and hydrogen clays, which are expansive in nature, respond better to lime stabilization. For these reasons, proper care should be exercised in selecting the stabilizing material.

For field compaction, the proper amount of cement can be mixed with soil either at the site or at a mixing plant. If the latter approach is adopted, the mixture can then be carried to the site. The soil is compacted to the required unit weight with a predetermined amount of water.

TABLE 5.11 Typical Compressive Strengths of Soil and Soil–Cement Mixtures[a]

Material	Unconfined compressive strength range	
	kN/m^2	lb/in^2
Untreated soil:		
Clay, peat	Less than 350	Less than 50
Well-compacted sandy clay	70–280	10–40
Well-compacted gravel, sand, and clay mixtures	280–700	40–100
Soil–cement (10% cement by weight):		
Clay, organic soil	Less than 350	Less than 50
Silts, silty clays, very poorly graded sands, and slightly organic soil	350–1050	50–150
Silty clays, sandy clays, very poorly graded sands, and gravels	700–1730	100–250
Silty sands, sandy clays, sands, and gravels	1730–3460	250–500
Well-graded sand–clay or gravel–sand–clay mixtures and sands and gravels	3460–10,350	500–1500

[a]Based on data from Mitchell, J. K. and Freitag, D. R. (1959). "A Review and Evaluation of Soil-Cement Pavements," *Journal of the Soil Mechanics and Foundations Division*, American Society of Civil Engineers, Vol. 85, No. SM6, pp. 49–73.

Similar to lime injection, cement slurry made of portland cement and water (in a water–cement ratio of 0.5:5.0) can be used for pressure grouting of poor soil under foundations of buildings and other structures. Grouting decreases the hydraulic conductivity of soil and increases their strength and load-bearing capacity. For the design of low-frequency machine foundations subjected to vibrating forces, stiffening the foundation soil by grouting and thereby increasing the resonant frequency is sometimes necessary.

5.13 Fly-Ash Stabilization

Fly ash is a by-product of the pulverized coal combustion process usually associated with electric power-generating plants. It is a fine-grained dust and is composed primarily of silica, alumina, and various oxides and alkalies. Fly ash is pozzolanic in nature and can react with hydrated lime to produce cementitious products. For that reason, lime–fly-ash mixtures can be used to stabilize highway bases and subbases. Effective mixes can be prepared with 10 to 35% fly ash and 2 to 10% lime. Soil–lime–fly-ash mixes are compacted under controlled conditions, with proper amounts of moisture to obtain stabilized soil layers.

A certain type of fly ash, referred to as "Type C" fly ash, is obtained from the burning of coal primarily from the western United States. This type of fly ash contains a fairly large proportion (up to about 25%) of free lime that, with the addition of water, will react with other fly-ash compounds to form cementitious products. Its use may eliminate the need to add manufactured lime. The other type of fly ash, known as "Type F," is pozzolanic too but requires a cementing agent such as cement or lime in the presence of water to form a cementitious material. It has a lower lime content than Type C.

5.14 Stone Columns

A method now being used to increase the load-bearing capacity of shallow foundations on soft clay layers is the construction of stone columns. This generally consists of water-jetting a vibroflot (see Section 5.6) into the soft clay layer to make a circular hole that extends through the clay to firmer soil. The hole is then filled with an imported gravel. The gravel in the hole is gradually compacted as the vibrator is withdrawn. The gravel used for the stone column has a size range of 6 to 40 mm (0.25 to 1.6 in.). Stone columns usually have diameters of 0.5 to 0.75 m (1.6 to 2.5 ft) and are spaced at about 1.5 to 3 m (5 to 10 ft) center to center. Figure 5.32 shows the construction of a stone column.

After stone columns are constructed, a fill material should always be placed over the ground surface and compacted before the foundation is constructed. The stone columns tend to reduce the settlement of foundations at allowable loads. Several case histories of construction projects using stone columns are presented in Hughes and Withers (1974), Hughes et al. (1975), Mitchell and Huber (1985), and other works.

Stone columns work more effectively when they are used to stabilize a large area where the undrained shear strength of the subsoil is in the range of 10 to 50 kN/m^2 (200 to 1000 lb/ft^2) than to improve the bearing capacity of structural foundations (Bachus and Barksdale, 1989). Subsoils weaker than that may not provide sufficient lateral support for the columns. For large-site improvement, stone columns are most effective to a depth of 6 to 10 m (20 to 30 ft). However, they have been constructed to a depth of 31 m (100 ft). Bachus and Barksdale provided general guidelines for the design of stone columns to stabilize large areas.



FIGURE 5.32 Construction of a stone column [DGI-Menard (USA)]

Figure 5.33a shows the plan view of several stone columns. The area replacement ratio for the stone columns may be expressed as

$$a_s = \frac{A_s}{A} \tag{5.49}$$

where

A_s = area of the stone column

A = total area within the unit cell

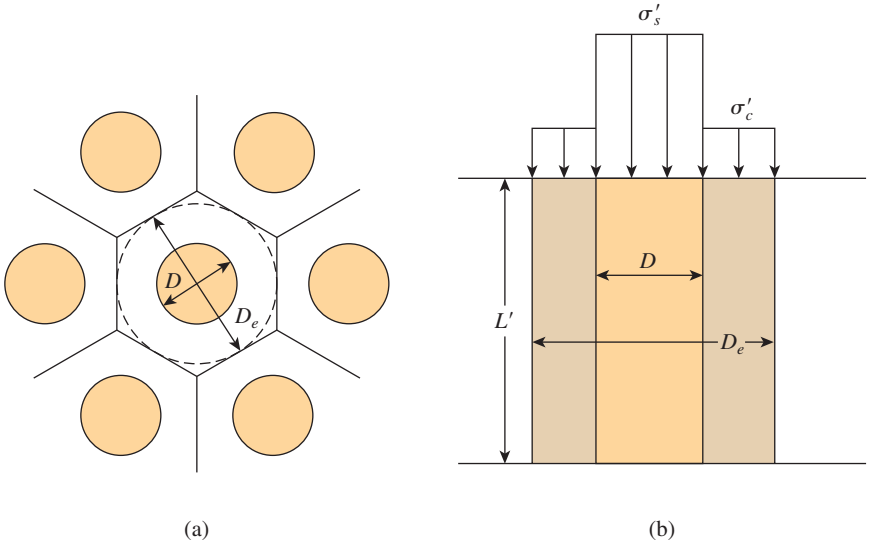


FIGURE 5.33 (a) Stone columns in a triangular pattern; (b) stress concentration due to change in stiffness

For an *equilateral triangular pattern* of stone columns,

$$a_s = 0.907\left(\frac{D}{s}\right)^2 \tag{5.50}$$

where

D = diameter of the stone column

s = spacing between the columns

Combining Eqs. (5.49) and (5.50),

$$\frac{A_s}{A} = \frac{\frac{\pi}{4}D^2}{\frac{\pi}{4}D_e^2} = a_s = 0.907\left(\frac{D}{s}\right)^2$$

or

$$D_e = 1.05s \tag{5.51}$$

Similarly, it can be shown that, for a square pattern of stone columns,

$$D_e = 1.13s \tag{5.52}$$

When a uniform stress by means of a fill operation is applied to an area with stone columns to induce consolidation, a stress concentration occurs due to the change in the stiffness between the stone columns and the surrounding soil. (See Figure 5.33b.) The stress concentration factor is defined as

$$n' = \frac{\sigma_s'}{\sigma_c'} \tag{5.53}$$

where

σ_s' = effective stress in the stone column

σ_c' = effective stress in the subgrade soil

The relationships for σ_s' and σ_c' are

$$\sigma_s' = \sigma'\left[\frac{n'}{1 + (n' - 1)a_s}\right] = \mu_s\sigma' \tag{5.54}$$

and

$$\sigma_c' = \sigma'\left[\frac{1}{1 + (n' - 1)a_s}\right] = \mu_c\sigma' \tag{5.55}$$

where

σ' = average effective vertical stress

μ_s, μ_c = stress concentration coefficients

The improvement in the soil owing to the stone columns may be expressed as

$$\frac{S_{e(t)}}{S_e} = \mu_c \tag{5.56}$$

where

$S_{e(t)}$ = settlement of the treated soil

S_e = total settlement of the untreated soil

LOAD-BEARING CAPACITY OF STONE COLUMNS

When the length L' of the stone column is less than about $3D$ and a foundation is constructed over it, failure occurs by plunging, similar to short piles in soft to medium-stiff clays. For longer columns sufficient to prevent plunging, the load-carrying capacity is governed by the ultimate radial confining pressure and the shear strength of the surrounding matrix soil. In those cases, failure at ultimate load occurs by bulging, as shown in Figure 5.34. Mitchell (1981) proposed that the ultimate bearing capacity (q_u) of a stone column can be given as

$$q_u = c_u N_p \tag{5.57}$$

where

c_u = undrained shear strength of clay

N_p = bearing capacity factor

Mitchell (1981) recommended that

$$N_p \approx 25 \tag{5.58}$$

Based on several field case studies, Stuedlein and Holtz (2013) recommended that

$$N_p = \exp(-0.0096c_u + 3.5) \tag{5.59}$$

where c_u is in kN/m^2.

If a foundation is constructed measuring $B \times L$ in plan over a group of stone columns, as shown in Figure 5.35, the ultimate bearing capacity q_u can be expressed as (Stuedlein and Holtz, 2013)

$$q_u = N_p c_u a_s + N_c c_u (1 - a_s) F_{cs} F_{cd} \tag{5.60}$$

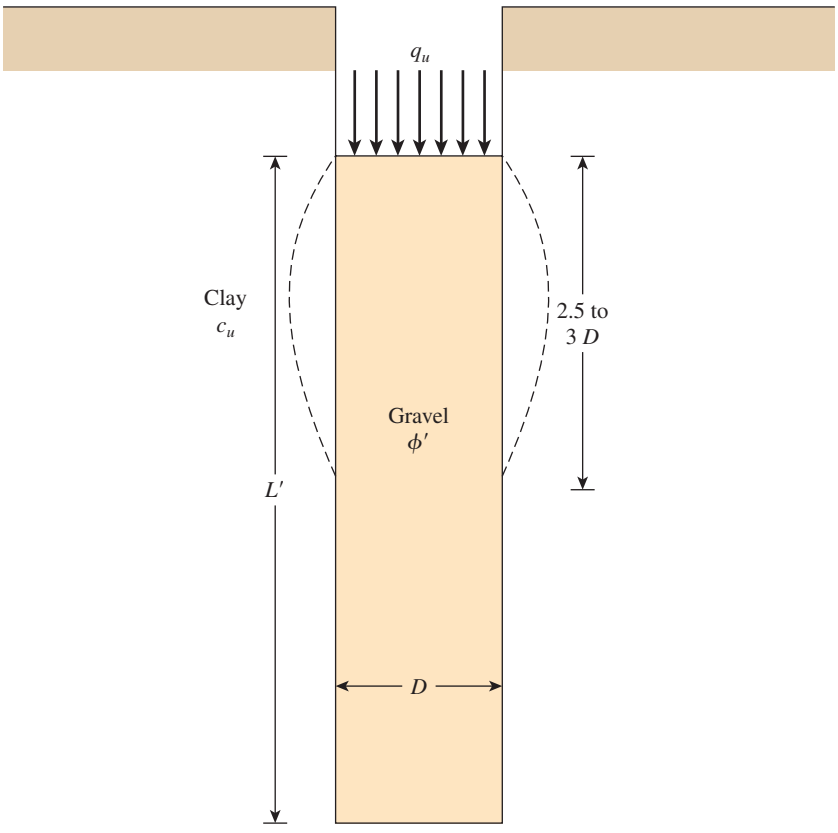


FIGURE 5.34 Bearing capacity of stone column

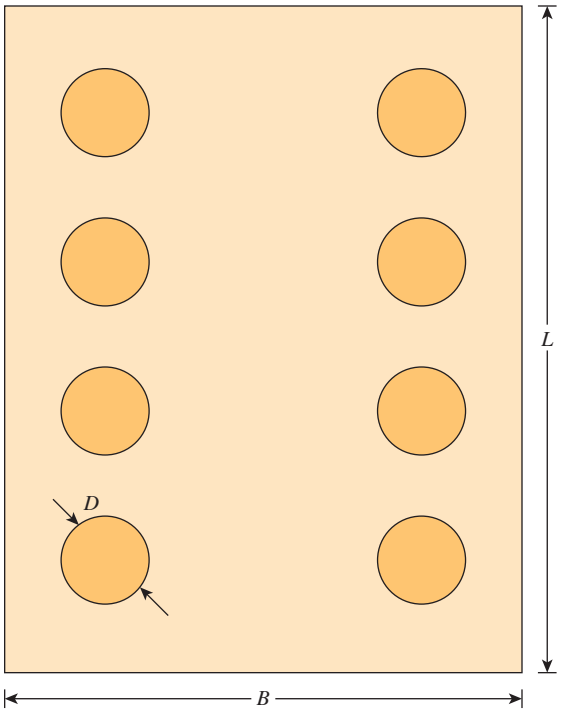


FIGURE 5.35 Shallow foundation over a group of stone columns

where N_p is expressed by Eq. (5.59):

$$N_c = 5.14$$

F_{cs} and F_{cd} = shape and depth factors (see Table 6.6)

Then

$$F_{cs} = 1 + 0.2\frac{B}{L} \tag{5.61}$$

and

$$F_{cd} = 1 + 0.2\frac{D_f}{B} \tag{5.62}$$

where D_f = depth of the foundation.

EXAMPLE 5.7

Consider a foundation 4 m × 2 m in plan constructed over a group of stone columns in a square pattern in soft clay. Given

Stone columns: $D = 0.4$ m
Area ratio, $a_s = 0.3$
$L' = 4.8$ m
Clay: $c_u = 36$ kN/m^2
Foundation: $D_f = 0.75$ m

Estimate the ultimate load Q_u for the foundation.

SOLUTION

From Eq. (5.60),

$$Q_u = N_p c_u a_s + N_c c_u (1 - a_s) F_{cs} F_{cd}$$

From Eq. (5.59),

$$N_p = \exp(-0.0096 c_u + 3.5) = \exp[(-0.0096)(36) + 3.5] = 23.44$$

$$F_{cs} = 1 + 0.2\left(\frac{B}{L}\right) = 1 + 0.2\left(\frac{2}{4}\right) = 1.1$$

$$F_{cd} = 1 + 0.2\left(\frac{D_f}{B}\right) = 1 + 0.2\left(\frac{0.75}{2}\right) = 1.075$$

and

$$q_u = (23.44)(36)(0.3) + (5.14)(36)(1 - 0.3)(1.1)(1.075) = 406.31 \text{ kN/m}^2$$

Thus, the ultimate load is

$$Q_u = q_u BL = (406.31)(2)(4) = \mathbf{3250.48\ kN}$$

5.15 Sand Compaction Piles

Sand compaction piles are similar to stone columns, and they can be used in marginal sites to improve stability, control liquefaction, and reduce the settlement of various structures. Built in soft clay, these piles can significantly accelerate the pore water pressure-dissipation process and hence the time for consolidation.

Sand piles were first constructed in Japan between 1930 and 1950 (Ichimoto, 1981). Large-diameter compacted sand columns were constructed in 1955, using the Compozer technique (Aboshi et al., 1979). The Vibro-Compozer method of sand pile construction was developed by Murayama in Japan in 1958 (Murayama, 1962).

Sand compaction piles are constructed by driving a hollow mandrel with its bottom closed during driving. On partial withdrawal of the mandrel, the bottom doors open. Sand is poured from the top of the mandrel and is compacted in steps by applying air pressure as the mandrel is withdrawn. The piles are usually 0.46 to 0.76 m (1.5 to 2.5 ft) in diameter and are placed at about 1.5 to 3 m (5 to 10 ft) center to center. The pattern of layout of sand compaction piles is the same as for stone columns. Figure 5.36 shows the construction of sand compaction piles in the harbor of Yokohama, Japan.

Basore and Boitano (1969) reported a case history on the densification of a granular subsoil having a thickness of about 9 m (30 ft) at the Treasure Island Naval Station in San Francisco, California, using sand compaction piles. The sand piles had diameters of 356 mm (14 in.). Figure 5.37a shows the layout of the sand piles. The spacing, S', between the piles was varied. The standard penetration resistance, N_{60}, before and after the construction of piles is shown in Figure 5.37b (see location of SPT test in Figure 5.37a). From this figure, it can be seen that the effect of densification at any given depth decreases with the increase in S' (or S'/D). These tests show that when S'/D exceeds about 4 to 5, the effect of densification is practically negligible.



FIGURE 5.36 Construction of sand compaction pile in Yokohama, Japan Harbor (Courtesy of E. C. Shin, University of Incheon, Korea)

5.16 Dynamic Compaction

Dynamic compaction is a technique that has gained popularity in the United States for densification of granular soil deposits. The process primarily involves dropping a heavy weight repeatedly on the ground at regular intervals. The weight of the hammer used varies from 8 to 35 metric tons, and the height of the hammer drop varies between 7.5 and 30.5 m ($\simeq$ 25 and 100 ft). The stress waves generated by the hammer drops help in the densification. The degree of compaction achieved depends on

- The weight of the hammer
- The height of the drop
- The spacing of the locations at which the hammer is dropped

Leonards et al. (1980) suggested that the significant depth of influence for compaction is approximately

$$\text{DI} \simeq \tfrac{1}{2}\sqrt{W_H h} \tag{5.63a}$$

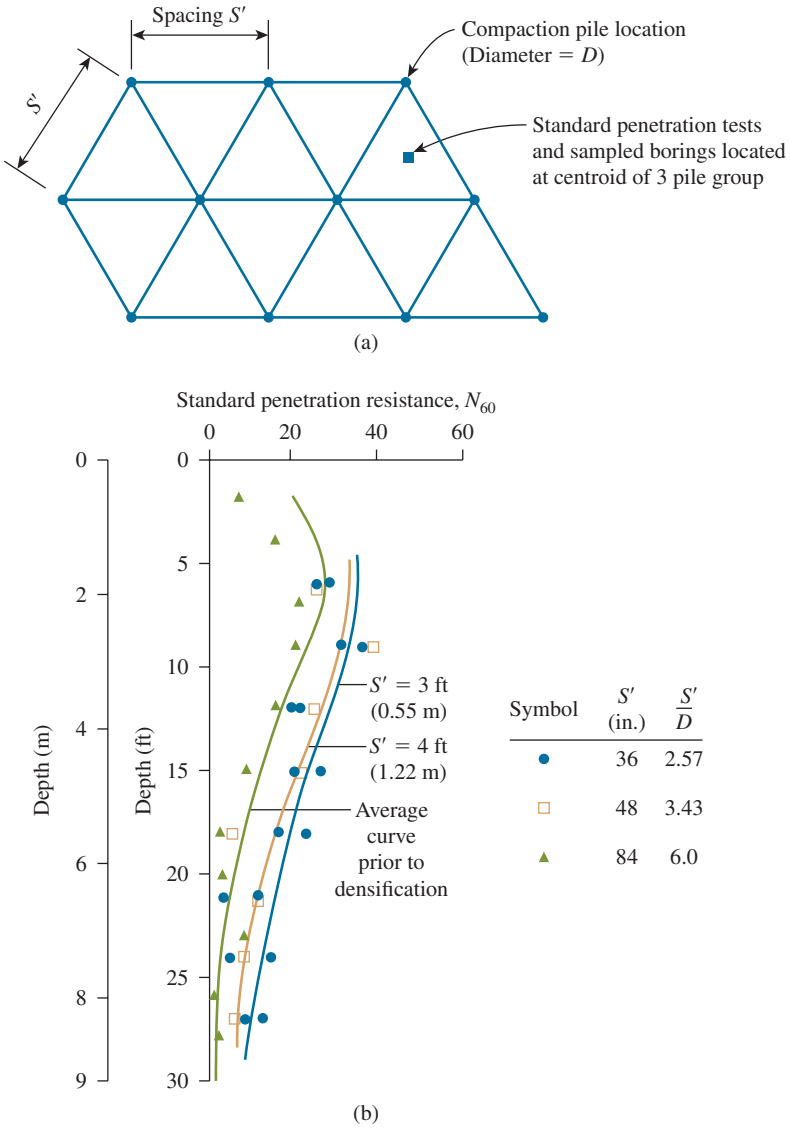


FIGURE 5.37 Sand compaction pile test of Basore and Boitano (1969): (a) layout of the compaction piles; (b) standard penetration resistance variation with depth and S'

where

DI = significant depth of densification (m)

W_H = dropping weight (metric ton)

h = height of drop (m)

In English units, Eq. (5.63a) becomes

$$\text{DI} = 0.61\sqrt{W_H h} \tag{5.63b}$$

where DI and h are in ft and W_H is in kip.

Partos et al. (1989) provided several case histories of site improvement that used dynamic compaction. Poran and Rodriguez (1992) suggested a rational method for conducting dynamic compaction for granular soil in the field. According to their

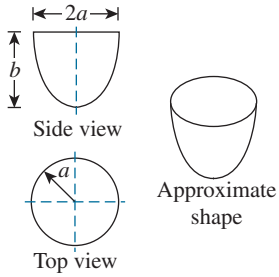


FIGURE 5.38 Approximate shape of the densified area due to dynamic compaction (Poran, C. J. and Rodriguez, J. A. (1992). "Design of Dynamic Compaction," *Canadian Geotechnical Journal*, Vol. 29, No. 5, pp. 796–802.)

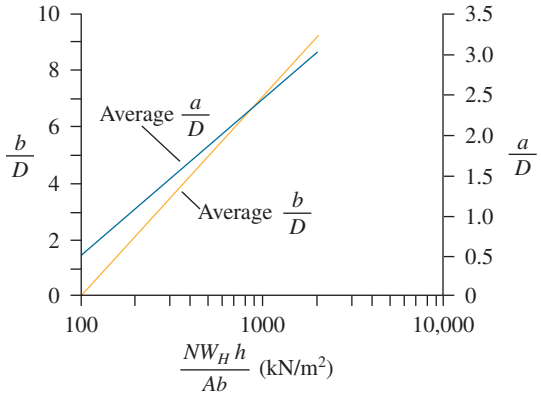


FIGURE 5.39 Plot of a/D and b/D versus NW_Hh/Ab (Based on Poran, C. J. and Rodriguez, J. A. (1992) "Design of Dynamic Compaction," *Canadian Geotechnical Journal*, Vol. 29, No. 5, pp. 796–802.)

method, for a hammer of width D having a weight W_H and a drop h, the approximate shape of the densified area will be of the type shown in Figure 5.38 (i.e., a semiprolate spheroid). Note that in this figure b = DI. Figure 5.39 gives the design chart for a/D and b/D versus NW_Hh/Ab (D = width of the hammer if not circular in cross section; A = area of cross section of the hammer; N = number of required hammer drops). The method uses the following steps:

Step 1. Determine the required significant depth of densification, DI($=b$).

Step 2. Determine the hammer weight (W_H), height of drop (h), dimensions of the cross section, and thus the area A and the width D.

Step 3. Determine $\text{DI}/D = b/D$.

Step 4. Use Figure 5.39 and determine the magnitude of NW_Hh/Ab for the value of b/D obtained in Step 3.

Step 5. Since the magnitudes of W_H, h, A, and b are known (or assumed) from Step 2, the number of hammer drops can be estimated from the value of NW_Hh/Ab obtained from Step 4.

Step 6. With known values of NW_Hh/Ab, determine a/D and thus a from Figure 5.39.

Step 7. The grid spacing, S_g, for dynamic compaction may now be assumed to be equal to or somewhat less than a. (See Figure 5.40.)

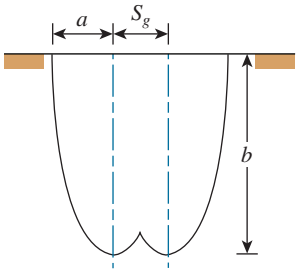


FIGURE 5.40 Approximate grid spacing for dynamic compaction

5.17 Jet Grouting

Jet grouting is a soil stabilization process whereby cement slurry is injected into soil at a high velocity to form a soil–concrete matrix. Conceptually, the process of jet grouting was first developed in the 1960s. Most of the research work after that was conducted in Japan (Ohta and Shibazaki, 1982). The technique was introduced into Europe in the late 1970s, whereas the process was first used in the United States in the early 1980s (Welsh et al., 1986).

Three basic systems of jet grouting have been developed—single, double, and triple rod systems. In all cases, hydraulic rotary drilling is used to reach the design depth at which the soil has to be stabilized. Figure 5.41a shows the *single rod system* in which a cement slurry is injected at a high velocity to form a soil–cement matrix. In the *double rod system* (Figure 5.41b), the cement slurry is injected at a high velocity sheathed in a cone of air at an equally high velocity to erode and mix the soil well. The *triple rod system* (Figure 5.41c) uses high-pressure water shielded in a cone of air to erode the soil. The void created in this process is then filled with a pre-engineering cement slurry.

The effectiveness of the jet grouting is very much influenced by the nature of erodibility of soil. Gravelly soil and clean sand are highly erodible, whereas highly plastic clays are difficult to erode. A summary of the range of parameters generally encountered for the three systems above follows (Burke, 2004; Welsh and Burke, 1991):

Single Rod System:

A. Grout slurry
- Pressure . . . . . 0.4–0.7 MN/m^2 (58–101.5 lb/in^2)
- Volume . . . . . 100–300 l/min (3.5–10.5 ft^3/min)
- Specific gravity 1.25–1.6
- Number of nozzles 1–6

B. Lift
- Step height . . . . . 5–600 mm (0.2–24 in.)
- Step time . . . . . 4–30 s

C. Rotation . . . . . 7–20 rpm

D. Stabilized soil column diameter
- Soft clay . . . . . 0.4–0.9 m (1.3–2.95 ft)
- Silt . . . . . 0.6–1.1 m (1.97–3.6 ft)
- Sand . . . . . 0.8–1.2 m (2.6–3.9 ft)

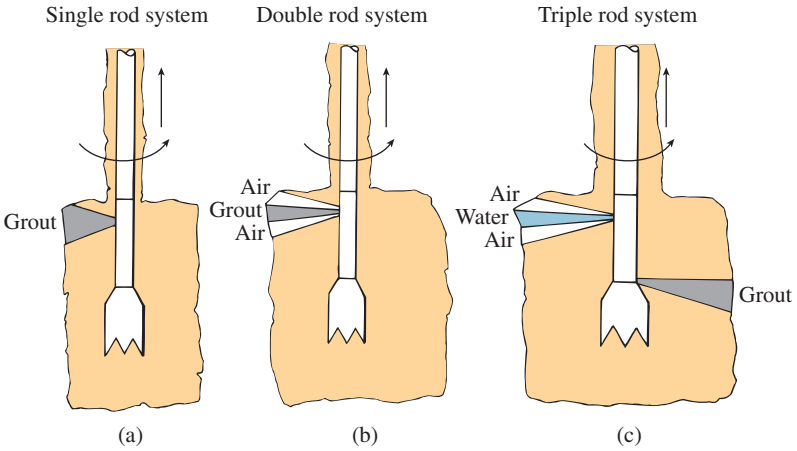


FIGURE 5.41 Jet grouting

Double Rod System:

A. Grout slurry
- Pressure . . . . . 0.3–0.7 MN/m^2 (43.5–101.5 lb/in^2)
- Volume . . . . . 100–600 l/min (3.5–21.2 ft^3/min)
- Specific gravity 1.25–1.8
- Number of nozzles 1–2

B. Air
- Pressure . . . . . 0.7–1.5 MN/m^2 (101.5–217.5 lb/in^2)
- Volume . . . . . 8–30 m^3/min (282.5–1060 ft^3/min)

C. Lift
- Step height . . . . . 25–400 mm (1–15.7 in.)
- Step time . . . . . 4–30 s

D. Rotation . . . . . 7–15 rpm

E. Stabilized soil column diameter
- Soft clay . . . . . 0.9–1.8 m (2.95–6.23 ft)
- Silt . . . . . 0.9–1.8 m (2.95–6.23 ft)
- Sand . . . . . 1.2–2.1 m (3.94–6.9 ft)

Triple Rod System:

A. Grout slurry
- Pressure . . . . . 0.7–1.0 MN/m^2 (101.5–145 lb/in^2)
- Volume . . . . . 120–200 l/min (4.24–7.06 ft^3/min)
- Specific gravity 1.5–2.0
- Number of nozzles 1–3

B. Air
- Pressure . . . . . 0.7–1.5 MN/m^2 (101.5–217.5 lb/in^2)
- Volume . . . . . 4–15 m^3/min (141.3–530 ft^3/min)

C. Water
- Pressure . . . . . 0.3–0.4 MN/m^2 (43.5–58 lb/in^2)
- Volume . . . . . 80–200 l/min (2.83–7.06 ft^3/min)

D. Lift
- Step height . . . . . 20–50 mm (0.79–2 in.)
- Step time . . . . . 4–20 s

E. Rotation . . . . . 7–15 rpm

F. Stabilized soil column diameter
- Soft clay . . . . . 0.9–1.2 m (2.95–3.94 ft)
- Silt . . . . . 0.9–1.4 m (2.95–4.59 ft)
- Sand . . . . . 0.9–2.5 m (2.95–8.2 ft)

5.18 Deep Mixing

Deep mixing method (DMM) refers to a ground modification technology in which soft, compressible, or other unstable soil are treated *in situ* for safely and economically improving the physical and mechanical properties of the natural soil to meet the design requirements of various geotechnical applications. The treated soil generally has higher strength, lower compressibility, and lower permeability than the native soil. The technology involves mechanically blending *in situ* soil with cementitious binder materials that are injected into the soil either in a dry form called *dry mixing* or in a slurry form called *wet mixing* through hollow rotating mixing shafts that are often mounted as multi-axis augers equipped with mixing paddles and cutting tools. Treated soil may be constructed as columns in various grid patterns or as overlapping columns to create soil mix walls. The columns are

typically 0.6 to 1.5 m (2–5 ft) in diameter and may extend up to 40 m (130 ft) in depth (FHWA, 2000).

At the present time, *deep mixing* is used more as a generic name to describe the concept of deep soil mixing by using mechanical rotating shafts—as opposed to jet grouting, which uses hydraulically powered high pressure jets to achieve similar objectives. Depending on the characteristics of the mixing equipment, binder materials, treatment patterns, geographic locations, and the specialty contractors implementing the technique, a variety of acronyms and trade names are used globally to refer to the general concept of deep mixing.

BRIEF HISTORY OF DMM

Various deep mixing methods evolved throughout the second half of the 20th century, primarily in Japan, the Scandinavian countries, and the United States. A chronological history of these developments and their applications is summarized by FHWA (2000). A brief review of those developments is given here.

DMM was first introduced in 1954 by Intrusion Prepakt Co. (USA) in the form of a single-auger *mixed in place* (MIP) piling technique. The MIP technique was used in Japan by the Seiko Kogyo Company of Osaka for excavation support and groundwater control (1961–early part of 1970s). Japan played pioneering roles in the development of several well-known deep mixing techniques. In 1972, the Seiko Kogyo Company developed the *soil mixed wall* (SMW) method for retaining walls by using overlapping multiple-auger techniques for the first time. The Port and Harbor Research Institute of Japan developed the *deep lime mixing* (DLM) methods through extensive laboratory and field research (1967–1977); the *cement deep mixing* (CDM) method using fluid cement grout in offshore soft marine soil (1975–1977); and other similar methods, such as *deep chemical mixing* (DCM), *deep cement continuous mixing* (DCCM), and *deep mixing improvement by cement stabilization* (DEMIC) over the following five years. The Public Works Research Institute of Japan developed the *dry jet mixing* (DJM) method using dry powdered cement (1976–1980). In 1979, the Tenox Company developed the *soil cement column* (SCC) system in Japan. The *spreadable wing* (SWING) method of deep mixing was developed in Japan in 1984, followed by various jet-assisted methods (1986–1991). In 1992, Fudo Company and Chemical Grout Company of Japan developed the *jet and churning system management* (JACSMAN), which combined the procedures of mechanical mixing (core of the column) and cross jet mixing (outside zone of the column).

The first major DMM development in Scandinavia was the *Swedish lime column* method to treat soft clays under embankments (1967 by Kjeld Paus, Linden–Alimak AB, in cooperation with Swedish Geotechnical Institute, Euroc AB, and BPA Byggproduktion AB). The first commercial applications were in excavation support, embankment stabilization, and shallow foundations near Stockholm in 1975. The *lime cement column* method was first used commercially in Finland and Norway in the mid-1980s. Outside Scandinavia, the first European developments appear to be in France with the introduction of a compacted soil–cement mix called "*Colmix*" by Bachy Company in 1987 (constructed by reverse rotation of multiple augers during withdrawal), and in the UK at around the same time with the single-auger deep-mixing system developed by Cementation Ltd. In 1991, the City of Helsinki, Finland, and contractor YIT introduced block stabilization of soft clays to a depth of 5 m. In 1995, Finnish researchers introduced new binders such as slag and pulverized fly ash in addition to cement.

Major developments related to DMM in the United States include: (a) introduction of deep soil mixing (DSM) in 1987; (b) shallow soil mixing (SSM) in 1988 (both by Geo-Con, Inc.); (c) inclusion of DMM in the U.S. EPA Superfund Innovative Technology Evaluation Program for *in situ* stabilization of contaminated soil (1989); and (d) first full-scale demonstration of VERTwall DMM concept in Texas by Geo-Con, Inc. (1998).

DMM TREATMENT PATTERNS

Deep mixing techniques can be used to produce a wide range of patterns in the treated soil structure. The selected pattern depends on the construction location (land or marine), the purpose of the DMM applications, and the characteristics and capabilities of the method used. The treatment patterns can be single element (column), rows of overlapping elements (walls or panels), grids or lattices, or blocks.

DRY AND WET MIXING METHODS

Deep mixing is carried out using either the dry method or the wet method. Dry mixing is possible when the natural moisture content of the *in situ* soil is quite high, so the cement hydration reaction can take place for strength development. Deep deposits of organic and peat soil (with high water content) can be effectively stabilized with the dry method. The column diameter is typically 0.6 to 0.8 m (2.0–2.6 ft) with the depth of treatment reaching up to 25 m (82 ft). Release of dry binder and the soil mixing occur during the withdrawal of the mixing rod, where the rotational direction is reversed compared to the direction during penetration. The binder dosage is maintained as desired by controlling the air pressure and the amount of binder during construction.

Wet mixing is more appropriate when the natural water content is low. Soft clays, silts, and fine sands are suitable for this method. The binder is introduced in a slurry form through a nozzle placed generally at the end of the auger. The specialized mixing tool contains transverse beams and can move vertically along the column length to achieve homogeneous mixing. The composition and the amount of slurry can be controlled to achieve design specifications. The column diameters are typically 0.4 to 2.4 m (1.3 to 8.2 ft), depending on the application. Steel reinforcements can be inserted into the soft columns to improve bending resistance.

Cement injected in the wet method is typically in the range of 100 to 500 kg/m^3 of untreated soil (Bruce and Bruce, 2003). In the dry method, this range is 100 to 300 kg/m^3, provided the natural moisture content is in the range of 40 to 200%.

5.19 Summary

When the soil conditions at the site are not suitable or when the project can be constructed more economically by improving the ground conditions, the geotechnical engineer has several alternatives. The different ground improvement techniques discussed in this chapter include field compaction, vibroflotation, blasting, precompression, prefabricated vertical drains, chemical stabilization, stone columns, and dynamic compaction. Every technique has its limitations, and it is necessary to understand them before selecting the most suitable method for modifying ground conditions.

PROBLEMS

5.1 From the test specifications given in Table 5.2, show that the compactive energy in method C is 2700 kN · m/m^3.

5.2 In a sandy soil, the maximum and minimum void ratios were determined to be 0.725 and 0.465, respectively. The specific gravity of the soil grains is 2.65.

a. What would be the relative density of this sand compacted to a dry unit weight of 104.7 lb/ft^3?

b. Assuming the maximum dry unit weight of the sand determined from the compaction is the same as the one corresponding to e_{min}, determine the relative compaction of the soil.

5.3 For a cohesive soil with LL = 45 and PL = 25, estimate the difference in the w_{opt} and $\gamma_{d(max)}$ values between standard and modified compaction tests. Use Gurtug and Sridharan (2004) correlations.

5.4 Repeat Problem 5.3 using Osman et al. (2008) correlations.

5.5 The undisturbed soil at a given borrow pit is found to have the following properties: w = 15%; γ = 19.1 kN/m^3; G_s = 2.70. The soil from this borrow is to be used to construct a rolled fill having a finished volume of 38,500 m^3. The soil is excavated by means of a shovel and dumped onto trucks having a capacity of 4.80 m^3 each. When loaded to capacity,

these trucks are found to contain, on average, a net weight of soil and water equal to 72.7 kN.

In the construction process, the trucks dump their load on the fill, the material is spread and broken up, after which a sprinkler adds water until the moisture content is equal to 18%. The soil and water are thoroughly mixed by a disc (or similar equipment) and then compacted until the dry unit weight is equal to 17.3 kN/m^3.

a. Assuming that each load is a full-capacity load, how many truckloads are required to construct the fill?
b. What should be the volume of the pit that remains in the borrow area after all the material required for the fill has been removed?
c. How many liters of water will have to be added per truckload, assuming that the moisture lost by evaporation during excavation, haulage, and handling is negligible?
d. If the fill should become saturated at some time subsequent to the construction and does not change volume appreciably, what will be its saturation water content?

5.6 For a vibroflotation work, the backfill to be used has the following characteristics:
$D_{50} = 2$ mm
$D_{20} = 0.7$ mm
$D_{10} = 0.65$ mm

Determine the suitability number of the backfill. How would you rate the material?

5.7 For the soil A, B, and C in Problem 2.7, find the suitability numbers using Eq. (5.17) and the suitability of these soil for densification using vibroflotation method. What are these soil?

5.8 A 5 m thick doubly drained normally consolidated clay layer at a site has $e_o = 0.95$, $C_c = 0.54$, and $c_v = 4.0$ m^2/year. The effective overburden pressure at the middle of the clay layer is 70.0 kN/m^2. Some proposed construction work is expected to impose a 60.0 kN/m^2 load at the ground level.

a. Determine the primary consolidation settlement.
b. Noting that the expected primary consolidation settlement is high, it is proposed to apply a surcharge over a period of one year. What should the magnitude of this temporary surcharge be so there will be no postconstruction consolidation settlement?

5.9 In Problem 5.8, the client sees the one-year duration of the preload as too long and wants to limit this to 6 months. What should the total surcharge be during this period?

5.10 A 3.0 m thick singly drained normally consolidated clay layer has $e_o = 0.89$, $C_c = 0.46$, and $c_v = 3.5$ m^2/year. The effective overburden pressure at the middle of the layer is 105.0 kN/m^2. It is proposed to build a large warehouse that is expected to impose a pressure of 50.0 kN/m^2 at the ground level.

a. What would the primary consolidation settlement be?
b. If the engineer proposes to preload the site with a pressure of 90.0 kN/m^2, how long should this surcharge be left to ensure there is no postconstruction settlement when the warehouse is built?

5.11 The diagram of a sand drain is shown in Figures 5.21 and 5.22. Given: $r_w = 0.25$ m, $r_s = 0.35$ m, $d_e = 4.5$ m, $c_v = c_{vr} = 0.3$ m^2/month, $k_h/k_s = 2$, and $H_c = 9$ m. Determine:

a. The degree of consolidation for the clay layer caused only by the sand drains after six months of surcharge application
b. The degree of consolidation for the clay layer that is caused by the combination of vertical drainage (drained on top and bottom) and radial drainage after six months of the application of surcharge

Assume that the surcharge is applied instantaneously.

5.12 A 10 ft thick clay layer is drained at the top and bottom. Its characteristics are $c_{vr} = c_v$ (for vertical drainage) = 0.042 ft^2/day, $r_w = 8$ in., and $d_e = 6$ ft. Estimate the degree of consolidation of the clay layer caused by the combination of vertical and radial drainage at $t = 0.2$, 0.4, 0.8, and 1 year. Assume that the surcharge is applied instantaneously and there is no smear.

5.13 For a sand drain project (Figure 5.20), the following are given:

Clay: Normally consolidated
$H_c = 5.5$ m (one-way drainage)
$C_c = 0.3$
$e_o = 0.76$
$c_v = 0.015$ m^2/day
Effective overburden pressure at the middle of clay layer = 80 kN/m^2

Sand drain: $r_w = 0.07$ m
$r_w = r_s$
$d_e = 2.5$ m
$c_v = c_{vr}$

A surcharge is applied as shown in Figure P5.13. Calculate the degree of consolidation and the consolidation settlement 50 days after the beginning of the surcharge application.

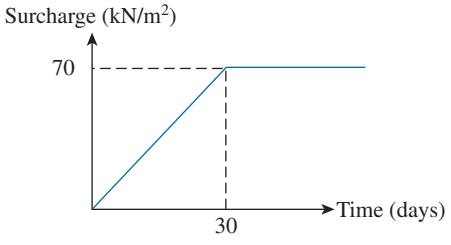


FIGURE P.5.13

REFERENCES

Aboshi, H., Ichimoto, E., and Harada, K. (1979). "The Compozer—a Method to Improve Characteristics of Soft Clay by Inclusion of Large Diameter Sand Column," *Proceedings, International Conference on Soil Reinforcement, Reinforced Earth and Other Techniques*, Vol. 1, Paris, pp. 211–216.

American Society for Testing and Materials (2007). *Annual Book of Standards*, Vol. 04.08, West Conshohocken, PA.

Bachus, R. C. and Barksdale, R. D. (1989). "Design Methodology for Foundations on Stone Columns," *Proceedings, Foundation Engineering: Current Principles and Practices*, American Society of Civil Engineers, Vol. 1, pp. 244–257.

Barron, R. A. (1948). "Consolidation of Fine-Grained Soils by Drain Wells," *Transactions*, American Society of Civil Engineers, Vol. 113, pp. 718–754.

Basore, C. E. and Boitano, J. D. (1969). "Sand Densification by Piles and Vibroflotation," *Journal of the Soil Mechanics and Foundations Division*, American Society of Civil Engineers, Vol. 95, No. SM6, pp. 1303–1323.

Brown, R. E. (1977). "Vibroflotation Compaction of Cohesionless Soils," *Journal of the Geotechnical Engineering Division*, American Society of Civil Engineers, Vol. 103, No. GT12, pp. 1437–1451.

Bruce, D. A. and Bruce, E. C. (2003). "The Practitioner's Guide to Deep Mixing," *Grouting and Ground Treatment, Proceedings of the Third International Conference*, New Orleans, LA, pp. 474–488.

Burke, G. K. (2004). "Jet Grouting Systems: Advantages and Disadvantages," *Proceedings, GeoSupport 2004: Drilled Shafts, Micropiling, Deep Mixing, Remedial Methods, and Special Foundation Systems*, American Society of Civil Engineers, pp. 875–886.

D'Appolonia, D. J., Whitman, R. V., and D'Appolonia, E. (1969). "Sand Compaction with Vibratory Rollers," *Journal of the Soil Mechanics and Foundations Division*, American Society of Civil Engineers, Vol. 95, No. SM1, pp. 263–284.

FHWA (2000). "An Introduction to the Deep Soil Mixing Methods as used in Geotechnical Applications," FHWA-RD-99-138, *Federal Highway Administration*, U.S. Department of Transportation, p. 135.

Gurtug, Y. and Sridharan, A. (2004). "Compaction Behaviour and Prediction of Its Characteristics of Fine Grained Soils with Particular Reference to Compaction Energy," *Soils and Foundations*, Vol. 44, No. 5, pp. 27–36.

Hausmann, M. (1990). *Engineering Principles of Ground Modification*, McGraw-Hill, Singapore.

Hughes, J. M. O., and Withers, N. J. (1974). "Reinforcing of Soft Cohesive Soil with Stone Columns," *Ground Engineering*, Vol. 7, pp. 42–49.

Hughes, J. M. O., Withers, N. J., and Greenwood, D. A. (1975). "A Field Trial of Reinforcing Effects of Stone Columns in Soil," *Geotechnique*, Vol. 25, No. 1, pp. 31–34.

Ichimoto, A. (1981). "Construction and Design of Sand Compaction Piles," *Soil Improvement*, *General Civil Engineering Laboratory* (in Japanese), Vol. 5. pp. 37–45.

Johnson, S. J. (1970a). "Precompression for Improving Foundation Soils," *Journal of the Soil Mechanics and Foundations Division*, American Society of Civil Engineers. Vol. 96, No. SM1, pp. 114–144.

Johnson, S. J. (1970b). "Foundation Precompression with Vertical Sand Drains," *Journal of the Soil Mechanics and Foundations Division*, American Society of Civil Engineers. Vol. 96, No. SM1, pp. 145–175.

Leonards, G. A., Cutter, W. A., and Holtz, R. D. (1980). "Dynamic Compaction of Granular Soils," *Journal of Geotechnical Engineering Division*, ASCE, Vol. 96, No. GT1, pp. 73–110.

Matteo, L. D., Bigotti, F., and Ricco, R. (2009). "Best-Fit Model to Estimate Proctor Properties of Compacted Soil," *Journal of Geotechnical and Geoenvironmental Engineering*, American Society of Civl Engineers, Vol. 135, No. 7, pp. 992–996.

Mitchell, J. K. (1970). "In-Place Treatment of Foundation Soils," *Journal of the Soil Mechanics and Foundations Division*, American Society of Civil Engineers, Vol. 96, No. SM1, pp. 73–110.

Mitchell, J. K. (1981). "Soil Improvement—State-of-the-Art Report," *Proceedings*, *10th International Conference on Soil Mechanics and Foundation Engineering,* Stockholm, Sweden, Vol. 4, pp. 506–565.

Mitchell, J. K. and Freitag, D. R. (1959). "A Review and Evaluation of Soil–Cement Pavements," *Journal of the Soil Mechanics and Foundations Division*, American Society of Civil Engineers, Vol. 85, No. SM6, pp. 49–73.

Mitchell, J. K. and Huber, T. R. (1985). "Performance of a Stone Column Foundation," *Journal of Geotechnical Engineering*, American Society of Civil Engineers, Vol. 111, No. GT2, pp. 205–223.

Murayama, S. (1962). "An Analysis of Vibro-Compozer Method on Cohesive Soils," *Construction in Mechanization* (in Japanese), No. 150, pp. 10–15.

Ohta, S. and Shibazaki, M. (1982). "A Unique Underpinning of Soil Specification Utilizing Super-High Pressure Liquid Jet," *Proceedings, Conference on Grouting in Geotechnical Engineering*, New Orleans, LA.

Olson, R. E. (1977). "Consolidation under Time-Dependent Loading," *Journal of Geotechnical Engineering Division*, ASCE, Vol. 102, No. GT1, pp. 55–60.

Omar, M., Abdallah, S., Basma, A., and Barakat, S. (2003). "Compaction Characteristics of Granular Soils in the United Arab Emirates," *Geotechnical and Geological Engineering*, Vol. 21, No. 3, pp. 283–295.

Osman, S., Togrol, E., and Kayadelen, C. (2008). "Estimating Compaction Behavior of Fine-Grained Soils Based on Compaction Energy," *Canadian Geotechnical Journal*, Vol. 45, No. 6, pp. 877–887.

Othman, M. A. and Luettich, S. M. (1994). "Compaction Control Criteria for Clay Hydraulic Barriers," *Transportation Research Record*, No. 1462, National Research Council, Washington, DC, pp. 28–35.

Partos, A., Welsh, J. P., Kazaniwsky, P. W., and Sander, E. (1989). "Case Histories of Shallow Foundation on Improved Soil," *Proceedings, Foundation Engineering: Current Principles and Practices*, American Society of Civil Engineers, Vol. 1, pp. 313–327.

Patra, C. R., Sivakugan, N., Das, B. M., and Rout, S. K. (2010). "Correlations of Relative Density of Clean Sand with Median Grain Size and Compaction Energy," *International Journal of Geotechnical Engineering*, Vol. 4, No. 2, pp. 195–203.

Poran, C. J. and Rodriguez, J. A. (1992). "Design of Dynamic Compaction," *Canadian Geotechnical Journal*, Vol. 2, No. 5, pp. 796–802.

Shibuya, S. and Hanh, L. T. (2001). "Estimating Undrained Shear Strength of Soft Clay Ground Improved by Preloading with PVD—Case History in Bangkok," *Soils and Foundations*, Vol. 41, No. 4, pp. 95–101.

Steudlein, A. W. and Holtz, R. D. (2013). "Bearing Capacity of Spread Footings on Aggregate Pier Reinforced Clay," *Journal of Geotechnical and Geoenvironmental Engineering*, American Society of Civil Engineers, Vol. 139, No. 1, pp. 49–58.

Thompson, M. R. (1967). *Bulletin 492*, *Factors Influencing the Plasticity and Strength of Lime-Soil Mixtures*, Engineering Experiment Station, University of Illinois.

Thompson, M. R. (1966). "Shear Strength and Elastic Properties of Lime-Soil Mixtures," *Highway Research Record 139*, National Research Council, Washington, DC, pp. 1–14.

Transportation Research Board (1987). *Lime Stabilization: Reactions, Properties, Design and Construction*, National Research Council, Washington, DC.

Tullock, W. S., II, Hudson, W. R., and Kennedy, T. W. (1970). *Evaluation and Prediction of the Tensile Properties of Lime-Treated Materials*, Research Report 98-5, Center for Highway Research, University of Texas, Austin, TX.

U.S. Navy (1982). *Soil mechanics—Design manual 7.1*, Department of the Navy, Naval Facilities Engineering Command, U.S. Government Printing Office, Washington, DC.

Welsh, J. P. and Burke, G. K. (1991). "Jet Grouting–Uses for Soil Improvement," *Proceedings*, *Geotechnical Engineering Congress*, American Society of Civil Engineers, Vol. 1, pp. 334–345.

Welsh, J. P., Rubright, R. M., and Coomber, D. B. (1986). "Jet Grouting for Support of Structures," presented at the Spring Convention of the American Society of Civil Engineers, Seattle, WA.

Yeung, A. T. (1997). "Design Curves for Prefabricated Vertical Drains," *Journal of Geotechnical and Geoenvironmental Engineering*, Vol. 123, No. 8, pp. 755–759.

PART 3

Foundation Analysis

Chapter 6: Shallow Foundations: Ultimate Bearing Capacity

Chapter 7: Ultimate Bearing Capacity of Shallow Foundations: Special Cases

Chapter 8: Vertical Stress Increase in Soil

Chapter 9: Settlement of Shallow Foundations

Chapter 10: Mat Foundations

Chapter 11: Load and Resistance Factor Design (LRFD)

Chapter 12: Pile Foundations

Chapter 13: Drilled-Shaft Foundations

Chapter 14: Piled Raft: An Overview

Chapter 15: Foundations on Difficult Soil

Aisyah Iumaranas/Shutterstock.com

6

Shallow Foundations: Ultimate Bearing Capacity



stockthrone.com/Shutterstock.com

6.1 Introduction 207
6.2 General Concept 208
6.3 Terzaghi's Bearing Capacity Theory 212
6.4 Factor of Safety 216
6.5 Modification of Bearing Capacity Equations for Water Table 217
6.6 The General Bearing Capacity Equation 218
6.7 Other Solutions for Bearing Capacity, Shape, and Depth Factors 225
6.8 Case Studies on Ultimate Bearing Capacity 227
6.9 Effect of Soil Compressibility 231
6.10 Eccentrically Loaded Foundations 235
6.11 Ultimate Bearing Capacity Under Eccentric Loading—One-Way Eccentricity 236
6.12 Bearing Capacity—Two-Way Eccentricity 242
6.13 A Simple Approach for Bearing Capacity with Two-Way Eccentricity 249
6.14 Bearing Capacity of a Continuous Foundation Subjected to Eccentrically Inclined Loading 251
6.15 Plane-Strain Correction of Friction Angle 254
6.16 Summary 254

PROBLEMS 254
REFERENCES 256

6.1 Introduction

Foundations are structural elements like beams and columns, which are designed to transfer building loads safely to the underlying ground. They must satisfy the following two design criteria:

1. *Bearing capacity*: There must be no failure within the surrounding soil; soil failure would jeopardize the integrity of the foundation.
2. *Settlement*: The settlement must be within tolerable limits.

Foundations are of two types: *shallow* and *deep foundations*. A shallow foundation is generally placed within the soil at a depth less than the width of the foundation. A deep foundation can extend to a depth much larger than the width. Shallow foundations include *pad, strip*, and *mat* (or *raft*) foundations. Pad foundations, also known as *pad footings* or *spread footings*, can be square, circular, or rectangular in plan and carry column loads (Figure 6.1a). They spread the column load evenly into the underlying ground. Strip foundations or footings, also known as *continuous foundations*, support wall loads (Figure 6.1b). Mat foundations can carry multiple column or wall loads (Figure 6.1c). Deep foundations include single piles, pile groups, and drilled shafts. The width and length of the foundation are denoted by B and L, respectively, and the depth at which the foundation is placed by D_f. The *contact pressure* or *load per unit area* (q) at the interface between the pad foundation and the soil is given by

$$q = \frac{Q}{BL} \tag{6.1}$$

where Q is the column load. The contact pressure (q) beneath a strip foundation carrying wall load of Q (unit of kN/m or kip/ft) is given by

$$q = \frac{Q}{B} \tag{6.2}$$

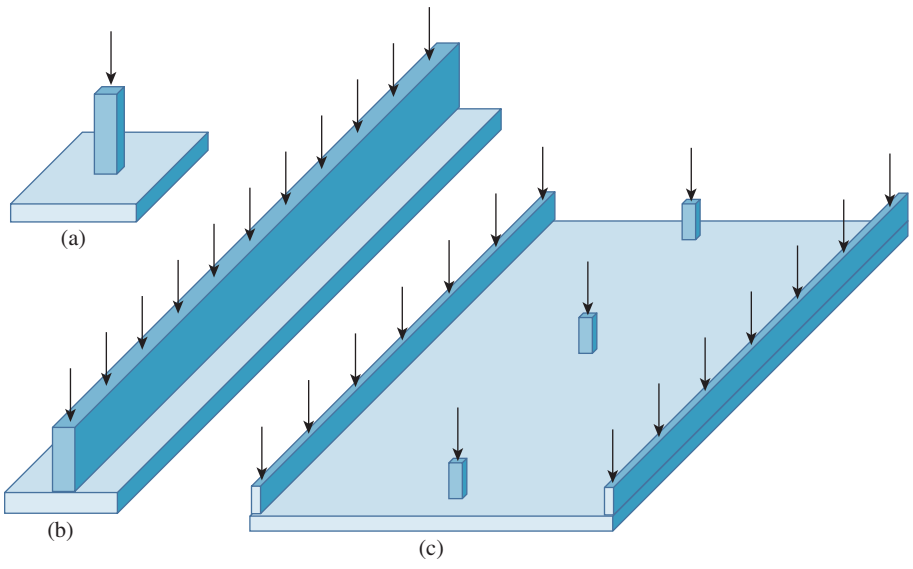


FIGURE 6.1 Shallow foundations: (a) pad; (b) strip; and (c) raft or mat

The contact pressure at which shear failure takes place within the surrounding soil is known as the *ultimate bearing capacity* (q_u), which is the subject of this chapter. In this chapter, we will discuss the following:

- Theoretical developments related to Terzaghi's ultimate bearing capacity equation and its modifications
- Effects of water table location
- Ultimate and allowable bearing capacities and factor of safety
- Methods to account for eccentricity and inclination in the applied loads

6.2 General Concept

Consider a strip foundation with a width of B resting on the surface of a dense sand or stiff cohesive soil, as shown in Figure 6.2a. Now, if a load is gradually applied to the foundation, settlement will increase. The variation of the load per unit area on the foundation (q) with the foundation settlement is also shown in Figure 6.2a. At a certain point—when the load per unit area equals q_u—a sudden failure in the soil supporting the foundation will take place, and the failure surface in the soil will extend to the ground surface. When such sudden failure in soil takes place, it is called *general shear failure*.

If the foundation under consideration rests on sand or clayey soil of medium compaction (Figure 6.2b), an increase in the load on the foundation will also be accompanied by an increase in settlement. However, in this case the failure surface in the soil will gradually extend outward from the foundation, as shown by the solid lines in Figure 6.2b.

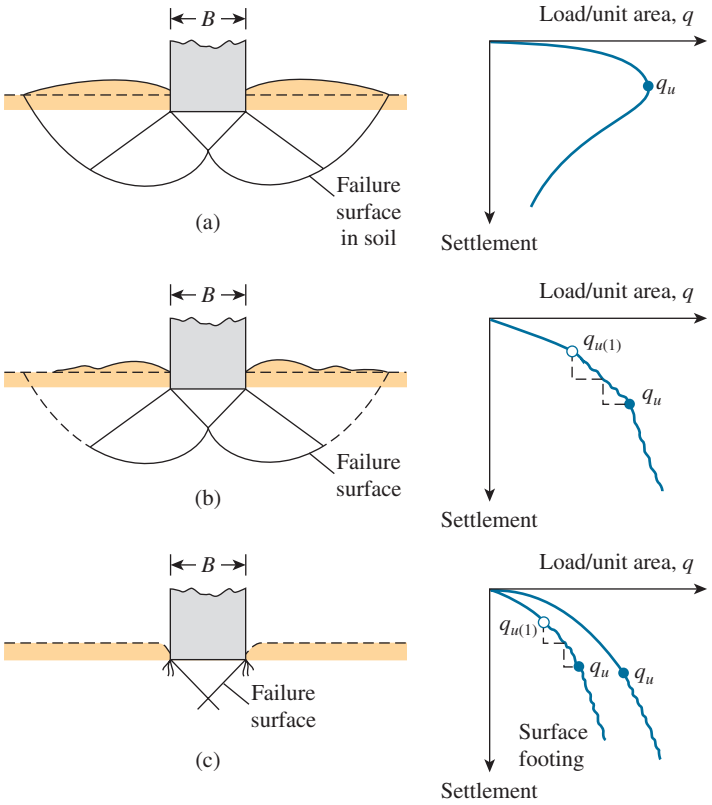


FIGURE 6.2 Nature of bearing capacity failure in soil: (a) general shear failure: (b) local shear failure; (c) punching shear failure (Redrawn after Vesic, 1973) (Based on Vesic, A. S. (1973). "Analysis of Ultimate Loads of Shallow Foundations," *Journal of Soil Mechanics and Foundations Division*, American Society of Civil Engineers, Vol. 99, No. SM1, pp. 45–73.)

When the load per unit area on the foundation equals $q_{u(1)}$, movement of the foundation will be accompanied by sudden jerks. A considerable movement of the foundation is then required for the failure surface in soil to extend to the ground surface (as shown by the broken lines in the figure). The load per unit area at which this happens is the *ultimate bearing capacity*, q_u. Beyond that point, an increase in load will be accompanied by a large increase in foundation settlement. The load per unit area of the foundation, $q_{u(1)}$, is referred to as the *first failure load* (Vesic, 1963). Note that a peak value of q is not realized in this type of failure, which is called the *local shear failure* in soil.

If the foundation is supported by a fairly loose soil, the load-settlement plot will be like the one in Figure 6.2c. In this case, the failure surface in soil will not extend to the ground surface. Beyond the ultimate failure load, q_u, the load-settlement plot will be steep and practically linear. This type of failure in soil is called the *punching shear failure*.

Vesic (1963) conducted several laboratory load-bearing tests on circular and rectangular plates supported by a sand at various relative densities of compaction, D_r. The variations of $q_{u(1)}/\frac{1}{2}\gamma B$ and $q_u/\frac{1}{2}\gamma B$ obtained from those tests, where B is the diameter of a circular plate or width of a rectangular plate and γ is a dry unit weight of sand, are shown in Figure 6.3. It is important to note from this figure that, for $D_r \geq$ about 70%, the general shear type of failure in soil occurs.

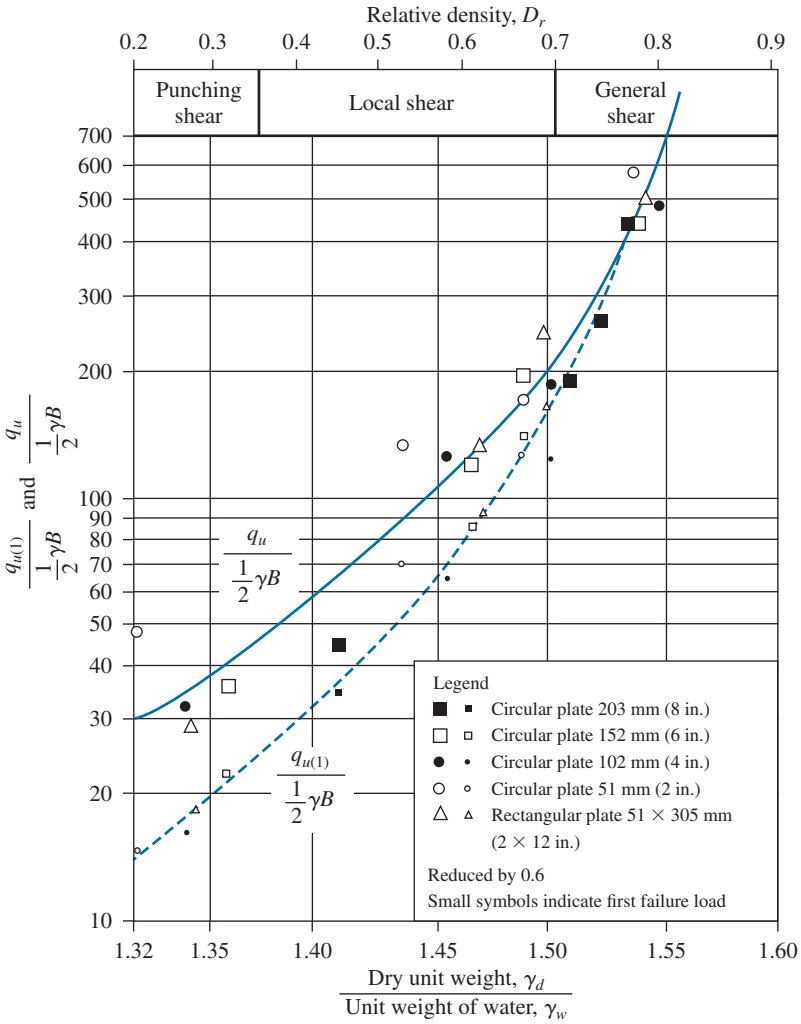


FIGURE 6.3 Variation of $q_{u(1)}/0.5\gamma B$ and $q_u/0.5\gamma B$ for circular and rectangular plates on the surface of a sand (Adapted from Vesic, 1963) (Based on Vesic, A. B. Bearing Capacity of Deep Foundations in Sand. In *Highway Research Record 39*, Highway Research Board, National Research Council, Washington, D.C., 1963, Figure 28, p. 137.)

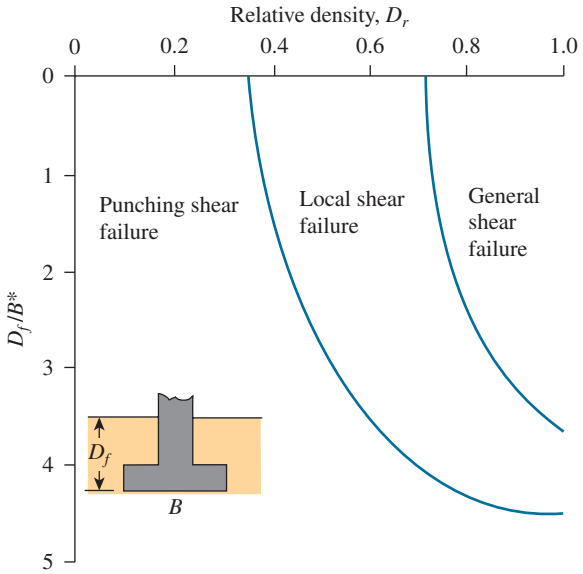


FIGURE 6.4 Modes of foundation failure in sand (Based on Vesic, A. S. (1973). "Analysis of Ultimate Loads of Shallow Foundations," *Journal of Soil Mechanics and Foundations Division*, American Society of Civil Engineers, Vol. 99, No. SM1, pp. 45–73.)

On the basis of experimental results, Vesic (1973) proposed a relationship for the mode of bearing capacity failure of foundations resting on sands. Figure 6.4 shows this relationship, which involves the notation

D_r = relative density of sand

D_f = depth of foundation measured from the ground surface

$$B^* = \frac{2BL}{B + L} \tag{6.3}$$

where

B = width of foundation

L = length of foundation

(*Note:* L is always greater than B.)

For square foundations, $B = L$; for circular foundations, $B = L$ = diameter, so

$$B^* = B \tag{6.4}$$

B^* varies between B and $2B$, depending on B/L.

Figure 6.5 shows the settlement S_u of the circular and rectangular plates on the surface of a sand ($D_f = 0$) at *ultimate load*, as described in Figure 6.3. The figure indicates a general range of S_u/B with the relative density of compaction of sand. So, in general, we can say that, for foundations at a shallow depth (i.e., small D_f/B^*), under general shear failure the ultimate load may occur at a foundation settlement of 4 to 10% of B. In the case of local or punching shear failure, the ultimate load may occur at settlements of 15 to 25% of the width of the foundation (B).

DeBeer (1967) provided laboratory experimental results of S_u/B (B = diameter of circular plate) for $D_f/B = 0$ as a function of γB and relative density D_r. These results, expressed in a nondimensional form as plots of S_u/B versus $\gamma B/p_a$ (p_a = atmospheric pressure $\approx$ 100 kN/m^2), are shown in Figure 6.6. Patra et al. (2013) approximated the plots as

$$\left(\frac{S_u}{B}\right)_{(D_f/B=0)} (\%) = 30\,e^{(-0.9D_r)} + 1.67 \ln\left(\frac{\gamma B}{p_a}\right) - 1 \qquad \left(\text{for } \frac{\gamma B}{p_a} \leq 0.025\right) \tag{6.5a}$$

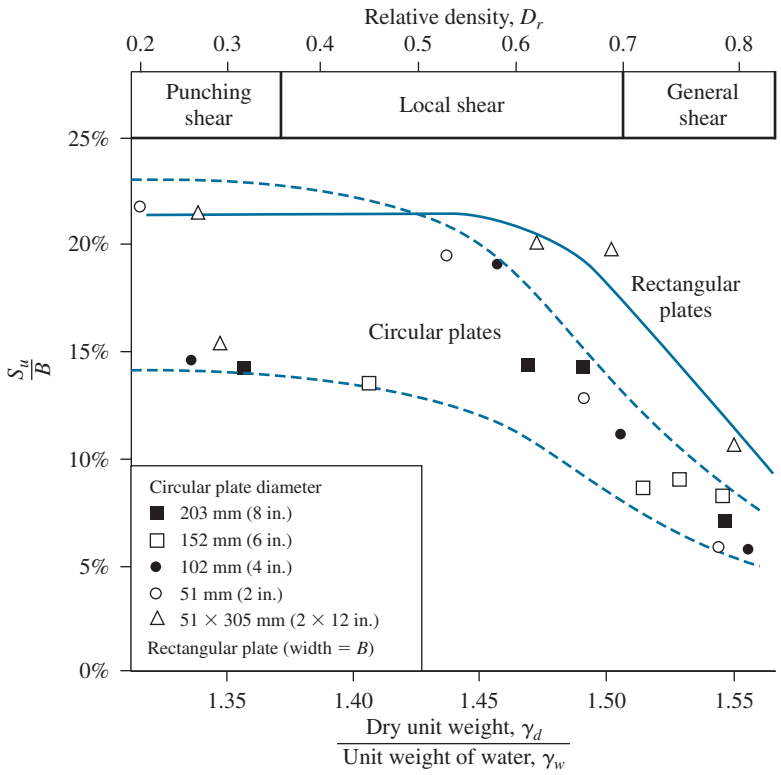


FIGURE 6.5 Range of settlement of circular and rectangular plates at ultimate load ($D_f/B = 0$) in sand (Based on Vesic, A. B. Bearing Capacity of Deep Foundations in Sand. In *Highway Research Record 39*, Highway Research Board, National Research Council, Washington, D.C., 1963, Figure 29, p. 138.)

and

$$\left(\frac{S_u}{B}\right)_{(D_f/B=0)} (\%) = 30e^{(-0.9D_r)} - 7.16 \quad \left(\text{for } \frac{\gamma B}{p_a} > 0.025\right) \tag{6.5b}$$

where D_r is expressed as a fraction. For comparison purposes, Eq. (6.5a) is also plotted in Figure 6.6. For $D_f/B > 0$, the magnitude of S_u/B in sand will be somewhat higher.

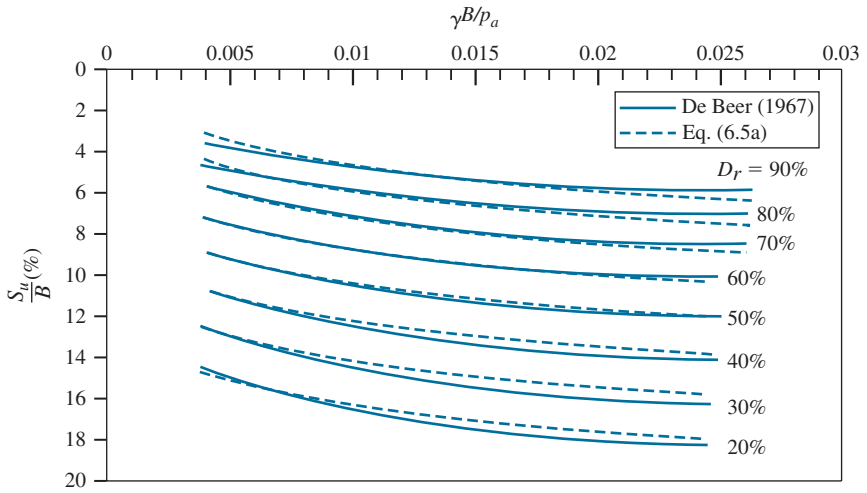


FIGURE 6.6 Variation of S_u/B with $\gamma B/p_a$ and D_r for circular plates in sand (*Note:* $D_f/B = 0$)

6.3 Terzaghi's Bearing Capacity Theory

Terzaghi (1943) was the first to present a comprehensive theory for the evaluation of the ultimate bearing capacity of rough shallow foundations. According to this theory, a foundation is *shallow* if its depth, D_f (Figure 6.7), is less than or equal to its width. Later investigators, however, have suggested that foundations with D_f as high as 3 to 4 times their width may also be defined as *shallow foundations*.

Terzaghi suggested that for a *continuous*, or *strip, foundation* (i.e., one whose width-to-length ratio approaches zero), the failure surface in soil at ultimate load may be assumed to be similar to that shown in Figure 6.7. (Note that this is the case of general shear failure, as defined in Figure 6.2a.) Foundations are generally placed on ground that is well compacted, and hence the assumption of general shear failure is valid. The effect of soil above the bottom of the foundation may also be assumed to be replaced by an equivalent surcharge, $q = \gamma D_f$ (where γ is the unit weight of soil above the foundation level). The failure zone under the foundation can be separated into three parts (see Figure 6.7):

1. The *triangular zone ACD* immediately under the foundation
2. The *radial shear zones ADF* and *CDE*, with the curves *DE* and *DF* being arcs of a logarithmic spiral
3. Two triangular *Rankine passive zones AFH* and *CEG*

The angles *CAD* and *ACD* are assumed to be equal to the soil friction angle ϕ'. Note that with the replacement of the soil above the bottom of the foundation by an equivalent surcharge q, the shear resistance of the soil along the failure surfaces *GI* and *HJ* was neglected.

The ultimate bearing capacity, q_u, of the foundation now can be obtained by considering the equilibrium of the triangular wedge *ACD* shown in Figure 6.7. This is shown on a larger scale in Figure 6.8. If the load per unit area, q_u, is applied to the foundation and general shear failure occurs, the passive force, P_p, will act on each of the faces of the soil wedge, *ACD*. This is easy to conceive if we imagine that *AD* and *CD* are two walls that are pushing the soil wedges *ADFH* and *CDEG*, respectively, to cause passive failure. P_p should be inclined at an angle δ' (which is the angle of wall friction) to the perpendicular drawn to the wedge faces (that is, *AD* and *CD*). With soil on both sides of *AD* and *CD*, δ' should be equal to the angle of friction of soil, ϕ'. Because *AD* and *CD* are inclined at an angle ϕ' to the horizontal, the direction of P_p should be vertical.

Considering a unit length of the foundation, we have for equilibrium

$$(q_u)(2b)(1) = -W + 2C \sin \phi' + 2P_p \tag{6.6}$$

where

$b = B/2$

$W =$ weight of soil wedge $ACD = \gamma b^2 \tan \phi'$

$C =$ cohesive force acting along each face, *AD* and *CD*, that is equal to the unit cohesion times the length of each face $= c'b/(\cos \phi')$

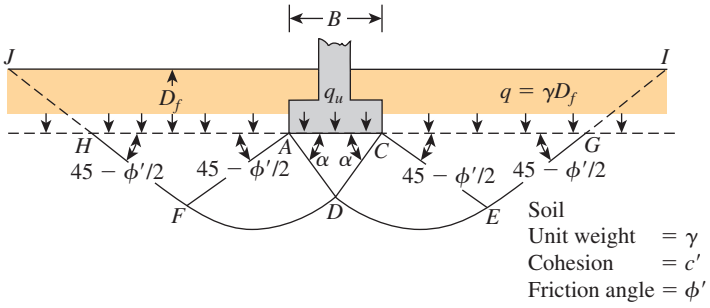


FIGURE 6.7 Bearing capacity failure in soil under a rough rigid continuous (strip) foundation

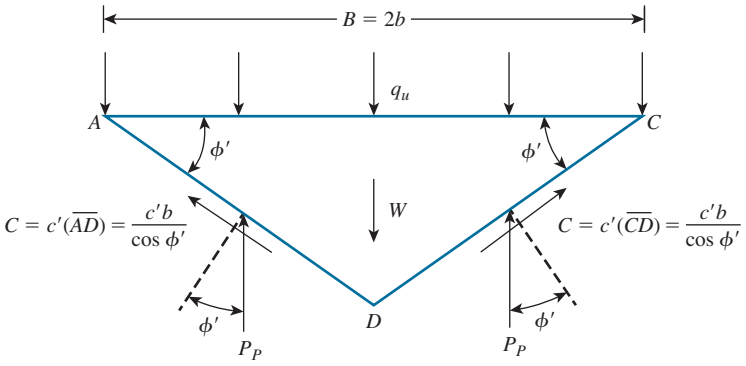


FIGURE 6.8 Derivation of Eq. (6.10)

Thus,

$$2bq_u = 2P_p + 2bc' \tan\phi' - \gamma b^2 \tan\phi' \tag{6.7}$$

or

$$q_u = \frac{P_p}{b} + c' \tan\phi' - \frac{\gamma b}{2} \tan\phi' \tag{6.8}$$

The passive force P_p in Eq. (6.8) is the sum of the contribution of the weight of soil γ, cohesion c', and surcharge q. Figure 6.9 shows the distribution of passive pressure from each of these components on the wedge face CD. Thus, we can write

$$P_p = \frac{1}{2}\gamma(b\tan\phi')^2 K_\gamma + c'(b\tan\phi')K_c + q(b\tan\phi')K_q \tag{6.9}$$

where K_γ, K_c, and K_q are earth pressure coefficients that are functions of the soil friction angle, ϕ'.

Combining Eqs. (6.8) and (6.9), we obtain

$$q_u = c'N_c + qN_q + \frac{1}{2}\gamma B N_\gamma \tag{6.10}$$

where

$$N_c = \tan\phi'(K_c + 1) \tag{6.11}$$

$$N_q = K_q \tan\phi' \tag{6.12}$$

and

$$N_\gamma = \frac{1}{2}\tan\phi'(K_\gamma \tan\phi' - 1) \tag{6.13}$$

where N_c, N_q, and N_γ are called *bearing capacity factors*.

The bearing capacity factors N_c, N_q, and N_γ are, respectively, the contributions of cohesion, surcharge, and unit weight of soil to the ultimate load-bearing capacity. It is extremely tedious to evaluate K_c, K_q, and K_γ. For this reason, Terzaghi used an approximate method to determine the ultimate bearing capacity, q_u. The principles of this approximation are given here.

1. If $\gamma = 0$ (weightless soil) and $c = 0$, then

$$q_u = q_q = qN_q \tag{6.14}$$

where

$$N_q = \frac{e^{2(3\pi/4 - \phi'/2)\tan\phi'}}{2\cos^2\left(45 + \frac{\phi'}{2}\right)} \tag{6.15}$$

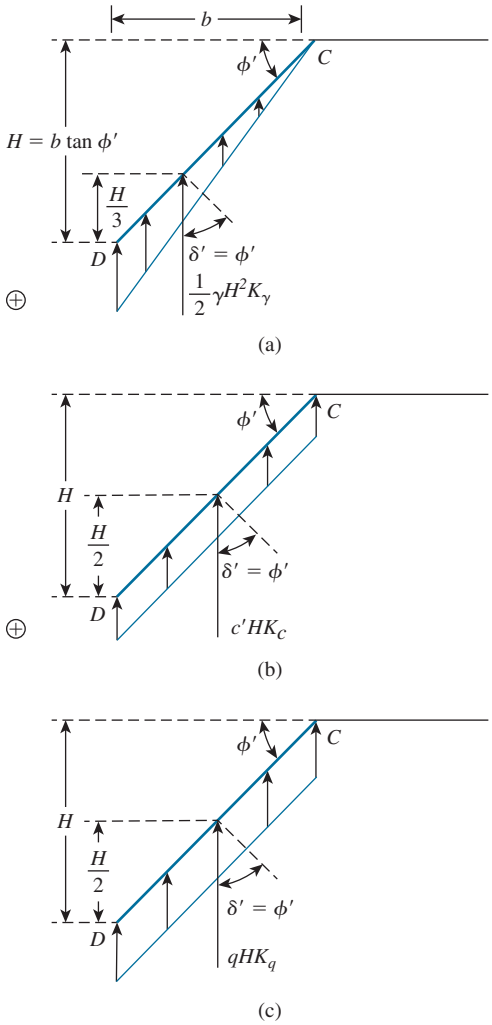


FIGURE 6.9 Passive force distribution on the wedge face *CD* shown in Figure 6.8: (a) contribution of soil weight γ; (b) contribution of cohesion c'; (c) contribution of surcharge q

2. If $\gamma = 0$ (that is, weightless soil) and $q = 0$, then

$$q_u = q_c = c' N_c \tag{6.16}$$

where

$$N_c = \cot \phi' \left[\frac{e^{2(3\pi/4 - \phi'/2)\tan \phi'}}{2\cos^2\left(\frac{\pi}{4} + \frac{\phi'}{2}\right)} - 1 \right] = \cot \phi' (N_q - 1) \tag{6.17}$$

3. If $c' = 0$ and surcharge $q = 0$ (that is, $D_f = 0$), then

$$q_u = q_\gamma = \frac{1}{2} \gamma B N_\gamma \tag{6.18}$$

The magnitude of N_γ for various values of ϕ' is determined by trial and error.

The variations of the bearing capacity factors defined by Eqs. (6.17), (6.15), and (6.13) are given in Table 6.1.

TABLE 6.1 Terzaghi's Bearing Capacity Factors—Eqs. (6.17), (6.15), and (6.13)[a]

ϕ'	N_c	N_q	N_γ[a]	ϕ'	N_c	N_q	N_γ[a]
0	5.70	1.00	0.00	26	27.09	14.21	9.84
1	6.00	1.10	0.01	27	29.24	15.90	11.60
2	6.30	1.22	0.04	28	31.61	17.81	13.70
3	6.62	1.35	0.06	29	34.24	19.98	16.18
4	6.97	1.49	0.10	30	37.16	22.46	19.13
5	7.34	1.64	0.14	31	40.41	25.28	22.65
6	7.73	1.81	0.20	32	44.04	28.52	26.87
7	8.15	2.00	0.27	33	48.09	32.23	31.94
8	8.60	2.21	0.35	34	52.64	36.50	38.04
9	9.09	2.44	0.44	35	57.75	41.44	45.41
10	9.61	2.69	0.56	36	63.53	47.16	54.36
11	10.16	2.98	0.69	37	70.01	53.80	65.27
12	10.76	3.29	0.85	38	77.50	61.55	78.61
13	11.41	3.63	1.04	39	85.97	70.61	95.03
14	12.11	4.02	1.26	40	95.66	81.27	115.31
15	12.86	4.45	1.52	41	106.81	93.85	140.51
16	13.68	4.92	1.82	42	119.67	108.75	171.99
17	14.60	5.45	2.18	43	134.58	126.50	211.56
18	15.12	6.04	2.59	44	151.95	147.74	261.60
19	16.56	6.70	3.07	45	172.28	173.28	325.34
20	17.69	7.44	3.64	46	196.22	204.19	407.11
21	18.92	8.26	4.31	47	224.55	241.80	512.84
22	20.27	9.19	5.09	48	258.28	287.85	650.67
23	21.75	10.23	6.00	49	298.71	344.63	831.99
24	23.36	11.40	7.08	50	347.50	415.14	1072.80
25	25.13	12.72	8.34				

[a]From Kumbhojkar (1993)

To estimate the ultimate bearing capacity of *square* and *circular foundations*, Eq. (6.10) may be respectively modified to

$$q_u = 1.3c'N_c + qN_q + 0.4\gamma BN_\gamma \quad \text{(square foundation)} \tag{6.19}$$

and

$$q_u = 1.3c'N_c + qN_q + 0.3\gamma BN_\gamma \quad \text{(circular foundation)} \tag{6.20}$$

In Eq. (6.19), B equals the dimension of each side of the foundation; in Eq. (6.20), B equals the diameter of the foundation.

Terzaghi's bearing capacity equation [Eq. (6.10)] and the bearing capacity factors have been modified. While recognizing the three components from cohesion,

surcharge, and the soil weight that contribute to the ulimate bearing capacity, the equation has been modified to account for the effects of the foundation shape (B/L), foundation depth (D_f), and inclination in the applied load. These are discussed in Section 6.6. Terzaghi's original bearing capacity equation [Eq. (6.10)] still provides fairly good estimates of the ultimate bearing capacity, but these estimates can be conservative.

6.4 Factor of Safety

Once the ultimate bearing capacity of a foundation is computed, it is necessary to determine the *allowable bearing capacity* (q_{all}), which is the load per unit area the foundation applies on the underlying soil when the structure is constructed. Allowing for an adequate *factor of safety* (FS), q_{all} is defined as

$$q_{all} = \frac{q_u}{FS} \tag{6.21}$$

The ultimate bearing capacity q_u computed from Eqs. (6.10), (6.19), or (6.20) is the *gross* ultimate bearing capacity. However, some practicing engineers prefer to use a factor of safety such that

$$\text{Net stress increase on soil} = \frac{\text{net ultimate bearing capacity}}{FS} \tag{6.22}$$

The net ultimate bearing capacity is defined as the ultimate pressure per unit area of the foundation that can be supported by the soil in excess of the pressure caused by the surrounding soil at the foundation level.

Similarly, the net pressure applied by the foundation to the underlying soil is the pressure in excess of the overburden pressure q ($= \gamma D_f$). For shallow foundations with D_f = 0–2 m, there is very little difference between the net and gross values. Only in situations with deep basements, where D_f is large and significant overburden is removed, it is necessary to distinguish between the net and gross values. If the difference between the unit weight of concrete used in the foundation and the unit weight of soil surrounding is assumed to be negligible, then

$$q_{u(net)} = q_u - q \tag{6.23}$$

where

$q_{u(net)}$ = net ultimate bearing capacity

$q = \gamma D_f$

So

$$q_{all(net)} = \frac{q_u - q}{FS} \tag{6.24}$$

Considering the uncertainties associated with the shear strength parameters and the simplifications used in the bearing capacity theory, a relatively large factor of safety of 3 is used with shallow foundations.

EXAMPLE 6.1

A 2.0 m wide strip foundation is placed at a depth of 1.5 m within a sandy clay, where $c' = 10$ kN/m^2, $\phi' = 26°$, and $\gamma = 19.0$ kN/m^3. Determine the maximum wall load that can be allowed on the foundation with a factor of safety of 3, assuming general shear failure. Use gross values.

SOLUTION

From Eq. (6.10),

$$q_u = c'N_c + qN_q + 0.5\gamma BN_\gamma$$

From Table 6.1, $N_c = 27.09$, $N_q = 14.21$, and $N_\gamma = 9.84$. Thus,

$$q_u = (10)(27.09) + (19.0 \times 1.5)(14.21) + (0.5)(19.0)(2.0)(9.84) = 862.8 \text{ kN/m}^2$$

$$q_{all} = \frac{q_u}{FS} = \frac{862.8}{3} = 287.6 \text{ kN/m}^2$$

Therefore, the maximum allowable load $Q = 287.6 \times 2 = \mathbf{575 \text{ kN/m}}$.

EXAMPLE 6.2

A design requires placing a square foundation at 1.0 m depth to carry a column load of 1500 kN. The soil properties are: $c' = 15$ kN/m^2, $\phi' = 24°$, and $\gamma = 18.5$ kN/m^3. What should be the width B of the foundation?

SOLUTION

From Eq. (6.19),

$$q_u = 1.3c'N_c + qN_q + 0.4\gamma BN_\gamma$$

From Table 6.1, $N_c = 23.36$, $N_q = 11.40$, and $N_\gamma = 7.08$.

$$q_u = (1.3)(15)(23.36) + (18.5 \times 1.0)(11.40) + (0.4)(18.5)(B)(7.08)$$
$$= 52.4\,B + 666.4 \text{ kN/m}^2$$

$$q_{all} = \frac{q_u}{FS} = \frac{52.4B + 666.4}{3} = 17.5B + 222.1$$

The applied pressure to the ground is $\frac{1500}{B^2}$ kN/m^2. Therefore, $\frac{1500}{B^2} = 17.5B + 222.1$.

By trial and error (or use of a graphics calculator), $B = \mathbf{2.4 \text{ m}}$.

6.5 Modification of Bearing Capacity Equations for Water Table

Equations (6.10) and (6.19) through (6.20) give the ultimate bearing capacity, based on the assumption that the water table is located well below the foundation. However, if the water table is close to the foundation, it reduces the unit weight of soil, so some modifications of the bearing capacity equations will be necessary. (See Figure 6.10.)

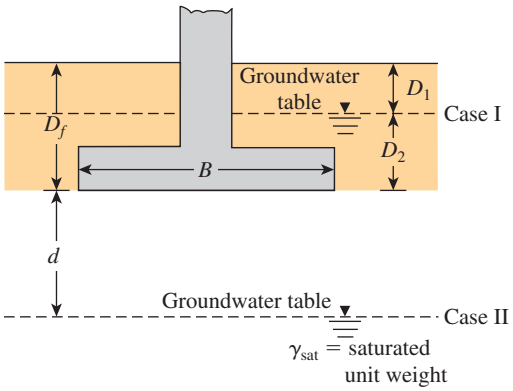


FIGURE 6.10 Modification of bearing capacity equations for water table

Case I. If the water table is located so that $0 \le D_1 \le D_f$, the factor q in the bearing capacity equations takes the form

$$q = \text{effective surcharge} = D_1\gamma + D_2(\gamma_{sat} - \gamma_w) \tag{6.25}$$

where

γ_{sat} = saturated unit weight of soil

γ_w = unit weight of water

Also, the value of γ in the last term of the equations has to be replaced by $\gamma' = \gamma_{sat} - \gamma_w$.

Case II. For a water table located so that $0 \le d \le B$,

$$q = \gamma D_f \tag{6.26}$$

In this case, the factor γ in the last term of the bearing capacity equations must be replaced by the weighted average value of the effective unit weight within B below the foundation, which is given by

$$\bar{\gamma} = \gamma' + \frac{d}{B}(\gamma - \gamma') \tag{6.27}$$

The preceding modifications are based on the assumption that there is no seepage force in the soil.

Case III. When the water table is located so that $d \ge B$, the water will have no effect on the ultimate bearing capacity.

In cases II and III, it is recognized that the failure surface (see Figure 6.7) is confined within a depth B below the foundation level.

6.6 The General Bearing Capacity Equation

The ultimate bearing capacity equations (6.10), (6.19), and (6.20) are for continuous, square, and circular foundations only; they do not address the case of rectangular foundations ($0 < B/L < 1$). Also, the equations do not take into account the shearing resistance along the failure surface in soil above the bottom of the foundation (the portion of the failure surface marked as dashed lines *GI* and *HJ* in Figure 6.7). In addition, the load on the foundation may be inclined. To account for all these shortcomings, Meyerhof (1963) suggested the following form of the general bearing capacity equation:

$$q_u = c'N_cF_{cs}F_{cd}F_{ci} + qN_qF_{qs}F_{qd}F_{qi} + \tfrac{1}{2}\gamma BN_\gamma F_{\gamma s}F_{\gamma d}F_{\gamma i} \tag{6.28}$$

In this equation:

c' = cohesion

q = effective stress at the level of the bottom of the foundation

γ = unit weight of soil

B = width of foundation (= diameter for a circular foundation)

$F_{cs}, F_{qs}, F_{\gamma s}$ = shape factors

$F_{cd}, F_{qd}, F_{\gamma d}$ = depth factors

$F_{ci}, F_{qi}, F_{\gamma i}$ = load inclination factors

N_c, N_q, N_γ = bearing capacity factors

The equations for determining the various factors given in Eq. (6.28) are described briefly in the sections that follow. Note that the original equation for ultimate bearing capacity is derived only for the plane-strain case (i.e., for continuous foundations). The shape, depth, and load inclination factors are empirical factors based on experimental data.

It is important to recognize the fact that in the *case of inclined loading on a foundation*, Eq. (6.28) provides the vertical component.

BEARING CAPACITY FACTORS

The basic nature of the failure surface in soil suggested by Terzaghi now appears to have been borne out by laboratory and field studies of bearing capacity (Vesic, 1973). However, the angle α shown in Figure 6.7 is closer to $45 + \phi'/2$ than to ϕ'. If this change is accepted, the values of N_c, N_q, and N_γ for a given soil friction angle will also change from those given in Table 6.1. With $\alpha = 45 + \phi'/2$, it can be shown that

$$N_q = \tan^2\left(45 + \frac{\phi'}{2}\right) e^{\pi \tan \phi'} \tag{6.29}$$

and

$$N_c = (N_q - 1)\cot \phi' \tag{6.30}$$

Equation (6.30) for N_c was originally derived by Prandtl (1921), and Eq. (6.29) for N_q was presented by Reissner (1924). Caquot and Kerisel (1953) and Vesic (1973) gave the relation for N_γ as

$$N_\gamma = 2(N_q + 1)\tan \phi' \tag{6.31}$$

Table 6.2 shows the variation of the preceding bearing capacity factors with soil friction angles.

TABLE 6.2 Bearing Capacity Factors From Eqs. (6.30), (6.29), and (6.31)

ϕ'	N_c	N_q	N_γ	ϕ'	N_c	N_q	N_γ
0	5.14	1.00	0.00	11	8.80	2.71	1.44
1	5.38	1.09	0.07	12	9.28	2.97	1.69
2	5.63	1.20	0.15	13	9.81	3.26	1.97
3	5.90	1.31	0.24	14	10.37	3.59	2.29
4	6.19	1.43	0.34	15	10.98	3.94	2.65
5	6.49	1.57	0.45	16	11.63	4.34	3.06
6	6.81	1.72	0.57	17	12.34	4.77	3.53
7	7.16	1.88	0.71	18	13.10	5.26	4.07
8	7.53	2.06	0.86	19	13.93	5.80	4.68
9	7.92	2.25	1.03	20	14.83	6.40	5.39
10	8.35	2.47	1.22	21	15.82	7.07	6.20

(continued)

TABLE 6.2 Bearing Capacity Factors From Eqs. (6.30), (6.29), and (6.31) (*Continued*)

ϕ'	N_c	N_q	N_γ	ϕ'	N_c	N_q	N_γ
22	16.88	7.82	7.13	37	55.63	42.92	66.19
23	18.05	8.66	8.20	38	61.35	48.93	78.03
24	19.32	9.60	9.44	39	67.87	55.96	92.25
25	20.72	10.66	10.88	40	75.31	64.20	109.41
26	22.25	11.85	12.54	41	83.86	73.90	130.22
27	23.94	13.20	14.47	42	93.71	85.38	155.55
28	25.80	14.72	16.72	43	105.11	99.02	186.54
29	27.86	16.44	19.34	44	118.37	115.31	224.64
30	30.14	18.40	22.40	45	133.88	134.88	271.76
31	32.67	20.63	25.99	46	152.10	158.51	330.35
32	35.49	23.18	30.22	47	173.64	187.21	403.67
33	38.64	26.09	35.19	48	199.26	222.31	496.01
34	42.16	29.44	41.06	49	229.93	265.51	613.16
35	46.12	33.30	48.03	50	266.89	319.07	762.89
36	50.59	37.75	56.31				

SHAPE, DEPTH, AND INCLINATION FACTORS

Commonly used shape, depth, and inclination factors are given in Table 6.3.

TABLE 6.3 Shape, Depth, and Inclination Factors [DeBeer (1970); Hansen (1970); Meyerhof (1963); Meyerhof and Hanna (1981)]

Factor	Relationship	Reference
Shape	$F_{cs} = 1 + \left(\frac{B}{L}\right)\left(\frac{N_q}{N_c}\right)$ $F_{qs} = 1 + \left(\frac{B}{L}\right)\tan\phi'$ $F_{\gamma s} = 1 - 0.4\left(\frac{B}{L}\right)$	DeBeer (1970)
Depth	$\frac{D_f}{B} \le 1$ For $\phi = 0$: $F_{cd} = 1 + 0.4\left(\frac{D_f}{B}\right)$ $F_{qd} = 1$ $F_{\gamma d} = 1$ For $\phi' > 0$: $F_{cd} = F_{qd} - \frac{1 - F_{qd}}{N_c \tan\phi'}$ $F_{qd} = 1 + 2\tan\phi'(1 - \sin\phi')^2\left(\frac{D_f}{B}\right)$ $F_{\gamma d} = 1$	Hansen (1970)

TABLE 6.3 Shape, Depth, and Inclination Factors [DeBeer (1970); Hansen (1970); Meyerhof (1963); Meyerhof and Hanna (1981)] (*Continued*)

Factor	Relationship	Reference
	$\frac{D_f}{B} > 1$ For $\phi = 0$: $F_{cd} = 1 + 0.4 \underbrace{\tan^{-1}\left(\frac{D_f}{B}\right)}_{\text{radians}}$ $F_{qd} = 1$ $F_{\gamma d} = 1$ For $\phi' > 0$: $F_{cd} = F_{qd} - \frac{1 - F_{qd}}{N_c \tan \phi'}$ $F_{qd} = 1 + 2 \tan \phi'(1 - \sin \phi')^2 \underbrace{\tan^{-1}\left(\frac{D_f}{B}\right)}_{\text{radians}}$ $F_{\gamma d} = 1$	
Inclination	$F_{ci} = F_{qi} = \left(1 - \frac{\beta^\circ}{90^\circ}\right)^2$ $F_{\gamma i} = \left(1 - \frac{\beta^\circ}{\phi'}\right)^2$ β = inclination of the load on the foundation with respect to the vertical	Meyerhof (1963); Hanna and Meyerhof (1981)

DRAINED AND UNDRAINED CONDITIONS

The equations for the ultimate bearing capacity [Eqs. (6.10), (6.19), (6.20), and (6.28)] can be applied for drained conditions in terms of effective stresses and for undrained conditions in terms of total stresses. When applying the equation in terms of effective stresses, c' and ϕ' are used. When applying the equation in terms of total stresses for analyzing undrained loading, undrained cohesion c_u and $\phi = 0$ are used. For $\phi = 0$, $N_c = 5.14$, $N_q = 1$, and $N_\gamma = 0$ (see Table 6.2).

In the case of strip foundation in clay under undrained conditions carrying vertical wall loads, with $D_f = 0$,

$$F_{cs} = F_{qs} = F_{\gamma s} = 1;\ F_{cd} = F_{qd} = F_{\gamma d} = 1; \text{ and } F_{ci} = F_{qi} = F_{\gamma i} = 1$$

From Eq. (6.28), the gross ultimate bearing capacity is given by

$$q_u = 5.14c_u + q \tag{6.32}$$

$$q_{u(\text{net})} = 5.14c_u \tag{6.33}$$

EXAMPLE 6.3

Solve Example 6.1 using Eq. (6.28).

SOLUTION

From Eq. (6.28), the ultimate bearing capacity is given by

$$q_u = c'N_cF_{cs}F_{cd}F_{ci} + qN_qF_{qs}F_{qd}F_{qi} + 0.5\gamma B\, N_\gamma F_{\gamma s}F_{\gamma d}F_{\gamma i}$$

For $\phi' = 26^\circ$, from Table 6.2, $N_c = 22.25$, $N_q = 11.85$, and $N_\gamma = 12.54$. Since the load is vertical, the inclination factors are unity.

For strip foundation, $L > B$ and, hence, all three shape factors are unity.

$$F_{qd} = 1 + 2\tan\phi'(1 - \sin\phi')^2\left(\frac{D_f}{B}\right) = 1 + 2\tan 26(1 - \sin 26)^2 \times \frac{1.5}{2.0} = 1.23$$

$$F_{cd} = F_{qd} - \frac{1 - F_{qd}}{N_c \tan\phi'} = 1.23 - \frac{1 - 1.23}{22.25\tan 26} = 1.25$$

$$F_{\gamma d} = 1$$

Hence,

$$\begin{aligned} q_u &= (10)(22.25)(1)(1.25)(1) + (19.0\times 1.5)(11.85)(1)(1.23)(1.0) \\ &\quad + (0.5)(19.0)(2.0)(12.54)(1)(1)(1) \\ &= 931.8 \text{ kN/m}^2 \end{aligned}$$

$$q_{all} = \frac{q_u}{\text{FS}} = \frac{931.8}{3} = 310.6 \text{ kN/m}^2$$

Therefore, the maximum allowable load $Q = 310.6 \times 2 = \mathbf{621\ kN/m}$.

■

EXAMPLE 6.4

A square foundation ($B \times B$) has to be constructed as shown in Figure 6.11. Assume that $\gamma = 105$ lb/ft^3, $\gamma_{sat} = 118$ lb/ft^3, $\phi' = 34°$, $D_f = 4$ ft, and $D_1 = 2$ ft. The gross allowable load, Q_{all}, with FS = 3 is 150,000 lb. Determine the size of the foundation. Use Eq. (6.28).

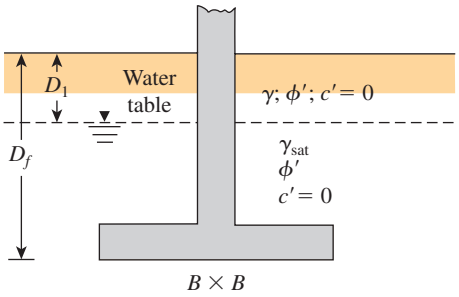


FIGURE 6.11 A square foundation

SOLUTION

We have

$$q_{\text{all}} = \frac{Q_{\text{all}}}{B^2} = \frac{150{,}000}{B^2} \text{ lb/ft}^2 \tag{a}$$

From Eq. (6.28) (with $c' = 0$), for vertical loading, we obtain

$$q_{\text{all}} = \frac{q_u}{\text{FS}} = \frac{1}{3}\left(qN_qF_{qs}F_{qd} + \frac{1}{2}\gamma' BN_\gamma F_{\gamma s}F_{\gamma d}\right)$$

For $\phi' = 34°$, from Table 6.2, $N_q = 29.44$ and $N_\gamma = 41.06$. Hence,

$$F_{qs} = 1 + \left(\frac{B}{L}\right)\tan\phi' = 1 + \tan 34 = 1.67$$

$$F_{\gamma s} = 1 - 0.4\left(\frac{B}{L}\right) = 1 - 0.4 = 0.6$$

$$F_{qd} = 1 + 2\tan\phi'(1 - \sin\phi')^2\frac{D_f}{B} = 1 + 2\tan 34\,(1 - \sin 34)^2\frac{4}{B} = 1 + \frac{1.05}{B}$$

$$F_{\gamma d} = 1$$

and

$$q = (2)(105) + 2(118 - 62.4) = 321.2 \text{ lb/ft}^2$$

So

$$q_{all} = \frac{1}{3}\left[(321.2)(29.44)(1.67)\left(1 + \frac{1.05}{B}\right) + \left(\frac{1}{2}\right)(118 - 62.4)(B)(41.06)(0.6)(1)\right] \quad \text{(b)}$$

$$= 5263.9 + \frac{5527.1}{B} + 228.3B$$

Combining Eqs. (a) and (b) results in

$$\frac{150{,}000}{B^2} = 5263.9 + \frac{5527.1}{B} + 228.3B$$

By trial and error, we find that $B \approx$ **4.5 ft**.

EXAMPLE 6.5

A square column foundation (Figure 6.12) is to be constructed on a sand deposit. The allowable load Q will be inclined at an angle $\beta = 20°$ with the vertical. The standard penetration numbers N_{60} obtained from the field are as follows. Determine Q. Use FS = 3, Eq. (3.13), Eq. (3.29), and Eq. (6.28).

Depth (m)	N_{60}
1.5	3
3.0	6
4.5	9
6.0	10
7.5	10
9.0	8

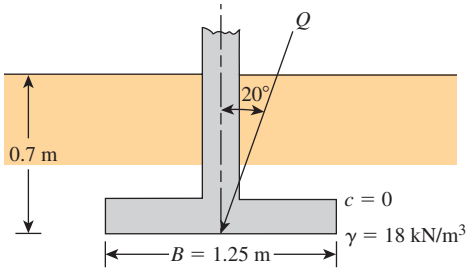


FIGURE 6.12

SOLUTION

From Eq. (3.29),

$$\phi' \text{ (deg)} = 27.1 + 0.3(N_1)_{60} - 0.00054[(N_1)_{60}]^2$$

The following is an estimation of ϕ' in the field using Eq. (3.29).

Depth (m)	σ_o'(kN/m^2)	C_N from Eq. (3.13)	N_{60}	$(N_1)_{60}$	ϕ' (°) from Eq. (3.29)
1.5	27.0	1.92	3	5.8	28.8
3.0	54.0	1.36	6	8.2	29.5
4.5	81.0	1.11	9	10.0	30.0
6.0	108.0	0.96	10	9.6	29.9
7.5	135.0	0.86	10	8.6	29.6
9.0	162.0	0.79	8	6.3	29.0

Average $\phi' = 29.5° \approx 30°$

With $c' = 0$, the ultimate bearing capacity [Eq. (6.28)] becomes

$$q_u = qN_qF_{qs}F_{qd}F_{qi} + \frac{1}{2}\gamma BN_\gamma F_{\gamma s}F_{\gamma d}F_{\gamma i}$$

$$q = (0.7)(18) = 12.6 \text{ kN/m}^2$$

$$\gamma = 18 \text{ kN/m}^3$$

From Table 6.2 for $\phi' = 30°$,

$$N_q = 18.4$$

$$N_\gamma = 22.4$$

From Table 6.3 (*Note:* $B = L$),

$$F_{qs} = 1 + \left(\frac{B}{L}\right)\tan\phi' = 1 + 0.577 = 1.577$$

$$F_{\gamma s} = 1 - 0.4\left(\frac{B}{L}\right) = 0.6$$

$$F_{qd} = 1 + 2\tan\phi'(1 - \sin\phi')^2\frac{D_f}{B} = 1 + \frac{(0.289)(0.7)}{1.25} = 1.162$$

$$F_{\gamma d} = 1$$

$$F_{qi} = \left(1 - \frac{\beta^\circ}{90^\circ}\right)^2 = \left(1 - \frac{20}{90}\right)^2 = 0.605$$

$$F_{\gamma i} = \left(1 - \frac{\beta^\circ}{\phi'}\right)^2 = \left(1 - \frac{20}{30}\right)^2 = 0.11$$

Hence,

$$q_u = (12.6)(18.4)(1.577)(1.162)(0.605) + \left(\frac{1}{2}\right)(18)(1.25)(22.4)(0.6)(1)(0.11)$$

$$= 273.66 \text{ kN/m}^2$$

$$q_{\text{all}} = \frac{q_u}{\text{FS}} = \frac{273.66}{3} = 91.22 \text{ kN/m}^2$$

Now,

$$Q\cos 20 = q_{\text{all}}B^2 = (91.22)(1.25)^2$$

$$Q \approx \mathbf{151.7 \text{ kN}}$$



6.7 Other Solutions for Bearing Capacity, Shape, and Depth Factors

BEARING CAPACITY FACTOR, $N\gamma$

The bearing capacity factor, N_γ, given in Eq. (6.31) will be used in this text. There are, however, several other expressions for N_γ that can be found in the literature. Some of those are given in Table 6.4.

The variations of N_γ with soil friction angle ϕ' for these relationships are given in Table 6.5.

TABLE 6.4 N_γ Relationships

Investigator	Relationship
Meyerhof (1963)	$N_\gamma = (N_q - 1)\tan 1.4\phi'$
Hansen (1970)	$N_\gamma = 1.5(N_q - 1)\tan \phi'$
Biarez (1961)	$N_\gamma = 1.8(N_q - 1)\tan \phi'$
Booker (1969)	$N_\gamma = 0.1045e^{9.6\phi'}$ (ϕ' is in radians)
Michalowski (1997)	$N_\gamma = e^{(0.66+5.1\tan\phi')}\tan\phi'$
Hjiaj et al. (2005)	$N_\gamma = e^{(1/6)(\pi+3\pi^2\tan\phi')} \times (\tan\phi')^{2\pi/5}$
Martin (2005)	$N_\gamma = (N_q - 1)\tan 1.32\phi'$

Note: N_q is given by Eq. (6.29)

TABLE 6.5 Comparison of N_γ Values Provided by Various Investigators

Soil friction angle, ϕ' (deg)	Meyerhof (1963)	Hansen (1970)	Biarez (1961)	Booker (1969)	Michalowski (1997)	Hjiaj et al. (2005)	Martin (2005)
0	0.00	0	0.00	0.10	0.00	0.00	0.00
1	0.00	0.00	0.00	0.12	0.04	0.01	0.00
2	0.01	0.01	0.01	0.15	0.08	0.03	0.01
3	0.02	0.02	0.03	0.17	0.13	0.05	0.02
4	0.04	0.05	0.05	0.20	0.19	0.08	0.04
5	0.07	0.07	0.09	0.24	0.26	0.12	0.07
6	0.11	0.11	0.14	0.29	0.35	0.17	0.10
7	0.15	0.16	0.19	0.34	0.44	0.22	0.14
8	0.21	0.22	0.27	0.40	0.56	0.29	0.20
9	0.28	0.30	0.36	0.47	0.69	0.36	0.26
10	0.37	0.39	0.47	0.56	0.84	0.46	0.35
11	0.47	0.50	0.60	0.66	1.01	0.56	0.44
12	0.60	0.63	0.76	0.78	1.22	0.69	0.56
13	0.75	0.79	0.94	0.92	1.45	0.84	0.70
14	0.92	0.97	1.16	1.09	1.72	1.01	0.87
15	1.13	1.18	1.42	1.29	2.04	1.21	1.06
16	1.38	1.44	1.72	1.53	2.40	1.45	1.29

(continued)

TABLE 6.5 Comparison of N_γ Values Provided by Various Investigators (*Continued*)

Soil friction angle, ϕ' (deg)	Meyerhof (1963)	Hansen (1970)	Biarez (1961)	Booker (1969)	Michalowski (1997)	Hjiaj et al. (2005)	Martin (2005)
17	1.67	1.73	2.08	1.81	2.82	1.72	1.56
18	2.01	2.08	2.49	2.14	3.30	2.05	1.88
19	2.41	2.48	2.98	2.52	3.86	2.42	2.25
20	2.88	2.95	3.54	2.99	4.51	2.86	2.69
21	3.43	3.50	4.20	3.53	5.27	3.38	3.20
22	4.07	4.14	4.97	4.17	6.14	3.98	3.80
23	4.84	4.89	5.87	4.94	7.17	4.69	4.50
24	5.73	5.76	6.91	5.84	8.36	5.51	5.32
25	6.78	6.77	8.13	6.90	9.75	6.48	6.29
26	8.02	7.96	9.55	8.16	11.37	7.63	7.43
27	9.49	9.35	11.22	9.65	13.28	8.97	8.77
28	11.22	10.97	13.16	11.41	15.52	10.57	10.35
29	13.27	12.87	15.45	13.50	18.15	12.45	12.22
30	15.71	15.11	18.13	15.96	21.27	14.68	14.44
31	18.62	17.74	21.29	18.87	24.95	17.34	17.07
32	22.09	20.85	25.02	22.31	29.33	20.51	20.20
33	26.25	24.52	29.42	26.39	34.55	24.30	23.94
34	31.25	28.86	34.64	31.20	40.79	28.86	28.41
35	37.28	34.03	40.84	36.90	48.28	34.34	33.79
36	44.58	40.19	48.23	43.63	57.31	40.98	40.28
37	53.47	47.55	57.06	51.59	68.22	49.03	48.13
38	64.32	56.38	67.65	61.00	81.49	58.85	57.67
39	77.64	67.01	80.41	72.14	97.69	70.87	69.32
40	94.09	79.85	95.82	85.30	117.57	85.67	83.60
41	114.49	95.44	114.53	100.87	142.09	103.97	101.21
42	139.96	114.44	137.33	119.28	172.51	126.75	123.04
43	171.97	137.71	165.25	141.04	210.49	155.25	150.26
44	212.47	166.34	199.61	166.78	258.21	191.13	184.40
45	264.13	201.78	242.13	197.21	318.57	236.63	227.53

SHAPE AND DEPTH FACTORS

The shape and depth factors given in Table 6.3 recommended, respectively, by DeBeer (1970) and Hansen (1970) will be used in this text for solving problems. Many geotechnical engineers presently use the shape and depth factors proposed by Meyerhof (1963). These are given in Table 6.6. More recently, Zhu and Michalowski (2005) evaluated the shape factors based on the elastoplastic model of soil and finite element analysis. They are

$$F_{cs} = 1 + (1.8 \tan^2 \phi' + 0.1)\left(\frac{B}{L}\right)^{0.5} \tag{6.34}$$

TABLE 6.6 Meyerhof's Shape and Depth Factors

Factor	Relationship
Shape	
For $\phi = 0$,	
F_{cs}	$1 + 0.2\ (B/L)$
$F_{qs} = F_{\gamma s}$	1
For $\phi' \geq 10°$,	
F_{cs}	$1 + 0.2\ (B/L) \tan^2(45 + \phi'/2)$
$F_{qs} = F_{\gamma s}$	$1 + 0.1\ (B/L) \tan^2(45 + \phi'/2)$
Depth	
For $\phi = 0$,	
F_{cd}	$1 + 0.2\ (D_f/B)$
$F_{qd} = F_{\gamma d}$	1
For $\phi \geq 10°$,	
F_{cd}	$1 + 0.2\ (D_f/B) \tan (45 + \phi'/2)$
$F_{qd} = F_{\gamma d}$	$1 + 0.1\ (D_f/B) \tan (45 + \phi'/2)$

$$F_{qs} = 1 + 1.9 \tan^2\phi' \left(\frac{B}{L}\right)^{0.5} \tag{6.35}$$

$$F_{\gamma s} = 1 + (0.6 \tan^2 \phi' - 0.25)\left(\frac{B}{L}\right) \quad (\text{for } \phi' \leq 30°) \tag{6.36}$$

and

$$F_{\gamma s} = 1 + (1.3 \tan^2\phi' - 0.5)\left(\frac{L}{B}\right)^{1.5} e^{-\left(\frac{L}{B}\right)} \quad (\text{for } \phi' > 30°) \tag{6.37}$$

Equations (6.34) through (6.37) have been derived based on sound theoretical background and may be used for bearing capacity calculation.

6.8 Case Studies on Ultimate Bearing Capacity

In this section, we will consider two field observations related to the ultimate bearing capacity of foundations on soft clay. The failure loads on the foundations in the field will be compared with those estimated from the theory presented in Section 6.6.

FOUNDATION FAILURE OF A CONCRETE SILO

An excellent case of bearing capacity failure of a 6-m (20-ft) diameter concrete silo was provided by Bozozuk (1972). The concrete tower silo was 21 m (70 ft) high and was constructed over soft clay on a ring foundation. Figure 6.13 shows the variation of the undrained shear strength (c_u) obtained from field vane shear tests at the site. The groundwater table was located at about 0.6 m (2 ft) below the ground surface.

On September 30, 1970, just after it was filled to capacity for the first time with corn silage, the concrete tower silo suddenly overturned due to bearing

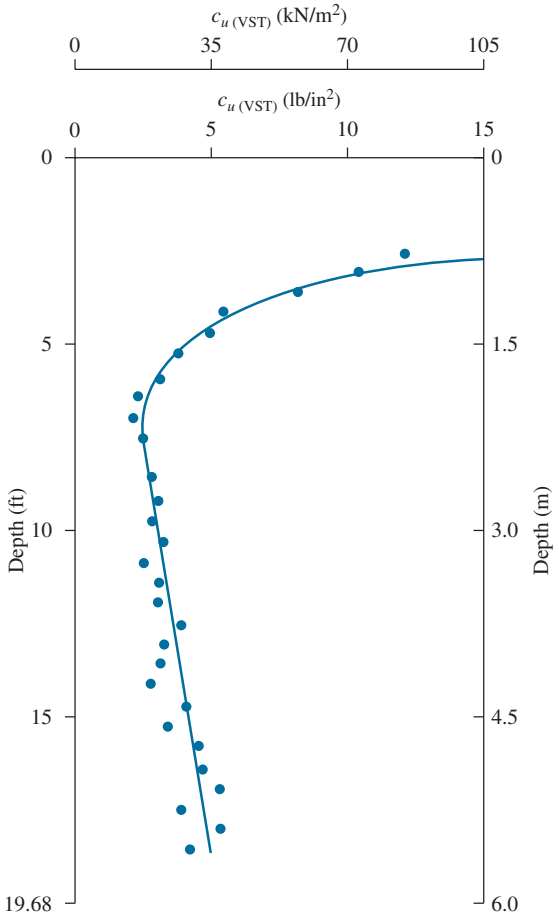


FIGURE 6.13 Variation of c_u with depth obtained from field vane shear test

capacity failure. Figure 6.14 shows the approximate profile of the failure surface in soil. The failure surface extended to about 7 m (23 ft) below the ground surface. Bozozuk (1972) provided the following average parameters for the soil in the failure zone and the foundation:

- Load per unit area on the foundation when failure occurred $\approx$ 160 kN/m^2 (23.2 1b/in^2)
- Average plasticity index of clay (PI) $\approx$ 36
- Average undrained shear strength (c_u) from 0.6 to 7 m depth obtained from field vane shear tests $\approx$ 27.1 kN/m^2 (3.9 1b/in^2)
- From Figure 6.14, $B \approx 7.2$ m (23.6 ft) and $D_f \approx 1.52$ m (5 ft)

We can now calculate the factor of safety against bearing capacity failure. From Eq. (6.28),

$$q_u = c' N_c F_{cs} F_{cd} F_{ci} + q N_c F_{qs} F_{qd} F_{qi} + \tfrac{1}{2} \gamma B N_\gamma F_{\gamma s} F_{\gamma d} F_{\gamma i}$$

For $\phi = 0$ condition and vertical loading, $c = c_u$, $N_c = 5.14$, $N_q = 1$, $N_\gamma = 0$, and $F_{ci} = F_{qi} = F_{\gamma i} = 0$. Also, from Table 6.3,

$$F_{cs} = 1 + \left(\frac{7.2}{7.2}\right)\left(\frac{1}{5.14}\right) = 1.195$$

$$F_{qs} = 1$$

$$F_{cd} = 1 + (0.4)\left(\frac{1.52}{7.2}\right) = 1.08$$

$$F_{qd} = 1$$

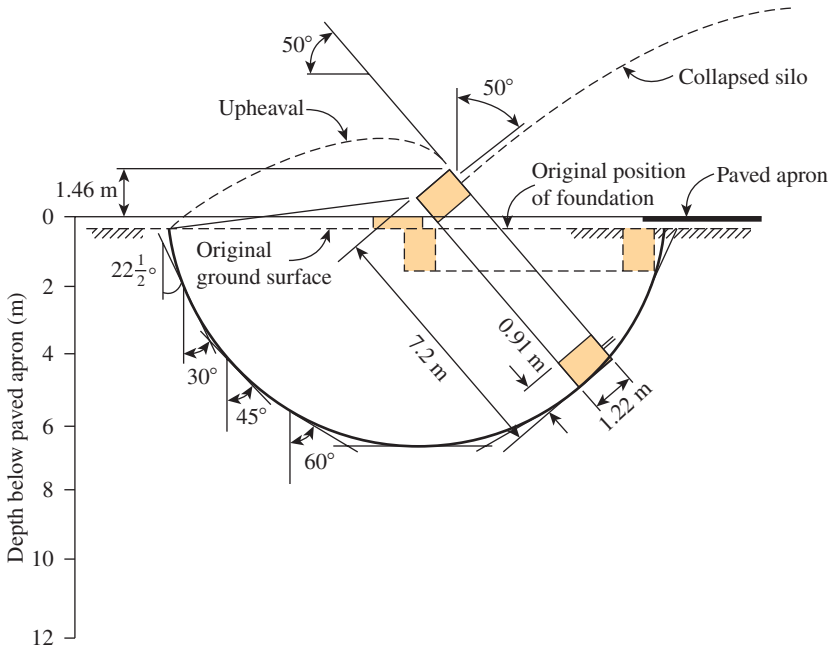


FIGURE 6.14 Approximate profile of silo failure (Based on Bozozuk, 1972)

Thus,

$$q_u = (c_u)(5.14)(1.195)(1.08)(1) + (\gamma)(1.52)$$

Assuming $\gamma \approx 18$ kN/m^3,

$$q_u = 6.63c_u + 27.36 \tag{6.38}$$

According to Eqs. (3.39) and (3.40a),

$$c_{u(\text{corrected})} = \lambda\, c_{u(\text{VST})}$$

$$\lambda = 1.7 - 0.54 \log [\text{PI}(\%)]$$

For this case, PI $\approx$ 36 and $c_{u(\text{VST})} = 27.1$ kN/m^2. So

$$c_{u(\text{corrected})} = \{1.7 - 0.54 \log [\text{PI}(\%)]\} c_{u(\text{VST})}$$

$$= (1.7 - 0.54 \log 36)(27.1) \approx 23.3 \text{ kN/m}^2$$

Substituting this value of c_u in Eq. (6.38),

$$q_u = (6.63)(23.3) + 27.36 = 181.8 \text{ kN/m}^2$$

So,

$$q_{u(\text{net})} \approx 154.5 \text{ kN/m}^2$$

The factor of safety against bearing capacity failure is

$$\text{FS} = \frac{q_{u(\text{net})}}{\text{applied load per unit area}} = \frac{154.5}{160} \approx 0.97$$

This factor of safety is too low and approximately equals one, for which the failure occurred.

LOAD TESTS ON SMALL FOUNDATIONS IN SOFT BANGKOK CLAY

Brand et al. (1972) reported load test results for five small square foundations in soft Bangkok clay in Rangsit, Thailand. The foundations were 0.6 m $\times$ 0.6 m,

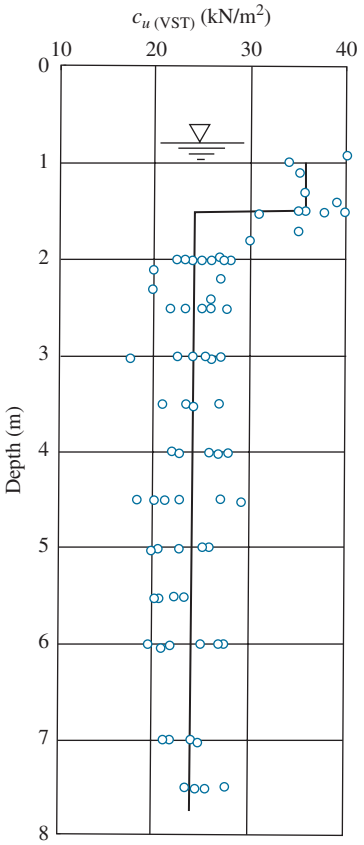


FIGURE 6.15 Variation of $c_{u(VST)}$ with depth for soft Bangkok clay

0.675 m × 0.675 m, 0.75 m × 0.75 m, 0.9 m × 0.9 m, and 1.05 m × 1.05 m. The depth of the foundations (D_f) was 1.5 m in all cases.

Figure 6.15 shows the vane shear test results for clay. Based on the variation of $c_{u(VST)}$ with depth, it can be approximated that $c_{u(VST)}$ is about 35 kN/m^2 for depths between zero to 1.5 m measured from the ground surface, and $c_{u(VST)}$ is approximately equal to 24 kN/m^2 for depths varying from 1.5 to 8 m. Other properties of the clay are

- Liquid limit = 80
- Plastic limit = 40
- Sensitivity ≈ 5

Figure 6.16 shows the load-settlement plots obtained from the bearing-capacity tests on all five foundations. The ultimate loads, Q_u, obtained from each test are shown in Figure 6.16 and given in Table 6.7. The ultimate load is defined as the point where the load-settlement plot becomes practically linear.

From Eq. (6.30),

$$q_u = c'N_cF_{cs}F_{cd}F_{ci} + qN_qF_{qs}F_{qd}F_{qi} + \frac{1}{2}\gamma BN_\gamma F_{\gamma s}F_{\gamma d}F_{\gamma i}$$

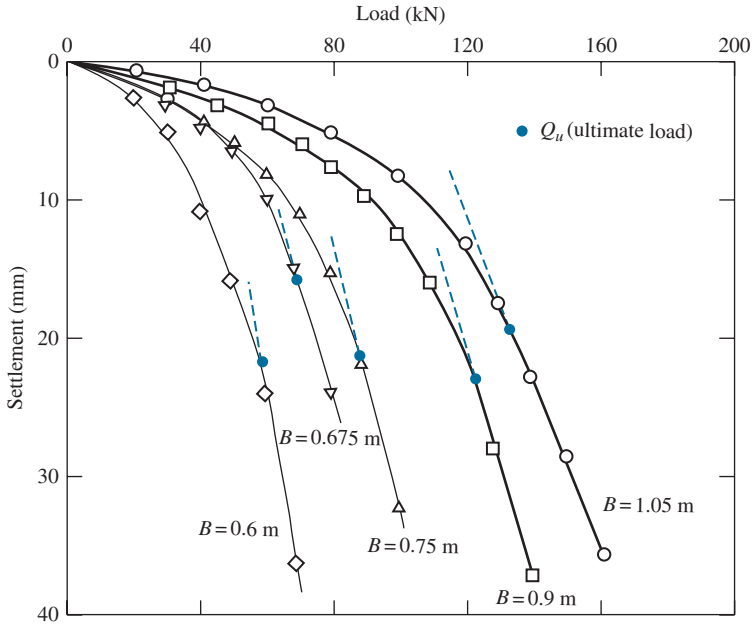


FIGURE 6.16 Load-settlement plots obtained from bearing capacity tests

TABLE 6.7 Comparison of Ultimate Bearing Capacity—Theory Versus Field Test Results

B (m) (1)	D_f (m) (2)	F_{cd} ‡ (3)	$q_{u(theory)}$ ‡‡ (kN/m^2) (4)	$Q_{u(field)}$ (kN) (5)	$q_{u(field)}$ ‡‡‡ (kN/m^2) (6)	$\frac{q_{u(field)} - q_{u(theory)}}{q_{u(field)}}$ (%) (7)
0.600	1.5	1.476	158.3	60	166.6	4.98
0.675	1.5	1.459	156.8	71	155.8	−0.64
0.750	1.5	1.443	155.4	90	160.6	2.87
0.900	1.5	1.412	152.6	124	153.0	0.27
1.050	1.5	1.384	150.16	140	127.0	−18.24

‡Eq. (6.39); ‡‡Eq. (6.41); ‡‡‡$Q_{u(field)}/B^2 = q_{u(field)}$

For undrained condition and vertical loading (that is, $\phi = 0$), from Tables 6.2 and 6.3,

- $F_{ci} = F_{qi} = F_{\gamma i} = 1$
- $c' = c_u$, $N_c = 5.14$, $N_q = 1$, and $N_\gamma = 0$
- $F_{cs} = 1 + \left(\frac{B}{L}\right)\left(\frac{N_q}{N_c}\right) = 1 + (1)\left(\frac{1}{5.14}\right) = 1.195$
- $F_{qs} = 1$
- $F_{qd} = 1$
- $F_{cd} = 1 + 0.4 \tan^{-1}\left(\frac{D_f}{B}\right) = 1 + 0.4 \tan^{-1}\left(\frac{1.5}{B}\right)$ (6.39)

(*Note:* $D_f/B > 1$ in all cases). Thus,

$$q_u = (5.14)(c_u)(1.195)F_{cd} + q \tag{6.40}$$

The values of $c_{u(\text{VST})}$ need to be corrected for use in Eq. (6.40). From Eq. (3.39),

$$c_u = \lambda c_{u(\text{VST})}$$

From Eq. (3.40b),

$$\lambda = 1.18e^{-0.08(\text{PI})} + 0.57 = 1.18e^{-0.08(80\,-\,40)} + 0.57 = 0.62$$

From Eq. (3.40c),

$$\lambda = 7.01e^{-0.08(\text{LL})} + 0.57 = 7.01e^{-0.08(80)} + 0.57 = 0.58$$

So the average value of $\lambda \approx 0.6$. Hence,

$$c_u = \lambda c_{u(\text{VST})} = (0.6)(24) = 14.4 \text{ kN/m}^2$$

Let us assume $\gamma = 18.5$ kN/m^2. So

$$q = \gamma D_f = (18.5)(1.5) = 27.75 \text{ kN/m}^2$$

Substituting $c_u = 14.4$ kN/m^2 and $q = 27.75$ kN/m^2 into Eq. (6.40), we obtain

$$q_u(\text{kN/m}^2) = 88.4F_{cd} + 27.75 \tag{6.41}$$

The values of q_u calculated using Eq. (6.41) are given in column 4 of Table 6.7. Also, the q_u determined from the field tests are given in column 6. The theoretical and field values of q_u compare very well. The important lessons learned from this study are

1. The ultimate bearing capacity is a function of c_u. If Eq. (3.40a) would have been used to correct the undrained shear strength, the theoretical values of q_u would have varied between 200 kN/m^2 and 210 kN/m^2. These values are about 25 to 55% more than those obtained from the field and are on the unsafe side.
2. It is important to recognize that empirical correlations like those given in Eqs. (3.40a), (3.40b), and (3.40c) are sometimes site specific. Thus, proper engineering judgment and any record of past studies would be helpful in the evaluation of bearing capacity.

6.9 Effect of Soil Compressibility

In Section 6.2, we have discussed the mode of bearing-capacity failure such as general shear failure, local shear failure, and punching shear failure. The change of failure mode is due to soil compressibility, to account for which Vesic (1973) proposed the following modification of Eq. (6.28):

$$q_u = c'N_cF_{cs}F_{cd}F_{cc} + qN_qF_{qs}F_{qd}F_{qc} + \tfrac{1}{2}\gamma BN_\gamma F_{\gamma s}F_{\gamma d}F_{\gamma c} \tag{6.42}$$

In this equation, F_{cc}, F_{qc}, and $F_{\gamma c}$ are soil compressibility factors.

The soil compressibility factors were derived by Vesic (1973) by analogy to the expansion of cavities. According to that theory, in order to calculate F_{cc}, F_{qc}, and $F_{\gamma c}$, the following steps should be taken:

Step 1. Calculate the *rigidity index*, I_r, of the soil at a depth approximately $B/2$ below the bottom of the foundation, or

$$I_r = \frac{G_s}{c' + q' \tan \phi'} \tag{6.43}$$

where

G_s = shear modulus of the soil

q' = effective overburden pressure at a depth of $D_f + B/2$

Step 2. The critical rigidity index, $I_{r(\text{cr})}$, can be expressed as

$$I_{r(\text{cr})} = \frac{1}{2}\left\{\exp\left[\left(3.30 - 0.45\frac{B}{L}\right)\cot\left(45 - \frac{\phi'}{2}\right)\right]\right\} \tag{6.44}$$

The variations of $I_{r(\text{cr})}$ with B/L are given in Table 6.8.

Step 3. If $I_r \geq I_{r(\text{cr})}$, then

$$F_{cc} = F_{qc} = F_{\gamma c} = 1$$

However, if $I_r < I_{r(\text{cr})}$, then

$$F_{\gamma c} = F_{qc} = \exp\left\{\left(-4.4 + 0.6\frac{B}{L}\right)\tan \phi' + \left[\frac{(3.07 \sin \phi')(\log 2I_r)}{1 + \sin \phi'}\right]\right\} \tag{6.45}$$

Figure 6.17 shows the variation of $F_{\gamma c} = F_{qc}$ [see Eq. (6.45)] with ϕ' and I_r. For $\phi = 0$,

$$F_{cc} = 0.32 + 0.12\frac{B}{L} + 0.60 \log I_r \tag{6.46}$$

TABLE 6.8 Variation of $I_{r(\text{cr})}$ with ϕ' and B/L

ϕ' (deg)	$I_{r(\text{cr})}$					
	$B/L = 0$	$B/L = 0.2$	$B/L = 0.4$	$B/L = 0.6$	$B/L = 0.8$	$B/L = 1.0$
0	13.56	12.39	11.32	10.35	9.46	8.64
5	18.30	16.59	15.04	13.63	12.36	11.20
10	25.53	22.93	20.60	18.50	16.62	14.93
15	36.85	32.77	29.14	25.92	23.05	20.49
20	55.66	48.95	43.04	37.85	33.29	29.27
25	88.93	77.21	67.04	58.20	50.53	43.88
30	151.78	129.88	111.13	95.09	81.36	69.62
35	283.20	238.24	200.41	168.59	141.82	119.31
40	593.09	488.97	403.13	332.35	274.01	225.90
45	1440.94	1159.56	933.19	750.90	604.26	486.26

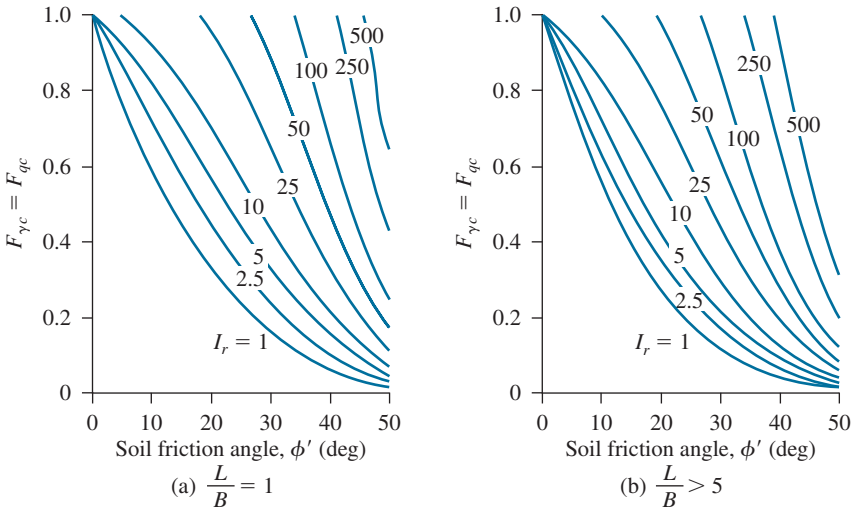


FIGURE 6.17 Variation of $F_{\gamma c} = F_{qc}$ with I_r and ϕ'

For $\phi' > 0$,

$$F_{cc} = F_{qc} - \frac{1 - F_{qc}}{N_q \tan \phi'} \tag{6.47}$$

EXAMPLE 6.6

For a shallow foundation, $B = 0.6$ m, $L = 1.2$ m, and $D_f = 0.6$ m. The known soil characteristics are

Soil:

$$\phi' = 25^\circ$$
$$c' = 48 \text{ kN/m}^2$$
$$\gamma = 18 \text{ kN/m}^3$$

Modulus of elasticity, $E_s = 620 \text{ kN/m}^2$

Poisson's ratio, $\mu_s = 0.3$

Calculate the ultimate bearing capacity.

SOLUTION

From Eq. (6.43),

$$I_r = \frac{G_s}{c' + q' \tan \phi'}$$

However,

$$G_s = \frac{E_s}{2(1 + \mu_s)}$$

So

$$I_r = \frac{E_s}{2(1 + \mu_s)[c' + q' \tan \phi']}$$

Now,

$$q' = \gamma\left(D_f + \frac{B}{2}\right) = 18\left(0.6 + \frac{0.6}{2}\right) = 16.2 \text{ kN/m}^2$$

Thus,

$$I_r = \frac{620}{2(1 + 0.3)[48 + 16.2 \tan 25]} = 4.29$$

From Eq. (6.44),

$$I_{r(\text{cr})} = \frac{1}{2}\left\{\exp\left[\left(3.3 - 0.45\frac{B}{L}\right)\cot\left(45 - \frac{\phi'}{2}\right)\right]\right\}$$

$$= \frac{1}{2}\left\{\exp\left[\left(3.3 - 0.45\frac{0.6}{1.2}\right)\cot\left(45 - \frac{25}{2}\right)\right]\right\} = 62.41$$

Since $I_{r(\text{cr})} > I_r$, we use Eqs. (6.45) and (6.47) to obtain

$$F_{\gamma c} = F_{qc} = \exp\left\{\left(-4.4 + 0.6\frac{B}{L}\right)\tan\phi' + \left[\frac{(3.07\sin\phi')\log(2I_r)}{1 + \sin\phi'}\right]\right\}$$

$$= \exp\left\{\left(-4.4 + 0.6\frac{0.6}{1.2}\right)\tan 25 + \left[\frac{(3.07\sin 25)\log(2 \times 4.29)}{1 + \sin 25}\right]\right\} = 0.347$$

and

$$F_{cc} = F_{qc} - \frac{1 - F_{qc}}{N_c \tan\phi'}$$

For $\phi' = 25°$, $N_c = 20.72$ (see Table 6.2); therefore,

$$F_{cc} = 0.347 - \frac{1 - 0.347}{20.72 \tan 25} = 0.279$$

Now, from Eq. (6.42),

$$q_u = c'N_cF_{cs}F_{cd}F_{cc} + qN_qF_{qs}F_{qd}F_{qc} + \tfrac{1}{2}\gamma BN_\gamma F_{\gamma s}F_{\gamma d}F_{\gamma c}$$

From Table 6.2, for $\phi' = 25°$, $N_c = 20.72$, $N_q = 10.66$, and $N_\gamma = 10.88$. Consequently,

$$F_{cs} = 1 + \left(\frac{N_q}{N_c}\right)\left(\frac{B}{L}\right) = 1 + \left(\frac{10.66}{20.72}\right)\left(\frac{0.6}{1.2}\right) = 1.257$$

$$F_{qs} = 1 + \frac{B}{L}\tan\phi' = 1 + \frac{0.6}{1.2}\tan 25 = 1.233$$

$$F_{\gamma s} = 1 - 0.4\left(\frac{B}{L}\right) = 1 - 0.4\,\frac{0.6}{1.2} = 0.8$$

$$F_{qd} = 1 + 2\tan\phi'(1 - \sin\phi')^2\left(\frac{D_f}{B}\right)$$

$$= 1 + 2\tan 25(1 - \sin 25)^2\left(\frac{0.6}{0.6}\right) = 1.311$$

$$F_{cd} = F_{qd} - \frac{1 - F_{qd}}{N_c\tan\phi'} = 1.311 - \frac{1 - 1.311}{20.72\tan 25}$$

$$= 1.343$$

and

$$F_{\gamma d} = 1$$

Thus,

$$q_u = (48)(20.72)(1.257)(1.343)(0.279) + (0.6 \times 18)(10.66)(1.233)(1.311)$$
$$(0.347) + \left(\tfrac{1}{2}\right)(18)(0.6)(10.88)(0.8)(1)(0.347) = \mathbf{549.32\ kN/m^2}$$

6.10 Eccentrically Loaded Foundations

In several instances, as with the base of a retaining wall, foundations are subjected to moments in addition to the vertical load, as shown in Figure 6.18a. In such cases, the distribution of pressure by the foundation on the soil is not uniform. The nominal distribution of pressure is

$$q_{\max} = \frac{Q}{BL} + \frac{6M}{B^2L} \tag{6.48}$$

and

$$q_{\min} = \frac{Q}{BL} - \frac{6M}{B^2L} \tag{6.49}$$

where

Q = total vertical load

M = moment on the foundation

Figure 6.18b shows a force system equivalent to that shown in Figure 6.18a. The distance

$$e = \frac{M}{Q} \tag{6.50}$$

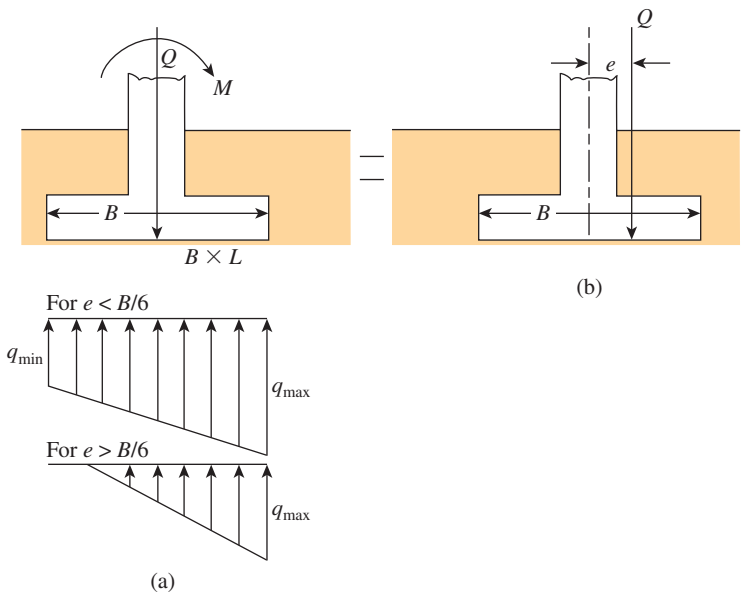


FIGURE 6.18 Eccentrically loaded foundations

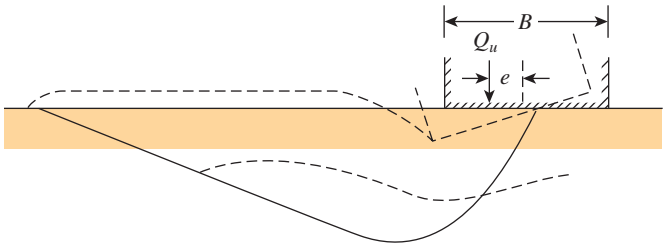


FIGURE 6.19 Nature of failure surface in soil supporting a strip foundation subjected to eccentric loading (*Note:* $D_f = 0$; Q_u is ultimate load per unit length of foundation)

is the eccentricity. Substituting Eq. (6.50) into Eqs. (6.48) and (6.49) gives

$$q_{\max} = \frac{Q}{BL}\left(1 + \frac{6e}{B}\right) \tag{6.51}$$

and

$$q_{\min} = \frac{Q}{BL}\left(1 - \frac{6e}{B}\right) \tag{6.52}$$

Note that, in these equations, when the eccentricity e becomes $B/6$, $q_{\min}$ is zero. For $e > B/6$, $q_{\min}$ will be negative, which means that tension will develop. Because soil cannot take any tension, there will then be a separation between the foundation and the soil underlying it. The nature of the pressure distribution on the soil will be as shown in Figure 6.18a. The value of $q_{\max}$ is then (Tomlinson, 1978)

$$q_{\max} = \frac{4Q}{3L(B - 2e)} \tag{6.53}$$

The exact distribution of pressure is difficult to estimate.

Figure 6.19 shows the nature of failure surface in soil for a surface strip foundation subjected to an eccentric load. The factor of safety for such type of loading against bearing capacity failure can be evaluated as

$$\text{FS} = \frac{Q_u}{Q} \tag{6.54}$$

where Q_u = ultimate load-carrying capacity.

The following sections describe several theories for determining Q_u.

6.11 Ultimate Bearing Capacity Under Eccentric Loading—One-Way Eccentricity

EFFECTIVE AREA METHOD (MEYERHOFF, 1953)

In 1953, Meyerhof proposed a theory that is generally referred to as the *effective area method*.

The following is a step-by-step procedure for determining the ultimate load that the soil can support and the factor of safety against bearing capacity failure:

Step 1. Determine the effective dimensions of the foundation (Figure 6.20a):

$$B' = \text{effective width} = B - 2e$$
$$L' = \text{effective length} = L$$

Note that if the eccentricity were in the direction of the length of the foundation, the value of L' would be equal to $L - 2e$. The value of B' would equal B. The smaller of the two dimensions (i.e., L' and B') is the effective width of the foundation.

Step 2. Use Eq. (6.28) for the ultimate bearing capacity:

$$q'_u = c'N_cF_{cs}F_{cd}F_{ci} + qN_qF_{qs}F_{qd}F_{qi} + \tfrac{1}{2}\gamma B'N_\gamma F_{\gamma s}F_{\gamma d}F_{\gamma i} \qquad (6.55)$$

To evaluate F_{cs}, F_{qs}, and $F_{\gamma s}$, use the relationships given in Table 6.3 with *effective length* and *effective width* dimensions instead of L and B, respectively. To determine F_{cd}, F_{qd}, and $F_{\gamma d}$, use the relationships given in Table 6.3. However, do not replace B with B'.

Step 3. The total ultimate load that the foundation can sustain is

$$Q_u = q'_u\overbrace{(B')(L')}^{A'} \qquad (6.56)$$

where $A' =$ effective area.

Step 4. The factor of safety against bearing capacity failure is

$$\text{FS} = \frac{Q_u}{Q}$$

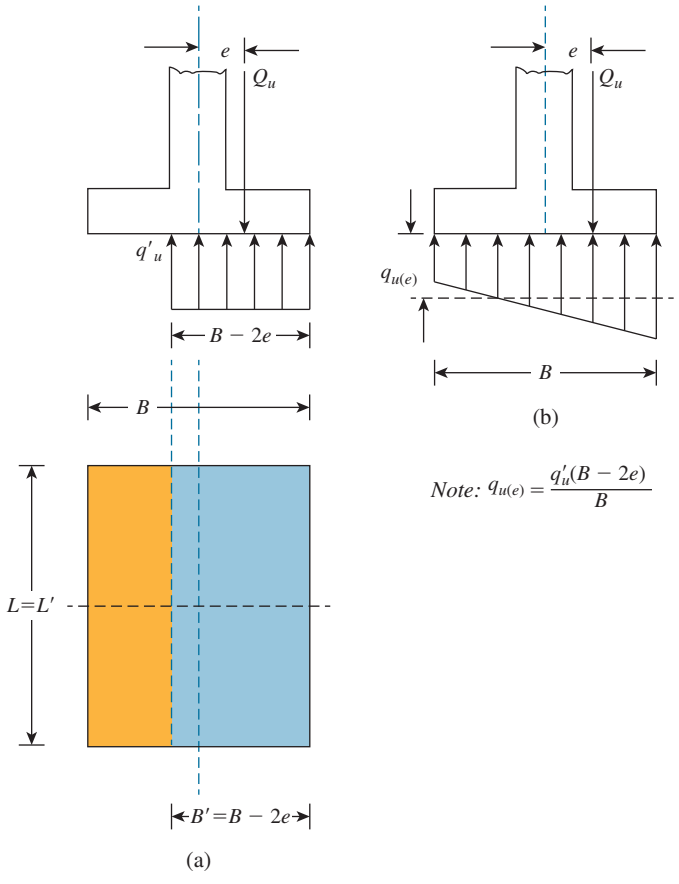


FIGURE 6.20 Definition of q'_u and $q_{u(e)}$

It is important to note that q'_u is the ultimate bearing capacity of a foundation of width $B' = B - 2e$ with a centric load (Figure 6.20a). However, the actual distribution of soil reaction at ultimate load will be of the type shown in Figure 6.20b. In Figure 6.20b, $q_{u(e)}$ is the average load per unit area of the foundation. Thus,

$$q_{u(e)} = \frac{q'_u(B - 2e)}{B} \tag{6.57}$$

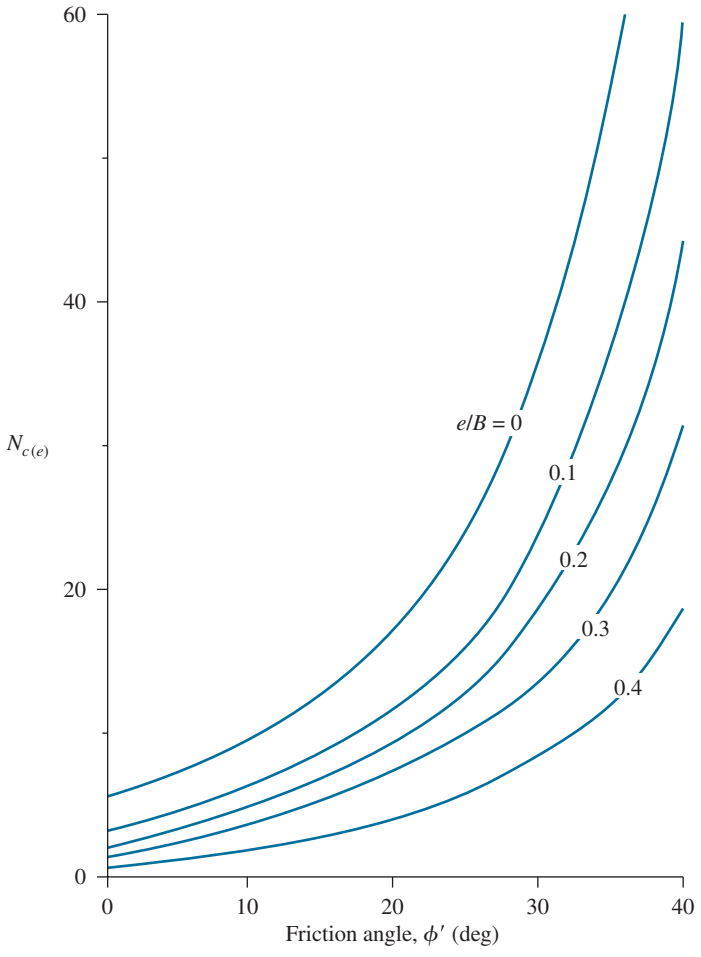
PRAKASH AND SARAN THEORY

Prakash and Saran (1971) analyzed the problem of ultimate bearing capacity of eccentrically and vertically loaded continuous (strip) foundations by using the one-sided failure surface in soil, as shown in Figure 6.19. According to this theory, the ultimate load *per unit length of a continuous foundation* can be estimated as

$$Q_u = q_{u(e)}B = B\left[c'N_{c(e)} + qN_{q(e)} + \frac{1}{2}\gamma BN_{\gamma(e)}\right] \tag{6.58}$$

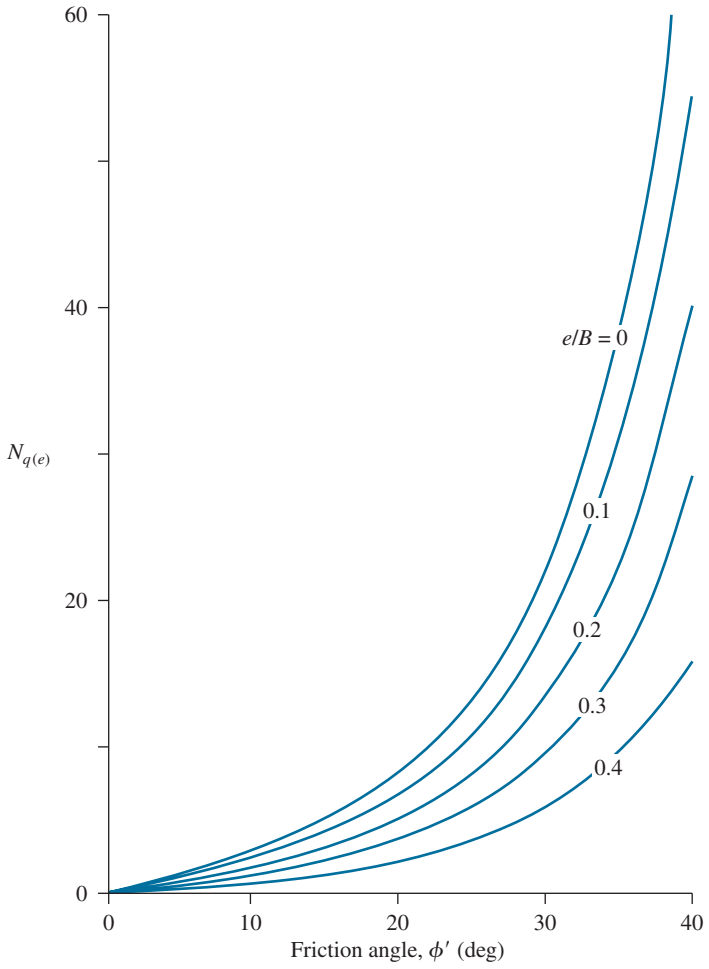
where $N_{c(e)}$, $N_{q(e)}$, $N_{\gamma(e)}$ = bearing capacity factors under eccentric loading.

The variations of $N_{c(e)}$, $N_{q(e)}$, and $N_{\gamma(e)}$ with soil friction angle ϕ' are given in Figures 6.21, 6.22, and 6.23. For rectangular foundations, the ultimate load can be given as



$\phi' = 40°$	
e/B	$N_{c(e)}$
0	94.83
0.1	66.60
0.2	54.45
0.3	36.3
0.4	18.15

FIGURE 6.21 Variation of $N_{c(e)}$ with ϕ'



$\phi' = 40°$	
e/B	$N_{q(e)}$
0	81.27
0.1	56.09
0.2	45.18
0.3	30.18
0.4	15.06

FIGURE 6.22 Variation of $N_{q(e)}$ with ϕ'

$$Q_u = BL\left[c'N_{c(e)}F_{cs(e)} + qN_{q(e)}F_{qs(e)} + \frac{1}{2}\gamma BN_{\gamma(e)}F_{\gamma s(e)}\right] \tag{6.59}$$

where $F_{cs(e)}$, $F_{qs(e)}$, and $F_{\gamma s(e)}$ = shape factors.

Prakash and Saran (1971) also recommended the following for the shape factors:

$$F_{cs(e)} = 1.2 - 0.025\frac{L}{B} \text{ (with a minimum of 1.0)} \tag{6.60}$$

$$F_{qs(e)} = 1 \tag{6.61}$$

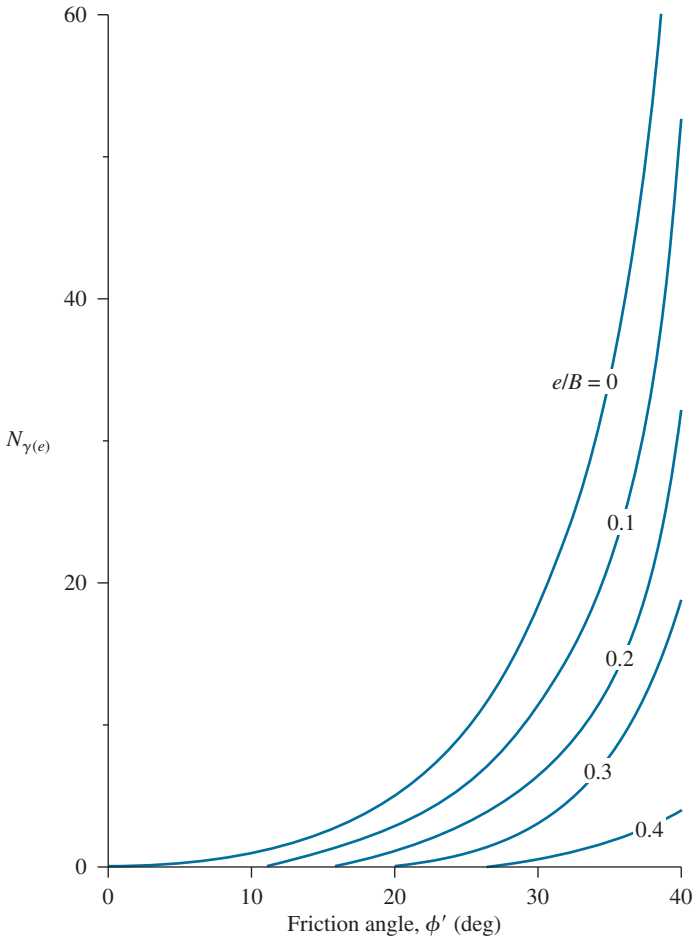
and

$$F_{\gamma s(e)} = 1.0 + \left(\frac{2e}{B} - 0.68\right)\frac{B}{L} + \left[0.43 - \left(\frac{3}{2}\right)\left(\frac{e}{B}\right)\right]\left(\frac{B}{L}\right)^2 \tag{6.62}$$

REDUCTION FACTOR METHOD (FOR GRANULAR SOIL)

Purkayastha and Char (1977) carried out stability analysis of eccentrically loaded *continuous foundations supported by a layer of sand* using the method of slices. Based on that analysis, they proposed

$$R_k = 1 - \frac{q_{u(e)}}{q_{u(\text{centric})}} \tag{6.63}$$



$\phi' = 40°$	
e/B	$N_{\gamma(e)}$
0	115.80
0.1	71.80
0.2	41.60
0.3	18.50
0.4	4.62

FIGURE 6.23 Variation of $N_{\gamma(e)}$ with ϕ'

where

R_k = reduction factor

$q_{u(e)}$ = average ultimate bearing capacity of eccentrically loaded continuous foundations (See Figure 6.20.)

q_u = ultimate bearing capacity of centrally loaded continuous foundations

The magnitude of R_k can be expressed as

$$R_k = a\left(\frac{e}{B}\right)^k \tag{6.64}$$

where a and k are functions of the embedment ratio D_f/B (Table 6.9).

TABLE 6.9 Variations of a and k [Eq. (6.64)]

D_f/B	a	k
0.00	1.862	0.73
0.25	1.811	0.785
0.50	1.754	0.80
1.00	1.820	0.888

Hence, combining Eqs. (6.63) and (6.64),

$$q_{u(e)} = q_u(1 - R_k) = q_u\left[1 - a\left(\frac{e}{B}\right)^k\right] \tag{6.65}$$

where

$$q_u = qN_qF_{qd} + \frac{1}{2}\gamma BN_\gamma F_{\gamma d} \tag{6.66}$$

The relationships for F_{qd} and $F_{\gamma d}$ are given in Table 6.3.

Based on several laboratory model tests, Patra et al. (2012a) have concluded that

$$q_{u(e)} \approx q_u\left(1 - \frac{2e}{B}\right) \tag{6.67}$$

The ultimate load *per unit length* of the foundation can then be given as

$$Q_u = Bq_{u(e)} \tag{6.68}$$

EXAMPLE 6.7

A continuous foundation is shown in Figure 6.24. If the load eccentricity is 0.2 m, determine the ultimate load, Q_u, per unit length of the foundation. Use Meyerhof's effective area method.

SOLUTION

For $c' = 0$, Eq. (6.55) gives

$$q'_u = qN_qF_{qs}F_{qd}F_{qi} + \frac{1}{2}\gamma' B' N_\gamma F_{\gamma s}F_{\gamma d}F_{\gamma i}$$

where $q = (16.5)\,(1.5) = 24.75$ kN/m^2.

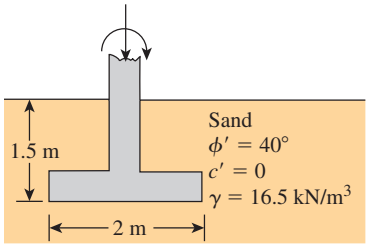


FIGURE 6.24 A continuous foundation with load eccentricity

For $\phi' = 40°$, from Table 6.2, $N_q = 64.2$ and $N_\gamma = 109.41$. Also,

$$B' = 2 - (2)(0.2) = 1.6 \text{ m}$$

Because the foundation in question is a continuous foundation, B'/L' is zero. Hence, $F_{qs} = 1$, $F_{\gamma s} = 1$. From Table 6.3,

$$F_{qi} = F_{\gamma i} = 1$$

$$F_{qd} = 1 + 2\tan\phi'(1 - \sin\phi')^2\frac{D_f}{B} = 1 + 0.214\left(\frac{1.5}{2}\right) = 1.16$$

$$F_{\gamma d} = 1$$

and

$$q'_u = (24.75)(64.2)(1)(1.16)(1) + \left(\frac{1}{2}\right)(16.5)(1.6)(109.41)(1)(1)(1) = 3287.39 \text{ kN/m}^2$$

Consequently,

$$Q_u = (B')(1)(q'_u) = (1.6)(1)(3287.39) \approx \mathbf{5260\ kN}$$

■

EXAMPLE 6.8

Solve Example 6.7 using Eq. (6.58).

SOLUTION

Since $c' = 0$,

$$Q_u = B\left[qN_{q(e)} + \frac{1}{2}\gamma BN_{\gamma(e)}\right]$$

$$\frac{e}{B} = \frac{0.2}{2} = 0.1$$

For $\phi' = 40°$ and $e/B = 0.1$, Figures 6.22 and 6.23 give $N_{q(e)} \approx 56.09$ and $N_{\gamma(e)} \approx 71.8$. Hence,

$$Q_u = 2[(24.75)(56.09) + (\tfrac{1}{2})(16.5)(2)(71.8)] = \mathbf{5146\ kN}$$

■

EXAMPLE 6.9

Solve Example 6.7 using Eq. (6.67).

SOLUTION

With $c' = 0$,

$$q_{u(e)} = qN_qF_{qd} + \frac{1}{2}\gamma BN_\gamma F_{\gamma d}$$

For $\phi' = 40°$, $N_q = 64.2$ and $N_\gamma = 109.41$ (see Table 6.2). Hence,

$$F_{qd} = 1.16 \text{ and } F_{\gamma d} = 1 \text{ (see Example 6.7)}$$

$$q_u = (24.75)(64.2)(1.16) + \frac{1}{2}(16.5)(2)(109.41)(1)$$

$$= 1843.18 + 1805.27 = 3648.45\ \text{kN/m}^2$$

From Eq. (6.67),

$$q_{u(e)} = q_u\left(1 - \frac{2e}{B}\right)$$

$$= 3648.45\left[1 - 2\left(\frac{0.2}{2}\right)\right]$$

$$= 2918.76\ \text{kN/m}^2$$

$$Q_u = Bq_{u(e)} = (2)(2918.76) \approx \mathbf{5838\ kN}$$

■

6.12 Bearing Capacity—Two-Way Eccentricity

Consider a situation in which a foundation is subjected to a vertical ultimate load Q_{ult} and a moment M, as shown in Figures 6.25a and b. For this case, the components of the moment M about the x- and y-axes can be determined as M_x and M_y, respectively. (See Figure 6.25c.) This condition is equivalent to a load Q_u placed eccentrically on the foundation with $x = e_B$ and $y = e_L$ (Figure 6.25d). Note that

$$e_B = \frac{M_y}{Q_u} \tag{6.69}$$

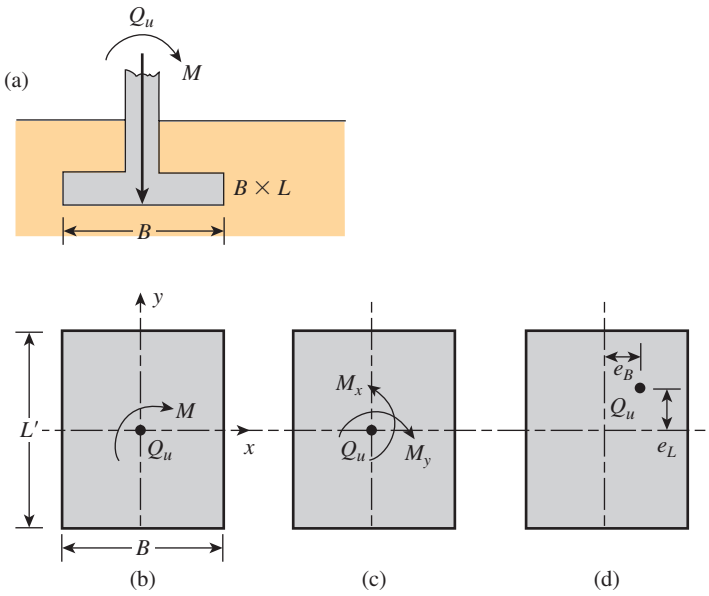


FIGURE 6.25 Analysis of foundation with two-way eccentricity

and

$$e_L = \frac{M_x}{Q_u} \tag{6.70}$$

If Q_u is needed, it can be obtained from Eq. (6.56); that is,

$$Q_u = q'_u A'$$

where, from Eq. (6.55),

$$q'_u = c' N_c F_{cs} F_{cd} F_{ci} + q N_q F_{qs} F_{qd} F_{qi} + \tfrac{1}{2} \gamma B' N_\gamma F_{\gamma s} F_{\gamma d} F_{\gamma i}$$

and

$$A' = \text{effective area} = B' L'$$

As before, to evaluate F_{cs}, F_{qs}, and $F_{\gamma s}$ (Table 6.3), we use the effective length L' and effective width B' instead of L and B, respectively. To calculate F_{cd}, F_{qd}, and $F_{\gamma d}$, we do not replace B with B'. In determining the effective area A', effective width B', and effective length L', five possible cases may arise (Highter and Anders, 1985).

Case I. $e_L/L \geq \frac{1}{6}$ and $e_B/B \geq \frac{1}{6}$. The effective area for this condition is shown in Figure 6.26, or

$$A' = \tfrac{1}{2} B_1 L_1 \tag{6.71}$$

where

$$B_1 = B\left(1.5 - \frac{3e_B}{B}\right) \tag{6.72}$$

and

$$L_1 = L\left(1.5 - \frac{3e_L}{L}\right) \tag{6.73}$$

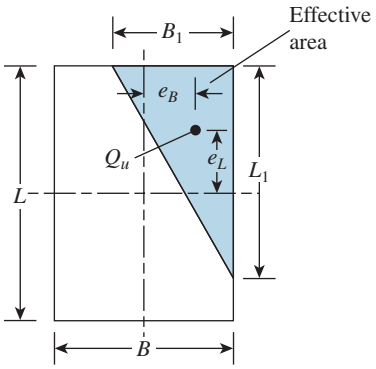


FIGURE 6.26 Effective area for the case of $e_L/L \geq \frac{1}{6}$ and $e_B/B \geq \frac{1}{6}$

The effective length L' is the larger of the two dimensions B_1 and L_1. So the effective width is

$$B' = \frac{A'}{L'} \tag{6.74}$$

Case II. $\frac{1}{6} < e_L/L < 0.5$ and $e_B/B < \frac{1}{6}$. The effective area for this case, shown in Figure 6.27a, is

$$A' = \tfrac{1}{2}(L_1 + L_2)B \tag{6.75}$$

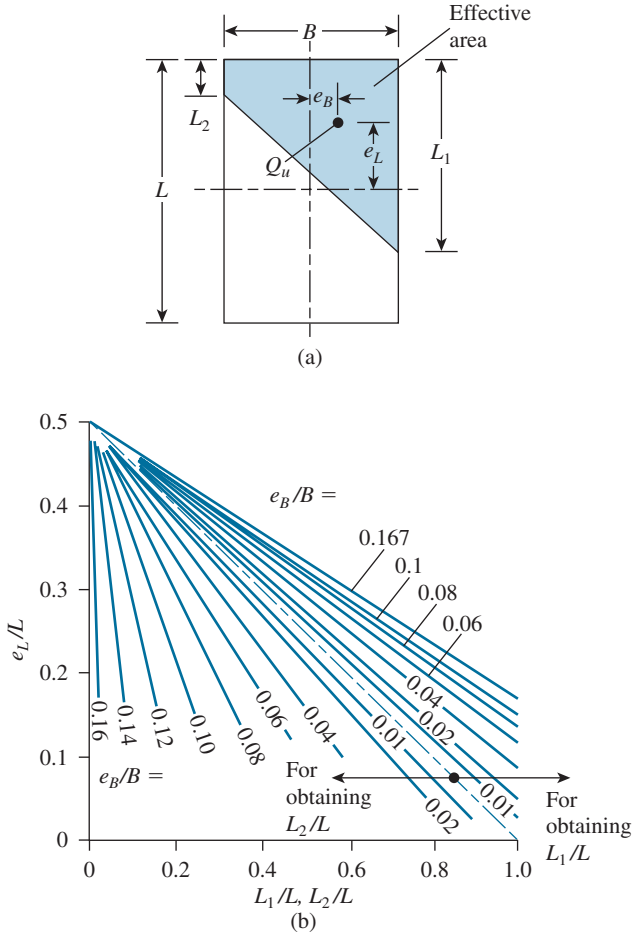


FIGURE 6.27 Effective area for case II where $\frac{1}{6} < e_L/L < 0.5$ and $e_B/B < \frac{1}{6}$ (Based on Highter, W. H. and Anders, J. C. (1985). "Dimensioning Footings Subjected to Eccentric Loads," *Journal of Geotechnical Engineering*, American Society of Civil Engineers, Vol. 111, No. GT5, pp. 659–665)

The magnitudes of L_1 and L_2 can be determined from Figure 6.27b. The effective width is

$$B' = \frac{A'}{L_1 \text{ or } L_2 \quad \text{(whichever is larger)}} \tag{6.76}$$

The effective length is

$$L' = L_1 \text{ or } L_2 \quad \text{(whichever is larger)} \tag{6.77}$$

Case III. $e_L/L < \frac{1}{6}$ and $\frac{1}{6} < e_B/B < 0.5$. The effective area, shown in Figure 6.28a, is

$$A' = \tfrac{1}{2}(B_1 + B_2)L \tag{6.78}$$

The effective width is

$$B' = \frac{A'}{L} \tag{6.79}$$

The effective length is

$$L' = L \tag{6.80}$$

The magnitudes of B_1 and B_2 can be determined from Figure 6.28b.

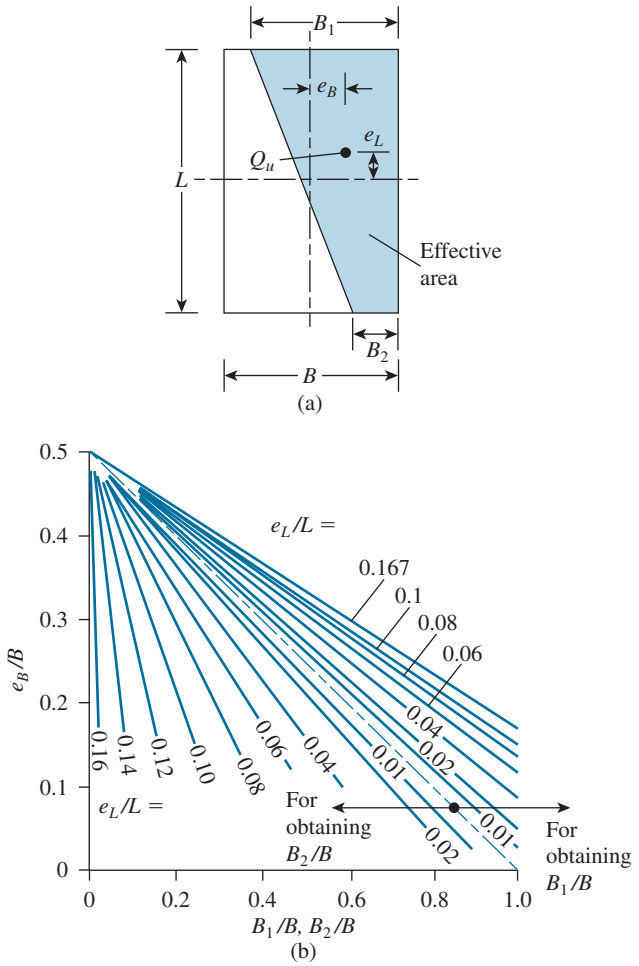


FIGURE 6.28 Effective area for case III where $e_L/L < \frac{1}{6}$ and $\frac{1}{6} < e_B/B < 0.5$ (Based on Highter, W. H. and Anders, J. C. (1985). "Dimensioning Footings Subjected to Eccentric Loads," *Journal of Geotechnical Engineering*, American Society of Civil Engineers, Vol. 111, No. GT5, pp. 659–665)

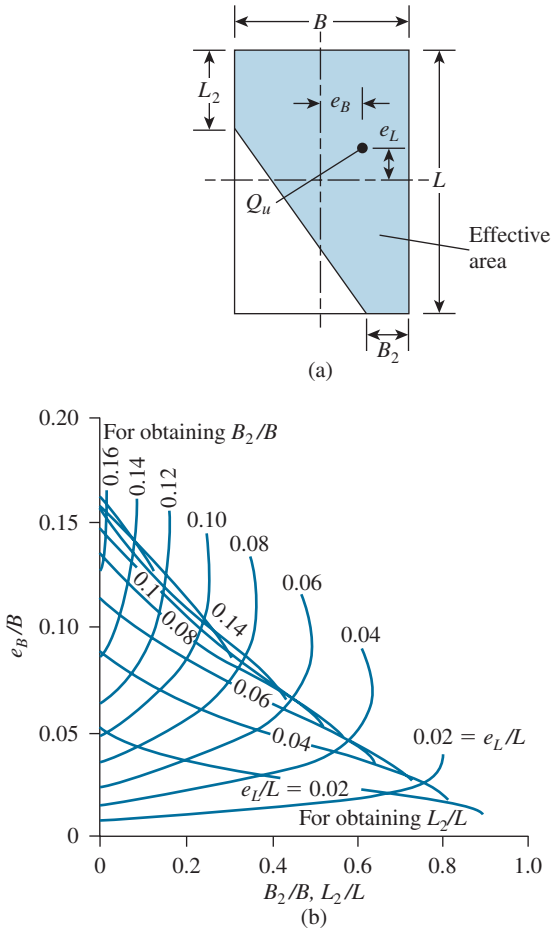


FIGURE 6.29 Effective area for case IV where $e_L/L < \frac{1}{6}$ and $e_B/B < \frac{1}{6}$ (Based on Highter, W. H. and Anders, J. C. (1985). "Dimensioning Footings Subjected to Eccentric Loads," *Journal of Geotechnical Engineering*, American Society of Civil Engineers, Vol. 111, No. GT5, pp. 659–665.)

Case IV. $e_L/L < \frac{1}{6}$ and $e_B/B < \frac{1}{6}$. Figure 6.29a shows the effective area for this case. The ratio B_2/B, and thus B_2, can be determined by using the e_L/L curves that slope upward. Similarly, the ratio L_2/L, and thus L_2, can be determined by using the e_L/L curves that slope downward. The effective area is then

$$A' = L_2B + \tfrac{1}{2}(B + B_2)(L - L_2) \tag{6.81}$$

The effective width is

$$B' = \frac{A'}{L} \tag{6.82}$$

The effective length is

$$L' = L \tag{6.83}$$

Case V. (Circular Foundation) In the case of circular foundations under eccentric loading (Figure 6.30a), the eccentricity is always one way. The effective area A' and the effective width B' for a circular foundation are given in a nondimensional form in Table 6.10. Once A' and B' are determined, the effective length can be obtained as

$$L' = \frac{A'}{B'} \tag{6.84}$$

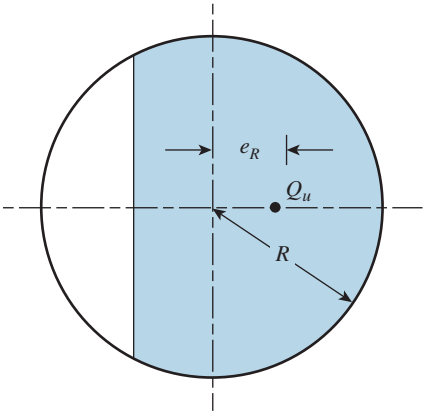


FIGURE 6.30 Effective area for circular foundation

TABLE 6.10 Variation of A'/R^2 and B'/R with e_R/R for Circular Foundations

e_R/R	A'/R^2	B'/R
0.1	2.8	1.85
0.2	2.4	1.32
0.3	2.0	1.2
0.4	1.61	0.80
0.5	1.23	0.67
0.6	0.93	0.50
0.7	0.62	0.37
0.8	0.35	0.23
0.9	0.12	0.12
1.0	0	0

EXAMPLE 6.10

A square foundation is shown in Figure 6.31, with $e_L = 0.3$ m and $e_B = 0.15$ m. Assume two-way eccentricity, and determine the ultimate load, Q_u.

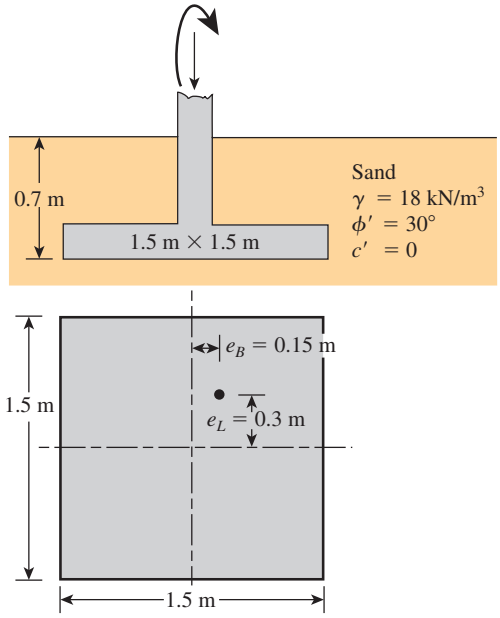


FIGURE 6.31 An eccentrically loaded foundation

SOLUTION

We have

$$\frac{e_L}{L} = \frac{0.3}{1.5} = 0.2$$

and

$$\frac{e_B}{B} = \frac{0.15}{1.5} = 0.1$$

This case is similar to that shown in Figure 6.27a. From Figure 6.27b, for $e_L/L = 0.2$ and $e_B/B = 0.1$,

$$\frac{L_1}{L} \approx 0.85; \qquad L_1 = (0.85)(1.5) = 1.275 \text{ m}$$

and

$$\frac{L_2}{L} \approx 0.21; \qquad L_2 = (0.21)(1.5) = 0.315 \text{ m}$$

From Eq. (6.75),

$$A' = \tfrac{1}{2}(L_1 + L_2)B = \tfrac{1}{2}(1.275 + 0.315)(1.5) = 1.193 \text{ m}^2$$

From Eq. (6.77),

$$L' = L_1 = 1.275 \text{ m}$$

From Eq. (6.76),

$$B' = \frac{A'}{L'} = \frac{1.193}{1.275} = 0.936 \text{ m}$$

Note from Eq. (6.55) with $c' = 0$,

$$q'_u = qN_qF_{qs}F_{qd}F_{qi} + \tfrac{1}{2}\gamma B'N_\gamma F_{\gamma s}F_{\gamma d}F_{\gamma i}$$

where $q = (0.7)(18) = 12.6 \text{ kN/m}^2$.

For $\phi' = 30°$, from Table 6.2, $N_q = 18.4$ and $N_\gamma = 22.4$. Thus from Table 6.3,

$$F_{qs} = 1 + \left(\frac{B'}{L'}\right)\tan\phi' = 1 + \left(\frac{0.936}{1.275}\right)\tan 30° = 1.424$$

$$F_{\gamma s} = 1 - 0.4\left(\frac{B'}{L'}\right) = 1 - 0.4\left(\frac{0.936}{1.275}\right) = 0.706$$

$$F_{qd} = 1 + 2\tan\phi'(1 - \sin\phi')^2\frac{D_f}{B} = 1 + \frac{(0.289)(0.7)}{1.5} = 1.135$$

and

$$F_{\gamma d} = 1$$

So

$$\begin{aligned} Q_u = A'q'_u &= A'(qN_qF_{qs}F_{qd} + \tfrac{1}{2}\gamma B'N_\gamma F_{\gamma s}F_{\gamma d}) \\ &= (1.193)[(12.6)(18.4)(1.424)(1.135) \\ &\quad + (0.5)(18)(0.936)(22.4)(0.706)(1)] \approx \mathbf{606 \text{ kN}} \end{aligned}$$

EXAMPLE 6.11

Consider the foundation shown in Figure 6.31 with the following changes:

$$e_L = 0.18 \text{ m}$$

$$e_B = 0.12 \text{ m}$$

For the soil, $\gamma = 16.5 \text{ kN/m}^3$.

$$\phi' = 25°$$

$$c' = 25 \text{ kN/m}^2$$

Determine the ultimate load, Q_u.

SOLUTION

$$\frac{e_L}{L} = \frac{0.18}{1.5} = 0.12; \qquad \frac{e_B}{B} = \frac{0.12}{1.5} = 0.08$$

This is the case shown in Figure 6.29a. From Figure 6.29b,

$$\frac{B_2}{B} \approx 0.1; \qquad \frac{L_2}{L} \approx 0.32$$

So

$$B_2 = (0.1)(1.5) = 0.15 \text{ m}$$

$$L_2 = (0.32)(1.5) = 0.48 \text{ m}$$

From Eq. (6.81),

$$A' = L_2 B + \frac{1}{2}(B + B_2)(L - L_2) = (0.48)(1.5) + \frac{1}{2}(1.5 + 0.15)(1.5 - 0.48)$$

$$= 0.72 + 0.8415 = 1.5615 \text{ m}^2$$

$$B' = \frac{A'}{L} = \frac{1.5615}{1.5} = 1.041 \text{ m}$$

$$L' = 1.5 \text{ m}$$

From Eq. (6.55),

$$q'_u = c' N_c F_{cs} F_{ed} + q N_q F_{qs} F_{qd} + \frac{1}{2}\gamma B' N_\gamma F_{\gamma s} F_{\gamma d}$$

For $\phi' = 25°$, Table 6.2 gives $N_c = 20.72$, $N_q = 10.66$, and $N_\gamma = 10.88$. From Table 6.3,

$$F_{cs} = 1 + \left(\frac{B'}{L'}\right)\left(\frac{N_q}{N_c}\right) = 1 + \left(\frac{1.041}{1.5}\right)\left(\frac{10.66}{20.72}\right) = 1.357$$

$$F_{qs} = 1 + \left(\frac{B'}{L'}\right)\tan\phi' = 1 + \left(\frac{1.041}{1.5}\right)\tan 25 = 1.324$$

$$F_{\gamma s} = 1 - 0.4\left(\frac{B'}{L'}\right) = 1 - 0.4\left(\frac{1.041}{1.5}\right) = 0.722$$

$$F_{qd} = 1 + 2\tan\phi'(1 - \sin\phi')^2\left(\frac{D_f}{B}\right) = 1 + 2\tan 25(1 - \sin 25)^2\left(\frac{0.7}{1.5}\right) = 1.145$$

$$F_{cd} = F_{qd} - \frac{1 - F_{qd}}{N_c \tan\phi'} = 1.145 - \frac{1 - 1.145}{20.72 \tan 25} = 1.16$$

$$F_{\gamma d} = 1$$

Hence,

$$q'_u = (25)(20.72)(1.357)(1.16) + (16.5 \times 0.7)(10.66)(1.324)(1.145) + \frac{1}{2}(16.5)(1.041)(10.88)(0.722)(1)$$

$$= 815.39 + 186.65 + 67.46 = 1069.5 \text{ kN/m}^2$$

$$Q_u = A' q_u' = (1069.5)(1.5615) = \mathbf{1670 \text{ kN}}$$

6.13 A Simple Approach for Bearing Capacity with Two-Way Eccentricity

A simpler approach to compute the ultimate bearing capacity q'_u under a two-way eccentric load is discussed here. The foundation of dimensions $B \times L$, with the column load acting with eccentricities e_B and e_L, is shown in Figure 6.32. Based on

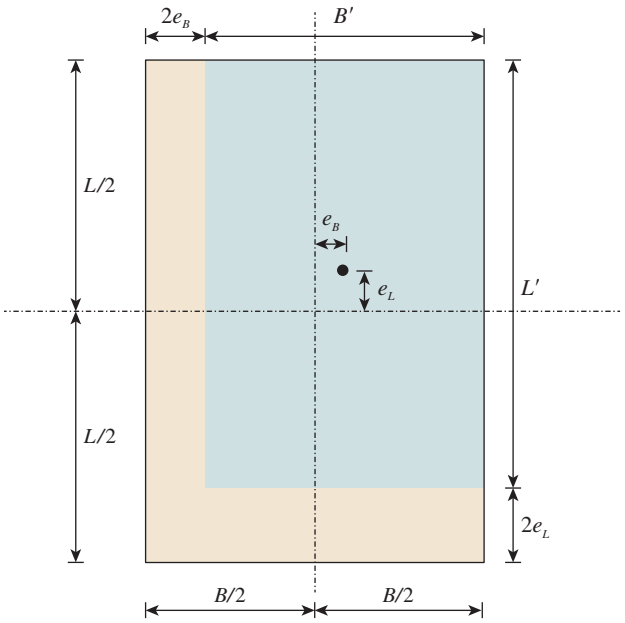


FIGURE 6.32 Effective area of a foundation with two-way eccentricity

Meyerhof's suggestion, by neglecting the light yellow area in the figure, the load is acting at the centroid of the remaining area. The light yellow area consists of two strips of widths $2e_B$ and $2e_L$, as shown in the figure. The effective area of the foundation is thus $B' \times L'$. As discussed in Section 6.12, in the bearing capacity equation and in computing the shape factors, B' and L' should be used. In computing the depth factors, B should be used. In computing the column load, the effective area of the foundation must be used.

EXAMPLE 6.12

A 2 m × 3 m foundation is expected to carry a column load with eccentricities e_B = 0.15 m and e_L = 0.2 m. It is placed in a soil where c' = 10.0 kN/m^2, ϕ' = 22°, and γ = 18.0 kN/m^3, at 1.0 m depth. Determine the maximum load the foundation can carry with factor of safety of 3.

SOLUTION

B = 2.0 m, and L = 3.0 m
e_B = 0.15 m, and e_L = 0.20 m
$B' = B - 2e_B = 2.0 - 2 \times 0.15 = 1.70$ m; $L' = L - 2e_L = 3.0 - 2 \times 0.20 = 2.60$ m

For $\phi' = 22°$, from Table 6.2, $N_c = 16.88$, $N_q = 7.82$, and $N_\gamma = 7.13$.

Shape factors:

$$F_{cs} = 1 + \left(\frac{B'}{L'}\right)\left(\frac{N_q}{N_c}\right) = 1 + \left(\frac{1.70}{2.60}\right)\left(\frac{7.82}{16.88}\right) = 1.30$$

$$F_{qs} = 1 + \left(\frac{B'}{L'}\right)\tan\phi' = 1 + \left(\frac{1.70}{2.60}\right)\tan 22 = 1.26$$

$$F_{\gamma s} = 1 - 0.4\left(\frac{B'}{L'}\right) = 1 - 0.4\left(\frac{1.7}{2.6}\right) = 0.74$$

Depth factors:

$$F_{qd} = 1 + 2\tan\phi'(1 - \sin\phi')^2\frac{D_f}{B} = 1 + 2\tan 22(1 - \sin 22)^2\frac{1}{2} = 1.16$$

$$F_{cd} = F_{qd} - \frac{1 - F_{qd}}{N_c\tan\phi'} = 1.16 - \frac{1 - 1.16}{16.88\tan 22} = 1.18$$

$$F_{\gamma d} = 1.00$$

With the load being vertical, $F_{ci} = F_{qi} = F_{\gamma i} = 1$. From Eq. (6.55),

$$q'_u = c'N_cF_{cs}F_{cd}F_{ci} + qN_qF_{qs}F_{qd}F_{qi} + 0.5\gamma B'F_{\gamma s}F_{\gamma d}F_{\gamma i}$$

$$q'_u = (10.0)(16.88)(1.30)(1.18)(1) + (18 \times 1)(7.82)(1.26)(1.16)(1) + 0.5(18)(1.70)(0.74)(1.0)(1)$$

$$= 258.9 + 205.7 + 11.3 = 475.9\ \text{kN/m}^2$$

The effective area $A' = B' \times L' = 1.70 \times 2.60 = 4.42\ \text{m}^2$. Therefore, $Q_u = 475.9 \times 4.42 = 2103.5$ kN. The allowable load, with FS = 3, is 2103.5/3 = **701 kN**.

■

6.14 Bearing Capacity of a Continuous Foundation Subjected to Eccentrically Inclined Loading

Shallow continuous foundations are at times subjected to eccentrically inclined loads. Figure 6.33 shows two possible modes of load application. In this figure, B is the width of the foundation, e is the load eccentricity, and $Q_{u(ei)}$ is the ultimate load per unit length of the foundation. In Figure 6.33a, the line of load application of the foundation is inclined toward the center line of the foundation and was referred to as *partially compensated* by Perloff and Baron (1976). It is also possible for the line of load application on the foundation to be inclined away from the center line of the foundation, as shown in Figure 6.33b. Perloff and Baron (1976) called this type of loading a *reinforced* case.

The results of practically all studies relating to the bearing capacity of a shallow foundation subjected to an eccentrically inclined load presently available in literature—though fairly limited—consider the *partially compensated* case. The following are the procedures used to estimate the ultimate load $Q_{u(ei)}$ for both of these cases.

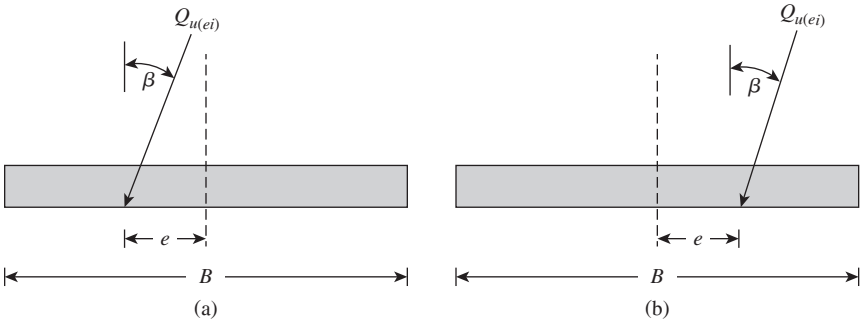


FIGURE 6.33 Continuous foundation subjected to eccentrically inclined load: (a) partially compensated case and (b) reinforced case

PARTIALLY COMPENSATED CASE (FIGURE 6.33a)

Meyerhof's effective area method can be used to determine the ultimate load $Q_{u(ei)}$. From Eq. (6.55),

$$q'_u = c'N_cF_{cd}F_{ci} + qN_qF_{qd}F_{qi} + \frac{1}{2}\gamma N_\gamma B'F_{\gamma d}F_{\gamma i} \tag{6.85}$$

Note that, for continuous foundations, $F_{cs} = F_{qs} = F_{\gamma s} = 1$, and $B' = B - 2e$. Using the values of the bearing capacity factors given in Table 6.2 and the depth and inclination factors given in Table 6.3, the value of q'_u can be estimated. Note that q'_u is the vertical component of the soil reaction. So,

$$Q_{u(ei)} = \frac{(q'_u)(B')(1)}{\cos\beta} = \frac{q'_u(B - 2e)}{\cos\beta} \tag{6.86}$$

Based on a larger number of model test results, Patra et al. (2012a) proposed a reduction factor to estimate $Q_{u(ei)}$ for a foundation on granular soil, according to which

$$Q_{u(ei)} = q_uB(RF) \tag{6.87}$$

where RF = reduction factor

q_u = ultimate bearing capacity of the foundation with centric vertical loading (i.e., $e = 0, \beta = 0$)

The reduction factor can be expressed as

$$RF = \left(1 - 2\frac{e}{B}\right)\left(1 - \frac{\beta^\circ}{\phi'}\right)^{2-(D_f/B)} \tag{6.88}$$

Combining Eqs. (6.87) and (6.88), we have

$$Q_{u(ei)} = q_uB\left(1 - 2\frac{e}{B}\right)\left(1 - \frac{\beta^\circ}{\phi'}\right)^{2-(D_f/B)} \tag{6.89}$$

REINFORCED CASE (GRANULAR SOIL)

Patra et al. (2012b) conducted several model tests on continuous foundations on granular soil and gave the following correlation to estimate $Q_{u(ei)}$.

$$Q_{u(ei)} = q_uB\left(1 - 2\frac{e}{B}\right)\left(1 - \frac{\beta^\circ}{\phi'}\right)^{1.5-0.7(D_f/B)} \tag{6.90}$$

EXAMPLE 6.13

A continuous foundation is shown in Figure 6.34. Estimate the inclined ultimate load, $Q_{u(ei)}$, per unit length of the foundation. Use Eqs. (6.85) and (6.86).

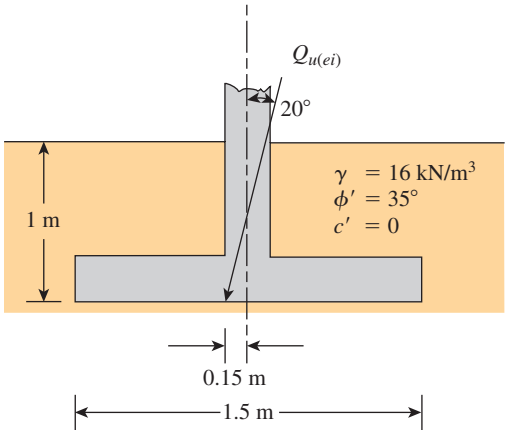


FIGURE 6.34

SOLUTION

From Eq. (6.85) with $c' = 0$, we have

$$q'_u = qN_qF_{qd}F_{qi} + \frac{1}{2}\gamma B'N_\gamma F_{\gamma d}F_{\gamma i}$$

$$q = \gamma D_f = (16)(1) = 16 \text{ kN/m}^2$$

and

$$B' = B - 2e = 1.5 - (2)(0.15) = 1.2 \text{ m}$$

From Table 6.2 for $\phi' = 35°$, $N_q = 33.3$, and $N_\gamma = 48.03$, we have

$$F_{qd} = 1 + 2\tan\phi'(1 - \sin\phi')^2\left(\frac{D_f}{B}\right) = 1 + 2\tan 35(1 - \sin 35)^2\left(\frac{1}{1.5}\right) = 1.17$$

$$F_{\gamma d} = 1$$

$$F_{qi} = \left(1 - \frac{\beta°}{90°}\right)^2 = \left(1 - \frac{20}{90}\right)^2 = 0.605$$

$$F_{\gamma i} = \left(1 - \frac{\beta°}{\phi'}\right)^2 = \left(1 - \frac{20}{35}\right)^2 = 0.184$$

$$q'_u = (16)(33.3)(1.17)(0.605) + \left(\frac{1}{2}\right)(16)(1.2)(48.03)(1)(0.184) = 461.98 \text{ kN/m}^2$$

and

$$Q_{u(ei)} = \frac{q'_u(B - 2e)}{\cos\beta} = \frac{(461.98)(1.2)}{\cos 20} = 589.95 \text{ kN} \approx \mathbf{590 \text{ kN/m}}$$

EXAMPLE 6.14

Solve Example 6.13 using Eq. (6.89).

SOLUTION

From Eq. (6.28) with $c = 0$, we have

$$F_{qs} = F_{\gamma s} = 1 \text{ (continuous foundation)}$$

$$F_{qi} = F_{\gamma i} = 1 \text{ (vertical centric loading)}$$

and

$$q_u = qN_qF_{qd} + \frac{1}{2}\gamma BN_\gamma F_{\gamma d}$$

From Example 6.13, $q = 16 \text{ kN/m}^2$, $N_q = 33.3$, $N_\gamma = 48.03$, $F_{qd} = 1.17$, and $F_{\gamma d} = 1$. Hence,

$$q_u = (16)(33.3)(1.17) + \left(\frac{1}{2}\right)(16)(1.5)(48.03)(1) = 1199.74 \text{ kN/m}^2$$

and

$$Q_{u(ei)} = q_uB\left[1 - 2\left(\frac{e}{B}\right)\right]\left(1 - \frac{\beta°}{\phi'}\right)^{2-(D_f/B)}$$

$$= (1199.74)(1.5)\left[1 - (2)\left(\frac{0.15}{1.5}\right)\right]\left[1 - \left(\frac{20}{35}\right)\right]^{2-\left(\frac{1}{1.5}\right)}$$

$$\approx \mathbf{465 \text{ kN/m}}$$

6.15 Plane-Strain Correction of Friction Angle

The friction angle of a soil can be obtained from triaxial or direct shear tests in the laboratory, or *in situ* tests such as standard penetration or cone penetration tests. Depending on the test method, there can be some difference in the friction angle. The interrelationships among the various friction angles have been summarized by Ameratunga et al. (2016). It has been reported by many researchers that the friction angle obtained from a test representing plane-strain compression loading (ϕ'_{ps}) is greater than that obtained from tests such as the triaxial test ($\phi'_{triaxial}$) representing axisymmetric loading.

The soil beneath the vertical center line of a circular or square foundation is subjected to axisymmetric loading condition, where the stresses are approximately equal all around. The soil beneath the center line of the strip foundation is subjected to plane-strain compression and, hence, ϕ'_{ps} should be used in the bearing capacity equation. Noting that ϕ'_{ps} is about 10% greater than $\phi'_{triaxial}$, Meyerhof (1963) suggested the following equation to interpolate the friction angle for rectangular foundations.

$$\phi'_{rectangle} = \phi'_{triaxial}\left(1.1 - 0.1\frac{B}{L}\right) \tag{6.91}$$

The bearing capacity factors N_c, N_q, and N_γ are very sensitive to the friction angle. Therefore, it is necessary to select the appropriate friction angle.

6.16 Summary

Depending on the strength of the soil, the shallow foundations can fail in three different modes; general shear, local shear, and punching shear. In firm ground, the failure is in general shear mode. The original bearing capacity theory was developed by Terzaghi for general shear mode. This was later modified by many others, with correction factors to account for the shape and depth of the foundation, soil compressibility, and the inclination and eccentricity of the applied load. There are several widely varying expressions for the bearing capacity factor N_γ and some correction factors.

PROBLEMS

6.1 For the following cases, determine the allowable gross vertical load-bearing capacity of the foundation. Use Terzaghi's equation and assume general shear failure in soil. Use FS = 4.

6.2 A 5.0 ft wide square footing is placed at 3.0 ft depth within the ground where $c' = 200$ lb/ft^2, $\phi' = 25°$, and $\gamma = 115.0$ lb/ft^3. Determine the ultimate bearing capacity of the footing using Terzaghi's bearing capacity equation and the bearing capacity factors from Table 6.1. What is the maximum column load that can be allowed with a factor of safety of 3.0?

6.3 Use the general bearing capacity equation [Eq. (6.28)] to solve the following:
- **a.** Problem 6.1a
- **b.** Problem 6.1b
- **c.** Problem 6.1c

6.4 Redo Problem 6.2 using the general bearing capacity equation [Eq. (6.28)].

6.5 The applied load on a shallow square foundation makes an angle of 20° with the vertical. Given: $B = 5$ ft, $D_f = 3$ ft, $\gamma = 115$ lb/ft^3, $\phi' = 25°$, and $c' = 600$ lb/ft^2. Use FS = 3

Parameters for Problem 6.1

Part	B	D_f	ϕ'	c'	γ	Foundation type
a.	3 ft	3 ft	28°	400 lb/ft^2	110 lb/ft^3	Continuous
b.	1.5 m	1.2 m	35°	0	17.8 kN/m^3	Continuous
c.	3 m	2 m	30°	0	16.5 kN/m^3	Square

and determine the gross inclined allowable load. Use Eq. (6.28).

6.6 A 2.0 m wide continuous foundation carries a wall load of 350 kN/m in a clayey soil where $\gamma = 19.0$ kN/m^3, $c' = 5.0$ kN/m^2, and $\phi' = 23°$. The foundation depth is 1.5 m. Determine the factor of safety of this foundation using Eq. (6.28).

6.7 Determine the maximum column load that can be applied on a 1.5 m × 1.5 m square foundation placed at a depth of 1.0 m within a soil, where $\gamma = 19.0$ kN/m^3, $c' = 10$ kN/m^2, and $\phi' = 24°$. Allow a factor of safety of 3.0.

6.8 A 2.0 m wide strip foundation is placed in sand at 1.0 m depth. The properties of the sand are: $\gamma = 19.5$ kN/m^3, $c' = 0$, and $\phi' = 34°$. Determine the maximum wall load that the foundation can carry, with a factor of safety of 3.0, using

a. Terzaghi's original bearing capacity equation with his bearing capacity factors, and

b. Meyerhof's general bearing capacity equation with shape, depth, and inclination factors from Table 6.3.

6.9 A column foundation (Figure P6.9) is 3 m × 2 m in plan. Given: $D_f = 1.5$ m, $\phi' = 25°$, $c' = 70$ kN/m^2. Using Eq. (6.28) and FS = 3, determine the net allowable load [see Eq. (6.24)] the foundation could carry.

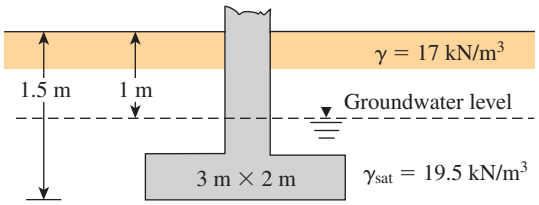


FIGURE P6.9

6.10 For the design of a shallow foundation, given the following:

Soil: $\phi' = 20°$
$c' = 72$ kN/m^2
Unit weight, $\gamma = 17$ kN/m^3
Modulus of elasticity, $E_s = 1400$ kN/m^2
Poisson's ratio, $\mu_s = 0.35$

Foundation: $L = 2$ m
$B = 1$ m
$D_f = 1$ m

Calculate the ultimate bearing capacity. Use Eq. (6.42).

6.11 An eccentrically loaded foundation is shown in Figure P6.11. Use FS of 4 and determine the maximum allowable load that the foundation can carry. Use Meyerhof's effective area method.

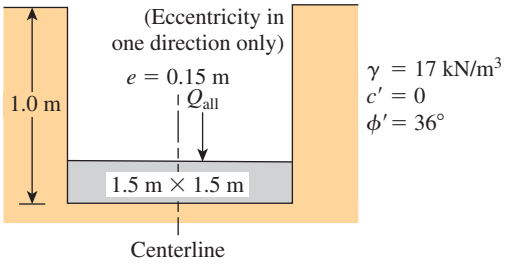


FIGURE P6.11

6.12 Repeat Problem 6.11 using Prakash and Saran's method.

6.13 For an eccentrically loaded continuous foundation on sand, given $B = 1.8$ m, $D_f = 0.9$ m, $e/B = 0.12$ (one-way eccentricity), $\gamma = 16$ kN/m^3, and $\phi' = 35°$. Using the reduction factor method [Eq. (6.64)], estimate the ultimate load per unit length of the foundation.

6.14 A 2 m × 3 m spread footing placed at a depth of 2 m carries a vertical load of 3000 kN and a moment of 300 kN·m, as shown in Figure P6.14. Determine the factor of safety using Meyerhof's effective area method.

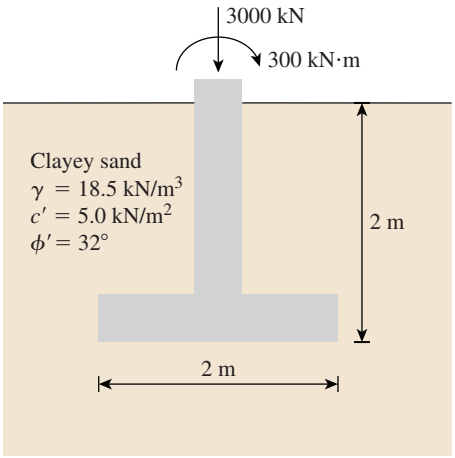


FIGURE P6.14

6.15 Three continuous foundations are shown in Figure P6.15. For each of them, what values would you use for their eccentricity and inclination in the bearing capacity calculations?

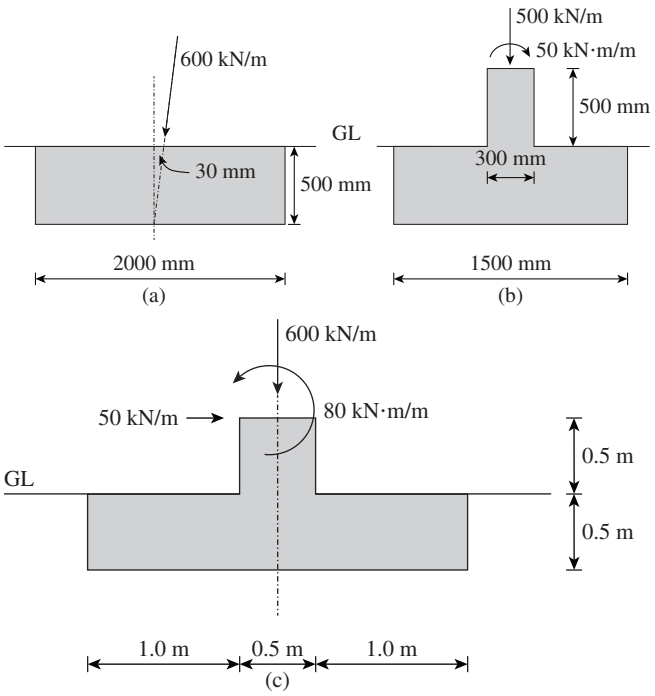


FIGURE P6.15

6.16 A tall cylindrical silo carrying flour is to be supported by a 1.5 m wide ring beam that can be designed as a continuous foundation. The inner and outer diameters of the ring are 10 m and 13 m, respectively. The soil at the site is entirely sand ($\phi' = 35°$, $\gamma = 19$ kN/m^3) and the ring beam is placed on the ground with $D_f = 0$. Determine the maximum silo load that can be carried by the ring beam, assuming that the entire load is transferred to the ground through the ring beam.

6.17 A 2.0 m × 2.0 m square pad footing will be placed in a normally consolidated clay soil to carry a column load Q. The depth of the footing is 1.0 m. The soil parameters are: $c' = 0$, $\phi' = 26°$, $\gamma = 19$ kN/m^3, and $c_u = 60$ kN/m^2. Determine the maximum possible value for Q, considering short-term and long-term stability of the footing.

6.18 An eccentrically loaded continuous foundation is shown in Figure P6.18. Determine the ultimate load Q_u per unit length that the foundation can carry. Use the reduction factor method [Eq. (6.67)].

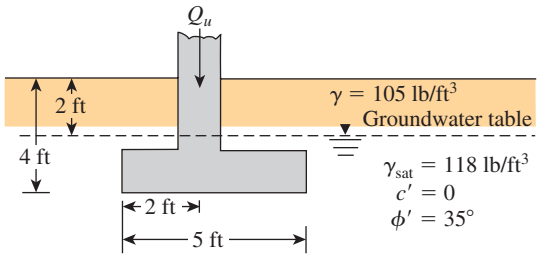


FIGURE P6.18

6.19 A square foundation is shown in Figure P6.19. Use FS = 6, and determine the size of the foundation. Use Prakash and Saran's method [Eq. (6.59)].

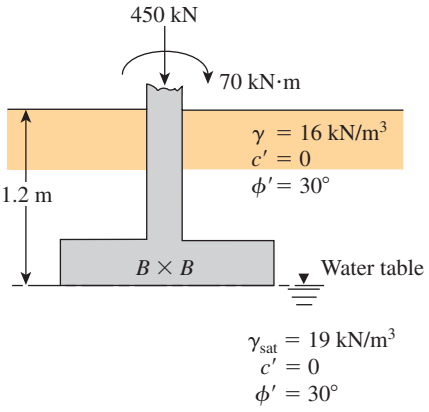


FIGURE P6.19

6.20 The shallow foundation shown in Figure 6.25 measures 1.5 m × 2.25 m and is subjected to a centric load and a moment. If $e_B = 0.12$ m, $e_L = 0.36$ m, and the depth of the foundation is 0.8 m, determine the allowable load the foundation can carry. Use a factor of safety of 4. For the soil, we are told that unit weight $\gamma = 17$ kN/m^3, friction angle $\phi' = 35°$, and cohesion $c' = 0$. Use Eqs (6.75), (6.76), and (6.77).

6.21 Consider a continuous foundation of width $B = 1.4$ m on a sand deposit with $c' = 0$, $\phi' = 38°$, and $\gamma = 17.5$ kN/m^3. The foundation is subjected to an eccentrically inclined load (see Figure 6.33). Given: load eccentricity $e = 0.15$ m, $D_f = 1$ m, and load inclination $\beta = 18°$. Estimate the failure load $Q_{u(ei)}$ per unit length of the foundation
a. for a partially compensated type of loading [Eq. (6.89)]
b. for a reinforced type of loading [Eq. (6.90)]

REFERENCES

Ameratunga, J., Sivakugan, N., and Das, B. M. (2016). *Correlations of Soil and Rock Properties in Geotechnical Engineering*, Springer, New Delhi.

Biarez, J., Burel, M., and Wack, B. (1961). "Contribution á l'étude de la Force Portante des Fondations," *Proceedings, Fifth International Conference on Soil Mechanics and Foundation Engineering*, Paris, Vol. 1, pp. 603–609.

Booker, J. R. (1969). Application of theories of plasticity for cohesive frictional soils. Ph.D. thesis, University of Sydney, Australia.

Bozozuk, M. (1972). "Foundation Failure of the Vankleek Hill Tower Site," *Proceedings*, Specialty Conference on Performance of Earth and Earth-Supported Structures, Vol. 1, Part 2, pp. 885–902.

Brand, E. W., Muktabhant, C., and Taechanthummarak, A. (1972). "Load Test on Small Foundations in Soft Clay," *Proceedings, Specialty Conference on Performance of Earth and Earth-Supported Structures*, American Society of Civil Engineers, Vol. 1, Part 2, pp. 903–928.

Caquot, A. and Kerisel, J. (1953). "Sur le terme de surface dans le calcul des fondations en milieu pulverulent," *Proceedings, Third International Conference on Soil Mechanics and Foundation Engineering*, Zürich, Vol. I, pp. 336–337.

DeBeer, E. E. (1970). "Experimental Determination of the Shape Factors and Bearing Capacity Factors of Sand," *Geotechnique*, Vol. 20, No. 4, pp. 387–411.

Hanna, A. M. and Meyerhof, G. G. (1981). "Experimental Evaluation of Bearing Capacity of Footings Subjected to Inclined Loads," *Canadian Geotechnical Journal*, Vol. 18, No. 4, pp. 599–603.

Hansen, J. B. (1970). *A Revised and Extended Formula for Bearing Capacity*, Bulletin 28, Danish Geotechnical Institute, Copenhagen.

Highter, W. H. and Anders, J. C. (1985). "Dimensioning Footings Subjected to Eccentric Loads," *Journal of Geotechnical Engineering*, American Society of Civil Engineers, Vol. 111, No. GT5, pp. 659–665.

Hjiaj, M., Lyamin, A. V., and Sloan, S. W. (2005). "Numerical Limit Analysis Solutions for the Bearing Capacity Factor N_γ," *International Journal of Solids and Structures*, Vol. 42, No. 5–6, pp. 1681–1804.

Kumbhojkar, A. S. (1993). "Numerical Evaluation of Terzaghi's N_γ," *Journal of Geotechnical Engineering*, American Society of Civil Engineers, Vol. 119, No. 3, pp. 598–607.

Martin, C. M. (2005). "Exact Bearing Capacity Calculations Using the Method of Characteristics," *Proceedings, Eleventh International Conference of the International Association for Computer Methods and Advances in Geomechanics*, Turin, Italy, Vol. 4, pp. 441–450.

Michalowski, R. L. (1997). "An Estimate of the Influence of Soil Weight on Bearing Capacity Using Limit Analysis," *Soils and Foundations*, Vol. 37, No. 4, pp. 57–64.

Meyerhof, G. G. (1953). "The Bearing Capacity of Foundations Under Eccentric and Inclined Loads," *Proceedings, Third International Conference on Soil Mechanics and Foundation Engineering*, Zürich, Vol. 1, pp. 440–445.

Meyerhof, G. G. (1963). "Some Recent Research on the Bearing Capacity of Foundations," *Canadian Geotechnical Journal*, Vol. 1, No. 1, pp. 16–26.

Patra, C. R., Behera, R. N., Sivakugan, N., and Das, B. M. (2012a). "Ultimate Bearing Capacity of Shallow Strip Foundation under Eccentrically Inclined Load: Part I," *International Journal of Geotechnical Engineering*, Vol. 6, No. 3, pp. 342–352.

Patra, C. R., Behera, R. N., Sivakugan, N., and Das, B. M. (2012b). "Ultimate Bearing Capacity of Shallow Strip Foundation under Eccentrically Inclined Load: Part II," *International Journal of Geotechnical Engineering*, Vol. 6, No. 4, pp. 507–514.

Patra, C. R., Behera, R. N., Sivakugan, N., and Das, B. M. (2013). "Estimation of Average Settlement of Shallow Strip Foundation on Granular Soil under Eccentric Load," *International Journal of Geotechnical Engineering*, Vol. 7, No. 2, pp. 218–222.

Perloff, W. H. and Barron, W. (1976). *Soil Mechanics: Principles and Applications*, Ronald Press, New York.

Prakash, S. and Saran, S. (1971). "Bearing Capacity of Eccentrically Loaded Footings," *Journal of the Soil Mechanics and Foundations Division*, ASCE, Vol. 97, No. SM1, pp. 95–117.

Prandtl, L. (1921). "Über die Eindringungsfestigkeit (Härte) plastischer Baustoffe und die Festigkeit von Schneiden," *Zeitschrift für angewandte Mathematik und Mechanik*, Vol. 1, No. 1, pp. 15–20.

Purkayastha, R. D. and Char, R. A. N. (1977). "Stability Analysis of Eccentrically Loaded Footings," *Journal of Geotechnical Engineering Div*., ASCE, Vol. 103, No. 6, pp. 647–651.

Reissner, H. (1924). "Zum Erddruckproblem," *Proceedings, First International Congress of Applied Mechanics*, Delft, pp. 295–311.

Terzaghi, K. (1943). *Theoretical Soil Mechanics*, John Wiley & Sons, New York.

Tomlinson, M. J. (1978). *Foundation Design and Construction*, 3rd ed., Pitman, London.

Vesic, A. S. (1963). "Bearing Capacity of Deep Foundations in Sand," *Highway Research Record* No. 39, National Academy of Sciences, pp. 112–153.

Vesic, A. S. (1973). "Analysis of Ultimate Loads of Shallow Foundations," *Journal of the Soil Mechanics and Foundations Division*, American Society of Civil Engineers, Vol. 99, No. SM1, pp. 45–73.

Zhu, M. and Michalowski, R. L. (2005). "Shape Factors for Limit Loads on Square and Rectangular Footings," *Journal of Geotechnical and Geoenvironmental Engineering*, American Society of Civil Engineering, Vol. 131, No. 2, pp. 223–231.

7

Ultimate Bearing Capacity of Shallow Foundations: Special Cases



PHATR/Shutterstock.com

7.1 Introduction 259
7.2 Foundation Supported by a Soil with a Rigid Base at Shallow Depth 259
7.3 Foundations on Layered Clay 266
7.4 Bearing Capacity of Layered Soil: Stronger Soil Underlain by Weaker Soil ($c' - \phi'$ soil) 268
7.5 Bearing Capacity of Layered Soil: Weaker Soil Underlain by Stronger Soil 275
7.6 Continuous Foundation on Weak Clay with a Granular Trench 278
7.7 Closely Spaced Foundations—Effect on Ultimate Bearing Capacity 280
7.8 Bearing Capacity of Foundations on Top of a Slope 282
7.9 Bearing Capacity of Foundations on a Slope 285
7.10 Seismic Bearing Capacity and Settlement in Granular Soil 286
7.11 Foundations on Rock 289
7.12 Ultimate Bearing Capacity of Wedge-Shaped Foundations 291
7.13 Uplift Capacity of Foundations 293
7.14 Summary 298

PROBLEMS 299
REFERENCES 300

7.1 Introduction

The ultimate bearing capacity problems described in Chapter 6 assume that the soil supporting the foundation is homogeneous and extends to a great depth below the bottom of the foundation. They also assume that the ground surface is horizontal. However, that is not true in all cases: It is possible to encounter a rigid layer at a shallow depth, or the soil may be layered and have different shear strength parameters. In some instances, it may be necessary to construct foundations on or near a slope, or it may be required to design a foundation subjected to uplifting load. In earthquake-prone areas, it is necessary to consider the additional seismic loads these events might impose on the structure.

This chapter discusses the methods for determining the bearing capacities under these special circumstances.

7.2 Foundation Supported by a Soil with a Rigid Base at Shallow Depth

CONTINUOUS FOUNDATION

Figure 7.1a shows a shallow, rough *continuous* foundation supported by a soil that extends to a great depth. Neglecting the depth factor, for vertical loading Eq. (6.28) will take the form

$$q_u = c'N_c + qN_q + \frac{1}{2}\gamma BN_\gamma \tag{7.1}$$

The general approach for obtaining expressions for N_c, N_q, and N_γ was outlined in Chapter 6. The extent of the failure zone in soil, D, at ultimate load obtained in the derivation of N_c and N_q by Prandtl (1921) and Reissner (1924) is given in Figure 7.1b. Similarly, the magnitude of D obtained by Lundgren and Mortensen (1953) in evaluating N_γ is given in the figure. When the friction angle increases, the failure zone extends deeper and D increases.

Now, if a rigid rough base is located at a depth of $H < D$ below the bottom of the foundation, full development of the failure surface in soil will be restricted. In such a case, the soil failure zone and the development of slip lines at ultimate load will be as shown in Figure 7.2. Mandel and Salencon (1972) determined the bearing capacity factors applicable to this case by numerical integration, using the theory of plasticity. According to their theory, the ultimate bearing capacity of a rough continuous foundation with a rigid rough base located at a shallow depth can be given by the relation

$$q_u = c'N_c^* + qN_q^* + \frac{1}{2}\gamma BN_\gamma^* \tag{7.2}$$

where

N_c^*, N_q^*, N_γ^* = modified bearing capacity factors

B = width of foundation

γ = unit weight of soil

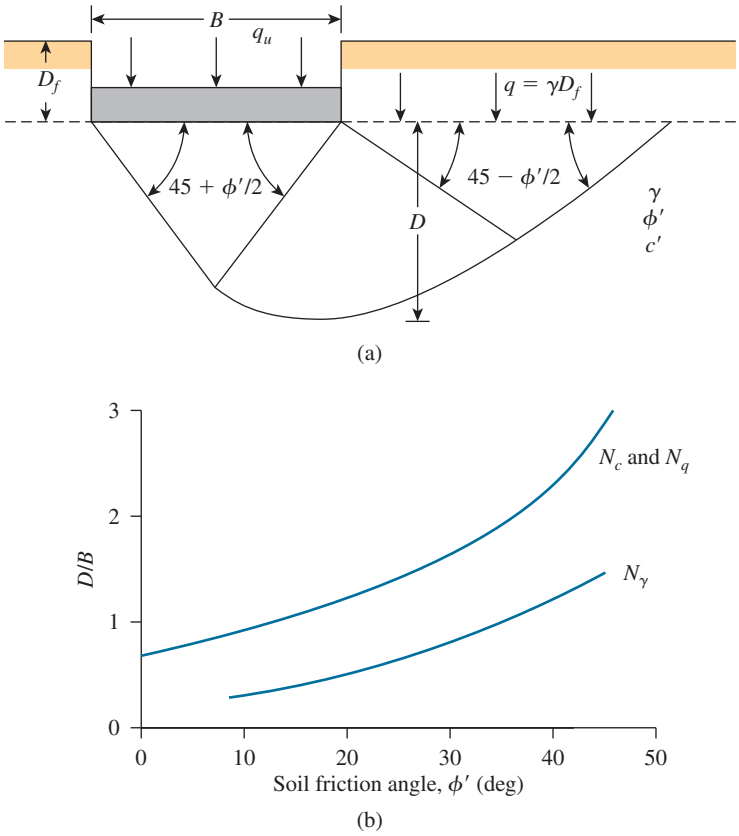


FIGURE 7.1 (a) Failure surface under a rough continuous foundation; (b) variation of D/B with soil friction angle ϕ'

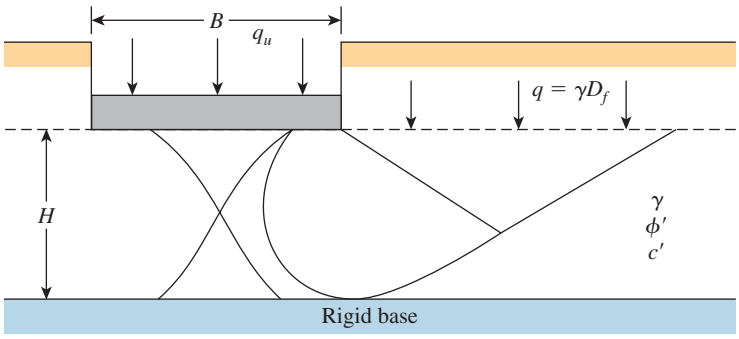


FIGURE 7.2 Failure surface under a rough continuous foundation with a rigid rough base located at a shallow depth

Note that for $H \geq D$, $N_c^* = N_c$, $N_q^* = N_q$, and $N_\gamma^* = N_\gamma$ (Lundgren and Mortensen, 1953). The variations of N_c^*, N_q^*, and N_γ^* with H/B and the soil friction angle ϕ' are given in Figures 7.3, 7.4, and 7.5, respectively.

It can be seen from Figures 7.3 to 7.5 that when the depth to the rigid base H decreases, the bearing capacity factors and hence the ultimate bearing capacity of the foundation increase. It can also be seen that when $H > B$, especially for lower friction angles, one can conservatively ignore the presence of the rigid base and use the general bearing capacity factors N_c, N_q, and N_γ (Table 6.2).

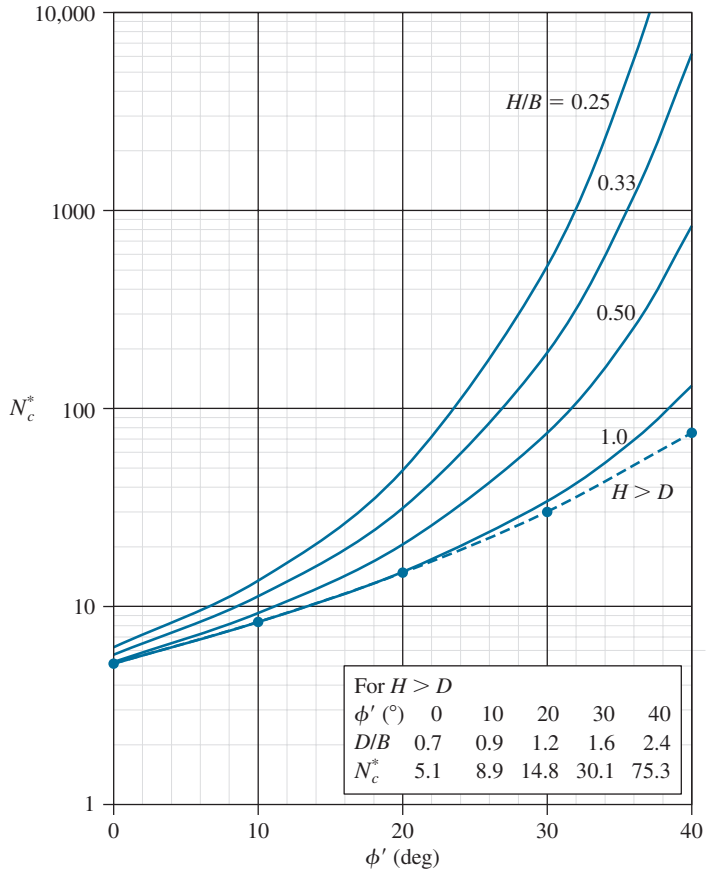


FIGURE 7.3 Mandel and Salencon's bearing capacity factor N_c^* for Eq. (7.2)

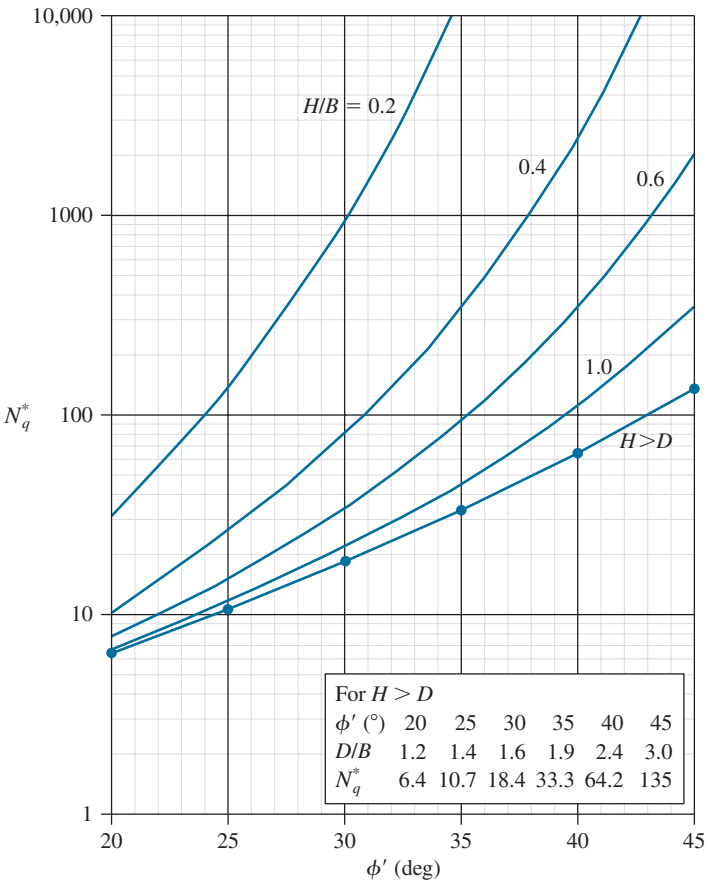


FIGURE 7.4 Mandel and Salencon's bearing capacity factor N_q^* for Eq. (7.2)

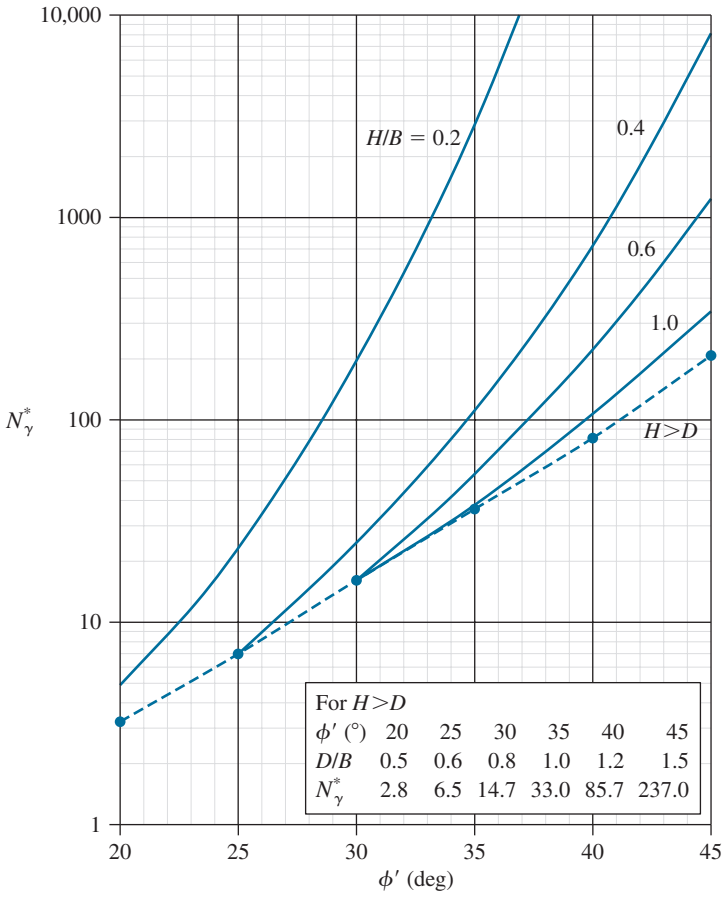


FIGURE 7.5 Mandel and Salencon's bearing capacity factor N^*_γ for Eq. (7.2)

RECTANGULAR FOUNDATION ON GRANULAR SOIL

Neglecting the depth factors, the ultimate bearing capacity of rough circular and rectangular foundations on a sand layer ($c' = 0$) with a rough rigid base located at a shallow depth can be given as

$$q_u = qN^*_q F^*_{qs} + \frac{1}{2}\gamma B N^*_\gamma F^*_{\gamma s} \tag{7.3}$$

where F^*_{qs}, $F^*_{\gamma s}$ are modified shape factors considering the presence of the rigid base.

The shape factors F^*_{qs} and $F^*_{\gamma s}$ are functions of H/B and ϕ'. On the basis of the work of Meyerhof and Chaplin (1953) and simplifying the assumption that in radial planes, the stresses and shear zones are identical to those in transverse planes, Meyerhof (1974) proposed that

$$F^*_{qs} \approx 1 - m_1\left(\frac{B}{L}\right) \tag{7.4}$$

and

$$F^*_{\gamma s} \approx 1 - m_2\left(\frac{B}{L}\right) \tag{7.5}$$

where L = length of the foundation. The variations of m_1 and m_2 with H/B and ϕ' are shown in Figure 7.6.

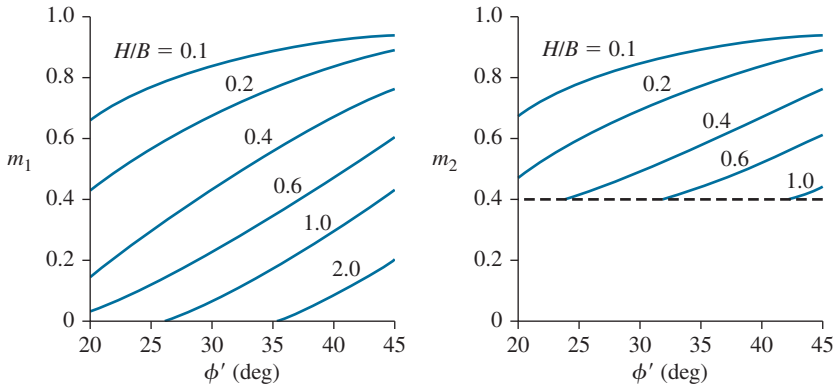


FIGURE 7.6 Variation of m_1 and m_2 with H/B and ϕ'

More recently, Cerato and Lutenegger (2006) provided some test results for the bearing capacity factor N_γ^*. These tests were conducted using *square* and *circular* plates with B varying from 0.152 m (6 in.) to 0.305 m (12 in.). It was assumed that Terzaghi's bearing-capacity equations for *square and circular foundations* can be used. Or, from Eqs. (6.19) and (6.20) with $c' = 0$,

$$q_u = qN_q^* + 0.4\gamma BN_\gamma^* \text{ (square foundation)} \tag{7.6}$$

and

$$q_u = qN_q^* + 0.3\gamma BN_\gamma^* \text{ (circular foundation)} \tag{7.7}$$

The experimentally determined variation of N_γ^* is shown in Figure 7.7. It also was observed in this study that N_γ^* becomes equal to N_γ at $H/B \approx 3$ instead of $D/B \approx 1$, as shown in Figure 7.5. For that reason, Figure 7.7 shows the variation of N_γ^* for $H/B = 0.5$ to 3.0.

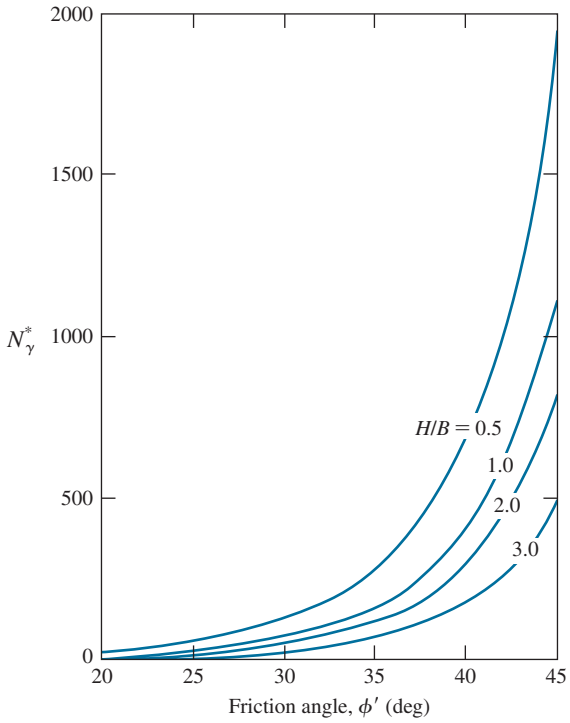


FIGURE 7.7 Cerato and Lutenegger's test results for N_γ^*

TABLE 7.1 Values of N_c^* for Continuous and Square Foundations ($\phi = 0$)

$\frac{B}{H}$	N_c^*	
	Square[a]	Continuous[b]
2	5.43	5.24
3	5.93	5.71
4	6.44	6.22
5	6.94	6.68
6	7.43	7.20
8	8.43	8.17
10	9.43	9.05

[a]Buisman's analysis (1940)
[b]Mandel and Salencon's analysis (1972)

FOUNDATION ON SATURATED CLAY

For a continuous foundation on saturated clay (i.e., under the undrained condition, or $\phi = 0$), Eq. (7.2) will simplify to the form

$$q_u = c_u N_c^* + q \tag{7.8}$$

Mandel and Salencon (1972) performed calculations to evaluate N_c^* for *continuous foundations*. Similarly, Buisman (1940) gave the following relationship for obtaining the ultimate bearing capacity of square foundations:

$$q_{u(\text{square})} = \left(\pi + 2 + \frac{B}{2H} - \frac{\sqrt{2}}{2}\right)c_u + q \qquad (\text{for } H < 0.707B) \tag{7.9}$$

In this equation, c_u is the undrained shear strength.

Equation (7.9) can be rewritten as

$$q_{u(\text{square})} = \underbrace{5.14\left(1 + \frac{0.5\dfrac{B}{H} - 0.707}{5.14}\right)}_{N_{c(\text{square})}^*} c_u + q \tag{7.10}$$

Table 7.1 gives the values of N_c^* for continuous and square foundations. The N_c^* values for the square foundations from Eq. 7.10 and Table 7.1 include the shape factors, which should not be applied separately.

EXAMPLE 7.1

A square foundation measuring 1.2 m × 1.2 m is constructed on a layer of sand. We are given that $D_f = 1$ m, $\gamma = 15.5$ kN/m^3, $\phi' = 35°$, and $c' = 0$. A rock layer is located at a depth of 0.48 m below the bottom of the foundation. Using a factor of safety of 4, determine the gross allowable load the foundation can carry.

SOLUTION

From Eq. (7.3),

$$q_u = qN_q^* F_{qs}^* + \frac{1}{2}\gamma B N_\gamma^* F_{\gamma s}^*$$

and we also have

$$q = 15.5 \times 1 = 15.5 \text{ kN/m}^3$$

For $\phi' = 35°$, $H/B = 0.48/1.2 = 0.4$, $N_q^* \approx 336$ (Figure 7.4), and $N_\gamma^* \approx 138$ (Figure 7.5), and we have

$$F_{qs}^* = 1 - m_1\left(\frac{B}{L}\right)$$

From Figure 7.6a for $\phi' = 35°$, $H/B = 0.4$. The value of $m_1 \approx 0.58$, so

$$F_{qs}^* = 1 - (0.58)(1.2/1.2) = 0.42$$

Similarly,

$$F_{\gamma s}^* = 1 - m_2(B/L)$$

From Figure 7.6b, $m_2 = 0.6$, so

$$F_{\gamma s}^* = 1 - (0.6)\,(1.2/1.2) = 0.4$$

Hence,

$$q_u = (15.5)\,(336)\,(0.42) + (1/2)\,(15.5)\,(1.2)\,(138)\,(0.4) = 2700.72 \text{ kN/m}^2$$

and

$$Q_{\text{all}} = \frac{q_u B^2}{\text{FS}} = \frac{(2700.72)\,(1.2 \times 1.2)}{4} = \mathbf{972.3\ kN}$$

■

EXAMPLE 7.2

Consider a square foundation 1 m × 1 m in plan located on a saturated clay layer underlain by a layer of rock. Given:

Clay: $c_u = 72 \text{ kN/m}^2$
Unit weight: $\gamma = 18 \text{ kN/m}^3$
Distance between the bottom of foundation and the rock layer = 0.25 m
$D_f = 1$ m

Estimate the gross allowable bearing capacity of the foundation. Use FS = 3.

SOLUTION

From Eq. (7.10),

$$q_u = 5.14\left(1 + \frac{0.5\dfrac{B}{H} - 0.707}{5.14}\right)c_u + q$$

For $B/H = 1/0.25 = 4$; $c_u = 72 \text{ kN/m}^2$; and $q = \gamma D_f = (18)\,(1) = 18 \text{ kN/m}^3$.

$$q_u = 5.14\left[1 + \frac{(0.5)(4) - 0.707}{5.14}\right]72 + 18 = 481.2 \text{ kN/m}^2$$

$$q_{\text{all}} = \frac{q_u}{\text{FS}} = \frac{481.2}{3} = \mathbf{160.4\ kN/m^2}$$

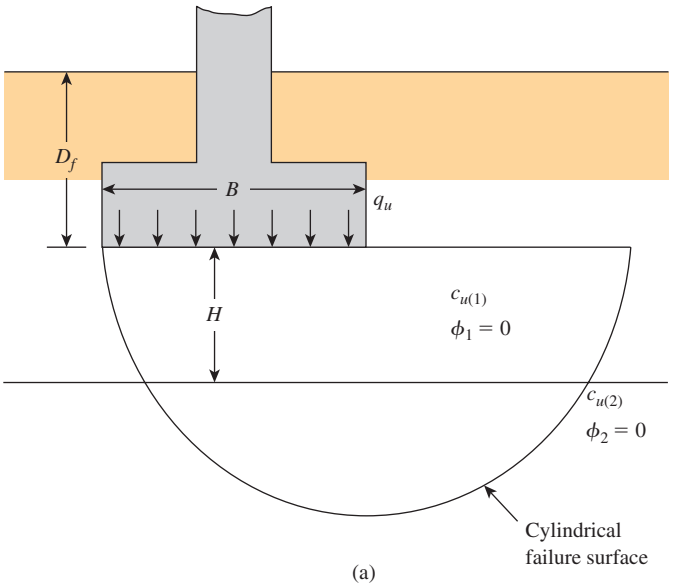
■

7.3 Foundations on Layered Clay

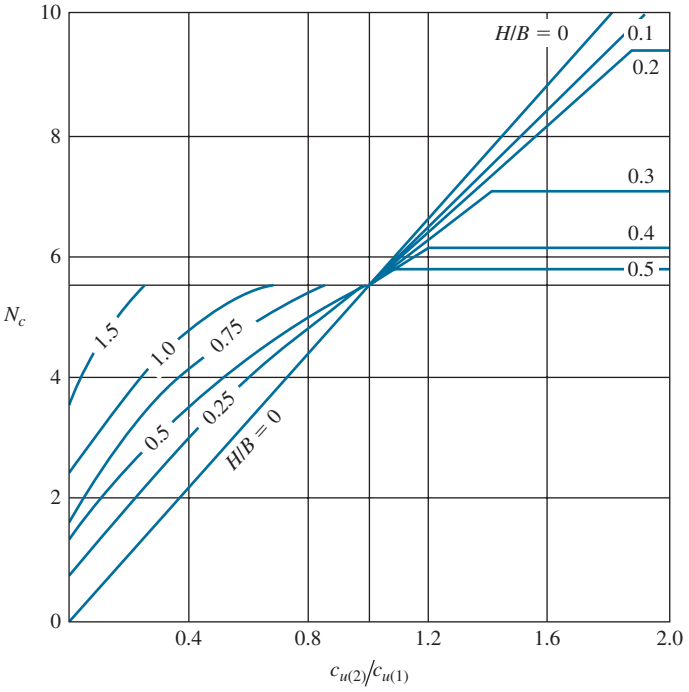
Reddy and Srinivasan (1967) have derived the equation for the bearing capacity of foundations on layered clay soil, assuming the failure mode as shown in Figure 7.8a. For undrained loading ($\phi = 0$ condition), let $c_{u(1)}$ and $c_{u(2)}$ be the shear strength of the upper and lower clay layers, respectively. In such a case, the ultimate bearing capacity of a foundation can be given as [similar to Eq. (6.28)]

$$q_u = c_{u(1)} N_c F_{cs} F_{cd} + q \tag{7.11}$$

The relationships for F_{cs} and F_{cd} are the same as given in Table 6.3 (for $\phi = 0$ condition). For layered soil, the value of the bearing capacity factor, N_c, is not a constant. It is a function of $c_{u(2)}/c_{u(1)}$ and H/B (*note:* H = depth measured from the bottom of the foundation



(a)



(b)

FIGURE 7.8 Bearing capacity on layered clay soil—$\phi = 0$ (Figure 7.8b based on Reddy and Srinivasan, 1967)

to the interface of the two clay layers). The variation of N_c is given in Figure 7.8b. It can be seen from this figure that if the lower layer of clay is softer than the top one (that is, $c_{u(2)}/c_{u(1)} < 1$), the value of the bearing capacity factor (N_c) is lower than when the soil is not layered (that is, when $c_{u(2)}/c_{u(1)} = 1$). This means that the ultimate bearing capacity is reduced by the presence of a softer clay layer below the top layer.

Vesic (1975) proposed that the ultimate bearing capacity of a foundation supported by a weaker clay layer [$c_{u(1)}$] underlain by a stronger clay layer [$c_{u(2)}$] can be expressed as

$$q_u = c_{u(1)} m N_c F_{cs} F_{cd} + q \tag{7.12}$$

where

$$N_c F_{cs} = \begin{cases} 5.14 \text{ for continous foundation} \\ 6.17 \text{ for square or circular foundation} \end{cases}$$

F_{cs} = shape factor

F_{cd} = depth factor

$$m = f\left[\frac{c_{u(1)}}{c_{u(2)}}, \frac{H}{B}, \text{ and } \frac{B}{L}\right] \tag{7.13}$$

The variation of m for continuous foundations is given in Table 7.2, and the variation of m for square and circular foundations is given in Table 7.3.

TABLE 7.2 Variation of m [Eq. (7.12)] for Continuous Foundation ($B/L \leq 0.2$)

	H/B				
$c_{u(1)}/c_{u(2)}$	≥ 0.5	0.25	0.167	0.125	0.1
1	1	1	1	1	1
0.667	1	1.033	1.064	1.088	1.109
0.5	1	1.056	1.107	1.152	1.193
0.333	1	1.088	1.167	1.241	1.311
0.25	1	1.107	1.208	1.302	1.389
0.2	1	1.121	1.235	1.342	1.444
0.1	1	1.154	1.302	1.446	1.584

Based on Vesic (1975)

TABLE 7.3 Variation of m [Eq. (7.12)] for Square Foundation ($B/L = 1$)

	H/B				
$c_{u(1)}/c_{u(2)}$	≥ 0.25	0.125	0.083	0.063	0.05
1	1	1	1	1	1
0.667	1	1.028	1.052	1.075	1.096
0.5	1	1.047	1.091	1.131	1.167
0.333	1	1.075	1.143	1.207	1.267
0.25	1	1.091	1.177	1.256	1.334
0.2	1	1.102	1.199	1.292	1.379
0.1	1	1.128	1.254	1.376	1.494

Based on Vesic (1975)

EXAMPLE 7.3

Refer to Figure 7.8a. A foundation 1.5 m × 1 m is located at a depth (D_f) of 1 m in a clay. A softer clay layer is located at a depth (H) of 1 m measured from the bottom of the foundation. Given:

For the top clay layer,

Undrained shear strength = 120 kN/m^2
Unit weight = 16.8 kN/m^3

For the bottom clay layer,

Undrained shear strength = 48 kN/m^2
Unit weight = 16.2 kN/m^3

Determine the gross allowable load for the foundation with a factor of safety of 4. Use Eq. (7.11).

SOLUTION

From Eq. (7.11),

$$q_u = c_{u(1)} N_c F_{cs} F_{cd} + q$$

$$c_{u(1)} = 120 \text{ kN/m}^2$$

$$q = \gamma D_f = (16.8)(1) = 16.8 \text{ kN/m}^2$$

$$\frac{c_{u(2)}}{c_{u(1)}} = \frac{48}{120} = 0.4; \frac{H}{B} = \frac{1}{1} = 1$$

From Figure 7.8b, for $H/B = 1$ and $c_{u(2)}/c_{u(1)} = 0.4$, the value of N_c is equal to 4.6. From Table 6.3,

$$F_{cs} = 1 + \left(\frac{B}{L}\right)\left(\frac{N_q}{N_c}\right) = 1 + \left(\frac{1}{1.5}\right)\left(\frac{1}{4.6}\right) = 1.145$$

$$F_{cd} = 1 + 0.4\frac{D_f}{B} = 1 + 0.4\left(\frac{1}{1}\right) = 1.4$$

Thus,

$$q_u = (120)(4.6)(1.145)(1.4) + 16.8 = 884.8 + 16.8 = 901.6 \text{ kN/m}^2$$

So

$$q_{all} = \frac{q_u}{FS} = \frac{901.6}{4} = 225.4 \text{ kN/m}^2$$

Total allowable load = $(q_{all})(B \times L) = (225.4)(1 \times 1.5) =$ **338.1 kN**

7.4 Bearing Capacity of Layered Soil: Stronger Soil Underlain by Weaker Soil ($c' - \phi'$ soil)

The bearing capacity equations presented in Chapter 6 involve cases in which the soil supporting the foundation is homogeneous and extends to a considerable depth. The cohesion, angle of friction, and unit weight of soil were assumed to remain constant for the bearing capacity analysis. However, in practice, layered soil profiles are often encountered. In such instances, the failure surface at ultimate load may extend through two or more soil layers, making it difficult to determine the ultimate bearing capacity in layered soil. This section features the procedure for estimating

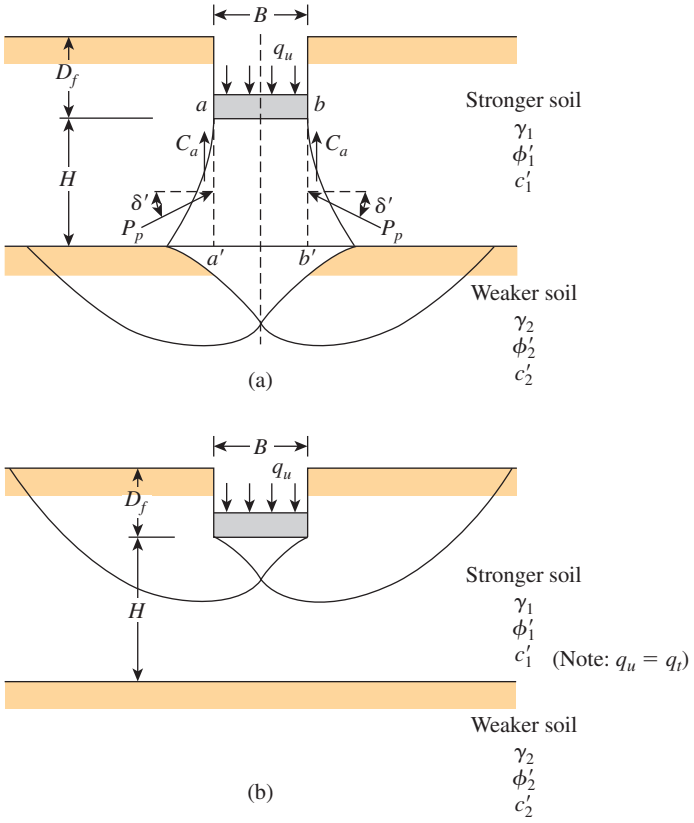


FIGURE 7.9 Bearing capacity of a continuous foundation on layered soil: (a) small H; and (b) large H

the bearing capacity for layered soil proposed by Meyerhof and Hanna (1978) and Meyerhof (1974) in a $c'-\phi'$ soil.

Figure 7.9 shows a shallow, continuous foundation supported by a *stronger soil layer*, underlain by a weaker soil that extends to a large depth. For the two soil layers, the physical parameters are as follows:

	Soil properties		
Layer	**Unit weight**	**Friction angle**	**Cohesion**
Top	γ_1	ϕ_1'	c_1'
Bottom	γ_2	ϕ_2'	c_2'

At ultimate load per unit area (q_u), the failure surface in soil will be as shown in the figure. If the depth H is relatively small compared with the foundation width B, a punching shear failure will occur in the top soil layer, followed by a general shear failure in the bottom soil layer. This is shown in Figure 7.9a. However, if the depth H is relatively large, then the failure surface will be completely located in the top soil layer with no influence from the weaker bottom layer, giving the maximum possible value for the ultimate bearing capacity q_t. This is shown in Figure 7.9b.

The ultimate bearing capacity for this problem, as shown in Figure 7.9a, can be given as

$$q_u = q_b + \frac{2(C_a + P_p \sin \delta')}{B} - \gamma_1 H \tag{7.14}$$

where

B = width of the foundation

C_a = adhesive force

P_p = passive force per unit length of the faces aa' and bb'

q_b = bearing capacity of the bottom soil layer

δ' = inclination of the passive force P_p with the horizontal

Note that, in Eq. (7.14),

$$C_a = c'_a H$$

where c'_a is the adhesion

Equation (7.14) can be simplified to the form

$$q_u = q_b + \frac{2c'_a H}{B} + \gamma_1 H^2 \left(1 + \frac{2D_f}{H}\right) \frac{K_{pH} \tan \delta'}{B} - \gamma_1 H \tag{7.15}$$

where K_{pH} is the horizontal component of passive earth pressure coefficient.

However, let

$$K_{pH} \tan \delta' = K_s \tan \phi'_1 \tag{7.16}$$

where K_s is the punching shear coefficient. Then,

$$q_u = q_b + \frac{2c'_a H}{B} + \gamma_1 H^2 \left(1 + \frac{2D_f}{H}\right) \frac{K_s \tan \phi'_1}{B} - \gamma_1 H \tag{7.17}$$

The punching shear coefficient, K_s, is a function of q_2/q_1 and ϕ'_1, or, specifically,

$$K_s = f\left(\frac{q_2}{q_1}, \phi'_1\right)$$

Note that q_1 and q_2 are the ultimate bearing capacities of a continuous foundation of width B under vertical load on the surfaces of homogeneous thick beds of upper and lower soil, or

$$q_1 = c'_1 N_{c(1)} + \tfrac{1}{2}\gamma_1 B N_{\gamma(1)} \tag{7.18}$$

and

$$q_2 = c'_2 N_{c(2)} + \tfrac{1}{2}\gamma_2 B N_{\gamma(2)} \tag{7.19}$$

where

$N_{c(1)}$, $N_{\gamma(1)}$ are the bearing capacity factors for friction angle ϕ'_1 (Table 6.2)

$N_{c(2)}$, $N_{\gamma(2)}$ are the bearing capacity factors for friction angle ϕ'_2 (Table 6.2)

Observe that, for the top layer to be a stronger soil, q_2/q_1 should be less than unity.

The variation of K_s with q_2/q_1 and ϕ'_1 is shown in Figure 7.10. The variation of c'_a/c'_1 with q_2/q_1 is shown in Figure 7.11. If the height H is relatively large, then the failure surface in soil will be completely located in the stronger upper-soil layer (Figure 7.9b). For this case,

$$q_u = q_t = c'_1 N_{c(1)} + q N_{q(1)} + \tfrac{1}{2}\gamma_1 B N_{\gamma(1)} \tag{7.20}$$

where $N_{c(1)}$, $N_{q(1)}$, and $N_{\gamma(1)}$ are the bearing capacity factors for $\phi' = \phi'_1$ (Table 6.2) and $q = \gamma_1 D_f$.

Combining Eqs. (7.17) and (7.20) yields

$$q_u = q_b + \frac{2c'_a H}{B} + \gamma_1 H^2 \left(1 + \frac{2D_f}{H}\right) \frac{K_s \tan \phi'_1}{\mathrm{B}} - \gamma_1 H \le q_t \tag{7.21}$$

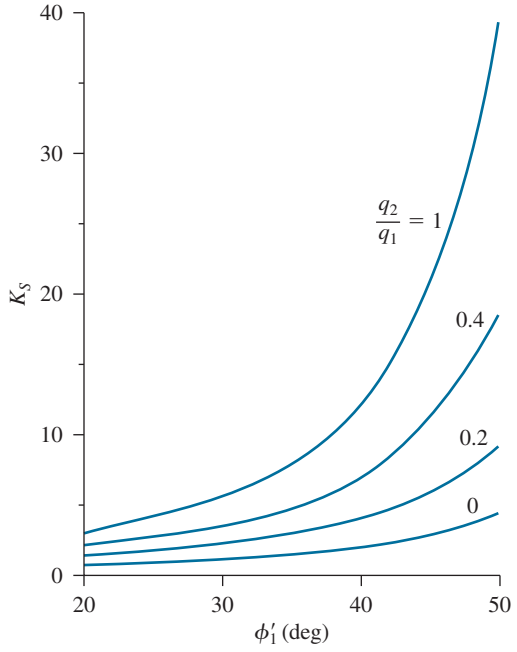


FIGURE 7.10 Meyerhof and Hanna's punching shear coefficient K_s

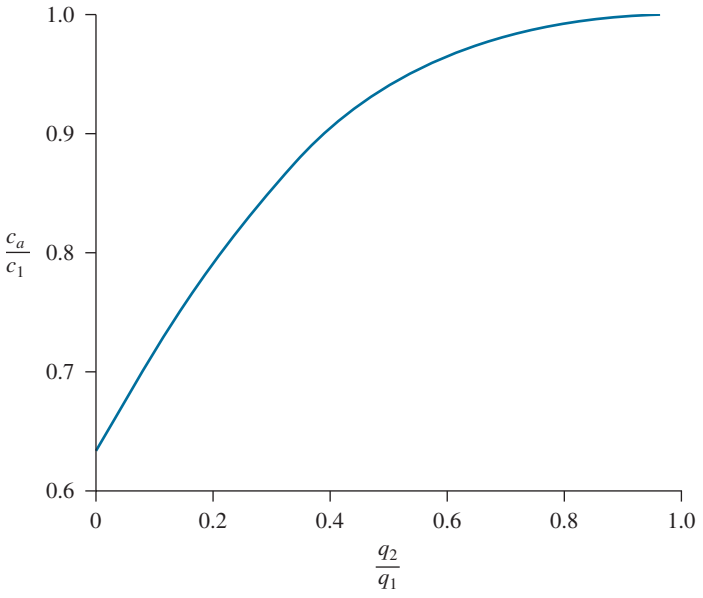


FIGURE 7.11 Variation of c_a/c_1 with q_2/q_1 based on the theory of Meyerhof and Hanna (1978)

Here q_t, determined from the properties of the upper layer (neglecting the influence of the lower layer), is the upper limit for the ultimate bearing capacity value calculated using Eq. (7.21). The depth factors are not considered here.

For rectangular foundations, the preceding equation can be extended to the form

$$q_u = q_b + \left(1 + \frac{B}{L}\right)\left(\frac{2c_a' H}{B}\right) + \gamma_1 H^2 \left(1 + \frac{B}{L}\right)\left(1 + \frac{2D_f}{H}\right)\left(\frac{K_s \tan \phi_1'}{B}\right) - \gamma_1 H \le q_t \tag{7.22}$$

where

$$q_b = c'_2 N_{c(2)} F_{cs(2)} + \gamma_1 (D_f + H)\, N_{q(2)} F_{qs(2)} + \frac{1}{2}\gamma_2 B N_{\gamma(2)} F_{\gamma s(2)} \tag{7.23}$$

and

$$q_t = c'_1 N_{c(1)} F_{cs(1)} + \gamma_1 D_f N_{q(1)} F_{qs(1)} + \frac{1}{2}\gamma_1 B N_{\gamma(1)} F_{\gamma s(1)} \tag{7.24}$$

in which

$F_{cs(1)}, F_{qs(1)}, F_{\gamma s(1)}$ = shape factors with respect to top soil layer (Table 6.3)
$F_{cs(2)}, F_{qs(2)}, F_{\gamma s(2)}$ = shape factors with respect to bottom soil layer (Table 6.3)

SPECIAL CASES

1. *The top layer is strong sand and the weaker bottom layer is saturated soft clay* ($\phi_2 = 0$). From Eqs. (7.22), (7.23), and (7.24),

$$q_b = \left(1 + 0.2\frac{B}{L}\right) 5.14 c_{u(2)} + \gamma_1 (D_f + H) \tag{7.25}$$

and

$$q_t = \gamma_1 D_f N_{q(1)} F_{qs(1)} + \tfrac{1}{2}\gamma_1 B N_{\gamma(1)} F_{\gamma s(1)} \tag{7.26}$$

Hence,

$$\begin{aligned} q_u = {} & \left(1 + 0.2\frac{B}{L}\right) 5.14 c_{u(2)} + \gamma_1 H^2 \left(1 + \frac{B}{L}\right)\left(1 + \frac{2D_f}{H}\right)\frac{K_s \tan \phi'_1}{B} \\ & + \gamma_1 D_f \le \gamma_1 D_f N_{q(1)} F_{qs(1)} + \frac{1}{2}\gamma_1 B N_{\gamma(1)} F_{\gamma s(1)} \end{aligned} \tag{7.27}$$

where $c_{u(2)}$ is the undrained cohesion.

For a determination of K_s from Figure 7.10,

$$\frac{q_2}{q_1} = \frac{c_{u(2)} N_{c(2)}}{\frac{1}{2}\gamma_1 B N_{\gamma(1)}} = \frac{5.14 c_{u(2)}}{0.5 \gamma_1 B N_{\gamma(1)}} \tag{7.28}$$

2. *The top layer is stronger sand and the bottom layer is weaker sand* ($c'_1 = 0$, $c'_2 = 0$). The ultimate bearing capacity can be given as

$$\begin{aligned} q_u = {} & \left[\gamma_1 (D_f + H) N_{q(2)} F_{qs(2)} + \frac{1}{2}\gamma_2 B N_{\gamma(2)} F_{\gamma s(2)}\right] \\ & + \gamma_1 H^2 \left(1 + \frac{B}{L}\right)\left(1 + \frac{2D_f}{H}\right)\frac{K_s \tan \phi'_1}{B} - \gamma_1 H \le q_t \end{aligned} \tag{7.29}$$

where

$$q_t = \gamma_1 D_f N_{q(1)} F_{qs(1)} + \frac{1}{2}\gamma_1 B N_{\gamma(1)} F_{\gamma s(1)} \tag{7.30}$$

Then

$$\frac{q_2}{q_1} = \frac{\frac{1}{2}\gamma_2 B N_{\gamma(2)}}{\frac{1}{2}\gamma_1 B N_{\gamma(1)}} = \frac{\gamma_2 N_{\gamma(2)}}{\gamma_1 N_{\gamma(1)}} \tag{7.31}$$

3. *The top layer is stronger saturated clay* ($\phi_1 = 0$) *and the bottom layer is weaker saturated clay* ($\phi_2 = 0$). The ultimate bearing capacity can be given as

$$q_u = \left(1 + 0.2\frac{B}{L}\right)5.14c_{u(2)} + \left(1 + \frac{B}{L}\right)\left(\frac{2c_a H}{B}\right) + \gamma_1 D_f \le q_t \tag{7.32}$$

where

$$q_t = \left(1 + 0.2\frac{B}{L}\right)5.14c_{u(1)} + \gamma_1 D_f \tag{7.33}$$

and $c_{u(1)}$ and $c_{u(2)}$ are undrained cohesions. For this case,

$$\frac{q_2}{q_1} = \frac{5.14c_{u(2)}}{5.14c_{u(1)}} = \frac{c_{u(2)}}{c_{u(1)}} \tag{7.34}$$

EXAMPLE 7.4

Refer to Figure 7.9a and consider the case of a continuous foundation with $B = 2$ m, $D_f = 1.2$ m, and $H = 1.5$ m. The following are given for the two soil layers:

Top sand layer:

Unit weight $\gamma_1 = 17.5$ kN/m^3
$\phi_1' = 40°$
$c_1' = 0$

Bottom clay layer:

Unit weight $\gamma_2 = 16.5$ kN/m^3
$\phi_2' = 0$
$c_{u(2)} = 30$ kN/m^2

Determine the gross ultimate load per unit length of the foundation.

SOLUTION

For this case, Eqs. (7.27) and (7.28) apply. For $\phi_1' = 40°$, from Table 6.2, $N_\gamma = 109.41$ and

$$\frac{q_2}{q_1} = \frac{c_{u(2)}N_{c(2)}}{0.5\gamma_1 B N_{\gamma(1)}} = \frac{(30)(5.14)}{(0.5)(17.5)(2)(109.41)} = 0.081$$

From Figure 7.10, for $c_{u(2)}N_{c(2)}/0.5\gamma_1 B N_{\gamma(1)} = 0.081$ and $\phi_1' = 40°$, the value of $K_s \approx 2.5$. Equation (7.27) then gives

$$\begin{aligned} q_u &= \left[1 + (0.2)\left(\frac{B}{L}\right)\right]5.14c_{u(2)} + \left(1 + \frac{B}{L}\right)\gamma_1 H^2\left(1 + \frac{2D_f}{H}\right)K_s\frac{\tan\phi_1'}{\mathrm{B}} + \gamma_1 D_f \\ &= [1 + (0.2)(0)](5.14)(30) + (1 + 0)(17.5)(1.5)^2 \\ &\quad \times \left[1 + \frac{(2)(1.2)}{1.5}\right](2.5)\frac{\tan 40}{2.0} + (17.5)(1.2) \\ &= 154.2 + 107.4 + 21 = 282.6 \text{ kN/m}^2 \end{aligned}$$

Again, from Eq. (7.26),

$$q_t = \gamma_1 D_f N_{q(1)} F_{qs(1)} + \frac{1}{2}\gamma_1 B N_{\gamma(1)} F_{\gamma s(1)}$$

From Table 6.2, for $\phi_1' = 40°$, $N_\gamma = 109.4$ and $N_q = 64.20$.
From Table 6.3,

$$F_{qs(1)} = 1 + \left(\frac{B}{L}\right)\tan\phi_1' = 1 + (0)\tan 40 = 1$$

and

$$F_{\gamma s(1)} = 1 - 0.4\frac{B}{L} = 1 - (0.4)(0) = 1$$

so that

$$q_t = (17.5)(1.2)(64.20)(1) + \left(\frac{1}{2}\right)(17.5)(2)(109.4)(1) = 3262.7 \text{ kN/m}^2$$

Hence,

$$q_u = 282.6 \text{ kN/m}^2$$

$$Q_u = (282.6)(B) = (282.6)(2) = \mathbf{565.2 \text{ kN/m}}$$

■

EXAMPLE 7.5

A foundation 1.5 m × 1 m is located at a depth, D_f, of 1 m in a stronger clay. A softer clay layer is located at a depth, H, of 1 m measured from the bottom of the foundation. For the top clay layer,

Undrained shear strength = 120 kN/m^2
Unit weight = 16.8 kN/m^3

and for the bottom clay layer,

Undrained shear strength = 48 kN/m^2
Unit weight = 16.2 kN/m^3

Determine the gross allowable load for the foundation with an FS of 4. Use Eqs. (7.32), (7.33), and (7.34).

SOLUTION

For this problem, Eqs. (7.32), (7.33), and (7.34) will apply, or

$$q_u = \left(1 + 0.2\frac{B}{L}\right)5.14c_{u(2)} + \left(1 + \frac{B}{L}\right)\left(\frac{2c_a H}{B}\right) + \gamma_1 D_f$$

$$\leq \left(1 + 0.2\frac{B}{L}\right)5.14c_{u(1)} + \gamma_1 D_f$$

Given:

$B = 1$ m $\quad H = 1$ m $\quad D_f = 1$ m
$L = 1.5$ m $\quad \gamma_1 = 16.8$ kN/m^3

From Figure 7.11, $c_{u(2)}/c_{u(1)} = 48/120 = 0.4$, the value of $c_a/c_{u(1)} \approx 0.9$, so

$$c_a = (0.9)(120) = 108 \text{ kN/m}^2$$

$$q_u = \left[1 + (0.2)\left(\frac{1}{1.5}\right)\right](5.14)(48) + \left(1 + \frac{1}{1.5}\right)\left[\frac{(2)(108)(1)}{1}\right] + (16.8)(1)$$

$$= 279.6 + 360 + 16.8 = 656.4 \text{ kN/m}^2$$

Check: From Eq. (7.33),

$$q_t = \left[1 + (0.2)\left(\frac{1}{1.5}\right)\right](5.14)(120) + (16.8)(1)$$

$$= 699 + 16.8 = 715.8 \text{ kN/m}^2$$

Thus $q_u = 656.4$ kN/m^2 (q_t is always larger than q_u) and

$$q_{all} = \frac{q_u}{FS} = \frac{656.4}{4} = 164.1 \text{ kN/m}^2$$

The total allowable load is

$$(q_{all})(1 \times 1.5) = \mathbf{246.15\ kN}$$

Note: This is the same problem as in Example 7.3. The allowable load is about 40% lower than that calculated in Example 7.3. This is due to the different failure surface in the soil assumed at the ultimate load.

■

7.5 Bearing Capacity of Layered Soil: Weaker Soil Underlain by Stronger Soil

When a foundation is supported by a weaker soil layer underlain by a stronger layer (Figure 7.12a), the ratio of q_2/q_1 defined by Eqs. (7.18) and (7.19) will be greater than one. Also, if H/B is relatively small, as shown in the left-hand half of Figure 7.12a, the failure surface in soil at ultimate load will pass through both soil layers. However, for larger H/B ratios, the failure surface will be fully located in the weaker top soil layer, as shown in the right-hand half of Figure 7.12a. For this condition, the ultimate bearing capacity (Meyerhof, 1974; Meyerhof and Hanna, 1978) can be given by the empirical equation

$$q_u = q_t + (q_b - q_t)\left(\frac{H}{D}\right)^2 \geq q_t \tag{7.35}$$

where

D = depth of failure surface beneath the foundation in the thick bed of the upper weaker soil layer

q_t = ultimate bearing capacity in a thick bed of the upper soil layer

q_b = ultimate bearing capacity in a thick bed of the lower soil layer

So

$$q_t = c_1' N_{c(1)} F_{cs(1)} + \gamma_1 D_f N_{q(1)} F_{qs(1)} + \frac{1}{2}\gamma_1 B N_{\gamma(1)} F_{\gamma s(1)} \tag{7.36}$$

and

$$q_b = c_2' N_{c(2)} F_{cs(2)} + \gamma_2 D_f N_{q(2)} F_{qs(2)} + \frac{1}{2}\gamma_2 B N_{\gamma(2)} F_{\gamma s(2)} \tag{7.37}$$

where

$N_{c(1)}, N_{q(1)}, N_{\gamma(1)}$ = bearing capacity factors corresponding to the soil friction angle ϕ_1'

$N_{c(2)}, N_{q(2)}, N_{\gamma(2)}$ = bearing capacity factors corresponding to the soil friction angle ϕ_2'

$F_{cs(1)}, F_{qs(1)}, F_{\gamma s(1)}$ = shape factors corresponding to the soil friction angle ϕ_1'

$F_{cs(2)}, F_{qs(2)}, F_{\gamma s(2)}$ = shape factors corresponding to the soil friction angle ϕ_2'

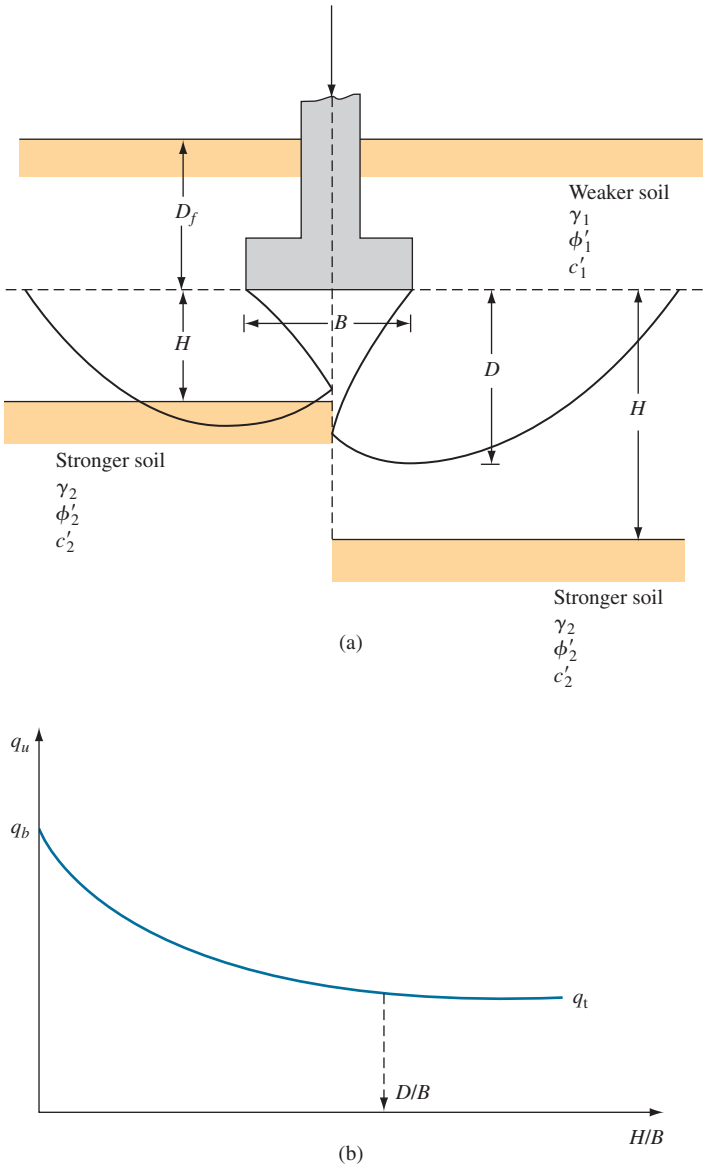


FIGURE 7.12 (a) Foundation on weaker soil layer underlain by stronger sand layer; (b) nature of variation of q_u with H/B

Meyerhof and Hanna (1978) suggested that

- $D \approx B$ for loose sand and clay
- $D \approx 2B$ for dense sand

Equations (7.35), (7.36), and (7.37) imply that the maximum and minimum values of q_u will be q_b and q_t, respectively, as shown in Figure 7.12b, and q_u lies between the two.

EXAMPLE 7.6

Refer to Figure 7.12a. For a layered saturated-clay profile, given: $L = 6$ ft, $B = 4$ ft, $D_f = 3$ ft, $H = 2$ ft, $\gamma_1 = 110$ lb/ft^3, $\phi_1 = 0$, $c_{u(1)} = 1200$ lb/ft^2, $\gamma_2 = 125$ lb/ft^3, $\phi_2 = 0$, and $c_{u(2)} = 2500$ lb/ft^2. Determine the ultimate bearing capacity of the foundation.

SOLUTION

From Eqs. (7.18) and (7.19),

$$\frac{q_2}{q_1} = \frac{c_{u(2)}N_c}{c_{u(1)}N_c} = \frac{c_{u(2)}}{c_{u(1)}} = \frac{2500}{1200} = 2.08 > 1$$

So, Eq. (7.35) will apply.

From Eqs. (7.36) and (7.37) with $\phi_1 = \phi_2 = 0$,

$$q_t = \left(1 + 0.2\frac{B}{L}\right)N_c c_{u(1)} + \gamma_1 D_f$$

$$= \left[1 + (0.2)\left(\frac{4}{6}\right)\right](5.14)(1200) + (3)(110) = 6990.4 + 330 = 7320.4 \text{ lb/ft}^2$$

and

$$q_b = \left(1 + 0.2\,\frac{B}{L}\right)N_c c_{u(2)} + \gamma_2 D_f$$

$$= \left[1 + (0.2)\left(\frac{4}{6}\right)\right](5.14)(2500) + (3)(125)$$

$$= 14{,}563.3 + 375 = 14{,}938.3 \text{ lb/ft}^2$$

From Eq. (7.35),

$$q_u = q_t + (q_b - q_t)\left(\frac{H}{D}\right)^2$$

$$D \approx B$$

$$q_u = 7320.4 + (14{,}938.3 - 7320.4)\left(\frac{2}{4}\right)^2 \approx 9225 \text{ lb/ft}^2 > q_t$$

Hence,

$$q_u = \mathbf{9225\ lb/ft^2}$$

EXAMPLE 7.7

Solve Example 7.6 using Vesic's theory [Eq. (7.12)]. For the value of m, use Table 7.3.

SOLUTION

From Eq. (7.12),

$$q_u = c_{u(1)} m N_c F_{cs} F_{cd} + q$$

From Table 6.3,

$$F_{cs} = 1 + \left(\frac{B}{L}\right)\left(\frac{N_q}{N_c}\right) = 1 + \left(\frac{4}{6}\right)\left(\frac{1}{5.14}\right) = 1.13$$

$$F_{cd} = 1 + 0.4\left(\frac{D_f}{B}\right) = 1 + 0.4\left(\frac{3}{4}\right) = 1.3$$

From Table 7.3, for $c_{u(1)}/c_{u(2)} = 1200/2500 = 0.48$ and $H/B = 2/4 = 0.5$, the value of $m \approx 1$. Thus,

$$q_u = (1200)(1)(5.14)(1.13)(1.3) + (110)(3) = \mathbf{9390\ lb/ft^2}$$

7.6 Continuous Foundation on Weak Clay with a Granular Trench

In practice, there are several techniques to improve the load-bearing capacity and settlement of shallow foundations on weak compressible soil layers. One of those techniques is the use of a granular trench under a foundation. Figure 7.13 shows a continuous rough foundation on a granular trench made in a weak soil extending to a great depth. The width of the trench is W, the width of the foundation is B, and the depth of the trench is H. The width W of the trench can be smaller or larger than B. The parameters of the stronger trench material and the weak soil for bearing capacity calculation are as follows.

	Trench material	Weak soil
Angle of friction	ϕ_1'	ϕ_2'
Cohesion	c_1'	c_2'
Unit weight	γ_1	γ_2

Madhav and Vitkar (1978) assumed a general shear failure mechanism in the soil under the foundation to analyze the ultimate bearing capacity using the upper-bound limit analysis, and this is shown in Figure 7.13. The failure zone in the soil can be divided into subzones:

1. An active Rankine zone ABC with a wedge angle of ξ
2. A mixed transition zone such as BCD bounded by angle θ_1. CD is an arc of a log spiral
3. A transition zone such as BDF with a central angle θ_2. DF is an arc of a log spiral
4. A Rankine passive zone like BFG

Note that θ_1 and θ_2 are functions of ξ, η, W/B, and ϕ_1.

By using the upper-bound limit analysis theorem, Madhav and Vitkar (1978) expressed the ultimate bearing capacity of the foundation as

$$q_u = c_2' N_{c(T)} + D_f \gamma_2 N_{q(T)} + \left(\frac{\gamma_2 B}{2}\right) N_{\gamma(T)} \tag{7.38}$$

where $N_{c(T)}$, $N_{q(T)}$, $N_{\gamma(T)}$ = bearing-capacity factors with the presence of the trench.

The variations of the bearing-capacity factors [that is, $N_{c(T)}$, $N_{q(T)}$, and $N_{\gamma(T)}$] for purely granular trench soil ($c_1' = 0$) in a soft saturated clay (with $\phi_2 = 0$ and $c_2' = c_u$) determined by Madhav and Vitkar (1978) are given in Figures 7.14, 7.15, and 7.16.

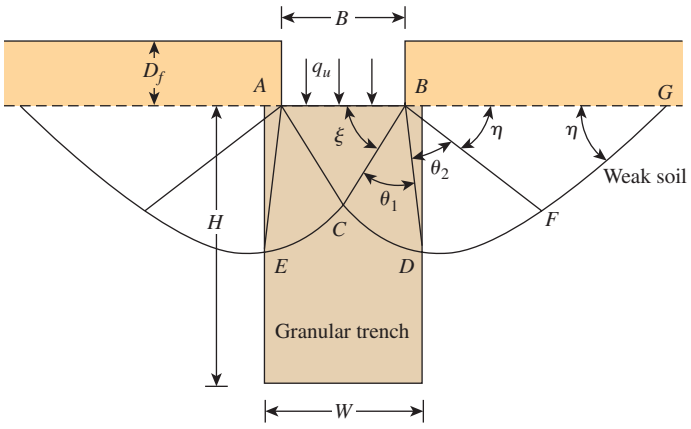


FIGURE 7.13 Continuous rough foundation on weak soil with a granular trench

The values of $N_{q(T)}$ given in Figure 7.16 are for $\gamma_1/\gamma_2 = 1$. In an actual case, the ratio γ_1/γ_2 may be different than one; however, the error for this assumption is less than 10%.

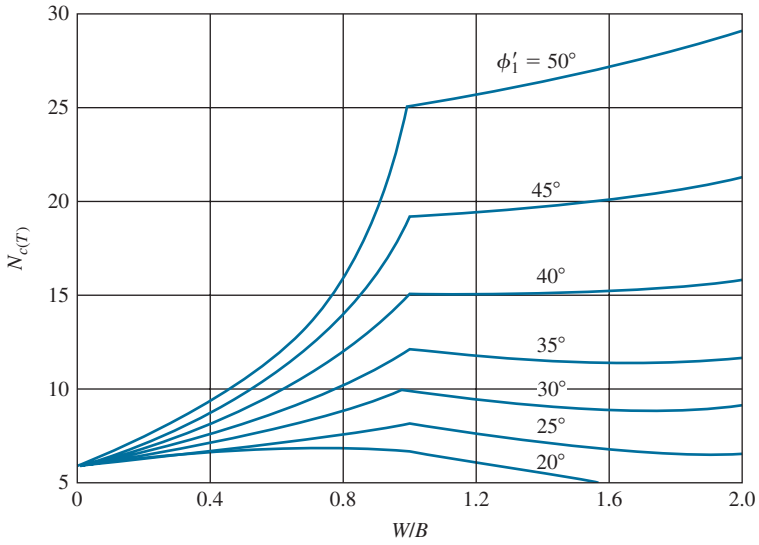


FIGURE 7.14 Madhav and Vitkar's bearing-capacity factor $N_{c(T)}$

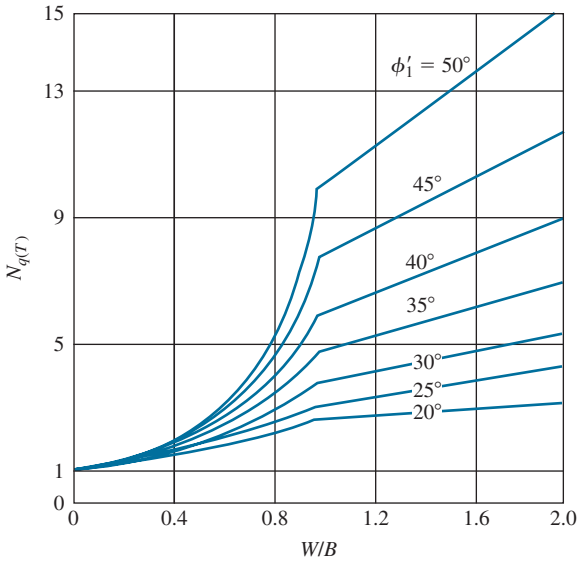


FIGURE 7.15 Madhav and Vitkar's bearing-capacity factor $N_{q(T)}$

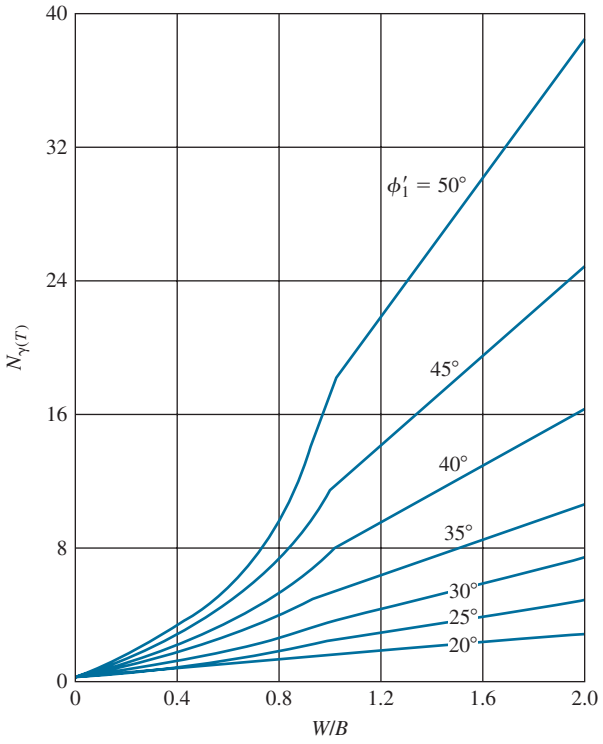


FIGURE 7.16 Madhav and Vitkar's bearing-capacity factor $N_{\gamma(T)}$

7.7 Closely Spaced Foundations—Effect on Ultimate Bearing Capacity

In Chapter 6, theories relating to the ultimate bearing capacity of single rough continuous foundations supported by a homogeneous soil extending to a great depth were discussed. However, if foundations are placed close to each other with similar soil conditions, the ultimate bearing capacity of each foundation may change due to the interference effect of the failure surface in the soil. This was theoretically investigated by Stuart (1962) for *granular soil*. It was assumed that the geometry of the rupture surface in the soil mass would be the same as that assumed by Terzaghi (Figure 6.7). According to Stuart, the following conditions may arise (Figure 7.17):

Case I. (Figure 7.17a) If the center-to-center spacing of the two foundations is $x \geq x_1$, the rupture surface in the soil under each foundation will not overlap. So the ultimate bearing capacity of each continuous foundation can be given by Terzaghi's equation [Eq. (6.10)]. For ($c' = 0$),

$$q_u = qN_q + \frac{1}{2}\gamma BN_\gamma \tag{7.39}$$

where N_q, N_γ are Terzaghi's bearing capacity factors (Table 6.1).

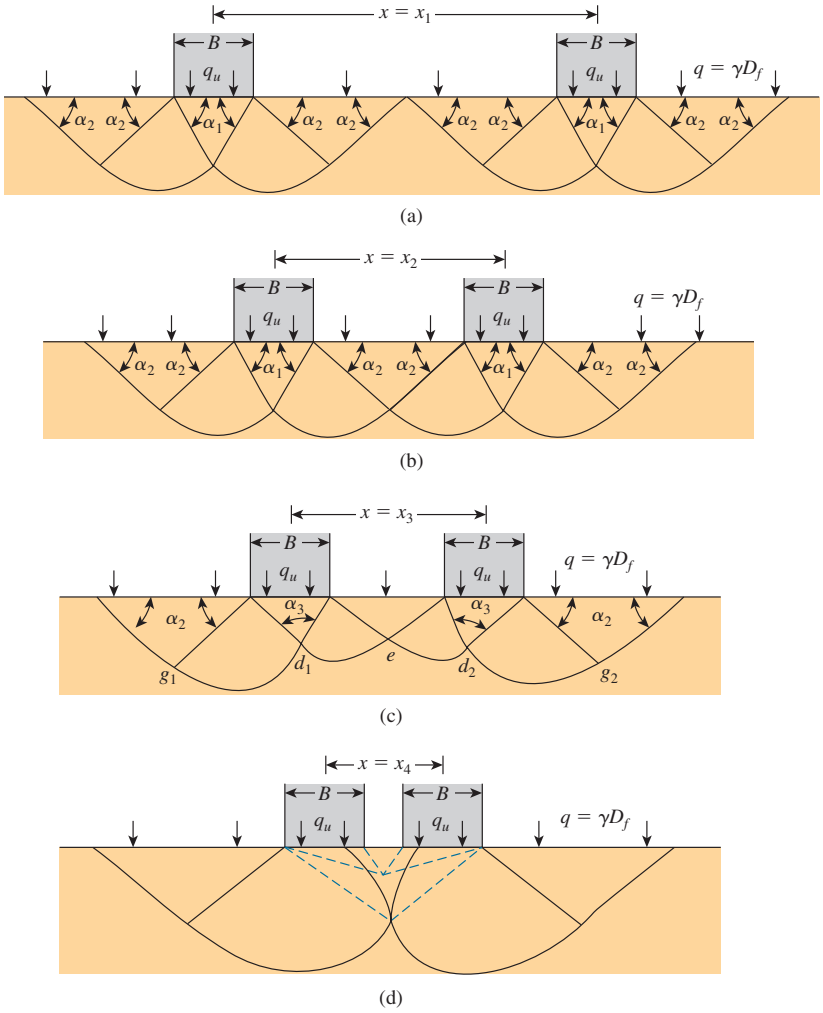


FIGURE 7.17 Assumptions for the failure surface in granular soil under two closely spaced rough continuous foundations
(*Note:* $\alpha_1 = \phi'$, $\alpha_2 = 45 - \phi'/2$, $\alpha_3 = 180 - 2\phi'$)

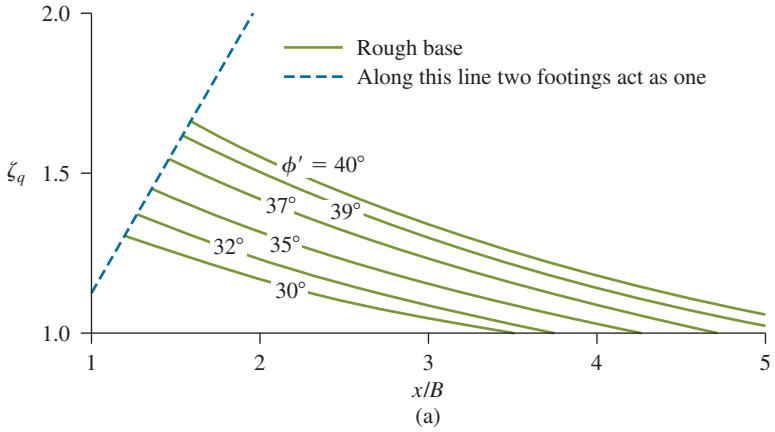
Case II. (Figure 7.17b) If the center-to-center spacing of the two foundations ($x = x_2 < x_1$) is such that the Rankine passive zones between the two just overlap, then the magnitude of q_u will still be given by Eq. (7.39). However, the foundation settlement at ultimate load will change (compared to the case of an isolated foundation).

Case III. (Figure 7.17c) This is the case where the center-to-center spacing of the two continuous foundations is $x = x_3 < x_2$. Note that the triangular wedges in the soil under the foundations make angles of $180° - 2\phi'$ at points d_1 and d_2. The arcs of the logarithmic spirals d_1g_1 and d_1e are tangent to each other at d_1. Similarly, the arcs of the logarithmic spirals d_2g_2 and d_2e are tangent to each other at d_2. For this case, the ultimate bearing capacity of each foundation can be given as ($c' = 0$)

$$q_u = qN_q\zeta_q + \frac{1}{2}\gamma BN_\gamma\,\zeta_\gamma \tag{7.40}$$

where ζ_q, ζ_γ are the efficiency ratios.

The efficiency ratios are functions of x/B and soil friction angle ϕ'. The theoretical variations of ζ_q and ζ_γ are given in Figure 7.18.



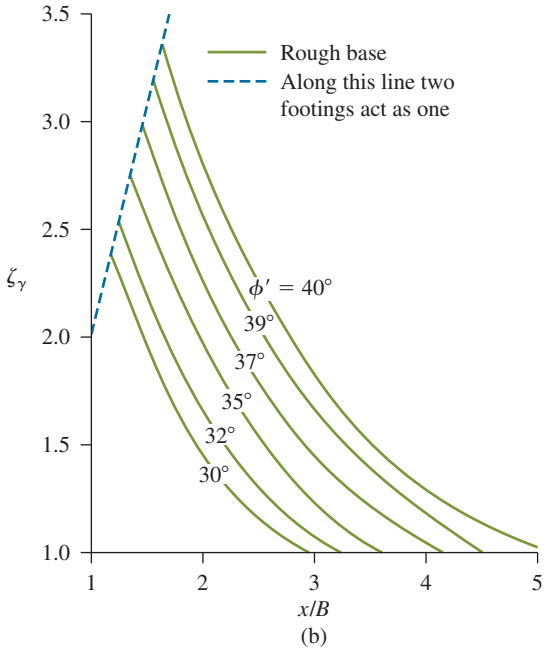


FIGURE 7.18 Variation of efficiency ratios with x/B and ϕ'

Case IV. (Figure 7.17d): If the spacing of the foundation is further reduced such that $x = x_4 < x_3$, blocking will occur and the pair of foundations will act as a single foundation. The soil between the individual units will form an inverted arch which travels down with the foundation as the load is applied. When the two foundations touch, the zone of arching disappears and the system behaves as a single foundation with a width equal to $2B$. The ultimate bearing capacity for this case can be given by Eq. (7.39), with B being replaced by $2B$ in the second term.

The ultimate bearing capacity of two continuous foundations spaced close to each other may increase since the efficiency ratios are greater than one. However, when the closely spaced foundations are subjected to a similar load per unit area, the settlement S_e will be larger when compared to that for an isolated foundation.

7.8 Bearing Capacity of Foundations on Top of a Slope

In some instances, shallow foundations need to be constructed on top of a slope. In Figure 7.19, the height of the slope is H, and the slope makes an angle β with the horizontal. The edge of the foundation is located at a distance b from the top of the slope. At ultimate load, q_u, the failure surface will be as shown in the figure.

Meyerhof (1957) developed the following theoretical relation for the ultimate bearing capacity for *continuous foundations*:

$$q_u = c' N_{cq} + \frac{1}{2}\gamma B N_{\gamma q} \tag{7.41}$$

For purely granular soil, $c' = 0$; thus,

$$q_u = \frac{1}{2}\gamma B N_{\gamma q} \tag{7.42}$$

Again, for purely cohesive soil, $\phi = 0$ (the undrained condition); hence,

$$q_u = c_u N_{cq} \tag{7.43}$$

where c_u is the undrained cohesion.

The variations of $N_{\gamma q}$ and N_{cq} defined by Eqs. (7.42) and (7.43) are shown in Figures 7.20 and 7.21, respectively. In using N_{cq} in Eq. (7.43) as given in Figure 7.21, the following points need to be kept in mind:

1. The term

$$N_s = \frac{\gamma H}{c_u} \tag{7.44}$$

   is defined as the stability number.
2. If $B < H$, use the curves for $N_s = 0$.
3. If $B \geq H$, use the curves for the calculated stability number N_s.

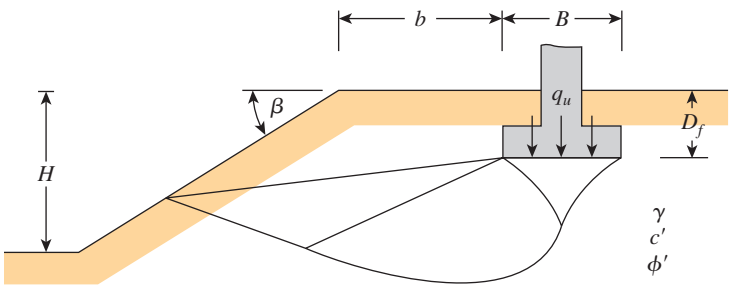


FIGURE 7.19 Shallow foundation on top of a slope

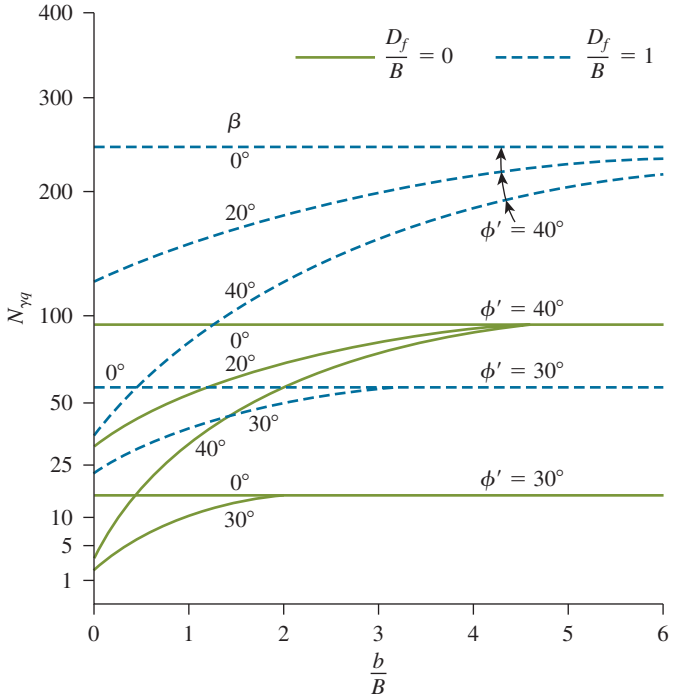


FIGURE 7.20 Meyerhof's bearing capacity factor $N_{\gamma q}$ for granular soil ($c' = 0$)

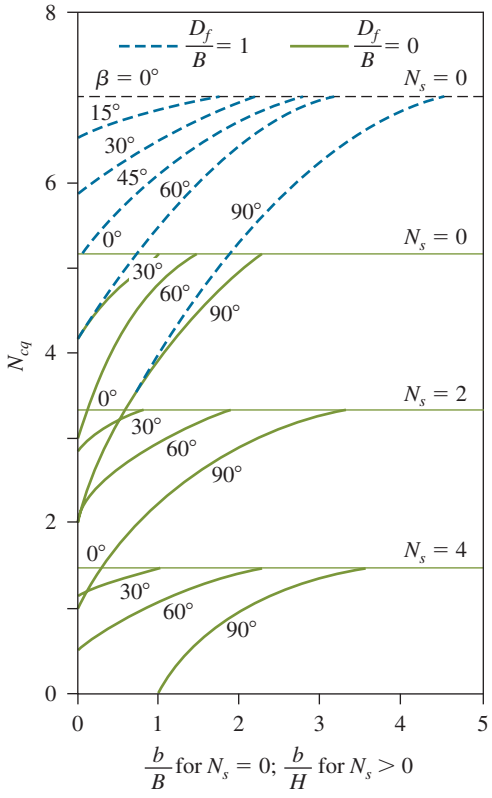


FIGURE 7.21 Meyerhof's bearing capacity factor N_{cq} for purely cohesive soil

EXAMPLE 7.8

In Figure 7.19, for a shallow continuous foundation in a clay, the following data are given: $B = 1.2$ m; $D_f = 1.2$ m; $b = 0.8$ m; $H = 6.2$ m; $\beta = 30°$; unit weight of soil $= 17.5$ kN/m^3; $\phi = 0$; and $c_u = 50$ kN/m^2. Determine the gross allowable bearing capacity with a factor of safety FS $= 4$.

SOLUTION

Since $B < H$, we will assume the stability number $N_s = 0$. From Eq. (7.43),

$$q_u = c_u N_{cq}$$

We are given that

$$\frac{D_f}{B} = \frac{1.2}{1.2} = 1$$

and

$$\frac{b}{B} = \frac{0.8}{1.2} = 0.67$$

For $\beta = 30°$, $D_f/B = 1$, and $b/B = 0.67$, Figure 7.21 gives $N_{cq} = 6.3$. Hence,

$$q_u = (50)(6.3) = 315 \text{ kN/m}^2$$

and

$$q_{all} = \frac{q_u}{\text{FS}} = \frac{315}{4} = \mathbf{78.8 \text{ kN/m}^2}$$

EXAMPLE 7.9

Figure 7.22 shows a continuous foundation on a slope of a granular soil. Estimate the ultimate bearing capacity.

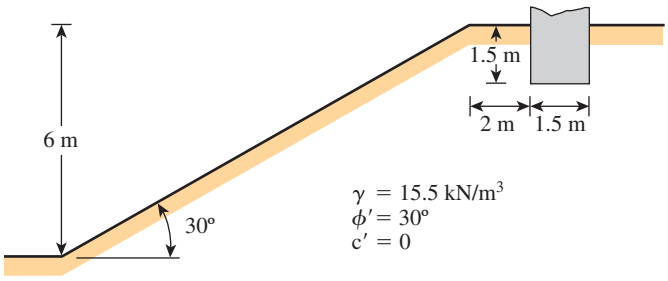


FIGURE 7.22 Foundation on a granular slope

SOLUTION

For granular soil ($c' = 0$), from Eq. (7.42),

$$q_u = \frac{1}{2}\gamma B N_{\gamma q}$$

We are given that $b/B = 2/1.5 = 1.33$, $D_f/B = 1.5/1.5 = 1$, $\phi' = 30°$, and $\beta = 30°$.

From Figure 7.20, $N_{\gamma q} \approx 41$. So,

$$q_u = \frac{1}{2}(15.5)(1.5)(41) = \mathbf{476.6 \text{ kN/m}^2}$$

7.9 Bearing Capacity of Foundations on a Slope

A theoretical solution for the ultimate bearing capacity of a shallow foundation located on the face of a slope was developed by Meyerhof (1957). Figure 7.23 shows the nature of the plastic zone developed under a rough continuous foundation of width B. In Figure 7.23, *abc* is an elastic zone, *acd* is a radial shear zone, and *ade* is a mixed shear zone. Based on this solution, the ultimate bearing capacity can be expressed as

$$q_u = c_u N_{cqs} \text{ (for purely cohesive soil, that is, } \phi = 0) \tag{7.45}$$

and

$$q_u = \tfrac{1}{2}\gamma B N_{\gamma qs} \text{ (for granular soil, that is } c' = 0) \tag{7.46}$$

The variations of N_{cqs} and $N_{\gamma qs}$ with slope angle β are given in Figures 7.24 and 7.25.

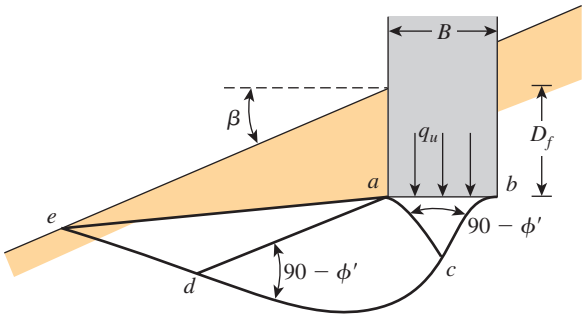


FIGURE 7.23 Nature of plastic zone under a rough continuous foundation on the face of a slope

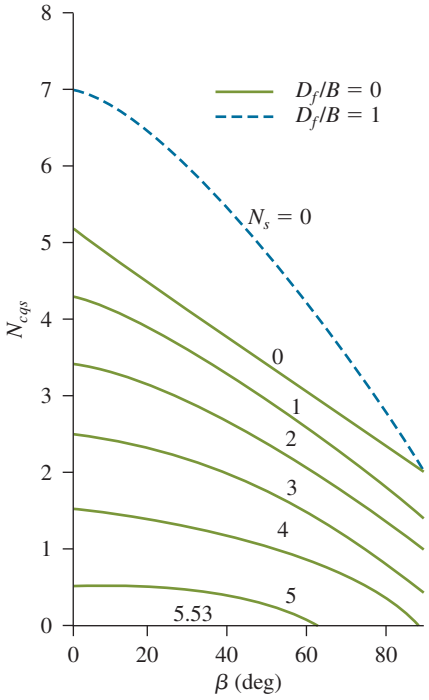


FIGURE 7.24 Variation of N_{cqs} with β. (*Note:* $N_s = \gamma H/c_u$)

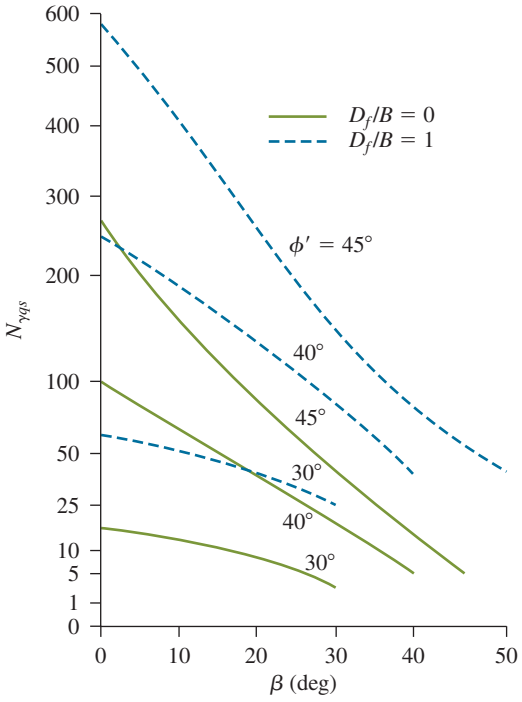


FIGURE 7.25 Variation of $N_{\gamma qs}$ with β

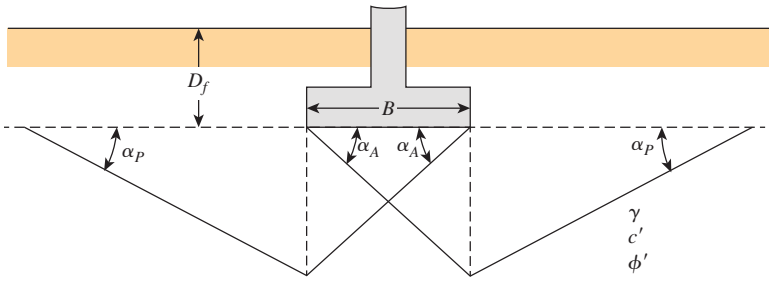


FIGURE 7.26 Failure surface in soil for static bearing-capacity analysis

7.10 Seismic Bearing Capacity and Settlement in Granular Soil

In some instances, shallow foundations may fail during seismic events. Published studies relating to the bearing capacity of shallow foundations in such instances are rare. Richards et al. (1993) developed a seismic bearing-capacity theory that is presented in this section. It needs to be pointed out that this theory has not yet been supported by field data.

Figure 7.26 shows the nature of failure in soil assumed for this analysis for static conditions. Similarly, Figure 7.27 shows the failure surface under earthquake conditions. Note that, in Figures 7.26 and 7.27,

α_A, α_{AE} = inclination angles for active pressure conditions
α_P, α_{PE} = inclination angles for passive pressure conditions

According to this theory, the ultimate bearing capacities for *continuous foundations* in granular soil are

$$\text{Static conditions: } q_u = qN_q + \frac{1}{2}\gamma BN_\gamma \tag{7.47}$$

$$\text{Earthquake conditions: } q_{uE} = qN_{qE} + \frac{1}{2}\gamma BN_{\gamma E} \tag{7.48}$$

where

N_q, N_γ, N_{qE}, $N_{\gamma E}$ = bearing capacity factors

$$q = \gamma D_f$$

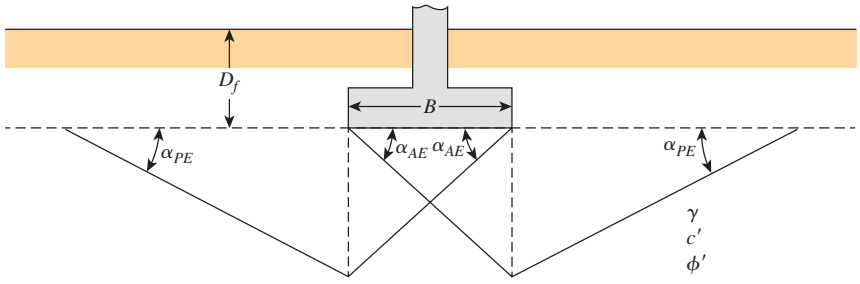


FIGURE 7.27 Failure surface in soil for seismic bearing-capacity analysis

Note that

$$N_q \text{ and } N_\gamma = f(\phi')$$

and

$$N_{qE} \text{ and } N_{\gamma E} = f(\phi', \tan\theta)$$

where

$$\tan\theta = \frac{k_h}{1 - k_v}$$

k_h = horizontal coefficient of acceleration due to an earthquake

k_v = vertical coefficient of acceleration due to an earthquake

The variations of N_q and N_γ with ϕ' are shown in Figure 7.28. Figure 7.29 shows the variations of $N_{\gamma E}/N_\gamma$ and N_{qE}/N_q with $\tan\theta$ and the soil friction angle ϕ'.

For static conditions, bearing-capacity failure can lead to substantial sudden downward movement of the foundation. However, bearing-capacity–related settlement in an earthquake takes place when the ratio $k_h/(1 - k_v)$ reaches a critical value $(k_h/1 - k_v)^*$. If $k_v = 0$, then $(k_h/1 - k_v)^*$ becomes equal to k_h^*. Figure 7.30 shows the variation of k_h^* (for $k_v = 0$ and $c' = 0$; granular soil) with the factor of safety (FS) applied to the ultimate static bearing capacity [Eq. (7.47)], ϕ', and D_f/B.

The settlement of a continuous foundation due to an earthquake (S_{Eq}) can be estimated (Richards et al., 1993) as

$$S_{\text{Eq}}(\text{m}) = 0.174\frac{V^2}{Ag}\left|\frac{k_h^*}{A}\right|^{-4}\tan\alpha_{AE} \tag{7.49}$$

where

V = peak velocity for the design earthquake (m/s)

A = acceleration coefficient for the design earthquake

g = acceleration due to gravity (9.81 m/s^2)

The values of k_h^* and α_{AE} can be obtained from Figures 7.30 and 7.31, respectively.

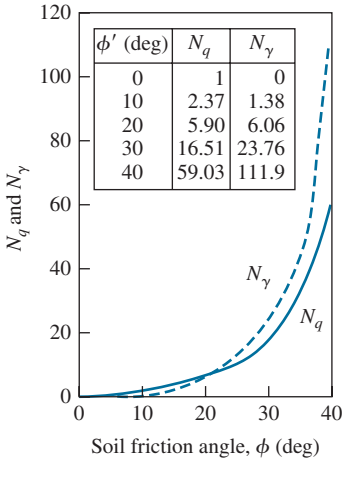


FIGURE 7.28 Variation of N_q and N_γ based on failure surface assumed in Figure 7.26

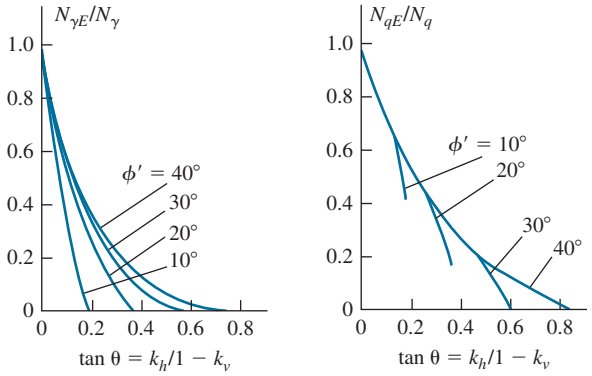


FIGURE 7.29 Variation of $N_{\gamma E}/N_\gamma$ and N_{qE}/N_q (Based on Richards et al., 1993)

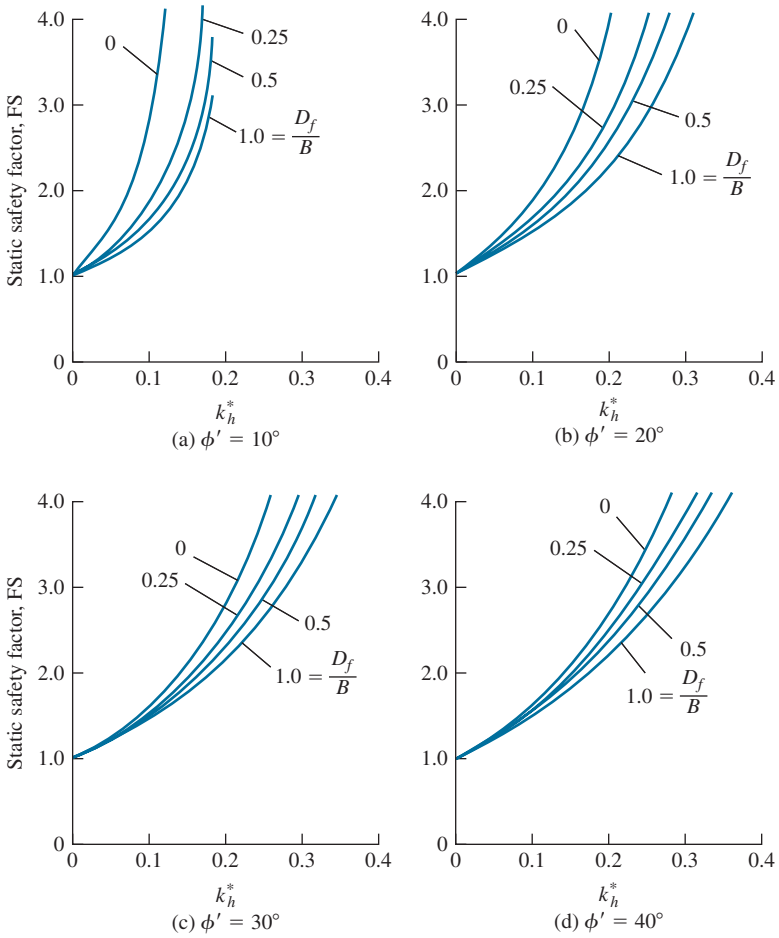


FIGURE 7.30 Critical acceleration k_h^* for $c = 0$ (Based on Richards et al., 1993)

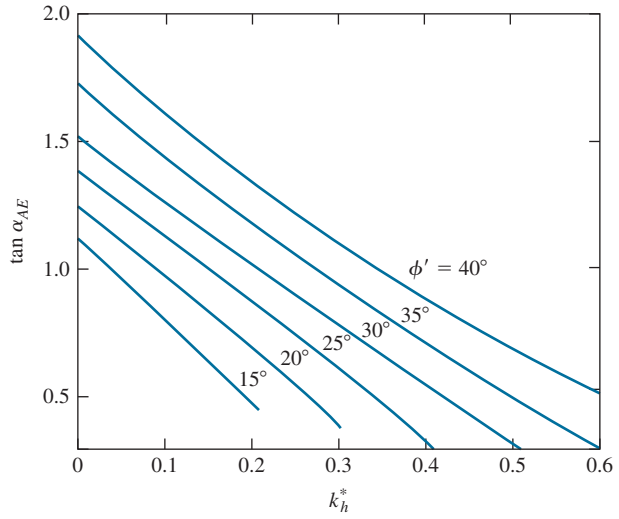


FIGURE 7.31 Variation of tan α_{AE} with k_h^* and soil friction angle, ϕ' (Based on Richards et al., 1993)

EXAMPLE 7.10

A continuous foundation is to be constructed on a sandy soil with $B = 2$ m, $D_f = 1.5$ m, $\gamma = 18$ kN/m^3, and $\phi' = 30°$. Determine the gross ultimate bearing capacity q_{uE}. Assume $k_v = 0$ and $k_h = 0.176$.

SOLUTION

From Figure 7.28, for $\phi' = 30°$, $N_q = 16.51$ and $N_\gamma = 23.76$.

$$\tan\theta = \frac{k_h}{1 - k_v} = 0.176$$

For $\tan\theta = 0.176$, Figure 7.29 gives

$$\frac{N_{\gamma E}}{N_\gamma} = 0.4 \text{ and } \frac{N_{qE}}{N_q} = 0.6$$

Thus,

$$N_{\gamma E} = (0.4)(23.76) = 9.5$$

$$N_{qE} = (0.6)(16.51) = 9.91$$

$$q_{uE} = qN_{qE} + \tfrac{1}{2}\gamma B N_{\gamma E}$$

$$= (1.5 \times 18)(9.91) + \left(\tfrac{1}{2}\right)(18)(2)(9.5) = \mathbf{438.6\ kN/m^2}$$

EXAMPLE 7.11

Refer to Example 7.10. If the design earthquake parameters are $V = 0.4$ m/s and $A = 0.32$, determine the seismic settlement of the foundation. Use FS = 3 for obtaining allowable static bearing capacity.

SOLUTION

For the foundation,

$$\frac{D_f}{B} = \frac{1.5}{2} = 0.75$$

From Figure 7.30c for $\phi' = 30°$, FS = 3, and $D_f/B = 0.75$, the value of $k_h^* = 0.26$. Also from Figure 7.31 for $k_h^* = 0.26$ and $\phi' = 30°$, the value of $\tan\alpha_{AE} = 0.88$. From Eq. (7.49),

$$S_{\text{Eq}} = 0.174\left|\frac{k_h^*}{A}\right|^{-4}\tan\alpha_{AE}\left(\frac{V^2}{Ag}\right)$$

$$= 0.174\frac{(0.4)^2}{(0.32)(9.81)}\left|\frac{0.26}{0.32}\right|^{-4}(0.88) = 0.0179\text{ m} = \mathbf{17.9\ mm}$$

7.11 Foundations on Rock

On some occasions, shallow foundations may have to be built on rocks, as shown in Figure 7.32. For estimation of the ultimate bearing capacity of shallow foundations on rock, we may use Terzaghi's bearing capacity equations

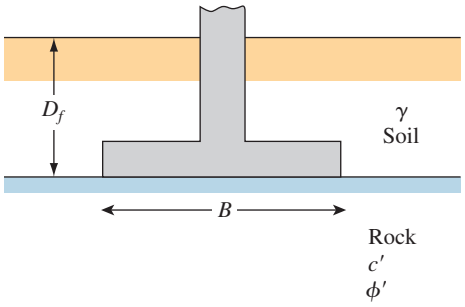


FIGURE 7.32 Foundation on rock

[Eqs. (6.10), (6.19), and (6.20)] with the bearing capacity factors given here (Bowles, 1996; Stagg and Zienkiewicz, 1968):

$$N_c = 5\tan^4\left(45 + \frac{\phi'}{2}\right) \tag{7.50}$$

$$N_q = \tan^6\left(45 + \frac{\phi'}{2}\right) \tag{7.51}$$

$$N_\gamma = N_q + 1 \tag{7.52}$$

In an unconfined compression test (also called a uniaxial compression test) on a dry rock specimen, where $\sigma_3' = 0$ and $\sigma_1' = q_{uc}$, Eq. (2.91) becomes

$$q_{uc} = 2c'\tan\left(45 + \frac{\phi'}{2}\right) \tag{7.53}$$

where

q_{uc} = unconfined (uniaxial) compression strength of rock

ϕ' = angle of friction

The unconfined compression strength and the friction angle of rocks can vary widely. Table 7.4 gives a general range of q_{uc} for various types of rocks. It is important to keep in mind that the magnitude of q_{uc} and ϕ' (hence c') reported from laboratory tests is for intact rock specimens. The reported magnitude does not account for the effect of discontinuities. Therefore, the ultimate bearing capacity q_u, computed using Eqs. (6.10), (6.19), and, (6.20) for the intact rock, can be significantly higher than that of the rock mass containing discontinuities. To account for discontinuities, Bowles (1996) suggested that the ultimate bearing capacity q_u should be modified as

$$q_{u(\text{modified})} = q_u(\text{RQD})^2 \tag{7.54}$$

where RQD = rock quality designation (see Section 3.26).

TABLE 7.4 Range of the Unconfined Compression Strength of Various Types of Rocks

Rock type	q_{uc} MN/m²	q_{uc} kip/in²	ϕ' (deg)
Granite	65–250	9.5–36	45–55
Limestone	30–150	4–22	35–45
Sandstone	25–130	3.5–19	30–45
Shale	5–40	0.75–6	15–30

In any case, the upper limit of the allowable bearing capacity should not exceed f_c' (28-day compressive strength of concrete).

EXAMPLE 7.12

Refer to Figure 7.32. A square column foundation is to be constructed over siltstone. Given:

Foundation: $B \times B = 2.5\text{ m} \times 2.5\text{ m}$
$D_f = 2\text{ m}$
Soil: $\gamma = 17\text{ kN/m}^3$
Siltstone: $c' = 32\text{ MN/m}^2$
$\phi' = 31°$
$\gamma = 25\text{ kN/m}^3$
RQD = 50%

Estimate the allowable load-bearing capacity. Use FS = 4. Also, for concrete, use $f_c' = 30\text{ MN/m}^2$.

SOLUTION

From Eq. (6.19),

$$q_u = 1.3c'N_c + qN_q + 0.4\gamma BN_\gamma$$

$$N_c = 5\tan^4\left(45 + \frac{\phi'}{2}\right) = 5\tan^4\left(45 + \frac{31}{2}\right) = 48.8$$

$$N_q = \tan^6\left(45 + \frac{\phi'}{2}\right) = \tan^6\left(45 + \frac{31}{2}\right) = 30.5$$

$$N_\gamma = N_q + 1 = 30.5 + 1 = 31.5$$

Hence,

$$\begin{aligned} q_u &= (1.3)(32 \times 10^3\text{ kN/m}^2)(48.8) + (17 \times 2)(30.5) + (0.4)(25)(2.5)(31.5) \\ &= 2030.08 \times 10^3 + 1.037 \times 10^3 + 0.788 \times 10^3 \\ &= 2031.9 \times 10^3\text{ kN/m}^2 \approx 2032\text{ MN/m}^2 \end{aligned}$$

$$q_{u(\text{modified})} = q_u(\text{RQD})^2 = (2032)(0.5)^2 = 508\text{ MN/m}^2$$

$$q_{\text{all}} = \frac{508}{4} = 127\text{ MN/m}^2$$

Since 127 MN/m^2 is greater than f_c', use $q_{\text{all}} = \mathbf{30\ MN/m^2}$.

■

7.12 Ultimate Bearing Capacity of Wedge-Shaped Foundations

Meyerhof (1961) proposed a theory to estimate the ultimate bearing capacity of a wedge-shaped shallow continuous foundation. Figure 7.33 shows the nature of the failure surface in soil below a blunt *rough* wedge at ultimate load. In Figure 7.33, D_f is the depth of embedment, and B is the width of the foundation. Note that α is the semi-angle of the wedge. Also, p_o and s_o are the normal and shear stresses on the failure plane BF inclined at angle β with the horizontal.

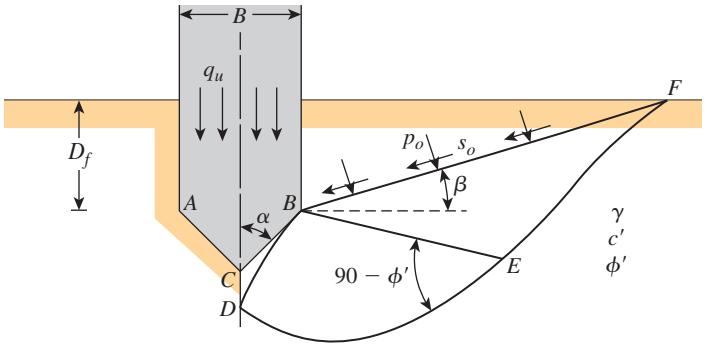


FIGURE 7.33 Failure surface in soil for blunt rough wedge (or cone) at ultimate load

Meyerhof expressed the ultimate bearing capacity, q_u, for a wedge-shaped foundation as

$$q_u = c'N_c + p_oN_q + \frac{1}{2}\gamma BN_\gamma \text{ (for wedge-shaped foundation)} \qquad (7.55)$$

where N_c, N_q, and N_γ are bearing capacity factors that are functions of β and ϕ'.

For $D_f/B \leq 1$, p_o can be taken as γD_f. Hence,

$$q_u = c'N_c + \gamma D_fN_q + \frac{1}{2}\gamma BN_\gamma \quad (\text{for } D_f/B \leq 1) \qquad (7.56)$$

The variations of N_c, N_q, and N_γ with α and ϕ' are given in Figures 7.34, 7.35, and 7.36, respectively.

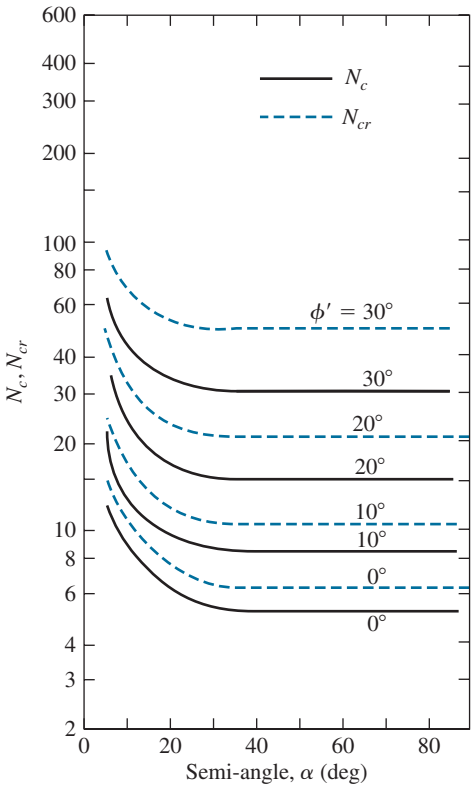


FIGURE 7.34 Variation of N_c and N_{cr} [Eqs. (7.55) and (7.57)]

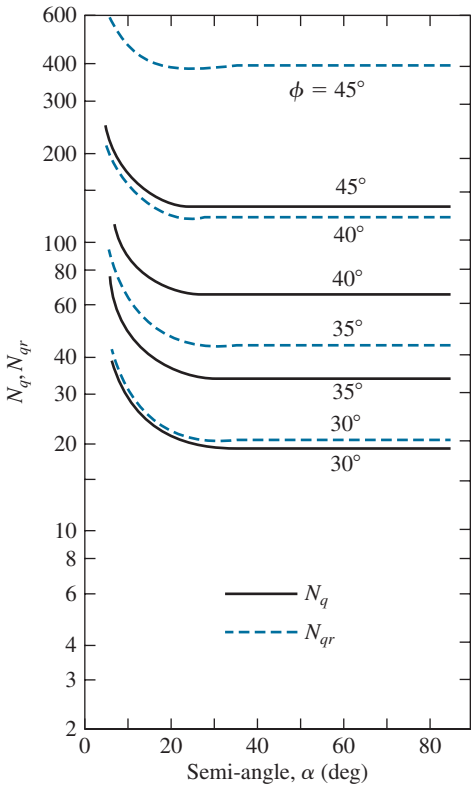


FIGURE 7.35 Variation of N_q and N_{qr} [Eqs. (7.55) and (7.57)]

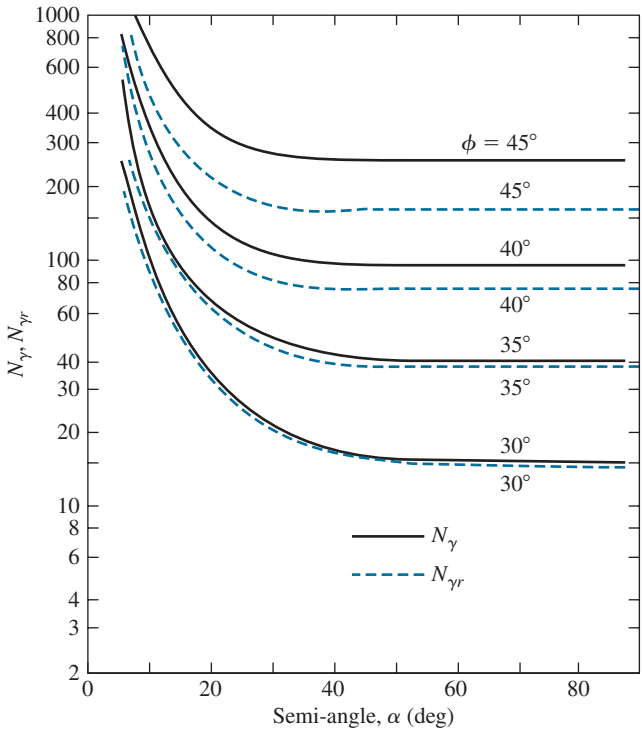


FIGURE 7.36 Variation of N_γ and $N_{\gamma r}$ [Eqs. (7.55) and (7.57)]

Equation (7.56) can be modified to obtain the ultimate bearing capacity of a circular foundation, the base of which will be a *rough* cone. For this case, $(D_f/B \leq 1)$.

$$q_u = c'N_{cr} + \gamma D_f N_{qr} + \frac{1}{2}\gamma B N_{\gamma r} \quad \text{(for conical base foundation)} \tag{7.57}$$

where N_{cr}, N_{qr}, and $N_{\gamma r}$ are bearing capacity factors.

The variations of N_{cr}, N_{qr}, and $N_{\gamma r}$ with α and ϕ' are given in Figures 7.34, 7.35, and 7.36.

7.13 Uplift Capacity of Foundations

Foundations may be subjected to uplift forces under special circumstances. During the design process for those foundations, it is desirable to provide a sufficient factor of safety against failure by uplift. This section will provide the relationships for the uplift capacity of foundations in granular and cohesive soil.

FOUNDATIONS IN GRANULAR SOIL ($c' = 0$)

Figure 7.37 shows a shallow continuous foundation that is being subjected to an uplift force. At ultimate load, Q_u, the failure surface in soil will be as shown in the figure. The ultimate load can be expressed in the form of a nondimensional *breakout factor*, F_q. Or

$$F_q = \frac{Q_u}{A\gamma D_f} \tag{7.58}$$

where A = area of the foundation.

The breakout factor is a function of the soil friction angle ϕ' and D_f/B. For a given soil friction angle, F_q increases with D_f/B to a maximum at $D_f/B = (D_f/B)_{\text{cr}}$

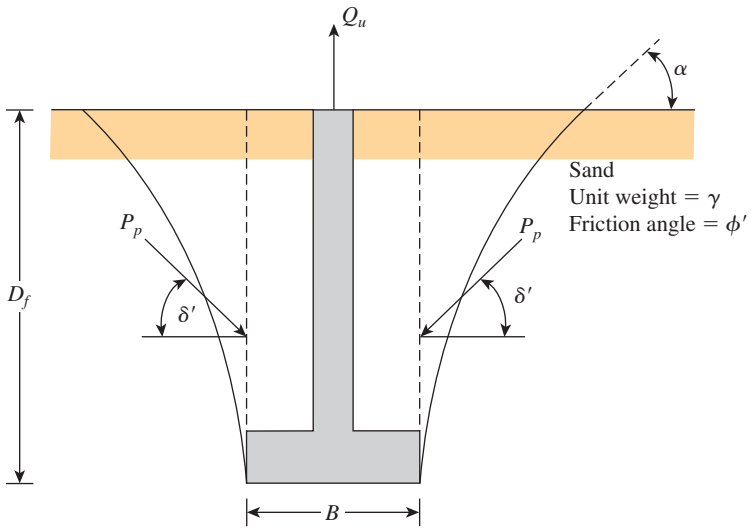


FIGURE 7.37 Shallow continuous foundation subjected to uplift

and remains constant thereafter. For foundations subjected to uplift, $D_f/B \le (D_f/B)_{cr}$ is considered a shallow foundation condition. When a foundation has an embedment ratio of $D_f/B > (D_f/B)_{cr}$, it is referred to as a deep foundation. Meyerhof and Adams (1968) provided relationships to estimate the ultimate uplifting load Q_u for shallow [that is, $D_f/B \le (D_f/B)_{cr}$], circular, and rectangular foundations. Using these relationships and Eq. (7.58), Das and Seeley (1975) expressed the breakout factor F_q in the following form:

$$F_q = 1 + 2\left[1 + m\left(\frac{D_f}{B}\right)\right]\left(\frac{D_f}{B}\right)K_u \tan\phi' \tag{7.59}$$

(for shallow circular and square foundations)

$$F_q = 1 + \left\{\left[1 + 2m\left(\frac{D_f}{B}\right)\right]\left(\frac{B}{L}\right) + 1\right\}\left(\frac{D_f}{B}\right)K_u \tan\phi' \tag{7.60}$$

(for shallow rectangular foundations)

where

m = a coefficient which is a function of ϕ'

K_u = nominal uplift coefficient

The variations of K_u, m, and $(D_f/B)_{cr}$ for square and circular foundations are given in Table 7.5 (Meyerhof and Adams, 1968).

TABLE 7.5 Variation of K_u, m, and $(D_f/B)_{cr}$

Soil friction angle, ϕ' (deg)	K_u	m	$(D_f/B)_{cr}$ for square and circular foundations
20	0.856	0.05	2.5
25	0.888	0.10	3
30	0.920	0.15	4
35	0.936	0.25	5
40	0.960	0.35	7
45	0.960	0.50	9

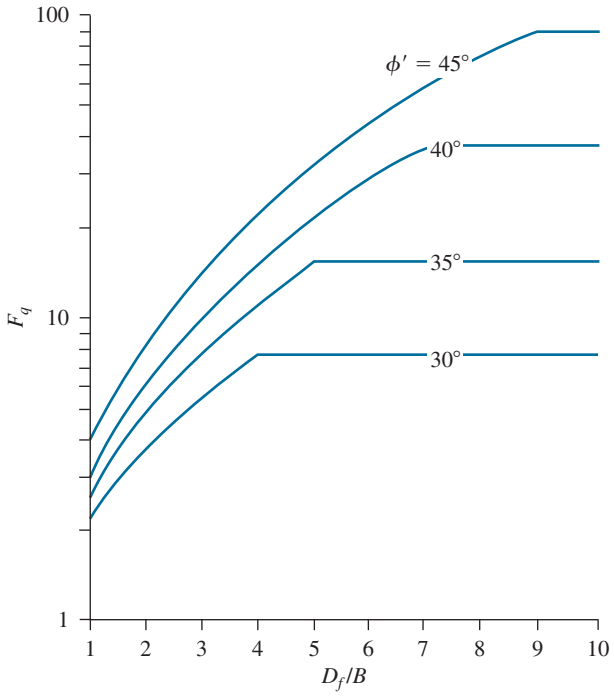


FIGURE 7.38 Variation of F_q with D_f/B and ϕ' [Eq. (7.59)]

For rectangular foundations, Das and Jones (1982) recommended that

$$\left(\frac{D_f}{B}\right)_{\text{cr-rectangular}} = \left(\frac{D_f}{B}\right)_{\text{cr-square}}\left[0.133\left(\frac{L}{B}\right) + 0.867\right] \le 1.4\left(\frac{D_f}{B}\right)_{\text{cr-square}} \tag{7.61}$$

Using the values of K_u, m, and $(D_f/B)_{cr}$ in Eq. (7.59), the variations of F_q for square and circular foundations have been calculated and are shown in Figure 7.38. Given here is a step-by-step procedure to estimate the uplift capacity of foundations in granular soil.

Step 1. Determine D_f, B, L, and ϕ'.

Step 2. Calculate D_f/B.

Step 3. Using Table 7.5 and Eq. (7.61), calculate $(D_f/B)_{cr}$.

Step 4. If D_f/B is less than or equal to $(D_f/B)_{cr}$, it is a shallow foundation.

Step 5. If $D_f/B > (D_f/B)_{cr}$, it is a deep foundation.

Step 6. For shallow foundations, use D_f/B calculated in Step 2 in Eq. (7.59) or (7.60) to estimate F_q. Thus, $Q_u = F_q A\gamma D_f$.

Step 7. For deep foundations, substitute $(D_f/B)_{cr}$ for D_f/B in Eq. (7.59) or (7.60) to obtain F_q, from which the ultimate load Q_u may be obtained.

FOUNDATIONS IN COHESIVE SOIL ($\phi = 0, c = c_u$)

The ultimate uplift capacity, Q_u, of a foundation in a purely cohesive soil can be expressed as

$$Q_u = A(\gamma D_f + c_u F_c) \tag{7.62}$$

where

A = area of the foundation

c_u = undrained shear strength of soil

F_c = breakout factor

As in the case of foundations in granular soil, the breakout factor F_c increases with embedment ratio and reaches a maximum value of $F_c = F_c^*$ at $D_f/B = (D_f/B)_{cr}$ and remains constant thereafter.

Das (1978) also reported some model test results with square and rectangular foundations. Based on these test results, it was proposed that

$$\left(\frac{D_f}{B}\right)_{\text{cr-square}} = 0.107c_u + 2.5 \leq 7 \tag{7.63}$$

where

$\left(\frac{D_f}{B}\right)_{\text{cr-square}}$ = critical embedment ratio of square (or circular) foundations

c_u = undrained cohesion, in kN/m^2

It was also observed by Das (1980) that

$$\left(\frac{D_f}{B}\right)_{\text{cr-rectangular}} = \left(\frac{D_f}{B}\right)_{\text{cr-square}}\left[0.73 + 0.27\left(\frac{L}{B}\right)\right] \leq 1.55\left(\frac{D_f}{B}\right)_{\text{cr-square}} \tag{7.64}$$

where

$\left(\frac{D_f}{B}\right)_{\text{cr-rectangular}}$ = critical embedment ratio of rectangular foundations

L = length of foundation

Based on these findings, Das (1980) proposed an empirical procedure to obtain the breakout factors for shallow and deep foundations. According to this procedure, α' and β' are two nondimensional factors defined as

$$\alpha' = \frac{\dfrac{D_f}{B}}{\left(\dfrac{D_f}{B}\right)_{\text{cr}}} \tag{7.65}$$

and

$$\beta' = \frac{F_c}{F_c^*} \tag{7.66}$$

For a given foundation, the critical embedment ratio can be calculated using Eqs. (7.63) and (7.64). The magnitude of F_c^* can be given by the following empirical relationship:

$$F^*_{c\text{-rectangular}} = 7.56 + 1.44\left(\frac{B}{L}\right) \tag{7.67}$$

where $F^*_{c\text{-rectangular}}$ = breakout factor for deep rectangular foundations.

Figure 7.39 shows the experimentally derived plots relating α' and β' (upper limit, lower limit, and average of β' and α'). The following is a step-by-step procedure to estimate the ultimate uplift capacity.

Step 1. Determine the representative value of the undrained cohesion, c_u.

Step 2. Determine the critical embedment ratio using Eqs. (7.63) and (7.64).

Step 3. Determine the D_f/B ratio for the foundation.

Step 4. If $D_f/B > (D_f/B)_{cr}$, as determined in Step 2, it is a deep foundation. However, if $D_f/B \leq (D_f/B)_{cr}$, it is a shallow foundation.

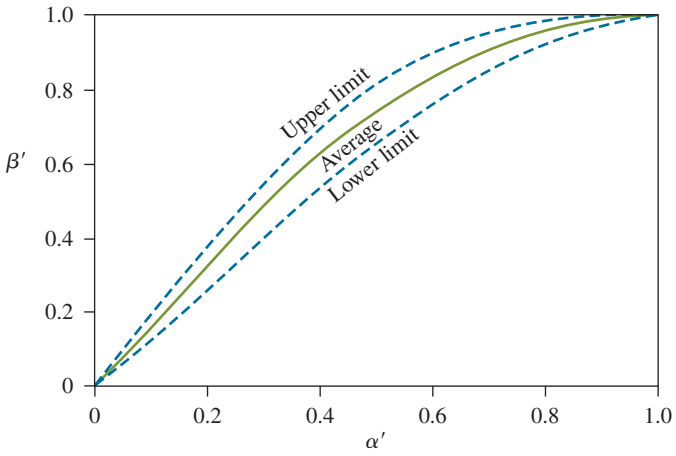


FIGURE 7.39 Plot of β' versus α'

Step 5. For $D_f/B > (D_f/B)_{cr}$,

$$F_c = F_c^* = 7.56 + 1.44\left(\frac{B}{L}\right)$$

Thus,

$$Q_u = A\left\{\left[7.56 + 1.44\left(\frac{B}{L}\right)\right]c_u + \gamma D_f\right\} \tag{7.68}$$

where A = area of the foundation.

Step 6. For $D_f/B \le (D_f/B)_{cr}$,

$$Q_u = A(\beta' F_c^* c_u + \gamma D_f) = A\left\{\beta'\left[7.56 + 1.44\left(\frac{B}{L}\right)\right]c_u + \gamma D_f\right\} \tag{7.69}$$

The value of β' can be obtained from the average curve of Figure 7.39. The procedure outlined above gives fairly good results for estimating the net ultimate uplift capacity of foundations and agrees reasonably well with the theoretical solution of Merifield et al. (2003).

EXAMPLE 7.13

Consider a circular foundation in sand. Given for the foundation: diameter, $B = 1.5$ m and depth of embedment, $D_f = 1.5$ m. Given for the sand: unit weight, $\gamma = 17.4$ kN/m^3, and friction angle, $\phi' = 35°$. Calculate the ultimate bearing capacity.

SOLUTION

$D_f/B = 1.5/1.5 = 1$ and $\phi' = 35°$. For circular foundation, $(D_f/B)_{cr} = 5$. Hence, it is a shallow foundation. From Eq. (7.59),

$$F_q = 1 + 2\left[1 + m\left(\frac{D_f}{B}\right)\right]\left(\frac{D_f}{B}\right)K_u \tan\phi'$$

For $\phi' = 35°$, $m = 0.25$, and $K_u = 0.936$ (Table 7.5). So

$$F_q = 1 + 2[1 + (0.25)(1)](1)(0.936)(\tan 35) = 2.638$$

So

$$Q_u = F_q \gamma A D_f = (2.638)(17.4)\left[\left(\frac{\pi}{4}\right)(1.5)^2\right](1.5) = \mathbf{121.7\ kN}$$

■

EXAMPLE 7.14

A rectangular foundation in a saturated clay measures 1.5 m × 3 m. Given: $D_f = 1.8$ m, $c_u = 52$ kN/m^2, and $\gamma = 18.9$ kN/m^3. Estimate the ultimate uplift capacity.

SOLUTION

From Eq. (7.63),

$$\left(\frac{D_f}{B}\right)_{\text{cr-square}} = 0.107 c_u + 2.5 = (0.107)(52) + 2.5 = 8.06$$

So use $(D_f/B)_{\text{cr-square}} = 7$. Again from Eq. (7.64),

$$\left(\frac{D_f}{B}\right)_{\text{cr-rectangular}} = \left(\frac{D_f}{B}\right)_{\text{cr-square}}\left[0.73 + 0.27\left(\frac{L}{B}\right)\right]$$

$$= 7\left[0.73 + 0.27\left(\frac{3}{1.5}\right)\right] = 8.89$$

Check: $1.55\left(\frac{D_f}{B}\right)_{\text{cr-square}} = (1.55)(7) = 10.85$

So use $(D_f/B)_{\text{cr-rectangular}} = 8.89$. The actual embedment ratio is $D_f/B = 1.8/1.5 = 1.2$. Hence, this is a shallow foundation.

$$\alpha' = \frac{\dfrac{D_f}{B}}{\left(\dfrac{D_f}{B}\right)_{\text{cr}}} = \frac{1.2}{8.89} = 0.135$$

Referring to the average curve of Figure 7.39, for $\alpha' = 0.135$, the magnitude of $\beta' = 0.2$. From Eq. (7.69),

$$Q_u = A\left\{\beta'\left[7.56 + 1.44\left(\frac{B}{L}\right)\right]c_u + \gamma D_f\right\}$$

$$= (1.5)(3)\left\{(0.2)\left[7.56 + 1.44\left(\frac{1.5}{3}\right)\right](52) + (18.9)(1.8)\right\} = \mathbf{540.6\ kN}$$

■

7.14 Summary

The general bearing capacity equations, correction factors, and the procedures discussed in Chapter 6 are for situations where the soil properties are the same for the entire region under consideration. In reality, the soil properties at a site vary, and there can be a hard stratum such as bedrock or very stiff clay lying at a short depth below the foundation. Some special cases were considered in this chapter, and the ways to compute the bearing capacities were discussed. These include situations where the

soil is underlain by a hard stratum, weak soil underlain by a stronger soil, and a stronger soil underlain by weaker soil. Procedures to determine the uplift capacity of the foundations were also discussed. While the theoretical framework required in developing these procedures involves some mathematics, the design charts and the step-by-step procedures suggested in this chapter simplify the computations significantly.

PROBLEMS

7.1 A 7.5 ft wide rough continuous foundation is placed in the ground at 3.0 ft depth. There is bedrock present at 3 ft depth below the bottom of the foundation. The soil properties are $c' = 210$ lb/ft^2, $\phi' = 25°$, and $\gamma = 115.0$ lb/ft^3. Determine the ultimate bearing capacity of the foundation.

7.2 In Problem 7.1, if there was no bedrock present for at least 12.0 ft below the foundation, what would the ultimate bearing capacity be?

7.3 A 1.5 m $\times$ 2.0 m rectangular foundation is placed at 1.0 m depth in sand where $\phi' = 40°$ and $\gamma = 18.5$ kN/m^3. Bedrock is present at 1.0 m below the foundation. Using Eq. (7.3), determine the ultimate bearing capacity of the foundation.

7.4 In Problem 7.3, if no bedrock was present for at least 4 m below the foundation, determine the ultimate bearing capacity.

7.5 A 2.0 m wide square foundation is placed at 0.5 m depth in a saturated clay where $c_u = 40$ kN/m^2 and $\gamma = 19.0$ kN/m^3. There is a very stiff stratum present at 1.0 m below the foundation. Determine the ultimate bearing capacity using Buisman's (1940) equation.

7.6 A 2.0 m wide continuous foundation is placed at 1.5 m depth in a saturated clay where $c_u = 40$ kN/m^2 and $\gamma = 18.5$ kN/m^3. At 2.0 m below the ground level, this clay layer is underlain by a stiffer clay where $c_u = 60$ kN/m^2 and $\gamma = 19.0$ kN/m^3. What would be the maximum wall load allowed with FS = 3? Use Eq. (7.11).

7.7 Redo Problem 7.6 using Vesic's (1975) solution [Eq. (7.12)].

7.8 A 2 m wide continuous foundation is placed at 1 m depth within a 1.5 m thick sand layer that is underlain by a weaker clay layer. The soil properties are as follows:

Upper sand layer: unit weight = 18.0 kN/m^3, $\phi' = 38°$
Lower clay layer: unit weight = 19.0 kN/m^3, undrained shear strength = 25 kN/m^2
Determine the maximum wall load that can be allowed on the foundation with FS = 3.

7.9 A 3 m thick clay layer ($c_u = 60$ kN/m^2 and $\gamma = 19.0$ kN/m^3) is underlain by a weaker clay ($c_u = 30$ kN/m^2 and $\gamma = 18.0$ kN/m^3) to a large depth. A 2.0 m wide square foundation is placed at 1.5 m depth below the ground level. Determine the maximum column load that can be allowed on the foundation with FS = 3.

7.10 A continuous foundation having a width of 1.5 m is placed at 1.0 m depth within a loose sand deposit where $\phi' = 32°$ and $\gamma = 17.0$ kN/m^3. This sand is underlain by a thick dense sand deposit ($\phi' = 40°$ and $\gamma = 18.0$ kN/m^3) at 2.5 m depth below the ground level. Determine the ultimate bearing capacity of the foundation.

7.11 A 2 m wide continuous foundation is to be placed in a saturated clay at 1.5 m depth where $c_u = 40$ kN/m^2 and $\gamma = 18.0$ kN/m^3.

a. What is the ultimate bearing capacity of the foundation?

b. To increase the ultimate bearing capacity, it is proposed to place dense sand ($\phi' = 42°$ and $\gamma = 18.5$ kN/m^3) in a trench directly beneath the foundation to a depth of 4.0 m. The width of the trench is the same as the width of the foundation. What is the new ultimate bearing capacity of the foundation?

7.12 Two continuous foundations are constructed alongside each other in a granular soil. Given for the foundation: $B = 1.2$ m, $D_f = 1$ m, and center-to-center spacing = 2 m. The soil friction angle $\phi' = 35°$. Estimate the net allowable bearing capacity of the foundations. Use FS = 4 and a unit weight of soil, $\gamma = 16.8$ kN/m^3.

7.13 A continuous foundation with a width of 1 m is located on a slope made of clay soil. Refer to Figure 7.19 and let $D_f = 1$ m, $H = 4$ m, $b = 2$ m, $\gamma = 16.8$ kN/m^3, $c = c_u = 68$ kN/m^2, $\phi = 0$, and $\beta = 60°$.

a. Determine the allowable bearing capacity of the foundation. Let FS = 3.

b. Plot a graph of the ultimate bearing capacity q_u if b is changed from 0 to 6 m.

7.14 A continuous foundation is to be constructed near a slope made of granular soil (see Figure 7.19). If $B = 4$ ft, $b = 6$ ft, $H = 15$ ft, $D_f = 4$ ft, $\beta = 30°$, $\phi' = 40°$, and $\gamma = 110$ lb/ft^3, estimate the ultimate bearing capacity of the foundation.

7.15 The following are the average values of cone penetration resistance in a granular soil deposit.

Depth (m)	Cone penetration resistance, q_c (MN/m^2)
2	1.73
4	3.6
6	4.9
8	6.8
10	8.7
15	13

For the soil deposit, assume γ to be 16.5 kN/m^3 and estimate the seismic ultimate bearing capacity, q_{uE}, for a continuous foundation with $B = 1.5$ m, $D_f = 1.0$ m, $k_h = 0.2$, and $k_v = 0$. Use Eqs. (7.47) and (7.48).

7.16 Refer to Problem 7.15. If the design earthquake parameters are $V = 0.35$ m/s and $A = 0.3$, determine the seismic settlement of the foundation. Assume FS = 4 for obtaining static allowable bearing capacity.

7.17 A sandstone rock specimen has $q_{uc} = 50$ MN/m^2 and $\phi' = 35°$. Find c'.

7.18 A sandstone bed with RQD = 70% and $\gamma = 26.0$ kN/m^3 lies beneath 1.5 m of overburden soil. A 2.0 m × 2.0 m square foundation is to be placed on top of the sandstone rock (i.e., at a 1.5 depth below the ground level) to carry a column load. The unit weight of the soil is 18.0 kN/m^3. Assuming the rock strength parameters from Problem 7.17, determine the maximum load that can be allowed on the foundation with the safety factor FS = 3. The compressive strength f'_c of concrete is 30.0 MN/m^2.

7.19 A square foundation in a sand deposit measures 4 ft × 4 ft in plan. Given: $D_f = 5$ ft, soil friction angle = 35°, and unit weight of soil = 112 lb/ft^3. Estimate the ultimate uplift capacity of the foundation.

7.20 A foundation measuring 1.2 m × 2.4 m in plan is constructed in a saturated clay. Given: depth of embedment of the foundation = 2 m, unit weight of soil = 18 kN/m^3, and undrained cohesion of clay = 74 kN/m^2. Estimate the ultimate uplift capacity of the foundation.

REFERENCES

Bowles, J. E. (1996). *Foundation Analysis and Design*, 5th ed., McGraw-Hill, New York.

Buisman, A. S. K. (1940). *Grondmechanica*, Waltman, Delft, The Netherlands.

Cerato, A. B. and Lutenegger, A. J. (2006). "Bearing Capacity of Square and Circular Footings on a Finite Layer of Granular Soil Underlain by a Rigid Base," *Journal of Geotechnical and Geoenvironmental Engineering*, American Society of Civil Engineers, Vol. 132, No. 11, pp. 1496–1501.

Das, B. M. (1978). "Model Tests for Uplift Capacity of Foundations in Clay," *Soils and Foundations*, Vol. 18, No. 2, pp. 17–24.

Das, B. M. (1980). "A Procedure for Estimation of Ultimate Uplift Capacity of Foundations in Clay," *Soils and Foundations*, Vol. 20, No. 1, pp. 77–82.

Das, B. M. and Jones, A. D. (1982). "Uplift Capacity of Rectangular Foundations in Sand," *Transportation Research Record 884*, National Research Council, Washington, DC, pp. 54–58.

Das, B. M. and Seeley, G. R. (1975). "Breakout Resistance of Horizontal Anchors," *Journal of Geotechnical Engineering Division*, ASCE, Vol. 101, No. 9, pp. 999–1003.

Lundgren, H. and Mortensen, K. (1953). "Determination by the Theory of Plasticity on the Bearing Capacity of Continuous Footings on Sand," *Proceedings, Third International Conference on Soil Mechanics and Foundation Engineering*, Zurich, Vol. 1, pp. 409–412.

Madhav, M. R. and Vitkar, P. P. (1978). "Strip Footing on Weak Clay Stabilized with a Granular Trench," *Canadian Geotechnical Journal*, Vol. 15, No. 4, pp. 605–609.

Mandel, J. and Salencon, J. (1972). "Force portante d'un sol sur une assise rigide (étude théorique)," *Geotechnique*, Vol. 22, No. 1, pp. 79–93.

Merifield, R. S., Lyamin, A. and Sloan, S. W. (2003). "Three Dimensional Lower Bound Solutions for the Stability of Plate Anchors in Clay," *Journal of Geotechnical and Geoenvironmental Engineering*, ASCE, Vo. 129, No. 3, pp. 243–253.

Meyerhof, G. G. (1957). "The Ultimate Bearing Capacity of Foundations on Slopes," *Proceedings, Fourth International Conference on Soil Mechanics and Foundation Engineering*, London, Vol. 1, pp. 384–387.

Meyerhof, G. G. (1961). "The Ultimate Bearing Capacity of Wedge-Shaped Foundations," *Proceedings, Fourth International Conference on Soil Mechanics and Foundation Engineering*, Paris, Vol. 2, pp. 105–109.

Meyerhof, G. G. (1974). "Ultimate Bearing Capacity of Footings on Sand Layer Overlying Clay," *Canadian Geotechnical Journal*, Vol. 11, No. 2, pp. 224–229.

Meyerhof, G. G. and Adams, J. I. (1968). "The Ultimate Uplift Capacity of Foundations," *Canadian Geotechnical Journal*, Vol. 5, No. 4, pp. 225–244.

Meyerhof, G. G. and Chaplin, T. K. (1953). "The Compression and Bearing Capacity of Cohesive Soils," *British Journal of Applied Physics*, Vol. 4, pp. 20–26.

Meyerhof, G. G. and Hanna, A. M. (1978). "Ultimate Bearing Capacity of Foundations on Layered Soil under Inclined Load," *Canadian Geotechnical Journal*, Vol. 15, No. 4, pp. 565–572.

Prandtl, L. (1921). "Über die Eindringungsfestigkeit (Härte) plastischer Baustoffe und die Festigkeit von Schneiden," *Zeitschrift für angewandte Mathematik und Mechanik*, Vol. 1, No. 1, pp. 15–20.

Reddy, A. S. and Srinivasan, R. J. (1967). "Bearing Capacity of Footings on Layered Clay," *Journal of the Soil Mechanics and Foundations Division*, American Society of Civil Engineers, Vol. 93, No. SM2, pp. 83–99.

Reissner, H. (1924). "Zum Erddruckproblem," *Proceedings, First International Congress of Applied Mechanics*, Delft, The Netherlands, pp. 295–311.

Richards, R., Jr., Elms, D. G., and Budhu, M. (1993). "Seismic Bearing Capacity and Settlement of Foundations," *Journal of Geotechnical Engineering*, American Society of Civil Engineers, Vol. 119, No. 4, pp. 662–674.

Stagg, K. G. and Zienkiewicz, O. C. (1968). *Rock Mechanics in Engineering Practice*, John Wiley & Sons, New York.

Vesic, A. S. (1975). "Bearing Capacity of Shallow Foundations," in *Foundation Engineering Handbook*, ed. R. F. Winterkorn and H. Y. Fang, Van Nostrand Reinhold Company, New York.

8

Vertical Stress Increase in Soil



Bertold Werkmann/Shutterstock.com

8.1 Introduction 303
8.2 Stress Due to a Concentrated Load 303
8.3 Stress Due to a Circularly Loaded Area 304
8.4 Stress Due to a Line Load 305
8.5 Stress Below a Vertical Strip Load of Finite Width and Infinite Length 306
8.6 Stress Below a Horizontal Strip Load of Finite Width and Infinite Length 310
8.7 Stress Below a Rectangular Area 312
8.8 Stress Isobars 317
8.9 Average Vertical Stress Increase Due to a Rectangularly Loaded Area 318
8.10 Average Vertical Stress Increase Below the Center of a Circularly Loaded Area 323
8.11 Stress Increase Under an Embankment 325
8.12 Westergaard's Solution for Vertical Stress Due to a Point Load 328
8.13 Stress Distribution for Westergaard Material 330
8.14 Summary 333

PROBLEMS 333

REFERENCES 335

8.1 Introduction

All foundations are designed to satisfy bearing capacity requirements and settlement considerations. While it is necessary to ensure an adequate factor of safety against any shear failure in the surrounding soil, it is also necessary to limit the amount of settlement. Generally the factor of safety of a shallow foundation in terms of bearing capacity is about 3, and the settlement is limited to 25–75 mm (1–3 in.), depending on the type of foundation, soil conditions, and the type of structure. Under bearing capacity considerations, the allowable bearing pressure is determined as q_u/FS. In terms of settlement, the allowable bearing pressure is the one that corresponds to the maximum allowable settlement. Thus we have two different values for q_{all} and select the lower one. In many cases, the allowable bearing pressure of the foundation is controlled by the settlement rather than the bearing capacity. Therefore, it is necessary to compute the settlement correctly.

The foundation settlement depends on the loading, size, and shape of the foundation, along with the properties of the underlying soil. To compute the settlement, it is necessary to know the vertical stress increase within the underlying soil due to the foundation load. Hence, in this chapter, we will discuss the general principles for estimating the increase of vertical stress at various depths in soil due to the application of (on the ground surface):

- Point load
- Circularly loaded area
- Vertical line load
- Strip load
- Rectangularly loaded area
- Embankment type of loading

Various procedures for estimating foundation settlement will be discussed in Chapter 9. The soil mass is generally treated as an *elastic half-space* that is a homogeneous, isotropic, linear elastic continuum, with Young's modulus of E_s and Poisson's ratio μ_s. That is, the elastic medium is extending to infinite lengths laterally and to an infinite depth. Since these are elastic solutions, the principle of superposition is valid.

8.2 Stress Due to a Concentrated Load

In 1885, Boussinesq developed the mathematical relationships for determining the normal and shear stresses at any point inside a *homogeneous, elastic*, and *isotropic* mediums due to a *concentrated point load* located at the surface, as shown in Figure 8.1. According to these relationships, the *vertical stress increase* at point *A* caused by a point load of magnitude *P* is given by

$$\Delta\sigma = \frac{3P}{2\pi z^2\left[1 + \left(\frac{r}{z}\right)^2\right]^{5/2}} \tag{8.1}$$

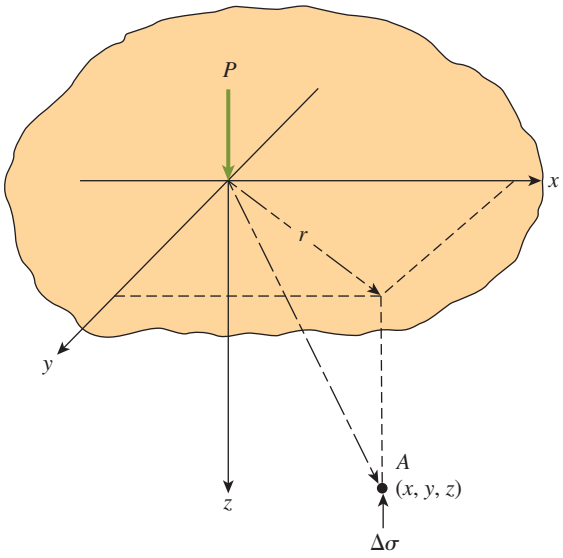


FIGURE 8.1 Vertical stress at a point A caused by a point load on the surface

where

$$r = \sqrt{x^2 + y^2}$$

x, y, z = coordinates of the point A

Note that Eq. (8.1) is not a function of Poisson's ratio of the soil.

8.3 Stress Due to a Circularly Loaded Area

The Boussinesq equation (8.1) can also be used to determine the vertical stress below the center of a flexible circularly loaded area, as shown in Figure 8.2. Let the radius of the loaded area be $B/2$, and let q_o be the uniformly distributed load per unit area. To determine the stress increase at a point A, located at a depth z below the center of the circular area, consider an elemental area on the circle. The load on this elemental area may be taken to be a point load and expressed as $q_o r\, d\theta\, dr$. The stress increase at A caused by this load can be determined from Eq. (8.1) as

$$d\sigma = \frac{3(q_o r\, d\theta\, dr)}{2\pi z^2\left[1 + \left(\frac{r}{z}\right)^2\right]^{5/2}} \tag{8.2}$$

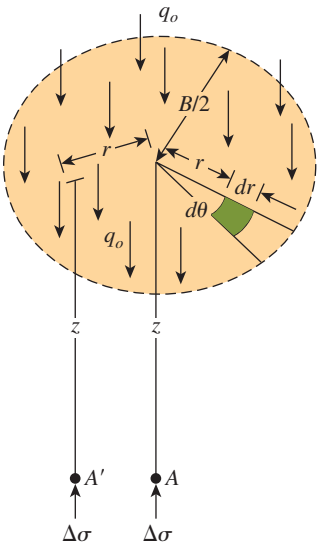


FIGURE 8.2 Increase in vertical stress under a uniformly loaded flexible circular area

The total increase in stress at A caused by the entire loaded area may be obtained by integrating Eq. (8.2), or

$$\Delta\sigma = \int d\sigma = \int_{\theta=0}^{\theta=2\pi}\int_{r=0}^{r=B/2} \frac{3(q_o r\, d\theta\, dr)}{2\pi z^2\left[1 + \left(\frac{r}{z}\right)^2\right]^{5/2}}$$

$$= q_o\left\{1 - \frac{1}{\left[1 + \left(\frac{B}{2z}\right)^2\right]^{3/2}}\right\} \tag{8.3}$$

TABLE 8.1 Variation of $\Delta\sigma/q_o$ for a Uniformly Loaded Flexible Circular Area

	$r/(B/2)$					
$z/(B/2)$	0	0.2	0.4	0.6	0.8	1.0
0	1.000	1.000	1.000	1.000	1.000	1.000
0.1	0.999	0.999	0.998	0.996	0.976	0.484
0.2	0.992	0.991	0.987	0.970	0.890	0.468
0.3	0.976	0.973	0.963	0.922	0.793	0.451
0.4	0.949	0.943	0.920	0.860	0.712	0.435
0.5	0.911	0.902	0.869	0.796	0.646	0.417
0.6	0.864	0.852	0.814	0.732	0.591	0.400
0.7	0.811	0.798	0.756	0.674	0.545	0.367
0.8	0.756	0.743	0.699	0.619	0.504	0.366
0.9	0.701	0.688	0.644	0.570	0.467	0.348
1.0	0.646	0.633	0.591	0.525	0.434	0.332
1.2	0.546	0.535	0.501	0.447	0.377	0.300
1.5	0.424	0.416	0.392	0.355	0.308	0.256
2.0	0.286	0.286	0.268	0.248	0.224	0.196
2.5	0.200	0.197	0.191	0.180	0.167	0.151
3.0	0.146	0.145	0.141	0.135	0.127	0.118
4.0	0.087	0.086	0.085	0.082	0.080	0.075

Similar integrations could be performed to obtain the vertical stress increase at A', located a distance r from the center of the loaded area at a depth z (Ahlvin and Ulery, 1962). Table 8.1 gives the variation of $\Delta\sigma/q_o$ with $r/(B/2)$ and $z/(B/2)$ [for $0 \le r/(B/2) \le 1$]. Note that the variation of $\Delta\sigma/q_o$ with depth at $r/(B/2) = 0$ can be obtained from Eq. (8.3).

8.4 Stress Due to a Line Load

Figure 8.3 shows a vertical flexible line load of infinite length that has an intensity q/unit length on the surface of a semi-infinite soil mass. The vertical stress increase, $\Delta\sigma$, inside the soil mass can be determined by using the principles of the theory of elasticity, or

$$\Delta\sigma = \frac{2qz^3}{\pi(x^2 + z^2)^2} \tag{8.4}$$

This equation can be rewritten as

$$\Delta\sigma = \frac{2q}{\pi z[(x/z)^2 + 1]^2}$$

$$\frac{\Delta\sigma}{(q/z)} = \frac{2}{\pi[(x/z)^2 + 1]^2} \tag{8.5}$$

Note that Eq. (8.5) is in a nondimensional form. Using this equation, we can calculate the variation of $\Delta\sigma/(q/z)$ with x/z. This is given in Table 8.2. The value of

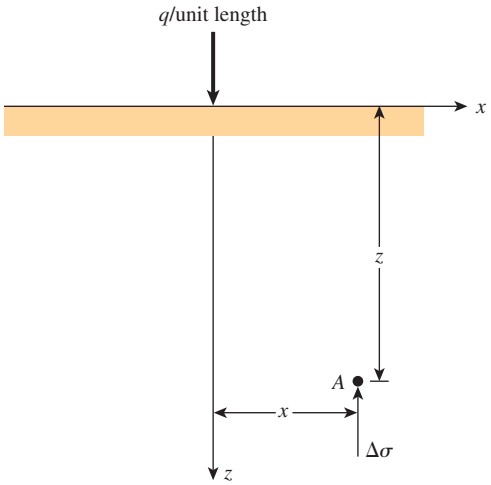


FIGURE 8.3 Line load over the surface of a semi-infinite soil mass

TABLE 8.2 Variation of $\Delta\sigma/(q/z)$ with x/z [Eq. (8.5)]

x/z	$\Delta\sigma/(q/z)$	x/z	$\Delta\sigma/(q/z)$
0	0.637	1.3	0.088
0.1	0.624	1.4	0.073
0.2	0.589	1.5	0.060
0.3	0.536	1.6	0.050
0.4	0.473	1.7	0.042
0.5	0.407	1.8	0.035
0.6	0.344	1.9	0.030
0.7	0.287	2.0	0.025
0.8	0.237	2.2	0.019
0.9	0.194	2.4	0.014
1.0	0.159	2.6	0.011
1.1	0.130	2.8	0.008
1.2	0.107	3.0	0.006

$\Delta\sigma$ calculated by using Eq. (8.5) is the *additional* stress on the soil caused by the line load. The value of $\Delta\sigma$ does not include the overburden pressure of the soil above point A.

8.5 Stress Below a Vertical Strip Load of Finite Width and Infinite Length

The fundamental equation for the vertical stress increase at a point in a soil mass as the result of a line load (Section 8.4) can be used to determine the vertical stress at a point caused by a flexible strip load of width B. (See Figure 8.4.) Let the load per unit area of the strip shown in Figure 8.4 be equal to q_o. If we consider an elemental strip of width dr, the load per unit length of this strip is equal to $q_o\, dr$. This elemental strip can be treated as a line load. Eq. (8.4) gives the vertical stress increase $d\sigma$ at point A inside the soil mass caused by this elemental

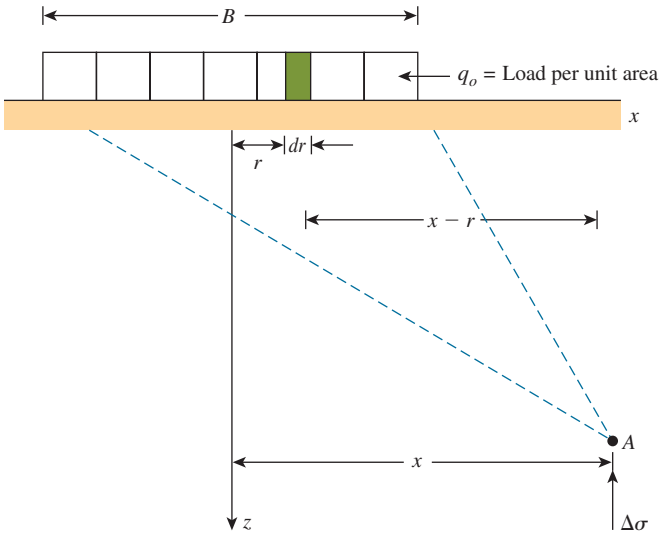


FIGURE 8.4 Vertical stress caused by a flexible vertical strip load

strip load. To calculate the vertical stress increase, we need to substitute $q_o\,dr$ for q and $(x - r)$ for x. So,

$$d\sigma = \frac{2(q_o\,dr)z^3}{\pi[(x-r)^2 + z^2]^2} \tag{8.6}$$

The total increase in the vertical stress ($\Delta\sigma$) at point A caused by the entire strip load of width B can be determined by integration of Eq. (8.6) with limits of r from $-B/2$ to $+B/2$, or

$$\begin{aligned}\Delta\sigma = \int d\sigma &= \int_{-B/2}^{+B/2}\left(\frac{2q}{\pi}\right)\left\{\frac{z^3}{[(x-r)^2+z^2]^2}\right\}dr \\ &= \frac{q_o}{\pi}\left\{\tan^{-1}\left[\frac{z}{x-(B/2)}\right] - \tan^{-1}\left\{\frac{z}{x+(B/2)}\right\}\right. \\ &\quad \left. - \frac{Bz[x^2 - z^2 - (B^2/4)]}{[x^2+z^2-(B^2/4)]^2 + B^2z^2}\right\}\end{aligned} \tag{8.7}$$

With respect to Eq. (8.7), the following should be kept in mind:

1. $\tan^{-1}\left[\dfrac{z}{x-\left(\dfrac{B}{2}\right)}\right]$ and $\tan^{-1}\left[\dfrac{z}{x+\left(\dfrac{B}{2}\right)}\right]$ are in radians.
2. The magnitude of $\Delta\sigma$ depends on the absolute value of x/z.
3. Equation (8.7) is valid as shown in Figure 8.4; that is, for point A, $x \geq B/2$.

However, for $0 \leq x < B/2$, the magnitude of $\tan^{-1}\left[\dfrac{z}{x-\left(\dfrac{B}{2}\right)}\right]$ becomes negative.

For this case, that should be replaced by $\pi + \tan^{-1}\left[\dfrac{z}{x-\left(\dfrac{B}{2}\right)}\right]$.

Table 8.3 shows the variation of $\Delta\sigma/q_o$ with $2z/B$ and $2x/B$. This table can be used conveniently for the calculation of vertical stress at a point caused by a flexible strip load.

TABLE 8.3 Variation of $\Delta\sigma/q_o$ with $2z/B$ and $2x/B$ [Eq. (8.7)]

	$2x/B$										
$2z/B$	0.0	0.1	0.2	0.3	0.4	0.5	0.6	0.7	0.8	0.9	1.0
0.00	1.000	1.000	1.000	1.000	1.000	1.000	1.000	1.000	1.000	1.000	0.000
0.10	1.000	1.000	0.999	0.999	0.999	0.998	0.997	0.993	0.980	0.909	0.500
0.20	0.997	0.997	0.996	0.995	0.992	0.988	0.979	0.959	0.909	0.775	0.500
0.30	0.990	0.989	0.987	0.984	0.978	0.967	0.947	0.908	0.833	0.697	0.499
0.40	0.977	0.976	0.973	0.966	0.955	0.937	0.906	0.855	0.773	0.651	0.498
0.50	0.959	0.958	0.953	0.943	0.927	0.902	0.864	0.808	0.727	0.620	0.497
0.60	0.937	0.935	0.928	0.915	0.896	0.866	0.825	0.767	0.691	0.598	0.495
0.70	0.910	0.908	0.899	0.885	0.863	0.831	0.788	0.732	0.662	0.581	0.492
0.80	0.881	0.878	0.869	0.853	0.829	0.797	0.755	0.701	0.638	0.566	0.489
0.90	0.850	0.847	0.837	0.821	0.797	0.765	0.724	0.675	0.617	0.552	0.485
1.00	0.818	0.815	0.805	0.789	0.766	0.735	0.696	0.650	0.598	0.540	0.480
1.10	0.787	0.783	0.774	0.758	0.735	0.706	0.670	0.628	0.580	0.529	0.474
1.20	0.755	0.752	0.743	0.728	0.707	0.679	0.646	0.607	0.564	0.517	0.468
1.30	0.725	0.722	0.714	0.699	0.679	0.654	0.623	0.588	0.548	0.506	0.462
1.40	0.696	0.693	0.685	0.672	0.653	0.630	0.602	0.569	0.534	0.495	0.455
1.50	0.668	0.666	0.658	0.646	0.629	0.607	0.581	0.552	0.519	0.484	0.448
1.60	0.642	0.639	0.633	0.621	0.605	0.586	0.562	0.535	0.506	0.474	0.440
1.70	0.617	0.615	0.608	0.598	0.583	0.565	0.544	0.519	0.492	0.463	0.433
1.80	0.593	0.591	0.585	0.576	0.563	0.546	0.526	0.504	0.479	0.453	0.425
1.90	0.571	0.569	0.564	0.555	0.543	0.528	0.510	0.489	0.467	0.443	0.417
2.00	0.550	0.548	0.543	0.535	0.524	0.510	0.494	0.475	0.455	0.433	0.409
2.10	0.530	0.529	0.524	0.517	0.507	0.494	0.479	0.462	0.443	0.423	0.401
2.20	0.511	0.510	0.506	0.499	0.490	0.479	0.465	0.449	0.432	0.413	0.393
2.30	0.494	0.493	0.489	0.483	0.474	0.464	0.451	0.437	0.421	0.404	0.385
2.40	0.477	0.476	0.473	0.467	0.460	0.450	0.438	0.425	0.410	0.395	0.378
2.50	0.462	0.461	0.458	0.452	0.445	0.436	0.426	0.414	0.400	0.386	0.370
2.60	0.447	0.446	0.443	0.439	0.432	0.424	0.414	0.403	0.390	0.377	0.363
2.70	0.433	0.432	0.430	0.425	0.419	0.412	0.403	0.393	0.381	0.369	0.355
2.80	0.420	0.419	0.417	0.413	0.407	0.400	0.392	0.383	0.372	0.360	0.348
2.90	0.408	0.407	0.405	0.401	0396	0.389	0.382	0.373	0.363	0.352	0.341
3.00	0.396	0.395	0.393	0.390	0.385	0.379	0.372	0.364	0.355	0.345	0.334
3.10	0.385	0.384	0.382	0.379	0.375	0.369	0.363	0.355	0.347	0.337	0.327
3.20	0.374	0.373	0.372	0.369	0.365	0.360	0.354	0.347	0.339	0.330	0.321
3.30	0.364	0.363	0.362	0.359	0.355	0.351	0.345	0.339	0.331	0.323	0.315
3.40	0.354	0.354	0.352	0.350	0.346	0.342	0.337	0.331	0.324	0.316	0.308
3.50	0.345	0.345	0.343	0.341	0.338	0.334	0.329	0.323	0.317	0.310	0.302
3.60	0.337	0.336	0.335	0.333	0.330	0.326	0.321	0.316	0.310	0.304	0.297
3.70	0.328	0.328	0.327	0.325	0.322	0.318	0.314	0.309	0.304	0.298	0.291
3.80	0.320	0.320	0.319	0.317	0.315	0.311	0.307	0.303	0.297	0.292	0.285
3.90	0.313	0.313	0.312	0.310	0.307	0.304	0.301	0.296	0.291	0.286	0.280
4.00	0.306	0.305	0.304	0.303	0.301	0.298	0.294	0.290	0.285	0.280	0.275
4.10	0.299	0.299	0.298	0.296	0.294	0.291	0.288	0.284	0.280	0.275	0.270
4.20	0.292	0.292	0.291	0.290	0.288	0.285	0.282	0.278	0.274	0.270	0.265
4.30	0.286	0.286	0.285	0.283	0.282	0.279	0.276	0.273	0.269	0.265	0.260
4.40	0.280	0.280	0.279	0.278	0.276	0.274	0.271	0.268	0.264	0.260	0.256
4.50	0.274	0.274	0.273	0.272	0.270	0.268	0.266	0.263	0.259	0.255	0.251
4.60	0.268	0.268	0.268	0.266	0.265	0.263	0.260	0.258	0.254	0.251	0.247
4.70	0.263	0.263	0.262	0.261	0.260	0.258	0.255	0.253	0.250	0.246	0.243
4.80	0.258	0.258	0.257	0.256	0.255	0.253	0.251	0.248	0.245	0.242	0.239
4.90	0.253	0.253	0.252	0.251	0.250	0.248	0.246	0.244	0.241	0.238	0.235
5.00	0.248	0.248	0.247	0.246	0.245	0.244	0.242	0.239	0.237	0.234	0.231

TABLE 8.3 Variation of $\Delta\sigma/q_o$ with $2z/B$ and $2x/B$ [Eq. (8.7)] *(Continued)*

	$2x/B$									
$2z/B$	1.1	1.2	1.3	1.4	1.5	1.6	1.7	1.8	1.9	2.0
0.00	0.000	0.000	0.000	0.000	0.000	0.000	0.000	0.000	0.000	0.000
0.10	0.091	0.020	0.007	0.003	0.002	0.001	0.001	0.000	0.000	0.000
0.20	0.225	0.091	0.040	0.020	0.011	0.007	0.004	0.003	0.002	0.002
0.30	0.301	0.165	0.090	0.052	0.031	0.020	0.013	0.009	0.007	0.005
0.40	0.346	0.224	0.141	0.090	0.059	0.040	0.027	0.020	0.014	0.011
0.50	0.373	0.267	0.185	0.128	0.089	0.063	0.046	0.034	0.025	0.019
0.60	0.391	0.298	0.222	0.163	0.120	0.088	0.066	0.050	0.038	0.030
0.70	0.403	0.321	0.250	0.193	0.148	0.113	0.087	0.068	0.053	0.042
0.80	0.411	0.338	0.273	0.218	0.173	0.137	0.108	0.086	0.069	0.056
0.90	0.416	0.351	0.291	0.239	0.195	0.158	0.128	0.104	0.085	0.070
1.00	0.419	0.360	0.305	0.256	0.214	0.177	0.147	0.122	0.101	0.084
1.10	0.420	0.366	0.316	0.271	0.230	0.194	0.164	0.138	0.116	0.098
1.20	0.419	0.371	0.325	0.282	0.243	0.209	0.178	0.152	0.130	0.111
1.30	0.417	0.373	0.331	0.291	0.254	0.221	0.191	0.166	0.143	0.123
1.40	0.414	0.374	0.335	0.298	0.263	0.232	0.203	0.177	0.155	0.135
1.50	0.411	0.374	0.338	0.303	0.271	0.240	0.213	0.188	0.165	0.146
1.60	0.407	0.373	0.339	0.307	0.276	0.248	0.221	0.197	0.175	0.155
1.70	0.402	0.370	0.339	0.309	0.281	0.254	0.228	0.205	0.183	0.164
1.80	0.396	0.368	0.339	0.311	0.284	0.258	0.234	0.212	0.191	0.172
1.90	0.391	0.364	0.338	0.312	0.286	0.262	0.239	0.217	0.197	0.179
2.00	0.385	0.360	0.336	0.311	0.288	0.265	0.243	0.222	0.203	0.185
2.10	0.379	0.356	0.333	0.311	0.288	0.267	0.246	0.226	0.208	0.190
2.20	0.373	0.352	0.330	0.309	0.288	0.268	0.248	0.229	0.212	0.195
2.30	0.366	0.347	0.327	0.307	0.288	0.268	0.250	0.232	0.215	0.199
2.40	0.360	0.342	0.323	0.305	0.287	0.268	0.251	0.234	0.217	0.202
2.50	0.354	0.337	0.320	0.302	0.285	0.268	0.251	0.235	0.220	0.205
2.60	0.347	0.332	0.316	0.299	0.283	0.267	0.251	0.236	0.221	0.207
2.70	0.341	0.327	0.312	0.296	0.281	0.266	0.251	0.236	0.222	0.208
2.80	0.335	0.321	0.307	0.293	0.279	0.265	0.250	0.236	0.223	0.210
2.90	0.329	0.316	0.303	0.290	0.276	0.263	0.249	0.236	0.223	0.211
3.00	0.323	0.311	0.299	0.286	0.274	0.261	0.248	0.236	0.223	0.211
3.10	0.317	0.306	0.294	0.283	0.271	0.259	0.247	0.235	0.223	0.212
3.20	0.311	0.301	0.290	0.279	0.268	0.256	0.245	0.234	0.223	0.212
3.30	0.305	0.296	0.286	0.275	0.265	0.254	0.243	0.232	0.222	0.211
3.40	0.300	0.291	0.281	0.271	0.261	0.251	0.241	0.231	0.221	0.211
3.50	0.294	0.286	0.277	0.268	0.258	0.249	0.239	0.229	0.220	0.210
3.60	0.289	0.281	0.273	0.264	0.255	0.246	0.237	0.228	0.218	0.209
3.70	0.284	0.276	0.268	0.260	0.252	0.243	0.235	0.226	0.217	0.208
3.80	0.279	0.272	0.264	0.256	0.249	0.240	0.232	0.224	0.216	0.207
3.90	0.274	0.267	0.260	0.253	0.245	0.238	0.230	0.222	0.214	0.206
4.00	0.269	0.263	0.256	0.249	0.242	0.235	0.227	0.220	0.212	0.205
4.10	0.264	0.258	0.252	0.246	0.239	0.232	0.225	0.218	0.211	0.203
4.20	0.260	0.254	0.248	0.242	0.236	0.229	0.222	0.216	0.209	0.202
4.30	0.255	0.250	0.244	0.239	0.233	0.226	0.220	0.213	0.207	0.200
4.40	0.251	0.246	0.241	0.235	0.229	0.224	0.217	0.211	0.205	0.199
4.50	0.247	0.242	0.237	0.232	0.226	0.221	0.215	0.209	0.203	0.197
4.60	0.243	0.238	0.234	0.229	0.223	0.218	0.212	0.207	0.201	0.195
4.70	0.239	0.235	0.230	0.225	0.220	0.215	0.210	0.205	0.199	0.194
4.80	0.235	0.231	0.227	0.222	0.217	0.213	0.208	0.202	0.197	0.192
4.90	0.231	0.227	0.223	0.219	0.215	0.210	0.205	0.200	0.195	0.190
5.00	0.227	0.224	0.220	0.216	0.212	0.207	0.203	0.198	0.193	0.188

EXAMPLE 8.1

Refer to Figure 8.4. Given: $B = 4$ m and $q_o = 100$ kN/m^2. For point A, $z = 1$ m and $x = 1$ m. Determine the vertical stress $\Delta\sigma$ at A. Use Eq. (8.7).

SOLUTION

Since $x = 1 \text{ m} < B/2 = 2$ m,

$$\Delta\sigma = \frac{q_o}{\pi}\left\{\tan^{-1}\left[\frac{z}{x-\left(\frac{B}{2}\right)}\right] + \pi - \tan^{-1}\left[\frac{z}{x+\left(\frac{B}{2}\right)}\right] - \frac{Bz\left[x^2 - z^2 - \left(\frac{B^2}{4}\right)\right]}{\left[x^2 + z^2 - \left(\frac{B^2}{4}\right)\right]^2 + B^2z^2}\right\}$$

$$\tan^{-1}\left[\frac{z}{x-\left(\frac{B}{2}\right)}\right] = \tan^{-1}\left(\frac{1}{1-2}\right) = -45° = -0.785 \text{ rad}$$

$$\tan^{-1}\left[\frac{z}{x+\left(\frac{B}{2}\right)}\right] = \tan^{-1}\left(\frac{1}{1+2}\right) = 18.43° = 0.322 \text{ rad}$$

$$\frac{Bz\left[x^2 - z^2 - \left(\frac{B^2}{4}\right)\right]}{\left[x^2 + z^2 - \left(\frac{B^2}{4}\right)\right]^2 + B^2z^2} = \frac{(4)(1)\left[(1)^2 - (1)^2 - \left(\frac{16}{4}\right)\right]}{\left[(1)^2 + (1)^2 - \left(\frac{16}{4}\right)\right]^2 + (16)(1)} = -0.8$$

Hence,

$$\frac{\Delta\sigma}{q_o} = \frac{1}{\pi}[-0.785 + \pi - 0.322 - (-0.8)] = 0.902$$

Now, compare with Table 8.3. For this case, $\frac{2x}{B} = \frac{(2)(1)}{4} = 0.5$ and $\frac{2z}{B} = \frac{(2)(1)}{4} = 0.5$. So, $\frac{\Delta\sigma}{q_o} = 0.902$. (Check)

$$\Delta\sigma = 0.902q_o = (0.902)(100) = \mathbf{90.2\ kN/m^2}$$

8.6 Stress Below a Horizontal Strip Load of Finite Width and Infinite Length

Figure 8.5 shows a horizontal flexible strip load of width B on a semi-infinite soil mass. The load per unit area is equal to q_o. The vertical stress $\Delta\sigma$ at a point $A(x, z)$ can be given as (see Harr, 1966)

$$\Delta\sigma = \frac{4bq_o xz^2}{\pi[(x^2 + z^2 - b^2)^2 + 4b^2z^2]} \tag{8.8}$$

where $b = B/2$. Table 8.4 gives the variation of $\Delta\sigma/q_o$ with z/b and x/b.

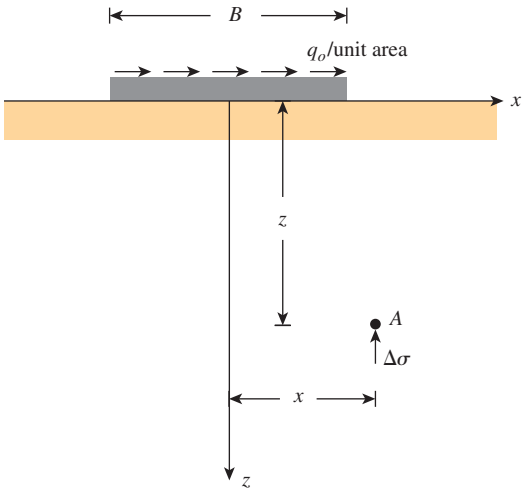


FIGURE 8.5 Vertical stress caused by a flexible horizontal strip load

TABLE 8.4 Variation of $\Delta\sigma/q_o$ with z/b and x/b [Eq. (8.8)]

	x/b					
z/b	0	0.5	1.0	1.5	2.0	2.5
0	—	—	—	—	—	—
0.25	—	0.052	0.313	0.061	0.616	
0.5	—	0.127	0.300	0.147	0.055	0.025
1.0	—	0.159	0.255	0.210	0.131	0.074
1.5	—	0.128	0.204	0.202	0.157	0.110
2.0	—	0.096	0.159	0.175	0.157	0.126
2.5	—	0.072	0.124	0.147	0.144	0.127

EXAMPLE 8.2

Consider the inclined strip load shown in Figure 8.6. Determine the vertical stress $\Delta\sigma$ at A ($x = 2.25$ m, $z = 3$ m) and B ($x = -2.25$ m, $z = 3$ m).

SOLUTION

Vertical component of $q_o = q_v = q\cos 30 = 150\cos 30 = 129.9\ \text{kN/m}^2$

Horizontal component of $q_o = q_h = q\sin 30 = 150\sin 30 = 75\ \text{kN/m}^2$

$\Delta\sigma$ due to q_v:

$$\frac{2z}{B} = \frac{(2)(3)}{3} = 2$$

$$\frac{2x}{B} = \frac{(2)(\pm 2.25)}{3} = \pm 1.5$$

From Table 8.3, $\Delta\sigma/q_v = 0.288$.

$$\Delta\sigma_v = (0.288)(129.9) = 37.4\ \text{kN/m}^2 \quad \text{(same at } A \text{ and at } B\text{)}$$

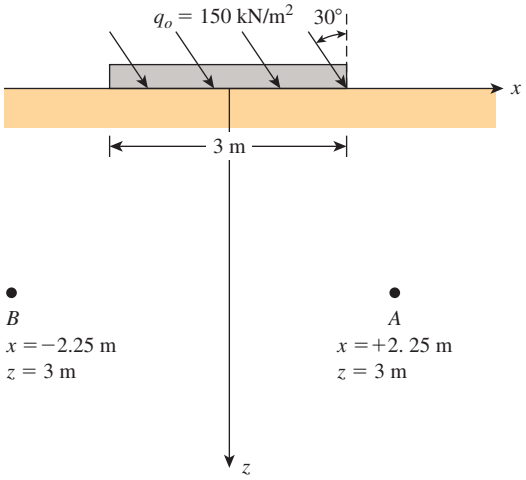


FIGURE 8.6

$\Delta\sigma$ due to q_h:

$$b = \frac{B}{2} = \frac{3}{2} = 1.5$$
$$\frac{z}{b} = \frac{3}{1.5} = 2$$
$$\frac{x}{b} = \frac{\pm 2.25}{1.5} = \pm 1.5$$

From Table 8.4, $\Delta\sigma/q_h = \pm 0.175$. So at A

$$\Delta\sigma = (+0.175)q_h = (0.175)(75) = 13.13 \text{ kN/m}^2$$

and at B

$$\Delta\sigma = (-0.175)q_h = (-0.175)(75) = -13.13 \text{ kN/m}^2$$

Hence, at A

$$\Delta\sigma = \Delta\sigma_v + \Delta\sigma_h = 37.4 + 13.13 = \mathbf{50.53 \text{ kN/m}^2}$$

At B

$$\Delta\sigma = \Delta\sigma_v + \Delta\sigma_h = 37.4 + (-13.13) = \mathbf{24.27 \text{ kN/m}^2}$$

8.7 Stress Below a Rectangular Area

The integration technique of Boussinesq's equation also allows the vertical stress at any point A below the corner of a flexible rectangular loaded area to be evaluated. (See Figure 8.7.) To do so, consider an elementary area $dA = dx\,dy$ on the flexible loaded area. If the load per unit area is q_o, the total load on the elemental area is

$$dP = q_o\,dx\,dy \tag{8.9}$$

This elemental load, dP, may be treated as a point load. The increase in vertical stress at point A caused by dP may be evaluated by using Eq. (8.1). Note, however, the need to substitute $dP = q_o\,dx\,dy$ for P and $x^2 + y^2$ for r^2 in that equation. Thus,

$$\text{The stress increase at } A \text{ caused by } dP = \frac{3q_o(dx\,dy)z^3}{2\pi(x^2 + y^2 + z^2)^{5/2}}$$

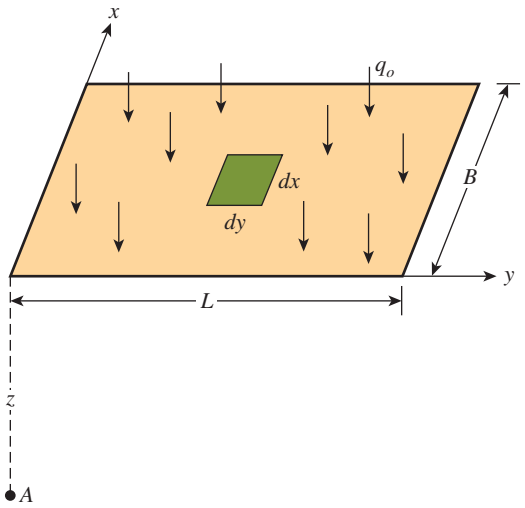


FIGURE 8.7 Determination of vertical stress below the corner of a flexible rectangular loaded area

The total stress increase $\Delta\sigma$ caused by the entire loaded area at point A may now be obtained by integrating the preceding equation:

$$\Delta\sigma = \int_{y=0}^{L}\int_{x=0}^{B} \frac{3q_o\,(dx\,dy)z^3}{2\pi(x^2 + y^2 + z^2)^{5/2}} = q_o I \tag{8.10}$$

Here,

$$I = \text{influence factor} = \frac{1}{4\pi}\left(\frac{2mn\sqrt{m^2 + n^2 + 1}}{m^2 + n^2 + m^2n^2 + 1}\cdot\frac{m^2 + n^2 + 2}{m^2 + n^2 + 1} + \tan^{-1}\frac{2mn\sqrt{m^2 + n^2 + 1}}{m^2 + n^2 + 1 - m^2n^2}\right) \tag{8.11}$$

where

$$m = \frac{B}{z} \tag{8.12}$$

and

$$n = \frac{L}{z} \tag{8.13}$$

The arctangent term in Eq. (8.11) must be a positive angle in radians. When $m^2 + n^2 + 1 < m^2n^2$, it becomes a negative angle. So a term π should be added to that angle. The variations of the influence values with m and n are given in Table 8.5.

The stress increase at any point below a rectangular loaded area can also be found by using Eq. (8.10) in conjunction with Figure 8.8. To determine the stress at a depth z below point O, divide the loaded area into four rectangles, with O the corner common to each. Then use Eq. (8.10) to calculate the increase in stress at a depth z below O caused by each rectangular area. The total stress increase caused by the entire loaded area may now be expressed as

$$\Delta\sigma = q_o\,(I_1 + I_2 + I_3 + I_4) \tag{8.14}$$

where I_1, I_2, I_3, and I_4 = the influence values of rectangles 1, 2, 3, and 4, respectively.

TABLE 8.5 Variation of Influence Value I [Eq. (8.11)][a]

	n											
m	0.1	0.2	0.3	0.4	0.5	0.6	0.7	0.8	0.9	1.0	1.2	1.4
0.1	0.00470	0.00917	0.01323	0.01678	0.01978	0.02223	0.02420	0.02576	0.02698	0.02794	0.02926	0.03007
0.2	0.00917	0.01790	0.02585	0.03280	0.03866	0.04348	0.04735	0.05042	0.05283	0.05471	0.05733	0.05894
0.3	0.01323	0.02585	0.03735	0.04742	0.05593	0.06294	0.06858	0.07308	0.07661	0.07938	0.08323	0.08561
0.4	0.01678	0.03280	0.04742	0.06024	0.07111	0.08009	0.08734	0.09314	0.09770	0.10129	0.10631	0.10941
0.5	0.01978	0.03866	0.05593	0.07111	0.08403	0.09473	0.10340	0.11035	0.11584	0.12018	0.12626	0.13003
0.6	0.02223	0.04348	0.06294	0.08009	0.09473	0.10688	0.11679	0.12474	0.13105	0.13605	0.14309	0.14749
0.7	0.02420	0.04735	0.06858	0.08734	0.10340	0.11679	0.12772	0.13653	0.14356	0.14914	0.15703	0.16199
0.8	0.02576	0.05042	0.07308	0.09314	0.11035	0.12474	0.13653	0.14607	0.15371	0.15978	0.16843	0.17389
0.9	0.02698	0.05283	0.07661	0.09770	0.11584	0.13105	0.14356	0.15371	0.16185	0.16835	0.17766	0.18357
1.0	0.02794	0.05471	0.07938	0.10129	0.12018	0.13605	0.14914	0.15978	0.16835	0.17522	0.18508	0.19139
1.2	0.02926	0.05733	0.08323	0.10631	0.12626	0.14309	0.15703	0.16843	0.17766	0.18508	0.19584	0.20278
1.4	0.03007	0.05894	0.08561	0.10941	0.13003	0.14749	0.16199	0.17389	0.18357	0.19139	0.20278	0.21020
1.6	0.03058	0.05994	0.08709	0.11135	0.13241	0.15028	0.16515	0.17739	0.18737	0.19546	0.20731	0.21510
1.8	0.03090	0.06058	0.08804	0.11260	0.13395	0.15207	0.16720	0.17967	0.18986	0.19814	0.21032	0.21836
2.0	0.03111	0.06100	0.08867	0.11342	0.13496	0.15326	0.16856	0.18119	0.19152	0.19994	0.21235	0.22058
2.5	0.03138	0.06155	0.08948	0.11450	0.13628	0.15483	0.17036	0.18321	0.19375	0.20236	0.21512	0.22364
3.0	0.03150	0.06178	0.08982	0.11495	0.13684	0.15550	0.17113	0.18407	0.19470	0.20341	0.21633	0.22499
4.0	0.03158	0.06194	0.09007	0.11527	0.13724	0.15598	0.17168	0.18469	0.19540	0.20417	0.21722	0.22600
5.0	0.03160	0.06199	0.09014	0.11537	0.13737	0.15612	0.17185	0.18488	0.19561	0.20440	0.21749	0.22632
6.0	0.03161	0.06201	0.09017	0.11541	0.13741	0.15617	0.17191	0.18496	0.19569	0.20449	0.21760	0.22644
8.0	0.03162	0.06202	0.09018	0.11543	0.13744	0.15621	0.17195	0.18500	0.19574	0.20455	0.21767	0.22652
10.0	0.03162	0.06202	0.09019	0.11544	0.13745	0.15622	0.17196	0.18502	0.19576	0.20457	0.21769	0.22654
∞	0.03162	0.06202	0.09019	0.11544	0.13745	0.15623	0.17197	0.18502	0.19577	0.20458	0.21770	0.22656

(continued)

TABLE 8.5 Variation of Influence Value I [Eq. (8.11)] *(Continued)*

	n										
m	1.6	1.8	2.0	2.5	3.0	4.0	5.0	6.0	8.0	10.0	∞
0.1	0.03058	0.03090	0.03111	0.03138	0.03150	0.03158	0.03160	0.03161	0.03162	0.03162	0.03162
0.2	0.05994	0.06058	0.06100	0.06155	0.06178	0.06194	0.06199	0.06201	0.06202	0.06202	0.06202
0.3	0.08709	0.08804	0.08867	0.08948	0.08982	0.09007	0.09014	0.09017	0.09018	0.09019	0.09019
0.4	0.11135	0.11260	0.11342	0.11450	0.11495	0.11527	0.11537	0.11541	0.11543	0.11544	0.11544
0.5	0.13241	0.13395	0.13496	0.13628	0.13684	0.13724	0.13737	0.13741	0.13744	0.13745	0.13745
0.6	0.15028	0.15207	0.15326	0.15483	0.15550	0.15598	0.15612	0.15617	0.15621	0.15622	0.15623
0.7	0.16515	0.16720	0.16856	0.17036	0.17113	0.17168	0.17185	0.17191	0.17195	0.17196	0.17197
0.8	0.17739	0.17967	0.18119	0.18321	0.18407	0.18469	0.18488	0.18496	0.18500	0.18502	0.18502
0.9	0.18737	0.18986	0.19152	0.19375	0.19470	0.19540	0.19561	0.19569	0.19574	0.19576	0.19577
1.0	0.19546	0.19814	0.19994	0.20236	0.20341	0.20417	0.20440	0.20449	0.20455	0.20457	0.20458
1.2	0.20731	0.21032	0.21235	0.21512	0.21633	0.21722	0.21749	0.21760	0.21767	0.21769	0.21770
1.4	0.21510	0.21836	0.22058	0.22364	0.22499	0.22600	0.22632	0.22644	0.22652	0.22654	0.22656
1.6	0.22025	0.22372	0.22610	0.22940	0.23088	0.23200	0.23236	0.23249	0.23258	0.23261	0.23263
1.8	0.22372	0.22736	0.22986	0.23334	0.23495	0.23617	0.23656	0.23671	0.23681	0.23684	0.23686
2.0	0.22610	0.22986	0.23247	0.23614	0.23782	0.23912	0.23954	0.23970	0.23981	0.23985	0.23987
2.5	0.22940	0.23334	0.23614	0.24010	0.24196	0.24344	0.24392	0.24412	0.24425	0.24429	0.24432
3.0	0.23088	0.23495	0.23782	0.24196	0.24394	0.24554	0.24608	0.24630	0.24646	0.24650	0.24654
4.0	0.23200	0.23617	0.23912	0.24344	0.24554	0.24729	0.24791	0.24817	0.24836	0.24842	0.24846
5.0	0.23236	0.23656	0.23954	0.24392	0.24608	0.24791	0.24857	0.24885	0.24907	0.24914	0.24919
6.0	0.23249	0.23671	0.23970	0.24412	0.24630	0.24817	0.24885	0.24916	0.24939	0.24946	0.24952
8.0	0.23258	0.23681	0.23981	0.24425	0.24646	0.24836	0.24907	0.24939	0.24964	0.24973	0.24980
10.0	0.23261	0.23684	0.23985	0.24429	0.24650	0.24842	0.24914	0.24946	0.24973	0.24981	0.24989
∞	0.23263	0.23686	0.23987	0.24432	0.24654	0.24846	0.24919	0.24952	0.24980	0.24989	0.25000

[a]After Newmark, 1935

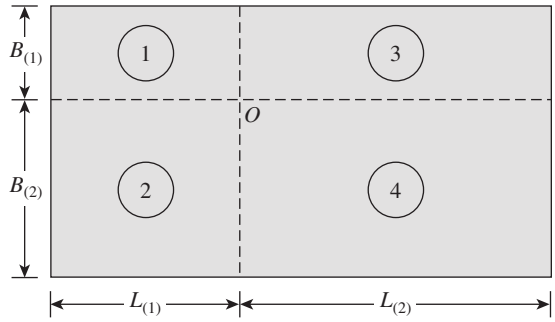


FIGURE 8.8 Stress below any point of a loaded flexible rectangular area

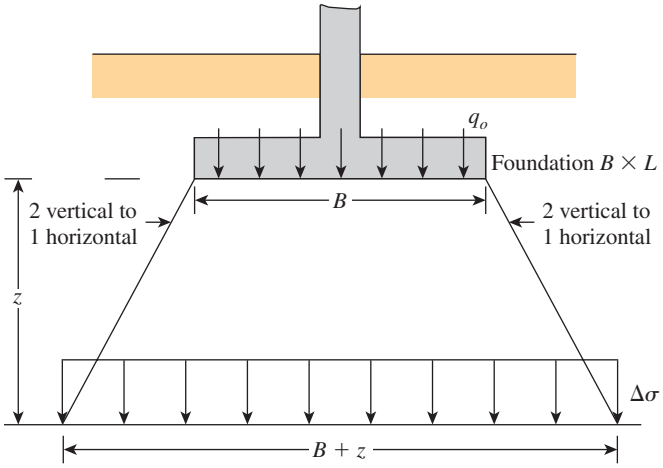


FIGURE 8.9 2:1 method of finding stress increase under a foundation

Foundation engineers often use an approximate method to determine the increase in vertical stress with depth caused by the construction of a foundation. The method is referred to as the *2:1 method*. (See Figure 8.9.) According to this method, the increase in stress at depth z is

$$\Delta\sigma = \frac{q_o \times B \times L}{(B + z)(L + z)} \tag{8.15}$$

Note that Eq. (8.15) is based on the assumption that the stress from the foundation spreads out along lines with a *vertical-to-horizontal slope of 2:1*.

For strip loads of infinite length, Eq. (8.15) becomes

$$\Delta\sigma = \frac{q_o B}{(B + z)} \tag{8.15a}$$

EXAMPLE 8.3

A flexible rectangular area measures 2.5 m × 5 m in plan. It supports a load of 150 kN/m^2.

Determine the vertical stress increase due to the load at a depth of 6.25 m below the center of the rectangular area.

SOLUTION

Refer to Figure 8.8. For this case,

$$B_1 = B_2 = \frac{2.5}{2} = 1.25 \text{ m}$$

$$L_1 = L_2 = \frac{5}{2} = 2.5 \text{ m}$$

From Eqs. (8.12) and (8.13),

$$m = \frac{B_1}{z} = \frac{B_2}{z} = \frac{1.25}{6.25} = 0.2$$

$$n = \frac{L_1}{z} = \frac{L_2}{z} = \frac{2.5}{6.25} = 0.4$$

From Table 8.5, for $m = 0.2$ and $n = 0.4$, the value of $I = 0.0328$. Thus,

$$\Delta\sigma = q_o(4I) = (150)(4)(0.0328) = \mathbf{19.68\ kN/m^2}$$

From Eq. (8.15),

$$\Delta\sigma = \frac{q_o BL}{(B + z)(L + z)} = \frac{(150)(2.5)(5.0)}{(2.5 + 6.25)(5.0 + 6.25)} = \mathbf{19.05\ kN/m^3}$$

8.8 Stress Isobars

Using Eq. (8.7), it is possible to determine the variation of $\Delta\sigma/q_o$ at various points below a uniform strip load of width B. The results can be used to plot *stress isobars* (i.e., contours of $\Delta\sigma/q_o$), as shown in Figure 8.10. In a similar manner, Eq. (8.10) can

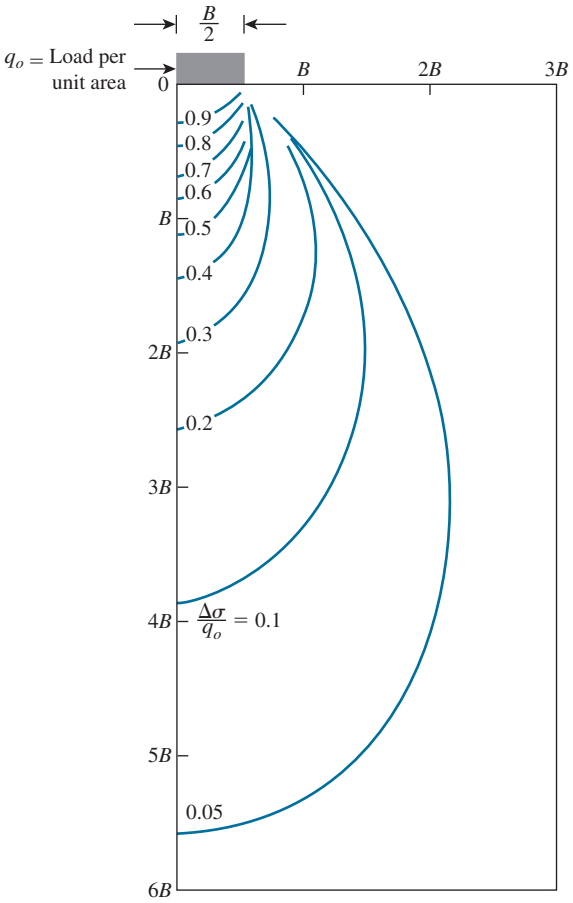


FIGURE 8.10 Contours of $\Delta\sigma/q_o$ below a strip load

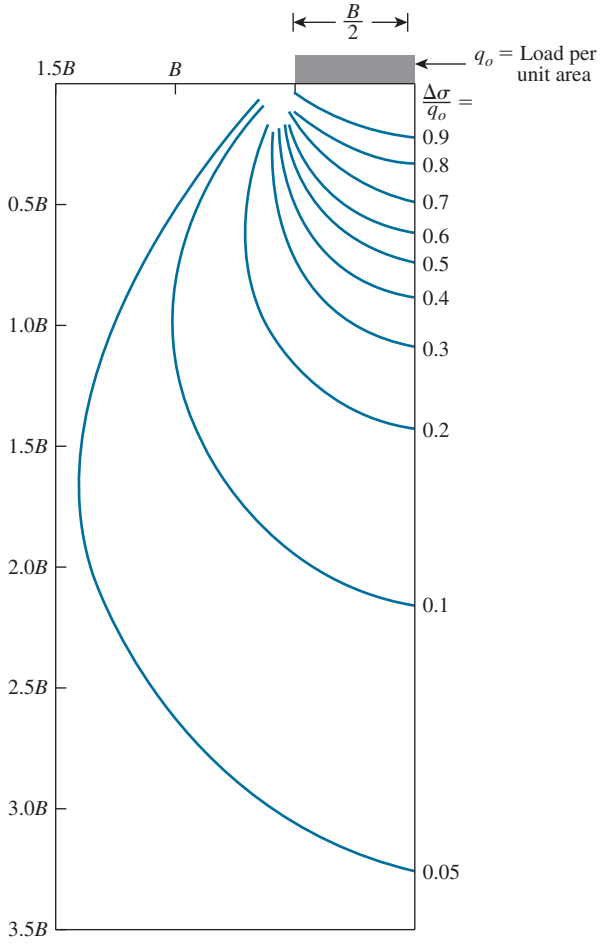


FIGURE 8.11 Contours of $\Delta\sigma/q_o$ below the center line of a square loaded area ($B \times B$)

be used to determine the variation of $\Delta\sigma/q_o$ below a square loaded area measuring $B \times B$, and stress isobars can be plotted as shown in Figure 8.11. These stress isobars are sometimes helpful in the design of shallow foundations.

8.9 Average Vertical Stress Increase Due to a Rectangularly Loaded Area

In Section 8.7, the vertical stress increase below the corner of a uniformly loaded rectangular area was given as

$$\Delta\sigma = q_o I$$

In many cases, one must find the average stress increase, $\Delta\sigma_{av}$, below the corner of a uniformly loaded rectangular area with limits of $z = 0$ to $z = H$, as shown in Figure 8.12. This can be evaluated as

$$\Delta\sigma_{av} = \frac{1}{H}\int_0^H (q_o I)\,dz = q_o I_a \tag{8.16}$$

where

$$I_a = f(m_2, n_2) \tag{8.17}$$

$$m_2 = \frac{B}{H} \tag{8.18}$$

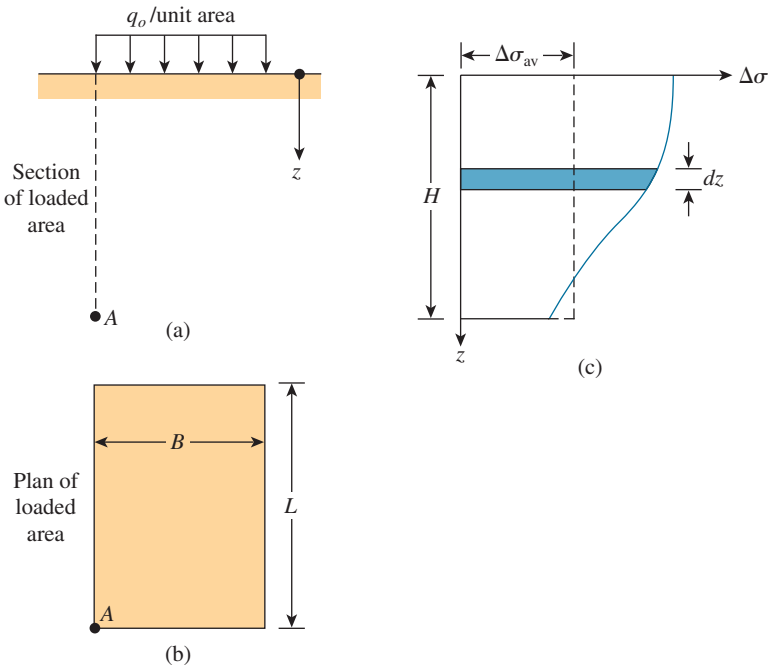


FIGURE 8.12 Average vertical stress increase due to a rectangularly loaded flexible area

and

$$n_2 = \frac{L}{H} \tag{8.19}$$

The variation of I_a with m_2 and n_2 is shown in Figure 8.13, as proposed by Griffiths (1984).

In estimating the consolidation settlement under a foundation, it may be required to determine the average vertical stress increase in only a given layer—that is,

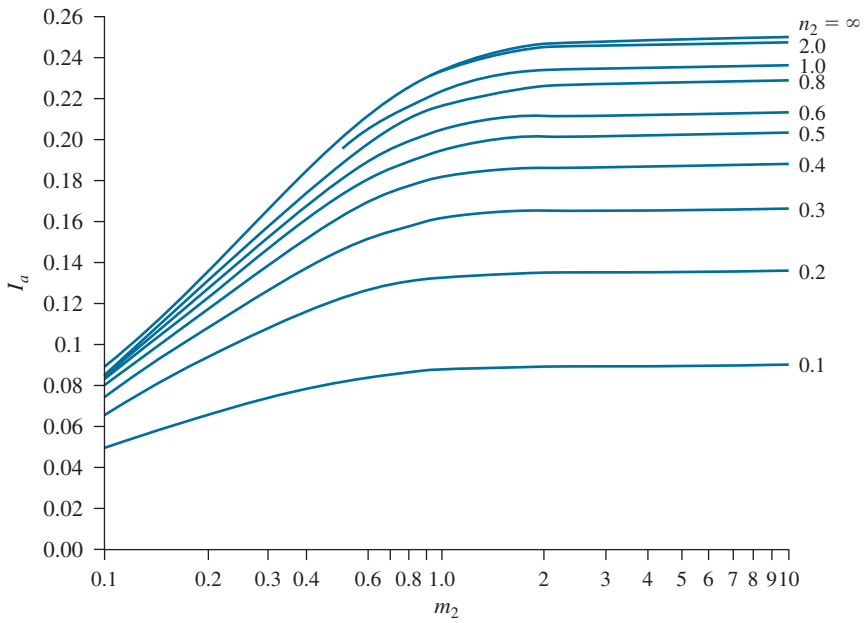


FIGURE 8.13 Griffiths' influence factor I_a

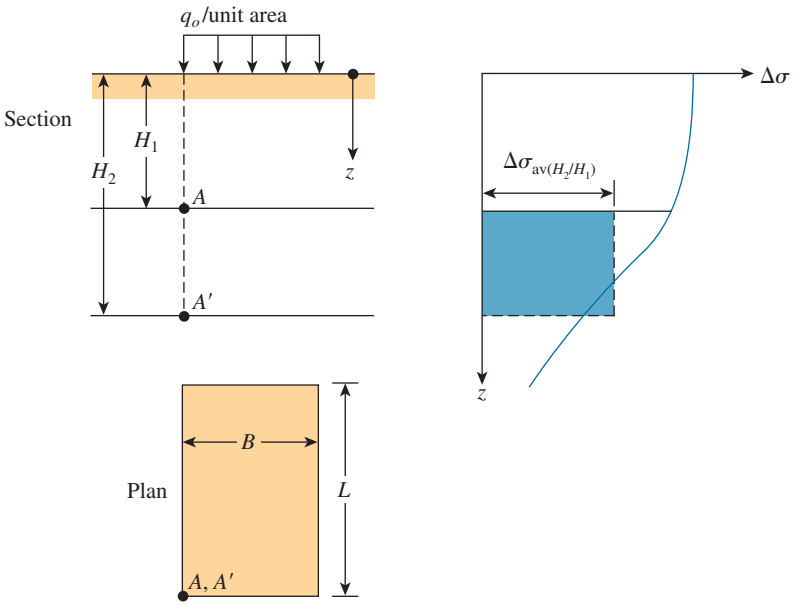


FIGURE 8.14 Average pressure increase between $z = H_1$ and $z = H_2$ below the corner of a uniformly loaded rectangular area

between $z = H_1$ and $z = H_2$, as shown in Figure 8.14. This can be done as (Griffiths, 1984)

$$\Delta\sigma_{av(H_2/H_1)} = q_o\left[\frac{H_2 I_{a(H_2)} - H_1 I_{a(H_1)}}{H_2 - H_1}\right] \tag{8.20}$$

where

$\Delta\sigma_{av(H_2/H_1)}$ = average stress increase immediately below the corner of a uniformly loaded rectangular area between depths $z = H_1$ and $z = H_2$

$$I_{a(H_2)} = I_a \text{ for } z = 0 \text{ to } z = H_2 = f\left(m_2 = \frac{B}{H_2}, n_2 = \frac{L}{H_2}\right) \tag{8.21}$$

$$I_{a(H_1)} = I_a \text{ for } z = 0 \text{ to } z = H_1 = f\left(m_2 = \frac{B}{H_1}, n_2 = \frac{L}{H_1}\right) \tag{8.22}$$

In most practical cases, however, we will need to determine the average stress increase between $z = H_1$ and $z = H_2$ below the center of a loaded area. The procedure for doing this can be explained with reference to Figure 8.15, which shows the plan of a loaded area measuring $L \times B$. The loaded area can be divided into four rectangular areas measuring $B' \times L'$ (note: $B' = B/2$ and $L' = L/2$), and the point O is the common corner for each of the four rectangles. The average stress increase below O between $z = H_1$ to H_2 due to each loaded area then can be given by Eq. (8.20), where

$$I_{a(H_2)} = f\left(m_2 = \frac{B'}{H_2};\ n_2 = \frac{L'}{H_2}\right) \tag{8.23}$$

and

$$I_{a(H_1)} = f\left(m_2 = \frac{B'}{H_1};\ n_2 = \frac{L'}{H_1}\right) \tag{8.24}$$

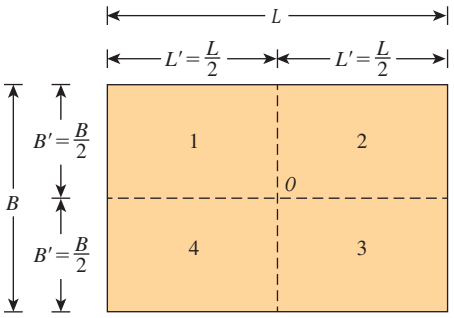


FIGURE 8.15 Average stress increase calculation below a flexible loaded rectangular area

Now the total average stress increase due to the four loaded areas (each measuring $L' \times B'$) between $z = H_1$ to H_2 can be given as

$$\Delta\sigma_{\text{av}(H_2/H_1)} = 4q_o\left[\frac{H_2 I_{a(H_2)} - H_1 I_{a(H_1)}}{H_2 - H_1}\right] \qquad (8.25)$$

(Eq. (8.23) and Eq. (8.24) refer to $I_{a(H_2)}$ and $I_{a(H_1)}$, respectively.)

This procedure for the determination of $\Delta\sigma_{\text{av}(H_2/H_1)}$ is shown in Example 8.4.

Another approximate procedure to determine $\Delta\sigma_{\text{av}(H_2/H_1)}$ is to use the relationship

$$\Delta\sigma_{\text{av}(H_2/H_1)} = \frac{\Delta\sigma_t + 4\Delta\sigma_m + \Delta\sigma_b}{6} \qquad (8.26)$$

where $\Delta\sigma_t$, $\Delta\sigma_m$, and $\Delta\sigma_b$ = stress increase below the center of the loaded area ($L \times B$), respectively, at depths $z = H_1$, $H_1 + H_2/2$, and $H_1 + H_2$.

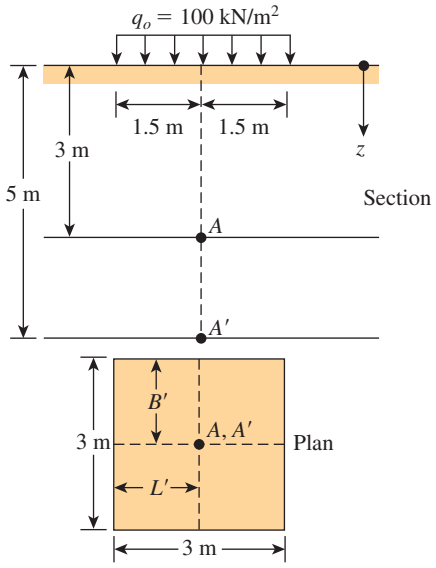


FIGURE 8.16 Determination of average increase in stress below a rectangular area

EXAMPLE 8.4

Refer to Figure 8.16. Determine the *average* stress increase below the center of the loaded area between $z = 3$ m to $z = 5$ m (that is, between points A and A').

SOLUTION

Refer to Figure 8.16. The loaded area can be divided into four rectangular areas, each measuring 1.5 m × 1.5 m ($L' \times B'$). Using Eq. (8.25), the average stress increase (between the required depths) below the center of the entire loaded area can be given as

$$\Delta\sigma_{\text{av}(H_2/H_1)} = 4q_o\left[\frac{H_2 I_{a(H_2)} - H_1 I_{a(H_1)}}{H_2 - H_1}\right] = (4)(100)\left[\frac{(5)I_{a(H_2)} - (3)I_{a(H_1)}}{5 - 3}\right]$$

For $I_{a(H_2)}$ [Eq. (8.23)],

$$m_2 = \frac{B'}{H_2} = \frac{1.5}{5} = 0.3$$

$$n_2 = \frac{L'}{H_2} = \frac{1.5}{5} = 0.3$$

Referring to Figure 8.13, for $m_2 = 0.3$ and $n_2 = 0.3$, $I_{a(H_2)} = 0.126$. For $I_{a(H_1)}$ [Eq. (8.24)],

$$m_2 = \frac{B'}{H_1} = \frac{1.5}{3} = 0.5$$

$$n_2 = \frac{L'}{H_1} = \frac{1.5}{3} = 0.5$$

Referring to Figure 8.13, $I_{a(H_1)} = 0.175$, so

$$\Delta\sigma_{\text{av}\,(H_2/H_1)} = (4)(100)\left[\frac{(5)(0.126) - (3)(0.175)}{5 - 3}\right] = \mathbf{21\ kN/m^2}$$

EXAMPLE 8.5

Solve Example 8.4 using Eqs. (8.10) and (8.26) and Table 8.5.

SOLUTION

Consider a quarter of the square and multiply by four for the I-value for the center.

$$q_o = 100\ \text{kN/m}^2$$

z(m)	$B' = B/2$ (m)	$L' = L/2$ (m)	m	n	I (Table 8.5)	$\Delta\sigma = 4q_oI$ (kN/m^2)
3.0	1.5	1.5	0.5	0.5	0.08403	33.6
4.0	1.5	1.5	0.375	0.375	0.0540	21.6
5.0	1.5	1.5	0.3	0.3	0.03735	14.9

From Eq. (8.26),

$$\Delta\sigma_{\text{av}(H_2/H_1)} = \frac{\Delta\sigma_t + 4\Delta\sigma_m + \Delta\sigma_b}{6} = \frac{33.6 + 4 \times 21.6 + 14.9}{6} = \mathbf{22.5\ kN/m^2}$$

EXAMPLE 8.6

Solve Example 8.4 using Eqs. (8.15) and (8.26).

SOLUTION

From Eq. (8.15) for a square loaded area,

$$\sigma_t = \frac{q_oB^2}{(B + z)^2} = \frac{(100)(3)^2}{(3 + 3)^2} = 25\ \text{kN/m}^2$$

$$\sigma_m = \frac{(100)(3)^2}{(3 + 4)^2} = 18.37\ \text{kN/m}^2$$

$$\sigma_b = \frac{(100)(3)^2}{(3 + 5)^2} = 14.06\ \text{kN/m}^2$$

$$\Delta\sigma_{\text{av}(H_2/H_1)} = \frac{25 + 4(18.37) + 14.06}{6} = \mathbf{18.76\ kN/m^2}$$

8.10 Average Vertical Stress Increase Below the Center of a Circularly Loaded Area

The average vertical stress increase below the center of a flexible circularly loaded area of diameter B between $z = H_1$ and $z = H_2$ (see inset in Figure 8.17) can be estimated using Eq. (8.26). The values of σ_t, σ_m, and σ_b can be obtained by using Eq. (8.3).

Saika (2012) has also provided a mathematical solution to obtain $\Delta\sigma_{av(H_2/H_1)}$ below the center of a flexible circularly loaded (intensity = q_o) area. This is shown in a nondimensional form in Figure 8.17.

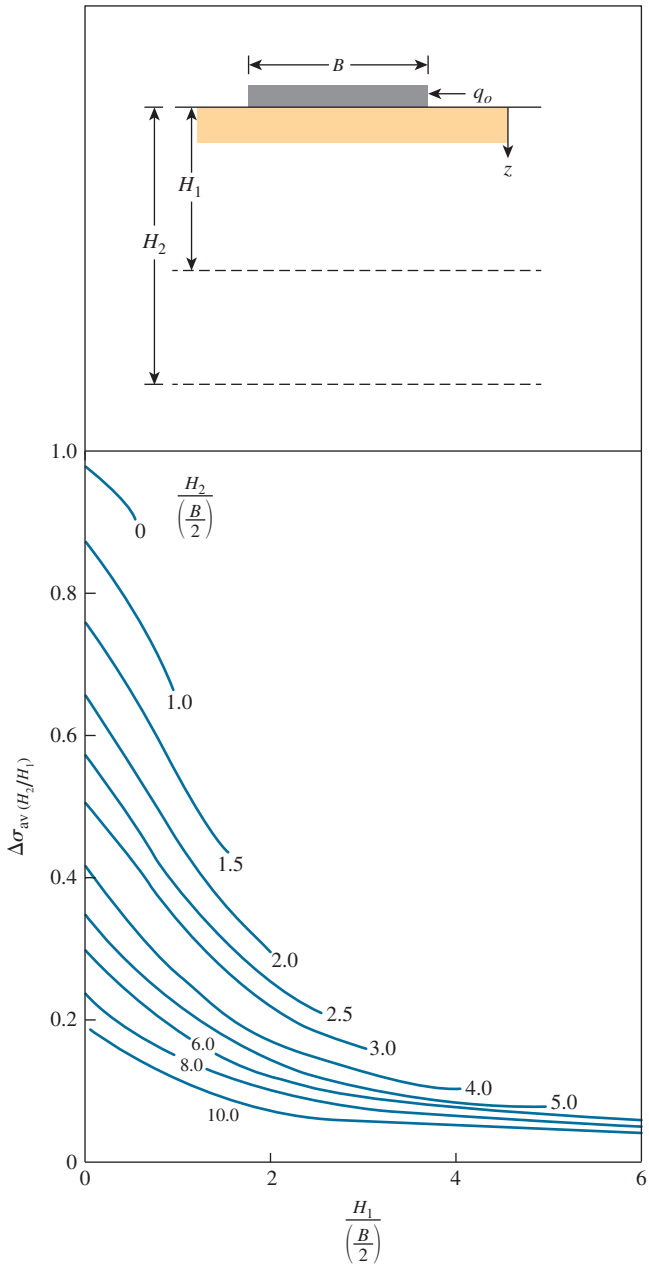


FIGURE 8.17 Average stress increase below the center of a flexible circularly loaded area between $z = H_1$ to $z = H_2$ (Based on Saika, 2012)

EXAMPLE 8.7

Figure 8.18 shows a flexible circularly loaded area with $B = 2$ m and $q_o = 150$ kN/m^2. Estimate the average stress ($\Delta\sigma_{av}$) increase in the clay layer below the center of the loaded area. Use Eqs. (8.3) and (8.26).

SOLUTION

From Eq. (8.3),

$$\Delta\sigma = q_o\left\{1 - \frac{1}{\left[1 + \left(\frac{B}{2z}\right)^2\right]^{3/2}}\right\}$$

Hence (at $z = H_1 = 1$ m),

$$\Delta\sigma_t = 150\left\{1 - \frac{1}{\left[1 + \left(\frac{2}{2 \times 1}\right)^2\right]^{3/2}}\right\} = 96.97 \text{ kN/m}^2$$

At $z = 3.5$ m,

$$\Delta\sigma_m = 150\left\{1 - \frac{1}{\left[1 + \left(\frac{2}{2 \times 3.5}\right)^2\right]^{3/2}}\right\} = 16.66 \text{ kN/m}^2$$

At $z = 6$ m,

$$\Delta\sigma_b = 150\left\{1 - \frac{1}{\left[1 + \left(\frac{2}{2 \times 6}\right)^2\right]^{3/2}}\right\} = 6.04 \text{ kN/m}^2$$

From Eq. (8.26),

$$\Delta\sigma_{av} = \frac{\Delta\sigma_t + 4\Delta\sigma_m + \Delta\sigma_b}{6} = \frac{96.97 + (4)(16.66) + 6.04}{6} = \mathbf{28.28 \text{ kN/m}^2}$$

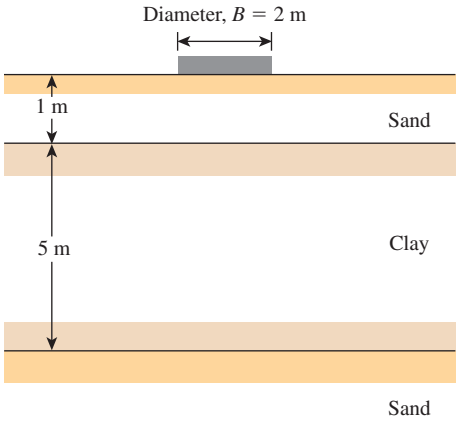


FIGURE 8.18

EXAMPLE 8.8

Solve Example 8.7 by using Figure 8.17.

SOLUTION

$$\frac{H_1}{\left(\frac{B}{2}\right)} = \frac{1}{\left(\frac{2}{2}\right)} = 1$$

$$\frac{H_2}{\left(\frac{B}{2}\right)} = \frac{6}{\left(\frac{2}{2}\right)} = 6$$

From Figure 8.17, for $H_1/(B/2) = 1$ and $H_2/(B/2) = 6$, the value of $\Delta\sigma_{av}/q_o \approx 0.175$. Hence,

$$\Delta\sigma_{av} = (150)(0.175) = \mathbf{26.25\ kN/m^2}$$

8.11 Stress Increase Under an Embankment

Figure 8.19 shows the cross section of an embankment of height H. For this two-dimensional loading condition, the vertical stress increase may be expressed as

$$\Delta\sigma = \frac{q_o}{\pi}\left[\left(\frac{B_1 + B_2}{B_2}\right)(\alpha_1 + \alpha_2) - \frac{B_1}{B_2}(\alpha_2)\right] \tag{8.27}$$

where

$q_o = \gamma H$

γ = unit weight of the embankment soil

H = height of the embankment

$$\alpha_1 = \tan^{-1}\left(\frac{B_1 + B_2}{z}\right) - \tan^{-1}\left(\frac{B_1}{z}\right) \tag{8.28}$$

$$\alpha_2 = \tan^{-1}\left(\frac{B_1}{z}\right) \tag{8.29}$$

(Note that α_1 and α_2 are in radians.)

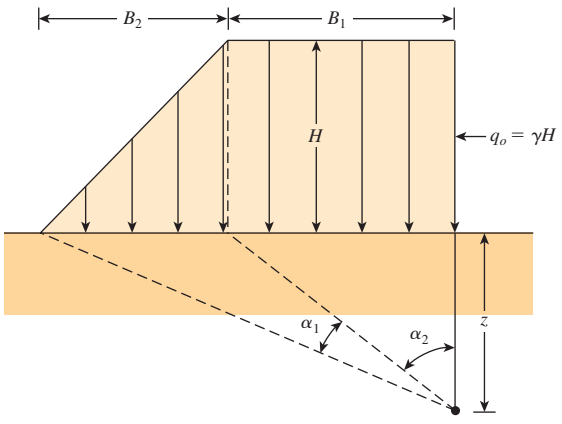


FIGURE 8.19 Embankment loading

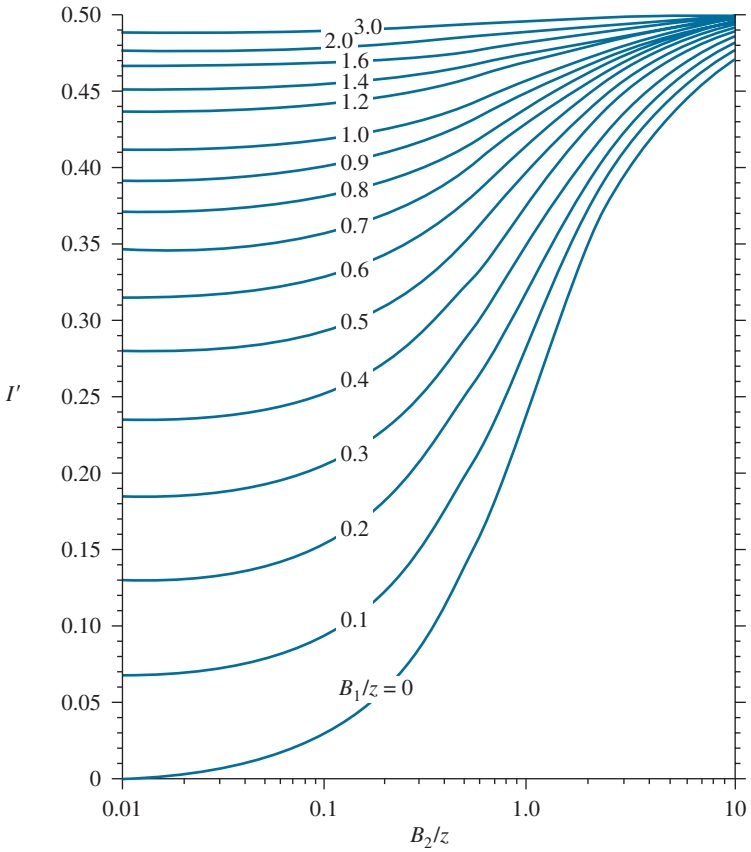


FIGURE 8.20 Influence value I' for embankment loading (Osterberg, J. O. (1957). "Influence Values for Vertical Stresses in Semi-Infinite Mass Due to Embankment Loading," *Proceedings, Fourth International Conference on Soil Mechanics and Foundation Engineering*, London, Vol. 1. pp. 393–396. With permission from ASCE.)

For a detailed derivation of Eq. (8.27), see Das (2014). A simplified form of the equation is

$$\Delta\sigma = q_o I' \tag{8.30}$$

where I' = a function of B_1/z and B_2/z.

The variation of I' with B_1/z and B_2/z is shown in Figure 8.20. An application of this diagram is given in Example 8.9.

EXAMPLE 8.9

An embankment is shown in Figure 8.21a. Determine the stress increase under the embankment at points A_1 and A_2.

SOLUTION

We have

$$\gamma H = (17.5)(7) = 122.5 \text{ kN/m}^2$$

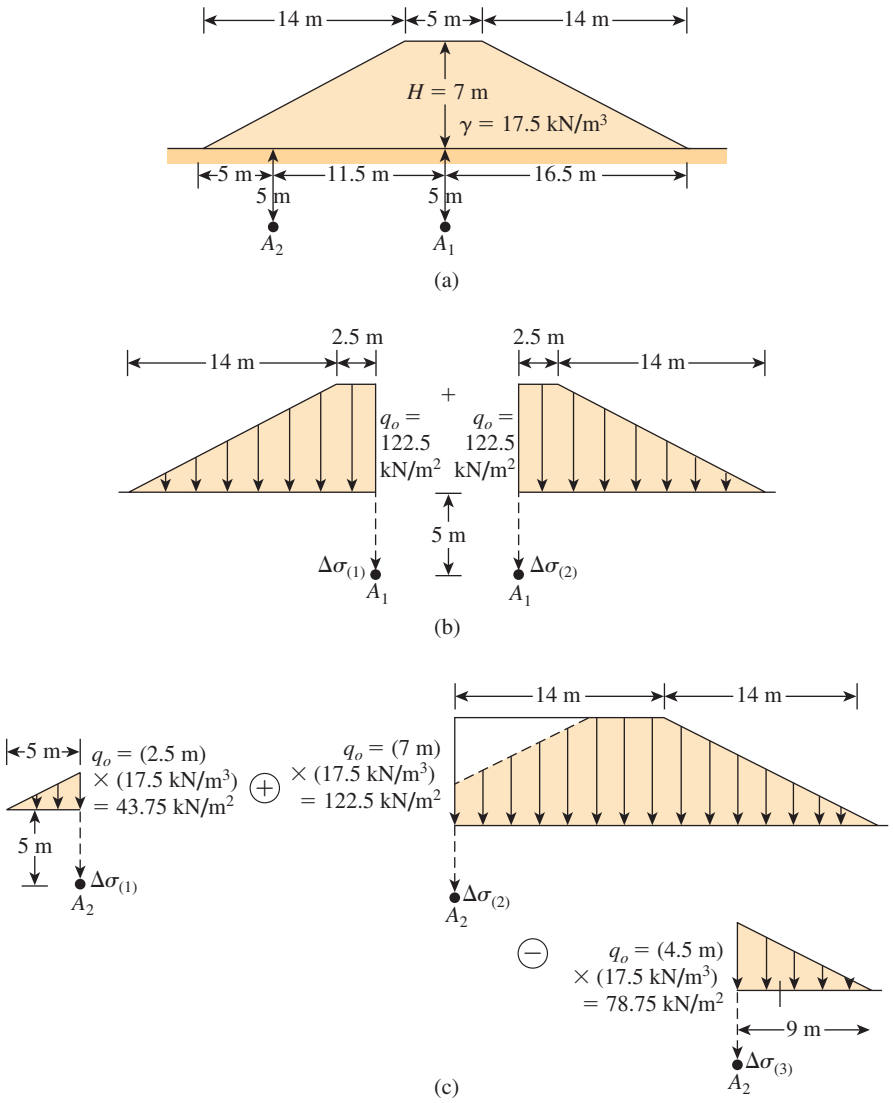


FIGURE 8.21 Stress increase due to embankment loading

Stress Increase at A_1

The left side of Figure 8.21b indicates that $B_1 = 2.5$ m and $B_2 = 14$ m, so

$$\frac{B_1}{z} = \frac{2.5}{5} = 0.5$$

and

$$\frac{B_2}{z} = \frac{14}{5} = 2.8$$

According to Figure 8.20, in this case $I' = 0.445$. Because the two sides in Figure 8.21b are symmetrical, the value of I' for the right side will also be 0.445, so

$$\Delta\sigma = \Delta\sigma_{(1)} + \Delta\sigma_{(2)} = q_o[I'_{(\text{left side})} + I'_{(\text{right side})}]$$

$$= 122.5[0.445 + 0.445] = \mathbf{109.03\ kN/m^2}$$

Stress Increase at A_2

In Figure 8.21c, for the left side, $B_2 = 5$ m and $B_1 = 0$, so

$$\frac{B_2}{z} = \frac{5}{5} = 1$$

and

$$\frac{B_1}{z} = \frac{0}{5} = 0$$

According to Figure 8.20, for these values of B_2/z and B_1/z, $I' = 0.24$; hence,

$$\Delta\sigma_{(1)} = 43.75(0.24) = 10.5 \text{ kN/m}^2$$

For the middle section,

$$\frac{B_2}{z} = \frac{14}{5} = 2.8$$

and

$$\frac{B_1}{z} = \frac{14}{5} = 2.8$$

Thus, $I' = 0.495$, so

$$\Delta\sigma_{(2)} = 0.495(122.5) = 60.64 \text{ kN/m}^2$$

For the right side,

$$\frac{B_2}{z} = \frac{9}{5} = 1.8$$
$$\frac{B_1}{z} = \frac{0}{5} = 0$$

and $I' = 0.335$, so

$$\Delta\sigma_{(3)} = (78.75)(0.335) = 26.38 \text{ kN/m}^2$$

The total stress increase at point A_2 is

$$\Delta\sigma = \Delta\sigma_{(1)} + \Delta\sigma_{(2)} - \Delta\sigma_{(3)} = 10.5 + 60.64 - 26.38 = \mathbf{44.76 \text{ kN/m}^2}$$

8.12 Westergaard's Solution for Vertical Stress Due to a Point Load

Boussinesq's solution for stress distribution due to a point load was presented in Section 8.2. The stress distribution due to various types of loading discussed in previous sections is based on integration of Boussinesq's solution.

Westergaard (1938) has proposed a solution for the determination of the vertical stress due to a point load P in an elastic solid medium in which there exist alternating layers with thin rigid reinforcements (Figure 8.22a). This type of assumption may be

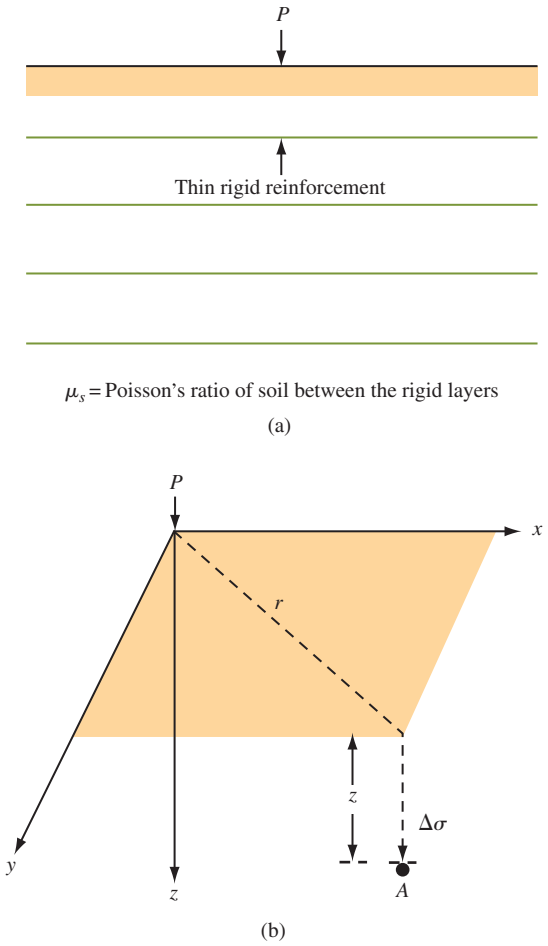


FIGURE 8.22 Westergaard's solution for vertical stress due to a point load

an idealization of a clay layer with thin seams of sand. For such an assumption, the vertical stress increase at a point A (Figure 8.22b) can be given as

$$\Delta\sigma = \frac{P\eta}{2\pi z^2}\left[\frac{1}{\eta^2 + (r/z)^2}\right]^{3/2} \tag{8.31}$$

where

$$\eta = \sqrt{\frac{1 - 2\mu_s}{2 - 2\mu_s}} \tag{8.32}$$

μ_s = Poisson's ratio of the solid between the rigid reinforcements

$r = \sqrt{x^2 + y^2}$

Equation (8.31) can be rewritten as

$$\Delta\sigma = \left(\frac{P}{z^2}\right)I_1 \tag{8.33}$$

TABLE 8.6 Variation of I_1 [Eq. (8.34)]

	I_1		
r/z	$\mu_s = 0$	$\mu_s = 0.2$	$\mu_s = 0.4$
0	0.3183	0.4244	0.9550
0.1	0.3090	0.4080	0.8750
0.2	0.2836	0.3646	0.6916
0.3	0.2483	0.3074	0.4997
0.4	0.2099	0.2491	0.3480
0.5	0.1733	0.1973	0.2416
0.6	0.1411	0.1547	0.1700
0.7	0.1143	0.1212	0.1221
0.8	0.0925	0.0953	0.0897
0.9	0.0751	0.0756	0.0673
1.0	0.0613	0.0605	0.0516
1.5	0.0247	0.0229	0.0173
2.0	0.0118	0.0107	0.0076
2.5	0.0064	0.0057	0.0040
3.0	0.0038	0.0034	0.0023
4.0	0.0017	0.0015	0.0010
5.0	0.0009	0.0008	0.0005

where

$$I_1 = \frac{1}{2\pi\eta^2}\left[\left(\frac{r}{\eta z}\right)^2 + 1\right]^{-3/2} \tag{8.34}$$

Table 8.6 gives the variation of I_1 with μ_s.

8.13 Stress Distribution for Westergaard Material

STRESS DUE TO A CIRCULARLY LOADED AREA

Referring to Figure 8.2, if the circular area is located on a Westergaard-type material, the increase in vertical stress, $\Delta\sigma$, at a point located at a depth z directly below the center of the area can be given as

$$\Delta\sigma = q_o\left\{1 - \frac{\eta}{\left[\eta^2 + \left(\frac{B}{2z}\right)^2\right]^{1/2}}\right\} \tag{8.35}$$

The term η has been defined in Eq. (8.32). The variations of $\Delta\sigma/q_o$ with $B/2z$ and $\mu_s = 0$ are given in Table 8.7.

TABLE 8.7 Variation of $\Delta\sigma/q_o$ with $B/2z$

	$\Delta\sigma/q_o$		
$B/2z$	$\mu_s = 0$	$\mu_s = 0.2$	$\mu_s = 0.4$
0.00	0.0000	0.0000	0.0000
0.25	0.0572	0.0742	0.1472
0.33	0.0955	0.1217	0.2254
0.50	0.1835	0.2254	0.3675
0.75	0.3140	0.3675	0.5219
1.00	0.4226	0.4778	0.6220
1.25	0.5076	0.5601	0.6895
1.50	0.5736	0.6220	0.7374
1.75	0.6254	0.6697	0.7728
2.00	0.6667	0.7072	0.8000
2.25	0.7002	0.7374	0.8215
2.50	0.7278	0.7621	0.8388
2.75	0.7510	0.7826	0.8532
3.00	0.7706	0.8000	0.8652
4.00	0.8259	0.8487	0.8985
5.00	0.8600	0.8784	0.9186
6.00	0.8830	0.8985	0.9321
7.00	0.8995	0.9129	0.9418
8.00	0.9120	0.9237	0.9490
9.00	0.9217	0.9321	0.9547
10.00	0.9295	0.9389	0.9592

STRESS DUE TO A UNIFORMLY LOADED FLEXIBLE RECTANGULAR AREA

Refer to Figure 8.7. If the flexible rectangular area is located on a Westergaard-type material, the stress increase at point A can be given as

$$\Delta\sigma = \frac{q_o}{2\pi}\left[\cot^{-1}\sqrt{\eta^2\left(\frac{1}{m^2}+\frac{1}{n^2}\right)+\eta^4\left(\frac{1}{m^2n^2}\right)}\right] \tag{8.36a}$$

where

$$m = \frac{B}{z}$$

$$n = \frac{L}{z}$$

or

$$\frac{\Delta\sigma}{q_o} = \frac{1}{2\pi}\left[\cot^{-1}\sqrt{\eta^2\left(\frac{1}{m^2}+\frac{1}{n^2}\right)+\eta^4\left(\frac{1}{m^2n^2}\right)}\right] = I_w \tag{8.36b}$$

Table 8.8 gives the variation of I_w with m and n (for $\mu_s = 0$). Figure 8.23 also provides a plot of I_w (for $\mu_s = 0$) for various values of m and n.

TABLE 8.8 Variation of I_w with m and n ($\mu_s = 0$)

	n								
m	0.1	0.2	0.4	0.5	0.6	1.0	2.0	5.0	10.0
0.1	0.0031	0.0061	0.0110	0.0129	0.0144	0.0182	0.0211	0.0211	0.0223
0.2	0.0061	0.0118	0.0214	0.0251	0.0282	0.0357	0.0413	0.0434	0.0438
0.4	0.0110	0.0214	0.0390	0.0459	0.0516	0.0658	0.0768	0.0811	0.0847
0.5	0.0129	0.0251	0.0459	0.0541	0.0610	0.0781	0.0916	0.0969	0.0977
0.6	0.0144	0.0282	0.0516	0.0610	0.0687	0.0886	0.1044	0.1107	0.1117
1.0	0.0183	0.0357	0.0658	0.0781	0.0886	0.1161	0.1398	0.1491	0.1515
2.0	0.0211	0.0413	0.0768	0.0916	0.1044	0.1398	0.1743	0.1916	0.1948
5.0	0.0221	0.0435	0.0811	0.0969	0.1107	0.1499	0.1916	0.2184	0.2250
10.0	0.0223	0.0438	0.0817	0.0977	0.1117	0.1515	0.1948	0.2250	0.2341

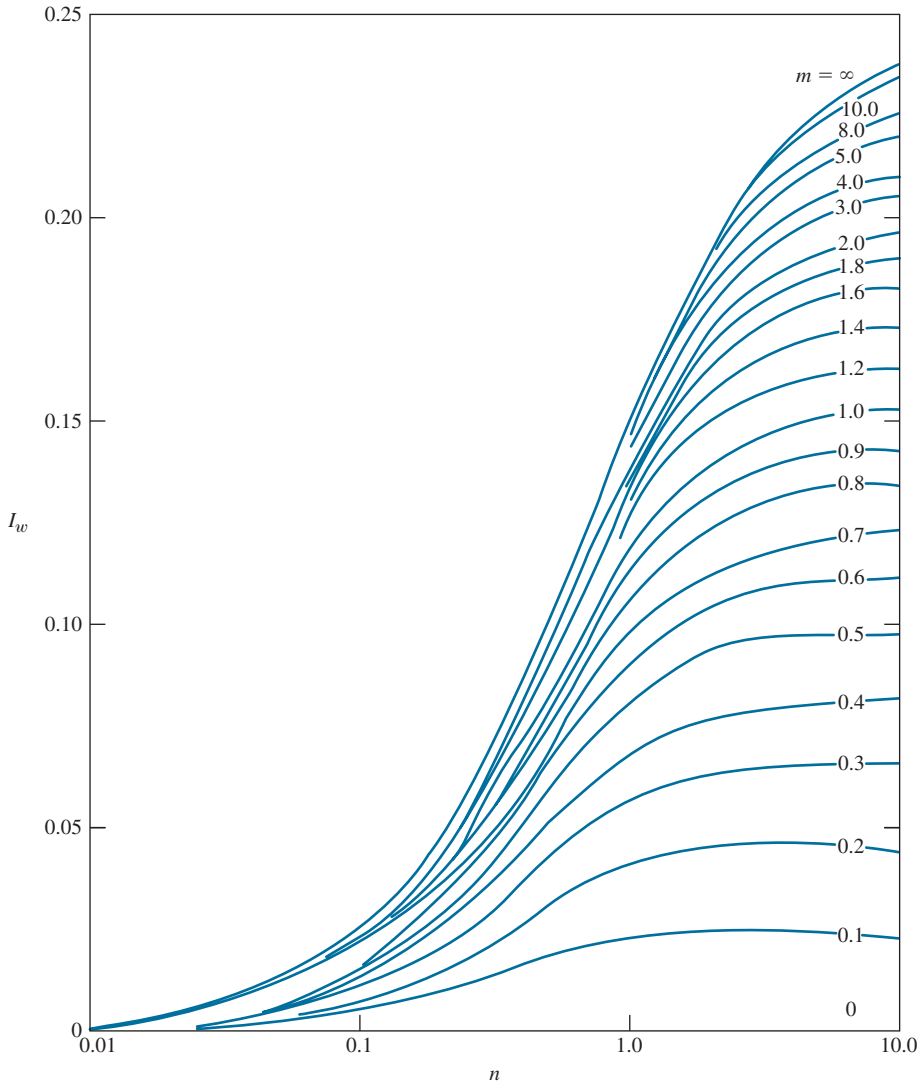


FIGURE 8.23 Variation of I_w ($\mu_s = 0$) [Eq. (8.36b)] for various values of m and n

EXAMPLE 8.10

Solve Example 8.3 using Eq. (8.36). Assume $\mu_s = 0$.

SOLUTION

From Example 8.3,

$$m = 0.2$$
$$n = 0.4$$
$$\Delta\sigma = q_o(4I_w)$$

From Table 8.8, for $m = 0.2$ and $n = 0.4$, the value of $I_w \approx 0.0214$. So

$$\Delta\sigma = (150)(4 \times 0.0214) = \mathbf{12.84\ kN/m^2}$$

8.14 Summary

When a foundation, embankment, or retaining wall is placed on the ground, the stresses within the subsoil are increased. Such increases can lead to deformations (e.g., settlements) of the soil mass that can jeopardize the integrity of the structure. To determine the deformations, it is necessary to know the stress increases within the soil mass.

The loading at the ground level can be in the form of a point load, line load, or area loads. Techniques to determine the vertical stress increases due to these different types of loads were discussed in this chapter. In deriving the expressions for computing the vertical stress increase, the soil was treated as an elastic continuum.

PROBLEMS

8.1 Four point loads with the same magnitude of P are applied as shown in the plan view in Figure P8.1 and are separated by distance b.

a. Find the vertical stress increase $\Delta\sigma$ at a depth of $0.5b$ below the points O and A in terms of P and b. Use Boussinesq's solution given by Eq. (8.1).

b. Determine $\Delta\sigma$ if $P = 500$ kN and $b = 5$ m. Use the results of Part a.

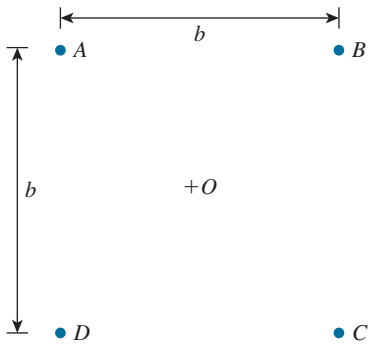


FIGURE P8.1

8.2 A point load of 500 kN is applied at the ground level. Plot the lateral variation of the vertical stress increase $\Delta\sigma$ at depths of 2 m, 3 m, and 4 m below the ground level.

8.3 A point load of 1000 kN is applied at the ground level. Plot the variation of the vertical stress increase $\Delta\sigma$ with depth at horizontal distance of 1 m, 2 m, and 4 m from the load.

8.4 A 10 ft diameter flexible loaded area is subjected to a uniform pressure of 1200 lb/ft^2.

a. Plot the variation of the vertical stress increase beneath the center with depth $z = 0$ to 20 ft.

b. In the same plot, show the variation beneath the edge of the loaded area.

8.5 For the flexible loaded area in Problem 8.4, plot the vertical stress variation with the radial distance at 2.5 ft below the ground level.

8.6 Two line loads q_1 and q_2 of infinite lengths are acting on top of an elastic medium, as shown in Figure P8.6. Find the vertical stress increase at A.

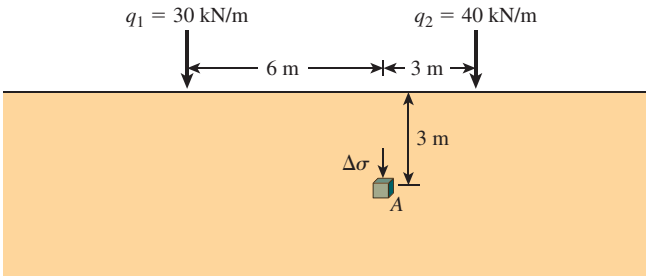


FIGURE P8.6

8.7 A 9 ft wide and infinitely long flexible strip load of 800 lb/ft^2 is placed on an elastic medium as shown in Figure P8.7. Find the vertical stress increase at points *A*, *B*, and *C* located 3 ft below the surface.

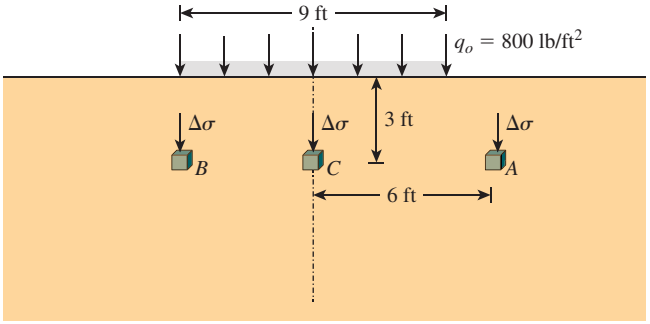


FIGURE P8.7

8.8 Figure P8.8 shows a flexible rectangular raft that is 8 m × 16 m and applies a uniform pressure of 80 kN/m^2 to the underlying ground. Find the vertical stress increase Δσ at 4 m below *A*, *B*, *C*, and *D*.

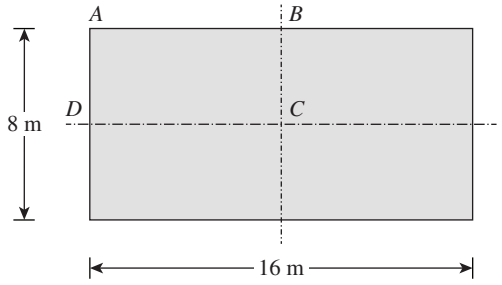


FIGURE P8.8

8.9 A flexible L-shaped raft shown in Figure P8.9 applies a uniform pressure of 60 kN/m^2 to the underlying ground. Find the vertical stress increase at 4 m below *A*, *B*, and *C*.

8.10 A square flexible foundation of width *B* applies a uniform pressure q_o to the underlying ground. Determine the vertical stress increase at a depth of *B*/2 below the center using:

a. Δσ beneath the corner of a uniform rectangular load [Eq. (8.10) and Table 8.5],
b. 2:1 method [Eq. (8.15)], and
c. Stress isobars (Figure 8.11).

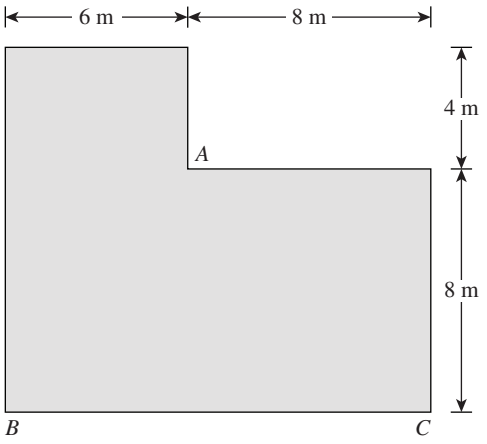


FIGURE P8.9

8.11 A square foundation, 5 ft wide, carries a net column load of 50 tons as shown in Figure P8.11. Determine the average stress increase beneath the center of the foundation in the clay layer:

a. Using Eq. (8.25),
b. Using Eqs. (8.26) and (8.10), and
c. Using Eqs. (8.26) and (8.15).

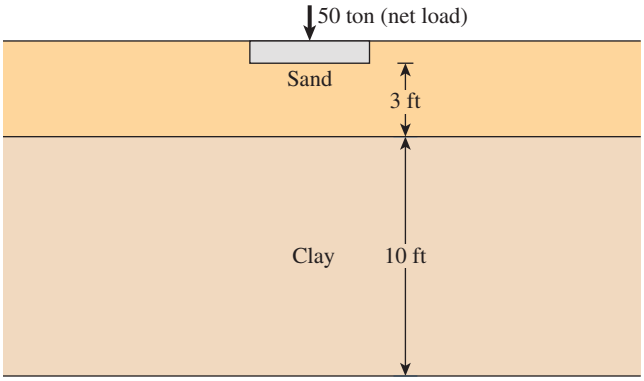


FIGURE P8.11

8.12 Figure P.8.12 shows an embankment load on a silty clay soil layer. Determine the stress increase at points *A*, *B*, and *C*, which are located at a depth of 5 m below the ground surface.

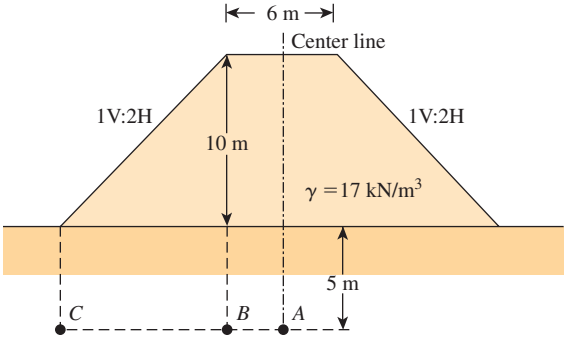


FIGURE P8.12

8.13 A point load of 50 tons is applied on an elastic medium with Poisson's ratio of 0.2. Compare the vertical stress increase at the following locations as determined by the Boussinesq ($\Delta\sigma_B$) and Westergaard ($\Delta\sigma_W$) solutions.

Point	***A***	***B***	***C***	***D***	***E***	***F***
***z* (ft)**	6	6	6	12	12	12
***r* (ft)**	0	6	12	0	6	12

8.14 A 6 ft diameter flexible foundation applies a uniform pressure to the underlying soil of 2 ton/ft^2. Plot the variation of the vertical stress increase below the center of the foundation as determined using both the Boussinesq ($\Delta\sigma_B$) and Westergaard ($\Delta\sigma_W$) solutions up to a depth of $z = 15$ ft. (*Note:* $\mu_s = 0.2$.)

REFERENCES

Ahlvin, R. G. and Ulery, H. H. (1962). "Tabulated Values for Determining the Complete Pattern of Stresses, Strains, and Deflections Beneath a Uniform Circular Load on a Homogeneous Half Space," in *Highway Research Bulletin 342*, Transportation Research Board, National Research Council, Washington, DC, pp. 1–13.

Boussinesq, J. (1883). *Application des Potentials á L'Étude de L'Équilibre et du Mouvement des Solides Élastiques*, Gauthier-Villars, Paris.

Das, B. (2014). *Advanced Soil Mechanics*, 4th ed., CRC Press, Boca Raton, FL.

Griffiths, D. V. (1984). "A Chart for Estimating the Average Vertical Stress Increase in an Elastic Foundation below a Uniformly Loaded Rectangular Area," *Canadian Geotechnical Journal*, Vol. 21, No. 4, pp. 710–713.

Harr, M. E. (1966). *Foundations of Theoretical Soil Mechanics*, McGraw-Hill, New York.

Newmark, N. M. (1935). *Simplified Computation of Vertical Pressure in Elastic Foundation*, Circular 24, University of Illinois Engineering Experiment Station, Urbana, IL.

Osterberg, J. O. (1957). "Influence Values for Vertical Stresses in Semi-Infinite Mass Due to Embankment Loading," *Proceedings, Fourth International Conference on Soil Mechanics and Foundation Engineering*, London, Vol. 1, pp. 393–396.

Saika, A. (2012). "Vertical Stress Averaging over a Layer Depth Down the Axis of Symmetry of Uniformly Loaded Circular Regime: An Analytical-cum-Graphical Solution," *International Journal of Geotechnical Engineering*, Vol. 6, No. 3, pp. 359–363.

Westergaard, H. M. (1938)."A Problem of Elasticity Suggested by a Problem in Soil Mechanics: Soft Material Reinforced by Numerous Strong Horizontal Sheets," *Contributions to the Mechanics of Solids, Dedicated to Stephen Timoshenko*, pp. 268–277, Macmillan, New York.

9

Settlement of Shallow Foundations



Rachata Kietsirikul/Shutterstock.com

9.1 Introduction 337
9.2 Elastic Settlement of Shallow Foundation on Saturated Clay ($\mu_s = 0.5$) 337
9.3 Settlement Based on the Theory of Elasticity 339
9.4 Improved Equation for Elastic Settlement 350
9.5 Settlement of Sandy Soil: Use of Strain Influence Factor 354
9.6 Settlement of Foundation on Sand Based on Standard Penetration Resistance 361
9.7 Settlement Considering Soil Stiffness Variation with Stress Level 366
9.8 Settlement Based on Pressuremeter Test (PMT) 370
9.9 Settlement Estimation Using the $L_1 - L_2$ Method 375
9.10 Effect of the Rise of Water Table on Elastic Settlement 378
9.11 Primary Consolidation Settlement Relationships 380
9.12 Three-Dimensional Effect on Primary Consolidation Settlement 382
9.13 Settlement Due to Secondary Consolidation 386
9.14 Field Load Test 388
9.15 Presumptive Bearing Capacity 389
9.16 Tolerable Settlement of Buildings 390
9.17 Summary 392

PROBLEMS 392

REFERENCES 394

9.1 Introduction

The settlement process is different in granular and cohesive soil. In granular soil, such as sand and gravel, the settlement occurs almost immediately upon applying the load. This is referred to as immediate (or elastic) settlement and is computed by using elastic theories. In clay, while there is a small immediate (or elastic) settlement component, most of the settlement occurs during the consolidation process, which includes *primary* and *secondary consolidation*.

The fundamentals of primary consolidation were summarized in Chapter 2. The secondary consolidation is assumed to occur on completion of primary consolidation, when the excess pore water pressure has fully dissipated. During the secondary consolidation, the settlement continues indefinitely, due to the realignment of the clay particles and the resulting change in the clay fabric. Primary consolidation settlement is more significant than secondary settlement in inorganic clays and silty soil. However, in organic soil, secondary consolidation settlement is more significant.

This chapter presents various theories presently available for estimating elastic and consolidation settlements of shallow foundations. In computing the elastic settlement, the modulus of elasticity (E_s) and Poisson's ratio (μ_s) are the two key design parameters. The modulus of elasticity of the soil can vary over a wide range (1–50 MPa), and it is often determined from *in situ* tests. Poisson's ratio varies in the range of 0–0.5. For *all* saturated clays subjected to undrained loading, which implies no volume change, it can be shown from elastic analysis that $\mu_s = 0.50$.

9.2 Elastic Settlement of Shallow Foundation on Saturated Clay ($\mu_s = 0.5$)

Janbu et al. (1956) proposed an equation for evaluating the average settlement of flexible foundations on saturated clay soil (Poisson's ratio, $\mu_s = 0.5$). Referring to Figure 9.1, this relationship can be expressed as

$$S_e = A_1 A_2 \frac{q_o B}{E_s} \tag{9.1}$$

where

$A_1 = f(H/B, L/B)$

$A_2 = f(D_f/B)$

L = length of the foundation

B = width of the foundation

D_f = depth of the foundation

H = depth of the bottom of the foundation to a rigid layer

q_o = net load per unit area of the foundation

Christian and Carrier (1978) modified the values of A_1 and A_2 to some extent, and these are presented in Figure 9.1.

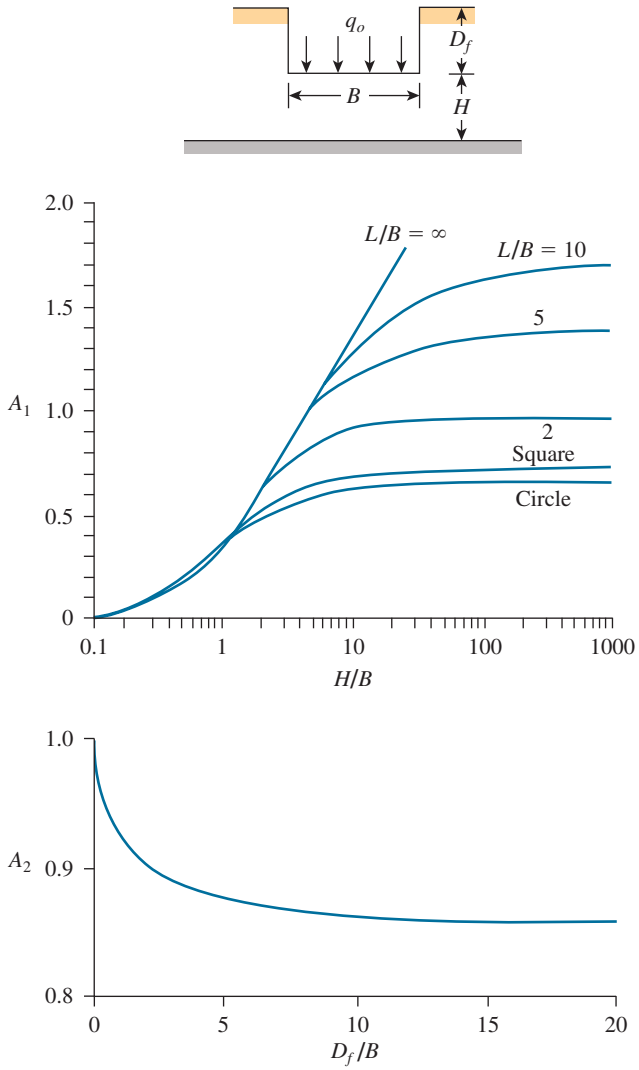


FIGURE 9.1 Values of A_1 and A_2 for elastic settlement calculation—Eq. (9.1) (Based on Christian, J. T. and Carrier, W. D. (1978). "Janbu, Bjerrum and Kjaernsli's chart reinterpreted," *Canadian Geotechnical Journal*, Vol. 15, pp. 123–128)

The modulus of elasticity (E_s) for saturated clays under undrained conditions can, in general, be given as

$$E_s = \beta c_u \tag{9.2}$$

where c_u = undrained shear strength.

The parameter β is primarily a function of the plasticity index and overconsolidation ratio (OCR). Table 9.1 provides a general range for β based on that proposed

TABLE 9.1 Range of β for Saturated Clay [Eq. (9.2)][a]

Plasticity index	β				
	OCR = 1	OCR = 2	OCR = 3	OCR = 4	OCR = 5
<30	1500–600	1380–500	1200–580	950–380	730–300
30 to 50	600–300	550–270	580–220	380–180	300–150
>50	300–150	270–120	220–100	180–90	150–75

[a]Based on Duncan and Buchignani (1976)

by Duncan and Buchignani (1976). In any case, proper judgment should be used in selecting the magnitude of β.

EXAMPLE 9.1

Consider a shallow foundation 2 m × 1 m in plan in a saturated clay layer. A rigid rock layer is located 8 m below the bottom of the foundation. Given:

Foundation: $D_f = 1$ m, $q_o = 120$ kN/m^2

Clay: $c_u = 150$ kN/m^2, OCR = 2, and plasticity index, PI = 35

Estimate the elastic settlement of the foundation.

SOLUTION

From Eq. (9.1),

$$S_e = A_1 A_2 \frac{q_o B}{E_s}$$

Given:

$$\frac{L}{B} = \frac{2}{1} = 2$$
$$\frac{D_f}{B} = \frac{1}{1} = 1$$
$$\frac{H}{B} = \frac{8}{1} = 8$$
$$E_s = \beta c_u$$

For OCR = 2 and PI = 35, the value of $\beta \approx 480$ (Table 9.1). Hence,

$$E_s = (480)(150) = 72{,}000 \text{ kN/m}^2$$

Also, from Figure 9.1, $A_1 = 0.9$ and $A_2 = 0.92$. Hence,

$$S_e = A_1 A_2 \frac{q_o B}{E_s} = (0.9)(0.92)\frac{(120)(1)}{72{,}000} = 0.00138 \text{ m} = \mathbf{1.38 \text{ mm}}$$

Elastic Settlement in Granular Soil

9.3 Settlement Based on the Theory of Elasticity

In this section, the procedure to compute the elastic settlement in a granular soil is discussed. Here, the soil is treated as an elastic continuum. The settlement profiles of rigid and flexible foundations are shown in Figure 9.2. A flexible foundation applies uniform pressure to the underlying soil, but its settlement is nonuniform. A rigid foundation settles uniformly, but the pressure applied to the underlying soil is nonuniform.

In the first part of this section, an expression is developed for a flexible surface foundation ($D_f = 0$) resting on an elastic half-space, as shown in Figure 9.3a. This is further modified to account for

a. the presence of a rigid layer at a finite depth H (Figure 9.3b), and
b. embedment depth D_f (Figure 9.3c).

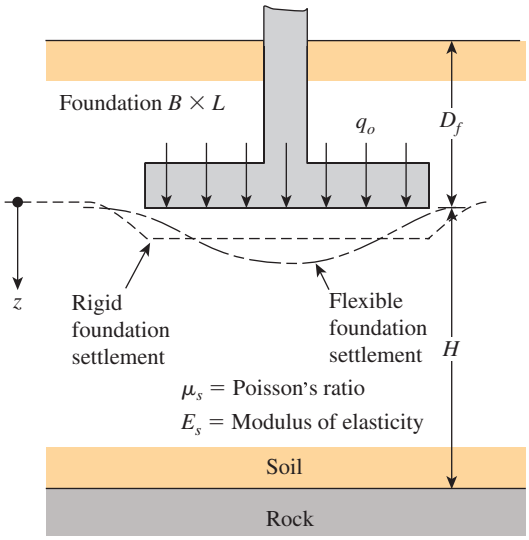


FIGURE 9.2 Elastic settlement of flexible and rigid foundations

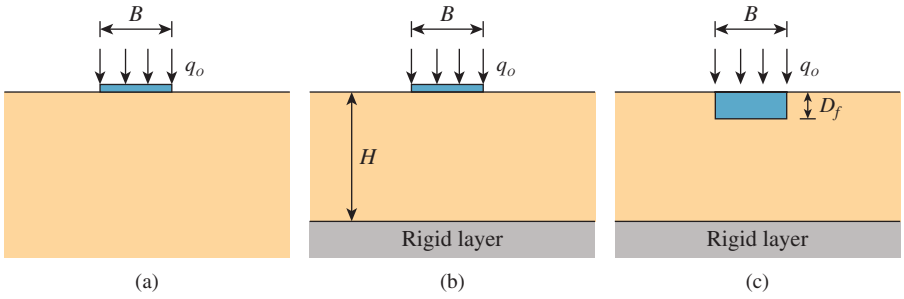


FIGURE 9.3 Elastic settlement of a flexible foundation: (a) elastic half-space, (b) underlain by a rigid layer, and (c) with embedment

SURFACE FOUNDATIONS ON ELASTIC HALF-SPACE

For a flexible rectangular foundation of dimensions $B \times L$ lying on an elastic half-space as shown in Figure 9.3a, the elastic settlement under a point on the foundation is given by

$$S_e = \frac{q_o B}{E_s}(1 - \mu_s^2)I \tag{9.3}$$

where I is the influence factor that depends on the location of the point of interest on the foundation. Here q_o is the net pressure applied by the foundation to the underlying soil, B is the width of the foundation, E_s is the modulus of elasticity of the soil, and μ_s is Poisson's ratio of the soil.

Schleicher (1926) expressed the influence factor for the *corner of a flexible foundation* as

$$I_{\text{corner}} = \frac{1}{\pi}\left[m' \ln\left(\frac{1 + \sqrt{m'^2 + 1}}{m'}\right) + \ln\left(m' + \sqrt{m'^2 + 1}\right)\right] \tag{9.4}$$

where $m' = L/B$. The influence factors for the other locations on the foundation can be determined by dividing the foundation into four rectangles and using the principle of superposition. It can be deduced that the influence factor for the center is twice that of the corner. The influence factors for the corner, center, midpoint of the short side, and midpoint of the long side, as determined from Eq. (9.4), are shown in Figure 9.4 for $1 \leq m' \leq 1000$. The values computed here are the same as those

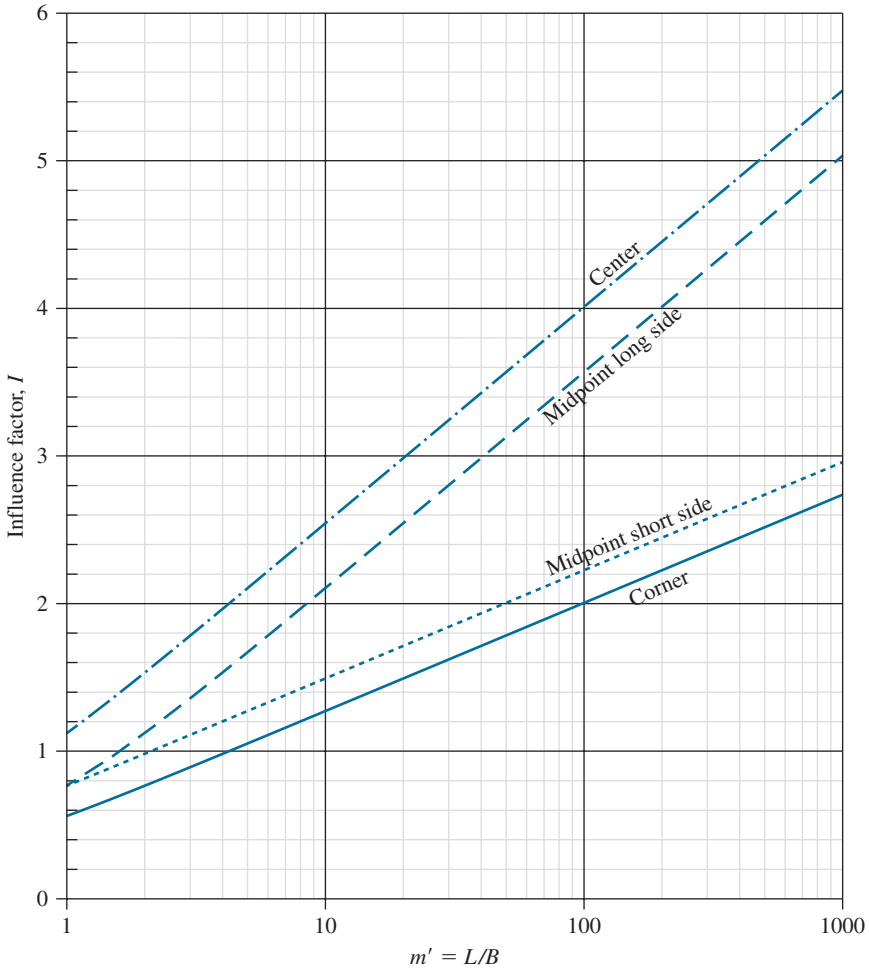


FIGURE 9.4 Variation of I versus m' for a flexible foundation

reported by Poulos and Davis (1974), who refer the work of Giroud (1968). The authors note that these values can be approximated as follows.

Corner: $$I = 0.7283 \log m' + 0.5469 \quad (9.5)$$

Center: $$I = 1.4566 \log m' + 1.0939 \quad (9.6)$$

Midpoint short side: $$I = 0.7318 \log m' + 0.7617 \quad (9.7)$$

Midpoint long side: $$I = 1.4357 \log m' + 0.6894 \quad (9.8)$$

The settlements under the center and the perimeter of a uniformly loaded *flexible circular foundation* of diameter B are given by:

Center: $$S_e = \frac{q_o B}{E_s}(1 - \mu_s^2) \quad (9.9)$$

Perimeter: $$S_e = \frac{q_o B}{E_s}(1 - \mu_s^2)\frac{2}{\pi} \quad (9.10)$$

From Eqs. (9.9) and (9.10), it can be seen that the influence factors for the center and a point on the perimeter of a flexible circular foundation are 1.00 and $2/\pi$, respectively.

TABLE 9.2 Influence Factors to Compute *Average* Settlement of Flexible and Rigid Foundation

$m' = L/B$	Flexible	Rigid
Circle	0.85	0.79
1	0.95	0.82
1.5	1.20	1.07
2	1.30	1.21
3	1.52	1.42
5	1.82	1.60
10	2.24	2.00
100	2.96	3.40

Flexible foundations apply uniform pressure and settle nonuniformly. Rigid foundations apply nonuniform pressure and settle uniformly. Some influence factors for estimating the average values of the settlements of flexible and rigid foundations, as reported in the literature, are given in Table 9.2.

Based on the work of Timoshenko and Goodier (1951), Bowles (1987) suggested that the settlement of the rigid foundation can be *estimated as 93% of the settlement computed for a flexible foundation under the center*. The average values of I reported by Giroud (1968) and Poulos and Davis (1974) suggest that the average value of the settlement of a flexible foundation can be computed using 84–88% of the I-value for the center.

EFFECTS OF A RIGID LAYER ON THE SETTLEMENTS OF SURFACE FOUNDATIONS

When the soil is underlain by a rigid layer, as shown in Figure 9.3b, the settlement computed by Eq. (9.3) has to be reduced. Steinbrenner (1934) suggested the following expression for the influence factor for the corner of a rectangular flexible surface foundation, taking into consideration the presence of the rigid layer, at depth of H below the foundation and $n' = H/B$.

$$I_s = F_1 + \left(\frac{1 - 2\mu_s}{1 - \mu_s}\right)F_2 \tag{9.11}$$

where

$$F_1 = \frac{1}{\pi}(A_0 + A_1) \tag{9.12}$$

$$F_2 = \frac{n'}{2\pi}\tan^{-1}A_2 \tag{9.13}$$

A_0, A_1, and A_2 are given by

$$A_0 = m' \ln \frac{\left(1 + \sqrt{m'^2 + 1}\right)\sqrt{m'^2 + n'^2}}{m'\left(1 + \sqrt{m'^2 + n'^2 + 1}\right)} \tag{9.14}$$

$$A_1 = \ln \frac{\left(m' + \sqrt{m'^2 + 1}\right)\sqrt{1 + n'^2}}{m' + \sqrt{m'^2 + n'^2 + 1}} \tag{9.15}$$

$$A_2 = \frac{m'}{n' + \sqrt{m'^2 + n'^2 + 1}} \tag{9.16}$$

The influence factor determined using Eqs. (9.11) to (9.16) is for the corner of a uniformly loaded flexible rectangular surface foundation. The influence factor for any other point on the foundation can be determined using the principle of superposition as before. For $H = \infty$, $n' = \infty$, and Eqs. (9.14) to (9.16) become

$$A_0 = m' \ln \frac{1 + \sqrt{m'^2 + 1}}{m'} \tag{9.17}$$

$$A_1 = \ln \left(m' + \sqrt{m'^2 + 1}\right) \tag{9.18}$$

$$A_2 = 0 \tag{9.19}$$

Substituting these in Eqs. (9.12) and (9.13),

$$F_1 = \frac{1}{\pi}\left[m' \ln \left(\frac{1 + \sqrt{m'^2 + 1}}{m'}\right) + \ln \left(m' + \sqrt{m'^2 + 1}\right)\right] \tag{9.20}$$

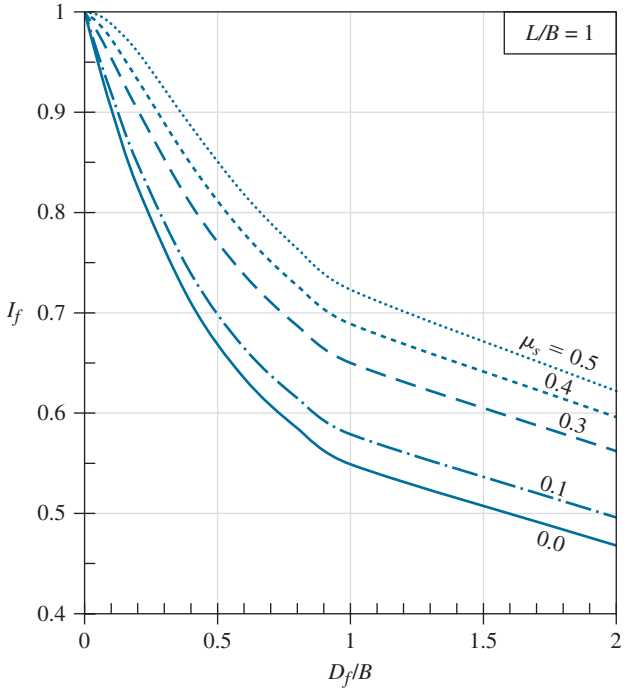
$$F_2 = 0 \tag{9.21}$$

Substituting Eqs. (9.20) and (9.21) in Eq. (9.11) gives the same expression we had from Schleicher (1926) in Eq. (9.4). The variations of F_1 and F_2 [see Eqs. (9.12) to (9.16)] with m' and n' are given in Tables 9.3 and 9.4.

EFFECT OF EMBEDMENT

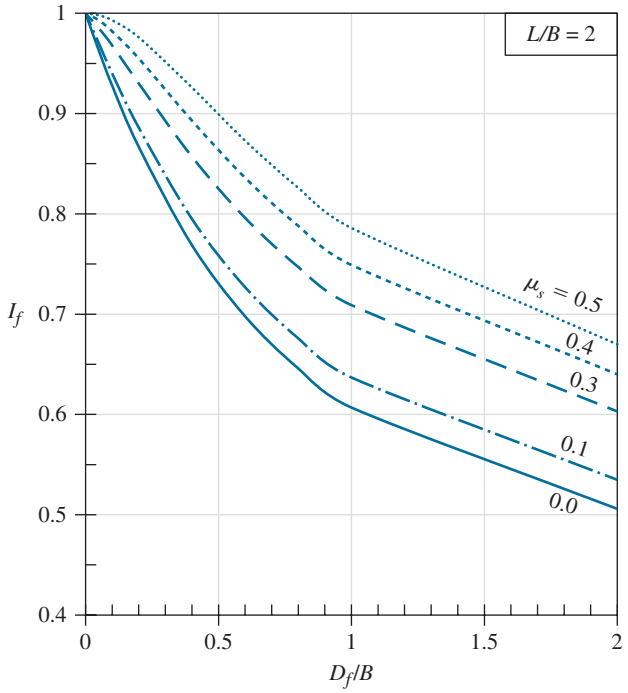
When the foundation base is located at some depth beneath the ground level, the embedment reduces the settlement further. Fox (1948) proposed the reduction factor I_f to account for this reduction in settlement. The settlement computed in Eq. (9.3) using the Schleicher (1926) or Steinbrenner (1934) influence factors must be multiplied by I_f to account for the settlement reduction due to embedment. I_f values for different values of D_f/B, L/B, and μ_s are given in Figure 9.5. Therefore, Eq. (9.3) becomes

$$S_e = \frac{q_o B}{E_s}(1 - \mu_s^2) I_s I_f \tag{9.22}$$

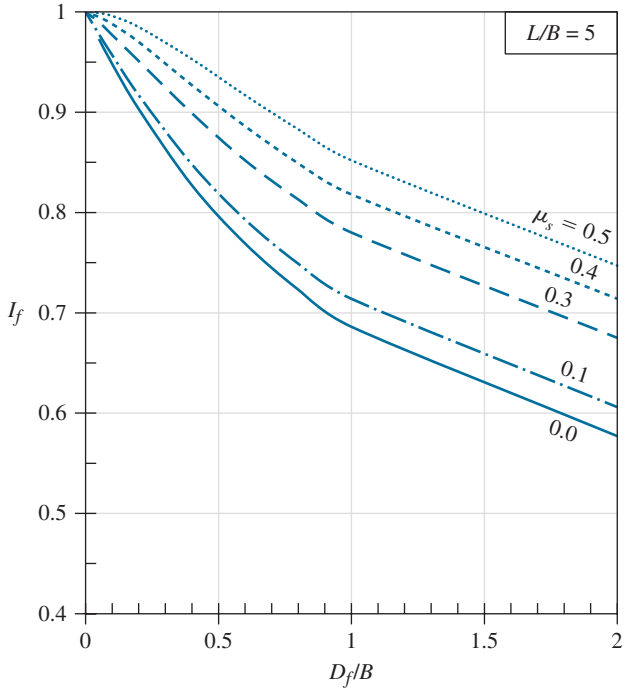


(a)

FIGURE 9.5 Variation of I_f with D_f/B: (a) $L/B = 1$; (b) $L/B = 2$; (c) $L/B = 5$



(b)



(c)

FIGURE 9.5 (*Continued*)

TABLE 9.3 Variation of F_1 with m' and n'

	m'									
n'	1.0	1.2	1.4	1.6	1.8	2.0	2.5	3.0	3.5	4.0
0.25	0.014	0.013	0.012	0.011	0.011	0.011	0.010	0.010	0.010	0.010
0.50	0.049	0.046	0.044	0.042	0.041	0.040	0.038	0.038	0.037	0.037
0.75	0.095	0.090	0.087	0.084	0.082	0.080	0.077	0.076	0.074	0.074
1.00	0.142	0.138	0.134	0.130	0.127	0.125	0.121	0.118	0.116	0.115
1.25	0.186	0.183	0.179	0.176	0.173	0.170	0.165	0.161	0.158	0.157
1.50	0.224	0.224	0.222	0.219	0.216	0.213	0.207	0.203	0.199	0.197
1.75	0.257	0.259	0.259	0.258	0.255	0.253	0.247	0.242	0.238	0.235
2.00	0.285	0.290	0.292	0.292	0.291	0.289	0.284	0.279	0.275	0.271
2.25	0.309	0.317	0.321	0.323	0.323	0.322	0.317	0.313	0.308	0.305
2.50	0.330	0.341	0.347	0.350	0.351	0.351	0.348	0.344	0.340	0.336
2.75	0.348	0.361	0.369	0.374	0.377	0.378	0.377	0.373	0.369	0.365
3.00	0.363	0.379	0.389	0.396	0.400	0.402	0.402	0.400	0.396	0.392
3.25	0.376	0.394	0.406	0.415	0.420	0.423	0.426	0.424	0.421	0.418
3.50	0.388	0.408	0.422	0.431	0.438	0.442	0.447	0.447	0.444	0.441
3.75	0.399	0.420	0.436	0.447	0.454	0.460	0.467	0.458	0.466	0.464
4.00	0.408	0.431	0.448	0.460	0.469	0.476	0.484	0.487	0.486	0.484
4.25	0.417	0.440	0.458	0.472	0.481	0.484	0.495	0.514	0.515	0.515
4.50	0.424	0.450	0.469	0.484	0.495	0.503	0.516	0.521	0.522	0.522
4.75	0.431	0.458	0.478	0.494	0.506	0.515	0.530	0.536	0.539	0.539
5.00	0.437	0.465	0.487	0.503	0.516	0.526	0.543	0.551	0.554	0.554
5.25	0.443	0.472	0.494	0.512	0.526	0.537	0.555	0.564	0.568	0.569
5.50	0.448	0.478	0.501	0.520	0.534	0.546	0.566	0.576	0.581	0.584
5.75	0.453	0.483	0.508	0.527	0.542	0.555	0.576	0.588	0.594	0.597
6.00	0.457	0.489	0.514	0.534	0.550	0.563	0.585	0.598	0.606	0.609
6.25	0.461	0.493	0.519	0.540	0.557	0.570	0.594	0.609	0.617	0.621
6.50	0.465	0.498	0.524	0.546	0.563	0.577	0.603	0.618	0.627	0.632
6.75	0.468	0.502	0.529	0.551	0.569	0.584	0.610	0.627	0.637	0.643
7.00	0.471	0.506	0.533	0.556	0.575	0.590	0.618	0.635	0.646	0.653
7.25	0.474	0.509	0.538	0.561	0.580	0.596	0.625	0.643	0.655	0.662
7.50	0.477	0.513	0.541	0.565	0.585	0.601	0.631	0.650	0.663	0.671
7.75	0.480	0.516	0.545	0.569	0.589	0.606	0.637	0.658	0.671	0.680
8.00	0.482	0.519	0.549	0.573	0.594	0.611	0.643	0.664	0.678	0.688
8.25	0.485	0.522	0.552	0.577	0.598	0.615	0.648	0.670	0.685	0.695
8.50	0.487	0.524	0.555	0.580	0.601	0.619	0.653	0.676	0.692	0.703
8.75	0.489	0.527	0.558	0.583	0.605	0.623	0.658	0.682	0.698	0.710
9.00	0.491	0.529	0.560	0.587	0.609	0.627	0.663	0.687	0.705	0.716
9.25	0.493	0.531	0.563	0.589	0.612	0.631	0.667	0.693	0.710	0.723
9.50	0.495	0.533	0.565	0.592	0.615	0.634	0.671	0.697	0.716	0.719
9.75	0.496	0.536	0.568	0.595	0.618	0.638	0.675	0.702	0.721	0.735
10.00	0.498	0.537	0.570	0.597	0.621	0.641	0.679	0.707	0.726	0.740
20.00	0.529	0.575	0.614	0.647	0.677	0.702	0.756	0.797	0.830	0.858
50.00	0.548	0.598	0.640	0.678	0.711	0.740	0.803	0.853	0.895	0.931
100.00	0.555	0.605	0.649	0.688	0.722	0.753	0.819	0.872	0.918	0.956

(*Continued*)

TABLE 9.3 Variation of F_1 with m' and n' (*Continued*)

	m'									
n'	4.5	5.0	6.0	7.0	8.0	9.0	10.0	25.0	50.0	100.0
0.25	0.010	0.010	0.010	0.010	0.010	0.010	0.010	0.010	0.010	0.010
0.50	0.036	0.036	0.036	0.036	0.036	0.036	0.036	0.036	0.036	0.036
0.75	0.073	0.073	0.072	0.072	0.072	0.072	0.071	0.071	0.071	0.071
1.00	0.114	0.113	0.112	0.112	0.112	0.111	0.111	0.110	0.110	0.110
1.25	0.155	0.154	0.153	0.152	0.152	0.151	0.151	0.150	0.150	0.150
1.50	0.195	0.194	0.192	0.191	0.190	0.190	0.189	0.188	0.188	0.188
1.75	0.233	0.232	0.229	0.228	0.227	0.226	0.225	0.223	0.223	0.223
2.00	0.269	0.267	0.264	0.262	0.261	0.260	0.259	0.257	0.256	0.256
2.25	0.302	0.300	0.296	0.294	0.293	0.291	0.291	0.287	0.287	0.287
2.50	0.333	0.331	0.327	0.324	0.322	0.321	0.320	0.316	0.315	0.315
2.75	0.362	0.359	0.355	0.352	0.350	0.348	0.347	0.343	0.342	0.342
3.00	0.389	0.386	0.382	0.378	0.376	0.374	0.373	0.368	0.367	0.367
3.25	0.415	0.412	0.407	0.403	0.401	0.399	0.397	0.391	0.390	0.390
3.50	0.438	0.435	0.430	0.427	0.424	0.421	0.420	0.413	0.412	0.411
3.75	0.461	0.458	0.453	0.449	0.446	0.443	0.441	0.433	0.432	0.432
4.00	0.482	0.479	0.474	0.470	0.466	0.464	0.462	0.453	0.451	0.451
4.25	0.516	0.496	0.484	0.473	0.471	0.471	0.470	0.468	0.462	0.460
4.50	0.520	0.517	0.513	0.508	0.505	0.502	0.499	0.489	0.487	0.487
4.75	0.537	0.535	0.530	0.526	0.523	0.519	0.517	0.506	0.504	0.503
5.00	0.554	0.552	0.548	0.543	0.540	0.536	0.534	0.522	0.519	0.519
5.25	0.569	0.568	0.564	0.560	0.556	0.553	0.550	0.537	0.534	0.534
5.50	0.584	0.583	0.579	0.575	0.571	0.568	0.585	0.551	0.549	0.548
5.75	0.597	0.597	0.594	0.590	0.586	0.583	0.580	0.565	0.583	0.562
6.00	0.611	0.610	0.608	0.604	0.601	0.598	0.595	0.579	0.576	0.575
6.25	0.623	0.623	0.621	0.618	0.615	0.611	0.608	0.592	0.589	0.588
6.50	0.635	0.635	0.634	0.631	0.628	0.625	0.622	0.605	0.601	0.600
6.75	0.646	0.647	0.646	0.644	0.641	0.637	0.634	0.617	0.613	0.612
7.00	0.656	0.658	0.658	0.656	0.653	0.650	0.647	0.628	0.624	0.623
7.25	0.666	0.669	0.669	0.668	0.665	0.662	0.659	0.640	0.635	0.634
7.50	0.676	0.679	0.680	0.679	0.676	0.673	0.670	0.651	0.646	0.645
7.75	0.685	0.688	0.690	0.689	0.687	0.684	0.681	0.661	0.656	0.655
8.00	0.694	0.697	0.700	0.700	0.698	0.695	0.692	0.672	0.666	0.665
8.25	0.702	0.706	0.710	0.710	0.708	0.705	0.703	0.682	0.676	0.675
8.50	0.710	0.714	0.719	0.719	0.718	0.715	0.713	0.692	0.686	0.684
8.75	0.717	0.722	0.727	0.728	0.727	0.725	0.723	0.701	0.695	0.693
9.00	0.725	0.730	0.736	0.737	0.736	0.735	0.732	0.710	0.704	0.702
9.25	0.731	0.737	0.744	0.746	0.745	0.744	0.742	0.719	0.713	0.711
9.50	0.738	0.744	0.752	0.754	0.754	0.753	0.751	0.728	0.721	0.719
9.75	0.744	0.751	0.759	0.762	0.762	0.761	0.759	0.737	0.729	0.727
10.00	0.750	0.758	0.766	0.770	0.770	0.770	0.768	0.745	0.738	0.735
20.00	0.878	0.896	0.925	0.945	0.959	0.969	0.977	0.982	0.965	0.957
50.00	0.962	0.989	1.034	1.070	1.100	1.125	1.146	1.265	1.279	1.261
100.00	0.990	1.020	1.072	1.114	1.150	1.182	1.209	1.408	1.489	1.499

TABLE 9.4 Variation of F_2 with m' and n'

	m'									
n'	1.0	1.2	1.4	1.6	1.8	2.0	2.5	3.0	3.5	4.0
0.25	0.049	0.050	0.051	0.051	0.051	0.052	0.052	0.052	0.052	0.052
0.50	0.074	0.077	0.080	0.081	0.083	0.084	0.086	0.086	0.0878	0.087
0.75	0.083	0.089	0.093	0.097	0.099	0.101	0.104	0.106	0.107	0.108
1.00	0.083	0.091	0.098	0.102	0.106	0.109	0.114	0.117	0.119	0.120
1.25	0.080	0.089	0.096	0.102	0.107	0.111	0.118	0.122	0.125	0.127
1.50	0.075	0.084	0.093	0.099	0.105	0.110	0.118	0.124	0.128	0.130
1.75	0.069	0.079	0.088	0.095	0.101	0.107	0.117	0.123	0.128	0.131
2.00	0.064	0.074	0.083	0.090	0.097	0.102	0.114	0.121	0.127	0.131
2.25	0.059	0.069	0.077	0.085	0.092	0.098	0.110	0.119	0.125	0.130
2.50	0.055	0.064	0.073	0.080	0.087	0.093	0.106	0.115	0.122	0.127
2.75	0.051	0.060	0.068	0.076	0.082	0.089	0.102	0.111	0.119	0.125
3.00	0.048	0.056	0.064	0.071	0.078	0.084	0.097	0.108	0.116	0.122
3.25	0.045	0.053	0.060	0.067	0.074	0.080	0.093	0.104	0.112	0.119
3.50	0.042	0.050	0.057	0.064	0.070	0.076	0.089	0.100	0.109	0.116
3.75	0.040	0.047	0.054	0.060	0.067	0.073	0.086	0.096	0.105	0.113
4.00	0.037	0.044	0.051	0.057	0.063	0.069	0.082	0.093	0.102	0.110
4.25	0.036	0.042	0.049	0.055	0.061	0.066	0.079	0.090	0.099	0.107
4.50	0.034	0.040	0.046	0.052	0.058	0.063	0.076	0.086	0.096	0.104
4.75	0.032	0.038	0.044	0.050	0.055	0.061	0.073	0.083	0.093	0.101
5.00	0.031	0.036	0.042	0.048	0.053	0.058	0.070	0.080	0.090	0.098
5.25	0.029	0.035	0.040	0.046	0.051	0.056	0.067	0.078	0.087	0.095
5.50	0.028	0.033	0.039	0.044	0.049	0.054	0.065	0.075	0.084	0.092
5.75	0.027	0.032	0.037	0.042	0.047	0.052	0.063	0.073	0.082	0.090
6.00	0.026	0.031	0.036	0.040	0.045	0.050	0.060	0.070	0.079	0.087
6.25	0.025	0.030	0.034	0.039	0.044	0.048	0.058	0.068	0.077	0.085
6.50	0.024	0.029	0.033	0.038	0.042	0.046	0.056	0.066	0.075	0.083
6.75	0.023	0.028	0.032	0.036	0.041	0.045	0.055	0.064	0.073	0.080
7.00	0.022	0.027	0.031	0.035	0.039	0.043	0.053	0.062	0.071	0.078
7.25	0.022	0.026	0.030	0.034	0.038	0.042	0.051	0.060	0.069	0.076
7.50	0.021	0.025	0.029	0.033	0.037	0.041	0.050	0.059	0.067	0.074
7.75	0.020	0.024	0.028	0.032	0.036	0.039	0.048	0.057	0.065	0.072
8.00	0.020	0.023	0.027	0.031	0.035	0.038	0.047	0.055	0.063	0.071
8.25	0.019	0.023	0.026	0.030	0.034	0.037	0.046	0.054	0.062	0.069
8.50	0.018	0.022	0.026	0.029	0.033	0.036	0.045	0.053	0.060	0.067
8.75	0.018	0.021	0.025	0.028	0.032	0.035	0.043	0.051	0.059	0.066
9.00	0.017	0.021	0.024	0.028	0.031	0.034	0.042	0.050	0.057	0.064
9.25	0.017	0.020	0.024	0.027	0.030	0.033	0.041	0.049	0.056	0.063
9.50	0.017	0.020	0.023	0.026	0.029	0.033	0.040	0.048	0.055	0.061
9.75	0.016	0.019	0.023	0.026	0.029	0.032	0.039	0.047	0.054	0.060
10.00	0.016	0.019	0.022	0.025	0.028	0.031	0.038	0.046	0.052	0.059
20.00	0.008	0.010	0.011	0.013	0.014	0.016	0.020	0.024	0.027	0.031
50.00	0.003	0.004	0.004	0.005	0.006	0.006	0.008	0.010	0.011	0.013
100.00	0.002	0.002	0.002	0.003	0.003	0.003	0.004	0.005	0.006	0.006

(*Continued*)

TABLE 9.4 Variation of F_2 with m' and n' (*Continued*)

	m'									
n'	4.5	5.0	6.0	7.0	8.0	9.0	10.0	25.0	50.0	100.0
0.25	0.053	0.053	0.053	0.053	0.053	0.053	0.053	0.053	0.053	0.053
0.50	0.087	0.087	0.088	0.088	0.088	0.088	0.088	0.088	0.088	0.088
0.75	0.109	0.109	0.109	0.110	0.110	0.110	0.110	0.111	0.111	0.111
1.00	0.121	0.122	0.123	0.123	0.124	0.124	0.124	0.125	0.125	0.125
1.25	0.128	0.130	0.131	0.132	0.132	0.133	0.133	0.134	0.134	0.134
1.50	0.132	0.134	0.136	0.137	0.138	0.138	0.139	0.140	0.140	0.140
1.75	0.134	0.136	0.138	0.140	0.141	0.142	0.142	0.144	0.144	0.145
2.00	0.134	0.136	0.139	0.141	0.143	0.144	0.145	0.147	0.147	0.148
2.25	0.133	0.136	0.140	0.142	0.144	0.145	0.146	0.149	0.150	0.150
2.50	0.132	0.135	0.139	0.142	0.144	0.146	0.147	0.151	0.151	0.151
2.75	0.130	0.133	0.138	0.142	0.144	0.146	0.147	0.152	0.152	0.153
3.00	0.127	0.131	0.137	0.141	0.144	0.145	0.147	0.152	0.153	0.154
3.25	0.125	0.129	0.135	0.140	0.143	0.145	0.147	0.153	0.154	0.154
3.50	0.122	0.126	0.133	0.138	0.142	0.144	0.146	0.153	0.155	0.155
3.75	0.119	0.124	0.131	0.137	0.141	0.143	0.145	0.154	0.155	0.155
4.00	0.116	0.121	0.129	0.135	0.139	0.142	0.145	0.154	0.155	0.156
4.25	0.113	0.119	0.127	0.133	0.138	0.141	0.144	0.154	0.156	0.156
4.50	0.110	0.116	0.125	0.131	0.136	0.140	0.143	0.154	0.156	0.156
4.75	0.107	0.113	0.123	0.130	0.135	0.139	0.142	0.154	0.156	0.157
5.00	0.105	0.111	0.120	0.128	0.133	0.137	0.140	0.154	0.156	0.157
5.25	0.102	0.108	0.118	0.126	0.131	0.136	0.139	0.154	0.156	0.157
5.50	0.099	0.106	0.116	0.124	0.130	0.134	0.138	0.154	0.156	0.157
5.75	0.097	0.103	0.113	0.122	0.128	0.133	0.136	0.154	0.157	0.157
6.00	0.094	0.101	0.111	0.120	0.126	0.131	0.135	0.153	0.157	0.157
6.25	0.092	0.098	0.109	0.118	0.124	0.129	0.134	0.153	0.157	0.158
6.50	0.090	0.096	0.107	0.116	0.122	0.128	0.132	0.153	0.157	0.158
6.75	0.087	0.094	0.105	0.114	0.121	0.126	0.131	0.153	0.157	0.158
7.00	0.085	0.092	0.103	0.112	0.119	0.125	0.129	0.152	0.157	0.158
7.25	0.083	0.090	0.101	0.110	0.117	0.123	0.128	0.152	0.157	0.158
7.50	0.081	0.088	0.099	0.108	0.115	0.121	0.126	0.152	0.156	0.158
7.75	0.079	0.086	0.097	0.106	0.114	0.120	0.125	0.151	0.156	0.158
8.00	0.077	0.084	0.095	0.104	0.112	0.118	0.124	0.151	0.156	0.158
8.25	0.076	0.082	0.093	0.102	0.110	0.117	0.122	0.150	0.156	0.158
8.50	0.074	0.080	0.091	0.101	0.108	0.115	0.121	0.150	0.156	0.158
8.75	0.072	0.078	0.089	0.099	0.107	0.114	0.119	0.150	0.156	0.158
9.00	0.071	0.077	0.088	0.097	0.105	0.112	0.118	0.149	0.156	0.158
9.25	0.069	0.075	0.086	0.096	0.104	0.110	0.116	0.149	0.156	0.158
9.50	0.068	0.074	0.085	0.094	0.102	0.109	0.115	0.148	0.156	0.158
9.75	0.066	0.072	0.083	0.092	0.100	0.107	0.113	0.148	0.156	0.158
10.00	0.065	0.071	0.082	0.091	0.099	0.106	0.112	0.147	0.156	0.158
20.00	0.035	0.039	0.046	0.053	0.059	0.065	0.071	0.124	0.148	0.156
50.00	0.014	0.016	0.019	0.022	0.025	0.028	0.031	0.071	0.113	0.142
100.00	0.007	0.008	0.010	0.011	0.013	0.014	0.016	0.039	0.071	0.113

It is suggested that the settlement be computed for the surface foundations ($D_f = 0$) using Eq. (9.3) and then multiplied by I_f to account for the embedment.

Due to the nonhomogeneous nature of soil deposits, the magnitude of E_s may vary with depth. For that reason, Bowles (1987) recommended using a weighted average of E_s in Eqs. (9.3) and (9.22), or

$$E_s = \frac{\Sigma E_{s(i)} \Delta z}{\bar{z}} \tag{9.23}$$

where

$E_{s(i)}$ = soil modulus of elasticity within a depth Δz

$\bar{z} = H$ or $5B$, whichever is smaller

EXAMPLE 9.2

A flexible shallow foundation 1 m × 2 m is shown in Figure 9.6. Calculate the elastic settlement at the center of the foundation.

SOLUTION

We are given that $B = 1$ m and $L = 2$ m. Note that $\bar{z} = 5$ m $= 5B$. From Eq. (9.23),

$$E_s = \frac{\Sigma E_{s(i)} \Delta z}{\bar{z}}$$

$$= \frac{(10{,}000)(2) + (8000)(1) + (12{,}000)(2)}{5} = 10{,}400 \text{ kN/m}^2$$

For one of the four quarters of the foundation, $B = 0.5$ m and $L = 1.0$ m. Also, $H = 6.0$ m (*Note:* The Steinbrenner factors in Tables 9.3 and 9.4 are for surface foundations with $D_f = 0$.)

$$m' = L/B = 2.0 \text{ and } n' = H/B = 12.0$$

From Table 9.3, $F_1 = 0.653$, and from Table 9.4, $F_2 = 0.028$.

From Eq. (9.11), with $\mu_s = 0.3$,

$$I_s = F_1 + \left(\frac{1 - 2\mu_s}{1 - \mu_s}\right) F_2 = 0.653 + \left(\frac{1 - 2 \times 0.3}{1 - 0.3}\right)(0.028) = 0.669$$

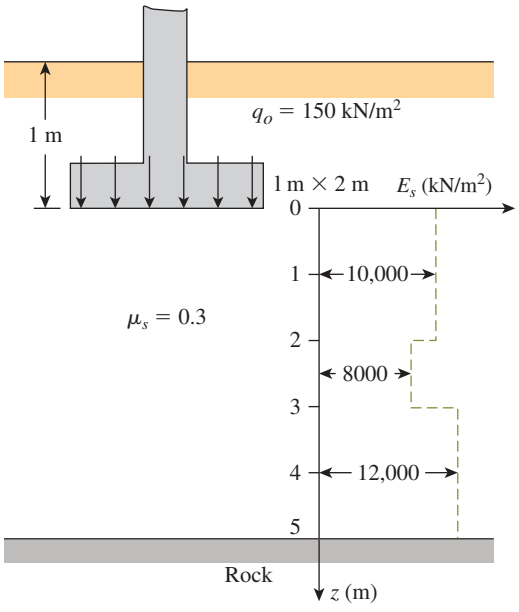


FIGURE 9.6 Elastic settlement below the center of a foundation

For $\mu_s = 0.3$, $L/B = 2$ and $D_f/B = 1$ (using $B = 1$ m for the entire foundation); from Figure 9.5b, $I_f = 0.71$.

From Eq. (9.22) and considering the four quarters,

$$S_e = \frac{q_0 B}{E_s}(1 - \mu_s^2) I_s I_f$$

$$= \frac{(150)(0.5)}{(10{,}400)}(1 - 0.3^2)(0.669 \times 4)(0.71) = 0.0124 \text{ m} = \mathbf{12.4 \text{ mm}}$$

9.4 Improved Equation for Elastic Settlement

In 1999, Mayne and Poulos presented an improved formula for calculating the elastic settlement of foundations. The formula takes into account the rigidity of the foundation, the depth of embedment of the foundation, the increase in the modulus of elasticity of the soil with depth, and the presence of a rigid layer at a limited depth. To use Mayne and Poulos' equation, one needs to determine the equivalent diameter B_e of a rectangular foundation, or

$$B_e = \sqrt{\frac{4BL}{\pi}} \tag{9.24}$$

where

B = width of foundation

L = length of foundation

For circular foundations,

$$B_e = B \tag{9.25}$$

where B = diameter of foundation.

Figure 9.7 shows a foundation with an equivalent diameter B_e located at a depth D_f below the ground surface. Let the thickness of the foundation be t and the modulus of elasticity of the foundation material be E_f. A rigid layer is located at a depth H below the bottom of the foundation. The modulus of elasticity of the compressible soil layer can be given as

$$E_s = E_o + kz \tag{9.26}$$

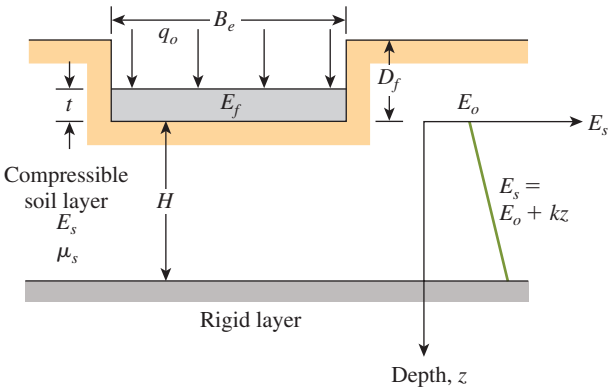


FIGURE 9.7 Improved equation for calculating elastic settlement: general parameters

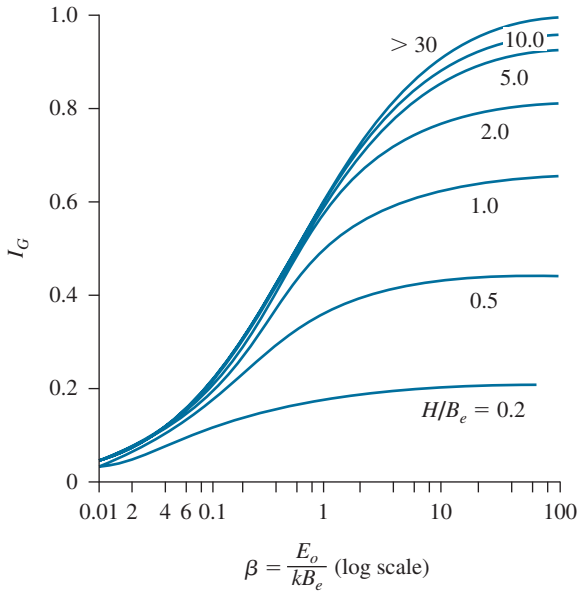


FIGURE 9.8 Variation of I_G with β

With the preceding parameters defined, the elastic settlement below the center of the foundation is

$$S_e = \frac{q_o B_e I_G I_F I_E}{E_o}(1 - \mu_s^2) \tag{9.27}$$

where

I_G = influence factor for the variation of E_s with depth

$$= f\left(\beta = \frac{E_o}{kB_e}, \frac{H}{B_e}\right)$$

I_F = foundation rigidity correction factor

I_E = foundation embedment correction factor

Figure 9.8 shows the variation of I_G with $\beta = E_o/kB_e$ and H/B_e. The foundation rigidity correction factor can be expressed as

$$I_F = \frac{\pi}{4} + \frac{1}{4.6 + 10\left(\dfrac{E_f}{E_o + \dfrac{B_e}{2}k}\right)\left(\dfrac{2t}{B_e}\right)^3} \tag{9.28}$$

Similarly, the embedment correction factor is

$$I_E = 1 - \frac{1}{3.5\exp(1.22\mu_s - 0.4)\left(\dfrac{B_e}{D_f} + 1.6\right)} \tag{9.29}$$

Figures 9.9 and 9.10 show the variation of I_F and I_E with terms expressed in Eqs. (9.28) and (9.29).

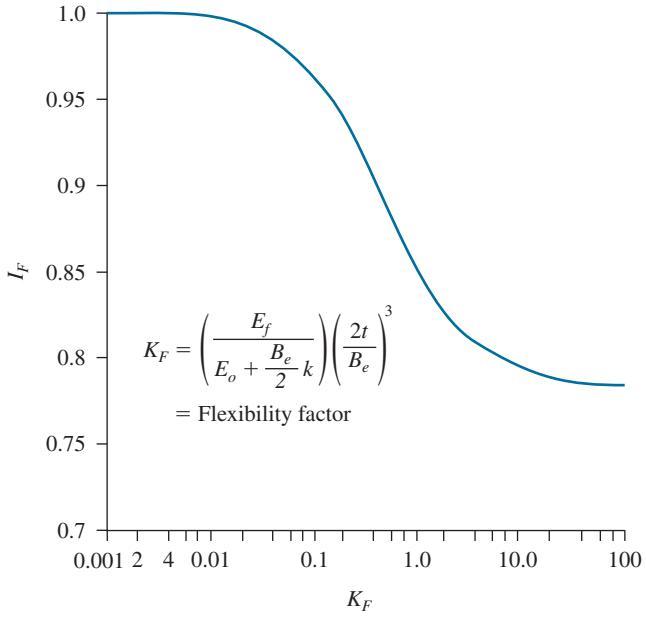


FIGURE 9.9 Variation of rigidity correction factor I_F with flexibility factor K_F [Eq. (9.28)]

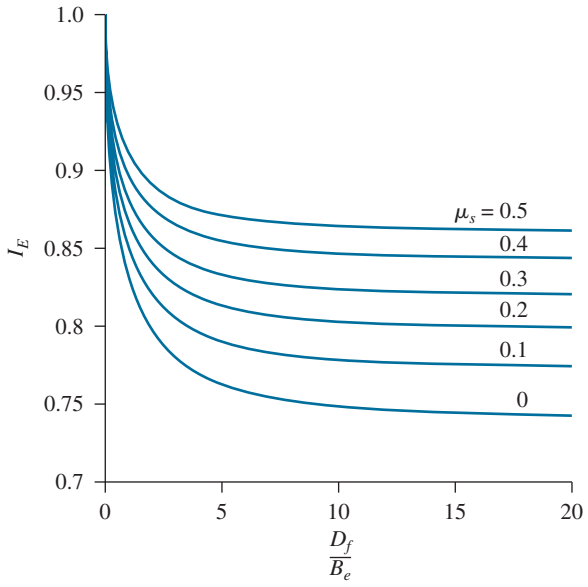


FIGURE 9.10 Variation of embedment correction factor I_E with D_f/B_e [Eq (9.29)]

EXAMPLE 9.3

For a shallow foundation supported by a silty sand, as shown in Figure 9.7,

Length = L = 3 m

Width = B = 1.5 m

Depth of foundation = D_f = 1.5 m

Thickness of foundation = t = 0.3 m

Load per unit area = q_o = 240 kN/m^2

$E_f = 16 \times 10^6$ kN/m^2

The silty sand soil has the following properties:

H = 3.7 m

μ_s = 0.3

$E_o = 9700\ \text{kN/m}^2$

$k = 575\ \text{kN/m}^2\text{/m}$

Estimate the elastic settlement of the foundation.

SOLUTION

From Eq. (9.24), the equivalent diameter is

$$B_e = \sqrt{\frac{4BL}{\pi}} = \sqrt{\frac{(4)(1.5)(3)}{\pi}} = 2.39\ \text{m}$$

so

$$\beta = \frac{E_o}{kB_e} = \frac{9700}{(575)(2.39)} = 7.06$$

and

$$\frac{H}{B_e} = \frac{3.7}{2.39} = 1.55$$

From Figure 9.8, for $\beta = 7.06$ and $H/B_e = 1.55$, the value of $I_G \approx 0.7$. From Eq. (9.28),

$$I_F = \frac{\pi}{4} + \frac{1}{4.6 + 10\left(\dfrac{E_f}{E_o + \dfrac{B_e}{2}k}\right)\left(\dfrac{2t}{B_e}\right)^3}$$

$$= \frac{\pi}{4} + \frac{1}{4.6 + 10\left[\dfrac{16 \times 10^6}{9700 + \left(\dfrac{2.39}{2}\right)(575)}\right]\left[\dfrac{(2)(0.3)}{2.39}\right]^3} = 0.789$$

From Eq. (9.29),

$$I_E = 1 - \frac{1}{3.5\exp(1.22\mu_s - 0.4)\left(\dfrac{B_e}{D_f} + 1.6\right)}$$

$$= 1 - \frac{1}{3.5\exp[(1.22)(0.3) - 0.4]\left(\dfrac{2.39}{1.5} + 1.6\right)} = 0.907$$

From Eq. (9.27),

$$S_e = \frac{q_o B_e I_G I_F I_E}{E_o}(1 - \mu_s^2)$$

so, with $q_o = 240\ \text{kN/m}^2$, it follows that

$$S_e = \frac{(240)(2.39)(0.7)(0.789)(0.907)}{9700}(1 - 0.3^2) \approx 0.02696\ \text{m} \approx \mathbf{27\ mm}$$

9.5 Settlement of Sandy Soil: Use of Strain Influence Factor

SOLUTION OF SCHMERTMANN ET AL. (1978)

The settlement of granular soil can also be evaluated by the use of a semiempirical *strain influence factor* proposed by Schmertmann et al. (1978). According to this method (Figure 9.11), the settlement is

$$S_e = C_1 C_2 (\bar{q} - q) \sum_{0}^{z_2} \frac{I_z}{E_s} \Delta z \tag{9.30}$$

where

I_z = strain influence factor

C_1 = a correction factor for the depth of foundation embedment
$= 1 - 0.5\,[q/(\bar{q} - q)]$

C_2 = a correction factor to account for creep in soil
$= 1 + 0.2 \log$ (time in years/0.1)

$\bar{q}$ = stress at the level of the foundation

$q = \gamma D_f$ = effective stress at the base of the foundation

E_s = modulus of elasticity of soil

The recommended variation of the strain influence factor I_z for square ($L/B = 1$) or circular foundations and for foundations with $L/B \geq 10$ is shown in Figure 9.11. The I_z diagrams for $1 < L/B < 10$ can be interpolated.

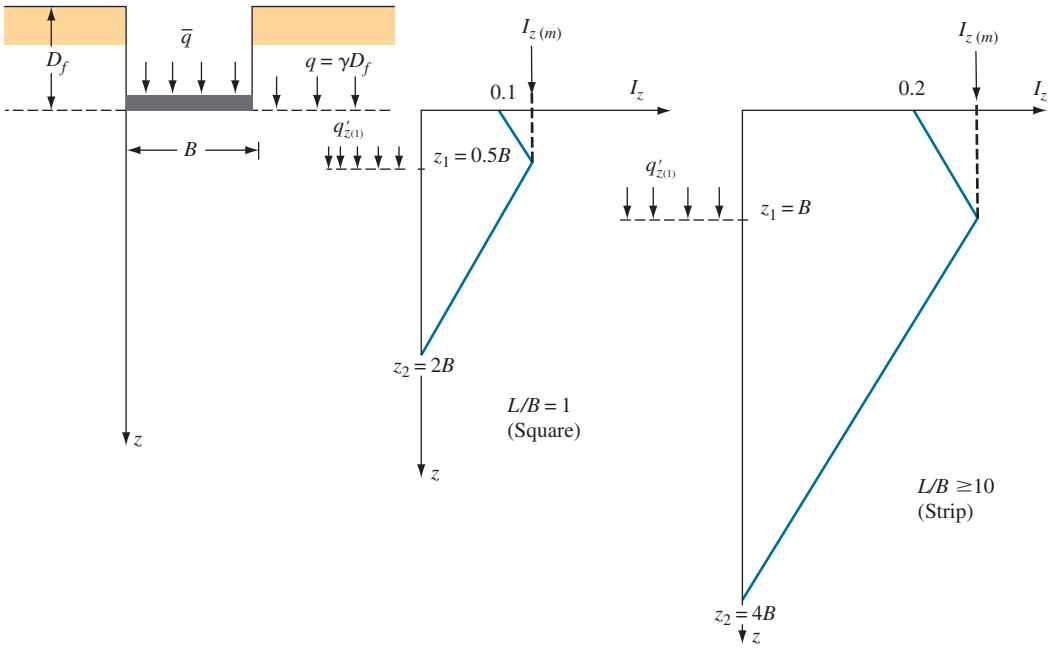


FIGURE 9.11 Variation of strain influence factor with depth and L/B

Note that the maximum value of I_z [that is, $I_{z(m)}$] occurs at $z = z_1$ and then reduces to zero at $z = z_2$. The maximum value of I_z can be calculated as

$$I_{z(m)} = 0.5 + 0.1\sqrt{\frac{\bar{q} - q}{q'_{z(1)}}} \tag{9.31}$$

where

$q'_{z(1)}$ = effective stress at a depth of z_1 before construction of the foundation

The following relations are suggested by Salgado (2008) for interpolation of I_z at $z = 0$, z_1/B, and z_2/B for rectangular foundations.

- I_z at $z = 0$

$$I_z = 0.1 + 0.0111\left(\frac{L}{B} - 1\right) \leq 0.2 \tag{9.32}$$

- z_1/B

$$\frac{z_1}{B} = 0.5 + 0.0555\left(\frac{L}{B} - 1\right) \leq 1 \tag{9.33}$$

- z_2/B

$$\frac{z_2}{B} = 2 + 0.222\left(\frac{L}{B} - 1\right) \leq 4 \tag{9.34}$$

Schmertmann et al. (1978) suggested that

$$E_s = 2.5q_c \text{ (for square foundation)} \tag{9.35}$$

and

$$E_s = 3.5q_c \text{ (for } L/B \geq 10) \tag{9.36}$$

where q_c is the cone penetration resistance.

It appears reasonable to write (Terzaghi et al., 1996)

$$E_{s(\text{rectangle})} = \left(1 + 0.4 \log\frac{L}{B}\right)E_{s(\text{square})} \tag{9.37}$$

The procedure for calculating elastic settlement using Eq. (9.30) is given here (Figure 9.12).

Step 1. Plot the foundation and the variation of I_z with depth to scale (Figure 9.12a).

Step 2. Using the correlation from standard penetration resistance (N_{60}) or cone penetration resistance (q_c), plot the actual variation of E_s with depth (Figure 9.12b).

Step 3. Approximate the actual variation of E_s into a number of layers of soil having a constant E_s, such as $E_{s(1)}$, $E_{s(2)}$, . . . , $E_{s(i)}$, . . . $E_{s(n)}$ (Figure 9.12b).

Step 4. Divide the soil layer from $z = 0$ to $z = z_2$ into a number of layers by drawing horizontal lines. The number of layers will depend on the break in continuity in the I_z and E_s diagrams.

Step 5. Prepare a table (such as Table 9.5) to obtain $\Sigma\frac{I_z}{E_s}\Delta z$.

Step 6. Calculate C_1 and C_2.

Step 7. Calculate S_e from Eq. (9.30).

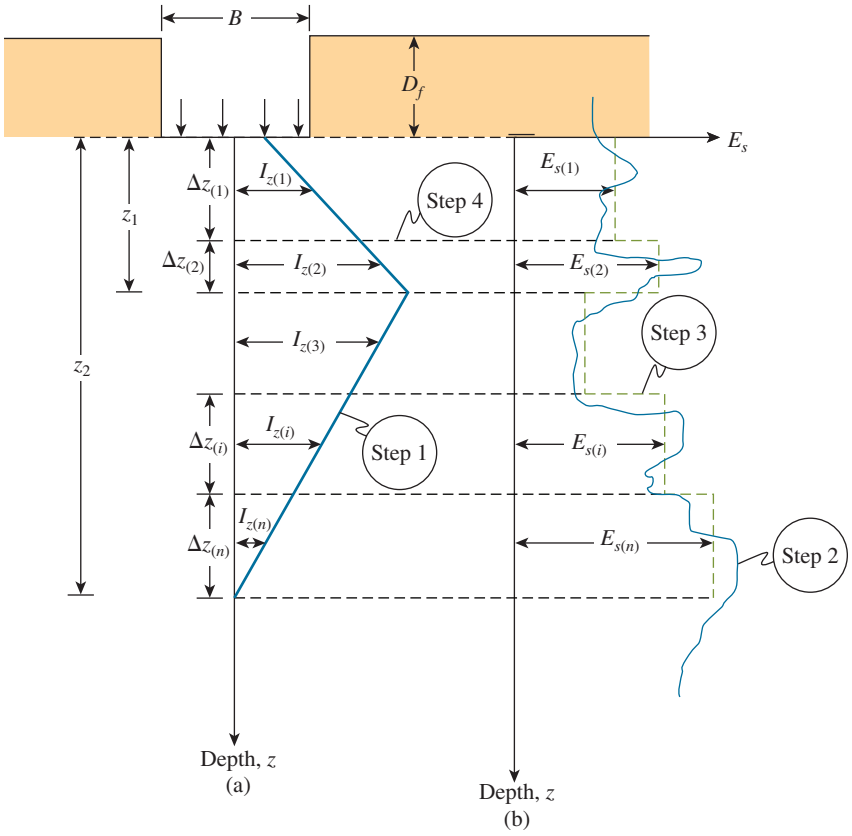


FIGURE 9.12 Procedure for calculation of S_e using the strain influence factor

TABLE 9.5 Calculation of $\Sigma \frac{I_z}{E_s} \Delta z$

Layer no.	Δz	E_s	I_z at the middle of the layer	$\frac{I_z}{E_s} \Delta z$
1	$\Delta z_{(1)}$	$E_{s(1)}$	$I_{z(1)}$	$\frac{I_{z(1)}}{E_{s(1)}} \Delta z_1$
2	$\Delta z_{(2)}$	$E_{s(2)}$	$I_{z(2)}$	
⋮	⋮	⋮	⋮	
i	$\Delta z_{(i)}$	$E_{s(i)}$	$I_{z(i)}$	$\frac{I_{z(i)}}{E_{s(i)}} \Delta z_i$
⋮	⋮	⋮	⋮	⋮
n	$\Delta z_{(n)}$	$E_{s(n)}$	$I_{z(n)}$	$\frac{I_{z(n)}}{E_{s(n)}} \Delta z_n$
				$\Sigma \frac{I_z}{E_s} \Delta z$

EXAMPLE 9.4

Consider a rectangular foundation 2 m × 4 m in plan at a depth of 1.2 m in a sand deposit, as shown in Figure 9.13a. Given: $\gamma = 17.5$ kN/m^3, $\bar{q} = 145$ kN/m^2, and the following approximated variation of q_c with z:

z (m)	q_c (kN/m^2)
0–0.5	2250
0.5–2.5	3430
2.5–6.0	2950

Estimate the elastic settlement of the foundation using the strain influence factor method.

SOLUTION

From Eq. (9.33),

$$\frac{z_1}{B} = 0.5 + 0.0555\left(\frac{L}{B} - 1\right) = 0.5 + 0.0555\left(\frac{4}{2} - 1\right) \approx 0.56$$

$$z_1 = (0.56)(2) = 1.12 \text{ m}$$

From Eq. (9.34),

$$\frac{z_2}{B} = 2 + 0.222\left(\frac{L}{B} - 1\right) = 2 + 0.222(2 - 1) = 2.22$$

$$z_2 = (2.22)(2) = 4.44 \text{ m}$$

From Eq. (9.32), at $z = 0$,

$$I_z = 0.1 + 0.0111\left(\frac{L}{B} - 1\right) = 0.1 + 0.0111\left(\frac{4}{2} - 1\right) \approx 0.11$$

From Eq. (9.31),

$$I_{z(m)} = 0.5 + 0.1\sqrt{\frac{\bar{q} - q}{q'_{z(1)}}} = 0.5 + 0.1\left[\frac{145 - (1.2 \times 17.5)}{(1.2 + 1.12)(17.5)}\right]^{0.5} = 0.675$$

The plot of I_z versus z is shown in Figure 9.13c. Again, from Eq. (9.37),

$$E_{s(\text{rectangle})} = \left(1 + 0.4 \log\frac{L}{B}\right)E_{s(\text{square})} = \left[1 + 0.4 \log\left(\frac{4}{2}\right)\right](2.5 \times q_c) = 2.8q_c$$

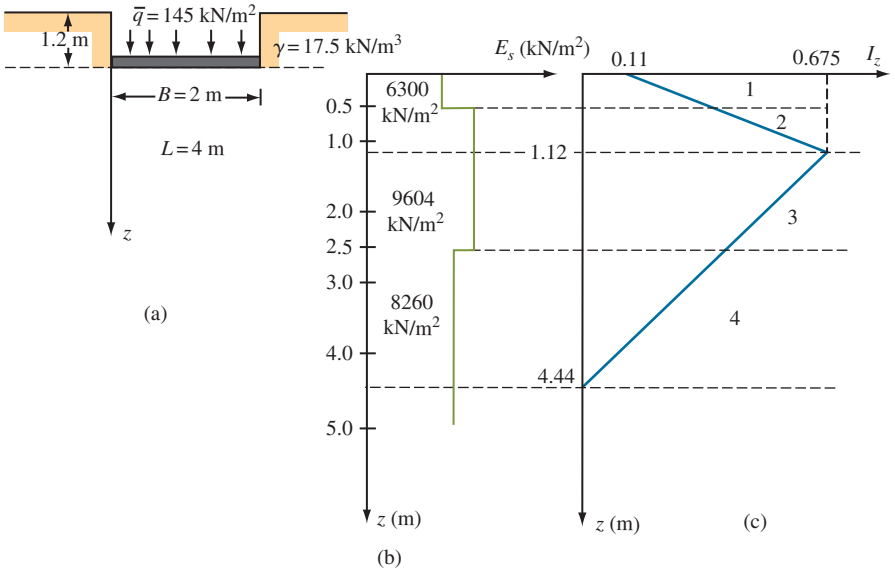


FIGURE 9.13

Hence, the approximated variation of E_s with z is as follows:

z (m)	q_c (kN/m^2)	E_s (kN/m^2)
0–0.5	2250	6300
0.5–2.5	3430	9604
2.5–6.0	2950	8260

The plot of E_s versus z is shown in Figure 9.13b.

The soil layer is divided into four layers as shown in Figures 9.13b and 9.13c. Now the following table can be prepared.

Layer no.	Δz (m)	E_s (kN/m^2)	I_z at middle of layer	$\frac{I_z}{E_s}\Delta z$ (m^3/kN)
1	0.50	6300	0.236	1.87×10^{-5}
2	0.62	9604	0.519	3.35×10^{-5}
3	1.38	9604	0.535	7.68×10^{-5}
4	1.94	8260	0.197	4.62×10^{-5}
				$\Sigma 17.52 \times 10^{-5}$

$$S_e = C_1 C_2 (\bar{q} - q) \sum \frac{I_z}{E_s} \Delta z$$

$$C_1 = 1 - 0.5\left(\frac{q}{\bar{q} - q}\right) = 1 - 0.5\left(\frac{21}{145 - 21}\right) = 0.915$$

Assume the time for creep is 10 years. So,

$$C_2 = 1 + 0.2 \log\left(\frac{10}{0.1}\right) = 1.4$$

Hence,

$$S_e = (0.915)(1.4)(145 - 21)(17.52 \times 10^{-5}) = 2783 \times 10^{-5} \text{ m} = \mathbf{27.83 \text{ mm}}$$

SOLUTION OF TERZAGHI ET AL. (1996)

Terzaghi et al. (1996) proposed a slightly different form of the strain influence factor diagram, as shown in Figure 9.14. According to Terzaghi et al. (1996),

At $z = 0$, $I_z = 0.2$ (for all L/B values)

At $z = z_1 = 0.5B$, $I_z = 0.6$ (for all L/B values)

At $z = z_2 = 2B$, $I_z = 0$ (for $L/B = 1$)

At $z = z_2 = 4B$, $I_z = 0$ (for $L/B \geq 10$)

For L/B between 1 and 10 (or > 10),

$$\frac{z_2}{B} = 2\left[1 + \log\left(\frac{L}{B}\right)\right] \tag{9.38}$$

The elastic settlement can be given as

$$S_e = C_d(\bar{q} - q)\sum_0^{z_2} \frac{I_z}{E_s}\Delta z + \underbrace{0.02\left[\frac{0.1}{\frac{\sum(q_c \Delta z)}{z_2}}\right] z_2 \log\left(\frac{t \text{ days}}{1 \text{ day}}\right)}_{\text{Postconstruction settlement}} \tag{9.39}$$

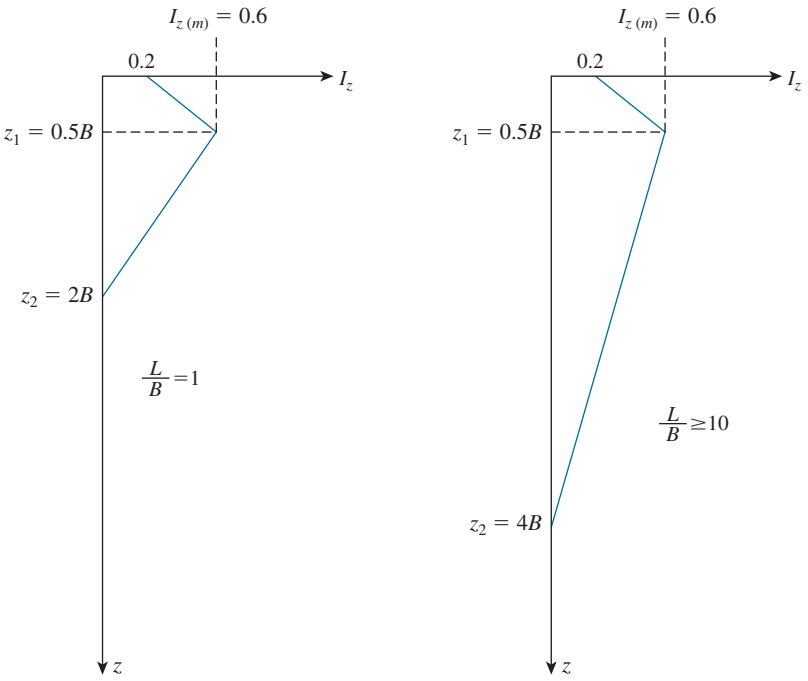


FIGURE 9.14 Strain influence factor diagram proposed by Terzaghi et al. (1996)

In Eq. (9.39), q_c is in MN/m^2.

The relationships for E_s are

$$E_s = 3.5q_c \text{ (for square and circular foundations)} \tag{9.40}$$

and

$$E_{s(\text{rectangular})} = \left[1 + 0.4 \log\left(\frac{L}{B}\right)\right] E_{s(\text{square})} \leq 1.4E_{s(\text{square})} \tag{9.41}$$

In Eq. (9.38), C_d is the depth factor. Table 9.6 gives the interpolated values of C_d for values of D_f/B.

TABLE 9.6 Variation of C_d with D_f/B*

D_f/B	C_d
0.1	1
0.2	0.96
0.3	0.92
0.5	0.86
0.7	0.82
1.0	0.77
2.0	0.68
3.0	0.65

*Based on data from Terzaghi et al. (1996)

EXAMPLE 9.5

Solve Example 9.4 using the method of Terzaghi et al. (1996).

SOLUTION

Given: $L/B = 4/2 = 2$.

Figure 9.15a shows the plot of I_z with depth below the foundation. Note that

$$\frac{z_2}{B} = 2\left[1 + \log\left(\frac{L}{B}\right)\right] = 2[1 + \log(2)] = 2.6$$

or

$$z_2 = (2.6)(B) = (2.6)(2) = 5.2 \text{ m}$$

Also, from Eqs. (9.40) and (9.41),

$$E_s = \left[1 + 0.4 \log\left(\frac{L}{B}\right)\right](3.5q_c) = \left[1 + 0.4 \log\left(\frac{4}{2}\right)\right](3.5q_c) = 3.92$$

The following table can be prepared and shows the variation of E_s with depth, which is shown in Figure 9.15b.

z (m)	q_c (kN/m^2)	E_s (kN/m^2)
0–0.5	2250	8820
0.5–2.5	3430	14,445.6
2.5–6	2950	11,564

Again, $D_f/B = 1.2/2 = 0.6$. From Table 9.6, $C_d \approx 0.85$.

The following table is used to calculate $\sum_0^{z_2} \frac{I_z}{E_s}\Delta z$.

Layer no.	Δz (m)	E_s (kN/m^2)	I_z at the middle of the layer	$\frac{I_z}{E_s}\Delta z$ (m^2/kN)
1	0.5	8820	0.3	1.7×10^{-5}
2	0.5	14,445.6	0.5	1.73×10^{-5}
3	1.5	14,445.6	0.493	5.12×10^{-5}
4	2.7	11,564	0.193	4.5×10^{-5}
				Σ 13.06×10^{-5} m^2/kN

Thus,

$$C_d(\bar{q} - q)\sum_0^{z_2} \frac{I_z}{E_s}\Delta_z = (0.85)(145 - 21)(13.06 \times 10^{-5}) = 1376.5 \times 10^{-5} \text{ m}$$

Postconstruction creep is

$$0.02\left[\frac{0.1}{\frac{\sum(q_c\Delta z)}{z_2}}\right] z_2 \log\left(\frac{t \text{ days}}{1 \text{ day}}\right)$$

$$\frac{\sum(q_c\Delta z)}{z_2} = \frac{(2250 \times 0.5) + (3430 \times 2) + (2950 \times 2.7)}{5.2}$$

$$= 3067.3 \text{ kN/m}^2 \approx 3.07 \text{ MN/m}^2$$

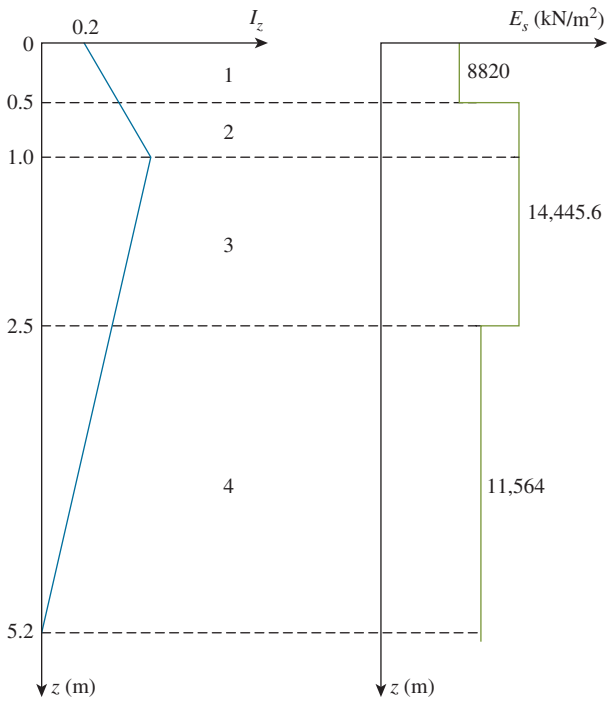


FIGURE 9.15

Hence, the elastic settlement is

$$S_e = 1376.5 \times 10^{-5} + 0.02\left[\frac{0.1}{3.07}\right](5.2)\log\left(\frac{10 \times 365 \text{ days}}{1 \text{ day}}\right)$$
$$= 2583.3 \times 10^{-5} \text{ m}$$
$$\approx \mathbf{25.83 \text{ mm}}$$

Note: The magnitude of S_e is about 93% of that found in Example 9.4. In Example 9.4, the elastic settlement was about 19.88 mm, and settlement due to creep was about 7.95 mm. However, in Example 9.5, elastic settlement is about 13.77 mm, and the settlement due to creep is about 12.07 mm. Thus the magnitude of creep settlement is about 50% more in Example 9.5. However, the magnitude of elastic settlement in Example 9.4 is about 30% more compared to that in Example 9.5. This is because of the assumption of the $E_s - q_c$ relationship.

■

Leonards (1986) and Holtz (1991) noted that the method of Schmertmann et al. (1978) is based on settlement records from Florida, where sands are interbedded with clays and silts that exhibit creep. In sands and gravels that do not contain any fines, they suggest using $C_2 = 1$.

9.6 Settlement of Foundation on Sand Based on Standard Penetration Resistance

TERZAGHI AND PECK'S METHOD

Terzaghi and Peck (1967) proposed the first rational method for predicting settlement of a shallow foundation in a granular soil. They related the elastic settlement of

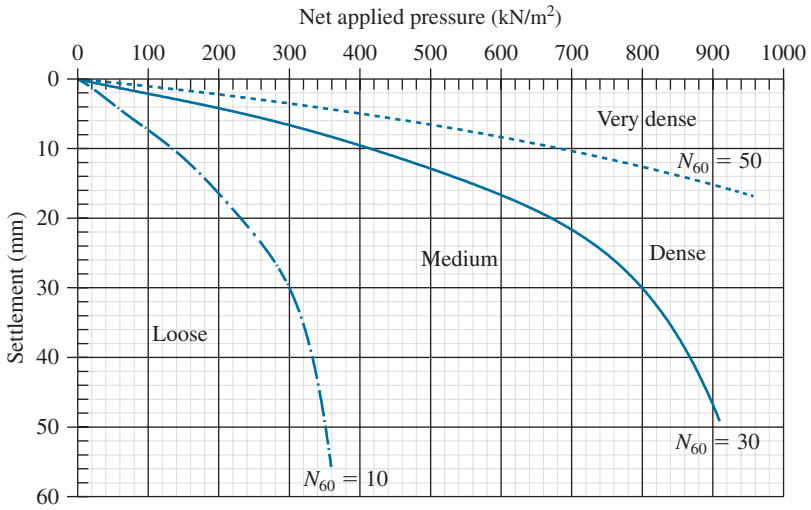


FIGURE 9.16 Settlement of 300 mm (1 ft) × 300 mm (1 ft) plate (Load test data from Late Professor G.A. Leonards, Purdue University)

a square foundation ($S_{e,\text{ foundation}}$) of width B to the settlement of a 300 mm (1 ft) wide square plate ($S_{e,\text{ plate}}$) under the same pressure by

$$S_{e,\text{ foundation}} = S_{e,\text{ plate}}\left(\frac{2B}{B+1}\right)^2\left(1-\frac{1}{4}\frac{D_f}{B}\right) \tag{9.42}$$

where B is in feet. In SI units, Eq. (9.42) becomes

$$S_{e,\text{ foundation}} = S_{e,\text{ plate}}\left(\frac{2B}{B+0.3}\right)^2\left(1-\frac{1}{4}\frac{D_f}{B}\right) \tag{9.43}$$

where B is in meters.

In Eqs. (9.42) and (9.43), the last term takes into account the reduction in settlement with the increase in foundation depth. Leonards (1986) suggested replacing 1/4 by 1/3, based on additional load test data. The values of $S_{e,\text{ plate}}$ can be obtained from Figure 9.16, which summarizes the plate loading test data given by Terzaghi and Peck (1967). These load tests were carried out on thick deposits of normally consolidated drained sand. This method was originally proposed for square foundations but can be applied to rectangular and strip foundations with caution. The deeper influence zone and increase in the stresses within the underlying soil mass in the case of rectangular or strip foundations are compensated by the increase in the soil stiffness.

EXAMPLE 9.6

A 2.5 m square foundation placed at a depth of 1.5 m within a sandy soil applies a net pressure of 120 kN/m^2 to the underlying ground. The sand has $\gamma = 18.5$ kN/m^3 and $N_{60} = 25$. What would be the settlement?

SOLUTION

For net applied pressure = 120 kN/m^2 and $N_{60} = 25$; from Figure 9.16, $S_{e,\text{ plate}} = 4$ mm.

From Eq. (9.43),

$$S_{e,\text{ foundation}} = S_{e,\text{ plate}}\left(\frac{2B}{B+0.3}\right)^2\left(1-\frac{1}{3}\frac{D_f}{B}\right)$$

$$= (4)\left(\frac{2\times 2.5}{2.5+0.3}\right)^2\left(1-\frac{1}{3}\times\frac{1.5}{2.5}\right) = \mathbf{10.2\ mm}$$

■

MEYERHOF'S METHOD

Meyerhof (1956) proposed a correlation for the *net bearing pressure* for foundations with the standard penetration resistance, N_{60}. The net pressure has been defined as

$$q_{net} = \bar{q} - \gamma D_f$$

where $\bar{q}$ is the stress at the level of the foundation.

For a long time, 25 mm (1 in.) has been considered the maximum allowable settlement for shallow foundations (see Section 9.16). According to Meyerhof's theory, for 25 mm (1 in.) of estimated maximum settlement,

$$q_{net}(\text{kip/ft}^2) = \frac{N_{60}}{4} \quad (\text{for } B \le 4 \text{ ft}) \tag{9.44}$$

and

$$q_{net}(\text{kip/ft}^2) = \frac{N_{60}}{6}\left(\frac{B+1}{B}\right)^2 \quad (\text{for } B > 4 \text{ ft}) \tag{9.45}$$

Since the time that Meyerhof proposed his original correlations, researchers have observed that its results are rather conservative. Later, Meyerhof (1965) suggested that the net allowable bearing pressure should be increased by about 50%. Bowles (1977) proposed that the modified form of the bearing equations be expressed as

$$q_{net}(\text{kip/ft}^2) = \frac{N_{60}}{2.5} F_d S_e \quad (\text{for } B \le 4 \text{ ft}) \tag{9.46}$$

and

$$q_{net}(\text{kip/ft}^2) = \frac{N_{60}}{4}\left(\frac{B+1}{B}\right)^2 F_d S_e \quad (\text{for } B > 4 \text{ ft}) \tag{9.47}$$

where

F_d = depth factor = $1 + 0.33(D_f/B)$

B = foundation width, in feet

S_e = settlement, in inches

Hence,

$$S_e(\text{in.}) = \frac{2.5 q_{net}(\text{kip/ft}^2)}{N_{60} F_d} \quad (\text{for } B \le 4 \text{ ft}) \tag{9.48}$$

and

$$S_e(\text{in.}) = \frac{4 q_{net}(\text{kip/ft}^2)}{N_{60} F_d}\left(\frac{B}{B+1}\right)^2 \quad (\text{for } B > 4 \text{ ft}) \tag{9.49}$$

In SI, units, Eqs. (9.46) and (9.47) can be written as

$$q_{net}(\text{kN/m}^2) = \frac{N_{60}}{0.05} F_d\left(\frac{S_e}{25}\right) \quad (\text{for } B \le 1.22 \text{ m}) \tag{9.50}$$

and

$$q_{net}(\text{kN/m}^2) = \frac{N_{60}}{0.08}\left(\frac{B+0.3}{B}\right)^2 F_d\left(\frac{S_e}{25}\right) \quad (\text{for } B > 1.22 \text{ m}) \tag{9.51}$$

where B is in meters and S_e is in mm. Hence,

$$S_e(\text{mm}) = \frac{1.25 q_{net}(\text{kN/m}^2)}{N_{60} F_d} \quad (\text{for } B \le 1.22 \text{ m}) \tag{9.52}$$

and

$$S_e(\text{mm}) = \frac{2q_{\text{net}}(\text{kN/m}^2)}{N_{60}F_d}\left(\frac{B}{B+0.3}\right)^2 \quad (\text{for } B > 1.22 \text{ m}) \tag{9.53}$$

The N_{60} referred to in the preceding equations is the standard penetration resistance between the bottom of the foundation and $2B$ below the bottom.

BURLAND AND BURBIDGE'S METHOD

Burland and Burbidge (1985) proposed a method of calculating the elastic settlement of sandy soil using the *field standard penetration number*, N_{60}. (See Chapter 3.) The method can be summarized as follows:

1. **Variation of Standard Penetration Number with Depth**
   Obtain the field penetration numbers (N_{60}) with depth at the location of the foundation. The following adjustments of N_{60} may be necessary, depending on the field conditions:

   For gravel or sandy gravel,

   $$N_{60(a)} \approx 1.25N_{60} \tag{9.54}$$

   For fine sand or silty sand below the groundwater table and $N_{60} > 15$,

   $$N_{60(a)} \approx 15 + 0.5(N_{60} - 15) \tag{9.55}$$

   where $N_{60(a)}$ = adjusted N_{60} value.

2. **Determination of Depth of Stress Influence (z')**
   In determining the depth of stress influence, the following three cases may arise:

   Case I. If N_{60} [or $N_{60(a)}$] is approximately constant with depth, calculate z' from

   $$\frac{z'}{B_R} = 1.4\left(\frac{B}{B_R}\right)^{0.75} \tag{9.56}$$

   where

   $$B_R = \text{reference width}\begin{cases} = 1 \text{ ft (if } B \text{ is in ft)} \\ = 0.3 \text{ m (if } B \text{ is in m)} \end{cases}$$

   B = width of the actual foundation

   Case II. If N_{60} [or $N_{60(a)}$] is increasing with depth, use Eq. (9.56) to calculate z'.

   Case III. If N_{60} [or $N_{60(a)}$] is decreasing with depth, $z' = 2B$ or the depth to the bottom of soft soil layer measured from the bottom of the foundation (whichever is smaller).

3. **Calculation of Elastic Settlement S_e**
   The elastic settlement of the foundation, S_e, can be calculated from

   $$\frac{S_e}{B_R} = \alpha_1\alpha_2\alpha_3\left[\frac{1.25\left(\frac{L}{B}\right)}{0.25 + \left(\frac{L}{B}\right)}\right]^2\left(\frac{B}{B_R}\right)^{0.7}\left(\frac{q'}{p_a}\right) \tag{9.57}$$

   where

   α_1 = a constant

   α_2 = compressibility index

TABLE 9.7 Summary of q', α_1, α_2, and α_3

Soil type	q'	α_1	α_2	α_3
Normally consolidated sand	q_{net}	0.14	$\dfrac{1.71}{\left[\overline{N}_{60} \text{ or } \overline{N}_{60(a)}\right]^{1.4}}$	
Overconsolidated sand ($q_{net} \le \sigma_c'$)	q_{net}	0.047	$\dfrac{0.57}{\left[\overline{N}_{60} \text{ or } \overline{N}_{60(a)}\right]^{1.4}}$	$\alpha_3 = \dfrac{H}{z'}\left(2 - \dfrac{H}{z'}\right)$ (if $H \le z'$) or $\alpha_3 = 1$ (if $H > z'$)
where σ_c' = preconsolidation pressure				where H = depth of compressible layer
Overconsolidated sand ($q_{net} > \sigma_c'$)	$q_{net} - 0.67\sigma_c'$	0.14	$\dfrac{0.57}{\left[\overline{N}_{60} \text{ or } \overline{N}_{60(a)}\right]^{1.4}}$	

α_3 = correction for the depth of influence

p_a = atmospheric pressure = 100 kN/m^2 (≈2000 lb/ft^2)

L = length of the foundation

Table 9.7 summarizes the values of q', α_1, α_2, and α_3 to be used in Eq. (9.57) for various types of soil. Note that in this table, $\overline{N}_{60}$ or $\overline{N}_{60(a)}$ = average value of N_{60} or $N_{60(a)}$ in the depth of stress influence.

EXAMPLE 9.7

A shallow foundation measuring 1.75 m × 1.75 m is to be constructed over a layer of sand. Given $D_f = 1$ m; N_{60} is generally increasing with depth; $\overline{N}_{60}$ within the depth of stress influence = 10; $q_{net} = 120$ kN/m^2. The sand is normally consolidated. Estimate the elastic settlement of the foundation. Use the Burland and Burbidge method.

SOLUTION

From Eq. (9.56),

$$\frac{z'}{B_R} = 1.4\left(\frac{B}{B_R}\right)^{0.75}$$

Depth of stress influence,

$$z' = 1.4\left(\frac{B}{B_R}\right)^{0.75} B_R = (1.4)(0.3)\left(\frac{1.75}{0.3}\right)^{0.75} \approx 1.58 \text{ m}$$

From Eq. (9.57),

$$\frac{S_e}{B_R} = \alpha_1\alpha_2\alpha_3\left[\frac{1.25\left(\frac{L}{B}\right)}{0.25 + \left(\frac{L}{B}\right)}\right]^2\left(\frac{B}{B_R}\right)^{0.7}\left(\frac{q'}{p_a}\right)$$

For normally consolidated sand (Table 9.7),

$$\alpha_1 = 0.14$$

$$\alpha_2 = \frac{1.71}{(\overline{N}_{60})^{1.4}} = \frac{1.71}{(10)^{1.4}} = 0.068$$

$$\alpha_3 = 1$$

$$q' = q_{net} = 120 \text{ kN/m}^2$$

So,

$$\frac{S_e}{0.3} = (0.14)(0.068)(1)\left[\frac{(1.25)\left(\frac{1.75}{1.75}\right)}{0.25 + \left(\frac{1.75}{1.75}\right)}\right]^2 \left(\frac{1.75}{0.3}\right)^{0.7}\left(\frac{120}{100}\right)$$

$$S_e \approx 0.0118 \text{ m} = \mathbf{11.8 \text{ mm}}$$

■

EXAMPLE 9.8

Solve Example 9.6 using Meyerhof's method.

SOLUTION

From Eq. (9.53),

$$S_e = \frac{2q_{\text{net}}}{(N_{60})(F_d)}\left(\frac{B}{B + 0.3}\right)^2$$

$$F_d = 1 + 0.33(D_f/B) = 1 + 0.33(1/1.75) = 1.19$$

$$S_e = \frac{(2)(120)}{(10)(1.19)}\left(\frac{1.75}{1.75 + 0.3}\right)^2 = \mathbf{14.7 \text{ mm}}$$

■

9.7 Settlement Considering Soil Stiffness Variation with Stress Level

In most settlement prediction methods, the stiffness is determined from penetration tests, such as SPT or CPT, and a constant value is assumed for the modulus of elasticity (e.g., $E_s = 2.5q_c$). Berardi and Lancellotta (1991) recognized that the soil stiffness varies with the stress level, with the modulus of elasticity decreasing with increasing strain levels. They proposed an improved method for predicting settlement; this method incorporates the stress level in determining the soil stiffness.

Figure 9.17 shows a foundation resting on sand where the influence zone is extending to a depth Z below the foundation. Berardi et al. (1991) noted that Z varies in the range of $B-2B$. For square foundations $Z = B$, and for strip foundations $Z = 2B$. For rectangular foundations, Z can be logarithmically interpolated as

$$\frac{Z}{B} = 1 + \log\left(\frac{L}{B}\right) \tag{9.58}$$

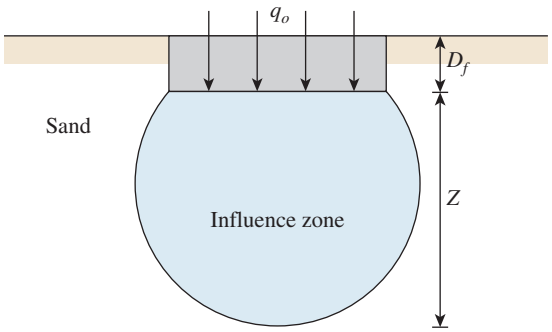


FIGURE 9.17 Foundation and the influence zone

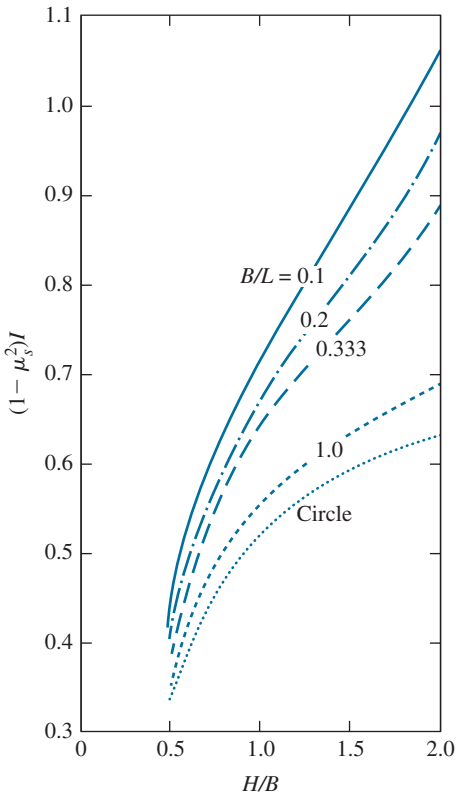


FIGURE 9.18 Variation of $(1 - \mu_s^2)I$ with H/B and B/L (Based on Berardi et al., 1991)

where L/B is limited to 10 in the case of a strip foundation.

From elastic analysis, the settlement of a foundation with dimensions B and L resting on an elastic body is given by

$$S_e = \frac{q_o B}{E_s}(1 - \mu_s^2)I \tag{9.59}$$

where q_o is the net applied pressure, B is the foundation width, E_s is the modulus of elasticity, μ_s is Poisson's ratio, and I is the influence factor that depends on the dimensions of the foundation. Assuming Poisson's ratio to be 0.15 and the foundation to be rigid, values of $(1 - \mu_s^2)I$ are given in Figure 9.18. Here H is the depth of the compressible soil stratum.

Application of the load to the foundation will increase the soil stiffness. Janbu (1963) suggested that the modulus of elasticity can be written as

$$E_s = K_E p_a \left(\frac{\sigma'_o + 0.5\Delta\sigma'_o}{p_a}\right)^{0.5} \tag{9.60}$$

where K_E is a dimensionless *modulus number* for the sand which depends on the relative density, strain level, and the influence depth Z; σ'_o is the initial overburden pressure at the center of the influence zone; $\Delta\sigma'_o$ is the vertical effective stress increase at the center of the influence zone due to the foundation load; and p_a is the atmospheric pressure ($\approx$ 2000 lb/ft^2 or 100 kN/m^2).

According to Lancellotta (2009), at 0.1% strain level (S_e/B)

$$K_{E,\,0.1\%} = 9.1D_r + 92.5 \quad (\text{for } Z = B) \tag{9.61}$$

and

$$K_{E,\,0.1\%} = 11.44D_r - 76.5 \quad (\text{for } Z = 2B) \tag{9.62}$$

where D_r is the relative density of sand (%) (see Figure 9.19).

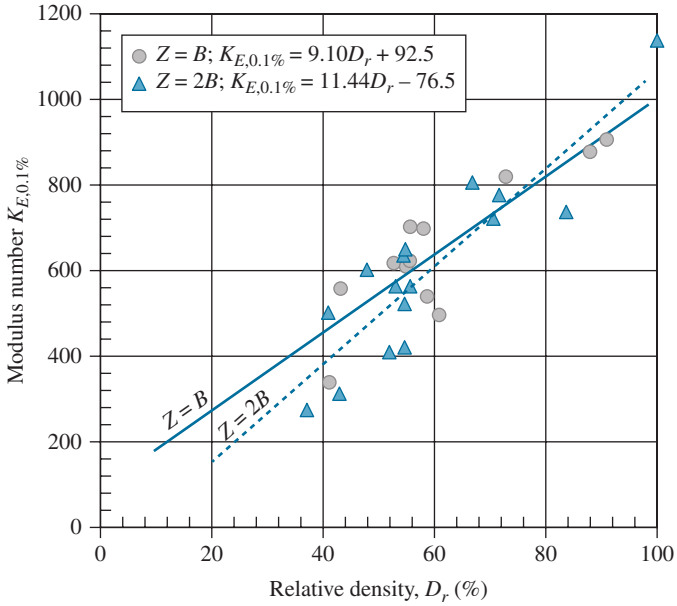


FIGURE 9.19 Variation of $K_{E,\,0.1\%}$ with relative density for $Z = B$ and $Z = 2B$ (Based on Lancellotta, 2009)

It is important to note that at $D_r = 60\%$, Eqs. (9.61) and (9.62) will give values of $K_{E,0.1\%}$ as 638.5 and 609.9, respectively. Similarly, at $D_r = 80\%$, Eqs. (9.61) and (9.62) will give $K_{E,0.1\%}$ as 820.5 and 838.7, respectively. These values of $K_{E,\,0.1\%}$ are relatively close. Most of the foundations are analyzed within a range of $D_r = 60$ to 80%. So, $K_{E,\,0.1\%}$ values for the range of $Z = B$ and $2B$ can be reasonably interpolated.

The magnitude of D_r can be estimated as (Skempton, 1986)

$$D_r = \left[\frac{(N_1)_{60}}{60}\right]^{0.5} \tag{9.63}$$

where $(N_1)_{60}$ is the average corrected standard penetration resistance in the zone of influence [see Eq. (3.12)].

According to Berardi et al. (1991), the modulus number K_E, at any other strain level, can be estimated as (Berardi et al. 1991) (also see Figure 9.20)

$$\frac{K_{E\left(\frac{S_e}{B}\%\right)}}{K_{E,0.1\%}} = 0.008\left(\frac{S_e}{B}\right)^{-0.7} \tag{9.64}$$

Based on the work of Berardi (1999), Lancellotta (2009) has suggested that

$$\frac{E_s}{E_{s,0.1\%}} = 0.008\left(\frac{S_e}{B}\right)^{-0.7} \tag{9.65}$$

where $E_{s,0.1\%}$ is the modulus of elasticity of sand when the vertical strain level $\varepsilon_v = S_e/B = 0.1\%$. The value of $K_{E,0.1\%}$ determined from Figure 9.19 or Eqs. (9.61) and (9.62) can be substituted into Eq. (9.60) for the estimation of $E_{s,0.1}$.

Again, from Eqs. (9.59) and (9.65),

$$\left(\frac{S_e}{B}\right)^{0.3} = \frac{125q_o(1-\mu_s^2)I}{E_{s,\,0.1\%}} \tag{9.66}$$

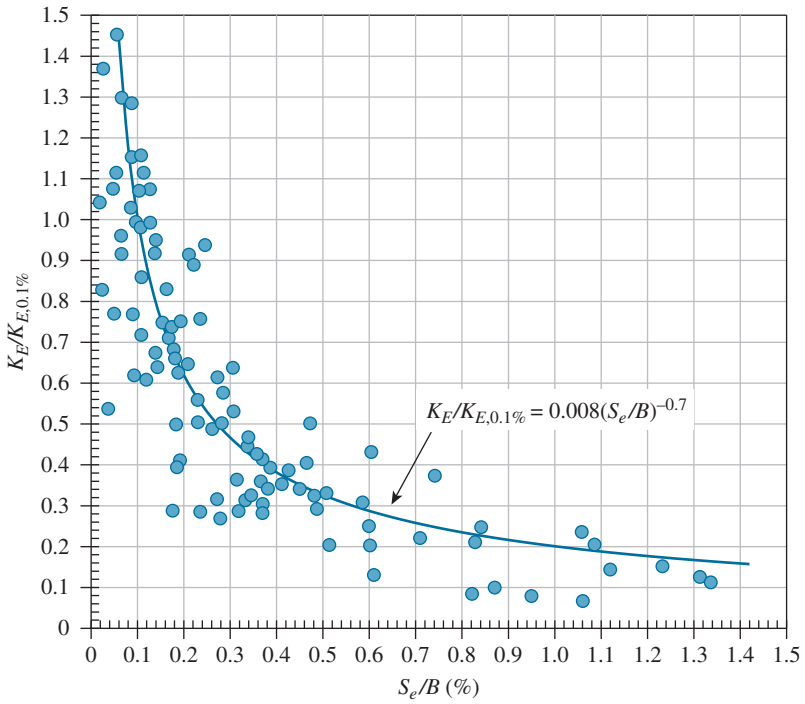


FIGURE 9.20 $K_E/K_{E,0.1\%}$ ratio versus S_e/B (Based on Berardi et al., 1991)

EXAMPLE 9.9

A 2 m × 2 m square foundation placed on sand at a depth of 0.5 m carries a column load of 1000 kN. The sand has a unit weight of 19 kN/m^3 and $(N_1)_{60}$ of 28. Estimate the settlement. Assume Poisson's ratio of the sand to be 0.15.

SOLUTION

Refer to Figure 9.21. The applied pressure at the foundation level $= \dfrac{600}{2 \times 2} = 150$ kN/m^2.

From Eq. (9.63), $D_r = \sqrt{\dfrac{(N_1)_{60}}{60}} = \sqrt{\dfrac{28}{60}} = 0.683$ or 68.3%. At X, $\sigma'_o = 1.5 \times 19 = 28.5$ kN/m^2. At X, estimate that $\Delta\sigma'_o = \dfrac{150 \times 2 \times 2}{(2 + 1)(2 + 1)} = 66.7$ kN/m^2 (based on the 2V:1H method; see Section 8.6). The influence depth $Z = B = 2.0$ m.

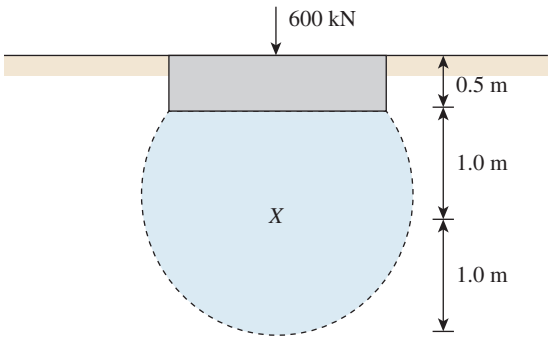


FIGURE 9.21

From Figure 9.18, for $H/B = 1$ and $L/B = 1$, $(1 - \mu_s^2)I = 0.56$. Also, $p_a \approx 100$ kN/m^2.

$$\left(\frac{\sigma'_o + 0.5\Delta\sigma'_o}{p_a}\right)^{0.5} = \left(\frac{28.5 + 0.5 \times 66.7}{100}\right)^{0.5} = 0.786$$

For $D_r = 68.3\%$ and $Z = B$, from Eq. (9.61), we obtain $K_{E,0.1\%} = 714.03$. From Eq. (9.60),

$$E_{s,\,0.1\%} = K_{E,\,0.1\%}\, p_a \left(\frac{\sigma'_o + 0.5\Delta\sigma'_o}{p_a}\right)^{0.5} = 714.3 \times 100 \times 0.786 \approx 56{,}144 \text{ kN/m}^2$$

Substituting these in Eq. (9.66),

$$\left(\frac{S_e}{B}\right)^{0.3} = \frac{125 \times 150 \times 0.56}{56{,}144} = 0.187$$

Therefore, $S_e/B = 0.00375$, and settlement $= 0.00374 \times 2000 =$ **7.48 mm**.

9.8 Settlement Based on Pressuremeter Test (PMT)

Briaud (2007) proposed a method based on pressuremeter tests (Section 3.22) from which the load-settlement diagrams of foundations can be derived. The following is a step-by-step procedure for performing the analysis.

Step 1. Conduct pressuremeter tests at varying depths at the desired location and obtain plots of p_p (pressure in the measuring cell for cavity expansion; see Figure 3.31) versus $\Delta R/R_o$ (R_o is the initial radius of the PMT cavity, and ΔR is the increase in the cavity radius), as shown in Figure 9.22a.

Step 2. Extend the straight line part of the PMT curve to zero pressure and shift the vertical axis, as shown in Figure 9.22a. Re-zero the $\Delta R/R_o$ axis.

Step 3. Draw a strain influence factor diagram for the desired foundation (Section 9.5). Using all pressuremeter test curves within the depth of influence, develop a mean PMT curve. Referring to Figure 9.22b, this can be done as follows:

For each value of $\Delta R/R_o$, let the p_p values be $p_{p(1)}$, $p_{p(2)}$, $p_{p(3)}$,.... The mean value of p_p can be obtained as

$$p_{p(m)} = \frac{A_1}{A}p_{p(1)} + \frac{A_2}{A}p_{p(2)} + \frac{A_3}{A}p_{p(3)} + \cdots \tag{9.67}$$

where A_1, A_2, and A_3 are the areas tributary to each test under the strain influence factor diagram.

$$A = A_1 + A_2 + A_3 + \cdots \tag{9.68}$$

Step 4. Based on the results of Step 3, develop a mean $p_{p(m)}$ versus $\Delta R/R_o$ plot (Figure 9.22c).

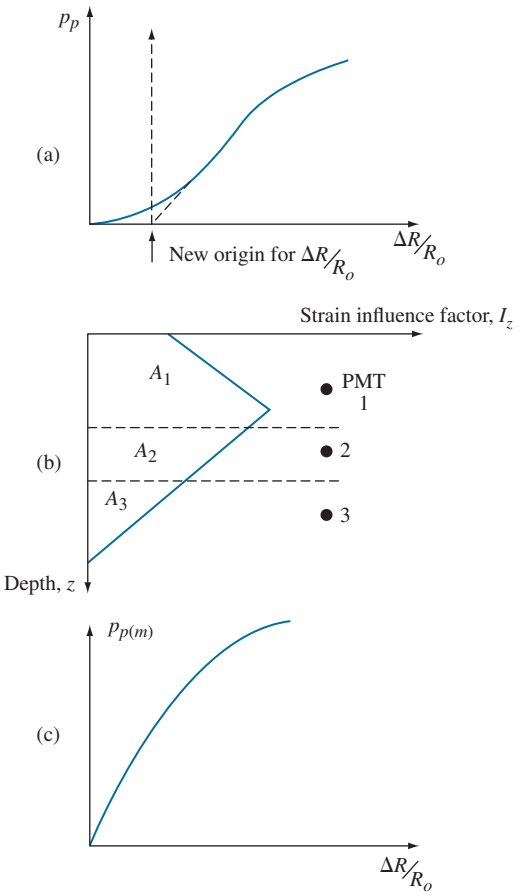


FIGURE 9.22 (a) Plot of p_p versus $\Delta R/R_o$; (b) averaging the pressuremeter curves within the foundation zone of influence; (c) plot of $p_{p(m)}$ versus $\Delta R/R_o$

Step 5. The mean PMT curve now can be used to develop the load-settlement plot for the foundation via the following equations.

$$\frac{S_e}{B} = 0.24\frac{\Delta R}{R_o} \tag{9.69}$$

and

$$q_o = f_{L/B} f_e f_\delta f_{\beta,d} \Gamma p_{p(m)} \tag{9.70}$$

where

S_e = elastic settlement of the foundation

B = width of foundation

L = length of foundation

q_o = net load per unit area on the foundation

Γ = gamma function linking q_o and $p_{p(m)}$

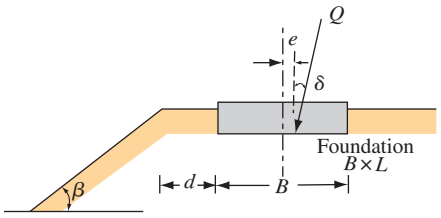


FIGURE 9.23 Definition of parameters—β, L, d, δ, β, e, and β

$$f_{L/B} = \text{shape factor} = 0.8 + 0.2\left(\frac{B}{L}\right) \tag{9.71}$$

$$f_e = \text{eccentricity factor} = 1 - 0.33\left(\frac{e}{B}\right)(\text{center}) \tag{9.72}$$

$$f_e = \text{eccentricity factor} = 1 - \left(\frac{e}{B}\right)^{0.5} (\text{edge}) \tag{9.73}$$

$$f_\delta = \text{load inclination factor} = 1 - \left[\frac{\delta(\text{deg})}{90}\right]^2 (\text{center}) \tag{9.74}$$

$$f_\delta = \text{load inclination factor} = 1 - \left[\frac{\delta(\text{deg})}{360}\right]^{0.5} (\text{edge}) \tag{9.75}$$

$$f_{\beta,d} = \text{slope factor} = 0.8\left(1 + \frac{d}{B}\right)^{0.1} (\text{3H:1V slope}) \tag{9.76}$$

$$f_{\beta,d} = \text{slope factor} = 0.7\left(1 + \frac{d}{B}\right)^{0.15} (\text{2H:1V slope}) \tag{9.77}$$

δ = inclination of load with respect to the vertical

β = inclination of a slope with the horizontal if the foundation is located on top of a slope

d = distance of the edge of the foundation from the edge of the slope

The parameters δ, β, d, and e are defined in Figure 9.23. Figure 9.24 shows the design plot for Γ with S_e/B or $0.24\dfrac{\Delta R}{R_o}$.

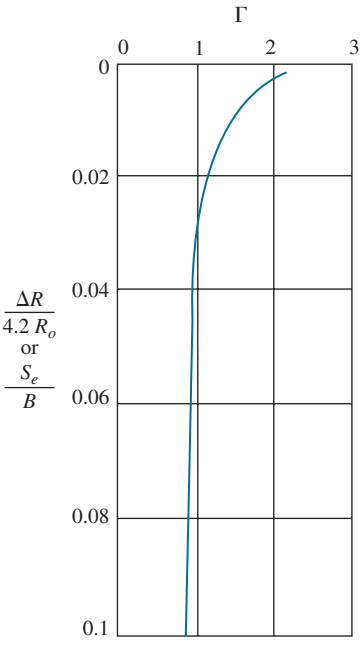


FIGURE 9.24 Variation of Γ with $S_e/B = 0.24\ \Delta R/R_o$

Step 6. Based on the values of B/L, e/B, δ, and d/B, calculate the values of $f_{L/B}$, f_e, f_δ, and $f_{\beta,d}$ as needed. Let

$$f = (f_{L/B})(f_e)(f_\delta)(f_{\beta,d}) \tag{9.78}$$

Thus,

$$q_o = f\Gamma p_{p(m)} \tag{9.79}$$

Step 7. Now prepare a table, as shown in Table 9.8.

Step 8. Complete Table 9.8 as follows:

a. Column 1—Assume several values of $\Delta R/R_o$.
b. Column 2—For given values of $\Delta R/R_o$, obtain $p_{p(m)}$ from Figure 9.22c.

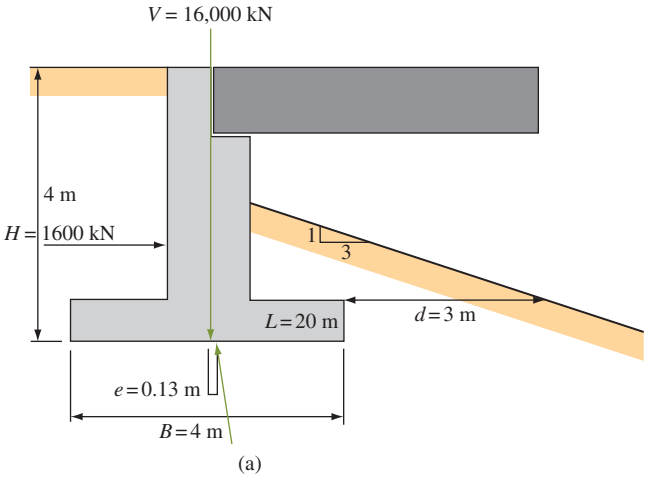
TABLE 9.8 Calculations to Obtain the Load-Settlement Plot

$\Delta R/R_o$ (1)	$p_{p(m)}$ (2)	S_e/B (3)	S_e (4)	Γ (5)	q_o (6)

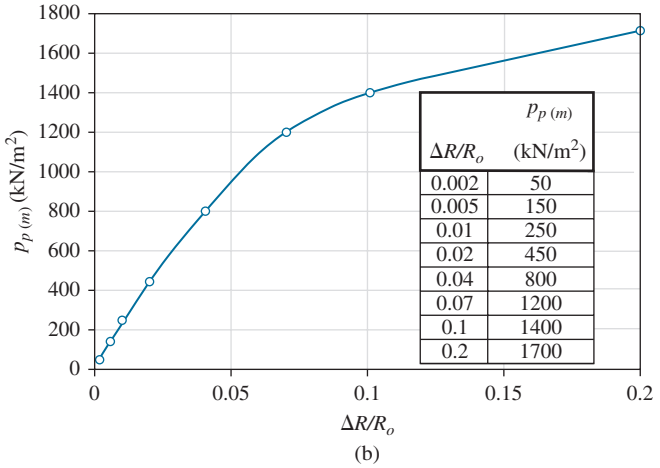
c. Column 3—From Eq. (9.69), calculate the values of S_e/B from values of $\Delta R/R_o$ given in Column 1.
d. Column 4—With known values of B, calculate the values of S_e.
e. Column 5—From Figure 9.24, obtain the desired values of Γ.
f. Column 6—Use Eq. (9.79) to obtain q_o.
g. Now plot a graph of S_e (Column 4) versus q_o (Column 6) from which the magnitude of S_e for a given q_o can be determined.

EXAMPLE 9.10

A foundation, shown in Figure 9.25a, with a width of 4 m and a length of 20 m serves as a bridge abutment foundation. The soil is medium dense sand. A 16,000 kN



(a)



(b)

FIGURE 9.25

vertical load acts on the foundation. The active pressure on the abutment wall develops a 1600 kN horizontal load. The resultant reaction force due to the vertical and horizontal load is applied at an eccentricity of 0.13 m. PMT testing at the site produced a mean pressuremeter curve characterizing the soil and is shown in Figure 9.25b. What is the settlement at the current loading?

SOLUTION

Given: $B = 4$ m, $L = 20$ m, $d = 3$ m, and slope = 3H:1V. So

$$f_{L/B} = 0.8 + 0.2\left(\frac{B}{L}\right) = 0.8 + 0.2\left(\frac{4}{20}\right) = 0.84$$

$$f_{e(\text{center})} = 1 - 0.33\left(\frac{e}{B}\right) = 1 - 0.33\left(\frac{0.13}{4}\right) = 0.99$$

$$f_{\delta(\text{center})} = 1 - \left(\frac{\delta}{90}\right)^2$$

$$\delta = \tan^{-1}\left(\frac{H}{V}\right) = \tan^{-1}\left(\frac{1600}{16{,}000}\right) = 5.71^\circ$$

$$f_\delta = 1 - \left(\frac{5.71}{90}\right)^2 = 0.996$$

$$f_{\beta,d} = 0.8\left(1 + \frac{d}{B}\right)^{0.1} = 0.8\left(1 + \frac{3}{4}\right)^{0.1} = 0.846$$

$$f = f_{L/B} f_e f_\delta f_{\beta,d} = (0.84)(0.99)(0.996)(0.845) = 0.7$$

Now the following table can be prepared.

$\Delta R/R_o$ (1)	$p_{p(m)}$ (kN/m^2) (2)	S_e/B (3)	S_e (mm) (4)	Γ (5)	q_o (kN/m^2) (6)	Q_o (MN) (7)
0.002	50	0.0005	2.0	2.27	79.45	6.36
0.005	150	0.0012	4.8	2.17	227.85	18.23
0.01	250	0.0024	9.6	2.07	362.25	28.98
0.02	450	0.0048	19.2	1.83	576.45	46.12
0.04	800	0.0096	38.4	1.40	784.00	62.72
0.07	1200	0.0168	67.2	1.17	982.8	78.62
0.10	1400	0.024	96.0	1.07	1048.6	83.89
0.20	1700	0.048	192.0	0.90	1071.0	85.68

Note: Columns 1 and 2: From Figure 9.25b
Column 3: (Column 1)(0.24) = S_e/B
Column 4: (Column 3)(B = 4000 mm) = S_e
Column 5: From Figure 9.24
Column 6: $f\Gamma p_{p(m)} = (0.7)(\Gamma)p_{p(m)} = q_o$
Column 7: (Column 6)($B \times L$) = Q_o

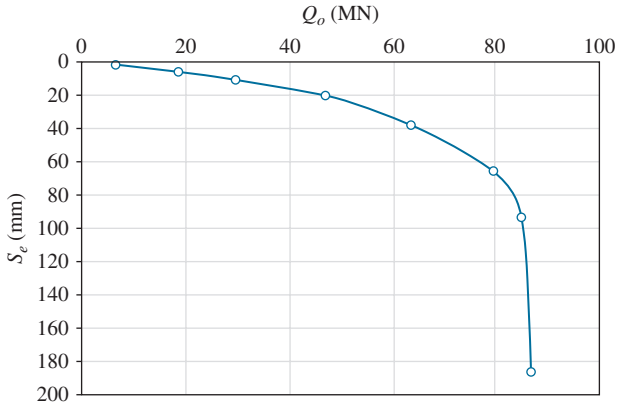


FIGURE 9.26

Figure 9.26 shows the plot of Q_o versus S_e. From this plot it can be seen that for a vertical loading of 16,000 kN (16 MN), the value of $S_e \approx$ **4.2 mm**.

9.9 Settlement Estimation Using the $L_1 - L_2$ Method

Akbas and Kulhawy (2009) evaluated 167 load–displacement relationships obtained from field tests. Based on those tests, the general nature of the load (Q) versus settlement (S_e) is shown in Figure 9.27. Tangents are drawn to the initial and final portions of the Q versus S_e plot. In the figure, note that the load Q_{L_1} occurs at a settlement level of $S_{e(L_1)} = 0.23B(\%)$ and the load Q_{L_2} occurs at $S_{e(L_2)} = 5.39B\ (\%)$. It is also important

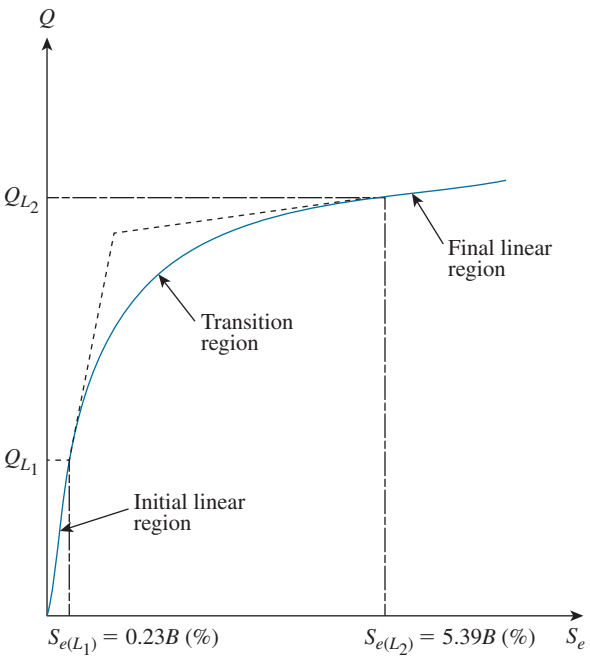


FIGURE 9.27 General nature of Q versus S_e plot

to note that Q_{L_2} is the *ultimate load* (Q_u) on the foundation. Also, the mean plot of Q versus S_e can be expressed as:

$$\frac{Q}{Q_{L_2}} = \frac{\left(\frac{S_e}{B}\right)}{0.69\left(\frac{S_e}{B}\right) + 1.68} \tag{9.80}$$

where S_e/B is in percent.

In order to find Q for a given settlement level, one needs to know Q_u. This can be done using Eq. (6.42) given in Section 6.9. Akbas and Kulhawy (2009) recommended that

- For $B > 1$ m [from Eq. (6.42) with $c' = 0$]

$$Q_{L_2} = Q_u = \left[\frac{1}{2}\gamma B N_\gamma F_{\gamma s} F_{\gamma d} F_{\gamma c} + q N_q F_{qs} F_{qd} F_{qc}\right] A \tag{9.81}$$

where

A = area of the foundation

- For $B \leq 1$ m,

$$Q_{L_2} = \left[\frac{1}{2}\gamma N_\gamma F_{\gamma s} F_{\gamma d} F_{\gamma c} + q N_q F_{qs} F_{qd} F_{qc}\right] A \tag{9.82}$$

EXAMPLE 9.11

For a square foundation supported by a sand layer, the following are given:

Foundation: $B = 1.5$ m; $D_f = 1$ m

Sand: $\gamma = 16.5$ kN/m^3; $\phi' = 35°$; $G_s = 280$ kN/m^2

Load on foundation: $Q = 800$ kN

Estimate:

a. $S_{e(L_1)}$
b. $S_{e(L_2)}$
c. Settlement S_e with application of load $Q = 800$ kN

SOLUTION

Part a

$$S_{e(L_1)} = 0.23B\ (\%) = \frac{(0.23)(1.5 \times 1000)}{100} = \mathbf{3.45\ mm}$$

Part b

$$S_{e(L_2)} = 5.39B\ (\%) = \frac{(5.39)(1.5 \times 1000)}{100} = \mathbf{80.85\ mm}$$

Part c

B is greater than 1 m. Hence, from Eq. (9.81),

$$Q_{L_2} = \left[\frac{1}{2}\gamma B N_\gamma F_{\gamma s} F_{\gamma d} F_{\gamma c} + q N_q F_{qs} F_{qd} F_{qc}\right] A$$

$\gamma = 16.5$ kN/m^3; $B = 1.5$ m; $q = \gamma D_f = (16.5)(1) = 16.5$ kN/m^2

From Table 6.2, for $\phi' = 35°$, $N_\gamma = 48.03$ and $N_q = 33.3$. From Table 6.3,

$$F_{qs} = 1 + \left(\frac{B}{L}\right)\tan\phi' = 1 + \left(\frac{1.5}{1.5}\right)\tan 35 = 1.7$$

$$F_{\gamma s} = 1 - 0.4\left(\frac{B}{L}\right) = 1 - (0.4)\left(\frac{1.5}{1.5}\right) = 0.6$$

$$F_{qd} = 1 + 2\tan\phi'(1 - \sin\phi')^2\left(\frac{D_f}{B}\right) = 1 + 2\tan 35(1 - \sin 35)^2\left(\frac{1}{1.5}\right) \approx 1.17$$

$$F_{\gamma d} = 1$$

In order to calculate F_{qc} and $F_{\gamma c}$, refer to Eq. (6.43) (with $c' = 0$):

$$I_r = \frac{G_s}{q\tan\phi'} = \frac{280}{(16.5)(\tan 35)} = 24.23$$

From Eq. (6.44),

$$I_{r(\text{cr})} = \frac{1}{2}\left\{\exp\left[\left(3.3 - 0.45\frac{B}{L}\right)\cot\left(45 - \frac{\phi'}{2}\right)\right]\right\}$$

$$= \frac{1}{2}\left\{\exp\left[\left(3.3 - 0.45\frac{1.5}{1.5}\right)\cot\left(45 - \frac{35}{2}\right)\right]\right\} = 119.3$$

So, $I_r < I_{r(\text{cr})}$. From Eq. (6.45),

$$F_{\gamma c} = F_{qc} = \exp\left\{\left[-4.4 + 0.6\left(\frac{B}{L}\right)\right]\tan\phi' + \frac{(3.07\sin\phi')(\log 2I_r)}{1 + \sin\phi'}\right\}$$

$$= \exp\left\{\left[-4.4 + 0.6\left(\frac{1.5}{1.5}\right)\right]\tan 35 + \frac{(3.07\sin 35)(\log 2 \times 24.23)}{1 + \sin 35}\right\}$$

$$= 0.461$$

Thus,

$$Q_{L_2} = \left[\begin{array}{c}\left(\frac{1}{2}\right)(16.5)(1.5)(48.03)(0.6)(1)(0.461) \\ + (16.5)(33.3)(1.7)(1.7)(0.461)\end{array}\right](1.5 \times 1.5) = 1467.4 \text{ kN}$$

Substituting the values of Q and Q_{L_2} in Eq. (9.80),

$$\frac{800}{1467.4} = \frac{\left(\frac{S_e}{B}\right)}{0.69\left(\frac{S_e}{B}\right) + 1.68};\ \frac{S_e}{B} = 1.467\%$$

$$S_e = (1.467)\left(\frac{1.5 \times 1000}{100}\right) \approx \mathbf{22.0\ mm}$$

9.10 Effect of the Rise of Water Table on Elastic Settlement

Terzaghi (1943) suggested that the submergence of soil mass reduces the soil stiffness by about half, which in turn doubles the settlement. In most cases of foundation design, it is considered that if the groundwater table is located $1.5B$ to $2B$ below the bottom of the foundation, it will not have any effect on the settlement. The total elastic settlement (S'_e) due to the rise of the groundwater table can be given as

$$S'_e = S_e C_w \tag{9.83}$$

where

S_e = elastic settlement before the rise of groundwater table

C_w = water correction factor

The following are some empirical relationships for C_w (refer to Figure 9.28).

- Peck, Hansen, and Thornburn (1974):

$$C_w = \frac{1}{0.5 + 0.5\left(\dfrac{D_w}{D_f + B}\right)} \geq 1 \tag{9.84}$$

- Teng (1982):

$$C_w = \frac{1}{0.5 + 0.5\left(\dfrac{D_w - D_f}{B}\right)} \leq 2 \qquad \left(\begin{matrix}\text{for water table below the} \\ \text{base of the foundation}\end{matrix}\right) \tag{9.85}$$

- Bowles (1977):

$$C_w = 2 - \left(\frac{D_w}{D_f + B}\right) \tag{9.86}$$

In any case, these relationships could be considered approximate, since there is a lack of agreement among geotechnical engineers about the true magnitude of C_w.

METHOD OF SHAHRIAR ET AL. (2014)

When the water table is present in the vicinity of the foundation, the unit weight of the soil has to be reduced for calculation of bearing capacity. Any future rise in the

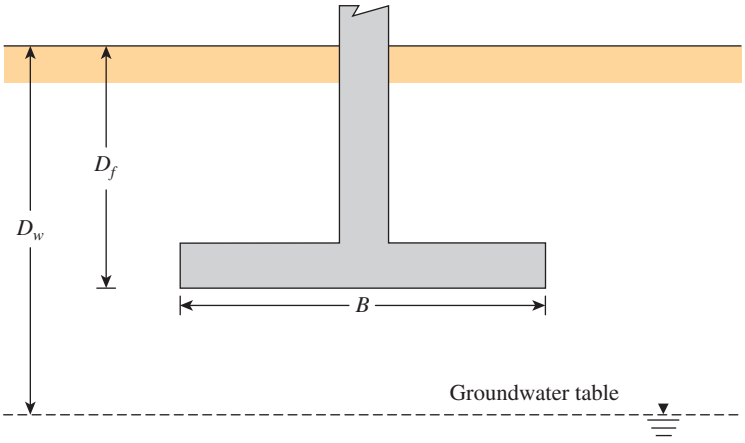


FIGURE 9.28 Effect of rise of groundwater table on elastic settlement in granular soil

water table can reduce the ultimate bearing capacity. A future water table rise in the vicinity of the foundation in granular soil can reduce the soil stiffness and, hence, produce additional settlement. Terzaghi (1943) concluded that when the water table rises from very deep to the foundation level, the settlement will be doubled in granular soil. Provided that the settlement is doubled when the entire sand layer beneath the foundation is submerged, laboratory model test results and numerical modeling work by Shahriar et al. (2014) show that the additional settlement produced by the rise of water table to any height can be expressed as

$$S_{e,\,\text{additional}} = \frac{A_w}{A_t} S_e \tag{9.87}$$

where S_e is the elastic settlement computed in dry soil, A_w is the area of the strain influence diagram submerged due to water table rise, and A_t is the total area of the strain influence diagram under the foundation. Example 9.13 shows the application of this method.

EXAMPLE 9.12

Consider the shallow foundation given in Example 9.7. Due to flooding, the groundwater table rose from $D_w = 4$ m to 2 m (Figure 9.28). Estimate the total elastic settlement S'_e after the rise of the water table. Use Eq. (9.84).

SOLUTION

From Eq. (9.83),

$$S'_e = S_e C_w$$

From Eq. (9.84),

$$C_w = \frac{1}{0.5 + 0.5\left(\dfrac{D_w}{D_f + B}\right)} = \frac{1}{0.5 + 0.5\left(\dfrac{2}{1 + 1.75}\right)} = 1.158$$

Hence,

$$S'_e = (11.8\text{ mm})(1.158) = \mathbf{13.66\text{ mm}}$$

EXAMPLE 9.13

A pad foundation 2.5 m × 2.5 m in plan, when placed at a depth of 1.5 m in sand, applies 175 kN/m^2 pressure to the underlying ground. Given: $\gamma = 18.0$ kN/m^3. Currently the water table is at 6.5 m below the foundation, and the expected settlement is 15.0 mm. In the future, as the worst-case scenario, it is expected that the water table could rise by 4.0 m, as shown in Figure 9.29a. What would be the total settlement of the foundation if this occurs? Use Eq. (9.37).

SOLUTION

The influence factor diagram needs to be drawn first. From Eq. (9.31) and Figure 9.11,

$$I_{z(m)} = 0.5 + 0.1\sqrt{\frac{\bar{q} - q}{q'_{z(1)}}} = 0.5 + 0.1\sqrt{\frac{175 - (18.0)(1.5)}{(18.0)\left[1.5 + \left(\dfrac{2.5}{2}\right)\right]}} = 0.67$$

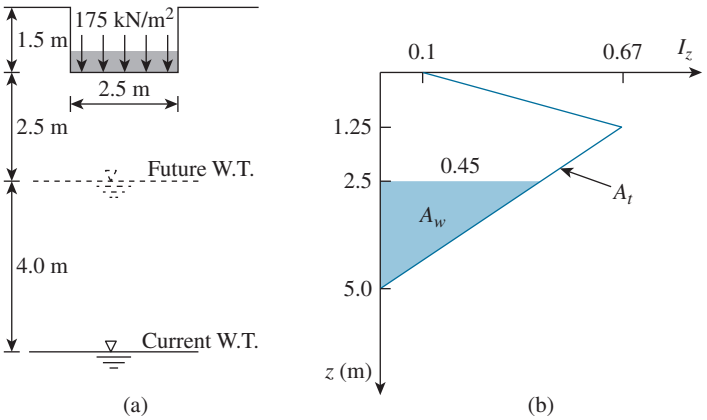


FIGURE 9.29

The I_z versus z diagram is shown in Figure 9.29b. Currently, the water table is below the influence zone. $S_e = 15.0$ mm. The total area of the influence diagram A_t is given by

$$A_t = \left(\frac{0.10 + 0.67}{2}\right) \times 1.25 + \frac{1}{2} \times 0.67 \times 3.75 = 1.738 \text{ m}$$

$$A_w = \frac{1}{2} \times 2.5 \times 0.45 = 0.563 \text{ m}$$

From Eq. (9.87),

$$S_{e,\text{ additional}} = \frac{A_w}{A_t} S_e = \frac{0.563}{1.738} \times 15.0 = 4.9 \text{ mm}$$

The total settlement would be $15.0 + 4.9 =$ **19.9 mm.**

Consolidation Settlement

9.11 Primary Consolidation Settlement Relationships

As mentioned before, consolidation settlement occurs over time in saturated clayey soil subjected to an increased load caused by construction of the foundation. (See Figure 9.30.) On the basis of the one-dimensional consolidation settlement equations given in Chapter 2, we write

$$S_{c(p)} = \int \varepsilon_z \, dz$$

where

ε_z = vertical strain

$$= \frac{\Delta e}{1 + e_o}$$

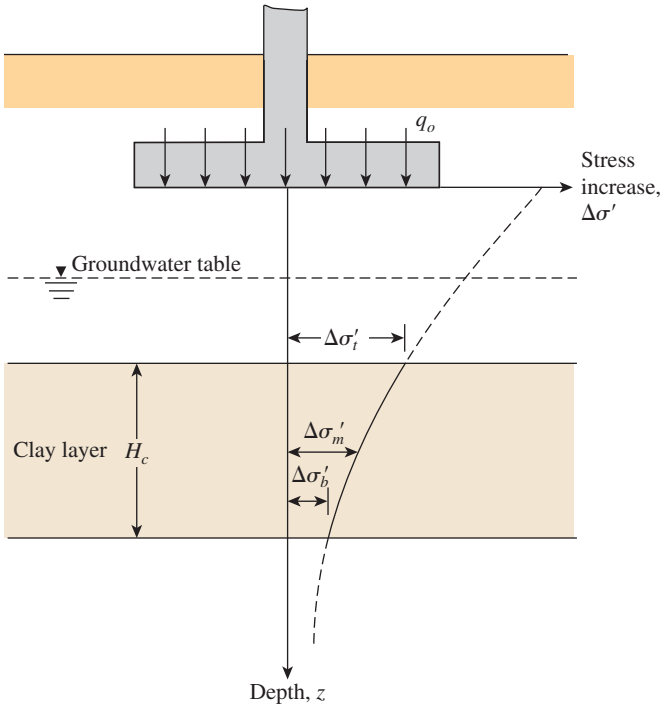


FIGURE 9.30 Consolidation settlement calculation

Δe = change of void ratio

$= f(\sigma_o', \sigma_c', \text{and } \Delta\sigma')$

So,

$$S_{c(p)} = \frac{C_c H_c}{1 + e_o} \log \frac{\sigma_o' + \Delta\sigma_{\text{av}}'}{\sigma_o'}$$ (for normally consolidated clays) [Eq. (2.65)]

$$S_{c(p)} = \frac{C_s H_c}{1 + e_o} \log \frac{\sigma_o' + \Delta\sigma_{\text{av}}'}{\sigma_o'}$$ for overconsolidated clays with $\sigma_o' + \Delta\sigma_{\text{av}}' < \sigma_c'$ [Eq. (2.67)]

$$S_{c(p)} = \frac{C_s H_c}{1 + e_o} \log \frac{\sigma_c'}{\sigma_o'} + \frac{C_c H_c}{1 + e_o} \log \frac{\sigma_o' + \Delta\sigma_{\text{av}}'}{\sigma_c'}$$ for overconsolidated clays with $\sigma_o' < \sigma_c' < \sigma_o' + \Delta\sigma_{\text{av}}'$ [Eq. (2.69)]

where

σ_o' = average effective pressure on the clay layer before the construction of the foundation

$\Delta\sigma_{\text{av}}'$ = average increase in effective pressure on the clay layer caused by the construction of the foundation

σ_c' = preconsolidation pressure

e_o = initial void ratio of the clay layer

C_c = compression index

C_s = swelling index

H_c = thickness of the clay layer

The procedures for determining the compression and swelling indexes were discussed in Chapter 2.

Note that the increase in effective pressure, $\Delta\sigma'$, on the clay layer is not constant with depth: The magnitude of $\Delta\sigma'$ will decrease with the increase in depth measured from the bottom of the foundation. However, the average increase in pressure may be approximated by

$$\Delta\sigma'_{av} = \frac{1}{6}(\Delta\sigma'_t + 4\Delta\sigma'_m + \Delta\sigma'_b) \tag{8.26}$$

where $\Delta\sigma'_t$, $\Delta\sigma'_m$, and $\Delta\sigma'_b$ are, respectively, the effective pressure increases at the *top, middle*, and *bottom* of the clay layer that are caused by the construction of the foundation.

The method of determining the pressure increase caused by various types of foundation load using Boussinesq's solution is discussed in Sections 8.2 through 8.10. $\Delta\sigma'_{av}$ can also be directly obtained from the method presented in Section 8.9.

9.12 Three-Dimensional Effect on Primary Consolidation Settlement

The consolidation settlement calculation presented in the preceding section is based on Eqs. (2.65), (2.67), and (2.69). These equations, as shown in Chapter 2, are in turn based on one-dimensional laboratory consolidation tests. The underlying assumption is that the increase in pore water pressure, Δu, immediately after application of the load equals the increase in stress, $\Delta\sigma$, at any depth. In this case,

$$S_{c(p)-\text{oed}} = \int \frac{\Delta e}{1 + e_o}\, dz = \int m_v \Delta\sigma'_{(1)}\, dz$$

where

$S_{c(p)-\text{oed}}$ = one-dimensional consolidation settlement calculated by using oedometer data and Eqs. (2.65), (2.67), and (2.69)

$\Delta\sigma'_{(1)}$ = effective vertical stress increase

m_v = volume coefficient of compressibility (see Chapter 2)

In the field, however, when a load is applied over a limited area on the ground surface, such an assumption will not be correct. Consider the case of a circular foundation on a clay layer, as shown in Figure 9.31. The vertical and the horizontal stresses' increase at a point in the layer immediately below the center of the foundation are $\Delta\sigma_{(1)}$ and $\Delta\sigma_{(3)}$, respectively. For a saturated clay, the pore water pressure increase at that depth (see Chapter 2) is

$$\Delta u = \Delta\sigma_{(3)} + A[\Delta\sigma_{(1)} - \Delta\sigma_{(3)}] \tag{9.88}$$

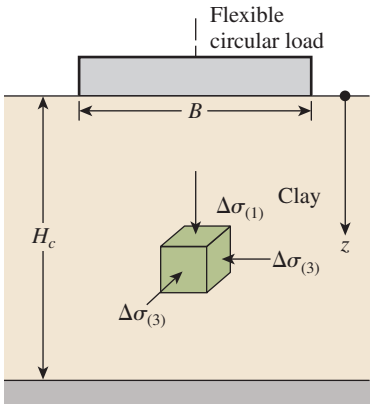


FIGURE 9.31 Circular foundation on a clay layer

where A = pore water pressure parameter. For this case, the consolidation settlement considering three-dimensional effects is given by

$$S_{c(p)} = \int m_v \, \Delta u \, dz = \int (m_v)\{\Delta\sigma_{(3)} + A[\Delta\sigma_{(1)} - \Delta\sigma_{(3)}]\} \, dz \tag{9.89}$$

Thus, we can write

$$K_{\text{cir}} = \frac{S_{c(p)}}{S_{c(p)-\text{oed}}} = \frac{\displaystyle\int_0^{H_c} m_v \, \Delta u \, dz}{\displaystyle\int_0^{H_c} m_v \, \Delta\sigma'_{(1)} \, dz} = A + (1 - A)\left[\frac{\displaystyle\int_0^{H_c} \Delta\sigma'_{(3)} \, dz}{\displaystyle\int_0^{H_c} \Delta\sigma'_{(1)} \, dz}\right] \tag{9.90}$$

where K_{cir} = settlement ratio for circular foundations.

The settlement ratio for a continuous foundation, K_{str}, can be determined in a manner similar to that for a circular foundation. The variation of K_{cir} and K_{str} with A and H_c/B is given in Figure 9.32. (*Note:* B is the diameter of a circular foundation, and B is the width of a continuous foundation.)

The preceding technique is generally referred to as the *Skempton–Bjerrum modification* (1957) for a consolidation settlement calculation.

Leonards (1976) examined the correction factor K_{cr} for a three-dimensional consolidation effect in the field for a circular foundation located over *overconsolidated clay*. Referring to Figure 9.31, we have

$$S_{c(p)} = K_{\text{cr(OC)}} \, S_{c(p)-\text{oed}} \tag{9.91}$$

where

$$K_{\text{cir(OC)}} = f\left(\text{OCR}, \frac{B}{H_c}\right) \tag{9.92}$$

in which

$$\text{OCR} = \text{overconsolidation ratio} = \frac{\sigma'_c}{\sigma'_o} \tag{9.93}$$

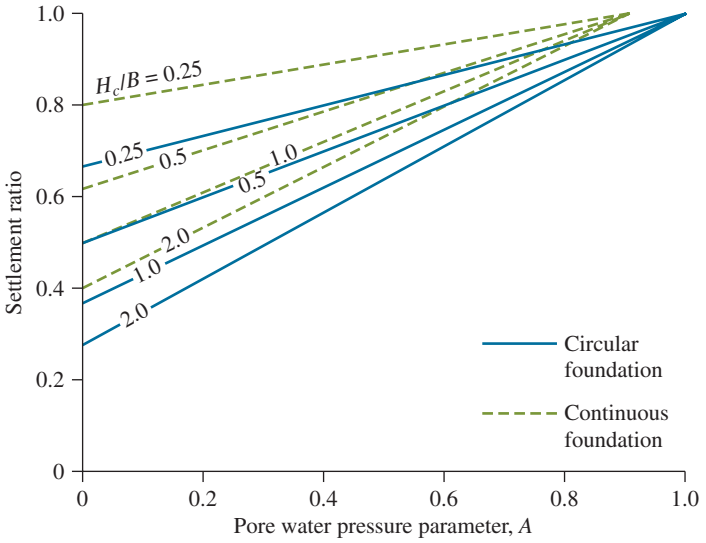


FIGURE 9.32 Settlement ratios for circular (K_{cir}) and continuous (K_{str}) foundations

TABLE 9.9 Variation of $K_{cir(OC)}$ with OCR and B/H_c

	$K_{cir(OC)}$		
OCR	$B/H_c = 4.0$	$B/H_c = 1.0$	$B/H_c = 0.2$
1	1	1	1
2	0.986	0.957	0.929
3	0.972	0.914	0.842
4	0.964	0.871	0.771
5	0.950	0.829	0.707
6	0.943	0.800	0.643
7	0.929	0.757	0.586
8	0.914	0.729	0.529
9	0.900	0.700	0.493
10	0.886	0.671	0.457
11	0.871	0.643	0.429
12	0.864	0.629	0.414
13	0.857	0.614	0.400
14	0.850	0.607	0.386
15	0.843	0.600	0.371
16	0.843	0.600	0.357

where

σ'_c = preconsolidation pressure

σ'_o = present average effective pressure

The interpolated values of $K_{cr(OC)}$ from Leonard's 1976 work are given in Table 9.9.

EXAMPLE 9.14

A plan of a foundation 1 m × 2 m is shown in Figure 9.33. Estimate the consolidation settlement of the foundation, taking into account the three-dimensional effect. Given: $A = 0.6$.

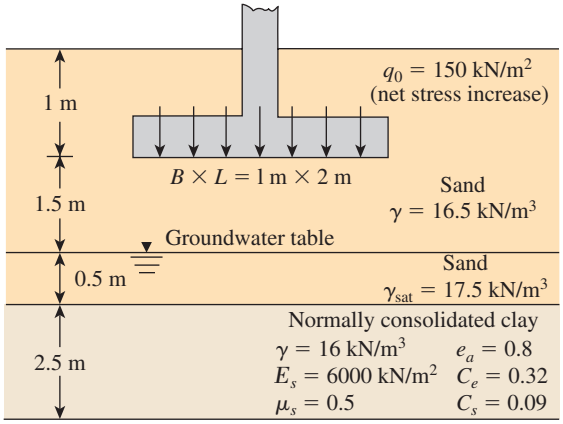


FIGURE 9.33 Calculation of primary consolidation settlement for a foundation

SOLUTION

The clay is normally consolidated. Thus,

$$S_{c(p)-\text{oed}} = \frac{C_c H_c}{1 + e_o} \log \frac{\sigma'_o + \Delta\sigma'_{\text{av}}}{\sigma'_o}$$

so

$$\begin{aligned}\sigma'_o &= (2.5)(16.5) + (0.5)(17.5 - 9.81) + (1.25)(16 - 9.81)\\ &= 41.25 + 3.85 + 7.74 = 52.84 \text{ kN/m}^2\end{aligned}$$

From Eq. (8.26),

$$\Delta\sigma'_{\text{av}} = \tfrac{1}{6}(\Delta\sigma'_t + 4\Delta\sigma'_m + \Delta\sigma'_b)$$

We divide the foundation into four quarters, compute the stress increase under a corner of each quarter using Eq. (8.10), and multiply by four. For each quarter, $B = 0.5$ m and $L = 1.0$ m.

Location	z (m)	$m = B/z$	$n = L/z$	I	$\Delta\sigma' = 4q_o I$
Top	2.0	0.25	0.50	0.0475	$28.5 = \Delta\sigma'_t$
Middle	3.25	0.154	0.308	≈ 0.0213	$12.75 = \Delta\sigma'_m$
Bottom	4.5	0.111	0.222	≈ 0.0113	$6.75 = \Delta\sigma'_b$

Now,

$$\Delta\sigma'_{\text{av}} = \tfrac{1}{6}(28.5 + 4 \times 12.75 + 6.75) = 14.38 \text{ kN/m}^2$$

so

$$S_{c(p)-\text{oed}} = \frac{(0.32)(2.5)}{1 + 0.8} \log\left(\frac{52.84 + 14.38}{52.84}\right) = 0.0465 \text{ m}$$

$$= \mathbf{46.5 \text{ mm}}$$

Now assuming that the 2:1 method of stress increase (see Figure 8.9) holds, the area of distribution of stress at the top of the clay layer will have dimensions

$$B' = \text{width} = B + z = 1 + (1.5 + 0.5) = 3 \text{ m}$$

and

$$L' = \text{width} = L + z = 2 + (1.5 + 0.5) = 4 \text{ m}$$

The diameter of an equivalent circular area, B_{eq}, can be given as

$$\frac{\pi}{4} B_{\text{eq}}^2 = B'L'$$

so that

$$B_{\text{eq}} = \sqrt{\frac{4B'L'}{\pi}} = \sqrt{\frac{(4)(3)(4)}{\pi}} = 3.91 \text{ m}$$

Also,

$$\frac{H_c}{B_{\text{eq}}} = \frac{2.5}{3.91} = 0.64$$

From Figure 9.32, for $A = 0.6$ and $H_c/B_{\text{eq}} = 0.64$, the magnitude of $K_{\text{cr}} \approx 0.78$. Hence,

$$S_{e(p)} = K_{\text{cir}} S_{e(p)-\text{oed}} = (0.78)(46.5) \approx \mathbf{36.3 \text{ mm}}$$

■

9.13 Settlement Due to Secondary Consolidation

At the end of primary consolidation (i.e., after the complete dissipation of excess pore water pressure), some settlement is observed that is due to the plastic adjustment of soil fabrics. This stage of consolidation is called *secondary consolidation*. A plot of deformation against the logarithm of time during secondary consolidation is practically linear, as shown in Figure 9.34. From the figure, the secondary compression index can be defined as

$$C_\alpha = \frac{\Delta e}{\log t_2 - \log t_1} = \frac{\Delta e}{\log(t_2/t_1)} \tag{9.94}$$

where

C_α = secondary compression index

Δe = change of void ratio

t_1, t_2 = time

The magnitude of the secondary consolidation can be calculated as

$$S_{c(s)} = C'_\alpha H_c \log(t_2/t_1) \tag{9.95}$$

where

$$C'_\alpha = C_\alpha/(1 + e_p) \tag{9.96}$$

e_p = void ratio at the end of primary consolidation

H_c = thickness of clay layer

Mesri (1973) correlated C'_α with the natural moisture content (w) of several soil, from which it appears that

$$C'_\alpha \approx 0.0001w \tag{9.97}$$

where w = natural moisture content, in percent. For most overconsolidated soil, C'_α varies between 0.0005 to 0.001.

Mesri and Godlewski (1977) compiled the magnitude of C_α/C_c (C_c = compression index) for a number of soil. Based on their compilation, it can be summarized that

- For inorganic clays and silts:

$$C_\alpha/C_c \approx 0.04 \pm 0.01$$

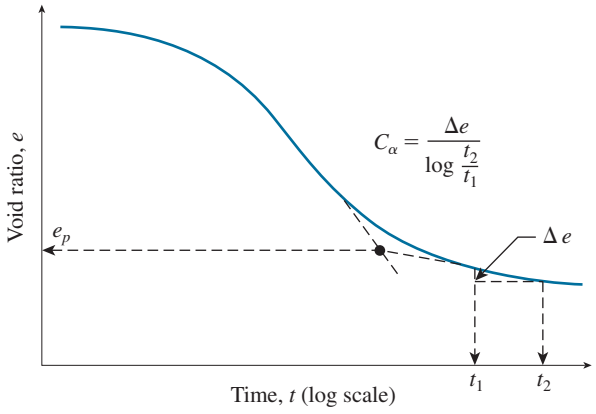


FIGURE 9.34 Variation of e with log t under a given load increment, and definition of secondary compression index

- For organic clays and silts:

$$C_\alpha/C_c \approx 0.05 \pm 0.01$$

- For peats:

$$C_\alpha/C_c \approx 0.075 \pm 0.01$$

Secondary consolidation settlement is more important in the case of all organic and highly compressible inorganic soil. In overconsolidated inorganic clays, the secondary compression index is very small and of less practical significance.

There are several factors that might affect the magnitude of secondary consolidation, some of which are not yet very clearly understood (Mesri, 1973). The ratio of secondary to primary compression for a given thickness of soil layer is dependent on the ratio of the stress increment, $\Delta\sigma'$, to the initial effective overburden stress, σ'_o. For small $\Delta\sigma'/\sigma'_o$ ratios, the secondary-to-primary compression ratio is larger.

EXAMPLE 9.15

Refer to Example 9.14. Given for the clay layer: $C_\alpha = 0.02$. Estimate the total consolidation settlement five years after the completion of the primary consolidation settlement. (*Note:* Time for completion of primary consolidation settlement is 1.3 years.)

SOLUTION

From Eq. (2.53),

$$C_c = \frac{e_1 - e_2}{\log\left(\frac{\sigma'_2}{\sigma'_1}\right)}$$

For this problem, $e_1 - e_2 = \Delta e$. Referring to Example 9.14, we have

$$\sigma'_2 = \sigma'_o + \Delta\sigma' = 52.84 + 14.38 = 67.22 \text{ kN/m}^2$$
$$\sigma'_1 = \sigma'_o = 52.84 \text{ kN/m}^2$$
$$C_c = 0.32$$

Hence,

$$\Delta e = C_c \log\left(\frac{\sigma'_o + \Delta\sigma}{\sigma'_o}\right) = 0.32 \log\left(\frac{67.22}{52.84}\right) = 0.0335$$

Given: $e_o = 0.8$. Hence,

$$e_p = e_o - e = 0.8 - 0.0335 = 0.7665$$

From Eq. (9.96),

$$C'_\alpha = \frac{C_\alpha}{1 + e_p} = \frac{0.02}{1 + 0.7665} = 0.0113$$

From Eq. (9.95),

$$S_{c(s)} = C'_\alpha H_c \log\left(\frac{t_2}{t_1}\right)$$

Note: $t_1 = 1.3$ years; $t_2 = 1.3 + 5 = 6.3$ years.

Thus,

$$S_{c(s)} = (0.0113)(2.5 \text{ m}) \log\left(\frac{6.3}{1.3}\right) = 0.0194 \text{ m} = 19.4 \text{ mm}$$

Total consolidation settlement is

$$\underbrace{36.3 \text{ mm}}_{\substack{\uparrow \\ \text{Example 9.14} \\ \text{(primary} \\ \text{consolidation} \\ \text{settlement)}}} + 19.4 = \mathbf{55.7\ m}$$

9.14 Field Load Test

The ultimate load-bearing capacity of a foundation, as well as the allowable bearing capacity based on tolerable settlement considerations, can be effectively determined from the field load test, generally referred to as the *plate load test*. The plates that are used for tests in the field are usually made of steel and are 25 mm (1 in.) thick and 150 mm to 762 mm (6 in. to 30 in.) in diameter. Occasionally, square plates that are 305 mm × 305 mm (12 in. × 12 in.) are also used.

To conduct a plate load test, a hole is excavated with a minimum diameter of $4B$ (B is the diameter of the test plate) to a depth of D_f, the depth of the proposed foundation. The plate is placed at the center of the hole, and a load that is about one-fourth to one-fifth of the estimated ultimate load is applied to the plate in steps by means of a jack. A schematic diagram of the test arrangement is shown in Figure 9.35a. During each step of the application of the load, the settlement of the plate is observed on dial gauges. At least one hour is allowed to elapse between each application. The test should be conducted until failure, or at least until the plate has gone through 25 mm (1 in.) of settlement. Figure 9.35b shows the nature of the load-settlement curve obtained from such tests, from which the ultimate load per unit area can be determined. Figure 9.36 shows a plate load test conducted in the field.

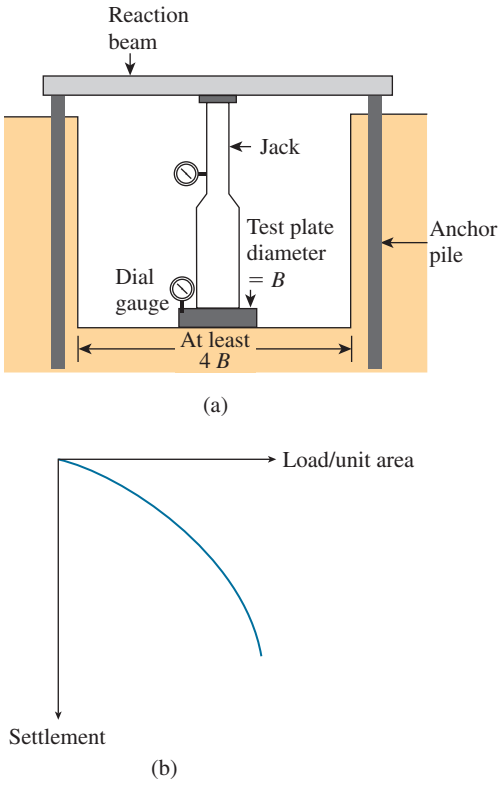


FIGURE 9.35 Plate load test: (a) test arrangement; (b) nature of load-settlement curve



FIGURE 9.36 Plate load test in the field (Courtesy of Braja M. Das, Henderson, Nevada)

For tests in clay,

$$q_{u(F)} = q_{u(P)} \tag{9.98}$$

where

$q_{u(F)}$ = ultimate bearing capacity of the proposed foundation

$q_{u(P)}$ = ultimate bearing capacity of the test plate

Equation (9.98) implies that the ultimate bearing capacity in clay is virtually independent of the size of the plate.

For tests in sandy soil,

$$q_{u(F)} = q_{u(P)}\frac{B_F}{B_P} \tag{9.99}$$

where

B_F = width of the foundation

B_P = width of the test plate

The allowable bearing capacity of a foundation, based on settlement considerations and for a given intensity of load, q_o, is

$$S_F = S_P\frac{B_F}{B_P} \quad \text{(for clayey soil)} \tag{9.100}$$

and

$$S_F = S_P\left(\frac{2B_F}{B_F + B_P}\right)^2 \quad \text{(for sandy soil)} \tag{9.101}$$

9.15 Presumptive Bearing Capacity

Several building codes (e.g., the Uniform Building Code, Chicago Building Code, and New York City Building Code) specify the allowable bearing capacity of foundations on various types of soil. For minor construction, they often provide

fairly acceptable guidelines. However, these bearing capacity values are based primarily on the *visual classification* of near-surface soil and generally do not take into consideration factors such as the stress history of the soil, the location of the water table, the depth of the foundation, and the tolerable settlement. So for large construction projects, the codes' presumptive values should be used only as guides.

9.16 Tolerable Settlement of Buildings

The subsoil is often not homogeneous. In addition, the load transferred to the foundation can vary widely. As a result, the settlement can vary between any two adjacent columns. These *differential settlements* can induce additional moments and hence bending stresses in the structural system that can cause damage to the structure. Early stages of the damage are architectural, such as cracking of the plaster or partitions, and those affecting alignments, serviceability, and aesthetics. More serious damage includes structural cracks that can expose the reinforcements and lead to corrosion, which can jeopardize the safety of the building.

The differential settlement and the *angular distortion* can cause structural distress when they are excessive. The angular distortion is defined as the ratio of the differential settlement between two adjacent foundations to the span length. The serviceability limit state can be threatened when the angular distortion reaches a specific value in the range of 1/300 to 1/500. When it gets as high as 1/150 to 1/250, the ultimate limit state can also be threatened (O'Brien 2012). These limiting values depend on the type of structure and the material of construction. Tilt is different from angular distortion. It does not cause structural distress. The Leaning Tower of Pisa in Italy is an example of tilt that is on the order of 1/10. There are structures that have undergone large total settlement but with insignificant differential settlement, making them still functional. Even when there is no structural damage, the total settlement can cause problems with utility lines, drainage, and alignment.

It is difficult to predict the differential settlement due to the complicated soil–structure interaction and redistribution of the loading during the differential settlement. Therefore, a limit is generally placed on the total settlement in an attempt to control the differential settlement. A rule of thumb is that the differential settlement is less than 75% of the total settlement.

Limiting values for the settlement have been discussed in the literature since the 1950s by Polshin and Tokar (1957) and Skempton and MacDonald (1956). The settlement in clay is slower than in sand, occurring over many years; hence, the structural system can gradually adjust to the settlement and sustain less damage. Therefore, larger settlement is generally allowed in clay than in sand. Similarly, raft foundations are subject to relatively lower differential settlement due to their rigidity and, hence, can tolerate larger total settlement than pad foundations. The limiting values for total settlement in routine design of shallow foundations (O'Brien, 2012; Skempton and MacDonald, 1956) are as follows:

Pad foundations in clay	65 mm (2.6 in.)
Pad foundations in sand	40 mm (1.6 in.)
Raft foundations in clay	100 mm (4 in.)
Raft foundations in sand	65 mm (2.6 in.)

These limiting values are larger than those provided by Terzaghi and Peck (1948), who suggested an allowable settlement limiting value of 25 mm (1 in.) for isolated foundations and 50 mm (2 in.) for rafts.

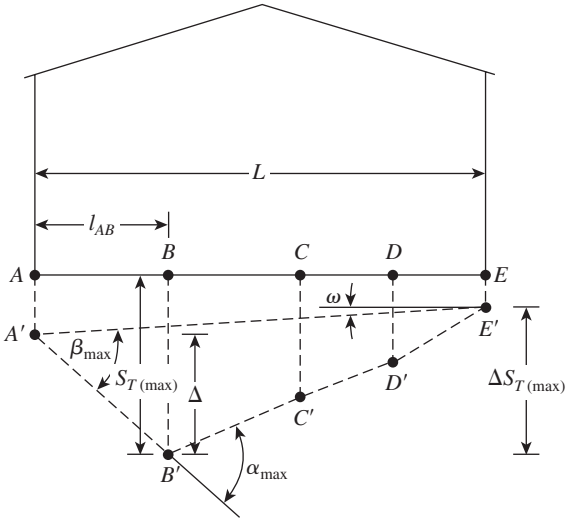


FIGURE 9.37 Definition of parameters for differential settlement

Burland and Wroth (1974) defined some parameters relevant to foundation settlement that are explained through Figure 9.37. The points *A, B, C, D*, and *E* represent points on a raft foundation or isolated pad foundation that have settled to *A′, B′, C′, D′*, and *E′*, respectively. The definitions of these parameters are as follows:

- *Settlement* (S_T)—Often known as *total settlement*, it is the downward movement of a point.
- *Differential settlement* (ΔS_T)—Difference in total settlement between two points. Generally, two adjacent points are considered.
- *Angular distortion* (β)—Ratio of the differential settlement to the distance between the two points.
- *Tilt* (ω)—Rigid body rotation of the entire structure.
- *Relative deflection* (Δ)—The vertical displacement from the tilt plane.
- *Deflection ratio* (Δ/L)—Can be sagging or hogging. It provides a better measure than angular distortion in quantifying structural distress. Unlike angular distortion, the deflection ratio is not affected by tilt.

Bjerrum (1963) recommended the limiting angular distortion, β_{max} for various structures, as shown in Table 9.10. If the maximum allowable values of β_{max} are known, the magnitude of the allowable $S_{T(max)}$ can be calculated with the use of the foregoing correlations. The European Committee for Standardization has also provided limiting values for serviceability and the maximum accepted foundation movements. (See Table 9.11.)

TABLE 9.10

Category of potential damage	β_{max}
Safe limit for flexible brick wall ($L/H > 4$)	1/150
Danger of structural damage to most buildings	1/150
Cracking of panel and brick walls	1/150
Visible tilting of high rigid buildings	1/250
First cracking of panel walls	1/300
Safe limit for no cracking of building	1/500
Danger to frames with diagonals	1/600

TABLE 9.11 Recommendations of European Committee for Standardization on Differential Settlement Parameters

Item	Parameter	Magnitude	Comments
Limiting values for serviceability	S_T	25 mm 50 mm	Isolated shallow foundation Raft foundation
(European Committee for Standardization, 1994a)	ΔS_T	5 mm 10 mm 20 mm	Frames with rigid cladding Frames with flexible cladding Open frames
	β	1/500	—
Maximum acceptable foundation movement	S_T ΔS_T	50 20	Isolated shallow foundation Isolated shallow foundation
(European Committee for Standardization, 1994b)	β	≈1/500	—

9.17 Summary

Settlement plays an important role in the designs of shallow foundations. For the structure to perform satisfactorily, the settlement of pad and strip foundations has to be limited to specific values on the order of 25–65 mm (1–2.5 in.). Therefore, a realistic estimate of the settlement has to be made in every foundation design. Considering the rigidity of the foundation and the difficulties in estimating the soil stiffness in the case of granular soil, as well as other variables associated with the soil in general, predicting future settlement accurately is a difficult task.

When soil mass is considered as an elastic continuum, it is important to note the following:

- Rigid foundations settle uniformly, but the pressure applied to the ground is nonuniform. Flexible foundations apply uniform pressure to the ground, and the settlement is nonuniform.
- The immediate (or elastic) settlement of a rigid foundation can be estimated as 93% of the settlement beneath the center of a flexible foundation.

Some methods for estimating the settlement beneath flexible and rigid foundations were discussed. This was followed by the different settlement prediction methods specifically developed for foundations on granular soil.

Settlement in clay soil includes three separate components: (a) immediate (or elastic), (b) primary consolidation, and (c) secondary consolidation. The methods for estimating these components were discussed in this chapter.

PROBLEMS

9.1 Refer to Figure 9.1, where a 2.0 m × 3.0 m flexible foundation is placed in a saturated clay at 1.5 m depth. Bedrock lies at 4.0 m below the foundation. The clay is overconsolidated with OCR = 2, undrained shear strength = 60 kN/m^2, and plasticity index = 45. If the pressure applied by the foundation to the underlying soil is 80.0 kN/m^2, determine the average elastic settlement.

9.2 For an elastic material, the bulk modulus (K) and Young's modulus (E) are related by

$$K = \frac{1}{3(1 - 2\mu_s)}E$$

For undrained loading, deduce that $\mu_s = 0.5$.

9.3 A 6.0 ft × 12.0 ft flexible foundation is placed on a granular soil with $D_f = 0$. The foundation applies a pressure q_o = 2.4 kip/ft^2. Assuming the soil mass to be infinitely thick, with E_s = 300 kip/ft^2 and $\mu_s = 0.1$, determine the expected settlement beneath the center of the foundation.

9.4 Redo Problem 9.3 for the situation where the same soil is underlain by bedrock at 9.0 ft below the surface.

9.5 Redo Problem 9.4 with D_f = 3.0 ft.

9.6 A 2.0 m × 4.0 m flexible loaded area shown in Figure P9.6 applies a uniform pressure of 150 kN/m^2 to the underlying silty sand. Estimate the elastic settlement below the center of the foundation.

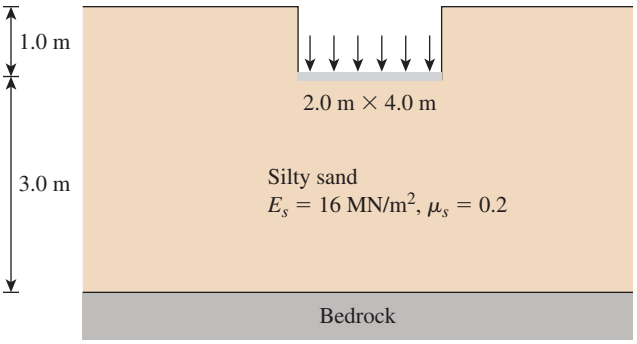


FIGURE P9.6

9.7 Refer to Figure 9.7. Estimate the elastic settlement of the foundation in sand for the following data using the method of Mayne and Poulos [Eq. (9.27)].

Foundation:	length L = 3 m, width B = 2 m, depth D_f = 1 m, thickness t = 0.25 m, $E_f = 25 \times 10^3$ MN/m²
Loading:	net applied pressure q_o = 125 kN/m²
Sand:	H = 3 m, μ_s = 0.2, E_o = 12 MN/m², k = 400 kN/m²/m

9.8 A plan calls for a square foundation measuring 3 m × 3 m supported by a layer of sand (see Figure 9.7). Let D_f = 1.5 m, t = 0.25 m, E_o = 16,000 kN/m², k = 400 kN/m²/m, μ_s = 0.3, H = 20 m, $E_f = 15 \times 10^6$ kN/m², and q_o = 150 kN/m². Calculate the elastic settlement. Use Eq. (9.27).

9.9 A 2 m wide square foundation is placed at a depth of 1.5 m, in a very thick homogeneous sand deposit where q_c = 10 MN/m² and γ = 18.5 kN/m³. The stress level at the foundation is 140 kN/m². Estimate the settlement in 25 years, using the method of Schmertmann et al. [Eq. (9.30)]. How much of this settlement is due to creep?

9.10 A continuous foundation on a deposit of sand layer is shown in Figure P9.10 along with the variation of the cone penetration resistance q_c. Assuming γ = 18 kN/m³ and creep is at the end of ten years after construction, calculate the elastic settlement of the foundation using the strain influence factor method. Use Eqs. (9.30) and (9.36).

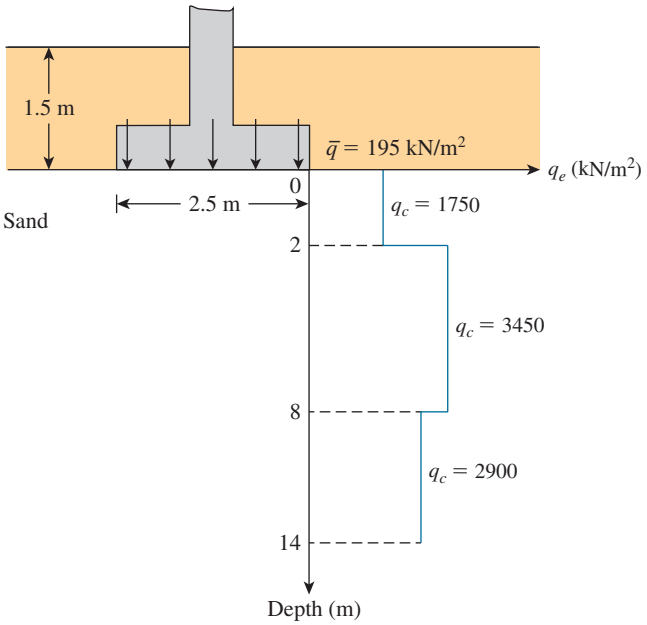


FIGURE P9.10

9.11 Solve Problem 9.10 using Eqs. (9.39), (9.40), and (9.41).

9.12 Find the settlement of a 2.0 m wide square foundation (D_f = 1.0 m) applying a net pressure of 150 kN/m² to the underlying sand, where N_{60} = 20 and γ = 18.5 kN/m³. Use Eq. (9.43). In the last term of the equation, replace 1/4 by 1/3 (Leonards, 1986).

9.13 It is proposed to place a 9 ft × 9 ft foundation at 6 ft depth in a sandy soil, where the average N_{60} is 25 and the unit weight is 115.0 lb/ft³. Using Meyerhof's expressions presented in Section 9.6, estimate the allowable net pressure that would give 1.2 in. of settlement.

9.14 A shallow foundation measuring 1 m × 2 m in plan is to be constructed over a normally consolidated sand layer. Given: D_f = 1 m, N_{60} increases with depth, $\overline{N}_{60}$ (in the depth of stress influence) = 12, and q_{net} = 153 kN/m². Estimate the elastic settlement using Burland and Burbidge's method (Section 9.6).

9.15 A 2 m wide continuous foundation carrying a 260 kN/m wall load is placed at a depth of 1.0 m in sand where the unit weight is 19.0 kN/m³ and $(N_1)_{60}$ is 32. Assuming Poisson's ratio of 0.15, estimate the settlement of the foundation. Use the procedure outlined in Section 9.7.

9.16 A 2.0 m × 2.0 m foundation carrying a 1000 kN column load is placed at 1.0 m below the ground level in a sand where γ = 19 kN/m³ and $(N_1)_{60}$ = 25. Estimate the settlement using the Berardi and Lancellotta method (1991) (Section 9.7). Assume μ_s = 0.15.

9.17 Refer to Figure 9.23. For a foundation on a layer of sand, given: B = 5 ft, L = 10 ft, d = 5 ft, β = 26.6°, e = 0.5 ft, and δ = 10°. The pressuremeter testing at the site produced a mean pressuremeter curve for which the $p_{p(m)}$ versus $\Delta R/R_o$ points are as follows.

$\Delta R/R_o$ (1)	$p_{p(m)}$ (lb/in²) (2)
0.002	7.2
0.004	24.2
0.008	32.6
0.012	42.4
0.024	68.9
0.05	126.1
0.08	177.65
0.1	210.5
0.2	369.6

What should be the magnitude of Q_o for a settlement (center) of 1 in.?

9.18 A 3.0 m wide square foundation is placed at 1.5 m depth in sand where γ = 18.5 kN/m³. The water table lies well below the foundation level. Under the applied pressure of

200 kN/m^2 at the foundation level, the settlement recorded was 14.0 mm. It is expected that the water table will rise in the future to unknown levels. Plot the expected additional settlement against the water table rise. Discuss the rate of rise in the additional settlement with the water table rise. Use the method of Shahriar et al. (2014) (Section 9.10).

REFERENCES

Akbas, S. O. and Kulhawy, F. H. (2009). "Axial Compression of Footings in Cohesionless Soils. I: Load-Settlement Behavior," *Journal of Geotechnical and Geoenvironmental Engineering*, American Society of Civil Engineers, Vol. 135, No. 11, pp. 1562–1574.

Berardi, R. (1999). "Nonlinear Elastic Approaches in Foundation Design," *Proceedings, II International Symposium on Pre-Failure Deformation Characteristics of Geomaterials, IS Torino 99*, Eds., M. Jamiolkowski, R. Lancellotta, and D. Lo Presti, A.A. Balkema., pp. 733–740.

Berardi, R. and Lancellotta, R. (1991). "Stiffness of Granular Soil from Field Performance," *Geotechnique*, Vol. 1, pp. 149–157.

Berardi, R., Jamiolkowski, M., and Lancellotta, R. (1991). "Settlement of Shallow Foundations in Sands: Selection of Stiffness on the Basis of Penetration Resistance," Proceedings, Geotechnical Engineering Congress, Boulder, Colorado, *ASCE Geotechnical Special Publication No. 27*, 1, pp. 185–200.

Bjerrum, L. (1963). "Allowable Settlement of Structures," *Proceedings, European Conference on Soil Mechanics and Foundation Engineering*, Wiesbaden, Germany, Vol. III, pp. 135–139.

Bowles, J. E. (1987). "Elastic Foundation Settlement on Sand Deposits," *Journal of Geotechnical Engineering*, ASCE, Vol. 113, No. 8, pp. 846–860.

Bowles, J. E. (1977). *Foundation Analysis and Design*, 2nd ed., McGraw-Hill, New York.

Briaud, J. L. (2007). "Spread Footings in Sand: Load Settlement Curve Approach," *Journal of Geotechnical and Geoenvironmental Engineering*, American Society of Civil Engineers, Vol. 133, No. 8, pp. 905–920.

Burland, J. B. and Burbidge, M. C. (1985). "Settlement of Foundations on Sand and Gravel," *Proceedings, Institute of Civil Engineers*, Part I, Vol. 7, pp. 1325–1381.

Burland, J. B. and Wroth, C. P. (1974). "Allowable and Differential Settlement of Structures Including Damage and Soil-Structure Interaction," *Proceedings, Conference on Settlement of Structures*, Cambridge University, England, pp. 611–654.

Christian, J. T. and Carrier, W. D. (1978). "Janbu, Bjerrum, and Kjaernsli's Chart Reinterpreted," *Canadian Geotechnical Journal*, Vol. 15, pp. 124–128.

Duncan, J. M. and Buchignani, A. N. (1976). *An Engineering Manual for Settlement Studies*, Department of Civil Engineering, University of California, Berkeley.

European Committee for Standardization (1994a). *Basis of Design and Actions on Structures*, Eurocode 1, Brussels, Belgium.

European Committee for Standardization (1994b). *Geotechnical Design, General Rules—Part 1*, Eurocode 7, Brussels, Belgium.

Fox, E. N. (1948). "The Mean Elastic Settlement of a Uniformly Loaded Area at a Depth below the Ground Surface," *Proceedings, 2nd International Conference on Soil Mechanics and Foundation Engineering*, Rotterdam, Vol. 1, pp. 129–132.

Giroud, J. P. (1968). "Settlement of Linearly Loaded Rectangular Area", *Journal of Soil Mechanics and Foundations Division*, American Society of Civil Engineers, Vol. 94, No. SM4, pp. 813–831.

Holtz, R. D. (1991). "Stress Distribution and Settlement of Shallow Foundations," Chapter 5, *Foundation Engineering Handbook*, Ed., H-Y. Fang, 2nd ed., Van Nostrand Reinhold, New York, pp. 166–222.

Janbu, N. (1963). "Soil Compressibility as Determined by Oedometer and Triaxial Tests," *Proceedings*, *III European Conference on Soil Mechanics and Foundation Engineering*, Wiesbaden, Germany, Vol. 1, pp. 19–25.

Janbu, N., Bjerrum, L., and Kjaernsli, B. (1956). "Veiledning vedlosning av fundamentering—soppgaver," *Publication No. 18*, Norwegian Geotechnical Institute, pp. 30–32.

Lancellotta, R. (2009). *Geotechnical Engineering*, 2nd ed., Taylor & Francis, London.

Leonards, G. A. (1976). *Estimating Consolidation Settlement of Shallow Foundations on Overconsolidated Clay*, Special Report No. 163, Transportation Research Board, Washington, DC, pp. 13–16.

Leonards, G. A. (1986). *Advanced Foundation Engineering—CE 683*, Lecture Notes, Purdue University.

Mayne, P. W. and Poulos, H. G. (1999). "Approximate Displacement Influence Factors for Elastic Shallow Foundations," *Journal of Geotechnical and Geoenvironmental Engineering*, ASCE, Vol. 125, No. 6, pp. 453–460.

Mesri, G. (1973). "Coefficient of Secondary Compression," *Journal of the Soil Mechanics and Foundations Division*, American Society of Civil Engineers, Vol. 99, No. SM1, pp. 122–137.

Mesri, G. and Godlewski, P. M. (1977). "Time and Stress—Compressibility Interrelationship," *Journal of Geotechnical Engineering Division*, American Society of Civil Engineers, Vol. 103, No. GT5, pp. 417–430.

Meyerhof, G. G. (1956). "Penetration Tests and Bearing Capacity of Cohesionless Soils," *Journal of the Soil Mechanics and Foundations Division*, American Society of Civil Engineers, Vol. 82, No. SM1, pp. 1–19.

Meyerhof, G. G. (1965). "Shallow Foundations," *Journal of the Soil Mechanics and Foundations Division*, American Society of Civil Engineers, Vol. 91, No. SM2, pp. 21–31.

O'Brien, A. S. (2012). "Foundation Types and Conceptual Design Principles," Chapter 52, *ICE Manual of Geotechnical Engineering*, Eds., J. B. Burland, T. Chapman, H. Skinner, and M. Brown, ICE Publishing, Vol. II, pp. 733–764.

Peck, R. B., Hanson, W. E., and Thornburn, T. H. (1974). *Foundation Engineering*, 2nd ed., John Wiley & Sons, New York.

Polshin, D. E. and Tokar, R. A. (1957). "Maximum Allowable Nonuniform Settlement of Structures," *Proceedings, Fourth International Conference on Soil Mechanics and Foundation Engineering*, London, Vol. 1, pp. 402–405.

Poulos, H. G. and Davis, E. H. (1974). *Elastic Solutions for Soil and Rock Mechanics*, John Wiley & Sons, New York.

Salgado, R. (2008). *The Engineering of Foundations*, McGraw-Hill, New York.

Schleicher, F. (1926). "Zur Theorie des Baurundes." *Bauingenieur*, Vol. 7, No. 48, pp. 931–935.

Schmertmann, J. H., Hartman, J. P., and Brown, P. R. (1978). "Improved Strain Influence Factor Diagrams," *Journal of the Geotechnical Engineering Division*, American Society of Civil Engineers, Vol. 104, No. GT8, pp. 1131–1135.

Shahriar, M. A., Sivakugan, N., Das, B. M., Urquardt, A., and Tapiolas, M. (2014). "Water Table Correction Factors for Settlements of Shallow Foundations in Granular Soils," *International Journal of Geomechanics*, American Society of Civil Engineers, Vol. 15, No. 1, 7 p. DOI:10,1061/(ASCE)GM.1943-5622.0000391.

Skempton, A. W. (1986). "Standard Penetration Test Procedures and the Effects in Sands of Overburden Pressure, Relative Density, Particle Size, Ageing and Overconsolidation," *Geotechnique*, Vol. 36, No. 3, pp. 425–447.

Skempton, A. W. and Bjerrum, L. (1957). "A Contribution to Settlement Analysis of Foundations in Clay," *Geotechnique*, London, Vol. 7, p. 178.

Skempton, A. W. and McDonald, D. M. (1956). "The Allowable Settlement of Buildings," *Proceedings of Institute of Civil Engineers*, Vol. 5, Part III, p. 727.

Steinbrenner, W. (1934). "Tafeln zur Setzungsberechnung," *Die Strasse*, Vol. 1, pp. 121–124.

Teng, W. C. (1962). *Foundation Design*, Prentice-Hall, Englewood Cliffs, NJ.

Terzaghi, K. (1943). *Theoretical Soil Mechanics*, John Wiley & Sons, New York.

Terzaghi, K. and Peck, R. B. (1948). *Soil Mechanics in Engineering Practice*. John Wiley & Sons, New York.

Terzaghi, K. and Peck, R. B. (1967). *Soil Mechanics in Engineering Practice*, 2nd ed., John Wiley & Sons, New York.

Terzaghi, K., Peck, R. B., and Mesri, G. (1996). *Soil Mechanics in Engineering Practice*, 3rd ed., John Wiley & Sons, New York.

Timoshenko, S. and Goodier, J. N. (1951). *Theory of Elasticity*, 2nd ed., McGraw-Hill, New York.

10

Mat Foundations



Kekyalyaynen/Shutterstock.com

10.1 Introduction 397
10.2 Combined Footings 397
10.3 Common Types of Mat Foundations 401
10.4 Bearing Capacity of Mat Foundations 403
10.5 Differential Settlement of Mats 406
10.6 Field Settlement Observations for Mat Foundations 407
10.7 Compensated Foundation 407
10.8 Structural Design of Mat Foundations 411
10.9 Summary 424
PROBLEMS 425
REFERENCES 425

10.1 Introduction

The types of shallow foundations discussed in Chapters 6 and 7 are called footings. Under normal conditions, these square and rectangular footings are economical for supporting columns and walls. However, under certain circumstances, it may be desirable to construct a footing that supports a line of two or more columns. These footings are referred to as *combined footings*. When more than one line of columns is supported by a concrete slab, it is called a *mat* or *raft foundation*. Combined footings can be classified generally under the following categories:

a. Rectangular combined footing
b. Trapezoidal combined footing
c. Strap footing

Mat foundations are generally used with soil that has a low bearing capacity. Mat foundations are used under the following circumstances:

a. When more than 50% of the structure's footprint will otherwise be constructed as pad or strip footings,
b. When the type of structure requires that the differential settlements be limited to very small values, or
c. When there are nonuniform soil conditions or soil where pockets of weak soil are present.

A brief overview of the principles of combined footings is given in Section 10.2, followed by a more detailed discussion of mat foundations.

10.2 Combined Footings

RECTANGULAR COMBINED FOOTING

In several instances, the load to be carried by a column and the soil bearing capacity are such that the standard spread footing design will require extension of the column foundation beyond the property line. This can be avoided by having two or more columns supported on a single rectangular foundation, as shown in Figure 10.1. If the net allowable soil pressure is known, the size of the foundation ($B \times L$) can be determined in the following manner:

a. Determine the area of the foundation

$$A = \frac{Q_1 + Q_2}{q_{all(net)}} \tag{10.1}$$

where

Q_1, Q_2 = column loads

$q_{all(net)}$ = net allowable soil bearing capacity

b. Determine the location of the resultant of the column loads. From Figure 10.1,

$$X = \frac{Q_2 L_3}{Q_1 + Q_2} \tag{10.2}$$

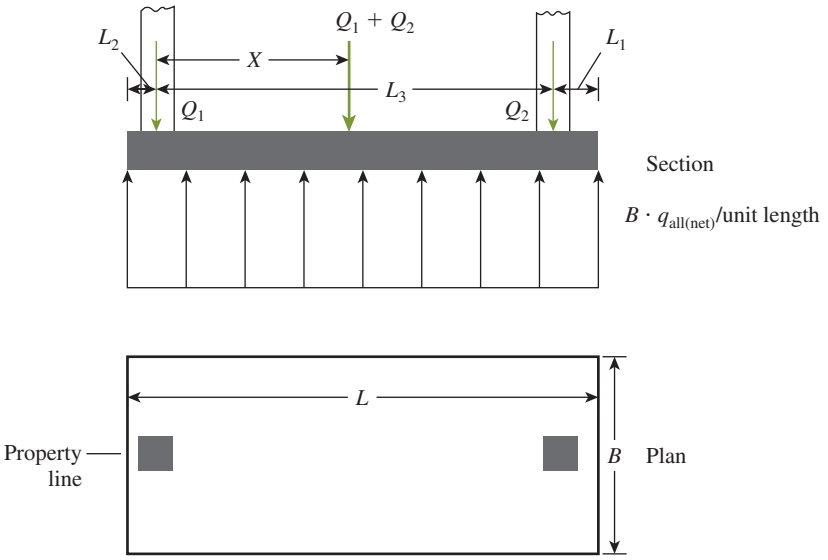


FIGURE 10.1 Rectangular combined footing

c. For a uniform distribution of soil pressure under the foundation, the resultant of the column loads should pass through the centroid of the foundation. Thus,

$$L = 2(L_2 + X) \tag{10.3}$$

where L = length of the foundation.

d. Once the length L is determined, the value of L_1 can be obtained as follows:

$$L_1 = L - L_2 - L_3 \tag{10.4}$$

Note that the magnitude of L_2 will be known and depends on the location of the property line.

e. The width of the foundation is then

$$B = \frac{A}{L} \tag{10.5}$$

If L as computed in Eq. (10.3) is less than $L_2 + L_3$, it should be increased to encompass the two columns. Here, the resultant is not acting on the centroid of the base anymore, and the pressure distribution becomes nonuniform.

TRAPEZOIDAL COMBINED FOOTING

A trapezoidal combined footing (see Figure 10.2) is sometimes used as an isolated spread foundation of columns carrying large loads where space is tight. The size of the foundation that will uniformly distribute pressure on the soil can be obtained in the following manner:

a. If the net allowable soil pressure is known, determine the area of the foundation:

$$A = \frac{Q_1 + Q_2}{q_{all(net)}} \tag{10.6}$$

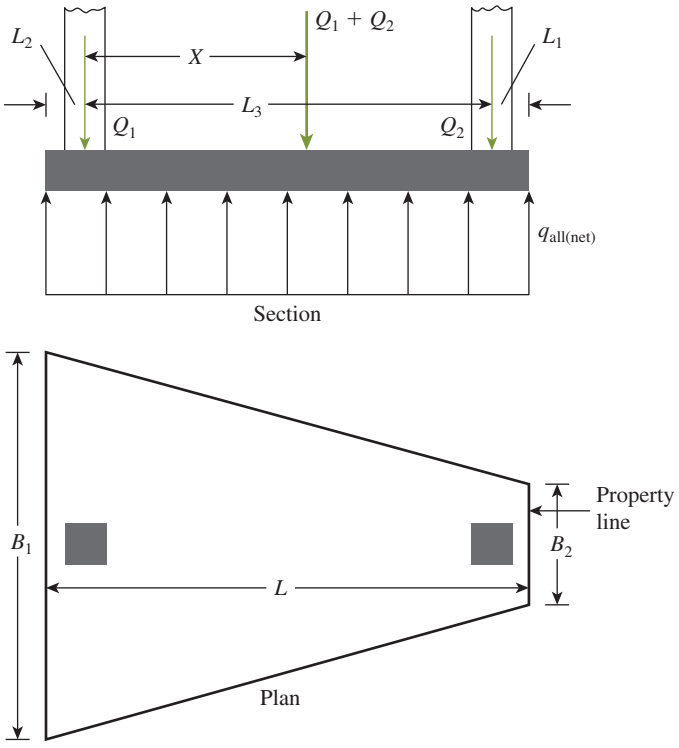


FIGURE 10.2 Trapezoidal combined footing

From Figure 10.2,

$$A = \frac{B_1 + B_2}{2} L \tag{10.7}$$

b. Determine the location of the resultant for the column loads:

$$X = \frac{Q_2 L_3}{Q_1 + Q_2} \tag{10.8}$$

c. From the property of a trapezoid, where the resultant column load passes through the centroid,

$$X + L_2 = \left(\frac{B_1 + 2B_2}{B_1 + B_2}\right)\frac{L}{3} \tag{10.9}$$

With known values of A, L, X, and L_2, Eqs. (10.7) and (10.9) can be solved to obtain B_1 and B_2. Note that, for a trapezoid,

$$\frac{L}{3} < X + L_2 < \frac{L}{2}$$

CANTILEVER FOOTING

Cantilever footing construction uses a *strap beam* to connect an eccentrically loaded column foundation to the foundation of an interior column. (See Figure 10.3.) Cantilever footings may be used in place of trapezoidal or rectangular combined footings when the allowable soil bearing capacity is high and the distances between the columns are large.

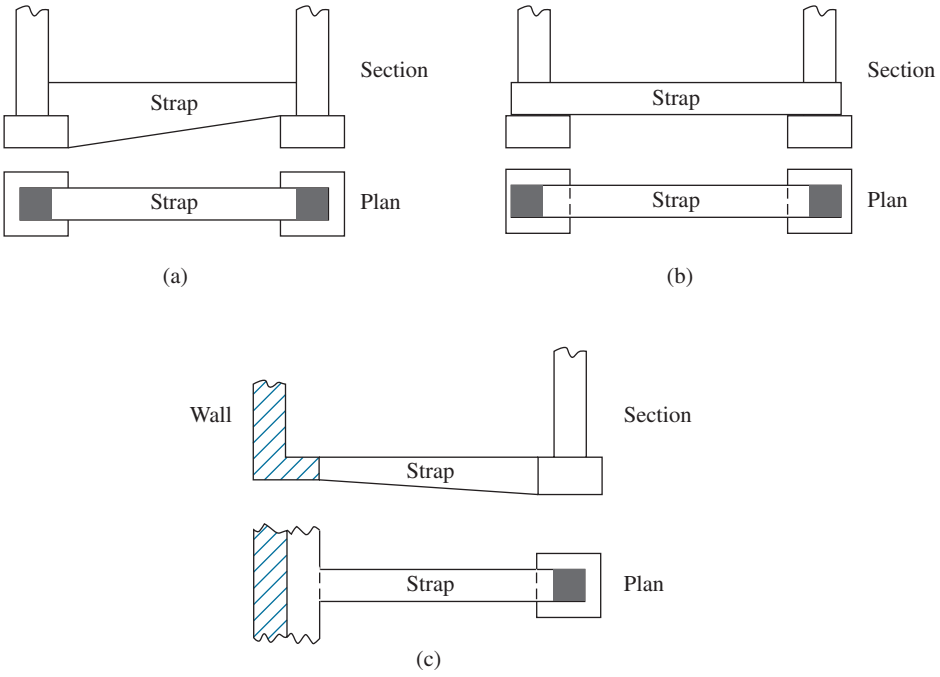


FIGURE 10.3 Cantilever footing—use of strap beam

EXAMPLE 10.1

Refer to Figure 10.1. Given:

$$Q_1 = 400 \text{ kN}$$
$$Q_2 = 500 \text{ kN}$$
$$q_{all(net)} = 140 \text{ kN/m}^2$$
$$L_3 = 3.5 \text{ m}$$

Based on the location of the property line, it is required that L_2 be 1.5 m. Determine the size ($B \times L$) of the rectangular combined footing.

SOLUTION

Area of the foundation required is

$$A = \frac{Q_1 + Q_2}{q_{all(net)}} = \frac{400 + 500}{140} = 6.43 \text{ m}^2$$

Location of the resultant [Eq. (10.2)] is

$$X = \frac{Q_2 L_3}{Q_1 + Q_2} = \frac{(500)(3.5)}{400 + 500} \approx 1.95 \text{ m}$$

For uniform distribution of soil pressure under the foundation from Eq. (10.3), we have

$$L = 2(L_2 + X) = 2(1.5 + 1.95) = \mathbf{6.9\ m}$$

Again, from Eq. (10.4),

$$L_1 = L - L_2 - L_3 = 6.9 - 1.5 - 3.5 = 1.9 \text{ m}$$

Thus,

$$B = \frac{A}{L} = \frac{6.43}{6.9} = \mathbf{0.93\ m}$$

EXAMPLE 10.2

Refer to Figure 10.2. Given:

$$Q_1 = 1000 \text{ kN}$$
$$Q_2 = 400 \text{ kN}$$
$$L_3 = 3 \text{ m}$$
$$q_{all(net)} = 120 \text{ kN/m}^2$$

Based on the space available for construction, it is required that $L_2 = 1.2$ m and $L_1 = 1$ m. Determine B_1 and B_2.

SOLUTION

The area of the trapezoidal combined footing required is [Eq. (10.6)]

$$A = \frac{Q_1 + Q_2}{Q_{all(net)}} = \frac{1000 + 400}{120} = 11.67 \text{ m}^2$$

$$L = L_1 + L_2 + L_3 = 1 + 1.2 + 3 = 5.2 \text{ m}$$

From Eq. (10.7),

$$A = \frac{B_1 + B_2}{2} L$$

$$11.67 = \left(\frac{B_1 + B_2}{2}\right)(5.2)$$

or

$$B_1 + B_2 = 4.49 \text{ m} \tag{a}$$

From Eq. (10.8),

$$X = \frac{Q_2 L_3}{Q_1 + Q_2} = \frac{(400)(3)}{1000 + 400} = 0.857 \text{ m}$$

Again, from Eq. (10.9),

$$X + L_2 = \left(\frac{B_1 + 2B_2}{B_1 + B_2}\right)\frac{L}{3}$$

$$0.857 + 1.2 = \left(\frac{B_1 + 2B_2}{B_1 + B_2}\right)\left(\frac{5.2}{3}\right)$$

$$\frac{B_1 + 2B_2}{B_1 + B_2} = 1.187 \tag{b}$$

From Eqs. (a) and (b), we have

$$B_1 = \mathbf{3.65 \text{ m}}$$
$$B_2 = \mathbf{0.84 \text{ m}}$$

10.3 Common Types of Mat Foundations

The mat foundation, which is sometimes referred to as a *raft foundation*, is a combined footing that may cover the entire area under a structure, supporting several columns and walls. Mat foundations are sometimes preferred for soil that have low load-bearing capacities, but will have to support high column or wall loads. Under some conditions, spread footings would have to cover more than half the building

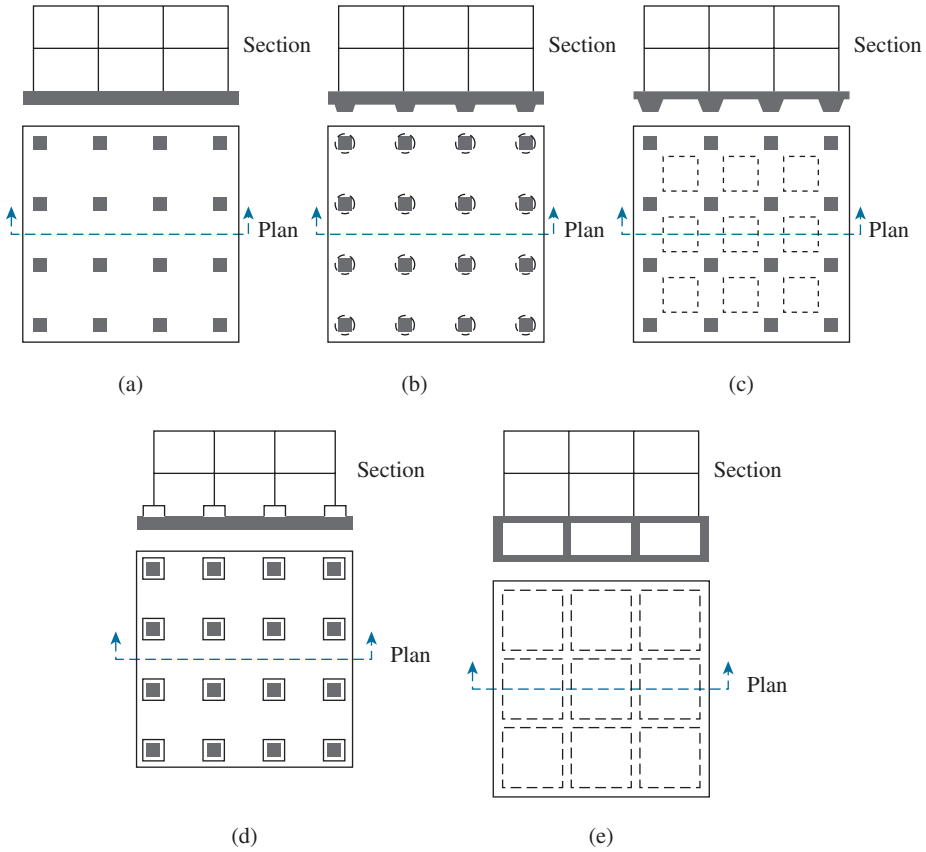


FIGURE 10.4 Common types of mat foundations

area, and mat foundations might be more economical. Several types of mat foundations are used currently. Some of the common ones are shown schematically in Figure 10.4 and include the following:

1. Flat plate (Figure 10.4a). The mat is of uniform thickness.
2. Flat plate thickened under columns (Figure 10.4b).
3. Beams and slab (Figure 10.4c). The beams run both ways, and the columns are located at the intersections of the beams.
4. Flat plates with pedestals (Figure 10.4d).
5. Slab with basement walls as a part of the mat (Figure 10.4e). The walls act as stiffeners for the mat.

Mats may be supported by piles, which help reduce the settlement of a structure built over highly compressible soil. Where the water table is high, mats are often placed over piles to control buoyancy. Figure 10.5 shows the difference between the

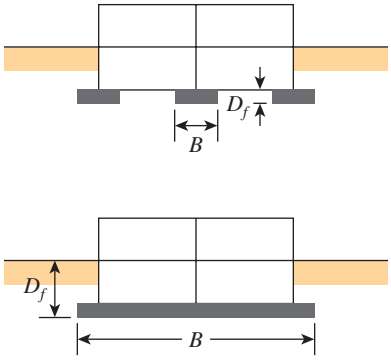


FIGURE 10.5 Comparison of isolated foundation and mat foundation (B = width, D_f = depth)



FIGURE 10.6 A flat plate mat foundation under construction (Courtesy of Dharma Shakya, Geotechnical Solutions, Inc., Irvine, California)

depth D_f and the width B of isolated foundations and mat foundations. Figure 10.6 shows a flat-plate mat foundation under construction.

10.4 Bearing Capacity of Mat Foundations

The *gross ultimate bearing capacity* of a mat foundation can be determined by the same equation used for shallow foundations (see Section 6.6), or

$$q_u = c' N_c F_{cs} F_{cd} F_{ci} + q N_q F_{qs} F_{qd} F_{qi} + \tfrac{1}{2} \gamma B N_\gamma F_{\gamma s} F_{\gamma d} F_{\gamma i} \qquad \text{Eq. (6.28)}$$

(Chapter 6 gives the proper values of the bearing capacity factors, as well as the shape, depth, and load inclination factors.) The term B in Eq. (6.28) is the smallest dimension of the mat. The *net ultimate capacity* of a mat foundation is

$$q_{u(\text{net})} = q_u - q \qquad \text{Eq. (6.23)}$$

A suitable factor of safety should be used to calculate the net *allowable* bearing capacity. For mats on clay, the factor of safety should not be less than 3 under dead load or maximum live load. However, under the most extreme conditions, the factor of safety should be at least 1.75 to 2. For mats constructed over sand, a factor of safety of 3 should normally be used. Under most working conditions, the factor of safety against bearing capacity failure of mats on sand is very large. Here settlement considerations dominate in the design.

For saturated clays with $\phi = 0$ (*Note:* $N_c = 5.14$, $N_q = 1$, and $N_\gamma = 0$) and a vertical loading condition, Eq. (6.28) gives

$$q_u = c_u N_c F_{cs} F_{cd} + q \qquad (10.10)$$

where c_u = undrained cohesion.

From Table 6.3, for $\phi = 0$,

$$F_{cs} = 1 + \frac{B}{L}\left(\frac{N_q}{N_c}\right) = 1 + \left(\frac{B}{L}\right)\left(\frac{1}{5.14}\right) = 1 + 0.195\left(\frac{B}{L}\right)$$

and

$$F_{cd} = 1 + 0.4\left(\frac{D_f}{B}\right)$$

Substitution of the preceding shape and depth factors into Eq. (10.10) yields

$$q_u = 5.14c_u\left(1 + 0.195\frac{B}{L}\right)\left(1 + 0.4\frac{D_f}{B}\right) + q \tag{10.11}$$

Hence, the net ultimate bearing capacity is

$$q_{u(\text{net})} = q_u - q = 5.14c_u\left(1 + 0.195\frac{B}{L}\right)\left(1 + 0.4\frac{D_f}{B}\right) \tag{10.12}$$

For FS = 3, the net allowable soil bearing capacity becomes

$$q_{\text{all(net)}} = \frac{q_{u(\text{net})}}{\text{FS}} = 1.713c_u\left(1 + 0.195\frac{B}{L}\right)\left(1 + 0.4\frac{D_f}{B}\right) \tag{10.13}$$

For mats in sands, since the factor of safety against bearing capacity failure is very large, the designs are governed by the settlement considerations. From Eq. (9.51) given below, with N_{60} and substituting the allowable settlement for S_e, the net allowable bearing pressure can be determined by

$$q_{\text{net}}(\text{kN/m}^2) = \frac{N_{60}}{0.08}\left(\frac{B + 0.3}{B}\right)^2 F_d\left(\frac{S_e}{25}\right) \qquad \text{Eq. (9.51)}$$

where

N_{60} = standard penetration resistance

B = width (m)

$F_d = 1 + 0.33(D_f/B) \le 1.33$

S_e = settlement (mm)

When the width B is large, assuming $D_f/B = 1$, the preceding equation can be approximated as

$$\begin{aligned} q_{\text{net}}(\text{kN/m}^2) &= \frac{N_{60}}{0.08}F_d\left(\frac{S_e}{25}\right) \\ &= \frac{N_{60}}{0.08}\left[1 + 0.33\left(\frac{D_f}{B}\right)\right]\left[\frac{S_e(\text{mm})}{25}\right] \\ &\le 0.67N_{60}[S_e(\text{mm})] \end{aligned} \tag{10.14}$$

In English units, assuming $D_f/B = 1$, Eq. (10.14) may be expressed as

$$\begin{aligned} q_{\text{net}}(\text{kip/ft}^2) &= 0.25N_{60}\left[1 + 0.33\left(\frac{D_f}{B}\right)\right][S_e(\text{in.})] \\ &\le 0.33N_{60}[S_e(\text{in.})] \end{aligned} \tag{10.15}$$

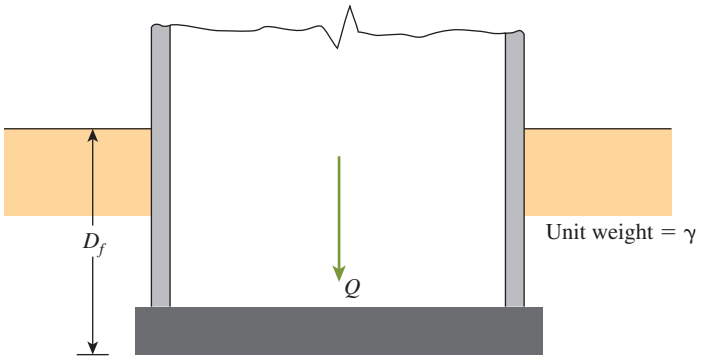


FIGURE 10.7 Definition of net pressure on soil caused by a mat foundation

Terzaghi and Peck (1948) suggested limiting the total settlement of pad and strip foundations to 25 mm (1 in.), which would limit the differential settlement to 19 mm (0.75 in.). However, the width of the raft foundations are larger than those of the isolated spread footings. As shown in Figures 8.10 and 8.11, the depth of significant stress increase in the soil below a foundation depends on the width of the foundation. Hence, for a raft foundation, the depth of the zone of influence is likely to be much larger than that of a spread footing. Thus, the loose soil pockets under a raft may be more evenly distributed with further stiffening of the soil taking place, resulting in a smaller differential settlement. Based on this concept, Terzaghi and Peck (1948) suggested allowing for a maximum raft settlement of 50 mm (2 in.), which would still limit the differential settlement to 19 mm (0.75 in.). Nowadays, even higher values are allowed for the limiting settlements (see Section 9.16). Using this logic and conservatively assuming that $F_d = 1$, we can respectively approximate Eqs. (10.14) and (10.15) as

$$q_{all(net)} = q_{net}(kN/m^2) \approx 25N_{60} \tag{10.16a}$$

and

$$q_{all(net)} = q_{net}(kip/ft^2) = 0.5N_{60} \tag{10.16b}$$

The net pressure applied on a foundation (see Figure 10.7) may be expressed as

$$q = \frac{Q}{A} - \gamma D_f \tag{10.17}$$

where

Q = dead weight of the structure and the live load

A = area of the raft

In all cases, q should be less than or equal to allowable $q_{all(net)}$.

EXAMPLE 10.3

Determine the net ultimate bearing capacity of a mat foundation measuring 20 m × 8 m on a saturated clay with $c_u = 85$ kN/m^2, $\phi = 0$, and $D_f = 1.5$ m.

SOLUTION

From Eq. (10.12),

$$q_{u(net)} = 5.14c_u\left[1 + \left(\frac{0.195B}{L}\right)\right]\left[1 + 0.4\,\frac{D_f}{B}\right]$$

$$= (5.14)(85)\left[1 + \left(\frac{0.195 \times 8}{20}\right)\right]\left[1 + \left(\frac{0.4 \times 1.5}{8}\right)\right]$$

$$= \mathbf{506.3\ kN/m^2}$$

EXAMPLE 10.4

What will be the net allowable bearing capacity of a mat foundation with dimensions of 45 ft × 30 ft constructed over a sand deposit? Here, $D_f = 6.5$ ft, the allowable settlement is 2 in., and the average penetration number $N_{60} = 10$.

SOLUTION

From Eq. (10.15),

$$q_{all(net)} = 0.25\, N_{60}\left[1 + 0.33\left(\frac{D_f}{B}\right)\right] S_e \text{ (in.)}$$

or

$$q_{all(net)} = (0.25)(10)\left[1 + \frac{0.33 \times 6.5}{30}\right](2) = \mathbf{5.36\ kip/ft^2}$$

10.5 Differential Settlement of Mats

In 1988, the American Concrete Institute Committee 336 suggested a method for calculating the differential settlement of mat foundations. According to this method, the rigidity factor K_r is calculated as

$$K_r = \frac{E' I_b}{E_s B^3} \tag{10.18}$$

where

E' = modulus of elasticity of the material used in the structure

E_s = modulus of elasticity of the soil

B = width of foundation

I_b = moment of inertia of the structure per unit length at right angles to B

The term $E'I_b$ can be expressed as

$$E' I_b = E'\left(I_F + \sum I'_b + \sum \frac{ah^3}{12}\right) \tag{10.19}$$

where

$E'I_b$ = flexural rigidity of the superstructure and foundation per unit length at right angles to B

$\Sigma E'I'_b$ = flexural rigidity of the framed members at right angles to B

$\Sigma(E'ah^3/12)$ = flexural rigidity of the shear walls

a = shear wall thickness

h = shear wall height

$E'I_F$ = flexibility of the foundation

Based on the value of K_r, the ratio (δ) of the differential settlement to the total settlement can be estimated in the following manner:

1. If $K_r > 0.5$, it can be treated as a rigid mat, and $\delta = 0$.
2. If $K_r = 0.5$, then $\delta \approx 0.1$.
3. If $K_r = 0$, then $\delta = 0.35$ for square mats ($B/L = 1$), and $\delta = 0.5$ for long foundations ($B/L = 0$).

10.6 Field Settlement Observations for Mat Foundations

Several field settlement observations for mat foundations are currently available in the literature. In this section, we compare the observed settlements for some mat foundations constructed over granular soil deposits with those obtained from Eqs. (10.14) and (10.15).

Meyerhof (1965) compiled the observed maximum settlements for mat foundations constructed on sand and gravel, as listed in Table 10.1. In Eq. (10.14), if the depth factor, $1 + 0.33(D_f/B)$, is assumed to be approximately unity, then

$$S_e(\text{mm}) \approx \frac{2q_{\text{all(net)}}}{N_{60}} \tag{10.20}$$

From the values of $q_{\text{all(net)}}$ and N_{60} given in Columns 6 and 5, respectively, of Table 10.1, the magnitudes of S_e were calculated and are given in Column 8.

Column 9 of Table 10.1 gives the ratios of calculated to measured values of S_e. These ratios vary from about 0.79 to 3.39. Thus, calculating the net allowable bearing capacity with the use of Eq. (10.14) or (10.15) will yield safe and conservative values.

10.7 Compensated Foundation

Figure 10.7 and Eq. (10.17) indicate that the net pressure increase in the soil under a mat foundation can be reduced by increasing the depth D_f of the mat. This approach is generally referred to as the *compensated foundation design* and is extremely useful when structures are to be built on very soft clays. In this design, a deeper basement is made below the higher portion of the superstructure, so that the net pressure increase in soil at any depth is small and relatively uniform. (See Figure 10.8.) From Eq. (10.17) and Figure 10.7, the net average applied pressure on soil is

$$q = \frac{Q}{A} - \gamma D_f$$

For no increase in the net pressure on soil below a mat foundation, q should be zero. Thus,

$$D_f = \frac{Q}{A\gamma} \tag{10.21}$$

This relation for D_f is usually referred to as the depth of a *fully compensated foundation*.

The factor of safety against bearing capacity failure for partially compensated foundations (i.e., $D_f < Q/A\gamma$) may be given as

$$\text{FS} = \frac{q_{u(\text{net})}}{q} = \frac{q_{u(\text{net})}}{\dfrac{Q}{A} - \gamma D_f} \tag{10.22}$$

where $q_{u(\text{net})}$ = net ultimate bearing capacity.

For saturated clays, the factor of safety against bearing capacity failure can thus be obtained by substituting Eq. (10.12) into Eq. (10.22):

$$\text{FS} = \frac{5.14c_u\left(1 + \dfrac{0.195B}{L}\right)\left(1 + 0.4\,\dfrac{D_f}{B}\right)}{\dfrac{Q}{A} - \gamma D_f} \tag{10.23}$$

TABLE 10.1 Settlement of Mat Foundations on Sand and Gravel [Based on Meyerhof, G. G., (1965). "Shallow Foundations," *Journal of the Soil Mechanics and Foundation Engineering Division*, American Society of Civil Engineers, Vol. 91, pp. 21–31, Table 1.]

Case No. (1)	Structure (2)	Reference (3)	B m (ft) (4)	Average N_{60} (5)	$q_{all(net)}$ kN/m^2 (kip/ft^2) (6)	Observed maximum settlement, S_e mm (in.) (7)	Calculated maximum settlement, S_e mm (in.) (8)	Calculated S_e / Observed S_e (9)
1	T. Edison São Paulo, Brazil	Rios and Silva (1948)	18.29 (60)	15	229.8 (4.8)	15.24 (0.6)	30.64 (1.21)	2.01
2	Banco do Brazil São Paulo, Brazil	Rios and Silva (1948); Vargas (1961)	22.86 (75)	18	239.4 (5.0)	27.94 (1.1)	26.6 (1.05)	0.95
3	Iparanga São Paulo, Brazil	Vargas (1948)	9.14 (30)	9	304.4 (6.4)	35.56 (1.4)	67.64 (2.66)	1.9
4	C.B.I., Esplanda São Paulo, Brazil	Vargas (1961)	14.63 (48)	22	383.0 (8.0)	27.94 (1.1)	34.82 (1.37)	1.25
5	Riscala São Paulo, Brazil	Vargas (1948)	3.96 (13)	20	229.8 (4.8)	12.7 (0.5)	22.98 (0.9)	1.81
6	Thyssen Düsseldorf, Germany	Schultze (1962)	22.55 (74)	25	239.4 (5)	24.13 (0.95)	19.15 (0.75)	0.79
7	Ministry Düsseldorf, Germany	Schultze (1962)	15.85 (52)	20	220.2 (4.6)	20.32 (0.8)	22.02 (0.87)	1.08
8	Chimney Cologne, Germany	Schultze (1962)	20.42 (67)	10	172.4 (3.6)	10.16 (0.4)	34.48 (1.36)	3.39

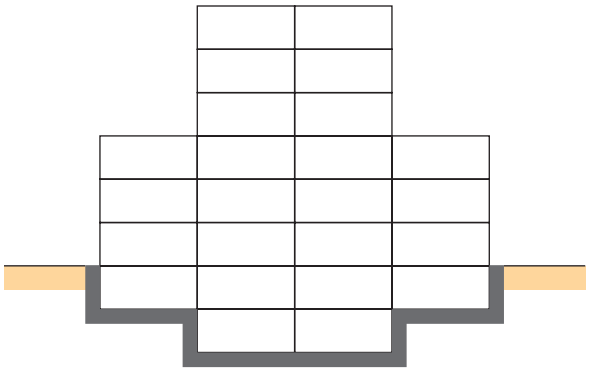


FIGURE 10.8 Compensated foundation

EXAMPLE 10.5

The mat shown in Figure 10.7 has dimensions of 20 m × 30 m. The total dead and live load on the mat is 110 MN. The mat is placed over a saturated clay having a unit weight of 18 kN/m^3 and $c_u = 140$ kN/m^2. Given that $D_f = 1.5$ m, determine the factor of safety against bearing capacity failure.

SOLUTION

From Eq. (10.23), the factor of safety

$$\text{FS} = \frac{5.14c_u\left(1 + \dfrac{0.195B}{L}\right)\left(1 + 0.4\dfrac{D_f}{B}\right)}{\dfrac{Q}{A} - \gamma D_f}$$

We are given that $c_u = 140$ kN/m^2, $D_f = 1.5$ m, $B = 20$ m, $L = 30$ m, and $\gamma = 18$ kN/m^3. Hence,

$$\text{FS} = \frac{(5.14)(140)\left[1 + \dfrac{(0.195)(20)}{30}\right]\left[1 + 0.4\left(\dfrac{1.5}{20}\right)\right]}{\left(\dfrac{110{,}000 \text{ kN}}{20 \times 30}\right) - (18)(1.5)} = \mathbf{5.36}$$

EXAMPLE 10.6

Consider a mat foundation 30 m × 40 m in plan, as shown in Figure 10.9. The total dead load and live load on the raft is 200 × 10^3 kN. Estimate the consolidation settlement at the center of the foundation.

SOLUTION

From Eq. (2.65),

$$S_{c(p)} = \frac{C_c H_c}{1 + e_o}\log\left(\frac{\sigma'_o + \Delta\sigma'_{\text{av}}}{\sigma'_o}\right)$$

$$\sigma'_o = (3.67)(15.72) + (13.33)(19.1 - 9.81) + \frac{6}{2}(18.55 - 9.81) \approx 208 \text{ kN/m}^2$$

$$H_c = 6 \text{ m}$$

$$C_c = 0.28$$

$$e_o = 0.9$$

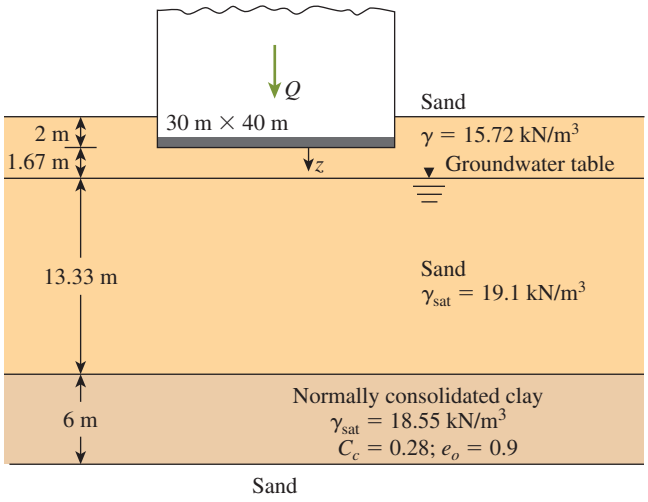


FIGURE 10.9 Consolidation settlement under a mat foundation

For $Q = 200 \times 10^3$ kN, the net load per unit area is

$$q = \frac{Q}{A} - \gamma D_f = \frac{200 \times 10^3}{30 \times 40} - (15.72)(2) \approx 135.2 \text{ kN/m}^2$$

In order to calculate $\Delta\sigma'_{av}$, we refer to Section 8.9. The loaded area can be divided into four areas, each measuring 15 m × 20 m. Now using Eq. (8.20), we can calculate the average stress increase in the clay layer below the corner of each rectangular area, or

$$\Delta\sigma'_{av(H_2/H_1)} = q_o\left[\frac{H_2 I_{a(H_2)} - H_1 I_{a(H_1)}}{H_2 - H_1}\right]$$

$$= 135.2\left[\frac{(1.67 + 13.33 + 6)I_{a(H_2)} - (1.67 + 13.33)I_{a(H_1)}}{6}\right]$$

For $I_{a(H_2)}$,

$$m_2 = \frac{B}{H_2} = \frac{15}{1.67 + 13.33 + 6} = 0.71$$

$$n_2 = \frac{L}{H_2} = \frac{20}{21} = 0.95$$

From Figure 8.11, for $m_2 = 0.71$ and $n_2 = 0.95$ the value of $I_{a(H_2)}$ is 0.21. Again, for $I_{a(H_1)}$,

$$m_2 = \frac{B}{H_1} = \frac{15}{15} = 1$$

$$n_2 = \frac{L}{H_1} = \frac{20}{15} = 1.33$$

From Figure 8.11, $I_{a(H_1)} = 0.225$, so

$$\Delta\sigma'_{av(H_2/H_1)} = 135.2\left[\frac{(21)(0.21) - (15)(0.225)}{6}\right] = 23.32 \text{ kN/m}^2$$

So, the stress increase below the center of the 30 m × 40 m area is (4)(23.32) = 93.28 kN/m^2. Thus

$$S_{c(p)} = \frac{(0.28)(6))}{1 + 0.9} \log\left(\frac{208 + 93.28}{208}\right) = 0.142 \text{ m}$$

$$= \mathbf{142 \text{ mm}}$$

10.8 Structural Design of Mat Foundations

The structural design of mat foundations can be carried out by two conventional methods: the conventional rigid method and the approximate flexible method. Finite-difference and finite-element methods can also be used, but this section covers only the basic concepts of the first two design methods.

CONVENTIONAL RIGID METHOD

The *conventional rigid method* of mat foundation design can be explained step by step with reference to Figure 10.10. In the conventional rigid method, the entire raft is assumed to be rigid. The bottom of the mat remains horizontal. The pressure applied to the underlying soil is assumed to vary linearly. The mat is divided into rectangular beams (i.e., a strip) in both x and y directions, considering the tributary areas. Each beam is analyzed as a structural member, and reinforcements are provided from the structural design considerations based on the bending moment and shear force diagrams.

Step 1. Figure 8.10a shows mat dimensions of $L \times B$ and column loads of Q_1, Q_2, Q_3, ... Calculate the total column load as

$$Q = Q_1 + Q_2 + Q_3 + \cdots \tag{10.24}$$

Step 2. Determine the pressure on the soil, q, below the mat at points A, B, C, D, ..., by using the equation

$$q = \frac{Q}{A} + \frac{M_y x}{I_y} + \frac{M_x y}{I_x} \tag{10.25}$$

where

$A = BL$

$I_x = (1/12)BL^3$ = moment of inertia about the x-axis

$I_y = (1/12)LB^3$ = moment of inertia about the y-axis

M_x = moment of the column loads about the x-axis = Qe_y

M_y = moment of the column loads about the y-axis = Qe_x

x, y = coordinates with appropriate +/− signs

The load eccentricities, e_x and e_y, in the x and y directions can be determined by using (x', y') coordinates:

$$x' = \frac{Q_1 x_1' + Q_2 x_2' + Q_3 x_3' + \cdots}{Q} \tag{10.26}$$

and

$$e_x = x' - \frac{B}{2} \tag{10.27}$$

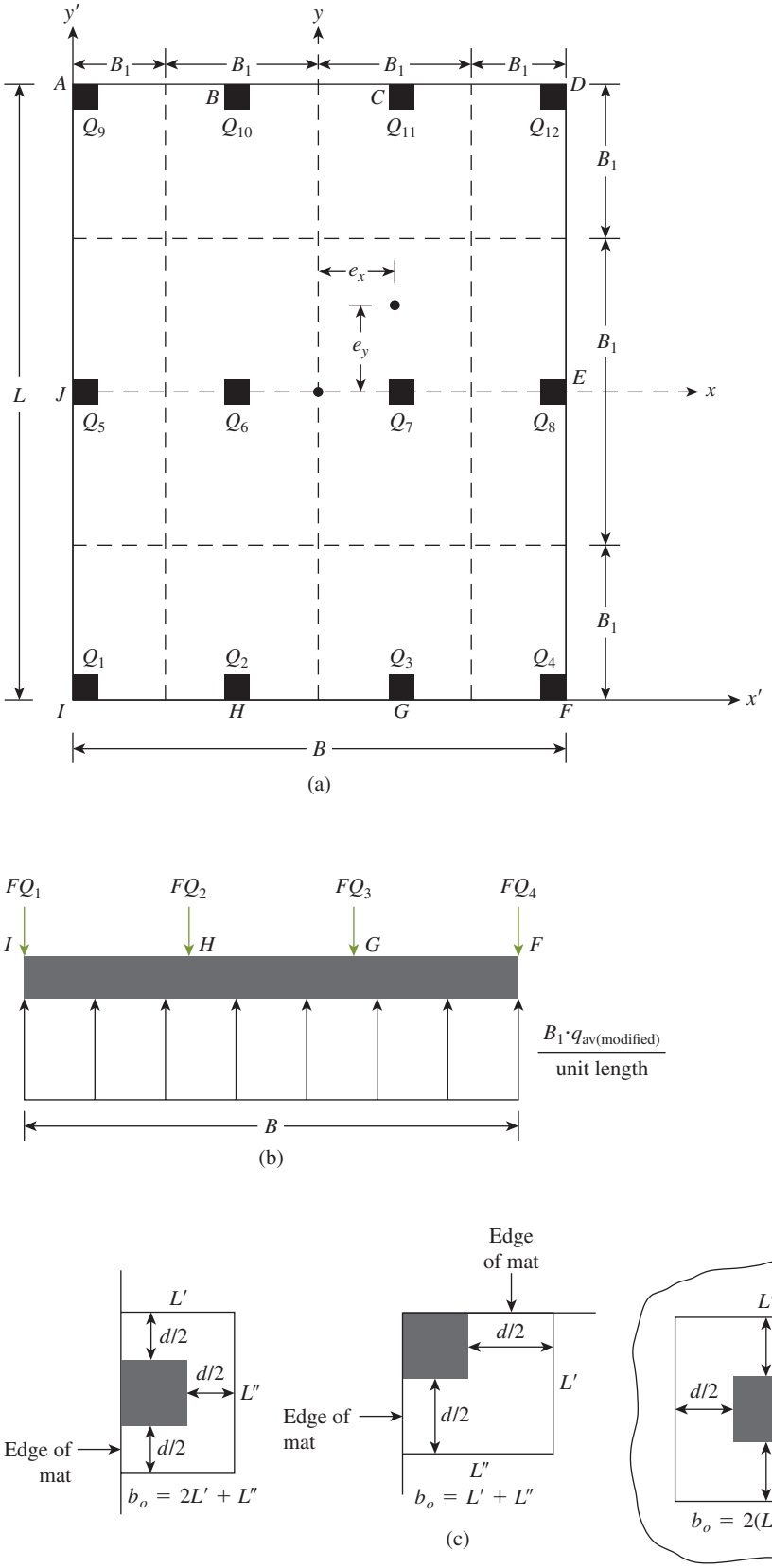


FIGURE 10.10 Conventional rigid mat foundation design

Similarly,

$$y' = \frac{Q_1 y_1' + Q_2 y_2' + Q_3 y_3' + \cdots}{Q} \tag{10.28}$$

and

$$e_y = y' - \frac{L}{2} \tag{10.29}$$

It is also possible to determine e_x, e_y using (x, y) coordinates.

Step 3. Compare the values of the soil pressures determined in Step 2 with the net allowable soil pressure to determine whether $q \leq q_{\text{all(net)}}$.

Step 4. Divide the mat into several strips in the x and y directions. (See Figure 10.10.) Let the width of any strip be B_1.

Step 5. Draw the shear, V, and the moment, M, diagrams for each individual strip (in the x and y directions). For example, the average soil pressure of the bottom strip in the x direction of Figure 10.10a is

$$q_{\text{av}} \approx \frac{q_I + q_F}{2} \tag{10.30}$$

where q_I and q_F = soil pressures at points I and F, as determined from Step 2.

The total soil reaction is equal to $q_{\text{av}} B_1 B$. Now obtain the total column load on the strip as $Q_1 + Q_2 + Q_3 + Q_4$. The sum of the column loads on the strip will not equal $q_{\text{av}} B_1 B$, because the shear between the adjacent strips has not been taken into account. For this reason, the soil reaction and the column loads need to be adjusted, or

$$\text{Average load} = \frac{q_{\text{av}} B_1 B + (Q_1 + Q_2 + Q_3 + Q_4)}{2} \tag{10.31}$$

Now, the modified average soil reaction becomes

$$q_{\text{av(modified)}} = \frac{\text{average load}}{B_1 B} \tag{10.32}$$

and the column load modification factor is

$$F = \frac{\text{average load}}{Q_1 + Q_2 + Q_3 + Q_4} \tag{10.33}$$

So the modified column loads are FQ_1, FQ_2, FQ_3, and FQ_4. This modified loading on the strip under consideration is shown in Figure 10.10b. The shear and the moment diagram for this strip can now be drawn, and the procedure is repeated in the x and y directions for all strips. From here, the thickness of the mat and the reinforcement details can be determined through sturctural design considerations according to the American Concrete Institute (ACI) or equivalent codes or design standards.

Examples 10.7 and 10.8 illustrate the use of the conventional rigid method of mat foundation design.

APPROXIMATE FLEXIBLE METHOD

In the conventional rigid method of design, the mat is assumed to be infinitely rigid. Also, the soil pressure is distributed in a straight line, and the centroid of the soil pressure is coincident with the line of action of the resultant column loads.

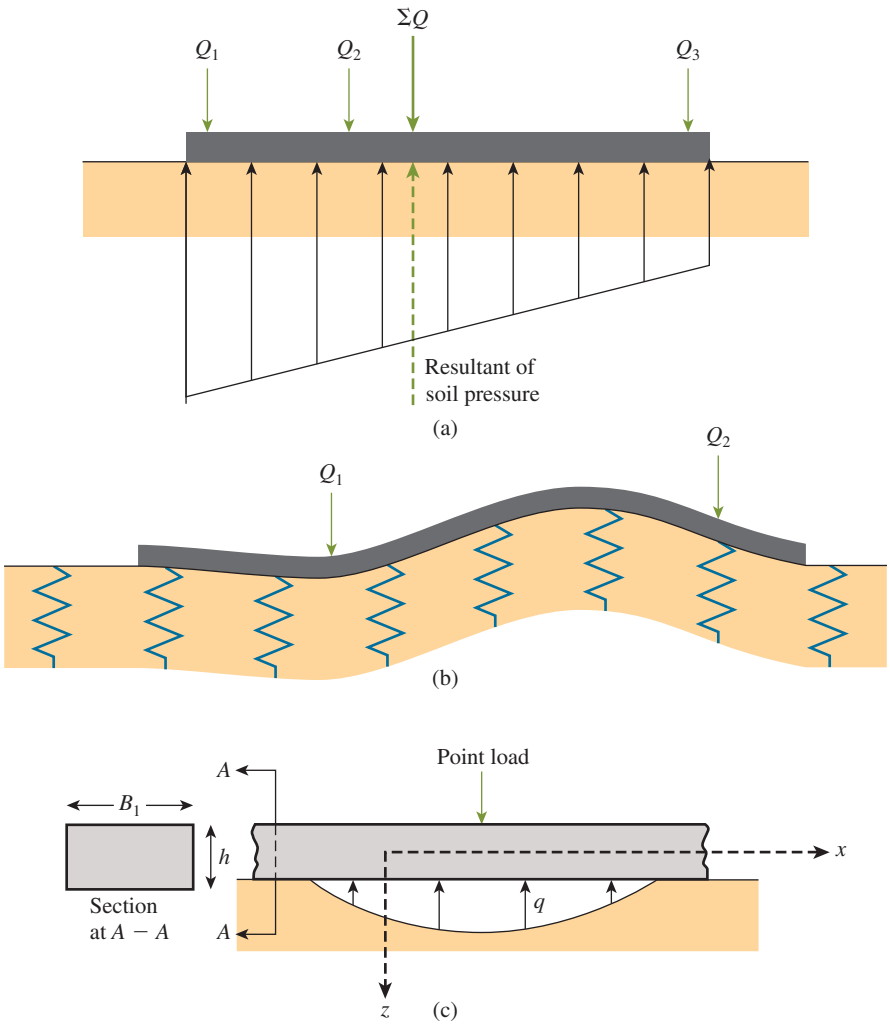


FIGURE 10.11 (a) Principles of design by conventional rigid method; (b) principles of approximate flexible method; (c) derivation of Eq. (10.38) for beams on elastic foundation

(See Figure 10.11a.) In the *approximate flexible method* of design, the soil is assumed to be equivalent to an infinite number of elastic springs, as shown in Figure 10.11b. This arrangement is sometimes referred to as the *Winkler foundation*. The elastic constant of these assumed springs is referred to as the *coefficient of subgrade reaction, k*.

To understand the fundamentals behind flexible foundation design, consider a beam of width B_1 having infinite length, as shown in Figure 10.11c. The beam is subjected to a single concentrated load Q. From the fundamentals of mechanics of materials,

$$M = E_F I_F \frac{d^2z}{dx^2} \tag{10.34}$$

where

M = moment at any section

E_F = modulus of elasticity of foundation material

I_F = moment of inertia of the cross section of the beam $= \left(\frac{1}{12}\right) B_1 h^3$ (see Figure 10.11c)

However,

$$\frac{dM}{dx} = \text{shear force} = V$$

and

$$\frac{dV}{dx} = q = \text{soil reaction}$$

Hence,

$$\frac{d^2M}{dx^2} = q \tag{10.35}$$

Combining Eqs. (10.34) and (10.35) yields

$$E_F I_F \frac{d^4z}{dx^4} = q \tag{10.36}$$

However, the soil reaction is

$$q = -zk'$$

where

z = deflection

$k' = kB_1$

k = coefficient of subgrade reaction (kN/m^3 or lb/in^3)

So,

$$E_F I_F \frac{d^4z}{dx^4} = -zkB_1 \tag{10.37}$$

Solving Eq. (10.37) yields

$$z = e^{-\alpha x}(A' \cos \beta x + A'' \sin \beta x) \tag{10.38}$$

where A' and A'' are constants and

$$\beta = \sqrt[4]{\frac{B_1 k}{4E_F I_F}} \tag{10.39}$$

The unit of the term β, as defined by the preceding equation, is $(\text{length})^{-1}$. This parameter is very important in determining whether a mat foundation should be designed by the conventional rigid method or the approximate flexible method. According to the American Concrete Institute Committee 336 (1988), mats should be designed by the conventional rigid method if the spacing of columns in a strip is less than $1.75/\beta$. If the spacing of columns is larger than $1.75/\beta$, the approximate flexible method may be used.

To perform the analysis for the structural design of a flexible mat, one must know the principles involved in evaluating the coefficient of subgrade reaction, k. Before proceeding with the discussion of the approximate flexible design method, let us discuss this coefficient in more detail.

If a foundation of width B (see Figure 10.12) is subjected to a load per unit area of q, it will undergo a settlement Δ. The coefficient of subgrade reaction can be defined as

$$k = \frac{q}{\Delta} \tag{10.40}$$

It is the pressure that produces a unit of settlement.

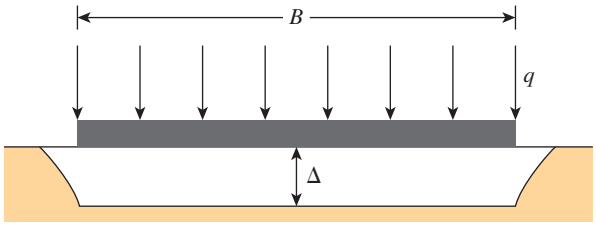


FIGURE 8.12 Definition of coefficient of subgrade reaction, k

The unit of k is kN/m^3 (or lb/in^3). The value of the coefficient of subgrade reaction is not a constant for a given soil, but rather depends on several factors, such as the length L and width B of the foundation and also the depth of embedment of the foundation. A comprehensive study by Terzaghi (1955) of the parameters affecting the coefficient of subgrade reaction indicated that the value of the coefficient decreases with the width of the foundation. In the field, load tests can be carried out by means of square plates measuring 0.3 m × 0.3 m (1 ft × 1 ft), and values of k can be calculated. The value of k can be related to large foundations measuring $B \times B$ in the following ways:

FOUNDATIONS ON SANDY SOIL

For foundations on sandy soil,

$$k = k_{0.3}\left(\frac{B + 0.3}{2B}\right)^2 \tag{10.41}$$

where $k_{0.3}$ and k are the coefficients of subgrade reaction of foundations measuring 0.3 m × 0.3 m and B (m) × B (m), respectively (unit is kN/m^3).

In English units, Eq. (10.41) may be expressed as

$$k = k_1\left(\frac{B + 1}{2B}\right)^2 \tag{10.42}$$

where k_1 and k are the coefficients of subgrade reaction of foundations measuring 1 ft × 1 ft and B (ft) × B (ft), respectively (unit is lb/in^3).

FOUNDATIONS ON CLAYS

For foundations on clays,

$$k(\text{kN/m}^3) = k_{0.3}(\text{kN/m}^3)\left[\frac{0.3\ (\text{m})}{B\ (\text{m})}\right] \tag{10.43a}$$

The definitions of k and $k_{0.3}$ in Eq. (10.43a) are the same as in Eq. (10.41).

In English units,

$$k(\text{lb/in}^3) = k_1\ (\text{lb/in}^3)\left[\frac{1\ (\text{ft})}{B\ (\text{ft})}\right] \tag{10.43b}$$

The definitions of k and k_1 are the same as in Eq. (10.42).

For rectangular foundations having dimensions of $B \times L$ (for similar value of q), in all soil,

$$k = \frac{k_{(B\times B)}\left(1 + 0.5\frac{B}{L}\right)}{1.5} \tag{10.44}$$

where

k = coefficient of subgrade reaction of the rectangular foundation ($L \times B$)

$k_{(B\times B)}$ = coefficient of subgrade reaction of a square foundation having dimension of $B \times B$

Equation (10.44) indicates that the value of k for a very long foundation with a width B is approximately $0.67k_{(B\times B)}$.

The modulus of elasticity of granular soil increases with depth. Because the settlement of a foundation depends on the modulus of elasticity, the value of k increases with the depth of the foundation.

Table 10.2 provides typical ranges of values for the coefficient of subgrade reaction, $k_{0.3}(k_1)$, for sandy and clayey soil.

For long beams, Vesic (1961) proposed an equation for estimating subgrade reaction, namely,

$$k' = Bk = 0.65\sqrt[12]{\frac{E_s B^4}{E_F I_F}}\frac{E_s}{1-\mu_s^2}$$

or

$$k = 0.65\sqrt[12]{\frac{E_s B^4}{E_F I_F}}\frac{E_s}{B(1-\mu_s^2)} \tag{10.45}$$

TABLE 10.2 Typical Subgrade Reaction Values, $k_{0.3}(k_1)$

Soil type	$k_{0.3}$(MN/m^3)	k_1(lb/in^3)
Dry or moist sand:		
Loose	8–25	30–90
Medium	25–125	90–450
Dense	125–375	450–1350
Saturated sand:		
Loose	10–15	35–55
Medium	35–40	125–145
Dense	130–150	475–550
Clay:		
Stiff	10–25	40–90
Very stiff	25–50	90–185
Hard	>50	>185

where

E_s = modulus of elasticity of soil

B = foundation width

E_F = modulus of elasticity of foundation material

I_F = moment of inertia of the cross section of the foundation

μ_s = Poisson's ratio of soil

For most practical purposes, Eq. (10.45) can be approximated as

$$k = \frac{E_s}{B(1 - \mu_s^2)} \tag{10.46}$$

Now that we have discussed the coefficient of subgrade reaction, we will proceed with the discussion of the approximate flexible method of designing mat foundations. This method, as proposed by the American Concrete Institute Committee 336 (1988), is described step by step. The use of the design procedure, based primarily on the theory of plates, allows the effects (i.e., moment, shear, and deflection) of a concentrated column load in the area surrounding it to be evaluated. If the zones of influence of two or more columns overlap, superposition can be employed to obtain the net moment, shear, and deflection at any point. The method is as follows:

Step 1. Assume a thickness h for the mat, which is determined from structural design considerations.

Step 2. Determine the flexural ridigity R of the mat as given by the formula

$$R = \frac{E_F h^3}{12(1 - \mu_F^2)} \tag{10.47}$$

where

E_F = modulus of elasticity of foundation material

μ_F = Poisson's ratio of foundation material

Step 3. Determine the radius of effective stiffness—that is,

$$L' = \sqrt[4]{\frac{R}{k}} \tag{10.48}$$

where k is the coefficient of subgrade reaction. The zone of influence of any column load will be on the order of 3 to 4 times L'.

Step 4. Determine the moment (in polar coordinates at a point) caused by a column load (see Figure 10.13a). The formulas to use are

$$M_r = \text{radial moment} = -\frac{Q}{4}\left[A_1 - \frac{(1 - \mu_F)A_2}{\frac{r}{L'}}\right] \tag{10.49}$$

and

$$M_t = \text{tangential moment} = -\frac{Q}{4}\left[\mu_F A_1 + \frac{(1 - \mu_F)A_2}{\frac{r}{L'}}\right] \tag{10.50}$$

where

r = radial distance from the column load

Q = column load

A_1, A_2 = functions of r/L'

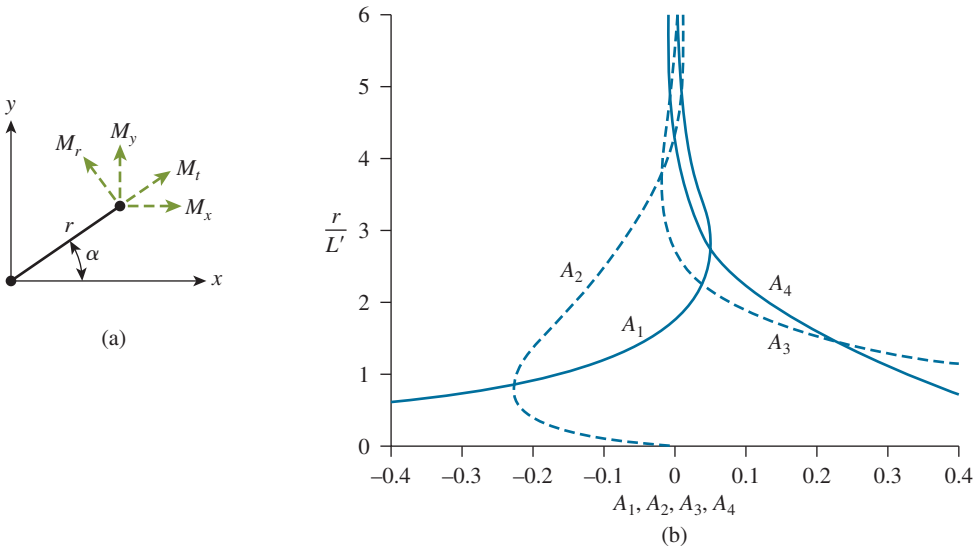


FIGURE 10.13 Approximate flexible method of mat design

The variations of A_1 and A_2 with r/L' are shown in Figure 10.13b. (For details see Hetenyi, 1946.)

In the Cartesian coordinate system (see Figure 10.13a),

$$M_x = M_t \sin^2\alpha + M_r \cos^2\alpha \tag{10.51}$$

and

$$M_y = M_t \cos^2\alpha + M_r \sin^2\alpha \tag{10.52}$$

Step 5. For the unit width of the mat, determine the shear force V caused by a column load:

$$V = \frac{Q}{4L'}A_3 \tag{10.53}$$

The variation of A_3 with r/L' is shown in Figure 10.13b.

Step 6. If the edge of the mat is located in the zone of influence of a column, determine the moment and shear along the edge. (Assume that the mat is continuous.) Moment and shear opposite in sign to those determined are applied at the edges to satisfy the known conditions.

Step 7. The deflection at any point is given by

$$\delta = \frac{QL'^2}{4R}A_4 \tag{10.54}$$

The variation of A_4 is presented in Figure 10.13b.

EXAMPLE 10.7

The plan of a mat foundation is shown in Figure 10.14. Calculate the soil pressure at points *A, B, C, D, E,* and *F*. (*Note:* All column sections are planned to be 0.5 m × 0.5 m.)

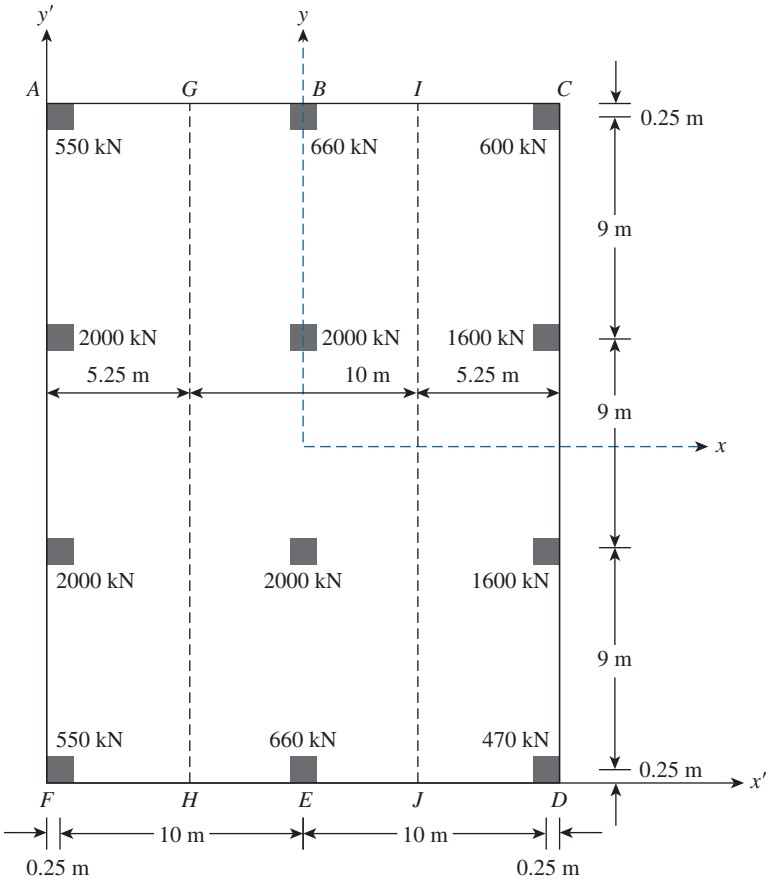


FIGURE 10.14 Plan of a mat foundation

SOLUTION

Eq. (10.25): $q = \dfrac{Q}{A} + \dfrac{M_y x}{I_y} + \dfrac{M_x y}{I_x}$

$$A = (20.5)(27.5) = 563.75 \text{ m}^2$$

$$I_x = \frac{1}{12}BL^3 = \frac{1}{12}(20.5)(27.5)^3 = 35{,}528 \text{ m}^4$$

$$I_y = \frac{1}{12}LB^3 = \frac{1}{12}(27.5)(20.5)^3 = 19{,}743 \text{ m}^4$$

$$Q = 470 + (2)(550) + 600 + (2)(660) + (2)(1600) + (4)(2000) = 14{,}690 \text{ kN}$$

$$M_y = Qe_x; \quad e_x = x' - \frac{B}{2}$$

$$x' = \frac{Q_1x_1' + Q_2x_2' + Q_3x_3' + \cdots}{Q}$$

$$= \frac{1}{14{,}690}\begin{bmatrix}(10.25)(660 + 2000 + 2000 + 660)\\ + (20.25)(470 + 1600 + 1600 + 600)\\ + (0.25)(550 + 2000 + 2000 + 550)\end{bmatrix} = 9.686 \text{ m}$$

$$e_x = x' - \frac{B}{2} = 9.686 - 10.25 = -0.565 \text{ m} \approx -0.57 \text{ m}$$

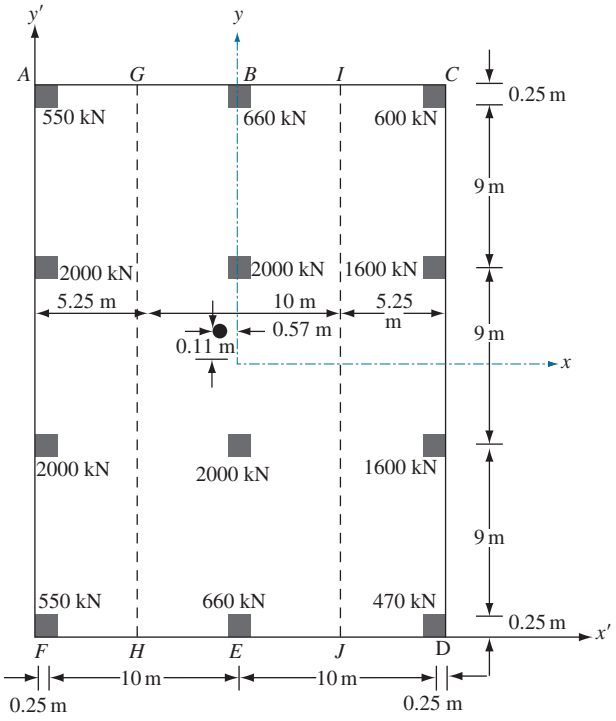


FIGURE 10.15

Hence, the resultant line of action is located to the left of the center of the mat. So $M_y = (14{,}690)(-0.57) = -8373\ \text{kN}\cdot\text{m}$. Similarly,

$$M_x = Qe_y; \quad e_y = y' - \frac{L}{2}$$

$$y' = \frac{Q_1 y_1' + Q_2 y_2' + Q_3 y_3' + \cdots}{Q}$$

$$= \frac{1}{14{,}690}\left[\begin{matrix}(0.25)(550 + 660 + 470) + (9.25)(2000 + 2000 + 1600) \\ +(18.25)(2000 + 2000 + 1600) + (27.25)(550 + 660 + 600)\end{matrix}\right]$$

$$= 13.86\ \text{m}$$

$$e_y = y' - \frac{L}{2} = 13.86 - 13.75 = 0.11\ \text{m}$$

The location of the line of action of the resultant column loads is shown in Figure 10.15.

$$M_x = (14{,}690)(0.11) = 1616\ \text{kN}\cdot\text{m}$$

So

$$q = \frac{14{,}690}{563.75} - \frac{8373x}{19743} + \frac{1616y}{35{,}528} = 26.0 - 0.42x + 0.05y\ (\text{kN/m}^2)$$

Therefore,

At *A*: $q = 26 - (0.42)(-10.25) + (0.05)(13.75) =$ **31.0 kN/m²**
At *B*: $q = 26 - (0.42)(0) + (0.05)(13.75) =$ **26.68 kN/m²**
At *C*: $q = 26 - (0.42)(10.25) + (0.05)(13.75) =$ **22.38 kN/m²**
At *D*: $q = 26 - (0.42)(10.25) + (0.05)(-13.75) =$ **21.0 kN/m²**
At *E*: $q = 26 - (0.42)(0) + (0.05)(-13.75) =$ **25.31 kN/m²**
At *F*: $q = 26 - (0.42)(-10.25) + (0.05)(-13.75) =$ **29.61 kN/m²**

EXAMPLE 10.8

Divide the mat shown in Figure 10.14 into three strips, such as *AGHF* ($B_1 = 5.25$ m), *GIJH* ($B_1 = 10$ m), and *ICDJ* ($B_1 = 5.25$ m). Using the result of Example 10.7, determine the bending moment and shear force diagrams in the y direction.

SOLUTION

Determination of Shear and Moment Diagrams for Strips:
Strip *AGHF*:

$$\text{Average soil pressure} = q_{av} = q_{(\text{at } A)} + q_{(\text{at } F)} = \frac{31 + 29.61}{2} = 30.305 \text{ kN/m}^2$$

$$\text{Total soil reaction} = q_{av} B_1 L = (30.305)\,(5.25)\,(27.5) = 4375 \text{ kN}$$

$$\text{Average load} = \frac{\text{load due to soil reaction} + \text{column loads}}{2}$$

$$= \frac{4375 + 5100}{2} = 4737.5 \text{ kN}$$

So, modified average soil pressure [from Eq. 10.32)],

$$q_{av(\text{modified})} = \frac{4737.5}{(5.25)(27.5)} = 32.81 \text{ kN/m}^2$$

The column loads can be modified in a similar manner by multiplying factor

$$F = \frac{4737.5}{5100} = 0.929$$

Figure 10.16 shows the loading on the strip and corresponding shear and moment diagrams. Note that the column loads shown in this figure have been multiplied by

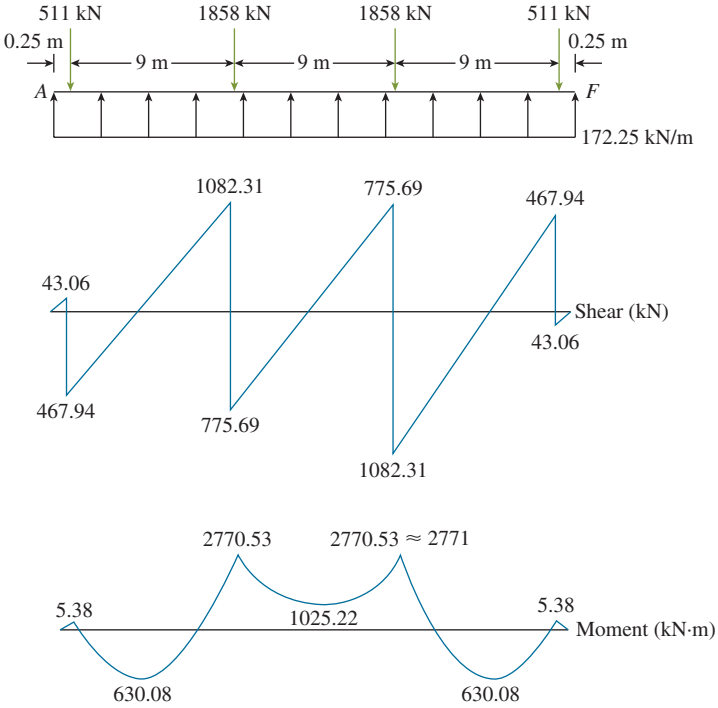


FIGURE 10.16 Load, shear, and moment diagrams for strip *AGHF*

$F = 0.929$. Also the load per unit length of the beam is equal to $B_1 q_{av(modified)} = (5.25)(32.81) = 172.25$ kN/m.

Strip *GIJH*: In a similar manner,

$$q_{av} = \frac{q_{(at\ B)} + q_{(at\ E)}}{2} = \frac{26.68 + 25.31}{2} = 26.0\ \text{kN/m}^2$$

$$\text{Total soil reaction} = (26)(10)(27.5) = 7150\ \text{kN}$$

$$\text{Total column load} = 5320\ \text{kN}$$

$$\text{Average load} = \frac{7150 + 5320}{2} = 6235\ \text{kN}$$

$$q_{av(modified)} = \frac{6235}{(10)(27.5)} = 22.67\ \text{kN/m}^2$$

$$F = \frac{6235}{5320} = 1.17$$

The load, shear, and moment diagrams are shown in Figure 10.17.

Strip *ICDJ*: Figure 10.18 shows the load, shear, and moment diagrams for this strip.

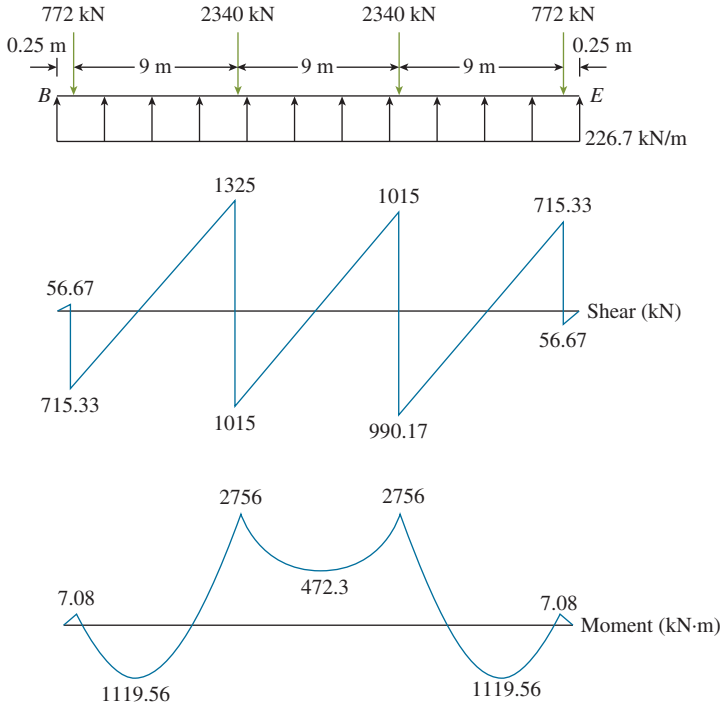


FIGURE 10.17 Load, shear, and moment diagrams for strip *GIJH*

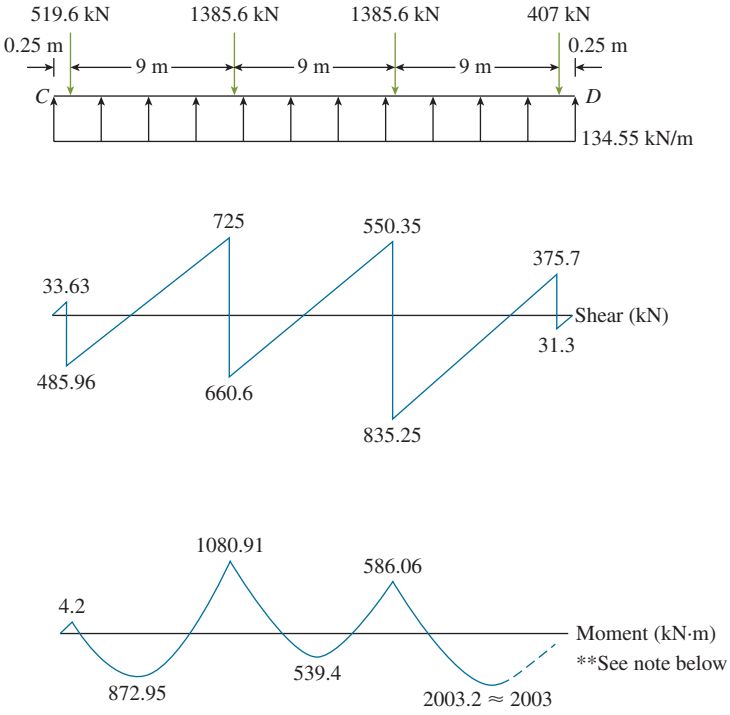


FIGURE 10.18 Load, shear, and moment diagrams for strip *ICDJ*

**Note: In view of the assumption of uniform soil reaction to nonsymmetric loading, there is a discrepancy in the moment values at the right column. As a result, the moment diagram will not "close." This is ignored since it is not the governing design moment.

10.9 Summary

When the columns are located too close to the property line and the loads are high, it may not be possible to provide pad footings without eccentricity that remain within the property line. Under these circumstances combined footings, either rectangular or trapezoidal, work well. Simple methods for determining the dimensions of rectangular and trapezoidal combined footings were discussed in this chapter.

A mat foundation may carry multiple columns and walls. The excavation required in placing the mat in the ground causes removal of overburden and thus reduces the net applied pressure significantly. The mat becomes partially or fully compensated, depending on the depth of excavation.

Designs of mat foundations are often governed by the settlement considerations rather than the bearing capacity. The tolerable settlement for mats can be on the order of 50–100 mm (see Section 9.16), depending on the structure.

The design of mat foundations is not straightforward because of the complex soil–structure interaction taking place. Two simplified methods, namely the conventional rigid method and the approximate flexible method, were presented in this chapter. The modulus of subgrade reaction k is the key parameter in the flexible method.

PROBLEMS

10.1 Refer to the rectangular combined footing in Figure 10.1, with $Q_1 = 100$ kip and $Q_2 = 150$ kip. The distance between the two column loads $L_3 = 13.5$ ft. The proximity of the property line at the left edge requires that $L_2 = 3.0$ ft. The net allowable soil pressure is 2500 lb/ft^2. Determine the breadth and length of a rectangular combined footing.

10.2 Refer to the trapezoidal combined footing in Figure 10.2, with $Q_1 = 200$ kip and $Q_2 = 100$ kip. The distance between the columns L_3 is 12.0 ft, and the net allowable soil pressure is 2600 lb/ft^2. It is required to maintain L_2 as 4.5 ft and L_1 as 3.0 ft. Determine the values for B_1 and B_2.

10.3 A 30 ft × 24 ft mat foundation is to be placed at 9 ft depth in a saturated clay where $c_u = 1200$ lb/ft^2 and $\phi = 0$. Determine the net ultimate bearing capacity.

10.4 A 10 m × 6 m mat foundation is placed at 2.0 m depth in sand where the average value of N_{60} is 23. Determine the allowable net pressure that would limit the settlement to 75 mm, using Eqs. (9.51) and (10.14).

10.5 A 36 ft × 27 ft mat foundation is placed at a depth of 9 ft within sand where N_{60} is 20. Using Eq. (10.15), estimate the elastic settlement when the net applied pressure is 5.2 kip/ft^2.

10.6 It is proposed to build an 8 story building with a footprint of 15 m × 20 m, resting on a mat foundation of the same dimensions, in a saturated clay where $c_u = 50$ kN/m^2, $\gamma = 19.0$ kN/m^3. Assume approximately 15 kN/m^2 per floor for the live and dead loads.

a. At what depth would you place the mat to make this a fully compensated foundation?

b. What should be the factor of safety if the mat is placed at 3.0 m depth?

10.7 A 15 m × 20 m mat foundation shown in Figure P10.7 carries a building load of 36 MN and is placed at 3.0 m depth below the ground level.

For the clay layer, the consolidation tests show that the preconsolidation pressure at the middle of the clay layer is 210 kN/m^2.

a. Find the net applied pressure on the underlying ground.

b. Is the clay overconsolidated?

c. What would be the consolidation settlement beneath the center of the mat?

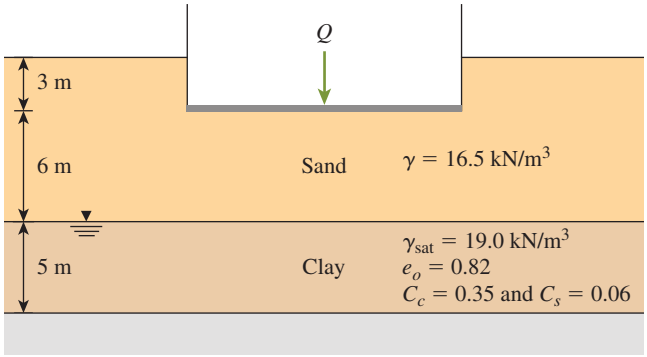


FIGURE P10.7

10.8 In Problem 10.7, determine the consolidation settlement under the corner of the mat.

10.9 A plate loading test was carried out on a medium dense sand, using a 1 ft wide square plate, and k_1 was determined as 350 lb/in^3. Determine the coefficient of subgrade reaction for a 7.5 ft wide square foundation and a 7.5 ft × 10.5 ft rectangular foundation.

10.10 A 300 mm × 450 mm plate was used in carrying out a plate loading test in a sand, during which the plate settled 5 mm under the applied pressure of 250 kN/m^2.

a. What is the coefficient of subgrade reaction for a 300 mm wide square plate?

b. What would be the coefficient of subgrade reaction of a 2 m × 3 m foundation?

10.11 For a 2.0 m wide and 0.40 m thick beam on an elastic foundation, determine the coefficient of subgrade reaction k using Eqs. (10.45) and (10.46), assuming the following parameters: $E_s = 30$ MN/m^2, $E_F = 30{,}000$ MN/m^2, $\mu_s = 0.25$.

REFERENCES

American Concrete Institute (2011). *ACI Standard Building Code Requirements for Reinforced Concrete*, ACI 318–11, Farmington Hills, MI.

American Concrete Institute Committee 336 (1988). "Suggested Design Procedures for Combined Footings and Mats," *Journal of the American Concrete Institute*, Vol. 63, No. 10, pp. 1041–1077.

Hetenyi, M. (1946). *Beams of Elastic Foundations*, University of Michigan Press, Ann Arbor, MI.

Meyerhof, G. G. (1965). "Shallow Foundations," *Journal of the Soil Mechanics and Foundations Division*, American Society of Civil Engineers, Vol. 91, No. SM2, pp. 21–31.

Rios, L. and Silva, F. P. (1948). "Foundations in Downtown São Paulo (Brazil)," *Proceedings, Second International Conference on Soil Mechanics and Foundation Engineering*, Rotterdam, Vol. 4, p. 69.

SCHULTZE, E. (1962). "Probleme bei der Auswertung von Setzungsmessungen," *Proceedings, Baugrundtagung*, Essen, Germany, p. 343.

TERZAGHI, K. (1955). "Evaluation of the Coefficient of Subgrade Reactions," *Geotechnique*, Institute of Engineers, London, Vol. 5, No. 4, pp. 197–226.

TERZAGHI, K. and PECK, R. B. (1948). *Soil Mechanics in Engineering Practice*. John Wiley & Sons, New York

VARGAS, M. (1948). "Building Settlement Observations in São Paulo," *Proceedings, Second International Conference on Soil Mechanics and Foundation Engineering*, Rotterdam, Vol. 4, p. 13.

VARGAS, M. (1961). "Foundations of Tall Buildings on Sand in São Paulo (Brazil)," *Proceedings, Fifth International Conference on Soil Mechanics and Foundation Engineering*, Paris, Vol. 1, p. 841.

VESIC, A. S. (1961). "Bending of Beams Resting on Isotropic Solid," *Journal of the Engineering Mechanics Division*, American Society of Civil Engineers, Vol. 87, No. EM2, pp. 35–53.

11

Load and Resistance Factor Design (LRFD)



Oliver Foerstner/Shutterstock.com

11.1 Introduction 428
11.2 Design Philosophy 429
11.3 Allowable Stress Design (ASD) 431
11.4 Limit State Design (LSD) and Partial Safety Factors 432
11.5 Load and Resistance Factor Design (LRFD) 433
11.6 Summary 436
PROBLEMS 436
REFERENCES 436

11.1 Introduction

Geotechnical engineers play an important role in the design and construction of buildings, bridges, dams, roads, and other infrastructure facilities. One of the main concerns in every design is the safety of the structure throughout its design life. An equally important consideration in any project is the cost. While an adequate level of safety must be maintained, its cost should not be excessive. Figure 11.1 shows the typical relationship between the level of safety and the project cost.

The level of safety required in a structure depends on the consequences of failure, design life, and the importance of the structure. Nuclear power plants require a very high level of safety, as the consequences of failure can be catastrophic. As seen in Figure 11.1, increasing the level of safety also increases the project cost significantly. In addition to safety and cost, it is also necessary to ensure that the structure or facility serves its intended purpose and meets the necessary criteria (e.g., settlement).

Most structures can be designed and built in various ways. These alternatives may have different levels of safety and cost. The other factors that influence decision making when selecting the best option are environmental issues and construction time.

In this chapter, we will discuss two different ways of carrying out the design:

- Allowable stress design (ASD), and
- Limit state design (LSD).

The allowable stress design method is the older of the two and has been presented in most textbooks, including this book. Limit state design is relatively new in geotechnical engineering and is becoming increasingly popular worldwide. This chapter provides only a general introduction to the limit state design approach in geotechnical engineering, known as *load and resistance factor design* (LRFD).

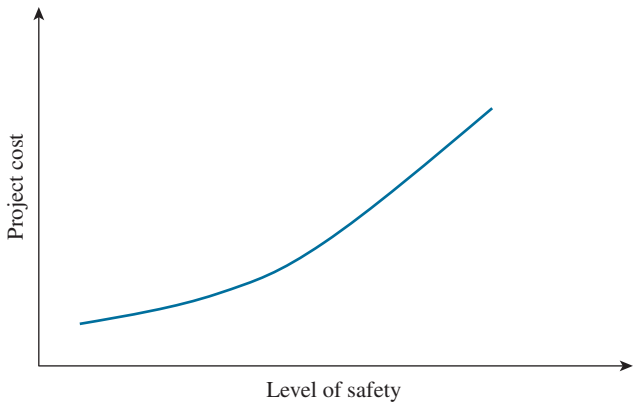


FIGURE 11.1 Safety versus cost

11.2 Design Philosophy

Any civil engineering design can be seen as a struggle between *capacity* and *demand*. When the capacity exceeds the demand throughout the design life, the design is satisfactory. In the case of a spread footing, the pressure applied by the footing to the underlying soil is the *demand*, and the ultimate bearing capacity is the *capacity*. Capacity depends on the material properties, and demand depends on the loadings. Due to the variability associated with the material properties and loadings, both capacity and demand are not deterministic—they are probabilistic variables, as seen in Figure 11.2, and follow specific probability distributions (e.g., normal, log-normal, or beta). Table 11.1 lists the capacities and demands associated with some typical geotechnical problems.

In Figure 11.2, $\overline{C}$ and $\overline{D}$ are the mean values of the capacity and demand, respectively. In the traditional *allowable stress design* (ASD) approach, the mean values $\overline{C}$ and $\overline{D}$ are estimated from material properties and the loadings. Considering the uncertainties associated with their determinations and the simplifications in the design methodology, a conservative factor of safety is used as

$$\text{FS} = \frac{\overline{C}}{\overline{D}} \tag{11.1}$$

Here, a single *lumped* factor of safety is used to account for (a) the variability associated with the different loads, including dead load, live load, wind load, and earthquake load; (b) variabilities in the soil parameters; and (c) the uncertainty arising from the design methodology. This factor of safety, typically in

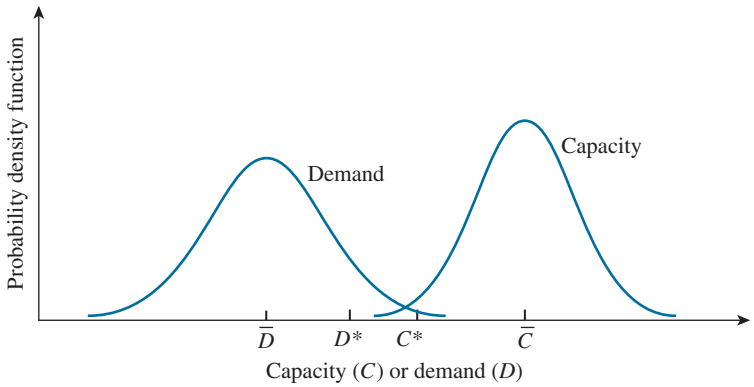


FIGURE 11.2 Capacity–demand model

TABLE 11.1 Some Simple Capacity–Demand Analogies

Problem	Capacity	Demand
Sliding of retaining wall	Resistance to sliding	Horizontal component of active load
Overturning of retaining wall	Moment resisting overturning	Driving moment in opposite direction, causing overturning
Piping due to seepage	Critical hydraulic gradient	Exit hydraulic gradient
Bearing capacity failure of a foundation	Ultimate bearing capacity	Pressure applied to the underlying soil

the range of 1.5–4.0, is based on experience, judgment, design method, quality and quantity of site investigation, and type of structure. As long as the factor of safety computed in Eq. (11.1) is greater than a recommended minimum value, the design is considered satisfactory.

The second and more modern approach is the limit state design, known as LRFD. Here, the capacity C^* under the worst-case scenario is estimated (i.e., underestimated) such that there is very little likelihood that the actual capacity will be less than this value. Similarly, the demand D^* is estimated (i.e., overestimated) such that there is very little likelihood that the actual demand will be more than this. The design is considered satisfactory if C^* is still greater than D^*. The factors to be used in underestimating the capacity and overestimating the demand are specified by the different design standards.

Compared with other engineering materials, such as steel or concrete, soil and rock have significant variability. This variability increases the risk associated with our predictions. Table 11.2 summarizes the coefficient of variation values of some

TABLE 11.2 Typical Values of Coefficient of Variation

Parameter	Coefficient of variation (%)
Void ratio, e	20–30
Porosity, n	20–30
Relative density, D_r	10–40
Specific gravity, G_s	2–3
Unit weight, γ	3–7
Buoyant unit weight, γ'	0–10
Liquid limit, LL	10–20
Plastic limit, PL	10–20
Plasticity index, PI	30–70 †
Optimum water (moisture) content, w_{opt}	20–40 ‡
Maximum dry density, $\gamma_{d(max)}$	5
California bearing ratio, CBR	25
Permeability (saturated), k	70–90
Permeability (unsaturated), k	130–240
Coefficient of consolidation, c_v	25–70
Compression index, C_c	10–40
Preconsolidation pressure, σ'_c	10–35
Friction angle (sand), ϕ'	10
Friction angle (clay), ϕ'	10–50
Friction angle (mine tailings), ϕ'	5–20
Undrained shear strength of clay, c_u	20–40
Standard penetration test blow count, N	20–40
Cone (electric) resistance, q_c	5–15
Cone (mechanical) resistance, q_c	15–35
Undrained shear strength of clay from field vane, c_u	10–30

† Lower values for clay and higher ones for sandy/gravelly clay
‡ Lower values for clay and higher ones for granular soil

geotechnical parameters reported in the literature (Duncan 2000; Sivakugan 2011). Here, the coefficient of variation is defined as

$$\text{Coefficient of variation (\%)} = \frac{\text{Standard deviation}}{\text{Mean}} \times 100 \tag{11.2}$$

11.3 Allowable Stress Design (ASD)

The allowable stress design (ASD), also known as the *working stress design*, has been used in civil engineering since the early 1800s. Here, the loading (S) is compared against the resistance (R) provided by the structure, and a factor of safety (FS) is defined as follows:

$$\text{FS} = \frac{R}{S} \tag{11.3}$$

There can be considerable uncertainties associated with the magnitudes of the parameters required for determining the loading (S) and the resistance (R). In addition, there are many assumptions, idealizations, and approximations made in the design method that introduce further uncertainty. For example, we often treat soil as a homogeneous isotropic linear elastic continuum, which is rarely true. To account for the variability in the design parameters and the uncertainty introduced by the design methods, a single lumped factor of safety, FS, is used, which can be tweaked to account for the importance of the structure and the consequence of any possible failure. These lumped factors of safety can be in the range of 1.5–4.0. The larger values are common in geotechnical engineering, where the uncertainties in the design parameters and the approximations are high or the risk of failure is high (e.g., bearing capacity of a foundation, piping beneath a dam). In the case of earthworks and temporary structures, like cofferdams or excavations, we live with lower factors of safety on the order of 1.2–1.5. Table 11.3 summarizes some typical values of lumped factors of safety used in practice. The safety factor is a reflection of the probability of failure during the service life. For example, it is expected that the probability of failure during the service life is on the order of 1×10^{-2} for earthworks, 1×10^{-3} for earth retaining structures, and 1×10^{-4} for foundations (Meyerhof, 1984).

TABLE 11.3 Typical Values of Factors of Safety

Structure	FS	Reference
Shallow foundations		
Spread footings in compression	2.0–3.0	Bowles 1988
Mat foundations	1.7–2.5	Bowles 1988
Uplift	1.7–2.5	Bowles 1988
Pile foundations in compression		
Verified by static load tests	2.0	USACE 1991
Verified by pile driving analyser (PDA)	2.5	USACE 1991
Not verified by static load tests or PDA	3.0	USACE 1991
From pile driving equations	3.0–6.0	
Retaining walls		
Sliding (if passive resistance neglected)	1.5	Goodman and Karol 1968
Sliding (if passive resistance included)	2.0	Goodman and Karol 1968

(Continued)

TABLE 11.3 Typical Values of Factors of Safety (*Continued*)

Structure	FS	Reference
Overturning (granular backfill)	1.5	Teng 1962
Overturning (cohesive backfill)	2.0	Teng 1962
Seepage		
Piping	3.0–5.0	Bowles 1988
Heave or uplift	1.5–2.5	Bowles 1988
Earthworks	1.2–1.6	Bowles 1988
Temporary braced excavations	1.2–1.5	Bowles 1988
Sheet piling coffer dams	1.2–1.6	Bowles 1988

11.4 Limit State Design (LSD) and Partial Safety Factors

Limit state design (LSD) in structural engineering was first introduced in the 1980s, but the geotechnical counterparts have been much slower in adopting this. In the context of structural engineering, the *limit state* is the state at which a structural component ceases to perform as intended. The two subsets of limit state are the *ultimate limit state* (ULS) and *serviceability limit state* (SLS). These are checked by using design loads (denoted by S) and design resistances (denoted by R) that are factored conservatively, where the loads are overestimated and the resistances are underestimated. No separate factor of safety is used in limit state designs, since the loads and resistances are already adjusted using *partial factors of safety* (ψ for loads and Φ for resistance parameters). The load factors are greater than 1, and the resistance factors are less than 1. Some of the factors suggested by the *Canadian Foundation Engineering Manual* (1992) are given in Table 11.4.

The ultimate limit state implies failure or collapse, which can be in tension, compression, shear, or bending. These different *modes of failure* should be checked separately, each constituting a limit state. The serviceability limit state has nothing to do with failure or collapse. This is introduced to address the other concerns, such as deflection, settlement, tilt, vibration, noise, etc., which must be within tolerable limits so the structure remains functional for its intended use. There may be no signs of imminent failure when the serviceability limits are reached. The tolerance values used for deflection, differential settlement, vibration, etc. depend on the purpose for which the structure or facility is built and can vary significantly between structures.

TABLE 11.4 Typical Values for Load Factor (ψ) and Resistance Factor (Φ) (Based on *Canadian Foundation Engineering Manual*, 1992)

Category	Item	Factor
Loads:	Dead loads	$\psi = 1.25$
	Live, wind, or earthquake load	$\psi = 1.50$
	Water pressure	$\psi = 1.25$
Shear strength:	Cohesion (stability, earth pressure)	$\Phi = 0.65$
	Cohesion (foundations)	$\Phi = 0.50$
	Friction ($\tan \phi'$)	$\Phi = 0.80$

For any geotechnical problem, the factored loading S^* (similar to demand) is computed as

$$S^* = \sum_{i=1}^{n} \psi_i S_i \tag{11.4}$$

where S_i accounts for the effects from various permanent, variable, and accidental loads and ψ_i are the corresponding load factors. Permanent loads include dead loads and water thrust that act throughout the design life. Variable loads include live loads, wind loads, snow loads, and traffic loads that act only over a limited duration. Accidental loads include seismic loads, explosions, and vehicle impacts.

The factored resistance R^* (similar to capacity) is computed using the factored material properties as

$$R^* = \sum_{i=1}^{n} \Phi_i R_i \tag{11.5}$$

The design is considered adequate if

$$S^* \leq R^* \tag{11.6}$$

The limit state designs for geotechnical designs work better with the structural engineering codes that have been based on the same design philosophy for decades. In addition, they make it possible to compute the probability of failure and quantify risk more rationally, in a move toward reliability-based designs.

11.5 Load and Resistance Factor Design (LRFD)

Load and resistance factor design (LRFD) is a limit state design approach that is becoming increasingly popular in geotechnical engineering. The load effects are computed by considering several possible loading scenarios: the range of load combinations, the magnitudes of the load and resistance factors, the varying ways they are applied among countries, the different agencies (e.g., AASHTO, IBC), and the type of the problem (e.g., shallow foundations, retaining walls, etc.).

There are two slightly different approaches to LRFD. In both methods, the factored load S^* [Eq. (11.4)] is computed the same way. It is the way the factored resistance R^* is computed that differs.

Method 1: Partial resistance factor

Equations (11.4), (11.5), and (11.6) form the basis for this method. It can be seen from Eq. (11.5) that separate resistance factors are applied to the different strength parameters, such as cohesion and friction angle. These reduced strength parameters are used in computing the final resistance R^*. This method is illustrated in Example 11.1.

Method 2: Total resistance factor

Here a single strength reduction factor Φ is applied to the resistance value R computed using the unadjusted material parameters. Therefore, Eq. (11.5) becomes

$$R^* = \Phi R \tag{11.7}$$

This method is illustrated in Example 11.2. Some of the strength reduction factors for LRFD, as recommended by the AASHTO bridge design specifications, are given in Table 11.5.

When computing the load effects in Eq. (11.4), it is necessary to consider all possible load combinations and use the worst-case scenario. Scott et al. (2003) summarized the load factors for foundation designs suggested by some major institutions. These factors are given in Table 11.6.

TABLE 11.5 Resistance Factors Suggested by AASHTO (2012)

Structure	Resistance factor
Bearing capacity of shallow foundations	0.45–0.55
Bearing capacity of driven piles	
From load tests	0.75–0.80
From pile driving formulas	0.10–0.40
From static analysis: clay and mixed soil	
α-method	0.35
β-method	0.25
λ-method	0.40
From static analysis in sands	0.45

TABLE 11.6 Load Factors for Foundation Designs

	United States				Canada		Europe	
Load type	**AASHTO**	**ACI**	**AISC**	**API**	**MOT**	**NRC**	**DGI**	**ECS**
Dead	1.25–1.95	1.4	1.2–1.4	1.1–1.3	1.1–1.5	1.25	1.0	1.0–1.35
	(0.65–0.9)	(0.9)	(0.9)	(0.9)	(0.65–0.95)	(0.85)	(0.85)	(0.95)
Live	1.35–1.75	1.7	1.6	1.1–1.5	1.15–1.4	1.5	1.3	1.3–1.5
				(0.8)				
Wind	1.4	1.3	1.3	1.2–1.35	1.3	1.5	1.3	1.3–1.5
Seismic	1.0	1.4	1.0	0.9	1.3	1.0	1.0	1.0

Note: Values in parentheses apply when the load is favorable and resists failure.

AASHTO = American Association of State Highway Transportation Officials
ACI = American Concrete Institute
AISC = American Institute of Steel Construction
API = American Petroleum Institute
MOT = Ministry of Transportation
NRC = National Research Council of Canada
DGI = Danish Geotechnical Institute
ECS = Eurocode

Some of the common load combinations that are considered in the designs are:

$$Q = 1.25\,Q_D + 1.75\,Q_L \tag{11.8}$$

$$Q = 1.25\,Q_D + 1.35\,Q_L + 0.4\,Q_W \tag{11.9}$$

where Q = design load, Q_D = dead load, Q_L = live load, and Q_W = wind load.

EXAMPLE 11.1

A square pad foundation of 2.0 m width is placed at a depth of 1.0 m in a granular soil where $\phi' = 35°$ and $\gamma = 19.0$ kN/m^3. It is expected that the live load is 80% of the dead load. Determine the maximum dead load that can be applied to the footing based on

a. an allowable stress design with FS = 3, and
b. a limit state design using load and resistance factors in Table 11.4.

Use the bearing capacity equation [Eq. (6.19)] and the bearing capacity factors (Table 6.1) in Section 6.3 for simplicity.

SOLUTION

Part a: Allowable stress design

For $\phi' = 35°$, from Table 6.1, $N_q = 41.44$ and $N_\gamma = 45.41$. From Eq. (6.19),

$$q_u = 1.3c'N_c + qN_q + 0.4\gamma BN_\gamma$$
$$q_u = (19.0 \times 1)(41.44) + 0.4(19.0)(2.0)(45.45) = 1477.6 \text{ kN/m}^2$$
$$q_{all} = \frac{1477.6}{3} = 492.5 \text{ kN/m}^2$$

Assume the dead load is P kN. The live load is then $0.8P$ kN, so the total load acting on the footing is $1.8P$. The pressure applied to the soil is $\frac{1.8P}{2 \times 2} = 0.45P$ kN/m^2.

$$0.45P \leq 492.5$$

Therefore, $\boldsymbol{P \leq 1094.4 \text{ kN}}$.

Part b: Limit state design

Applying the resistance factors from Table 11.4,

$$\tan \phi' = 0.8 \times \tan 35 = 0.560; \phi' = 29.3°$$

From Table 6.1, $N_q = 20.72$ and $N_\gamma = 17.07$. From Eq. (6.19),

$$q_u = 1.3c'N_c + qN_q + 0.4\gamma BN_\gamma$$
$$q_u = (19.0 \times 1)(20.72) + 0.4(19.0)(2.0)(17.07) = 653.1 \text{ kN/m}^2$$

Applying the load factors from Table 11.4, Total load $= 1.25(P) + 1.5(0.8P) = 2.45P$. The pressure applied to the soil is $\frac{2.45P}{2 \times 2} = 0.6125P$ kN/m^2.

$$0.6125P \leq 653.1$$

Therefore, $\boldsymbol{P \leq 1066.3 \text{ kN}}$.

Both methods give similar results. ■

EXAMPLE 11.2

Based on LRFD, determine the maximum dead load that can be applied on the 2.0 m wide footing from Example 11.1. Assume the following load/resistance factors:

load factor for dead load = 1.25

load factor for live load = 1.75

strength reduction factor on the ultimate bearing capacity = 0.50

SOLUTION

Total load = 1.25 (P) + 1.75 (0.8P) = 2.65P. The pressure applied to the soil is $\frac{2.65P}{2 \times 2} = 0.6625P$ kN/m^2.

Thus, $S^* = 0.6625P$ kN/m^2. For $\phi' = 35°$, from Table 6.1, $N_q = 41.44$ and $N_\gamma = 45.41$. From Eq. (6.19),

$$q_u = 1.3c'N_c + qN_q + 0.4\gamma BN_\gamma$$

$$q_u = (19.0 \times 1)(41.44) + 0.4(19.0)(2.0)(45.45) = 1477.6 \text{ kN/m}^2$$

$$R^* = 0.5 \times 1477.6 = 738.8 \text{ kN/m}^2$$

For $S^* \leq R^*$, $0.6625P \leq 738.8$.

$$\boldsymbol{P \leq 1115.2 \text{ kN}}$$

It can be seen that the two different approaches in Example 11.1 and the one adopted in this example give similar results.

11.6 Summary

These were the main points covered in this chapter:

1. Allowable stress design (ASD) is older than load and resistance factor design (LRFD).
2. There is a notable difference in the way the *resistance factors* can be applied in LRFD: (a) multiple resistance factors applied to the strength parameters (such as cohesion and friction angle), and (b) one single resistance factor applied to the final computed soil resistance.
3. LRFD is a limit state design approach.
4. In LRFD, the factor of safety is built into the load and resistance factors. No separate factor of safety is used.
5. LRFD requires that the factored load is less than the factored resistance.

PROBLEMS

11.1 A continuous foundation is required in a soil where $c' = 10$ kN/m^2, $\phi' = 26°$, and $\gamma = 19.0$ kN/m^3. The depth of the footing will be 1.0 m. The dead load and the live load are 600 kN/m and 400 kN/m, respectively. Determine the required width for the foundation based on allowable stress design with FS = 3, using Eq. (6.10) and Table 6.1.

11.2 Repeat Problem 11.1 based on limit state design, using the factors given in Table 11.4.

11.3 Repeat Problem 11.1 based on LRFD using the following factors:

load factor for dead load = 1.25
load factor for live load = 1.75
strength reduction factor on the ultimate bearing capacity = 0.50

REFERENCES

AASHTO (2012). *AASHTO LRFD Bridge Design Specifications*, Washington, DC.

Bowles, J. E. (1988). *Foundation Analysis and Design*, 4th ed., McGraw-Hill, New York.

CFEM (1992). *Canadian Foundation Engineering Manual*, 3rd ed., Canadian Geotechnical Society, Canada.

Duncan, J. M. (2000). "Factor of Safety and Reliability in Geotechnical Engineering," *Journal of Geotechnical and Geoenvironmental Engineering*, American Society of Civil Engineers, Vol. 126, No. 4, pp. 307–316.

Goodman, L. J., and Karol, R.H. (1968). *Theory and Practice of Foundation Engineering*, Macmillan Publishing Co., New York.

Meyerhof, G. G. (1984). "Safety Factors and Limit States Analysis in Geotechnical Engineering," *Canadian Geotechnical Journal*, Vol. 21, pp. 1–7.

Scott, B., Kim, B. J., and Salgado, R. (2003). "Assessment of Current Load Factors for Use in Geotechnical Load and Resistance Factor Design," *Journal of Geotechnical and Geoenvironmental Engineering*, American Society of Civil Engineers, Vol. 129, No. 4, pp. 287–295.

Sivakugan, N. (2011). "Engineering Properties of Soil," Chapter 1 in *Geotechnical Engineering Handbook*, Ed. B. M. Das, J. Ross Publishing, Florida.

Teng, W. C. (1962). *Foundation Design*, Prentice Hall, Englewood Cliffs, NJ.

USACE (1991). *Design of Pile Foundations*, Engineering Design Manual EM 1110-2-2906, U.S. Army Corps of Engineers, Washington, DC.

12

Pile Foundations



DESIGNFACTS/Shutterstock.com

12.1 Introduction 439
12.2 Pile Materials 440
12.3 Continuous Flight Auger (CFA) Piles 450
12.4 Point Bearing and Friction Piles 451
12.5 Installation of Piles 452
12.6 Pile Driving 453
12.7 Load Transfer Mechanism 458
12.8 Equations for Estimating Pile Capacity 461
12.9 Meyerhof's Method for Estimating Q_p 463
12.10 Vesic's Method for Estimating Q_p 466
12.11 Coyle and Castello's Method for Estimating Q_p in Sand 469
12.12 Correlations for Calculating Q_p with SPT and CPT Results in Granular Soil 473
12.13 Frictional Resistance (Q_s) in Sand 474
12.14 Frictional (Skin) Resistance in Clay 480
12.15 Ultimate Capacity of Continuous Flight Auger Pile 485
12.16 Point Bearing Capacity of Piles Resting on Rock 487
12.17 Pile Load Tests 493
12.18 Elastic Settlement of Piles 497
12.19 Laterally Loaded Piles 502
12.20 Pile-Driving Formulas 514
12.21 Pile Capacity for Vibration-Driven Piles 520
12.22 Wave Equation Analysis 521
12.23 Negative Skin Friction 524
12.24 Group Efficiency 528
12.25 Ultimate Capacity of Group Piles in Saturated Clay 531
12.26 Elastic Settlement of Group Piles 534
12.27 Consolidation Settlement of Group Piles 536
12.28 Piles in Rock 538
12.29 Summary 539

PROBLEMS 539

REFERENCES 543

12.1 Introduction

Piles are structural members made of steel, concrete, or timber. They are deep foundations where the depth (or length) is significantly larger than the width. Unlike the shallow foundations discussed in Chapters 6, 7, and 8, deep foundations require special equipment and skill and hence cost more. Therefore, piles are considered only in situations where shallow foundations prove to be inadequate (e.g., large loads or poor soil conditions). Piles are recommended in the following situations:

1. *In weak ground conditions*
   When the soil conditions near the surface are poor, shallow foundations will not be able to carry the building loads, and deep foundations are required. If bedrock is present at reasonable depth, it is possible to drive the pile into the bedrock and transfer the entire load to the bedrock (Figure 12.1a). Generally, when the pile is driven into a thick deposit of soil, the load applied on the *pile head* is transferred to the soil through the *pile tip* (or *point*) and the *pile shaft*, as shown in Figure 12.1b.
2. *For carrying lateral loads*
   Tall buildings, earth-retaining structures, transmission towers, and chimneys can be subjected to large lateral loading due to wind loads, earth pressures,

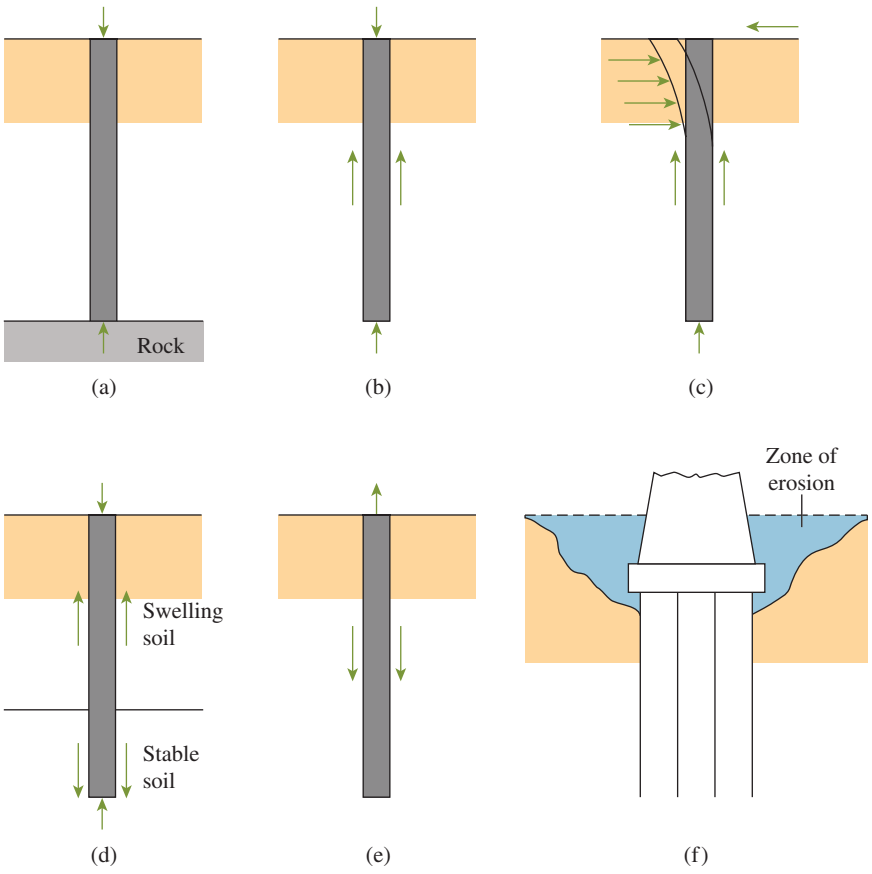


FIGURE 12.1 Conditions that require the use of pile foundations

or seismic loads. Unlike shallow foundations, the piles can resist lateral loads very effectively (Figure 12.1c). Sometimes these piles are installed at an angle to the vertical to resist the lateral load and are known as *batter piles*.

3. *In expansive or collapsible soil*
   Expansive soil pose a significant threat to low-rise buildings, roads, and other infrastructure in many parts of the world. Shallow foundations placed in expansive soil can undergo repeated swelling and shrinkage due to seasonal variations, which cause considerable damage to the superstructure. Piles can be driven well beyond the depths where the expansive soil are present, so this problem can be avoided (Figure 12.1d).

   Collapsible soil such as loess become weaker when saturated and undergo large settlements. Here, too, piles can be driven beyond the depths where such problematic soil are present.

4. *For resisting uplift*
   In transmission towers, offshore platforms, and situations where the basement or pump house lies below the water table, the foundations must be able to resist uplift. Piles can be very effective for such situations (Figure 12.1e). Sometimes, the bottoms of the piles are enlarged to provide anchorage against uplift. Such piles are known as "belled" or "underreamed" piles. These are discussed further in Chapter 13.

5. *For bridge abutments*
   Bridge abutments and piers are usually constructed over pile foundations to avoid the loss of bearing capacity that a shallow foundation may suffer because of soil erosion at the ground level (Figure 12.1f).

6. *As compaction piles*
   Under certain circumstances, piles are driven into granular soil to achieve proper compaction of soil close to the ground surface. These piles are called compaction piles. The lengths of compaction piles depend on the relative density of the soil before and after the compaction and the required depth of compaction. These piles are generally short; however, some field tests are necessary to determine a reasonable length.

Although numerous investigations, both theoretical and experimental, have been conducted in the past to predict the behavior and the load-bearing capacity of piles in granular and cohesive soil, the mechanisms are not yet entirely understood and may never be. The design and analysis of pile foundations may thus be considered somewhat of an art as a result of the uncertainties involved in working with some subsoil conditions. This chapter discusses the present state of the art.

12.2 Pile Materials

Different types of piles are used in practice, depending on the type of load to be carried, soil conditions, location of the water table, and the installation technique that is required. The three major materials used for making piles are steel, concrete, and timber. They are discussed in this section, along with their structural characteristics.

STEEL PILES

Steel piles generally are either *pipe piles* or *rolled steel* H-*section piles* that are installed by driving. Pipe piles can be driven into the ground with their ends open or closed. Wide-flange and I-section steel beams can also be used as piles. However, H-section piles are usually preferred because their web and flange thicknesses are equal. (In wide-flange and I-section beams, the web thicknesses are smaller than the thicknesses of the flange.) Table 12.1 gives the dimensions of some standard H-section steel piles used in the United States. Table 12.2 shows selected pipe sections frequently used for piling purposes. In many cases, the pipe piles are filled with concrete after they have been driven and they become *composite piles*.

TABLE 12.1a Common H-Pile Sections Used in the United States (SI Units)

Designation, size (mm) × weight (kg/m	Depth d_1 (mm)	Section area ($m^2 \times 10^{-3}$)	Flange and web thickness w (mm)	Flange width d_2 (mm)	Moment of inertia ($m^4 \times 10^{-6}$)	
					I_{xx}	I_{yy}
HP 200 × 53	204	6.84	11.3	207	49.4	16.8
HP 250 × 85	254	10.8	14.4	260	123	42
× 62	246	8.0	10.6	256	87.5	24
HP 310 × 125	312	15.9	17.5	312	271	89
× 110	308	14.1	15.49	310	237	77.5
× 93	303	11.9	13.1	308	197	63.7
× 79	299	10.0	11.05	306	164	62.9
HP 330 × 149	334	19.0	19.45	335	370	123
× 129	329	16.5	16.9	333	314	104
× 109	324	13.9	14.5	330	263	86
× 89	319	11.3	11.7	328	210	69
HP 360 × 174	361	22.2	20.45	378	508	184
× 152	356	19.4	17.91	376	437	158
× 132	351	16.8	15.62	373	374	136
× 108	346	13.8	12.82	371	303	109

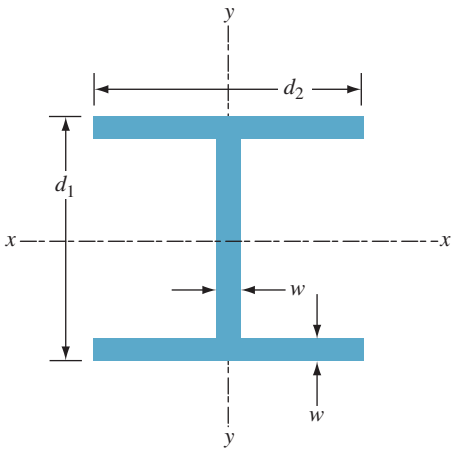


TABLE 12.1b Common H-Pile Sections Used in the United States (English Units)

Designation size (in.) × weight (lb/ft)	Depth d_1 (in.)	Section area (in^2)	Flange and web thickness w (in.)	Flange width d_2 (in.)	Moment of inertia (in^4)	
					I_{xx}	I_{yy}
HP 8 × 36	8.02	10.6	0.445	8.155	119	40.3
HP 10 × 57	9.99	16.8	0.565	10.225	294	101
× 42	9.70	12.4	0.420	10.075	210	71.7
HP 12 × 84	12.28	24.6	0.685	12.295	650	213
× 74	12.13	21.8	0.610	12.215	570	186
× 63	11.94	18.4	0.515	12.125	472	153
× 53	11.78	15.5	0.435	12.045	394	127
HP 13 × 100	13.15	29.4	0.766	13.21	886	294
× 87	12.95	25.5	0.665	13.11	755	250
× 73	12.74	21.6	0.565	13.01	630	207
× 60	12.54	17.5	0.460	12.90	503	165
HP 14 × 117	14.21	34.4	0.805	14.89	1220	443
× 102	14.01	30.0	0.705	14.78	1050	380
× 89	13.84	26.1	0.615	14.70	904	326
× 73	13.61	21.4	0.505	14.59	729	262

TABLE 12.2a Selected Pipe Pile Sections (SI Units)

Outside diameter (mm)	Wall thickness (mm)	Area of steel (cm^2)
219	3.17	21.5
	4.78	32.1
	5.56	37.3
	7.92	52.7
254	4.78	37.5
	5.56	43.6
	6.35	49.4
305	4.78	44.9
	5.56	52.3
	6.35	59.7
406	4.78	60.3
	5.56	70.1
	6.35	79.8
457	5.56	80
	6.35	90
	7.92	112
508	5.56	88
	6.35	100
	7.92	125
610	6.35	121
	7.92	150
	9.53	179
	12.70	238

TABLE 12.2b Selected Pipe Pile Sections (English Units)

Outside diameter (in.)	Wall thickness (in.)	Area of steel (in^2)
$8\frac{5}{8}$	0.125	3.34
	0.188	4.98
	0.219	5.78
	0.312	8.17
10	0.188	5.81
	0.219	6.75
	0.250	7.66
12	0.188	6.96
	0.219	8.11
	0.250	9.25
16	0.188	9.34
	0.219	10.86
	0.250	12.37
18	0.219	12.23
	0.250	13.94
	0.312	17.34
20	0.219	13.62
	0.250	15.51
	0.312	19.30
24	0.250	18.7
	0.312	23.2
	0.375	27.8
	0.500	36.9

The allowable structural capacity for steel piles is

$$Q_{all} = A_s f_s \tag{12.1}$$

where

A_s = cross-sectional area of the steel

f_s = allowable stress of steel ($\approx 0.33–0.5 f_y$)

Once the design load is determined from geotechnical consideration, it is necessary to ensure that it does not exceed the allowable load defined by Eq. (12.1).

When necessary, steel piles are spliced by welding or by riveting. Figure 12.2a shows a typical splice by welding for an H-pile. A typical splice by welding for a pipe pile is shown in Figure 12.2b. Figure 12.2c is a diagram of a splice of an H-pile by rivets or bolts.

When hard driving conditions are expected, such as driving through dense gravel, shale, or soft rock, steel piles can be fitted with driving points or shoes. Figures 12.2d and 12.2e are diagrams of two types of shoes used for pipe piles.

Steel piles may be subject to corrosion. For example, swamps, peats, and other organic soil are corrosive. Soil that have a pH greater than 7 are not so corrosive. To offset the effect of corrosion, an additional thickness of steel (over the actual

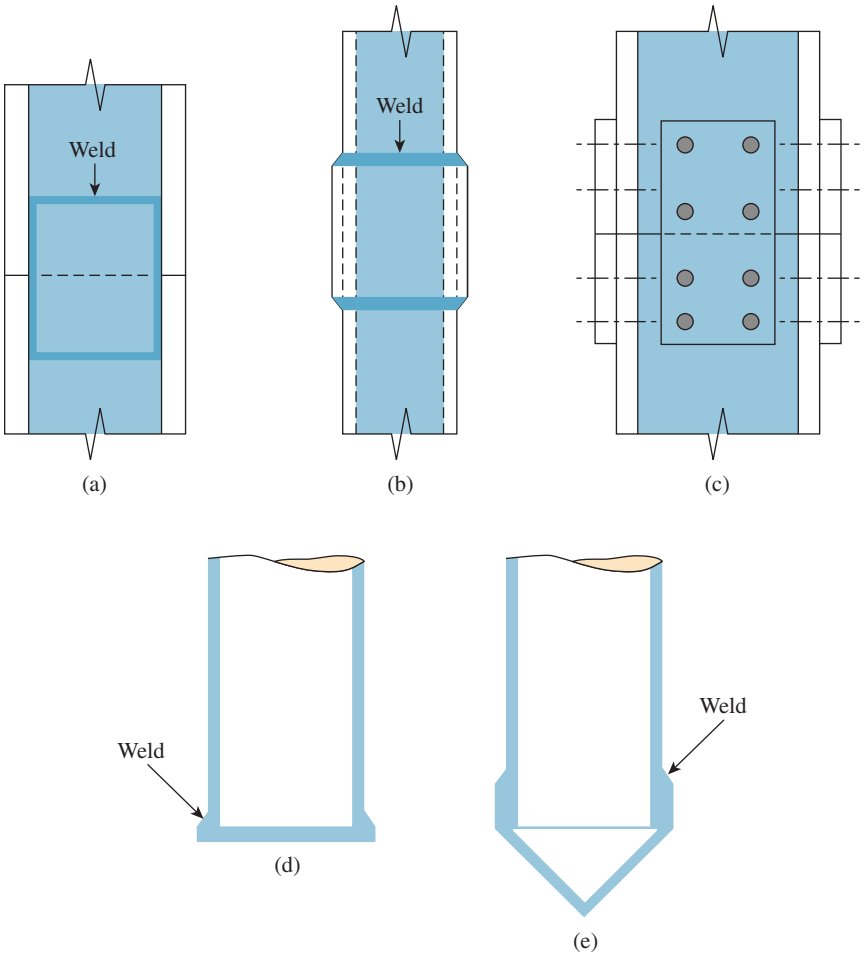


FIGURE 12.2 Steel piles: (a) splicing of H-pile by welding; (b) splicing of pipe pile by welding; (c) splicing of H-pile by rivets and bolts; (d) flat driving point of pipe pile; (e) conical driving point of pipe pile



(a) (b)

FIGURE 12.3 Installation of steel piles: (a) H-pile; (b) pipe pile (Courtesy of N. Sivakugan, James Cook University, Australia)

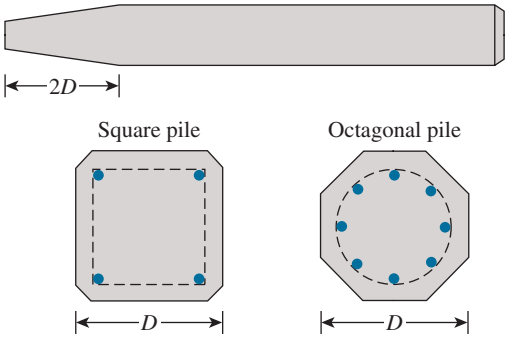
designed cross-sectional area) is generally recommended. In many circumstances, factory-applied epoxy coatings on piles work satisfactorily against corrosion. These coatings are not easily damaged by pile driving. Concrete encasement of steel piles in most corrosive zones also protects against corrosion. Figure 12.3 shows the installation of steel piles, which is generally by driving.

Here are some general facts about steel piles:

- Usual length: 15 m to 60 m (50 ft to 200 ft)
- Usual load: 300 kN to 1200 kN (67 kip to 265 kip)
- Advantages:
  - **a.** Easy to handle with respect to cutoff and extension to the desired length through splicing
  - **b.** Can stand high driving stresses
  - **c.** Can penetrate hard layers such as dense gravel and soft rock
  - **d.** High load-carrying capacity
- Disadvantages:
  - **a.** Relatively costly
  - **b.** High level of noise during pile driving
  - **c.** Subject to corrosion
  - **d.** H-piles may be damaged or deflected from the vertical during driving through hard layers or past major obstructions

CONCRETE PILES

Concrete piles may be divided into two basic categories: (a) precast piles and (b) cast-*in-situ* piles. *Precast piles* can be prepared by using ordinary reinforcement, and they can be square or octagonal in cross section (see Figure 12.4). Reinforcement is provided to enable the pile to resist the bending moment developed during pickup and transportation, the vertical load, and the bending moment caused by a lateral load. The piles are cast to desired lengths and cured before being transported to the work sites.



(a)



(b)

FIGURE 12.4 Precast piles with ordinary reinforcement: (a) schematic diagram; (b) photograph of 24 m long octagonal piles ready for driving (Courtesy of N. Sivakugan, James Cook University, Australia)

Some general facts about concrete piles are as follows:

- Usual length: 10 m to 15 m (30 ft to 50 ft)
- Usual load: 300 kN to 3000 kN (67 kip to 675 kip)
- Advantages:
  - **a.** Can be subjected to hard driving
  - **b.** Corrosion resistant
  - **c.** Can be easily combined with a concrete superstructure
- Disadvantages:
  - **a.** Difficult to achieve proper cutoff
  - **b.** Difficult to transport

Precast piles can also be prestressed by the use of high-strength steel prestressing cables. The ultimate strength of these cables is about 1800 MN/m^2 (≈260 ksi). During casting of the piles, the cables are pretensioned to about 900 to 1300 MN/m^2 (≈130 to 190 ksi), and concrete is poured around them. After curing, the cables are cut, producing a compressive force on the pile section. Table 12.3 gives additional information about prestressed concrete piles with square and octagonal cross sections.

Some general facts about precast prestressed piles are as follows:

- Usual length: 10 m to 45 m (30 ft to 150 ft)
- Maximum length: 60 m (200 ft)
- Maximum load: 7500 kN to 8500 kN (1700 kip to 1900 kip)

The advantages and disadvantages are the same as those of precast piles.

Cast-in-situ, or *cast-in-place, piles* are built by making a hole in the ground and then filling it with concrete. Various types of cast-in-place concrete piles are currently used in construction, and most of them have been patented by their manufacturers. These piles may be divided into two broad categories: (a) cased and (b) uncased. Both types may have a pedestal at the bottom.

Cased piles are made by driving a steel casing into the ground with the help of a mandrel placed inside the casing. When the pile reaches the proper depth, the mandrel is withdrawn and the casing is filled with concrete. Figures 12.5a, 12.5b, 12.5c, and 12.5d show some examples of cased piles without a pedestal. Figure 12.5e shows a cased pile with a pedestal. The pedestal is an expanded concrete bulb that is formed by dropping a hammer on fresh concrete. For a cased or uncased cast-in-place pile, a reinforcement cage is generally provided for the upper part.

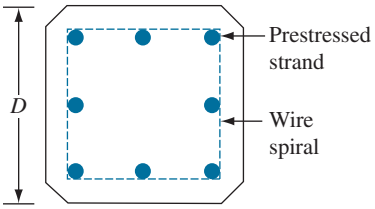
Some general facts about cased cast-in-place piles are as follows:

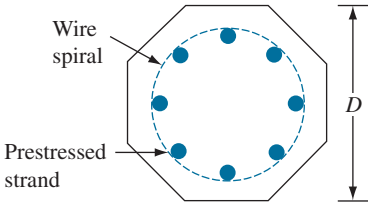
- Usual length: 5 m to 15 m (15 ft to 50 ft)
- Maximum length: 30 m to 40 m (100 ft to 130 ft)

TABLE 12.3a Typical Prestressed Concrete Pile in Use (SI Units)

Pile shape[a]	D (mm)	Area of cross section (cm^2)	Perimeter (mm)	Number of strands		Minimum effective prestress force (kN)	Section modulus ($m^3 \times 10^{-3}$)	Design bearing capacity (kN)	
				12.7 mm diameter	11.1 mm diameter			Strength of concrete (MN/m^2)	
								34.5	41.4
S	254	645	1016	4	4	312	2.737	556	778
O	254	536	838	4	4	258	1.786	462	555
S	305	929	1219	5	6	449	4.719	801	962
O	305	768	1016	4	5	369	3.097	662	795
S	356	1265	1422	6	8	610	7.489	1091	1310
O	356	1045	1168	5	7	503	4.916	901	1082
S	406	1652	1626	8	11	796	11.192	1425	1710
O	406	1368	1346	7	9	658	7.341	1180	1416
S	457	2090	1829	10	13	1010	15.928	1803	2163
O	457	1729	1524	8	11	836	10.455	1491	1790
S	508	2581	2032	12	16	1245	21.844	2226	2672
O	508	2136	1677	10	14	1032	14.355	1842	2239
S	559	3123	2235	15	20	1508	29.087	2694	3232
O	559	2587	1854	12	16	1250	19.107	2231	2678
S	610	3658	2438	18	23	1793	37.756	3155	3786
O	610	3078	2032	15	19	1486	34.794	2655	3186

[a]S = square section; O = octagonal section





- Usual load: 200 kN to 500 kN (45 kip to 115 kip)
- Approximate maximum load: 800 kN (180 kip)
- Advantages:
  - **a.** Relatively cheap
  - **b.** Allow for inspection before pouring concrete
  - **c.** Easy to extend
- Disadvantages:
  - **a.** Difficult to splice after concreting
  - **b.** Thin casings may be damaged during driving
- Structural load capacity:

$$Q_{all} = A_s f_s + A_c f_c \tag{12.2}$$

where

A_s = area of cross section of steel

A_c = area of cross section of concrete

f_s = allowable stress of steel

f_c = allowable stress of concrete

TABLE 12.3b Typical Prestressed Concrete Pile in Use (English Units)

Pile shape[a]	D (in.)	Area of cross section (in^2)	Perimeter (in.)	Number of strands		Minimum effective prestress force (kip)	Section modulus (in^3)	Design bearing capacity (kip)	
				$\frac{1}{2}$ in. diameter	$\frac{7}{16}$ in. diameter			Strength of concrete	
								5000 psi	6000 psi
S	10	100	40	4	4	70	167	125	175
O	10	83	33	4	4	58	109	104	125
S	12	144	48	5	6	101	288	180	216
O	12	119	40	4	5	83	189	149	178
S	14	196	56	6	8	137	457	245	295
O	14	162	46	5	7	113	300	203	243
S	16	256	64	8	11	179	683	320	385
O	16	212	53	7	9	148	448	265	318
S	18	324	72	10	13	227	972	405	486
O	18	268	60	8	11	188	638	336	402
S	20	400	80	12	16	280	1333	500	600
O	20	331	66	10	14	234	876	414	503
S	22	484	88	15	20	339	1775	605	727
O	22	401	73	12	16	281	1166	502	602
S	24	576	96	18	23	403	2304	710	851
O	24	477	80	15	19	334	2123	596	716

[a]S = square section; O = octagonal section

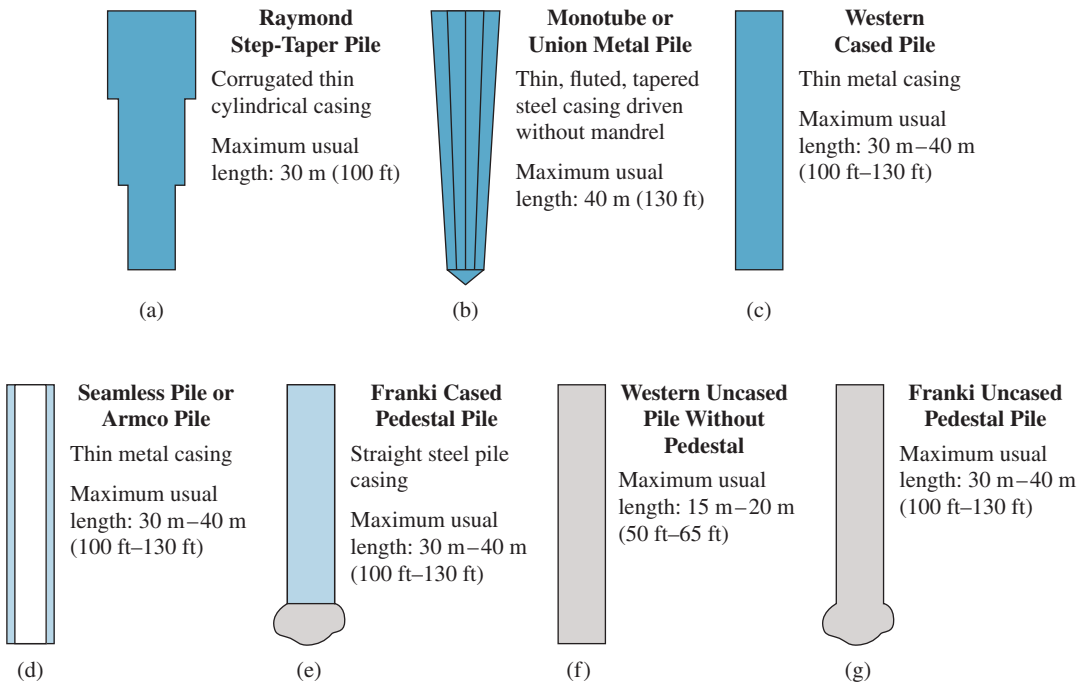


FIGURE 12.5 Cast-in-place concrete piles

Figures 12.5f and 12.5g are two types of uncased pile, one with a pedestal and the other without. The uncased piles are made by first driving the casing to the desired depth and then filling it with fresh concrete. The casing is then gradually withdrawn.

Following are some general facts about uncased cast-in-place concrete piles:

- Usual length: 5 m to 15 m (15 ft to 50 ft)
- Maximum length: 30 m to 40 m (100 ft to 130 ft)
- Usual load: 300 kN to 500 kN (67 kip to 115 kip)
- Approximate maximum load: 700 kN (160 kip)
- Advantages:
  a. Initially economical
  b. Can be finished at any elevation
- Disadvantages:
  a. Voids may be created if concrete is placed rapidly
  b. Difficult to splice after concreting
  c. In soft soil, the sides of the hole may cave in, squeezing the concrete
- Structural load capacity:

$$Q_{\text{all}} = A_c f_c \tag{12.3}$$

where

A_c = area of cross section of concrete

f_c = allowable stress of concrete

TIMBER PILES

Timber piles are tree trunks that have had their branches and bark carefully trimmed off. The maximum length of most timber piles is 10 to 20 m (30 to 65 ft). To qualify for use as a pile, the timber should be straight, sound, and without any defects. The American Society of Civil Engineers' *Manual of Practice*, No. 17 (1959), divided timber piles into three classes:

1. *Class A piles* carry heavy loads. The minimum diameter of the butt should be 356 mm (14 in.).
2. *Class B piles* are used to carry medium loads. The minimum butt diameter should be 305 to 330 mm (12 to 13 in.).
3. *Class C piles* are used in temporary construction work. They can be used permanently for structures when the entire pile is below the water table. The minimum butt diameter should be 305 mm (12 in.).

In any case, a pile tip should not have a diameter less than 150 mm (6 in.).

Timber piles cannot withstand hard driving stress; therefore, the pile capacity is generally limited. Steel shoes may be used to avoid damage at the pile tip (bottom). The tops of timber piles may also be damaged during the driving operation. The crushing of the wooden fibers caused by the impact of the hammer is referred to as *brooming*. To avoid damage to the top of the pile, a metal band or a cap may be used.

Splicing of timber piles should be avoided, particularly when they are expected to carry a tensile load or a lateral load. However, if splicing is necessary, it can be done by using *pipe sleeves* (see Figure 12.6a) or *metal straps and bolts* (see Figure 12.6b). The length of the sleeve should be at least five times the diameter of the pile. The butting ends should be cut square so that full contact can be maintained. The spliced portions should be carefully trimmed so that they fit tightly to the inside of the pipe sleeve. In the case of metal straps and bolts, the butting ends should also be cut square. The sides of the spliced portion should be trimmed plane for putting the straps on.

Timber piles can stay undamaged indefinitely if they are surrounded by saturated soil. However, in a marine environment, timber piles are subject to attack by various organisms and can be damaged extensively in a few months. When located above the water table, the piles are subject to attack by insects. The life of the piles may be increased by treating them with preservatives such as creosote.

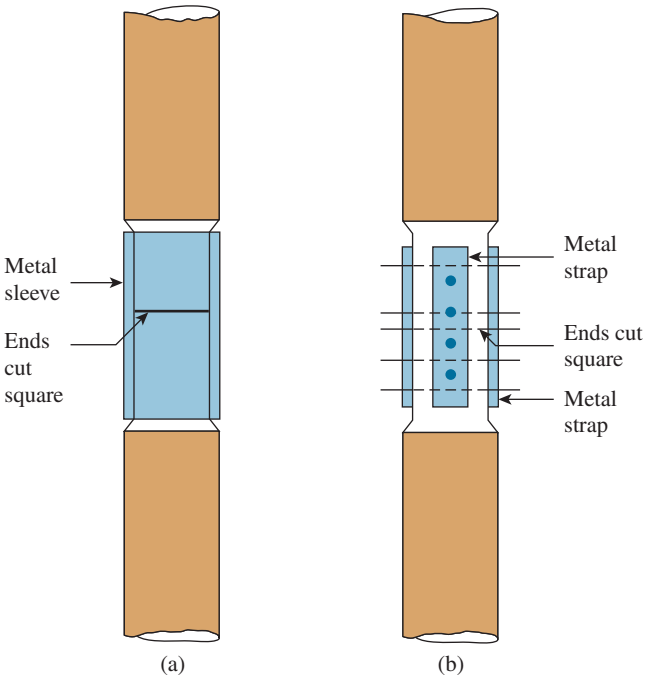


FIGURE 12.6 Splicing of timber piles: (a) use of pipe sleeves; (b) use of metal straps and bolts

The allowable load-carrying capacity of wooden piles is

$$Q_{\text{all}} = A_p f_w \tag{12.4}$$

where

A_p = average area of cross section of the pile

f_w = allowable stress on the timber

The following allowable stresses are for pressure-treated round timber piles made from Pacific Coast Douglas fir and Southern pine used in hydraulic structures (ASCE, 1993):

PACIFIC COAST DOUGLAS FIR

- Compression parallel to grain: 6.04 MN/m^2 (875 lb/in^2)
- Bending: 11.7 MN/m^2 (1700 lb/in^2)
- Horizontal shear: 0.66 MN/m^2 (95 lb/in^2)
- Compression perpendicular to grain: 1.31 MN/m^2 (190 lb/in^2)

SOUTHERN PINE

- Compression parallel to grain: 5.7 MN/m^2 (825 lb/in^2)
- Bending: 11.4 MN/m^2 (1650 lb/in^2)
- Horizontal shear: 0.62 MN/m^2 (90 lb/in^2)
- Compression perpendicular to grain: 1.41 MN/m^2 (205 lb/in^2)

The usual length of wooden piles is 5 m to 15 m (15 ft to 50 ft). The maximum length is about 30 m to 40 m (100 ft to 130 ft). The usual load carried by wooden piles is 300 kN to 500 kN (67 kip to 115 kip).

COMPOSITE PILES

The upper and lower portions of *composite piles* are made of different materials. For example, composite piles may be made of steel and concrete or timber and concrete.

Steel-and-concrete piles consist of a lower portion of steel and an upper portion of cast-in-place concrete. This type of pile is used when the length of the pile required for adequate bearing exceeds the capacity of simple cast-in-place concrete piles. Timber-and-concrete piles usually consist of a lower portion of timber pile below the permanent water table and an upper portion of concrete. In any case, forming proper joints between two dissimilar materials is difficult, and for that reason, composite piles are not widely used. Nowadays, fiber reinforced polymer (FRP) composite piles are widely used for waterfront structures.

12.3 Continuous Flight Auger (CFA) Piles

The continuous flight auger (CFA) piles are also referred to as auger-cast, auger-cast-in-place, and auger-pressure grout piles. CFA piles are constructed by using continuous flight augers and by drilling to the final depth in one continuous process. When the drilling to the final depth is complete, the auger is gradually withdrawn as concrete or sand/cement grout is pumped into the hole through the hollow center of the auger pipe to the base of the auger. Reinforcement, if needed, can be placed in CFA piles immediately after the withdrawal of the auger. The reinforcement is usually confined to the top 10 to 15 m (30 to 50 ft) of the pile.

In general, CFA piles are usually 0.3 to 0.9 m (1 to 3 ft) in diameter with a length up to about 30 m (100 ft). In the United States, smaller-diameter piles [i.e., 0.3 to 0.5 m (1 to 2 ft)] are generally used. However, piles with larger diameters [up to about 1.5 m (5 ft)] have been used. Typical center-to-center pile spacing is kept at 3 to 5 pile diameters. The following is a list of advantages and disadvantages of CFA piles.

- Advantages:
  a. Noise and vibration during construction are minimized
  b. Eliminate splicing and cutoff
- Disadvantages:
  a. Structural integrity is less reliable
  b. Soil spoils require collection and disposal

More recently, continuous flight auger (CFA) piles have been used worldwide and also in the commercial market in the United States. Figure 12.7 shows the construction of a CFA pile using a hollow-stem continuous flight auger. A detailed description



FIGURE 12.7 CFA pile construction (Courtesy of N. Sivakugan, James Cook University, Australia)

of the construction procedure for CFA piles can be found in the Federal Highway Administration (FHWA) *Geotechnical Engineering Circular* (*GEC*) No. 8 (2007).

12.4 Point Bearing and Friction Piles

Piles generally carry the applied column load through skin friction along the pile shaft and the bearing capacity at the pile point (or tip). When the pile carries the ultimate load Q_u, the ultimate shaft resistance and ultimate point resistance are denoted by Q_s and Q_p, respectively. From equilibrium considerations,

$$Q_u = Q_p + Q_s \tag{12.5}$$

Two extreme cases are *point bearing piles* (or *end bearing piles*) and *friction piles*, discussed here. In point bearing piles, it is assumed that the entire load is transferred to the soil as through the point, so $Q_s \approx 0$. In friction piles, it is assumed that the entire load is transferred through the pile shaft in the form of friction or adhesion, with $Q_p \approx 0$.

POINT BEARING PILES

In situations where the soil near the ground surface is weak and cannot support shallow foundations, pile foundations can be used. Especially when there is bedrock or a stiff stratum (e.g., stiff clay or dense sand) located at relatively shallow depths, it is possible to drive the piles through the weak soil and transfer the load to the underlying stiff stratum, as shown in Figure 12.8a. The pile can socket into the stiff stratum by extending a few meters. In point bearing piles,

$$Q_u = Q_p \tag{12.6}$$

FRICTION PILES

When there is no stiff stratum within reasonable depth, point bearing piles can become expensive. Here it is necessary to rely on the shaft resistance, which comes from skin friction or adhesion. The point resistance becomes insignificant; hence $Q_p \approx 0$ (Figure 12.8b). Therefore, in friction piles,

$$Q_u \approx Q_s \tag{12.7}$$

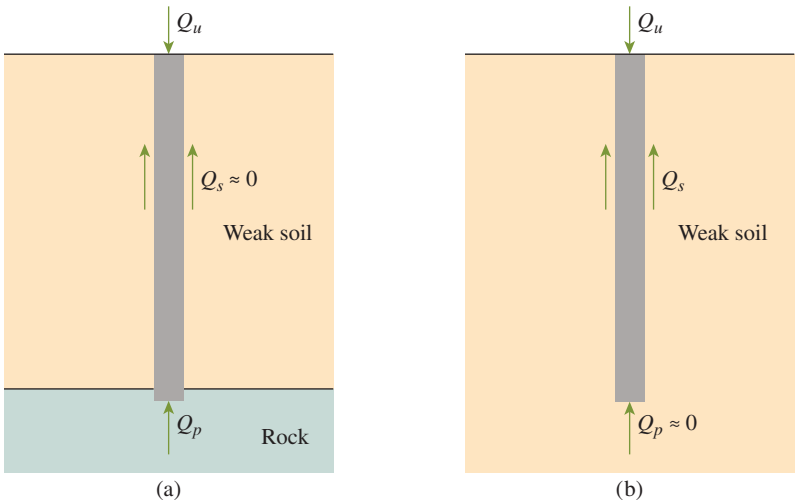


FIGURE 12.8 (a) Point bearing piles; (b) friction piles

12.5 Installation of Piles

There are different ways of installing piles, depending on the type of pile and the ground conditions. Steel, timber, and precast concrete piles are generally driven into the ground using an *impact hammer* or a *vibratory hammer*. A traditional impact pile driver allows a heavy hammer to slide up and down between guide rails, hitting the pile head and making the tip penetrate the ground by a few millimeters for every blow. The weight is raised by power from compressed air, steam, hydraulics, diesel, or simply by manual labor, as in ancient civilizations (Figures 12.9a and 12.9b).

The vibratory hammer was developed in the Soviet Union during World War II. Vibratory pile drivers produce less noise and are preferred near residential or office buildings. They are effective in medium-dense granular soil and with steel piles. Figure 12.9 shows the schematic diagrams of two impact hammers and a vibratory hammer. In Figures 12.9a and 12.9b, the pile is driven into the ground by raising and dropping a heavy weight, known as the *ram*. In the vibratory hammer, two counter-rotating weights produce a vertical sinusoidal load that drives the pile into the ground (Figure 12.9c). The horizontal components of the centrifugal forces induced by the two rotating weights cancel each other out. Figure 12.3b shows a steel pipe pile driven into the ground by a vibratory pile driver.

Cast-in-place (or *bored*) *concrete piles* are installed by placing a reinforcement cage into a cylindrical hole in the ground and pouring fresh concrete. The drilled shaft foundations discussed in Chapter 13 come under this category. Continuous flight auger (CFA) piles discussed in Section 12.3 are also special cases of cast-in-place piles.

Jetting is a technique that is sometimes used in pile driving when the pile needs to penetrate a thin layer of hard soil (such as sand and gravel) overlying a layer of softer soil. In this technique, water is discharged at the pile point by means of a pipe 50 to 75 mm (2 to 3 in.) in diameter to wash and loosen the sand and gravel. Piles also may be advanced by partial augering, with power augers (see Chapter 3) used to predrill holes part of the way.

Installation of piles generally causes lateral displacement of the surrounding soil. The extent of displacement depends on the method of installation and other factors. Driven piles generally cause high displacements: the larger the diameter, the larger the displacements. Cast-in-place piles (or bored piles) literally cause no displacement and are known as *nondisplacement piles*. H-piles and open-ended pipe piles cause little displacement and are known as *low-displacement piles*. Precast

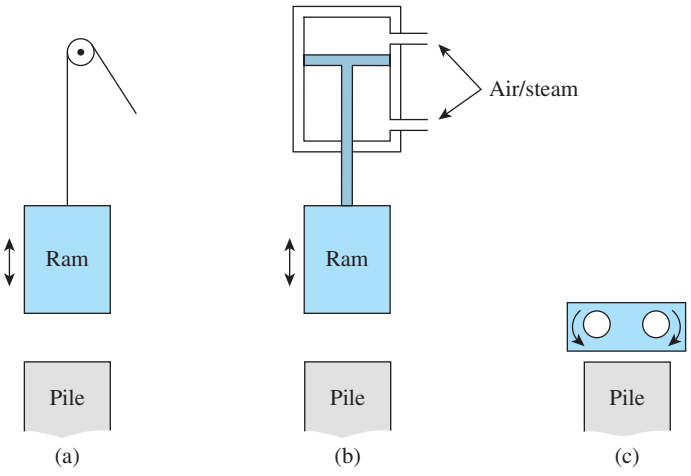


FIGURE 12.9 Pile-driving hammers: (a) drop hammer; (b) pneumatic hammer; (c) vibratory hammer

concrete, timber, or closed-end pipe piles that are driven into the ground are often *medium-* to *high-displacement piles*, depending on the diameter.

12.6 Pile Driving

There are several types of hammers used in pile driving. The pile hammer is selected based on the pile weight and the soil characteristics. The hammer will be most effective when the ram weight is 25–200% of the pile weight. Figure 12.10 shows a single-acting air/steam hammer driving a pile into the ground. Here compressed air or steam is sent into the cylinder to lift the ram, which is then allowed to fall freely.

The pile-driving setup includes the pile ram (piston), anvil (striker plate), hammer cushion (cap block or dolly), helmet (pile cap), and pile cushion (packing). The pile ram is the falling heavy weight that drives the pile into the ground through repeated blows. Typically the ram weighs 15–1500 kN (1.5–150 tons), with stroke length of 500–1500 mm (1.5–4.5 ft), and deliver 30–60 blows/min. The other accessories are there to protect the ram and the pile and to ensure that the impact energy is transferred to the pile in an efficient manner.

A good rule of thumb is to use a ram weight of 1/50th of the ultimate bearing capacity of the pile. Pile-driving formulas are useful in assessing whether a specific hammer can drive the pile into the ground to the desired depth without excessive driving that can damage the pile and the hammer. Such a situation arises when the blow count exceeds 120–150 blows per 250 mm (10 in.) for diesel or hydraulic hammers (Tomlinson and Woodward, 2008). The American Petroleum Institute (2000) defines refusal as the point where the blow count exceeds 300 blows per 300 mm (≈1 ft) for 1.5 m (≈ 4.5 ft) depth, or 800 blows per 300 mm (≈1 ft) for 0.3 m (1 ft) depth.

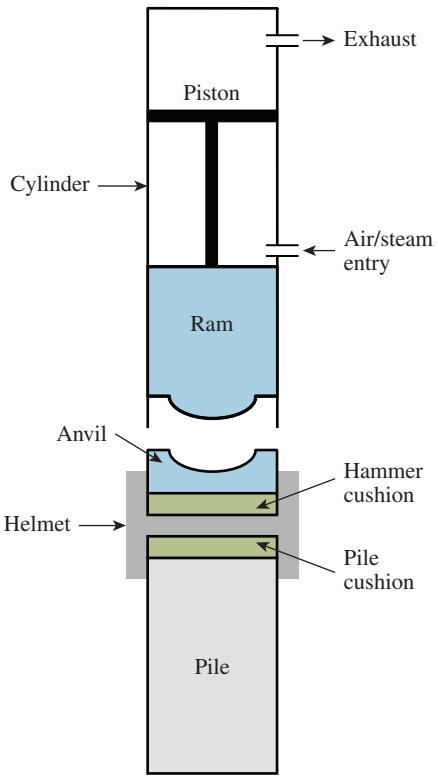


FIGURE 12.10 A single-acting hammer with possible accessories

HELMET AND CUSHIONS

Air or steam hammers do not require an anvil; they can strike the hammer cushion directly. The helmet is a rigid steel block used to hold the pile head in the right position under the ram. It distributes the hammer blow evenly to the pile. There are two types of cushions—*hammer cushions* and *pile cushions*—for different purposes. The first one is to protect the hammer and the second is to protect the pile.

The hammer cushion, sometimes called the *cap block* or *dolly*, protects the striking parts from excessive driving stresses caused by the considerable rebound which can damage the hammer. It is used between the ram and the helmet. It is made of relatively stiff and resilient materials. About 150 mm (6 in.) thick hardwood, fitted within a steel ring and with grain parallel to the pile axis to provide maximum stiffness, has been used in the past for hammer cushions. It can get crushed and burned quickly, requiring that it be replaced. Laminated blocks with alternating layers of aluminum and nylon-like material are commonly used as pile cushions. Aluminum has no cushioning effect and is only used to extract heat from the cushion stack. These materials have greater *coefficient of restitution* (e.g., 0.8) than hardwood (e.g., 0.5). Plywood is not suitable for hammer cushions.

A pile helmet, also known as the driving head, holds the pile aligned under the ram, thereby distributing the impact evenly. For H-piles and tubular piles, the helmet should fit snugly to avoid bulging and distortion. For concrete piles, a snug fit is not recommended, since that would prevent pile rotation.

Pile cushions, used between the pile and the helmet, are mostly used with concrete piles to reduce stress concentrations during driving at the hammer–pile contact as well as the peak stresses within the pile. In addition, they enable the impact energy to be transferred through the pile efficiently. Pile cushions are often made of low-stiffness material, such as plywood. They can be 150–500 mm (6–20 in.) in thickness.

Heat generated during driving is a major factor that can break down the cushion. In addition, the repeated hammer blows compress the cushion, making it stiffer and less effective in protecting the hammer. The cushions have to be replaced from time to time and are consumable items in pile driving.

DROP HAMMERS

The early piling works from the Roman times to the late 19th century relied on timber piles driven by drop hammers on wooden rigs. *Drop hammers*, also known as gravity hammers, are the oldest type of pile driving hammers. The hammer is connected to a cable attached to a winch or crane and is repeatedly raised to the required height and dropped on the pile head (Figure 12.9a). The ram weighs about 5–50 kN (0.5–5 tons), and the drop height is about 0.5–2.0 m (1.5–6.5 ft). The ram weight is typically 0.5 to 2.0 times the pile weight. In ancient times, the hammer was raised by humans and horses and dropped on the pile head, where the piles were mainly made of wood. While drop hammers are simple, their operation can be relatively slow, with 5–10 blows per minute. They are usually meant for small piles, small projects, or work in remote locations where other equipment is unavailable. Drop hammers are not very common in modern times. They cannot be used to drive battered piles. Their efficiency is reduced due to rope friction along the drum surface.

STEAM AND AIR HAMMERS

Steam hammers were introduced in the 1840s in Scotland (1887 in the United States), followed by *air hammers*. Steam from boilers or air from compressors is used for lifting the ram in the case of *single-acting hammers* and also to push them down in addition to gravity in *double-acting hammers* (also known as "downward-assist" hammers). Double-acting hammers are popular for driving sheet piles when

vibratory hammers cannot penetrate the soil. Steam hammers require a continuous supply of water for the boiler. Some steam hammers can be operated by compressed air. Hydraulic and vibratory hammers are also powered by internal combustion engines or electric motors and may not require boilers.

The original steam hammers were single acting. Single-acting hammers are essentially drop hammers in which the ram is raised by steam or compressed air instead of the hoisting cable. A single-acting air or steam hammer has a ram weighing about 15–1500 kN (1.5–150 tons) and stroke length of 0.5–1.5 m (1.5–4.5 ft), with an energy rating of 10–2250 kN·m (300–67,500 ton·ft), delivering about 30–60 blows per minute. Double-acting hammers were developed to increase the blow rate and deliver 60–120 blows/min. *Differential hammers* use steam or compressed air to raise the ram and to force it down. Unlike the air or steam hammers, a constant pressure is maintained in differential hammers. Differential hammers are a special form of double-acting hammers. Differential and double-acting hammers generally have half the stroke and twice the blow rate of comparable single-acting hammers.

DIESEL HAMMERS

Diesel hammers were introduced in the 1920s in Germany by DELMAG. They are smaller, lighter, and more efficient than air or steam hammers. When the ram strikes the anvil, a fuel–air mixture is ignited in the cylinder and the resulting explosion drives the ram up. Diesel hammers can be *single acting* (open end) or *double acting* (closed end). While the steam hammer requires a separate steam generator and an air hammer requires a compressor, a diesel hammer is a self-contained unit. Diesel hammers are also lighter but provide comparable striking energy.

Diesel hammers are effective under hard driving conditions. Timber piles are often driven by drop hammers or single-acting hammers. Diesel hammers may be too powerful and may damage the pile. The Swedish piling code suggests a minimum of a 1 tonne hammer with at least 1.5 times the weight of the pile and helmet.

HYDRAULIC HAMMERS

Hydraulic hammers use hydraulic fluid (e.g., pressurized oil) to lift the ram; they generate less noise and pollutants and hence are environmentally friendlier. This can make them favored over diesel hammers, which can be noisy and have environmental impacts. The hammer may be allowed to fall freely or be forced down. Hydraulic hammers can be single acting, double acting, or differential.

Hydraulic hammers and diesel hammers can have efficiencies on the order of 80%, which is higher than those of air hammers. Single-acting air or diesel hammer efficiency is about 67%; their double-acting counterparts have 50% efficiency but operate more quickly and deliver more blows per minute. The efficiency of a vibratory hammer can be as high as 100%. Hydraulic hammers are suitable for pile extraction.

An air, steam, diesel, or hydraulic hammer can be single acting or double acting. In double-acting hammers, air, steam, or diesel is used to accelerate the downward travel of the ram. This makes them faster and more productive than their single-acting counterparts. Double-acting hammers require less headroom than single-acting ones.

Single-acting hammers are driven by compressed air or steam and are suitable for timber piles or precast concrete piles. Double-acting hammers are more effective in granular soil and are commonly used for driving sheet piles. Diesel hammers are suitable for all soil except soft clays. Figure 12.11 summarizes the different types of impact pile-driving hammers used in practice. Here, external combustion requires external power sources (e.g., cranes, air compressors, steam boilers, or hydraulic power packs) that provide the hammer energy. Internal combustion requires fuel to be burned within the hammer itself to provide the energy.

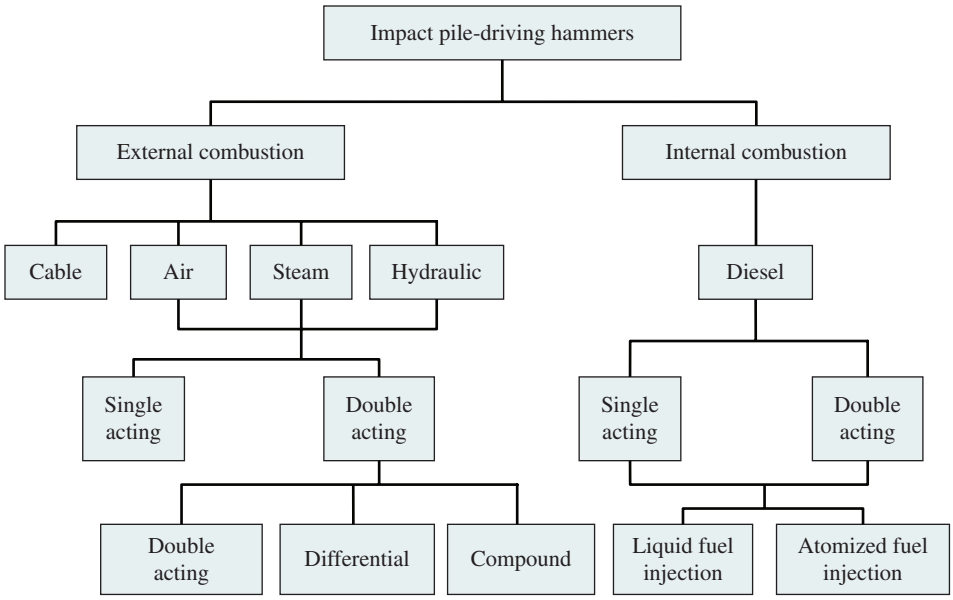


FIGURE 12.11 Hammer categories (Based on Rausche et al., 1986)

Vulcan, Conmaco, Menck, Raymond, DELMAG, MKT (McKiernan Terry Corporation), ICE (International Construction Equipment), and Junttan are some of the pile-driving equipment manufacturers worldwide. Table 12.4 lists the specifications of some of the commercially available pile-driving hammers. Figure 12.12 shows a pile-driving operation in the field.



FIGURE 12.12 A pile-driving operation in the field (Courtesy of E. C. Shin, University of Incheon, Korea)

TABLE 12.4 Specifications of Commercially Available Pile-Driving Hammers

Rated energy		Hammer				Ram weight*		Nominal stroke	
kN·m	kip·ft	Make	Model	Type	Blows/min	kN	kip	m	in.
11.9	8.75	MKT	9B3	DA (A/S)	145	7.1	1.6	0.432	17
17.8	13.1	MKT	10B3	DA (A/S)	105	13.3	3.0	0.483	19
20.3	15.0	Vulcan	305	SA (A/S)	60	22.2	5.0	0.914	36
26.0	19.15	MKT	11B3	DA (A/S)	95	22.2	5.0	0.483	19
26.44	19.5	Raymond	65C	DA/Differential (S)	100–110	28.93	6.5	0.406	16
33.2	24.5	Raymond	80C	DA/Differential (S)	95–105	35.6	8.0	0.419	16.5
44.1	32.5	Vulcan	010	SA (A/S)	50	44.5	10.0	0.991	39
44.6	32.9	Vulcan	100C	DA/Differential (A/S)	103	44.5	10.0	0.419	16.5
48.8	36.0	Vulcan	140C	DA/Differential (A/S)	103	62.3	14.0	0.394	15.5
66.1	48.75	Raymond	150C	DA/Differential (A/S)	95–105	66.75	15.0	0.457	18.0
68.1	50.2	Vulcan	200C	DA/Differential (A/S)	98	89.0	20.0	0.394	15.5
77.1	56.9	Raymond	5/O	SA (A/S)	44	77.9	17.5	0.991	39.0
81.3	60.0	Vulcan	320	SA (A/S)	55	89.0	20.0	0.914	36
107.1	79.0	Kobe	K-42	SA Diesel	45–60	41.2	9.26	2.600	102.4
110.2	81.25	Raymond	8/O	SA (A/S)	33–38	111.3	25.0	0.991	39
122.3	90.2	Delmag	D-44	SA Diesel	37–56	42.27	9.50	2.893	113.9
132.0	97.3	Junttan	HHK 9S	Hydraulic	30–100	88.29	19.84	1.500	59.1
135.6	100.0	Vulcan	520	SA (A/S)	42	89.0	20.0	1.524	60
141.3	104.2	Junttan	HHK 12A	Hydraulic	40–100	117.72	26.46	1.200	47.2
153.9	113.5	Vulcan	400C	DA (A/S)	100	178.0	40.0	0.419	16.5
165.0	121.6	Junttan	HHK 14A	Hydraulic	40–100	137.3	30.9	1.200	47.2
203.4	150.0	MKT	DE150	SA Diesel	40–50	66.75	15.0	3.05	120
204	150.0	Vulcan	530	SA (A/S)	42	133.5	30.0	1.524	60

*Weight of the striking parts

12.7 Load Transfer Mechanism

The load transfer mechanism from a pile to the soil is complicated. To understand it, consider a pile of length L, as shown in Figure 12.13a. The load on the pile is gradually increased from zero to $Q_{(z=0)}$ at the ground surface. Part of this load will be resisted by the side friction developed along the shaft, Q_1, and the rest by the soil below the tip of the pile, Q_2. Now, how is the total load $Q_{(z=0)}$ shared between Q_1 and Q_2? If measurements are made to obtain the load carried by the pile shaft, $Q_{(z)}$, at any depth z, the nature of the variation found will be like that shown in curve 1 of Figure 12.13b. The *frictional resistance per unit area* at any depth z may be determined as

$$f_{(z)} = \frac{\Delta Q_{(z)}}{(p)(\Delta z)} \tag{12.8}$$

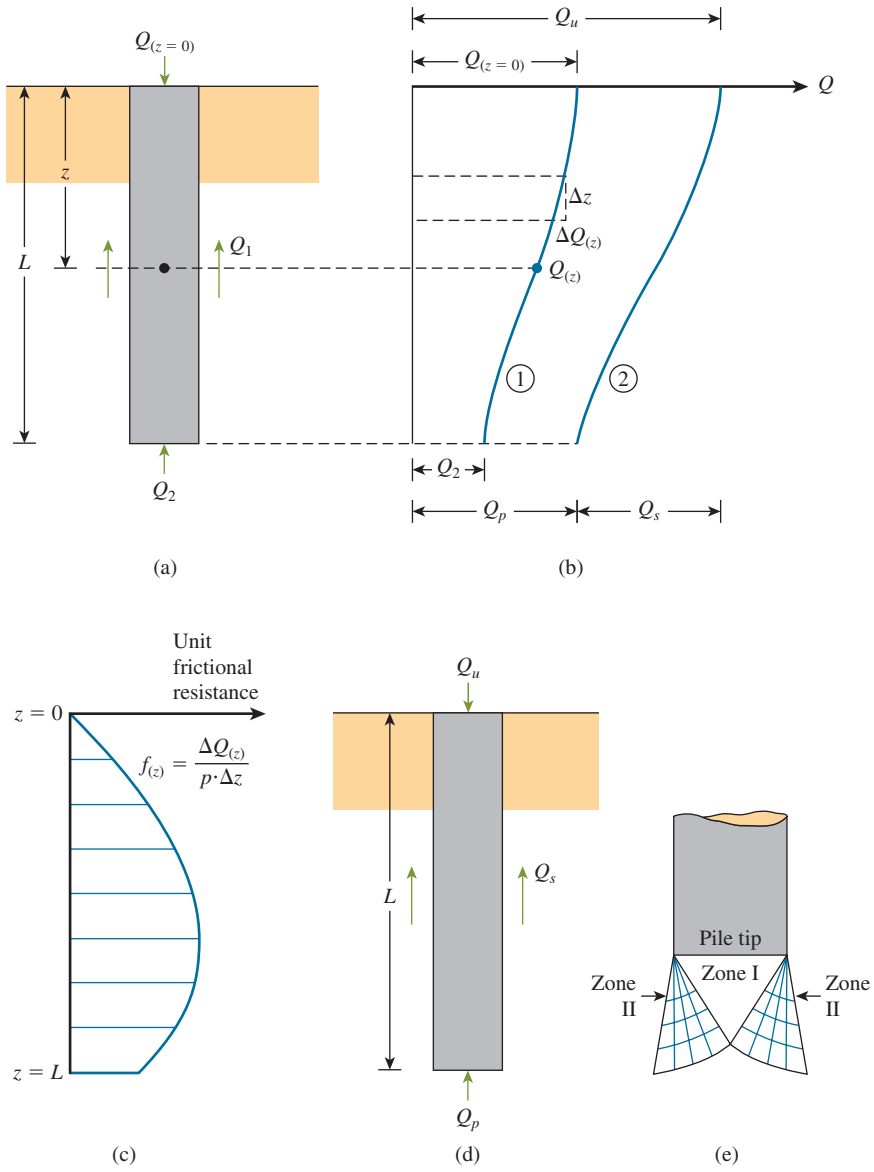


FIGURE 12.13 Load transfer mechanism for piles

where p = perimeter of the cross section of the pile. Figure 12.13c shows the variation of $f_{(z)}$ with depth. Noting that the pile load $Q_{(z)}$ decreases with depth, Eq. (12.8) can be written as

$$f_{(z)} = -\frac{1}{p}\frac{dQ_{(z)}}{dz} \tag{12.9}$$

If the load Q at the ground surface is gradually increased, maximum frictional resistance along the pile shaft will be fully mobilized when the relative displacement between the soil and the pile is about 5 to 10 mm (0.2 to 0.3 in.), irrespective of the pile size and length L. However, the maximum point resistance $Q_2 = Q_p$ will not be mobilized until the tip of the pile has moved about 10 to 25% of the pile width (or diameter). (The lower limit applies to driven piles and the upper limit to bored piles.) At ultimate load (Figure 12.13d and curve 2 in Figure 12.13b), $Q_{(z=0)} = Q_u$. Thus,

$$Q_1 = Q_s$$

and

$$Q_2 = Q_p$$

The preceding explanation indicates that Q_s (or the unit skin friction, f, along the pile shaft) is developed at a *much smaller pile displacement compared with the point resistance, Q_p*. In order to demonstrate this point, let us consider the results of a pile load test conducted in the field by Mansur and Hunter (1970). The details of the pile and subsoil conditions are as follows:

Type of pile: Steel pile with 406 mm (16 in.) outside diameter with 8.15 mm (0.321 in.) wall thickness
Type of subsoil: Sand
Length of pile embedment: 16.8 m (55 ft)

Figure 12.14a shows the load test results and is a plot of load at the top of the pile $[Q_{(z=0)}]$ versus settlement(s). Figure 12.14b shows the plot of the load carried by the pile shaft $[Q_{(z)}]$ at any depth. It was reported by Mansur and Hunter (1970) that, for this test, at failure

$$Q_u \approx 1601\,\text{kN}\,(360\ \text{kip})$$
$$Q_p \approx 416\,\text{kN}\,(93.6\ \text{kip})$$

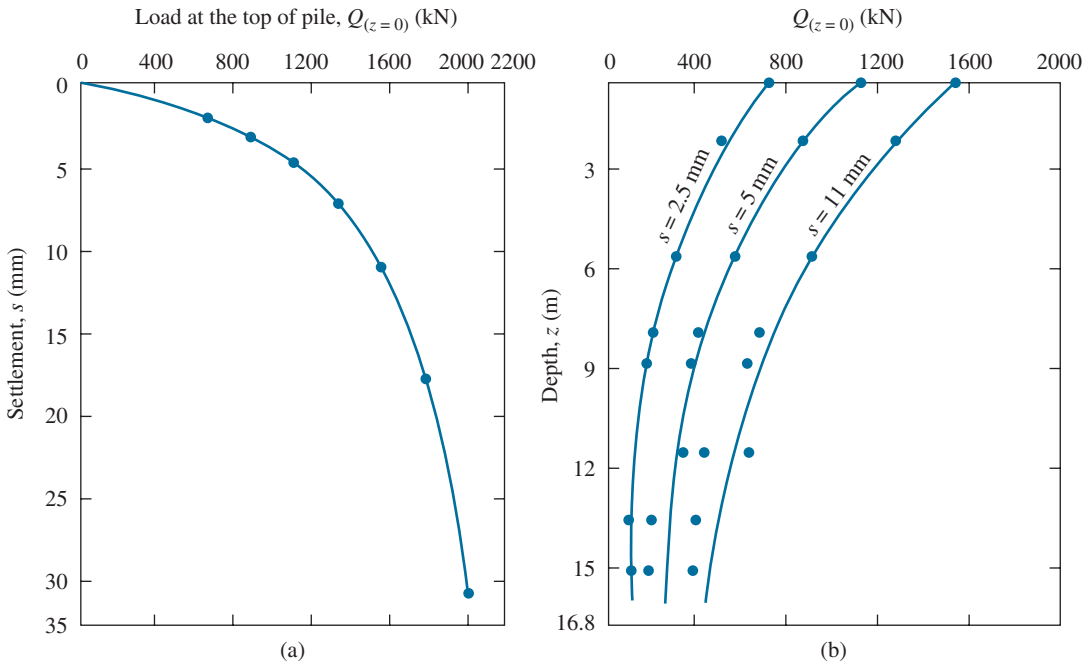


FIGURE 12.14

and

$$Q_s \approx 1185 \text{ kN} (266.4 \text{ kip})$$

Now, let us consider the load distribution in Figure 12.14b when the pile settlement(s) is about 2.5 mm. For this condition,

$$\begin{aligned} Q_{(z=0)} &\approx 667 \text{ kN} \\ Q_2 &\approx 93 \text{ kN} \\ Q_1 &\approx 574 \text{ kN} \end{aligned}$$

Hence, at $s = 2.5\,\text{mm}$

$$\frac{Q_2}{Q_p} = \frac{93}{416}(100) = 22.4\%$$

and

$$\frac{Q_1}{Q_s} = \frac{574}{1185}(100) = 48.4\%$$

Thus, it is obvious that the skin friction is mobilized faster at low settlement levels as compared to the point load.

At ultimate load, the failure surface in the soil at the pile tip (a bearing capacity failure caused by Q_p) is like that shown in Figure 12.13e. Note that pile foundations are deep foundations and that the soil fails mostly in a *punching mode*, as illustrated previously in Figures 6.2c and 6.4. That is, a *triangular zone*, I, is developed at the pile tip, which is pushed downward without producing any other visible slip surface. In dense sands and stiff clayey soil, a *radial shear zone*, II, may partially develop. Hence, the load-displacement curves of piles will resemble those shown in Figure 6.2c.

From Eq. (12.9), it is possible to deduce frictional resistance per unit area $f_{(z)}$ from the pile load $Q_{(z)}$ at any depth and vice versa. Figure 12.15 shows the $f_{(z)}$-z variation deduced from the $Q_{(z)}$-z plot for four special cases.

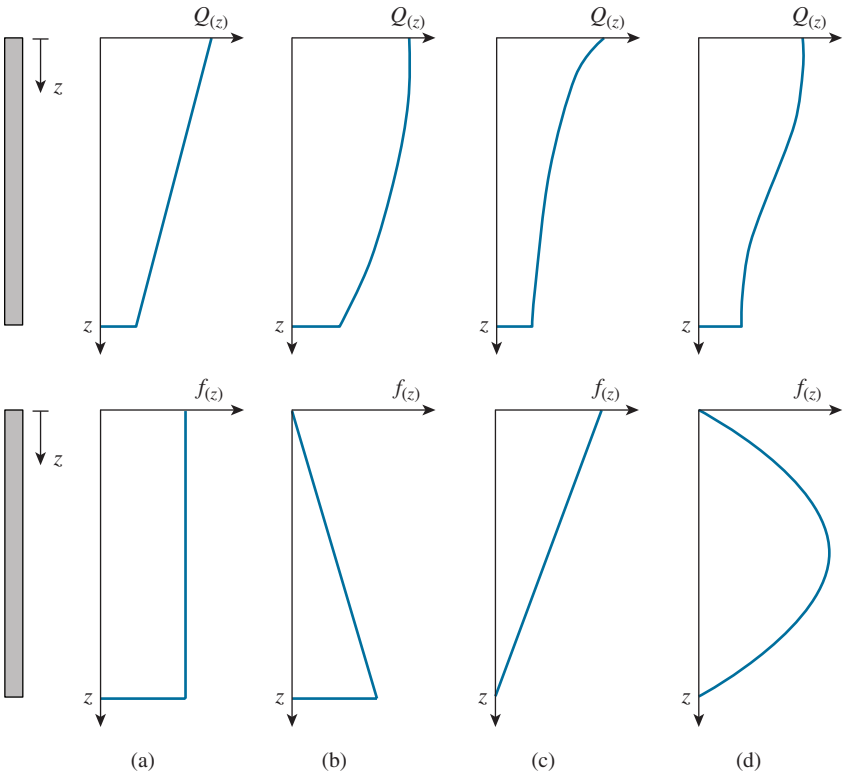


FIGURE 12.15 Variation of pile load $Q_{(z)}$ and skin friction $f_{(z)}$ with depth z

12.8 Equations for Estimating Pile Capacity

The ultimate load-carrying capacity Q_u of a pile is given by the equation

$$Q_u = Q_p + Q_s \tag{12.10}$$

where

Q_p = load-carrying capacity of the pile point

Q_s = frictional resistance (skin friction) derived from the soil–pile interface (see Figure 12.16)

Numerous published studies cover the determination of the values of Q_p and Q_s. Excellent reviews of many of these investigations have been provided by Vesic (1977), Meyerhof (1976), and Coyle and Castello (1981). These studies afford an insight into the problem of determining the ultimate pile capacity.

The ultimate load-carrying capacity relationships for CFA piles (Section 12.3) will be discussed separately in Section 12.15.

POINT BEARING CAPACITY, Q_p

The ultimate bearing capacity of shallow foundations was discussed in Chapter 6. According to Terzaghi's equations,

$$q_u = 1.3c'N_c + qN_q + 0.4\gamma BN_\gamma \qquad \text{(for shallow square foundations)}$$

and

$$q_u = 1.3c'N_c + qN_q + 0.3\gamma BN_\gamma \qquad \text{(for shallow circular foundations)}$$

Similarly, the general bearing capacity equation for shallow foundations was given in Chapter 6 (for vertical loading) as

$$q_u = c'N_cF_{cs}F_{cd} + qN_qF_{qs}F_{qd} + \tfrac{1}{2}\gamma BN_\gamma F_{\gamma s}F_{\gamma d}$$

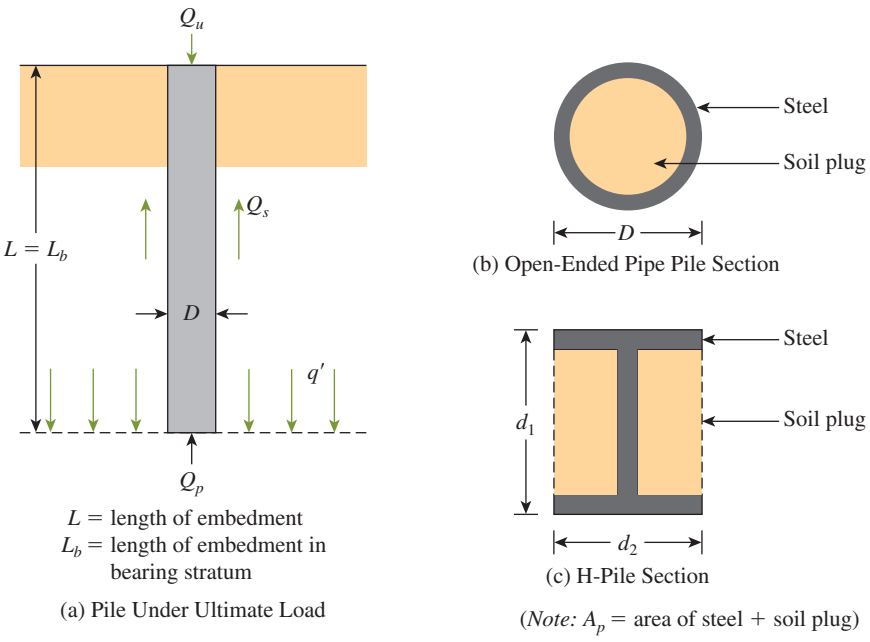


FIGURE 12.16 Ultimate load-carrying capacity of pile

Hence, in general, the ultimate load-bearing capacity for piles may be expressed as

$$q_u = c'N_c^* + qN_q^* + \gamma BN_\gamma^* \tag{12.11}$$

where N_c^*, N_q^*, and N_γ^* are the bearing capacity factors that include the necessary shape and depth factors.

Pile foundations are deep. However, the ultimate resistance per unit area developed at the pile tip, q_p, may be expressed by an equation similar in form to Eq. (12.11), although the values of N_c^*, N_q^*, and N_γ^* will change. The notation used in this chapter for the width of a pile is D. Hence, substituting D for B in Eq. (12.11) gives

$$q_u = q_p = c'N_c^* + qN_q^* + \gamma DN_\gamma^* \tag{12.12}$$

Because the width D of a pile is relatively small, the term γDN_γ^* may be dropped from the right side of the preceding equation without introducing a serious error; thus, we have

$$q_p = c'N_c^* + q'N_q^* \tag{12.13}$$

Note that the term q has been replaced by q' in Eq. (12.13) to signify effective vertical stress. Thus, the point bearing of piles is

$$Q_p = A_p q_p = A_p(c'N_c^* + q'N_q^*) \tag{12.14}$$

where

A_p = area of the pile tip

c' = cohesion of the soil supporting the pile tip

q_p = unit point resistance or ultimate bearing capacity of the pile point

q' = effective vertical stress at the level of the pile tip

N_c^*, N_q^* = the bearing capacity factors for piles

FRICTIONAL RESISTANCE, Q_s

The frictional, or skin, resistance of a pile may be written as

$$Q_s = \Sigma p\,\Delta L f \tag{12.15}$$

where

p = perimeter of the pile section

ΔL = incremental pile length over which p and f are taken to be constant

f = unit friction resistance at any depth z

The various methods for estimating Q_p and Q_s are discussed in the next several sections. It needs to be reemphasized that, in the field, for full mobilization of the point resistance (Q_p), the pile tip must go through a displacement of 10 to 25% of the pile width (or diameter).

ALLOWABLE LOAD, Q_{all}

After the total ultimate load-carrying capacity of a pile has been determined by summing the point bearing capacity and the frictional (or skin) resistance, a

TABLE 12.5 Factor of Safety for Axially Loaded Piles Suggested by USACE (1991)

Method of determining/ verifying pile capacity	Loading condition	Minimum factor of safety	
		In compression	In tension
Theoretical or empirical prediction, to be verified by pile load test	Usual	2.00	2.00
	Unusual	1.50	1.50
	Extreme	1.15	1.15
Theoretical or empirical prediction to be verified by pile-driving analyzer (PDA)	Usual	2.50	3.00
	Unusual	1.90	2.25
	Extreme	1.40	1.70
Theoretical or empirical prediction, not verified by load tests	Usual	3.00	3.00
	Unusual	2.25	2.25
	Extreme	1.70	1.70

reasonable factor of safety should be used to obtain the total allowable load for each pile, or

$$Q_{\text{all}} = \frac{Q_u}{\text{FS}} \tag{12.16}$$

where

Q_{all} = allowable load-carrying capacity for each pile

FS = factor of safety

The factor of safety generally used ranges from 2 to 3, depending on the uncertainties surrounding the calculation of ultimate load. The factors of safety suggested by the U.S. Army Corps of Engineers are given in Table 12.5.

12.9 Meyerhof's Method for Estimating Q_p

SAND

The point bearing capacity, q_p, of a pile in sand generally increases with the depth of embedment in the bearing stratum and reaches a maximum value at an embedment ratio of $L_b/D = (L_b/D)_{\text{cr}}$. Note that in a homogeneous soil, L_b is equal to the actual embedment length of the pile, L. However, where a pile has penetrated into a bearing stratum, $L_b < L$. Beyond the critical embedment ratio, $(L_b/D)_{\text{cr}}$, the value of q_p remains constant ($q_p = q_l$). That is, as shown in Figure 12.17 for the case of a homogeneous soil, $L = L_b$.

For piles in sand, $c' = 0$, and Eq. (12.14) simpifies to

$$Q_p = A_p q_p = A_p q' N_q^* \tag{12.17}$$

The variation of N_q^* with soil friction angle ϕ' is shown in Figure 12.18. The interpolated values of N_q^* for various friction angles are also given in Table 12.6. However, Q_p should not exceed the limiting value $A_p q_l$; that is,

$$Q_p = A_p q' N_q^* \le A_p q_l \tag{12.18}$$

The limiting point resistance is

$$q_l = 0.5\, p_a N_q^* \tan \phi' \tag{12.19}$$

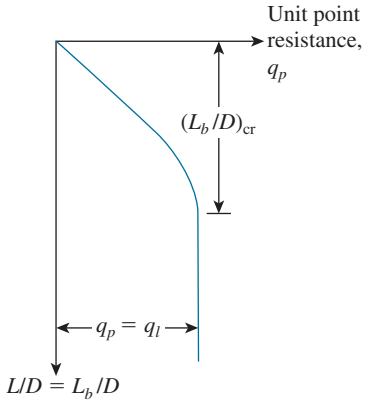


FIGURE 12.17 Nature of variation of unit point resistance in a homogeneous sand

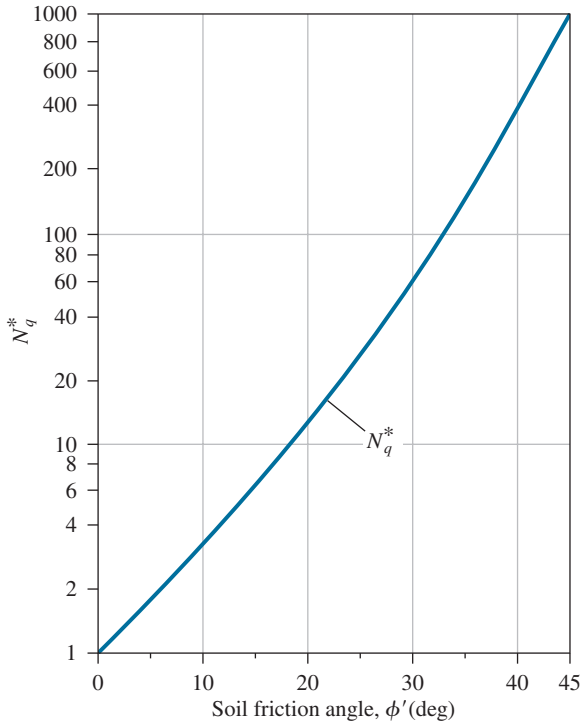


FIGURE 12.18 Variation of the maximum values of N_q^* with soil friction angle ϕ' (Based on Meyerhof, G. G. (1976). "Bearing Capacity and Settlement of Pile Foundations," *Journal of the Geotechnical Engineering Division*, American Society of Civil Engineers, Vol. 102, No. GT3, pp. 197–228.)

TABLE 12.6 Interpolated Values of N_q^* Based on Meyerhof's Theory

Soil friction angle, ϕ' (deg)	N_q^*
20	12.4
21	13.8
22	15.5
23	17.9
24	21.4
25	26.0
26	29.5
27	34.0
28	39.7
29	46.5
30	56.7
31	68.2
32	81.0
33	96.0
34	115.0
35	143.0
36	168.0
37	194.0
38	231.0
39	276.0
40	346.0
41	420.0
42	525.0
43	650.0
44	780.0
45	930.0

TABLE 12.7 Ultimate Point Resistance, q_p, of Test Pile at the Ogeechee River Site as Reported by Vesic (1970)

Pile diameter, D(m)	Depth of embedment, L (m)	L/D	q_p(kN/m^2)
0.457	3.02	6.61	3,304
0.457	6.12	13.39	9,365
0.457	8.87	19.4	11,472
0.457	12.0	26.26	11,587
0.457	15.00	32.82	13,971

where

p_a = atmospheric pressure (=100 kN/m^2 or 2000 lb/ft^2)

ϕ' = effective soil friction angle of the bearing stratum

A good example of the concept of the critical embedment ratio can be found from the field load tests on a pile in sand at the Ogeechee River site reported by Vesic (1970). The pile tested was a steel pile with a diameter of 457 mm (18 in.). Table 12.7 shows the ultimate resistance at various depths. Figure 12.19 shows the plot of q_p with depth obtained from the field tests along with the range of standard penetration resistance at the site. From the figure, the following observations can be made:

1. There is a limiting value of q_p. For the tests under consideration, it is about 12,000 kN/m^2.
2. The $(L/D)_{cr}$ value is about 16 to 18.

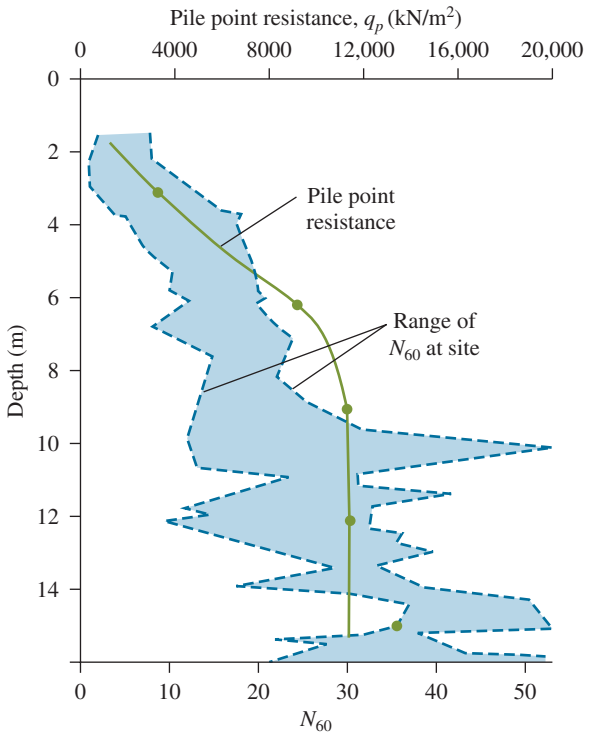


FIGURE 12.19 Vesic's pile test (1970) result—variation of q_p and N_{60} with depth

3. The average N_{60} value is about 30 for $L/D \geq (L/D)_{cr}$. Using Eq. (12.39), the limiting point resistance is $4p_a N_{60} = (4)(100)(30) = 12{,}000$ kN/m^2. This value is generally consistent with the field observation.

CLAY ($\phi = 0$)

For piles in *saturated clays* under undrained conditions ($\phi = 0$), the net ultimate load can be given as

$$Q_p \approx N_c^* c_u A_p = 9 c_u A_p \tag{12.20}$$

where c_u = undrained cohesion of the soil below the tip of the pile.

12.10 Vesic's Method for Estimating Q_p

SAND

Vesic (1977) proposed a method for estimating the pile point bearing capacity based on the theory of *expansion of cavities*. According to this theory, on the basis of effective stress parameters, we may write

$$Q_p = A_p q_p = A_p \, \overline{\sigma}'_o N_\sigma^* \tag{12.21}$$

where

$\overline{\sigma}'_o$ = mean effective normal ground stress at the level of the pile point

$$= \left(\frac{1 + 2K_o}{3}\right) q' \tag{12.22}$$

K_o = earth pressure coefficient at rest = $1 - \sin \phi'$ (12.23)

and

N_σ^* = bearing capacity factor

Note that Eq. (12.21) is a modification of Eq. (12.17) with

$$N_\sigma^* = \frac{3N_q^*}{(1 + 2K_o)} \tag{12.24}$$

According to Vesic's theory,

$$N_\sigma^* = f(I_{rr}) \tag{12.25}$$

where I_{rr} = reduced rigidity index for the soil. However,

$$I_{rr} = \frac{I_r}{1 + I_r \Delta} \tag{12.26}$$

where

$$I_r = \text{rigidity index} = \frac{E_s}{2(1 + \mu_s)\, q' \tan \phi'} = \frac{G_s}{q' \tan \phi'} \tag{12.27}$$

E_s = modulus of elasticity of soil

μ_s = Poisson's ratio of soil

G_s = shear modulus of soil

Δ = average volumetric strain in the plastic zone below the pile point

The general ranges of I_r for various soil are

Sand (relative density = 50% to 80%): 75 to 150
Silt: 50 to 75

In order to estimate I_r [Eq. (12.27)] and hence I_{rr} [Eq. (12.26)], the following approximations may be used (Chen and Kulhawy, 1994):

$$\frac{E_s}{p_a} = m \tag{12.28}$$

where

p_a = atmospheric pressure ($\approx$100 kN/m^2 or 2000 lb/ft^2)

$$m = \begin{cases} 100 \text{ to } 200 \text{ (loose soil)} \\ 200 \text{ to } 500 \text{ (medium dense soil)} \\ 500 \text{ to } 1000 \text{ (dense soil)} \end{cases}$$

$$\mu_s = 0.1 + 0.3\left(\frac{\phi' - 25}{20}\right) \text{(for } 25^\circ \le \phi' \le 45^\circ\text{)} \tag{12.29}$$

$$\Delta = 0.005\left(1 - \frac{\phi' - 25}{20}\right)\frac{q'}{p_a} \tag{12.30}$$

On the basis of cone penetration tests in the field, Baldi et al. (1981) gave the following correlations for I_r:

$$I_r = \frac{300}{F_r(\%)} \quad \text{(for mechanical cone penetration)} \tag{12.31}$$

and

$$I_r = \frac{170}{F_r(\%)} \quad \text{(for electric cone penetration)} \tag{12.32}$$

where $F_r(\%)$ is the friction ratio in a cone penetration test. Table 12.8 gives the values of N_σ^* for various values of I_{rr} and ϕ'.

CLAY ($\phi = 0$)

In saturated clay ($\phi = 0$ condition), the net ultimate point bearing capacity of a pile can be approximated as

$$Q_p = A_p q_p = A_p c_u N_c^* \tag{12.33}$$

where c_u = undrained cohesion.

According to the *expansion of cavity* theory of Vesic (1977),

$$N_c^* = \frac{4}{3}(\ln I_{rr} + 1) + \frac{\pi}{2} + 1 \tag{12.34}$$

The variations of N_c^* with I_{rr} for $\phi = 0$ condition are given in Table 12.9.

TABLE 12.8 Bearing Capacity Factors N_σ^* Based on the Theory of Expansion of Cavities

	I_{rr}									
ϕ'	10	20	40	60	80	100	200	300	400	500
25	12.12	15.95	20.98	24.64	27.61	30.16	39.70	46.61	52.24	57.06
26	13.18	17.47	23.15	27.30	30.69	33.60	44.53	52.51	59.02	64.62
27	14.33	19.12	25.52	30.21	34.06	37.37	49.88	59.05	66.56	73.04
28	15.57	20.91	28.10	33.40	37.75	41.51	55.77	66.29	74.93	82.40
29	16.90	22.85	30.90	36.87	41.79	46.05	62.27	74.30	84.21	92.80
30	18.24	24.95	33.95	40.66	46.21	51.02	69.43	83.14	94.48	104.33
31	19.88	27.22	37.27	44.79	51.03	56.46	77.31	92.90	105.84	117.11
32	21.55	29.68	40.88	49.30	56.30	62.41	85.96	103.66	118.39	131.24
33	23.34	32.34	44.80	54.20	62.05	68.92	95.46	115.51	132.24	146.87
34	25.28	35.21	49.05	59.54	68.33	76.02	105.90	128.55	147.51	164.12
35	27.36	38.32	53.67	65.36	75.17	83.78	117.33	142.89	164.33	183.16
36	29.60	41.68	58.68	71.69	82.62	92.24	129.87	158.65	182.85	204.14
37	32.02	45.31	64.13	78.57	90.75	101.48	143.61	175.95	203.23	227.26
38	34.63	49.24	70.03	86.05	99.60	111.56	158.65	194.94	225.62	252.71
39	37.44	53.50	76.45	94.20	109.24	122.54	175.11	215.78	250.23	280.71
40	40.47	58.10	83.40	103.05	119.74	134.52	193.13	238.62	277.26	311.50
41	43.74	63.07	90.96	112.68	131.18	147.59	212.84	263.67	306.94	345.34
42	47.27	68.46	99.16	123.16	143.64	161.83	234.40	291.13	339.52	382.53
43	51.08	74.30	108.08	134.56	157.21	177.36	257.99	321.22	375.28	423.39
44	55.20	80.62	117.76	146.97	172.00	194.31	283.80	354.20	414.51	468.28
45	59.66	87.48	128.28	160.48	188.12	212.79	312.03	390.35	457.57	517.58

Based on data from "Design of Pile Foundations," by A. S. Vesic. *Synthesis of Highway Practice* by American Association of State Highway and Transportation, 1977

TABLE 12.9 Variation of N_c^* with I_{rr} for $\phi = 0$ Condition Based on Vesic's Theory

I_{rr}	N_c^*
10	6.97
20	7.90
40	8.82
60	9.36
80	9.75
100	10.04
200	10.97
300	11.51
400	11.89
500	12.19

Now, referring to Eq. (12.26) for saturated clay with no volume change, $\Delta = 0$. Hence,

$$I_{rr} = I_r \tag{12.35}$$

For $\phi = 0$,

$$I_r = \frac{E_s}{3c_u} \tag{12.36}$$

O'Neill and Reese (1999) suggested the following approximate relationships for I_r and the undrained cohesion, c_u.

$\frac{c_u}{p_a}$	I_r
0.24	50
0.48	150
≥0.96	250−300

Note: p_a = atmospheric pressure ≈ 100 kN/m^2 or 2000 lb/ft^2.

The preceding values can be approximated as

$$I_r = 347\left(\frac{c_u}{p_a}\right) - 33 \leq 300 \tag{12.37}$$

12.11 Coyle and Castello's Method for Estimating Q_p in Sand

Coyle and Castello (1981) analyzed 24 large-scale field load tests of driven piles in sand. On the basis of the test results, they suggested that, in sand,

$$Q_p = q' N_q^* A_p \tag{12.38}$$

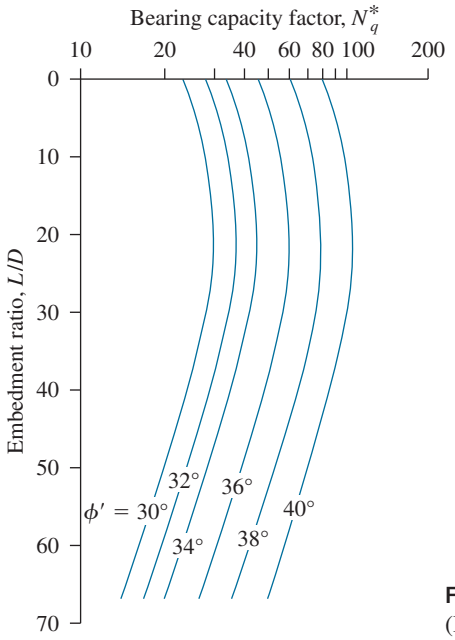


FIGURE 12.20 Variation of N_q^* with L/D (Based on Coyle and Castello, 1981)

where

q' = effective vertical stress at the pile tip

N_q^* = bearing capacity factor

Figure 12.20 shows the variation of N_q^* with L/D and the soil friction angle ϕ'.

EXAMPLE 12.1

Consider a 20 m long concrete pile with a cross section of 0.407 m × 0.407 m fully embedded in sand. For the sand, given: unit weight, $\gamma = 18$ kN/m^3; and soil friction angle, $\phi' = 35°$. Estimate the ultimate point Q_p with each of the following:

a. Meyerhof's method
b. Vesic's method
c. The method of Coyle and Castello
d. Based on the results of parts a, b, and c, adopt a value for Q_p

SOLUTION

Part a

From Eqs. (12.18) and (12.19),

$$Q_p = A_p q' N_q^* \le A_p(0.5 p_a N_q^* \tan \phi')$$

For $\phi' = 35°$, the value of $N_q^* \approx 143$ (Table 12.6). Also, $q' = \gamma L = (18)(20) = 360$ kN/m^2. Thus,

$$A_p q' N_q^* = (0.407 \times 0.407)(360)(143) \approx 8528 \text{ kN}$$

Again,

$$A_p(0.5 p_a N_q^* \tan \phi') = (0.407 \times 0.407)[(0.5)(100)(143)(\tan 35)] \approx 829 \text{ kN}$$

Hence, $Q_p =$ **829 kN**.

Part b

From Eq. (12.21),

$$Q_p = A_p \bar{\sigma}'_o N^*_\sigma$$

$$\bar{\sigma}'_o = \left[\frac{1 + 2(1 - \sin\phi')}{3}\right] q' = \left[\frac{1 + 2(1 - \sin 35)}{3}\right](18 \times 20)$$

$$= 222.34 \text{ kN/m}^2$$

From Eq. (12.28),

$$\frac{E_s}{p_a} = m$$

Assume $m \approx 250$ (medium sand). So,

$$E_s = (250)(100) = 25{,}000 \text{ kN/m}^2$$

From Eq. (12.29),

$$\mu_s = 0.1 + 0.3\left(\frac{\phi' - 25}{20}\right) = 0.1 + 0.3\left(\frac{35 - 25}{20}\right) = 0.25$$

From Eq. (12.30),

$$\Delta = 0.005\left(1 - \frac{\phi' - 25}{20}\right)\left(\frac{q'}{p_a}\right) = 0.005\left(1 - \frac{35 - 25}{20}\right)\left(\frac{18 \times 20}{100}\right) = 0.009$$

From Eq. (12.27),

$$I_r = \frac{E_s}{2(1 + \mu_s)q' \tan\phi'} = \frac{25{,}000}{(2)(1 + 0.25)(18 \times 20)(\tan 35)} = 39.67$$

From Eq. (12.26),

$$I_{rr} = \frac{I_r}{1 + I_r\Delta} = \frac{39.67}{1 + (39.67)(0.009)} = 29.23$$

From Table 12.8, for $\phi' = 35°$ and $I_{rr} = 29.23$, the value of $N^*_\sigma \approx 47$

$$Q_p = A_p \bar{\sigma}'_o N^*_\sigma = (0.407 \times 0.407)(222.34)(47) \approx \mathbf{1731 \text{ kN}}$$

Part c

From Eq. (12.38),

$$Q_p = q' N^*_q A_p$$

$$\frac{L}{D} = \frac{20}{0.407} = 49.1$$

For $\phi' = 35°$ and $L/D = 49.1$ N^*_q is about 34 (Figure 12.20). Thus,

$$Q_p = q' N^*_q A_p = (20 \times 18)(34)(0.407 \times 0.407) \approx \mathbf{2028 \text{ kN}}$$

Part d

It appears that Q_p obtained from the method of Coyle and Castello is too large. Thus, the average of the results from parts a and b is

$$\frac{829 + 1731}{2} = 1280 \text{ kN}$$

Use $Q_p = \mathbf{1280 \text{ kN}}$.

EXAMPLE 12.2

Consider a pipe pile (flat driving point—see Figure 12.2d) having an outside diameter of 457 mm. The embedded length of the pile in layered saturated clay is 20 m. The following are the details of the subsoil:

Depth from ground surface (m)	Saturated unit weight, γ (kN/m^3)	c_u (kN/m^2)
0–3	16	25
3–10	17	40
10–30	18	90

The groundwater table is located at a depth of 3 m from the ground surface. Estimate Q_p by using

a. Meyerhof's method
b. Vesic's method

SOLUTION

Part a

From Eq. (12.20),

$$Q_p = 9c_u A_p$$

The tip of the pile is resting on a clay with $c_u = 90$ kN/m^2. So,

$$Q_p = (9)(90)\left[\left(\frac{\pi}{4}\right)\left(\frac{457}{1000}\right)^2\right] = \mathbf{132.9\ kN}$$

Part b

From Eq. (12.33),

$$Q_p = A_p c_u N_c^*$$

From Eq. (12.37),

$$I_r = I_{rr} = 347\left(\frac{c_u}{p_a}\right) - 33 = 347\left(\frac{90}{100}\right) - 33 = 279.3$$

So use $I_{rr} = 279.3$.

From Table 12.9, for $I_{rr} = 279.3$, the value of $N_c^* \approx 11.4$. Thus,

$$Q_p = A_p c_u N_c^* = \left[\left(\frac{\pi}{4}\right)\left(\frac{457}{1000}\right)^2\right](90)(11.4) = \mathbf{168.3\ kN}$$

Note: The average value of Q_p is

$$\frac{132.9 + 168.3}{2} \approx \mathbf{151\ kN}$$

12.12 Correlations for Calculating Q_p with SPT and CPT Results in Granular Soil

On the basis of field observations, Meyerhof (1976) also suggested that the ultimate point resistance q_p in a homogeneous granular soil ($L = L_b$) may be obtained from standard penetration numbers as

$$q_p = 0.4 p_a N_{60} \frac{L}{D} \le 4 p_a N_{60} \tag{12.39}$$

where

N_{60} = the average value of the standard penetration number near the pile point (about $10D$ above to $4D$ below the pile point)

p_a = atmospheric pressure ($\approx$ 100 kN/m^2 or 2000 lb/ft^2)

Briaud et al. (1985) suggested the following correlation for q_p in granular soil with the standard penetration resistance N_{60}.

$$q_p = 19.7 p_a (N_{60})^{0.36} \tag{12.40}$$

Meyerhof (1956) also suggested that

$$q_p \approx q_c \tag{12.41}$$

where q_c = cone penetration resistance.

EXAMPLE 12.3

Consider a concrete pile that is 0.305 m $\times$ 0.305 m in cross section in sand. The pile is 12 m long. The following are the variations of N_{60} with depth.

Depth below ground surface (m)	N_{60}
1.5	8
3.0	10
4.5	9
6.0	12
7.5	14
9.0	18
10.5	11
12.0	17
13.5	20
15.0	28
16.5	29
18.0	32
19.5	30
21.0	27

a. Estimate Q_p using Eq. (12.39).
b. Estimate Q_p using Eq. (12.40).

SOLUTION

Part a

The tip of the pile is 12 m below the ground surface. For the pile, $D = 0.305$ m. The average of N_{60} $10D$ above and about $5D$ below the pile tip is

$$N_{60} = \frac{18 + 11 + 17 + 20}{4} = 16.5 \approx 17$$

From Eq. (12.39),

$$Q_p = A_p(q_p) = A_p\left[0.4p_aN_{60}\left(\frac{L}{D}\right)\right] \le A_p(4p_aN_{60})$$

$$A_p\left[0.4p_aN_{60}\left(\frac{L}{D}\right)\right] = (0.305 \times 0.305)\left[(0.4)(100)(17)\left(\frac{12}{0.305}\right)\right] = 2488.8 \text{ kN}$$

$$A_p(4p_aN_{60}) = (0.305 \times 0.305)[(4)(100)(17)] = 632.6 \text{ kN} \approx 633 \text{ kN}$$

Thus, $Q_p = \mathbf{633\ kN}$.

Part b

From Eq. (12.40),

$$Q_p = A_pq_p = A_p[19.7p_a(N_{60})^{0.36}] = (0.305 \times 0.305)[(19.7)(100)(17)^{0.36}]$$
$$= \mathbf{508.2\ kN}$$

12.13 Frictional Resistance (Q_s) in Sand

According to Eq. (12.15), the frictional resistance

$$Q_s = \Sigma p\,\Delta L\,f$$

The unit frictional resistance, f, is hard to estimate. In making an estimation of f, several important factors must be kept in mind:

1. The nature of the pile installation. For driven piles in sand, the vibration caused during pile driving helps densify the soil around the pile. The zone of sand densification may be as much as 2.5 times the pile diameter in the sand surrounding the pile.
2. It has been observed that the nature of variation of f in the field is approximately as shown in Figure 12.21. The unit skin friction increases with depth more or less linearly to a depth of L' and remains constant thereafter. The magnitude of the critical depth L' may be 15 to 20 pile diameters. A conservative estimate would be

$$L' \approx 15D \tag{12.42}$$

3. At similar depths, the unit skin friction in loose sand is higher for a high-displacement pile compared with a low-displacement pile.
4. At similar depths, bored, or jetted, piles will have a lower unit skin friction compared with driven piles.

Taking into account the preceding factors, we can give the following approximate relationship for f (see Figure 12.21):

For $z = 0$ to L',

$$f = K\sigma_o' \tan \delta' \tag{12.43}$$

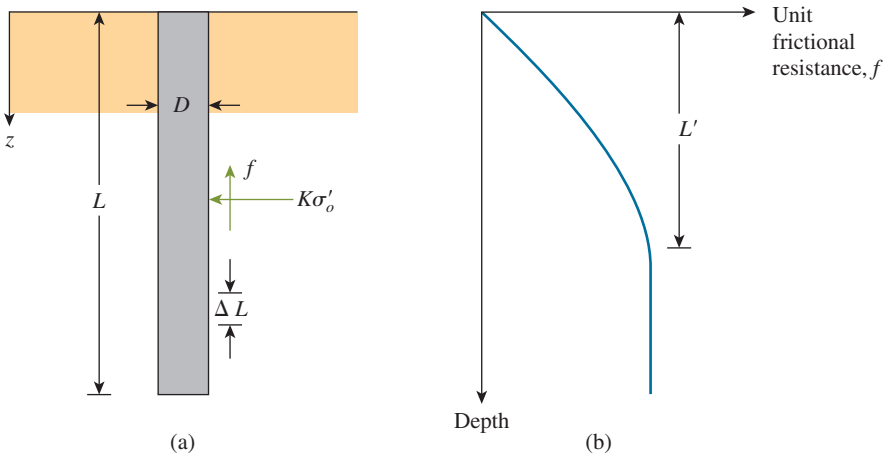


FIGURE 12.21 Unit frictional resistance for piles in sand

and for $z = L'$ to L,

$$f = f_{z=L'} \tag{12.44}$$

In these equations,

K = effective earth pressure coefficient

σ'_o = effective vertical stress at the depth under consideration

δ' = soil–pile friction angle

In reality, the magnitude of K varies with depth; it is approximately equal to the Rankine passive earth pressure coefficient, K_p, at the top of the pile and may be less than the at-rest pressure coefficient, K_o, at a greater depth. Based on presently available results, the following average values of K are recommended for use in Eq. (12.43):

Pile type	K
Bored or jetted	$\approx K_o = 1 - \sin\phi'$
Low-displacement driven	$\approx K_o = 1 - \sin\phi'$ to $1.4K_o = 1.4(1 - \sin\phi')$
High-displacement driven	$\approx K_o = 1 - \sin\phi'$ to $1.8K_o = 1.8(1 - \sin\phi')$

The values of δ' from various investigations appear to be in the range from $0.5\phi'$ to $0.8\phi'$.

Based on load test results in the field, Mansur and Hunter (1970) reported the following average values of K:

H-piles: $K = 1.65$
Steel pipe piles: $K = 1.26$
Precast concrete piles: $K = 1.5$

Coyle and Castello (1981), in conjunction with the material presented in Section 12.11, proposed that

$$Q_s = f_{av}pL = (K\overline{\sigma}'_o \tan\delta')pL \tag{12.45}$$

where

$\overline{\sigma}'_o$ = average effective overburden pressure

δ' = soil–pile friction angle = $0.8\phi'$

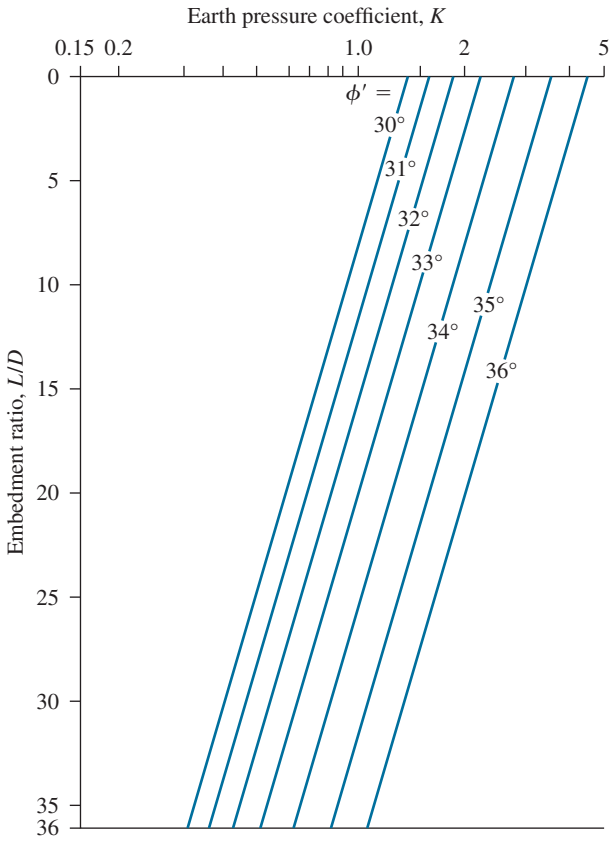


FIGURE 12.22 Variation of K with L/D (Redrawn after Coyle and Castello, 1981)

The lateral earth pressure coefficient K, which was determined from field observations, is shown in Figure 12.22. Thus, if that figure is used,

$$Q_s = K\,\overline{\sigma}'_o \tan(0.8\phi')pL \tag{12.46}$$

CORRELATION WITH STANDARD PENETRATION TEST RESULTS

Meyerhof (1976) indicated that the average unit frictional resistance, f_{av}, for high-displacement driven piles may be obtained from average standard penetration resistance values as

$$f_{av} = 0.02p_a(\overline{N}_{60}) \tag{12.47}$$

where

$(\overline{N}_{60})$ = average value of standard penetration resistance

p_a = atmospheric pressure ($\approx$100 kN/m^2 or 2000 lb/ft^2)

For low-displacement driven piles,

$$f_{av} = 0.01p_a(\overline{N}_{60}) \tag{12.48}$$

Briaud et al. (1985) suggested that

$$f_{av} \approx 0.224\,p_a(\overline{N}_{60})^{0.29} \tag{12.49}$$

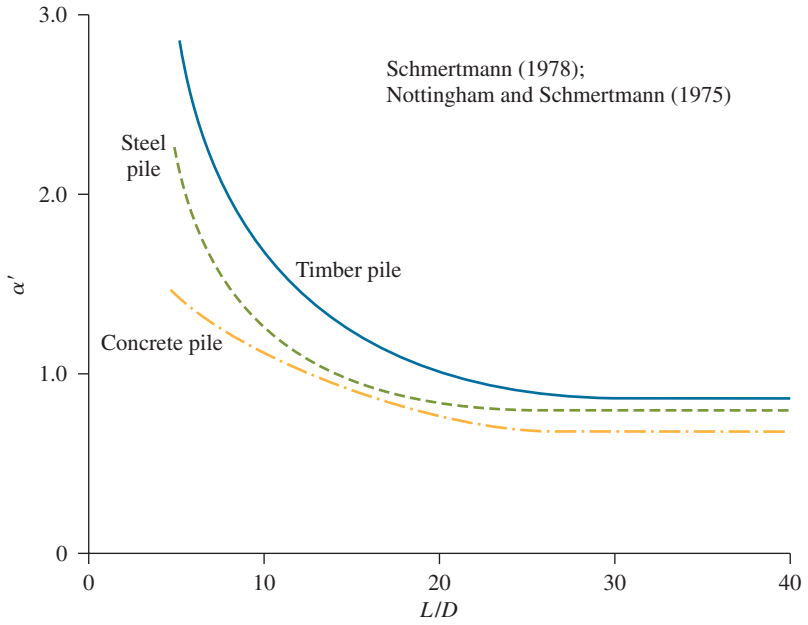


FIGURE 12.23 Variation of α' with embedment ratio for pile in sand: electric cone penetrometer

Thus,

$$Q_s = pLf_{av} \tag{12.50}$$

CORRELATION WITH CONE PENETRATION TEST RESULTS

Nottingham and Schmertmann (1975) and Schmertmann (1978) provided correlations for estimating Q_s using the frictional resistance (f_c) obtained during cone penetration tests. According to this method

$$f = \alpha' f_c \tag{12.51}$$

The variations of α' with L/D for electric cone and mechanical cone penetrometers are shown in Figures 12.23 and 12.24, respectively. We have

$$Q_s = \Sigma p(\Delta L) f = \Sigma p(\Delta L)\alpha' f_c \tag{12.52}$$

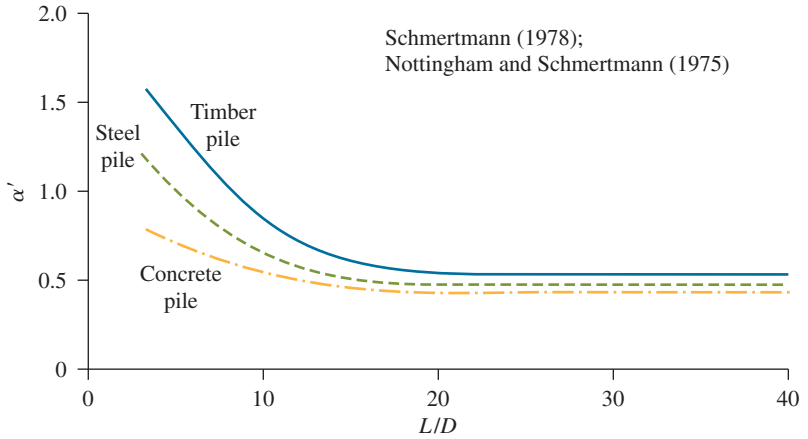


FIGURE 12.24 Variation of α' with embedment ratio for piles in sand: mechanical cone penetrometer

EXAMPLE 12.4

Refer to the pile described in Example 12.3. Estimate the magnitude of Q_s for the pile.

a. Use Eq. (12.47).
b. Use Eq. (12.49).
c. Considering the results in Example 12.3, determine the allowable load-carrying capacity of the pile based on Meyerhof's method and Briaud's method. Use a factor of safety FS = 3.

SOLUTION

The average N_{60} value for the sand for the top 12 m is

$$\overline{N}_{60} = \frac{8 + 10 + 9 + 12 + 14 + 18 + 11 + 17}{8} = 10.25 \approx 10$$

Part a
From Eq. (12.47),

$$f_{av} = 0.02 p_a(\overline{N}_{60}) = (0.02)(100)(10) = 20 \text{ kN/m}^2$$
$$Q_s = pLf_{av} = (4 \times 0.305)(12)(20) = \mathbf{292.8\ kN}$$

Part b
From Eq. (12.49),

$$f_{av} = 0.224\, p_a(\overline{N}_{60})^{0.29} = (0.224)(100)(10)^{0.29} = 43.68 \text{ kN/m}^2$$
$$Q_s = pLf_{av} = (4 \times 0.305)(12)(43.68) = \mathbf{639.5\ kN}$$

Part c

$$\text{Meyerhof's method: } Q_{all} = \frac{Q_p + Q_s}{FS} = \frac{633 + 292.8}{3} = \mathbf{308.6\ kN}$$
$$\text{Briaud's method: } Q_{all} = \frac{Q_p + Q_s}{FS} = \frac{508.2 + 639.5}{3} = \mathbf{382.6\ kN}$$

So the allowable pile capacity may be taken to be about **345 kN**.

EXAMPLE 12.5

Refer to Example 12.1. For the pile, estimate the frictional resistance Q_s.

a. Based on Eqs. (12.43) and (12.44). Use $K = 1.3$ and $\delta' = 0.8\phi'$.
b. Based on Eq. (12.46).
c. Using the results of Part d of Example 12.1, estimate the allowable bearing capacity of the pile. Use FS = 3.

SOLUTION

Part a
From Eq. (12.42), $L' = 15D = (15)(0.407) \approx 6.1$ m. Refer to Eq. (12.43):

At $z = 0$: $\sigma'_o = 0$, $f = 0$

At $z = 6.1$ m: $\sigma'_o = (6.1)(18) = 109.8 \text{ kN/m}^2$

So

$$f = K\sigma'_o \tan\delta' = (1.3)(109.8)[\tan(0.8 \times 35)] \approx 75.9 \text{ kN/m}^2$$

Thus,

$$Q_s = \frac{(f_{z=0} + f_{z=6.1\text{m}})}{2} pL' + f_{z=6.1\text{m}} p(L - L')$$

$$= \left(\frac{0 + 75.9}{2}\right)(4 \times 0.407)(6.1) + (75.9)(4 \times 0.407)(20 - 6.1)$$

$$= 376.87 + 1717.56 = 2094.43 \text{ kN} \approx \mathbf{2094 \text{ kN}}$$

Part b

From Eq. (12.46),

$$Q_s = K\bar{\sigma}'_o \tan(0.8\phi')pL$$

$$\bar{\sigma}'_o = \frac{(20)(18)}{2} = 180 \text{ kN/m}^2$$

$$\frac{L}{D} = \frac{20}{0.407} = 49.1; \phi' = 35^\circ$$

From Figure 12.22, $K \approx 0.41$ (by projection)

$$Q_s = (0.41)(180)\tan[(0.8 \times 35)](4 \times 0.407)(20) = \mathbf{1277.66 \text{ kN}}$$

Part c

The average value of Q_s from parts a and b is

$$Q_{s(\text{average})} = \frac{2094 + 1277.66}{2} = 1685.83 \approx 1686 \text{ kN—USE}$$

From part d of Example 12.1, $Q_p = 1280$ kN

$$Q_{\text{all}} = \frac{Q_p + Q_s}{\text{FS}} = \frac{1280 + 1686}{3} = \mathbf{988.7 \text{ kN}}$$

EXAMPLE 12.6

Consider an 18 m long concrete pile (cross section: 0.305 m × 0.305 m) fully embedded in a sand layer. For the sand layer, the following is an approximation of the cone penetration resistance q_c (mechanical cone) and the frictional resistance f_c with depth. Estimate the allowable load that the pile can carry. Use FS = 3.

Depth from ground surface (m)	q_c (kN/m^2)	f_c (kN/m^2)
0–5	3040	73
5–15	4560	102
15–25	9500	226

SOLUTION

$$Q_u = Q_p + Q_s$$

From Eq. (12.41),

$$q_p \approx q_c$$

At the pile tip (i.e., at a depth of 18 m), $q_c \approx 9500$ kN/m^2. Thus,

$$Q_p = A_p q_c = (0.305 \times 0.305)(9500) = 883.7 \text{ kN}$$

To determine Q_s, the following table can be prepared. (*Note:* $L/D = 18/0.305 = 59$.)

Depth from ground surface (m)	ΔL (m)	f_c (kN/m^2)	α' (Figure 12.24)	$p\,\Delta L\,\alpha' f_c$ (kN)
0–5	5	73	0.44	195.9
5–15	10	102	0.44	547.5
15–18	3	226	0.44	363.95
				Q_s = **1107.35 kN**

Hence,

$$Q_u = Q_p + Q_s = 883.7 + 1107.35 = 1991.05 \text{ kN}$$

$$Q_{\text{all}} = \frac{Q_u}{\text{FS}} = \frac{1991.05}{3} = 663.68 \approx \mathbf{664\ kN}$$

12.14 Frictional (Skin) Resistance in Clay

Estimating the frictional (or skin) resistance of piles in clay is as difficult a task as estimating that in sand (see Section 12.13) due to the presence of several variables that cannot easily be quantified. Several methods for obtaining the unit frictional resistance of piles are described in the literature. We examine some of them next.

λ METHOD

This is a *total stress* method, proposed by Vijayvergiya and Focht (1972), and is based on the assumption that the displacement of soil caused by pile driving results in a passive lateral pressure at any depth and that the average unit skin resistance is

$$f_{\text{av}} = \lambda(\bar{\sigma}'_o + 2c_u) \tag{12.53}$$

where

$\bar{\sigma}'_o$ = mean effective vertical stress for the entire embedment length

c_u = mean undrained shear strength ($\phi = 0$)

The value of λ decreases with the depth of penetration of the pile. (See Table 12.10.) Thus, the total frictional resistance may be calculated as

$$Q_s = pLf_{\text{av}}$$

Care should be taken in obtaining the values of $\bar{\sigma}'_o$ and c_u in layered soil. Figure 12.25 helps explain the reason. Figure 12.25a shows a pile penetrating three layers of clay. According to Figure 12.25b, the mean value of c_u is $(c_{u(1)}L_1 + c_{u(2)}L_2 + \cdots)/L$. Similarly, Figure 12.25c shows the plot of the variation of effective stress with depth. The mean effective stress is

$$\bar{\sigma}'_o = \frac{A_1 + A_2 + A_3 + \cdots}{L} \tag{12.54}$$

where $A_1, A_2, A_3, \cdots$ = areas of the vertical effective stress diagrams.

TABLE 12.10 Variation of λ with Pile Embedment Length, L

Embedment length, L (m)	λ
0	0.5
5	0.336
10	0.245
15	0.200
20	0.173
25	0.150
30	0.136
35	0.132
40	0.127
50	0.118
60	0.113
70	0.110
80	0.110
90	0.110

α METHOD

This is a total stress method where the unit skin resistance is expressed as

$$f = \alpha c_u \tag{12.55}$$

where α is an empirical adhesion factor that lies in the range of 0–1, decreasing with the undrained shear strength c_u. Generally, overconsolidated clays have larger c_u and hence lower α. Nevertheless, clay deposits at very large depths can be normally consolidated while having high c_u due to the overburden stress. Here, α can still be closer to unity in spite of large c_u. The stress history (i.e., OCR) comes into play here.

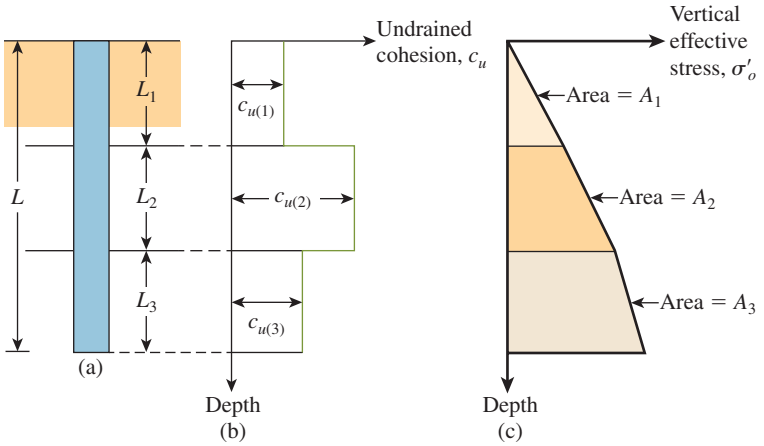


FIGURE 12.25 Application of λ method in layered soil

TABLE 12.11 Variation of α (Interpolated Values Based on Terzaghi et al., 1996)

$\frac{c_u}{p_a}$	α
≤ 0.1	1.00
0.2	0.92
0.3	0.82
0.4	0.74
0.6	0.62
0.8	0.54
1.0	0.48
1.2	0.42
1.4	0.40
1.6	0.38
1.8	0.36
2.0	0.35
2.4	0.34
2.8	0.34

Note: p_a = atmospheric pressure ≈ 100 kN/m^2 or 2000 lb/ft^2

The approximate variation of the value of α is shown in Table 12.11. It is important to realize that the values of α given in Table 12.11 may vary somewhat, since α is actually a function of vertical effective stress and the undrained cohesion. Sladen (1992) has shown that

$$\alpha = C\left(\frac{\overline{\sigma}'_o}{c_u}\right)^{0.45} \tag{12.56}$$

where

$\overline{\sigma}'_o$ = average vertical effective stress

$C \approx 0.4$ to 0.5 for bored piles; and ≥ 0.5 for driven piles

A correlation proposed by Randolph and Murphy (1987) was incorporated into the code of the American Petroleum Institute (API) in 1987 as

$$\alpha = 0.5\left(\frac{c_u}{\overline{\sigma}'_o}\right)^{-0.5} \qquad \left(\text{for } \frac{c_u}{\overline{\sigma}'_o} \leq 1\right) \tag{12.57a}$$

and

$$\alpha = 0.5\left(\frac{c_u}{\overline{\sigma}'_o}\right)^{-0.25} \qquad \left(\text{for } \frac{c_u}{\overline{\sigma}'_o} > 1\right) \tag{12.57b}$$

It was further modified by API (2007) as

$$f_{\text{av}} = 0.5(c_u\overline{\sigma}'_o)^{0.5} \quad \text{or} \quad 0.5(c_u)^{0.75}(\overline{\sigma}'_o)^{0.25} \quad \text{(whichever is larger)} \tag{12.58}$$

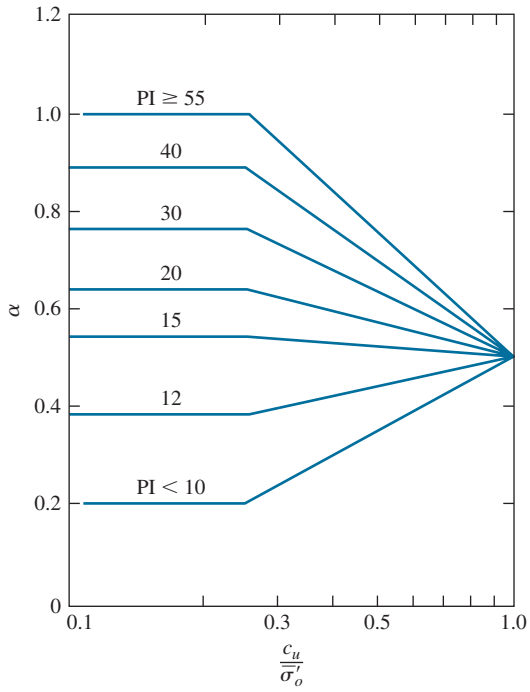


FIGURE 12.26 Variation of α with $c_u/\overline{\sigma}'_o$ for the NGI-99 method [Eqs. (12.59a) and (12.59b)]

Karlsrud et al. (2005) proposed an alternate relationship for α that is known as the Norwegian Geotechnical Institute (NGI)-99 method. According to this method,

$$\alpha = 0.32(\text{PI} - 10)^{0.3} (1 \geq \alpha \geq 0.2) \quad \left(\text{for } \frac{c_u}{\overline{\sigma}'_o} \leq 0.25\right) \tag{12.59a}$$

and

$$\alpha = 0.5 \quad \left(\text{for } \frac{c_u}{\overline{\sigma}'_o} = 1\right) \tag{12.59b}$$

The term α has a log–linear relationship with $c_u/\overline{\sigma}'_o$ between $c_u/\overline{\sigma}'_o = 0.25$ and 1. This is shown graphically in Figure 12.26. For $c_u/\overline{\sigma}'_o \geq 1$,

$$\alpha = 0.5\left(\frac{c_u}{\overline{\sigma}'_o}\right)^{-0.3} C \tag{12.60}$$

where C is the correction factor.

The interpolated values of α for open-ended and closed-ended piles are given in Table 12.12.

The ultimate side resistance can thus be given as

$$Q_s = \Sigma f p\, \Delta L = \Sigma \alpha c_u p\, \Delta L \tag{12.61}$$

β METHOD

When piles are driven into saturated clays, the pore water pressure in the soil around the piles increases. The excess pore water pressure in normally consolidated clays may be four to six times c_u. However, within a month or so, this pressure gradually dissipates. Hence, the unit frictional resistance for the pile can be determined on the basis of the effective stress parameters of the clay in a remolded state ($c' = 0$). Thus, at any depth,

$$f = \beta \sigma'_o \tag{12.62}$$

TABLE 12.12 Variation of α with $c_u/\overline{\sigma}'_o$

$\frac{c_u}{\overline{\sigma}'_o}$	α	
	Open-ended pile	Closed-ended pile
1	0.5	0.5
2	0.4	0.44
3	0.355	0.41
4	0.33	0.395
5	0.31	0.38
6	0.29	0.365
7	0.28	0.35
8	0.26	0.33
9	0.255	0.32
10	0.25	0.31

where

σ'_o = vertical effective stress

$\beta = K \tan \phi'_R$ (12.63)

ϕ'_R = drained friction angle of remolded clay

K = earth pressure coefficient

Conservatively, the magnitude of K is the earth pressure coefficient at rest, or

$$K = 1 - \sin \phi'_R \qquad \text{(for normally consolidated clays)} \tag{12.64}$$

and

$$K = (1 - \sin \phi'_R)\sqrt{\text{OCR}} \qquad \text{(for overconsolidated clays)} \tag{12.65}$$

where OCR is the overconsolidation ratio.

Combining Eqs. (12.62), (12.63), (12.64), and (12.65) for normally consolidated clays yields

$$f = (1 - \sin \phi'_R) \tan \phi'_R \sigma'_o \tag{12.66}$$

and for overconsolidated clays,

$$f = (1 - \sin \phi'_R) \tan \phi'_R \sqrt{\text{OCR}}\ \sigma'_o \tag{12.67}$$

With the value of f determined, the total frictional resistance may be evaluated as

$$Q_s = \Sigma f p\, \Delta L$$

CORRELATION WITH CONE PENETRATION TEST RESULTS

Nottingham and Schmertmann (1975) and Schmertmann (1978) found the correlation for unit skin friction in clay (with $\phi = 0$) to be

$$f = \alpha' f_c \tag{12.68}$$

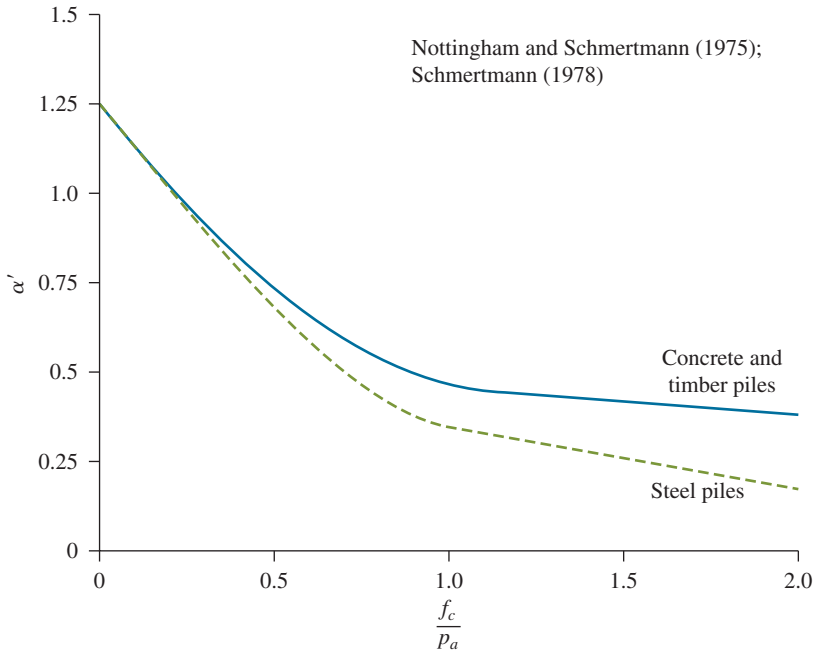


FIGURE 12.27 Variation of α' with f_c/p_a for piles in clay (p_a = atmospheric pressure $\approx$100 kN/m^2 or 2000 lb/ft^2)

The variation of α' with the frictional resistance f_c is shown in Figure 12.27. Thus,

$$Q_s = \Sigma fp(\Delta L) = \Sigma \alpha' f_c p(\Delta L) \tag{12.69}$$

12.15 Ultimate Capacity of Continuous Flight Auger Pile

In Section 12.3, a brief description of continuous flight auger piles was given. The procedure for estimating the ultimate bearing capacity (point and frictional/skin resistance) is briefly discussed in this section and is primarily based on the pile load test results in the field reported by Coleman and Arcement (2002) and the FHWA (2007).

GRANULAR SOIL

Based on the pile load tests in Mississippi and Louisiana conducted by Coleman and Arcement (2002), it has been suggested that the unit side-skin frictional resistance in sandy and silty soil (drained condition) can be given as

$$f = \beta \sigma_o' \leq 200 \text{ kN/m}^2 \text{ (4000 lb/ft}^2\text{)} \tag{12.70}$$

The values of β can be estimated as

$$\beta = 2.27 z_m^{-0.67} \quad \text{(silty soil)} \tag{12.71}$$

and

$$\beta = 10.72 z_m^{-1.3} \quad \text{(sandy soil)} \tag{12.72}$$

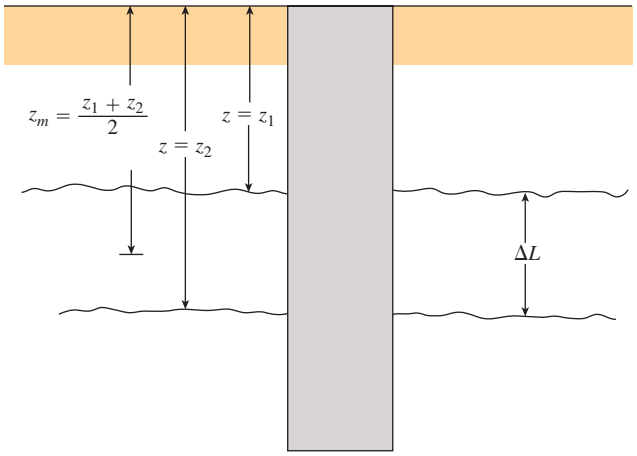


FIGURE 12.28 Definition of z_m [Eqs. (12.71) and (12.72)]

where z_m = depth in meters measured from the ground surface to the middle of the given soil layer (Figure 12.28).

The value of β is limited to $0.2 \leq \beta \leq 2.5$. Thus,

$$Q_s = \Sigma fp\, \Delta L \tag{12.73}$$

where p = pile diameter.

According to the FHWA (2007), the unit ultimate point load can be given as

$$q_p\ (\text{kN/m}^2) \approx 57.5N_{60} \quad (\text{for } 0 \leq N_{60} \leq 75) \tag{12.74a}$$

and

$$q_p = 4300\ \text{kN/m}^2 \quad (\text{for } N_{60} > 75) \tag{12.74b}$$

where N_{60} = field standard penetration number that is the average of the N_{60} values between one pile diameter above and 2 to 3 pile diameters below the pile tip. Also,

$$q_p\ (\text{MN/m}^2) = 0.375q_c\ (\text{MN/m}^2) \tag{12.75}$$

where q_c = average cone penetration resistance between 2 to 3 pile diameters below the pile tip.

COHESIVE SOIL

The CFA pile load test results of Coleman and Arcement (2002) in cohesive soil indicate [also see FHWA (2007)] that unit side-skin resistance can be expressed as [Eq. (12.55)]

$$f = \alpha c_u = 56.2\ \text{kN/m}^2 \quad (\text{for } 25\ \text{kN/m}^2 \leq c_u \leq 150\ \text{kN/m}^2) \tag{12.76}$$

The FHWA (2007) also recommends that the unit ultimate point resistance can be given as

$$q_p = 0.15q_c \tag{12.77}$$

where q_c = average cone resistance between 2 to 3 pile diameters below the pile tip.

12.16 Point Bearing Capacity of Piles Resting on Rock

Sometimes piles are driven to an underlying layer of rock. In such cases, the engineer must evaluate the bearing capacity of the rock. The ultimate unit point resistance in rock (Goodman, 1980) is approximately

$$q_p = q_u(N_\phi + 1) \tag{12.78}$$

where

$N_\phi = \tan^2(45 + \phi'/2)$

q_u = unconfined compression strength of rock

ϕ' = drained angle of friction

The unconfined compression strength of rock can be determined by laboratory tests on rock specimens collected during field investigation. However, extreme caution should be used in obtaining the proper value of q_u, because laboratory specimens usually are small in diameter. As the diameter of the specimen increases, the unconfined compression strength decreases—a phenomenon referred to as the *scale effect*. For specimens larger than about 1 m (3 ft) in diameter, the value of q_u remains approximately constant. There appears to be a fourfold to fivefold reduction of the magnitude of q_u in this process. The scale effect in rock is caused primarily by randomly distributed large and small fractures and also by progressive ruptures along the slip lines. Hence, we always recommend that

$$q_{u(\text{design})} = \frac{q_{u(\text{lab})}}{5} \tag{12.79}$$

Table 12.13 lists some representative values of (laboratory) unconfined compression strengths of rock. Representative values of the rock friction angle ϕ' are also given in Table 12.13.

A factor of safety of at least 3 should be used to determine the allowable point bearing capacity of piles. Thus,

$$Q_{p(\text{all})} = \frac{[q_{u(\text{design})}(N_\phi + 1)]A_p}{\text{FS}} \tag{12.80}$$

TABLE 12.13 Typical Unconfined Compressive Strength and Angle of Friction of Rocks

Type of rock	q_u (laboratory) MN/m^2	q_u (laboratory) lb/in^2	ϕ' (deg)
Sandstone	70–140	10,000–20,000	27–45
Limestone	105–210	15,000–30,000	30–40
Shale	35–70	5000–10,000	10–20
Granite	140–210	20,000–30,000	40–50
Marble	60–70	8500–10,000	25–30

EXAMPLE 12.7

Refer to the pipe pile in saturated clay shown in Figure 12.29. For the pile,

a. Calculate the skin resistance (Q_s) by (1) the α method, (2) the λ method, and (3) the β method. For the β method, use $\phi'_R = 30°$ for all clay layers. The top 10 m of clay is normally consolidated. The bottom clay layer has an OCR = 2. (*Note:* diameter of pile = 457 mm)

b. Using the results of Example 12.2 (same soil and pile data), estimate the allowable pile capacity (Q_{all}). Use FS = 3.

SOLUTION

Part a

(1) From Eq. (12.61),

$$Q_s = \Sigma \alpha\, c_u p\, \Delta L$$

[*Note:* $p = \pi(0.457) = 1.436$ m] Now the following table can be prepared.

Depth (m)	ΔL (m)	c_u (kN/m^2)	α (Table 12.11)	$\alpha c_u p\, \Delta L$ (kN)
0–3	3	25	0.87	93.7
3–10	7	40	0.74	297.5
10–20	10	90	0.51	659.1
				$Q_s \approx$ **1050 kN**

(2) From Eq. 12.53, $f_{av} = \lambda(\bar{\sigma}'_o + 2c_u)$. Now, the average value of c_u is

$$\frac{c_{u(1)}(3) + c_{u(2)}(7) + c_{u(3)}(10)}{20} = \frac{(25)(3) + (40)(7) + (90)(10)}{20} = 62.75 \text{ kN/m}^2$$

To obtain the average value of $\bar{\sigma}'_o$, the diagram for vertical effective stress variation with depth is plotted in Figure 12.29b. From Eq. (12.54),

$$\bar{\sigma}'_o = \frac{A_1 + A_2 + A_3}{L} = \frac{72 + 512.16 + 1392.8}{20} = 98.85 \text{ kN/m}^2$$

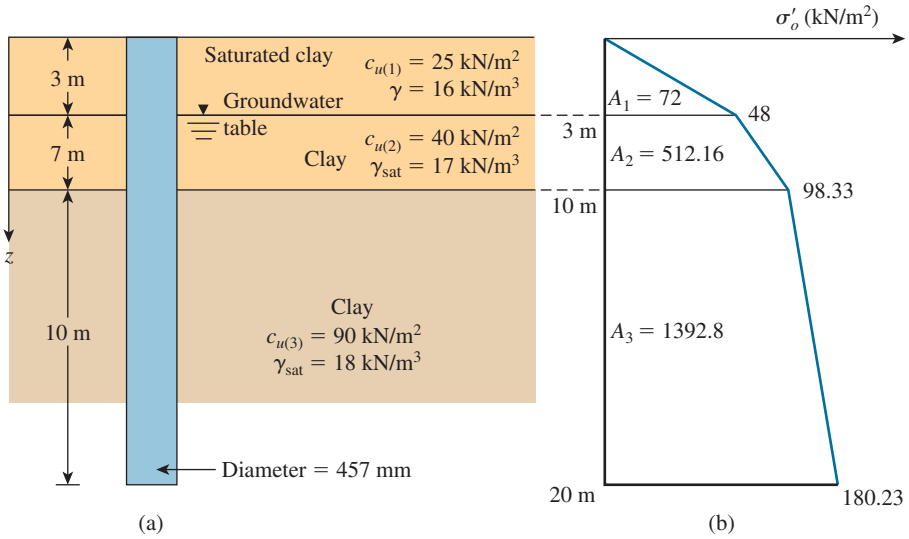


FIGURE 12.29 Estimation of the load bearing capacity of a driven-pipe pile

From Table 12.10, the magnitude of λ is 0.173. So

$$f_{av} = 0.173[98.85 + (2)(62.75)] = 38.81 \text{ kN/m}^2$$

Hence,

$$Q_s = pLf_{av} = \pi(0.457)(20)(38.81) = \mathbf{1114.4\ kN}$$

(3) The top layer of clay (10 m) is normally consolidated, and $\phi'_R = 30°$. For $z = 0–3$ m, from Eq. (12.66) we have

$$f_{av(1)} = (1 - \sin \phi'_R)\tan \phi'_R \, \overline{\sigma}'_o$$
$$= (1 - \sin 30°)(\tan 30°)\left(\frac{0 + 48}{2}\right) = 6.93 \text{ kN/m}^2$$

Similarly, for $z = 3–10$ m,

$$f_{av(2)} = (1 - \sin 30°)(\tan 30°)\left(\frac{48 + 98.33}{2}\right) = 21.12 \text{ kN/m}^2$$

For $z = 10–20$ m from Eq. (12.67),

$$f_{av} = (1 - \sin \phi'_R)\tan \phi'_R \sqrt{\text{OCR}}\, \overline{\sigma}'_o$$

For OCR = 2,

$$f_{av(3)} = (1 - \sin 30°)(\tan 30°)\sqrt{2}\left(\frac{98.33 + 180.23}{2}\right) = 56.86 \text{ kN/m}^2$$

So,

$$Q_s = p[f_{av(1)}(3) + f_{av(2)}(7) + f_{av(3)}(10)]$$
$$= (\pi)(0.457)[(6.93)(3) + (21.12)(7) + (56.86)(10)] = \mathbf{1058.45\ kN}$$

Part b

$$Q_u = Q_p + Q_s$$

From Example 12.2,

$$Q_p \approx 151 \text{ kN}$$

Again, the values of Q_s from the α method, λ method, and β method are close. So,

$$Q_s = \frac{1050 + 1114.4 + 1058.45}{3} \approx 1074 \text{ kN}$$

$$Q_{all} = \frac{Q_u}{FS} = \frac{151 + 1074}{3} = 408.3 \text{ kN} \approx \mathbf{408\ kN}$$

EXAMPLE 12.8

A concrete pile 305 mm × 305 mm in cross section is driven to a depth of 20 m below the ground surface in a saturated clay soil. A summary of the variation of frictional resistance f_c obtained from a cone penetration test is as follows:

Depth (m)	Friction resistance, f_c (kg/cm^2)
0–6	0.35
6–12	0.56
12–20	0.72

Estimate the frictional resistance Q_s for the pile.

SOLUTION

We can prepare the following table:

Depth (m)	f_c (kN/m^2)	α' (Figure 12.27)	ΔL (m)	$\alpha' f_c p(\Delta L)$ [Eq. (12.69)] (kN)
0–6	34.34	0.84	6	211.5
6–12	54.94	0.71	6	285.5
12–20	70.63	0.63	8	434.2

[*Note:* $p = (4)(0.305) = 1.22$ m]

Thus,

$$Q_s = \Sigma \alpha' f_c p(\Delta L) = \mathbf{931\ kN}$$

EXAMPLE 12.9

Refer to Example 12.7 and Figure 12.29. Using Eq. (12.58), estimate the skin resistance Q_s.

SOLUTION

For $z = 0$ to 3 m,

$$c_{u(1)} = 25\ \text{kN/m}^2;\quad \bar{\sigma}'_o = \frac{0 + 48}{2} = 24\ \text{kN/m}^2$$
$$f_{\text{av}} = 0.5(c_u \bar{\sigma}'_o)^{0.5} = 0.5[(25)(24)]^{0.5} = 12.25\ \text{kN/m}^2$$

Again,

$$f_{\text{av}} = 0.5(c_u)^{0.75}(\bar{\sigma}'_o)^{0.25} = 0.5(25)^{0.75}(24)^{0.25} = 12.37\ \text{kN/m}^2$$

Use $f_{\text{av}} = 12.37$ kN/m^2.

For $z = 3$ to 10 m,

$$c_{u(2)} = 40\ \text{kN/m}^2;\quad \bar{\sigma}'_o = \frac{48 + 98.33}{2} = 73.165\ \text{kN/m}^2$$
$$f_{\text{av}} = 0.5(c_u \bar{\sigma}'_o)^{0.5} = 0.5[(40)(73.165)]^{0.5} = 27.05\ \text{kN/m}^2$$
$$f_{\text{av}} = 0.5(c_u)^{0.75}(\bar{\sigma}'_o)^{0.25} = 0.5(40)^{0.75}(73.165)^{0.25} = 23.26\ \text{kN/m}^2$$

Use $f_{\text{av}} = 27.05$ kN/m^2.

For $z = 10$ to 20 m,

$$c_{u(3)} = 90\ \text{kN/m}^2;\ \bar{\sigma}'_o = \frac{98.33 + 180.23}{2} = 139.28\ \text{kN/m}^2$$
$$f_{\text{av}} = 0.5(c_u \bar{\sigma}'_o)^{0.5} = 0.5[(90)(139.28)]^{0.5} = 55.98\ \text{kN/m}^2$$
$$f_{\text{av}} = 0.5(c_u)^{0.75}(\bar{\sigma}'_o)^{0.25} = 0.5(90)^{0.75}(139.28)^{0.25} = 50.19\ \text{kN/m}^2$$

Use $f_{\text{av}} = 55.98$ kN/m^2.

Now,

$$Q_s = \Sigma f_{\text{av}} p\ \Delta L = (\pi \times 0.457)[(12.37)(3) + (27.05)(7) + (55.98)(10)] = \mathbf{1128.8\ kN}$$

EXAMPLE 12.10

Consider a CFA pile in granular soil (see Section 12.15) that has a nominal diameter of 0.6 m and length of 12 m. The average value of N_{60} between one pile diameter above and 3 pile diameters below the pile tips is 20. Use FS = 3 and estimate the allowable load-carrying capacity of the pile. Assume the unit weight of sand at $\gamma = 16$ kN/m^3.

SOLUTION

We will divide the pile into three segments (i.e., 4 m in length for each segment). Now we can prepare the following table.

Pile Segment no.	Depth (m)	z_m[a]	β[a]	β to be used
1	0–4	2	4.35	2.5
2	4–8	6	1.04	1.04
3	8–12	10	0.537	0.537

[a]Eq. (12.72) is $\beta = 10.72 z_m^{-1.3}$ $(0.2 < \beta < 2.5)$

Figure 12.30 shows the variation of σ'_o with depth. The average values of σ'_o (i.e., $\overline{\sigma}'_o$) for the three segments are

$$\text{Segment 1: } \frac{0 + 64}{2} = 32 \text{ kN/m}^2$$

$$\text{Segment 2: } \frac{64 + 128}{2} = 96 \text{ kN/m}^2$$

and

$$\text{Segment 3: } \frac{128 + 192}{2} = 160 \text{ kN/m}^2$$

Hence, the values of f_{av} [Eq. (12.70)] are

$$\text{Segment 1: } f_{av} = \beta\overline{\sigma}'_o = (2.5)(32) = 80 \text{ kN/m}^2$$

$$\text{Segment 2: } f_{av} = (1.04)(96) = 99.84 \text{ kN/m}^2$$

and

$$\text{Segment 3: } f_{av} = (0.537)(160) = 85.92 \text{ kN/m}^2$$

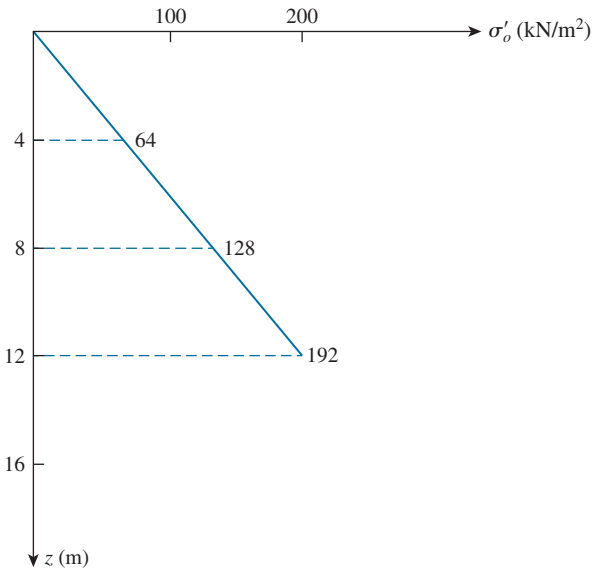


FIGURE 12.30

Hence,

$$Q_s = \Sigma f_{av} p\, \Delta L = (\pi \times 0.6)(4)(80 + 99.84 + 85.92) = \mathbf{2003.8\ kN}$$

From Eq. (12.74a),

$$q_p = 57.5N_{60} = (57.5)(20) = 1150\ \text{kN/m}^2$$

$$Q_p = \frac{\pi}{4}D^2 q_p = \left(\frac{\pi}{4}\right)(0.6)^2(1150) = 325.15\ \text{kN}$$

and

$$Q_{all} = \frac{Q_s + Q_p}{FS} = \frac{2003.8 + 325.15}{3} = \mathbf{776.3\ kN}$$

EXAMPLE 12.11

Figure 12.31 shows an idealized variation of c_u in a saturated clay. A CFA pile is to be constructed in this clay with a length of 10 m and a diameter of D of 0.45 m. Estimate the ultimate side-skin resistance Q_s and the point load Q_p for the pile. Assume a unit weight of γ for the clay to be 18 kN/m^3.

SOLUTION

From Eqs. (12.55) and (12.76),

$$f_{av} = \alpha c_u = 56.2\ \text{kN/m}^2$$

Hence,

$$Q_s = (\pi D)(f_{av})L = (\pi)(0.45)(56.2)(10) = \mathbf{252.9\ kN}$$

The magnitude of c_u at $z = 10$ m is 100 kN/m^2. Similarly, the magnitude of c_u at $z = 10\ \text{m} + 3D = 10 + (3)(0.45) = 10 + 1.35 = 11.35$ m is $100 + (7.14)(1.35) = 109.6$ kN/m^2. Thus, the average value of c_u within a distance of $3D$ below the pile tip is about $(100 + 109.6)/2 = 104.8$ kN/m^2. Again, from Eq. (3.56),

$$c_u = \frac{q_c - \sigma_o}{N_K}$$

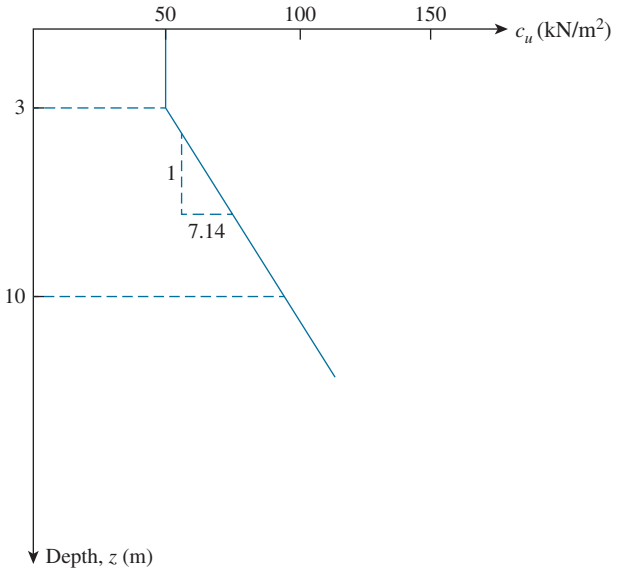


FIGURE 12.31

So, σ'_o at a depth of about 11 m below the ground surface is $(\gamma)(11) = (18)(11) = 198$ kN/m^2. For an electric cone, $N_K \approx 15$. Hence,

$$c_u = 104.8 = \frac{q_c - 198}{15}$$

and

$$q_c = (104.8)(15) + 198 = 1770 \text{ kN/m}^2$$

From Eq. (12.77),

$$q_p = 0.15q_c = (0.15)(1770) = 265.5 \text{ kN/m}^2$$

and

$$Q_p = \frac{\pi}{4}D^2q_p = \left(\frac{\pi}{4}\right)(0.45)^2(265.5) = \mathbf{42.2\ kN}$$

12.17 Pile Load Tests

High-rise buildings often require several piles to support the building loads. We have seen in previous sections that there are different methods for predicting the load-carrying capacities of the pile point and pile shaft, and the ultimate load Q_u thus determined can vary significantly depending on the method and the factors used. Varying soil conditions, unreliable soil parameters, and the assumptions and simplifications in the theoretical model used in the prediction contribute to the variability in the ultimate load Q_u. The pile load test is a good way to verify the load-carrying capacity of a pile.

Figure 12.32 shows schematic diagrams of two different pile load test arrangements for testing *axial compression* in the field. The main difference between the two is the way the horizontal reaction beam is held in place. In Figure 12.32a, a kentledge, consisting of heavy weights, is required to hold the reaction beam in place, and the hydraulic jack is used to jack against the beam and hence apply the pile load. In Figure 12.32b, two reaction piles, located far away from the test pile, anchor the horizontal reaction beam to the ground.

The loads are applied in increments as specified by the relevant standards, with sufficient time between the load increments. Generally, the piles are loaded well beyond their working loads (e.g., 2 times). On reaching the maximum load for the test, the pile is unloaded in steps. The dial gauges measure the settlement of the pile head where they are mounted. This is the *total* or *gross settlement*, denoted as s_t. Due to the compressibility of the pile material, the pile itself undergoes some elastic compression, known as the *elastic shortening* or *elastic compression of the pile*, denoted here as s_e. The *net settlement* of the pile is the settlement of the pile point, which is slightly less and is denoted as s_{net}. Therefore, at any load,

$$s_{\text{net}} = s_t - s_e \tag{12.81}$$

Figure 12.32c shows a load-settlement diagram obtained from field loading and unloading. For any load Q, the net pile settlement can be calculated as follows:

When $Q = Q_1$,

$$\text{Net settlement, } s_{\text{net}(1)} = s_{t(1)} - s_{e(1)}$$

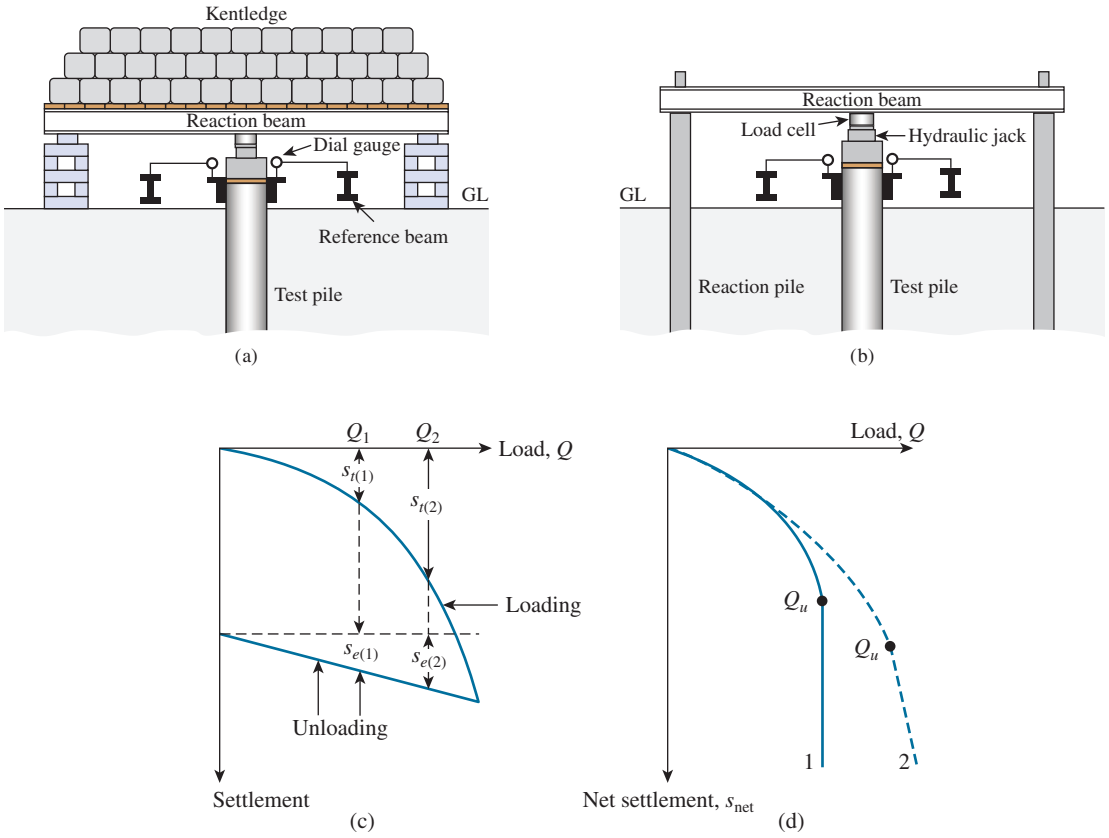


FIGURE 12.32 Pile load test: (a) using kentledge, (b) using reaction pile, (c) load vs. total settlement plots, and (d) load vs. net settlement

When $Q = Q_2$,

$$\text{Net settlement, } s_{\text{net}(2)} = s_{t(2)} - s_{e(2)}$$

$$\vdots$$

These values of Q can be plotted in a graph against the corresponding net settlement, s_{net}, as shown in Figure 12.32d. The ultimate load of the pile can then be determined from the graph. Pile settlement may increase with load to a certain point, beyond which the load-settlement curve becomes vertical. The load corresponding to the point where the curve of Q versus s_{net} becomes vertical is the ultimate load, Q_u, for the pile; it is shown by curve 1 in Figure 12.32d. In many cases, the latter stage of the load-settlement curve is almost linear, showing a large degree of settlement for a small increment of load; this is shown by curve 2 in the figure. The ultimate load, Q_u, for such a case is determined from the point of the curve of Q versus s_{net} where this steep linear portion starts.

One of the methods to obtain the ultimate load Q_u from the load-settlement plot is that proposed by Davisson (1973). Davisson's method is used more often in the field and is described here. Referring to Figure 12.33, the ultimate load occurs at a total settlement level (s_u) of

$$s_u\,(\text{mm}) = 4 + \frac{D\,(\text{mm})}{120} + \frac{Q_u L}{A_p E_p} \tag{12.82}$$

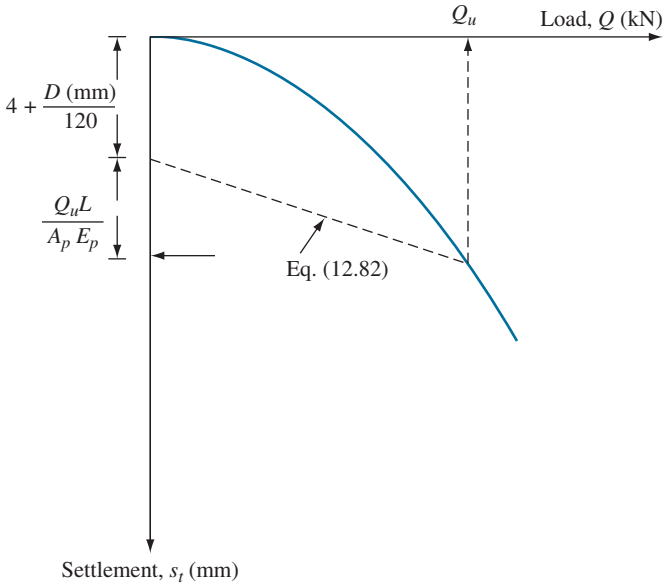


FIGURE 12.33 Davisson's method for determination of Q_u

where

Q_u = ultimate load (kN)

D = pile diameter or width (mm)

L = pile length (mm)

A_p = area of pile cross section (mm^2)

E_p = Young's modulus of pile material (kN/mm^2)

The application of this procedure is shown in Example 12.12.

The load test procedure just described requires the application of step loads on the piles and the measurement of settlement and is called a *load-controlled* test. Another technique used for a pile load test is the *constant-rate-of-penetration* test, wherein the load on the pile is continuously increased to maintain a constant rate of penetration, which can vary from 0.25 to 2.5 mm/min (0.01 to 0.1 in./min). This test gives a load-settlement plot similar to that obtained from the load-controlled test. Another type of pile load test is *cyclic loading*, in which an incremental load is repeatedly applied and removed.

In order to conduct a load test on piles, it is important to take into account the time lapse after the end of driving (EOD). When piles are driven into soft clay, a certain zone surrounding the clay becomes remolded or compressed, as shown in Figure 12.34a. This results in a reduction of undrained shear strength, c_u (Figure 12.34b). With time, the loss of undrained shear strength is partially or fully regained. The time lapse may range from 30 to 60 days.

For piles driven in dilative (dense to very dense) saturated fine sands, relaxation is possible. Negative pore water pressure, if developed during pile driving, will dissipate over time, resulting in a reduction in pile capacity with time after the driving operation is completed. At the same time, excess pore water pressure may be generated in contractive fine sands during pile driving. The excess pore water pressure will dissipate over time, which will result in greater pile capacity.

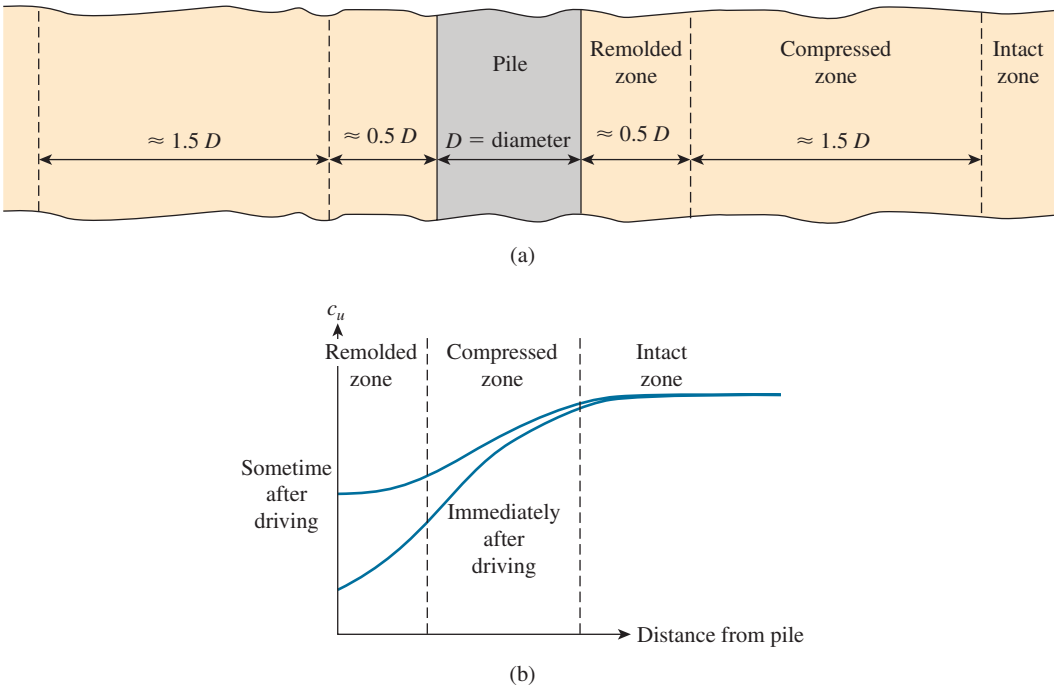


FIGURE 12.34 (a) Remolded or compacted zone around a pile driven into soft clay; (b) nature of variation of undrained shear strength (c_u) with time around a pile driven into soft clay

Several empirical relationships have been developed to predict changes in pile capacity with time. An excellent review of most of the works has been given by Sawant et al. (2013).

EXAMPLE 12.12

Figure 12.35 shows the load test results of a 20 m long concrete pile (406 mm × 406 mm) embedded in sand. Using Davisson's method, determine the ultimate load Q_u. Given: $E_p = 30 \times 10^6$ kN/m^2.

SOLUTION

From Eq. (12.82),

$$s_u = 4 + \frac{D}{120} + \frac{Q_u L}{A_p E_p}$$

$D = 406$ mm $L = 20$ m $= 20{,}000$ mm $A_p = 406$ mm $\times$ 406 mm $= 164{,}836$ mm^2, and $E_p = 30 \times 10^6$ kN/m^2. Hence,

$$s_u = 4 + \frac{406}{120} + \frac{(Q_u)(20{,}000)}{(30)(164{,}836)}$$

$$= 4 + 3.4 + 0.004Q_u = 7.4 + 0.004Q_u$$

The line s_u(mm) $= 7.4 + 0.004Q_u$ is drawn in Figure 12.35. The intersection of this line with the load-settlement curve gives the failure load $Q_u =$ **1630 kN**.

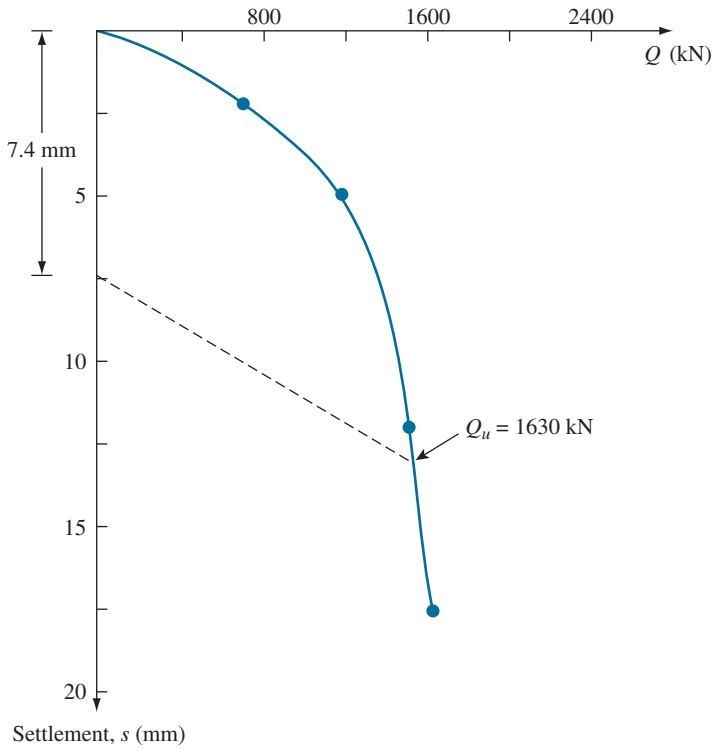


FIGURE 12.35

12.18 Elastic Settlement of Piles

The settlements in piles are relatively low when compared to their shallow foundation counterparts. Under working loads with a factor of safety on the order of 2–3, the settlement is about 1% of the pile diameter. Two methods of estimating the pile settlements are discussed in this section. The first one is a simplified method based on what was proposed by Poulos and Davis (1974). The second one is a more rational and rigorous method proposed by Vesic (1977). They are both based on elastic analysis.

METHOD OF POULOS AND DAVIS

First the pile is treated as incompressible, where there is no elastic compression ($s_e = 0$). The settlement of the pile head, which is the same as the settlement of the pile point, is obtained from Eq. (12.83).

$$s_{\text{net}} = \frac{Q}{LE_s} I_\rho \tag{12.83}$$

where Q is the load applied on the pile head, L is the pile length, E_s is the modulus of elasticity of the soil, and I_ρ is the influence factor from Figure 12.36. Here, H is the depth of the soil bed from the ground level to the stiff stratum. The elastic shortening of the pile can be computed using Eq. (12.84) and added to the value of s_{net} computed in Eq. (12.83) to obtain s_e.

$$s_e = \frac{Q_{\text{avg}} L}{A_p E_p} \tag{12.84}$$

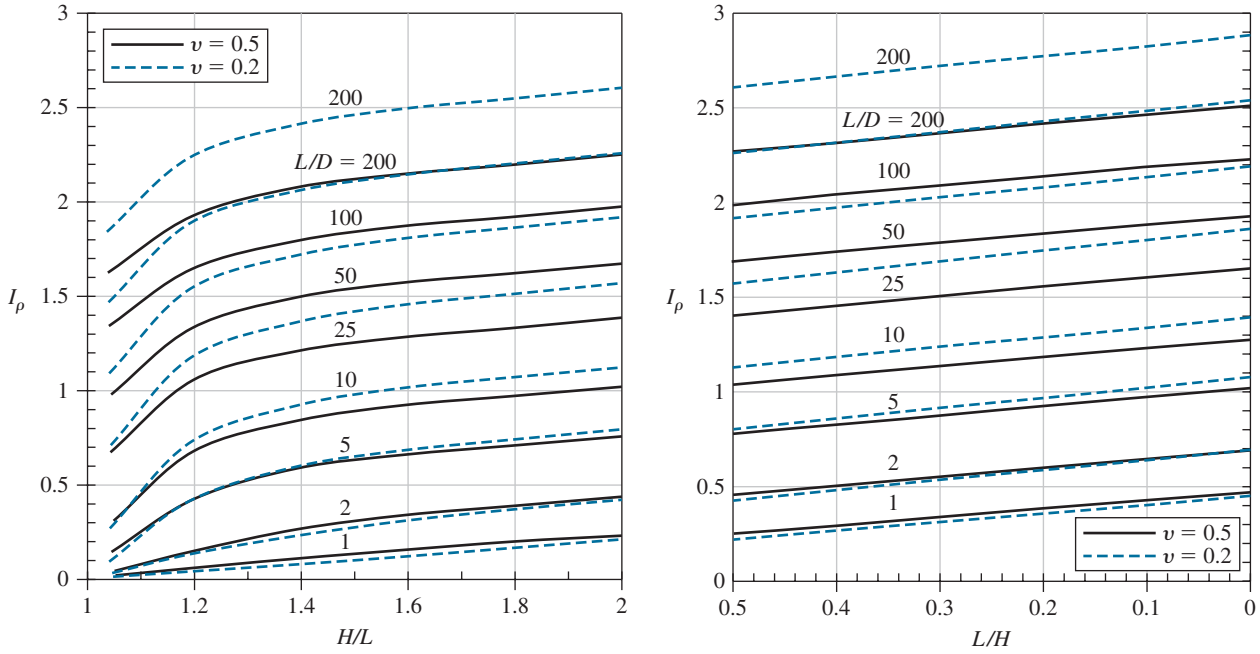


FIGURE 12.36 Influence factor I_ρ

where Q_{avg} is the average pile load carried by the pile shaft and E_p is the modulus of elasticity of the pile material. Note that the load carried by the pile cross section decreases with depth. Therefore, Q_{avg} can be taken as

$$Q_{avg} = \frac{Q + Q_{wp}}{2} \tag{12.85}$$

where Q_{wp} is the working load at the pile point. The total settlement or the settlement of the head s_t is given by

$$s_t = \frac{Q}{LE_s} I_\rho + \frac{Q_{avg} L}{A_p E_p} \tag{12.86}$$

EXAMPLE 12.13

A 500 mm diameter and 20 m long driven concrete pile carries a column load of 1000 kN. It is estimated the shaft carries 800 kN and the point carries 200 kN. Determine the settlement of the pile head using the following data: $E_s = 20$ MN/m^2, $E_p = 30 \times 10^3$ MN/m^2, $\mu_s = 0.2$.

SOLUTION

We first assume that the pile is incompressible and apply Eq. (12.83). $H = \infty$, $L = 20$ m, $D = 0.5$ m, and $\mu_s = 0.2$. Therefore, $L/D = 40$ and $L/H = 0$. From Figure 12.36, $I_\rho = 1.85$,

$$s_t = s_{net} = \frac{Q}{LE_s} I_\rho = \frac{1000 \times 10^3}{20(20 \times 10^6)} \times 1.85 \text{ m} = 0.0046 \text{ m} = 4.6 \text{ mm}$$

The average pile load on the cross-section can be taken as 0.5(1000 + 200) = 600 kN. From Eq. (12.84),

$$s_e = \frac{Q_{\text{avg}}L}{A_pE_p} = \frac{(600 \times 10^3)(20)}{\left(\frac{\pi}{4} \times 0.5^2\right)(30 \times 10^9)}\text{m} = 0.002037 \text{ m} \approx 2.0 \text{ mm}$$

Therefore, the settlement of the pile head = 4.6 + 2.0 = **6.6 mm**.

VESIC'S METHOD

Vesic (1977) separated the total settlement s_e of the pile head into three components and suggested expressions to determine them from elastic analysis. The three elastic components are:

1. Elastic shortening of the pile [$s_{e(1)}$]
2. Settlement of the pile due to the working load (Q_{wp}) at the pile point [$s_{e(2)}$]
3. Settlement of the pile due to the working load (Q_{ws}) along the pile shaft [$s_{e(3)}$]

The total elastic settlement of the pile head under the working load of Q_w is given by

$$s_e = s_{e(1)} + s_{e(2)} + s_{e(3)} \tag{12.87}$$

If there is no skin friction along the pile shaft, the pile load remains the same (i.e., Q_w) at all depths, and the elastic shortening becomes Q_wL/A_pE_p. Due to skin friction, $s_{e(1)}$ will be different and depends on the way the skin friction varies along the pile shaft. It can be shown theoretically that

$$s_{e(1)} = \frac{(Q_{\text{wp}} + \xi Q_{\text{ws}})L}{A_pE_p} \tag{12.88}$$

where

Q_{wp} = working load at the pile point

Q_{ws} = working load along the pile shaft

A_p = cross-sectional area of the pile point

L = pile length

E_p = modulus of elasticity of the pile material

ξ = a constant in the range of 0.50–0.67, depending on the skin friction distribution

Figure 12.15 shows four different possibilities for the variation of the skin friction $f_{(z)}$ with depth along the pile shaft. It can be shown theoretically that for $f_{(z)}$-z variation shown in Figures 12.15a and 12.15d (i.e., uniform or parabolic), $\xi = 0.50$, and for situations where the skin friction $f_{(z)}$ increases or decreases with depth, as shown in Figures 12.15b and 12.15c, $\xi = 0.67$.

The settlement of a pile caused by the load carried at the pile point may be expressed in the form:

$$s_{e(2)} = \frac{q_{\text{wp}}D}{E_s}(1 - \mu_s^2)I_{\text{wp}} \tag{12.89}$$

where

D = width or diameter of pile

q_{wp} = point load per unit area at the pile point = Q_{wp}/A_p

E_s = modulus of elasticity of soil at or below the pile point

μ_s = Poisson's ratio of soil

I_{wp} = influence factor ≈ 0.85

Vesic (1977) also proposed a semi-empirical method for obtaining the magnitude of the settlement of $s_{e(2)}$. His equation is

$$s_{e(2)} = \frac{Q_{wp}C_p}{Dq_p} \tag{12.90}$$

where

q_p = ultimate point resistance of the pile

C_p = an empirical coefficient

Representative values of C_p for various soil are given in Table 12.14.

The settlement of a pile caused by the load carried by the pile shaft is given by a relation similar to Eq. (12.89), namely,

$$s_{e(3)} = \left(\frac{Q_{ws}}{pL}\right)\frac{D}{E_s}(1 - \mu_s^2)I_{ws} \tag{12.91}$$

where

p = perimeter of the pile

L = embedded length of pile

I_{ws} = influence factor

Note that the term Q_{ws}/pL in Eq. (12.91) is the average value of f along the pile shaft. The influence factor, I_{ws}, has a simple empirical relation (Vesic, 1977):

$$I_{ws} = 2 + 0.35\sqrt{\frac{L}{D}} \tag{12.92}$$

TABLE 12.14 Typical Values of C_p [from Eq. (12.90)]

Type of soil	Driven pile	Bored pile
Sand (dense to loose)	0.02–0.04	0.09–0.18
Clay (stiff to soft)	0.02–0.03	0.03–0.06
Silt (dense to loose)	0.03–0.05	0.09–0.12

Based on "Design of Pile Foundations," by A. S. Vesic. *Synthesis of Highway Practice* by American Association of State Highway and Transportation, 1977.

Vesic (1977) also proposed a simple empirical relation similar to Eq. (12.90) for obtaining $s_{e(3)}$:

$$s_{e(3)} = \frac{Q_{ws} C_s}{L q_p} \tag{12.93}$$

In this equation, C_s = an empirical constant = $(0.93 + 0.16\sqrt{L/D})C_p$. (12.94)

The values of C_p for use in Eq. (12.94) may be estimated from Table 12.14.

EXAMPLE 12.14

The allowable working load on a prestressed concrete pile 21 m long that has been driven into sand is 502 kN. The pile is octagonal in shape with $D = 356$ mm (see Table 12.3a). Skin resistance carries 350 kN of the allowable load, and point bearing carries the rest. Use $E_p = 21 \times 10^6$ kN/m^2, $E_s = 25 \times 10^3$ kN/m^2, $\mu_s = 0.35$, and $\xi = 0.62$. Determine the settlement of the pile.

SOLUTION

From Eq. (12.88),

$$S_{e(1)} = \frac{(Q_{wp} + \xi Q_{ws})L}{A_p E_p}$$

From Table 12.3a, for $D = 356$ mm, the area of pile cross section, $A_p = 1045$ cm^2. Also, perimeter $p = 1.168$ m. Given: $Q_{ws} = 350$ kN, so

$$Q_{wp} = 502 - 350 = 152 \text{ kN}$$

$$s_{e(1)} = \frac{[152 + 0.62(350)](21)}{(0.1045 \text{ m}^2)(21 \times 10^6)} = 0.00353 \text{ m} = 3.35 \text{ mm}$$

From Eq. (12.89),

$$s_{e(2)} = \frac{q_{wp} D}{E_s}(1 - \mu_s^2) I_{wp} = \left(\frac{152}{0.1045}\right)\left(\frac{0.356}{25 \times 10^3}\right)(1 - 0.35^2)(0.85)$$

$$= 0.0155 \text{ m} = 15.5 \text{ mm}$$

Again, from Eq. (12.91),

$$s_{e(3)} = \left(\frac{Q_{ws}}{pL}\right)\left(\frac{D}{E_s}\right)(1 - \mu_s^2) I_{ws}$$

$$I_{ws} = 2 + 0.35\sqrt{\frac{L}{D}} = 2 + 0.35\sqrt{\frac{21}{0.356}} = 4.69$$

$$s_{e(3)} = \left[\frac{350}{(1.168)(21)}\right]\left(\frac{0.356}{25 \times 10^3}\right)(1 - 0.35^2)(4.69)$$

$$= 0.00084 \text{ m} = 0.84 \text{ mm}$$

Hence, total elastic settlement is

$$s_e = s_{e(1)} + s_{e(2)} + s_{e(3)} = 3.35 + 15.5 + 0.84 = \mathbf{19.69 \text{ mm}}$$

12.19 Laterally Loaded Piles

A vertical pile resists a lateral load by mobilizing passive pressure in the soil surrounding it. (See Figure 12.1c.) The degree of distribution of the soil's reaction depends on (a) the stiffness of the pile, (b) the stiffness of the soil, and (c) the fixity of the ends of the pile. In general, laterally loaded piles can be divided into two major categories: (1) short or rigid piles and (2) long or elastic piles. Figures 12.37a and 12.37b show the nature of the variation of the pile deflection and the distribution of the moment and shear force along the pile length when the pile is subjected to lateral loading. We next summarize the current solutions for laterally loaded piles.

ELASTIC SOLUTION

A general method for determining moments and displacements of a vertical pile embedded in a *granular soil* and subjected to lateral load and moment at the ground surface was given by Matlock and Reese (1960). Consider a pile of length L subjected to a lateral force Q_g and a moment M_g at the ground surface ($z = 0$), as shown in Figure 12.38a. Figure 12.38b shows the general deflected shape of the pile and the soil resistance caused by the applied load and the moment.

According to a simpler Winkler's model, an elastic medium (soil in this case) can be replaced by a series of infinitely close independent elastic springs. Based on this assumption,

$$k = \frac{p' \text{ (kN/m or lb/ft)}}{x \text{ (m or ft)}} \tag{12.95}$$

where

k = modulus of subgrade reaction

p' = pressure on soil

x = deflection

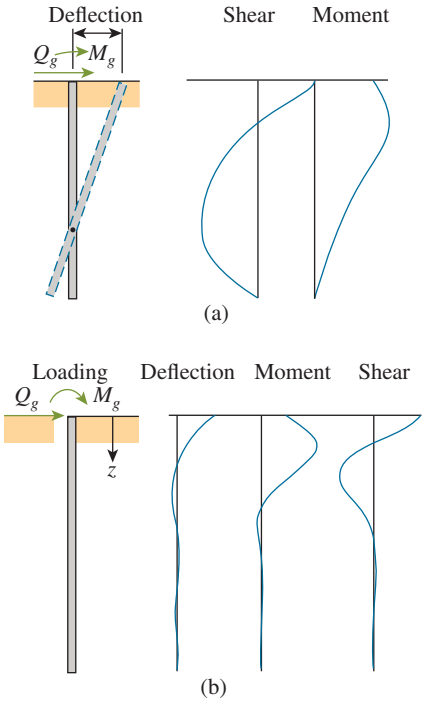


FIGURE 12.37 Nature of variation of pile deflection, moment, and shear force for (a) a rigid pile and (b) an elastic pile

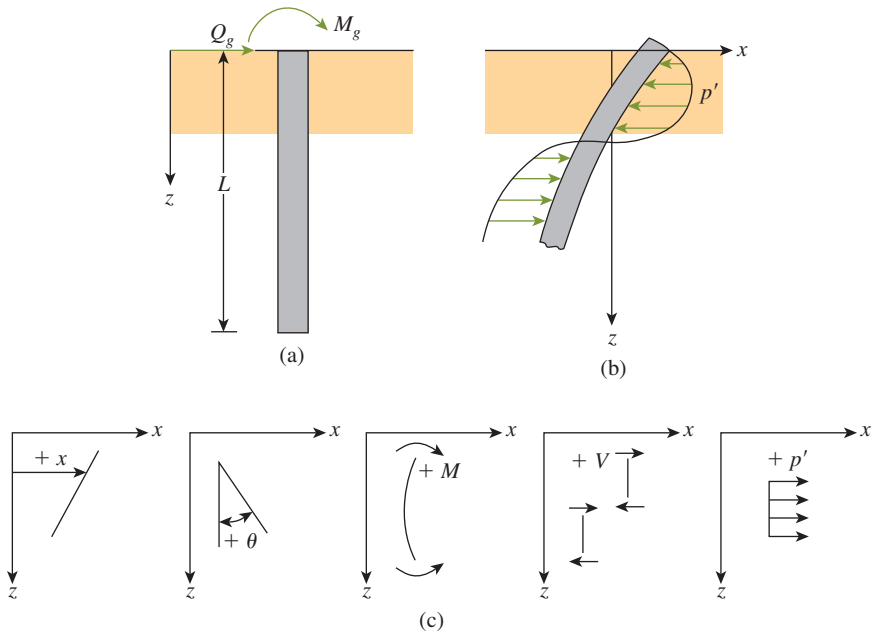


FIGURE 12.38 (a) Laterally loaded pile; (b) soil resistance on pile caused by lateral load; (c) sign conventions for displacement, slope, moment, shear, and soil reaction

The subgrade modulus for *granular soil* at a depth z is defined as

$$k_z = n_h z \tag{12.96}$$

where n_h is the constant modulus of horizontal subgrade reaction.

Referring to Figure 12.38b and using the theory of beams on an elastic foundation, we can write

$$E_p I_p \frac{d^4x}{dz^4} = p' \tag{12.97}$$

where

E_p = modulus of elasticity in the pile material

I_p = moment of inertia of the pile section

Based on Winkler's model,

$$p' = -kx \tag{12.98}$$

The sign in Eq. (12.98) is negative because the soil reaction is in the direction opposite that of the pile deflection.

Combining Eqs. (12.97) and (12.98) gives

$$E_p I_p \frac{d^4x}{dz^4} + kx = 0 \tag{12.99}$$

The solution of Eq. (12.99) results in the following expressions:

PILE DEFLECTION AT ANY DEPTH [$x_z(z)$]

$$x_z(z) = A_x \frac{Q_g T^3}{E_p I_p} + B_x \frac{M_g T^2}{E_p I_p} \tag{12.100}$$

SLOPE OF PILE AT ANY DEPTH [$\theta_z(z)$]

$$\theta_z(z) = A_\theta \frac{Q_g T^2}{E_p I_p} + B_\theta \frac{M_g T}{E_p I_p} \tag{12.101}$$

MOMENT OF PILE AT ANY DEPTH [$M_z(z)$]

$$M_z(z) = A_m Q_g T + B_m M_g \tag{12.102}$$

SHEAR FORCE ON PILE AT ANY DEPTH [$V_z(z)$]

$$V_z(z) = A_v Q_g + B_v \frac{M_g}{T} \tag{12.103}$$

SOIL REACTION AT ANY DEPTH [$p'_z(z)$]

$$p'_z(z) = A_{p'} \frac{Q_g}{T} + B_{p'} \frac{M_g}{T^2} \tag{12.104}$$

where

A_x, B_x, A_θ, B_θ, A_m, B_m, A_v, B_v, $A_{p'}$, and $B_{p'}$ are coefficients

T is the characteristic length of the soil–pile system

$$= \sqrt[5]{\frac{E_p I_p}{n_h}} \tag{12.105}$$

n_h has been defined in Eq. (12.96).

When $L \geq 5T$, the pile is considered to be a *long pile*. For $L \leq 2T$, the pile is considered to be a *rigid pile*. Table 12.15 gives the values of the coefficients for long piles ($L/T \geq 5$) in Eqs. (12.100) through (12.104). Note that, in the first column of the table,

$$Z = \frac{z}{T} \tag{12.106}$$

is the nondimensional depth.

The positive sign conventions for $x_z(z)$, $\theta_z(z)$, $M_z(z)$, $V_z(z)$, and $p'_z(z)$ assumed in the derivations in Table 12.15 are shown in Figure 12.38c. Figure 12.39 shows the variation of A_x, B_x, A_m, and B_m for various values of $L/T = Z_{\max}$. It indicates that when L/T is greater than about 5, the coefficients do not change, which is true of long piles only.

Calculating the characteristic length T for the pile requires assuming a proper value of n_h. Table 12.16 gives some representative values.

Elastic solutions similar to those given in Eqs. 12.100 through 12.104 for piles embedded in *cohesive soil* were developed by Davisson and Gill (1963). Their equations are

$$x_z(z) = A'_x \frac{Q_g R^3}{E_p I_p} + B'_x \frac{M_g R^2}{E_p I_p} \tag{12.107}$$

TABLE 12.15 Coefficients for Long Piles, $k_z = n_h z$

Z	A_x	A_θ	A_m	A_v	$A_{p'}$	B_x	B_θ	B_m	B_v	$B_{p'}$
0.0	2.435	−1.623	0.000	1.000	0.000	1.623	−1.750	1.000	0.000	0.000
0.1	2.273	−1.618	0.100	0.989	−0.227	1.453	−1.650	1.000	−0.007	−0.145
0.2	2.112	−1.603	0.198	0.956	−0.422	1.293	−1.550	0.999	−0.028	−0.259
0.3	1.952	−1.578	0.291	0.906	−0.586	1.143	−1.450	0.994	−0.058	−0.343
0.4	1.796	−1.545	0.379	0.840	−0.718	1.003	−1.351	0.987	−0.095	−0.401
0.5	1.644	−1.503	0.459	0.764	−0.822	0.873	−1.253	0.976	−0.137	−0.436
0.6	1.496	−1.454	0.532	0.677	−0.897	0.752	−1.156	0.960	−0.181	−0.451
0.7	1.353	−1.397	0.595	0.585	−0.947	0.642	−1.061	0.939	−0.226	−0.449
0.8	1.216	−1.335	0.649	0.489	−0.973	0.540	−0.968	0.914	−0.270	−0.432
0.9	1.086	−1.268	0.693	0.392	−0.977	0.448	−0.878	0.885	−0.312	−0.403
1.0	0.962	−1.197	0.727	0.295	−0.962	0.364	−0.792	0.852	−0.350	−0.364
1.2	0.738	−1.047	0.767	0.109	−0.885	0.223	−0.629	0.775	−0.414	−0.268
1.4	0.544	−0.893	0.772	−0.056	−0.761	0.112	−0.482	0.688	−0.456	−0.157
1.6	0.381	−0.741	0.746	−0.193	−0.609	0.029	−0.354	0.594	−0.477	−0.047
1.8	0.247	−0.596	0.696	−0.298	−0.445	−0.030	−0.245	0.498	−0.476	0.054
2.0	0.142	−0.464	0.628	−0.371	−0.283	−0.070	−0.155	0.404	−0.456	0.140
3.0	−0.075	−0.040	0.225	−0.349	0.226	−0.089	0.057	0.059	−0.213	0.268
4.0	−0.050	0.052	0.000	−0.106	0.201	−0.028	0.049	−0.042	0.017	0.112
5.0	−0.009	0.025	−0.033	0.015	0.046	0.000	−0.011	−0.026	0.029	−0.002

Based on *Drilled Pier Foundations*, by R. J. Woodward, W. S. Gardner, and D. M. Greer. McGraw-Hill, 1972.

and

$$M_z(z) = A'_m Q_g R + B'_m M_g \tag{12.108}$$

where A'_x, B_x, A'_m, and B'_m are coefficients; and R is the characteristic length given by Eq. (12.109).

TABLE 12.16 Representative Values of n_h

Soil	n_h kN/m³	n_h lb/in³
Dry or moist sand		
Loose	1800–2200	6.5–8.0
Medium	5500–7000	20–25
Dense	15,000–18,000	55–65
Submerged sand		
Loose	1000–1400	3.5–5.0
Medium	3500–4500	12–18
Dense	9000–12,000	32–45

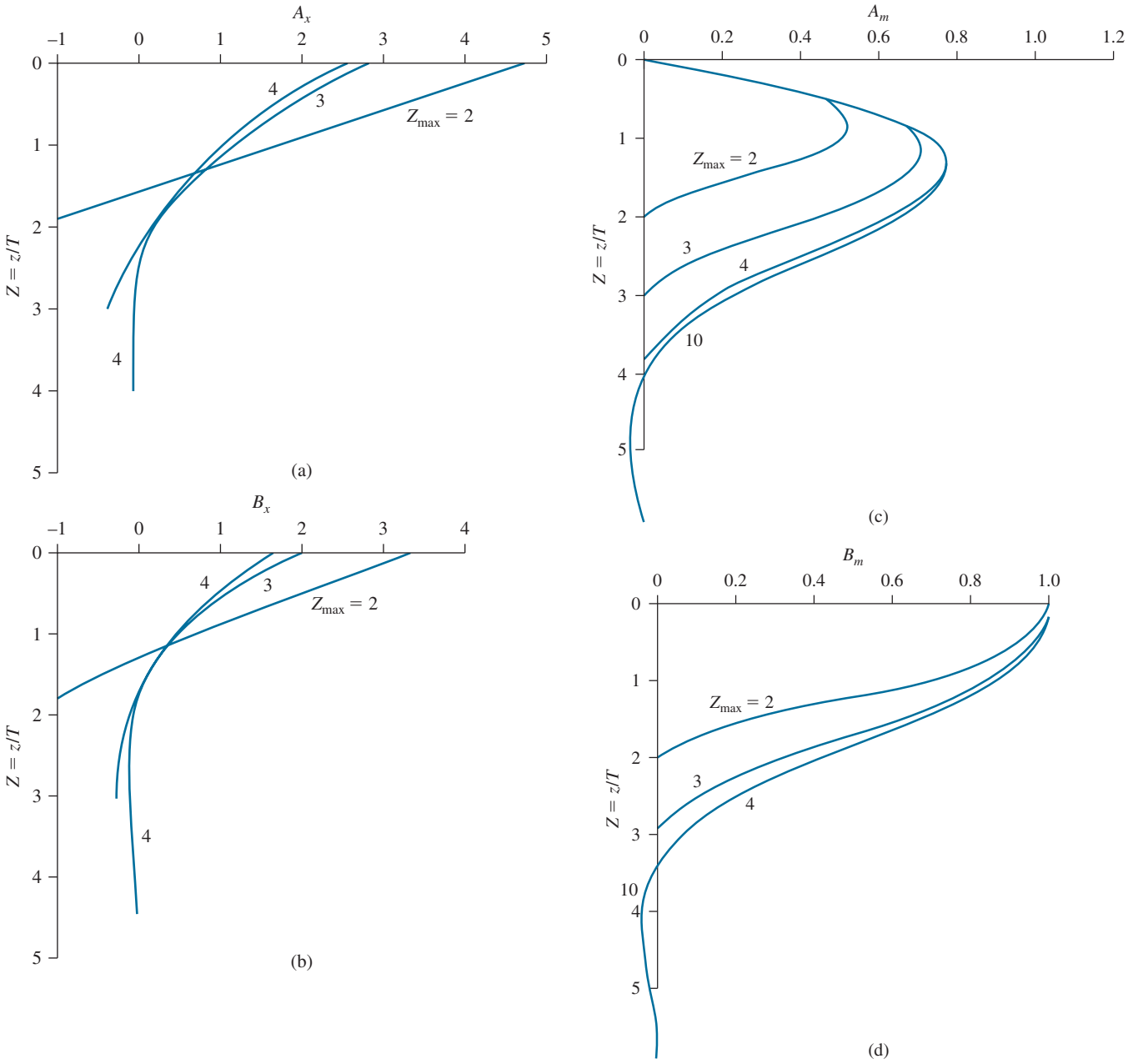


FIGURE 12.39 Variation of A_x, B_x, A_m, and B_m with Z (Based on Matlock, H. and Reese, L. C. (1960). "Generalized Solution for Laterally Loaded Piles," *Journal of the Soil Mechanics and Foundations Division*, American Society of Civil Engineers, Vol. 86, No. SM5, Part I, pp. 63–91.)

and

$$R = \sqrt[4]{\frac{E_p I_p}{k}} \tag{12.109}$$

The values of the coefficients A' and B' are given in Figure 12.40. Note that

$$Z = \frac{z}{R} \tag{12.110}$$

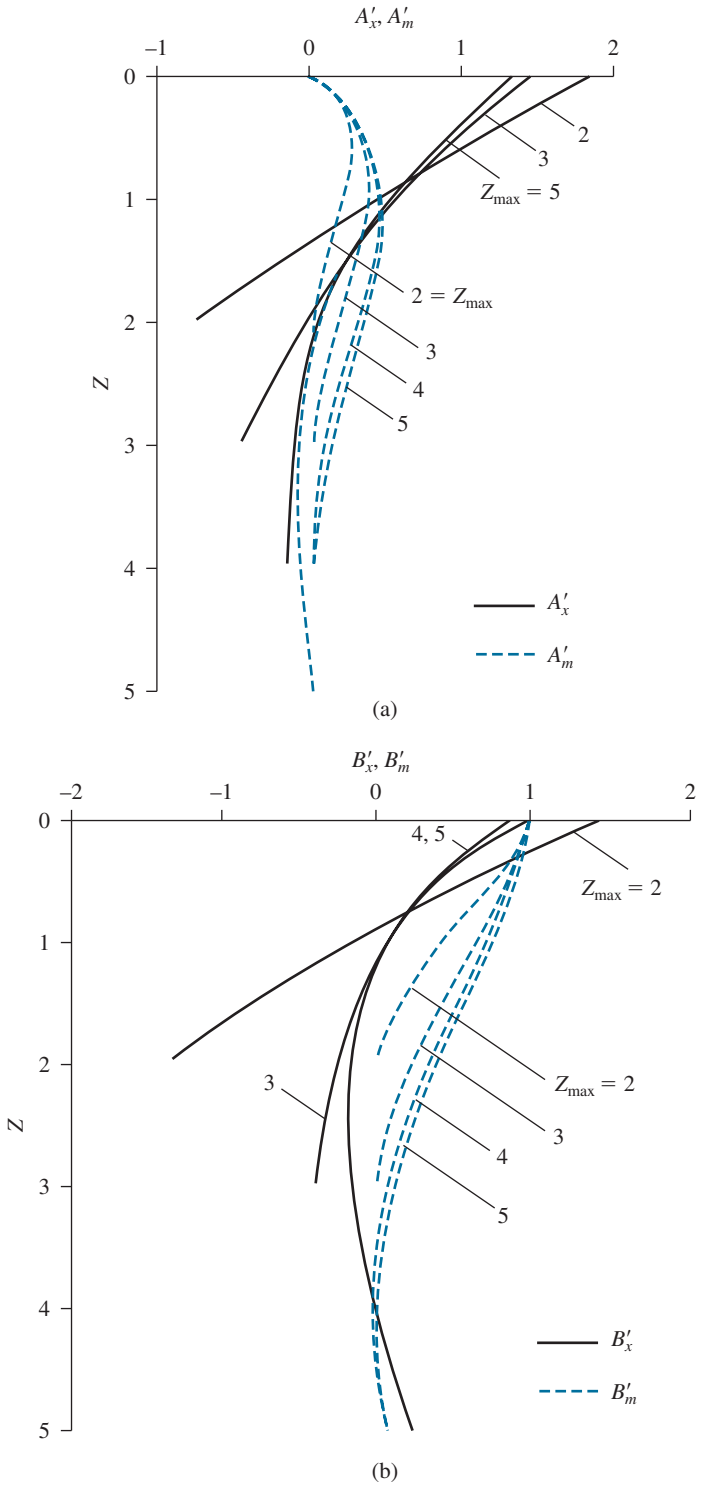


FIGURE 12.40 Variation of A_x, B'_x, A'_m, and B'_m with Z (Based on Davisson, M. T. and Gill, H. L. (1963). "Laterally Loaded Piles in a Layered Soil System," *Journal of the Soil Mechanics and Foundations Division*, American Society of Civil Engineers, Vol. 89, No. SM3, pp. 63–94.)

and

$$Z_{\max} = \frac{L}{R} \tag{12.111}$$

The use of Eqs. (12.107) and (12.108) requires knowing the magnitude of the characteristic length, R. This can be calculated from Eq. (12.109), provided that the coefficient of the subgrade reaction is known. For sands, the coefficient of the subgrade reaction was given by Eq. (12.96), which showed a linear variation with depth. However, in cohesive soil, the subgrade reaction may be assumed to be approximately constant with depth. Vesic (1961) proposed the following equation to estimate the value of k:

$$k = 0.65 \sqrt[12]{\frac{E_s D^4}{E_p I_p}} \frac{E_s}{1 - \mu_s^2} \tag{12.112}$$

Here,

E_s = modulus of elasticity of soil

D = pile width (or diameter)

μ_s = Poisson's ratio for the soil

For all practical purposes, Eq. (12.112) can be written as

$$k \approx \frac{E_s}{1 - \mu_s^2} \tag{12.113}$$

Eqs. (12.112) and (12.113) for laterally loaded piles are of the same form as Eqs. (10.45) and (10.46) developed for shallow foundations.

ULTIMATE LOAD ANALYSIS: METHOD OF BROMS

For laterally loaded piles, Broms (1965) developed a simplified solution based on the assumptions of (a) shear failure in soil, which is the case for short piles, and (b) bending of the pile, governed by the plastic yield resistance of the pile section, which is applicable to long piles. The solution of Broms for calculating the ultimate load resistance, $Q_{u(g)}$, for *short piles* in sand is given in Figure 12.41a. A similar solution for piles embedded in cohesive soil is shown in Figure 12.41b. In Figure 12.41a, note that

$$K_p = \text{Rankine passive earth pressure coefficient} = \tan^2\left(45 + \frac{\phi'}{2}\right) \tag{12.114}$$

Similarly, in Figure 12.41b,

$$c_u = \text{undrained cohesion} \approx \frac{0.75 q_u}{\text{FS}} = \frac{0.75 q_u}{2} = 0.375 q_u \tag{12.115}$$

where

FS = factor of safety (=2)

q_u = unconfined compression strength

Figure 12.42 shows the analysis of Broms for long piles. In the figure, the yield moment for the pile is

$$M_y = SF_Y \tag{12.116}$$

where

S = section modulus of the pile section

F_Y = yield stress of the pile material

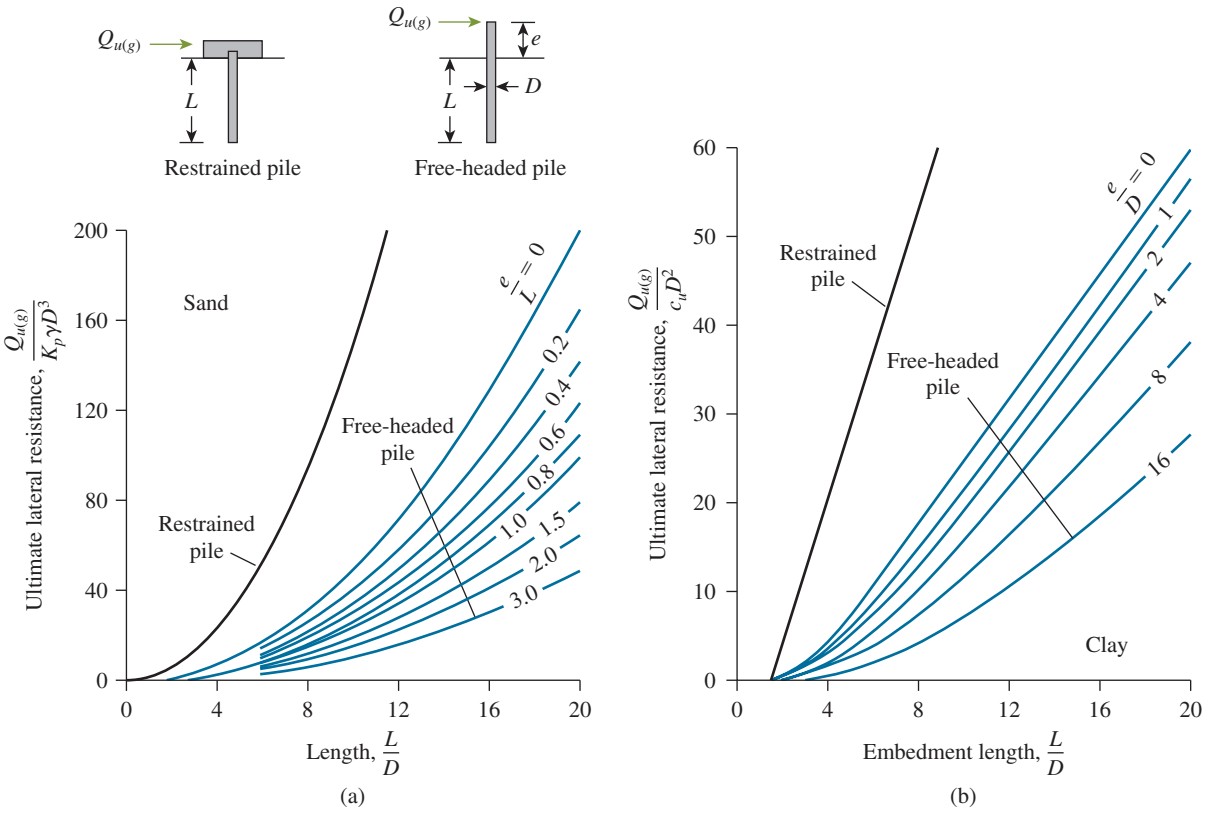


FIGURE 12.41 The solution of Broms for ultimate lateral resistance of short piles (a) in sand and (b) in clay

In solving a given problem, both cases (i.e., Figure 12.41 and Figure 12.42) should be checked.

The deflection of the pile head, $x_z(z = 0)$, under working load conditions can be estimated from Figure 12.43. In Figure 12.43a, the term η can be expressed as

$$\eta = \sqrt[5]{\frac{n_h}{E_p I_p}} \tag{12.117}$$

The range of n_h for granular soil is given in Table 12.16. Similarly, in Figure 12.43b, which is for clay, the term K is the horizontal soil modulus and can be defined as

$$K = \frac{\text{pressure (kN/m}^2 \text{ or lb/in}^2)}{\text{displacement (m or in.)}} \tag{12.118}$$

Also, the term β can be defined as

$$\beta = \sqrt[4]{\frac{KD}{4E_p I_p}} \tag{12.119}$$

Note that in Figure 12.43, Q_g is the working load.

The following is a general range of values of K for clay soil.

Unconfined compression strength, q_u		K	
kN/m^2	lb/in^2	kN/m^3	lb/in^3
200	≈ 30	10,000–20,000	37–75
200–800	30–120	20,000–40,000	75–150
> 800	> 120	> 40,000	> 150

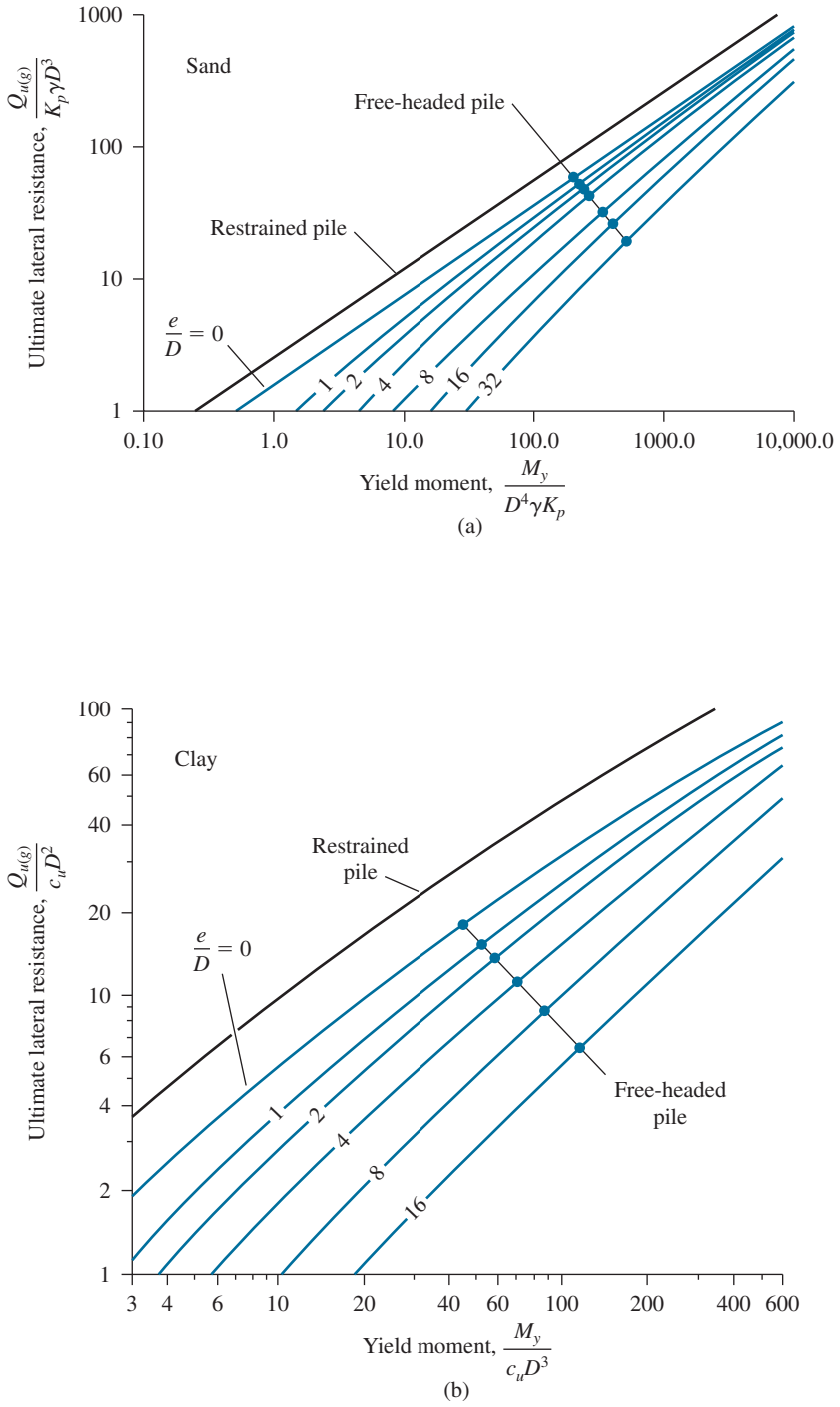
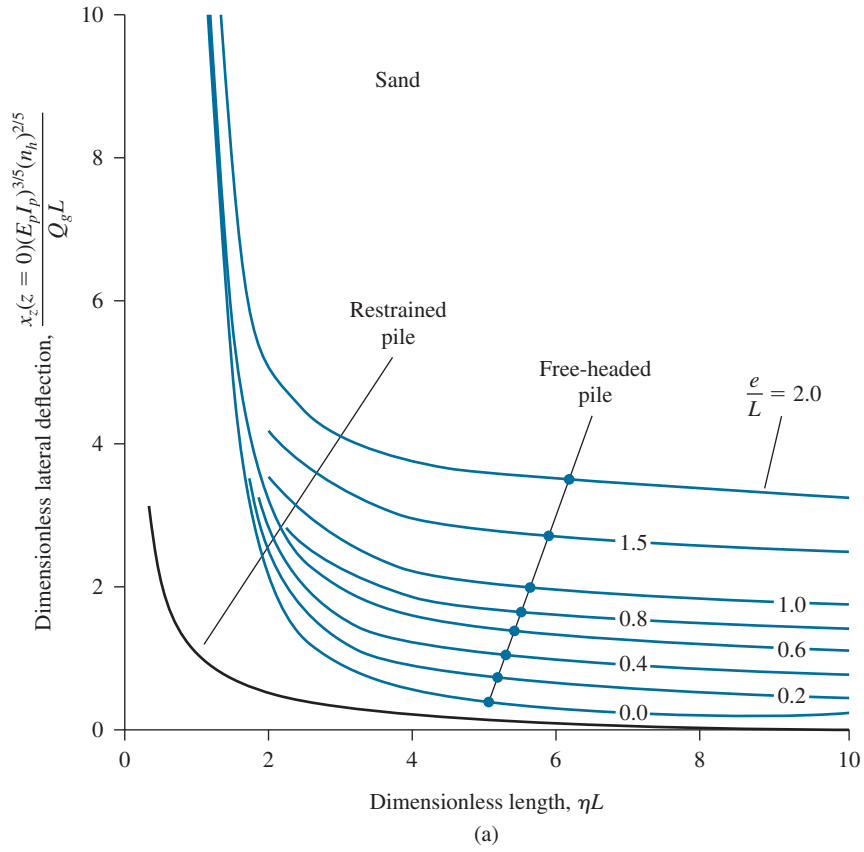


FIGURE 12.42 The solution of Broms for ultimate lateral resistance of long piles (a) in sand (b) in clay



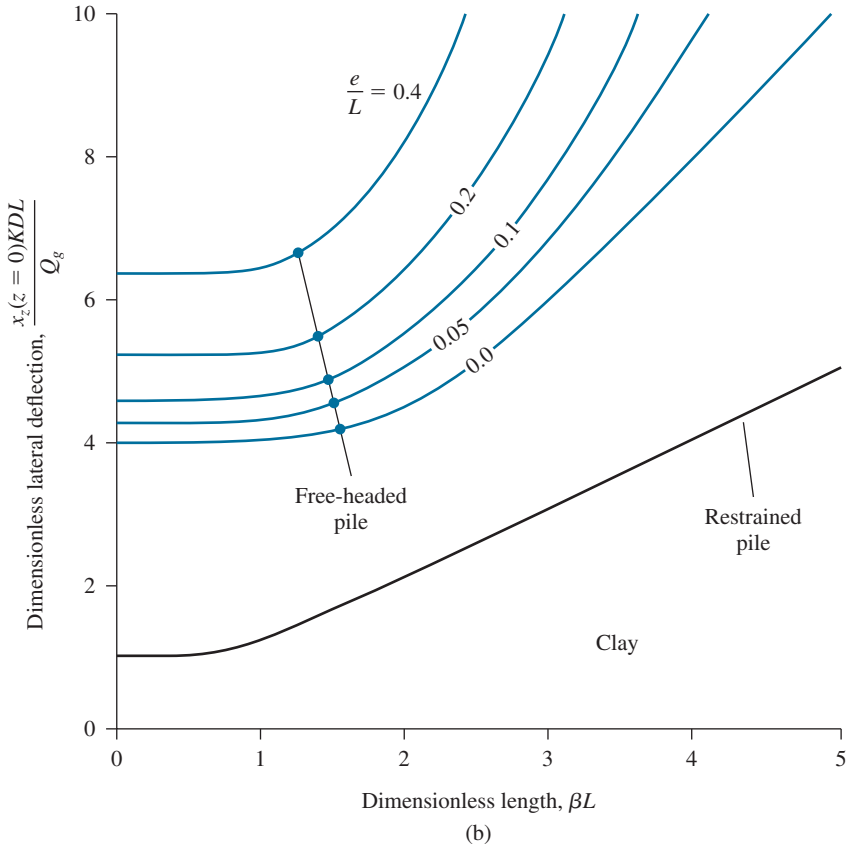


FIGURE 12.43 The solution of Broms for estimating deflection of pile head (a) in sand and (b) in clay

EXAMPLE 12.15

Consider a steel H-pile (HP 250 × 85) 25 m long, embedded fully in a granular soil. Assume that $n_h = 12{,}000$ kN/m^3. The allowable displacement at the top of the pile is 8 mm. Determine the allowable lateral load, Q_g. Let $M_g = 0$. Use the elastic solution.

SOLUTION

From Table 12.1a, for an HP 250 × 85 pile,

$$I_p = 123 \times 10^{-6}\,\text{m}^4 \qquad \text{(about the strong axis)}$$

and let

$$E_p = 207 \times 10^6\,\text{kN/m}^2$$

From Eq. (12.105),

$$T = \sqrt[5]{\frac{E_p I_p}{n_h}} = \sqrt[5]{\frac{(207 \times 10^6)(123 \times 10^{-6})}{12{,}000}} = 1.16\ \text{m}$$

Here, $L/T = 25/1.16 = 21.55 > 5$, so the pile is a long one. Because $M_g = 0$, Eq. (12.100) takes the form

$$x_z(z) = A_x \frac{Q_g T^3}{E_p I_p}$$

and it follows that

$$Q_g = \frac{x_z(z) E_p I_p}{A_x T^3}$$

At $z = 0$, $x_z = 8$ mm $= 0.008$ m and $A_x = 2.435$ (see Table 12.15), so

$$Q_g = \frac{(0.008)(207 \times 10^6)(123 \times 10^{-6})}{(2.435)(1.16^3)} = 53.59\ \text{kN}$$

This magnitude of Q_g is based on the *limiting displacement condition only*. However, the magnitude of Q_g based on the *moment capacity* of the pile also needs to be determined. For $M_g = 0$, Eq. (12.102) becomes

$$M_z(z) = A_m Q_g T$$

According to Table 12.15, the maximum value of A_m at any depth is 0.772. The maximum allowable moment that the pile can carry is

$$M_{z(\max)} = F_Y \frac{I_p}{\frac{d_1}{2}}$$

Let the yield stress $F_Y = 248{,}000$ kN/m^2. From Table 12.1a, $I_p = 123 \times 10^{-6}$ m^4 and $d_1 = 0.254$ m, so

$$\frac{I_p}{\left(\frac{d_1}{2}\right)} = \frac{123 \times 10^{-6}}{\left(\frac{0.254}{2}\right)} = 968.5 \times 10^{-6}\,\text{m}^3$$

Now,

$$Q_g = \frac{M_{z(\max)}}{A_m T} = \frac{(968.5 \times 10^{-6})(248{,}000)}{(0.772)(1.16)} = 268.2\ \text{kN}$$

Because $Q_g = 268.2$ kN > 53.59 kN, the deflection criteria apply. Hence, $Q_g =$ **53.59 kN**.

■

EXAMPLE 12.16

Solve Example 12.15 by the method of Broms. Assume that the pile is flexible and is free headed. Let the yield stress of the pile material $F_y = 248\ \text{MN/m}^2$; the unit weight of soil $\gamma = 18\ \text{kN/m}^3$; and the soil friction angle $\phi' = 35°$.

SOLUTION

We check for bending failure. From Eq. (12.116),

$$M_y = SF_y$$

From Table 12.1a,

$$S = \frac{I_p}{\frac{d_1}{2}} = \frac{123 \times 10^{-6}}{\frac{0.254}{2}}$$

Also,

$$M_y = \left[\frac{123 \times 10^{-6}}{\frac{0.254}{2}}\right](248 \times 10^3) = 240.2\ \text{kN}\cdot\text{m}$$

and

$$\frac{M_y}{D^4\gamma K_p} = \frac{M_y}{D^4\gamma \tan^2\left(45 + \frac{\phi'}{2}\right)} = \frac{240.2}{(0.254)^4(18)\tan^2\left(45 + \frac{35}{2}\right)} = 868.8$$

From Figure 12.42a, for $M_y/D^4\gamma K_p = 868.8$, the magnitude of $Q_{u(g)}/K_pD^3\gamma$ (for a free-headed pile with $e/D = 0$) is about 140, so

$$Q_{u(g)} = 140K_pD^3\gamma = 140\tan^2\left(45 + \frac{35}{2}\right)(0.254)^3(18) = 152.4\ \text{kN}$$

Next, we check for pile head deflection. From Eq. (12.117),

$$\eta = \sqrt[5]{\frac{n_h}{E_pI_p}} = \sqrt[5]{\frac{12{,}000}{(207 \times 10^6)(123 \times 10^{-6})}} = 0.86\ \text{m}^{-1}$$

so

$$\eta L = (0.86)(25) = 21.5$$

From Figure 12.43a, for $\eta L = 21.5$, $e/L = 0$ (free-headed pile): thus,

$$\frac{x_o(E_pI_p)^{3/5}(n_h)^{2/5}}{Q_gL} \approx 0.15 \qquad \text{(by interpolation)}$$

and

$$Q_g = \frac{x_o(E_pI_p)^{3/5}(n_h)^{2/5}}{0.15L}$$

$$= \frac{(0.008)[(207 \times 10^6)(123 \times 10^{-6})]^{3/5}(12{,}000)^{2/5}}{(0.15)(25)} = 40.2\ \text{kN}$$

Hence, $Q_g =$ **40.2 kN** (**< 152.4 kN**).

EXAMPLE 12.17

Assume that the 25 m long pile described in Example 12.15 is a restrained pile and is embedded in clay soil. Given: $c_u = 100$ kN/m^2 and $K = 5000$ kN/m^3. The allowable lateral displacement at the top of the pile is 10 mm. Determine the allowable lateral load Q_g. Given $M_g = 0$. Use the method of Broms.

SOLUTION

From Example 12.16, $M_y = 240.2$ kN·m. So

$$\frac{M_y}{c_u D^3} = \frac{240.2}{(100)(0.254)^3} = 146.6$$

For the unrestrained pile, from Figure 12.42b,

$$\frac{Q_{u(g)}}{c_u D^2} \approx 65$$

or

$$Q_{u(g)} = (65)(100)(0.254)^2 = 419.3 \text{ kN}$$

Check Pile-Head Deflection

From Eq. (12.119),

$$\beta = \sqrt[4]{\frac{KD}{4E_pI_p}} = \sqrt[4]{\frac{(5000)(0.254)}{(4)(207 \times 10^6)(123 \times 10^{-6})}} = 0.334$$

$$\beta L = (0.334)(25) = 8.35$$

From Figure 12.43b, for $\beta L = 8.35$

$$\frac{x_z(z = 0)KDL}{Q_g} \approx 8$$

$$Q_g = \frac{x_z(z = 0)KDL}{8} = \frac{\left(\frac{10}{1000}\right)(5000)(0.254)(25)}{8} = 39.7 \text{ kN}$$

Hence, $Q_g = \mathbf{39.7\ kN}$ (**<419.3 kN**).

12.20 Pile-Driving Formulas

When a pile is driven into the ground, the penetration of the pile point into the soil per blow is known as *set*, denoted by S. If a ram weighing W_R is dropped over a height of h and E is the efficiency of the hammer, the work done per blow is EW_Rh. For the pile point to penetrate the soil, the ultimate load (Q_u) carrying capacity has been developed, and the work done is then Q_uS. Equating the two,

$$Q_uS = EW_Rh \tag{12.120}$$

Equation (12.120) is the rationale behind the different pile-driving equations. Sometimes W_Rh is replaced by the *energy rating* (H_E) of the hammer.

There are several pile-driving equations reported in the literature. From the measured set and the hammer ratings, it is possible to estimate, though crudely, the ultimate load-carrying capacity of the pile. In light of the unreliable nature of the pile-driving equations for estimating Q_u, very large factors of safety are used in arriving at

the working loads. The set is continuously measured throughout pile driving and can be used as a guide to determine whether the pile has reached a satisfactory bearing capacity so that the driving can be stopped.

Pile-driving formulas were popular in the early 1900s for estimating the load-carrying capacity of driven piles. In the early days, the driven piles were mainly wooden and less than 12 inches in diameter. They were driven by drop hammers or single-acting steam hammers. The formulas were mainly for drop and single-acting hammers. Double-acting, differential, and diesel hammers were not in use then. One of the earliest pile-driving equations was the Engineering News Record (EN) formula for driving timber piles.

According to the EN formula, the pile resistance is the ultimate load Q_u, expressed as

$$Q_u = \frac{W_R h}{S + C} \tag{12.121}$$

where

W_R = weight of the ram

h = height of fall of the ram

S = penetration of pile per hammer blow

C = a constant

The pile penetration, known as set S, is usually based on the average value obtained from the last few driving blows. In the equation's original form, the following values of C were recommended:

For drop hammers,

$$C = \begin{cases} 25.4 \text{ mm if } S \text{ and } h \text{ are in mm} \\ 1 \text{ in. if } S \text{ and } h \text{ are in inches} \end{cases}$$

For steam hammers,

$$C = \begin{cases} 2.54 \text{ mm if } S \text{ and } h \text{ are in mm} \\ 0.1 \text{ in. if } S \text{ and } h \text{ are in inches} \end{cases}$$

Also, a factor of safety FS = 6 was recommended for estimating the allowable pile capacity. Note that, for single- and double-acting hammers, the term $W_R h$ can be replaced by EH_E, where E is the efficiency of the hammer and H_E is the rated energy of the hammer. Thus,

$$Q_u = \frac{EH_E}{S + C} \tag{12.122}$$

The EN formula has been revised several times over the years, and other pile-driving formulas also have been suggested. Three of the other relationships generally used are shown in Table 12.17.

The *coefficient of restitution n* used in some of the pile-driving formulas is a measure of the bounciness of the hammer, in the range of 0–1. It is the ratio of the relative velocity between the pile and the hammer after and before the impact.

The maximum stress developed on a pile during the driving operation can be estimated from the pile-driving formulas presented in Table 12.17. To illustrate, we use the modified EN formula:

$$Q_u = \frac{EW_R h}{S + C} \frac{W_R + n^2 W_p}{W_R + W_p}$$

TABLE 12.17 Pile-Driving Formulas

Name	Formula
Modified EN formula	$Q_u = \frac{EW_R h}{S + C} \frac{W_R + n^2 W_p}{W_R + W_p}$ where E = efficiency of hammer C = 2.54 mm if the units of S and h are in mm C = 0.1 in. if the units of S and h are in in. W_p = weight of the pile n = coefficient of restitution between the ram and the pile cap Typical values for E Single- and double-acting hammers 0.7–0.85 Diesel hammers 0.8–0.9 Drop hammers 0.7–0.9 Typical values for n Cast-iron hammer and concrete piles (without cap) 0.4–0.5 Wood cushion on steel piles 0.3–0.4 Wooden piles 0.25–0.3
Danish formula (Olson and Flaate, 1967)	$Q_u = \frac{EH_E}{S + \sqrt{\frac{EH_E L}{2A_p E_p}}}$ where E = efficiency of hammer H_E = rated hammer energy E_p = modulus of elasticity of the pile material L = length of the pile A_p = cross-sectional area of the pile
Janbu's formula (Janbu, 1953)	$Q_u = \frac{EH_E}{K'_u S}$ where $K'_u = C_d\left(1 + \sqrt{1 + \frac{\lambda'}{C_d}}\right)$ $C_d = 0.75 + 0.14\left(\frac{W_p}{W_R}\right)$ $\lambda' = \left(\frac{EH_E L}{A_p E_p S^2}\right)$
Hiley formula	Same formula as modified EN formula above, where C is the temporary compression of the pile head, given by $C = (C_1 + C_2 + C_3)/2$; C_1 = Temporary elastic compression of the pile cushion, head and cap ($\approx$ 1–5 mm); C_2 = Temporary elastic compression of the pile length [$\approx(0.2\text{–}1.0) \times 10^{-3} L$]; C_3 = Temporary elastic compression in the soil surrounding the pile and that lies beneath the tip, known as *quake* ($\approx$1–6 mm).

In this equation, S is the average penetration per hammer blow, which can also be expressed as

$$S = \frac{1}{N} \tag{12.123}$$

where

S is in inches

N = number of hammer blows per inch of penetration

Thus,

$$Q_u = \frac{EW_R h}{(1/N) + 0.1} \frac{W_R + n^2 W_p}{W_R + W_p} \tag{12.124}$$

Different values of N may be assumed for a given hammer and pile, and Q_u may be calculated. The driving stress Q_u/A_p can then be calculated for each value of N. This procedure can be demonstrated with a set of numerical values. Suppose that a prestressed concrete pile 80 ft in length has to be driven by a hammer. The pile sides measure 10 in. From Table 12.3b, for this pile,

$$A_p = 100 \text{ in}^2$$

The weight of the pile is

$$A_p L \gamma_c = \left(\frac{100 \text{ in}^2}{144}\right)(80 \text{ ft})(150 \text{ lb/ft}^3) = 8.33 \text{ kip}$$

If the weight of the cap is 0.67 kip, then

$$W_p = 8.33 + 0.67 = 9 \text{ kip}$$

For the hammer, let

$$\text{Rated energy} = 19.2 \text{ kip} \cdot \text{ft} = H_E = W_R h$$
$$\text{Weight of ram} = 5 \text{ kip}$$

Assume that the hammer efficiency is 0.85 and that $n = 0.35$. Substituting these values into Eq. (12.124) yields

$$Q_u = \left[\frac{(0.85)(19.2 \times 12)}{\frac{1}{N} + 0.1}\right]\left[\frac{5 + (0.35)^2(9)}{5 + 9}\right] = \frac{85.37}{\frac{1}{N} + 0.1} \text{ kip}$$

Now the following table can be prepared:

N	Q_u (kip)	A_p (in^2)	Q_u/A_p (kip/in^2)
0	0	100	0
2	142.3	100	1.42
4	243.9	100	2.44
6	320.1	100	3.20
8	379.4	100	3.79
10	426.9	100	4.27
12	465.7	100	4.66
20	569.1	100	5.69

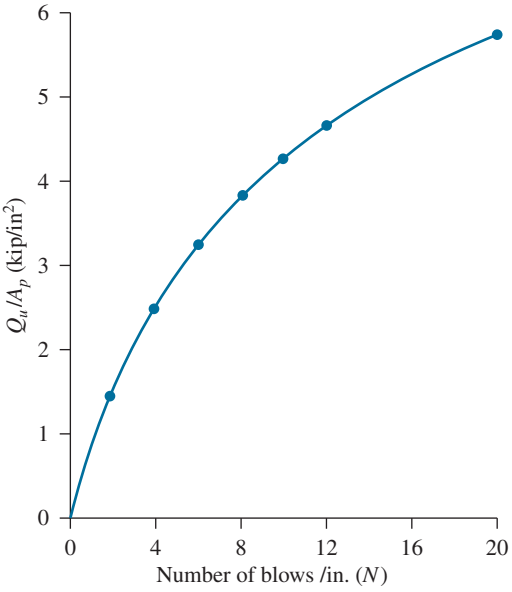


FIGURE 12.44 Plot of stress versus blows/in.

Both the number of hammer blows per inch and the stress can be plotted in a graph, as shown in Figure 12.44. If such a curve is prepared, the number of blows per inch of pile penetration corresponding to the allowable pile-driving stress can easily be determined.

Actual driving stresses in wooden piles are limited to about $0.7f_u$. Similarly, for concrete and steel piles, driving stresses are limited to about $0.6f_c'$ and $0.85f_y$, respectively.

In most cases, wooden piles are driven with a hammer energy of less than 60 kN·m (≈45 kip·ft). Driving resistances are limited mostly to 4 to 5 blows per inch of pile penetration. For concrete and steel piles, the usual values of N are 6 to 8 and 12 to 14, respectively.

PILE-DRIVING ANALYZER

These days, it is very common to see a pile-driving analyzer (PDA) used for monitoring pile driving. It can be used to determine the load-carrying capacity of a driven pile and is seen as an alternative to a pile load test. Figure 12.45 shows a pile-driving



(a) (b)

FIGURE 12.45 (a) Pile-driving analyzer; (b) a square pile connected to the PDA (Courtesy of N. Sivakugan, James Cook University, Australia)

analyzer connected to a square concrete pile that is being driven into the ground. In a typical project, a very limited number of piles (e.g., 1% of the piles) are subjected to static pile load test due to the high cost. A relatively larger proportion (e.g., 5–10% of the piles) are tested by PDA.

The PDA setup consists of strain gauges, acceleration transducers (accelerometers), and a portable computer. The impulse generated by the pile hammer, in the case of driven piles, or separately using a drop weight, in bored piles, is analyzed for determining the integrity of the pile and to estimate its load-carrying capacity. The analysis is carried out using a signal matching program known as Case Pile Wave Analysis Program (CAPWAP). These days, it is possible to have real-time monitoring from remote locations using the Internet and mobile phones.

EXAMPLE 12.18

A precast concrete pile 12 in. × 12 in. in cross section is driven by a hammer. Given

Maximum rated hammer energy = 30 kip·ft

Hammer efficiency = 0.8

Weight of ram = 7.5 kip

Pile length = 80 ft

Coefficient of restitution = 0.4

Weight of pile cap = 550 lb

$E_p = 3 \times 10^6$ lb/in^2

Number of blows for last 1 in. of penetration = 8

Estimate the allowable pile capacity by the

a. Modified EN formula (use FS = 6)
b. Danish formula (use FS = 4)

SOLUTION

Part a

$$Q_u = \frac{EW_R h}{S + C} \frac{W_R + n^2 W_p}{W_R + W_p}$$

$$\text{Weight of pile + cap} = \left(\frac{12}{12} \times \frac{12}{12} \times 80\right)(150 \text{ lb/ft}^3) + 550$$

$$= 12{,}550 \text{ lb} = 12.55 \text{ kip}$$

Given: $W_R h = 30$ kip·ft.

$$Q_u = \frac{(0.8)(30 \times 12 \text{ kip·in.})}{\frac{1}{8} + 0.1} \times \frac{7.5 + (0.4)^2(12.55)}{7.5 + 12.55} = 607 \text{ kip}$$

$$Q_{\text{all}} = \frac{Q_u}{\text{FS}} = \frac{607}{6} \approx \mathbf{101 \text{ kip}}$$

Part b

$$Q_u = \frac{EH_E}{S + \sqrt{\dfrac{EH_E L}{2A_p E_p}}}$$

Use $E_p = 3 \times 10^6$ lb/in^2.

$$\sqrt{\frac{EH_E L}{2A_p E_p}} = \sqrt{\frac{(0.8)(30 \times 12)(80 \times 12)}{2(12 \times 12)\left(\frac{3 \times 10^6}{1000}\text{ kip/in}^2\right)}} = 0.566 \text{ in.}$$

$$Q_u = \frac{(0.8)(30 \times 12)}{\frac{1}{8} + 0.566} \approx 417 \text{ kip}$$

$$Q_{\text{all}} = \frac{417}{4} \approx \mathbf{104\ kip}$$

12.21 Pile Capacity for Vibration-Driven Piles

The principles of vibratory pile drivers (Figure 12.9c) were discussed briefly in Section 12.5. As mentioned there, the driver essentially consists of two counterrotating weights. The amplitude of the centrifugal driving force generated by a vibratory hammer can be given as

$$F_c = me\omega^2 \tag{12.125}$$

where

m = total eccentric rotating mass

e = distance between the center of each rotating mass and the center of rotation

ω = operating circular frequency

Vibratory hammers typically include an isolated *bias weight*, which can range from 4 to 40 kN. The bias weight is isolated from oscillation by springs, so it acts as a net downward load helping the driving efficiency by increasing the penetration rate of the pile.

The use of vibratory pile drivers began in the early 1930s. Installing piles with vibratory drivers produces less noise and damage to the pile, compared with impact driving. However, because of a limited understanding of the relationships among the load, the rate of penetration, and the bearing capacity of piles, this method has not gained popularity in the United States.

Vibratory pile drivers are patented. Some examples are the Bodine Resonant Driver (BRD), the Vibro Driver of the McKiernan-Terry Corporation, and the Vibro Driver of the L. B. Foster Company. Davisson (1970) provided a relationship for estimating the ultimate pile capacity in granular soil:

In SI units,

$$Q_u(\text{kN}) = \frac{0.746(H_p) + 98(v_p \text{ m/s})}{(v_p \text{ m/s}) + (S_L \text{ m/cycle})(f \text{ Hz})} \tag{12.126}$$

In English units,

$$Q_u(\text{lb}) = \frac{550(H_p) + 22{,}000(v_p \text{ ft/s})}{(v_p \text{ ft/s}) + (S_L \text{ ft/cycle})(f \text{ Hz})} \tag{12.127}$$

where

H_p = horsepower delivered to the pile

v_p = final rate of pile penetration

S_L = loss factor

f = frequency, in Hz

The loss factor S_L for various types of granular soil is as follows (Bowles, 1996):

CLOSED-END PIPE PILES

- Loose sand: 0.244×10^{-3} m/cycle (0.0008 ft/cycle)
- Medium dense sand: 0.762×10^{-3} m/cycle (0.0025 ft/cycle)
- Dense sand: 2.438×10^{-3} m/cycle (0.008 ft/cycle)

H-PILES

- Loose sand: -0.213×10^{-3} m/cycle (-0.0007 ft/cycle)
- Medium dense sand: 0.762×10^{-3} m/cycle (0.0025 ft/cycle)
- Dense sand: 2.134×10^{-3} m/cycle (0.007 ft/cycle)

In 2000, Feng and Deschamps provided the following relationship for the ultimate capacity of vibrodriven piles in granular soil:

$$Q_u = \frac{3.6\,(F_c + 11W_B)}{1 + 1.8 \times 10^{10}\dfrac{v_p}{c}\sqrt{\text{OCR}}}\,\frac{L_E}{L} \tag{12.128}$$

Here,

F_c = centrifugal force

W_B = bias weight

v_p = final rate of pile penetration

c = speed of light [1.8×10^{10} m/min (5.91×10^{10} ft/min)]

OCR = overconsolidation ratio

L_E = embedded length of pile

L = pile length

EXAMPLE 12.19

Consider a 20 m long steel pile driven by a Bodine Resonant Driver (Section HP 310 × 125) in a medium dense sand. If $H_p = 350$ horsepower, $v_p = 0.0016$ m/s, and $f = 115$ Hz, calculate the ultimate pile capacity, Q_u.

SOLUTION

From Eq. (12.126),

$$Q_u = \frac{0.746H_p + 98v_p}{v_p + S_L f}$$

For an H-pile in medium dense sand, $S_L \approx 0.762 \times 10^{-3}$ m/cycle. So

$$Q_u = \frac{(0.746)\,(350) + (98)\,(0.0016)}{0.0016 + (0.762 \times 10^{-3})(115)} = \mathbf{2928\ kN}$$

12.22 Wave Equation Analysis

Pile-driving formulas presented in Section 12.20 are unreliable, and engineers have never been able to agree on which one is the best. These formulas are mostly empirical and apply only to certain types and lengths of piles. The availability of high-speed computing capabilities has given way to the development of wave equation analysis, which is pile-driving dynamics. It considers the stress wave–propagation

effect during the pile-driving process, which is somewhat similar to the propagation of stress waves along a long, slender rod and can be written as

$$\frac{\partial^2 u}{\partial t^2} = v_c^2 \frac{\partial^2 u}{\partial z^2} \tag{12.129}$$

where

u = displacement of pile at depth z measured from the ground surface

t = time

$v_c = \sqrt{\dfrac{E_p}{\rho}}$ = velocity of longitudinal stress wave propagation

ρ = mass density of the pile material

E_p = modulus of elasticity of the pile material

A detailed derivation of Eq. (12.129) can be found in any soil dynamics book (e.g., Das and Luo, 2017).

Smith (1960) used the wave propagation relationship given in Eq. (12.129), numerical modeling, and digital computers to develop the fundamentals of the wave equation analysis of piles. The wave equations given are

- Pile capacity
- Equipment compatibility
- Driving stresses

The numerical model of Smith (1960) is shown as an example in Figure 12.46. The pile is divided into several short sections (elements), such as 1.5 m (5 ft) or 3 m (10 ft) in length. In Figure 12.46, the pile is divided into ten sections. The individual weights of these sections are W_3, W_4, . . . , W_{12}. The weights of the ram and pile cap are W_1 and W_2, respectively. The elasticity of each pile element is represented by an individual spring, such as K_2, K_3, . . . , K_{11} in Figure 12.46. Also note that R_3, R_4, . . . , R_{11} represent side frictional resistance, and R_{12} represents the pile tip resistance. The soil–pile interface of the pile elements and the bottom of the lowest element are modeled using a series of springs and dashpots. The springs proposed by Smith (1960) are as shown in Figure 12.47a, for example, for the pile point. The spring resistance increases with displacement in a linear manner until it reaches point A. When the displacement is q, which is known as *quake*, the ultimate resistance is R_u; beyond this point the spring becomes plastic. The dashpot resistance is a linear function of the velocity and is defined by the term *damping coefficient*, J (resistance/velocity = J), as shown in Figure 12.47b. The numerical values of the quake, ultimate resistance, and damping coefficient for each element are primarily functions of soil type. Smith (1960) suggested a quake value of 2.5 mm (0.1 in.), which has been modified by other researchers since then.

This model simulates pile driving that is initiated by imparting hammer energy to the ram. The compression stress wave thus generated travels down to the bottom of the pile and reflects back as the compression wave moving upward. Tension may develop as two compression waves traveling in opposite directions pass each other. This can happen when the pile goes through a harder layer and the pile tip is located on a softer layer. With the dissipation of the stress waves, the pile advances downward through a certain distance called a *set*. Smith (1960) provided an example of time versus displacement of the pile elements, as shown in Figure 12.48. Referring to Figure 12.46, the following parameters were used:

- Steel H-pile: length 30 m (100 ft)
- Length of each unit of pile: 3 m (10 ft)
- At pile point: q = 2.5 m (0.1 m), R_u = 889.6 kN (200 kip)
- Ram impact velocity: 3.78 m/s (12.4 ft/s)

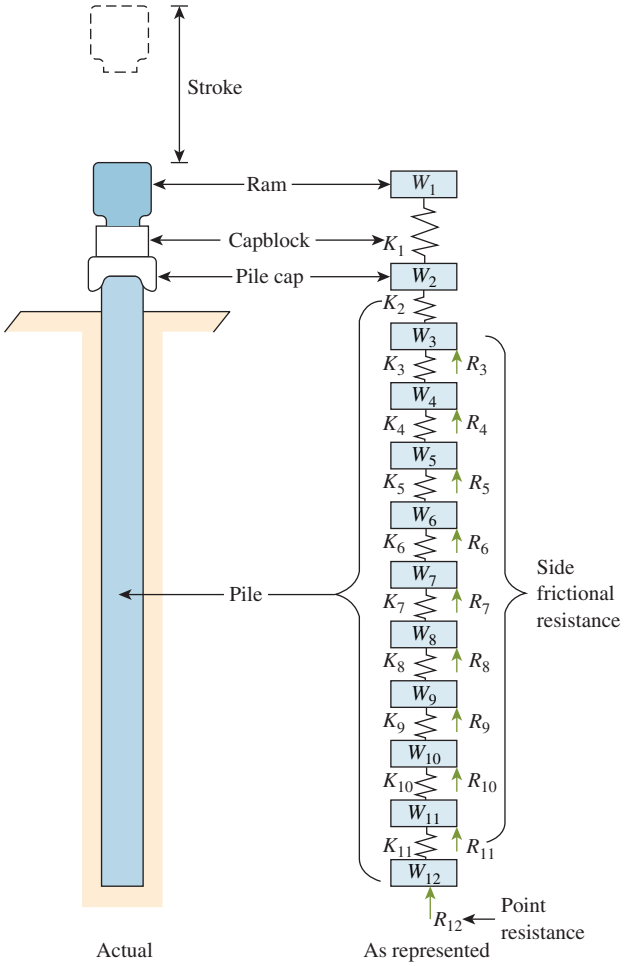


FIGURE 12.46 Wave equation model for driven piles (Based on Smith, 1960)

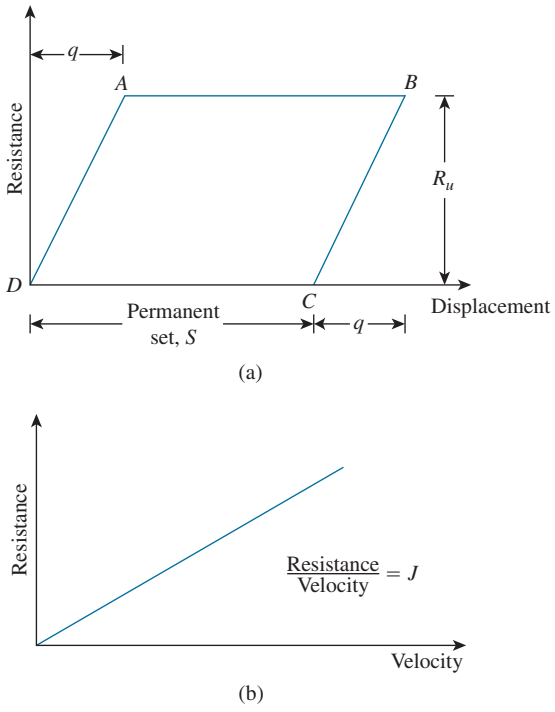


FIGURE 12.47 Model for soil–pile interface at pile point: (a) bilinear spring; (b) dashpot

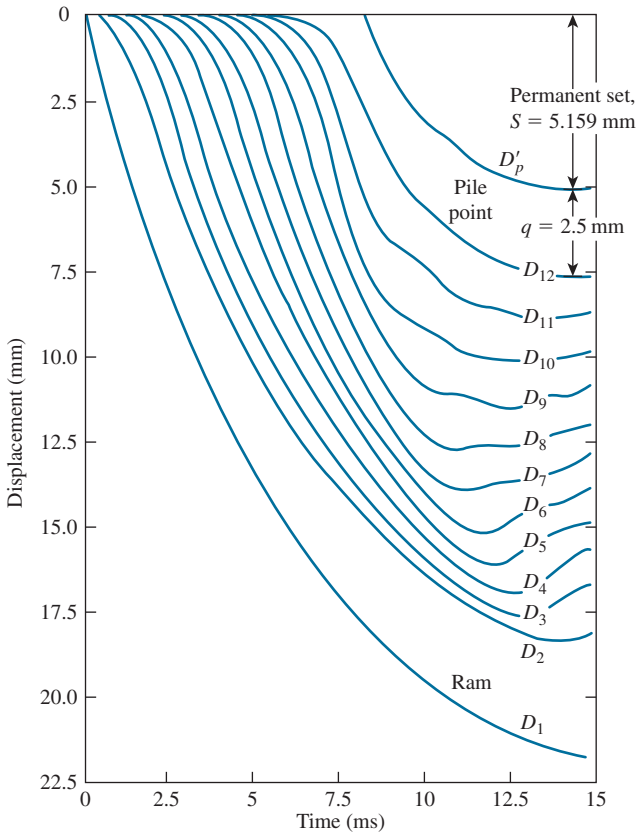


FIGURE 12.48 Example of wave equation analysis (Based on Smith, 1960)

In Figure 12.48, D_1 to D_{12} are the calculated displacements of weights W_1 to W_{12} as well as the plastic ground displacement D'_p, which is the permanent set of 5.159 mm (0.20311 in.).

The pile bearing capacity from the wave equation model is obtained by summing all of the R-values that represent both side friction and point bearing. The analysis is repeated with different assumed R-values to develop a plot of pile capacity versus blow count (N), which can be used in construction control.

12.23 Negative Skin Friction

Negative skin friction is a downward drag force exerted on a pile by the soil surrounding it. Such a force can exist under the following conditions, among others:

1. If a fill of clay soil is placed over a granular soil layer into which a pile is driven, the fill will gradually consolidate. The consolidation process will exert a downward drag force on the pile (see Figure 12.49a) during the period of consolidation.
2. If a fill of granular soil is placed over a layer of soft clay, as shown in Figure 12.49b, it will induce the process of consolidation in the clay layer and thus exert a downward drag on the pile.
3. Lowering of the water table will increase the vertical effective stress on the soil at any depth, which will induce consolidation settlement in clay. If a pile is located in the clay layer, it will be subjected to a downward drag force.

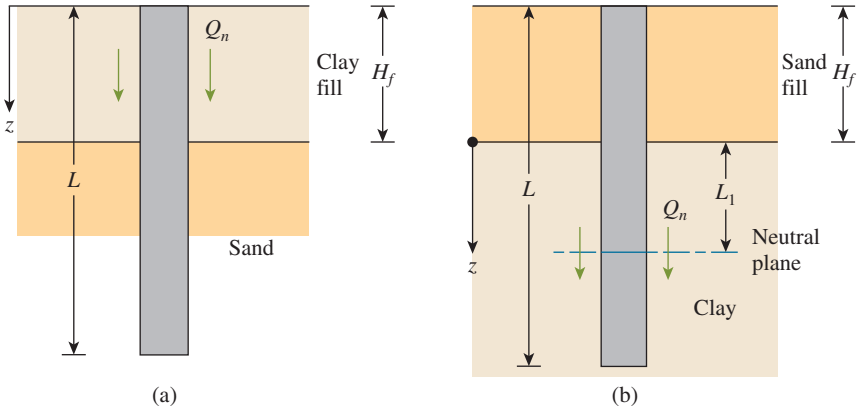


FIGURE 12.49 Negative skin friction

In some cases, the downward drag force may be excessive and cause foundation failure. This section outlines two tentative methods for the calculation of negative skin friction.

CLAY FILL OVER GRANULAR SOIL (FIGURE 12.49a)

Similar to the β method presented in Section 12.14, the negative (downward) skin stress on the pile is

$$f_n = K'\sigma'_o \tan \delta' \tag{12.130}$$

where

K' = earth pressure coefficient = $K_o = 1 - \sin \phi'$

σ'_o = vertical effective stress at any depth $z = \gamma'_f z$

γ'_f = effective unit weight of fill

δ' = soil–pile friction angle $\approx (0.5–0.7)\phi'$

Hence, the total downward drag force on a pile is

$$Q_n = \int_0^{H_f} (pK'\gamma'_f \tan \delta')z\, dz = \frac{pK'\gamma'_f H_f^2 \tan \delta'}{2} \tag{12.131}$$

where H_f = height of the clay fill. If the fill is above the water table, the effective unit weight, γ'_f, should be replaced by the moist unit weight.

GRANULAR SOIL FILL OVER CLAY (FIGURE 12.49b)

In this case, the evidence indicates that the negative skin stress on the pile may exist from $z = 0$ to $z = L_1$, which is referred to as the *neutral depth*. (See Vesic, 1977, pp. 25–26.) The neutral depth may be given as (Bowles, 1982)

$$L_1 = \frac{(L - H_f)}{L_1}\left[\frac{L - H_f}{2} + \frac{\gamma'_f H_f}{\gamma'}\right] - \frac{2\gamma'_f H_f}{\gamma'} \tag{12.132}$$

where γ'_f and γ' = effective unit weights of the fill and the underlying clay layer, respectively.

For end-bearing piles, the neutral depth may be assumed to be located at the pile tip (i.e., $L_1 = L - H_f$).

Once the value of L_1 is determined, the downward drag force is obtained in the following manner: The unit negative skin friction at any depth from $z = 0$ to $z = L_1$ is

$$f_n = K'\sigma'_o \tan \delta' \tag{12.133}$$

where

$$K' = K_o = 1 - \sin \phi'$$

$$\sigma'_o = \gamma'_f H_f + \gamma' z$$

$$\delta' = 0.5\text{–}0.7\phi'$$

$$\begin{aligned} Q_n &= \int_0^{L_1} pf_n \, dz = \int_0^{L_1} pK'(\gamma'_f H_f + \gamma' z)\tan \delta' \, dz \\ &= (pK'\gamma'_f H_f \tan \delta')L_1 + \frac{L_1^2 pK'\gamma' \tan \delta'}{2} \end{aligned} \tag{12.134}$$

If the soil and the fill are above the water table, the effective unit weights should be replaced by moist unit weights. In some cases, the piles can be coated with bitumen in the downdrag zone to avoid this problem.

A limited number of case studies of negative skin friction are available in the literature. Bjerrum et al. (1969) reported monitoring the downdrag force on a test pile at Sorenga in the harbor of Oslo, Norway (noted as pile G in the original paper). The study of Bjerrum et al. (1969) was also discussed by Wong and Teh (1995) in terms of the pile being driven to bedrock at 40 m. Figure 12.50a shows the soil profile and the pile. Wong and Teh estimated the following quantities:

- *Fill:* Moist unit weight, $\gamma_f = 16$ kN/m^3
  Saturated unit weight, $\gamma_{sat(f)} = 18.5$ kN/m^3
  So
  $$\gamma'_f = 18.5 - 9.81 = 8.69 \text{ kN/m}^3$$
  and
  $$H_f = 13 \text{ m}$$
- *Clay:* $K' \tan \delta' \approx 0.22$
  Saturated effective unit weight, $\gamma' = 19 - 9.81 = 9.19$ kN/m^3
- *Pile:* $L = 40$ m
  Diameter, $D = 500$ m

Thus, the maximum downdrag force on the pile can be estimated from Eq. (12.134). Since in this case the pile is a point bearing pile, the magnitude of $L_1 = 27$ m, and

$$Q_n = (p)(K' \tan \delta')[\gamma_f \times 2 + (13 - 2)\gamma'_f](L_1) + \frac{L_1^2 p\gamma'(K' \tan \delta')}{2}$$

or

$$\begin{aligned} Q_n &= (\pi \times 0.5)(0.22)[(16 \times 2) + (8.69 \times 11)](27) + \frac{(27)^2(\pi \times 0.5)(9.19)(0.22)}{2} \\ &= 2348 \text{ kN} \end{aligned}$$

The measured value of the maximum Q_n was about 2500 kN (Figure 12.50b), which is in good agreement with the calculated value.

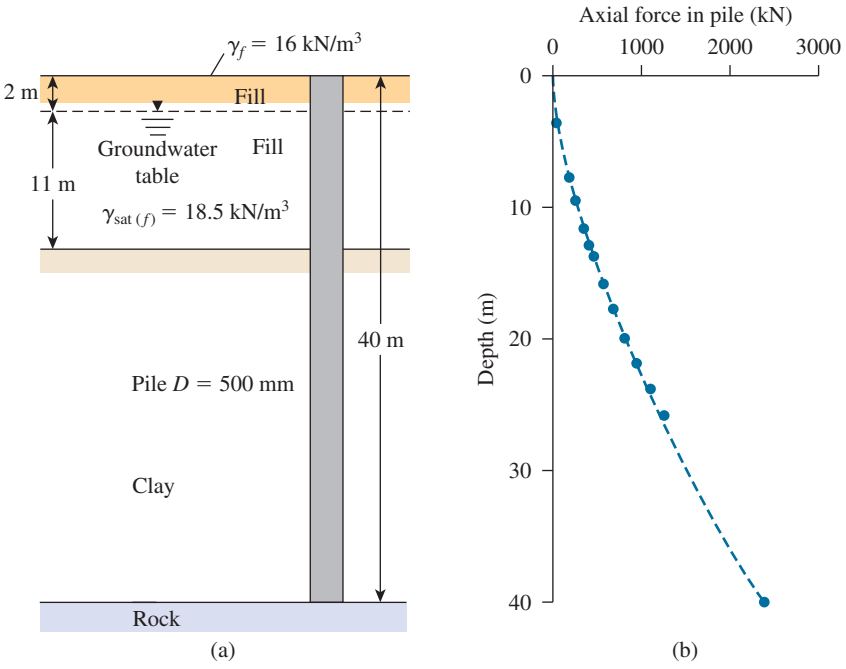


FIGURE 12.50 Negative skin friction on a pile in the harbor of Oslo, Norway (Based on Bjerrum et al. (1969) and Wong and Teh (1995))

EXAMPLE 12.20

In Figure 12.49a, let $H_f = 2$ m. The pile is circular in cross section with a diameter of 0.305 m. For the fill that is above the water table, $\gamma_f = 16$ kN/m^3 and $\phi' = 32°$. Determine the total drag force. Use $\delta' = 0.6\phi'$.

SOLUTION

From Eq. (12.131),

$$Q_n = \frac{pK'\gamma_f H_f^2 \tan \delta'}{2}$$

with

$$p = \pi(0.305) = 0.958 \text{ m}$$
$$K' = 1 - \sin \phi' = 1 - \sin 32 = 0.47$$

and

$$\delta' = (0.6)(32) = 19.2°$$

Thus,

$$Q_n = \frac{(0.958)(0.47)(16)(2)^2 \tan 19.2}{2} = \mathbf{5.02\ kN}$$

EXAMPLE 12.21

In Figure 12.49b, let $H_f = 2$ m, pile diameter = 0.305 m, $\gamma_f = 16.5$ kN/m^3, $\phi'_{clay} = 34°$, $\gamma_{sat(clay)} = 17.2$ kN/m^3, and $L = 20$ m. The water table coincides with the top of the clay layer. Determine the downward drag force. Assume that $\delta' = 0.6\phi'_{clay}$.

SOLUTION

The depth of the neutral plane is given in Eq. (12.132) as

$$L_1 = \frac{L - H_f}{L_1}\left(\frac{L - H_f}{2} + \frac{\gamma_f H_f}{\gamma'}\right) - \frac{2\gamma_f H_f}{\gamma'}$$

Note that γ_f' in Eq. (12.132) has been replaced by γ_f because the fill is above the water table, so

$$L_1 = \frac{(20-2)}{L_1}\left[\frac{(20-2)}{2} + \frac{(16.5)(2)}{(17.2-9.81)}\right] - \frac{(2)(16.5)(2)}{(17.2-9.81)}$$

or

$$L_1 = \frac{242.4}{L_1} - 8.93; \; L_1 = 11.75 \text{ m}$$

Now, from Eq. (12.134), we have

$$Q_n = (pK'\gamma_f H_f \tan\delta')L_1 + \frac{L_1^2 pK'\gamma' \tan\delta'}{2}$$

with

$$p = \pi(0.305) = 0.958 \text{ m}$$

and

$$K' = 1 - \sin 34^\circ = 0.44$$

Hence,

$$\begin{aligned} Q_n &= (0.958)(0.44)(16.5)(2)[\tan(0.6 \times 34)](11.75) \\ &\quad + \frac{(11.75)^2(0.958)(0.44)(17.2-9.81)[\tan(0.6\times 34)]}{2} \\ &= 60.78 + 79.97 = \mathbf{140.75 \text{ kN}} \end{aligned}$$

Group Piles

12.24 Group Efficiency

In most cases, piles are used in groups, as shown in Figure 12.51, to transmit the structural load to the soil. A *pile cap* is constructed over *group piles*. The cap can be in contact with the ground, as in most cases (see Figure 12.51a), or well above the ground, as in the case of offshore platforms (see Figure 12.51b).

Determining the load-bearing capacity of group piles is extremely complicated and has not yet been fully resolved. When the piles are placed close to each other, a reasonable assumption is that the stresses transmitted by the piles to the soil will overlap (see Figure 12.51c), reducing the load-bearing capacity of the piles. Ideally, the piles in a group should be spaced so that the load-bearing capacity of the group is not less than the sum of the bearing capacity of the individual piles. In practice, the minimum center-to-center pile spacing, d, is $2.5D$ and, in ordinary situations, is actually about 3 to $3.5D$.

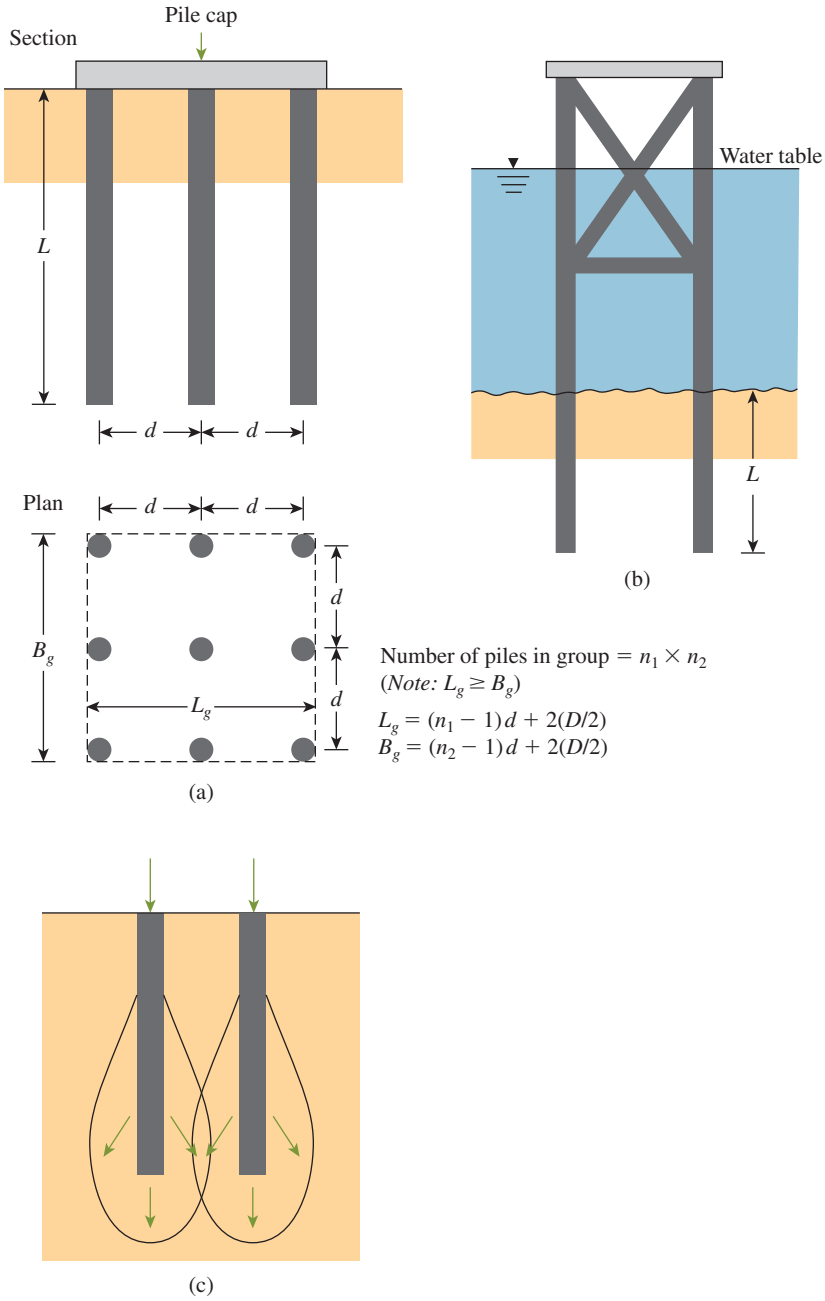


FIGURE 12.51 Group piles

The efficiency of the load-bearing capacity of a group pile may be defined as

$$\eta = \frac{Q_{g(u)}}{\Sigma Q_u} \tag{12.135}$$

where

η = group efficiency

$Q_{g(u)}$ = ultimate load-bearing capacity of the group pile

Q_u = ultimate load-bearing capacity of each pile without the group effect



(a) (b)

FIGURE 12.52 (a) Driving of piles in a group; (b) reinforcement cage for the pile cap over a 2×2 pile group (Courtesy of N. Sivakugan, James Cook University, Australia)

Figure 12.52a shows the driving of piles in a group. Figure 12.52b shows the reinforcement cage for the pile cap that will be cast on top of four concrete piles.

Many structural engineers use a simplified analysis to obtain the group efficiency for *friction piles*, particularly in sand. This type of analysis can be explained with the aid of Figure 12.51a. Depending on their spacing within the group, the piles may act in one of two ways: (1) as a *block*, with dimensions $L_g \times B_g \times L$, or (2) as *individual piles*. If the piles act as a block, the frictional capacity is $f_{av} p_g L \approx Q_{g(u)}$. [*Note:* p_g = perimeter of the cross section of the block = $2(n_1 + n_2 - 2)d + 4D$, and f_{av} = average unit frictional resistance.] Similarly, for each pile acting individually, $Q_u \approx pLf_{av}$. (*Note:* p = perimeter of the cross section of each pile.) Thus,

$$\eta = \frac{Q_{g(u)}}{\Sigma Q_u} = \frac{f_{av}[2(n_1 + n_2 - 2)d + 4D]L}{n_1 n_2 p L f_{av}} = \frac{2(n_1 + n_2 - 2)d + 4D}{p n_1 n_2} \tag{12.136}$$

Hence,

$$Q_{g(u)} = \left[\frac{2(n_1 + n_2 - 2)d + 4D}{p n_1 n_2}\right] \Sigma Q_u \tag{12.137}$$

From Eq. (12.137), if the center-to-center spacing d is large enough, $\eta > 1$. In that case, the piles will behave as individual piles. Thus, in practice, if $\eta < 1$, then

$$Q_{g(u)} = \eta \Sigma Q_u$$

and if $\eta \geq 1$, then

$$Q_{g(u)} = \Sigma Q_u$$

There are several other equations like Eq. (12.137) for calculating the group efficiency of friction piles. Some of these are given in Table 12.18.

It is important, however, to recognize that relationships such as Eq. (12.137) are simplistic.

TABLE 12.18 Equations for Group Efficiency of Friction Piles

Name	Equation
Converse–Labarre equation	$\eta = 1 - \left[\frac{(n_1 - 1)n_2 + (n_2 - 1)n_1}{90 n_1 n_2}\right]\theta$ where $\theta(\text{deg}) = \tan^{-1}(D/d)$
Los Angeles Group Action equation	$\eta = 1 - \frac{D}{\pi d n_1 n_2}[n_1(n_2 - 1) + n_2(n_1 - 1) + \sqrt{2}(n_1 - 1)(n_2 - 1)]$
Seiler–Keeney equation (Seiler and Keeney, 1944)	$\eta = \left\{1 - \left[\frac{11d}{7(d^2 - 1)}\right]\left[\frac{n_1 + n_2 - 2}{n_1 + n_2 - 1}\right]\right\} + \frac{0.3}{n_1 + n_2}$ where d is in ft

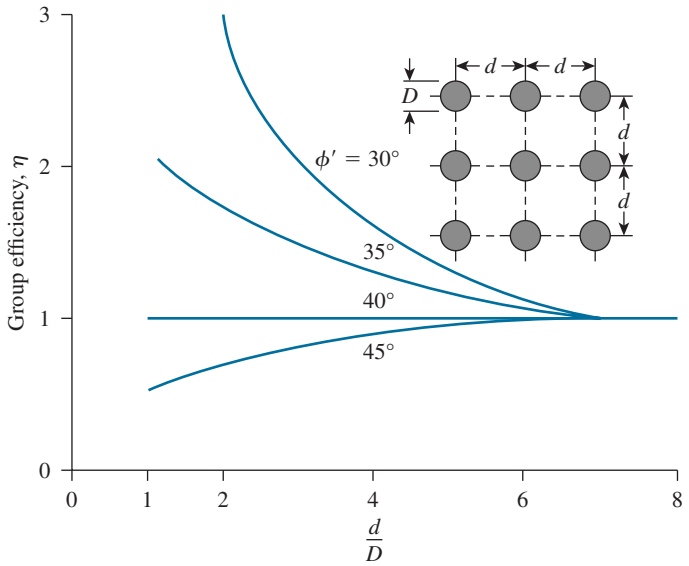


FIGURE 12.53 Variation of efficiency of pile groups in sand (Based on Kishida and Meyerhof, 1965)

Figure 12.53 shows the variation of the group efficiency η for a 3×3 group pile in sand (Kishida and Meyerhof, 1965). It can be seen that for loose and medium sands, the magnitude of the group efficiency can be larger than unity. This is due primarily to the densification of sand surrounding the pile. Dense sands can dilate and become loose during driving and hence the efficiency can be less than unity. When the spacing between the piles, d, is large, the group efficiency is close to unity, irrespective of the relative densities.

12.25 Ultimate Capacity of Group Piles in Saturated Clay

Figure 12.54 shows a group pile in saturated clay. Here the piles and the clay are treated as a monolithic block. Using the figure, one can estimate the ultimate load-bearing capacity of group piles in the following manner:

Step 1. Determine $\Sigma Q_u = n_1 n_2 (Q_p + Q_s)$. From Eq. (12.20),

$$Q_p = A_p[9c_{u(p)}]$$

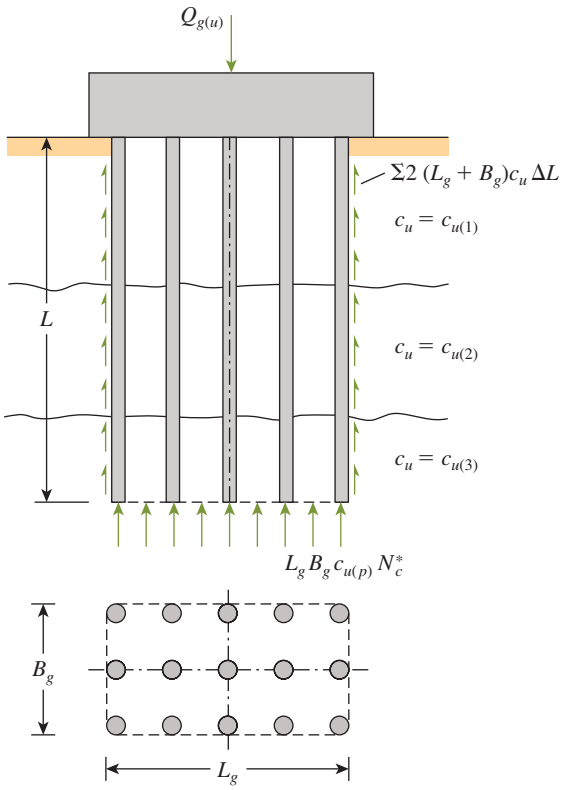


FIGURE 12.54 Ultimate capacity of group piles in clay

where $c_{u(p)}$ = undrained cohesion of the clay at the pile tip. Also, from Eq. (12.61), for a single pile,

$$Q_s = \Sigma\, \alpha p c_u\, \Delta L$$

So,

$$\Sigma\, Q_u = n_1 n_2 [9 A_p c_{u(p)} + \Sigma\, \alpha p c_u\, \Delta L] \tag{12.138}$$

Step 2. Determine the ultimate capacity by assuming that the piles in the group act as a block with dimensions $L_g \times B_g \times L$. The skin resistance of the block is

$$\Sigma\, p_g c_u\, \Delta L = \Sigma\, 2\,(L_g + B_g) c_u\, \Delta L$$

Calculate the point bearing capacity:

$$A_p q_p = A_p c_{u(p)} N_c^* = (L_g B_g) c_{u(p)} N_c^*$$

Obtain the value of the bearing capacity factor N_c^* from Figure 12.55. Thus, the ultimate load is

$$\Sigma\, Q_u = L_g B_g c_{u(p)} N_c^* + \Sigma\, 2(L_g + B_g) c_u\, \Delta L \tag{12.139}$$

Step 3. Compare the values obtained from Eqs. (12.138) and (12.139). The *lower* of the two values is $Q_{g(u)}$.

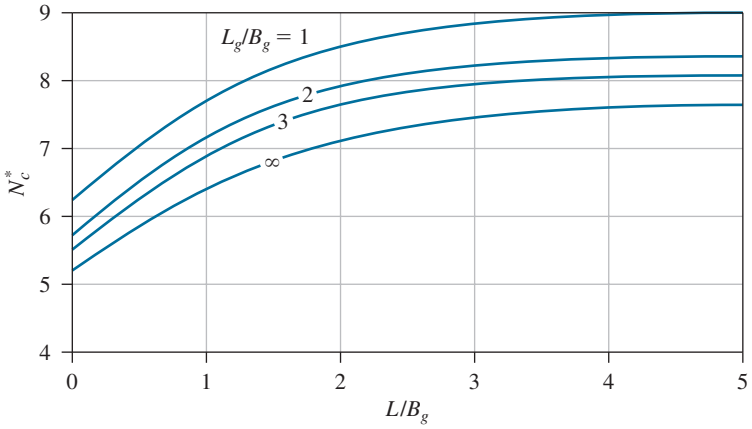


FIGURE 12.55 Variation of N_c^* with L_g/B_g and L/B_g

EXAMPLE 12.22

The section of a 3 × 4 group pile in a layered saturated clay is shown in Figure 12.56. The piles are square in cross section (14 in. × 14 in.). The center-to-center spacing, d, of the piles is 35 in. Determine the allowable load-bearing capacity of the pile group. Use FS = 4. Note that the groundwater table coincides with the ground surface.

SOLUTION

From Eq. (12.138),

$$\Sigma Q_u = n_1 n_2 [9A_p c_{u(p)} + \alpha_1 p c_{u(1)} L_1 + \alpha_2 p c_{u(2)} L_2]$$

From Figure 12.56, $c_{u(1)} = 1050$ lb/ft^2 and $c_{u(2)} = 1775$ lb/ft^2.

For the top layer with $c_{u(1)} = 1050$ lb/ft^2,

$$\frac{c_{u(1)}}{p_a} = \frac{1050}{2000} = 0.525$$

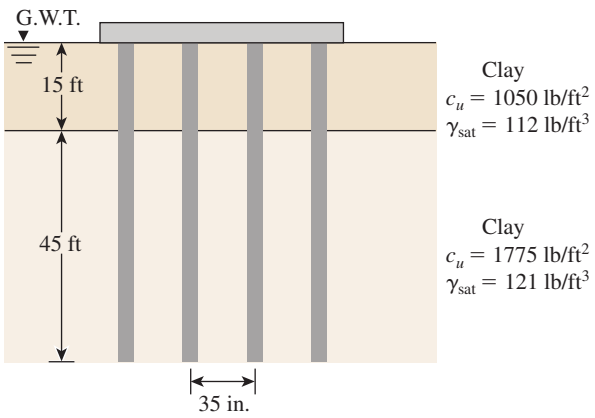


FIGURE 12.56 Group pile of layered saturated clay

From Table 12.11, $\alpha_1 \approx 0.68$

$$\frac{c_{u(2)}}{p_a} = \frac{1775}{2000} \approx 0.89$$

$$\alpha_2 = 0.51$$

$$\Sigma Q_u = \frac{(3)(4)}{1000}\left[\begin{array}{l}(9)\left(\frac{14}{12}\right)^2(1775) + (0.68)\left(4 \times \frac{14}{12}\right)(1050)(15) \\ + (0.51)\left(4 \times \frac{14}{12}\right)(1775)(45)\end{array}\right] = 3141.9 \text{ kip}$$

For piles acting as a group,

$$L_g = (3)(35) + 14 = 119 \text{ in.} = 9.92 \text{ ft}$$

$$B_g = (2)(35) + 14 = 84 \text{ in.} = 7 \text{ ft}$$

$$\frac{L_g}{B_g} = \frac{9.92}{7} = 1.42$$

$$\frac{L}{B_g} = \frac{60}{7} = 8.57$$

From Figure 12.55, $N_c^* = 8.75$. From Eq. (12.139),

$$\begin{aligned}\Sigma Q_u &= L_g B_g c_{u(p)} N_c^* + \Sigma 2(L_g + B_g) c_u \, \Delta L \\ &= (9.92)(7)(1775)(8.75) + (2)(9.92 + 7)[(1050)(15) + (1775)(45)] \\ &= 4{,}313{,}000 \text{ lb} = 4313 \text{ kip}\end{aligned}$$

Hence, $\Sigma Q_u = 3141.9$ kip.

$$\Sigma Q_{\text{all}} = \frac{3141.9}{\text{FS}} = \frac{3141.9}{4} \approx \mathbf{785.5 \text{ kip}}$$

12.26 Elastic Settlement of Group Piles

In general, the settlement of a group pile under a similar working load per pile increases with the width of the group (B_g) and the center-to-center spacing of the piles (d). Several investigations relating to the settlement of group piles have been reported in the literature, with widely varying results. The simplest relation for the settlement of group piles was given by Vesic (1969), namely,

$$s_{g(e)} = \sqrt{\frac{B_g}{D}} s_e \tag{12.140}$$

where

$s_{g(e)}$ = elastic settlement of group piles

B_g = width of group pile section

D = width or diameter of each pile in the group

s_e = elastic settlement of each pile at comparable working load (see Section 12.18)

For group piles in sand and gravel, for elastic settlement, Meyerhof (1976) suggested the empirical relation

$$s_{g(e)}(\text{in.}) = \frac{2q\sqrt{B_g}I}{N_{60}} \tag{12.141}$$

where

$$q = Q_g/(L_g B_g)\ (\text{in U.S. ton/ft}^2) \tag{12.142}$$

and

L_g and B_g = length and width of the group pile section, respectively (ft)

N_{60} = average standard penetration number within seat of settlement ($\approx B_g$ deep below the tip of the piles)

$$I = \text{influence factor} = 1 - L/8B_g \geq 0.5 \tag{12.143}$$

L = length of embedment of piles (ft)

In SI units,

$$S_{g(e)}(\text{mm}) = \frac{0.96q\sqrt{B_g}I}{N_{60}} \tag{12.144}$$

where q is in kN/m^2, B_g and L_g are in m, and

$$I = 1 - \frac{L(\text{m})}{8B_g(\text{m})}$$

Similarly, the group pile settlement is related to the cone penetration resistance by the formula

$$S_{g(e)} = \frac{qB_g I}{2q_c} \tag{12.145}$$

where q_c = average cone penetration resistance within the seat of settlement. [Note that in Eq. (12.145), all quantities are expressed in consistent units.]

EXAMPLE 12.23

Consider a 3 × 4 group of prestressed concrete piles, each 21 m long, in a sand layer. The details of each pile and the sand are similar to that described in Example 12.14. The working load for the pile group is 6024 kN (3 × 4 × Q_{all}—where Q_{all} = 502 kN as in Example 12.14), and $d/D = 3$. Estimate the elastic settlement of the pile group. Use Eq. (12.140).

SOLUTION

$$s_{e(g)} = \sqrt{\frac{B_g}{D}}s_e$$

$$B_g = (3-1)d + \frac{2D}{2} = (2)(3D) + D = 7D = (7)(0.356\ \text{m}) = 2.492\ \text{m}$$

From Example 12.14, s_e = 19.69 mm

$$s_{e(g)} = \sqrt{\frac{2.492}{0.356}}(19.69) = \mathbf{52.09\ mm}$$

12.27 Consolidation Settlement of Group Piles

The consolidation settlement of a group pile in clay can be estimated by using the 2:1 stress distribution method. The calculation involves the following steps (see Figure 12.57):

Step 1. Let the depth of embedment of the piles be L. The group is subjected to a total load of Q_g. If the pile cap is below the original ground surface, Q_g equals the total load of the superstructure on the piles, minus the effective weight of soil above the group piles removed by excavation.

Step 2. Assume that the load Q_g is transmitted to the soil beginning at a depth of $2L/3$ from the top of the pile, as shown in the figure. The load Q_g spreads out along two vertical to one horizontal line from this depth. Lines aa' and bb' are the two 2:1 lines.

Step 3. Calculate the increase in effective stress caused at the middle of each soil layer by the load Q_g. The formula is

$$\Delta\sigma_i' = \frac{Q_g}{(B_g + z_i)(L_g + z_i)} \tag{12.146}$$

where

$\Delta\sigma_i'$ = increase in effective stress at the middle of layer i

L_g, B_g = length and width, respectively of the planned group piles

z_i = distance from $z = 0$ to the middle of the clay layer i

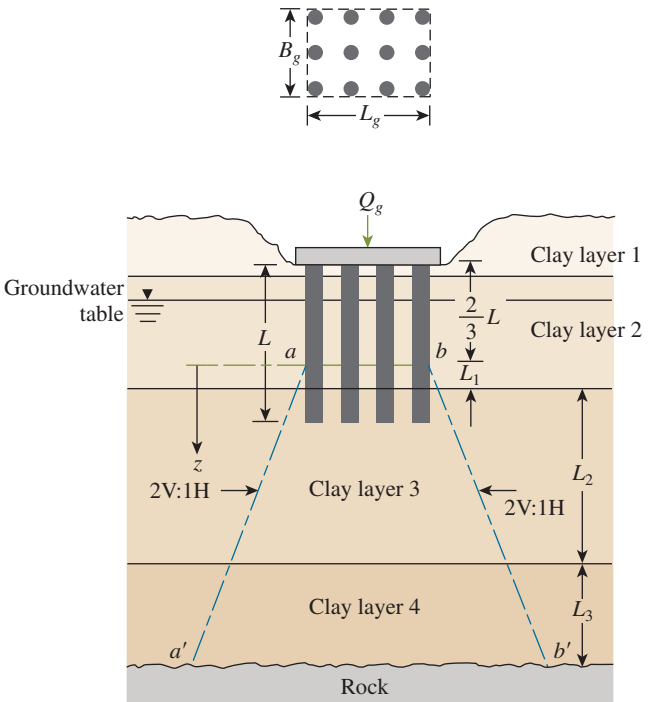


FIGURE 12.57 Consolidation settlement of group piles

For example, in Figure 12.57, for layer 2, $z_i = L_1/2$; for layer 3, $z_i = L_1 + L_2/2$; and for layer 4, $z_i = L_1 + L_2 + L_3/2$. Note, however, that there will be no increase in stress in clay layer 1, because it is above the horizontal plane ($z = 0$) from which the stress distribution to the soil starts.

Step 4. Calculate the consolidation settlement of each layer caused by the increased stress. The formula is

$$\Delta s_{c(i)} = \left[\frac{\Delta e_{(i)}}{1 + e_{o(i)}}\right] H_i \tag{12.147}$$

where

$\Delta s_{c(i)}$ = consolidation settlement of layer i

$\Delta e_{(i)}$ = change of void ratio caused by the increase in stress in layer i

$e_{o(i)}$ = initial void ratio of layer i (before construction)

H_i = thickness of layer i (*Note:* In Figure 12.57, for layer 2, $H_i = L_1$; for layer 3, $H_i = L_2$; and for layer 4, $H_i = L_3$.)

Relationships involving $\Delta e_{(i)}$ are given in Chapter 2.

Step 5. The total consolidation settlement of the group piles is then

$$\Delta s_{c(g)} = \Sigma \Delta s_{c(i)} \tag{12.148}$$

Note that the consolidation settlement of piles may be initiated by fills placed nearby, adjacent floor loads, or the lowering of water tables.

EXAMPLE 12.24

A group pile in clay is shown in Figure 12.58. Determine the consolidation settlement of the piles. All clays are normally consolidated.

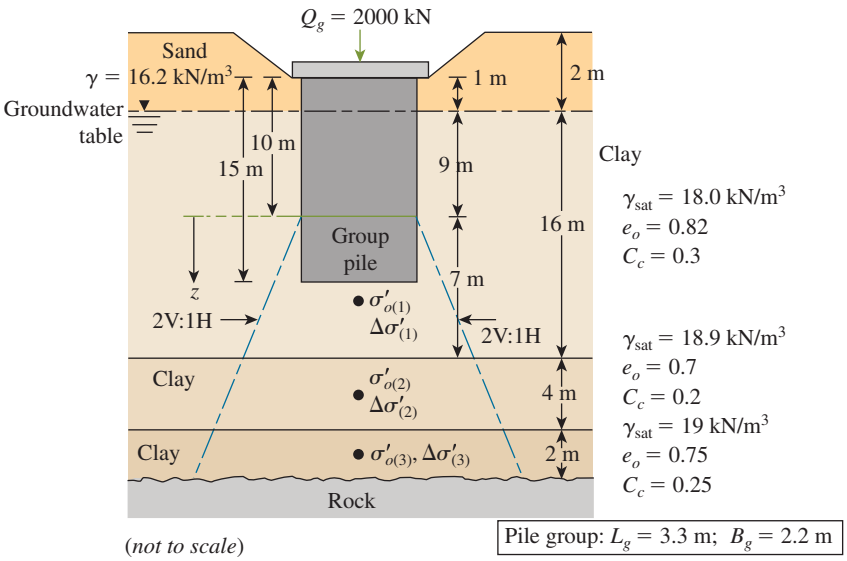


FIGURE 12.58 Consolidation settlement of a pile group

SOLUTION

Because the lengths of the piles are 15 m each, the stress distribution starts at a depth of 10 m below the top of the pile. We are given that $Q_g = 2000$ kN

Calculation of Settlement of Clay Layer 1

For normally consolidated clays,

$$\Delta s_{c(1)} = \left[\frac{(C_{c(1)}H_1)}{1 + e_{o(1)}}\right]\log\left[\frac{\sigma'_{o(1)} + \Delta\sigma'_{(1)}}{\sigma'_{o(1)}}\right]$$

$$\Delta\sigma'_{(1)} = \frac{Q_g}{(L_g + z_1)(B_g + z_1)} = \frac{2000}{(3.3 + 3.5)(2.2 + 3.5)} = 51.6 \text{ kN/m}^2$$

and

$$\sigma'_{o(1)} = 2(16.2) + 12.5(18.0 - 9.81) = 134.8 \text{ kN/m}^2$$

So

$$\Delta s_{c(1)} = \frac{(0.3)(7)}{1 + 0.82}\log\left[\frac{134.8 + 51.6}{134.8}\right] = 0.1624 \text{ m} = \mathbf{162.4 \text{ mm}}$$

Settlement of Layer 2

As with layer 1,

$$\Delta s_{c(2)} = \frac{C_{c(2)}H_2}{1 + e_{o(2)}}\log\left[\frac{\sigma'_{o(2)} + \Delta\sigma_{(2)}}{\sigma'_{o(2)}}\right]$$

$$\sigma'_{o(2)} = 2(16.2) + 16(18.0 - 9.81) + 2(18.9 - 9.81) = 181.62 \text{ kN/m}^2$$

and

$$\Delta\sigma'_{(2)} = \frac{2000}{(3.3 + 9)(2.2 + 9)} = 14.52 \text{ kN/m}^2$$

Hence,

$$\Delta s_{c(2)} = \frac{(0.2)(4)}{1 + 0.7}\log\left[\frac{181.62 + 14.52}{181.62}\right] = 0.0157 \text{ m} = \mathbf{15.7 \text{ mm}}$$

Settlement of Layer 3

Continuing analogously, we have

$$\sigma'_{o(3)} = 181.62 + 2(18.9 - 9.81) + 1(19 - 9.81) = 208.99 \text{ kN/m}^2$$

$$\Delta\sigma'_{(3)} = \frac{2000}{(3.3 + 12)(2.2 + 12)} = 9.2 \text{ kN/m}^2$$

$$\Delta s_{c(3)} = \frac{(0.25)(2)}{1 + 0.75}\log\left(\frac{208.99 + 9.2}{208.99}\right) = 0.0054 \text{ m} = \mathbf{5.4 \text{ mm}}$$

Hence, the total settlement is

$$\Delta s_{c(g)} = 162.4 + 15.7 + 5.4 = \mathbf{183.5 \text{ mm}}$$

12.28 Piles in Rock

For point bearing piles resting on rock, most building codes specify that $Q_{g(u)} = \Sigma Q_u$, provided that the minimum center-to-center spacing of the piles is $D + 300$ mm. For H-piles and piles with square cross sections, the magnitude of D is equal to the diagonal dimension of the cross section of the pile.

12.29 Summary

Piles can be classified based on their materials (e.g., steel, concrete, timber), method of installation (e.g., driven, bored, jetted), or the load transfer mechanism (e.g., end-bearing or friction piles). When the ultimate load Q_u is applied on top of a pile, it is shared by the pile point (Q_p) and pile shaft (Q_s). The first part of this chapter examined the different methods for computing these two components in sand and clay. These methods include rational ones based on simple theories as well as empirical methods based on *in situ* penetration test (e.g., SPT and CPT) data.

Pile load tests are carried out to verify the design loads. Interpretation of the load-settlement data obtained from the traditional pile load test was discussed. These days, pile-driving analyzers (PDAs) are widely used as an inexpensive, but less reliable, alternative. Pile-driving hammers and their accessories were also discussed in this chapter. Ways of estimating the load-carrying capacity of the pile based on the pile-driving equations were discussed.

When a fill is placed at the ground level, it can induce some downward drag on the pile, thus reversing the direction of the skin friction. Methods of determining the downward drag force were discussed.

When the column loads become very large, single piles may not be adequate. Here, more than one pile can be placed as a pile group, with a concrete pile cap, to carry the column load. The efficiency of a pile group compared to a single pile and the method of determining the load-carrying capacity of a pile group were discussed.

PROBLEMS

12.1 A 1500 kN load was applied on two 20 m long and 500 mm diameter piles that were instrumented for measuring the load variation with depth.

a. The variation of frictional resistance per unit area, $f_{(z)}$, with depth for the first pile is shown in Figure P12.1a. Using Eq. (12.9), draw the variation of pile load $Q_{(z)}$ with depth.

b. The variation of pile load $Q_{(z)}$ with depth for the second pile is shown in Figure P12.1b. Using Eq. (12.9), draw the variation of frictional resistance per unit area, $f_{(z)}$, with depth.

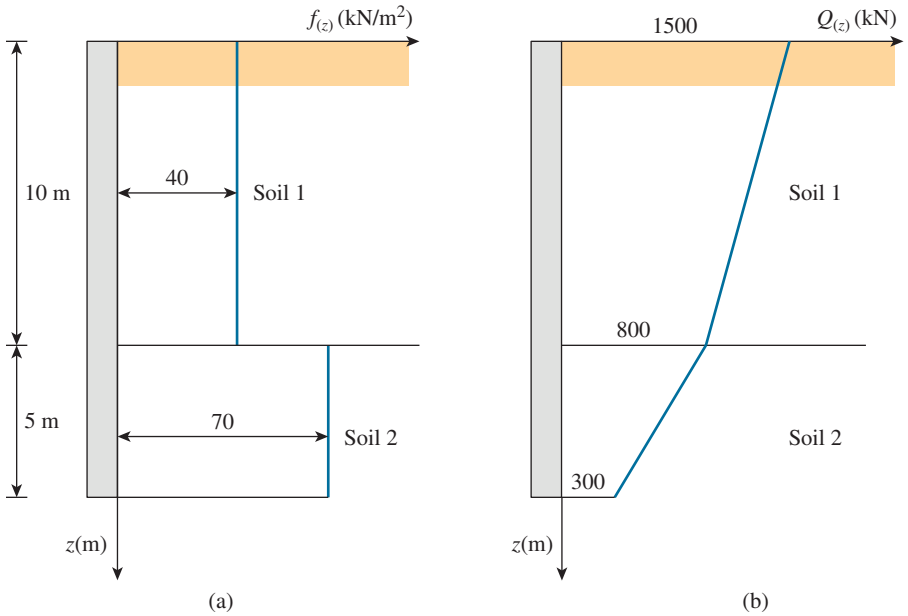


FIGURE P12.1

12.2 A 20 m long concrete pile is shown in Figure P12.2. Estimate the ultimate point load Q_p by
- **a.** Meyerhof's method
- **b.** Vesic's method
- **c.** Coyle and Castello's method

Use $m = 600$ in Eq. (12.28).

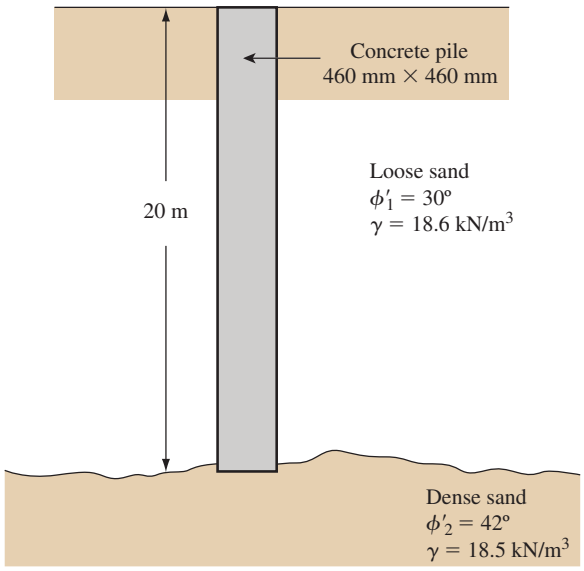


FIGURE P 12.2

12.3 A 500 mm diameter and 20 m long concrete pile is driven into a sand where $\gamma = 18.5$ kN/m^3 and $\phi' = 32°$. Assuming $\delta' = 0.7\phi'$ and $K = 1.5\ K_o$, determine the load-carrying capacity of the pile, with a factor of safety of 3. Use Meyerhof's method [Eq. (12.18)] for computing the point load-carrying capacity Q_p, and use Eqs. (12.42) and (12.43) for computing the load-carrying capacity of the pile shaft Q_s.

12.4 Redo Problem 12.3 using Coyle and Castello's methods for estimating both Q_p and Q_s.

12.5 A 400 mm × 400 mm square precast concrete pile of 15 m length is driven into a sand where $\gamma = 18.0$ kN/m^3 and $\phi' = 33°$. Assuming $\delta' = 0.7\phi'$ and $K = 1.4\ K_o$, determine the load-carrying capacity of the pile with a factor of safety of 3. Use Meyerhof's method [Eq. (12.18)] for computing the point load-carrying capacity Q_p, and Eqs. (12.42) and (12.43) for computing the load-carrying capacity of the pile shaft Q_s.

12.6 Determine the maximum load that can be allowed on a 450 mm diameter driven pile shown in Figure P12.6, allowing a factor of safety of 3. Use $K = 1.5\ K_o$ and $\delta' = 0.65\phi'$ in computing the shaft load. Use Meyerhof's method for computing the point load.

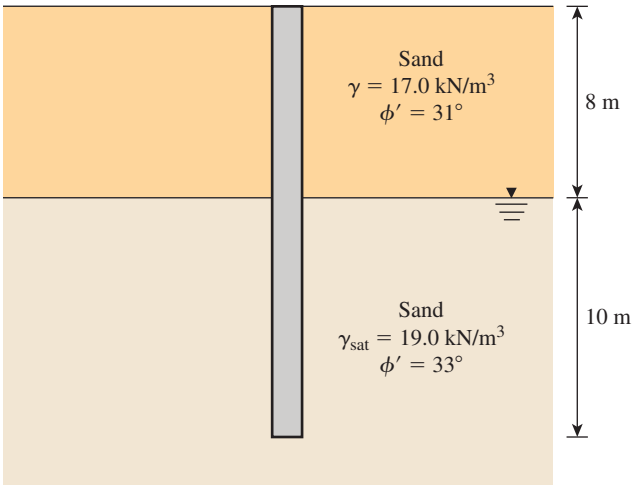


FIGURE P12.6

12.7 A driven closed-ended pile, circular in cross section, is shown in Figure P 12.7. Calculate the following.
- **a.** The ultimate point load using Meyerhof's procedure.
- **b.** The ultimate point load using Vesic's procedure. Take $I_{rr} = 50$
- **c.** An approximate ultimate point load on the basis of parts (a) and (b).
- **d.** The ultimate frictional resistance Q_s. [Use Eqs. (12.42) through (12.44), and take $K = 1.4$ and $\delta' = 0.6\phi'$.]
- **e.** The allowable load of the pile (use FS = 4).

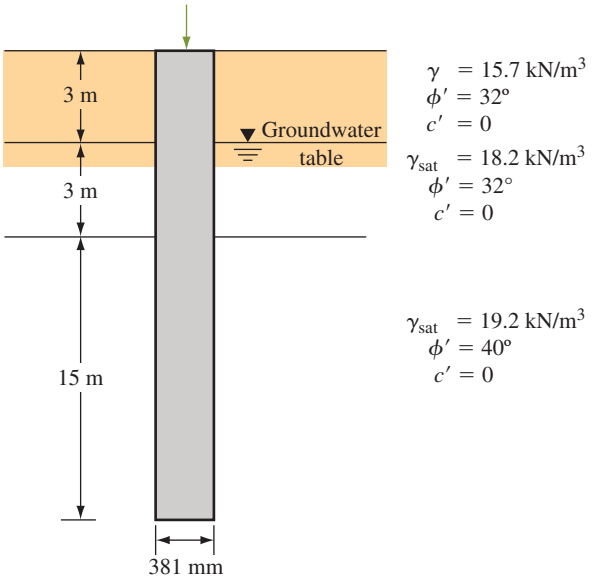


FIGURE P12.7

12.8 Consider a 500 mm diameter pile having a length of 18 m in a clay. Given: $\gamma = 20.0$ kN/m^3 and $c_u = 60$ kN/m^2.

a. Determine the maximum allowable load (Q_{all}) with FS = 3. Use the α method and Table 12.11 for determining the skin friction and Eq. (12.20) for determining the point load. Allow a factor of safety of 3.

b. What percentage of the ultimate load is being carried by the pile shaft? Is it a friction pile?

12.9 Determine the maximum load that can be allowed on the 450 mm diameter pile shown in Figure P12.9, with a factor of safety of 3. Use the α method and Table 12.11 for determining the skin friction and Eq. (12.20) for determining the point load.

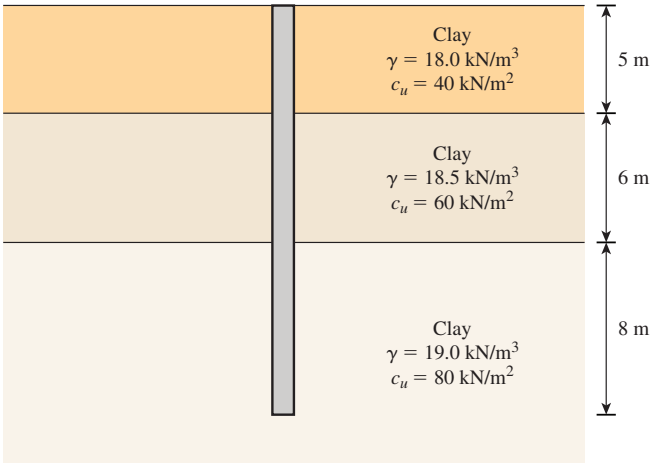


FIGURE P12.9

12.10 A concrete pile 50 ft long having a cross section of 15 in. × 15 in. is fully embedded in a saturated clay layer for which $\gamma_{sat} = 121$ lb/ft^3, $\phi = 0$, and $c_u = 1600$ lb/ft^2. Determine the allowable load that the pile can carry. (Let FS = 3.) Use the α method Eq. (12.61) and Table 12.11 to estimate the skin friction and Vesic's method for point load estimation.

12.11 Redo Problem 12.10 using the λ method for estimating the skin friction and Meyerhof's method for the point load estimation.

12.12 A concrete pile 20 m long having a cross section of 0.46 m × 0.46 m is fully embedded in a saturated clay layer. For the clay, given: $\gamma_{sat} = 18$ kN/m^3, $\phi = 0$, and $c_u = 80$ kN/m^2. Determine the allowable load that the pile can carry (FS = 3). Use the λ method to estimate the skin resistance.

12.13 A concrete pile 16 in. × 16 in. in cross section is shown in Figure P12.13. Calculate the ultimate skin friction resistance by using the

a. α method [use Eq. (12.61) and Table 12.11]

b. λ method

c. β method

Use $\phi'_R = 20°$ for all clays, which are normally consolidated.

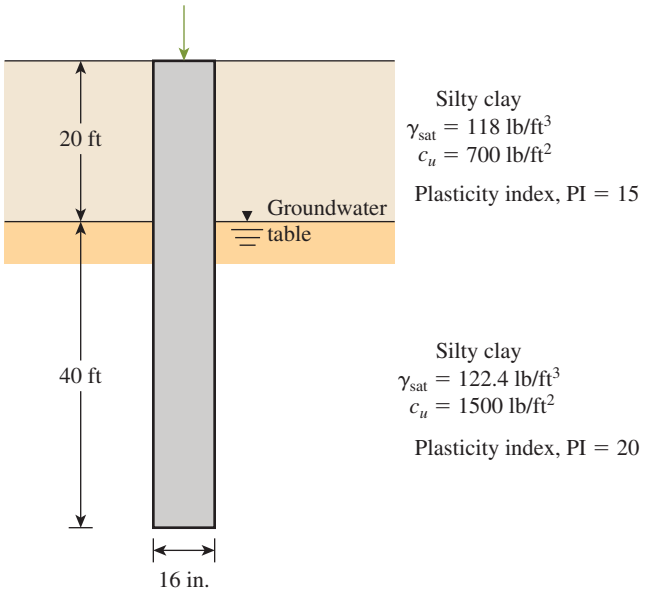


FIGURE P12.13

12.14 Solve Problem 12.13 using Eq. (12.58).

12.15 Solve Problem 12.13 using Eqs. (12.59) and (12.60).

12.16 Consider a continuous flight auger pile in a sandy soil deposit 10 m long with a diameter of 0.45 m. Following is the variation of standard penetration resistance values (N_{60}) with depth.

Depth (m)	N_{60}
1.5	6
3.0	7
4.5	5
6.0	8
7.5	10
9.0	10
10.5	13
12.0	15
13.5	18
15.0	20
17.0	17
18.5	18
20.0	21

Estimate the ultimate load-carrying capacity of the pile. Assume unit weight of soil, $\gamma = 15.5$ kN/m^3.

12.17 The average values of the undrained shear strength (c_u) with depth are given as follows:

Depth (m)	c_u (kN/m^2)
0–3	20
3–8	35
8–12	80
12–16	95

If a CFA pile having a diameter of 0.6 m and length of 10 m is to be constructed in this clayey soil, estimate the ultimate side skin resistance Q_s.

12.18 A steel pile (H-section; HP 310 × 125; see Table 12.1a) is driven into a layer of sandstone. The length of the pile is 25 m. Following are the properties of the sandstone: unconfined compression strength = $q_{u(\text{lab})}$ = 80 MN/m^2 and angle of friction = 36°. Using a factor of safety of 3, estimate the allowable point load that can be carried by the pile. Use [$q_{u(\text{design})} = q_{u(\text{lab})}/5$].

12.19 A 20 m long bored concrete pile having a diameter of 350 mm is load tested, and the data are given below:

Load (kN)	0	250	500	750	1000	1250	1000	750	500	250	0
Settlement (mm)	0	2.0	5.0	8.2	15.0	39.6	39.5	38.2	37.5	36.1	35.5

Also given: $E_{\text{concrete}} = 25 \times 10^3$ MN/m^2.

a. Estimate the allowable pile load using Davisson's (1973) method, with FS = 2.5.

b. At the maximum load of 1250 kN, what are the total and net settlements?

12.20 A 600 mm diameter and 25 m long driven concrete pile carries a column load of 1200 kN. It is estimated that the shaft carries 900 kN and the point carries 300 kN. Determine the settlement of the pile head using the Poulos and Davis method with the following data:
E_s = 25 MN/m^2, E_p = 30,000 MN/m^2, and μ_s = 0.2

12.21 Redo Problem 12.20 using Vesic's method, assuming that the skin friction is distributed uniformly along the shaft.

12.22 In Vesic's method of determining total settlement of a pile, elastic shortening of the pile $s_{e(1)}$ was determined by Eq. (12.88) as

$$s_{e(1)} = \frac{(Q_{wp} + \xi Q_{ws})L}{A_p E_p}$$

Show from the first principles that when the unit skin friction $f_{(z)}$ remains the same at all depths, $\xi = 0.5$.

12.23 A 30 m long concrete pile is 305 mm × 305 mm in cross section and is fully embedded in a sand deposit. If n_h = 9200 kN/m^2, the moment at ground level $M_g = 0$, the allowable displacement of pile head = 12 mm; $E_p = 21 \times 10^6$ kN/m^2, and $F_{Y\,(\text{pile})} = 21{,}000$ kN/m^2, calculate the allowable lateral load, Q_g, at the ground level. Use the elastic solution method.

12.24 Solve Problem 12.23 using the method of Broms. Assume that the pile is flexible and free headed. Let the soil unit weight, γ = 16 kN/m^3; the soil friction angle, $\phi' = 30°$; and the yield stress of the pile material, F_Y = 21 MN/m^2.

12.25 A steel H-pile (section HP 13 × 100) is driven by a hammer. The maximum rated hammer energy is 40 kip·ft, the weight of the ram is 12 kip, and the length of the pile is 90 ft. Also, we have coefficient of restitution = 0.35, weight of the pile cap = 2.4 kip, hammer efficiency = 0.85, number of blows for the last inch of penetration = 10, and $E_p = 30 \times 10^6$ lb/in^2. Estimate the pile capacity using Eq. (12.122). Take FS = 6.

12.26 Solve Problem 12.25 using the modified EN formula. (See Table 12.17.) Use FS = 3.

12.27 Solve Problem 12.25 using the Danish formula. (See Table 12.17.) Use FS = 3.

12.28 A single-acting steam hammer (Vulcan 08 model) is used to drive a 400 mm diameter and 20 m long precast concrete pile into the ground. The following data are recorded:

- Weight of ram = 35.6 kN
- Stroke (height of fall of the ram) = 1.0 m
- Maximum rated hammer energy = 35.6 kN·m
- Hammer efficiency = 0.8
- Coefficient of restitution = 0.4
- Weight of pile cap = 5 kN
- Number of blows recorded for the last 25 mm penetration = 6
- Unit weight of concrete = 24 kN/m^3

Determine the allowable load for the pile, with a factor of safety of 4, using the modified ENR formula.

12.29 A diesel hammer (Delmag D12) with a maximum energy rating of 30.0 kN·m and hammer efficiency of 85% is used to drive a 15 m long concrete pile having a square cross section of 400 mm × 400 mm. The following data are given:

- Weight of the ram = 12.2 kN
- Weight of the pile cap = 4.0 kN
- Coefficient of restitution = 0.35
- Unit weight of concrete = 24.0 kN/m^3

To derive an allowable load-carrying capacity of 400 kN from the pile, based on modified ENR formula and with factor of safety of 4, what should the set S be?

12.30 Figure 12.49a shows a pile. Let L = 15 m, D (pile diameter) = 305 mm, H_f = 3 m, γ_{fill} = 17.5 kN/m^3, and $\phi'_{\text{fill}} = 25°$. Determine the total downward drag force on the pile. Assume that the fill is located above the water table and that $\delta' = 0.5\phi'_{\text{fill}}$.

12.31 Redo Problem 12.30 assuming that the water table coincides with the top of the fill and that $\gamma_{\text{sat(fill)}}$ = 19.8 kN/m^3. If the other quantities remain the same, what would be the downward drag force on the pile? Assume $\delta' = 0.5\phi'_{\text{fill}}$.

12.32 Refer to Figure 12.49b. Let L = 18 m, γ_{fill} = 17 kN/m^3, $\gamma_{\text{sat(clay)}}$ = 19.8 kN/m^3, $\phi'_{\text{clay}} = 20°$, H_f = 3.5 m, and D (pile diameter) = 406 mm. The water table coincides with the top of the clay layer. Determine the total downward drag force on the pile. Assume $\delta' = 0.6\,\phi'_{\text{clay}}$.

12.33 Estimate the group efficiency of a 4 × 6 pile group, consisting of 400 mm diameter concrete piles at 1.2 m center-to-center spacing using

a. the Converse-Labarre equation

b. the Los Angeles Group Action equation

12.34 The plan of a group pile is shown in Figure P12.34. Assume that the piles are embedded in a saturated homogeneous clay having a c_u = 90 kN/m^2. Given: diameter of piles (D) = 316 mm, center-to-center spacing of piles = 600 mm, and length of piles = 20 m. Find the allowable load-carrying capacity of the pile group. Use Table 12.11 and FS = 3.

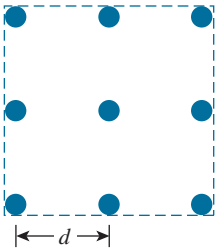


FIGURE P12.34

12.35 Redo Problem 12.34 with the following: center-to-center spacing of piles = 30 in., length of piles = 45 ft, D = 12 in., c_u = 860 lb/ft^2, and FS = 3. Use Table 12.11.

12.36 Figure P12.36 shows a 3 × 5 pile group consisting of 15 concrete piles of 400 mm diameter and 12 m in length. What would be the maximum load that can be allowed on the mat with a factor of safety of 3? The piles have a center-to-center spacing of 1200 mm.

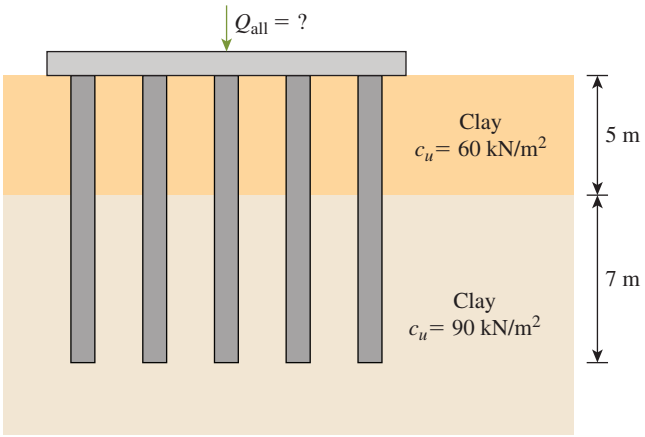


FIGURE P12.36

12.37 Figure P 12.37 shows a group pile in clay. Determine the consolidation settlement of the group. Use the 2:1 method to estimate the average effective stress in the clay layers.

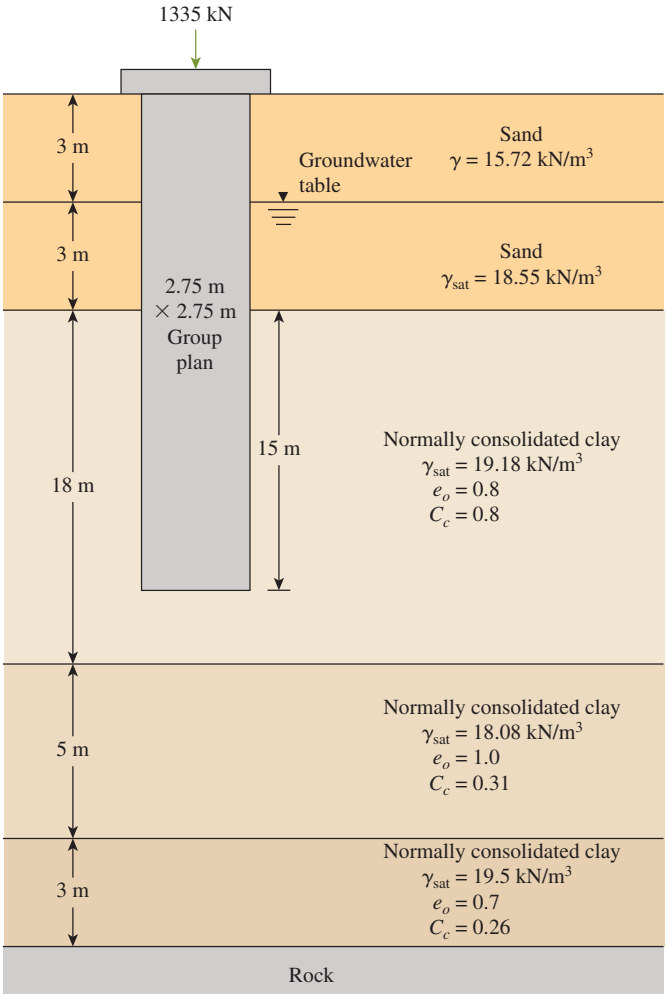


FIGURE P12.37

REFERENCES

American Petroleum Institute (API) (1987). *Recommended Practice for Planning, Designing, and Constructing Fixed Offshore Platforms*, API RP2A, 17th ed., American Petroleum Institute, Washington, DC.

American Petroleum Institute (API) (2000). *Recommended Practice for Planning, Designing, and Constructing Fixed Offshore Platforms*, API RP2A, 21st ed., Washington, DC.

American Petroleum Institute (API) (2007). *Recommended Practice for Planning, Designing, and Constructing Fixed Offshore Platforms*, API RP2A, 22nd ed., American Petroleum Institute, Washington, DC.

American Society of Civil Engineers (1959). "Timber Piles and Construction Timbers," *Manual of Practice*, No. 17, American Society of Civil Engineers, New York.

American Society of Civil Engineers (1993). *Design of Pile Foundations (Technical Engineering and Design Guides as Adapted from the U.S. Army Corps of Engineers*, No. 1), American Society of Civil Engineers, New York.

Baldi, G., Bellotti, R., Ghionna, V., Jamiolkowski, M., and Pasqualini, E. (1981). "Cone Resistance in Dry N.C. and O.C. Sands, Cone Penetration Testing and Experience," *Proceedings, ASCE Specialty Conference*, St. Louis, pp. 145–177.

Bjerrum, L., Johannessen, I. J., and Eide, O. (1969). "Reduction of Skin Friction on Steel Piles to Rock," *Proceedings, Seventh International Conference on Soil Mechanics and Foundation Engineering*, Mexico City, Vol. 2, pp. 27–34.

Bowles, J. E. (1982). *Foundation Analysis and Design*, 3rd ed., McGraw-Hill, New York.

Bowles, J. E. (1996). *Foundation Analysis and Design*, 5th ed., McGraw-Hill, New York.

Briaud, J. L., Tucker, L., Lytton, R. L., and Coyle, H. M. (1985). *Behavior of Piles and Pile Groups*, Report No. FHWA/RD-83/038, Federal Highway Administration, Washington, DC.

Broms, B. B. (1965). "Design of Laterally Loaded Piles," *Journal of the Soil Mechanics and Foundations Division*, American Society of Civil Engineers, Vol. 91, No. SM3, pp. 79–99.

Chen, Y. J. and Kulhawy, F. H. (1994). "Case History Evaluation of the Behavior of Drilled Shafts under Axial and Lateral Loading," *Final Report, Project 1493-04, EPRI TR-104601*, Geotechnical Group, Cornell University, Ithaca, NY, December.

Coleman D. M. and Arcement, B. J. (2002). "Evaluation of Design Methods for Auger Cast Piles in Mixed Soil Conditions." *Proceedings, International Deep Foundations Congress*, Orlando, FL, M. W. O'Neill and F. C. Townsends (eds.), American Society of Civil Engineers, pp. 1404–1420.

Coyle, H. M. and Castello, R. R. (1981). "New Design Correlations for Piles in Sand," *Journal of the Geotechnical Engineering Division*, American Society of Civil Engineers, Vol. 107, No. GT7, pp. 965–986.

Das, B. M. and Luo, Z. (2017). *Principles of Soil Dynamics*, 3rd ed., Cengage Learning, Boston, MA.

Davisson, M. T. (1973). "High Capacity Piles," in *Innovations in Foundation Construction*, Proceedings of a Lecture Series, Illinois Section, American Society of Civil Engineers, Chicago.

Davisson, M. T. (1970). "BRD Vibratory Driving Formula," *Foundation Facts*, Vol. VI, No. 1, pp. 9–11.

Davisson, M. T. and Gill, H. L. (1963). "Laterally Loaded Piles in a Layered Soil System," *Journal of the Soil Mechanics and Foundations Division*, American Society of Civil Engineers, Vol. 89, No. SM3, pp. 63–94.

Federal Highway Administration (FHWA) (2007). *Design and Construction of Continuous Flight Auger Piles*, Geotechnical Engineering Circular (GEC) No. 8, Washington, DC.

Feng, Z. and Deschamps, R. J. (2000). "A Study of the Factors Influencing the Penetration and Capacity of Vibratory Driven Piles," *Soils and Foundations*, Vol. 40, No. 3, pp. 43–54.

Goodman, R. E. (1980). *Introduction to Rock Mechanics*, John Wiley & Sons, New York.

Janbu, N. (1953). *An Energy Analysis of Pile Driving with the Use of Dimensionless Parameters*, Norwegian Geotechnical Institute, Oslo, Publication No. 3.

Karlsrud, K., Clausen, C. J. F., and Aas, P. M. (2005). "Bearing Capacity of Driven Piles in Clay, the NGI Approach." *Frontiers in Offshore Geotechnics: ISFOG*, S. Gourvenec and M. Cassidy, eds., Taylor and Francis Group, Perth, Australia, pp. 775–782.

Kishida, H. and Meyerhof, G. G. (1965). "Bearing Capacity of Pile Groups under Eccentric Loads in Sand," *Proceedings, Sixth International Conference on Soil Mechanics and Foundation Engineering*, Montreal, Vol. 2, pp. 270–274.

Liu, J. L., Yuan, Z. I., and Zhang, K. P. (1985). "Cap-Pile-Soil Interaction of Bored Pile Groups," *Proceedings, Eleventh International Conference on Soil Mechanics and Foundation Engineering*, San Francisco, Vol. 3, pp. 1433–1436.

Mansur, C. I. and Hunter, A. H. (1970). "Pile Tests—Arkansas River Project," *Journal of the Soil Mechanics and Foundations Division*, American Society of Civil Engineers, Vol. 96, No. SM6, pp. 1545–1582.

Matlock, H. and Reese, L. C. (1960). "Generalized Solution for Laterally Loaded Piles," *Journal of the Soil Mechanics and Foundations Division*, American Society of Civil Engineers, Vol. 86, No. SM5, Part I, pp. 63–91.

Meyerhof, G. G. (1976). "Bearing Capacity and Settlement of Pile Foundations," *Journal of the Geotechnical Engineering Division*, American Society of Civil Engineers, Vol. 102, No. GT3, pp. 197–228.

Nottingham, L. C. and Schmertmann, J. H. (1975). *An Investigation of Pile Capacity Design Procedures*, Research Report No. D629, Department of Civil Engineering, University of Florida, Gainesville, FL.

Olson, R. E. and Flaate, K. S. (1967). "Pile-Driving Formulas for Friction Piles in Sand," *Journal of the Soil Mechanics and Foundations Division*, American Society of Civil Engineers, Vol. 93, No. SM6, pp. 279–296.

O'Neill, M. W. and Reese, L. C. (1999). *Drilled Shafts: Construction Procedure and Design Methods*, FHWA Report No. IF-99-025.

Randolph M. F. and Murphy, B. S. (1985). "Shaft Capacity of Driven Piles in Clay," *Proceedings*, *17th Annual Offshore Technology Conference*, Houston, TX, pp. 371–378.

Rausche, F., Likins, G. E., Goble, G. G., and Hussein, M. (1986). "The Performance of Pile Driving Systems Inspection Manual," Federal Highway Administration, Report No. FHWA/RD-86/160, Washington, DC.

Sawant, V. A., Shukla, S. K., Sivakugan, N., and Das, B. M. (2013). "An Insight into the Pile Setup and the Load-Carrying Capacity of Driven Piles," *International Journal of Geotechnical Engineering*, Vol. 7, No. 1, pp. 71–83.

Schmertmann, J. H. (1978). *Guidelines for Cone Penetration Test: Performance and Design*, Report FHWA-TS-78-209, Federal Highway Administration, Washington, DC.

Seiler, J. F. and Keeney, W. D. (1944). "The Efficiency of Piles in Groups," *Wood Preserving News*, Vol. 22, No. 11 (November), pp. 109–118.

Sladen, J. A. (1992). "The Adhesion Factor: Applications and Limitations," *Canadian Geotechnical Journal*, Vol. 29, No. 2, pp. 323–326.

Smith, E. A. L. (1960). "Pile-Driving Analysis by the Wave Equation," *Journal of the Soil Mechanics and Foundations Division*, American Society of Civil Engineers, Vol. 86, No. SM4, pp. 35–61.

Terzaghi, K., Peck, R. B., and Mesri, G. (1996). *Soil Mechanics in Engineering Practice*, John Wiley & Sons, New York.

Tomlinson, M. J. and Woodward, J. (2008). *Pile Design and Construction Practice*, 5th ed., Taylor & Francis, UK.

USACE (1991). *Design of Pile Foundations*, Engineering Design Manual EM1110-2-2906, U.S. Army Corps of Engineers, Washington, DC.

Vesic, A. S. (1961). "Bending of Beams Resting on Isotropic Elastic Solids," *Journal of the Engineering Mechanics Division*, American Society of Civil Engineers, Vol. 87, No. EM2, pp. 35–53.

Vesic, A. S. (1969). *Experiments with Instrumented Pile Groups in Sand*, American Society for Testing and Materials, Special Technical Publication No. 444, pp. 177–222.

Vesic, A. S. (1970). "Tests on Instrumental Piles—Ogeechee River Site," *Journal of the Soil Mechanics and Foundations Division*, American Society of Civil Engineers, Vol. 96, No. SM2, pp. 561–584.

Vesic, A. S. (1977). *Design of Pile Foundations*, National Cooperative Highway Research Program Synthesis of Practice No. 42, Transportation Research Board, Washington, DC.

Vijayvergiya, V. N. and Focht, J. A., Jr. (1972). *A New Way to Predict Capacity of Piles in Clay*, Offshore Technology Conference Paper 1718, Fourth Offshore Technology Conference, Houston.

Wong, K. S. and Teh, C. I. (1995). "Negative Skin Friction on Piles in Layered Soil Deposit," *Journal of Geotechnical and Geoenvironmental Engineering*, American Society of Civil Engineers, Vol. 121, No. 6, pp. 457–465.

Woodward, R. J., Gardner, W. S., and Greer, D. M. (1972). *Drilled Pier Foundations*, McGraw-Hill, New York.

13

Drilled-Shaft Foundations



CHAIYA/Shutterstock.com

13.1 Introduction 547
13.2 Types of Drilled Shafts 547
13.3 Construction Procedures 548
13.4 Other Design Considerations 554
13.5 Load Transfer Mechanism 555
13.6 Estimation of Load-Bearing Capacity 556
13.7 Load-Bearing Capacity in Granular Soil 558
13.8 Load-Bearing Capacity in Granular Soil Based on Settlement 561
13.9 Load-Bearing Capacity in Clay 568
13.10 Load-Bearing Capacity in Clay Based on Settlement 570
13.11 Settlement of Drilled Shafts at Working Load 575
13.12 Lateral Load-Carrying Capacity—Characteristic Load and Moment Method 576
13.13 Drilled Shafts Extending into Rock 583
13.14 Summary 588
PROBLEMS 589
REFERENCES 590

13.1 Introduction

The terms *caisson, pier, drilled shaft*, and *drilled pier* are often used interchangeably in foundation engineering; all refer to a *cast-in-place* or *bored pile generally having a diameter of about 750 mm* (≈ 2.5 ft) or more, with or without steel reinforcement and with or without an enlarged bottom. Sometimes the diameter can be as small as 305 mm (≈ 1 ft).

To avoid confusion, we use the term *drilled shaft* for a hole drilled or excavated to the bottom of a structure's foundation and then filled with concrete. Depending on the soil conditions, casings may be used to prevent the soil around the hole from caving in during construction. The diameter of the shaft is usually large enough for a person to enter for inspection.

The use of drilled-shaft foundations has several advantages:

1. A single large diameter drilled shaft may be used instead of a group of piles and the pile cap.
2. Constructing drilled shafts in deposits of dense sand and gravel is easier than driving piles.
3. Drilled shafts may be constructed before grading operations are completed.
4. When piles are driven by a hammer, the ground vibration may cause damage to nearby structures. The use of drilled shafts avoids this problem.
5. Piles driven into clay soil may produce ground heaving and cause previously driven piles to move laterally. This does not occur during the construction of drilled shafts.
6. There is no hammer noise during the construction of drilled shafts; there is during pile driving.
7. Because the base of a drilled shaft can be enlarged, it provides anchorage and great resistance to the uplifting load.
8. The surface over which the base of the drilled shaft is constructed can be visually inspected.
9. The construction of drilled shafts generally utilizes mobile equipment, which, under poor soil conditions, may prove to be more economical than methods of constructing pile foundations.
10. Drilled shafts have high resistance to lateral loads.

There are also a couple of drawbacks to the use of drilled-shaft construction. For one thing, the concreting operation may be delayed by bad weather and always needs close supervision. For another, as in the case of braced cuts, deep excavations for drilled shafts may induce substantial ground loss and damage to nearby structures.

13.2 Types of Drilled Shafts

Drilled shafts are classified according to the ways in which they are designed to transfer the structural load to the substratum. Figure 13.1a shows a drilled *straight shaft*. It extends through the upper layer(s) of poor soil, and its tip rests on a strong load-bearing soil layer or rock. The shaft can be cased with a steel shell or pipe when

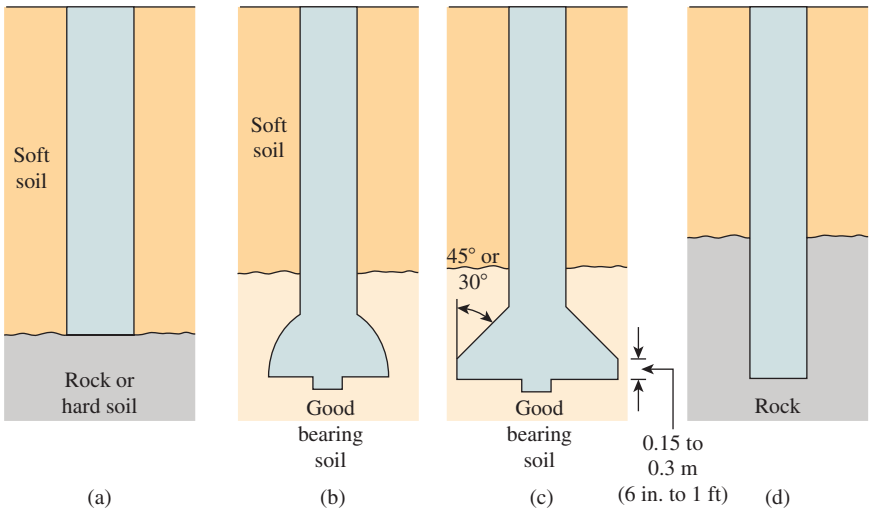


FIGURE 13.1 Types of drilled shafts: (a) straight shaft; (b) and (c) belled shaft; (d) straight shaft socketed into rock

required (as it is with cased, cast-in-place concrete piles). For such shafts, the resistance to the applied load may develop from end bearing and also from side friction at the shaft perimeter and soil interface.

A *belled shaft* (see Figures 13.1b and c) consists of a straight shaft with a bell at the bottom, which rests on good bearing soil. The bell can be constructed in the shape of a dome (see Figure 13.1b), or it can be angled (see Figure 13.1c). For angled bells, the underreaming tools that are commercially available can make 30 to 45° angles with the vertical.

Straight shafts can also be extended and socketed into an underlying rock layer. (See Figure 13.1d.) In the calculation of the load-bearing capacity of such shafts, the end bearing and the shear stress developed along the shaft perimeter and rock interface can be taken into account.

13.3 Construction Procedures

The most common construction procedure used in the United States involves rotary drilling. There are three major types of construction methods: the dry method, the casing method, and the wet method.

DRY METHOD OF CONSTRUCTION

This method is employed in soil and rocks that are above the water table and that will not cave in when the hole is drilled to its full depth. The sequence of construction, shown in Figure 13.2, is as follows:

Step 1. The excavation is completed (and belled if desired), using proper drilling tools, and the spoils from the hole are deposited nearby. (See Figure 13.2a.)

Step 2. Concrete is then poured into the cylindrical hole. (See Figure 13.2b.)

Step 3. If desired, a rebar cage is placed in the upper portion of the shaft. (See Figure 13.2c.)

Step 4. Concreting is then completed, and the drilled shaft will be as shown in Figure 13.2d.

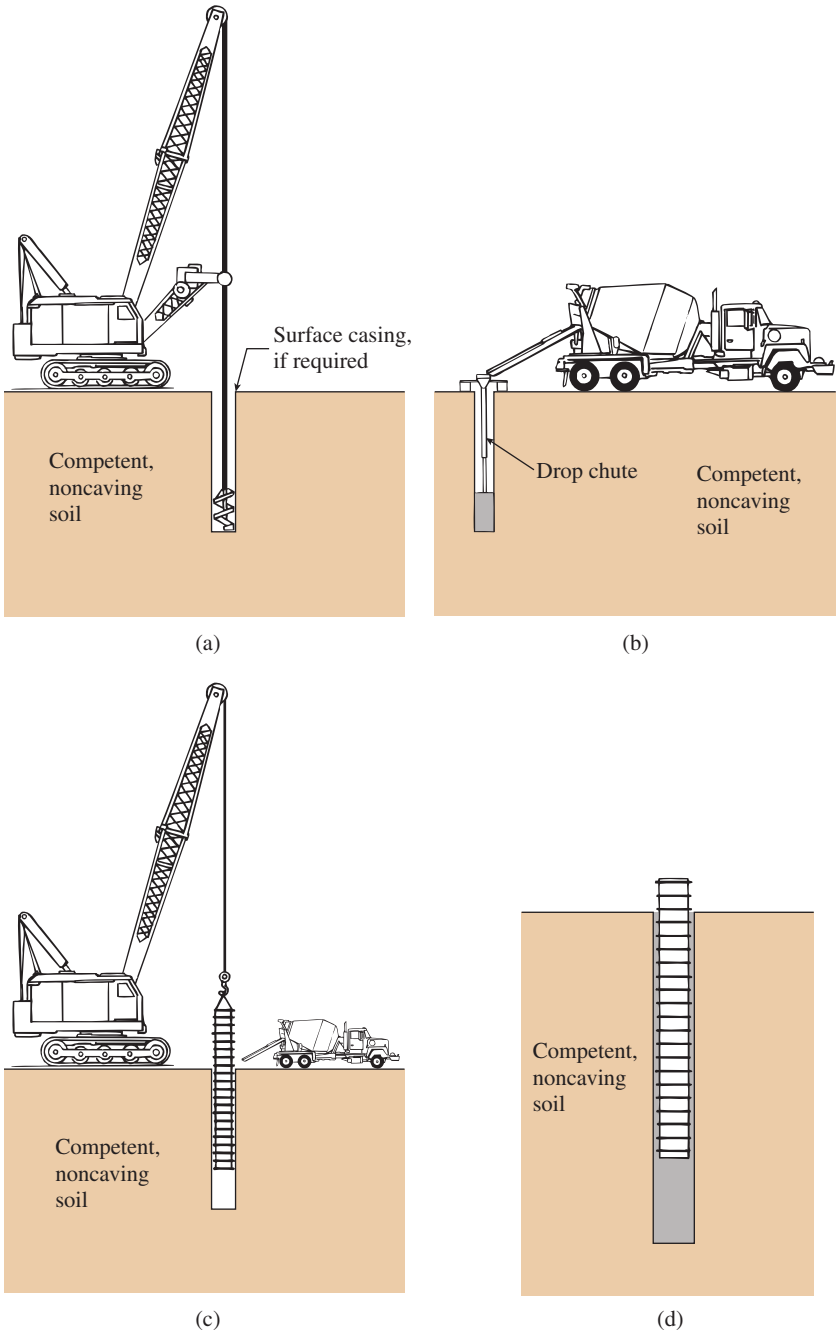


FIGURE 13.2 Dry method of construction: (a) initiating drilling; (b) starting concrete pour; (c) placing rebar cage; (d) completed shaft (After O'Neill and Reese, 1999)

CASING METHOD OF CONSTRUCTION

This method is used in soil or rocks in which caving or excessive deformation is likely to occur when the borehole is excavated. The sequence of construction is shown in Figure 13.3 and may be explained as follows:

Step 1. The excavation procedure is initiated as in the case of the dry method of construction. (See Figure 13.3a.)

Step 2. When the caving soil is encountered, bentonite slurry is introduced into the borehole. (See Figure 13.3b.) Drilling is continued until the excavation goes past the caving soil and a layer of impermeable soil or rock is encountered. The slurry supports the wall and helps prevent caving.

Step 3. A casing is then introduced into the hole from the ground level to bottom of the caving soil. (See Figure 13.3c.)

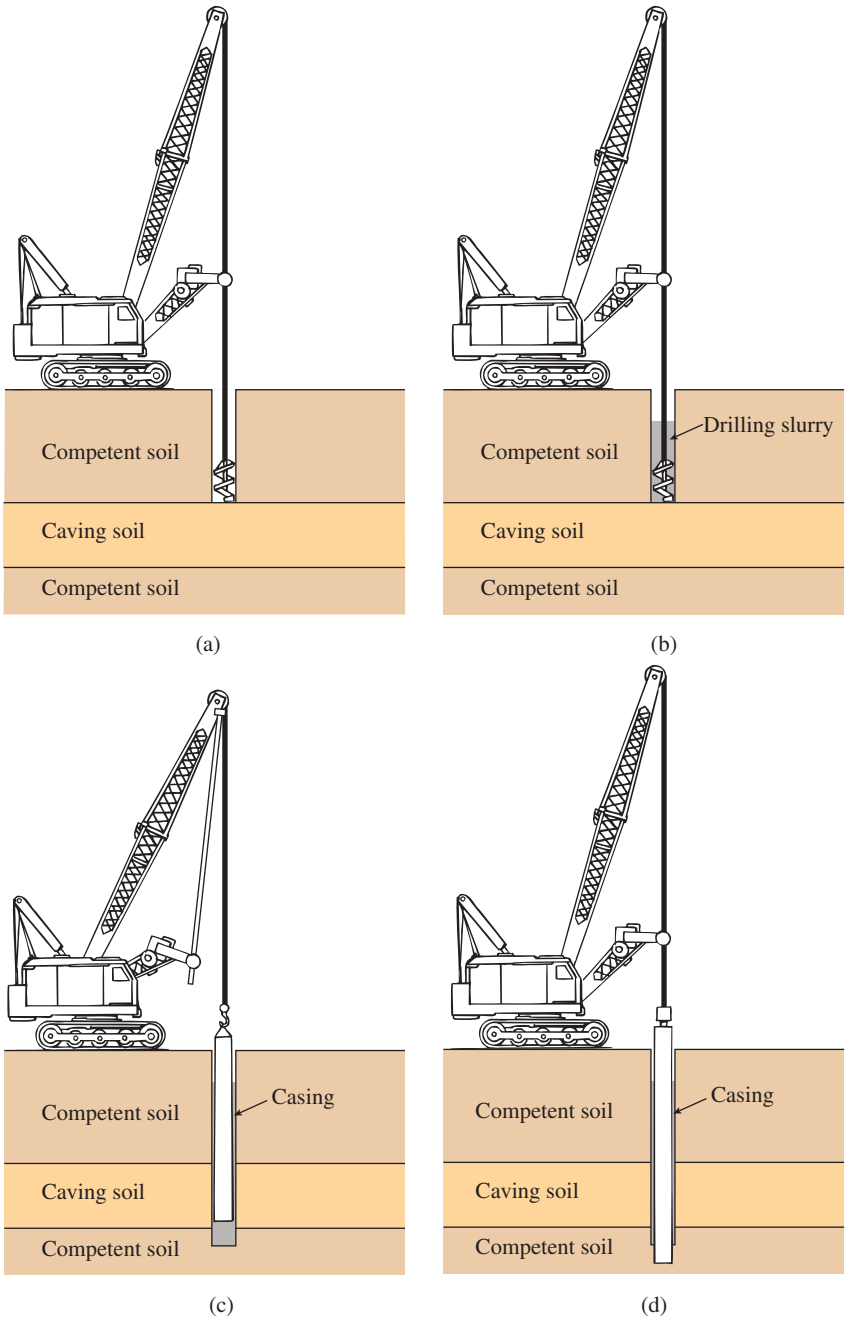


FIGURE 13.3 Casing method of construction: (a) initiating drilling; (b) drilling with slurry; (c) introducing casing; (d) casing is sealed and slurry is being removed from interior of casing; (e) drilling below casing; (f) underreaming; (g) removing casing; (h) completed shaft (After O'Neill and Reese, 1999)

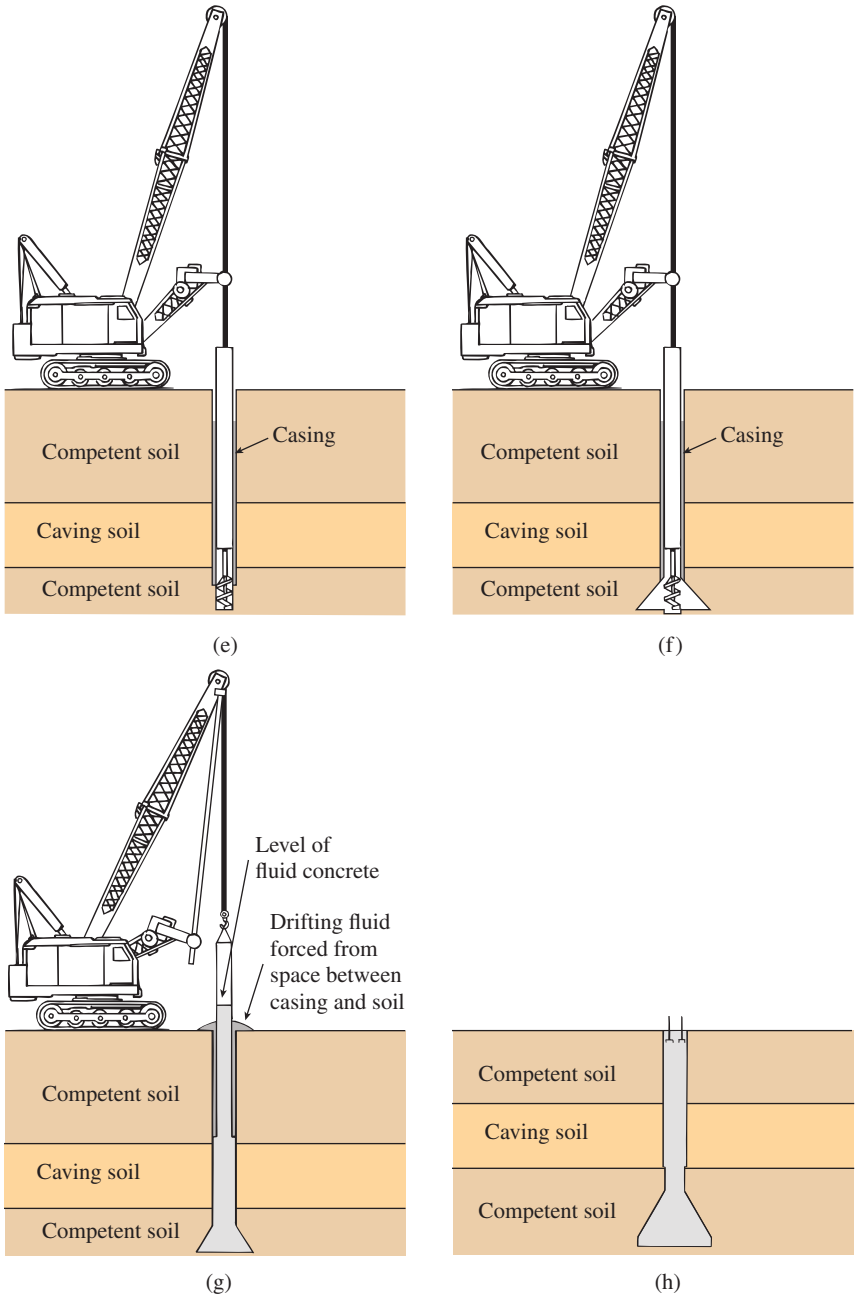


FIGURE 13.3 (*Continued*)

Step 4. The slurry is bailed out of the casing with a submersible pump. (See Figure 13.3d.)

Step 5. A smaller drill that can pass through the casing is introduced into the hole, and excavation continues. (See Figure 13.3e.)

Step 6. If needed, the base of the excavated hole can then be enlarged, using an underreamer. (See Figure 13.3f.)

Step 7. If reinforcing steel is needed, the rebar cage needs to extend the full length of the excavation. Concrete is then poured into the excavation, and the casing is gradually pulled out. (See Figure 13.3g.)

Step 8. Figure 13.3h shows the completed drilled shaft.

WET METHOD OF CONSTRUCTION

This method is sometimes referred to as the *slurry displacement method*. Slurry is used to keep the borehole open during the entire depth of excavation. (See Figure 13.4.) Following are the steps involved in the wet method of construction:

Step 1. Excavation continues to full depth with slurry. (See Figure 13.4a.)

Step 2. If reinforcement is required, the rebar cage is placed in the slurry. (See Figure 13.4b.)

Step 3. Concrete that will displace the volume of slurry is then placed in the drill hole. (See Figure 13.4c.)

Step 4. Figure 13.4d shows the completed drilled shaft.

Figure 13.5 shows a drilled shaft under construction using the dry method. The construction of a drilled shaft using the wet method is shown in Figure 13.6. A typical auger, a reinforcement cage, and clean-out bucket are shown in Figure 13.7.

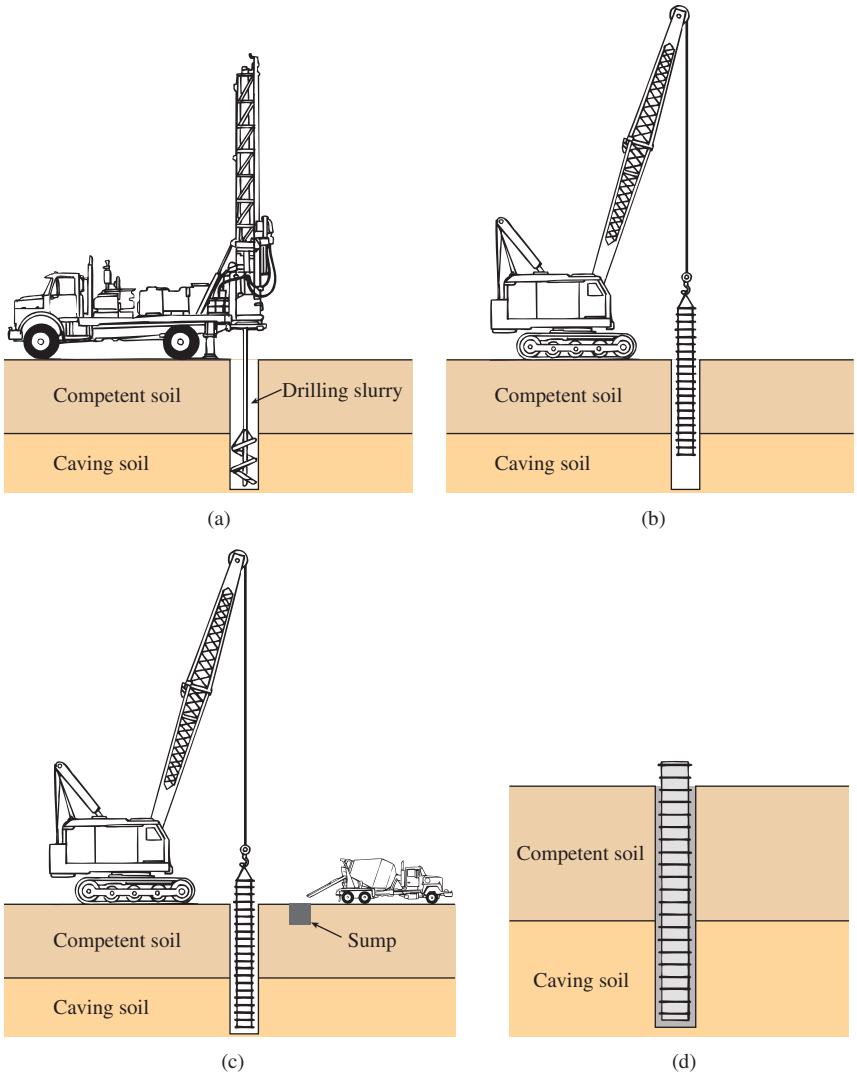


FIGURE 13.4 Slurry method of construction: (a) drilling to full depth with slurry; (b) placing rebar cage; (c) placing concrete; (d) completed shaft (After O'Neill and Reese, 1999)



FIGURE 13.5 Drilled-shaft construction using the dry method (Courtesy of Sanjeev Kumar, Southern Illinois University, Carbondale, Illinois)



FIGURE 13.6 Drilled-shaft construction using the wet method (Courtesy of Khaled Sobhan, Florida Atlantic University, Boca Raton, Florida)



(a)



(b)



(c)

FIGURE 13.7 Drilled-shaft construction: (a) a typical auger; (b) a reinforcement cage; (c) a clean-out bucket (Courtesy of Khaled Sobhan, Florida Atlantic University, Boca Raton, Florida)

13.4 Other Design Considerations

For the design of ordinary drilled shafts without casings, a minimum amount of vertical steel reinforcement is always desirable. Minimum reinforcement is 1% of the gross cross-sectional area of the shaft. For drilled shafts with nominal reinforcement, most building codes suggest using a design concrete strength, f_c, on the order of $f'_c/4$. Thus, the minimum shaft diameter becomes

$$f_c = 0.25f'_c = \frac{Q_w}{A_{gs}} = \frac{Q_w}{\frac{\pi}{4}D_s^2}$$

or

$$D_s = \sqrt{\frac{Q_w}{\left(\frac{\pi}{4}\right)(0.25)f'_c}} = 2.257\sqrt{\frac{Q_u}{f'_c}} \tag{13.1}$$

where

D_s = diameter of the shaft

f'_c = 28-day concrete strength

Q_w = working load of the drilled shaft

A_{gs} = gross cross-sectional area of the shaft

If drilled shafts are likely to be subjected to tensile loads, reinforcement should be continued for the entire length of the shaft. Due to their importance in carrying the building load, higher grade concrete is generally used.

CONCRETE MIX DESIGN

The concrete mix design for drilled shafts is not much different from that for any other concrete structure. When a reinforcing cage is used, consideration should be given to the ability of the concrete to flow through the reinforcement. In most cases, a concrete slump of about 15.0 mm (6 in.) is considered satisfactory. Also, the maximum size of the aggregate should be limited to about 20 mm (0.75 in.)

EXAMPLE 13.1

A straight drilled shaft is required to carry a load of 675 U.S. tons. The concrete used in the shaft is expected to have 28-day strength of 7250 psi.

a. What should be the diameter of the drilled shaft?
b. If a minimum reinforcement of 1% is to be provided, how many 5/8 in. diameter longitudinal reinforcing bars would be required along the perimeter of the rebar cage?

SOLUTION

Part a

$$f_c = 0.25f'_c = \frac{Q_w}{\frac{\pi}{4}D_s^2}$$

$$0.25(7250) = \frac{675 \times 2000}{\frac{\pi}{4}D_s^2};\ D_s = 30.8 \text{ in.}$$

Use 31 in. diameter drilled shaft.

Part b

If N number of 5/8 in. diameter bars are required,

$$\frac{\pi}{4} \times 31^2 \times \frac{1}{100} = N \times \frac{\pi}{4} \times 0.625^2$$

$$N = \mathbf{25}$$

13.5 Load Transfer Mechanism

The load transfer mechanism from drilled shafts to soil is similar to that of piles, as described in Section 12.7. Figure 13.8 shows the load test results of a drilled shaft, conducted in a clay soil by Reese et al. (1976). The shaft (Figure 13.8a) had a diameter of 762 mm (30 in.) and a depth of penetration of 6.94 m (22.75 ft). Figure 13.8b shows the load-settlement curves. It can be seen that the total load carried by the drilled shaft was 1246 kN (140 tons). The load carried by side resistance was about 800 kN (90 tons), and the rest was carried by point bearing. It is interesting to note that with a downward movement of about 6 mm (0.25 in.), full side resistance was mobilized. However, about 25 mm (≈1 in.) of downward movement was required for

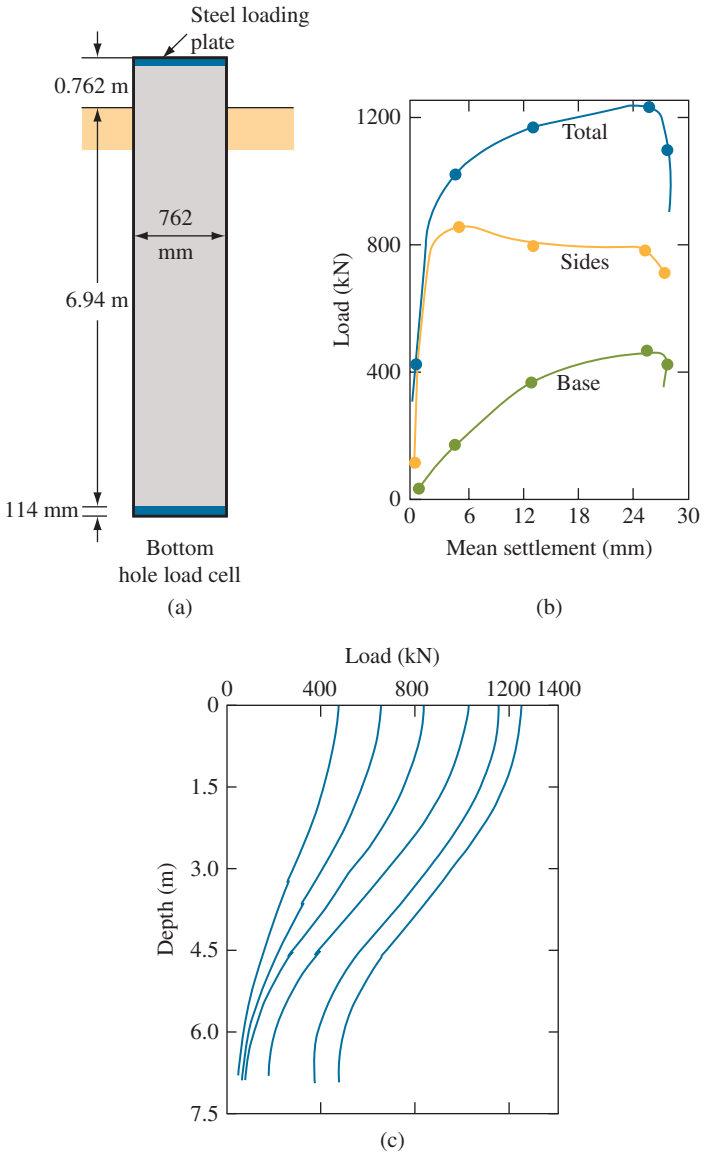


FIGURE 13.8 Load test results of Reese et al. (1976) on a drilled shaft: (a) dimensions of the shaft; (b) plot of base, sides, and total load with mean settlement; (c) plot of load-distribution curve with depth

mobilization of full point resistance. This situation is similar to that observed in the case of piles. Figure 13.8c shows the average load-distribution curves for different stages of the loading.

13.6 Estimation of Load-Bearing Capacity

As in the case of a pile foundation, the ultimate load-bearing capacity of a drilled shaft (see Figure 13.9) is

$$Q_u = Q_p + Q_s \tag{13.2}$$

where

Q_u = ultimate load

Q_p = ultimate load-carrying capacity at the base

Q_s = ultimate load-carrying capacity along the shaft

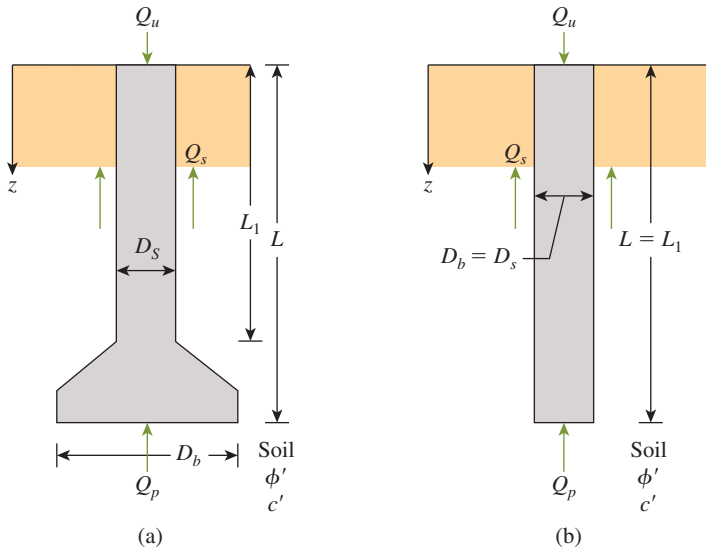


FIGURE 13.9 Ultimate bearing capacity of drilled shafts: (a) with bell and (b) straight shaft

The ultimate base load Q_p can be expressed in a manner similar to the way it is expressed in the case of shallow foundations considering soil compressibility (Section 6.9) [Eq. (6.42)], or

$$Q_p = A_p\left(c'N_cF_{cs}F_{cd}F_{cc} + q'N_qF_{qs}F_{qd}F_{qc} + \frac{1}{2}\gamma'BN_\gamma F_{\gamma s}F_{\gamma d}F_{\gamma c}\right) \tag{13.3}$$

where

c' = cohesion

N_c, N_q, N_γ = bearing capacity factors

$F_{cs}, F_{qs}, F_{\gamma s}$ = shape factors

$F_{cd}, F_{qd}, F_{\gamma d}$ = depth factors

$F_{cc}, F_{qc}, F_{\gamma c}$ = compressibility factors

γ' = effective unit weight of soil at the base of the shaft

q' = effective vertical stress at the base of the shaft

A_p = area of the base = $\frac{\pi}{4}D_b^2$

Equation (13.3) can be applied to deep foundations by substituting the pile diameter D for the foundation width B and taking the effective vertical stress at the base of the foundation (i.e., pile point) q' as $\gamma' L$. In piles where $L >> D$, $q' >> 0.5\, D\gamma'$. The bearing capacity factors (N_q and N_γ) and the F-factors in the second and third terms in Eq. (13.3) are of the same order of magnitude. Therefore, the third term (the one containing N_γ) becomes insignificant compared to the second term and can be neglected. Therefore, the ultimate load-bearing capacity Q_u of a drilled shaft can be written as

$$Q_u = A_p(c'N_cF_{cs}F_{cd}F_{cc} + q'N_qF_{qs}F_{qd}F_{qc}) + Q_s \tag{13.4}$$

The procedure to estimate the ultimate capacity of drilled shafts in granular and cohesive soil is described in the following sections.

13.7 Load-Bearing Capacity in Granular Soil

ESTIMATION OF Q_p

For a drilled shaft with its base located on a granular soil (that is, $c' = 0$), the *net ultimate load-carrying capacity* at the base can be obtained from Eq. (13.4) as

$$Q_{p(\text{net})} = A_p[q'(N_q - 1)F_{qs}F_{qd}F_{qc}] \tag{13.5}$$

The bearing capacity factor, N_q, for various soil friction angles (ϕ') can be taken from Table 6.2. It is also given in Table 13.1. Also,

$$F_{qs} = 1 + \tan\phi' \tag{13.6}$$

$$F_{qd} = 1 + C\underbrace{\tan^{-1}\left(\frac{L}{D_b}\right)}_{\text{radian}} \tag{13.7}$$

$$C = 2\tan\phi'(1 - \sin\phi')^2 \tag{13.8}$$

The variations of F_{qs} and C with ϕ' are given in Table 13.1.

TABLE 13.1 Variation of N_q, F_{qs}, C, I_{cr}, μ_s, and n with ϕ'

Soil friction angle, ϕ' (deg)	N_q (Table 6.2)	F_{qs} [Eq. (13.6)]	C [Eq. (13.8)]	I_{cr} [Eq. (13.9)]	μ_s [Eq. (13.13)]	n [Eq. (13.15)]
25	10.66	1.466	0.311	43.84	0.100	0.00500
26	11.85	1.488	0.308	47.84	0.115	0.00475
27	13.20	1.510	0.304	52.33	0.130	0.00450
28	14.72	1.532	0.299	57.40	0.145	0.00425
29	16.44	1.554	0.294	63.13	0.160	0.00400
30	18.40	1.577	0.289	69.63	0.175	0.00375
31	20.63	1.601	0.283	77.03	0.190	0.00350
32	23.18	1.625	0.276	85.49	0.205	0.00325
33	26.09	1.649	0.269	95.19	0.220	0.00300
34	29.44	1.675	0.262	106.37	0.235	0.00275
35	33.30	1.700	0.255	119.30	0.250	0.00250
36	37.75	1.727	0.247	134.33	0.265	0.00225
37	42.92	1.754	0.239	151.88	0.280	0.00200
38	48.93	1.781	0.231	172.47	0.295	0.00175
39	55.96	1.810	0.223	196.76	0.310	0.00150
40	64.20	1.839	0.214	225.59	0.325	0.00125
41	73.90	1.869	0.206	259.98	0.340	0.00100
42	85.38	1.900	0.197	301.29	0.355	0.00075
43	99.02	1.933	0.189	351.22	0.370	0.00050
44	115.31	1.966	0.180	412.00	0.385	0.00025
45	134.88	2.000	0.172	486.56	0.400	0.00000

According to Chen and Kulhawy (1994), F_{qc} can be calculated in the following manner.

Step 1. Calculate the critical rigidity index as

$$I_{cr} = 0.5 \exp\left[2.85 \cot\left(45 - \frac{\phi'}{2}\right)\right] \tag{13.9}$$

where I_{cr} = critical rigidity index (see Table 13.1).

Step 2. Calculate the reduced rigidity index as

$$I_{rr} = \frac{I_r}{1 + I_r \Delta} \tag{13.10}$$

where

$$I_r = \text{soil rigidity index} = \frac{E_s}{2(1 + \mu_s) q' \tan \phi'} \tag{13.11}$$

in which

$$E_s = \text{drained modulus of elasticity of soil} = mp_a \tag{13.12}$$

p_a = atmospheric pressure ($\approx$100 kN/m^2 or 2000 lb/ft^2)

$$m = \begin{cases} 100 \text{ to } 200 \text{ (loose soil)} \\ 200 \text{ to } 500 \text{ (medium dense soil)} \\ 500 \text{ to } 1000 \text{ (dense soil)} \end{cases}$$

$$\mu_s = \text{Poisson's ratio of soil} = 0.1 + 0.3\left(\frac{\phi' - 25}{20}\right)$$

$$(\text{for } 25^\circ \le \phi' \le 45^\circ) \text{ (see Table 13.1)} \tag{13.13}$$

$$\Delta = n \frac{q'}{p_a} \tag{13.14}$$

$$n = 0.005\left(1 - \frac{\phi' - 25}{20}\right) \text{(see Table 13.1)} \tag{13.15}$$

Step 3. If $I_{rr} \ge I_{cr}$, then

$$F_{qc} = 1 \tag{13.16}$$

However, if $I_{rr} < I_{cr}$, then

$$F_{qc} = \exp\left\{(-3.8 \tan \phi') + \left[\frac{(3.07 \sin \phi')(\log_{10} 2I_{rr})}{1 + \sin \phi'}\right]\right\} \tag{13.17}$$

The magnitude of $Q_{p(\text{net})}$ also can be reasonably estimated from a relationship based on the analysis of Berezantzev et al. (1961) that can be expressed as

$$Q_{p(\text{net})} = A_p q'(\omega N_q^* - 1) \tag{13.18}$$

where

$$N_q^* = \text{bearing capacity factor} = 0.21 e^{0.17\phi'} \text{ (see Table 13.2)} \tag{13.19}$$

ω = correction factor = $f(L/D_b)$

In Eq. (13.19), ϕ' is in degrees. The variation of ω (interpolated values) with L/D_b is given in Table 13.3.

TABLE 13.2 Variation of N_q^* with ϕ' [Eq. (13.19)]

ϕ' (deg)	N_q^*
25	14.72
26	17.45
27	20.68
28	24.52
29	29.06
30	34.44
31	40.83
32	48.39
33	57.36
34	67.99
35	80.59
36	95.52
37	113.22
38	134.20
39	159.07
40	188.55
41	223.49
42	264.90
43	313.99
44	372.17
45	441.14

TABLE 13.3 Berezantzev et al.'s Value of ω

Soil friction angle, ϕ' (deg)	L/D_b				
	5	10	15	20	25
26	0.744	0.619	0.546	0.49	0.439
28	0.757	0.643	0.572	0.525	0.475
30	0.774	0.671	0.606	0.568	0.525
32	0.787	0.697	0.641	0.615	0.581
34	0.804	0.727	0.680	0.654	0.632
36	0.822	0.753	0.716	0.692	0.675
38	0.839	0.774	0.746	0.723	0.712
40	0.849	0.796	0.770	0.744	0.735

ESTIMATION OF Q_s

The frictional resistance at ultimate load, Q_s, developed in a drilled shaft in granular soil may be calculated as

$$Q_s = \int_0^{L_1} p f \, dz \tag{13.20}$$

where

p = shaft perimeter = πD_s

f = unit frictional (or skin) resistance = $K\sigma'_o \tan \delta'$ (13.21)

K = earth pressure coefficient $\approx K_o = 1 - \sin \phi'$ (13.22)

σ'_o = effective vertical stress at any depth z

Thus,

$$Q_s = \int_0^{L_1} pf\, dz = \pi D_s (1 - \sin \phi') \int_0^{L_1} \sigma'_o \tan \delta'\, dz \tag{13.23}$$

The value of σ'_o will increase to a depth of about $15D_s$ and will remain constant thereafter, as shown in Figure 12.20.

For cast-in-pile concrete and good construction techniques, a rough interface develops and, hence, δ'/ϕ' may be taken to be one. With poor slurry construction, $\delta'/\phi' \approx 0.7$ to 0.8.

ALLOWABLE NET LOAD, $Q_{all(net)}$

An appropriate factor of safety should be applied to the ultimate load to obtain the net allowable load, or

$$Q_{all(net)} = \frac{Q_{p(net)} + Q_s}{FS} \tag{13.24}$$

13.8 Load-Bearing Capacity in Granular Soil Based on Settlement

On the basis of a database of 41 loading tests, Reese and O'Neill (1989) proposed a method for calculating the load-bearing capacity of drilled shafts that is based on settlement. The method is applicable to the following ranges:

1. Shaft diameter: D_s = 0.52 to 1.2 m (1.7 to 3.93 ft)
2. Bell depth: L = 4.7 to 30.5 m (15.4 to 100 ft)
3. Field standard penetration resistance: N_{60} = 5 to 60
4. Concrete slump = 100 to 225 mm (4 to 9 in.)

Reese and O'Neill's procedure (see Figure 13.10) gives

$$Q_{u(net)} = \sum_{i=1}^{N} f_i\, p\, \Delta L_i + q_p A_p \tag{13.25}$$

where

f_i = ultimate unit shearing resistance in layer i

p = perimeter of the shaft = πD_s

q_p = unit point resistance

A_p = area of the base = $(\pi/4)D_b^2$

$$f_i = \beta_1 \sigma'_{ozi} < \beta_2 \tag{13.26}$$

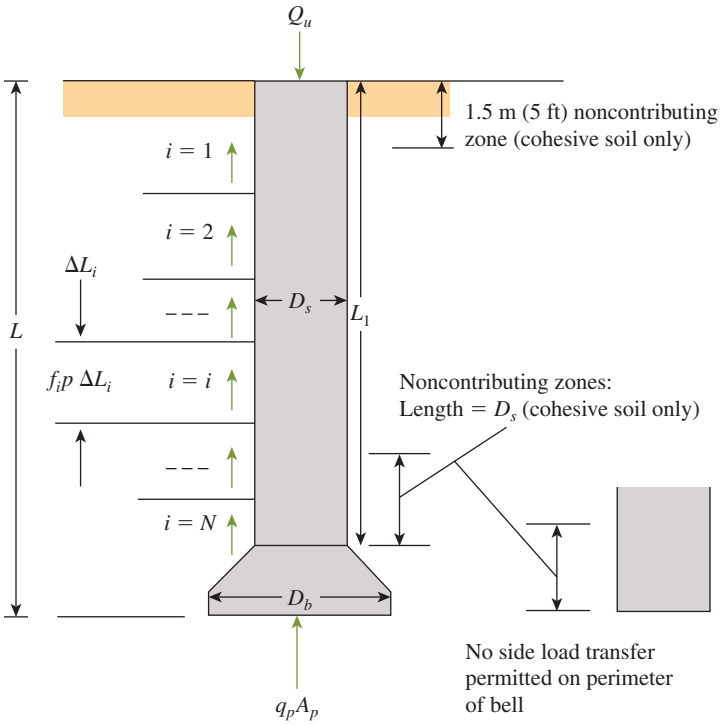


FIGURE 13.10 Development of Eq. (13.25)

where σ'_{ozi} = vertical effective stress at the middle of layer i.

$$\beta_1 = \beta_3 - \beta_4 z_i^{0.5} \text{ (for } 0.25 \le \beta_1 \le 1.2) \tag{13.27}$$

The units for f_i, z_i, and σ'_{ozi} and the magnitude of β_2, β_3, and β_4 in the SI and English systems are

Item	SI	English
f_i	kN/m^2	kip/ft^2
z_i	m	ft
σ'_{ozi}	kN/m^2	kip/ft^2
β_2	192 kN/m^2	4 kip/ft^2
β_3	1.5	1.5
β_4	0.244	0.135

The point bearing capacity is

$$q_p = \beta_5 N_{60} \le \beta_6 \quad [\text{for } D_b < 1.27\,\text{m (50 in.)}] \tag{13.28}$$

where N_{60} = field standard penetration number within a distance of $2D_b$ below the base of the drilled shaft.

The magnitudes of β_5 and β_6 and the unit of q_p in the SI and English systems are given here.

Item	SI	English
β_5	57.5 kN/m^2	1.2 kip/ft^2
β_6	4310 kN/m^2	90 kip/ft^2
q_p	kN/m^2	kip/ft^2

If D_b is equal to or greater than 1.27 m (50 in.), excessive settlement may occur. In that case, q_p may be reduced to q_{pr}.

SI Units:

$$q_{pr} = \frac{1.27}{D_b\,(\text{m})}\,q_p \tag{13.29a}$$

English Units:

$$q_{pr} = \frac{50}{D_b\,(\text{in.})}\,q_p \tag{13.29b}$$

Based on the desired level of settlement, Figures 13.11 and 13.12 may now be used to calculate the allowable load, $Q_{\text{all(net)}}$. Note that the trend lines given in these figures show the average of all test results.

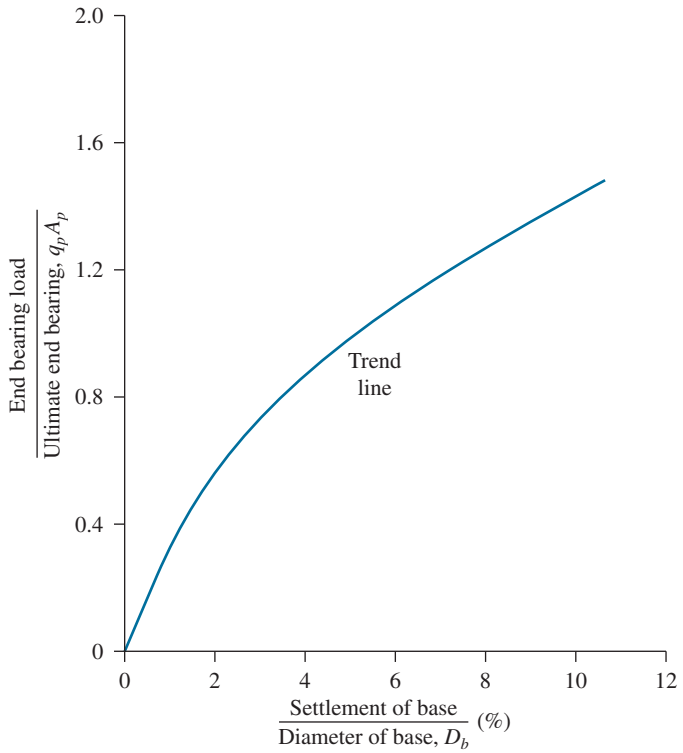
Rollins et al. (2005) have modified Eq. (13.27) for gravelly sands as follows.

- For sand with 25 to 50% gravel,

$$\beta_1 = \beta_7 - \beta_8 z_i^{0.75}\,(\text{for } 0.25 \le \beta_1 \le 1.8) \tag{13.30}$$

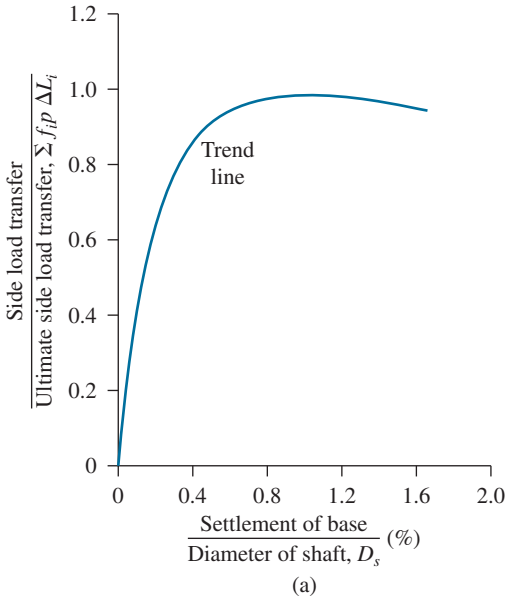
- For sand with more than 50% gravel,

$$\beta_1 = \beta_9 e^{-\beta_{10} z_i}\,(\text{for } 0.25 \le \beta_1 \le 3.0) \tag{13.31}$$



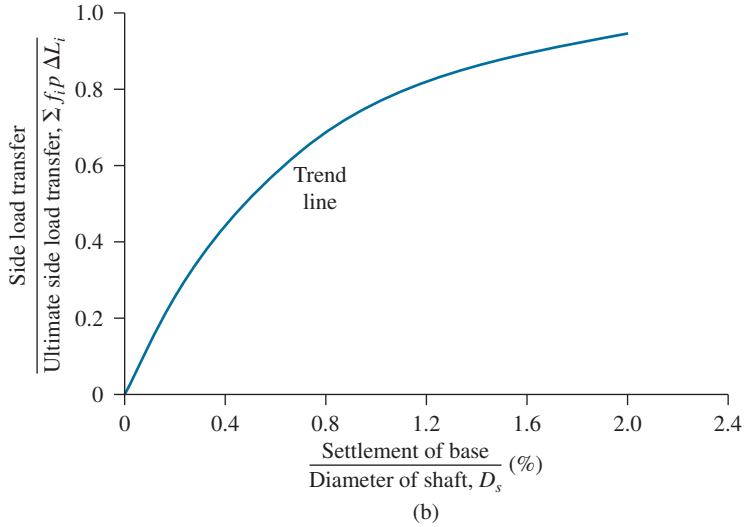
Settlement / D_b (%)	End bearing load / Ultimate end bearing
0	0
1	0.32
2	0.56
3	0.73
4	0.87
5	0.98
6	1.10
7	1.20
8	1.29
9	1.38
10	1.44

FIGURE 13.11 Normalized base-load transfer versus settlement in sand

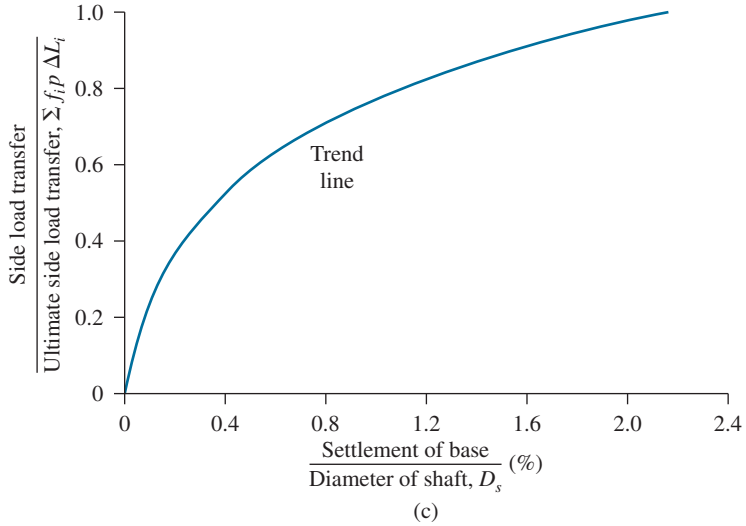


(a)

Settlement of base D_s	Side load transfer Ultimate side load
0	0
0.1	0.371
0.2	0.590
0.3	0.744
0.4	0.846
0.5	0.910
0.6	0.936
0.8	0.974
1.0	0.987
1.2	0.974
1.4	0.968
1.6	0.960
1.8	0.940



(b)



(c)

FIGURE 13.12 Normalized side load transfer versus settlement in (a) sand; (b) gravelly sand (gravel 25 to 50%); (c) gravel (more than 50%)

The magnitudes of β_7, β_8, β_9, and β_{10} and the unit of z_i in the SI and English systems are given here.

Item	SI	English
β_7	2.0	2.0
β_8	0.15	0.062
β_9	3.4	3.4
β_{10}	−0.085	−0.026
z_i	m	ft

EXAMPLE 13.2

A soil profile is shown in Figure 13.13. A point bearing drilled shaft with a bell is placed in a layer of dense sand and gravel. Determine the allowable load the drilled shaft could carry. Use Eq. (13.5) and a factor of safety of 4. Take $D_s = 1$ m and $D_b = 1.75$ m. For the dense sand layer, $\phi' = 36°$; $E_s = 500p_a$. Ignore the frictional resistance of the shaft, which is negligible compared to the end-bearing load.

SOLUTION

We have

$$Q_{p(\text{net})} = A_p[q'(N_q - 1)F_{qs}F_{qd}F_{qc}]$$

and

$$q' = (6)(16.2) + (2)(19.2) = 135.6 \text{ kN/m}^2$$

For $\phi' = 36°$, from Table 13.1, $N_q = 37.75$. Also,

$$F_{qs} = 1.727$$

and

$$F_{qd} = 1 + C \tan^{-1}\left(\frac{L}{D_b}\right)$$

$$= 1 + 0.247 \tan^{-1}\left(\frac{8}{1.75}\right) = 1.335$$

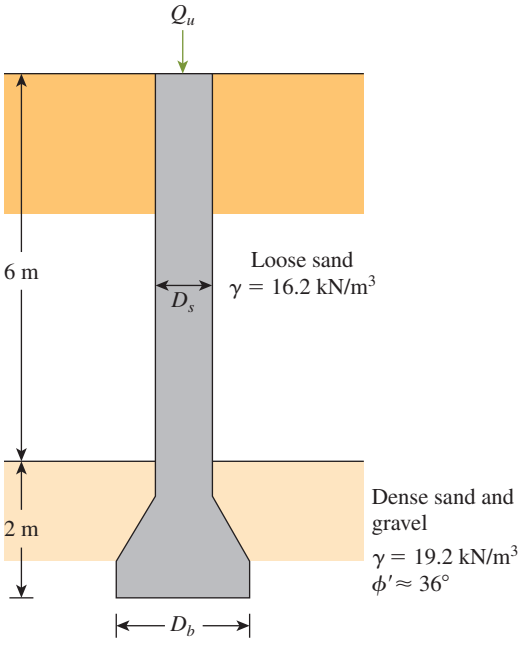


FIGURE 13.13 Allowable load of drilled shaft

From Eq. (13.9),

$$I_{cr} = 0.5 \exp\left[2.85 \cot\left(45 - \frac{\phi'}{2}\right)\right] = 134.3 \text{ (See Table 13.1)}$$

From Eq. (13.12), $E_s = mp_a$. With $m = 500$, we have

$$E_s = (500)(100) = 50{,}000 \text{ kN/m}^2$$

From Eq. (13.13) and Table 13.1,

$$\mu_s = 0.265$$

So

$$I_r = \frac{E_s}{2(1 + \mu_s)(q')(\tan \phi')} = \frac{50{,}000}{2(1 + 0.265)(135.6)(\tan 36)} = 200.6$$

From Eq. (13.10),

$$I_{rr} = \frac{I_r}{1 + I_r \Delta}$$

with

$$\Delta = n \frac{q'}{p_a} = 0.00225\left(\frac{135.6}{100}\right) = 0.0031$$

it follows that

$$I_{rr} = \frac{200.6}{1 + (200.6)(0.0031)} = 123.7$$

I_{rr} is less than I_{cr}. So, from Eq. (13.17),

$$F_{qc} = \exp\left\{(-3.8 \tan \phi') + \left[\frac{(3.07 \sin \phi')(\log_{10} 2I_{rr})}{1 + \sin \phi'}\right]\right\}$$

$$= \exp\left\{(-3.8 \tan 36) + \left[\frac{(3.07 \sin 36) \log (2 \times 123.7)}{1 + \sin 36}\right]\right\} = 0.958$$

Hence,

$$Q_{p(\text{net})} = \left[\left(\frac{\pi}{4}\right)(1.75)^2\right](135.6)(37.75 - 1)(1.727)(1.335)(0.958) = 26{,}474 \text{ kN}$$

and

$$Q_{p(\text{all})} = \frac{Q_{p(\text{net})}}{\text{FS}} = \frac{26{,}474}{4} \approx \mathbf{6619\ kN}$$

EXAMPLE 13.3

Solve Example 13.2 using Eq. (13.18).

SOLUTION

Equation (13.18) asserts that

$$Q_{p(\text{net})} = A_p q'(\omega N_q^* - 1)$$

We have (also see Table 13.2)

$$N_q^* = 0.21e^{0.17\phi'} = 0.21e^{(0.17)(36)} = 95.52$$

and

$$\frac{L}{D_b} = \frac{8}{1.75} = 4.57$$

From Table 13.3, for $\phi' = 36°$ and $L/D_b = 4.57$, the value of ω is about 0.83. So

$$Q_{p(\text{net})} = \left[\left(\frac{\pi}{4}\right)(1.75)^2\right](135.6)\,[\,(0.83)\,(95.52) - 1] = 25{,}532 \text{ kN}$$

and

$$Q_{p(\text{all})} = \frac{25{,}532}{4} = \mathbf{6383\ kN}$$

EXAMPLE 13.4

A drilled shaft is shown in Figure 13.14. The uncorrected average standard penetration number (N_{60}) within a distance of $2D_b$ below the base of the shaft is about 30. Determine

a. The ultimate load-carrying capacity. Use Eq. (13.30).
b. The load-carrying capacity for a settlement of 12 mm.

SOLUTION

Part a

From Eqs. (13.26) and (13.27),

$$f_i = \beta_1 \sigma'_{\text{ozi}}$$

and from Eq. (13.30),

$$\beta_1 = 2.0 - 0.15 z_i^{0.75}$$

We can divide the sandy gravel layer into two layers, each having a thickness of 3 m. Now the following table can be prepared.

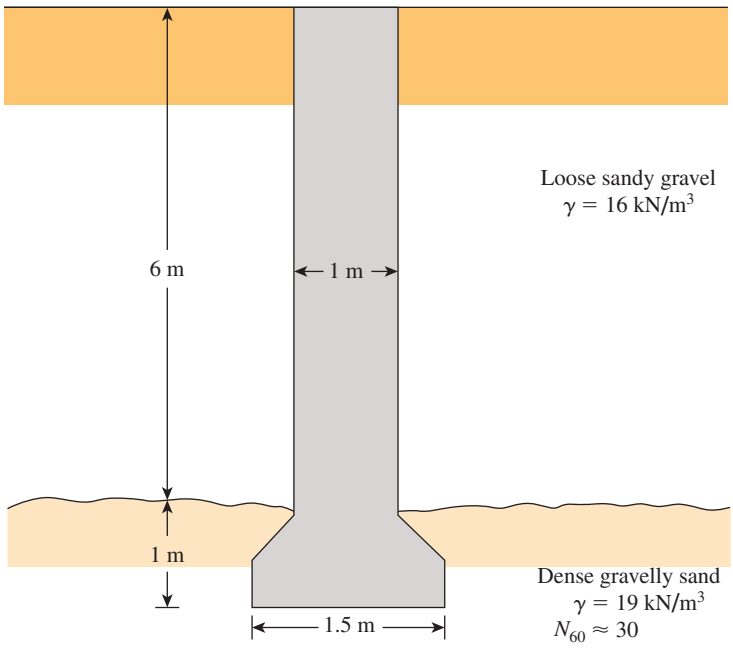


FIGURE 13.14 Drilled shaft supported by a dense layer of gravelly sand

Layer no.	Depth to the middle of the layer, z_i (m)	$\beta_1 = 2 - 0.15z_i^{0.75}$	$\sigma'_{ozi} = \gamma z_i$ (kN/m^2)	$f_i = \beta_1 \sigma'_{ozi}$ (kN/m^2)
1	1.5	1.797	24	43.13
2	4.5	1.537	72	110.66

Thus,

$$\Sigma f_i\, p\, \Delta L_i = (\pi \times 1)[(43.13)(3) + (110.66)(3)] = 1449.4 \text{ kN}$$

From Eq. (13.28),

$$q_p = 57.5N_{60} = (57.5)(30) = 1725 \text{ kN/m}^2$$

Note that D_b is greater than 1.27. So we will reduce q_p using Eq. (13.29a).

$$q_{pr} = \left(\frac{1.27}{D_b}\right) q_p = \left(\frac{1.27}{1.5}\right)(1725) \approx 1461 \text{ kN/m}^2$$

Now

$$q_{pr} A_p = (1461)\left(\frac{\pi}{4} \times 1.5^2\right) \approx 2582 \text{ kN}$$

Hence,

$$Q_{\text{ult(net)}} = q_{pr}A_p + \Sigma f_i\, p\, \Delta L_i = 2582 + 1449.4 = \mathbf{4031.4\ kN}$$

Part b
We have

$$\frac{\text{Allowable settlement}}{D_s} = \frac{12}{(1.0)(1000)} = 0.012 = 1.2\%$$

The trend line in Figure 13.12b shows that, for a normalized settlement of 1.2%, the normalized load is about 0.8. Thus, the side load transfer is (0.8)(1449.4) ≈ 1160 kN
Similarly,

$$\frac{\text{Allowable settlement}}{D_b} = \frac{12}{(1.5)(1000)} = 0.008 = 0.8\%$$

The trend line shown in Figure 13.11 indicates that, for a normalized settlement of 0.8%, the normalized base load is 0.235. So the base load is (0.235)(2582) = 606.77 kN. Hence, the total load is

$$Q = 1160 + 606.77 \approx \mathbf{1767\ kN}$$

13.9 Load-Bearing Capacity in Clay

For saturated clays with $\phi = 0$, the bearing capacity factor N_q in Eq. (13.4) is equal to unity. Thus, for this case,

$$Q_{p(\text{net})} \approx A_p c_u N_c F_{cs} F_{cd} F_{cc} \tag{13.32}$$

where c_u is the undrained cohesion.

Assuming that $L \geq 3D_b$, we can rewrite Eq. (13.32) as

$$Q_{p(\text{net})} = A_p c_u N_c^* \tag{13.33}$$

where $N_c^* = N_c F_{cs} F_{cd} F_{cc} = 1.33[(\ln I_r) + 1]$ in which $\left(\text{for } \frac{L}{D_b} > 3\right)$ I_r = soil rigidity index. (13.34)

The soil rigidity index was defined in Eq. (13.11). For $\phi = 0$,

$$I_r = \frac{E_s}{3c_u} \tag{13.35}$$

O'Neill and Reese (1999) provided an approximate relationship between c_u and $E_s/3c_u$. This is summarized in Table 13.4. For all practical purposes, if c_u/p_a is equal to or greater than unity (p_a = atmospheric pressure $\approx$ 100 kN/m^2 or 2000 lb/ft^2), then the magnitude of N_c^* can be taken to be 9.

For $L/D_b < 3$ (O'Neill and Reese, 1999),

$$Q_{p(\text{net})} = A_p \left\{ \frac{2}{3} \left[1 + \frac{1}{6} \left(\frac{L}{D_b} \right) \right] \right\} c_u N_c^* \tag{13.36}$$

Experiments by Whitaker and Cooke (1966) showed that, for belled shafts, the full value of $N_c^* = 9$ is realized with a base movement of about 10 to 15% of D_b. Similarly, for straight shafts ($D_b = D_s$), the full value of $N_c^* = 9$ is obtained with a base movement of about 20% of D_b.

The expression for the skin resistance of drilled shafts in clay is similar to Eq. (12.61), or

$$Q_s = \sum_{L=0}^{L=L_1} \alpha^* c_u p \, \Delta L \tag{13.37}$$

Kulhawy and Jackson (1989) reported the field-test result of 106 straight drilled shafts—65 in uplift and 41 in compression. The best correlation obtained from the results is

$$\alpha^* = 0.21 + 0.25 \left(\frac{p_a}{c_u} \right) \leq 1 \tag{13.38}$$

where p_a = atmospheric pressure $\approx$ 100 kN/m^2 ($\approx$2000 lb/ft^2).

So, conservatively, we may assume that

$$\alpha^* = 0.4 \tag{13.39}$$

TABLE 13.4 Approximate Variation of $E_s/3c_u$ with N_c^* and c_u/p_a (Based on data from O'Neill and Reese, 1999)

c_u/p_a	$E_s/3c_u$	N_c^*	c_u/p_a	$E_s/3c_u$	N_c^*
0.25	50	6.53	1.25	270	8.78
0.50	145	7.95	1.50	285	8.85
0.75	219	8.50	1.75	292	8.88
1.00	250	8.67	2.00	300	8.92

13.10 Load-Bearing Capacity in Clay Based on Settlement

Reese and O'Neill (1989) suggested a procedure for estimating the ultimate and allowable (based on settlement) bearing capacities for drilled shafts in clay. According to this procedure, we can use Eq. (13.25) for the net ultimate load, or

$$Q_{\text{ult(net)}} = \sum_{i=1}^{n} f_i p\, \Delta L_i + q_p A_p$$

The unit skin friction resistance can be given as

$$f_i = \alpha_i^* c_{u(i)} \tag{13.40}$$

The following values are recommended for α_i^*:

$\alpha_i^* = 0$ for the top 1.5 m (5 ft) and bottom 1 diameter, D_s, of the drilled shaft. (*Note:* If $D_b > D_s$, then $\alpha^* = 0$ for 1 diameter above the top of the bell and for the peripheral area of the bell itself.)

$\alpha_i^* = 0.55$ elsewhere.

The expression for q_p (point load per unit area) can be given as

$$q_p = 6c_{ub}\left(1 + 0.2\frac{L}{D_b}\right) \le 9c_{ub} \le 40p_a \tag{13.41}$$

where

c_{ub} = average undrained cohesion within a vertical distance of $2D_b$ below the base

p_a = atmospheric pressure

If D_b is large, excessive settlement will occur at the ultimate load per unit area, q_p, as given by Eq. (13.41). Thus, for $D_b > 1.91$ m (75 in.), q_p may be replaced by

$$q_{pr} = F_r q_p \tag{13.42}$$

where

$$F_r = \frac{2.5}{\psi_1 D_b + \psi_2} \le 1 \tag{13.43}$$

The relations for ψ_1 and ψ_2 along with the unit of D_b in the SI and English systems are given in Table 13.5.

Figures 13.15 and 13.16 may now be used to evaluate the allowable load-bearing capacity, based on settlement. (Note that the ultimate bearing capacity in Figure 13.15 is q_p, not q_{pr}.) To do so,

Step 1. Select a value of settlement, s.

Step 2. Calculate $\sum_{i=1}^{N} f_i p\, \Delta L_i$ and $q_p A_p$.

TABLE 13.5 Relationships for ψ_1 and ψ_2

Item	SI	English
ψ_1	$\psi_1 = 2.78 \times 10^{-4} + 8.26 \times 10^{-5}\left(\frac{L}{D_b}\right) \le 5.9 \times 10^{-4}$	$\psi_1 = 0.0071 + 0.0021\left(\frac{L}{D_b}\right) \le 0.015$
ψ_2	$\psi_2 = 0.065[c_{ub}(\text{kN/m}^2)]^{0.5}$	$\psi_2 = 0.45[c_{ub}(\text{kip/ft}^2)]^{0.5}$
	$(0.5 \le \psi_2 \le 1.5)$	$0.5 \le \psi_2 \le 1.5$
D_b	mm	in.

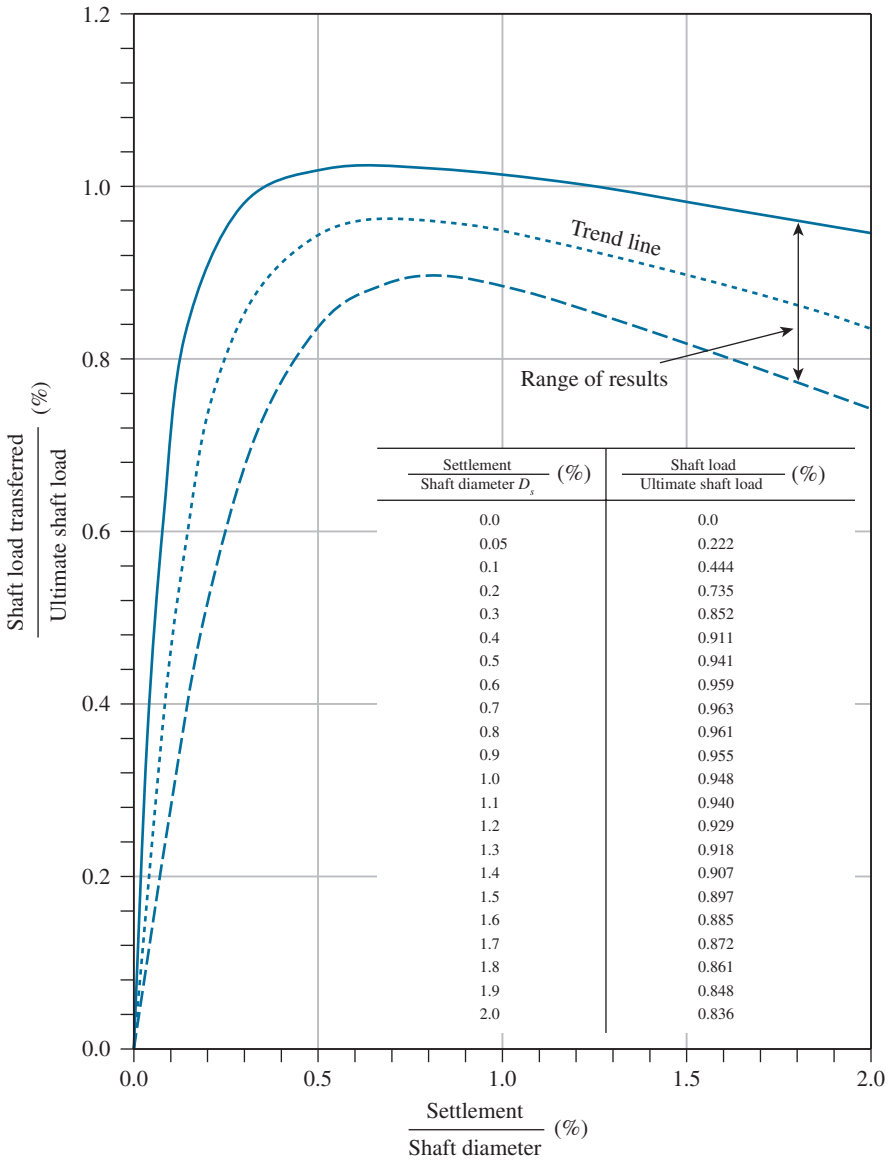
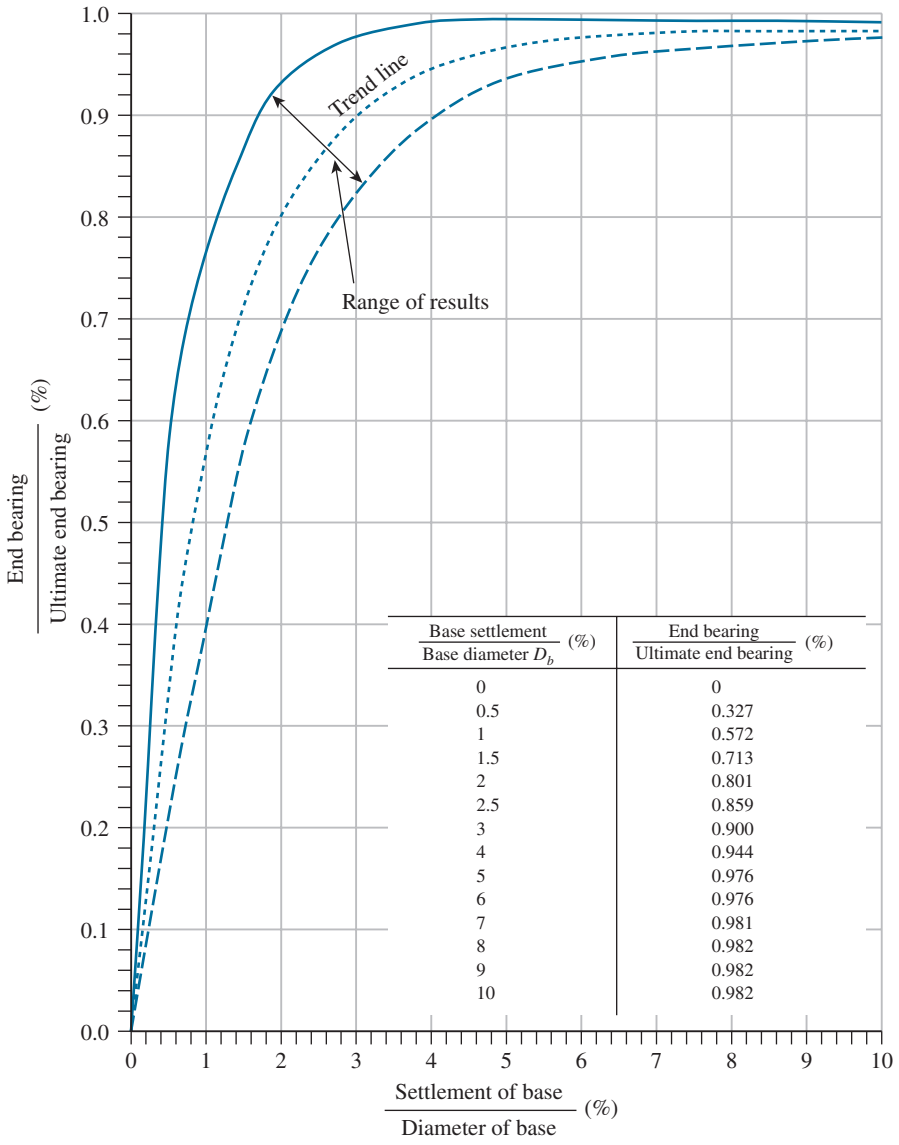


FIGURE 13.15 Normalized side load transfer versus settlement in cohesive soil

Step 3. Using Figures 13.15 and 13.16 and the calculated values in Step 2, determine the *side load* and the *end bearing load*.

Step 4. The sum of the side load and the end bearing load gives the total allowable load.



Base settlement / Base diameter D_b (%)	End bearing / Ultimate end bearing (%)
0	0
0.5	0.327
1	0.572
1.5	0.713
2	0.801
2.5	0.859
3	0.900
4	0.944
5	0.976
6	0.976
7	0.981
8	0.982
9	0.982
10	0.982

FIGURE 13.16 Normalized base-load transfer versus settlement in cohesive soil

EXAMPLE 13.5

Figure 13.17 shows a drilled shaft without a bell. Here, $L_1 = 27$ ft, $L_2 = 8.5$ ft, $D_s = 3.3$ ft, $c_{u(1)} = 1000$ lb/ft^2, and $c_{u(2)} = 2175$ lb/ft^2. Determine

a. The net ultimate point bearing capacity
b. The ultimate skin resistance
c. The working load, Q_w (FS = 3)

Use Eqs. (13.33), (13.37), and (13.39).

SOLUTION

Part a

From Eq. (13.33),

$$Q_{p(\text{net})} = A_p c_u N_c^* = A_p c_{u(2)} N_c^* = \left[\left(\frac{\pi}{4}\right)(3.3)^2\right](2175)(9) = \mathbf{167{,}425\ lb}$$

$$\approx \mathbf{167.4\ kip}$$

(*Note:* Since $c_{u(2)}/p_a > 1$, $N_c^* \approx 9$.

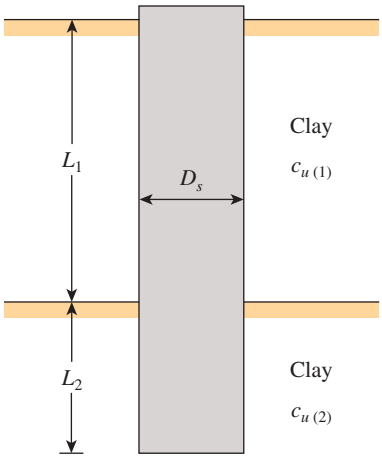


FIGURE 13.17 A drill shaft without a bell

Part b

From Eq. (13.37),

$$Q_s = \Sigma \alpha^* c_u p \, \Delta L$$

From Eq. (13.39),

$$\alpha^* = 0.4$$

$$p = \pi D_s = (3.14)(3.3) = 10.37 \text{ ft}$$

and

$$Q_s = (0.4)(10.37)[(1000 \times 27) + (2175 \times 8.5)] = \mathbf{188{,}682 \text{ lb}}$$

$$\approx \mathbf{188.7 \text{ kip}}$$

Part c

$$Q_w = \frac{Q_{p(\text{net})} + Q_s}{\text{FS}} = \frac{167.4 + 188.7}{3} = \mathbf{118.7 \text{ kip}}$$

EXAMPLE 13.6

A drilled shaft in a cohesive soil is shown in Figure 13.18. Use Reese and O'Neill's method, discussed in Section 13.10, to determine the following:

a. The ultimate load-carrying capacity
b. The load-carrying capacity for an allowable settlement of 12 mm

SOLUTION

Part a

From Eq. (13.40),

$$f_i = \alpha_i^* c_{u(i)}$$

From Figure 13.18,

$$\Delta L_1 = 3 - 1.5 = 1.5 \text{ m}$$

$$\Delta L_2 = (6 - 3) - D_s = (6 - 3) - 0.76 = 2.24 \text{ m}$$

$$c_{u(1)} = 40 \text{ kN/m}^2$$

and

$$c_{u(2)} = 60 \text{ kN/m}^2$$

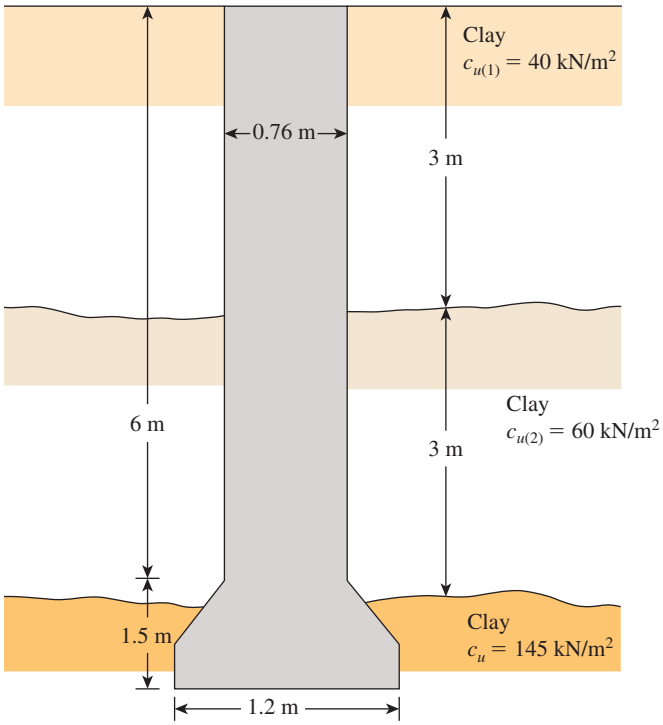


FIGURE 13.18 A drilled shaft in layered clay

Hence,

$$\begin{aligned}\Sigma f_i\, p\, \Delta L_i &= \Sigma \alpha_i^* c_{u(i)}\, p\, \Delta L_i \\ &= (0.55)\,(40)\,(\pi \times 0.76)\,(1.5) + (0.55)\,(60)\,(\pi \times 0.76)\,(2.24) \\ &= 255.28 \text{ kN}\end{aligned}$$

Again, from Eq. (13.41),

$$q_p = 6c_{ub}\left(1 + 0.2\,\frac{L}{D_b}\right) = (6)(145)\left[1 + 0.2\left(\frac{6 + 1.5}{1.2}\right)\right] = 1957.5 \text{ kN/m}^2$$

A check reveals that

$$q_p = 9c_{ub} = (9)(145) = 1305 \text{ kN/m}^2 < 1957.5 \text{ kN/m}^2$$

So we use $q_p = 1305$ kN/m^2.

$$q_p A_p = q_p\left(\frac{\pi}{4}D_b^2\right) = (1305)\left[\left(\frac{\pi}{4}\right)(1.2)^2\right] = 1475.9 \text{ kN}$$

Hence,

$$Q_{\text{ult}} = \Sigma \alpha_i^* c_{u(i)} p\, \Delta L_i + q_p A_p = 255.28 + 1475.9 \approx \mathbf{1731\ kN}$$

Part b

We have

$$\frac{\text{Allowable settlement}}{D_s} = \frac{12}{(0.76)(1000)} = 0.0158 = 1.58\%$$

The trend line shown in Figure 13.15 indicates that, for a normalized settlement of 1.58%, the normalized side load is about 0.9. Thus, the side load is

$$(0.9)\,(\Sigma f_i\, p\, \Delta L_i) = (0.9)\,(255.28) = 229.8 \text{ kN}$$

Again,

$$\frac{\text{Allowable settlement}}{D_b} = \frac{12}{(1.2)(1000)} = 0.01 = 1.0\%$$

The trend line shown in Figure 13.16 indicates that, for a normalized settlement of 1.0%, the normalized end bearing is about 0.572, so

$$\text{Base load} = (0.572)(q_p A_p) = (0.572)(1475.9) = 844.2 \text{ kN}$$

Thus, the total load is

$$Q = 229.8 + 844.2 = \mathbf{1074 \text{ kN}}$$

■

13.11 Settlement of Drilled Shafts at Working Load

The settlement of drilled shafts at working load is calculated in a manner similar to that outlined in Section 12.18. In many cases, the load carried by shaft resistance is small compared with the load carried at the base. In such cases, the contribution of s_3 may be ignored. [Note that in Eqs. (12.89) and (12.90) the term D should be replaced by D_b for drilled shafts.] In Eqs. (12.91) and (12.92), D should be replaced by D_s.

EXAMPLE 13.7

Refer to Figure 13.17. Given: $L_1 = 8$ m, $L_2 = 3$ m, $D_s = 1.5$ m, $c_{u(1)} = 50$ kN/m^2, $c_{u(2)} = 105$ kN/m^2, and working load $Q_w = 1005$ kN. Estimate the elastic settlement at the working load. Use Eqs. (12.88), (12.90), and (12.91). Take $\xi = 0.65$, $E_p = 21 \times 10^6$ kN/m^2, $E_s = 14{,}000$ kN/m^2, $\mu_s = 0.3$, and $Q_{wp} = 250$ kN.

SOLUTION

From Eq. (12.88),

$$s_{e(1)} = \frac{(Q_{wp} + \xi Q_{ws})L}{A_p E_p}$$

Now,

$$Q_{ws} = 1005 - 250 = 755 \text{ kN}$$

so

$$s_{e(1)} = \frac{[250 + (0.65)(755)](11)}{\left(\frac{\pi}{4} \times 1.5^2\right)(21 \times 10^6)} = 0.00022 \text{ m} = 0.22 \text{ mm}$$

From Eq. (12.90),

$$s_{e(2)} = \frac{Q_{wp} C_p}{D_b q_p}$$

From Table 12.14, for stiff clay, $C_p \approx 0.04$; also,

$$q_p = c_{u(b)} N_c^* = (105)(9) = 945 \text{ kN/m}^2$$

Hence,

$$s_{e(2)} = \frac{(250)(0.04)}{(1.5)(945)} = 0.0071 \text{ m} = 7.1 \text{ mm}$$

Again, from Eqs. (12.91) and (12.92),

$$s_{e(3)} = \left(\frac{Q_{ws}}{pL}\right)\left(\frac{D_s}{E_s}\right)(1 - \mu_s^2)I_{ws}$$

where

$$I_{ws} = 2 + 0.35\sqrt{\frac{L}{D_s}} = 2 + 0.35\sqrt{\frac{11}{1.5}} = 2.95$$

$$s_{e(3)} = \left[\frac{755}{(\pi \times 1.5)(11)}\right]\left(\frac{1.5}{14{,}000}\right)(1 - 0.3^2)(2.95) = 0.0042 \text{ m} = 4.2 \text{ mm}$$

The total settlement is

$$s_e = s_{e(1)} + s_{e(2)} + s_{e(3)} = 0.22 + 7.1 + 4.2 \approx \mathbf{11.52\ mm}$$

13.12 Lateral Load-Carrying Capacity—Characteristic Load and Moment Method

Several methods for analyzing the lateral load-carrying capacity of piles, as well as the load-carrying capacity of drilled shafts, were presented in Section 12.19; therefore, they will not be repeated here. In 1994, Duncan et al. developed a *characteristic load method* for estimating the lateral load capacity for drilled shafts that is fairly simple to use. We describe this method next.

According to the characteristic load method, the *characteristic load* Q_c and *moment* M_c form the basis for the dimensionless relationship that can be given by the following correlations:

CHARACTERISTIC LOAD

$$Q_c = 7.34D_s^2(E_pR_I)\left(\frac{c_u}{E_pR_I}\right)^{0.68} \quad \text{(for clay)} \tag{13.44}$$

$$Q_c = 1.57D_s^2(E_pR_I)\left(\frac{\gamma' D_s \phi' K_p}{E_pR_I}\right)^{0.57} \quad \text{(for sand)} \tag{13.45}$$

CHARACTERISTIC MOMENT

$$M_c = 3.86D_s^3(E_pR_I)\left(\frac{c_u}{E_pR_I}\right)^{0.46} \quad \text{(for clay)} \tag{13.46}$$

$$M_c = 1.33D_s^3(E_pR_I)\left(\frac{\gamma' D_s \phi' K_p}{E_pR_I}\right)^{0.40} \quad \text{(for sand)} \tag{13.47}$$

In these equations,

D_s = diameter of drilled shafts

E_p = modulus of elasticity of drilled shafts

R_I = ratio of moment of inertia of drilled shaft section to moment of inertia of a solid section (*Note:* $R_I = 1$ for uncracked shaft without central void.)

γ' = effective unit weight of sand

ϕ' = effective soil friction angle (degrees)

K_p = Rankine passive pressure coefficient = $\tan^2(45 + \phi'/2)$

DEFLECTION DUE TO LOAD Q_g APPLIED AT THE GROUND LINE

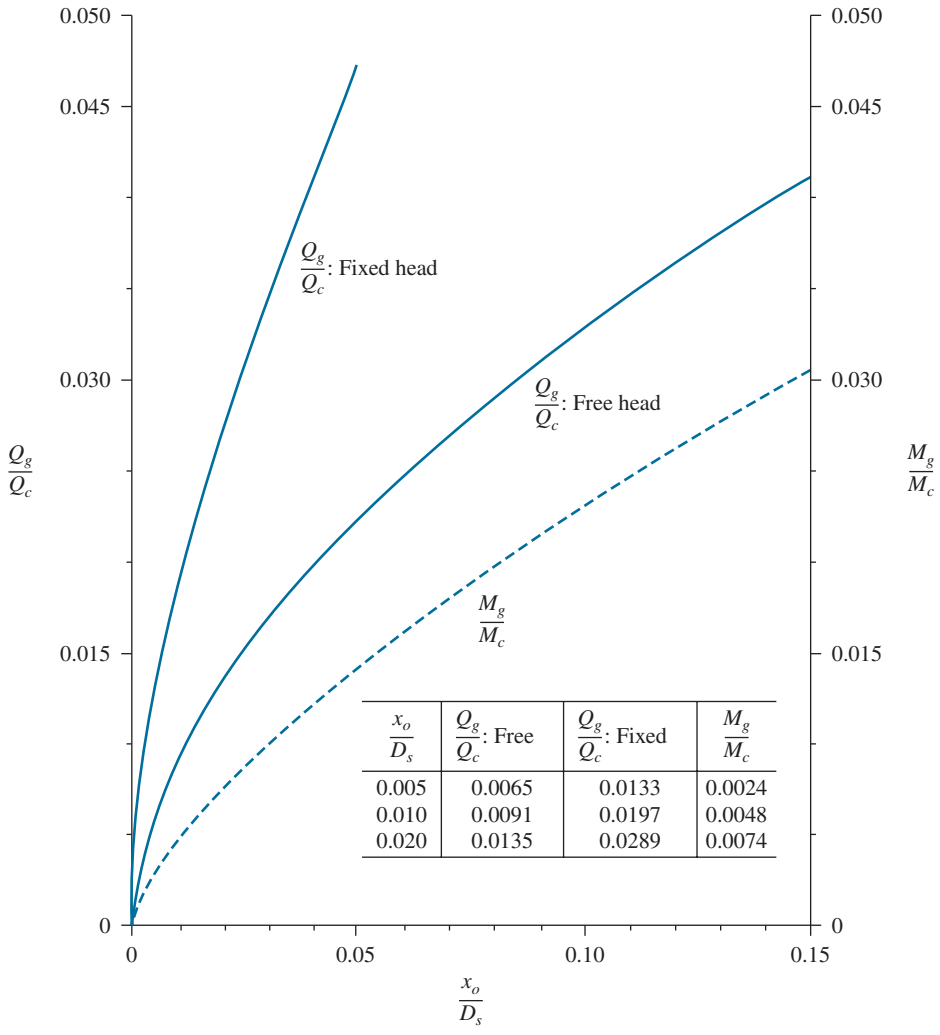
Figures 13.19 and 13.20 give the plot of Q_g/Q_c versus x_o/D_s for drilled shafts in sand and clay due to the load Q_g applied at the ground surface. Note that x_o is the ground line deflection. If the magnitudes of Q_g and Q_c are known, the ratio Q_g/Q_c can be calculated. The figure can then be used to estimate the corresponding value of x_o/D_s and, hence, x_o.

DEFLECTION DUE TO MOMENT APPLIED AT THE GROUND LINE

Figures 13.19 and 13.20 give the variation plot of M_g/M_c with x_o/D_s for drilled shafts in sand and clay due to an applied moment M_g at the ground line. Again, x_o is the ground line deflection. If the magnitudes of M_g, M_c, and D_s are known, the value of x_o can be calculated with the use of the figure.

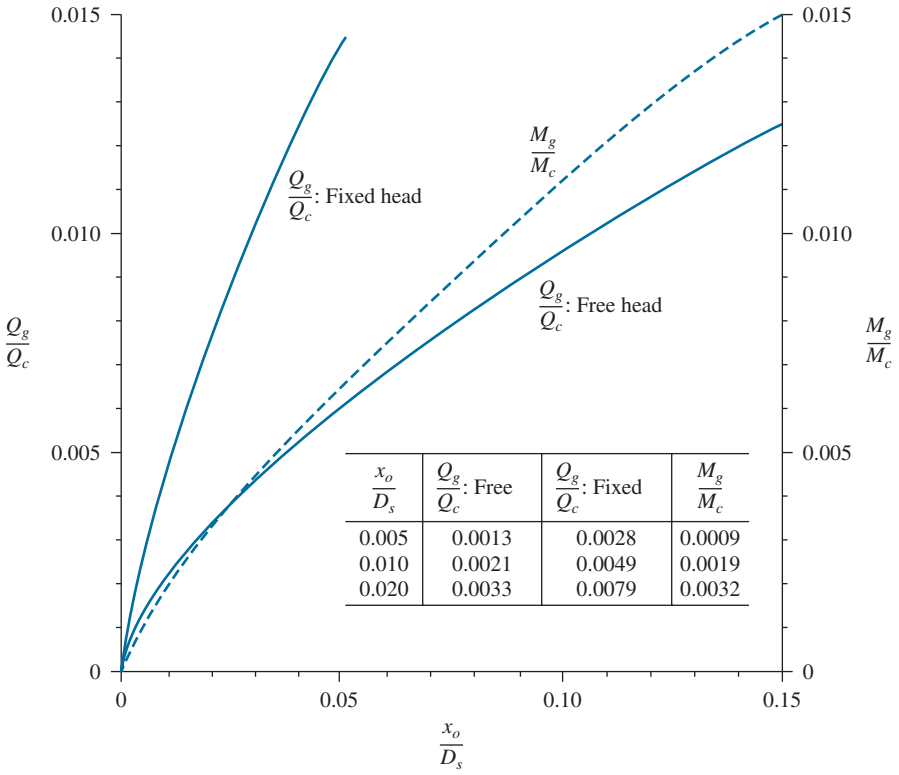
DEFLECTION DUE TO LOAD APPLIED ABOVE THE GROUND LINE

When a load Q is applied above the ground line, it induces both a load $Q_g = Q$ and a moment $M_g = Qe$ at the ground line, as shown in Figure 13.21a. A superposition



$\frac{x_o}{D_s}$	$\frac{Q_g}{Q_c}$: Free	$\frac{Q_g}{Q_c}$: Fixed	$\frac{M_g}{M_c}$
0.005	0.0065	0.0133	0.0024
0.010	0.0091	0.0197	0.0048
0.020	0.0135	0.0289	0.0074

FIGURE 13.19 Plot of $\frac{Q_g}{Q_c}$ and $\frac{M_g}{M_c}$ versus $\frac{x_o}{D_s}$ in clay



$\frac{x_o}{D_s}$	$\frac{Q_g}{Q_c}$: Free	$\frac{Q_g}{Q_c}$: Fixed	$\frac{M_g}{M_c}$
0.005	0.0013	0.0028	0.0009
0.010	0.0021	0.0049	0.0019
0.020	0.0033	0.0079	0.0032

FIGURE 13.20 Plot of $\frac{Q_g}{Q_c}$ and $\frac{M_g}{M_c}$ versus $\frac{x_o}{D_s}$ in sand

solution can now be used to obtain the ground line deflection. The step-by-step procedure is as follows (refer to Figure 13.21b):

Step 1. Calculate Q_g and M_g.

Step 2. Calculate the deflection x_{oQ} that would be caused by the load Q_g acting alone.

Step 3. Calculate the deflection x_{oM} that would be caused by the moment acting alone.

Step 4. Determine the value of a load Q_{gM} that would cause the same deflection as the moment (i.e., x_{oM}).

Step 5. Determine the value of a moment M_{gQ} that would cause the same deflection as the load (i.e., x_{oQ}).

Step 6. Calculate $(Q_g + Q_{gM})/Q_c$ and determine x_{oQM}/D_s.

Step 7. Calculate $(M_g + M_{gQ})/M_c$ and determine x_{oMQ}/D_s.

Step 8. Calculate the combined deflection:

$$x_{o(\text{combined})} = 0.5(x_{oQM} + x_{oMQ}) \tag{13.48}$$

MAXIMUM MOMENT IN DRILLED SHAFT DUE TO GROUND LINE LOAD ONLY

Figure 13.22 shows the plot of Q_g/Q_c with $M_{\max}/M_c$ for fixed- and free-headed drilled shafts due only to the application of a ground line load Q_g. For fixed-headed shafts, the maximum moment in the shaft, $M_{\max}$, occurs at the ground line. For this condition, if Q_c, M_c, and Q_g are known, the magnitude of $M_{\max}$ can be easily calculated.

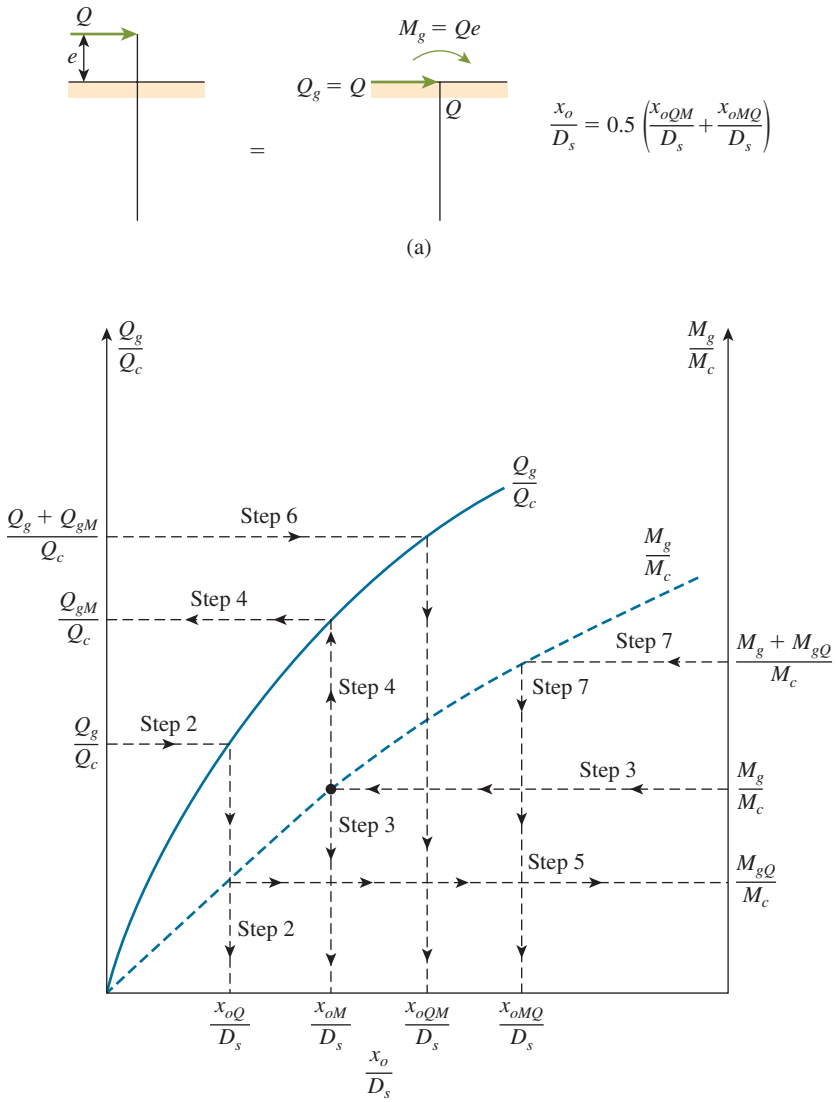


FIGURE 13.21 Superposition of deflection due to load and moment

MAXIMUM MOMENT DUE TO LOAD AND MOMENT AT GROUND LINE

If a load Q_g and a moment M_g are applied at the ground line, the maximum moment in the drilled shaft can be determined in the following manner:

Step 1. Using the procedure described before, calculate $x_{o(\text{combined})}$ from Eq. (13.48).

Step 2. To solve for the characteristic length T, use the following equation:

$$x_{o(\text{combined})} = \frac{2.43Q_g}{E_pI_p}T^3 + \frac{1.62M_g}{E_pI_p}T^2 \tag{13.49}$$

Step 3. The moment in the shaft at a depth z below the ground surface can be calculated as

$$M_z = A_mQ_gT + B_mM_g \tag{13.50}$$

where A_m, B_m = dimensionless moment coefficients (Matlock and Reese, 1961); see Figure 13.23.

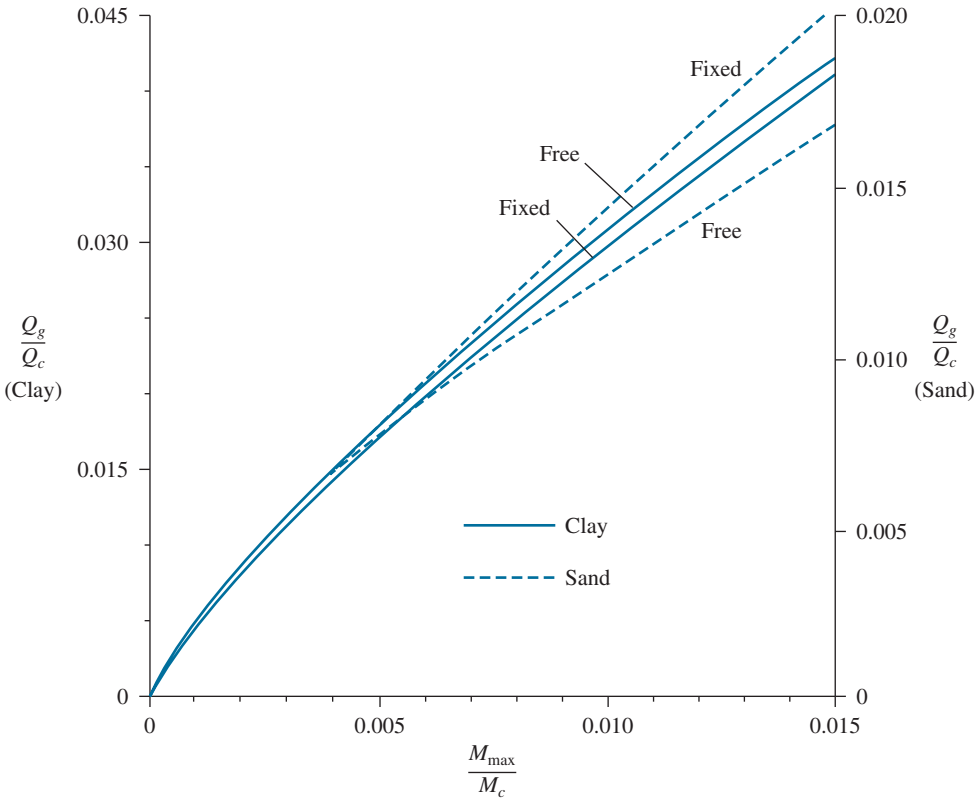


FIGURE 13.22 Variation of $\frac{Q_g}{Q_c}$ with $\frac{M_{max}}{M_c}$

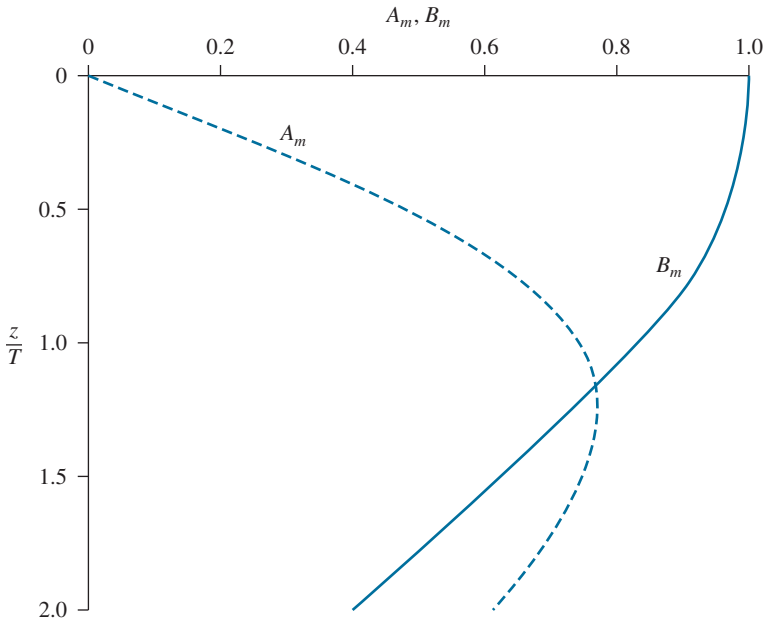


FIGURE 13.23 Variation of A_m and B_m with z/T

The value of the maximum moment M_{max} can be obtained by calculating M_z at various depths in the upper part of the drilled shaft.

The characteristic load method just described is valid only if L/D_s has a certain minimum value. If the actual L/D_s is less than $(L/D_s)_{min}$, then the ground line

deflections will be underestimated and the moments will be overestimated. The values of $(L/D_s)_{min}$ for drilled shafts in sand and clay are given in the following table:

Clay		Sand	
$\frac{E_pR_I}{c_u}$	$(L/D_s)_{min}$	$\frac{E_pR_I}{\gamma' D_s \phi' K_p}$	$(L/D_s)_{min}$
1×10^5	6	1×10^4	8
3×10^5	10	4×10^4	11
1×10^6	14	2×10^5	14
3×10^6	18		

EXAMPLE 13.8

A free-headed drilled shaft in clay is shown in Figure 13.24. Let $E_p = 22 \times 10^6$ kN/m^2. Determine

a. The ground line deflection, $x_{o(combined)}$
b. The maximum bending moment in the drilled shaft
c. The maximum tensile stress in the shaft
d. The minimum penetration of the shaft needed for this analysis

SOLUTION

We are given

$$D_s = 1 \text{ m}$$
$$c_u = 100 \text{ kN/m}^2$$
$$R_I = 1$$
$$E_p = 22 \times 10^6 \text{ kN/m}^2$$

and

$$I_p = \frac{\pi D_s^4}{64} = \frac{(\pi)(1)^4}{64} = 0.049 \text{ m}^4$$

Part a

From Eq. (13.44),

$$Q_c = 7.34 D_s^2 (E_p R_I) \left(\frac{c_u}{E_p R_I}\right)^{0.68}$$
$$= (7.34)(1)^2[(22 \times 10^6)(1)] \left[\frac{100}{(22 \times 10^6)(1)}\right]^{0.68}$$
$$= 37{,}607 \text{ kN}$$

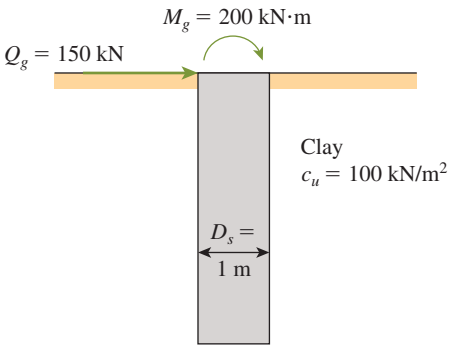


FIGURE 13.24 Free-headed drilled shaft

From Eq. (13.46),

$$M_c = 3.86 D_s^3 (E_p R_I)\left(\frac{c_u}{E_p R_I}\right)^{0.46}$$
$$= (3.86)(1)^3[(22 \times 10^6)(1)]\left[\frac{100}{(22 \times 10^6)(1)}\right]^{0.46}$$
$$= 296{,}139 \text{ kN} \cdot \text{m}$$

Thus,

$$\frac{Q_g}{Q_c} = \frac{150}{37{,}607} = 0.004$$

From Figure 13.19, $x_{oQ} \approx (0.0025) D_s = 0.0025$ m $= 2.5$ mm. Also,

$$\frac{M_g}{M_c} = \frac{200}{296{,}139} = 0.000675$$

From Figure 13.19, $x_{oM} \approx (0.0014) D_s = 0.0014$ m $= 1.4$ mm, so

$$\frac{x_{oM}}{D_s} = \frac{0.0014}{1} = 0.0014$$

From Figure 13.19, for $x_{oM}/D_s = 0.0014$, the value of $Q_{gM}/Q_c \approx 0.002$. Hence,

$$\frac{x_{oQ}}{D_s} = \frac{0.0025}{1} = 0.0025$$

From Figure 13.19, for $x_{oQ}/D_s = 0.0025$, the value of $M_{gQ}/M_c \approx 0.0013$, so

$$\frac{Q_g}{Q_c} + \frac{Q_{gM}}{Q_c} = 0.004 + 0.002 = 0.006$$

From Figure 13.19, for $(Q_g + Q_{gM})/Q_c = 0.006$, the value of $x_{oQM}/D_s \approx 0.0046$. Hence,

$$x_{oQM} = (0.0046)(1) = 0.0046 \text{ m} = 4.6 \text{ mm}$$

Thus, we have

$$\frac{M_g}{M_c} + \frac{M_{gQ}}{M_c} = 0.000675 + 0.0013 \approx 0.00198$$

From Figure 13.19, for $(M_g + M_{gQ})/M_c = 0.00198$, the value of $x_{oMQ}/D_s \approx 0.0041$. Hence,

$$x_{oMQ} = (0.0041)(1) = 0.0041 \text{ m} = 4.1 \text{ mm}$$

Consequently,

$$x_{o\,(\text{combined})} = 0.5(x_{oQM} + x_{oMQ}) = (0.5)(4.6 + 4.1) = \mathbf{4.35\ mm}$$

Part b

From Eq. (13.49),

$$x_{o\,(\text{combined})} = \frac{2.43 Q_g}{E_p I_p} T^3 + \frac{1.62 M_g}{E_p I_p} T^2$$

so

$$0.00435 \text{ m} = \frac{(2.43)(150)}{(22 \times 10^6)(0.049)} T^3 + \frac{(1.62)(200)}{(22 \times 10^6)(0.049)} T^2$$

or

$$0.00435 \text{ m} = 338 \times 10^{-6} T^3 + 300.6 \times 10^{-6} T^2$$

and it follows that

$$T \approx 2.05 \text{ m}$$

From Eq. (13.50),

$$M_z = A_m Q_g T + B_m M_g = A_m(150)(2.05) + B_m(200) = 307.5A_m + 200B_m$$

Now the following table can be prepared:

$\frac{z}{T}$	A_m (Figure 13.23)	B_m (Figure 13.23)	M_z (kN·m)
0	0	1.0	200
0.4	0.36	0.98	306.7
0.6	0.52	0.95	349.9
0.8	0.63	0.9	373.7
1.0	0.75	0.845	399.6
1.1	0.765	0.8	395.2
1.25	0.75	0.73	376.6

So the maximum moment is **399.4 kN·m ≈ 400 kN·m** and occurs at $z/T \approx 1$. Hence,

$$z = (1)(T) = (1)(2.05 \text{ m}) = \mathbf{2.05 \text{ m}}$$

Part c

The maximum tensile stress is

$$\sigma_{\text{tensile}} = \frac{M_{\max}\left(\frac{D_s}{2}\right)}{I_p} = \frac{(400)\left(\frac{1}{2}\right)}{0.049} = \mathbf{4081.6 \text{ kN/m}^2}$$

Part d

We have

$$\frac{E_p R_I}{c_u} = \frac{(22 \times 10^6)(1)}{100} = 2.2 \times 10^5$$

By interpolation, for $(E_p R_I)/c_u = 2.2 \times 10^5$, the value of $(L/D_s)_{\min} \approx 8.5$. So

$$L \approx (8.5)(1) = \mathbf{8.5 \text{ m}}$$

13.13 Drilled Shafts Extending into Rock

In Section 13.1, we noted that drilled shafts can be extended into rock. Figure 13.25 shows a drilled shaft whose depth of embedment in rock is equal to L. When considering drilled shafts in rock, we can find several correlations between the end bearing capacity and the *unconfined compression strength of intact rocks*, q_u. It is important to recognize that in the field there are cracks, joints, and other discontinuities in the rock, and the influence of those factors should be considered. Following are two procedures for determination of the ultimate bearing capacity of drilled shafts extending

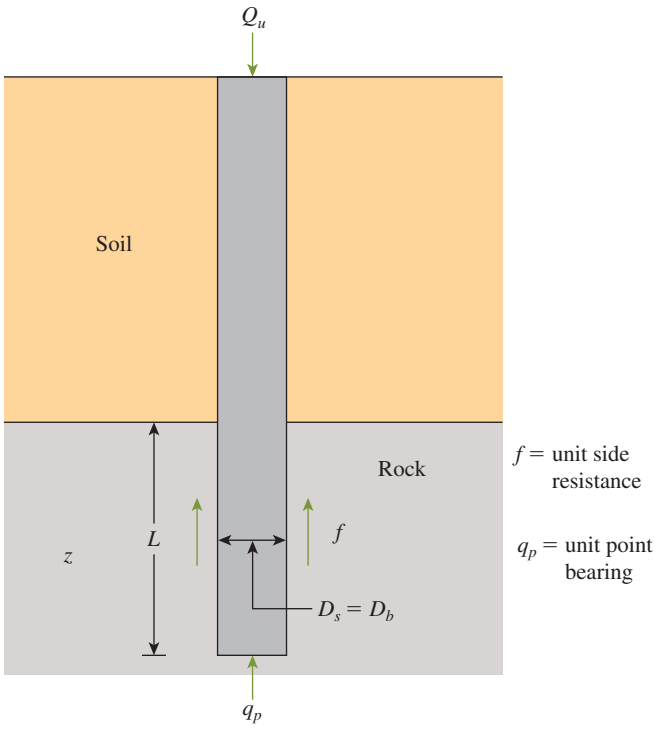


FIGURE 13.25 Drilled shaft socketed into rock

into rock. The procedures were developed by Reese and O'Neill (1988, 1989) and Zhang and Einstein (1998).

PROCEDURE OF REESE AND O'NEILL (1988, 1989)

Following is a step-by-step outline to estimate the ultimate bearing capacity. In this design procedure, it is assumed that there is either *side resistance between the shaft and the rock* or *point resistance at the bottom*.

Step 1. Calculate the ultimate unit side resistance as

$$f\,(\text{lb/in}^2) = 2.5q_u^{0.5} \leq 0.15q_u \tag{13.51a}$$

where q_u is the smaller of either (a) the unconfined compressive strength of NW or larger size rock core or (b) the unconfined compressive strength of the drilled shaft concrete in lb/in^2.

In SI units, Eq. (13.51a) can be expressed as

$$f\,(\text{kN/m}^2) = 6.564q_u^{0.5}\,(\text{kN/m}^2) \leq 0.15q_u\,(\text{kN/m}^2) \tag{13.51b}$$

Step 2. Calculate the ultimate capacity based on side resistance only, or

$$Q_u = \pi D_s L f \tag{13.52}$$

Step 3. Calculate the settlement s_e of the shaft at the top of the rock socket, or

$$s_e = s_{e(s)} + s_{e(b)} \tag{13.53}$$

where

$s_{e(s)}$ = elastic compression of the drilled shaft within the socket, assuming no side resistance

$s_{e(b)}$ = settlement of the base

However,

$$s_{e(s)} = \frac{Q_u L}{A_c E_c} \tag{13.54}$$

and

$$s_{e(b)} = \frac{Q_u I_f}{D_s E_{\text{mass}}} \tag{13.55}$$

where

Q_u = ultimate load obtained from Eq. (13.52) (this assumes that the contribution of the overburden to the side shear is negligible)

A_c = cross-sectional area of the drilled shaft in the socket $= \frac{\pi}{4} D_s^2$

E_c = Young's modulus of the concrete and reinforcing steel in the shaft

E_{mass} = Young's modulus of the rock mass into which the socket is drilled

I_f = elastic influence coefficient (see Table 13.6)

The magnitude of E_{mass} can be taken as

$$\frac{E_{\text{mass}}}{E_{\text{core}}} \approx 0.0266\,(\text{RQD}) - 1.66 \tag{13.56}$$

where

RQD = rock quality designation in %

E_{core} = Young's modulus of intact specimens of rock cores of NW size or larger

However, unless the socket is very long

$$s_e \approx s_{e(b)} = \frac{Q_u I_f}{D_s E_{\text{mass}}} \tag{13.57}$$

Step 4. If s_e is less than 10 mm ($\approx$ 0.4 in.), the ultimate load-carrying capacity is that calculated by Eq. (13.52). If $s_e \geq$ 10 mm (0.4 in.), then go to Step 5.

TABLE 13.6 Settlement Influence Factor, I_f (Interpolated values from O'Neill and Reese, 1989)

	I_f			
	E_c/E_{mass}			
L/D_s	10	50	100	5000
0	1.10	1.10	1.10	1.10
1	0.51	0.47	0.47	0.47
2	0.47	0.37	0.35	0.32
4	0.43	0.31	0.28	0.23
6	0.41	0.27	0.24	0.18
8	0.40	0.25	0.21	0.14
10	0.39	0.24	0.18	0.12
12	0.38	0.22	0.16	0.10
20	0.37	0.20	0.15	0.08

Step 5. If $s_e \geq 10$ mm (0.4 in.), there may be rapid progressive side shear failure in the rock socket resulting in a complete loss of side resistance. In that case, the ultimate capacity is equal to the point resistance, or (for hard rocks such as limestone, schist, etc.). Thus,

$$Q_u = 3A_p \left[\frac{3 + \frac{c_s}{D_s}}{10\left(1 + 300\frac{\delta}{c_s}\right)^{0.5}} \right] q_u \tag{13.58}$$

where

c_s = spacing of discontinuities (same unit as D_s)

δ = thickness of individual discontinuity (same unit as D_s)

q_u = unconfined compression strength of the rock beneath the base of the socket or the drilled shaft concrete, whichever is smaller

Note that Eq. (13.58) applies for horizontally stratified discontinuities with $c_s > 305$ mm (12 in.) and $\delta < 5$ mm (0.2 in.).

PROCEDURE OF ZHANG AND EINSTEIN (1998)

Zhang and Einstein (1988) analyzed a database of 39 full-scale drilled shaft tests in which shaft bases were cast on or in generally *soft rock* with some degree of jointing. Based on these results, they proposed

$$Q_{u(\text{net})} = Q_p + Q_s = q_p A_p + fpL \tag{13.59}$$

where end bearing capacity Q_p can be expressed as

$$Q_p\,(\text{MN}) = q_p A_p = [4.83(q_u\,\text{MN/m}^2)^{0.51}]\,[A_p\,(\text{m}^2)] \tag{13.60}$$

Also, the side resistance Q_s is

$$Q_s\,(\text{MN}) = fpL = [0.4\,(q_u\,\text{MN/m}^2)^{0.5}]\,[\pi D_s\,(\text{m})]\,[L\,(\text{m})] \quad \text{(for smooth socket)} \tag{13.61}$$

and

$$Q_s\,(\text{MN}) = fpL = [0.8(q_u\,\text{MN/m}^2)^{0.5}][\pi D_s\,(\text{m})][L\,(\text{m})] \quad \text{(for rough socket)} \tag{13.62}$$

EXAMPLE 13.9

Consider the case of drilled shaft extending into rock, as shown in Figure 13.26. Let $L = 4.5$ m, $D_s = 0.9$ m, q_u (rock) = 72,450 kN/m^2, q_u (concrete) = 20,700 kN/m^2, $E_c = 20.7 \times 10^6$ kN/m^2, RQD (rock) = 80%, E_{core} (rock) = 2.48×10^6 kN/m^2, c_s = 457 mm, and $\delta = 3.81$ mm. Estimate the allowable load-bearing capacity of the drilled shaft. Use a factor of safety (FS) = 3. Use the Reese and O'Neill method.

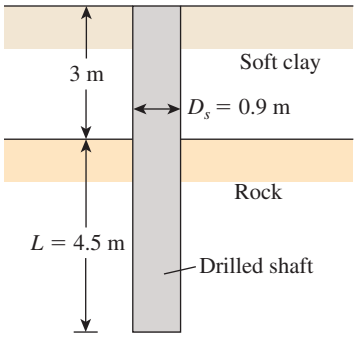


FIGURE 13.26 Drilled shaft extending into rock

SOLUTION

Step 1. From Eq. (13.51b),

$$f\ (\text{kN/m}^2) = 6.564\, q_u^{0.5} \leq 0.15 q_u$$

Since q_u (concrete) $<$ q_u (rock), use q_u (concrete) in Eq. (13.51b). Hence,

$$f = 6.564(20{,}700)^{0.5} = 944.4\ \text{kN/m}^2$$

As a check, we have

$$f = 0.15 q_u = (0.15)(20{,}700) = 3105\ \text{kN/m}^2 > 944.4\ \text{kN/m}^2$$

So use $f = 944.4\ \text{kN/m}^2$.

Step 2. From Eq. (13.52),

$$Q_u = \pi D_s L f = (\pi)(0.9)(4.5)(944.4) = 12{,}016\ \text{kN}$$

Step 3. From Eqs. (13.53), (13.54), and (13.55),

$$s_e = \frac{Q_u L}{A_c E_c} + \frac{Q_u I_f}{D_s E_{\text{mass}}}$$

From Eq. (13.56), for RQD = 80%,

$$\frac{E_{\text{mass}}}{E_{\text{core}}} = (0.0266)(80) - 1.66 = 0.468$$

$$E_{\text{mass}} = 0.468\, E_{\text{core}} = (0.468)(2.48 \times 10^6) = 1.16 \times 10^6\ \text{kN/m}^2$$

so

$$\frac{E_c}{E_{\text{mass}}} = \frac{20.7 \times 10^6}{1.16 \times 10^6} \approx 17.84$$

and

$$\frac{L}{D_s} = \frac{4.5}{0.9} = 5$$

From Table 13.6, for $E_c/E_{\text{mass}} = 17.84$ and $L/D_s = 5$, the magnitude of I_f is about 0.35. Hence,

$$s_e = \frac{(12{,}016)(4.5)}{\frac{\pi}{4}(0.9)^2(20.7 \times 10^6)} + \frac{(12{,}016)(0.35)}{(0.9)(1.16 \times 10^6)}$$

$$= 0.008128\ \text{m} \approx 8.13\ \text{mm} < 10\ \text{mm}$$

Therefore,

$$Q_u = 12{,}016\ \text{kN}$$

and

$$Q_{all} = \frac{Q_u}{FS} = \frac{12{,}016}{3} = 4005 \text{ kN} \approx \mathbf{4\ MN}$$

EXAMPLE 13.10

Figure 13.27 shows a drilled shaft extending into a shale formation. For the intact rock cores, given $q_u = 4.2$ MN/m^2. Estimate the allowable load-bearing capacity of the drilled shaft. Use a factor of safety (FS) = 3. Assume a smooth socket for side resistance. Use the Zhang and Einstein method.

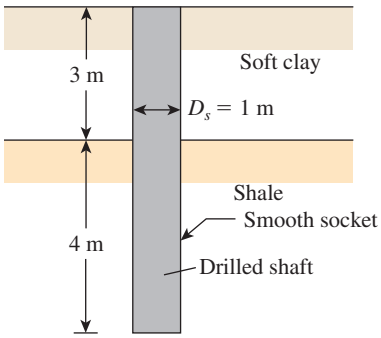


FIGURE 13.27 Drilled shaft extending into rock

SOLUTION

From Eq. (13.60),

$$Q_p = A_p\left[4.83(q_u)^{0.51}\right] = \frac{\pi}{4}(1)^2\left[(4.83)(4.2)^{0.51}\right] = 7.89 \text{ MN}$$

Again, from Eq. (13.61),

$$Q_s = 0.4(q_u)^{0.5}(\pi D_s L) = 0.4(4.2)^{0.5}[(\pi)(1)(4)] = 10.3 \text{ MN}$$

Hence,

$$Q_{all} = \frac{Q_u}{FS} = \frac{Q_p + Q_s}{FS} = \frac{7.89 + 10.3}{3} = \mathbf{6.06\ MN}$$

13.14 Summary

Drilled shafts are deep foundations, where holes excavated into the ground are filled with concrete and some reinforcement. The types of drilled shafts and the different construction methods were discussed in this chapter. This was followed by some discussion of the load transfer mechanisms in the drilled shafts and the methods for determining their load-carrying capacities in sand and clay. The load-carrying capacities can be determined solely from the bearing capacity considerations or from the allowable settlements. The lateral load-carrying capacity of drilled shafts and drilled shafts in rock was also discussed.

PROBLEMS

13.1 Figure P13.1 shows a drilled shaft in sand. Determine the maximum load that can be allowed on it. Assume $\delta' = 0.6\phi'$ and allow a factor of safety of 4. Use Berezantzev et al.'s Eq. (13.18) for computing the point load. What fraction of the load-carrying capacity is derived from the shaft?

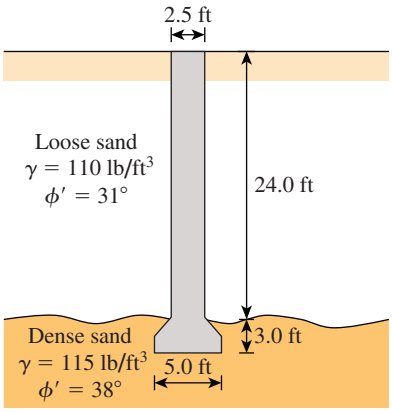


FIGURE P13.1

13.2 A straight drilled shaft 1.0 m in diameter and 15.0 m long is installed in a sand where $\phi' = 34°$ and $\gamma = 18.0$ kN/m^3.

- **a.** Determine the load-carrying capacity at the base using the Chen and Kulhawy (1994) method.
- **b.** Determine the load-carrying capacity at the base using the Berezantzev et al. (1961) method.
- **c.** Determine the load-carrying capacity of the shaft, assuming $\delta'/\phi' = 0.9$.
- **d.** With FS = 3, what would be the maximum load that can be allowed on the drilled shaft?

13.3 Figure P13.3 shows a drilled shaft with bell in a sandy soil. The soil properties are given in the figure.

- **a.** Determine the maximum load that can be allowed on the drilled shaft with a factor of safety of 4. Assume $\delta' = 0.5\phi'$. Use Eq. (13.18) for $Q_{p(\text{net})}$.
- **b.** What would be the allowable load if the settlement has to be limited to 15 mm?

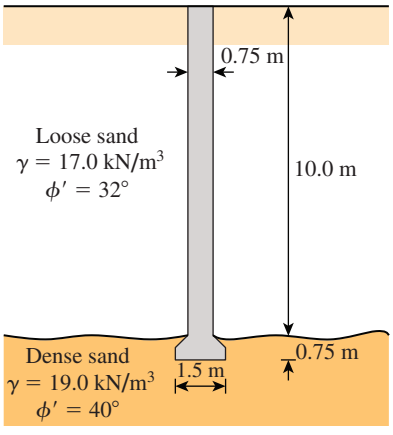


FIGURE P13.3

13.4 Determine the ultimate load-carrying capacity of the drilled shaft shown in Figure P13.4, using the Reese and O'Neill (1989) method.

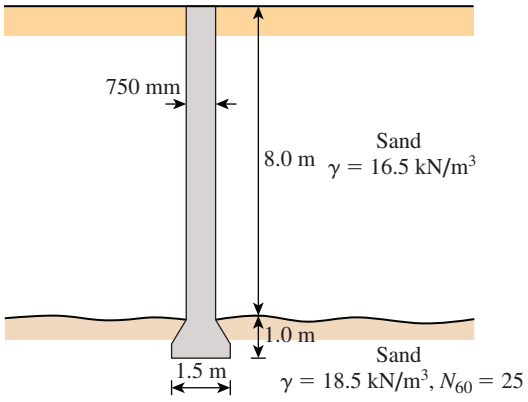


FIGURE P13.4

13.5 For the same data given in Problem 13.4, determine the load-carrying capacity of the drilled shaft, limiting the settlement to 10.0 mm.

13.6 The top 5 m in a site consists of a clay with $c_u = 80$ kN/m^2. This is underlain by a thick clay deposit with $c_u = 150$ kN/m^2. A 1.0 m diameter and 15 m long straight drilled shaft is constructed at this site. Determine the maximum load that can be allowed on this drilled shaft with a factor of safety of 3. Use Eqs. (13.33) and (13.37) to compute the point load and shaft load, respectively.

13.7 A 3 ft diameter straight drilled shaft is shown in Figure P13.7. Determine the load-carrying capacity of the drilled shaft with FS = 3. Take δ'/ϕ' as 0.8 for the sand.

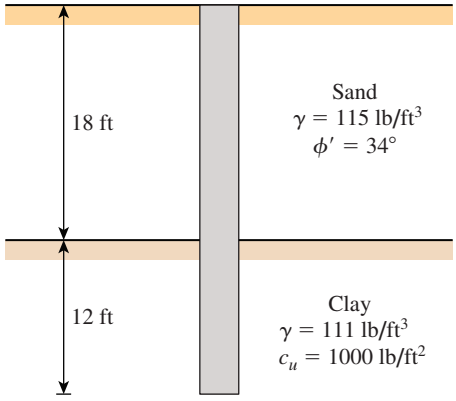


FIGURE P13.7

13.8 A straight drilled shaft of 2.5 ft diameter and 30 ft length is placed in a clay where $c_u = 2.4$ kip/ft^2, $E_s = 3600$ lb/in^2, and $\mu_s = 0.5$. When 220 kip is applied at the top, 160 kip is carried by the shaft and 60 kip is carried by the tip. Determine the settlement, assuming $\xi = 0.65$ and $E_p = 3.6 \times 10^6$ lb/in^2.

Determine $s_{e(2)}$ and $s_{e(3)}$, using the elastic equations [Eqs. (12.89) and (12.91)] and the semi-empirical relations [Eqs. (12.90) and (12.93)].

13.9 Figure P13.9 shows a drilled shaft extending into clay shale. Given: q_u (clay shale) = 1.81 MN/m^2. Considering the socket to be rough, estimate the allowable load-carrying capacity of the drilled shaft. Use FS = 4. Use the Zhang and Einstein procedure.

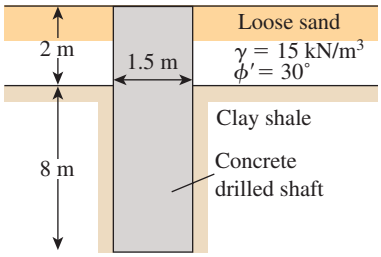


FIGURE P13.9

13.10 A free-headed drilled shaft is shown in Figure P13.10. Let Q_g = 260 kN, M_g = 0, γ = 17.5 kN/m^3, ϕ' = 35°, c' = 0, and $E_p = 22 \times 10^6$ kN/m^2. Determine

a. The ground line deflection, x_o
b. The maximum bending moment in the drilled shaft
c. The maximum tensile stress in the shaft
d. The minimum penetration of the shaft needed for this analysis

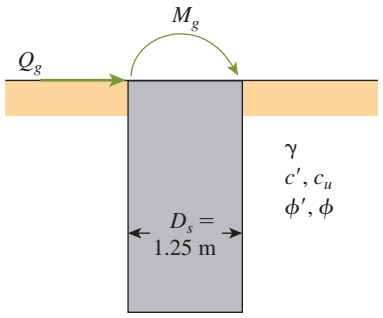


FIGURE P13.10

13.11 Refer to Figure P13.9. Assume the botton 8 m to be hard rock and the following values.

$q_{u(\text{concrete})}$ = 28,000 kN/m^2 $\quad$ $E_{(\text{concrete})} = 22 \times 10^6$ kN/m^2

$q_{u(\text{rock})}$ = 46,000 kN/m^2 $\quad$ $E_{\text{core(rock)}} = 12.1 \times 10^6$ kN/m^2

$\text{RQD}_{(\text{rock})}$ = 75%

Spacing of discontinuity in rock = 500 mm

Thickness of individual discontinuity in rock = 3 mm

Estimate the allowable load-bearing capacity of the drilled shaft using the procedure of Reese and O'Neill. Use FS = 3.

REFERENCES

Berezantzev, V. G., Khristoforov, V. S., and Golubkov, V. N. (1961). "Load-Bearing Capacity and Deformation of Piled Foundations," *Proceedings, Fifth International Conference on Soil Mechanics and Foundation Engineering*, Paris, Vol. 2, pp. 11–15.

Chen, Y.-J. and Kulhawy, F. H. (1994). "Case History Evaluation of the Behavior of Drilled Shafts under Axial and Lateral Loading," *Final Report, Project 1493-04, EPRI TR-104601*, Geotechnical Group, Cornell University, Ithaca, NY, December.

Duncan, J. M., Evans, L. T., Jr., and Ooi, P. S. K. (1994). "Lateral Load Analysis of Single Piles and Drilled Shafts," *Journal of Geotechnical Engineering*, ASCE, Vol. 120, No. 6, pp. 1018–1033.

Kulhawy, F. H. and Jackson, C. S. (1989). "Some Observations on Undrained Side Resistance of Drilled Shafts," *Proceedings, Foundation Engineering: Current Principles and Practices*, American Society of Civil Engineers, Vol. 2, pp. 1011–1025.

Matlock, H. and Reese, L. C. (1961). "Foundation Analysis of Offshore Pile-Supported Structures," *Proceedings, Fifth International Conference on Soil Mechanics and Foundation Engineering*, Vol. 2, Paris, pp. 91–97.

O'Neill, M. W. (1997). Personal communication.

O'Neill, M. W. and Reese, L. C. (1999). *Drilled Shafts: Construction Procedure and Design Methods*, FHWA Report No. IF-99-025.

Reese, L. C. and O'Neill, M. W. (1988). *Drilled Shafts: Construction and Design*, FHWA, Publication No. HI-88-042.

Reese, L. C. and O'Neill, M. W. (1989). "New Design Method for Drilled Shafts from Common Soil and Rock Tests," *Proceedings, Foundation Engineering: Current Principles and Practices*, American Society of Civil Engineers, Vol. 2, pp. 1026–1039.

Reese, L. C., Touma, F. T., and O'Neill, M. W. (1976). "Behavior of Drilled Piers under Axial Loading," *Journal of Geotechnical Engineering Division*, American Society of Civil Engineers, Vol. 102, No. GT5, pp. 493–510.

Rollins, K. M., Clayton, R. J., Mikesell, R. C., and Blaise, B. C. (2005). "Drilled Shaft Side Friction in Gravelly Soils," *Journal of Geotechnical and Geoenvironmental Engineering*, American Society of Civil Engineers, Vol. 131, No. 8, pp. 987–1003.

Whitaker, T. and Cooke, R. W. (1966). "An Investigation of the Shaft and Base Resistance of Large Bored Piles in London Clay," *Proceedings, Conference on Large Bored Piles*, Institute of Civil Engineers, London, pp. 7–49.

Zhang, L. and Einstein, H. H. (1998). "End Bearing Capacity of Drilled Shafts in Rock," *Journal of Geotechnical and Geoenvironmental Engineering*, American Society of Civil Engineers, Vol. 124, No. 7, pp. 574–584.

14

Piled Rafts: An Overview



1Roman Makedonsky/Shutterstock.com

14.1 Introduction 593

14.2 Load-Settlement Plots of Unpiled and Piled Rafts Under Different Design Conditions 594

14.3 Poulos–Davis–Randolph Simplified Design Method 595

14.4 Case Study: Burj Khalifa Tower in Dubai 600

14.5 Summary 602

PROBLEMS 602

REFERENCES 602

14.1 Introduction

Piled rafts optimize the advantages of pile foundations and raft foundations and have emerged as a way to provide economical foundation systems for very tall buildings, thereby satisfying the bearing capacity and settlement considerations in the best possible way. They are relatively new and are becoming increasingly popular. The Burj Khalifa tower in Dubai; the Petronas twin towers in Kuala Lumpur, Malaysia; and the Jeddah tower in Saudi Arabia are some of the prominent tall buildings that are built on piled rafts. As shown in Figure 14.1, the basement slab from the superstructure that is in contact with the soil and the numerous piles distributed over the footprint of the building act together with the raft in carrying the building load. As discussed later in this chapter, piles are used mainly to reduce settlement, but they also contribute to the bearing capacity.

Piled rafts are very effective in stiff clay and dense sand. They are not effective in loose sand, soft clay, or expansive soil and in situations where compressible layers are present at shallow depths.

RAFT ON PILE GROUP VERSUS GROUND-SUPPORTED PILED RAFT

There is a significant difference between a pile group and a piled raft. A pile group consists of a group of piles that are capped at the top by a pile cap made of reinforced concrete, which may or may not be in contact with the ground. While the pile cap often rests on the ground, in the case of offshore structures it is well above the ground level. It connects the pile heads together and transfers the column loads to the piles. The contribution of the pile cap to the bearing capacity is often ignored, even in circumstances where the cap is in contact with the soil, and the entire load is assumed to be carried by the piles.

The large dimensions of raft foundations make their bearing capacity relatively large in granular soil, enabling them to sustain loads at high contact pressure. The large dimensions of the raft and high contact pressures can make the settlement very large, so they exceed the tolerable limits, which are on the order of 50–100 mm

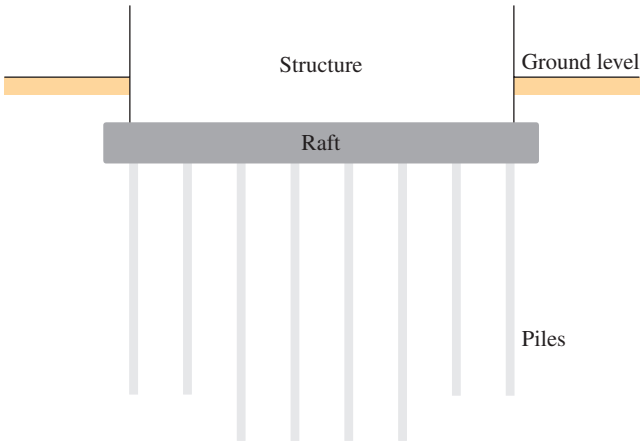


FIGURE 14.1 Piled raft

(2–4 in.) for rafts. By using piles with the raft, the settlement can be significantly reduced.

A piled raft is a raft foundation where a certain number of piles are located at the right places to reduce settlement. The major component of the bearing capacity comes from the raft, with the piles acting as *settlement reducers* by providing the necessary stiffness. Simply relying on piles without a raft would require more piles than a piled raft system needs. Piled rafts result in some reduction in the raft thickness and the bending moments and shear forces that would otherwise be present if the raft is placed without piles. In a piled raft, the raft typically carries about 20–40% of the total load applied.

14.2 Load-Settlement Plots of Unpiled and Piled Rafts Under Different Design Conditions

Randolph (1994) defined three different design philosophies for the design of piled rafts. Figure 14.2 shows the load-settlement plots for three curves (curves 1, 2, and 3), along with the case where the load is applied on a raft only (curve 0). These are discussed below to illustrate the advantages of piled rafts. For all four options, the design load is P_d, and the settlement has to be limited to S_a.

CURVE 0: RAFT ONLY

When the design load is carried only by the raft, the settlement exceeds the allowable value, but there is no problem with the bearing capacity. The raft may behave elastically in carrying the design load P_d.

CURVE 1: PILES DESIGNED WITH CONVENTIONAL FACTOR OF SAFETY PLUS RAFT

The piles are designed to carry most of the load with a conventional factor of safety (e.g., 2.0), allowing for a small fraction of the design load to be carried by the raft. The settlement is well within the limit. At the design load, the load-settlement plot is approximately linear. The bearing capacity is quite high, and the system could carry a larger load if not for the settlement, suggesting that the system is not fully utilized.

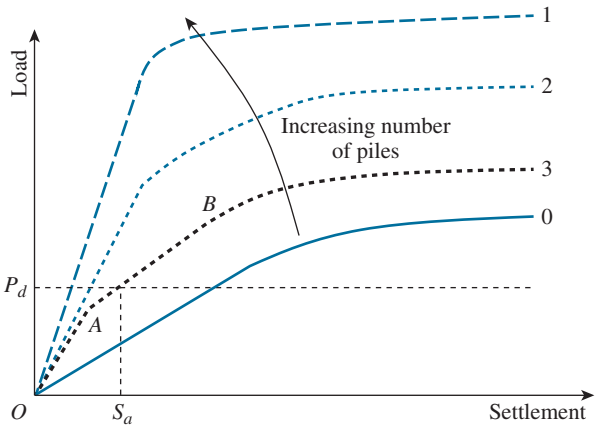


FIGURE 14.2 Load versus settlement for different scenarios (Based on Poulos, 2001)

CURVE 2: PILES DESIGNED WITH LOWER FACTOR OF SAFETY PLUS RAFT

The piles are designed to operate at lower factor of safety (e.g., 70–80% of the ultimate load capacity), so a smaller number of piles is required. The raft carries some of the design load. This situation is known as *creep piling*. Ideally, the number of piles should be selected to reduce the net contact pressure between the raft and the soil to below the preconsolidation pressure (Randolph, 1994).

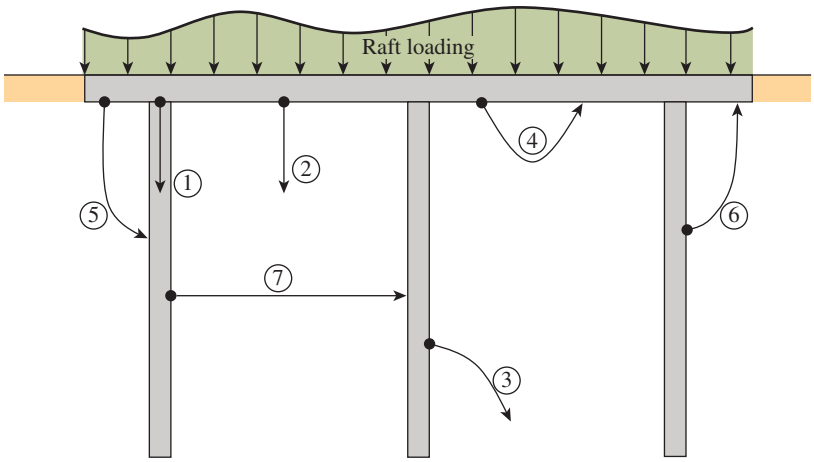
CURVE 3: PILES DESIGNED TO FULL CAPACITY PLUS RAFT

This is an extreme case of creep piling. All the piles are designed to operate at full capacity and yield, thus carrying the maximum possible load. The rest of the load is carried by the raft. The overall factor of safety of the piled raft system is adequate, and the settlement is less than the allowable limit. The piles act as settlement reducers and are located strategically in the heavily loaded areas to reduce differential settlements rather than the overall settlement. This gives a more economical solution than the others.

14.3 Poulos–Davis–Randolph Simplified Design Method

Three-way interaction takes place among the soil, pile, and the raft (Figure 14.3), which makes rigorous analysis of the problem very complex. The design requires more sophisticated modeling, such as a finite element analysis. Some simplified methods are adequate for the preliminary designs. Since settlements play a more important role than the bearing capacity in the design of piled rafts, we will focus more on the stiffness (K) defined as

$$\text{Stiffness } (K) = \frac{\text{Load } (P)}{\text{Settlement } (S)} \tag{14.1}$$



1 Raft–pile interaction
2 Raft–soil interaction
3 Pile–soil interaction
4 Raft–soil–raft interaction
5 Raft–soil–pile interaction
6 Pile–soil–raft interaction
7 Pile–soil–pile interaction

FIGURE 14.3 Soil–pile–raft interactions (Based on O'Brien et al., 2012)

The subscripts p and r refer to pile and raft, respectively. The approximate methods do not take the differential settlements into account.

The Poulos–Davis-Randolph (PDR) method suggests that the vertical bearing capacity of the piled raft may be taken as the lesser of the following:

a. The sum of the ultimate capacities of the raft and all piles
b. The ultimate capacity of the block containing the piles and the raft, plus the portion of the raft outside the perimeter of the piles

Figure 14.4 shows a simplified trilinear load-settlement plot $OABC$, represented by three straight line segments. Along OA, both the piles and the raft remain elastic, with the piles reaching their full capacity at A, where the total applied load on the piled raft is P_1. The slope of the line OA is the stiffness of the piled raft K_{pr}. At any point on OA, the total load (P_t) is shared by the raft (P_r) and the piles (P_p). (The subscripts p and r refer to pile and raft, respectively.) The relative proportion carried by the raft (X) is defined as

$$X = \frac{P_r}{P_t} = \frac{P_r}{P_r + P_p} \tag{14.2}$$

$$1 - X = \frac{P_p}{P_t} = \frac{P_p}{P_r + P_p} \tag{14.3}$$

where

$$P_t = P_p + P_r \tag{14.4}$$

If the ultimate load-carrying capacity of the piles alone is P_{up}, the load P_1 (see Figure 14.4) can be determined as

$$P_1 = \frac{P_{up}}{1 - X} \tag{14.5}$$

Based on elastic analysis, Clancy and Randolph (1996) define X as

$$X = \frac{K_r(1 - \alpha_{rp})}{K_p + K_r(1 - 2\alpha_{rp})} \tag{14.6}$$

where K_p is the stiffness of the pile group alone, K_r is the stiffness of the raft alone, and α_{rp} is the pile-raft interaction factor. Both K_r and K_p can be estimated from elastic theories (Fleming et al. 1992; Poulos and Davis, 1974). The piled raft stiffness K_{pr} is defined as (Poulos, 2001)

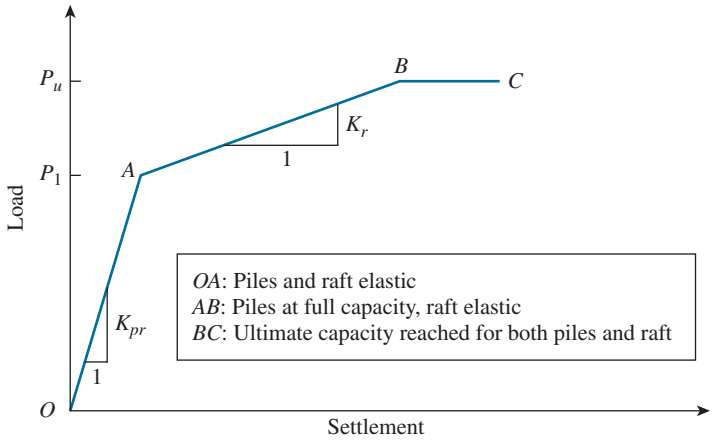


FIGURE 14.4 Simplified trilinear load-settlement plot for preliminary analysis (Based on Poulos, 2001)

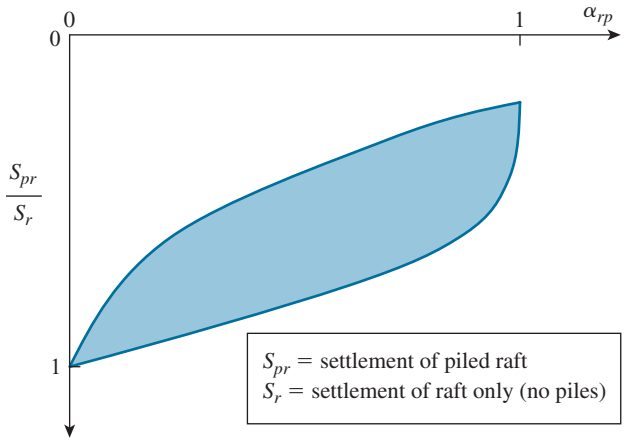


FIGURE 14.5 Qualitative illustration of possible settlement reduction and the value of α_{rp}

$$K_{pr} = \frac{K_p + K_r(1 - 2\alpha_{rp})}{1 - \alpha_{rp}^2 \dfrac{K_r}{K_p}} \tag{14.7}$$

The pile-raft interaction factor α_{rp} lies within the range of 0–1, with 0 when the structure is acting as a raft and 1 when it is acting as a fully piled foundation with no contact between the raft and the pile (e.g., offshore foundations). For the same raft size and soil conditions, α_{rp} depends on the number of piles, their lengths, and the stress level. Figure 14.5 shows the possible settlement reduction with the increasing value of α_{rp}.

From *A* to *B* in Figure 14.4, the piled raft relies only on the raft stiffness (K_r), as the piles have reached their full capacity at *A*. The raft behaves elastically along *AB*, where the slope is defined by the stiffness of the raft K_r, and it reaches its capacity at *B*. Beyond this the load-settlement plot is horizontal with no further capacity for any additional load. Until the pile capacity is fully mobilized at *A* (Figure 14.4), the piled raft stiffness (K_{pr}) can be used for determining the settlement along *OA*.

DETERMINATION OF α_{rp}

To determine the piled raft stiffness K_{pr}, it is necessary to determine the pile raft interaction factor α_{rp}.

Randolph (1994) proposed a simple piled-raft model shown in Figure 14.6, where a single pile is shown along with an equivalent raft or cap. The pile cap area

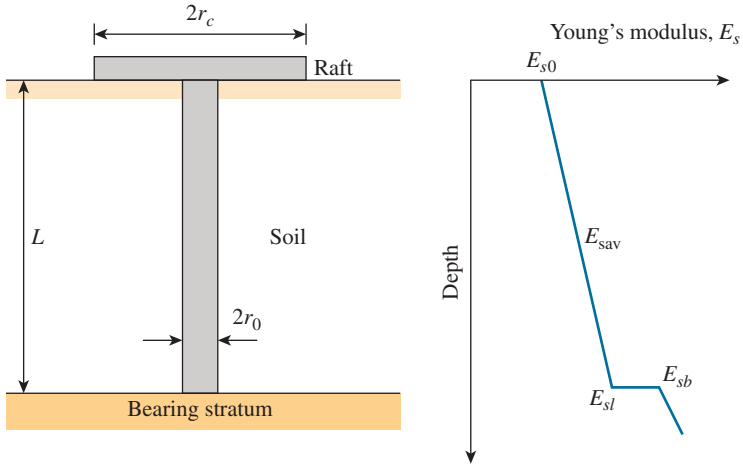


FIGURE 14.6 Simplified single pile-raft model proposed by Randolph (1994)

is defined as the raft area divided by the number of piles. In this figure the notations are as follows:

r_c = radius of pile cap (based on the raft area divided by the number of piles)

r_0 = radius of pile

L = pile length

E_{s0} = Young's modulus of the soil at the pile head

E_{sl} = Young's modulus of the soil at the pile tip

E_{sb} = Young's modulus of the bearing stratum below the pile tip

E_{sav} = average Young's modulus of the soil along the pile shaft

The pile–raft interaction factor α_{rp} can be determined as

$$\alpha_{rp} = 1 - \frac{\ln\left(\frac{r_c}{r_0}\right)}{\zeta} \tag{14.8}$$

where

$$\zeta = \ln\left(\frac{r_m}{r_0}\right) \tag{14.9}$$

The radius of influence of the pile r_m is defined as

$$r_m = \{0.25 + \xi[2.5\rho(1 - \mu_s) - 0.25]\}L \tag{14.10}$$

where

$$\xi = E_{sl}/E_{sb} \tag{14.11}$$

ρ is the inhomogeneity factor defined as

$$\rho = E_{\text{sav}}/E_{sl} \tag{14.12}$$

and μ_s is Poisson's ratio of the soil.

Some typical values used in the designs of tall buildings on piled rafts are as follows:

- Raft thickness = 2–4 m (≈ 6.5–13.0 ft)
- Pile spacing = 2.5–8.0 × pile diameter
- Slenderness ratio (length/diameter) = 10–100
- Pile load = 2–15 MN (≈ 225–1686 U.S. tons)
- Total building load = up to 5000 MN (≈ 562 × 10^3 U.S. tons)
- Observed maximum settlement = 50–150 mm (≈ 2–6 in.)
- Loading per floor
  - Residential buildings = 10 kN/m^2 (≈ 1.45 lb/in^2)
  - Office buildings = 12 kN/m^2 (≈ 1.75 lb/in^2)
  - Industrial buildings = 16 kN/m^2 (≈ 2.32 lb/in^2)
- Average contact pressure on the ground below the raft = 1–3 MN/m^2 (145–435 lb/in^2)
- Young's modulus of concrete = 30 GN/m^2 (435 × 10^4 lb/in^2)
- Modulus of subgrade reaction = 10–100 kN/m^2/mm (≈ 37–370 lb/in^2/in.)

EXAMPLE 14.1

It is proposed to build a 40-story building with a footprint of 1350 m^2 on a piled raft, with 1.0 m diameter bored piles placed at 3.0 m center to center. The average loading

per floor is about 12 kN/m^2. For the preliminary design, it can be assumed that the bored piles are distributed evenly.

a. How many bored piles will be required? What is the load per bored pile? Conservatively, neglect the contribution from the raft and assume that the entire building load is transferred to the piles.

b. Assuming uniform ground conditions, with a constant Young's modulus and Poisson's ratio of 0.25, estimate the pile-raft interaction factor α_{rp}, assuming the bored piles are 25 m long.

SOLUTION

Part a

$$\text{Weight of the building} = 40 \times 1350 \times 12 \text{ kN/m}^2 = 648 \text{ MN}$$

$$\text{Number of piles} = \frac{1350}{3 \times 3} = \mathbf{150}$$

$$\text{Load per pile} = \frac{648}{150} = \mathbf{4.32 \text{ MN}}$$

Part b

In uniform conditions, $\xi = 1$ and $\rho = 1$. From Eq. (14.10),

$$r_m = \{0.25 + 1[2.5 \times 1(1 - 0.25) - 0.25]\} \times 25 = 46.9 \text{ m}$$

From Eq. (14.9),

$$\xi = \ln\left(\frac{r_m}{r_0}\right) = \ln\left(\frac{46.9}{0.5}\right) = 4.54$$

The equivalent pile cap radius r_c can be determined as

$$\pi \times r_c^2 = \frac{1350}{150}; \; r_c = 1.69 \text{ m}$$

$$\alpha_{rp} = 1 - \frac{\ln\left(\frac{r_c}{r_0}\right)}{\xi} = 1 - \frac{\ln\left(\frac{1.69}{0.5}\right)}{4.54} = \mathbf{0.73}$$

■

EXAMPLE 14.2

In a piled raft, $K_p = 2500$ MN/m, $K_r = 800$ MN/m, and $\alpha_{rp} = 0.75$. Find the relative proportion of the load carried by the raft X and the stiffness of the piled raft K_{pr}.

SOLUTION

From Eq. (14.6),

$$X = \frac{K_r(1 - \alpha_{rp})}{K_p + K_r(1 - 2\alpha_{rp})} = \frac{800(1 - 0.75)}{2500 + 800(1 - 2 \times 0.75)} = 0.095$$

From Eq. (14.7),

$$K_{pr} = \frac{K_p + K_r(1 - 2\alpha_{rp})}{1 - \alpha_{rp}^2 \frac{K_r}{K_p}} = \frac{2500 + 800(1 - 2 \times 0.75)}{1 - 0.75^2 \frac{800}{2500}} = \mathbf{2561 \text{ MN/m}}$$

■

EXAMPLE 14.3

The simplified trilinear load-settlement plot of a piled raft is shown in Figure 14.7. The piles are designed to be utilized to their full capacity.

a. What are the values of K_{pr} and K_r used in this simplified model?
b. What is the settlement when the piles reach their full capacity?

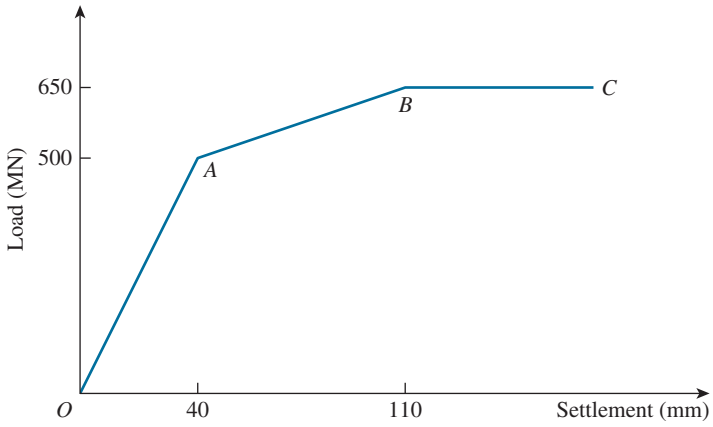


FIGURE 14.7 Simplified trilinear load settlement plot of the piled raft in Example 14.3

SOLUTION

Part a

K_{pr} and K_r are the slopes of the lines OA and AB, respectively. They are given by

$$K_{pr} = \frac{500}{40 \times 10^{-3}} = \mathbf{12{,}500\ MN/m}$$

$$K_r = \frac{650 - 500}{(110 - 40) \times 10^{-3}} = \mathbf{2143\ MN/m}$$

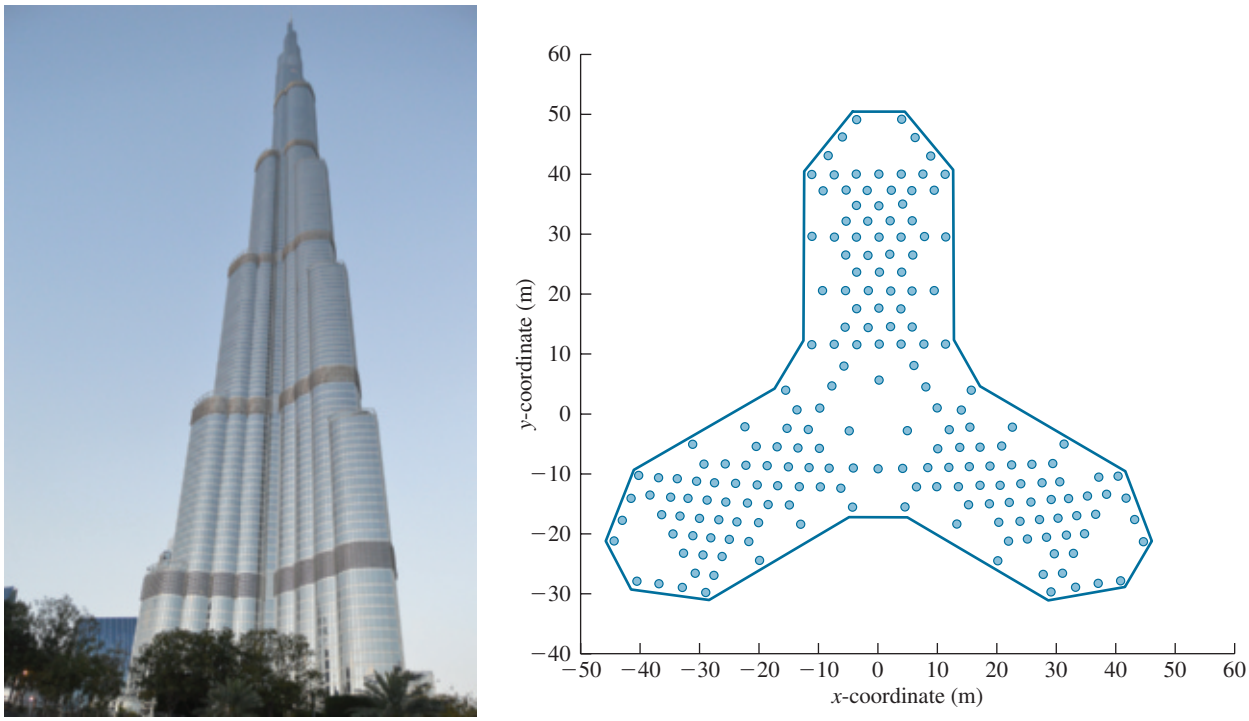
Part b

The piles reach their full capacity at A when the settlement is **40 mm**.

14.4 Case Study: Burj Khalifa Tower in Dubai

The Burj Khalifa Tower (Figure 14.8a), formerly known as Burj Dubai Tower, is presently the tallest building in the world. Located in Dubai, it was built at an approximate cost of $1.5 billion during the period 2004–2009. It consists of a 160 story and 828 m (≈ 2717 ft) high tower with a 4 to 6 story podium around the base. The podium also acts as a base, anchoring the tower to the ground. The triple-lobed footprint of the building (see Figure 14.8b) resembles a desert flower from the region, maximizes the views of the Persian Gulf, and provides good natural lighting. The entire construction used 330,000 m^3 (≈ 1166×10^4 ft^3) of concrete and 39,000 metric tons (≈ 86×10^6 lb) of rebar.

The site investigation was carried out in four stages during the second half of 2003, with a total of 33 boreholes extending to 60–90 m (≈ 197–295 ft), with one extending to 140 m (≈ 495 ft). Hundreds of standard penetration tests covering all boreholes and 60 pressuremeter tests limited to five boreholes were conducted, along with geophysical tests for measuring wave velocities and determining the soil profile.



(a) (b)

FIGURE 14.8 (a) Burj Khalifa Tower (Courtesy of Maher Omar, University of Sharjah, UAE); (b) piled raft showing the pile locations (Based on Poulos and Bunce, 2008)

The soil profile consisted of medium dense to very loose silty sand overlying weak calcareous sandstone interbedded with very weakly cemented sand, with the water table lying at 2.5 m (≈ 8.2 ft) below the ground level. The uniaxial compressive strength of the soil was on the order of 1–2 MN/m^2 (≈ 145–290 lb/in^2). The geotechnical consultant for the project, Hyder Consulting (UK), carried out the foundation design, which was verified by Coffey Geotechnics (Australia).

The foundation of the tower consists of a *piled raft* in which a 3.7 m (≈ 12.5 ft) thick raft is supported by 194 high-performance reinforced concrete bored piles of 1500 mm (≈ 59 in.) diameter and approximately 47.5 m (≈ 156 ft) length, with a minimum center-to-center spacing of 2.5 times the pile diameter; the piles were socketed into weak rock. Each bored pile had a capacity of 3000 metric tons (≈ 6614 kip). The raft and piles were made of self-compacting concrete with a water–cement ratio less than 0.30 and placed in a continuous pour using a tremie (Abdelrezaq, 2013). The podium area was supported by a 1.0 m (≈ 3.28 ft) thick piled raft on 734 bored piles of 900 mm (≈ 35.4 in.) diameter and 30 m (≈ 98 ft) in length. The construction of the raft and the bored piles required 12,500 m^3 (≈ 441.5 × 10^3 ft^3) and 32,500 m^3 (≈ 1148 × 10^3 ft^3) of concrete, respectively. High density low permeability concrete was used in the foundation, with a cathodic protection system under the raft to minimize corrosion. In piled raft systems, piles are used mainly to limit the settlement. One of the unique problems faced by the foundation designer(s) was the possibility of cyclic degradation of the skin friction due to the wind loads.

Static pile load tests were carried out on approximately 1% of the piles, which were loaded to 1.5 times the working load 4 weeks after construction. Dynamic pile load tests were carried out on approximately 5% of the piles.

Maximum long-term settlement is expected to be within 60 mm (≈ 2.36 in.). When the concrete structure of 156 stories was completed, 46 mm (≈ 1.81 in.) settlement was observed (Poulos and Bunce, 2008). Above the 156th floor, the structure is

a steel-braced frame that was topped by a 208 m (≈683 ft) long spire that tapers to 1.2 m (≈3.94 in.) diameter at the top (Abdelrazaq, 2013).

The excavation started in 2004, with piling commencing in February 2004, and the entire work was completed by December 2009.

14.5 Summary

Piled rafts optimize the advantages of piles and rafts and have emerged as the preferred solutions for tall buildings. The pile–raft–soil interaction is quite complex and often requires sophisticated computer modeling to carry out the detailed design. A simplified trilinear load-settlement plot was discussed in this chapter; this plot can be used to illustrate the load transfer in a simple way and can be used in the preliminary designs.

PROBLEMS

14.1 A piled raft has the pile-raft interaction factor $\alpha_{rp} = 0.85$. Determine the relative proportions of the loads carried by the piles and the raft in terms of K_r and K_p. Also, determine the stiffness of the piled raft in terms of K_r and K_p.

14.2 In a piled raft, 450 mm diameter and 13 m long piles are placed in a rectangular grid at 1.60 m × 1.63 m spacing. Find the pile-raft interaction factor α_{rp}, assuming uniform soil conditions with depth and $\mu_s = 0.1$

14.3 For the piled raft in Problem 14.2, if $K_r = 3250$ MN/m and $K_p = 5300$ MN/m, find K_{pr} and X, the fraction of the load carried by the raft.

14.4 In the piled raft described in Problems 14.2 and 14.3, if the design load is 345 MN, what would be the settlement?

14.5 In the piled raft described in Problems 14.2 and 14.3, the ultimate load-carrying capacity of the piles is estimated as 500 MN. What would be the total load on the piled raft when the piles are at their full capacity? What would be the settlement?

14.6 Prepare a case study on the new Kingdom Tower in Saudi Arabia, which will be the tallest building in the world when completed.

REFERENCES

Abdelrazaq, A. (2013). "Early Planning for the Concrete Work at Burj Khalifa, Dubai, UAE," *Proceedings of the R.N. Raikar Memorial International Conference on Advances in Science & Technology of Concrete*, Mumbai, India, pp. 21–29.

Fleming, W. G. K., Weltman, A. J., Randolph, M. F., and Elson, W. K. (1992). *Piling Engineering*, Blackie, Glasgow.

O'Brien, A. S., Burland, J. B., and Chapman, T. (2012). "Rafts and Piled Rafts," Chapter 6, *ICE Manual of Geotechnical Engineering*, Eds. J. Burland, T. Chapman, H. Skinner, and M. Brown, Institution of Civil Engineers, UK.

Poulos, H. G. (2001). "Pile Raft Foundations: Design and Applications," *Geotechnique*, Vol. 51, No. 2, pp. 95–113.

Poulos, H. G. and Bunce, G. (2008). "Foundation Design for the Burj Dubai—The World's Tallest Building," *Proceedings 6th International Conference on Case Histories in Geotechnical Engineering*, Paper 1.47.

Poulos, H. G. and Davis, E. H. (1974). *Elastic Solutions for Soil and Rock Mechanics*, Wiley, Chichester.

Randolph, M. F. (1994). Design Methods for Pile Groups and Piled Rafts. S.O.A. Report, *13th ICSMFE*, New Delhi, Vol. 5, pp. 61–82.

15

Foundations on Difficult Soil



CHAIYA/Shutterstock.com

15.1 Introduction 604
15.2 Definition and Types of Collapsible Soil 604
15.3 Physical Parameters for Identification 606
15.4 Procedure for Calculating Collapse Settlement 608
15.5 Foundations in Soil Not Susceptible to Wetting 609
15.6 Foundations in Soil Susceptible to Wetting 611
15.7 General Nature of Expansive Soil 612
15.8 Unrestrained Swell Test 615
15.9 Swelling Pressure Test 617
15.10 Classification of Expansive Soil on the Basis of Index Tests 621
15.11 Foundation Considerations for Expansive Soil 624
15.12 Construction on Expansive Soil 626
15.13 General Nature of Sanitary Landfills 630
15.14 Settlement of Sanitary Landfills 631
15.15 Summary 633
PROBLEMS 633
REFERENCES 634

15.1 Introduction

In many areas of the United States and other parts of the world, certain soil make the construction of foundations extremely difficult. For example, expansive or collapsible soil may cause high differential movements in structures through excessive heave or settlement. Similar problems can also arise when foundations are constructed over sanitary landfills. Foundation engineers must be able to identify difficult soil when they are encountered in the field. Although not all the problems caused by all soil can be solved, preventive measures can be taken to reduce the possibility of damage to structures built on them. This chapter outlines the fundamental properties of three major soil conditions—collapsible soil, expansive soil, and sanitary landfills—and methods of careful construction of foundations.

Collapsible Soil

15.2 Definition and Types of Collapsible Soil

Collapsible soil, which are sometimes referred to as *metastable soil*, are unsaturated soil that undergo a large change in volume upon saturation. The change may or may not be the result of the application of additional load. The behavior of collapsing soil under load is best explained by the typical void ratio versus effective pressure plot (e against log σ') for a collapsing soil, as shown in Figure 15.1. In branch ab, the vertical stress is increased to σ'_w, and the soil compresses at the natural water content to the void ratio of e_1. At this stage, the soil is not necessarily saturated and is in equilibrium under the effective stress of σ'_w at the void ratio e_1. If the soil is saturated by introducing water, the soil structure collapses to attain a lower void ratio of e_2, while the effective stress remains the same and the soil is in equilibrium. Now, cd is the branch of the e–log σ' curve under additional load after saturation. Foundations that are constructed on such soil may undergo large and sudden settlement if the soil under them becomes saturated with an unanticipated supply of moisture. The moisture may come from any of several sources, such as (a) broken water pipelines, (b) leaky sewers, (c) drainage from reservoirs and swimming pools, (d) a slow increase in groundwater, and so on. This type of settlement generally causes considerable structural damage. Hence, identifying collapsing soil during field exploration is crucial.

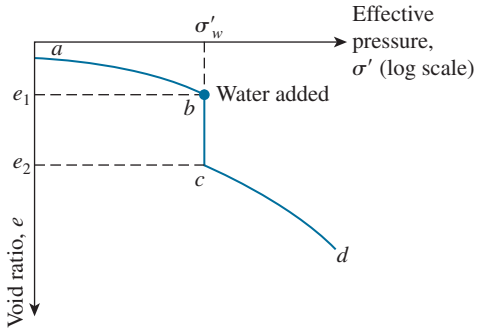


FIGURE 15.1 Nature of variation of void ratio with pressure for a collapsing soil

The majority of naturally occurring collapsing soil are *aeolian*—that is, wind-deposited sand or silt, such as loess, aeolic beaches, and volcanic dust deposits. The deposits have high void ratios and low unit weights and are cohesionless or only slightly cohesive. *Loess* deposits have silt-sized particles. The cohesion in loess may be the result of clay coatings surrounding the silt-size particles. The coatings hold the particles in a rather stable condition in an unsaturated state. The cohesion also may be caused by the presence of chemical precipitates leached by rainwater. When the soil becomes saturated, the clay binders lose their strength and undergo a structural collapse. In the United States, large parts of the Midwest and the arid West have such types of deposit. Loess deposits are also found over 15 to 20% of Europe and over large parts of China. The thickness of loess deposits can range up to about 10 m (33 ft) in the central United States. In parts of China it can be up to 100 m (330 ft). Figure 15.2 shows the extent of the loess deposits in the Mississippi River basin.

Many collapsing soil may be residual soil that are products of the weathering of parent rocks. Weathering produces soil with a large range of particle-size distribution. Soluble and colloidal materials are leached out by weathering, resulting in large void ratios and thus unstable structures. Many parts of South Africa and Zimbabwe have residual soil that are decomposed granites. Sometimes collapsing soil deposits may be left by flash floods and mudflows. These deposits dry out and are poorly consolidated. An excellent review of collapsing soil is that of Clemence and Finbarr (1981).



FIGURE 15.2 Loess deposit in Mississippi River basin

15.3 Physical Parameters for Identification

Several investigators have proposed various methods for evaluating the physical parameters of collapsing soil for identification. Some of these methods are discussed briefly in Table 15.1.

Jennings and Knight (1975) suggested a procedure for describing the *collapse potential* of a soil: An undisturbed soil specimen is taken at its natural moisture content in a consolidation ring. Step loads are applied to the specimen up to a pressure level σ'_w of 200 kN/m^2 ($\approx$ 29 lb/in^2). (In Figure 15.1, this is σ'_w.) At that pressure, the specimen is flooded for saturation and left for 24 hours. This test defines the void

TABLE 15.1 Reported Criteria for Identification of Collapsing Soil[a]

Investigator	Year	Criteria
Denisov	1951	Coefficient of subsidence: $K = \frac{\text{void ratio at liquid limit}}{\text{natural void ratio}}$ K = 0.5–0.75: highly collapsible K = 1.0: noncollapsible loam K = 1.5–2.0: noncollapsible soil
Clevenger	1958	If dry unit weight is less than 12.6 kN/m^3 ($\approx$ 80 lb/ft^3), settlement will be large; if dry unit weight is greater than 14 kN/m^3 ($\approx$ 90 lb/ft^3), settlement will be small.
Priklonski	1952	$K_D = \frac{\text{natural moisture content} - \text{plastic limit}}{\text{plasticity index}}$ $K_D < 0$: highly collapsible soil $K_D > 0.5$: noncollapsible soil $K_D > 1.0$: swelling soil
Gibbs	1961	Collapse ratio, $R = \frac{\text{saturation moisture content}}{\text{liquid limit}}$ This was put into graph form.
Soviet Building Code	1962	$L = \frac{e_o - e_L}{1 + e_o}$ where e_o = natural void ratio and e_L = void ratio at liquid limit. For natural degree of saturation less than 60%, if $L > -0.1$, the soil is a collapsing soil.
Feda	1964	$K_L = \frac{w_o}{S_r} - \frac{\text{PL}}{\text{PI}}$ where w_o = natural water content, S_r = natural degree of saturation, PL = plastic limit, and PI = plasticity index. For $S_r < 100\%$, if $K_L > 0.85$, the soil is a subsident soil.
Benites	1968	A dispersion test in which 2 g of soil are dropped into 12 ml of distilled water and specimen is timed until dispersed; dispersion times of 20 to 30 s were obtained for collapsing Arizona soil.
Handy	1973	Iowa loess with clay (<0.002 mm) contents: <16%: high probability of collapse 16–24%: probability of collapse 24–32%: less than 50% probability of collapse >32%: usually safe from collapse

[a]Based on data from Lutenegger and Saber (1988)

ratios e_1 and e_2 before and after flooding, respectively. The collapse potential may now be calculated as

$$C_p(\%) = \Delta\varepsilon = \frac{e_1 - e_2}{1 + e_o} \times 100 \tag{15.1}$$

where

e_o = natural void ratio of the soil

$\Delta\varepsilon$ = vertical strain

The stress level at which the saturation is initiated has a significant influence on the collapse potential. Stress levels in the range of 50 to 600 kPa (7 to 87 lb/in^2) have been reported in the literature. Lutenegger and Saber (1988) suggested applying a 300 kN/m^2 (43.5 lb/in^2) surcharge and replacing e_o in Eq. (15.1) by e_1, the void ratio just before saturation. Caution must be exercised in comparing C_p values determined under different stress levels.

The severity of foundation problems associated with a collapsible soil has been correlated with the collapse potential C_p by Jennings and Knight (1975). These problems were summarized by Clemence and Finbarr (1981) and are given in Table 15.2.

Holtz and Hilf (1961) suggested that a loessial soil that has a void ratio large enough to allow its moisture content to exceed its liquid limit upon saturation is susceptible to collapse. So, for collapse,

$$w_{(\text{saturated})} \geq \frac{\text{LL}(\%)}{100} \tag{15.2}$$

where LL = liquid limit.

However, for saturated soil,

$$e_o = wG_s \tag{15.3}$$

where G_s = specific gravity of soil solids.

Combining Eqs. (15.2) and (15.3) for collapsing soil yields

$$e_o \geq \left(\frac{\text{LL}}{100}\right)(G_s) \tag{15.4}$$

The natural dry unit weight of the soil required for its collapse is

$$\gamma_d \leq \frac{G_s\gamma_w}{1 + e_o} = \frac{G_s\gamma_w}{1 + \left(\frac{\text{LL}}{100}\right)(G_s)} \tag{15.5}$$

For an average value of $G_s = 2.65$, the limiting values of γ_d for various liquid limits may now be calculated from Eq. (15.5).

Figure 15.3 shows a plot of the preceding limiting values of dry unit weights against the corresponding liquid limits. For any soil, if the natural dry unit weight falls below the limiting line, the soil is likely to collapse.

TABLE 15.2 Relation of Collapse Potential to the Severity of Foundation Problems[a]

C_p (%)	Severity of problem
0–1	No problem
1–5	Moderate trouble
5–10	Trouble
10–20	Severe trouble
20	Very severe trouble

[a]Based on data from Clemence, S. P., and Finbarr, A. O. (1981). "Design Considerations for Collapsible Soils," *Journal of the Geotechnical Engineering Division*, American Society of Civil Engineers, Vol. 107, GT3 pp. 305–317.

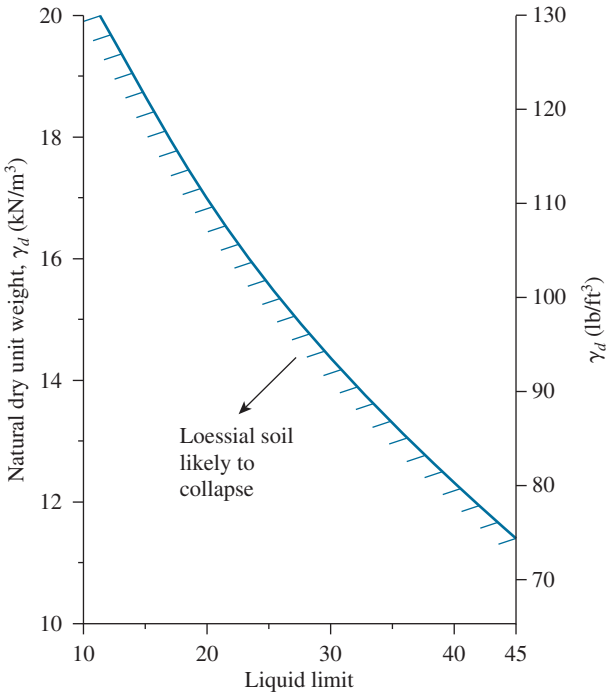


FIGURE 15.3 Loessial soil likely to collapse

Care should be taken to obtain undisturbed samples for determining the collapse potentials and dry unit weights—preferably block samples cut by hand. The reason is that samples obtained by thin-walled tubes may undergo some compression during the sampling process. However, if cut block samples are used, the boreholes should be made *without water*.

15.4 Procedure for Calculating Collapse Settlement

Jennings and Knight (1975) proposed the following laboratory procedure for determining the collapse settlement of structures upon saturation of soil:

Step 1. Obtain *two* undisturbed soil specimens for tests in a standard consolidation test apparatus (oedometer).

Step 2. Place the two specimens under 1 kN/m^2 (0.15 lb/in^2) pressure for 24 hours.

Step 3. After 24 hours, saturate one specimen by flooding. Keep the other specimen at its natural moisture content.

Step 4. After 24 hours of flooding, resume the consolidation test on both specimens by doubling the load (the same as in the standard consolidation test) to the desired pressure level.

Step 5. Plot the e–log σ' graphs for both specimens (Figures 15.4a and b).

Step 6. Calculate the *in situ* effective pressure, σ'_o. Draw a vertical line corresponding to the pressure σ'_o.

Step 7. From the e–log σ'_o curve of the soaked specimen, determine the preconsolidation pressure, σ'_c. If σ'_c/σ'_o is 0.8 to 1.5, the soil is normally consolidated; however, if $\sigma'_c/\sigma'_o > 1.5$, the soil is overconsolidated.

Step 8. Determine e'_o, corresponding to σ'_o from the e–log σ'_o curve of the soaked specimen. (This procedure for normally consolidated and overconsolidated soil is shown in Figures 15.4a and b, respectively.)

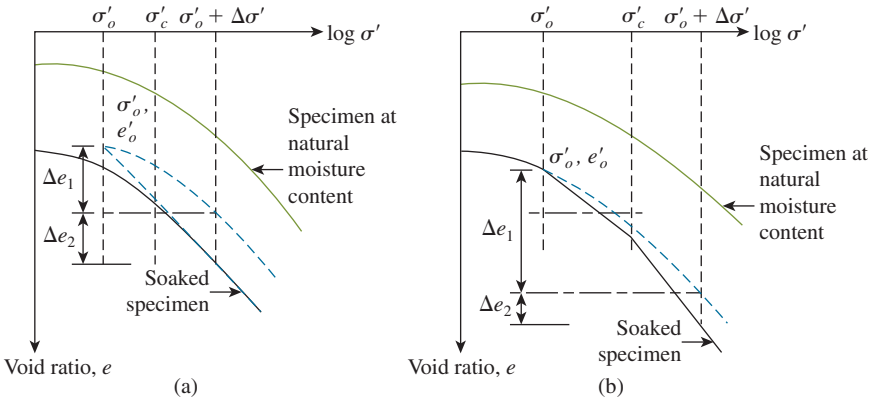


FIGURE 15.4 Settlement calculation from double oedometer test: (a) normally consolidated soil; (b) overconsolidated soil

Step 9. Through point (σ'_o, e'_o) draw a curve that is similar to the e–log σ'_o curve obtained from the specimen tested at its natural moisture content.

Step 10. Determine the incremental pressure, $\Delta\sigma'$, on the soil caused by the construction of the foundation. Draw a vertical line corresponding to the pressure of $\sigma'_o + \Delta\sigma'$ in the e–log σ' curve.

Step 11. Now, determine Δe_1 and Δe_2. The settlement of soil without change in the natural moisture content is

$$S_{c(1)} = \frac{\Delta e_1}{1 + e'_o}(H) \tag{15.6}$$

where H = thickness of soil susceptible to collapse.

Also, the settlement caused by collapse in the soil structure is

$$S_{c(2)} = \frac{\Delta e_2}{1 + e'_o}(H) \tag{15.7}$$

15.5 Foundations in Soil Not Susceptible to Wetting

For actual foundation design purposes, some standard field load tests may also be conducted. Figure 15.5 shows the relation of the nature of load per unit area versus settlement in a field load test in a loessial deposit. Note that the load-settlement

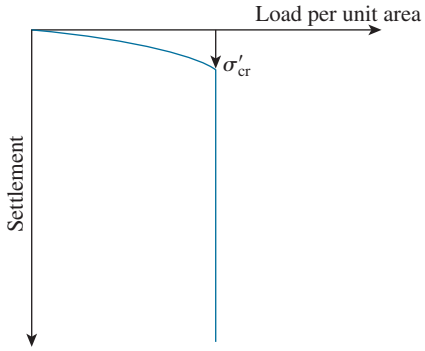


FIGURE 15.5 Field load test in loessial soil: load per unit area versus settlement

relationship is essentially linear up to a certain critical pressure, σ'_{cr}, at which there is a breakdown of the soil structure and hence a large settlement. Sudden breakdown of soil structure is more common with soil having a high natural moisture content than with normally dry soil.

If enough precautions are taken in the field to prevent moisture from increasing under structures, spread footings and mat foundations may be built on collapsible soil. However, the footings must be proportioned so that the critical stresses (see Figure 15.5) in the field are never exceeded. A factor of safety of about 2.5 to 3 should be used to calculate the allowable soil pressure, or

$$\sigma'_{all} = \frac{\sigma'_{cr}}{FS} \tag{15.8}$$

where

σ'_{all} = allowable soil pressure

FS = factor of safety

The differential and total settlements of these footings should be similar to those of foundations designed for sandy soil.

Continuous foundations may be safer than isolated footings over collapsible soil in that they can effectively minimize differential settlement. Figure 15.6 shows a typical procedure for constructing continuous foundations. This procedure uses footing beams and longitudinal load-bearing beams.

In the construction of heavy structures, such as grain elevators, over collapsible soil, settlements up to about 0.3 m (≈1 ft) are sometimes allowed (Peck et al., 1974). In this case, tilting of the foundation is not likely to occur, because there is no eccentric loading. The total expected settlement for such structures can be estimated from standard consolidation tests on specimens at field moisture content. Without eccentric loading, the foundations will exhibit uniform settlement over loessial deposits; however, if the soil is of residual or colluvial nature, settlement may not be uniform. The reason is the nonuniformity generally encountered in residual soil.

Extreme caution must be exercised in building heavy structures over collapsible soil. If large settlements are expected, drilled-shaft or pile foundations should be considered. These types of foundation can transfer the load to a stronger load-bearing stratum.

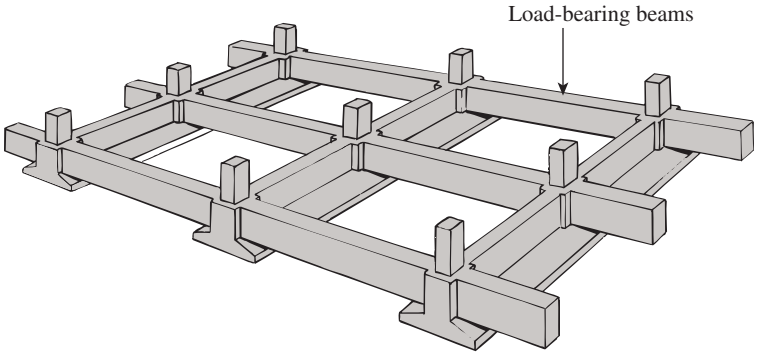


FIGURE 15.6 Continuous foundation with load-bearing beams (Based on data from Clemence, S. P., and Finbarr, A. O. (1981). "Design Considerations for Collapsible Soils," *Journal of the Geotechnical Engineering Division*, American Society of Civil Engineers, Vol. 107, GT3, pp. 305–317.)

15.6 Foundations in Soil Susceptible to Wetting

If the upper layer of soil is likely to get wet and collapse sometime after construction of the foundation, several design techniques to avoid failure of the foundation may be considered. They are as follows.

DYNAMIC COMPACTION

If the expected depth of wetting is about 1.5 to 2 m (≈5 to 6.5 ft) from the ground surface, the soil may be moistened and recompacted by heavy rollers. Spread footings and mats may be constructed over the compacted soil. An alternative to recompaction by heavy rollers is *heavy tamping*, which is sometimes referred to as *dynamic compaction*. (See Chapter 5.) Heavy tamping consists primarily of dropping a heavy weight repeatedly on the ground. The height of the drop can vary from 8 to 30 m (≈25 to 100 ft). The stress waves generated by the dropping weight help in the densification of the soil.

Lutenegger (1986) reported the use of dynamic compaction to stabilize a thick layer of friable loess before construction of a foundation in Russe, Bulgaria. During field exploration, the water table was not encountered to a depth of 10 m (33 ft), and the natural moisture content was below the plastic limit. Initial density measurements made on undisturbed soil specimens indicated that the moisture content at saturation would exceed the liquid limit, a property usually encountered in collapsible loess. For dynamic compaction of the soil, the upper 1.7 m (5.6 ft) of crust material was excavated. A circular concrete weight of 133 kN (≈15 ton) was used as a hammer. At each grid point, compaction was achieved by dropping the hammer 7 to 12 times through a vertical distance of 2.5 m (8.2 ft).

Figure 15.7 shows the dry unit weight of the soil before and after compaction. The increase in dry unit weight of the soil shows that dynamic compaction can be used effectively to stabilize collapsible soil.

CHEMICAL STABILIZATION

If conditions are favorable, foundation trenches can be flooded with solutions of sodium silicate and calcium chloride to stabilize the soil chemically. The soil will then behave like a soft sandstone and resist collapse upon saturation. This method

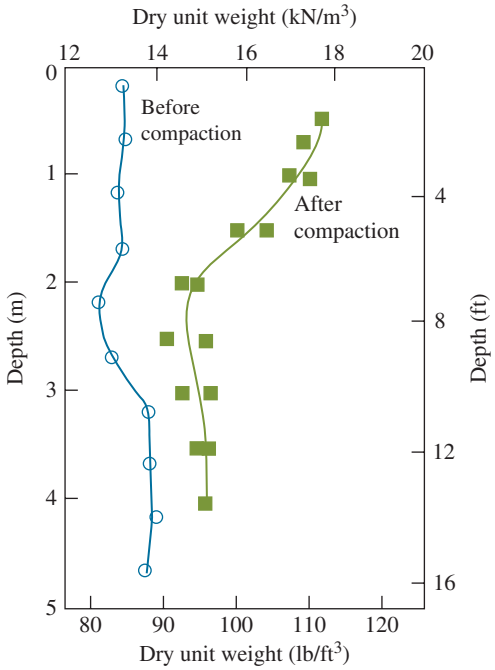


FIGURE 15.7 Dynamic compaction of a friable loess layer in Russe, Bulgaria (Based on Lutenegger, 1986)

is successful only if the solutions can penetrate to the desired depth; thus, it is most applicable to fine sand deposits. Silicates are rather costly and are not generally used. However, in some parts of Denver, silicates have been used successfully.

The injection of a sodium silicate solution to stabilize collapsible soil deposits has been used extensively in the former Soviet Union and Bulgaria (Houston and Houston, 1989). This process, which is used for dry collapsible soil and for wet collapsible soil that are likely to compress under the added weight of the structure to be built, consists of three steps:

Step 1. Injection of carbon dioxide to remove any water that is present and to perform preliminary activation of the soil

Step 2. Injection of sodium silicate grout

Step 3. Injection of carbon dioxide to neutralize alkalies

VIBROFLOTATION AND PONDING

When the soil layer is susceptible to wetting to a depth of about 10 m (≈30 ft), several techniques may be used to cause collapse of the soil *before* construction of the foundation is begun. Two of these techniques are *vibroflotation* and *ponding* (also called *flooding*). Vibroflotation is used successfully in free-draining soil. (See Chapter 5.) Ponding—by constructing low dikes—is utilized at sites that have no impervious layers. However, even after saturation and collapse of the soil by ponding, some additional settlement of the soil may occur after construction of the foundation is begun. Additional settlement may also be caused by incomplete saturation of the soil at the time of construction. Ponding may be used successfully in the construction of earth dams.

EXTENDING FOUNDATION BEYOND ZONE OF WETTING

If precollapsing the soil is not practical, foundations may be extended beyond the zone of possible wetting, although the technique may require drilled shafts or piles. The design of drilled shafts and piles must take into consideration the effect of negative skin friction resulting from the collapse of the soil structure and the associated settlement of the zone of subsequent wetting.

In some cases, a *rock-column type of foundation* (*vibroreplacement*) may be considered. Rock columns are built with large boulders that penetrate the collapsible soil layer. They act as piles in transferring the load to a more stable soil layer.

Expansive Soil

15.7 General Nature of Expansive Soil

Many plastic clays swell considerably when water is added to them and then shrink with the loss of water. Foundations constructed on such clays are subjected to large uplifting forces caused by the swelling. These forces induce heaving, cracking, and the breakup of both building foundations and slab-on-grade members. Figure 15.8 shows the cracks in a wall due to excessive heaving. Expansive clays cover large parts of the United States, South America, Africa, Australia, and India. In the United States, these clays are predominant in Texas, Oklahoma, and the upper Missouri Valley. In general, expansive clays have liquid limits and plasticity indices greater than about 40 and 15, respectively.

As noted, the increase and decrease in moisture content causes clay to swell and shrink. Figure 15.9 shows shrinkage cracks on the ground surface of a clay



FIGURE 15.8 Cracks in a wall due to heaving of an expansive clay (Courtesy of Anand Puppala, University of Texas at Arlington, Arlington, Texas)



FIGURE 15.9 Shrinkage cracks on ground surface in a clay weathered from the Eagle Ford shale formation in the Dallas–Fort Worth area (Courtesy of Thomas M. Petry, Missouri University of Science and Technology, Rolla, Missouri)

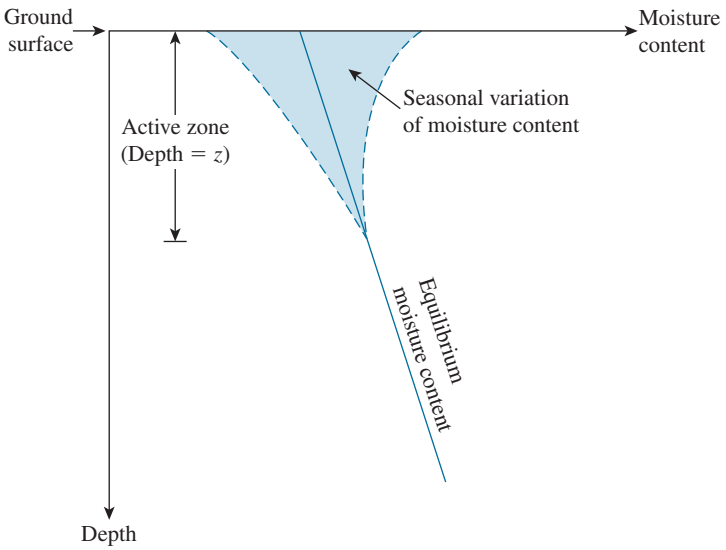


FIGURE 15.10 Definition of active zone

weathered from the Eagle Ford shale formation in the Dallas–Fort Worth, Texas area. The depth in a soil to which periodic changes of moisture occur is usually referred to as the *active zone* (see Figure 15.10). The fluctuation in the moisture content is highest near the ground level. The depth of the active zone varies, depending on the location of the site. Some typical active-zone depths in American cities are given in Table 15.3. In some clays and clay shales in the western United States, the depth of the active zone can be as much as 15 m (≈50 ft). The active-zone depth can easily be determined by plotting the liquidity index against the depth of the soil profile over several seasons. Figure 15.11 shows such a plot for the Beaumont formation in the Houston area.

Shrinkage cracks can extend deep into the active zone. Figure 15.12 shows interconnected shrinkage cracks extending from the ground surface into the active zone in an expansive clay.

To study the magnitude of possible swell in a clay, simple laboratory oedometer tests can be conducted on undisturbed specimens. Two common tests are the *unrestrained swell test* and the *swelling pressure test*. They are described in the following sections.

TABLE 15.3 Typical Active-Zone Depths in Some U.S. Cities[a]

City	Depth of active zone (m)	Depth of active zone (ft)
Houston	1.5 to 3	5 to 10
Dallas	2.1 to 4.6	7 to 15
San Antonio	3 to 9	10 to 30
Denver	3 to 4.6	10 to 15

[a]Based on data from O'Neill and Poormoayed (1980) (O'Neill, M. W., and Poormoayed, N. (1980). "Methodology for Foundations on Expansive Clays," *Journal of the Geotechnical Engineering Division*, American Society of Civil Engineers, Vol. 106, No. GT12, pp. 1345–1367.)

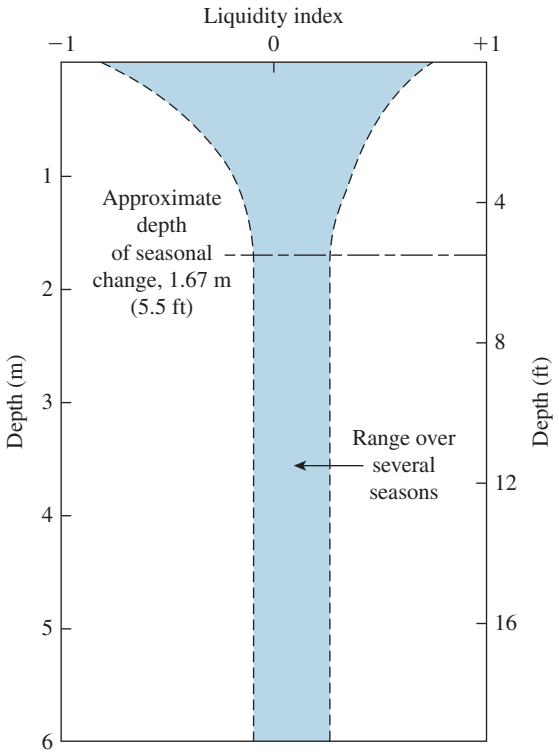


FIGURE 15.11 Active zone in Houston area, Beaumont formation (Based on O'Neill, M. W., and Poormoayed, N. (1980). "Methodology for Foundations on Expansive Clays," *Journal of the Geotechnical Engineering Division*, American Society of Civil Engineers, Vol. 106, No. GT12, pp. 1345–1367.)



FIGURE 15.12 Interconnected shrinkage cracks extended from the ground surface into the active zone (Courtesy of Thomas M. Petry, Missouri University of Science and Technology, Rolla, Missouri)

15.8 Unrestrained Swell Test

In the *unrestrained swell test*, the specimen is placed in an oedometer under a small surcharge of about 6.9 kN/m^2 (1 lb/in^2). Water is then added to the specimen to fully submerge it, and the expansion of the volume of the specimen (i.e., its height;

the area of cross section is constant) is measured until equilibrium is reached. The percentage of free swell may then be expressed as the ratio

$$s_{w(\text{free})}(\%) = \frac{\Delta H}{H}(100) \tag{15.9}$$

where

$s_{w(\text{free})}$ = free swell, as a percentage

ΔH = height of swell due to saturation

H = original height of the specimen

Vijayvergiya and Ghazzaly (1973) analyzed various soil test results obtained in this manner and prepared a correlation chart of the free swell, liquid limit, and natural moisture content, as shown in Figure 15.13. O'Neill and Poormoayed (1980) developed a relationship for calculating the free surface swell from this chart:

$$\Delta S_F = 0.0033 Z s_{w(\text{free})} \tag{15.10}$$

where

ΔS_F = free surface swell

Z = depth of active zone

$s_{w(\text{free})}$ = free swell, as a percentage

Free surface swell ΔS_F is a measure of the potential damage that can occur to the structure built on the expansive soil at the site.

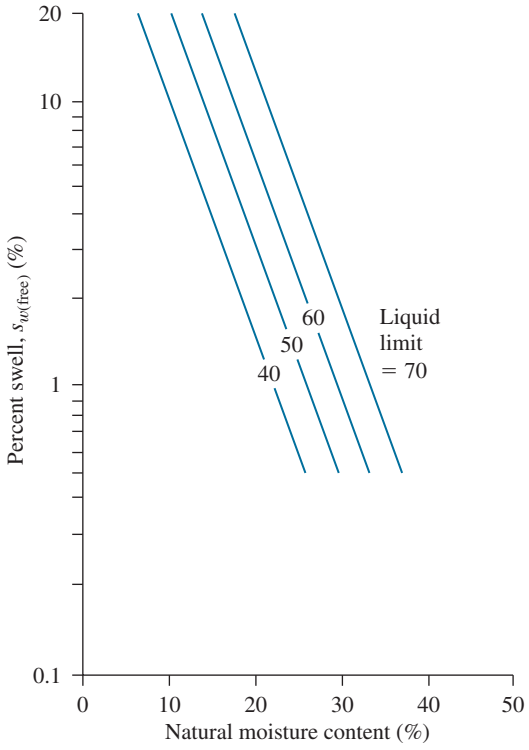


FIGURE 15.13 Relation among percentage of free swell, liquid limit, and natural moisture content (Based on Vijayvergiya, V. N. and Ghazzaly, O. I. (1973). "Prediction of Swelling Potential of Natural Clays," *Proceedings, Third International Research and Engineering Conference on Expansive Clays*, pp. 227–234.)

15.9 Swelling Pressure Test

Swelling pressure is the upward pressure exerted on the foundation. It is often quantified through zero swell pressure, which is the downward pressure required to ensure that the soil does not swell. The swelling pressure can be determined from two different types of tests:

- Conventional consolidation test
- Constant volume test

The two methods are briefly described here.

CONVENTIONAL CONSOLIDATION TEST

In this type of test, the specimen is placed in an oedometer under a small surcharge of about 6.9 kN/m^2 (1 lb/in^2). Water is added to the specimen, allowing it to swell and reach an equilibrium position after some time. Subsequently, loads are added in convenient steps, and the specimen is consolidated. The plot of specimen deformation (δ) versus log σ' is shown in Figure 15.14. The δ versus log σ' plot crosses the horizontal line through the point of initial condition. The pressure corresponding to the point of intersection is the *zero swell pressure,* σ'_{sw}.

CONSTANT VOLUME TEST

The *constant volume test* can be conducted by taking a specimen in a consolidation ring and applying a pressure equal to the effective overburden pressure, σ'_o, plus the approximate anticipated surcharge caused by the foundation, σ'_s. Water is then added to the specimen. As the specimen starts to swell, pressure is applied in small increments to prevent swelling. Pressure is maintained until full swelling pressure is developed on the specimen, at which time the total pressure is

$$\sigma'_{sw} = \sigma'_o + \sigma'_s + \sigma'_1 \tag{15.11}$$

where

σ'_{sw} = total pressure applied to prevent swelling, or zero swell pressure

σ'_1 = additional pressure applied to prevent swelling after addition of water

Figure 15.15 shows the variation of the percentage of swell with effective pressure during a swelling pressure test. (For more information on this type of test, see Sridharan et al., 1986.)

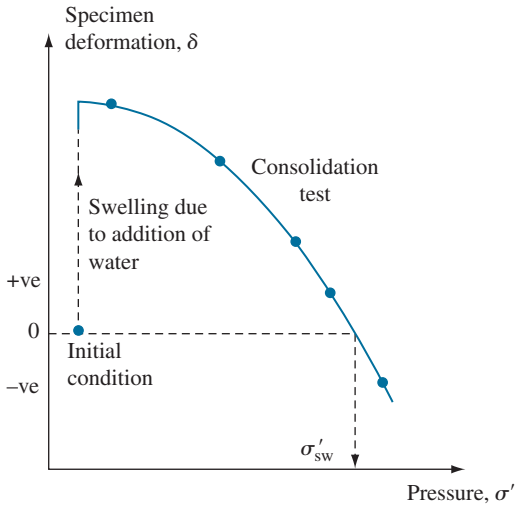


FIGURE 15.14 Zero swell pressure from conventional consolidation test

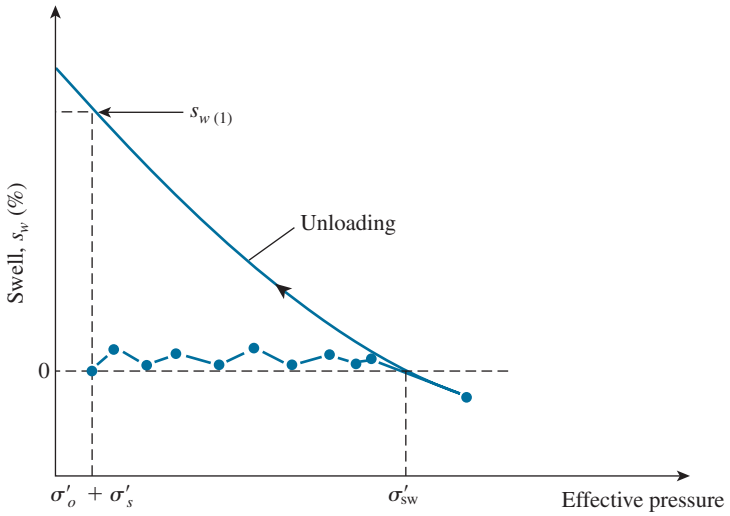


FIGURE 15.15 Swelling pressure test

A σ'_{sw} of about 20 to 30 kN/m^2 (400 to 650 lb/ft^2) is considered to be low, and a σ'_{sw} of 1500 to 2000 kN/m^2 (30,000 to 40,000 lb/ft^2) is considered to be high. After zero swell pressure is attained, the soil specimen can be unloaded in steps to the level of the effective overburden pressure, σ'_o. The unloading process will cause the specimen to swell. The equilibrium swell for each pressure level is also recorded. The variation of the swell, s_w in percent, and the applied pressure on the specimen will be like that shown in Figure 15.15.

The constant volume test can be used to determine the surface heave, ΔS, for a foundation (O'Neill and Poormoayed, 1980) as given by the formula

$$\Delta S = \sum_{i=1}^{n} [s_{w(1)}\,(\%)](H_i)(0.01) \tag{15.12}$$

where

$s_{w(1)}(\%)$ = swell, in percent, for layer i under a pressure of $\sigma'_o + \sigma'_s$ (see Figure 15.15)

H_i = thickness of layer i

It is important to point out that the zero swell pressure (σ'_{sw}) obtained from the conventional consolidation test and the constant volume test may not be the same. Table 15.4 summarizes some laboratory test results of Sridharan et al. (1986) to

TABLE 15.4 **Comparison of Zero Swell Pressure Obtained from Conventional Consolidation Tests and Constant Volume Tests—Summary of Test Results of Sridharan et al. (1986)**

Soil	Liquid limit	Plasticity index	Initial void ratio, e_i	σ'_{sw} (kN/m^2)	
				Consolidation test	Constant volume test
BC-1	80	44	0.893	294.3	186.4
BC-4	98	57	1.002	382.6	251.8
BC-5	96	65	0.742	500.3	304.1
BC-7	96	66	0.572	1275.3	372.8
BC-8	94	62	0.656	147.2	68.7

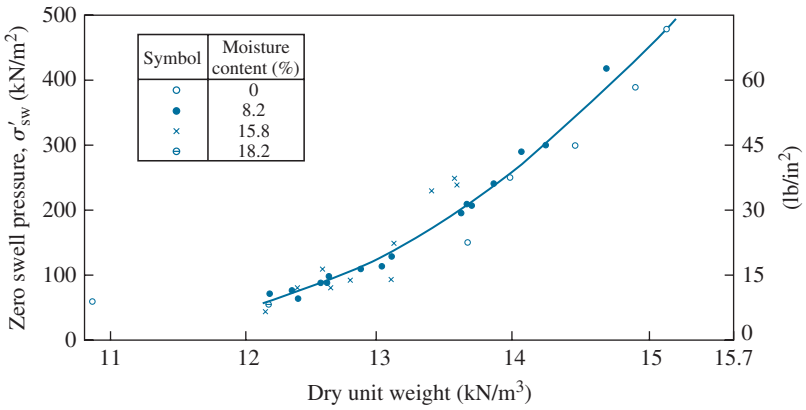


FIGURE 15.16 Plot of zero swell pressure with the dry unit weight of soil (Based on Sridharan et al., 1986)

illustrate this point. It also was shown by Sridharan et al. (1986) that the zero swell pressure is a function of the dry unit weight of soil but not of the initial moisture content (Figure 15.16).

While the free swell $s_{w(\text{free})}$ is measured under a small surcharge of 6.9 kN/m^2 (1.0 lb/in^2), the swell $s_{w(1)}$ obtained in a constant volume swell pressure test is measured under a pressure of $\sigma'_o + \sigma'_s$, replicating the overburden and foundation pressures in service. They are both strains expressed as a percentage.

EXAMPLE 15.1

A soil profile has an active zone of expansive soil of 2 m. The liquid limit and the average natural moisture content during the construction season are 60% and 30%, respectively. Determine the free surface swell.

SOLUTION

From Figure 15.13 for LL = 60% and w = 30%, $s_{w(\text{free})}$ = 1%. From Eq. (15.10),

$$\Delta S_F = 0.0033 Z s_{w(\text{free})}$$

Hence,

$$\Delta S_F = 0.0033(2)(1)(1000) = \mathbf{6.6\ mm}$$

EXAMPLE 15.2

An expansive soil profile has an active-zone thickness of 5.2 m. A shallow foundation is to be constructed 1.2 m below the ground surface. A swelling pressure test provided the following data:

Depth below ground surface (m)	Swell under overburden and estimated foundation surcharge pressure, $s_{w(1)}$(%)
1.2	3.0
2.2	2.0
3.2	1.2
4.2	0.55
5.2	0.0

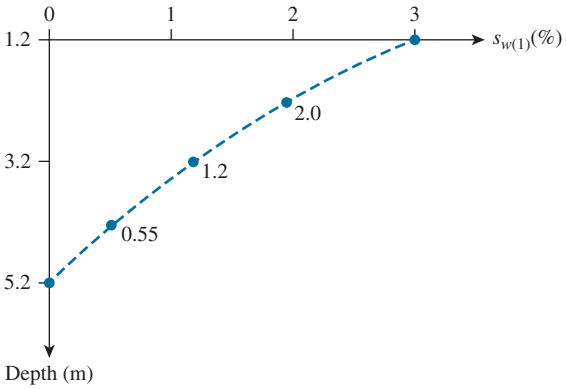


FIGURE 15.17

a. Estimate the total possible swell under the foundation.
b. If the allowable total swell is 15 mm, what would be the necessary undercut?

Note: The swelling soil within this undercut zone is replaced by nonswelling soil.

SOLUTION

Part a

Figure 15.17 shows the plot of depth versus $s_{w(1)}(\%)$. The area of this diagram will be the total swell. Thus

$$\Delta S = \frac{1}{100}\left[\left(\frac{1}{2}\right)(0.55 + 0)(1) + \left(\frac{1}{2}\right)(0.55 + 1.2)(1) + \left(\frac{1}{2}\right)(1.2 + 2)(1) + \left(\frac{1}{2}\right)(2 + 3)(1)\right]$$

$$= 0.0525 \text{ m} = \mathbf{52.5 \text{ mm}}$$

Part b

Total swell at various depths can be calculated as follows:

Depth (m)	Total swell, ΔS (m)
5.2	0
4.2	$0 + \frac{1}{2}(0.55 + 0)(1)(1/100) = 0.00275$
3.2	$0.00275 + \frac{1}{2}(1.2 + 0.55)(1)(1/100) = 0.0115$
2.2	$0.0115 + \frac{1}{2}(2 + 1.2)(1)(1/100) = 0.0275$
1.2	$0.0275 + \frac{1}{2}(2 + 3)(1)(1/100) = 0.0525$

The plot of ΔS versus depth is shown in Figure 15.18. From this figure, the depth of undercut is $2.91 - 1.2 =$ **1.71 m below the bottom of the foundation.**

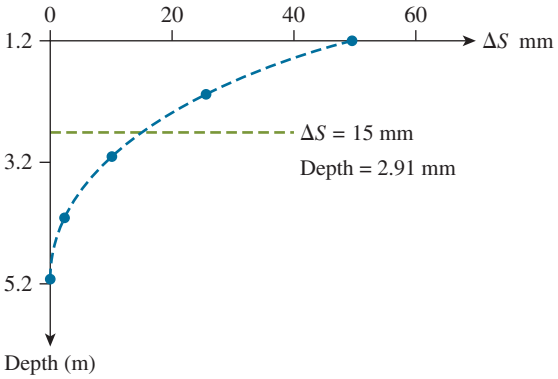


FIGURE 15.18

15.10 Classification of Expansive Soil on the Basis of Index Tests

Classification systems for expansive soil are based on the problems they create in the construction of foundations (potential swell). Most of the classifications contained in the literature are summarized in Figure 15.19 and Table 15.5. However, the classification system developed by the U.S. Army Waterways Experiment Station (Snethen et al., 1977) is the one most widely used in the United States. It has also been summarized by O'Neill and Poormoayed (1980); see Table 15.6. Sridharan (2005) proposed an index called the *free swell ratio* to predict the clay type, potential swell classification, and dominant clay minerals present in a given soil. The free swell ratio can be determined by finding the equilibrium sediment volumes of 10 grams of an oven-dried specimen passing a No. 40 U.S. sieve (0.425 mm opening) in distilled water (V_d) and in CCl_4 or kerosene (V_K). The free swell ratio (FSR) is defined as

$$\text{FSR} = \frac{V_d}{V_K} \tag{15.13}$$

Table 15.7 gives the expansive soil classification based on free swell ratio. Also, Figure 15.20 shows the classification of soil based on the free swell ratio.

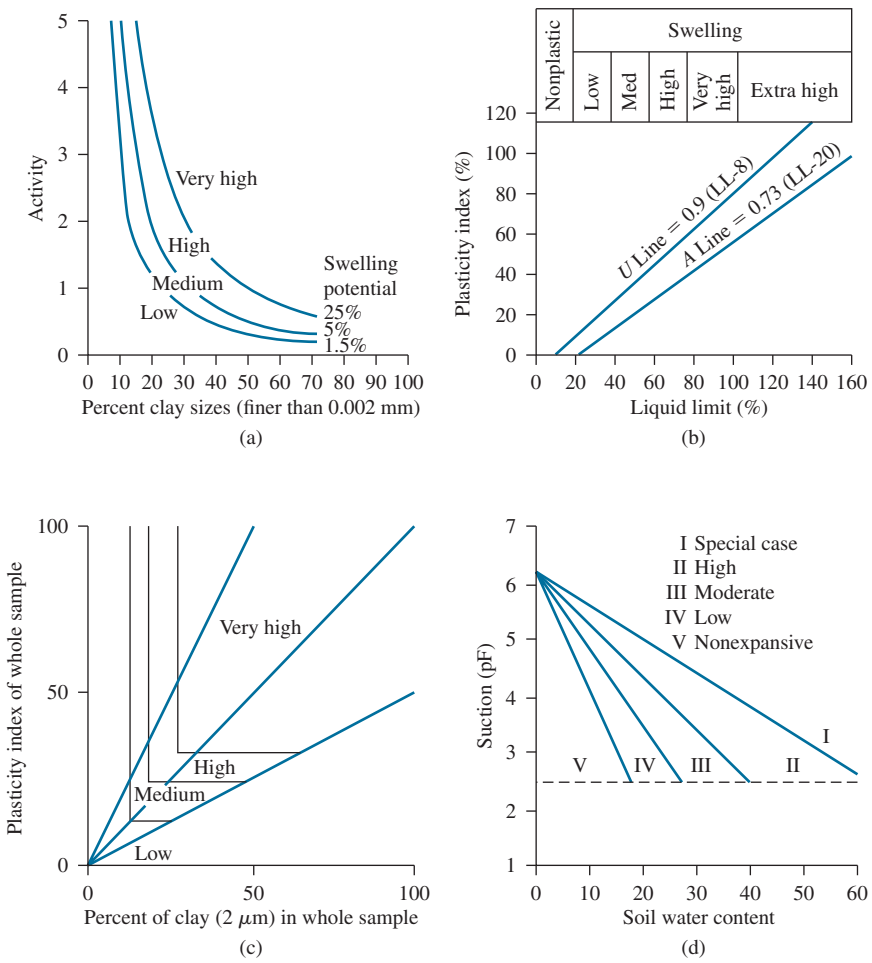


FIGURE 15.19 Commonly used criteria for determining swell potential (Based on Abduljauwad, S. N. and Al-Sulaimani, G. J. (1993). "Determination of Swell Potential of Al-Qatif Clay," *Geotechnical Testing Journal*, American Society for Testing and Materials, Vol. 16, No. 4, pp. 469–484.)

TABLE 15.5 Summary of Some Criteria for Identifying Swell Potential (Based on Abduljauwad, S. N. and Al-Sulaimani, G. J. (1993). "Determination of Swell Potential of Al-Qatif Clay," *Geotechnical Testing Journal*, American Society for Testing and Materials, Vol. 16, No. 4, pp. 469–484.)

Reference	Criteria	Remarks
Holtz (1959)	CC $>$ 28, PI $>$ 35, and SL $<$ 11 (very high) 20 $\leq$ CC $\leq$ 31, 25 $\leq$ PI $\leq$ 41, and 7 $\leq$ SL $\leq$ 12 (high) 13 $\leq$ CC $\leq$ 23, 15 $\leq$ PI $\leq$ 28, and 10 $\leq$ SL $\leq$ 16 (medium) CC $\leq$ 15, PI $\leq$ 18, and SL $\geq$ 15 (low)	Based on CC, PI, and SL
Seed et al. (1962)	See Figure 15.19a	Based on oedometer test using compacted specimen, percentage of clay $<$ 2 μm, and activity
Altmeyer (1955)	LS $<$ 5, SI $>$ 12, and PS $<$ 0.5 (noncritical) 5 $\leq$ LS $\leq$ 8, 10 $\leq$ SL $\leq$ 12, and 0.5 $\leq$ PS $\leq$ 1.5 (marginal) LS $>$ 8, SL $<$ 10, and PS $>$ 1.5 (critical)	Based on LS, SL, and PS Remolded sample ($\rho_{d(\max)}$ and w_{opt}) soaked under 6.9 kPa surcharge
Dakshanamanthy and Raman (1973)	See Figure 15.19b	Based on plasticity chart
Raman (1967)	PI $>$ 32 and SI $>$ 40 (very high) 23 $\leq$ PI $\leq$ 32 and 30 $\leq$ SI $\leq$ 40 (high) 12 $\leq$ PI $\leq$ 23 and 15 $\leq$ SI $\leq$ 30 (medium) PI $<$ 12 and SI $<$ 15 (low)	Based on PI and SI
Sowers and Sowers (1970)	SL $<$ 10 and PI $>$ 30 (high) 10 $\leq$ SL $\leq$ 12 and 15 $\leq$ PI $\leq$ 30 (moderate) SL $>$ 12 and PI $<$ 15 (low)	Little swell will occur when w_o results in LI of 0.25
Van Der Merwe (1964)	See Figure 15.19c	Based on PI, percentage of clay $<$ 2 μm, and activity
Uniform Building Code, 1968	EI $>$ 130 (very high) and 91 $\leq$ EI $\leq$ 130 (high) 51 $\leq$ EI $\leq$ 90 (medium) and 21 $\leq$ EI $\leq$ 50 (low) 0 $\leq$ EI $\leq$ 20 (very low)	Based on oedometer test on compacted specimen with degree of saturation close to 50% and surcharge of 6.9 kPa
Snethen (1984)	LL $>$ 60, PI $>$ 35, τ_{nat} $>$ 4, and SP $>$ 1.5 (high) 30 $\leq$ LL $\leq$ 60, 25 $\leq$ PI $\leq$ 35, 1.5 $\leq$ τ_{nat} $\leq$ 4, and 0.5 $\leq$ SP $\leq$ 1.5 (medium) LL $<$ 30, PI $<$ 25, τ_{nat} $<$ 1.5, and SP $<$ 0.5 (low)	PS is representative for field condition and can be used without τ_{nat}, but accuracy will be reduced
Chen (1988)	PI $\geq$ 35 (very high) and 20 $\leq$ PI $\leq$ 55 (high) 10 $\leq$ PI $\leq$ 35 (medium) and PI $\leq$ 15 (low)	Based on PI
McKeen (1992)	Figure 15.19d	Based on measurements of soil water content, suction, and change in volume on drying
Vijayvergiya and Ghazzaly (1973)	$\log SP = (1/12)(0.44\,LL - w_o + 5.5)$	Empirical equations
Nayak and Christensen (1974)	$SP = (0.00229\,PI)(1.45C)/w_o + 6.38$	Empirical equations
Weston (1980)	$SP = 0.00411(LL_w)^{4.17} q^{-3.86} w_o^{-2.33}$	Empirical equations

Note: C = clay, %
CC = colloidal content, %
EI = Expansion index = 100 × percent swell × fraction passing No. 4 sieve
LI = liquidity index, %
LL = liquid limit, %
LL_w = weighted liquid limit, %
LS = linear shrinkage, %
PI = plasticity index, %
PS = probable swell, %
q = surcharge
SI = shrinkage index = LL − SL, %
SL = shrinkage limit, %
SP = swell potential, %
w_o = natural soil moisture
w_{opt} = optimum moisture content, %
τ_{nat} = natural soil suction in ton/ft^2
$\rho_{d(\max)}$ = maximum dry density

TABLE 15.6 Expansive Soil Classification System[a]

Liquid limit	Plasticity index	Potential swell (%)	Potential swell classification
<50	<25	<0.5	Low
50–60	25–35	0.5–1.5	Marginal
>60	>35	>1.5	High

Potential swell = vertical swell under a pressure equal to overburden pressure

[a]Based on data from O'Neill and Poormoayed (1980)

TABLE 15.7 Expansive Soil Classification Based on Free Swell Ratio

Free swell ratio	Clay type	Potential swell classification	Dominant clay mineral
≤1.0	Nonswelling	Negligible	Kaolinite
1.0–1.5	Mixture of swelling and nonswelling	Low	Kaolinite and montmorillonite
1.5–2.0	Swelling	Moderate	Montmorillonite
2.0–4.0	Swelling	High	Montmorillonite
> 4.0	Swelling	Very High	Montmorillonite

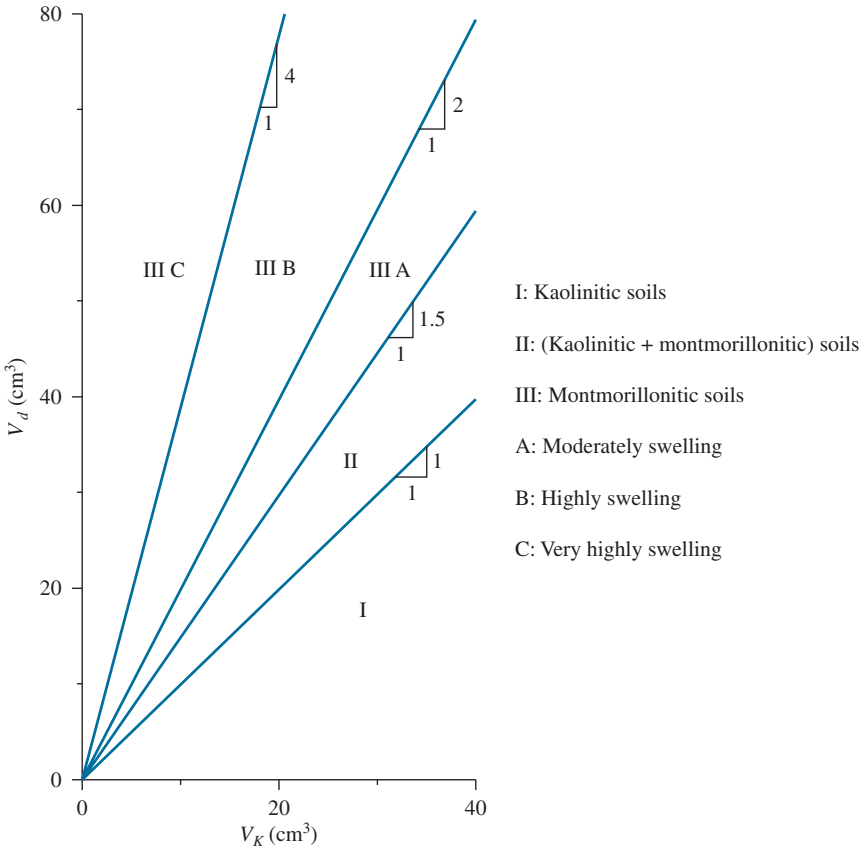


FIGURE 15.20 Classification based on free swell ratio (Based on Sridharan, 2005)

15.11 Foundation Considerations for Expansive Soil

If a soil has a low swell potential, standard construction practices may be followed. However, if the soil possesses a marginal or high swell potential, precautions need to be taken, which may entail

1. Replacing the expansive soil under the foundation
2. Changing the nature of the expansive soil by compaction control, prewetting, installation of moisture barriers, or chemical stabilization
3. Strengthening the structures to withstand heave, constructing structures that are flexible enough to withstand the differential soil heave without failure, or constructing isolated deep foundations below the depth of the active zone

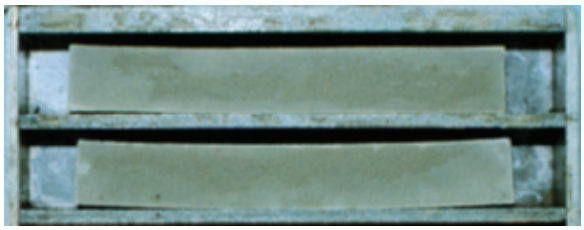
One particular method may not be sufficient in all situations. Combining several techniques may be necessary, and local construction experience should always be considered. Following are some details regarding the commonly used techniques for dealing with expansive soil.

REPLACEMENT OF EXPANSIVE SOIL

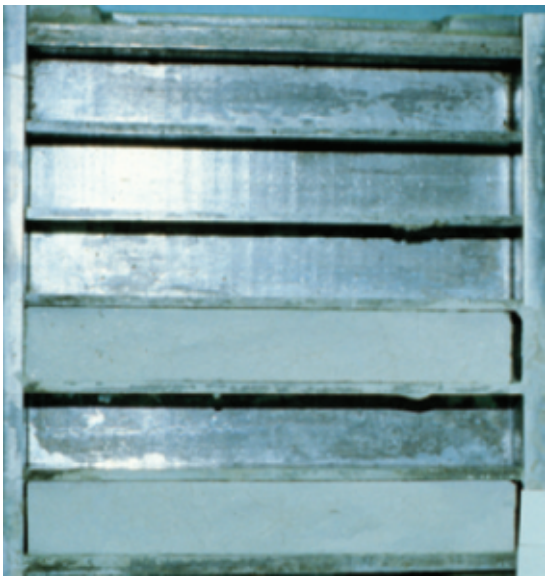
When shallow, moderately expansive soil are present at the surface, they can be removed and replaced by less expansive soil and then compacted properly.

CHANGING THE NATURE OF EXPANSIVE SOIL

1. *Compaction:* The heave of expansive soil decreases substantially when the soil is compacted to a lower unit weight on the wet side of the optimum moisture content (possibly 3 to 4% above the optimum moisture content). Even under such conditions, a slab-on-ground type of construction should not be considered when the total probable heave is expected to be about 38 mm (1.5 in.) or more.
2. *Prewetting:* One technique for increasing the moisture content of the soil is ponding and hence achieving most of the heave before construction. However, this technique may be time consuming because the seepage of water through highly plastic clays is slow. After ponding, 4 to 5% of hydrated lime may be added to the top layer of the soil to make it less plastic and more workable (Gromko, 1974).
3. *Installation of moisture barriers:* The long-term effect of the differential heave can be reduced by controlling the moisture variation in the soil. This is achieved by providing vertical moisture barriers about 1.5 m (≈5 ft) deep around the perimeter of slabs for the slab-on-grade type of construction. These moisture barriers may be constructed in trenches filled with gravel, lean concrete, or impervious membranes.
4. *Stabilization of soil:* Chemical stabilization with the aid of lime and cement has often proved useful. A mix containing about 5% lime is sufficient in most cases. The effect of lime in stabilizing expansive soil, thereby reducing the shrinking and swelling characteristics, can be demonstrated with the aid of Figure 15.21. For this, expansive clay weathered from the Eagle Ford shale formation in the Dallas–Fort Worth, Texas area was taken. Some of it was mixed with water to about its liquid limit. It was placed in two molds that were about 152 mm (6 in.) long and 12.7 mm × 12.7 mm (0.5 in. × 0.5 in.) in cross section. Figure 15.21a shows the shrinkage of the soil specimens in the mold in a *dry condition*. The same soil also was



(a)



(b)

FIGURE 15.21 Shrinkage of expansive clay (Eagle Ford soil) mixed with water to about its liquid limit in molds of 152 mm × 12.7 mm × 12.7 mm (6 in. × ½ in. × ½ in.): (a) without addition of lime; (b) with addition of 6% lime by weight (Courtesy of Thomas M. Petry, Missouri University of Science and Technology, Rolla, Missouri)

mixed with 6% lime (by dry weight) and then with a similar amount of water and placed in six similar molds. Figure 15.21b shows the shrinkage of the lime-stabilized specimens in a dry condition, which was practically negligible compared to that seen in Figure 15.21a. Lime or cement and water are mixed with the top layer of soil and compacted. The addition of lime or cement will decrease the liquid limit, the plasticity index, and the swell characteristics of the soil. This type of stabilization work can be done to a depth of 1 to 1.5 m (≈3 to 5 ft). Hydrated high-calcium lime and dolomite lime are generally used for lime stabilization.

Another method of stabilization of expansive soil is the *pressure injection* of lime slurry or lime–fly-ash slurry into the soil, usually to a depth of 4 to 5 m or (12 to 16 ft) and occasionally deeper to cover the active zone. Further details of the pressure injection technique were presented in Chapter 5. Depending on the soil conditions at a site, single or multiple injections can be planned, as shown in Figure 15.22. Figure 15.23 shows the slurry pressure injection work for a building pad. The stakes that are marked are the planned injection points. Figure 15.24 shows lime–fly-ash stabilization by pressure injection of the bank of a canal that has experienced sloughs and slides.

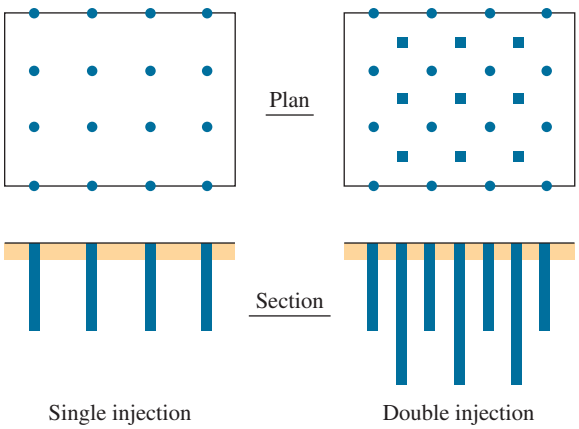


FIGURE 15.22 Multiple lime slurry injection planning for a building pad



FIGURE 15.23 Pressure injection of lime slurry for a building pad (Courtesy of Hayward Baker Inc., Odenton, Maryland)



FIGURE 15.24 Slope stabilization of a canal bank by pressure injection of lime–fly-ash slurry (Courtesy of Hayward Baker Inc., Odenton, Maryland)

15.12 Construction on Expansive Soil

Care must be exercised in choosing the type of foundation to be used on expansive soil. Table 15.8 shows some recommended construction procedures based on the total predicted heave, ΔS, and the length-to-height (L/H) ratio of the wall panels. For example, the table proposes the use of waffle slabs as an alternative in designing rigid buildings that are capable of tolerating movement. Figure 15.25 shows a schematic diagram of a waffle slab. In this type of construction, the ribs hold the structural load. The waffle voids allow the expansion of soil.

Table 15.8 also suggests the use of a drilled-shaft foundation with a suspended floor slab when structures are constructed independently of soil movement.

TABLE 15.8 Construction Procedures for Expansive Clay Soil[a]

Total predicted heave (mm)		Recommended construction	Method	Remarks
$L/H = 1.25$	$L/H = 2.5$			
0 to 6.35	12.7	No precaution		
6.35 to 12.7	12.7 to 50.8	Rigid building tolerating movement (steel reinforcement as necessary)	*Foundations:* Pads Strip footings mat (waffle)	Footings should be small and deep, consistent with the soil-bearing capacity. Mats should resist bending.
			Floor slabs: Waffle Tile	Slabs should be designed to resist bending and should be independent of grade beams.
			Walls:	Walls on a mat should be as flexible as the mat. There should be no vertical rigid connections. Brickwork should be strengthened with tie bars or bands.
12.7 to 50.8	50.8 to 101.6	Building damping movement	*Joints:* Clear Flexible	Contacts between structural units should be avoided, or flexible, waterproof material may be inserted in the joints.
			Walls: Flexible Unit construction Steel frame	Walls or rectangular building units should heave as a unit.
			Foundations: Three point Cellular Jacks	Cellular foundations allow slight soil expansion to reduce swelling pressure. Adjustable jacks can be inconvenient to owners. Three-point loading allows motion without duress.
>50.8	>101.6	Building independent of movement	*Foundation drilled shaft:* Straight shaft Bell bottom	Smallest-diameter and widely spaced shafts compatible with the load should be placed. Clearance should be allowed under grade beams.
			Suspended floor:	Floor should be suspended on grade beams 305 to 460 mm above the soil.

[a]Gromko, G. J., (1974). "Review of Expansive Soils," *Journal of the Geotechnical Engineering Division*, American Society of Civil Engineers, Vol. 100, No. GT6, pp. 667–687.

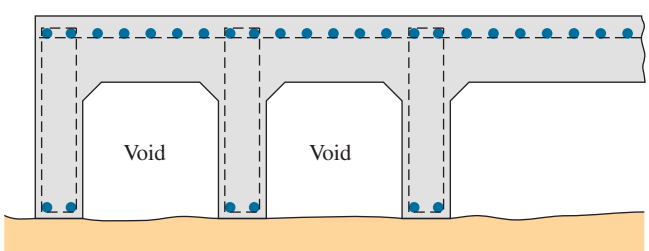


FIGURE 15.25 Waffle slab

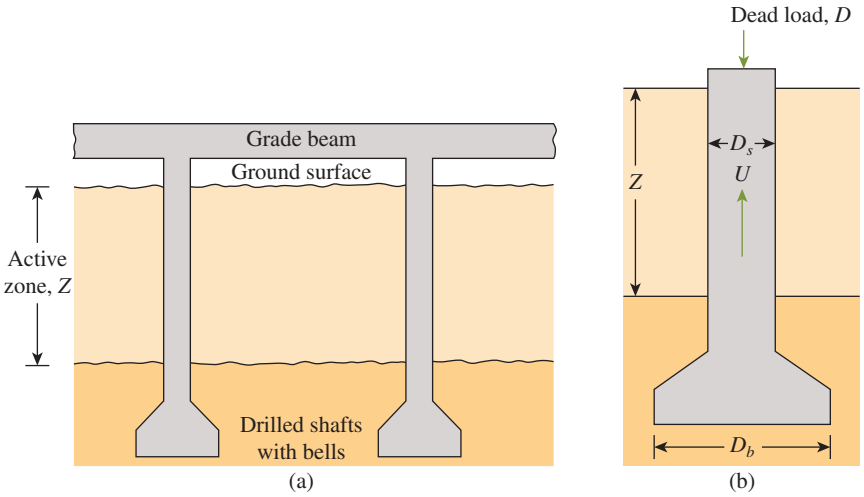


FIGURE 15.26 (a) Construction of drilled shafts with bells and grade beam; (b) definition of parameters in Eq. (15.14)

Figure 15.26a shows a schematic diagram of such an arrangement. The bottom of the shafts should be placed below the active zone of the expansive soil. For the design of the shafts, the uplifting force, U, may be estimated (see Figure 15.26b) from the equation

$$U = \pi D_s Z \sigma'_{sw} \tan \phi'_{ps} \tag{15.14}$$

where

D_s = diameter of the shaft

Z = depth of the active zone

ϕ'_{ps} = effective angle of plinth–soil friction

σ'_{sw} = pressure for zero swell (see Figures 15.14 and 15.15; $\sigma'_{sw} = \sigma'_o + \sigma'_s + \sigma'_1$)

In most cases, the value of ϕ'_{ps} varies between 10 and 20°. An average value of the zero horizontal swell pressure must be determined in the laboratory. In the absence of laboratory results, $\sigma'_{sw} \tan \phi'_{ps}$ may be considered equal to the undrained shear strength of clay, c_u, in the active zone.

The belled portion of the drilled shaft will act as an anchor to resist the uplifting force. Ignoring the weight of the drilled shaft, we have

$$Q_{net} = U - D \tag{15.15}$$

where

Q_{net} = net uplift load

D = dead load

Now,

$$Q_{net} \approx \frac{c_u N_c}{FS}\left(\frac{\pi}{4}\right)(D_b^2 - D_s^2) \tag{15.16}$$

where

c_u = undrained cohesion of the clay in which the bell is located

N_c = bearing capacity factor

FS = factor of safety

D_b = diameter of the bell of the drilled shaft

Combining Eqs. (15.15) and (15.16) gives

$$U - D = \frac{c_u N_c}{\text{FS}} \left(\frac{\pi}{4}\right)(D_b^2 - D_s^2) \tag{15.17}$$

Conservatively, from Tables 6.2 and 6.3,

$$N_c \approx N_{c(\text{strip})} F_{cs} = N_{c(\text{strip})} \left(1 + \frac{N_q B}{N_c L}\right) \approx 5.14 \left(1 + \frac{1}{5.14}\right) = 6.14$$

A drilled-shaft design is examined in Example 15.3.

EXAMPLE 15.3

Figure 15.27 shows a drilled shaft with a bell. The depth of the active zone is 5 m. The zero swell pressure of the swelling clay (σ'_{sw}) is 450 kN/m^2. For the drilled shaft, the dead load (D) is 600 kN and the live load is 300 kN. Assume $\phi'_{ps} = 12°$.

a. Determine the diameter of the bell, D_b.
b. Check the bearing capacity of the drilled shaft assuming zero uplift force.

SOLUTION

Part a: Determining the Bell Diameter, D_b

The uplift force, Eq. (15.14), is

$$U = \pi D_s Z \sigma'_{sw} \tan \phi'_{ps}$$

Given: $Z = 5$ m and $\sigma'_{sw} = 450$ kN/m^2. Then

$$U = \pi(0.8)(5)(450)\tan 12° = 1202 \text{ kN}$$

Conservatively assume the dead load and live load to be zero and FS in Eq. (15.17) to be 1.25. So, from Eq. (15.17),

$$U = \frac{c_u N_c}{\text{FS}} \left(\frac{\pi}{4}\right)(D_b^2 - D_s^2)$$

$$1202 = \frac{(450)(6.14)}{1.25} \left(\frac{\pi}{4}\right)(D_b^2 - 0.8^2); \quad D_b = \mathbf{1.15\ m}$$

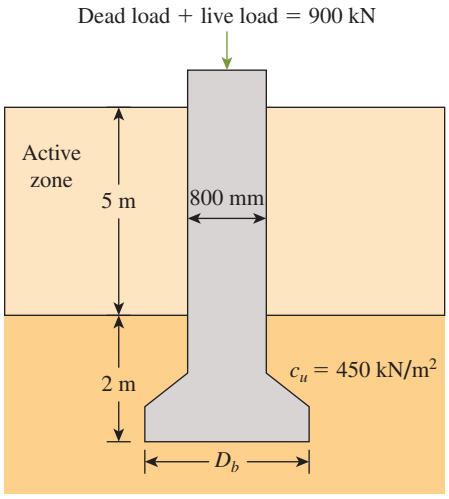


FIGURE 15.27 Drilled shaft in a swelling clay

The factor of safety against uplift with the dead load also should be checked. A factor of safety of at least 2 is desirable. So, from Eq. (15.17),

$$\text{FS} = \frac{c_u N_c \left(\frac{\pi}{4}\right)(D_b^2 - D_s^2)}{U - D}$$

$$= \frac{(450)(6.14)\left(\frac{\pi}{4}\right)(1.15^2 - 0.8^2)}{1202 - 600} = \mathbf{2.46 > 2—OK}$$

Part b: Check for Bearing Capacity

Assume that $U = 0$. Then

$$\text{Dead load + live load} = 600 + 300 = 900 \text{ kN}$$

$$\text{Downward load per unit area} = \frac{900}{\left(\frac{\pi}{4}\right)(D_b^2)} = \frac{900}{\left(\frac{\pi}{4}\right)(1.15^2)} = 866.5 \text{ kN/m}^2$$

$$\text{Net bearing capacity of the soil under the bell} = q_{u(\text{net})} = c_u N_c$$

$$= (450)(6.14) = 2763 \text{ kN/m}^2$$

Hence, the factor of safety against bearing capacity failure is

$$\text{FS} = \frac{2763}{866.5} = \mathbf{3.19 > 3—OK}$$

Sanitary Landfills

15.13 General Nature of Sanitary Landfills

Sanitary landfills provide a way to dispose of refuse on land without endangering public health. Sanitary landfills are used in almost all countries, to varying degrees of success. The refuse disposed of in sanitary landfills may contain organic, wood, paper, and fibrous wastes, or demolition wastes such as bricks and stones. The refuse is dumped and compacted at frequent intervals and is then covered with a layer of soil, as shown in Figure 15.28. In the compacted state, the average unit weight of the refuse may vary between 5 and 10 kN/m^3 (32 to 64 lb/ft^3). A typical

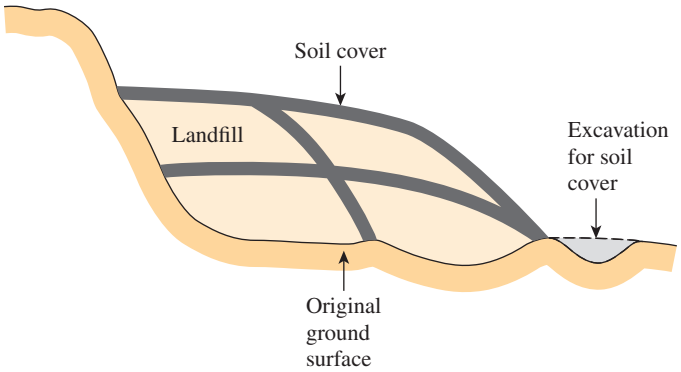


FIGURE 15.28 Schematic diagram of a sanitary landfill in progress

city in the United States, with a population of 1 million, generates about 3.8×10^6 m^3 ($\approx 135 \times 10^6$ ft^3) of compacted landfill material per year.

As property values continue to increase in densely populated areas, constructing structures over sanitary landfills becomes more and more tempting. In some instances, a visual site inspection may not be enough to detect an old sanitary landfill. However, construction of foundations over sanitary landfills is generally problematic because of poisonous gases (e.g., methane), excessive settlement, and low inherent bearing capacity.

15.14 Settlement of Sanitary Landfills

Sanitary landfills undergo large continuous settlements over a long time. Yen and Scanlon (1975) documented the settlement of several landfill sites in California. After completion of the landfill, the settlement rate (Figure 15.29) may be expressed as

$$m = \frac{\Delta H_f \text{ (m or ft)}}{\Delta t \text{ (month)}} \tag{15.18}$$

where

m = settlement rate

H_f = maximum height of the sanitary landfill

On the basis of several field observations, Yen and Scanlon determined the following empirical correlations for the settlement rate:

$$m = a - b \log t_1 \quad \text{[for fill heights ranging from 12 to 24 m (40 to 80 ft)]} \tag{15.19}$$

$$m = c - d \log t_1 \quad \text{[for fill heights ranging from 24 to 30 m (80 to l00 ft)]} \tag{15.20}$$

$$m = e - f \log t_1 \quad \text{[for fill heights larger than 30 m (l00 ft)]} \tag{15.21}$$

In these equations,

m is in m/month (ft/month)

t_1 is the median fill age (i.e., time since fill reached half height: see Figure 15.29), in months

In SI and English units, the values of *a, b, c, d, e*, and *f* given in Eqs. (15.19) through (15.21) are

Item	SI	English
a	0.0268	0.088
b	0.0116	0.038
c	0.038	0.125
d	0.0155	0.051
e	0.0435	0.142
f	0.0183	0.060

The median fill age may be defined from Figure 15.29 as

$$t_1 = t - \frac{t_c}{2} \tag{15.22}$$

where

t = time from the beginning of the landfill

t_c = time for completion of the landfill

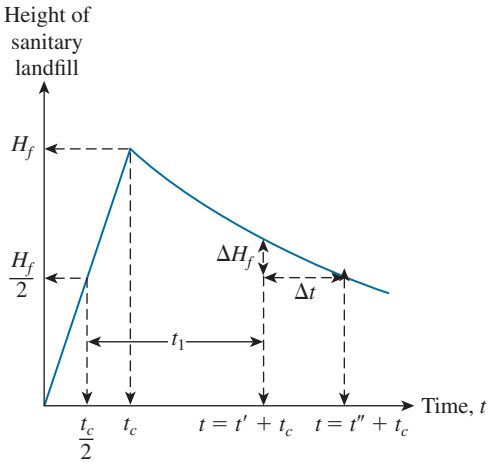


FIGURE 15.29 Settlement of sanitary landfills

Equations (15.19), (15.20), and (15.21) are based on field data from landfills for which t_c varied from 70 to 82 months. To get an idea of the approximate length of time required for a sanitary landfill to undergo complete settlement (i.e., no further settlement with $m = 0$), consider Eq. (15.19). For a fill 12 m high and for $t_c = 72$ months,

$$m = 0.0268 - 0.0116 \log t_1$$

so

$$\log t_1 = \frac{0.0268 - m}{0.0116}$$

If $m = 0$ (zero settlement rate), $\log t_1 = 2.31$, or $t_1 \approx 200$ months. Thus, settlement will continue for $t_1 - t_c/2 = 200 - 36 = 164$ months ($\approx$14 years) after completion of the fill—a fairly long time. This calculation emphasizes the need to pay close attention to the settlement of foundations constructed on sanitary landfills.

A comparison of Eqs. (15.19) through (15.21) for rates of settlement shows that the value of m increases with the height of the fill. However, for fill heights greater than about 30 m (100 ft), the rate of settlement should not be much different from that obtained from Eq. (15.21). The reason is that the decomposition of organic matter close to the surface is mainly the result of an anaerobic environment. For deeper fills, the decomposition is slower. Hence, for fill heights greater than about 30 m (100 ft), the rate of settlement does not exceed that for fills that are about 30 m in height.

Sowers (1973) also proposed a formula for calculating the settlement of a sanitary landfill, namely,

$$\Delta H_f = \frac{\alpha H_f}{1 + e} \log\left(\frac{t''}{t'}\right) \tag{15.23}$$

where

H_f = height of the fill

e = void ratio (at time t_c)

α = a coefficient for settlement

t', t'' = times (see Figure 15.29)

ΔH_f = settlement between times t' and t''

The coefficients α fall between

$$\alpha = 0.09e \quad \text{(for conditions favorable to decomposition)} \tag{15.24}$$

and

$$\alpha = 0.03e \quad \text{(for conditions unfavorable to decomposition)} \qquad (15.25)$$

Equation (15.23) is similar to the equation for secondary consolidation settlement.

15.15 Summary

Sometimes foundations have to be built in difficult soil conditions. This chapter discussed three problematic soil, namely, collapsible soil, expansive soil, and sanitary landfills. A good example of collapsible soil is loess, a wind-blown soil deposit, consisting of silt-sized grains. It is relatively stable when dry and loses its strength and collapses when saturated. Methods of identifying collapsible soil, computing settlement, and ground improvement and appropriate foundations for collapsible soil were discussed.

Expansive soil can exert upward pressures on foundations and can pose severe threats to buildings in many parts of the world. Free swell and swell pressure are two of the parameters used in quantifying the severity of the threat. Methods for calculating the surface heave (ΔS) were discussed. Classification of expansive soil and the design and construction of foundations in expansive soil were also discussed. Settlement of sanitary landfills continues for several years. An empirical equation was suggested for estimating the time beyond which no further settlement occurs.

PROBLEMS

15.1 For loessial soil with $G_s = 2.72$, plot a graph of γ_d (lb/ft^3) versus the liquid limit, similar to Figure 15.3, to identify the zone in which the soil is likely to collapse on saturation. If a soil has a liquid limit of 24, $G_s = 2.72$ and $\gamma_d = 92.2$ lb/ft^3, is collapse likely to occur?

15.2 The average effective overburden stress of a loessial soil deposit is 1565 lb/ft^2. An undisturbed specimen of this soil obtained from the middle of the layer was soaked for 24 hours and subjected to an oedometer test, where the preconsolidation pressure was determined as 2090.0 lb/ft^2. Is the *in situ* soil normally consolidated or overconsolidated?

15.3 A 4 m thick loessial deposit at a void ratio of 0.81 collapses to a void ratio of 0.68. What would be the settlement?

15.4 The thickness of the active zone in an expansive clay is 9.0 ft. The liquid limit of the clay is 50. If the natural moisture content is 20%, what would be the free swell at the ground level?

15.5 The expansive soil at the top of a soil profile consists of a 4.5 m thick active zone that is subjected to seasonal moisture variations. A shallow foundation is to be placed at 1.5 m depth. Constant volume swell pressure tests were carried out on specimens from different depths of this soil where the swell percentage $s_{w(1)}$ under the overburden and foundation pressures ($\sigma'_o + \sigma'_s$) were measured as follows.

Depth below ground level (m)	Swell percent under overburden + foundation pressure, $s_{w(1)}$ (%)
1.5	5.2
2.5	3.7
3.5	2.1
4.5	0.0

Estimate the total likely swell beneath the foundation.

15.6 In Problem 15.5, if the maximum allowable total swell is 25 mm, determine the undercut beneath the foundation that has to be replaced by nonswelling soil.

15.7 A shallow foundation is to be placed at 3.0 ft depth in an expansive soil where the active-zone thickness near the ground is 15.0 ft. Constant volume swell pressure tests were carried out on oedometer specimens at 3.0 ft intervals, and the results are as follows:

Depth below ground level (ft)	Swell percent under overburden + foundation pressure, $s_{w(1)}$ (%)
3.0	4.6
6.0	3.7
9.0	2.5
12.0	1.2
15.0	0.0

a. Estimate the expected swell of the foundation under the working loads.

b. If the maximum allowable swell is 1.0 in., what is the depth of the undercut?

15.8 Refer to Figure 15.26b. For the drilled shaft with bell, given:

Thickness of active zone, $Z = 9$ m

Dead load = 1500 kN

Live load = 300 kN

Diameter of the shaft, $D_s = 1$ m

Zero swell pressure for the clay in the active zone = 600 kN/m^2

Average angle of plinth–soil friction, $\phi'_{ps} = 20°$

Average undrained cohesion of the clay around the bell = 150 kN/m^2

Determine the diameter of the bell, D_b. A factor of safety of 3 against uplift is required with the assumption that dead load plus live load is equal to zero.

15.9 Refer to Problem 15.8. If an additional requirement is that the factor of safety against uplift is at least 4 with the dead load on (live load = 0), what should be the diameter of the bell?

REFERENCES

Abduljauwad, S. N. and Al-Sulaimani, G. J. (1993). "Determination of Swell Potential of Al-Qatif Clay," *Geotechnical Testing Journal*, American Society for Testing and Materials,Vol. 16, No. 4, pp. 469–484.

Altmeyer, W. T. (1955). "Discussion of Engineering Properties of Expansive Clays," *Journal of the Soil Mechanics and Foundations Division*, American Society of Civil Engineers, Vol. 81, No. SM2, pp. 17–19.

Benites, L. A. (1968). "Geotechnical Properties of the Soils Affected by Piping near the Benson Area, Cochise County, Arizona," M.S. Thesis, University of Arizona, Tucson.

Chen, F. H. (1988). *Foundations on Expansive Soils*, Elsevier, Amsterdam.

Clemence, S. P. and Finbarr, A. O. (1981). "Design Considerations for Collapsible Soils," *Journal of the Geotechnical Engineering Division*, American Society of Civil Engineers, Vol. 107, No. GT3, pp. 305–317.

Clevenger, W. (1958). "Experience with Loess as Foundation Material," *Transactions*, American Society of Civil Engineers, Vol. 123, pp. 151–170.

Dakshanamanthy, V. and Raman, V. (1973). "A Simple Method of Identifying an Expansive Soil," *Soils and Foundations*, Vol. 13, No. 1, pp. 97–104.

Denisov, N. Y. (1951). *The Engineering Properties of Loess and Loess Loams*, Gosstroiizdat, Moscow.

Feda, J. (1964). "Colloidal Activity, Shrinking and Swelling of Some Clays," *Proceedings, Soil Mechanics Seminar*, Loda, IL, pp. 531–546.

Gibbs, H. J. (1961). *Properties Which Divide Loose and Dense Uncemented Soils*, Earth Laboratory Report EM-658, Bureau of Reclamation, U.S. Department of the Interior, Washington, DC.

Gromko, G. J. (1974). "Review of Expansive Soils," *Journal of the Geotechnical Engineering Division*, American Society of Civil Engineers, Vol. 100, No. GT6, pp. 667–687.

Handy, R. L. (1973). "Collapsible Loess in Iowa," *Proceedings, Soil Science Society of America*, Vol. 37, pp. 281–284.

Holtz, W. G. (1959). "Expansive Clays—Properties and Problems," *Journal of the Colorado School of Mines*, Vol. 54, No. 4, pp. 89–125.

Holtz, W. G. and Hilf, J. W. (1961). "Settlement of Soil Foundations Due to Saturation," *Proceedings, Fifth International Conference on Soil Mechanics and Foundation Engineering*, Paris, Vol. 1, 1961, pp. 673–679.

Houston, W. N. and Houston, S. L. (1989). "State-of-the-Practice Mitigation Measures for Collapsible Soil Sites," *Proceedings, Foundation Engineering: Current Principles and Practices*, American Society of Civil Engineers, Vol. 1, pp. 161–175.

Jennings, J. E. and Knight, K. (1975). "A Guide to Construction on or with Materials Exhibiting Additional Settlements Due to 'Collapse' of Grain Structure," *Proceedings, Sixth Regional Conference for Africa on Soil Mechanics and Foundation Engineering*, Johannesburg, pp. 99–105.

Lutenegger, A. J. (1986). "Dynamic Compaction in Friable Loess," *Journal of Geotechnical Engineering*, American Society of Civil Engineers, Vol. 112, No. GT6, pp. 663–667.

Lutenegger, A. J. and Saber, R. T. (1988). "Determination of Collapse Potential of Soils," *Geotechnical Testing Journal*, American Society for Testing and Materials, Vol. 11. No. 3, pp. 173–178.

McKeen, R. G. (1992). "A Model for Predicting Expansive Soil Behavior," *Proceedings, Seventh International Conference on Expansive Soils*, Dallas, Vol. 1, pp. 1–6.

Nayak, N. V. and Christensen, R. W. (1974). "Swell Characteristics of Compacted Expansive Soils," *Clay and Clay Minerals*, Vol. 19, pp. 251–261.

O'Neill, M. W. and Poormoayed, N. (1980). "Methodology for Foundations on Expansive Clays," *Journal of the Geotechnical Engineering Division*, American Society of Civil Engineers, Vol. 106, No. GT12, pp. 1345–1367.

Peck, R. B., Hanson, W. E., and Thornburn, T. B. (1974). *Foundation Engineering*, John Wiley & Sons, New York.

Priklonskii, V. A. (1952). *Gruntovedenic, Vtoraya Chast*', Gosgeolzdat, Moscow.

Raman, V. (1967). "Identification of Expansive Soils from the Plasticity Index and the Shrinkage Index Data," *The Indian Engineer*, Vol. 11, No. 1, pp. 17–22.

Seed, H. B., Woodward, R. J., Jr., and Lundgren, R. (1962). "Prediction of Swelling Potential for Compacted Clays," *Journal of the Soil Mechanics and Foundations Division*, American Society of Civil Engineers, Vol. 88, No. SM3, pp. 53–87.

Semkin, V. V., Ermoshin, V. M., and Okishev, N. D. (1986). "Chemical Stabilization of Loess Soils in Uzbekistan," *Soil Mechanics and Foundation Engineering* (trans. from Russian), Vol. 23, No. 5, pp. 196–199.

Snethen, D. R. (1984). "Evaluation of Expedient Methods for Identification and Classification of Potentially Expansive Soils," *Proceedings, Fifth International Conference on Expansive Soils*, Adelaide, pp. 22–26.

Snethen, D. R., Johnson, L. D., and Patrick, D. M. (1977). *An Evaluation of Expedient Methodology for Identification of Potentially Expansive Soils*, Report No. FHWA-RD-77-94, U.S. Army Engineers Waterways Experiment Station, Vicksburg, MS.

Sowers, G. F. (1973). "Settlement of Waste Disposal Fills," *Proceedings, Eighth International Conference on Soil Mechanics and Foundation Engineering*, Moscow, pp. 207–210.

Sowers, G. B. and Sowers, G. F. (1970). *Introductory Soil Mechanics and Foundations*, 3rd ed., Macmillan, New York.

Sridharan, A. (2005). "On Swelling Behaviour of Clays," *Proceedings, International Conference on Problematic Soils*, North Cyprus, Vol. 2, pp. 499–516.

Sridharan, A., Rao, A. S., and Sivapullaiah, P. V. (1986), "Swelling Pressure of Clays," *Geotechnical Testing Journal*, American Society for Testing and Materials, Vol. 9, No. 1, pp. 24–33.

Uniform Building Code (1968). *UBC Standard No. 29-2.*

Van Der Merwe, D. H. (1964), "The Prediction of Heave from the Plasticity Index and Percentage Clay Fraction of Soils," *Civil Engineer in South Africa*, Vol. 6, No. 6, pp. 103–106.

Vijayvergiya, V. N. and Ghazzaly, O. I. (1973). "Prediction of Swelling Potential of Natural Clays," *Proceedings, Third International Research and Engineering Conference on Expansive Clays*, pp. 227–234.

Weston, D. J. (1980). "Expansive Roadbed Treatment for Southern Africa," *Proceedings, Fourth International Conference on Expansive Soils*, Vol. 1, pp. 339–360.

Yen, B. C. and Scanlon, B. (1975). "Sanitary Landfill Settlement Rates," *Journal of the Geotechnical Engineering Division*, American Society of Civil Engineers, Vol. 101, No. GT5, pp. 475–487.

PART 4

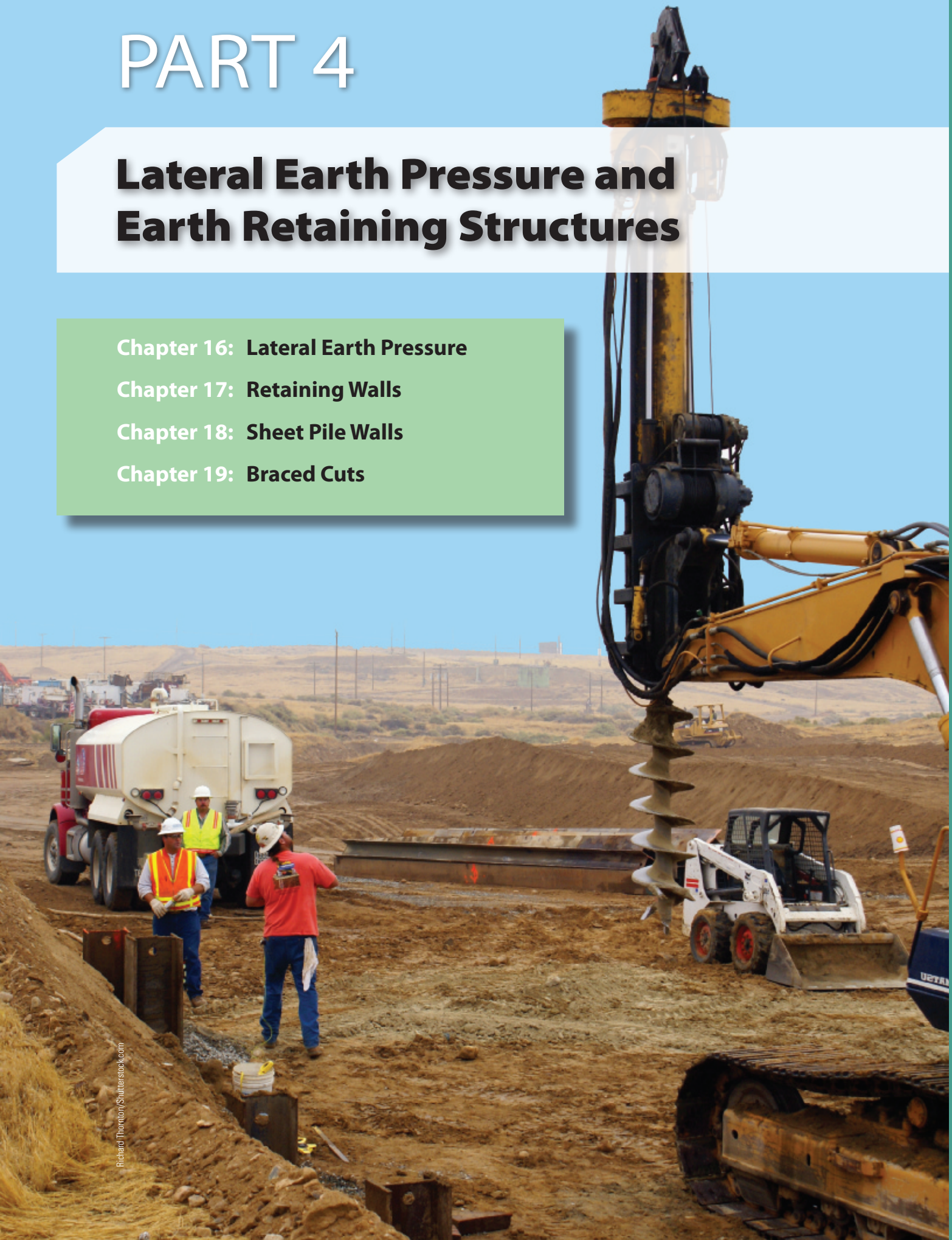
Lateral Earth Pressure and Earth Retaining Structures

Chapter 16: Lateral Earth Pressure

Chapter 17: Retaining Walls

Chapter 18: Sheet Pile Walls

Chapter 19: Braced Cuts



Richard Thornton/Shutterstock.com

16

Lateral Earth Pressure



Operation Shooting/Shutterstock.com

16.1 Introduction 639
16.2 Lateral Earth Pressure at Rest 640
16.3 Rankine Active Earth Pressure 644
16.4 A Generalized Case for Rankine Active Pressure—Granular Backfill 649
16.5 Generalized Case for Rankine Seismic Active Earth Pressure—Granular Backfill 653
16.6 Rankine Active Pressure with Vertical Wall Backface and Inclined $c' - \phi'$ Soil Backfill 655
16.7 Coulomb's Active Earth Pressure 658
16.8 Lateral Earth Pressure Due to Surcharge 665
16.9 Active Earth Pressure for Earthquake Conditions—Granular Backfill 668
16.10 Active Earth Pressure for Earthquake Condition (Vertical Backface of Wall and $c' - \phi'$ Backfill) 672
16.11 Rankine Passive Earth Pressure 676
16.12 Rankine Passive Earth Pressure—Vertical Backface and Inclined Backfill 679
16.13 Coulomb's Passive Earth Pressure 681
16.14 Comments on the Failure Surface Assumption for Coulomb's Pressure Calculations 683
16.15 Caquot and Kerisel Solution for Passive Earth Pressure (Granular Backfill) 684
16.16 Solution for Passive Earth Pressure by the Lower Bound Theorem of Plasticity (Granular Backfill) 686
16.17 Passive Force on Walls with Earthquake Forces 688
16.18 Summary 691

PROBLEMS 691
REFERENCES 693

16.1 Introduction

Vertical or near-vertical slopes of soil are supported by retaining walls, cantilever sheet-pile walls, sheet-pile bulkheads, braced cuts, and other similar structures. The proper design of those structures requires an estimation of lateral earth pressure, which is a function of several factors, such as (a) the type and amount of wall movement, (b) the shear strength parameters of the soil, (c) the unit weight of the soil, and (d) the drainage conditions in the backfill. Figure 16.1 shows a retaining wall of height H. For similar types of backfill,

a. The wall may be restrained from moving (Figure 16.1a). The lateral earth pressure on the wall at any depth is called the *at-rest earth pressure*.

b. The wall may tilt away from the soil that is retained (Figure 16.1b). With sufficient wall tilt, a triangular soil wedge behind the wall will fail. The lateral pressure for this condition is referred to as *active earth pressure*.

c. The wall may be pushed into the soil that is retained (Figure 16.1c). With sufficient wall movement, a soil wedge will fail. The lateral pressure for this condition is referred to as *passive earth pressure*.

Figure 16.2 shows the nature of variation of the lateral pressure, σ_h', at a certain depth of the wall with the magnitude of wall movement. The wall movement

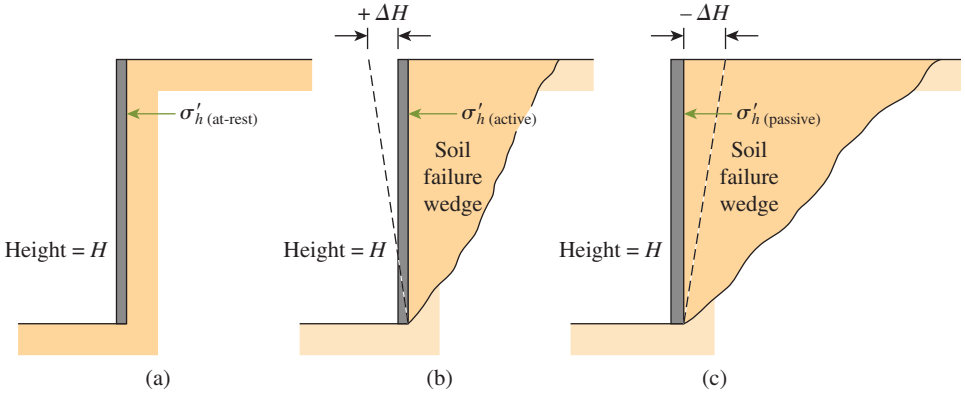


FIGURE 16.1 Nature of lateral earth pressure on a retaining wall

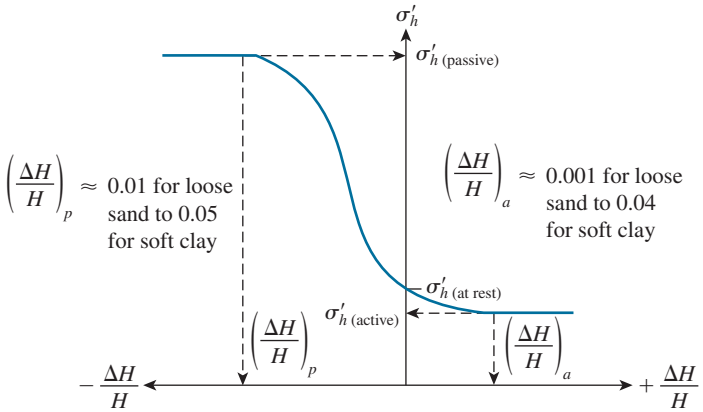


FIGURE 16.2 Nature of variation of lateral earth pressure at a certain depth



(a)



(b)



(c)

FIGURE 16.3 Earth retaining structures: (a) retaining wall; (b) crib wall; (c) basement wall (Courtesy of N. Sivakugan, James Cook University, Australia)

required to mobilize the active state is less than that required to mobilize the passive state.

In this chapter, we will focus on the three special cases of lateral earth pressures:

- At-rest earth pressure
- Active earth pressure
- Passive earth pressure

Here, active and passive pressures are the two extreme loadings where the soil is at failure. The principles and procedures for determining the lateral earth pressures under these special cases are discussed in this chapter. It is assumed that the reader has studied lateral earth pressure in the past, so this chapter will serve as a review. Figure 16.3 shows some examples of earth retaining structures.

16.2 Lateral Earth Pressure at Rest

In a homogeneous soil mass where the ground level is horizontal, the ratio of the effective horizontal stress (σ'_h) to the effective vertical stress (σ'_v) at any point within the soil is a constant, specific to the soil. The soil is known to be "at rest" and the constant is called the coefficient of earth pressure at rest, denoted by K_o. When the soil is at rest, there is no lateral strain within the soil. A clay element subjected to one-dimensional consolidation does not undergo any lateral strains and hence is in the K_o state (at rest).

Measuring K_o in the laboratory or *in situ* is not straightforward. It is often estimated using empirical correlations. For normally consolidated soil, K_o can be estimated by (Jaky, 1944)

$$K_o = 1 - \sin\phi' \tag{16.1}$$

Alpan (1967) suggested that for normally consolidated clays

$$K_o = 0.19 + 0.233 \log \text{PI} \tag{16.2}$$

Massarsch (1979) suggested that for normally consolidated clays,

$$K_o = 0.44 + 0.0042 \text{ PI} \tag{16.3}$$

K_o of an overconsolidated soil, either granular or cohesive, is greater than when it is normally consolidated. It is estimated by

$$K_{o(\text{overconsolidated})} = K_{o(\text{normally consolidated})}\text{OCR}^m \tag{16.4}$$

where OCR = overconsolidation ratio. Mayne and Kulhawy (1982) suggested that $m = \sin\phi'$, which is sometimes approximated as 0.5.

K_o of a normally consolidated soil is typically in the range of 0.4–0.6, and when soil are overconsolidated it can be larger and sometimes even exceed 1.0. When the soil mass is treated as a linear elastic continuum, the coefficient of earth pressure at rest is expressed as

$$K_o = \frac{\mu}{1 - \mu} \tag{16.5}$$

where μ is the Poisson's ratio of the elastic medium.

Consider a vertical wall of height H, as shown in Figure 16.4, retaining a soil having a unit weight of γ. A uniformly distributed load, q/unit area, is also applied at the ground surface. The shear strength of the soil is

$$s = c' + \sigma' \tan\phi'$$

where

c' = cohesion

ϕ' = effective angle of friction

σ' = effective normal stress

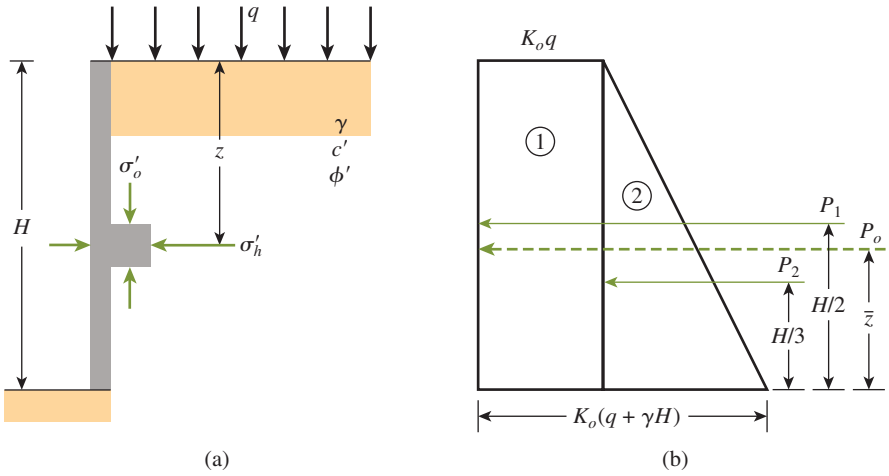


FIGURE 16.4 At-rest earth pressure

At any depth z below the ground surface, the vertical subsurface stress is

$$\sigma'_o = q + \gamma z \tag{16.6}$$

If the *wall is at rest and is not allowed to move at all*, either away from the soil mass or into the soil mass (i.e., there is zero horizontal strain), the lateral pressure at a depth z is

$$\sigma_h = K_o\sigma'_o + u \tag{16.7}$$

where

u = pore water pressure

With a properly selected value of the at-rest earth pressure coefficient, Eq. (16.7) can be used to determine the variation of lateral earth pressure with depth z. Figure 16.4b shows the variation of σ'_h with depth for the wall depicted in Figure 16.4a. Note that if the surcharge $q = 0$ and the pore water pressure $u = 0$, the pressure diagram will be a triangle. The total force, P_o, *per unit length* of the wall given in Figure 16.4a can now be obtained from the area of the pressure diagram given in Figure 16.4b and is

$$P_o = P_1 + P_2 = qK_oH + \tfrac{1}{2}\gamma H^2K_o \tag{16.8}$$

where

P_1 = area of rectangle 1

P_2 = area of triangle 2

The location of the line of action of the resultant force, P_o, can be obtained by taking the moment about the bottom of the wall. Thus,

$$\bar{z} = \frac{P_1\left(\frac{H}{2}\right) + P_2\left(\frac{H}{3}\right)}{P_o} \tag{16.9}$$

If the water table is located at a depth $z < H$, the at-rest pressure diagram shown in Figure 16.4b will have to be somewhat modified, as shown in Figure 16.5. If the effective unit weight of soil below the water table equals γ' (i.e., $\gamma_{sat} - \gamma_w$), then

at $z = 0$, $\quad \sigma'_h = K_o\sigma'_o = K_oq$

at $z = H_1$, $\quad \sigma'_h = K_o\sigma'_o = K_o(q + \gamma H_1)$

and

at $z = H_2$, $\quad \sigma'_h = K_o\sigma'_o = K_o(q + \gamma H_1 + \gamma' H_2)$

Note that in the preceding equations, σ'_o and σ'_h are effective vertical and horizontal pressures, respectively. Determining the total pressure distribution on the wall requires adding the hydrostatic pressure u, which is zero from $z = 0$ to $z = H_1$ and is $H_2\gamma_w$ at $z = H_2$. The variation of σ'_h and u with depth is shown in Figure 16.5b. Hence, the total force per unit length of the wall can be determined from the area of the pressure diagram. Specifically,

$$P_o = A_1 + A_2 + A_3 + A_4 + A_5$$

where A = area of the pressure diagram. (*Note:* A_5 is the horizontal load due to pore water pressure.)

So,

$$P_o = K_oqH_1 + \tfrac{1}{2}K_o\gamma H_1^2 + K_o(q + \gamma H_1)H_2 + \tfrac{1}{2}K_o\gamma' H_2^2 + \tfrac{1}{2}\gamma_w H_2^2 \tag{16.10}$$

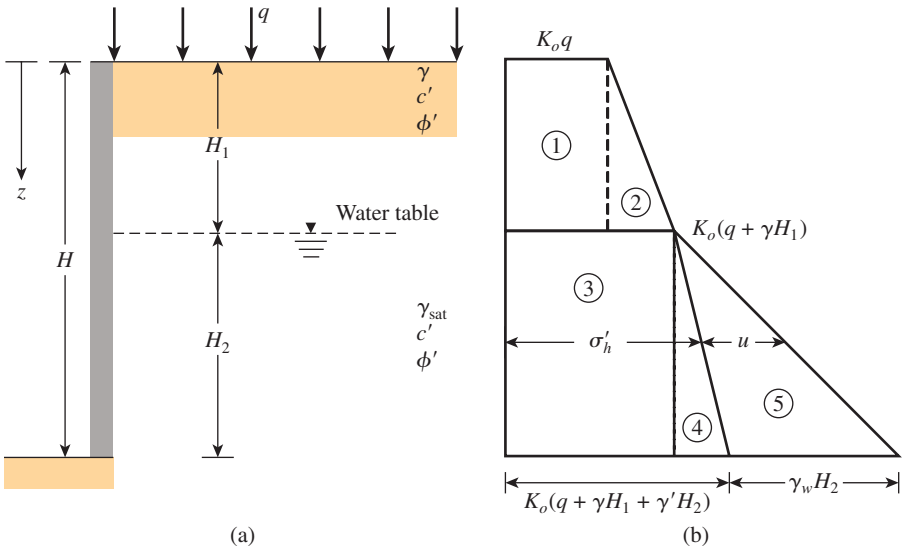


FIGURE 16.5 At-rest earth pressure with water table located at a depth $z < H$

EXAMPLE 16.1

For the retaining wall shown in Figure 16.6a, determine the lateral earth force at rest per unit length of the wall. Also determine the location of the resultant force. Assume OCR = 1.

SOLUTION

$$K_o = 1 - \sin\phi' = 1 - \sin 30^\circ = 0.5$$

At $z = 0$, $\sigma_o' = 0$; $\sigma_h' = 0$

At $z = 2.5$ m, $\sigma_o' = (16.5)(2.5) = 41.25$ kN/m^2;

$$\sigma_h' = K_o\sigma_o' = (0.5)(41.25) = 20.63 \text{ kN/m}^2$$

At $z = 5$ m, $\sigma_o' = (16.5)(2.5) + (19.3 - 9.81)2.5 = 64.98$ kN/m^2;

$$\sigma_h' = K_o\sigma_o' = (0.5)(64.98) = 32.49 \text{ kN/m}^2$$

The hydrostatic pressure distribution is as follows:

From $z = 0$ to $z = 2.5$ m, $u = 0$. At $z = 5$ m, $u = \gamma_w(2.5) = (9.81)(2.5) = 24.53$ kN/m^2.

The pressure distribution for the wall is shown in Figure 16.6b.

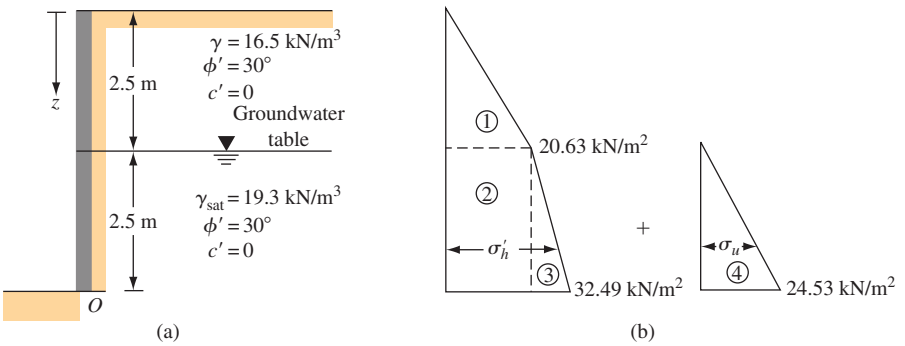


FIGURE 16.6

The total force per unit length of the wall can be determined from the area of the pressure diagram, or

$$\begin{aligned} P_o &= \text{Area 1} + \text{Area 2} + \text{Area 3} + \text{Area 4} \\ &= \tfrac{1}{2}(2.5)(20.63) + (2.5)(20.63) + \tfrac{1}{2}(2.5)(32.49 - 20.63) \\ &\quad + \tfrac{1}{2}(2.5)(24.53) = \mathbf{122.85\ kN/m} \end{aligned}$$

The location of the center of pressure measured from the bottom of the wall (point O) =

$$\begin{aligned} \bar{z} &= \frac{(\text{Area 1})\left(2.5 + \frac{2.5}{3}\right) + (\text{Area 2})\left(\frac{2.5}{2}\right) + (\text{Area 3} + \text{Area 4})\left(\frac{2.5}{3}\right)}{P_o} \\ &= \frac{(25.788)(3.33) + (51.575)(1.25) + (14.825 + 30.663)(0.833)}{122.85} \\ &= \frac{85.87 + 64.47 + 37.89}{122.85} = \mathbf{1.53\ m} \end{aligned}$$

Active Pressure

16.3 Rankine Active Earth Pressure

The lateral earth pressure described in Section 16.2 involves walls that do not yield at all. However, if a wall tends to move away from the soil a distance Δx, as shown in Figure 16.7a, the soil pressure on the wall at any depth will decrease while the vertical overburden pressure σ'_o remains the same. For a wall that is *frictionless*, the horizontal stress, σ'_h, at depth z will equal $K_o\sigma'_o$ $(=K_o\gamma z)$ when Δx is zero. However, with $\Delta x > 0$, σ'_h will be less than $K_o\sigma'_o$.

The Mohr's circles corresponding to wall displacements of $\Delta x = 0$ and $\Delta x > 0$ are shown as circles a and b, respectively, in Figure 16.7b. If the displacement of the wall, Δx, continues to increase, the corresponding Mohr's circle becomes larger and eventually will just touch the Mohr–Coulomb failure envelope defined by the equation

$$s = c' + \sigma' \tan \phi'$$

When failure occurs, the circle, marked c in the figure, represents the failure condition in the soil mass; the horizontal stress then equals σ'_a, referred to as the *Rankine active pressure*. The *slip lines* (failure planes) in the soil mass will then make angles of $\pm(45 + \phi'/2)$ with the horizontal, as shown in Figure 16.7a.

Equation (2.91) relates the principal stresses for a Mohr's circle that touches the Mohr–Coulomb failure envelope:

$$\sigma'_1 = \sigma'_3 \tan^2\left(45 + \frac{\phi'}{2}\right) + 2c' \tan\left(45 + \frac{\phi'}{2}\right)$$

For the Mohr's circle c in Figure 16.7b,

$$\text{Major principal stress, } \sigma'_1 = \sigma'_o$$

and

$$\text{Minor principal stress, } \sigma'_3 = \sigma'_a$$

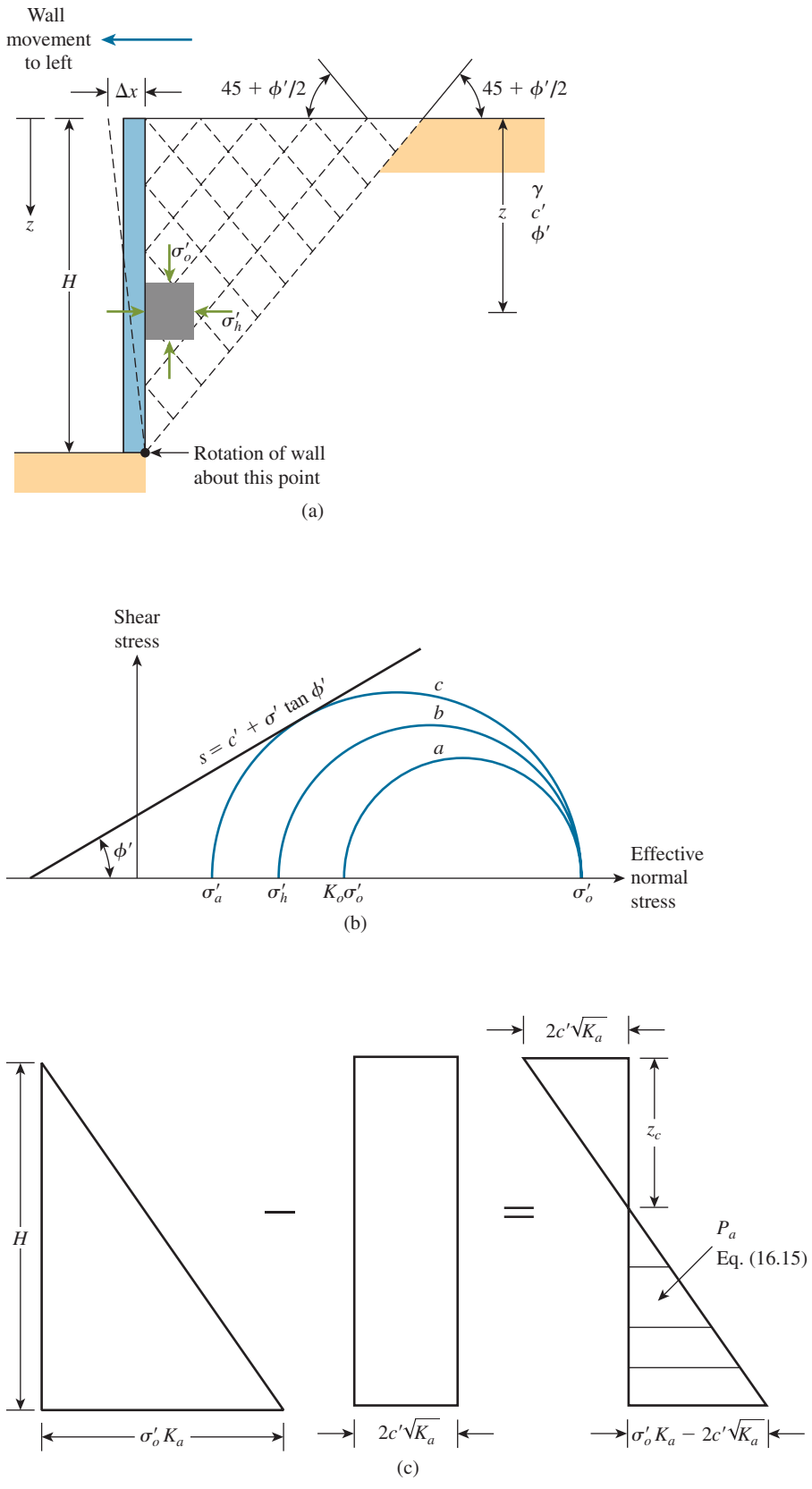


FIGURE 16.7 Rankine active pressure

Thus,

$$\sigma'_o = \sigma'_a \tan^2\left(45 + \frac{\phi'}{2}\right) + 2c' \tan\left(45 + \frac{\phi'}{2}\right)$$

$$\sigma'_a = \frac{\sigma'_o}{\tan^2\left(45 + \frac{\phi'}{2}\right)} - \frac{2c'}{\tan\left(45 + \frac{\phi'}{2}\right)}$$

or

$$\begin{aligned}\sigma'_a &= \sigma'_o \tan^2\left(45 - \frac{\phi'}{2}\right) - 2c' \tan\left(45 - \frac{\phi'}{2}\right) \\ &= \sigma'_o K_a - 2c'\sqrt{K_a}\end{aligned} \tag{16.11}$$

where $K_a = \tan^2(45 - \phi'/2) = \frac{1 - \sin\phi'}{1 + \sin\phi'}$ = Rankine active-pressure coefficient.

The variation of the active pressure with depth for the wall shown in Figure 16.7a is given in Figure 16.7c. Note that $\sigma'_o = 0$ at $z = 0$ and $\sigma'_o = \gamma H$ at $z = H$. The pressure distribution shows that at $z = 0$ the active pressure equals $-2c'\sqrt{K_a}$, indicating a tensile stress that decreases with depth and becomes zero at a depth $z = z_c$, or

$$\gamma z_c K_a - 2c'\sqrt{K_a} = 0$$

and

$$z_c = \frac{2c'}{\gamma\sqrt{K_a}} \tag{16.12}$$

The depth z_c is usually referred to as the *depth of tensile crack*, because the tensile stress in the soil will eventually cause a crack along the soil–wall interface. Thus, the total Rankine active force per unit length of the wall before the tensile crack occurs is

$$\begin{aligned}P_a &= \int_0^H \sigma'_a dz = \int_0^H \gamma z K_a dz - \int_0^H 2c'\sqrt{K_a} dz \\ &= \tfrac{1}{2}\gamma H^2 K_a - 2c' H\sqrt{K_a}\end{aligned} \tag{16.13}$$

After the tensile crack appears, the force per unit length on the wall will be caused only by the pressure distribution between depths $z = z_c$ and $z = H$, as shown by the hatched area in Figure 16.7c. This force may be expressed as

$$P_a = \tfrac{1}{2}(H - z_c)(\gamma H K_a - 2c'\sqrt{K_a}) \tag{16.14}$$

or

$$P_a = \frac{1}{2}\left(H - \frac{2c'}{\gamma\sqrt{K_a}}\right)\left(\gamma H K_a - 2c'\sqrt{K_a}\right) \tag{16.15}$$

Inclusion of the load component coming from the tensile zone reduces the active thrust P_a, which is generally seen as a load rather than resistance. Therefore, it is a conservative practice to completely neglect the tensile region in computing P_a.

However, it is important to realize that the active earth pressure condition will be reached only if the wall is allowed to "yield" sufficiently. The necessary amount of outward displacement of the wall is about $0.001H$ to $0.004H$ for granular soil backfills and about $0.01H$ to $0.04H$ for cohesive soil backfills.

Note further that if the *total stress* shear strength parameters (c, ϕ) were used, an equation similar to Eq. (16.11) could have been derived, namely,

$$\sigma_a = \sigma_o \tan^2\left(45 - \frac{\phi}{2}\right) - 2c \tan\left(45 - \frac{\phi}{2}\right)$$

EXAMPLE 16.2

A 6 m high retaining wall is to support a soil with unit weight $\gamma = 17.4$ kN/m^3, soil friction angle $\phi' = 26°$, and cohesion $c' = 5$ kN/m^2. Determine the Rankine active force per unit length of the wall both before and after the tensile crack occurs, and determine the line of action of the resultant in both cases.

SOLUTION

For $\phi' = 26°$,

$$K_a = \tan^2\left(45 - \frac{\phi'}{2}\right) = \tan^2(45 - 13) = 0.39$$

$$\sqrt{K_a} = 0.625$$

$$\sigma'_a = \gamma H K_a - 2c'\sqrt{K_a}$$

From Figure 16.7c, at $z = 0$,

$$\sigma'_a = -2c'\sqrt{K_a} = -2(5)(0.625) = -6.25 \text{ kN/m}^2$$

and at $z = 6$ m,

$$\sigma'_a = (17.4)(6)(0.39) - 2(5)(0.625)$$
$$= 40.72 - 6.25 = 34.47 \text{ kN/m}^2$$

Active Force Before the Tensile Crack Appeared: Eq. (16.13)

$$P_a = \tfrac{1}{2}\gamma H^2 K_a - 2c'H\sqrt{K_a}$$
$$= \tfrac{1}{2}(6)(40.72) - (6)(6.25) = 122.16 - 37.5 = \mathbf{84.66 \text{ kN/m}}$$

The line of action of the resultant can be determined by taking the moment of the area of the pressure diagrams about the bottom of the wall, or

$$P_a\bar{z} = (122.16)\left(\frac{6}{3}\right) - (37.5)\left(\frac{6}{2}\right)$$

Thus,

$$\bar{z} = \frac{244.32 - 112.5}{84.66} = \mathbf{1.56 \text{ m}}$$

Active Force After the Tensile Crack Appeared: Eq. (16.12)

$$z_c = \frac{2c'}{\gamma\sqrt{K_a}} = \frac{2(5.0)}{(17.4)(0.625)} = 0.92 \text{ m}$$

Using Eq. (16.14) gives

$$P_a = \tfrac{1}{2}(H - z_c)(\gamma H K_a - 2c'\sqrt{K_a}) = \tfrac{1}{2}(6 - 0.92)(34.47) = \mathbf{87.55 \text{ kN/m}}$$

Figure 16.7c indicates that the force $P_a = 87.55$ kN/m is the area of the hatched triangle. Hence, the line of action of the resultant will be located at a height $\bar{z} = (H - z_c)/3$ above the bottom of the wall, or

$$\bar{z} = \frac{6 - 0.92}{3} = \mathbf{1.69 \text{ m}}$$

EXAMPLE 16.3

Assume that the retaining wall shown in Figure 16.8a can yield sufficiently to develop an active state. Determine the Rankine active force per unit length of the wall and the location of the resultant line of action.

SOLUTION

If the cohesion, c', is zero, then

$$\sigma'_a = \sigma'_o K_a$$

For the top layer of soil, $\phi'_1 = 30°$, so

$$K_{a(1)} = \tan^2\left(45 - \frac{\phi'_1}{2}\right) = \tan^2(45 - 15) = \frac{1}{3}$$

Similarly, for the bottom layer of soil, $\phi'_2 = 36°$, and it follows that

$$K_{a(2)} = \tan^2\left(45 - \frac{36}{2}\right) = 0.26$$

The following table shows the calculation of σ'_a and u at various depths below the ground surface.

Depth, z (ft)	σ'_o (lb/ft^2)	K_a	$\sigma'_a = K_a \sigma'_o$ (lb/ft^2)	u (lb/ft^2)
0	0	1/3	0	0
10^-	(102)(10) = 1020	1/3	340	0
10^+	1020	0.26	265.2	0
20	(102)(10) + (121 − 62.4)(10) = 1606	0.26	417.6	(62.4)(10) = 624

The pressure distribution diagram is plotted in Figure 16.8b. The force per unit length is

$$\begin{aligned} P_a &= \text{area 1} + \text{area 2} + \text{area 3} + \text{area 4} \\ &= \tfrac{1}{2}(10)(340) + (265.2)(10) + \tfrac{1}{2}(417.6 - 265.2)(10) + \tfrac{1}{2}(624)(10) \\ &= 1700 + 2652 + 762 + 3120 = \mathbf{8234\ lb/ft} \end{aligned}$$

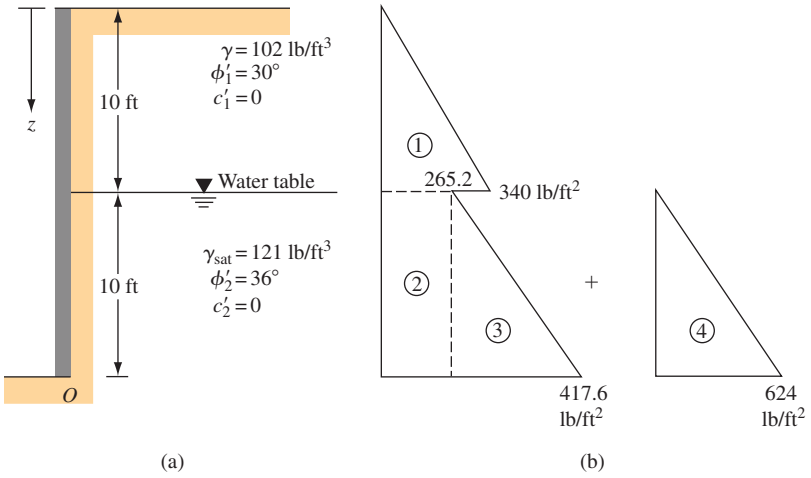


FIGURE 16.8 Rankine active force behind a retaining wall

The distance of the line of action of the resultant force from the bottom of the wall can be determined by taking the moments about the bottom of the wall (point O in Figure 16.8a) and is

$$\bar{z} = \frac{(1700)\left(10 + \frac{10}{2}\right) + (2652)\left(\frac{10}{2}\right) + (762 + 3120)\left(\frac{10}{3}\right)}{8234} = \mathbf{5.93\ ft}$$

16.4 A Generalized Case for Rankine Active Pressure—Granular Backfill

In Section 16.3, the relationship was developed for Rankine active pressure for a retaining wall with a vertical back and a horizontal backfill. That can be extended to general cases of frictionless walls with inclined backs and inclined backfills.

Figure 16.9 shows a retaining wall whose back is inclined at an angle θ with the vertical. The granular backfill is inclined at an angle α with the horizontal.

For a Rankine active case, the lateral earth pressure (σ'_a) at a depth z can be given as (Chu, 1991)

$$\sigma'_a = \frac{\gamma z \cos\alpha \sqrt{1 + \sin^2\phi' - 2\sin\phi'\cos\psi_a}}{\cos\alpha + \sqrt{\sin^2\phi' - \sin^2\alpha}} \tag{16.16}$$

where $\psi_a = \sin^{-1}\left(\frac{\sin\alpha}{\sin\phi'}\right) - \alpha + 2\theta.$ (16.17)

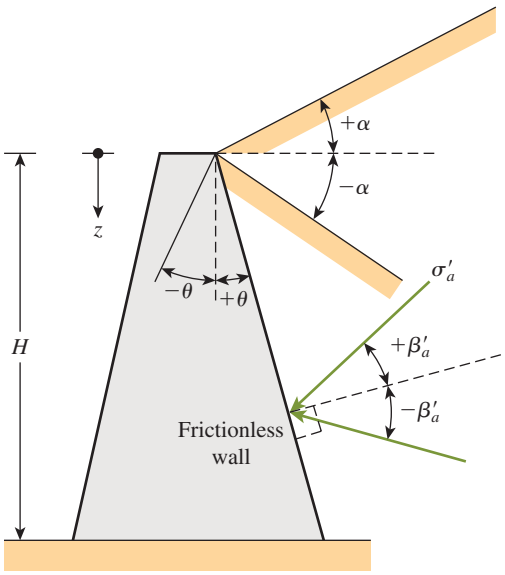


FIGURE 16.9 General case for a retaining wall with granular backfill

The pressure σ'_a will be inclined at an angle β'_a with the plane drawn at right angle to the backface of the wall, and

$$\beta'_a = \tan^{-1}\left(\frac{\sin\phi' \sin\psi_a}{1 - \sin\phi' \cos\psi_a}\right) \tag{16.18}$$

The active force, P_a, for unit length of the wall then can be calculated as

$$P_a = \frac{1}{2}\gamma H^2 K_{a(R)} \tag{16.19}$$

where

$$K_{asRd} = \frac{\cos(\alpha - \theta)\sqrt{1 + \sin^2\phi' - 2\sin\phi' \cos\psi_a}}{\cos^2\theta\left(\cos\alpha + \sqrt{\sin^2\phi' - \sin^2\alpha}\right)}$$
$$= \text{Rankine active earth-pressure coefficient for generalized case} \tag{16.20}$$

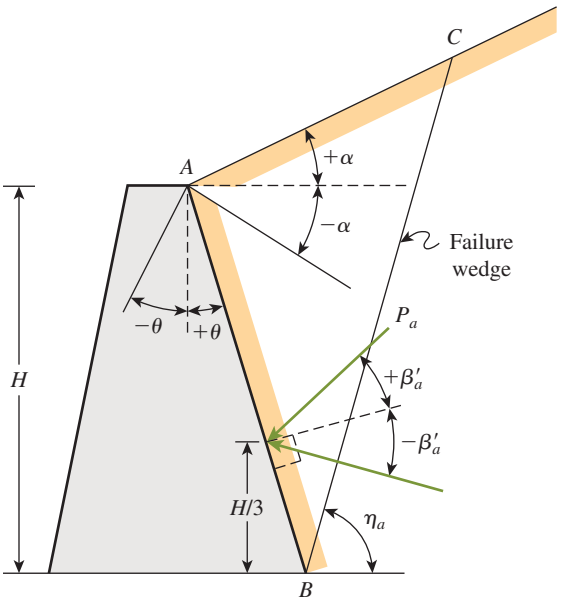
The location and direction of the resultant force P_a is shown in Figure 16.10. Also shown in this figure is the failure wedge, ABC. Note that BC will be inclined at an angle η_a. Or

$$\eta_a = \frac{\pi}{4} + \frac{\phi'}{2} + \frac{\alpha}{2} - \frac{1}{2}\sin^{-1}\left(\frac{\sin\alpha}{\sin\phi'}\right) \tag{16.21}$$

Tables 16.1 and 16.2 give the variations of $K_{a(R)}$ [Eq. (16.20)] and β'_a [Eq. (16.18)] for various values of α, θ, and ϕ'.

GRANULAR BACKFILL WITH VERTICAL BACK FACE OF WALL

As a special case, for a vertical backface of a wall (that is, $\theta = 0$), as shown in Figure 16.11, Eqs. (16.16), (16.19), and (16.20) simplify to the following:



$$\eta_a = \frac{\pi}{4} + \frac{\phi'}{2} + \frac{\alpha}{2} - \frac{1}{2}\sin^{-1}\left(\frac{\sin\alpha}{\sin\phi'}\right)$$

FIGURE 16.10 Location and direction of Rankine active force

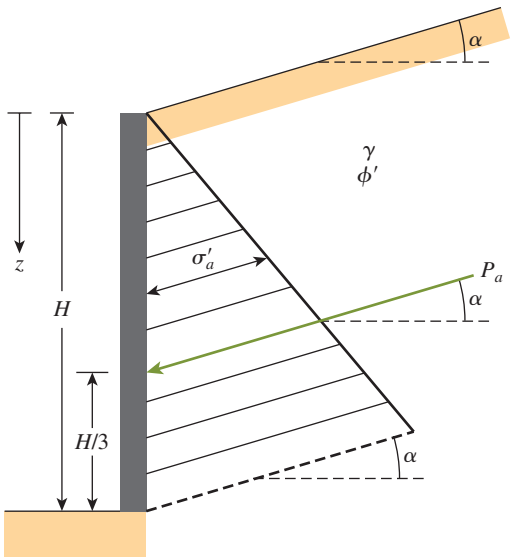


FIGURE 16.11 Notations for active pressure—Eqs. (16.22), (16.23), (16.24)

TABLE 16.1 Variation of $K_{a(R)}$ [Eq. (16.20)]

		$K_{a(R)}$						
		ϕ' (deg)						
α (deg)	θ (deg)	28	30	32	34	36	38	40
0	0	0.361	0.333	0.307	0.283	0.260	0.238	0.217
	2	0.363	0.335	0.309	0.285	0.262	0.240	0.220
	4	0.368	0.341	0.315	0.291	0.269	0.248	0.228
	6	0.376	0.350	0.325	0.302	0.280	0.260	0.242
	8	0.387	0.362	0.338	0.316	0.295	0.276	0.259
	10	0.402	0.377	0.354	0.333	0.314	0.296	0.280
	15	0.450	0.428	0.408	0.390	0.373	0.358	0.345
5	0	0.366	0.337	0.311	0.286	0.262	0.240	0.219
	2	0.373	0.344	0.317	0.292	0.269	0.247	0.226
	4	0.383	0.354	0.328	0.303	0.280	0.259	0.239
	6	0.396	0.368	0.342	0.318	0.296	0.275	0.255
	8	0.412	0.385	0.360	0.336	0.315	0.295	0.276
	10	0.431	0.405	0.380	0.358	0.337	0.318	0.300
	15	0.490	0.466	0.443	0.423	0.405	0.388	0.373
10	0	0.380	0.350	0.321	0.294	0.270	0.246	0.225
	2	0.393	0.362	0.333	0.306	0.281	0.258	0.236
	4	0.408	0.377	0.348	0.322	0.297	0.274	0.252
	6	0.426	0.395	0.367	0.341	0.316	0.294	0.273
	8	0.447	0.417	0.389	0.363	0.339	0.317	0.297
	10	0.471	0.441	0.414	0.388	0.365	0.344	0.324
	15	0.542	0.513	0.487	0.463	0.442	0.422	0.404
15	0	0.409	0.373	0.341	0.311	0.283	0.258	0.235
	2	0.427	0.391	0.358	0.328	0.300	0.274	0.250
	4	0.448	0.411	0.378	0.348	0.320	0.294	0.271
	6	0.472	0.435	0.402	0.371	0.344	0.318	0.295
	8	0.498	0.461	0.428	0.398	0.371	0.346	0.323
	10	0.527	0.490	0.457	0.428	0.400	0.376	0.353
	15	0.610	0.574	0.542	0.513	0.487	0.463	0.442
20	0	0.461	0.414	0.374	0.338	0.306	0.277	0.250
	2	0.486	0.438	0.397	0.360	0.328	0.298	0.271
	4	0.513	0.465	0.423	0.386	0.353	0.323	0.296
	6	0.543	0.495	0.452	0.415	0.381	0.351	0.324
	8	0.576	0.527	0.484	0.446	0.413	0.383	0.355
	10	0.612	0.562	0.518	0.481	0.447	0.417	0.390
	15	0.711	0.660	0.616	0.578	0.545	0.515	0.488

TABLE 16.2 Variation of β'_a [Eq. (16.18)]

		β'_a						
		ϕ' (deg)						
α (deg)	θ (deg)	28	30	32	34	36	38	40
0	0	0.000	0.000	0.000	0.000	0.000	0.000	0.000
	2	3.525	3.981	4.484	5.041	5.661	6.351	7.124
	4	6.962	7.848	8.821	9.893	11.075	12.381	13.827
	6	10.231	11.501	12.884	14.394	16.040	17.837	19.797
	8	13.270	14.861	16.579	18.432	20.428	22.575	24.876
	10	16.031	17.878	19.850	21.951	24.184	26.547	29.039
	15	21.582	23.794	26.091	28.464	30.905	33.402	35.940
5	0	5.000	5.000	5.000	5.000	5.000	5.000	5.000
	2	8.375	8.820	9.311	9.854	10.455	11.123	11.870
	4	11.553	12.404	13.336	14.358	15.482	16.719	18.085
	6	14.478	15.679	16.983	18.401	19.942	21.618	23.441
	8	17.112	18.601	20.203	21.924	23.773	25.755	27.876
	10	19.435	21.150	22.975	24.915	26.971	29.144	31.434
	15	23.881	25.922	28.039	30.227	32.479	34.787	37.140
10	0	10.000	10.000	10.000	10.000	10.000	10.000	10.000
	2	13.057	13.491	13.967	14.491	15.070	15.712	16.426
	4	15.839	16.657	17.547	18.519	19.583	20.751	22.034
	6	18.319	19.460	20.693	22.026	23.469	25.032	26.726
	8	20.483	21.888	23.391	24.999	26.720	28.559	30.522
	10	22.335	23.946	25.653	27.460	29.370	31.385	33.504
	15	25.683	27.603	29.589	31.639	33.747	35.908	38.114
15	0	15.000	15.000	15.000	15.000	15.000	15.000	15.000
	2	17.576	18.001	18.463	18.967	19.522	20.134	20.812
	4	19.840	20.631	21.485	22.410	23.417	24.516	25.719
	6	21.788	22.886	24.060	25.321	26.677	28.139	29.716
	8	23.431	24.778	26.206	27.722	29.335	31.052	32.878
	10	24.783	26.328	27.950	29.654	31.447	33.332	35.310
	15	27.032	28.888	30.793	32.747	34.751	36.802	38.894
20	0	20.000	20.000	20.000	20.000	20.000	20.000	20.000
	2	21.925	22.350	22.803	23.291	23.822	24.404	25.045
	4	23.545	24.332	25.164	26.054	27.011	28.048	29.175
	6	24.876	25.966	27.109	28.317	29.604	30.980	32.455
	8	25.938	27.279	28.669	30.124	31.657	33.276	34.989
	10	26.755	28.297	29.882	31.524	33.235	35.021	36.886
	15	27.866	29.747	31.638	33.552	35.498	37.478	39.491

If the backfill of a smooth retaining wall (with a vertical backface) is a *granular soil* ($c' = 0$) and rises at an angle α with respect to the horizontal (see Figure 16.11), the *active earth pressure coefficient* may be expressed in the form

$$K_{a(R)} = K_a = \cos\alpha \frac{\cos\alpha - \sqrt{\cos^2\alpha - \cos^2\phi'}}{\cos\alpha + \sqrt{\cos^2\alpha - \cos^2\phi'}} \tag{16.22}$$

where ϕ' = angle of friction of soil.

At any depth z, the *Rankine active pressure* may be expressed as

$$\sigma'_a = \gamma z K_a \tag{16.23}$$

Also, the total force per unit length of the wall is

$$P_a = \tfrac{1}{2}\gamma H^2 K_a \tag{16.24}$$

Note that in this case, the direction of the resultant force P_a is *inclined at an angle α with the horizontal* and intersects the wall at a distance $H/3$ from the base of the wall. Table 16.3 presents the values of K_a (active earth pressure) for various values of α and ϕ'.

16.5 Generalized Case for Rankine Seismic Active Earth Pressure—Granular Backfill

Iskander et al. (2003) have provided a solution for a generalized case for Rankine active earth pressure $P_{ae(R)}$ taking into consideration earthquake loading. This was based on the conjugate stress concept. For this analysis, we define:

a. Coefficient of horizontal acceleration,

$$k_h = \frac{\text{horizontal earthquake acceleration component}}{g} \tag{16.25}$$

and

b. Coefficient of vertical acceleration,

$$k_v = \frac{\text{vertical earthquake acceleration component}}{g} \tag{16.26}$$

where g is the acceleration due to gravity.

Now, referring to Figure 16.12,

$$P_{ae(R)} = \frac{1}{2}(1 - k_v)\gamma H^2 K_{ae(R)} \tag{16.27}$$

where $K_{ae(R)}$ = seismic Rankine active earth pressure coefficient.

The coefficient $K_{ae(R)}$ is given by the relationship

$$K_{ae(R)} = \frac{\cos^3(\alpha - \theta)m_a + \cos(\alpha - \theta)\sin^2(\theta' + \theta)}{\cos\beta''_a \cos^2\theta \cos(\alpha + \theta')\cos\theta'} \tag{16.28}$$

TABLE 16.3 Values of K_a for Wall with Vertical Backface and Inclined Backfill [Eq. (16.22)]

α (deg) ↓	ϕ' (deg) →												
	28	29	30	31	32	33	34	35	36	37	38	39	40
0	0.3610	0.3470	0.3333	0.3201	0.3073	0.2948	0.2827	0.2710	0.2596	0.2486	0.2379	0.2275	0.2174
1	0.3612	0.3471	0.3335	0.3202	0.3074	0.2949	0.2828	0.2711	0.2597	0.2487	0.2380	0.2276	0.2175
2	0.3618	0.3476	0.3339	0.3207	0.3078	0.2953	0.2832	0.2714	0.2600	0.2489	0.2382	0.2278	0.2177
3	0.3627	0.3485	0.3347	0.3214	0.3084	0.2959	0.2837	0.2719	0.2605	0.2494	0.2386	0.2282	0.2181
4	0.3639	0.3496	0.3358	0.3224	0.3094	0.2967	0.2845	0.2726	0.2611	0.2500	0.2392	0.2287	0.2186
5	0.3656	0.3512	0.3372	0.3237	0.3105	0.2978	0.2855	0.2736	0.2620	0.2508	0.2399	0.2294	0.2192
6	0.3676	0.3531	0.3389	0.3253	0.3120	0.2992	0.2868	0.2747	0.2631	0.2518	0.2409	0.2303	0.2200
7	0.3701	0.3553	0.3410	0.3272	0.3138	0.3008	0.2883	0.2761	0.2644	0.2530	0.2420	0.2313	0.2209
8	0.3730	0.3580	0.3435	0.3294	0.3159	0.3027	0.2900	0.2778	0.2659	0.2544	0.2432	0.2325	0.2220
9	0.3764	0.3611	0.3463	0.3320	0.3182	0.3049	0.2921	0.2796	0.2676	0.2560	0.2447	0.2338	0.2233
10	0.3802	0.3646	0.3495	0.3350	0.3210	0.3074	0.2944	0.2818	0.2696	0.2578	0.2464	0.2354	0.2247
11	0.3846	0.3686	0.3532	0.3383	0.3241	0.3103	0.2970	0.2841	0.2718	0.2598	0.2482	0.2371	0.2263
12	0.3896	0.3731	0.3573	0.3421	0.3275	0.3134	0.2999	0.2868	0.2742	0.2621	0.2503	0.2390	0.2281
13	0.3952	0.3782	0.3620	0.3464	0.3314	0.3170	0.3031	0.2898	0.2770	0.2646	0.2527	0.2412	0.2301
14	0.4015	0.3839	0.3671	0.3511	0.3357	0.3209	0.3068	0.2931	0.2800	0.2674	0.2552	0.2435	0.2322
15	0.4086	0.3903	0.3729	0.3564	0.3405	0.3253	0.3108	0.2968	0.2834	0.2705	0.2581	0.2461	0.2346
16	0.4165	0.3975	0.3794	0.3622	0.3458	0.3302	0.3152	0.3008	0.2871	0.2739	0.2612	0.2490	0.2373
17	0.4255	0.4056	0.3867	0.3688	0.3518	0.3356	0.3201	0.3053	0.2911	0.2776	0.2646	0.2521	0.2401
18	0.4357	0.4146	0.3948	0.3761	0.3584	0.3415	0.3255	0.3102	0.2956	0.2817	0.2683	0.2555	0.2433
19	0.4473	0.4249	0.4039	0.3842	0.3657	0.3481	0.3315	0.3156	0.3006	0.2862	0.2724	0.2593	0.2467
20	0.4605	0.4365	0.4142	0.3934	0.3739	0.3555	0.3381	0.3216	0.3060	0.2911	0.2769	0.2634	0.2504
21	0.4758	0.4498	0.4259	0.4037	0.3830	0.3637	0.3455	0.3283	0.3120	0.2965	0.2818	0.2678	0.2545
22	0.4936	0.4651	0.4392	0.4154	0.3934	0.3729	0.3537	0.3356	0.3186	0.3025	0.2872	0.2727	0.2590
23	0.5147	0.4829	0.4545	0.4287	0.4050	0.3832	0.3628	0.3438	0.3259	0.3091	0.2932	0.2781	0.2638
24	0.5404	0.5041	0.4724	0.4440	0.4183	0.3948	0.3731	0.3529	0.3341	0.3164	0.2997	0.2840	0.2692
25	0.5727	0.5299	0.4936	0.4619	0.4336	0.4081	0.3847	0.3631	0.3431	0.3245	0.3070	0.2905	0.2750

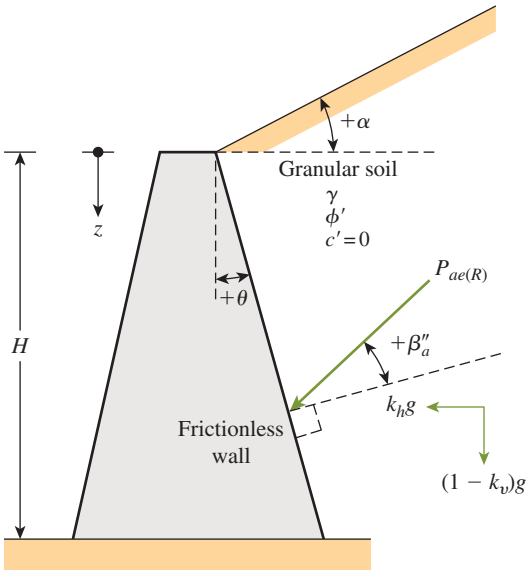


FIGURE 16.12 Generalized case for Rankine seismic active earth pressure

where

$$\theta' = \tan^{-1}\left(\frac{k_h}{1 - k_v}\right) \tag{16.29}$$

$$m_a = \frac{\cos(\alpha + \theta') - [\cos^2(\alpha + \theta') - \cos^2\phi']^{0.5}}{\cos(\alpha + \theta') + [\cos^2(\alpha + \theta') - \cos^2\phi']^{0.5}} \tag{16.30}$$

and

$$\beta_a'' = \tan^{-1}\left\{\frac{\sin 2(\theta' + \theta) + m_a \sin 2(\alpha - \theta)}{2[\sin^2(\theta' + \theta) + m_a \cos^2(\alpha - \theta)]}\right\} \tag{16.31}$$

Note that β_a'' is the inclination of $P_{ae(R)}$ with respect to the normal drawn to the backface of the wall.

16.6 Rankine Active Pressure with Vertical Wall Backface and Inclined $c' - \phi'$ Soil Backfill

For a frictionless retaining wall with a vertical backface ($\theta = 0$) and inclined backfill of $c' - \phi'$ soil (see Figure 16.11), the active pressure at any depth z can be given as (Mazindrani and Ganjali, 1997)

$$\sigma_a' = \gamma z K_a = \gamma z K_a' \cos\alpha \tag{16.32}$$

where

$$K_a' = \frac{1}{\cos^2\phi'}\left\{2\cos^2\alpha + 2\left(\frac{c'}{\gamma z}\right)\cos\phi'\sin\phi' - \sqrt{\left[4\cos^2\alpha(\cos^2\alpha - \cos^2\phi') + 4\left(\frac{c'}{\gamma z}\right)^2\cos^2\phi' + 8\left(\frac{c'}{\gamma z}\right)\cos^2\alpha\sin\phi'\cos\phi'\right]}\right\} - 1 \tag{16.33}$$

Selected values of K'_a are given in Table 16.4. Mazindrani and Ganjali (1997) also showed that in spite of the sloping backfill, the depth of the tensile crack is still given by the same expression [Eq. (16.12)] given for the horizontal backfill ($\alpha = 0$) and is expressed as

$$z_c = \frac{2c'}{\gamma}\sqrt{\frac{1 + \sin\phi'}{1 - \sin\phi'}} \tag{16.34}$$

The tensile zone should be neglected in determining the resultant active thrust P_a. The magnitude of the active pressure at any depth can be determined from Eq. (16.32). The active pressure is inclined at an angle α to the horizontal and is

TABLE 16.4 Values of K'_a

		$c'/\gamma z$						
α (deg)	ϕ' (deg)	0	0.025	0.05	0.075	0.1	0.2	0.5
0	15	0.5888	0.5504	0.5121	0.4737	0.4353	0.2819	−0.1785
0	20	0.4903	0.4553	0.4203	0.3853	0.3502	0.2102	−0.2099
0	25	0.4059	0.3740	0.3422	0.3103	0.2784	0.1510	−0.2312
0	30	0.3333	0.3045	0.2756	0.2467	0.2179	0.1024	−0.2440
0	35	0.2710	0.2450	0.2189	0.1929	0.1669	0.0628	−0.2496
0	40	0.2174	0.1941	0.1708	0.1475	0.1242	0.0309	−0.2489
5	15	0.6069	0.5658	0.5252	0.4849	0.4449	0.2867	−0.1804
5	20	0.5015	0.4650	0.4287	0.3925	0.3565	0.2133	−0.2119
5	25	0.4133	0.3805	0.3478	0.3152	0.2826	0.1530	−0.2332
5	30	0.3385	0.3090	0.2795	0.2501	0.2207	0.1036	−0.2460
5	35	0.2746	0.2481	0.2217	0.1952	0.1688	0.0634	−0.2515
5	40	0.2200	0.1964	0.1727	0.1491	0.1255	0.0312	−0.2507
10	15	0.6738	0.6206	0.5707	0.5230	0.4769	0.3022	−0.1861
10	20	0.5394	0.4974	0.4564	0.4162	0.3767	0.2230	−0.2180
10	25	0.4376	0.4015	0.3660	0.3308	0.2960	0.1590	−0.2394
10	30	0.3549	0.3233	0.2919	0.2607	0.2297	0.1072	−0.2522
10	35	0.2861	0.2581	0.2303	0.2025	0.1749	0.0654	−0.2575
10	40	0.2282	0.2034	0.1787	0.1541	0.1296	0.0321	−0.2564
15	15	1.0000	0.7762	0.6834	0.6102	0.5464	0.3324	−0.1962
15	20	0.6241	0.5666	0.5137	0.4639	0.4165	0.2411	−0.2287
15	25	0.4860	0.4428	0.4011	0.3606	0.3211	0.1700	−0.2503
15	30	0.3861	0.3502	0.3150	0.2803	0.2462	0.1137	−0.2628
15	35	0.3073	0.2764	0.2459	0.2158	0.1860	0.0690	−0.2678
15	40	0.2429	0.2161	0.1895	0.1632	0.1370	0.0338	−0.2662
20	20	1.0000	0.7432	0.6403	0.5608	0.4927	0.2718	−0.2449
20	25	0.5820	0.5207	0.4650	0.4133	0.3645	0.1879	−0.2665
20	30	0.4408	0.3964	0.3539	0.3130	0.2734	0.1241	−0.2787
20	35	0.3423	0.3064	0.2713	0.2371	0.2035	0.0746	−0.2831
20	40	0.2665	0.2363	0.2066	0.1773	0.1484	0.0363	−0.2807

parallel to the backfill slope. The K'_a value obtained from Eq. (16.33) (or Table 16.4) varies nonlinearly with depth; it is not a constant within the backfill. Mazindrani and Ganjali (1997) also showed that for $c' = 0$, Eqs. (16.23) and (16.32) give the same values of σ'_a.

EXAMPLE 16.4

Refer to the retaining wall in Figure 16.10. The backfill is granular soil. Given:

$$\begin{aligned} \text{Wall:} \quad & H = 10 \text{ ft} \\ & \theta = +10^\circ \\ \text{Backfill:} \quad & \alpha = 15^\circ \\ & \phi' = 35^\circ \\ & c' = 0 \\ & \gamma = 110 \text{ lb/ft}^3 \end{aligned}$$

Determine the Rankine active force, P_a, and its location and direction.

SOLUTION

From Table 16.1, for $\alpha = 15^\circ$ and $\theta = +10^\circ$, the value of $K_{a(R)} \approx 0.42$. From Eq. (16.19),

$$P_a = \frac{1}{2}\gamma H^2 K_{a(R)} = \left(\frac{1}{2}\right)(110)(10)^2(0.42) = \mathbf{2310 \text{ lb/ft}}$$

Again, from Table 16.2, for $\alpha = 15^\circ$ and $\theta = +10^\circ$, $\beta'_a \approx \mathbf{30.5^\circ}$.

The force P_a will act at a distance of $10/3 = 3.33$ ft above the bottom of the wall and will be inclined at an angle of $+30.5^\circ$ to the normal drawn to the backface of the wall.

■

EXAMPLE 16.5

For the retaining wall shown in Figure 16.11, $H = 7.5$ m, $\gamma = 18$ kN/m^3, $\phi' = 20^\circ$, $c' = 13.5$ kN/m^2, and $\alpha = 10^\circ$. Calculate the Rankine active force, P_a, per unit length of the wall and the location of the resultant force after the occurrence of the tensile crack.

SOLUTION

From Eq. (16.34).

$$z_r = \frac{2c'}{\gamma}\sqrt{\frac{1 + \sin\phi'}{1 - \sin\phi'}} = \frac{(2)(13.5)}{18}\sqrt{\frac{1 + \sin 20}{1 - \sin 20}} = 2.14 \text{ m}$$

At $z = 7.5$ m,

$$\frac{c'}{\gamma z} = \frac{13.5}{(18)(7.5)} = 0.1$$

From Table 16.4, for $\phi' = 20^\circ$, $c'/\gamma z = 0.1$, and $\alpha = 10^\circ$, the value of $K'_a \approx 0.377$, so at $z = 7.5$ m,

$$\sigma'_a = \gamma z K'_a \cos\alpha = (18)(7.5)(0.377)(\cos 10) = 50.1 \text{ kN/m}^2$$

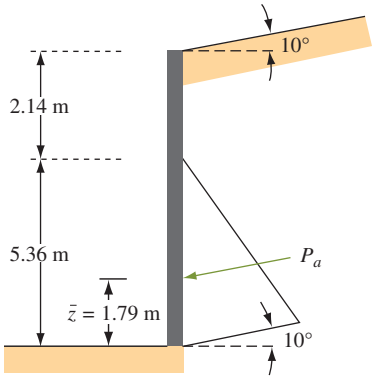


FIGURE 16.13 Calculation of Rankine active force, $c'-\phi'$ soil

After the occurrence of the tensile crack, the pressure distribution on the wall will be as shown in Figure 16.13, so

$$P_a = \left(\frac{1}{2}\right)(50.1)(7.5 - 2.14) = \mathbf{134.3\ kN/m}$$

and

$$\bar{z} = \frac{7.5 - 2.14}{3} = \mathbf{1.79\ m}$$

16.7 Coulomb's Active Earth Pressure

The Rankine active earth pressure calculations discussed in the preceding sections were based on the assumption that the wall is frictionless, which is not generally the case. In 1776, Coulomb proposed a theory for calculating the lateral earth pressure on a retaining wall with granular soil backfill. This theory takes wall friction into consideration.

To apply Coulomb's active earth pressure theory, let us consider a retaining wall with its backface inclined at an angle β with the horizontal, as shown in Figure 16.14a.

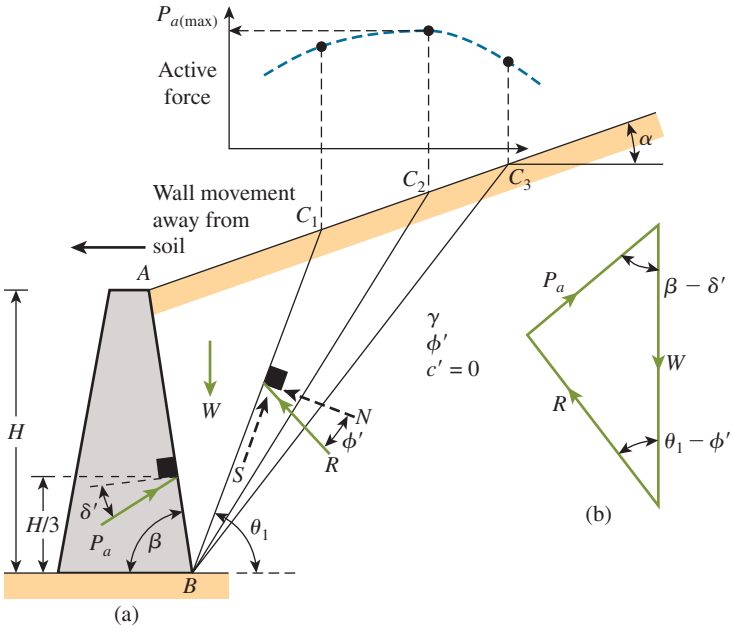


FIGURE 16.14 Coulomb's active pressure

The backfill is a granular soil that slopes at an angle α with the horizontal. Also, let δ' be the angle of friction between the soil and the wall (i.e., the angle of wall friction).

Under active pressure, the wall will move away from the soil mass (to the left in the figure). Coulomb assumed that, in such a case, the failure surface in the soil mass would be a plane passing through B (e.g., BC_1, BC_2, . . .). So to find the active force, consider a possible soil failure wedge ABC_1. The forces acting on this wedge (per unit length at right angles to the cross section shown) are as follows:

1. The weight of the wedge, W.
2. The resultant, R, of the normal and resisting shear forces along the surface, BC_1. The force R will be inclined at an angle ϕ' to the normal drawn to BC_1.
3. The active force per unit length of the wall, P_a, which will be inclined at an angle δ' to the normal drawn to the backface of the wall.

For equilibrium purposes, a force triangle can be drawn, as shown in Figure 16.14b. Note that θ_1 is the angle that BC_1 makes with the horizontal. Because the magnitude of W, as well as the directions of all three forces, is known, the value of P_a can now be determined. Similarly, the active forces of other trial wedges, such as ABC_2, ABC_3, . . . , can be determined. The maximum value of P_a thus determined is Coulomb's active force (see top part of Figure 16.14a), which may be expressed as

$$P_a = \tfrac{1}{2} K_a \gamma H^2 \tag{16.35}$$

where

$$K_a = \text{Coulomb's active earth pressure coefficient} = \frac{\sin^2(\beta + \phi')}{\sin^2\beta \sin(\beta - \delta')\left[1 + \sqrt{\dfrac{\sin(\phi' + \delta')\sin(\phi' - \alpha)}{\sin(\beta - \delta')\sin(\alpha + \beta)}}\right]^2} \tag{16.36}$$

and H = height of the wall.

The values of the active earth pressure coefficient, K_a, for a vertical retaining wall ($\beta = 90°$) with horizontal backfill ($\alpha = 0°$) are given in Table 16.5. For a smooth vertical wall ($\delta' = 0$), Rankine's and Coulomb's expressions give the same values for K_a. Note that the line of action of the resultant force (P_a) will act at a distance $H/3$ above the base of the wall and will be inclined at an angle δ' to the normal drawn to the back of the wall.

TABLE 16.5 Values of K_a [Eq. (16.36)] for $\beta = 90°$ and $\alpha = 0°$

	δ' (deg)					
ϕ' (deg)	0	5	10	15	20	25
28	0.3610	0.3448	0.3330	0.3251	0.3203	0.3186
30	0.3333	0.3189	0.3085	0.3014	0.2973	0.2956
32	0.3073	0.2945	0.2853	0.2791	0.2755	0.2745
34	0.2827	0.2714	0.2633	0.2579	0.2549	0.2542
36	0.2596	0.2497	0.2426	0.2379	0.2354	0.2350
38	0.2379	0.2292	0.2230	0.2190	0.2169	0.2167
40	0.2174	0.2098	0.2045	0.2011	0.1994	0.1995
42	0.1982	0.1916	0.1870	0.1841	0.1828	0.1831

In the actual design of retaining walls, the value of the wall friction angle δ' is assumed to be between $\frac{1}{2}\phi'$ and $\frac{2}{3}\phi'$. The active earth pressure coefficients for various values of ϕ', α, and β with $\delta' = \frac{2}{3}\phi'$ and $\frac{1}{2}\phi'$ are respectively given in Tables 16.6 and 16.7. These coefficients are very useful design considerations.

TABLE 16.6 Values of K_a [from Eq. (16.36)] for $\delta' = \frac{2}{3}\phi'$

		β (deg)					
α (deg)	ϕ' (deg)	90	85	80	75	70	65
0	28	0.3213	0.3588	0.4007	0.4481	0.5026	0.5662
	29	0.3091	0.3467	0.3886	0.4362	0.4908	0.5547
	30	0.2973	0.3349	0.3769	0.4245	0.4794	0.5435
	31	0.2860	0.3235	0.3655	0.4133	0.4682	0.5326
	32	0.2750	0.3125	0.3545	0.4023	0.4574	0.5220
	33	0.2645	0.3019	0.3439	0.3917	0.4469	0.5117
	34	0.2543	0.2916	0.3335	0.3813	0.4367	0.5017
	35	0.2444	0.2816	0.3235	0.3713	0.4267	0.4919
	36	0.2349	0.2719	0.3137	0.3615	0.4170	0.4824
	37	0.2257	0.2626	0.3042	0.3520	0.4075	0.4732
	38	0.2168	0.2535	0.2950	0.3427	0.3983	0.4641
	39	0.2082	0.2447	0.2861	0.3337	0.3894	0.4553
	40	0.1998	0.2361	0.2774	0.3249	0.3806	0.4468
	41	0.1918	0.2278	0.2689	0.3164	0.3721	0.4384
	42	0.1840	0.2197	0.2606	0.3080	0.3637	0.4302
5	28	0.3431	0.3845	0.4311	0.4843	0.5461	0.6190
	29	0.3295	0.3709	0.4175	0.4707	0.5325	0.6056
	30	0.3165	0.3578	0.4043	0.4575	0.5194	0.5926
	31	0.3039	0.3451	0.3916	0.4447	0.5067	0.5800
	32	0.2919	0.3329	0.3792	0.4324	0.4943	0.5677
	33	0.2803	0.3211	0.3673	0.4204	0.4823	0.5558
	34	0.2691	0.3097	0.3558	0.4088	0.4707	0.5443
	35	0.2583	0.2987	0.3446	0.3975	0.4594	0.5330
	36	0.2479	0.2881	0.3338	0.3866	0.4484	0.5221
	37	0.2379	0.2778	0.3233	0.3759	0.4377	0.5115
	38	0.2282	0.2679	0.3131	0.3656	0.4273	0.5012
	39	0.2188	0.2582	0.3033	0.3556	0.4172	0.4911
	40	0.2098	0.2489	0.2937	0.3458	0.4074	0.4813
	41	0.2011	0.2398	0.2844	0.3363	0.3978	0.4718
	42	0.1927	0.2311	0.2753	0.3271	0.3884	0.4625
10	28	0.3702	0.4164	0.4686	0.5287	0.5992	0.6834
	29	0.3548	0.4007	0.4528	0.5128	0.5831	0.6672
	30	0.3400	0.3857	0.4376	0.4974	0.5676	0.6516
	31	0.3259	0.3713	0.4230	0.4826	0.5526	0.6365
	32	0.3123	0.3575	0.4089	0.4683	0.5382	0.6219
	33	0.2993	0.3442	0.3953	0.4545	0.5242	0.6078
	34	0.2868	0.3314	0.3822	0.4412	0.5107	0.5942

TABLE 16.6 Values of K_a [from Eq. (16.36)] for $\delta' = \frac{2}{3}\phi'$ (*Continued*)

		β (deg)					
α (deg)	ϕ' (deg)	90	85	80	75	70	65
	35	0.2748	0.3190	0.3696	0.4283	0.4976	0.5810
	36	0.2633	0.3072	0.3574	0.4158	0.4849	0.5682
	37	0.2522	0.2957	0.3456	0.4037	0.4726	0.5558
	38	0.2415	0.2846	0.3342	0.3920	0.4607	0.5437
	39	0.2313	0.2740	0.3231	0.3807	0.4491	0.5321
	40	0.2214	0.2636	0.3125	0.3697	0.4379	0.5207
	41	0.2119	0.2537	0.3021	0.3590	0.4270	0.5097
	42	0.2027	0.2441	0.2921	0.3487	0.4164	0.4990
15	28	0.4065	0.4585	0.5179	0.5868	0.6685	0.7670
	29	0.3881	0.4397	0.4987	0.5672	0.6483	0.7463
	30	0.3707	0.4219	0.4804	0.5484	0.6291	0.7265
	31	0.3541	0.4049	0.4629	0.5305	0.6106	0.7076
	32	0.3384	0.3887	0.4462	0.5133	0.5930	0.6895
	33	0.3234	0.3732	0.4303	0.4969	0.5761	0.6721
	34	0.3091	0.3583	0.4150	0.4811	0.5598	0.6554
	35	0.2954	0.3442	0.4003	0.4659	0.5442	0.6393
	36	0.2823	0.3306	0.3862	0.4513	0.5291	0.6238
	37	0.2698	0.3175	0.3726	0.4373	0.5146	0.6089
	38	0.2578	0.3050	0.3595	0.4237	0.5006	0.5945
	39	0.2463	0.2929	0.3470	0.4106	0.4871	0.5805
	40	0.2353	0.2813	0.3348	0.3980	0.4740	0.5671
	41	0.2247	0.2702	0.3231	0.3858	0.4613	0.5541
	42	0.2146	0.2594	0.3118	0.3740	0.4491	0.5415
20	28	0.4602	0.5205	0.5900	0.6714	0.7689	0.8880
	29	0.4364	0.4958	0.5642	0.6445	0.7406	0.8581
	30	0.4142	0.4728	0.5403	0.6195	0.7144	0.8303
	31	0.3935	0.4513	0.5179	0.5961	0.6898	0.8043
	32	0.3742	0.4311	0.4968	0.5741	0.6666	0.7799
	33	0.3559	0.4121	0.4769	0.5532	0.6448	0.7569
	34	0.3388	0.3941	0.4581	0.5335	0.6241	0.7351
	35	0.3225	0.3771	0.4402	0.5148	0.6044	0.7144
	36	0.3071	0.3609	0.4233	0.4969	0.5856	0.6947
	37	0.2925	0.3455	0.4071	0.4799	0.5677	0.6759
	38	0.2787	0.3308	0.3916	0.4636	0.5506	0.6579
	39	0.2654	0.3168	0.3768	0.4480	0.5342	0.6407
	40	0.2529	0.3034	0.3626	0.4331	0.5185	0.6242
	41	0.2408	0.2906	0.3490	0.4187	0.5033	0.6083
	42	0.2294	0.2784	0.3360	0.4049	0.4888	0.5930

TABLE 16.7 Values of K_a [from Eq. (16.36)] for $\delta' = \frac{1}{2}\phi'$

		β (deg)					
α (deg)	ϕ' (deg)	90	85	80	75	70	65
0	28	0.3264	0.3629	0.4034	0.4490	0.5011	0.5616
	29	0.3137	0.3502	0.3907	0.4363	0.4886	0.5492
	30	0.3014	0.3379	0.3784	0.4241	0.4764	0.5371
	31	0.2896	0.3260	0.3665	0.4121	0.4645	0.5253
	32	0.2782	0.3145	0.3549	0.4005	0.4529	0.5137
	33	0.2671	0.3033	0.3436	0.3892	0.4415	0.5025
	34	0.2564	0.2925	0.3327	0.3782	0.4305	0.4915
	35	0.2461	0.2820	0.3221	0.3675	0.4197	0.4807
	36	0.2362	0.2718	0.3118	0.3571	0.4092	0.4702
	37	0.2265	0.2620	0.3017	0.3469	0.3990	0.4599
	38	0.2172	0.2524	0.2920	0.3370	0.3890	0.4498
	39	0.2081	0.2431	0.2825	0.3273	0.3792	0.4400
	40	0.1994	0.2341	0.2732	0.3179	0.3696	0.4304
	41	0.1909	0.2253	0.2642	0.3087	0.3602	0.4209
	42	0.1828	0.2168	0.2554	0.2997	0.3511	0.4177
5	28	0.3477	0.3879	0.4327	0.4837	0.5425	0.6115
	29	0.3337	0.3737	0.4185	0.4694	0.5282	0.5972
	30	0.3202	0.3601	0.4048	0.4556	0.5144	0.5833
	31	0.3072	0.3470	0.3915	0.4422	0.5009	0.5698
	32	0.2946	0.3342	0.3787	0.4292	0.4878	0.5566
	33	0.2825	0.3219	0.3662	0.4166	0.4750	0.5437
	34	0.2709	0.3101	0.3541	0.4043	0.4626	0.5312
	35	0.2596	0.2986	0.3424	0.3924	0.4505	0.5190
	36	0.2488	0.2874	0.3310	0.3808	0.4387	0.5070
	37	0.2383	0.2767	0.3199	0.3695	0.4272	0.4954
	38	0.2282	0.2662	0.3092	0.3585	0.4160	0.4840
	39	0.2185	0.2561	0.2988	0.3478	0.4050	0.4729
	40	0.2090	0.2463	0.2887	0.3374	0.3944	0.4620
	41	0.1999	0.2368	0.2788	0.3273	0.3840	0.4514
	42	0.1911	0.2276	0.2693	0.3174	0.3738	0.4410
10	28	0.3743	0.4187	0.4688	0.5261	0.5928	0.6719
	29	0.3584	0.4026	0.4525	0.5096	0.5761	0.6549
	30	0.3432	0.3872	0.4368	0.4936	0.5599	0.6385
	31	0.3286	0.3723	0.4217	0.4782	0.5442	0.6225
	32	0.3145	0.3580	0.4071	0.4633	0.5290	0.6071
	33	0.3011	0.3442	0.3930	0.4489	0.5143	0.5920
	34	0.2881	0.3309	0.3793	0.4350	0.5000	0.5775
	35	0.2757	0.3181	0.3662	0.4215	0.4862	0.5633
	36	0.2637	0.3058	0.3534	0.4084	0.4727	0.5495

(continued)

TABLE 16.7 Values of K_a [from Eq. (16.36)] for $\delta' = \frac{1}{2}\phi'$ (*Continued*)

		β (deg)					
α (deg)	ϕ' (deg)	90	85	80	75	70	65
	37	0.2522	0.2938	0.3411	0.3957	0.4597	0.5361
	38	0.2412	0.2823	0.3292	0.3833	0.4470	0.5230
	39	0.2305	0.2712	0.3176	0.3714	0.4346	0.5103
	40	0.2202	0.2604	0.3064	0.3597	0.4226	0.4979
	41	0.2103	0.2500	0.2956	0.3484	0.4109	0.4858
	42	0.2007	0.2400	0.2850	0.3375	0.3995	0.4740
15	28	0.4095	0.4594	0.5159	0.5812	0.6579	0.7498
	29	0.3908	0.4402	0.4964	0.5611	0.6373	0.7284
	30	0.3730	0.4220	0.4777	0.5419	0.6175	0.7080
	31	0.3560	0.4046	0.4598	0.5235	0.5985	0.6884
	32	0.3398	0.3880	0.4427	0.5059	0.5803	0.6695
	33	0.3244	0.3721	0.4262	0.4889	0.5627	0.6513
	34	0.3097	0.3568	0.4105	0.4726	0.5458	0.6338
	35	0.2956	0.3422	0.3953	0.4569	0.5295	0.6168
	36	0.2821	0.3282	0.3807	0.4417	0.5138	0.6004
	37	0.2692	0.3147	0.3667	0.4271	0.4985	0.5846
	38	0.2569	0.3017	0.3531	0.4130	0.4838	0.5692
	39	0.2450	0.2893	0.3401	0.3993	0.4695	0.5543
	40	0.2336	0.2773	0.3275	0.3861	0.4557	0.5399
	41	0.2227	0.2657	0.3153	0.3733	0.4423	0.5258
	42	0.2122	0.2546	0.3035	0.3609	0.4293	0.5122
20	28	0.4614	0.5188	0.5844	0.6608	0.7514	0.8613
	29	0.4374	0.4940	0.5586	0.6339	0.7232	0.8313
	30	0.4150	0.4708	0.5345	0.6087	0.6968	0.8034
	31	0.3941	0.4491	0.5119	0.5851	0.6720	0.7772
	32	0.3744	0.4286	0.4906	0.5628	0.6486	0.7524
	33	0.3559	0.4093	0.4704	0.5417	0.6264	0.7289
	34	0.3384	0.3910	0.4513	0.5216	0.6052	0.7066
	35	0.3218	0.3736	0.4331	0.5025	0.5851	0.6853
	36	0.3061	0.3571	0.4157	0.4842	0.5658	0.6649
	37	0.2911	0.3413	0.3991	0.4668	0.5474	0.6453
	38	0.2769	0.3263	0.3833	0.4500	0.5297	0.6266
	39	0.2633	0.3120	0.3681	0.4340	0.5127	0.6085
	40	0.2504	0.2982	0.3535	0.4185	0.4963	0.5912
	41	0.2381	0.2851	0.3395	0.4037	0.4805	0.5744
	42	0.2263	0.2725	0.3261	0.3894	0.4653	0.5582

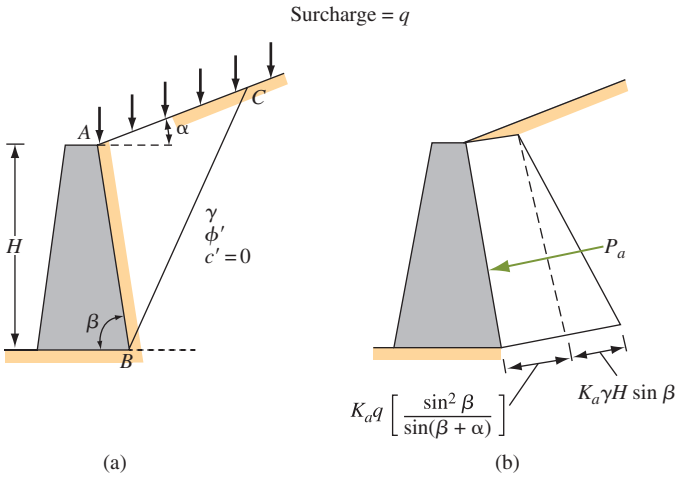


FIGURE 16.15 Coulomb's active pressure with a surcharge on the backfill

So far in Section 16.7, we have dealt with granular backfills where $c' = 0$, which are commonly used as backfills behind retaining walls for better drainage. When dealing with a backfill having cohesion and friction (i.e., $c' - \phi'$ soil), the wedge ABC_1 in Figure 16.14a will have two additional forces along BC_1 and BA, both acting upward. The force along BC_1 can be computed as $c' \times l_{BC_1}$, where l_{BC_1} is the length of the line BC_1. The force along BA can be computed as $c'_a \times l_{BA}$, where c'_a is the *adhesion* between the soil and the wall, which can be taken as 0.50–0.67 of c', and l_{BA} is the length of the line BA. Since these two forces are known in magnitude and direction, the force polygon for the five forces can be drawn, and P_a can be determined.

If a uniform surcharge of intensity q is located above the backfill, as shown in Figure 16.15, the active force, P_a, can be calculated as

$$P_a = \tfrac{1}{2} K_a \gamma_{eq} H^2 \quad \text{(Eq. (16.36))} \tag{16.37}$$

where

$$\gamma_{eq} = \gamma + \left[\frac{\sin\beta}{\sin(\beta + \alpha)}\right]\left(\frac{2q}{H}\right) \tag{16.38}$$

EXAMPLE 16.6

Consider the retaining wall shown in Figure 16.14a. Given: $H = 5$ m; unit weight of soil $= 17.6$ kN/m^3; angle of friction of soil $= 35°$; wall friction angle, $\delta' = \frac{2}{3}\phi'$; soil cohesion, $c' = 0$; $\alpha = 0$; and $\beta = 90°$. Calculate the Coulomb's active force per unit length of the wall.

SOLUTION

From Eq. (16.35),

$$P_a = \tfrac{1}{2}\gamma H^2 K_a$$

From Table 16.6, for $\alpha = 0°$, $\beta = 90°$, $\phi' = 35°$, and $\delta' = \frac{2}{3}\phi' = 23.33°$, $K_a = 0.2444$. Hence,

$$P_a = \tfrac{1}{2}(17.6)(5)^2(0.2444) = \mathbf{53.77\ kN/m}$$

■

EXAMPLE 16.7

Refer to Figure 16.15a. Given: $H = 20$ ft, $\phi' = 30°$, $\delta' = 20°$, $\alpha = 5°$, $\beta = 85°$, $q = 2000$ lb/ft^2, and $\gamma = 115$ lb/ft^3. Determine Coulomb's active force and the location of the line of action of the resultant P_a.

SOLUTION

For $\beta = 85°$, $\alpha = 5°$, $\delta' = 20°$, $\phi' = 30°$, and $K_a = 0.3578$ (Table 16.6). From Eqs. (16.37) and (16.38),

$$P_a = \frac{1}{2}K_a\gamma_{eq}H^2 = \frac{1}{2}K_a\left[\gamma + \frac{2q}{H}\frac{\sin\beta}{\sin(\beta+\alpha)}\right]H^2 = \underbrace{\frac{1}{2}K_a\gamma H^2}_{P_{a(1)}} + \underbrace{K_aHq\left[\frac{\sin\beta}{\sin(\beta+\alpha)}\right]}_{P_a(2)}$$

$$= (0.5)(0.3578)(115)(20)^2 + (0.3578)(20)(2000)\left[\frac{\sin 85}{\sin(85+5)}\right]$$

$$= 8229.4 + 14{,}257.5 = \mathbf{22{,}486.9\ lb/ft}$$

Location of the line of action of the resultant:

$$P_a\bar{z} = P_{a(1)}\frac{H}{3} + P_{a(2)}\frac{H}{2}$$

or

$$\bar{z} = \frac{(8229.4)\left(\frac{20}{3}\right) + (14{,}257.5)\left(\frac{20}{2}\right)}{22{,}486.9}$$

$$= \mathbf{8.78\ ft}\ \text{(measured vertically from the bottom of the wall)}$$

■

16.8 Lateral Earth Pressure Due to Surcharge

In several instances, the theory of elasticity is used to determine the lateral earth pressure on unyielding retaining structures caused by various types of surcharge loading, such as *line loading* (Figure 16.16a) and *strip loading* (Figure 16.16b).

According to the theory of elasticity, the stress at any depth, z, on a retaining structure caused by a line load of intensity q/unit length (Figure 16.16a) may be given as

$$\sigma = \frac{2q}{\pi H}\frac{a^2b}{(a^2+b^2)^2} \tag{16.39}$$

where σ = horizontal stress at depth $z = bH$. (See Figure 16.16a for explanations of the terms a and b.)

The lateral stress caused by the self-weight of the soil is not considered here.

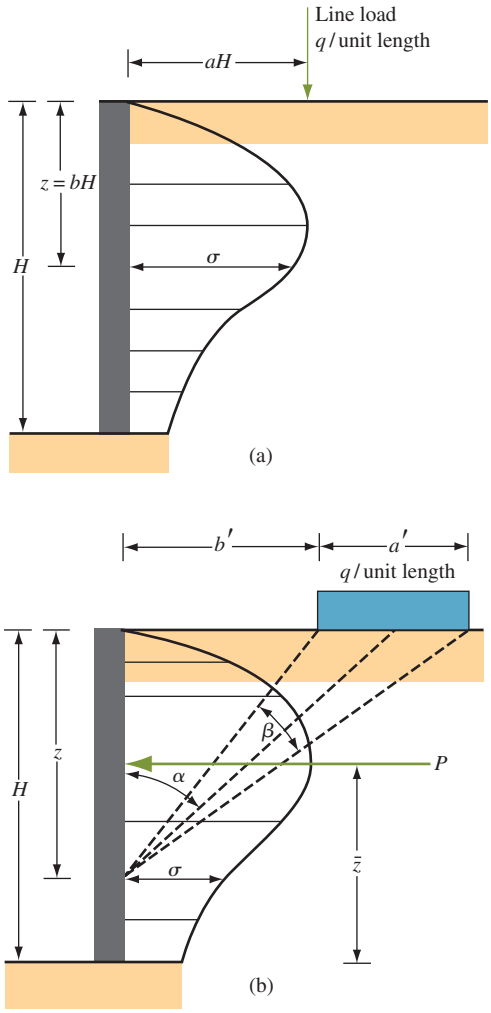


FIGURE 16.16 Lateral earth pressure caused by (a) line load and (b) strip load

However, because soil is not a perfectly elastic medium, some deviations from Eq. (16.39) may be expected. The modified forms of this equation generally accepted for use with soil are as follows:

$$\sigma = \frac{4a}{\pi H}\frac{a^2 b}{(a^2 + b^2)} \qquad \text{for } a > 0.4 \tag{16.40}$$

and

$$\sigma = \frac{q}{H}\frac{0.203b}{(0.16 + b^2)^2} \qquad \text{for } a \leq 0.4 \tag{16.41}$$

Figure 16.16b shows a strip load with an intensity of q/unit area located at a distance b' from a wall of height H. Based on the theory of elasticity, the horizontal stress, σ, at any depth z on a retaining structure is

$$\sigma = \frac{q}{\pi}(\beta - \sin\beta \cos 2\alpha) \tag{16.42}$$

(The angles α and β are defined in Figure 16.16b.)

However, in the case of soil, the right-hand side of Eq. (16.42) is doubled to account for the yielding soil continuum, or

$$\sigma = \frac{2q}{\pi}(\beta - \sin\beta\cos 2\alpha) \tag{16.43}$$

The total horizontal force per unit length (P) due to the *strip loading only* (Jarquio, 1981) may be expressed as

$$P = \frac{q}{90}[H(\theta_2 - \theta_1)] \tag{16.44}$$

where

$$\theta_1 = \tan^{-1}\left(\frac{b'}{H}\right)(\text{deg}) \tag{16.45}$$

$$\theta_2 = \tan^{-1}\left(\frac{a' + b'}{H}\right)(\text{deg}) \tag{16.46}$$

The location $\bar{z}$ (see Figure 16.16b) of the resultant force, P, can be given as

$$\bar{z} = H - \left[\frac{H^2(\theta_2 - \theta_1) + (R - Q) - 57.3a'H}{2H(\theta_2 - \theta_1)}\right] \tag{16.47}$$

where

$$R = (a' + b')^2(90 - \theta_2) \tag{16.48}$$

$$Q = b'^2(90 - \theta_1) \tag{16.49}$$

EXAMPLE 16.8

Refer to Figure 16.16a, which shows a line load surcharge. Given: $H = 6$ m, $a = 0.25$, and $q = 3$ kN/m. Calculate the variation of the lateral stress σ on the retaining structure at $z = 1$, 2, 3, 4, 5, and 6 m.

SOLUTION

For $a = 0.25$, which is less than 0.4, we will use Eq. (16.41). Now the following table can be prepared.

z (m)	H (m)	$b = z/H$	a	σ (kN/m^2)
1	6	0.167	0.25	**0.48**
2	6	0.333	0.25	**0.46**
3	6	0.5	0.25	**0.302**
4	6	0.667	0.25	**0.185**
5	6	0.833	0.25	**0.116**
6	6	1	0.25	**0.073**

EXAMPLE 16.9

Refer to Figure 16.16b. Here, $a' = 2$ m, $b' = 1$ m, $q = 40$ kN/m^2, and $H = 6$ m. Determine the total force on the wall (kN/m) caused by the strip loading only.

SOLUTION

From Eqs. (16.45) and (16.46),

$$\theta_1 = \tan^{-1}\left(\frac{1}{6}\right) = 9.46^\circ$$

$$\theta_2 = \tan^{-1}\left(\frac{2+1}{6}\right) = 26.57^\circ$$

From Eq. (16.44),

$$P = \frac{q}{90}[H(\theta_2 - \theta_1)] = \frac{40}{90}[6(26.57 - 9.46)] = \mathbf{45.63\ kN/m}$$

EXAMPLE 16.10

Refer to Example 16.9. Determine the location of the resultant $\bar{z}$.

SOLUTION

From Eqs. (16.48) and (16.49),

$$R = (a' + b')^2(90 - \theta_2) = (2+1)^2(90 - 26.57) = 570.87$$

$$Q = b'^2(90 - \theta_1) = (1)^2(90 - 9.46) = 80.54$$

From Eq. (16.47),

$$\bar{z} = H - \left[\frac{H^2(\theta_2 - \theta_1) + (R - Q) - 57.3a'H}{2H(\theta_2 - \theta_1)}\right]$$

$$= 6 - \left[\frac{(6)^2(26.57 - 9.46) + (570.87 - 80.54) - (57.3)(2)(6)}{(2)(6)(26.57 - 9.46)}\right] = \mathbf{3.96\ m}$$

16.9 Active Earth Pressure for Earthquake Conditions—Granular Backfill

Coulomb's active earth pressure theory (see Section 16.7) can be extended to take into account the forces caused by an earthquake. Figure 16.17 shows a condition of active pressure with a granular backfill ($c' = 0$). Note that the forces acting on the soil failure wedge in Figure 16.17 are essentially the same as those shown in Figure 16.14a with the addition of k_hW and k_vW in the horizontal and vertical direction, respectively; k_h and k_v have been defined in Eqs. (16.25) and (16.26), respectively, as

$$k_h = \frac{\text{horizontal earthquake acceleration component}}{\text{acceleration due to gravity, } g}$$

$$k_v = \frac{\text{vertical earthquake acceleration component}}{\text{acceleration due to gravity, } g}$$

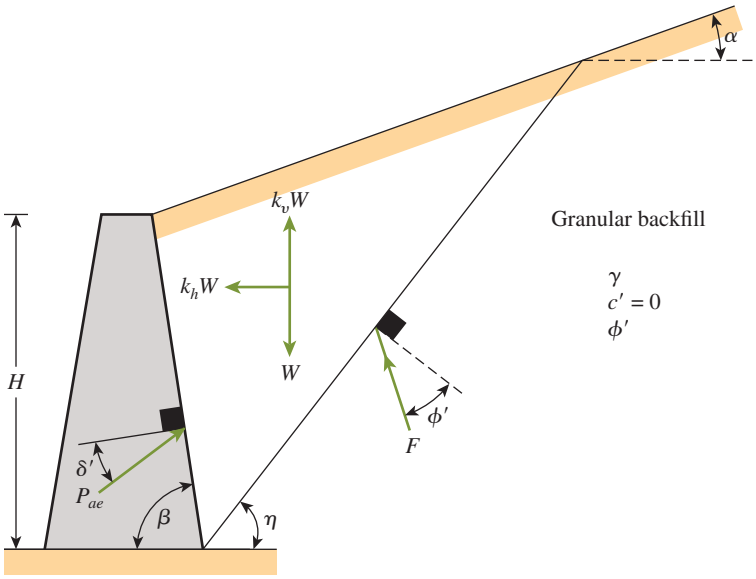


FIGURE 16.17 Derivation of Eq. (16.50)

As in Section 16.7, the relation for the active force per unit length of the wall (P_{ae}) can be determined as

$$P_{ae} = \tfrac{1}{2}\gamma H^2(1 - k_v)K_{ae} \tag{16.50}$$

where

$$K_{ae} = \text{active earth pressure coefficient} = \frac{\sin^2(\phi' + \beta - \theta')}{\cos\theta' \sin^2\beta \sin(\beta - \theta' - \delta')\left[1 + \sqrt{\dfrac{\sin(\phi' + \delta')\sin(\phi' - \theta' - \alpha)}{\sin(\beta - \delta' - \theta')\sin(\alpha + \beta)}}\right]^2} \tag{16.51}$$

$$\theta' = \tan^{-1}\left[\frac{k_h}{(1 - k_v)}\right] \text{ [See Eq. (16.29)]}$$

Note that for no earthquake condition, $k_h = 0$, $k_v = 0$, and $\theta' = 0$. Hence $K_{ae} = K_a$ [as given by Eq. (16.36)].

Some values of K_{ae} for $\beta = 90°$ and $k_v = 0$ are given in Table 16.8.

The magnitude of P_{ae} as given in Eq. (16.50) also can be determined as (Seed and Whitman, 1970)

$$P_{ae} = \frac{1}{2}\gamma H^2(1 - k_v)[K_a(\beta', \alpha')]\left(\frac{\sin^2\beta'}{\cos\theta'\sin^2\beta}\right) \tag{16.52}$$

where

$$\beta' = \beta - \theta' \tag{16.53}$$

$$\alpha' = \theta' + \alpha \tag{16.54}$$

TABLE 16.8 Values of K_{ae} [Eq. (16.51)] for $\beta = 90°$ and $k_v = 0$

			ϕ' (deg)				
k_h	δ' (deg)	α (deg)	28	30	35	40	45
0.1	0	0	0.427	0.397	0.328	0.268	0.217
0.2			0.508	0.473	0.396	0.382	0.270
0.3			0.611	0.569	0.478	0.400	0.334
0.4			0.753	0.697	0.581	0.488	0.409
0.5			1.005	0.890	0.716	0.596	0.500
0.1	0	5	0.457	0.423	0.347	0.282	0.227
0.2			0.554	0.514	0.424	0.349	0.285
0.3			0.690	0.635	0.522	0.431	0.356
0.4			0.942	0.825	0.653	0.535	0.442
0.5			—	—	0.855	0.673	0.551
0.1	0	10	0.497	0.457	0.371	0.299	0.238
0.2			0.623	0.570	0.461	0.375	0.303
0.3			0.856	0.748	0.585	0.472	0.383
0.4			—	—	0.780	0.604	0.486
0.5			—	—	—	0.809	0.624
0.1	$\phi'/2$	0	0.396	0.368	0.306	0.253	0.207
0.2			0.485	0.452	0.380	0.319	0.267
0.3			0.604	0.563	0.474	0.402	0.340
0.4			0.778	0.718	0.599	0.508	0.433
0.5			1.115	0.972	0.774	0.648	0.522
0.1	$\phi'/2$	5	0.428	0.396	0.326	0.268	0.218
0.2			0.537	0.497	0.412	0.342	0.283
0.3			0.699	0.640	0.526	0.438	0.367
0.4			1.025	0.881	0.690	0.568	0.475
0.5			—	—	0.962	0.752	0.620
0.1	$\phi'/2$	10	0.472	0.433	0.352	0.285	0.230
0.2			0.616	0.562	0.454	0.371	0.303
0.3			0.908	0.780	0.602	0.487	0.400
0.4			—	—	0.857	0.656	0.531
0.5			—	—	—	0.944	0.722
0.1	$\frac{2}{3}\phi'$	0	0.393	0.366	0.306	0.256	0.212
0.2			0.486	0.454	0.384	0.326	0.276
0.3			0.612	0.572	0.486	0.416	0.357
0.4			0.801	0.740	0.622	0.533	0.462
0.5			1.177	1.023	0.819	0.693	0.600
0.1	$\frac{2}{3}\phi'$	5	0.427	0.395	0.327	0.271	0.224
0.2			0.541	0.501	0.418	0.350	0.294
0.3			0.714	0.655	0.541	0.455	0.386
0.4			1.073	0.921	0.722	0.600	0.509
0.5			—	—	1.034	0.812	0.679
0.1	$\frac{2}{3}\phi'$	10	0.472	0.434	0.354	0.290	0.237
0.2			0.625	0.570	0.463	0.381	0.317
0.3			0.942	0.807	0.624	0.509	0.423
0.4			—	—	0.909	0.699	0.573
0.5			—	—	—	1.037	0.800

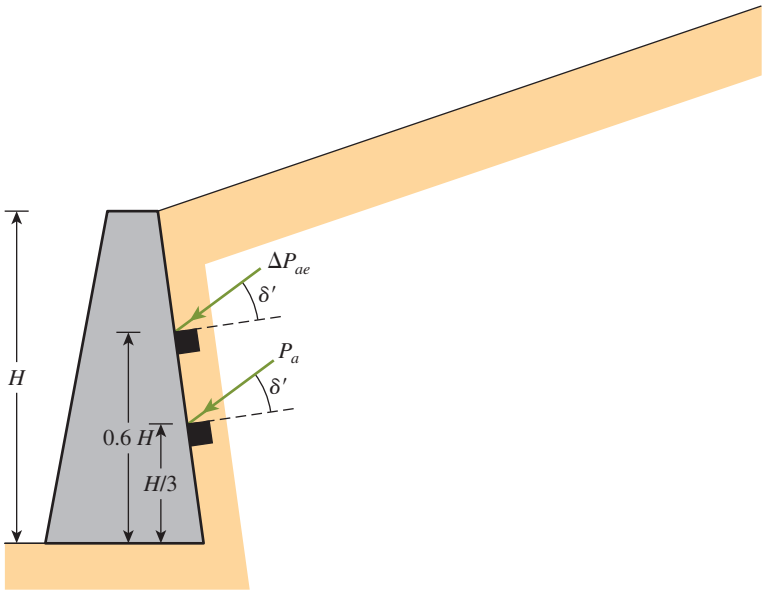


FIGURE 16.18 Determining the line of action of P_{ae}

$K_a(\beta', \alpha')$ = Coulomb's active earth pressure coefficient on a wall with a backface inclination of β' with the horizontal and with a backfill inclined at an angle α' with the horizontal (such as Tables 16.6 and 16.7)

Equation (16.50) is usually referred to as the *Mononobe–Okabe* solution. Unlike the case shown in Figure 16.14a, the resultant earth pressure in this situation, as calculated by Eq. (16.50), *does not act* at a distance of $H/3$ from the bottom of the wall. The following procedure may be used to obtain the location of the resultant force P_{ae}:

Step 1. Calculate P_{ae} by using Eq. (16.50).

Step 2. Calculate P_a by using Eq. (16.35).

Step 3. Calculate

$$\Delta P_{ae} = P_{ae} - P_a \tag{16.55}$$

Step 4. Assume that P_a acts at a distance of $H/3$ from the bottom of the wall (Figure 16.18) inclined at angle δ' to the normal drawn to the backface of the wall.

Step 5. Assume that ΔP_{ae} acts at a distance of $0.6H$ from the bottom of the wall (Figure 16.18) inclined at angle δ' to the normal drawn to the backface of the wall.

Step 6. Calculate the location of the resultant as

$$\bar{z} = \frac{(0.6H)(\Delta P_{ae}) + \left(\frac{H}{3}\right)(P_a)}{P_{ae}} \tag{16.56}$$

EXAMPLE 16.11

Refer to Figure 16.17. Given: $H = 10$ ft, $\beta = 85°$, $\alpha = 5°$, $k_v = 0$, and $k_h = 0.3$. For the backfill, $\phi' = 35°$, $\gamma = 105$ lb/ft^3, and $\delta' = 17.5°$. Determine:

a. P_{ae} using Eq. (16.52)
b. The location of the resultant, $\bar{z}$, from the bottom of the wall

SOLUTION

Part a

$$\theta' = \tan^{-1}\left(\frac{k_h}{1 - k_v}\right) = \tan^{-1}\left(\frac{0.3}{1 - 0}\right) = 16.7°$$

From Eqs. (16.53) and (16.54),

$$\beta' = \beta - \theta' = 85 - 16.7 = 68.3°$$
$$\alpha' = \theta' + \alpha = 16.7 + 5 = 21.7°$$
$$\frac{\delta'}{\phi'} = \frac{17.5}{35} = 0.5$$

We will refer to Eq. (16.36). For $\phi' = 35°$, $\delta'/\phi' = 0.5$, $\beta' = 68.3°$, and $\alpha' = 21.7°$, the value of $K_a(\beta', \alpha') \approx 0.642$. Thus, from Eq. (16.52),

$$P_{ae} = \frac{1}{2}\gamma H^2(1 - k_v)[K_a(\beta',\alpha')]\left(\frac{\sin^2\beta'}{\cos\theta'\sin^2\beta}\right)$$
$$= \frac{1}{2}(105)(10^2)(1 - 0)(0.642)\left(\frac{\sin^2 68.3}{\cos 21.7\,\sin^2 85}\right) = \mathbf{3155.6\ lb/ft}$$

Part b

From Eq. (16.35),

$$P_a = \tfrac{1}{2}\gamma H^2 K_a$$

From Eq. (16.36) with $\delta' = 17.5°$, $\beta = 85°$, and $\alpha = 5°$, $K_a \approx 0.2986$ (Table 16.7).

$$P_a = \tfrac{1}{2}(105)(10)^2(0.2986) = 1568\ \text{lb/ft}$$
$$\Delta P_{ae} = P_{ae} - P_a = 3155.6 - 1568 = 1587.6\ \text{lb/ft}$$

From Eq. (16.56),

$$\bar{z} = \frac{(0.6H)(\Delta P_{ae}) + (H/3)(P_a)}{P_{ae}}$$
$$= \frac{[(0.6)(10)](1587.6) + (10/3)(1568)}{3155.6} = \mathbf{4.67\ ft}$$

16.10 Active Earth Pressure for Earthquake Condition (Vertical Backface of Wall and $c' - \phi'$ Backfill)

Shukla et al. (2009) developed a procedure for estimation of P_{ae} for a retaining wall with a vertical backface and horizontal backfill with a $c' - \phi'$ soil (Figure 16.19a). In Figure 16.19a, ABC is the trial failure wedge. The following assumptions have been made in the analysis:

1. The effect of tensile crack is not taken into account.
2. The friction and adhesion between the backface of the wall and backfill are neglected.

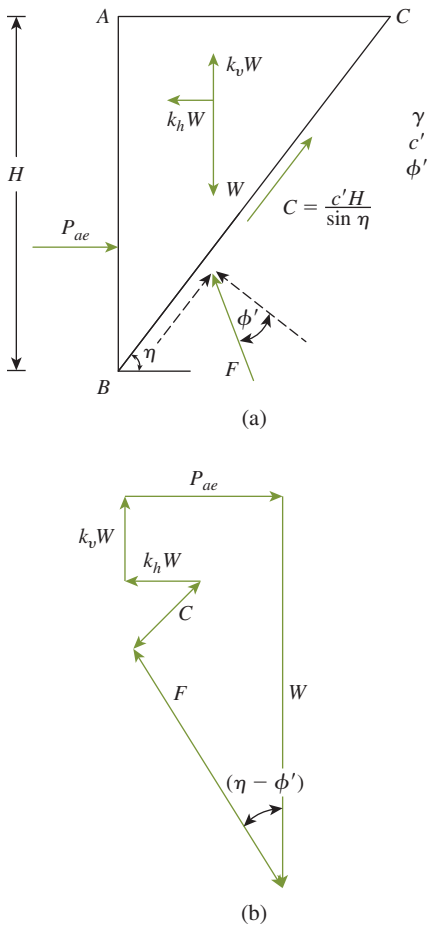


FIGURE 16.19 Estimation of P_{ae} with $c' - \phi'$ backfill: (a) trial failure wedge; (b) force polygon

Figure 16.19b shows the polygon for all the forces acting on the wedge *ABC*. The notations are similar to those shown in Figure 16.17. According to this analysis, the critical wedge angle $\eta = \eta_c$ for the maximum value of P_{ae} can be given as

$$\tan\eta_c = \frac{\sin\phi'\sin(\phi' - \theta') + m\sin 2\phi' + \left[\begin{array}{l}\sin\phi'\sin(\phi' - \theta')\cos\theta' \\ + 4m^2\cos^2\phi' + 2m\cos\phi' \\ \{\sin\phi'\cos\theta' + \sin(\phi' - \theta')\}\end{array}\right]^{0.5}}{\sin\phi'\cos(\phi' - \theta') + 2m\cos^2\phi'} \tag{16.57}$$

where

$$m = \frac{c'\cos\theta'}{\gamma H(1 - k_v)} \tag{16.58}$$

For the definition of θ', see Eq. (16.29).

Thus, the magnitude of P_{ae} can be expressed as

$$\frac{P_{ae}}{\gamma H^2} = P^*_{ae} = \frac{1}{2}(1 - k_v)K_{ae\gamma} - c^*K_{aec} \tag{16.59}$$

where

$$c^* = \frac{c'}{\gamma H} \tag{16.60}$$

$$K_{ae\gamma} = \frac{\cos(\phi' - \theta') - \dfrac{\sin(\phi' - \theta')}{\tan \eta_c}}{\cos\theta'(\cos\phi' + \tan\eta_c \sin\phi')} \tag{16.61}$$

$$K_{aec} = \frac{\cos\phi'(1 + \tan^2\eta_c)}{\tan\eta_c(\cos\phi' + \tan\eta_c \sin\phi')} \tag{16.62}$$

Figure 16.20 gives plots of P^*_{ae} against ϕ' for various values of c^* and k_h ($k_v = 0$).

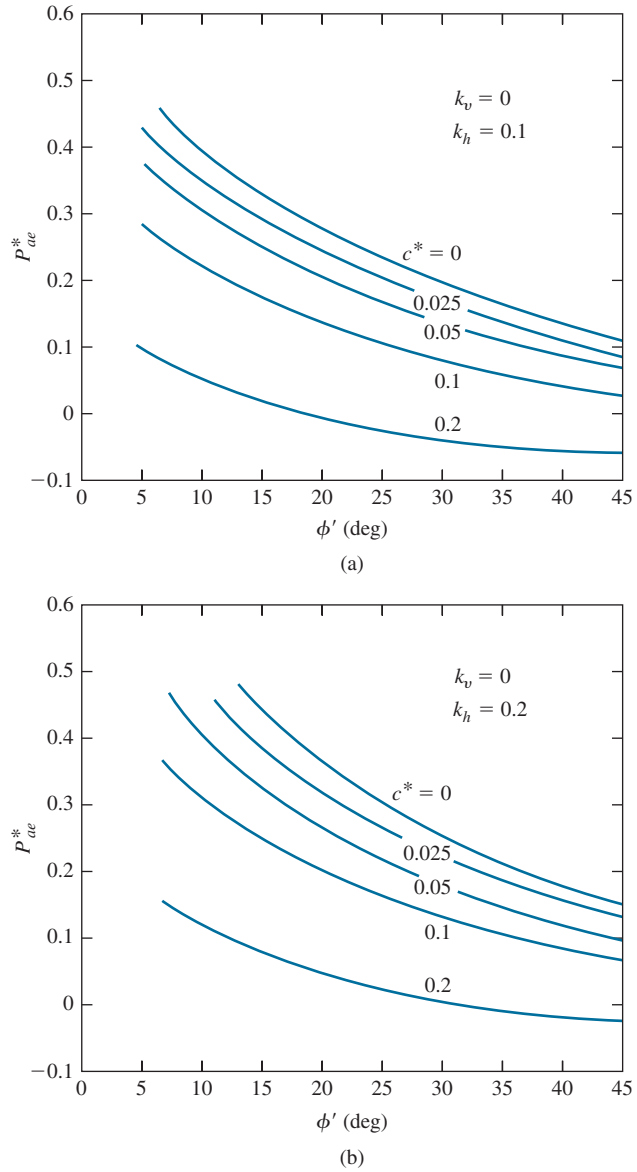
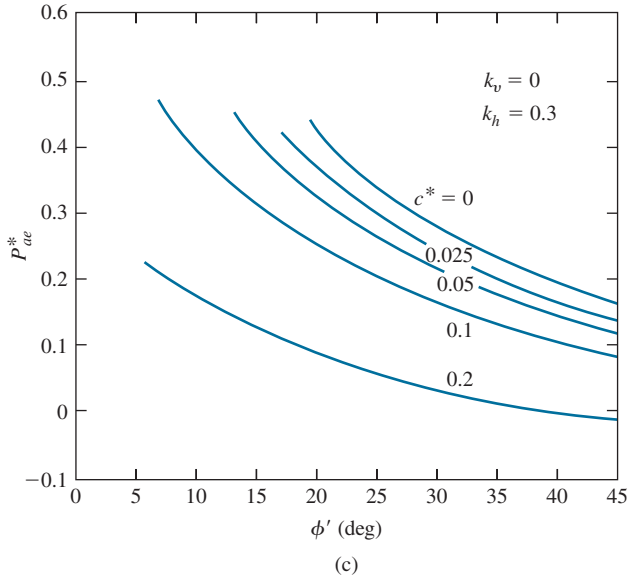
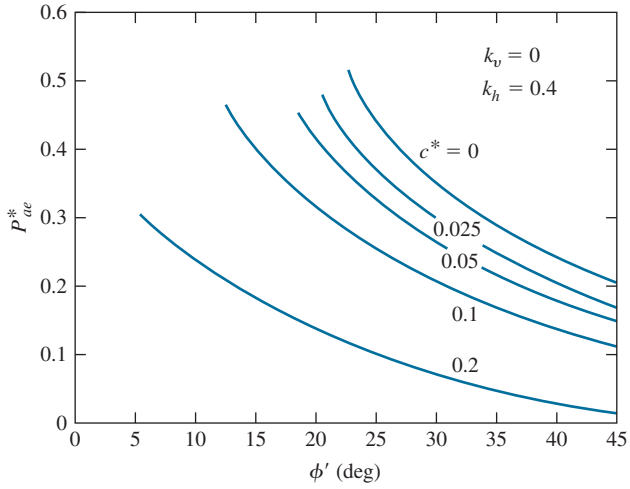


FIGURE 16.20 Plot of P^*_{ae} vs. ϕ' for various values of c^*: (a) $k_h = 0.1$; (b) $k_h = 0.2$; (c) $k_h = 0.3$; (d) $k_h = 0.4$ (*Note*: $k_v = 0$)



(c)



(d)

FIGURE 16.20 (*Continued*)

EXAMPLE 16.12

For a retaining wall with a vertical backface and horizontal backfill, the following are given:

- $H = 28$ ft
- $\phi' = 20°$
- $c' = 165$ lb/ft^2
- $\gamma = 118$ lb/ft^3
- $k_h = 0.1$

Determine the magnitude of the active force, P_{ae}.

SOLUTION

From Eq. (16.60),

$$c^* = \frac{c'}{\gamma H} = \frac{165}{(118)(28)} = 0.0499 \approx 0.05$$

$$\phi' = 20°$$

From Figure 16.20a, for $\phi' = 20°$ and $c^* = 0.05$, the value of $P_{ae}^* = 0.207$. Hence

$$P_{ae} = P_{ae}^* \gamma H^2 = (0.207)(118)(28)^2 = \mathbf{19{,}150\ lb/ft}$$

Passive Pressure

16.11 Rankine Passive Earth Pressure

Figure 16.21a shows a vertical frictionless retaining wall with a horizontal backfill. At depth z, the effective vertical pressure on a soil element is $\sigma_o' = \gamma z$. Initially, if the wall does not yield at all, the lateral stress at that depth will be $\sigma_h' = K_o \sigma_o'$. This state of stress is illustrated by the Mohr's circle a in Figure 16.21b. Now, if the wall is pushed into the soil mass by an amount Δx, as shown in Figure 16.21a, the vertical stress at depth z will stay the same; however, the horizontal stress will increase. Thus, σ_h' will be greater than $K_o \sigma_o'$. The state of stress can now be represented by the Mohr's circle b in Figure 16.21b. If the wall moves further inward (i.e., Δx is increased still more), the stresses at depth z will ultimately reach the state represented by Mohr's circle c. Note that this Mohr's circle touches the Mohr–Coulomb failure envelope, which implies that the soil behind the wall will fail by being pushed upward. The horizontal stress, σ_h', at this point is referred to as the *Rankine passive pressure*, or $\sigma_h' = \sigma_p'$.

For Mohr's circle c in Figure 16.21b, the major principal stress is σ_p', and the minor principal stress is σ_o'. Substituting these quantities into Eq. (2.91) yields

$$\sigma_p' = \sigma_o' \tan^2\left(45 + \frac{\phi'}{2}\right) + 2c' \tan\left(45 + \frac{\phi'}{2}\right) \tag{16.63}$$

Now, let

$$K_p = \text{Rankine passive earth pressure coefficient} = \tan^2\left(45 + \frac{\phi'}{2}\right) \tag{16.64}$$

Then, from Eq. (16.63), we have

$$\sigma_p' = \sigma_o' K_p + 2c' \sqrt{K_p} \tag{16.65}$$

Equation (16.65) produces Figure 16.21c, the passive pressure diagram for the wall shown in Figure 16.21a. Note that at $z = 0$,

$$\sigma_o' = 0 \quad \text{and} \quad \sigma_p' = 2c' \sqrt{K_p}$$

and at $z = H$,

$$\sigma_o' = \gamma H \quad \text{and} \quad \sigma_p' = \gamma H K_p + 2c' \sqrt{K_p}$$

The passive force per unit length of the wall can be determined from the area of the pressure diagram, or

$$P_p = \tfrac{1}{2} \gamma H^2 K_p + 2c' H \sqrt{K_p} \tag{16.66}$$

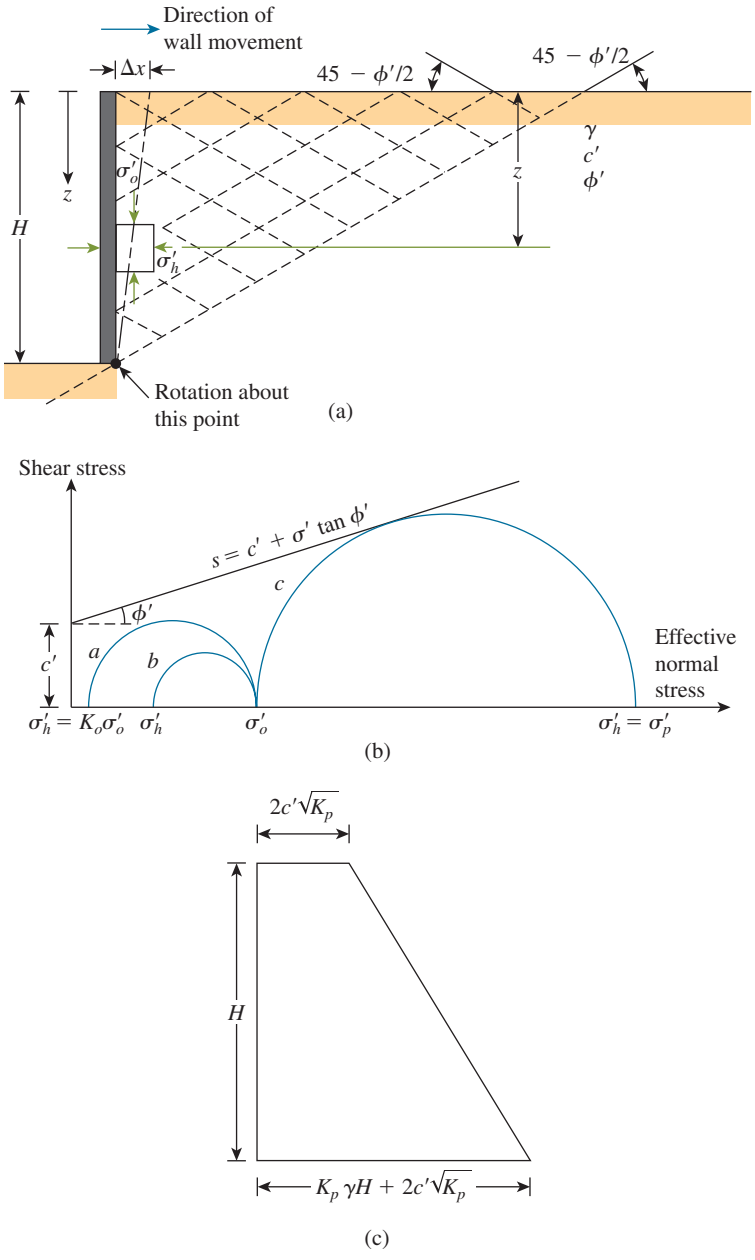


FIGURE 16.21 Rankine passive pressure

The approximate magnitudes of the wall movements, Δx, required to develop failure under passive conditions are as follows:

Soil type	Wall movement for passive condition, Δx
Dense sand	$0.005H$
Loose sand	$0.01H$
Stiff clay	$0.01H$
Soft clay	$0.05H$

Rankine's passive earth pressure coefficient is about an order of magnitude greater than the active earth pressure coefficient. The at-rest earth pressure coefficient lies between the two, being closer to the active earth pressure coefficient.

If the backfill behind the wall is a granular soil (i.e., $c' = 0$), then, from Eq. (16.66), the passive force per unit length of the wall will be

$$P_p = \frac{1}{2}\gamma H^2 K_p \tag{16.67}$$

EXAMPLE 16.13

A 3 m high wall is shown in Figure 16.22a. Determine the Rankine passive force per unit length of the wall.

SOLUTION

For the top layer,

$$K_{p(1)} = \tan^2\left(45 + \frac{\phi_1'}{2}\right) = \tan^2(45 + 15) = 3$$

From the bottom soil layer,

$$K_{p(2)} = \tan^2\left(45 + \frac{\phi_2'}{2}\right) = \tan^2(45 + 13) = 2.56$$

$$\sigma_p' = \sigma_o' K_p + 2c'\sqrt{K_p}$$

where

σ_o' = effective vertical stress

at $z = 0$, $\sigma_o' = 0$, $c_1' = 0$, $\sigma_p' = 0$

at $z = 2$ m, $\sigma_o' = (15.72)(2) = 31.44$ kN/m^2, $c_1' = 0$

So, for the top soil layer,

$$\sigma_p' = 31.44K_{p(1)} + 2(0)\sqrt{K_{p(1)}} = 31.44(3) = 94.32 \text{ kN/m}^2$$

At this depth (that is, $z = 2$ m), for the bottom soil layer,

$$\sigma_p' = \sigma_o' K_{p(2)} + 2c_2'\sqrt{K_{p(2)}} = 31.44(2.56) + 2(10)\sqrt{2.56}$$
$$= 80.49 + 32 = 112.49 \text{ kN/m}^2$$

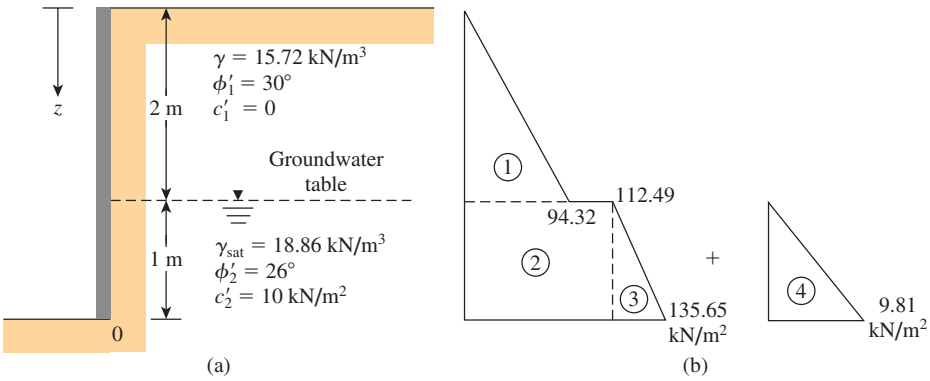


FIGURE 16.22

Again, at $z = 3$ m,

$$\sigma'_o = (15.72)(2) + (\gamma_{sat} - \gamma_w)(1)$$
$$= 31.44 + (18.86 - 9.81)(1) = 40.49 \text{ kN/m}^2$$

Hence,

$$\sigma'_p = \sigma'_o K_{p(2)} + 2c'_2\sqrt{K_{p(2)}} = 40.49(2.56) + (2)(10)(1.6)$$
$$= \mathbf{135.65 \text{ kN/m}^2}$$

Note that, because a water table is present, the hydrostatic stress, u, also has to be taken into consideration. For $z = 0$ to 2 m, $u = 0$; at $z = 3$ m, $u = (1)(\gamma_w) = 9.81$ kN/m^2.

The passive pressure diagram is plotted in Figure 16.22b. The passive force per unit length of the wall can be determined from the area of the pressure diagram as follows:

Area no.	Area	
1	$\left(\frac{1}{2}\right)(2)(94.32)$	$= 94.32$
2	$(112.49)(1)$	$= 112.49$
3	$\left(\frac{1}{2}\right)(1)(135.65 - 112.49)$	$= 11.58$
4	$\left(\frac{1}{2}\right)(9.81)(1)$	$= 4.905$
		$P_P \approx$ **223.3 kN/m**

16.12 Rankine Passive Earth Pressure—Vertical Backface and Inclined Backfill

GRANULAR SOIL

For a frictionless vertical retaining wall (Figure 16.11) with a *granular backfill* ($c' = 0$), the Rankine passive pressure at any depth can be determined in a manner similar to that done in the case of active pressure in Section 16.4. The pressure is

$$\sigma'_p = \gamma z K_p \tag{16.68}$$

and the passive force is

$$P_p = \tfrac{1}{2}\gamma H^2 K_p \tag{16.69}$$

where

$$K_p = \cos\alpha \frac{\cos\alpha + \sqrt{\cos^2\alpha - \cos^2\phi'}}{\cos\alpha - \sqrt{\cos^2\alpha - \cos^2\phi'}} \tag{16.70}$$

As in the case of the active force, the resultant force, P_p, is inclined at an angle α with the horizontal and intersects the wall at a distance $H/3$ from the bottom of the wall. The values of K_p (the passive earth pressure coefficient) for various values of α and ϕ' are given in Table 16.9.

$c' - \phi'$ SOIL

If the backfill of the frictionless vertical retaining wall is a $c - \phi'$ soil (see Figure 16.11), then (Mazindrani and Ganjali, 1997)

$$\sigma'_p = \gamma z K_p = \gamma z K'_p \cos\alpha \tag{16.71}$$

TABLE 16.9 Passive Earth Pressure Coefficient K_p [from Eq. (16.70)]

	ϕ' (deg) →						
↓α (deg)	28	30	32	34	36	38	40
0	2.770	3.000	3.255	3.537	3.852	4.204	4.599
5	2.715	2.943	3.196	3.476	3.788	4.136	4.527
10	2.551	2.775	3.022	3.295	3.598	3.937	4.316
15	2.284	2.502	2.740	3.003	3.293	3.615	3.977
20	1.918	2.132	2.362	2.612	2.886	3.189	3.526
25	1.434	1.664	1.894	2.135	2.394	2.676	2.987

where

$$K'_p = \frac{1}{\cos^2\phi'}\left\{2\cos^2\alpha + 2\left(\frac{c'}{\gamma z}\right)\cos\phi'\sin\phi' + \sqrt{4\cos^2\alpha(\cos^2\alpha - \cos^2\phi') + 4\left(\frac{c'}{\gamma z}\right)^2\cos^2\phi' + 8\left(\frac{c'}{\gamma z}\right)\cos^2\alpha\sin\phi'\cos\phi'}\right\} - 1 \tag{16.72}$$

The variation of K'_p with ϕ', α, and $c'/\gamma z$ is given in Table 16.10 (Mazindrani and Ganjali, 1997). Mazindrani and Ganjali (1997) also showed that for $c' = 0$, Eqs. (16.69) and (16.71) give the same values for σ'_p.

TABLE 16.10 Values of K'_p

		$c'/\gamma z$						
α (deg)	ϕ' (deg)	0	0.025	0.05	0.075	0.1	0.2	0.5
0	15	1.6984	1.7636	1.8287	1.8939	1.9590	2.2197	3.0016
0	20	2.0396	2.1110	2.1824	2.2538	2.3252	2.6109	3.4678
0	25	2.4639	2.5424	2.6209	2.6994	2.7778	3.0918	4.0336
0	30	3.0000	3.0866	3.1732	3.2598	3.3464	3.6928	4.7321
0	35	3.6902	3.7862	3.8823	3.9783	4.0744	4.4586	5.6112
0	40	4.5989	4.7061	4.8134	4.9206	5.0278	5.4567	6.7434
5	15	1.6477	1.7156	1.7830	1.8501	1.9169	2.1823	2.9709
5	20	1.9940	2.0669	2.1396	2.2122	2.2846	2.5734	3.4353
5	25	2.4195	2.4989	2.5782	2.6575	2.7367	3.0529	3.9986
5	30	2.9543	3.0416	3.1288	3.2159	3.3030	3.6511	4.6935
5	35	3.6412	3.7378	3.8342	3.9307	4.0271	4.4126	5.5678
5	40	4.5445	4.6521	4.7597	4.8672	4.9747	5.4046	6.6935
10	15	1.4841	1.5641	1.6408	1.7153	1.7882	2.0700	2.8799
10	20	1.8539	1.9323	2.0097	2.0863	2.1622	2.4615	3.3392
10	25	2.2854	2.3680	2.4502	2.5320	2.6135	2.9370	3.8950

(continued)

TABLE 16.10 Values of K_p' (*Continued*)

		$c'/\gamma z$						
α (deg)	ϕ' (deg)	0	0.025	0.05	0.075	0.1	0.2	0.5
10	30	2.8176	2.9070	2.9961	3.0850	3.1737	3.5272	4.5794
10	35	3.4953	3.5933	3.6912	3.7889	3.8866	4.2761	5.4393
10	40	4.3826	4.4913	4.5999	4.7084	4.8168	5.2500	6.5454
15	15	1.0000	1.2506	1.3702	1.4702	1.5608	1.8819	2.7321
15	20	1.6024	1.6962	1.7856	1.8717	1.9556	2.2766	3.1831
15	25	2.0575	2.1474	2.2357	2.3229	2.4090	2.7466	3.7264
15	30	2.5900	2.6836	2.7766	2.8689	2.9608	3.3242	4.3936
15	35	3.2546	3.3555	3.4559	3.5561	3.6559	4.0530	5.2300
15	40	4.1168	4.2275	4.3380	4.4483	4.5584	4.9973	6.3041
20	20	1.0000	1.2932	1.4325	1.5484	1.6529	2.0194	2.9728
20	25	1.7181	1.8260	1.9283	2.0267	2.1222	2.4853	3.4993
20	30	2.2687	2.3708	2.4710	2.5697	2.6670	3.0472	4.1429
20	35	2.9216	3.0275	3.1325	3.2368	3.3404	3.7494	4.9473
20	40	3.7525	3.8666	3.9802	4.0934	4.2062	4.6540	5.9779

16.13 Coulomb's Passive Earth Pressure

Coulomb (1776) also presented an analysis for determining the passive earth pressure (i.e., when the wall moves *into* the soil mass) for walls possessing friction ($\delta' =$ angle of wall friction) and retaining a granular backfill material similar to that discussed in Section 16.7.

To understand the determination of Coulomb's passive force, P_p, consider the wall shown in Figure 16.23a. As in the case of active pressure, Coulomb assumed that the potential failure surface in soil is a plane passing through B. For a trial failure wedge of soil, such as ABC_1, the forces per unit length of the wall acting on the wedge are

1. The weight of the wedge, W
2. The resultant, R, of the normal and shear forces on the plane BC_1
3. The passive force, P_p

Figure 16.23b shows the force triangle at equilibrium for the trial wedge ABC_1. From this force triangle, the value of P_p can be determined, because the direction of all three forces and the magnitude of one force are known.

Similar force triangles for several trial wedges, such as ABC_1, ABC_2, ABC_3, . . . , can be constructed, and the corresponding values of P_p can be determined. The top part of Figure 16.23a shows the nature of variation of the P_p values for different wedges. The *minimum value of* P_p in this diagram is *Coulomb's passive force*, mathematically expressed as

$$P_p = \tfrac{1}{2}\gamma H^2 K_p \tag{16.73}$$

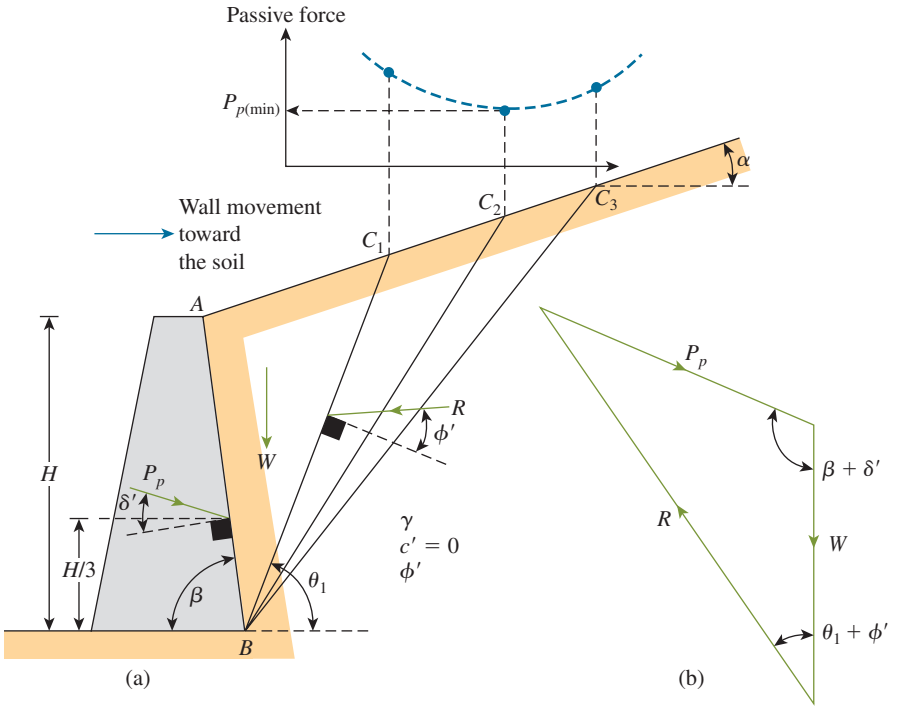


FIGURE 16.23 Coulomb's passive pressure

where

$$K_p = \text{Coulomb's passive pressure coefficient} = \frac{\sin^2(\beta - \phi')}{\sin^2\beta \sin(\beta + \delta')\left[1 - \sqrt{\dfrac{\sin(\phi' + \delta')\sin(\phi' + \alpha)}{\sin(\beta + \delta')\sin(\beta + \alpha)}}\right]^2} \tag{16.74}$$

The values of the passive pressure coefficient, K_p, for various values of ϕ' and δ' are given in Table 16.11 for a retaining wall with vertical backface retaining a horizontal granular backfill ($\beta = 90°$, $\alpha = 0°$).

TABLE 16.11 Values of K_p [from Eq. (16.74)] for $\beta = 90°$ and $\alpha = 0°$

	δ' (deg)				
ϕ' (deg)	0	5	10	15	20
15	1.698	1.900	2.130	2.405	2.735
20	2.040	2.313	2.636	3.030	3.525
25	2.464	2.830	3.286	3.855	4.597
30	3.000	3.506	4.143	4.977	6.105
35	3.690	4.390	5.310	6.854	8.324
40	4.600	5.590	6.946	8.870	11.772

Note that the resultant passive force, P_p, will act at a distance $H/3$ from the bottom of the wall and will be inclined at an angle δ' to the normal drawn to the backface of the wall.

16.14 Comments on the Failure Surface Assumption for Coulomb's Pressure Calculations

Coulomb's pressure calculation methods for active and passive pressure have been discussed in Sections 16.7 and 16.13. The fundamental assumption in these analyses is the acceptance of *plane failure surface*. However, for walls with friction, this assumption does not hold in practice. The nature of *actual* failure surface in the soil mass for active and passive pressure is shown in Figures 16.24a and b, respectively (for a vertical wall with a horizontal backfill). Note that the failure surface *BC* is curved and that the failure surface *CD* is a plane.

Although the actual failure surface in soil for the case of active pressure is somewhat different from that assumed in the calculation of the Coulomb pressure, the results are not greatly different. However, in the case of passive pressure, as the value of δ' increases, Coulomb's method of calculation gives increasingly erroneous values of P_p. This factor of error could lead to an unsafe condition because the values of P_p would become higher than the soil resistance.

Several studies have been conducted to determine the passive force P_p, assuming that the curved portion *BC* in Figure 16.24b is an arc of a circle, an ellipse, or a logarithmic spiral (e.g., Caquot and Kerisel, 1948; Shields and Tolunay, 1973; Terzaghi and Peck, 1967; Zhu and Qian, 2000). Section 16.15 presents the solution of Caquot and Kerisel (1948), which will suffice for the purpose of this text.

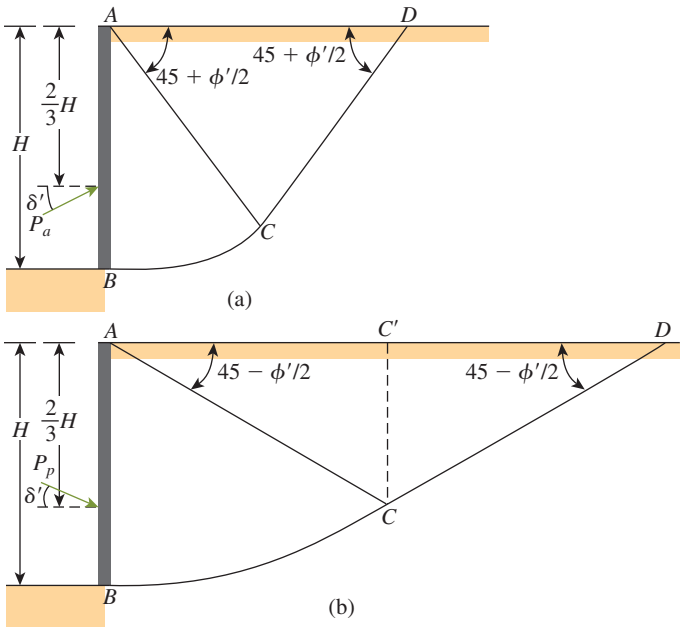


FIGURE 16.24 Nature of failure surface in soil with wall friction: (a) active pressure; (b) passive pressure

16.15 Caquot and Kerisel Solution for Passive Earth Pressure (Granular Backfill)

(a) INCLINED WALL WITH HORIZONTAL BACKFILL

Figure 16.25(b) shows a retaining wall with an inclined back and a horizontal backfill. For this case, the passive pressure per unit length of the wall can be calculated as

$$P_p = \tfrac{1}{2}\gamma H_1^2 K_p \tag{16.75}$$

where K_p = the passive pressure coefficient.

The variation of K_p determined by Caquot and Kerisel (1948) is shown in Figure 16.25a. For the definition of H_1, refer to Figure 16.25b. It is important to note that the K_p values shown are for $\delta'/\phi' = 1$. If $\delta'/\phi' \neq 1$, the following procedure must be used to determine K_p.

1. Assume δ' and ϕ'.
2. Calculate δ'/ϕ'.
3. Using the ratio of δ'/ϕ' (step 2), determine the reduction factor, R', from Table 16.12.
4. Determine K_p from Figure 16.25 for $\delta'/\phi' = 1$.
5. Calculate K_p for the required δ'/ϕ' as

$$K_p = (R')[K_{p(\delta'/\phi'=1)}] \tag{16.76}$$

(b) VERTICAL WALL WITH INCLINED BACKFILL

Figure 16.26b shows a vertical retaining wall with inclined granular backfill. For this case,

$$P_p = \frac{1}{2}\gamma H^2 K_p \tag{16.77}$$

The variation of K_p (for $\frac{\delta'}{\phi'} = 1$) with ϕ' and $\frac{\alpha}{\phi'}$ is shown in Figure 16.26a.

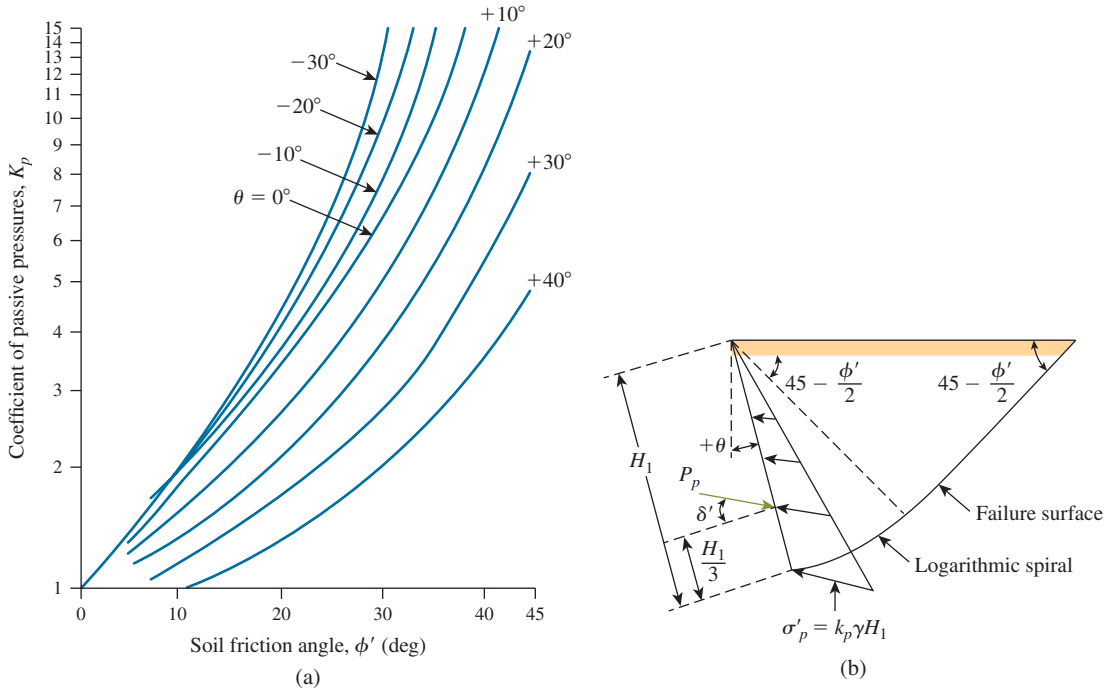
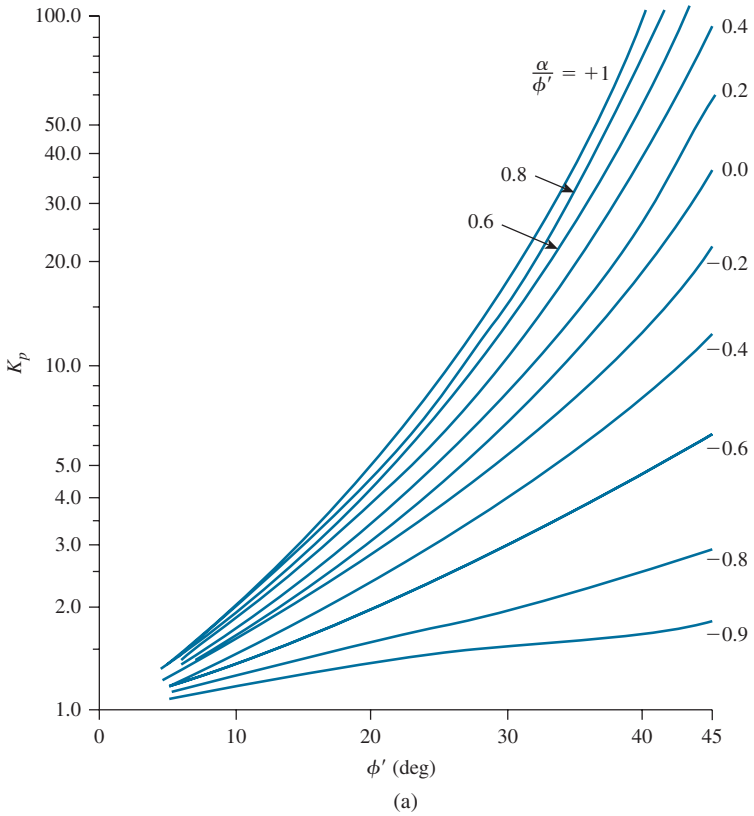


FIGURE 16.25 Caquot and Kerisel's solution for K_p [Eq.(16.75)] (*Note*: θ is the inclination of the backface of the wall with the vertical.)

TABLE 16.12 Caquot and Kerisel's Reduction Factor, R', for Passive Pressure Calculation

	δ'/ϕ'							
ϕ'	0.7	0.6	0.5	0.4	0.3	0.2	0.1	0.0
10	0.978	0.962	0.946	0.929	0.912	0.898	0.881	0.864
15	0.961	0.934	0.907	0.881	0.854	0.830	0.803	0.775
20	0.939	0.901	0.862	0.824	0.787	0.752	0.716	0.678
25	0.912	0.860	0.808	0.759	0.711	0.666	0.620	0.574
30	0.878	0.811	0.746	0.686	0.627	0.574	0.520	0.467
35	0.836	0.752	0.674	0.603	0.536	0.475	0.417	0.362
40	0.783	0.682	0.592	0.512	0.439	0.375	0.316	0.262
45	0.718	0.600	0.500	0.414	0.339	0.276	0.221	0.174



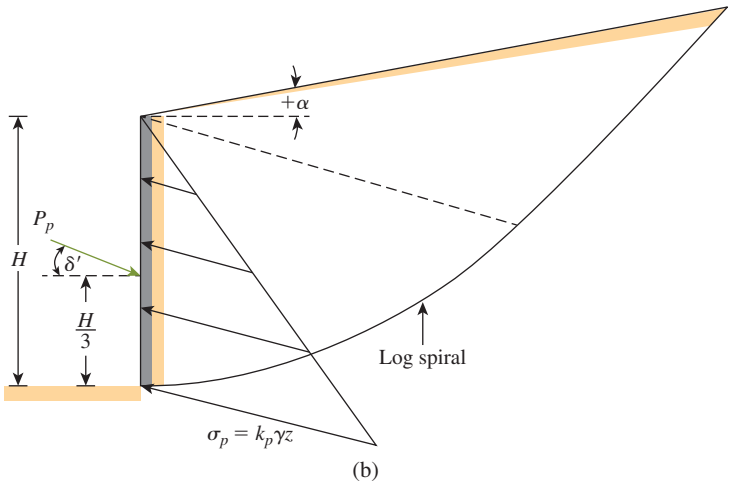


FIGURE 16.26 Caquot and Kerisel's solution for K_p [Eq. (16.77)]

Caquot and Kerisel's solution (1948) for K_p to use in Eq. (16.77) is given in Figure 16.26a for $\delta'/\phi' = 1$. In order to determine K_p via Figure 16.26a, the following steps are necessary:

Step 1. Determine α/ϕ' (note the sign of α).

Step 2. Knowing ϕ' and α/ϕ', use Figure 16.26a to determine K_p for $\delta'/\phi' = 1$.

Step 3. Calculate δ'/ϕ'.

Step 4. Go to Table 16.12 to determine the reduction factor, R'.

Step 5. $K_p = (R')\,[K_{p(\delta'/\phi'=1)}]$. (16.78)

EXAMPLE 16.14

Consider a 3 m high (H) retaining wall with a vertical back ($\theta = 0°$) and a horizontal granular backfill. Given: $\gamma = 15.7$ kN/m^3, $\delta' = 15°$, and $\phi' = 30°$. Estimate the passive force, P_p, by using

a. Coulomb's theory
b. Caquot and Kerisel's theory

SOLUTION

Part a

From Eq. (16.73),

$$P_p = \frac{1}{2}K_p\gamma H^2$$

From Table 16.11, for $\phi' = 30°$ and $\delta' = 15°$, the value of K_p is 4.977. Thus,

$$P_p = \left(\frac{1}{2}\right)(4.977)(15.7)(3)^2 = \mathbf{351.6\ kN/m}$$

Part b

From Eq. (16.75), with $\theta = 0, H_1 = H$,

$$P_p = \frac{1}{2}\gamma H^2 K_p$$

From Figure 16.25a, for $\phi' = 30°$ and $\delta'/\phi' = 1$, the value of $K_{p(\delta'/\phi'=1)}$ is about 5.9. Also, from Table 16.12, with $\phi' = 30°$ and $\delta'/\phi' = 0.5$, the value of R' is 0.746.

Hence,

$$P_p = \frac{1}{2}\gamma H^2 K_p = \frac{1}{2}(15.7)(3)^2(0.746 \times 5.9) \approx \mathbf{311\ kN/m}$$

16.16 Solution for Passive Earth Pressure by the Lower Bound Theorem of Plasticity (Granular Backfill)

Lancellotta (2002) analyzed the passive pressure problem by using the lower bound theorem of plasticity for retaining walls with a vertical backface ($\theta = 0$) and a horizontal granular backfill. Lancellotta (2002) provided the expression for K_p [as defined by Eq. (16.77)] as

$$K_p = \left[\left(\frac{1}{1 - \sin\phi'}\right)\left(\cos\delta' + \sqrt{\sin^2\phi' - \sin^2\delta'}\right)\right]e^{2\eta\tan\phi'} \qquad (16.79)$$

TABLE 16.13 Variation of K_p with ϕ' and δ' [Eq. (16.79)]

ϕ' (deg)	δ' (deg)	K_p
20	10	2.52
	20	2.92
30	15	4.44
	30	5.81
40	20	8.91
	40	14.4

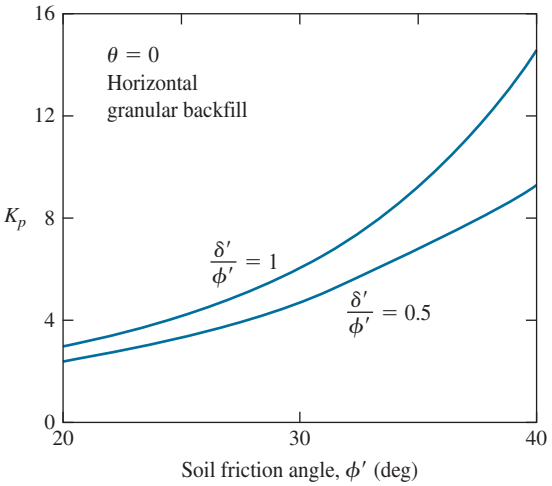


FIGURE 16.27 Lancellotta's solution for K_p—variation with ϕ' and $\frac{\delta'}{\phi'}$

where

$$2\eta \text{ (in radians)} = \sin^{-1}\left(\frac{\sin\delta'}{\sin\phi'}\right) + \delta' \tag{16.80}$$

The variation of K_p [Eq. (16.79)] with ϕ' and δ' is given in Table 16.13 and Figure 16.27.

EXAMPLE 16.15

Refer to Example 16.14. Estimate the passive force P_p using the analysis by Lancellotta (2002).

SOLUTION

From Table 16.13, for $\phi' = 30°$ and $\delta' = 15°$, the value of K_p is 4.44. So,

$$P_p = \frac{1}{2}K_p\gamma H^2 = \left(\frac{1}{2}\right)(4.44)(15.7)(3)^2 \approx \mathbf{314\ kN/m}$$

16.17 Passive Force on Walls with Earthquake Forces

The relationship for passive earth pressure on a retaining wall with a *horizontal backfill* and vertical backface under earthquake conditions (Figure 16.28) was evaluated by Subba Rao and Choudhury (2005) using the pseudostatic approach to the method of limit equilibrium. The failure surface in soil assumed in the analysis was similar to that shown in Figure 16.24b (with $\theta = 0$; that is, vertical backface) and in Figure 16.28. The notations used in the analysis were

H = Height of retaining wall
P_{pe} = Passive force per unit length of the wall
ϕ' = Soil friction angle
δ' = Angle of wall friction
c' = Cohesion
c'_a = Soil–wall interface adhesion
q = Surcharge

$$k_h = \frac{\text{Horizontal component of earthquake acceleration}}{\text{Acceleration due to gravity, } g}$$

$$k_v = \frac{\text{Vertical component of earthquake acceleration}}{\text{Acceleration due to gravity, } g}$$

Based on this analysis, the passive force P_{pe} can be expressed as

$$P_{pe} = \left[\frac{1}{2}\gamma H^2 K_{p\gamma(e)} + qHK_{pq(e)} + 2c'HK_{pc'(e)}\right]\frac{1}{\cos\delta'} \tag{16.81}$$

where $K_{p\gamma(e)}$, $K_{pq(e)}$, and $K_{pc'(e)}$ = passive earth pressure coefficients in the normal direction to the wall.

The variations of $K_{p\gamma(e)}$ and $K_{pq(e)}$ for $\delta'/\phi' = 0.5$ and 1 are shown in Figures 16.29 and 16.30.

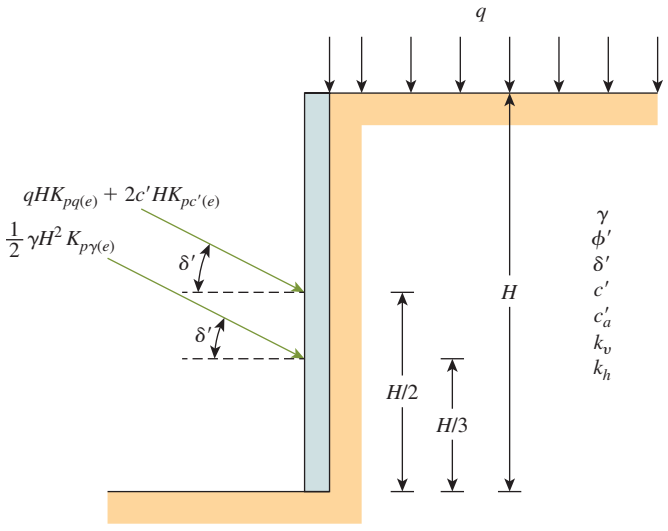


FIGURE 16.28 Passive pressure on wall (vertical backface and horizontal backfill) with earthquake forces

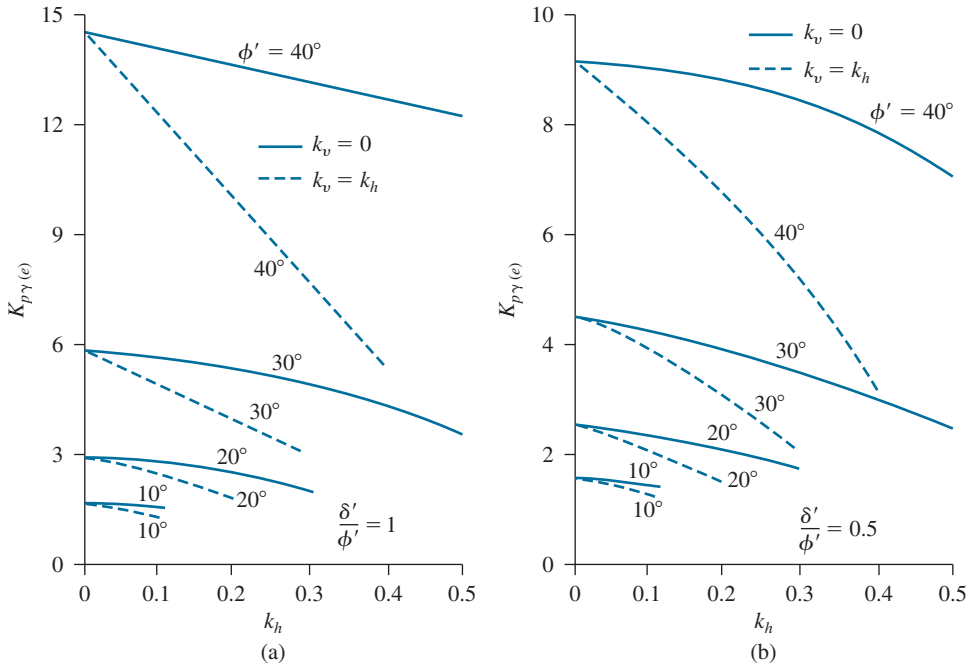


FIGURE 16.29 Variation of $K_{p\gamma(e)}$: (a) $\delta'/\phi' = 1$; (b) $\dfrac{\delta'}{\phi'} = 0.5$

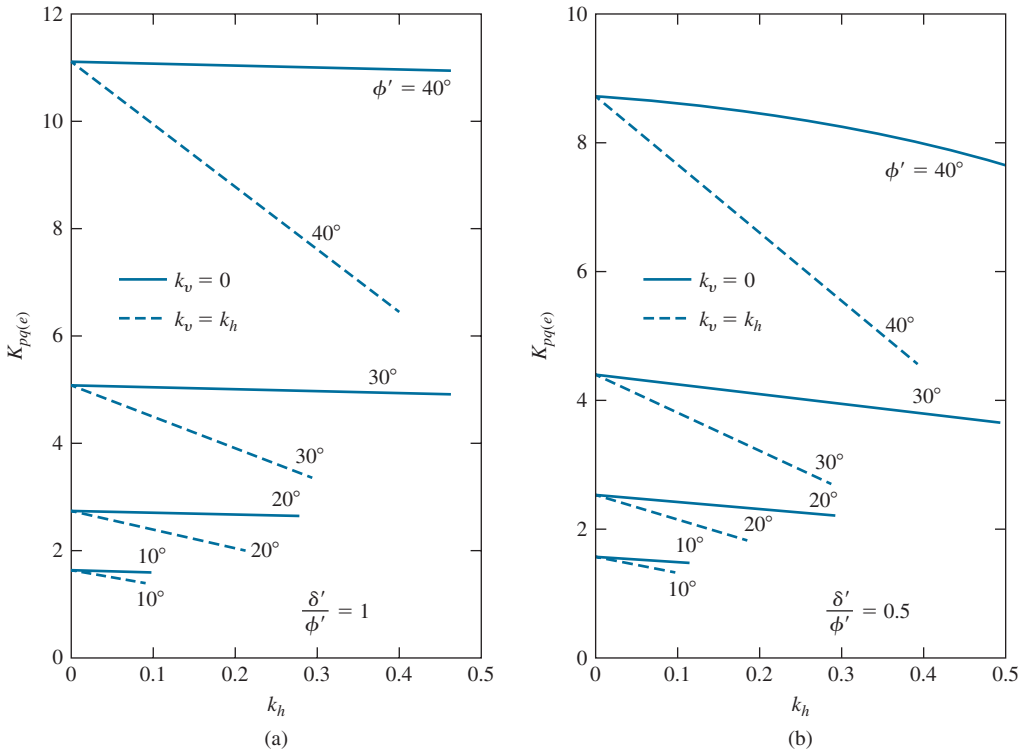


FIGURE 16.30 Variation of $K_{pq(e)}$: (a) $\dfrac{\delta'}{\phi'} = 1$, (b) $\dfrac{\delta'}{\phi'} = 0.5$

TABLE 16.14 Variation of $K_{pc'(e)}$

	$c'_a/c' = 0$		$c'_a/c' = \tan\delta'/\tan\phi'$	
ϕ' (deg)	$\delta'/\phi' = 0.5$	$\delta'/\phi' = 1.0$	$\delta'/\phi' = 0.5$	$\delta'/\phi' = 1.0$
10	1.32	1.45	1.55	1.69
20	1.81	2.18	2.07	2.33
30	2.66	3.42	2.94	3.49
40	4.33	5.95	4.65	5.97

The locations of the components of P_{pe},

$$\left[\frac{\frac{1}{2}\gamma H^2 K_{p\gamma(e)}}{\cos\delta'}\right] \text{ and } \left[\frac{qHK_{pq(e)} + 2c'HK_{pc'(e)}}{\cos\delta'}\right]$$

are shown in Figure 16.28. The variation of $K_{pc'(e)}$ is given in Table 16.14.

EXAMPLE 16.16

Refer to Figure 16.28. Let $H = 4$ m, $\phi' = \delta' = 40°$, $\gamma' = 17.5$ kN/m^3, $q = 10$ kN/m^2, $c' = 10$ kN/m^2, $c'_a = 0$, $k_v = 0$, $k_h = 0.3$. Determine the magnitude and location of P_{pe}.

SOLUTION

Given $k_h = 0.3$, $k_v = 0$, $\phi' = 40°$, $\delta'/\phi' = 1$. From Figures 16.29a and 16.30a, $K_{p\gamma(e)} \approx 13.7$ and $K_{pq(e)} \approx 11.15$.

Also, given $c'_a/c' = 0$, $\phi' = 40°$, $\delta'/\phi' = 1$. From Table 16.14, $K_{pc'(e)} = 5.95$. Now, using Eq. (16.81),

$$P_{pe} = \left[\left(\frac{1}{2}\right)(17.5)(4)^2(13.7) + (10)(4)(11.5) + (2)(10)(4)(5.95)\right]\frac{1}{\cos 40}$$

$$= (1918 + 446 + 476)\frac{1}{\cos 40} = \mathbf{3707.4\ kN/m}$$

Location of P_{pe}

$$\frac{1}{\cos\delta'}[qHK_{pq(e)} + 2c'HK_{pc'(e)}] = \frac{1}{\cos 40}(446 + 476) = 1203.6 \text{ kN/m}$$

The force 1203.6 kN/m acts at a distance of $H/2 = (4/2)$ m $= 2$ m above the bottom of the wall.

$$\frac{1}{\cos\delta'}\left[\frac{1}{2}\gamma H^2 K_{p\gamma(e)}\right] = \frac{1}{\cos 40}(1918) = 2503.8 \text{ kN/m}$$

The force 2503.8 kN/m acts at a distance of $H/3 = (4/3)$ m $= 1.33$ m above the bottom of the wall.

Hence,

$$\bar{z} = \frac{(1203.6)(2) + (2503.8)(1.33)}{3707.4} = \mathbf{1.548\ m}$$

16.18 Summary

When a wall retains a backfill, the loading on the wall depends on the following:

a. Roughness of the wall
b. Slope of the wall at the backfill–wall interface
c. Slope of the backfill at the ground level
d. Shear strength parameters c' and ϕ' and the unit weight of the backfill

Earthquakes can aggravate the situation by imposing an additional component to what is computed under static conditions.

The at-rest condition is a stable condition where the ratio of the effective horizontal to vertical stresses is a constant, K_o, known as the coefficient of earth pressure at rest. From the at-rest state, when the soil is allowed to expand laterally, it reaches the active state, where the soil fails. Likewise, from the at-rest state, when the soil is compressed laterally, the horizontal effective stresses increase until the passive state is reached, where the soil fails. In Rankine's theory, for a smooth vertical wall retaining a backfill that is horizontal at the ground level (i.e., $\alpha = 0$), it can be shown that

$$\sigma'_a = \sigma'_o K_a - 2c'\sqrt{K_a}$$
$$\sigma'_p = \sigma'_o K_p + 2c'\sqrt{K_p}$$

where σ'_o is the effective overburden stress acting vertically at the point of interest. K_a and K_p are Rankine's active and passive earth pressure coefficients given by

$$K_a = \tan^2\left(45 - \frac{\phi'}{2}\right) = \frac{1 - \sin\phi'}{1 + \sin\phi'}$$

$$K_p = \tan^2\left(45 + \frac{\phi'}{2}\right) = \frac{1 + \sin\phi'}{1 - \sin\phi'}$$

Rankine's earth equations above can be used in terms of total or effective stress parameters.

Coulomb's theory allows for friction along the wall, which can also be inclined. Methods to determine active and passive loadings using Coulomb's method were discussed. Finally, simple methods to compute the active and passive loadings under earthquake conditions were also presented.

PROBLEMS

16.1 A 15 ft high vertical wall retains an overconsolidated soil where OCR = 1.5, $c' = 0$, $\phi' = 33°$, and $\gamma = 115.0$ lb/ft^3. Determine the magnitude and location of the thrust on the wall, assuming that the soil is at rest.

16.2 In Problem 16.1, if the entire soil behind the wall is submerged with the water level at the ground surface, determine the magnitude and the location of the horizontal load on the wall, assuming the at-rest condition. Use $\gamma_{sat} = 127$ lb/ft^3.

16.3 The soil profile at a site is shown Figure P16.3. Find the total horizontal normal stresses at A and B, assuming at-rest conditions.

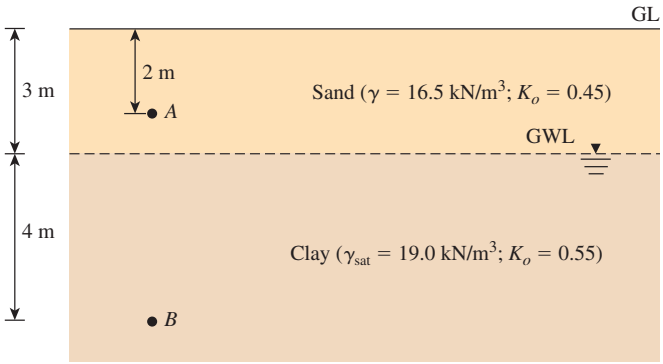


FIGURE P16.3

16.4 In Problem 16.3, if there was a surcharge of 20 kN/m^2 at the ground level, what would be the total horizontal normal stresses at A and B? Use the results from Problem 16.3.

16.5 The backfill retained by a gravity retaining wall shown in Figure P16.5 consists of two sand layers, compacted at different densities. The properties of the sand are shown in the figure. Assuming that the gravity wall does not move laterally (i.e., at-rest), determine the magnitude and location of the thrust on the wall.

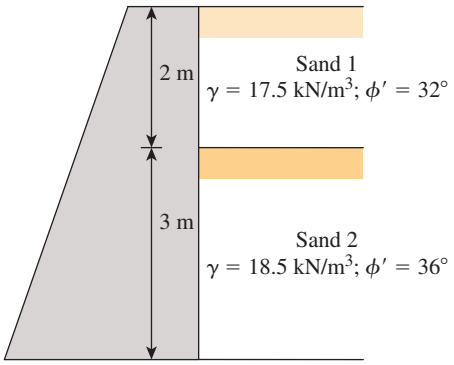


FIGURE P16.5

16.6 A 5 m high smooth vertical wall retains a clay backfill with $c' = 10$ kN/m^2, $\phi' = 25°$, and $\gamma = 19.0$ kN/m^3. If the clay is in active state, determine the following:

- **a.** The maximum tensile stress within the clay
- **b.** The depth of the tensile cracks
- **c.** The magnitude and location of the active thrust, neglecting the tensile zone

16.7 Determine the magnitude and the location of the active thrust on the smooth vertical wall shown in Figure P16.7, assuming that the entire backfill is in the active state.

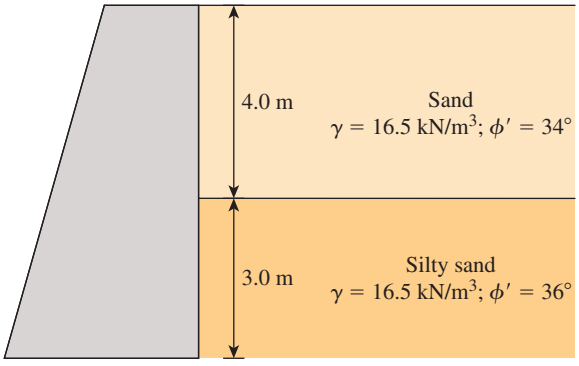


FIGURE P16.7

16.8 Figure P16.8 shows a smooth vertical wall retaining a sandy backfill underlain by clay. Assuming that the entire soil is in the active state, determine the magnitude and location of the resultant active force on the wall.

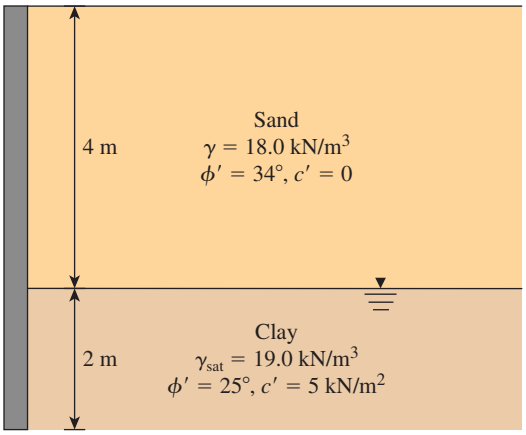


FIGURE P16.8

16.9 Develop a spreadsheet to compute the values of $K_{a(R)}$, β'_a, and η_a, using Eqs. (16.20), (16.18), and (16.21), respectively.

- **a.** Use this spreadsheet to compute the values for the following values of θ and α. Use $\phi' = 34°$.

θ (°)	0	0	0	0	0	10	10	10	20	20	20
α (°)	0	5	10	15	20	0	10	20	0	10	20

- **b.** Compare the values of $K_{a(R)}$ and β'_a with the values given in Tables 16.1 and 16.2.
- **c.** Discuss the trends in the magnitude and direction of the active thrust P_a with changes in θ and α.

16.10 For a smooth vertical wall supporting a granular backfill with $\phi' = 34°$, determine K_a using Eq. (16.22) for $\alpha = 0$, 5, 10, 15, and 20 degrees, and compare the results with the values calculated in Problem 16.9.

16.11 Refer to Figure 16.11. A 6.0 m high smooth wall retains a $c' - \phi'$ soil backfill, where $c' = 10.5$ kN/m^2, $\phi' = 15°$, and $\gamma = 17.5$ kN/m^3. The backfill is sloping at 5°.

- **a.** Determine the depth of tensile crack, z_c.
- **b.** Determine the active pressure variation with depth, based on Eqs. (16.32) and (16.33).
- **c.** Determine the magnitude, location, and direction of the resultant active thrust, P_a.

16.12 Refer to Figure 16.14a. For $H = 6$ m, $\gamma = 17.0$ kN/m^3, $\phi' = 36°$, $c' = 0$, $\beta = 85°$, $\alpha = 10°$, and $\delta' = 24°$, assume that the backfill is in the active state and use Coulomb's equation to determine the magnitude, location, and direction of the active thrust on the wall.

16.13 In Problem 16.12, what would be the active thrust P_a when there is a surcharge of 25 kN/m^2 at the ground level?

16.14 Refer to Figure 16.16a. Given $H = 15$ ft, $a = 0.3$, and $q = 600$ lb/ft, plot the variation of the horizontal earth pressures on the wall.

16.15 Refer to Figure 16.16b. Given $H = 6$ m, $a' = 1.5$ m, $b' = 2.0$ m, and $q = 40$ kN/m^2, find the magnitude and location of the resultant load on the wall.

16.16 Refer to Figure 16.17. Given $H = 6$ m, $\gamma = 18.5$ kN/m^3, $\phi' = 33°$, $\delta' = 22°$, $c' = 0$, $\alpha = 10°$, and $\beta = 80°$, use Eqs. (16.50) and (16.51) to determine the magnitude of the active thrust on the wall, assuming earthquake loading with the following parameters: $k_h = 0$ and $k_v = 0.15$.

16.17 Redo Problem 16.16 using Eqs. (16.52) and (16.56) to determine the magnitude and location of the active thrust on the wall.

16.18 For the data given in this problem, determine the magnitude of the active thrust on the wall retaining a $c' - \phi'$ soil, using the procedure discussed in Section 16.10. Given $H = 15.0$ ft, $c' = 100$ lb/ft^2, $\phi' = 26°$, $\gamma = 115$ lb/ft^3, $k_v = 0$, and $k_h = 0.3$.

16.19 A 15 ft high smooth vertical wall is pushed against a clay where the total stress parameters are given as $c = 300$ lb/ft^2, $\phi = 0°$, $\gamma = 115.0$ lb/ft^3. At the passive state, plot the variation of the lateral earth pressure with depth and determine the resultant load.

16.20 For a smooth vertical wall retaining a granular backfill inclined at an angle of $\alpha = 15°$, check whether Eqs. (16.70) and (16.72) (or Tables 16.9 and 16.10) give the same values for the passive earth pressure coefficient. Use $\phi' = 30°$ and 40°.

REFERENCES

Alpan, I. (1967). "The Empirical Evaluation of the Coefficients K_o and K_{oR}," *Soil and Foundations*, Vol. 7, No. 1, pp. 31–40.

Caquot, A. and Kerisel, J. (1948). *Tables for the Calculation of Passive Pressure, Active Pressure, and Bearing Capacity of Foundations*, Gauthier-Villars, Paris.

Chu, S. C. (1991). "Rankine Analysis of Active and Passive Pressures on Dry Sand," *Soils and Foundations*, Vol. 31, No. 4, pp. 115–120.

Coulomb, C. A. (1776). *Essai sur une Application des Règles de Maximis et Minimum à quelques Problemes de Statique Relatifs à l'Architecture*, Mem. Acad. Roy. des Sciences, Paris, Vol. 3, p. 38.

Iskander, M., Omidvar, M., and Elsherif, O. (2013). "Conjugate Stress Approach for Rankine Seismic Active Earth Pressure in Cohesionless Soils," *Journal of Geotechnical and Geoenvironmental Engineering*, American Society of Civil Engineers, Vol. 139, No. 7, pp. 1205–1210.

Jaky, J. (1944). "The Coefficient of Earth Pressure at Rest," *Journal for the Society of Hungarian Architects and Engineers*, October, pp. 355–358.

Jarquio, R. (1981). "Total Lateral Surcharge Pressure Due to Strip Load," *Journal of the Geotechnical Engineering Division*, American Society of Civil Engineers, Vol. 107, No. GT10, pp. 1424–1428.

Lancellotta, R. (2002). "Analytical Solution of Passive Earth Pressure," *Geotechnique*, Vol. 52, No. 8, pp. 617–619.

Massarsch, K. R. (1979). "Lateral Earth Pressure in Normally Consolidated Clay," *Proceedings of the Seventh European Conference on Soil Mechanics and Foundation Engineering*, Brighton, England, Vol. 2, pp. 245–250.

Mayne, P. W. and Kulhawy, F. H. (1982). "K_o–*OCR* Relationships in Soil," *Journal of the Geotechnical Engineering Division*, ASCE, Vol. 108, No. GT6, pp. 851–872.

Mazindrani, Z. H. and Ganjali, M. H. (1997). "Lateral Earth Pressure Problem of Cohesive Backfill with Inclined Surface," *Journal of Geotechnical and Geoenvironmental Engineering*, ASCE, Vol. 123, No. 2, pp. 110–112.

Seed, H. B. and Whitman, R. V. (1970). "Design of Earth Retaining Structures for Dynamic Loads," *Proceedings, Specialty Conference on Lateral Stresses in the Ground and Design of Earth Retaining Structures*, American Society of Civil Engineers, pp. 103–147.

Shields, D. H. and Tolunay, A. Z. (1973). "Passive Pressure Coefficients by Method of Slices," *Journal of the Soil Mechanics and Foundations Division*, ASCE, Vol. 99, No. SM12, pp. 1043–1053.

Shukla, S. K., Gupta, S. K., and Sivakugan, N. (2009). "Active Earth Pressure on Retaining Wall for c–ϕ Soil Backfill Under Seismic Loading Condition," *Journal of Geotechnical and Geoenvironmental Engineering*, ASCE, Vol. 135, No. 5, pp. 690–696.

Subba Rao, K. S. and Choudhury, D. (2005). "Seismic Passive Earth Pressures in Soil," *Journal of Geotechnical and Geoenvironmental Engineering*, ASCE, Vol. 131, No. 1, pp. 131–135.

Terzaghi, K. and Peck, R. B. (1967). *Soil Mechanics in Engineering Practice*, 2nd ed. John Wiley and Sons, New York.

Zhu, D. Y. and Qian, Q. (2000). "Determination of Passive Earth Pressure Coefficient by the Method of Triangular Slices," *Canadian Geotechnical Journal*, Vol. 37, No. 2, pp. 485–491.

17

Retaining Walls



Jarous/Shutterstock.com

17.1 Introduction 695
17.2 Proportioning Retaining Walls 697
17.3 Application of Lateral Earth Pressure Theories to Design 698
17.4 Stability of Retaining Walls 699
17.5 Check for Overturning 701
17.6 Check for Sliding Along the Base 703
17.7 Check for Bearing Capacity Failure 706
17.8 Construction Joints and Drainage from Backfill 714
17.9 Comments on Design of Retaining Walls and a Case Study 717
17.10 Gravity Retaining-Wall Design for Earthquake Conditions 720
17.11 Soil Reinforcement 723
17.12 Considerations in Soil Reinforcement 723
17.13 General Design Considerations 727
17.14 Retaining Walls with Metallic Strip Reinforcement 728
17.15 Step-by-Step-Design Procedure Using Metallic Strip Reinforcement 734
17.16 Retaining Walls with Geotextile Reinforcement 738
17.17 Retaining Walls with Geogrid Reinforcement—General 744
17.18 Design Procedure for Geogrid-Reinforced Retaining Wall 746
17.19 Summary 748
PROBLEMS 749
REFERENCES 750

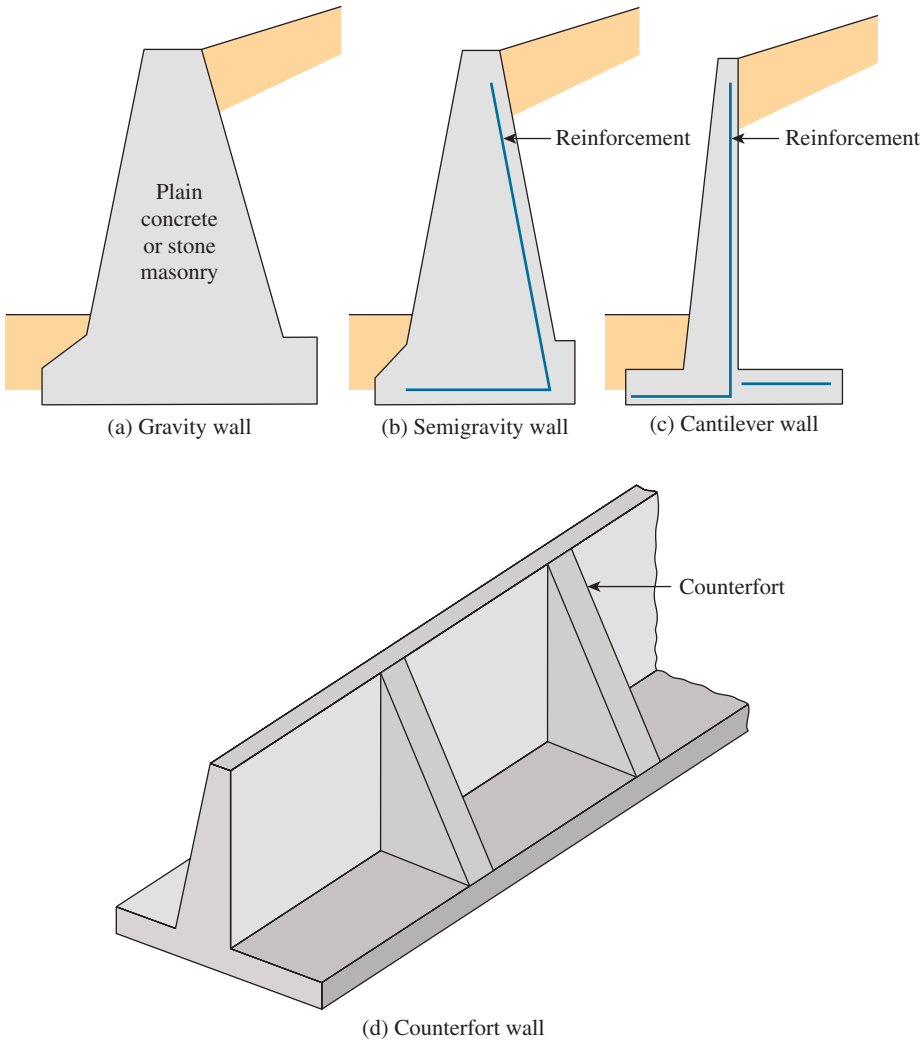
17.1 Introduction

In Chapter 16, you were introduced to various theories of lateral earth pressure. Those theories will be used in this chapter to design various types of retaining walls. In general, retaining walls can be divided into two major categories: (a) conventional retaining walls and (b) mechanically stabilized earth walls.

Conventional retaining walls can generally be classified into four varieties:

1. Gravity retaining walls
2. Semigravity retaining walls
3. Cantilever retaining walls
4. Counterfort retaining walls

Gravity retaining walls (Figure 17.1a) are constructed with plain concrete or stone masonry. They depend for stability on their own weight and any soil resting on the masonry. This type of construction is not economical for high walls.



(a) Gravity wall (b) Semigravity wall (c) Cantilever wall

(d) Counterfort wall

FIGURE 17.1 Types of retaining walls

In many cases, a small amount of steel may be used for the construction of gravity walls, thereby minimizing the size of wall sections. Such walls are generally referred to as *semigravity walls* (Figure 17.1b).

Cantilever retaining walls (Figure 17.1c) are made of reinforced concrete that consists of a thin stem and a base slab. Here, the retaining wall is acting like a vertical cantilever column fixed at the bottom end. This type of wall is economical to a height of about 8 m (25 ft). Figure 17.2 shows a cantilever retaining wall under construction.

Counterfort retaining walls (Figure 17.1d) are similar to cantilever walls. At regular intervals, however, they have thin vertical concrete slabs known as *counterforts* that tie the wall and the base slab together. The purpose of the counterforts is to reduce the shear and the bending moments.

To design retaining walls properly, an engineer must know the basic parameters—the *unit weight, angle of friction*, and *cohesion*—of the soil retained behind the wall and the soil below the base slab. Knowing the properties of the soil behind the wall enables the engineer to determine the lateral pressure distribution that has to be designed for.

There are two phases in the design of a conventional retaining wall—geotechnical and structural. In the first phase, with the lateral earth pressure known, the structure as a whole is checked for *stability*. The structure is examined for possible *overturning*, *sliding*, and *bearing capacity* failures. In the second phase, each component of the structure is checked for *strength*, and the *steel reinforcement* of each component is determined.

This chapter presents the procedures for determining the stability of the retaining wall. Checks for strength can be found in any textbook on reinforced concrete.



FIGURE 17.2 A cantilever retaining wall under construction (Courtesy of Dharma Shakya, Geotechnical Solutions, Inc., Irvine, California)

Some retaining walls have their backfills stabilized mechanically by including reinforcing elements such as metal strips, bars, welded wire mats, geotextiles, and geogrids. These walls are relatively flexible and can sustain large horizontal and vertical displacements without much damage.

Gravity and Cantilever Walls

17.2 Proportioning Retaining Walls

In designing retaining walls, an engineer must assume some of their dimensions. Called *proportioning*, such assumptions allow the engineer to check trial sections of the walls for stability. If the stability checks yield undesirable results, the sections can be changed and rechecked. Figure 17.3 shows the general proportions of various retaining-wall components that can be used in the preliminary design.

Note that the top of the stem of any retaining wall should not be less than about 0.3 m (≈12 in.) for proper placement of concrete. The depth, D, to the bottom of the base slab should be a minimum of 0.6 m (≈2 ft). However, the bottom of the base slab should be positioned below the seasonal frost line.

For counterfort retaining walls, the general proportion of the stem and the base slab is the same as for cantilever walls. However, the counterfort slabs may be about 0.3 m (≈12 in.) thick and spaced at center-to-center distances of $0.3H$ to $0.7H$.

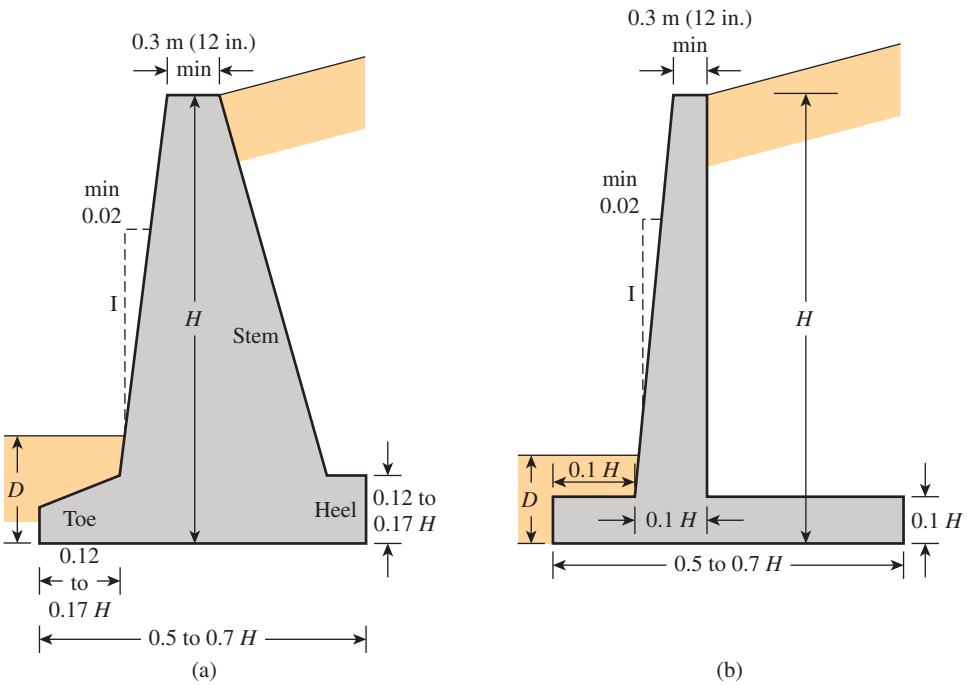


FIGURE 17.3 Approximate dimensions for various components of retaining walls for initial stability checks: (a) gravity wall; (b) cantilever wall

17.3 Application of Lateral Earth Pressure Theories to Design

The fundamental theories for calculating lateral earth pressure were presented in Chapter 16. Generally, Rankine's theory is preferred to that of Coulomb for its simplicity. To use these theories in design, an engineer must make several simple assumptions. In the case of cantilever walls, the use of the Rankine earth pressure theory for stability checks involves drawing a vertical line AB through point A, located at the edge of the heel of the base slab in Figure 17.4a. The Rankine active condition is assumed to exist along the vertical plane AB. Rankine active earth pressure equations may then be used to calculate the lateral pressure on the face AB of the wall. In the analysis of the wall's stability, the force $P_{a(\text{Rankine})}$, the weight of soil above the heel, and the weight W_c of the concrete all should be taken into consideration. Using Mohr's circles, Chu (1991) showed that the slip plane to the right of the heel in Rankine's active zone is inclined at an angle of $\left[45 + \frac{\alpha}{2} + \frac{\phi_1'}{2} - \frac{1}{2}\sin^{-1}\left(\frac{\sin\alpha}{\sin\phi_1'}\right)\right]$ to the horizontal [see Eq. (16.21) and Figure 16.10]. Terzaghi (1943) showed that for the active wedge formed within a sloping granular backfill, the angle between the slip planes is $90 - \phi_1'$. In Figure 17.4a, the slip plane AC' makes an angle of η to the vertical. This angle η can be calculated as $\eta = (90 - \phi_1') + \left[45 + \frac{\alpha}{2} + \frac{\phi_1'}{2} - \frac{1}{2}\sin^{-1}\left(\frac{\sin\alpha}{\sin\phi_1'}\right)\right] - 90.$

Therefore,

$$\eta = 45 + \frac{\alpha}{2} - \frac{\phi_1'}{2} - \frac{1}{2}\sin^{-1}\left(\frac{\sin\alpha}{\sin\phi_1'}\right) \tag{17.1}$$

The assumption for the development of Rankine active pressure along the soil face AB is theoretically correct if the shear zone bounded by the line AC is not obstructed by the stem of the wall.

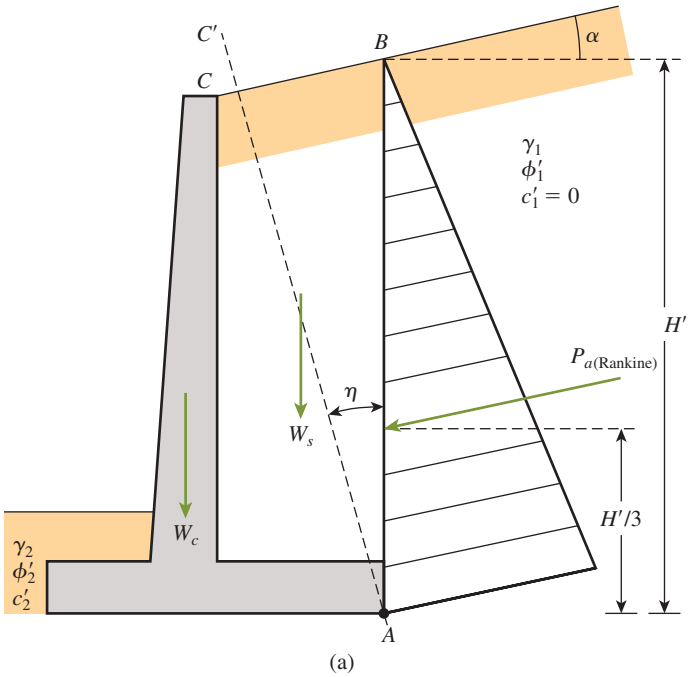


FIGURE 17.4 Assumption for the determination of lateral earth pressure: (a) cantilever wall; (b) and (c) gravity wall

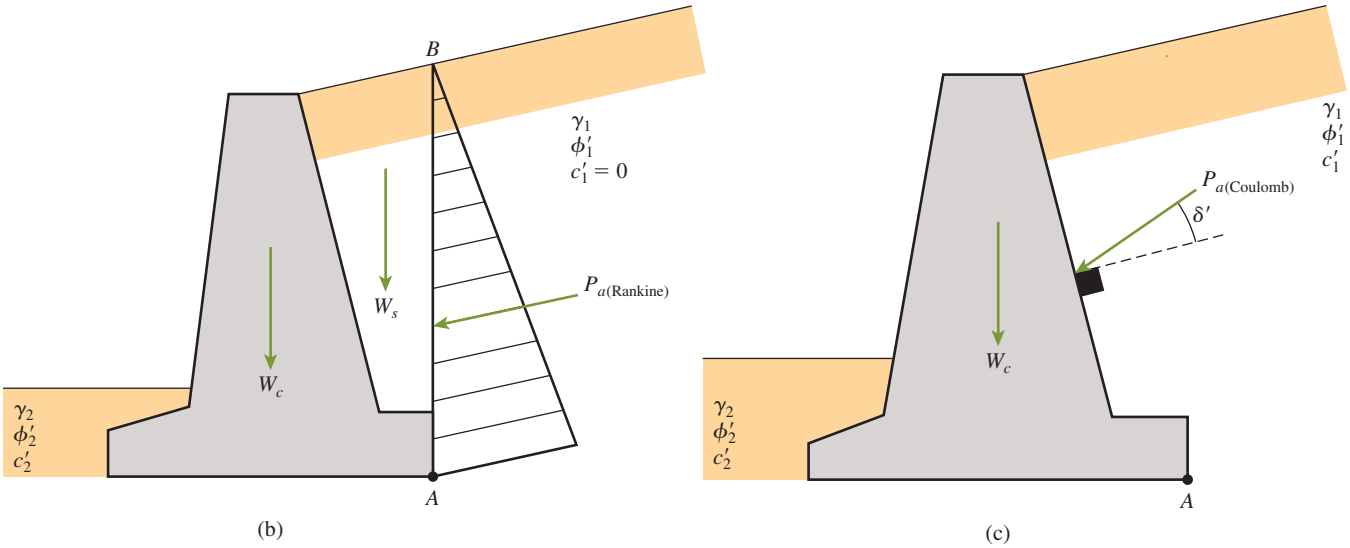


FIGURE 17.4 (*Continued*)

A similar type of analysis may be used for gravity walls, as shown in Figure 17.4b. However, *Coulomb's active earth pressure theory* also may be used, as shown in Figure 17.4c. If it is used, the only forces to be considered are $P_{a(\text{Coulomb})}$ and the weight of the wall, W_c.

If Coulomb's theory is used, it will be necessary to know the range of the wall friction angle δ' with various types of backfill material. Following are some ranges of wall friction angle for masonry or mass concrete walls:

Backfill material	Range of δ' (deg)
Gravel	27–30
Coarse sand	20–28
Fine sand	15–25
Stiff clay	15–20
Silty clay	12–16

In the case of ordinary retaining walls, water table problems and hence hydrostatic pressure are not encountered. Facilities for drainage from the soil that are retained are always provided.

17.4 Stability of Retaining Walls

A retaining wall may fail in any of the following ways:

- It may *overturn* about its toe. (See Figure 17.5a.)
- It may *slide* along its base. (See Figure 17.5b.)
- It may fail due to the loss of *bearing capacity* of the soil supporting the base. (See Figure 17.5c.)
- It may undergo deep-seated shear failure. (See Figure 17.5d.)
- It may go through excessive settlement.

The checks for stability against overturning, sliding, and bearing capacity failure will be described in Sections 17.5, 17.6, and 17.7. The principles used to estimate settlement were covered in Chapter 9 and will not be discussed further. When a weak

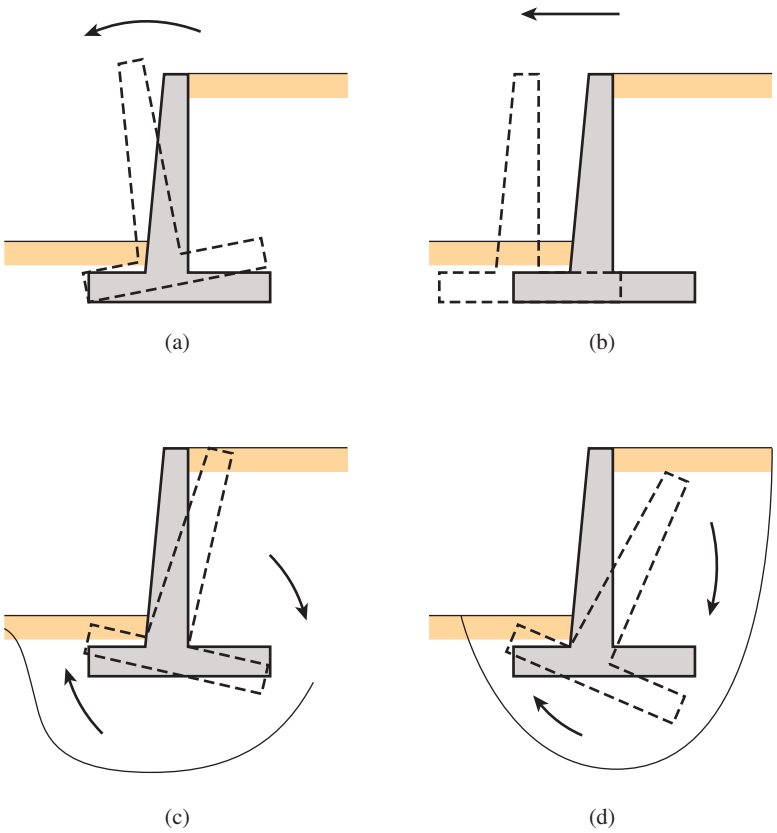


FIGURE 17.5 Failure of retaining wall: (a) by overturning; (b) by sliding; (c) by bearing capacity failure; (d) by deep-seated shear failure

soil layer is located at a shallow depth—that is, within a depth of 1.5 times the width of the base slab of the retaining wall—the possibility of excessive settlement should be considered. In some cases, the use of lightweight backfill material behind the retaining wall may solve the problem.

Deep shear failure can occur along a cylindrical surface, such as *abc* shown in Figure 17.6, as a result of the existence of a weak layer of soil underneath the wall within a depth of about 1.5 times the width of the base slab of the retaining wall. In such cases, the critical cylindrical failure surface *abc* has to be determined by trial

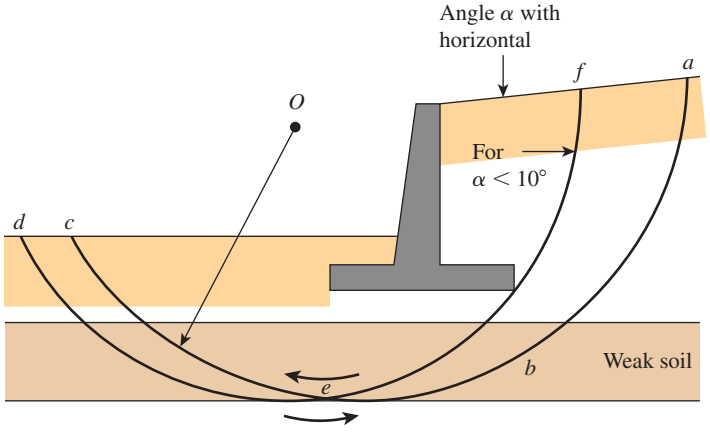


FIGURE 17.6 Deep-seated shear failure

and error, using various centers such as O. The failure surface along which the minimum factor of safety is obtained is the *critical surface of sliding*. For the backfill slope with α less than about 10°, the critical failure circle apparently passes through the edge of the heel slab (such as *def* in the figure). In this situation, the minimum factor of safety also has to be determined by trial and error by changing the center of the trial circle.

17.5 Check for Overturning

Figure 17.7 shows the forces acting on a cantilever and a gravity retaining wall, based on the assumption that the Rankine active pressure is acting along a vertical plane AB drawn through the heel of the structure. P_p is the Rankine passive pressure; recall that its magnitude is [from Eq. (16.66)]

$$P_p = \tfrac{1}{2}K_p\gamma_2 D^2 + 2c_2'\sqrt{K_p}D$$

where

γ_2 = unit weight of soil in front of the heel and under the base slab

K_p = Rankine passive earth pressure coefficient = $\tan^2(45 + \phi_2'/2)$

c_2', ϕ_2' = cohesion and effective soil friction angle, respectively

The factor of safety against overturning about the toe—that is, about point C in Figure 17.7—may be expressed as

$$\text{FS}_{(\text{overturning})} = \frac{\Sigma M_R}{\Sigma M_o} \tag{17.2}$$

where

ΣM_o = sum of the moments of forces tending to overturn about point C

ΣM_R = sum of the moments of forces tending to resist overturning about point C

The overturning moment is

$$\Sigma M_o = P_h\left(\frac{H'}{3}\right) \tag{17.3}$$

where $P_h = P_a \cos\alpha$.

To calculate the resisting moment about the toe, ΣM_R (neglecting P_p), a table such as Table 17.1 can be prepared. The weight of the soil above the heel and the weight of the concrete (or masonry) are both forces that contribute to the resisting moment. Note that the force P_v also contributes to the resisting moment. P_v is the vertical component of the active force P_a, or

$$P_v = P_a \sin\alpha$$

The moment of the force P_v about C is

$$M_v = P_v B = P_a \sin\alpha B \tag{17.4}$$

where B is the width of the base slab.

Once ΣM_R is known, the factor of safety can be calculated as

$$\text{FS}_{(\text{overturning})} = \frac{M_1 + M_2 + M_3 + M_4 + M_5 + M_6 + M_v}{P_a \cos\alpha(H'/3)} \tag{17.5}$$

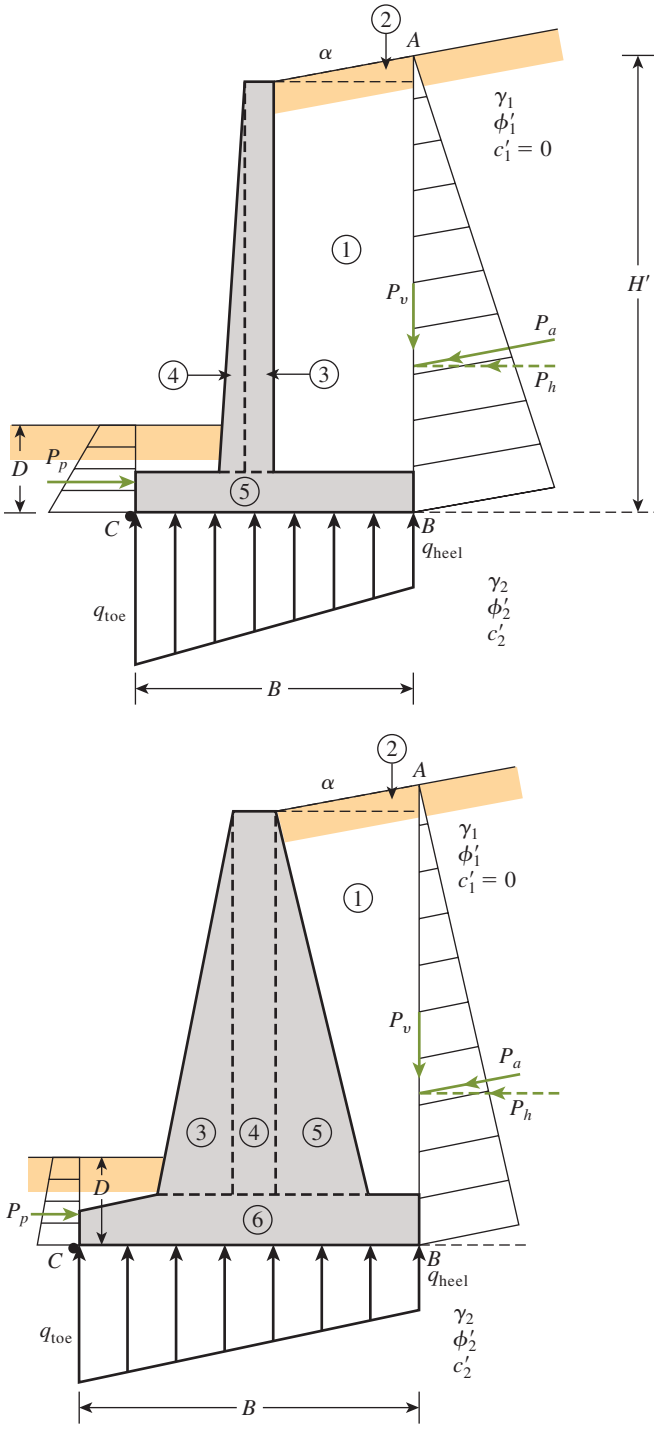


FIGURE 17.7 Check for overturning, assuming that the Rankine pressure is valid

The usual minimum desirable value of the factor of safety with respect to overturning is 2 to 3.

Some designers prefer to determine the factor of safety against overturning with the formula

$$\text{FS}_{(\text{overturning})} = \frac{M_1 + M_2 + M_3 + M_4 + M_5 + M_6}{P_a \cos\alpha (H'/3) - M_v} \tag{17.6}$$

TABLE 17.1 Procedure for Calculating ΣM_R

Section (1)	Area (2)	Weight/unit length of wall (3)	Moment arm measured from C (4)	Moment about C (5)
1	A_1	$W_1 = \gamma_1 \times A_1$	X_1	M_1
2	A_2	$W_2 = \gamma_1 \times A_2$	X_2	M_2
3	A_3	$W_3 = \gamma_c \times A_3$	X_3	M_3
4	A_4	$W_4 = \gamma_c \times A_4$	X_4	M_4
5	A_5	$W_5 = \gamma_c \times A_5$	X_5	M_5
6	A_6	$W_6 = \gamma_c \times A_6$	X_6	M_6
		P_v	B	M_v
		ΣV		ΣM_R

(*Note:* γ_l = unit weight of backfill
γ_c = unit weight of concrete
X_i = horizontal distance between C and the centroid of the section)

17.6 Check for Sliding Along the Base

The factor of safety against sliding may be expressed by the equation

$$\text{FS}_{(\text{sliding})} = \frac{\Sigma F_{R'}}{\Sigma F_d} \tag{17.7}$$

where

$\Sigma F_{R'}$ = sum of the horizontal resisting forces

ΣF_d = sum of the horizontal driving forces

Figure 17.8 indicates that the shear strength of the soil immediately below the base slab may be represented as

$$s = \sigma' \tan \delta' + c'_a$$

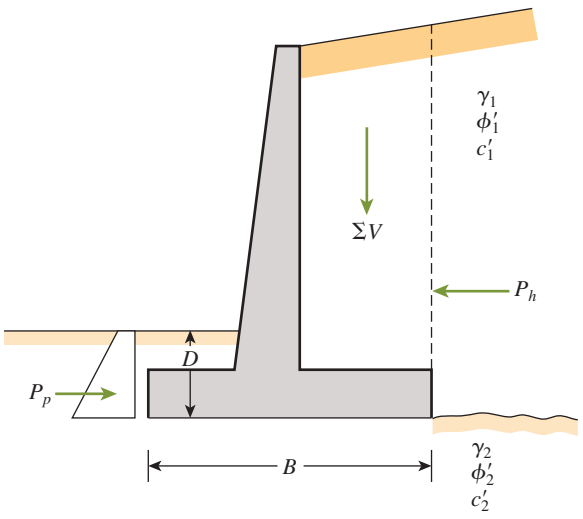


FIGURE 17.8 Check for sliding along the base

where

δ' = angle of friction between the soil and the base slab

c'_a = adhesion between the soil and the base slab

Thus, the maximum resisting force that can be derived from the soil per unit length of the wall along the bottom of the base slab is

$$R' = s(\text{area of cross section}) = s(B \times 1) = B\sigma' \tan \delta' + Bc'_a$$

However,

$$B\sigma' = \text{sum of the vertical force} = \Sigma V \text{ (see Table 17.1)}$$

so

$$R' = (\Sigma V) \tan \delta' + Bc'_a$$

Figure 17.8 shows that the passive force P_p is also a horizontal resisting force. Hence,

$$\Sigma F_{R'} = (\Sigma V) \tan \delta' + Bc'_a + P_p \tag{17.8}$$

The only horizontal force that will tend to cause the wall to slide (a *driving force*) is the horizontal component of the active force P_a, so

$$\Sigma F_d = P_a \cos \alpha \tag{17.9}$$

Combining Eqs. (17.7), (17.8), and (17.9) yields

$$\text{FS}_{(\text{sliding})} = \frac{(\Sigma V) \tan \delta' + Bc'_a + P_p}{P_a \cos \alpha} \tag{17.10}$$

A minimum factor of safety of 1.5 against sliding is generally required.

In many cases, the passive force P_p is ignored conservatively in calculating the factor of safety with respect to sliding. In general, we can write $\delta' = k_1 \phi'_2$ and $c'_a = k_2 c'_2$. In most cases, k_1 and k_2 are in the range from $\frac{1}{2}$ to $\frac{2}{3}$. Thus,

$$\text{FS}_{(\text{sliding})} = \frac{(\Sigma V) \tan (k_1 \phi'_2) + Bk_2 c'_2 + P_p}{P_a \cos \alpha} \tag{17.11}$$

If the desired value of $\text{FS}_{(\text{sliding})}$ is not achieved, several alternatives may be investigated (see Figure 17.9):

- Increase the width of the base slab (i.e., the heel of the footing).
- Use a key to the base slab. If a key is included, the passive force per unit length of the wall becomes

$$P_p = \frac{1}{2} \gamma_2 D_1^2 K_p + 2c'_2 D_1 \sqrt{K_p}$$

  where $K_p = \tan^2\left(45 + \frac{\phi'_2}{2}\right)$.
- Use a *deadman anchor* at the stem of the retaining wall.
- Another possible way to increase the value of $\text{FS}_{(\text{sliding})}$ is to consider reducing the value of P_a [see Eq. (17.11)]. One possible way to do so is to use the method developed by Elman and Terry (1988). The discussion here is limited to the case in which the retaining wall has a horizontal granular backfill (Figure 17.10). In Figure 17.10a, the active force, P_a, is horizontal ($\alpha = 0$) so that

$$P_a \cos \alpha = P_h = P_a$$

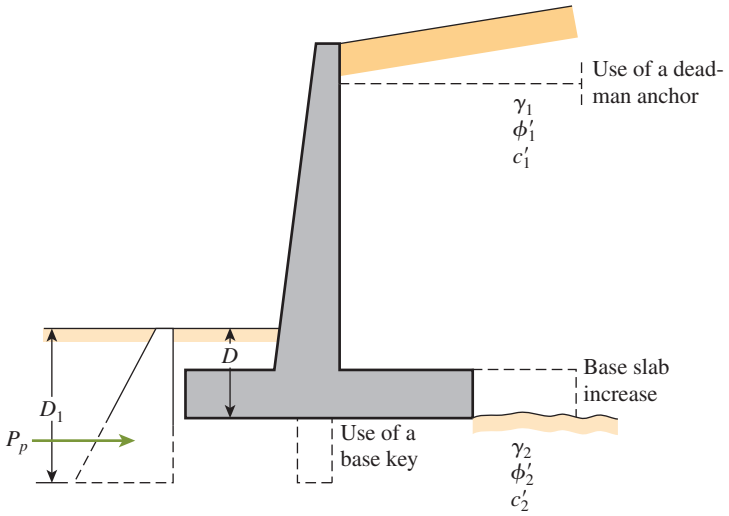


FIGURE 17.9 Alternatives for increasing the factor of safety with respect to sliding

and

$$P_a \sin \alpha = P_v = 0$$

However,

$$P_a = P_{a(1)} + P_{a(2)} \tag{17.12}$$

The magnitude of $P_{a(2)}$ can be reduced if the heel of the retaining wall is sloped as shown in Figure 17.10b. For this case,

$$P_a = P_{a(1)} + AP_{a(2)} \tag{17.13}$$

The magnitude of A, as shown in Table 17.2, is valid for $\alpha' = 45°$. However, note that in Figure 17.10a

$$P_{a(1)} = \frac{1}{2}\gamma_1 K_a (H' - D')^2$$

and

$$P_a = \frac{1}{2}\gamma_1 K_a H'^2$$

Hence,

$$P_{a(2)} = \frac{1}{2}\gamma_1 K_a [H'^2 - (H' - D')^2]$$

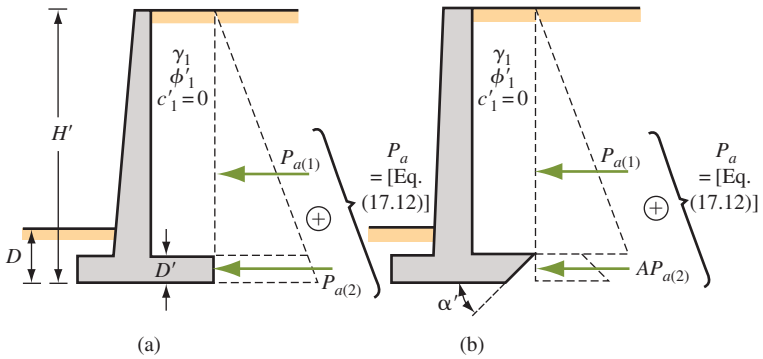


FIGURE 17.10 Retaining wall with sloped heel

TABLE 17.2 Variation of A with ϕ_1' (for $\alpha' = 45°$)

Soil friction angle, ϕ_1' (deg)	A
20	0.28
25	0.14
30	0.06
35	0.03
40	0.018

So, for the active pressure diagram shown in Figure 17.10b,

$$P_a = \frac{1}{2}\gamma_1 K_a (H' - D')^2 + \frac{A}{2}\gamma_1 K_a [H'^2 - (H' - D')^2] \qquad (17.14)$$

Sloping the heel of a retaining wall can thus be extremely helpful in some cases.

17.7 Check for Bearing Capacity Failure

Now that we have checked the retaining wall for stability against overturning and sliding, we will do the final check for possible bearing capacity failure. Here, the base of the retaining wall can be treated as a strip foundation that is subjected to a line load, which can act eccentrically and with some inclination to the vertical.

In the retaining wall shown in Figure 17.11, R is the resultant of ΣV and P_h, acting at E, at a distance of $\overline{X}$ from the toe C. Being an eccentric line load, it makes the

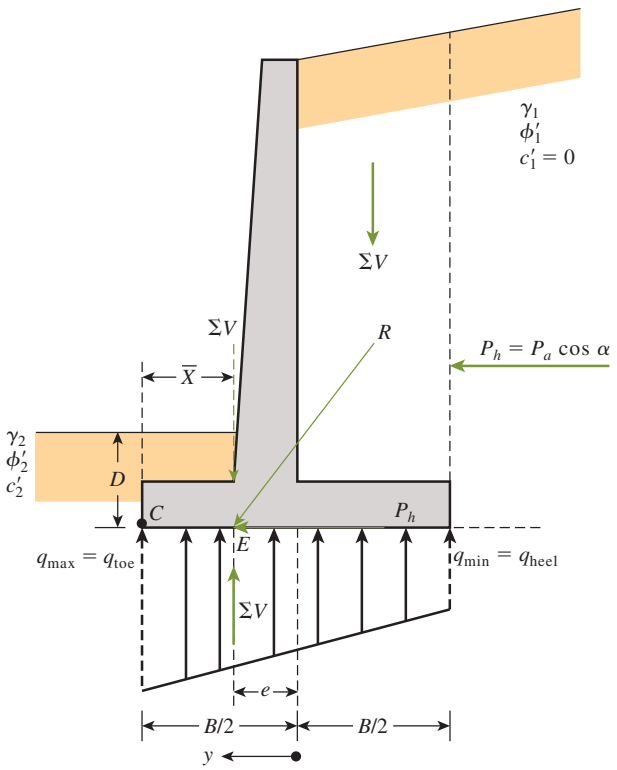


FIGURE 17.11 Check for bearing capacity failure

soil pressure distribution vary, as shown in the figure, from $q_{\min}$ at one end to $q_{\max}$ at the other end. The resultant of the soil pressure at the base of the wall has magnitude of ΣV, acting upward at E. Taking moments about C,

$$\Sigma M_R - \Sigma M_o - (\Sigma V)\overline{X} = 0$$

Therefore,

$$\overline{X} = \frac{\Sigma M_R - \Sigma M_o}{\Sigma V} \tag{17.15}$$

The values of ΣV, ΣM_R, and ΣM_o were already determined for the overturning analysis in Table 17.1. The eccentricity of the resultant force R is given by

$$e = \frac{B}{2} - \overline{X} \tag{17.16}$$

The effect of the vertical eccentric load ΣV on the soil pressure is the same as the effect of the same force at the center and a moment given by $(\Sigma V)e$. Using the simple principles from the mechanics of materials, the linearly varying pressure distribution under the base of the wall can be expressed as

$$q = \frac{\Sigma V}{A} + \frac{(\Sigma V)e}{I}y \tag{17.17}$$

where

y = distance from the center where q is computed (see Figure 17.11). Note the sign.

A = base area per unit length = B

I = moment of inertia per unit length = $B^3/12$

The maximum and minimum pressures occur at $y = B/2$ and $-B/2$, respectively. Substituting these values in Eq. (17.17),

$$q_{\max} = q_{\text{toe}} = \frac{\Sigma V}{A} + \frac{(\Sigma V)e}{I}y = \frac{\Sigma V}{B} + \frac{12(\Sigma V)e}{B^3}\left(\frac{B}{2}\right) = \frac{\Sigma V}{B}\left(1 + \frac{6e}{B}\right) \tag{17.18}$$

$$q_{\min} = q_{\text{heel}} = \frac{\Sigma V}{A} + \frac{(\Sigma V)e}{I}y = \frac{\Sigma V}{B} - \frac{12(\Sigma V)e}{B^3}\left(\frac{B}{2}\right) = \frac{\Sigma V}{B}\left(1 - \frac{6e}{B}\right) \tag{17.19}$$

It can be seen from Eq. (17.19) that when the eccentricity exceeds $B/6$, $q_{\min}$ becomes negative. Since soil have very little tensile strength in general, this situation is not desirable. Therefore, if the design shows that $e > B/6$, the wall should be reproportioned and the calculations redone to reduce e.

Computation of the ultimate bearing capacity q_u for shallow foundations was discussed in Chapter 6 in detail. Treating the base of the retaining wall as a continuous foundation (with shape factors F_{cs}, F_{qs}, and $F_{\gamma s}$ being unity), q_u can be written as

$$q_u = c_2' N_c F_{cd} F_{ci} + q N_q F_{qd} F_{qi} + \tfrac{1}{2}\gamma_2 B' N_\gamma F_{\gamma d} F_{\gamma i} \tag{17.20}$$

where

$$q = \gamma_2 D$$

$$B' = B - 2e$$

From Table 6.3,

$$F_{cd} = F_{qd} - \frac{1 - F_{qd}}{N_c \tan \phi_2'}$$

$$F_{qd} = 1 + 2 \tan \phi_2' (1 - \sin \phi_2')^2 \frac{D}{B'}$$

$$F_{\gamma d} = 1$$

$$F_{ci} = F_{qi} = \left(1 - \frac{\psi^\circ}{90^\circ}\right)^2$$

$$F_{\gamma i} = \left(1 - \frac{\psi^\circ}{\phi_2'^\circ}\right)^2$$

$$\psi^\circ = \tan^{-1}\left(\frac{P_a \cos\alpha}{\Sigma V}\right)$$

Once the ultimate bearing capacity of the soil has been calculated by using Eq. (17.20), the factor of safety against bearing capacity failure can be determined:

$$\text{FS}_{(\text{bearing capacity})} = \frac{q_u}{q_{\max}} \tag{17.21}$$

Generally, a factor of safety of 3 is required. In Chapter 6, we noted that the ultimate bearing capacity of shallow foundations occurs at a settlement of about 10% of the foundation width. In the case of retaining walls, the width B is large. Hence, the ultimate load q_u will occur at a fairly large foundation settlement. A factor of safety of 3 against bearing capacity failure may not ensure that settlement of the structure will be within the tolerable limit in all cases. Thus, this situation needs further investigation.

EXAMPLE 17.1

The cross section of a cantilever retaining wall is shown in Figure 17.12. Calculate the factors of safety with respect to overturning, sliding, and bearing capacity.

SOLUTION

From the figure,

$$H' = H_1 + H_2 + H_3 = 2.6 \tan 10^\circ + 6 + 0.7$$
$$= 0.458 + 6 + 0.7 = 7.158 \text{ m}$$

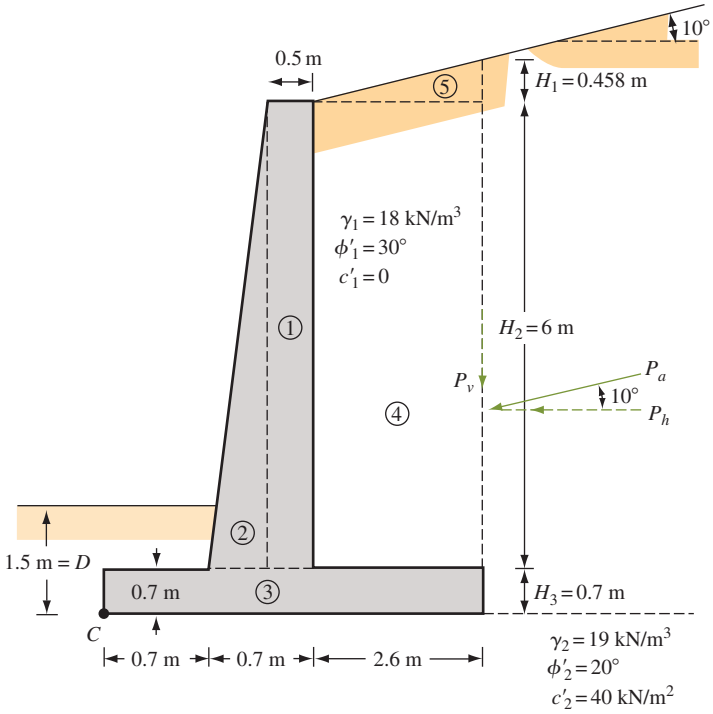


FIGURE 17.12 Calculation of stability of a retaining wall

The Rankine active force per unit length of wall $= P_p = \frac{1}{2}\gamma_1 H'^2 K_a$. For $\phi_1' = 30°$ and $\alpha = 10°$, K_a is equal to 0.3495. (See Table 16.1.) Thus,

$$P_a = \tfrac{1}{2}(18)(7.158)^2(0.3495) = 161.2 \text{ kN/m}$$

$$P_v = P_a \sin 10° = 161.2 (\sin 10°) = 28.0 \text{ kN/m}$$

and

$$P_h = P_a \cos 10° = 161.2 (\cos 10°) = 158.75 \text{ kN/m}$$

Factor of Safety Against Overturning

The following table can now be prepared for determining the resisting moment:

Section no.[a]	Area (m^2)	Weight/unit length (kN/m)	Moment arm from point C (m)	Moment (kN · m/m)
1	$6 \times 0.5 = 3$	70.74	1.15	81.35
2	$\frac{1}{2}(0.2)6 = 0.6$	14.15	0.833	11.79
3	$4 \times 0.7 = 2.8$	66.02	2.0	132.04
4	$6 \times 2.6 = 15.6$	280.80	2.7	758.16
5	$\frac{1}{2}(2.6)(0.458) = 0.595$	10.71	3.13	33.52
		$P_v = 28.0$	4.0	112.0
		$\Sigma V = 470.42$		$1128.86 = \Sigma M_R$

[a]For section numbers, refer to Figure 17.12.
Note: $\gamma_{\text{concrete}} = 23.58 \text{ kN/m}^3$

The overturning moment

$$M_o = P_h\left(\frac{H'}{3}\right) = 158.75\left(\frac{7.158}{3}\right) = 378.78 \text{ kN} \cdot \text{m/m}$$

and

$$\text{FS}_{\text{(overturning)}} = \frac{\Sigma M_R}{M_o} = \frac{1128.86}{378.78} = \mathbf{2.98 > 2, OK}$$

Factor of Safety Against Sliding

From Eq. (17.11),

$$\text{FS}_{\text{(sliding)}} = \frac{(\Sigma V)\tan(k_1\phi_2') + Bk_2c_2' + P_p}{P_a \cos\alpha}$$

Let $k_1 = k_2 = \frac{2}{3}$. Also,

$$P_p = \tfrac{1}{2}K_p\gamma_2 D^2 + 2c_2'\sqrt{K_p}D$$

$$K_p = \tan^2\left(45 + \frac{\phi_2'}{2}\right) = \tan^2(45 + 10) = 2.04$$

and

$$D = 1.5 \text{ m}$$

So

$$P_p = \tfrac{1}{2}(2.04)(19)(1.5)^2 + 2(40)(\sqrt{2.04})(1.5)$$
$$= 43.61 + 171.39 = 215 \text{ kN/m}$$

Hence,

$$\text{FS}_{\text{(sliding)}} = \frac{(470.42)\tan\left(\frac{2 \times 20}{3}\right) + (4)\left(\frac{2}{3}\right)(40) + 215}{158.75}$$

$$= \frac{111.49 + 106.67 + 215}{158.75} = \mathbf{2.73 > 1.5, OK}$$

Note: For some designs, the depth D in a passive pressure calculation may be taken to be *equal to the thickness of the base slab*.

Factor of Safety Against Bearing Capacity Failure

Combining Eqs. (17.15) and (17.16) yields

$$e = \frac{B}{2} - \frac{\Sigma M_R - \Sigma M_o}{\Sigma V} = \frac{4}{2} - \frac{1128.86 - 378.78}{470.42}$$

$$= 0.406 \text{ m} < \frac{B}{6} = \frac{4}{6} = 0.666 \text{ m}$$

Again, from Eqs. (17.18) and (17.19),

$$q_{\text{heel}} = \frac{\Sigma V}{B}\left(1 - \frac{6e}{B}\right) = \frac{470.42}{4}\left(1 - \frac{6 \times 0.406}{4}\right) = 45.98 \text{ kN/m}^2$$

$$q_{\text{toe}} = \frac{\Sigma V}{B}\left(1 + \frac{6e}{B}\right) = \frac{470.42}{4}\left(1 + \frac{6 \times 0.406}{4}\right)$$

$$= 189.2 \text{ kN/m}^2$$

The ultimate bearing capacity of the soil can be determined from Eq. (17.20).

$$q_u = c_2' N_c F_{cd} F_{ci} + q N_q F_{qd} F_{qi} + \frac{1}{2}\gamma_2 B' N_\gamma F_{\gamma d} F_{\gamma i}$$

For $\phi_2' = 20°$ (see Table 6.2), $N_c = 14.83$, $N_q = 6.4$, and $N_\gamma = 5.39$. Also,

$$q = \gamma_2 D = (19)\,(1.5) = 28.5 \text{ kN/m}^2$$

$$B' = B - 2e = 4 - 2(0.406) = 3.188 \text{ m}$$

From Table 6.3,

$$F_{cd} = F_{qd} - \frac{1 - F_{qd}}{N_c \tan \phi_2'} = 1.148 - \frac{1 - 1.148}{(14.83)(\tan 20)} = 1.175$$

$$F_{qd} = 1 + 2 \tan \phi_2'(1 - \sin \phi_2')^2\left(\frac{D}{B'}\right) = 1 + 0.315\left(\frac{1.5}{3.188}\right) = 1.148$$

$$F_{\gamma d} = 1$$

$$F_{ci} = F_{qi} = \left(1 - \frac{\psi°}{90°}\right)^2$$

and

$$\psi = \tan^{-1}\left(\frac{P_a \cos \alpha}{\Sigma V}\right) = \tan^{-1}\left(\frac{158.75}{470.42}\right) = 18.65°$$

So

$$F_{ci} = F_{qi} = \left(1 - \frac{18.65}{90}\right)^2 = 0.628$$

and

$$F_{\gamma i} = \left(1 - \frac{\psi}{\phi_2'}\right)^2 = \left(1 - \frac{18.65}{20}\right)^2 \approx 0$$

Hence,

$$\begin{aligned} q_u &= (40)(14.83)(1.175)(0.628) + (28.5)(6.4)(1.148)(0.628) \\ &\quad + \tfrac{1}{2}(19)(5.93)(3.188)(1)(0) \\ &= 437.72 + 131.5 + 0 = 569.22 \text{ kN/m}^2 \end{aligned}$$

and

$$\text{FS}_{\text{(bearing capacity)}} = \frac{q_u}{q_{\text{toe}}} = \frac{569.22}{189.2} = \textbf{3.0, OK}$$

EXAMPLE 17.2

A gravity retaining wall is shown in Figure 17.13. Use $\delta' = 2/3\phi_1'$ and Coulomb's active earth pressure theory. Determine:

a. The factor of safety against overturning
b. The factor of safety against sliding
c. The pressure on the soil at the toe and heel

SOLUTION

The height

$$H' = 5 + 1.5 = 6.5 \text{ m}$$

Coulomb's active force is

$$P_a = \tfrac{1}{2}\gamma_1 H'^2 K_a$$

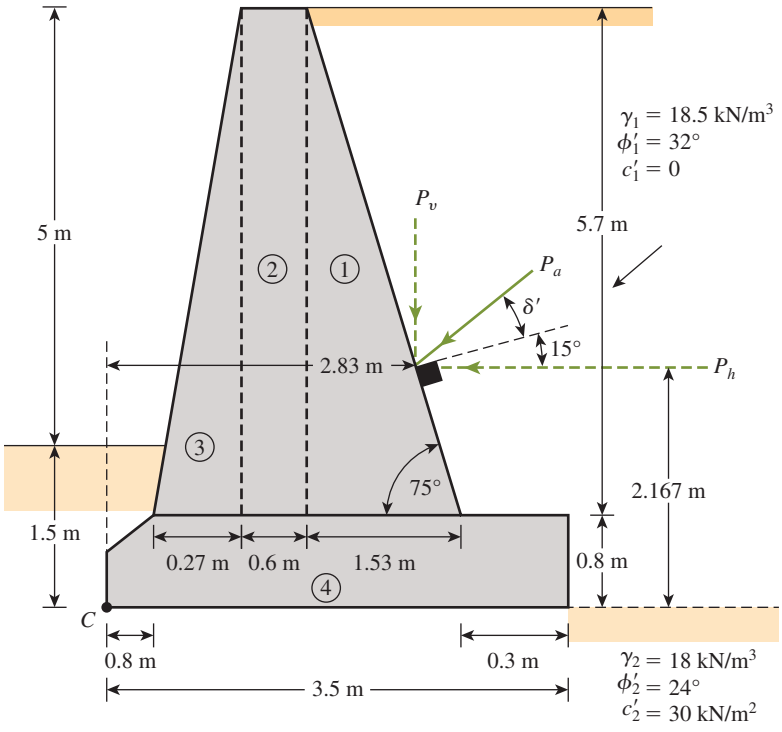


FIGURE 17.13 Gravity retaining wall (not to scale)

With $\alpha = 0°$, $\beta = 75°$, $\delta' = 2/3\phi_1'$, and $\phi_1' = 32°$, $K_a = 0.4023$. (See Table 16.6.) So,

$$P_a = \tfrac{1}{2}(18.5)(6.5)^2(0.4023) = 157.22 \text{ kN/m}$$

$$P_h = P_a \cos(15 + \tfrac{2}{3}\phi_1') = 157.22 \cos 36.33 = 126.65 \text{ kN/m}$$

and

$$P_v = P_a \sin(15 + \tfrac{2}{3}\phi_1') = 157.22 \sin 36.33 = 93.14 \text{ kN/m}$$

Part a: Factor of Safety Against Overturning

From Figure 17.13, we can prepare the following table:

Area no.	Area (m^2)	Weight* (kN/m)	Moment arm from C (m)	Moment (kN · m/m)
1	$\frac{1}{2}(5.7)(1.53) = 4.36$	102.81	2.18	224.13
2	$(0.6)(5.7) = 3.42$	80.64	1.37	110.48
3	$\frac{1}{2}(0.27)(5.7) = 0.77$	18.16	0.98	17.80
4	$\approx (3.5)(0.8) = 2.8$	66.02	1.75	115.54
		$P_v = 93.14$	2.83	263.59
		$\Sigma V = 360.77$ kN/m		$\Sigma M_R = 731.54$ kN · m/m

*$\gamma_{\text{concrete}} = 23.58 \text{ kN/m}^3$

Note that the weight of the soil above the backface of the wall is not taken into account in the preceding table. We have

$$\text{Overturning moment} = M_o = P_h\left(\frac{H'}{3}\right) = 126.65(2.167) = 274.45 \text{ kN} \cdot \text{m/m}$$

Hence,

$$\text{FS}_{(\text{overturning})} = \frac{\Sigma M_R}{\Sigma M_o} = \frac{731.54}{274.45} = \mathbf{2.67 > 2, OK}$$

Part b: Factor of Safety Against Sliding

We have

$$\text{FS}_{(\text{sliding})} = \frac{(\Sigma V)\tan\left(\frac{2}{3}\phi_2'\right) + \frac{2}{3}c_2'B + P_p}{P_h}$$

$$P_p = \tfrac{1}{2}K_p\gamma_2 D^2 + 2c_2'\sqrt{K_p}D$$

and

$$K_p = \tan^2\left(45 + \frac{24}{2}\right) = 2.37$$

Hence,

$$P_p = \tfrac{1}{2}(2.37)(18)(1.5)^2 + 2(30)(1.54)(1.5) = 186.59 \text{ kN/m}$$

So

$$\text{FS}_{(\text{sliding})} = \frac{360.77\tan\left(\frac{2}{3} \times 24\right) + \frac{2}{3}(30)(3.5) + 186.59}{126.65}$$

$$= \frac{103.45 + 70 + 186.59}{126.65} = \mathbf{2.84}$$

If P_p is ignored, the factor of safety is **1.37**.

Part c: Pressure on Soil at Toe and Heel

From Eqs. (17.15) and (17.16),

$$e = \frac{B}{2} - \frac{\Sigma M_R - \Sigma M_o}{\Sigma V} = \frac{3.5}{2} - \frac{731.54 - 274.45}{360.77} = 0.483 < \frac{B}{6} = 0.583$$

$$q_{\text{toe}} = \frac{\Sigma V}{B}\left[1 + \frac{6e}{B}\right] = \frac{360.77}{3.5}\left[1 + \frac{(6)(0.483)}{3.5}\right] = \mathbf{188.43\ kN/m^2}$$

and

$$q_{\text{heel}} = \frac{V}{B}\left[1 - \frac{6e}{B}\right] = \frac{360.77}{3.5}\left[1 - \frac{(6)(0.483)}{3.5}\right] = \mathbf{17.73\ kN/m^2}$$

EXAMPLE 17.3

Refer to the gravity wall described in Example 17.2 and redo the problem using Rankine active pressure.

SOLUTION

The retaining wall is redrawn in Figure 17.14. From the figure, $H' = 5 + 1.5 = 6.5$ m.

$$K_a = \tan^2\left(45 - \frac{\phi_1'}{2}\right) = \tan^2\left(45 - \frac{32}{2}\right) = 0.307$$

$$P_a = \frac{1}{2}\gamma H'^2 K_a = \frac{1}{2}(18.5)(6.5)^2(0.307) = 119.98\ \text{kN/m} \approx 120\ \text{kN/m}$$

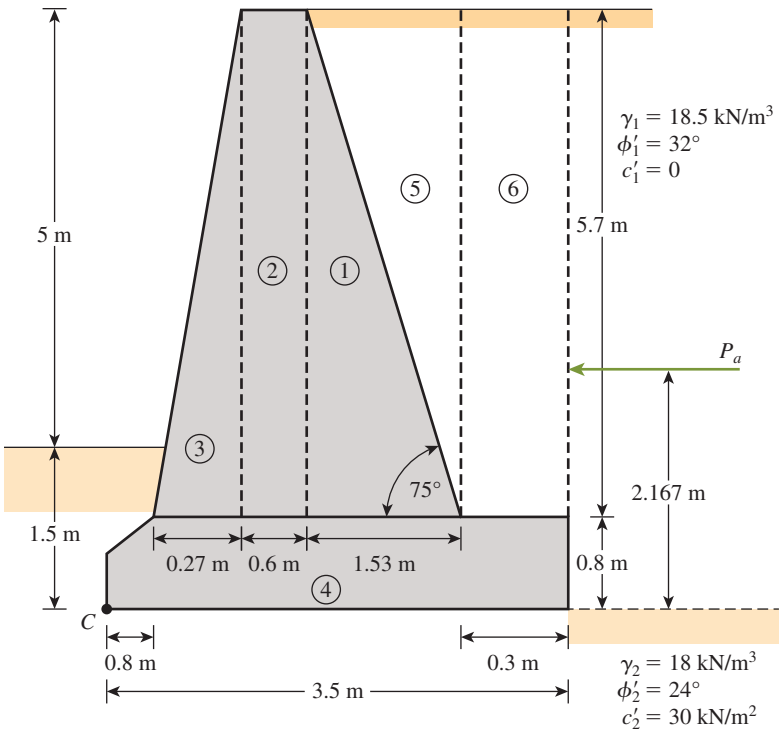


FIGURE 17.14

Part a: Factor of Safety Against Overturning

The following table can now be prepared.

Section no.	Area (m^2)	Weight per unit length (kN/m)	Moment arm from C (m)	Moment about C (kN · m/m)
*1	4.36	102.81	2.18	224.13
*2	3.42	80.64	1.37	110.48
*3	0.77	18.16	0.98	17.80
*4	2.8	66.02	1.75	115.54
5	(0.5)(1.53)(5.7) = 4.36	80.66	2.69	216.98
6	(5.7)(0.3) = 1.71	31.44	3.35	105.99
		$\Sigma V = 379.93$		$\Sigma M_R = 790.92$

*From Example 17.2

Overturning moment, $M_o = P_a\left(\frac{H'}{3}\right) = (120)(2.167) \approx 260.0$ kN · m/m.

$$\text{FS}_{(\text{overturning})} = \frac{\Sigma M_R}{\Sigma M_o} = \frac{790.92}{260.0} = \mathbf{3.04}$$

Part b: Factor of Safety Against Sliding

$$\text{FS}_{(\text{sliding})} = \frac{(\Sigma V)\tan\left(\frac{2}{3}\phi'_2\right) + \frac{2}{3}c'_2 + P_p}{P_h}$$

From Example 17.2, $P_p = 186.59$ kN/m

$$\text{FS}_{(\text{sliding})} = \frac{(379.93)(\tan 16) + \left(\frac{2}{3}\right)(30)(3.5) + 186.59}{120} = \mathbf{3.05}$$

Part c: Pressure on Soil at Toe and Heel

$$e = \frac{B}{2} - \frac{\Sigma M_R - \Sigma M_o}{\Sigma V} = \frac{3.5}{2} - \frac{(790.92 - 260.0)}{379.93} = 1.75 - 1.397 = 0.353 \text{ m}$$

$$q_{\text{toe}} = \frac{\Sigma V}{B}\left(1 + \frac{6e}{B}\right) = \frac{379.93}{3.5}\left(1 + \frac{6 \times 0.353}{3.5}\right) = \mathbf{174.24\ kN/m^2}$$

$$q_{\text{toe}} = \frac{\Sigma V}{B}\left(1 - \frac{6e}{B}\right) = \frac{379.93}{3.5}\left(1 - \frac{6 \times 0.353}{3.5}\right) = \mathbf{42.86\ kN/m^2}$$

17.8 Construction Joints and Drainage from Backfill

CONSTRUCTION JOINTS

A retaining wall may be constructed with one or more of the following joints:

1. *Construction joints* (see Figure 17.15a) are vertical and horizontal joints that

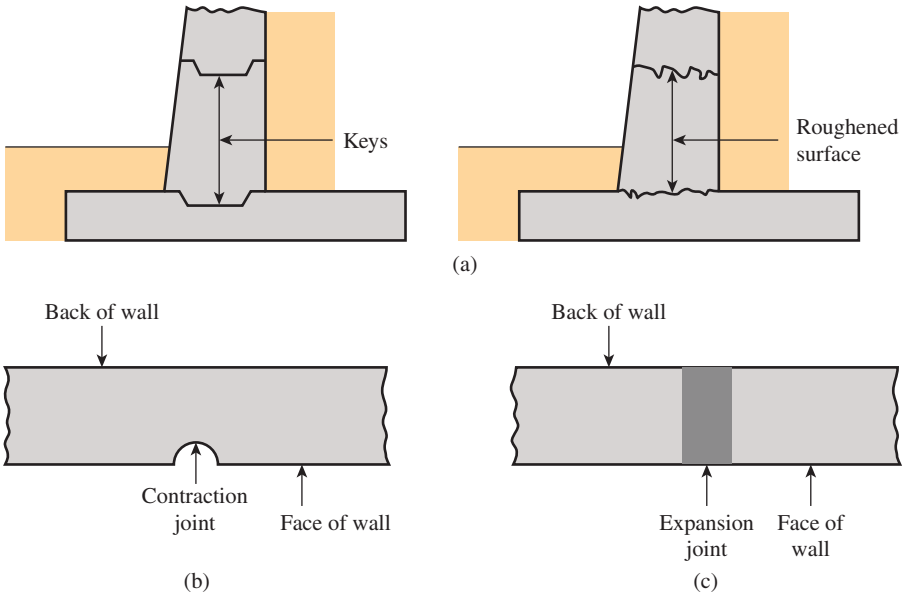


FIGURE 17.15 (a) Construction joints; (b) contraction joint; (c) expansion joint

resistance at the joints, keys may be used. If keys are not used, the surface of the first pour is cleaned and roughened before the next pour of concrete.

2. *Contraction joints* (Figure 17.15b) are vertical joints (grooves) placed in the face of a wall (from the top of the base slab to the top of the wall) that allow the concrete to shrink without noticeable harm. The grooves may be about 6 to 8 mm (≈0.25 to 0.3 in.) wide and 12 to 16 mm (≈0.5 to 0.6 in.) deep.
3. *Expansion joints* (Figure 17.15c) allow for the expansion of concrete caused by temperature changes; vertical expansion joints from the base to the top of the wall may also be used. These joints may be filled with flexible joint fillers. In most cases, horizontal reinforcing steel bars running across the stem are continuous through all joints. The steel is greased to allow the concrete to expand.

DRAINAGE FROM THE BACKFILL

As the result of rainfall or other wet conditions, the backfill material for a retaining wall may become saturated, thereby increasing the pressure on the wall and perhaps creating an unstable condition. For this reason, adequate drainage must be provided by means of *weep holes* or *perforated drainage pipes*. (See Figure 17.16.)

When provided, weep holes should have a minimum diameter of about 0.1 m (4 in.) and be adequately spaced. Note that there is always a possibility that backfill material may be washed into weep holes or drainage pipes and ultimately clog them. Thus, a filter material needs to be placed behind the weep holes or around the drainage pipes, as the case may be; geotextiles now serve that purpose.

When selecting the material for a granular filter, two contradicting criteria have to be satisfied. In the first one, known as the *retention criterion*, the filter material should be fine enough to prevent migration of fines from the soil into the filter. In the second one, known as the *permeability criterion*, the filter should be coarse enough compared to the soil being protected to act as a sink and avoid build-up of excess pore water pressure. To satisfy these two conditions, Terzaghi and Peck (1967) suggested ensuring the following conditions.

Retention criterion:

$$D_{15(F)} < 5D_{85(B)} \tag{17.22}$$

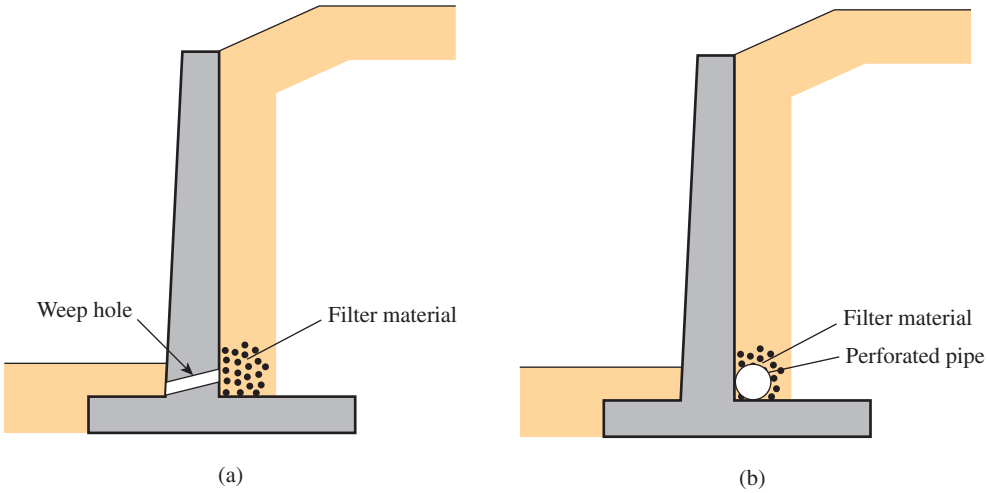


FIGURE 17.16 Drainage provisions for the backfill of a retaining wall: (a) by weep holes; (b) by a perforated drainage pipe

Permeability criterion:

$$D_{15(F)} > 4D_{15(B)} \tag{17.23}$$

In addition, the grain-size distributions of the filter and the base materials should have the same shape (i.e., approximately parallel).

In these relations, the subscripts F and B refer to the *filter* and the *base* material (i.e., the backfill soil), respectively. Also, D_{15} and D_{85} refer to the diameters through which 15% and 85% of the soil (filter or base, as the case may be) will pass. Here $D_{15(F)}$ is the average pore size of the filter material. Example 17.4 gives the procedure for designing a filter.

U.S. Navy (1982) suggests two additional conditions for the retention criterion: The

$$D_{50(F)} < 25D_{50(B)} \tag{17.24}$$

$$D_{15(F)} < 20D_{15(B)} \tag{17.25}$$

EXAMPLE 17.4

Figure 17.17 shows the grain-size distribution of a backfill material. Using the conditions outlined in Section 17.8, determine the range of the grain-size distribution for the filter material.

SOLUTION

From the grain-size distribution curve given in the figure, the following values can be determined:

$$D_{15(B)} = 0.04 \text{ mm}$$

$$D_{85(B)} = 0.25 \text{ mm}$$

$$D_{50(B)} = 0.13 \text{ mm}$$

Conditions of Filter

1. $D_{15(F)}$ should be less than $5D_{85(B)}$; that is, $5 \times 0.25 = 1.25$ mm.
2. $D_{15(F)}$ should be greater than $4D_{15(B)}$; that is, $4 \times 0.04 = 0.16$ mm.
3. $D_{50(F)}$ should be less than $25D_{50(B)}$; that is, $25 \times 0.13 = 3.25$ mm.
4. $D_{15(F)}$ should be less than $20D_{15(B)}$; that is, $20 \times 0.04 = 0.8$ mm.

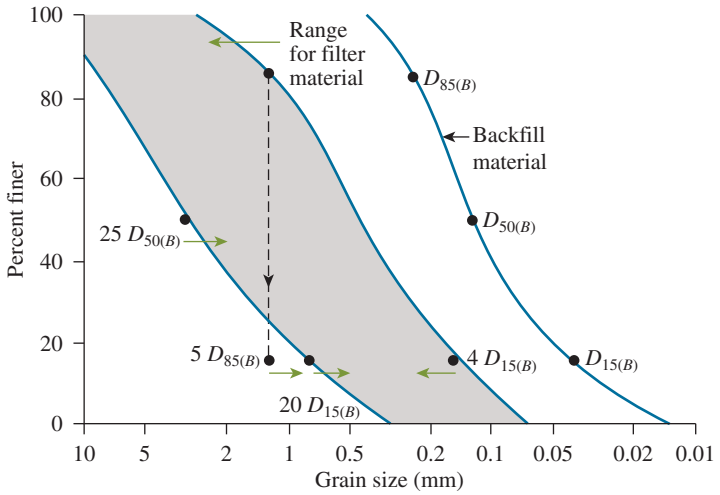


FIGURE 17.17 Determination of grain-size distribution of filter material

These limiting points are plotted in Figure 17.17. Through them, two curves can be drawn that are similar in nature to the grain-size distribution curve of the backfill material. These curves define the range of the filter material to be used.

17.9 Comments on Design of Retaining Walls and a Case Study

In Section 17.3, it was suggested that the *active earth pressure coefficient* be used to estimate the lateral force on a retaining wall due to the backfill. It is important to recognize the fact that the active state of the backfill can be established only if the wall yields sufficiently, which does not happen in all cases. The degree to which the wall yields depends on its *height* and the *section modulus*. Furthermore, the lateral force of the backfill depends on several factors identified by Casagrande (1973):

1. Effect of temperature
2. Groundwater fluctuation
3. Readjustment of the soil particles due to creep and prolonged rainfall
4. Tidal changes
5. Heavy wave action
6. Traffic vibration
7. Earthquakes

Insufficient wall yielding combined with other unforeseen factors may generate a larger lateral force on the retaining structure compared with that obtained from the active earth pressure theory. This is particularly true in the case of gravity retaining walls, bridge abutments, and other heavy structures that have a large section modulus.

An example to illustrate this case is shown in Figure 17.18, which is for a bridge abutment in Germany as reported by Casagrande (1973). The bridge abutment had a slag backfill that gave an angle of friction (ϕ') between 37° and 45°, depending on the degree of compaction. For purposes of comparison, the variation of the Rankine active earth pressure with $\phi' = 37°$ and 45° is shown in Figure 17.18, along with the measured variation of horizontal effective pressure with depth. This comparison indicates that:

a. The actual lateral earth pressure distribution may not be triangular.
b. The actual active force is greater than the minimum theoretical active force calculated by using Rankine theory.

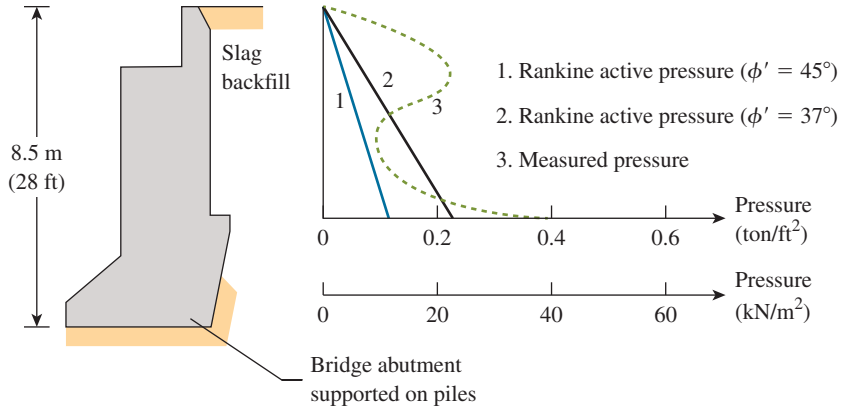


FIGURE 17.18 Pressure distribution behind a bridge abutment in Germany (Based on Casagrande, 1973)

CASE STUDY FOR THE PERFORMANCE OF A CANTILEVER RETAINING WALL

Bentler and Labuz (2006) have reported the performance of a cantilever retaining wall built along Interstate 494 in Bloomington, Minnesota. The retaining wall had 83 panels, each having a length of 9.3 m (30.5 ft). The panel height ranged from 4.0 m to 7.9 m (13 ft to 26 ft). One of the 7.9 m high (26 ft) panels was instrumented with earth pressure cells, tiltmeters, strain gauges, and inclinometer casings. Figure 17.19 shows a schematic diagram (cross section) of the wall panel. Some details on the backfill and the foundation material are:

- Granular Backfill
  Effective size, $D_{10} = 0.13$ mm
  Uniformity coefficient, $C_u = 3.23$
  Coefficient of gradation, $C_c = 1.4$
  Unified soil classification: SP
  Compacted unit weight, $\gamma_1 = 18.9$ kN/m^3 (120 lb/ft^3)
  Triaxial friction angle, ϕ_1': 35° to 39° (average 37°)
- Foundation Material
  Poorly graded sand and sand with gravel (medium dense to dense)

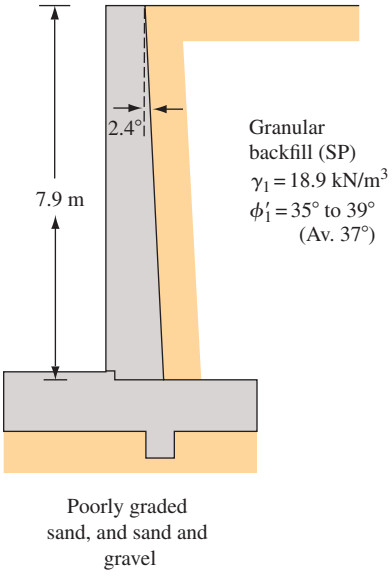


FIGURE 17.19 Schematic diagram of the retaining wall (drawn to scale)

The backfill and compaction of the granular material started on October 28, 2001 in stages and reached a height of 7.6 m (25 ft) on November 21, 2001. The final 0.3 m (1 ft) of soil was placed the following spring. During backfilling, the wall was continuously going through translation. Table 17.3 is a summary of the backfill height and horizontal translation of the wall.

TABLE 17.3 Horizontal Translation with Backfill Height

Day	Backfill height (m)	Horizontal translation (mm)
1	0.0	0
2	1.1	0
2	2.8	0
3	5.2	2
4	6.1	4
5	6.4	6
11	6.7	9
24	7.3	12
54	7.6	11

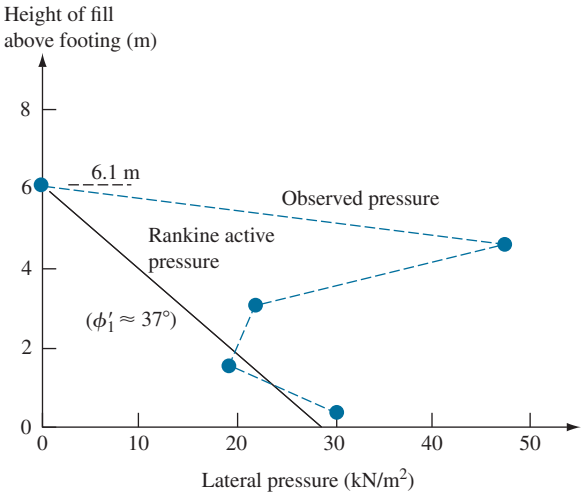


FIGURE 17.20 Observed lateral pressure distribution after fill height reached 6.1 m (Based on Bentler and Labuz, 2006)

Figure 17.20 shows a typical plot of the variation of lateral earth pressure *after compaction* on day 4, σ_a', when the backfill height was 6.1 m (October 31, 2001) along with the plot of Rankine active earth pressure ($\phi_1' = 37°$). Note that the measured lateral (horizontal) pressure is higher at most heights than that predicted by the Rankine active pressure theory, which may be due to residual lateral stresses caused by compaction. The measured lateral stress gradually reduced with time. This is demonstrated in Figure 17.21, which shows a plot of the variation of σ_a' with depth (November 27, 2001) when the height of the backfill was 7.6 m. The lateral pressure was lower at practically all depths compared to the Rankine active earth pressure.

Another point of interest is the nature of variation of q_{max} and q_{min} (see Figure 17.11). As shown in Figure 17.11, if the wall rotates about C, q_{max} will be at the toe and q_{min} will be at the heel. However, for the case of the retaining wall under consideration (undergoing horizontal translation), q_{max} was at the heel of the wall with q_{min} at the toe. On November 27, 2001, when the height of the fill was 7.6 m

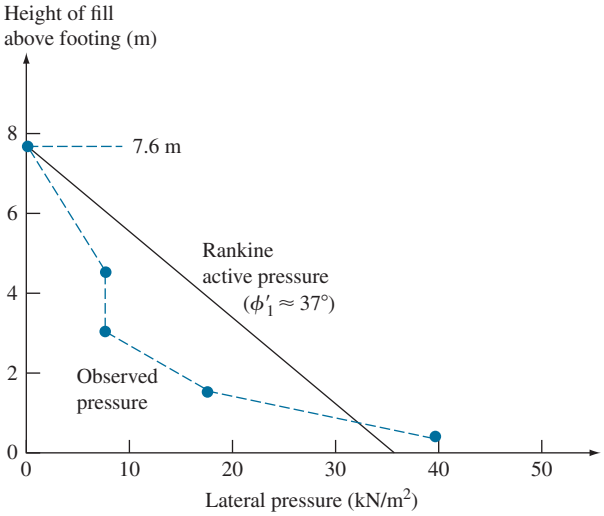


FIGURE 17.21 Observed pressure distribution on November 27, 2001 (Based on Bentler and Labuz, 2006)

(25 ft), q_{max} at the heel was about 140 kN/m^2 (2922 lb/ft^2), which was approximately equal to (γ_1)(height of fill) = (18.9)(7.6) = 143.6 kN/m^2. Also, at the toe, q_{min} was about 40 kN/m^2 (835 lb/ft^2), which suggests that the moment from lateral force had little effect on the vertical effective stress below the heel.

The lessons learned from this case study are the following:

a. Retaining walls may undergo lateral translation which will affect the variation of q_{max} and q_{min} along the base slab.
b. Initial lateral stress caused by compaction gradually decreases with time and lateral movement of the wall.

17.10 Gravity Retaining-Wall Design for Earthquake Conditions

Even in mild earthquakes, most retaining walls undergo limited lateral displacement. Richards and Elms (1979) proposed a procedure for designing gravity retaining walls for earthquake conditions that allows limited lateral displacement. This procedure takes into consideration the wall inertia effect. Figure 17.22 shows a retaining wall with various forces acting on it, which are as follows (per unit length of the wall):

a. W_w = weight of the wall
b. P_{ae} = active force with earthquake condition taken into consideration (Section 16.9)

The backfill of the wall and the soil on which the wall is resting are assumed cohesionless. Considering the equilibrium of the wall, it can be shown that

$$W_w = \left[\tfrac{1}{2}\gamma_1 H^2(1 - k_v)K_{ae}\right]C_{IE} \tag{17.26}$$

where γ_1 = unit weight of the backfill,

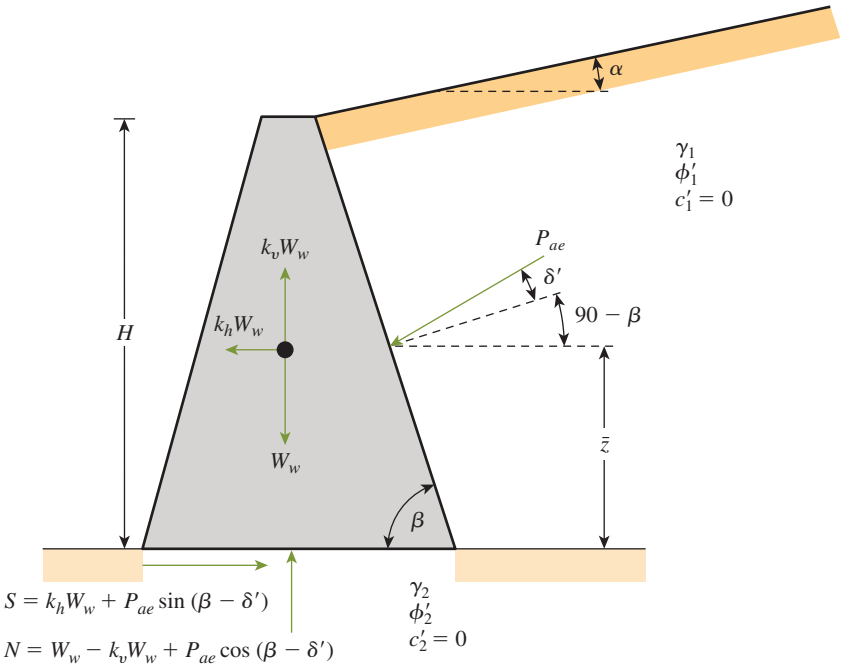


FIGURE 17.22 Stability of a retaining wall under earthquake forces

$$C_{IE} = \frac{\sin(\beta - \delta') - \cos(\beta - \delta')\tan \phi'_2}{(1 - k_v)(\tan \phi'_2 - \tan \theta')} \tag{17.27}$$

and $\theta' = \tan^{-1}\left(\frac{k_h}{1 - k_v}\right)$.

Based on Eqs. (17.26) and (17.27), the following procedure may be used to determine the weight of the retaining wall, W_w, for tolerable displacement that may take place during an earthquake.

1. Determine the tolerable displacement of the wall, Δ.
2. Obtain a design value of k_h from

$$k_h = A_a\left(\frac{0.2A_v^2}{A_a\Delta}\right)^{0.25} \tag{17.28}$$

   In Eq. (17.28), A_a and A_v are effective acceleration coefficients and Δ is displacement in inches. The magnitudes of A_a and A_v are given by the Applied Technology Council (1978) for various regions of the United States.
3. Assume that $k_v = 0$, and, with the value of k_h obtained, calculate K_{ae} from Eq. (16.51).
4. Use the value of K_{ae} determined in Step 3 to obtain the weight of the wall (W_w).
5. Apply a factor of safety to the value of W_w obtained in Step 4 [from Eq. (17.26)].

EXAMPLE 17.5

Refer to Figure 17.23. For $k_v = 0$ and $k_h = 0.3$, determine:

a. Weight of the wall for static condition
b. Weight of the wall for zero displacement during an earthquake
c. Weight of the wall for lateral displacement of 1.5 in. (≈38 mm) during an earthquake

For Part c, assume that $A_a = 0.2$ and $A_v = 0.2$. For Parts a, b, and c, use a factor of safety of 1.5.

SOLUTION

Part a

For static conditions, $\theta' = 0$ and Eq. (17.27) becomes

$$C_{IE} = \frac{\sin(\beta - \delta') - \cos(\beta - \delta')\tan \phi'_2}{\tan \phi'_2}$$

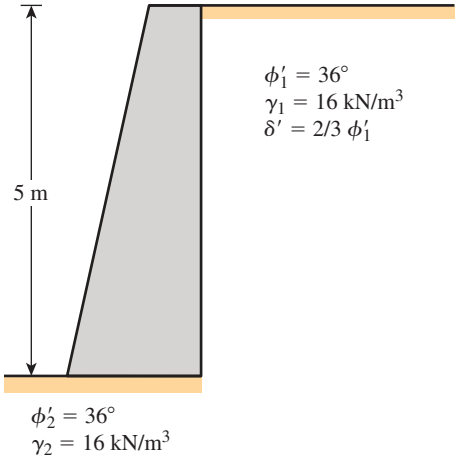


FIGURE 17.23

For $\beta = 90°$, $\delta' = 24°$ and $\phi_2' = 36°$,

$$C_{IE} = \frac{\sin(90 - 24) - \cos(90 - 24)\tan 36}{\tan 36} = 0.85$$

For static conditions, $K_{ae} = K_a$, so

$$W_w = \tfrac{1}{2}\gamma H^2 K_a C_{IE}$$

For $K_a \approx 0.2349$ [Table 16.6],

$$W_w = \tfrac{1}{2}(16)(5)^2(0.2349)(0.85) = 39.9 \text{ kN/m}$$

With a factor of safety of 1.5,

$$W_w = (39.9)(1.5) = \mathbf{59.9\ kN/m}$$

Part b

For zero displacement, $k_v = 0$,

$$C_{IE} = \frac{\sin(\beta - \delta') - \cos(\beta - \delta')\tan \phi_2'}{\tan \phi_2' - \tan \theta'}$$

$$\tan \theta' = \frac{k_h}{1 - k_v} = \frac{0.3}{1 - 0} = 0.3$$

$$C_{IE} = \frac{\sin(90 - 24) - \cos(90 - 24)\tan 36}{\tan 36 - 0.3} = 1.45$$

For $k_h = 0.3$, $\phi_1' = 36°$, and $\delta' = 2\phi_1'/3$, the value of $K_{ae} \approx 0.48$ (Table 16.8).

$$W_w = \tfrac{1}{2}\gamma_1 H^2(1 - k_v)K_{ae}C_{IE} = \tfrac{1}{2}(16)(5)^2(1 - 0)(0.48)(1.45) = 139.2 \text{ kN/m}$$

With a factor of safety of 1.5, $W_w = \mathbf{208.8\ kN/m.}$

Part c

For a lateral displacement of 1.5 in. (38 mm),

$$k_h = A_a\left(\frac{0.2A_v^2}{A_a\Delta}\right)^{0.25} = (0.2)\left[\frac{(0.2)(0.2)^2}{(0.2)(1.5)}\right]^{0.25} = 0.081$$

$$\tan \theta' = \frac{k_h}{1 - k_v} = \frac{0.081}{1 - 0} = 0.081$$

$$C_{IE} = \frac{\sin(90 - 24) - \cos(90 - 24)\tan 36}{\tan 36 - 0.081} = 0.957$$

$$W_w = \tfrac{1}{2}\gamma_1 H^2 K_{ae} C_{IE}$$

$K_{ae} \approx 0.29$ (Table 16.8)

$$W_w = \tfrac{1}{2}(16)(5)^2(0.29)(0.957) = 55.5 \text{ kN/m}$$

With a factor of safety of 1.5, $W_w = \mathbf{83.3\ kN/m.}$

Mechanically Stabilized Retaining Walls

Since the 1970s, soil reinforcement has been used in the construction and design of foundations, retaining walls, embankment slopes, and other structures. Depending on the type of construction, the reinforcements may be galvanized metal strips, geotextiles, geogrids, or geocomposites. Sections 17.11 and 17.12 provide a general overview of soil reinforcement and various reinforcement materials.

Reinforcement materials such as metallic strips, geotextiles, and geogrids are now being used to reinforce the backfill of retaining walls, which are generally

referred to as *mechanically stabilized retaining walls*. The general principles for designing these walls are given in the following sections.

17.11 Soil Reinforcement

The use of reinforced earth is a recent development in the design and construction of foundations and earth-retaining structures. *Reinforced earth* is a construction material made from soil that has been strengthened by tensile elements such as metal rods or strips, nonbiodegradable fabrics (geotextiles), geogrids, and the like. The fundamental idea of reinforcing soil is not new; in fact, it goes back several centuries. However, the present concept of systematic analysis and design was developed by a French engineer, H. Vidal (1966). The French Road Research Laboratory has done extensive research on the applicability and the beneficial effects of the use of reinforced earth as a construction material. This research has been documented in detail by Darbin (1970), Schlosser and Long (1974), and Schlosser and Vidal (1969). The tests that were conducted involved the use of metallic strips as reinforcing material.

Retaining walls with reinforced earth have been constructed around the world since Vidal began his work. The first reinforced-earth retaining wall with metal strips as reinforcement in the United States was constructed in 1972 in southern California.

The beneficial effects of soil reinforcement derive from (a) the soil's increased tensile strength and (b) the shear resistance developed from the friction at the soil-reinforcement interfaces. Such reinforcement is comparable to that of concrete structures. Currently, most reinforced-earth design is done with *free-draining granular soil only*. Thus, the effect of pore water development in cohesive soil, which, in turn, reduces the shear strength of the soil, is avoided.

17.12 Considerations in Soil Reinforcement

METAL STRIPS

In most instances, galvanized steel strips are used as reinforcement in soil. However, galvanized steel is subject to corrosion. The rate of corrosion depends on several environmental factors. Binquet and Lee (1975) suggested that the average rate of corrosion of galvanized steel strips varies between 0.025 and 0.050 mm/yr. So, in the actual design of reinforcement, allowance must be made for the rate of corrosion. Thus,

$$t_c = t_{\text{design}} + r\,(\text{life span of structure})$$

where

t_c = actual thickness of reinforcing strips to be used in construction

t_{design} = thickness of strips determined from design calculations

r = rate of corrosion

NONBIODEGRADABLE FABRICS

Nonbiodegradable fabrics are generally referred to as *geotextiles*. Since 1970, the use of geotextiles in construction has increased greatly around the world. The fabrics are usually made from petroleum products—polyester, polyethylene, and polypropylene. They may also be made from fiberglass. Geotextiles are not prepared from natural fabrics because they decay too quickly. Geotextiles may be woven, knitted, or nonwoven.

Woven geotextiles (Figure 17.24) are made of two sets of parallel filaments or strands of yarn systematically interlaced to form a planar structure. *Knitted*

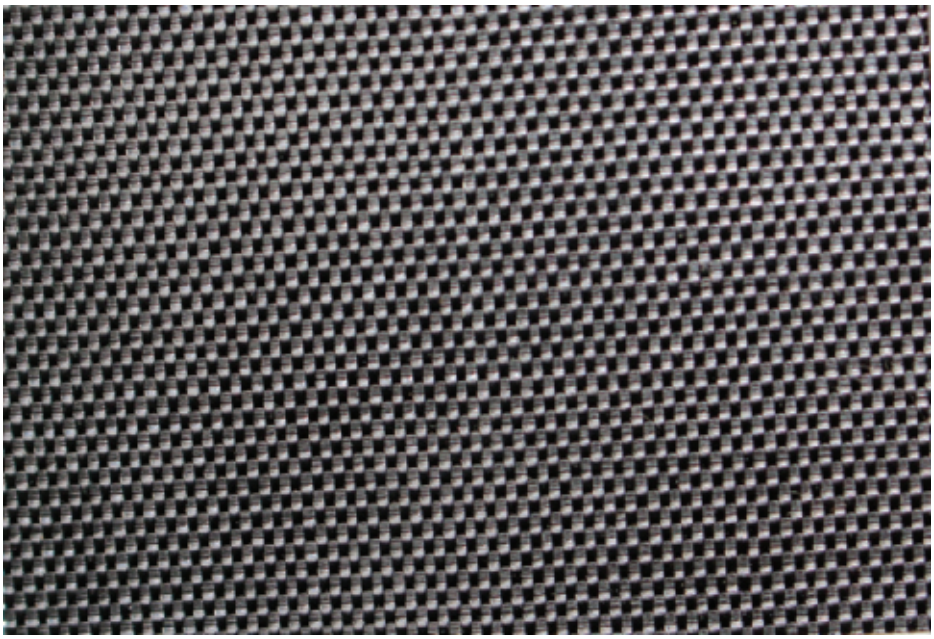


FIGURE 17.24 Woven geotextile (Courtesy of Reinaldo Vega-Meyer, San Antonio, Texas)

geotextiles are formed by interlocking a series of loops of one or more filaments or strands of yarn to form a planar structure. *Nonwoven geotextiles* (Figure 17.25) are formed from filaments or short fibers arranged in an oriented or random pattern in a planar structure. These filaments or short fibers are arranged into a loose web in the beginning and then are bonded by one or a combination of the following processes:

1. *Chemical bonding*—by glue, rubber, latex, a cellulose derivative, or the like
2. *Thermal bonding*—by heat for partial melting of filaments
3. *Mechanical bonding*—by needle punching



FIGURE 17.25 Nonwoven geotextile (Courtesy of Reinaldo Vega-Meyer, San Antonio, Texas)

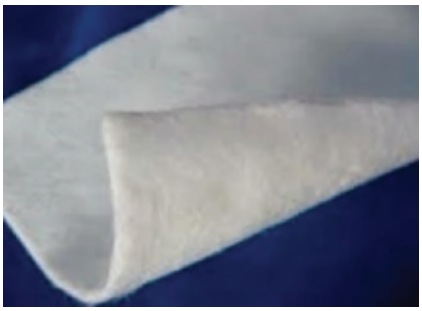


FIGURE 17.26 Nonwoven needle-punched geotextile (Courtesy of Reinaldo Vega-Meyer, San Antonio, Texas)

Needle-punched nonwoven (Figure 17.26) geotextiles are thick and have high in-plane permeability.

Geotextiles have four primary uses in foundation engineering:

1. *Drainage:* The fabrics can rapidly channel water from soil to various outlets, thereby providing a higher soil shear strength and hence stability.
2. *Filtration:* When placed between two soil layers, one coarse grained and the other fine grained, the fabric allows free seepage of water from one layer to the other. However, it protects the fine-grained soil from being washed into the coarse-grained soil.
3. *Separation:* Geotextiles help keep various soil layers separate after construction and during the projected service period of the structure. For example, in the construction of highways, a clayey subgrade can be kept separate from a granular base course.
4. *Reinforcement:* The tensile strength of geotextiles increases the load-bearing capacity of the soil.

The tensile strength depends on several parameters, such as manufacturing type, mass per unit area, thickness, and type of test. Table 17.4 gives the experimental results of some laboratory tests reported by Koerner (2005) that will provide a sense of the range of parameters encountered in various geotextiles. Table 17.5 gives some typical values of the tensile properties of geotextiles.

GEOGRIDS

Geogrids are high-modulus polymer materials, such as polypropylene and polyethylene, and are prepared by tensile drawing. Netlon, Ltd., of the United Kingdom was the first producer of geogrids. In 1982, the Tensar Corporation, presently Tensar International Corporation, introduced geogrids into the United States.

TABLE 17.4 Tensile Strength and Strain at Failure for Some Geotextiles [Interpolated Values from the Results of Koerner (2005)]

Manufacturing type	Mass/unit area (g/m^2)	Thickness (mm)	Tensile strength (kN/m)	Strain at failure (%)
Woven monofilament	200	0.38	37.7	21.9
Woven slit-film	170	0.25	28.2	26.3
Woven multi-filament	270	0.71	60.0	30.0
Nonwoven heat-bonded	135	0.33	24.1	68.8
Nonwoven needle-punched	200	0.63	27.3	72.5

TABLE 17.5 Typical Values of Tensile Properties of Some Geotextiles [Based on Shukla (2015)]

Type of geotextile	Tensile strength (kN/m)	Extension at maximum load (%)	Mass per unit area (g/cm^2)
Nonwoven			
Heat-bonded	3–30	20–60	60–360
Needle-punched	7–90	30–80	100–3000
Resin-bonded	5–30	25–50	125–800
Woven			
Monofilament	20–80	20–35	150–300
Multifilament	40–1200	10–30	250–1500
Flat tape	10–90	15–25	90–250

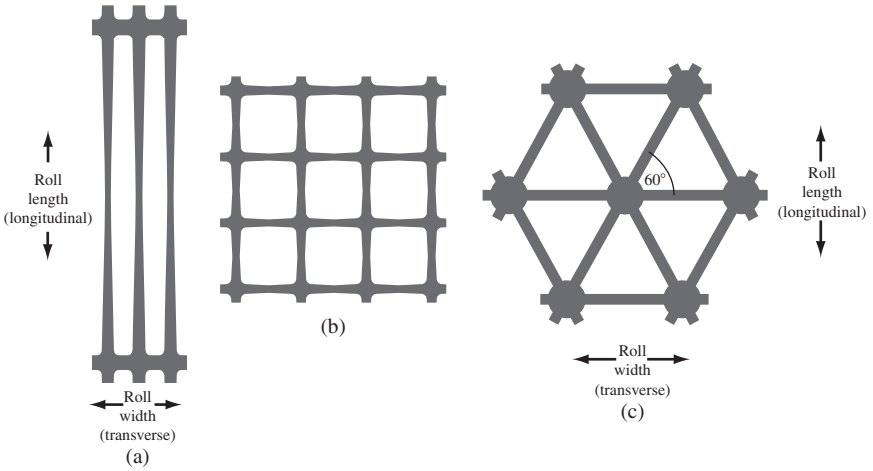


FIGURE 17.27 Extruded geogrid: (a) uniaxial; (b) biaxial; (c) with triangular apertures (Based on of Tensar International Corporation)

Geogrids generally are of two types: (a) uniaxial and (b) biaxial. Figures 17.27a and b show these two types of geogrids, which are produced by Tensar International Corporation.

Commercially available geogrids may be categorized by manufacturing process, principally: extruded, woven, and welded. Extruded geogrids are formed using a thick sheet of polyethylene or polypropylene that is punched and drawn to create apertures and to enhance engineering properties of the resulting ribs and nodes. Woven geogrids are manufactured by grouping polymeric strips—usually polyester and polypropylene—and weaving them into a mesh pattern that is then coated with a polymeric lacquer. Welded geogrids (Figure 17.28) are manufactured by fusing junctions of polymeric strips. Extruded geogrids have shown good performance when compared to other types for pavement reinforcement applications.

The commercial geogrids currently available for soil reinforcement have nominal rib thicknesses of about 0.5 to 1.5 mm (0.02 to 0.06 in.) and junctions of about 2.5 to 5 mm (0.1 to 0.2 in.). The grids used for soil reinforcement usually have openings

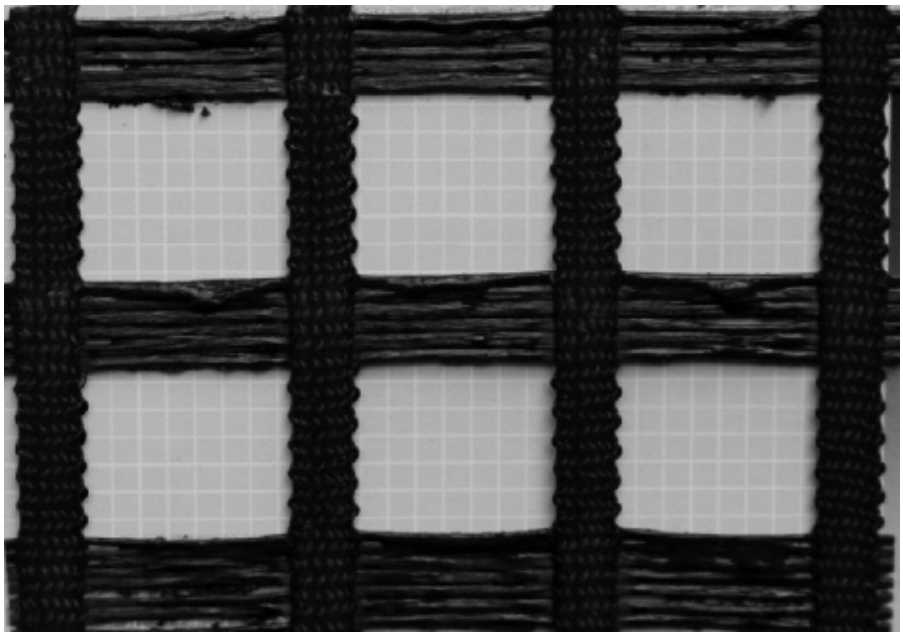


FIGURE 17.28 Thermowelded geogrid (Courtesy of Reinaldo Vega-Meyer, San Antonio, Texas)

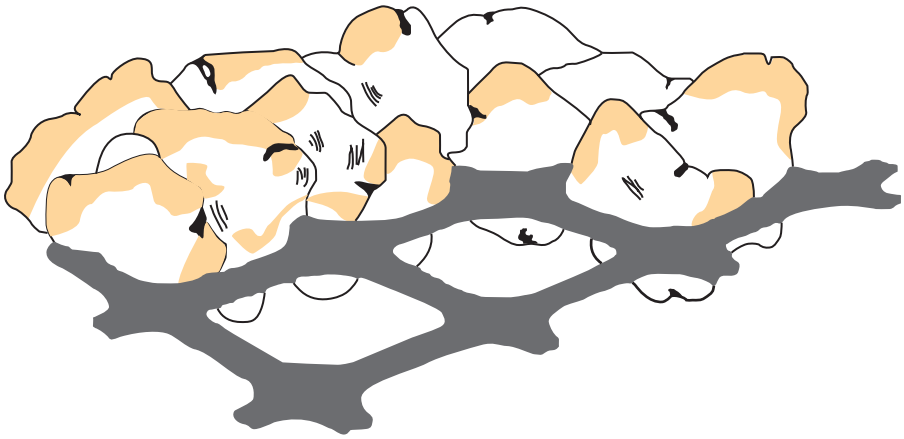


FIGURE 17.29 Geogrid apertures allowing interlocking with surrounding soil

or apertures that are rectangular or elliptical. The dimensions of the apertures vary from about 25 to 150 mm (1 to 6 in.). Geogrids are manufactured so that the open areas of the grids are greater than 50% of the total area. They develop reinforcing strength at low strain levels, such as 2% (Carroll, 1988).

The major function of geogrids is *reinforcement*. They are relatively stiff. The apertures are large enough to allow interlocking with surrounding soil or rock (Figure 17.29) to perform the function of reinforcement or segregation (or both). Sarsby (1985) investigated the influence of aperture size on the size of soil particles for maximum frictional efficiency (or efficiency against pullout). According to this study, the highest efficiency occurs when

$$B_{GG} > 3.5D_{50} \tag{17.29}$$

where

B_{GG} = minimum width of the geogrid aperture

D_{50} = the particle size through which 50% of the backfill soil passes (i.e., the average particle size)

More recently, extruded geogrids with triangular apertures (Figure 17.27c) have been introduced for construction purposes. Geogrids with triangular apertures are manufactured from a punched polypropylene sheet, which is then oriented in three substantially equilateral directions so that the resulting ribs shall have a high degree of molecular orientation.

17.13 General Design Considerations

The general design procedure of any mechanically stabilized retaining wall can be divided into two parts:

1. Satisfying *internal stability* requirements
2. Checking the *external stability* of the wall

The internal stability checks involve determining tension and pullout resistance in the reinforcing elements and ascertaining the integrity of facing elements. The external stability checks include checks for overturning, sliding, and bearing capacity failure (Figure 17.30). The sections that follow will discuss the retaining-wall design procedures for use with metallic strips, geotextiles, and geogrids.

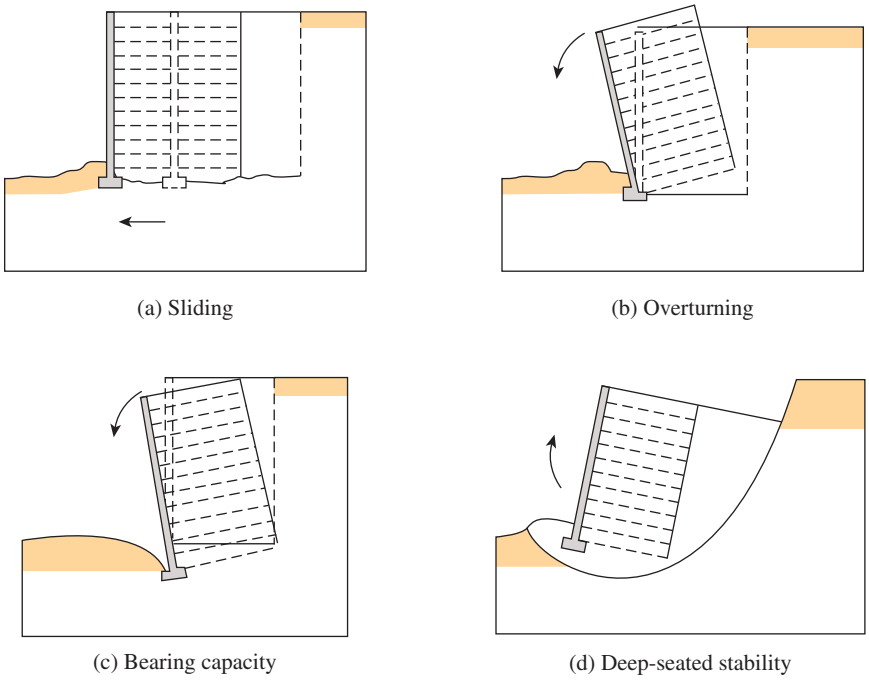


FIGURE 17.30 External stability checks (Based on Transportation Research Board, 1995) (From *Transportation Research Circular 444: Mechanically Stabilized Earth Walls*. Transportation Research Board, National Research Council, Washington, D.C., 1995.)

17.14 Retaining Walls with Metallic Strip Reinforcement

Reinforced-earth walls are flexible walls. Their main components are

1. *Backfill*, which is granular soil
2. *Reinforcing strips*, which are thin wide strips placed at regular intervals, and
3. *A cover* or *skin*, on the front face of the wall

Figure 17.31 is a diagram of a reinforced-earth retaining wall. Note that at any depth, the reinforcing strips or ties are placed with a horizontal spacing of S_H center

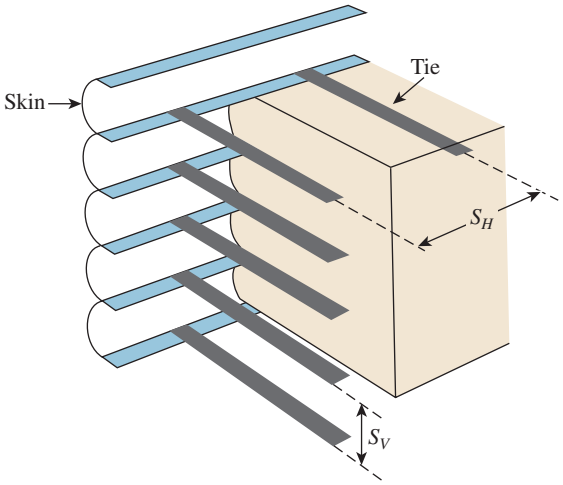


FIGURE 17.31 Reinforced-earth retaining wall

to center; the vertical spacing of the strips or ties is S_V center to center. The skin can be constructed with sections of relatively flexible thin material. Lee et al. (1973) showed that with a conservative design, a 5 mm thick (≈0.2 in.) galvanized steel skin would be enough to hold a wall about 14 to 15 m (45 to 50 ft) high. In most cases, precast concrete slabs also can be used as skin. The slabs are grooved to fit into each other so that soil cannot flow out between the joints. When metal skins are used, they are bolted together, and reinforcing strips are placed between the skins.

Figures 17.32 and 17.33 show a reinforced-earth retaining wall under construction; its skin (facing) is a precast concrete slab. Figure 17.34 shows a metallic reinforcement tie attached to the concrete slab.

The simplest and most common method for the design of ties is the *Rankine method*. We discuss this procedure next.

CALCULATION OF ACTIVE HORIZONTAL AND VERTICAL PRESSURE

Figure 17.35 shows a retaining wall with a granular backfill having a unit weight of γ_1 and a friction angle of ϕ_1'. Below the base of the retaining wall, the *in situ* soil has been excavated and recompacted, with granular soil used as backfill. Below the backfill, the *in situ* soil has a unit weight of γ_2, friction angle of ϕ_2', and cohesion of c_2'. A surcharge having an intensity of q per unit area lies atop the retaining wall, which has reinforcement ties at depths $z = 0, S_V, 2S_V, \ldots, NS_V$. The height of the wall is $NS_V = H$.



FIGURE 17.32 Reinforced-earth retaining wall (with metallic strip) under construction (Courtesy of Braja M. Das, Henderson, Nevada)



FIGURE 17.33 Another view of the retaining wall shown in Figure 17.32 (Courtesy of Braja M. Das, Henderson, Nevada)

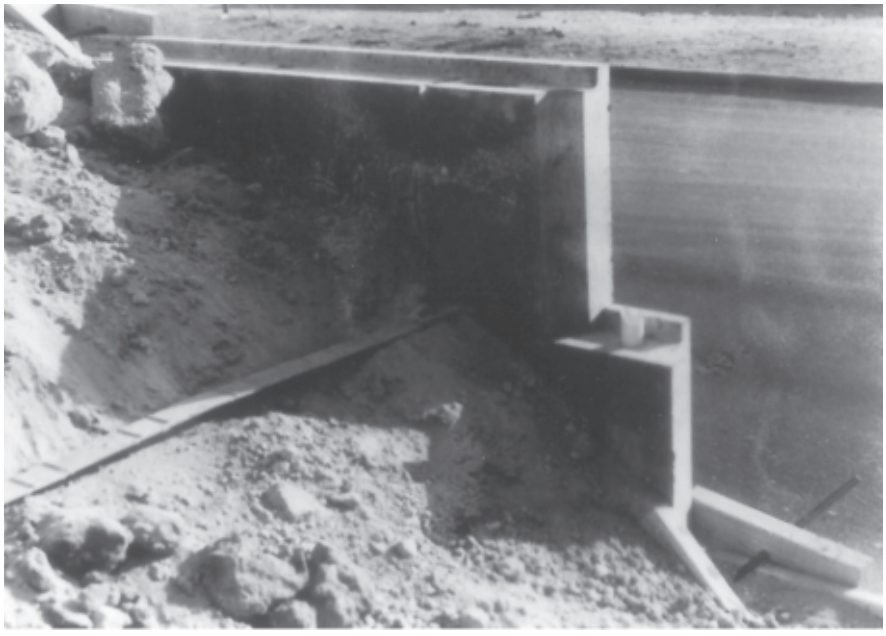


FIGURE 17.34 Metallic strip attachment to the precast concrete slab used as the skin (Courtesy of Braja M. Das, Henderson, Nevada)

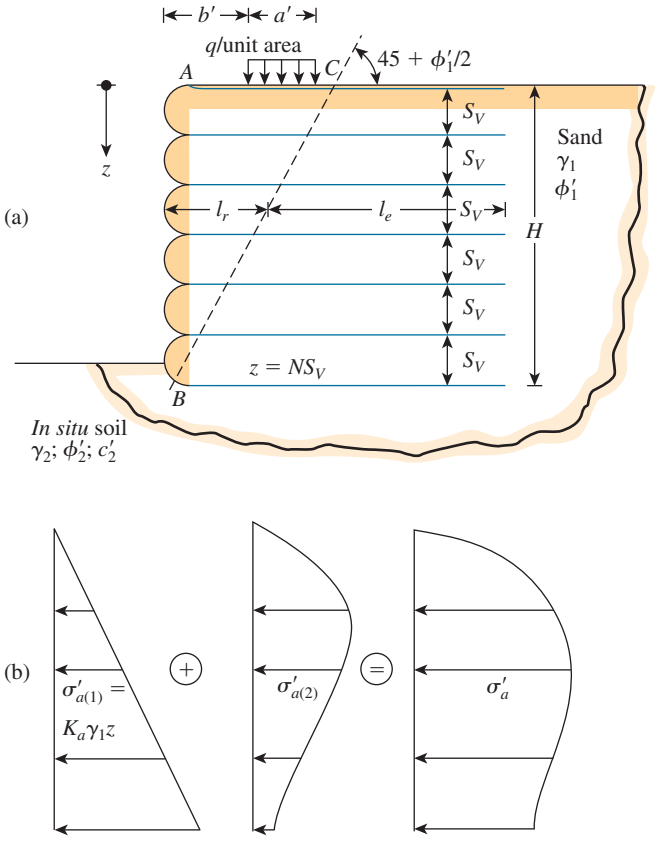


FIGURE 17.35 Analysis of a reinforced-earth retaining wall

According to the Rankine active pressure theory (Section 16.3),

$$\sigma'_a = \sigma'_o K_a - 2c'\sqrt{K_a}$$

where σ'_a is the Rankine active pressure at any depth z.

For dry granular soil with no surcharge at the top, $c' = 0$, $\sigma'_o = \gamma_1 z$, and $K_a = \tan^2(45 - \phi'_1/2)$. Thus,

$$\sigma'_{a(1)} = \gamma_1 z K_a \tag{17.30}$$

When a surcharge is added at the top, as shown in Figure 17.35,

$$\underset{\text{Due to soil only}}{\sigma'_o = \sigma'_{o(1)}} \quad \underset{\text{Due to the surcharge}}{+ \sigma'_{o(2)}}$$
$$= \gamma_1 z \tag{17.31}$$

The magnitude of $\sigma'_{o(2)}$ can be calculated by using the 2:1 method of stress distribution described in Eq. (8.15) and Figure 8.9. The 2:1 method of stress distribution is shown in Figure 17.36a. According to Laba and Kennedy (1986),

$$\sigma'_{o(2)} = \frac{qa'}{a' + z} \qquad (\text{for } z \le 2b') \tag{17.32}$$

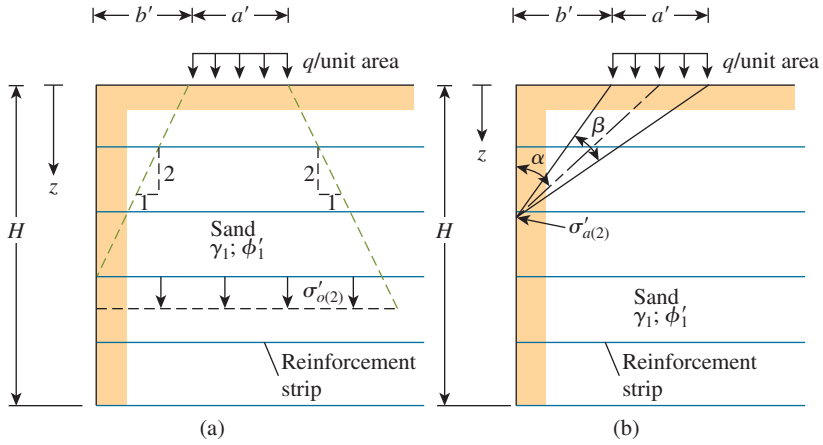


FIGURE 17.36 (a) Notation for the relationship of $\sigma'_{o(2)}$ in Eqs. (17.32) and (17.33); (b) notation for the relationship of $\sigma'_{a(2)}$ in Eqs. (17.35) and (17.36)

and

$$\sigma'_{o(2)} = \frac{qa'}{a' + \frac{z}{2} + b'} \qquad (\text{for } z > 2b') \tag{17.33}$$

Also, when a surcharge is added at the top, the lateral pressure at any depth is

$$\begin{aligned} \sigma'_a &= \sigma'_{a(1)} + \sigma'_{a(2)} \\ &\quad\uparrow \qquad\quad \uparrow \\ &= K_a \gamma_1 z \quad \text{Due to the} \\ &\quad \text{Due to} \quad \text{surcharge} \\ &\quad \text{soil only} \end{aligned} \tag{17.34}$$

According to Laba and Kennedy (1986), $\sigma'_{a(2)}$ may be expressed (see Figure 17.36b) as

$$\sigma'_{a(2)} = M\left[\frac{2q}{\pi}(\beta - \sin\beta \cos 2\alpha)\right] \tag{17.35}$$
$$\uparrow$$
$$(\text{in radians})$$

where

$$M = 1.4 - \frac{0.4b'}{0.14H} \geq 1 \tag{17.36}$$

The net active (lateral) pressure distribution on the retaining wall calculated by using Eqs. (17.34), (17.35), and (17.36) is shown in Figure 17.35b.

TIE FORCE

The tie force *per unit length of the wall* developed at any depth z (see Figure 17.35) is

$$\begin{aligned} T &= \text{active earth pressure at depth } z \\ &\quad \times \text{ area of the wall to be supported by the tie} \\ &= (\sigma'_a)(S_V S_H) \end{aligned} \tag{17.37}$$

FACTOR OF SAFETY AGAINST TIE FAILURE

The reinforcement ties at each level, and thus the walls, could fail by either (a) tie breaking or (b) tie pullout.

The factor of safety against *tie breaking* may be determined as

$$\text{FS}_{(B)} = \frac{\text{yield or breaking strength of each tie}}{\text{maximum force in any tie}} = \frac{wtf_y}{\sigma'_a S_V S_H} \tag{17.38}$$

where

w = width of each tie

t = thickness of each tie

f_y = yield or breaking strength of the tie material

A factor of safety of about 2.5 to 3 is generally recommended for ties at all levels.

Reinforcing ties at any depth z will fail by pullout if the frictional resistance developed along the surfaces of the ties is less than the force to which the ties are being subjected. The *effective length* of the ties along which frictional resistance is developed may be conservatively taken as the length that extends *beyond the limits of the Rankine active failure zone*, which is the zone *ABC* in Figure 17.35. Line *BC* makes an angle of $45 + \phi'_1/2$ with the horizontal. Now, the maximum friction force that can be realized for a tie at depth z is

$$F_R = 2l_e w\sigma'_o \tan\phi'_\mu \tag{17.39}$$

where

l_e = effective length

σ'_o = effective vertical pressure at a depth z

ϕ'_μ = soil–tie friction angle

Thus, the factor of safety against *tie pullout* at any depth z is

$$\text{FS}_{(P)} = \frac{F_R}{T} \tag{17.40}$$

Substituting Eqs. (17.37) and (17.39) into Eq. (17.40) yields

$$\text{FS}_{(P)} = \frac{2l_e w\sigma'_o \tan\phi'_\mu}{\sigma'_a S_V S_H} \tag{17.41}$$

TOTAL LENGTH OF TIE

The total length of ties at any depth is

$$L = l_r + l_e \tag{17.42}$$

where

l_r = length within the Rankine failure zone

l_e = effective length

For a given $\text{FS}_{(P)}$ from Eq. (17.41),

$$l_e = \frac{\text{FS}_{(P)}\sigma'_a S_V S_H}{2w\sigma'_o \tan\phi'_\mu} \tag{17.43}$$

Again, at any depth z,

$$l_r = \frac{(H - z)}{\tan\left(45 + \frac{\phi_1'}{2}\right)} \tag{17.44}$$

So, combining Eqs. (17.42), (17.43), and (17.44) gives

$$L = \frac{(H - z)}{\tan\left(45 + \frac{\phi_1'}{2}\right)} + \frac{\text{FS}_{(P)}\sigma_a' S_V S_H}{2w\sigma_o' \tan\phi_\mu'} \tag{17.45}$$

17.15 Step-by-Step-Design Procedure Using Metallic Strip Reinforcement

Following is a step-by-step procedure for the design of reinforced-earth retaining walls.

GENERAL

Step 1. Determine the height of the wall, H, and the properties of the granular backfill material, such as the unit weight (γ_1) and the angle of friction (ϕ_1').

Step 2. Obtain the soil–tie friction angle, ϕ_μ', and the required value of $\text{FS}_{(B)}$ and $\text{FS}_{(P)}$.

INTERNAL STABILITY

Step 3. Assume values for horizontal and vertical tie spacing, S_V and S_H. Also, assume the width of reinforcing strip, w, to be used.

Step 4. Calculate σ_a' from Eqs. (17.34), (17.35), and (17.36).

Step 5. Calculate the tie forces at various levels from Eqs. (17.34) and (17.37).

Step 6. For the known values of $\text{FS}_{(B)}$, calculate the thickness of ties, t, required to resist the tie breakout:

$$T = \sigma_a' S_V S_H = \frac{wtf_y}{\text{FS}_{(B)}}$$

or

$$t = \frac{(\sigma_a' S_V S_H)[\text{FS}_{(B)}]}{wf_y} \tag{17.46}$$

The conventional practice is to keep the magnitude of t the same at all levels (i.e., using the same strip), so σ_a' in Eq. (17.46) should equal $\sigma_{a(\max)}'$.

Step 7. For the known values of ϕ_μ' and $\text{FS}_{(P)}$, determine the length L of the ties at various levels from Eq. (17.45).

Step 8. The magnitudes of S_V, S_H, t, w, and L may be changed to obtain the most economical design.

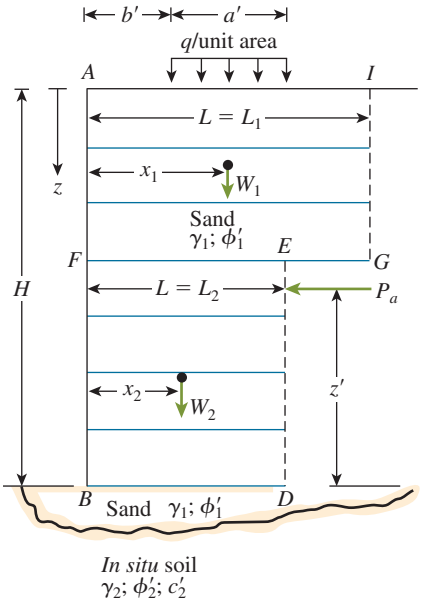


FIGURE 17.37 Stability check for the retaining wall

EXTERNAL STABILITY

Step 9. Check for *overturning*, using Figure 17.37 as a guide. Taking the moment about B yields the overturning moment for the unit length of the wall:

$$M_o = P_a z' \tag{17.47}$$

Here,

$$P_a = \text{active force} = \int_0^H \sigma'_a \, dz$$

The resisting moment per unit length of the wall is

$$M_R = W_1 x_1 + W_2 x_2 + \cdots + qa'\left(b' + \frac{a'}{2}\right) \tag{17.48}$$

where

$W_1 = (\text{area } AFEGI)(1)(\gamma_1)$

$W_2 = (\text{area } FBDE)(1)(\gamma_1)$

$\vdots$

So,

$$\text{FS}_{(\text{overturning})} = \frac{M_R}{M_o} = \frac{W_1 x_1 + W_2 x_2 + \cdots + qa'\left(b' + \frac{a'}{2}\right)}{\left(\int_0^H \sigma'_a \, dz\right) z'} \tag{17.49}$$

Step 10. The check for *sliding* can be done by using Eq. (17.11), or

$$\text{FS}_{(\text{sliding})} = \frac{(W_1 + W_2 + \cdots + qa')[\tan(k\phi'_1)]}{P_a} \tag{17.50}$$

where $k \approx \frac{2}{3}$.

Step 11. Check for ultimate bearing capacity failure, which can be given as

$$q_u = c'_2 N_c + \tfrac{1}{2}\gamma_2 L_2 N_\gamma \tag{17.51}$$

The bearing capacity factors N_c and N_γ correspond to the soil friction angle ϕ'_2. (See Table 6.2.) From Eq. 17.31, the vertical stress at $z = H$ is

$$\sigma'_{o(H)} = \gamma_1 H + \sigma'_{o(2)} \tag{17.52}$$

So the factor of safety against bearing capacity failure is

$$\text{FS}_{(\text{bearing capacity})} = \frac{q_{\text{ult}}}{\sigma'_{o(H)}} \tag{17.53}$$

Generally, minimum values of $\text{FS}_{(\text{overturning})} = 3$, $\text{FS}_{(\text{sliding})} = 3$, and $\text{FS}_{(\text{bearing capacity failure})} = 3$ to 5 are recommended.

EXAMPLE 17.5

A 10 m high retaining wall with galvanized steel strip reinforcement in a granular backfill has to be constructed. Referring to Figure 17.35, given:

Granular backfill: $\phi_1' = 36°$

$\gamma_1 = 16.5 \text{ kN/m}^3$

Foundation soil: $\phi_2' = 28°$

$\gamma_2 = 17.3 \text{ kN/m}^3$

$c_2' = 50 \text{ kN/m}^2$

Galvanized steel reinforcement:

Width of strip, $w = 75$ mm

$S_V = 0.6$ m center-to-center

$S_H = 1$ m center-to-center

$f_y = 240{,}000 \text{ kN/m}^2$

$\phi_\mu' = 20°$

Required $\text{FS}_{(B)} = 3$

Required $\text{FS}_{(P)} = 3$

Check for the external and internal stability. Assume the corrosion rate of the galvanized steel to be 0.025 mm/year and the life span of the structure to be 50 years.

SOLUTION

Internal Stability Check

Tie thickness: Maximum tie force, $T_{\max} = \sigma'_{a(\max)} S_V S_H$

$$\sigma_{a(\max)} = \gamma_1 H K_a = \gamma_1 H \tan^2\left(45 - \frac{\phi_1'}{2}\right)$$

so

$$T_{\max} = \gamma_1 H \tan^2\left(45 - \frac{\phi_1'}{2}\right) S_V S_H$$

From Eq. (17.46), for *tie break*,

$$t = \frac{(\sigma_a' S_V S_H)[\text{FS}_{(B)}]}{w f_y} = \frac{\left[\gamma_1 H \tan^2\left(45 - \frac{\phi_1'}{2}\right) S_V S_H\right] \text{FS}_{(B)}}{w f_y}$$

or

$$t = \frac{\left[(16.5)(10) \tan^2\left(45 - \frac{36}{2}\right)(0.6)(1)\right](3)}{(0.075 \text{ m})(240{,}000 \text{ kN/m}^2)} = 0.00428 \text{ m} = 4.28 \text{ mm}$$

If the rate of corrosion is 0.025 mm/yr and the life span of the structure is 50 yr, then the actual thickness, t, of the ties will be

$$t = 4.28 + (0.025)(50) = 5.53 \text{ mm}$$

So a **tie thickness of 6 mm** would be enough.

Tie length: Refer to Eq. (17.45). For this case, $\sigma'_a = \gamma_1 z K_a$ and $\sigma'_o = \gamma_1 z$, so

$$L = \frac{(H - z)}{\tan\left(45 + \frac{\phi'_1}{2}\right)} + \frac{\text{FS}_{(P)}\gamma_1 z K_a S_V S_H}{2w\gamma_1 z \tan\phi'_\mu}$$

Now the following table can be prepared. (*Note:* $\text{FS}_{(P)} = 3$, $H = 10$ m, $w = 75$ mm, and $\phi'_\mu = 20°$.)

z (m)	Tie length L (m) [Eq. (17.45)]
2	12.65
4	11.63
6	10.61
8	9.59
10	8.57

So use a **tie length of $L = 13$ m.**

External Stability Check

Check for overturning: Refer to Figure 17.38. For this case, using Eq. (17.49),

$$\text{FS}_{(\text{overturning})} = \frac{W_1 x_1}{\left[\int_0^H \sigma'_a\, dz\right] z'}$$

$$W_1 = \gamma_1 HL = (16.5)(10)(13) = 2145 \text{ kN/m}$$

$$x_1 = 6.5 \text{ m}$$

$$P_a = \int_0^H \sigma'_a\, dz = \tfrac{1}{2}\gamma_1 K_a H^2 = (\tfrac{1}{2})(16.5)(0.26)(10)^2 = 214.5 \text{ kN/m}$$

$$z' = \frac{10}{3} = 3.33 \text{ m}$$

$$\text{FS}_{(\text{overturning})} = \frac{(2145)(6.5)}{(214.5)(3.33)} = \mathbf{19.52 > 3—OK}$$

Check for sliding: From Eq. (17.50)

$$\text{FS}_{(\text{sliding})} = \frac{W_1 \tan(k\phi'_1)}{P_a} = \frac{2145 \tan\left[\left(\frac{2}{3}\right)(36)\right]}{214.5} = \mathbf{4.45 > 3—OK}$$

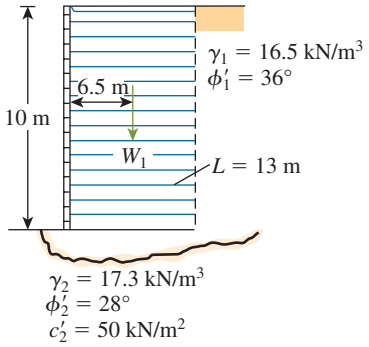


FIGURE 17.38 Retaining wall with galvanized steel strip reinforcement in the backfill

Check for bearing capacity: For $\phi_2' = 28°$, $N_c = 25.8$, $N_\gamma = 16.78$ (Table 6.2). From Eq. (17.51),

$$q_{ult} = c_2' N_c + \tfrac{1}{2}\gamma_2 L N_\gamma$$

$$q_{ult} = (50)(25.8) + (\tfrac{1}{2})(17.3)(13)(16.72) = 3170.16 \text{ kN/m}^2$$

From Eq. (17.52),

$$\sigma'_{o(H)} = \gamma_1 H = (16.5)(10) = 165 \text{ kN/m}^2$$

$$\text{FS}_{(\text{bearing capacity})} = \frac{q_{ult}}{\sigma'_{o(H)}} = \frac{3170.16}{165} = \mathbf{19.2 > 5—OK}$$

17.16 Retaining Walls with Geotextile Reinforcement

Figure 17.39 shows a retaining wall in which layers of geotextile have been used as reinforcement. As in Figure 17.37, the backfill is a granular soil. In this type of retaining wall, the facing of the wall is formed by lapping the sheets as shown with a lap length of l_l. When construction is finished, the exposed face of the wall must be covered; otherwise, the geotextile will deteriorate from exposure to ultraviolet light. *Bitumen emulsion* or *Gunite* is sprayed on the wall face. A wire mesh anchored to the geotextile facing may be necessary to keep the coating on. Figure 17.40 shows the construction of a geotextile-reinforced retaining wall. Figure 17.41 shows a completed geosynthetic-reinforced soil wall. The wall is in DeBeque Canyon, Colorado. Note the versatility of the facing type. In this case, single-tier concrete block facing is integrated with a three-tier facing via rock facing.

The design of geotextile-reinforced retaining walls is similar to that presented in Section 17.15. Following is a step-by-step procedure for design based on the recommendations of Bell et al. (1975) and Koerner (2005):

INTERNAL STABILITY

Step 1. Determine the active pressure distribution on the wall from the formula

$$\sigma'_a = K_a \sigma'_o = K_a \gamma_1 z \tag{17.54}$$

where

K_a = Rankine active pressure coefficient = $\tan^2(45 - \phi_1'/2)$

γ_1 = unit weight of the granular backfill

ϕ_1' = friction angle of the granular backfill

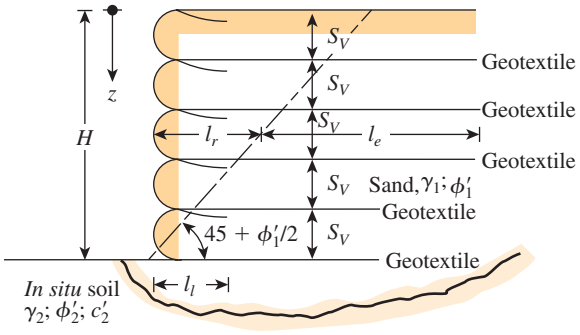


FIGURE 17.39 Retaining wall with geotextile reinforcement



FIGURE 17.40 Construction of a geotextile-reinforced retaining wall (Courtesy of Jonathan T. H. Wu, University of Colorado at Denver, Denver, Colorado)

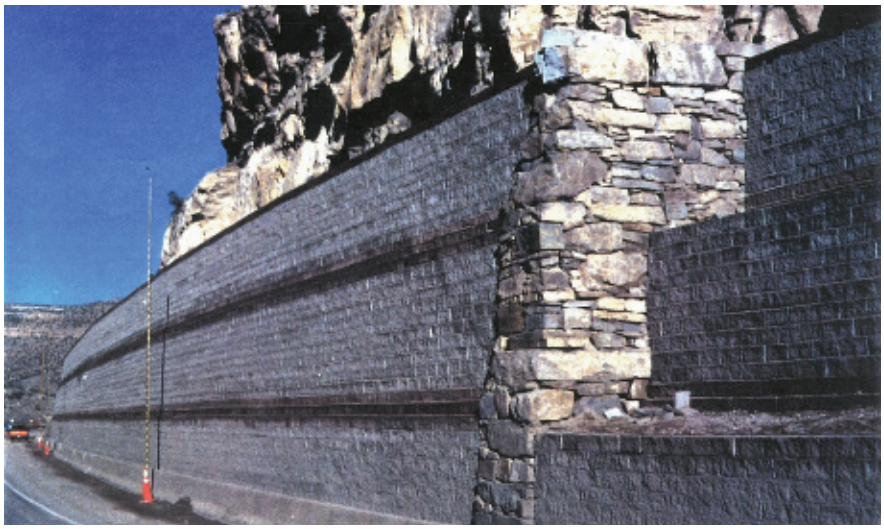


FIGURE 17.41 A completed geotextile-reinforced retaining wall in DeBeque Canyon, Colorado (Courtesy of Jonathan T. H. Wu, University of Colorado at Denver, Denver, Colorado)

Step 2. Select a geotextile fabric with an allowable tensile strength, T_{all} (lb/ft or kN/m

The allowable tensile strength for retaining wall construction may be expressed as (Koerner, 2005)

$$T_{all} = \frac{T_{ult}}{RF_{id} \times RF_{cr} \times RF_{cbd}} \tag{17.55}$$

where

T_{ult} = ultimate tensile strength

RF_{id} = reduction factor for installation damage

RF_{cr} = reduction factor for creep

RF_{cbd} = reduction factor for chemical and biological degradation

The recommended values of the reduction factor are as follows (Koerner, 2005):

RF_{id}	1.1–2.0
RF_{cr}	2–4
RF_{cbd}	1–1.5

Step 3. Determine the vertical spacing of the layers at any depth z from the formula

$$S_V = \frac{T_{all}}{\sigma'_a FS_{(B)}} = \frac{T_{all}}{(\gamma_1 z K_a)[FS_{(B)}]} \tag{17.56}$$

Note that Eq. (17.56) is similar to Eq. (17.38). The magnitude of $FS_{(B)}$ is generally 1.3 to 1.5.

Step 4. Determine the length of each layer of geotextile from the formula

$$L = l_r + l_e \tag{17.57}$$

where

$$l_r = \frac{H - z}{\tan\left(45 + \frac{\phi'_1}{2}\right)} \tag{17.58}$$

and

$$l_e = \frac{S_V \sigma'_a [FS_{(P)}]}{2\sigma'_o \tan \phi'_F} \tag{17.59}$$

in which

$$\sigma'_a = \gamma_1 z K_a$$

$$\sigma'_o = \gamma_1 z$$

$$FS_{(P)} = 1.3 \text{ to } 1.5$$

ϕ'_F = friction angle at geotextile–soil interface

$\approx \frac{2}{3}\phi'_1$

Note that Eqs. (17.57), (17.58), and (17.59) are similar to Eqs. (17.42), (17.44), and (17.43), respectively.

Based on the published results, the assumption of $\phi'_F/\phi'_1 \approx \frac{2}{3}$ is reasonable and appears to be conservative. Martin et al. (1984) presented the following laboratory test results for ϕ'_F/ϕ'_1 between various types of geotextiles and sand.

Type	ϕ'_F/ϕ'_1
Woven—monofilament/concrete sand	0.87
Woven—silt film/concrete sand	0.8
Woven—silt film/rounded sand	0.86
Woven—silt film/silty sand	0.92
Nonwoven—melt-bonded/concrete sand	0.87
Nonwoven—needle-punched/concrete sand	1.0
Nonwoven—needle-punched/rounded sand	0.93
Nonwoven—needle-punched/silty sand	0.91

Step 5. Determine the lap length, l_l (see Figure 17.39), from

$$l_l = \frac{S_V \sigma'_a \text{FS}_{(P)}}{4\sigma'_o \tan \phi'_F} \tag{17.60}$$

The minimum lap length should be 1 m (3 ft).

EXTERNAL STABILITY

Step 6. Check the factors of safety against overturning, sliding, and bearing capacity failure as described in Section 17.15 (Steps 9, 10, and 11).

EXAMPLE 17.6

A geotextile-reinforced retaining wall 5 m high is shown in Figure 17.42. For the granular backfill, $\gamma_1 = 15.7$ kN/m^3 and $\phi'_1 = 36°$. For the geotextile, $T_{\text{ult}} = 52.5$ kN/m. For the design of the wall, determine S_V, L, and l_l. Use $\text{RF}_{\text{id}} = 1.2$, $\text{RF}_{\text{cr}} = 2.5$, and $\text{RF}_{\text{cbd}} = 1.25$.

SOLUTION

We have

$$K_a = \tan^2\left(45 - \frac{\phi'_1}{2}\right) = 0.26$$

Determination of S_v

To find S_V, we make a few trials. From Eq. (17.56),

$$S_V = \frac{T_{\text{all}}}{(\gamma_1 z K_a)[\text{FS}_{(B)}]}$$

From Eq. (17.55),

$$T_{\text{all}} = \frac{T_{\text{uef}}}{\text{RF}_{\text{id}} \times \text{RF}_{\text{cr}} \times \text{RF}_{\text{cbd}}} = \frac{52.5}{1.2 \times 2.5 \times 1.25} = 14 \text{ kN/m}$$

With $\text{FS}_{(B)} = 1.5$ at $z = 2$ m,

$$S_V = \frac{14}{(15.7)\,(2)\,(0.26)\,(1.5)} = 1.14 \text{ m}$$

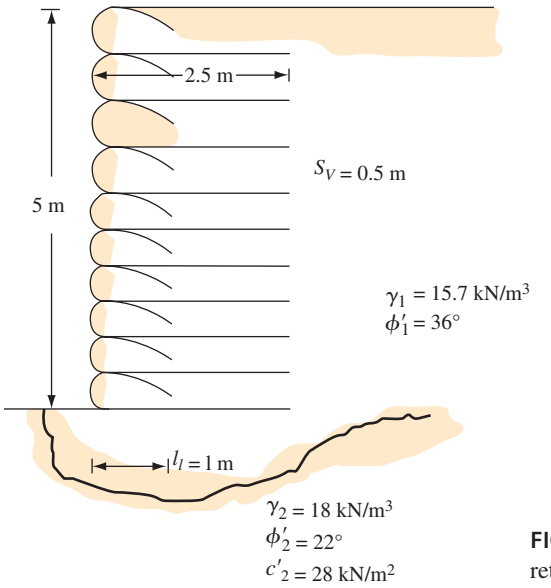


FIGURE 17.42 Geotextile-reinforced retaining wall

At $z = 4$ m,

$$S_V = \frac{14}{(15.7)(4)(0.26)(1.5)} = 0.57 \text{ m}$$

At $z = 5$ m,

$$S_V = \frac{14}{(15.7)(5)(0.26)(1.5)} = 0.46 \text{ m}$$

So, **use $S_V = 0.5$ m for $z = 0$ to $z = 5$ m** (see Figure 17.42).

Determination of L

From Eqs. (17.57), (17.58), and (17.59),

$$L = \frac{(H - z)}{\tan\left(45 + \frac{\phi_1'}{2}\right)} + \frac{S_V K_a [\text{FS}_{(P)}]}{2 \tan \phi_F'}$$

For $\text{FS}_{(P)} = 1.5$, $\tan\phi_F' = \tan\left[\left(\frac{2}{3}\right)(36)\right] = 0.445$, and it follows that

$$L = (0.51)(H - z) + 0.438 S_V$$

With $H = 5$ m, $S_V = 0.5$ m,

At $z = 0.5$ m: $L = (0.51)(5 - 0.5) + (0.438)(0.5) = 2.514$ m
At $z = 2.5$ m: $L = (0.51)(5 - 2.5) + (0.438)(0.5) = 1.494$ m

So, **use $L = 2.5$ m throughout**.

Determination of l_l

From Eq. (17.60),

$$l_l = \frac{S_V \sigma_a' [\text{FS}_{(P)}]}{4\sigma_o' \tan\phi_F'}$$

$\sigma_a' = \gamma_1 z K_a$, $\text{FS}_{(P)} = 1.5$; with $\sigma_o' = \gamma_1 z$, $\phi_F' = \frac{2}{3}\phi_1'$. So

$$l_l = \frac{S_V K_a [\text{FS}_{(P)}]}{4 \tan \phi_F'} = \frac{S_V (0.26)(1.5)}{4 \tan\left[\left(\frac{2}{3}\right)(36)\right]} = 0.219 S_V$$

$$l_l = 0.219 S_V = (0.219)(0.5) = 0.11 \text{ m} \leq 1 \text{ m}$$

So, use **$l_l = 1$ m.**

EXAMPLE 17.7

Consider the results of the internal stability check given in Example 17.6. For the geotextile-reinforced retaining wall, calculate the factor of safety against overturning, sliding, and bearing capacity failure.

SOLUTION

Refer to Figure 17.43.

Factor of Safety Against Overturning

From Eq. (17.49),

$$\text{FS}_{\text{(overturning)}} = \frac{W_1 x_1}{(P_a)\left(\frac{H}{3}\right)}$$

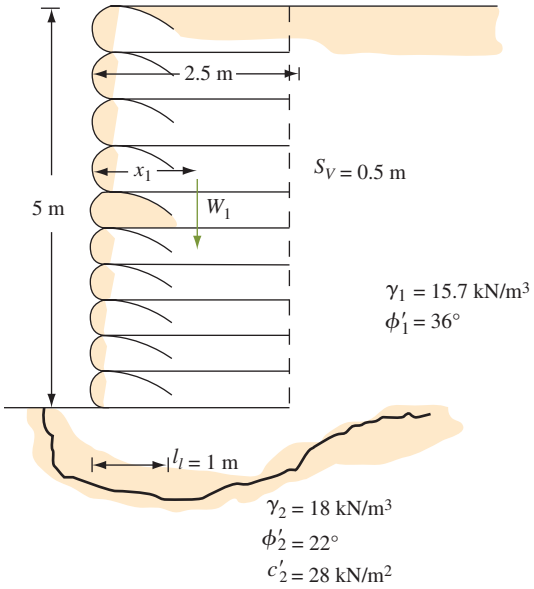


FIGURE 17.43 Stability check

$$W_1 = (5)(2.5)(15.7) = 196.25 \text{ kN/m}$$

$$x_1 = \frac{2.5}{2} = 1.25 \text{ m}$$

$$P_a = \frac{1}{2}\gamma H^2 K_a = \left(\frac{1}{2}\right)(15.7)(5)^2(0.26) = 51.03 \text{ kN/m}$$

Hence,

$$\text{FS}_{\text{(overturning)}} = \frac{(196.25)(1.25)}{51.03(5/3)} = 2.88 < 3$$

(increase length of geotextile layers to 3 m)

Factor of Safety Against Sliding

From Eq. (17.50),

$$\text{FS}_{\text{(sliding)}} = \frac{W_1 \tan\left(\frac{2}{3}\phi'_1\right)}{P_a} = \frac{(196.25)\left[\tan\left(\frac{2}{3} \times 36\right)\right]}{51.03} = \mathbf{1.71 > 1.5—OK}$$

Factor of Safety Against Bearing Capacity Failure

From Eq. (17.51), $q_u = c'_2 N_c + \frac{1}{2}\gamma_2 L_2 N_\gamma$. Given: $\gamma_2 = 18$ kN/m^3, $L_2 = 2.5$ m, $c'_2 = 28$ kN/m^2, and $\phi'_2 = 22°$. From Table 6.2, $N_c = 16.88$, and $N_\gamma = 7.13$.

$$q_u = (28)(16.88) + \left(\frac{1}{2}\right)(18)(2.5)(7.13) \approx 633 \text{ kN/m}^2$$

From Eq. (17.53),

$$\text{FS}_{\text{(bearing capacity)}} = \frac{q_u}{\sigma'_{o(H)}} = \frac{633}{\gamma_1 H} = \frac{633}{(15.7)(5)} = \mathbf{8.06 > 3—OK}$$

17.17 Retaining Walls with Geogrid Reinforcement—General

Geogrids can also be used as reinforcement in granular backfill for the construction of retaining walls. Figure 17.44 shows typical schematic diagrams of retaining walls with geogrid reinforcement. Figure 17.45 shows some photographs of geogrid-reinforced retaining walls in the field.

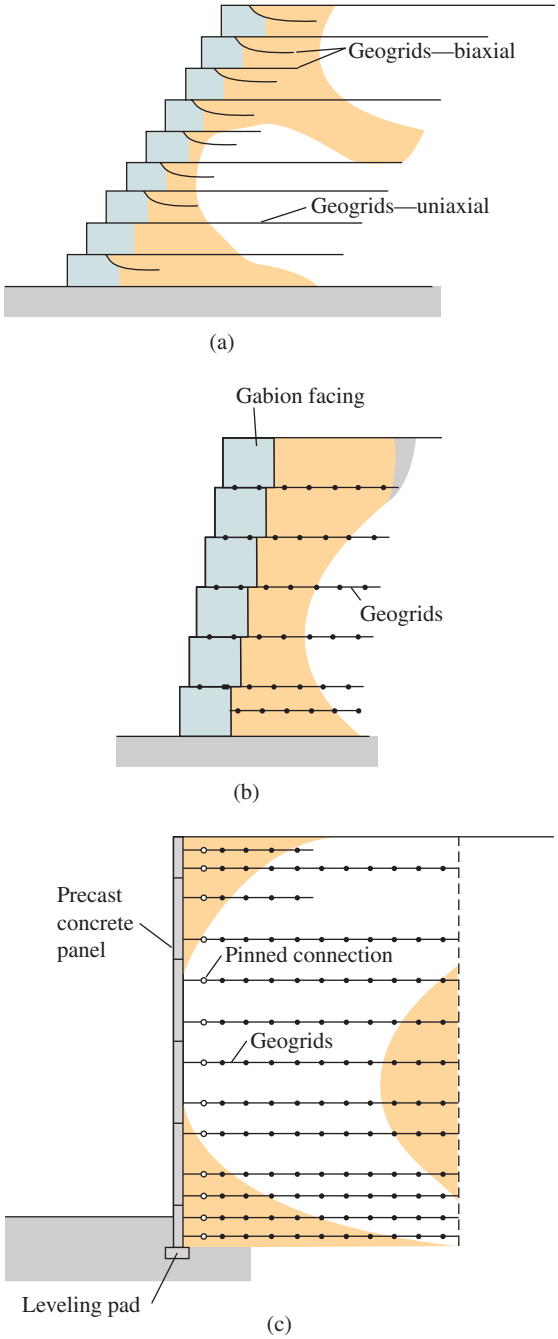


FIGURE 17.44 Typical schematic diagrams of retaining walls with geogrid reinforcement: (a) geogrid wraparound wall; (b) wall with gabion facing; (c) concrete panel–faced wall (Based on The Tensar Corporation, 1986)



(a)



(b)



(c)

FIGURE 17.45 (a) HDPE geogrid-reinforced wall with precast concrete panel facing under construction; (b) mechanical splice between two pieces of geogrid in the working direction; (c) segmented concrete-block faced wall reinforced with uniaxial geogrid (Courtesy of Tensar International Corporation, Atlanta, Georgia)

Relatively few field measurements are available for lateral earth pressure on retaining walls constructed with geogrid reinforcement. Figure 17.46 shows a comparison of measured and design lateral pressures (Berg et al. 1986) for two retaining walls constructed with precast panel facing. The figure indicates that the measured earth pressures were substantially smaller than those calculated for the Rankine active case.

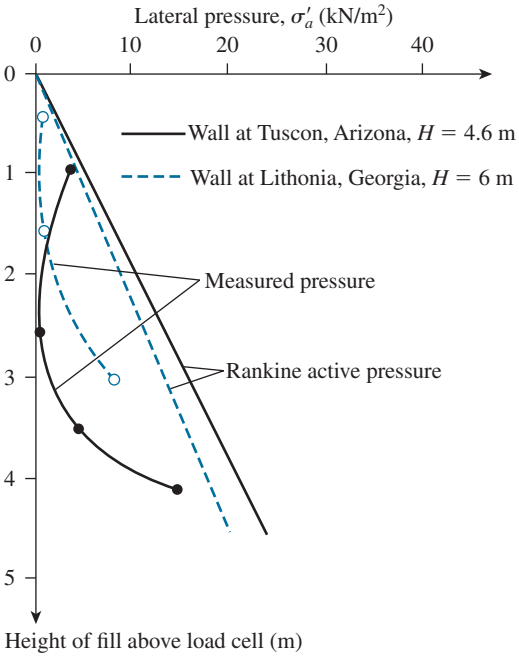


FIGURE 17.46 Comparison of theoretical and measured lateral pressures in geogrid-reinforced retaining walls (Based on Berg et al., 1986)

17.18 Design Procedure for Geogrid-Reinforced Retaining Wall

Figure 17.47 shows a schematic diagram of a concrete panel–faced wall with a granular backfill reinforced with layers of geogrid. The design process of the wall is essentially similar to that with geotextile reinforcement of the backfill given in Section 17.16. The following is a brief step-by-step procedure.

INTERNAL STABILITY

Step 1. Determine the active pressure at any depth z as [similar to Eq. (17.54)]:

$$\sigma'_a = K_a \gamma_1 z \tag{17.61}$$

where

K_a = Rankine active pressure coefficient $= \tan^2\left(45 - \dfrac{\phi'_1}{2}\right)$

Step 2. Select a geogrid with allowable tensile strength, T_{all} [similar to Eq. (17.55)] (Koerner, 2005):

$$T_{all} = \frac{T_{ult}}{RF_{id} \times RF_{cr} \times RF_{cbd}} \tag{17.62}$$

where

RF_{id} = reduction factor for installation damage (1.1 to 1.4)

RF_{cr} = reduction factor for creep (2.0 to 3.0)

RF_{cbd} = reduction factor for chemical and biological degradation (1.1 to 1.5).

Step 3. Obtain the vertical spacing of the geogrid layers, S_V, as

$$S_V = \frac{T_{all} C_r}{\sigma'_a \, FS_{(B)}} \tag{17.63}$$

where C_r is the coverage ratio for the geogrid.

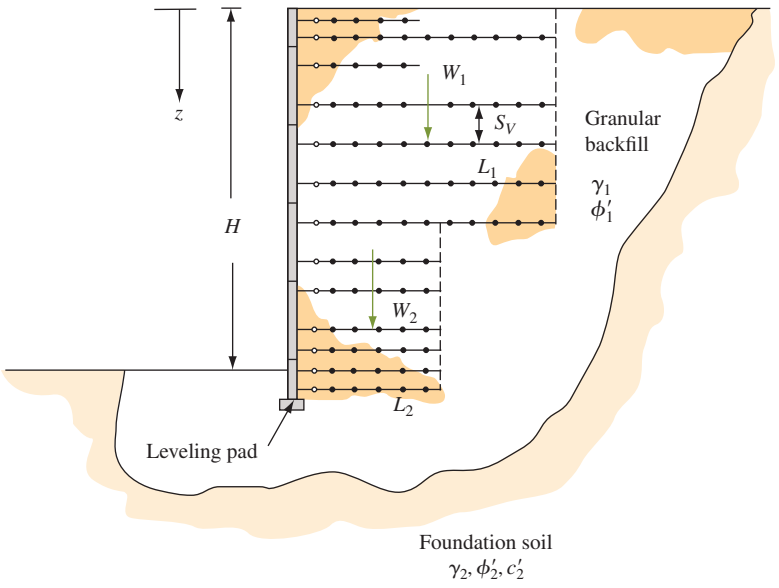


FIGURE 17.47 Design of geogrid-reinforced retaining wall

The *coverage ratio* is the fractional plan area at any particular elevation that is actually occupied by geogrid. For example, if there is a 0.3 m wide (1 ft) space between each 1.2 m wide (4 ft) piece of geogrid, the coverage ratio is

$$C_r = \frac{1.2\text{ m}}{1.2\text{ m} + 0.3\text{ m}} = 0.8$$

Step 4. Calculate the length of each layer of geogrid at a depth z as [Eq. (17.57)]

$$L = l_r + l_e$$

$$l_r = \frac{H - z}{\tan^2\left(45 - \frac{\phi_1'}{2}\right)} \tag{17.64}$$

For determination of l_e [similar to Eq. (17.59)],

$$\text{FS}_{(P)} = \frac{\text{resistance to pullout at a given normal effective stress}}{\text{pullout force}} \tag{17.65}$$

$$= \frac{(2)(l_e)(C_i\sigma_0' \tan\phi_1')(C_r)}{S_V\sigma_a'}$$

$$= \frac{(2)(l_e)(C_i \tan\phi_1')(C_r)}{S_V K_a}$$

where C_i = interaction coefficient or

$$l_e = \frac{S_V K_a \text{FS}_{(P)}}{2C_r C_i \tan\phi_1'} \tag{17.66}$$

Thus, at a given depth z, the total length, L, of the geogrid layer is

$$L = l_r + l_e = \frac{H - z}{\tan\left(45 + \frac{\phi_1'}{2}\right)} + \frac{S_V K_a\,\text{FS}_{(P)}}{2C_r C_i \tan\phi_1'} \tag{17.67}$$

The interaction coefficient, C_i, can be determined experimentally in the laboratory. The following is an approximate range for C_i for various types of backfill.

Gravel, sandy gravel	0.75–0.8
Well-graded sand, gravelly sand	0.7–0.75
Fine sand, silty sand	0.55–0.6

EXTERNAL STABILITY

Check the factors of safety against overturning, sliding, and bearing capacity failure as described in Section 17.15 (Steps 9, 10, and 11).

EXAMPLE 17.8

Consider a geogrid-reinforced retaining wall. Referring to Figure 17.47, given: $H = 6$ m, $\gamma_1 = 16.5$ kN/m^3, $\phi_1' = 35°$, $T_{all} = 45$ kN/m, $FS_{(B)} = 1.5$, $FS_{(P)} = 1.5$, $C_r = 0.8$, and $C_i = 0.75$. For the design of the wall, determine S_V and L.

SOLUTION

$$K_a = \tan^2\left(45 - \frac{\phi_1'}{2}\right) = \tan^2\left(45 - \frac{35}{2}\right) = 0.27$$

Determination of S_V

From Eq. (17.63),

$$S_v = \frac{T_{all}C_r}{\sigma_a' FS_{(B)}} = \frac{T_{all}C_r}{\gamma z K_a FS_{(B)}} = \frac{(45)(0.8)}{(16.5)(z)(0.27)(1.5)} = \frac{5.39}{z}$$

At $z = 2$ m: $S_v = \dfrac{5.39}{2} = 2.7$ m

At $z = 4$ m: $S_v = \dfrac{5.39}{4} = 1.35$ m

At $z = 5$ m: $S_v = \dfrac{5.39}{5} = 1.08$ m

Use $S_V \approx$ **1 m.**

Determination of L

From Eq. (17.67),

$$L = \frac{H - z}{\tan\left(45 + \frac{\phi_1'}{2}\right)} + \frac{S_V K_a FS_{(P)}}{2C_r C_i \tan\phi_1'} = \frac{6 - z}{\tan\left(45 + \frac{35}{2}\right)} + \frac{(1\text{ m})(0.27)(1.5)}{(2)(0.8)(0.75)(\tan 35°)}$$

At $z = 1$ m: $L = 0.52(6 - 1) + 0.482 = 3.08$ m ≈ 3.1 m
At $z = 3$ m: $L = 0.52(6 - 3) + 0.482 = 2.04$ m ≈ 2.1 m
At $z = 5$ m: $L = 0.52(6 - 5) + 0.482 = 1.0$ m

So, use $L = 3$ m for $z = 0$ to 6 m.

17.19 Summary

Rankine's and Coulomb's lateral earth pressure theories were discussed in Chapter 16. Rankine's analysis is generally simpler than Coulomb's. Therefore, in the designs of retaining walls and mechanically stabilized retaining walls, Rankine's theory is commonly used.

Designs of gravity and cantilever retaining walls and mechanically stabilized retaining walls were discussed in this chapter. The main modes of failure for cantilever and gravity retaining walls are (a) overturning, (b) sliding, and (c) bearing capacity. In addition, the settlements may be checked. In the case of mechanically stabilized retaining walls that are reinforced with metallic strips, geotextiles, or geogrids, in addition to these three checks it is necessary to check for breakages or slip (i.e., pullout) of the reinforcements.

PROBLEMS

17.1 Figure P17.1 shows a gravity retaining wall retaining a granular ($c' = 0$) backfill. The same soil is present at the bottom of the wall and on the left. The unit weight and the friction angle of the backfill are 18.5 kN/m^3 and 35°, respectively. The unit weight of the concrete is 24.0 kN/m^3 and $\delta' = \frac{2}{3}\phi'$. Determine the factors of safety with respect to overturning, sliding, and bearing capacity failure.

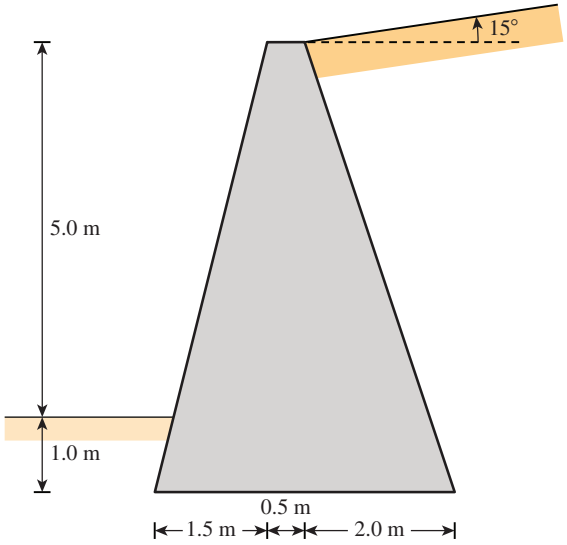


FIGURE P17.1

17.2 In Problem 17.1, if there is a possibility that the soil in front of the wall will be removed sometime later, neglect the passive resistance and compute the factors of safety.

17.3 Determine the factor of safety of the retaining wall shown in Figure P17.3 with respect to overturning, sliding, and bearing capacity failure. Given: unit weight of concrete = 24.0 kN/m^3, $\delta' = \frac{2}{3}\phi'$, and $c'_a = \frac{2}{3}c'$.

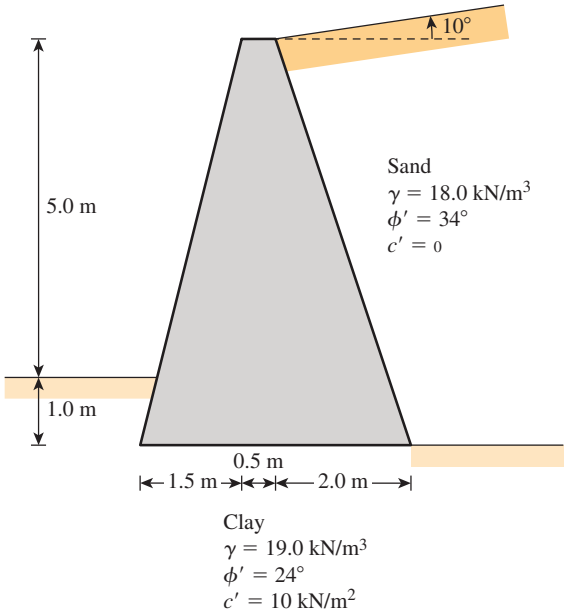


FIGURE P17.3

17.4 Using Rankine's earth pressures and neglecting the passive resistance, determine the factor of safety with respect to sliding and overturning for the gravity retaining wall shown in Figure P17.4. The unit weight of the concrete is 24 kN/m^3. Take δ' as $\frac{2}{3}\phi'$.

If the design requirement is that the eccentricity should be less than $B/6$, check whether this is satisfied.

Find the soil pressures at the toe and the heel.

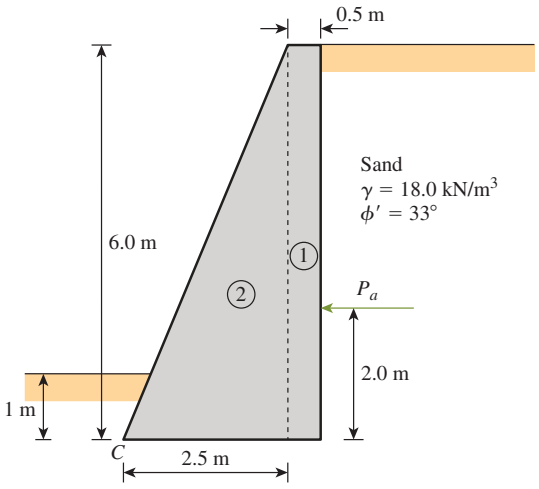


FIGURE P17.4

17.5 Redo Problem 17.4 using Coulomb's earth pressures.

17.6 It is required to design a cantilever retaining wall to retain a 5.0 m high sandy backfill. The consultant suggests the dimensions and soil properties shown in Figure P17.6 and requires that the wall be checked for stability with respect to sliding and overturning based on the active earth pressures determined using

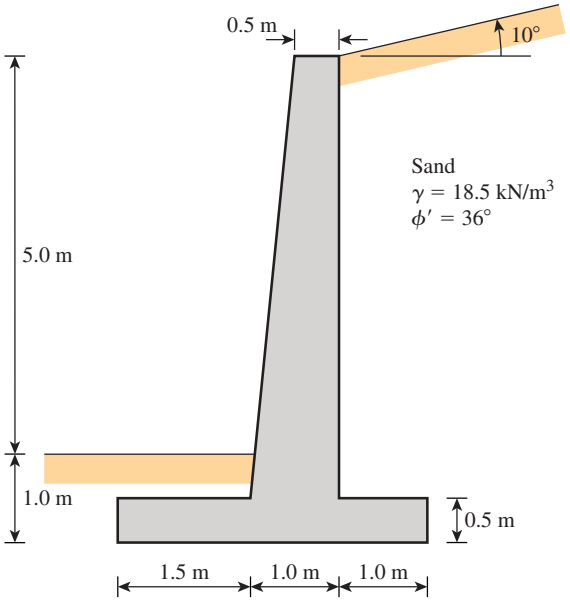


FIGURE P

a. Coulomb's earth pressure theory ($\delta' = 24°$), and
b. Rankine's earth pressure theory.

The unit weight of the concrete is 24 .0 kN/m^3.

17.7 A reinforced earth retaining wall (Figure 17.35) is to be 10 m high. Here,

Backfill:	unit weight, $\gamma_1 = 16$ kN/m^3 and soil friction angle, $\phi_1' = 34°$
Reinforcement:	vertical spacing, $S_V = 1$ m; horizontal spacing, $S_H = 1.25$ m; width of reinforcement = 120 mm; $f_y = 260$ MN/m^2; $\phi_\mu = 25°$; factor of safety against tie pullout = 3; and factor of safety against tie breaking = 3

Determine:
a. The required thickness of ties
b. The required maximum length of ties

17.8 In Problem 17.7 assume that the ties at all depths are the length determined in Part b. For the *in situ* soil, $\phi_2' = 25°$, $\gamma_2 = 15.5$ kN/m^3, $c_2' = 30$ kN/m^2. Calculate the factor of safety against (a) overturning, (b) sliding, and (c) bearing capacity failure.

17.9 A retaining wall with geotextile reinforcement is 6 m high. For the granular backfill, $\gamma_1 = 15.9$ kN/m^3 and $\phi_1' = 30°$. For the geotextile, $T_{all} = 16$ kN/m. For the design of the wall, determine S_V, L, and l_l. Use $FS_{(B)} = FS_{(P)} = 1.5$.

17.10 With the S_V, L, and l_l determined in Problem 17.9, check the overall stability (i.e., factor of safety against overturning, sliding, and bearing capacity failure) of the wall. For the *in situ* soil, $\gamma_2 = 16.8$ kN/m^3, $\phi_2' = 20°$, and $c_2' = 55$ kN/m^2.

REFERENCES

Applied Technology Council (1978). "Tentative Provisions for the Development of Seismic Regulations for Buildings," *Publication ATC-3-06*.

Bell, J. R., Stilley, A. N., and Vandre, B. (1975). "Fabric Retaining Earth Walls," *Proceedings*, *Thirteenth Engineering Geology and Soils Engineering Symposium*, Moscow, ID, pp. 271–287.

Bentler, J. G. and Labuz, J. F. (2006). "Performance of a Cantilever Retaining Wall," *Journal of Geotechnical and Geoenvironmental Engineering*, American Society of Civil Engineers, Vol. 132, No. 8, pp. 1062–1070.

Berg, R. R., Bonaparte, R., Anderson, R. P., and Chouery, V. E. (1986). "Design Construction and Performance of Two Tensar Geogrid Reinforced Walls," *Proceedings, Third International Conference on Geotextiles*, Vienna, pp. 401–406.

Binquet, J. and Lee, K. L. (1975). "Bearing Capacity Analysis of Reinforced Earth Slabs," *Journal of the Geotechnical Engineering Division*, American Society of Civil Engineers, Vol. 101, No. GT12, pp. 1257–1276.

Carroll, R., Jr. (1988). "Specifying Geogrids," *Geotechnical Fabric Report*, Industrial Fabric Association International, St. Paul, March/April.

Casagrande, L. (1973). "Comments on Conventional Design of Retaining Structure," *Journal of the Soil Mechanics and Foundations Division*, ASCE, Vol. 99, No. SM2, pp. 181–198.

Chu, S. C. (1991). "Rankine Analysis of Active and Passive Pressures on Dry Sand," *Soils and Foundations*, Vol. 31, No. 4, pp. 115–120.

Darbin, M. (1970). "Reinforced Earth for Construction of Freeways" (in French), *Revue Générale des Routes et Aerodromes*, No. 457, September.

Elman, M. T. and Terry, C. F. (1988). "Retaining Walls with Sloped Heel," *Journal of Geotechnical Engineering*, American Society of Civil Engineers, Vol. 114, No. GT10, pp. 1194–1199.

Koerner, R. B. (2005). *Design with Geosynthetics*, 5th. ed., Pearson Education, Upper Saddle River, NJ.

Laba, J. T. and Kennedy, J. B. (1986). "Reinforced Earth Retaining Wall Analysis and Design," *Canadian Geotechnical Journal*, Vol. 23, No. 3, pp. 317–326.

Lee, K. L., Adams, B. D., and Vagneron, J. J. (1973). "Reinforced Earth Retaining Walls," *Journal of the Soil Mechanics and Foundations Division*, American Society of Civil Engineers, Vol. 99, No. SM10, pp. 745–763.

Martin, J. P., Koerner, R. M., and Whitty, J. E. (1984). "Experimental Friction Evaluation of Slippage Between Geomembranes, Geotextiles, and Soils," *Proceedings, International Conference on Geomembranes*, Denver, pp. 191–196.

Richards, R. and Elms, D. G. (1979). "Seismic Behavior of Gravity Retaining Walls," *Journal of the Geotechnical Engineering Division*, American Society of Civil Engineers, Vol. 105, No. GT4, pp. 449–464.

Sarsby, R. W. (1985). "The Influence of Aperture Size/Particle Size on the Efficiency of Grid Reinforcement," *Proceedings, 2nd Canadian Symposium on Geotextiles and Geomembranes*, Edmonton, pp. 7–12.

Schlosser, F. and Long, N. (1974). "Recent Results in French Research on Reinforced Earth," *Journal of the Construction Division*, American Society of Civil Engineers, Vol. 100, No. CO3, pp. 113–237.

Schlosser, F. and Vidal, H. (1969). "Reinforced Earth" (in French), *Bulletin de Liaison des Laboratoires Routier*, Ponts et Chassées, Paris, France, November, pp. 101–144.

Shukla, S. K. (2015). Personal communication.

Tensar Corporation (1986). Tensar Technical Note. No. TTN:RW1, August.

Terzaghi, K. (1943). *Theoretical Soil Mechanics*, John Wiley & Sons, New York.

Terzaghi, K. and Peck, R. B. (1967). *Soil Mechanics in Engineering Practice*, John Wiley & Sons, New York.

Transportation Research Board (1995). Transportation Research Circular No. 444, National Research Council, Washington, DC.

U.S. Navy (1982). *Soil Mechanics, Design Manual NAVFAC DM 7.1*, Department of the Navy, Naval Facilities Engineering Command, Alexandria, VA 22332.

Vidal, H. (1966). "La terre Armée," *Annales de l'Institut Technique du Bâtiment et des Travaux Publiques*, France, July–August, pp. 888–938.

18

Sheet-Pile Walls



Aisyaqilumaranas/Shutterstock.com

18.1 Introduction 753
18.2 Construction Methods 756
18.3 Cantilever Sheet-Pile Walls 757
18.4 Cantilever Sheet Piling Penetrating Sandy Soil 758
18.5 Special Cases for Cantilever Walls Penetrating a Sandy Soil 764
18.6 Cantilever Sheet Piling Penetrating Clay 767
18.7 Special Cases for Cantilever Walls Penetrating Clay 772
18.8 Cantilever Sheet Piles Penetrating Sandy Soil—A Simplified Approach 775
18.9 Anchored Sheet-Pile Walls 779
18.10 Free Earth Support Method for Penetration of Sandy Soil—A Simplified Approach 780
18.11 Free Earth Support Method for Penetration of Sandy Soil—Net Lateral Pressure Method 782
18.12 Design Charts for Free Earth Support Method (Penetration into Sandy Soil) 785
18.13 Moment Reduction for Anchored Sheet-Pile Walls Penetrating into Sand 789
18.14 Computational Pressure Diagram Method for Penetration into Sandy Soil 792
18.15 Field Observations for Anchor Sheet-Pile Walls 795
18.16 Free Earth Support Method for Penetration of Clay 797
18.17 Anchors 802
18.18 Holding Capacity of Deadman Anchors 804
18.19 Holding Capacity of Anchor Plates in Sand 804
18.20 Holding Capacity of Anchor Plates in Clay ($\phi = 0$ Condition) 811
18.21 Ultimate Resistance of Tiebacks 811
18.22 Summary 812

PROBLEMS 812

REFERENCES 813

18.1 Introduction

When excavation takes place within a limited area such as a trench and often for excavations for temporay works, it is common to use braced cuts, where the two walls are covered by sheets that are supported by struts between them. These are discussed in Chapter 19. When the excavation is over a wider area, sheet piles are driven into the ground to support the walls of the excavation against the lateral earth pressures. Depending on the depth of the excavation, the sheet pile can be anchored or cantilevered. This chapter covers the design and analysis of sheet-pile walls.

Connected or semiconnected sheet piles are often used to build continuous walls for waterfront structures that range from small waterfront pleasure boat launching facilities to large dock facilities. (See Figure 18.1.) In contrast to the construction of other types of retaining walls, the building of sheet-pile walls does not usually require dewatering of the site. Sheet piles are also used for some temporary structures, such as braced cuts. (See Chapter 19.) The principles of sheet-pile wall design are discussed in the current chapter.

Several types of sheet pile are commonly used in construction: (a) wooden sheet piles, (b) precast concrete sheet piles, and (c) steel sheet piles. Aluminum sheet piles are also marketed.

Wooden sheet piles are used only for temporary light structures that are above the water table. The most common types are ordinary wooden planks and *Wakefield piles*. The wooden planks are about 50 mm × 300 mm (2 in. × 12 in.) in cross section and are driven edge to edge (Figure 18.2a). Wakefield piles are made by nailing three planks together, with the middle plank offset by 50 to 75 mm (2 to 3 in.) (Figure 18.2b). Wooden planks can also be milled to form *tongue-and-groove piles*, as shown in Figure 18.2c. Figure 18.2d shows another type of wooden sheet pile that has precut grooves. Metal *splines* are driven into the grooves of the adjacent sheetings to hold them together after they are sunk into the ground.

Precast concrete sheet piles are heavy and are designed with reinforcements to withstand the permanent stresses to which the structure will be subjected after construction and also to handle the stresses produced during construction. In cross section, these piles are about 500 to 800 mm (20 to 32 in.) wide and 150 to

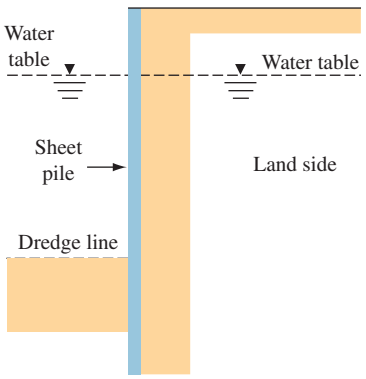


FIGURE 18.1 Example of waterfront sheet-pile wall

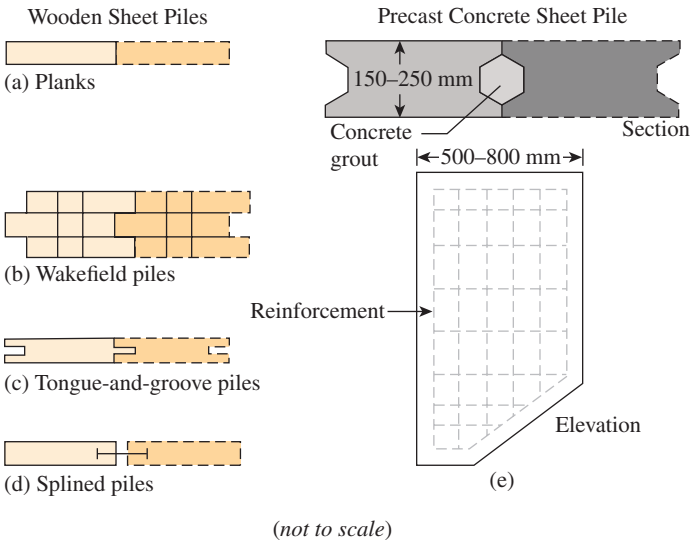


FIGURE 18.2 Various types of wooden and concrete sheet piles

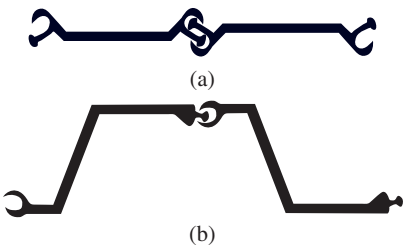


FIGURE 18.3 (a) Thumb-and-finger type sheet-pile connection; (b) ball-and-socket type sheet-pile connection

250 mm (6 to 10 in.) thick. Figure 18.2e is a schematic diagram of the elevation and the cross section of a reinforced concrete sheet pile.

Steel sheet piles in the United States are about 10 to 13 mm (0.4 to 0.5 in.) thick. European sections may be thinner and wider. Sheet-pile sections may be *Z, deep arch, low arch*, or *straight web* sections. The interlocks of the sheet-pile sections are shaped like a *thumb-and-finger* or *ball-and-socket* joint for watertight connections. Figure 18.3a is a schematic diagram of the thumb-and-finger type of interlocking for straight web sections. The ball-and-socket type of interlocking for *Z* section piles is shown in Figure 18.3b. Figure 18.4 shows a photograph of interlocking sheet piles at a construction site. Figure 18.5 shows a small enclosure with steel sheet piles for an excavation work. Table 18.1 lists the properties



FIGURE 18.4 Interlocking sheet piles at a construction site (Courtesy of N. Sivakugan, James Cook University, Australia)

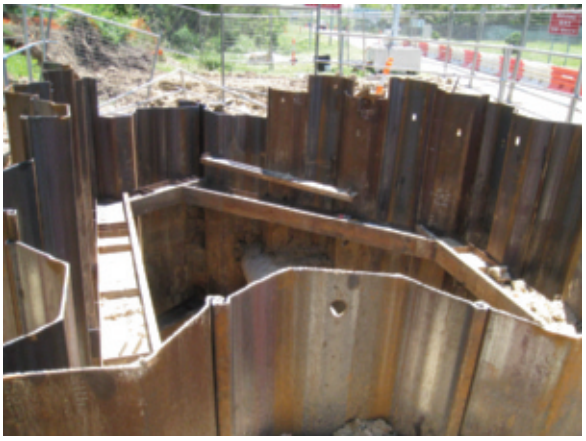
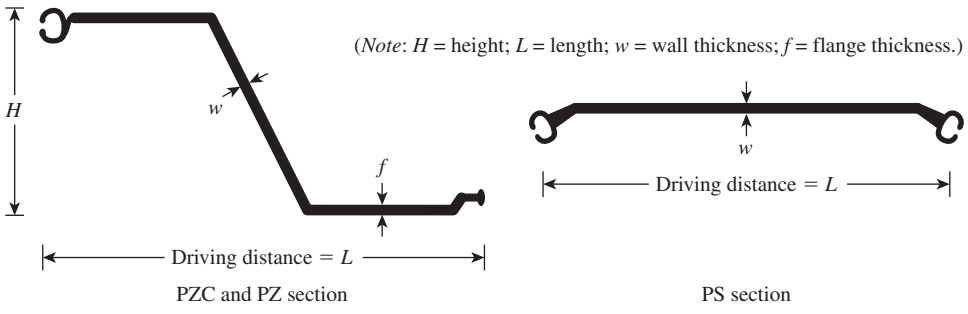


FIGURE 18.5 A small enclosure with steel sheet piles for an excavation work (Courtesy of N. Sivakugan, James Cook University, Australia)

TABLE 18.1 Properties of Some Commercially Available Sheet-Pile Sections (Adapted after Hammer and Steel, Inc., Hazelwood, Missouri, USA)

Section designation	*H* mm (in.)	*L* mm (in.)	*f* mm (in.)	*w* mm (in.)	Section modulus m^3/m of wall (in^3/ft of wall)	Moment of inertia m^4/m of wall (in^4/ft of wall)
PZC-12	318.0 (12.52)	708.2 (27.88)	8.51 (0.335)	8.51 (0.335)	120.42×10^{-5} (22.4)	192.06×10^{-6} (140.6)
PZC-13	319.0 (12.56)	708.2 (27.88)	9.53 (0.375)	9.53 (0.375)	130.1×10^{-5} (24.2)	207.63×10^{-6} (152.0)
PZC-14	320.0 (12.6)	708.2 (27.88)	10.67 (0.420)	10.67 (0.420)	139.78×10^{-5} (26.0)	225.12×10^{-6} (164.8)
PZC-17	386.3 (15.21)	635.0 (25.00)	8.51 (0.335)	8.51 (0.335)	166.67×10^{-5} (31.0)	322.38×10^{-6} (236.6)
PZC-18	387.4 (15.25)	635.0 (25.00)	9.53 (0.375)	9.53 (0.375)	180.1×10^{-5} (33.5)	349.01×10^{-6} (255.5)
PZC-19	388.6 (15.30)	635.0 (25.00)	10.67 (0.420)	10.67 (0.420)	194.07×10^{-5} (36.1)	377.97×10^{-6} (276.7)
PZC-26	449.6 (17.70)	708.2 (27.88)	15.24 (0.60)	13.34 (0.525)	260.2×10^{-5} (48.4)	584.78×10^{-6} (428.1)
PZ-22	235.0 (9.25)	558.8 (22.00)	9.53 (0.375)	9.53 (0.375)	98.92×10^{-5} (18.4)	116.2×10^{-6} (85.1)
PZ-27	307.3 (12.1)	457.2 (18.00)	9.53 (0.375)	9.53 (0.375)	166.66×10^{-5} (31.00)	255.9×10^{-6} (187.3)
PZ-35	383.5 (15.1)	575.1 (22.64)	15.37 (0.605)	12.7 (0.5)	262.9×10^{-5} (48.9)	504.6×10^{-6} (369.4)
PZ-40	416.6 (16.4)	499.1 (19.69)	15.24 (0.6)	12.7 (0.5)	329.5×10^{-5} (61.3)	686.7×10^{-6} (502.7)
PS-27.5	— —	500 (19.69)	— —	10.16 (0.4)	10.21×10^{-5} (1.9)	4.1×10^{-6} (3.0)
PS-31	— —	500 (19.69)	— —	12.7 (0.5)	10.21×10^{-5} (1.9)	4.1×10^{-6} (3.0)



of the steel sheet-pile sections produced by Hammer & Steel, Inc. of Hazelwood, Missouri. The allowable stress of the sheet pile is selected to be about 65% (87% for earthquake loading) of the yield strength. The basic grade is ASTM A-328, with a minimum yield strength of 38.5 ksi (265.5 MN/m^2). ASTM A-572 is a higher-strength section with a minimum yield strength of 50 ksi (344.8 MN/m^2). ASTM A-690 is developed as the corrosion-resistant grade (e.g., marine applications) with a minimum yield strength of 50 ksi (344.8 MN/m^2).

The allowable stresses for ASTM A-328, ASTM A-572, and ASTM A-690 are as follows:

Type of steel	Allowable stress	
ASTM A-328	170 MN/m^2	(25,000 lb/in^2)
ASTM A-572	225 MN/m^2	(32,500 lb/in^2)
ASTM A-690	225 MN/m^2	(32,500 lb/in^2)

Steel sheet piles are convenient to use because of their resistance to the high driving stress that is developed when they are being driven into hard soil. Sheet piles are often installed by vibrating hammers, diesel impact hammers, or hydraulic presses. Sometimes, water jetting or preboring is used to assist penetration through hard layers. Steel sheet piles are also lightweight and reusable.

18.2 Construction Methods

Sheet-pile walls may be divided into two basic categories: (a) cantilever and (b) anchored.

In the construction of sheet-pile walls, the sheet pile may be driven into the ground and then the backfill placed on the land side, or the sheet pile may first be driven into the ground and the soil in front of the sheet pile dredged. In either case, the soil used for backfill behind the sheet-pile wall is usually granular for better drainage. The soil below the dredge line may be sandy or clayey. The surface of soil on the water side is referred to as the *mud line* or *dredge line*.

Thus, construction methods generally can be divided into two categories (Tsinker, 1983):

1. Backfilled structure
2. Dredged structure

The sequence of construction for a *backfilled structure* is as follows (see Figure 18.6):

Step 1. Dredge the *in situ* soil in front and back of the proposed structure.

Step 2. Drive the sheet piles.

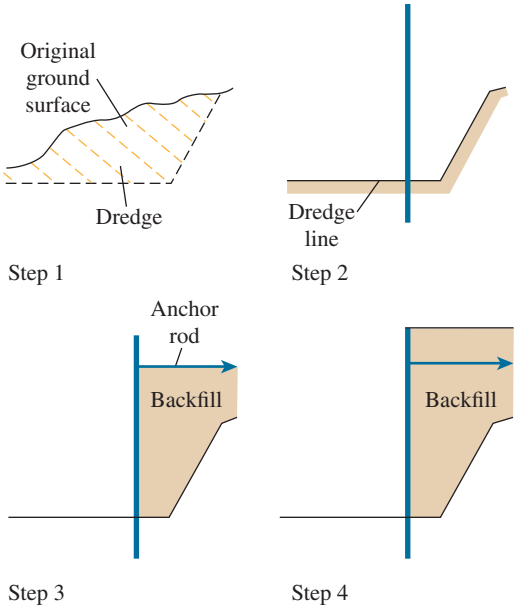


FIGURE 18.6 Sequence of construction for a backfilled structure

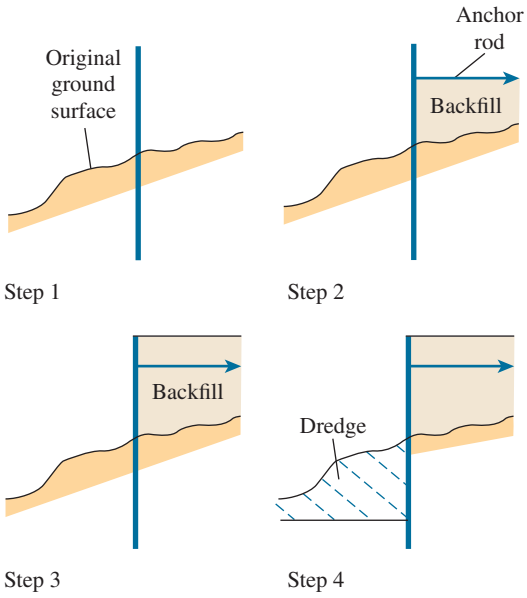


FIGURE 18.7 Sequence of construction for a dredged structure

Step 3. Backfill up to the level of the anchor, and place the anchor system.

Step 4. Backfill up to the top of the wall.

For a cantilever type of wall, where an anchor is not required, only Steps 1, 2, and 4 apply. The sequence of construction for a *dredged structure* is as follows (see Figure 18.7):

Step 1. Drive the sheet piles.

Step 2. Backfill up to the anchor level, and place the anchor system.

Step 3. Backfill up to the top of the wall.

Step 4. Dredge the front side of the wall.

With cantilever sheet-pile walls, Step 2 is not required.

18.3 Cantilever Sheet-Pile Walls

Cantilever sheet-pile walls are usually recommended for walls of moderate height—about 6 m (≈20 ft) or less, measured above the dredge line. In such walls, the sheet piles act as a wide vertical cantilever beam above the dredge line. The basic principles for estimating net lateral pressure distribution on a cantilever sheet-pile wall can be explained with the aid of Figure 18.8. The figure shows the nature of lateral yielding of a cantilever wall penetrating a sand layer below the dredge line. The wall rotates about point O (Figure 18.8a). Because the hydrostatic pressures at any depth from both sides of the wall will cancel each other, we consider only the effective lateral soil pressures. In zone A, the lateral pressure is just the active pressure from the land side. In zone B, because of the nature of yielding of the wall, there will be active pressure from the land side and passive pressure from the water side. The condition is reversed in zone C—that is, below the point of rotation, O. The net actual pressure distribution on the wall is like that shown in Figure 18.8b. However, for design purposes, Figure 18.8c shows a simplified version.

Sections 18.4 through 18.7 present the mathematical formulation of the analysis of cantilever sheet-pile walls. Note that in some waterfront structures, the water level may fluctuate as the result of tidal effects. Care should be taken in determining the water level that will affect the net pressure diagram.

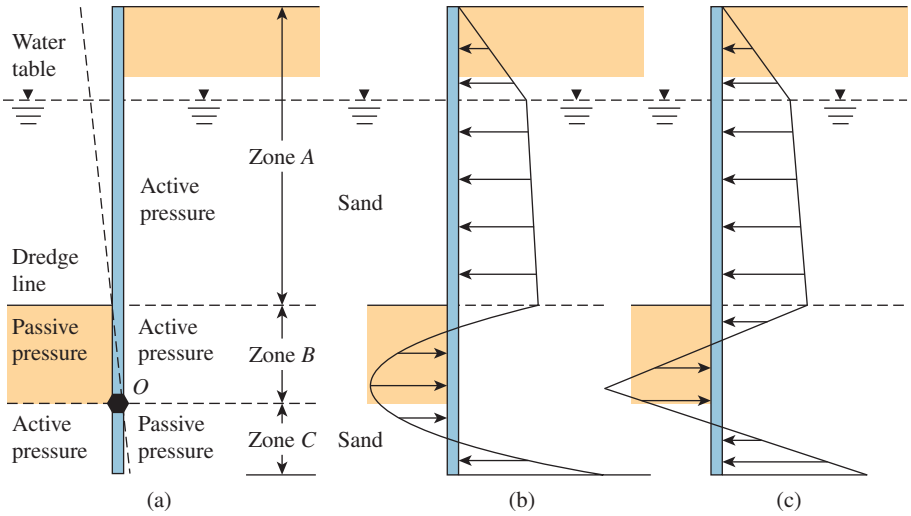


FIGURE 18.8 Cantilever sheet pile penetrating sand

18.4 Cantilever Sheet Piling Penetrating Sandy Soil

To develop the relationships for the proper depth of embedment of sheet piles driven into a granular soil, examine Figure 18.9a. The soil retained by the sheet piling above the dredge line also is sand. The water table is at a depth L_1 below the top of the wall.

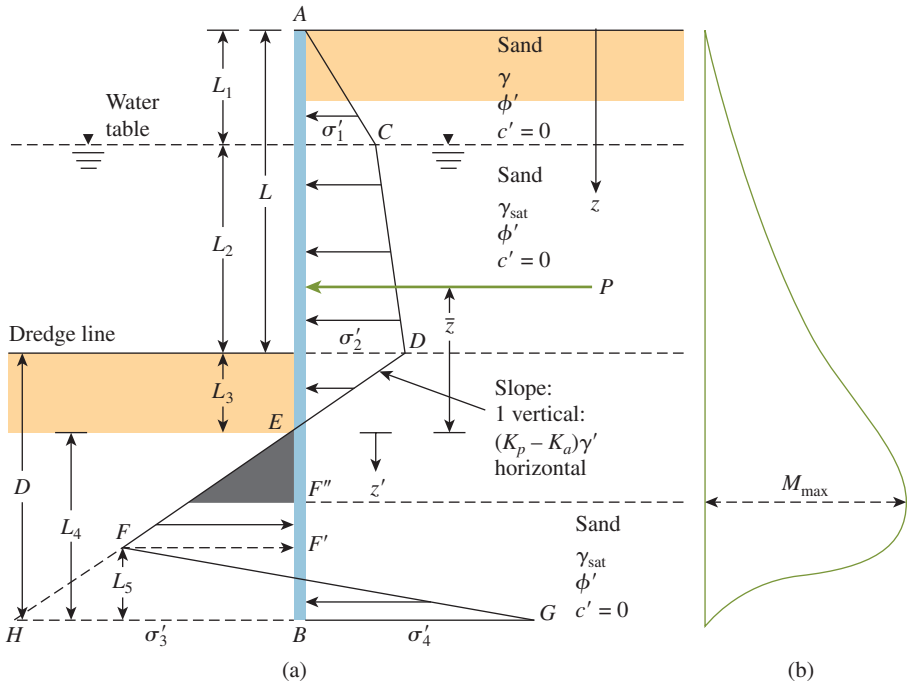


FIGURE 18.9 Cantilever sheet pile penetrating sand: (a) variation of net pressure diagram; (b) variation of bending moment

Let the effective angle of friction of the sand be ϕ'. The intensity of the active pressure at a depth $z = L_1$ is

$$\sigma'_1 = \gamma L_1 K_a \tag{18.1}$$

where

K_a = Rankine active pressure coefficient = $\tan^2(45 - \phi'/2)$

γ = unit weight of soil above the water table

Similarly, the active pressure at a depth $z = L_1 + L_2$ (i.e., at the level of the dredge line) is

$$\sigma'_2 = (\gamma L_1 + \gamma' L_2) K_a \tag{18.2}$$

where γ' = effective unit weight of soil = $\gamma_{sat} - \gamma_w$.

Note that at the level of the dredge line, the hydrostatic pressures from both sides of the wall are the same magnitude and cancel each other.

To determine the net lateral pressure below the dredge line up to the point of rotation, O, as shown in Figure 18.8a, an engineer has to consider the passive pressure acting from the left side (the water side) toward the right side (the land side) of the wall and also the active pressure acting from the right side toward the left side of the wall. For such cases, ignoring the hydrostatic pressure from both sides of the wall, the active pressure at depth z is

$$\sigma'_a = [\gamma L_1 + \gamma' L_2 + \gamma'(z - L_1 - L_2)] K_a \tag{18.3}$$

Also, the passive pressure at depth z is

$$\sigma'_p = \gamma'(z - L_1 - L_2) K_p \tag{18.4}$$

where K_p = Rankine passive pressure coefficient = $\tan^2(45 + \phi'/2)$. The depth z is measured from the top (see Figure 18.9).

Combining Eqs. (18.3) and (18.4) yields the net lateral pressure, namely,

$$\begin{aligned} \sigma' &= \sigma'_a - \sigma'_p = (\gamma L_1 + \gamma' L_2) K_a - \gamma'(z - L_1 - L_2)(K_p - K_a) \\ &= \sigma'_2 - \gamma'(z - L)(K_p - K_a) \end{aligned} \tag{18.5}$$

where $L = L_1 + L_2$.

The net pressure, σ', equals zero at a depth L_3 below the dredge line, so

$$\sigma'_2 - \gamma'(z - L)(K_p - K_a) = 0$$

or

$$(z - L) = L_3 = \frac{\sigma'_2}{\gamma'(K_p - K_a)} \tag{18.6}$$

Equation (18.6) indicates that the slope of the net pressure distribution line DEF is 1 vertical to $(K_p - K_a)\gamma'$ horizontal, so, in the pressure diagram,

$$\overline{HB} = \sigma'_3 = L_4(K_p - K_a)\gamma' \tag{18.7}$$

At the bottom of the sheet pile, passive pressure, σ'_p, acts from the right toward the left side, and active pressure acts from the left toward the right side of the sheet pile, so at $z = L + D$,

$$\sigma'_p = (\gamma L_1 + \gamma' L_2 + \gamma' D) K_p \tag{18.8}$$

At the same depth,

$$\sigma'_a = \gamma' D K_a \tag{18.9}$$

Hence, the net lateral pressure at the bottom of the sheet pile is

$$\begin{aligned}\sigma'_p - \sigma'_a = \sigma'_4 &= (\gamma L_1 + \gamma' L_2)K_p + \gamma' D(K_p - K_a) \\ &= (\gamma L_1 + \gamma' L_2)K_p + \gamma' L_3(K_p - K_a) + \gamma' L_4(K_p - K_a) \\ &= \sigma'_5 + \gamma' L_4(K_p - K_a) \end{aligned} \tag{18.10}$$

where

$$\sigma'_5 = (\gamma L_1 + \gamma' L_2)K_p + \gamma' L_3(K_p - K_a) \tag{18.11}$$

$$D = L_3 + L_4 \tag{18.12}$$

For the stability of the wall, the principles of statics can now be applied:

$$\Sigma \text{ horizontal forces per unit length of wall} = 0$$

and

$$\Sigma \text{ moment of the forces per unit length of wall about point } B = 0$$

Looking at the net pressure diagram shown in Figure 18.9, it can be seen that there are two unknowns: L_4 and L_5. These can be determined from equilibrium equations, as follows. We can include the area *HBGF* on both sides so that the computations are simpler.

For the summation of the horizontal forces, we have

$$\text{Area of the pressure diagram } ACDE - \text{area of } EFHB + \text{area of } FHBG = 0$$

or

$$P - \tfrac{1}{2}\sigma'_3 L_4 + \tfrac{1}{2}L_5(\sigma'_3 + \sigma'_4) = 0 \tag{18.13}$$

where P is the area of the pressure diagram *ACDE*. Summing the moment of all the forces about point B yields

$$P(L_4 + \bar{z}) - \left(\frac{1}{2}L_4\sigma'_3\right)\left(\frac{L_4}{3}\right) + \frac{1}{2}L_5(\sigma'_3 + \sigma'_4)\left(\frac{L_5}{3}\right) = 0 \tag{18.14}$$

From Eq. (18.13),

$$L_5 = \frac{\sigma'_3 L_4 - 2P}{\sigma'_3 + \sigma'_4} \tag{18.15}$$

Combining Eqs. (18.7), (18.10), (18.14), and (18.15) and simplifying them further, we obtain the following fourth-degree equation in terms of L_4:

$$L_4^4 + A_1 L_4^3 - A_2 L_4^2 - A_3 L_4 - A_4 = 0 \tag{18.16}$$

In this equation,

$$A_1 = \frac{\sigma'_5}{\gamma'(K_p - K_a)} \tag{18.17}$$

$$A_2 = \frac{8P}{\gamma'(K_p - K_a)} \tag{18.18}$$

$$A_3 = \frac{6P[2\bar{z}\gamma'(K_p - K_a) + \sigma'_5]}{\gamma'^2(K_p - K_a)^2} \tag{18.19}$$

$$A_4 = \frac{P(6\bar{z}\sigma_5' + 4P)}{\gamma'^2(K_p - K_a)^2} \tag{18.20}$$

STEP-BY-STEP PROCEDURE FOR OBTAINING THE PRESSURE DIAGRAM

Based on the preceding theory, a step-by-step procedure for obtaining the pressure diagram for a cantilever sheet-pile wall penetrating a granular soil is as follows:

Step 1. Calculate K_a and K_p.

Step 2. Calculate σ_1' [Eq. (18.1)] and σ_2' [Eq. (18.2)]. (*Note:* L_1 and L_2 will be given.)

Step 3. Calculate L_3 [Eq. (18.6)].

Step 4. Calculate P.

Step 5. Calculate $\bar{z}$ (i.e., the center of pressure for the area $ACDE$) by taking the moment about E.

Step 6. Calculate σ_5' [Eq. (18.11)].

Step 7. Calculate A_1, A_2, A_3, and A_4 [Eqs. (18.17) through (18.20)].

Step 8. Solve Eq. (18.16) by trial and error to determine L_4.

Step 9. Calculate σ_4' [Eq. (18.10)].

Step 10. Calculate σ_3' [Eq. (18.7)].

Step 11. Obtain L_5 from Eq. (18.15).

Step 12. Draw a pressure distribution diagram like the one shown in Figure 18.9a.

Step 13. Obtain the theoretical depth [see Eq. (18.12)] of penetration as $L_3 + L_4$. The actual depth of penetration is increased by about 20 to 30%.

Note that some designers prefer to use a factor of safety on the passive earth pressure coefficient at the beginning. In that case, in Step 1,

$$K_{p(\text{design})} = \frac{K_p}{\text{FS}}$$

where FS is the factor of safety (usually between 1.5 and 2).

For this type of analysis, follow Steps 1 through 12 with the value of $K_a = \tan^2(45 - \phi'/2)$ and $K_{p(\text{design})}$ (instead of K_p). The actual depth of penetration can now be determined by adding L_3, obtained from Step 3, and L_4, obtained from Step 8.

CALCULATION OF MAXIMUM BENDING MOMENT

The nature of the variation of the moment diagram for a cantilever sheet-pile wall is shown in Figure 18.9b. The maximum moment will occur between points E and F'. Obtaining the maximum moment ($M_{\max}$) per unit length of the wall requires determining the point of zero shear. For a new axis z' (with origin at point E) for zero shear,

$$P = \tfrac{1}{2}(z')^2(K_p - K_a)\gamma'$$

or

$$z' = \sqrt{\frac{2P}{(K_p - K_a)\gamma'}} \tag{18.21}$$

Once the point of zero shear force is determined (point F'' in Figure 18.9a), the magnitude of the maximum moment can be obtained as

$$M_{max} = P(\bar{z} + z') - [\tfrac{1}{2}\gamma' z'^2(K_p - K_a)](\tfrac{1}{3})z' \tag{18.22}$$

The necessary profile of the sheet piling is then sized according to the allowable flexural stress of the sheet-pile material, or

$$S = \frac{M_{max}}{\sigma_{all}} \tag{18.23}$$

where

S = section modulus of the sheet pile required per unit length of the structure

σ_{all} = allowable flexural stress of the sheet pile

The required sheet pile can be selected on the basis of the section modulus, which is generally provided in the sheet piling catalogs (see Table 18.1).

EXAMPLE 18.1

Figure 18.10 shows a cantilever sheet-pile wall penetrating a granular soil. Here, $L_1 = 2$ m, $L_2 = 3$ m, $\gamma = 15.9$ kN/m^3, $\gamma_{sat} = 19.33$ kN/m^3, and $\phi' = 32°$.

a. What is the theoretical depth of embedment, D?
b. For a 30% increase in D, what should be the total length of the sheet piles?
c. What should be the minimum section modulus of the sheet piles? Use $\sigma_{all} = 172$ MN/m^2. Also select a suitable section from Table 18.1.

SOLUTION

Part a

Using Figure 18.9a for the pressure distribution diagram, one can now prepare the following table for a step-by-step calculation.

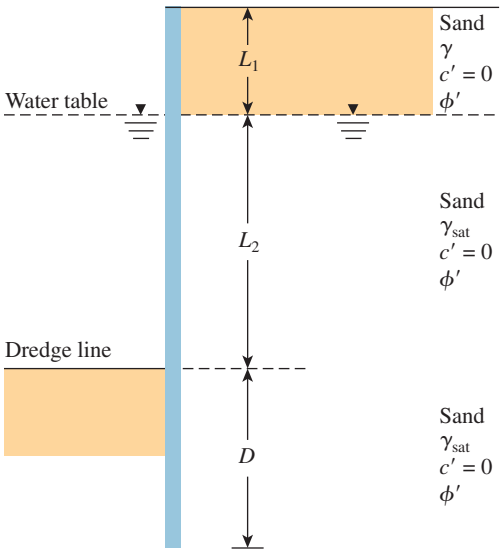


FIGURE 18.10 Cantilever sheet-pile wall

Quantity required	Eq. no.	Equation and calculation
K_a	—	$\tan^2\left(45 - \frac{\phi'}{2}\right) = \tan^2\left(45 - \frac{32}{2}\right) = 0.307$
K_p	—	$\tan^2\left(45 + \frac{\phi'}{2}\right) = \tan^2\left(45 + \frac{32}{2}\right) = 3.25$
σ_1'	18.1	$\gamma L_1 K_a = (15.9)(2)(0.307) = 9.763 \text{ kN/m}^2$
σ_2'	18.2	$(\gamma L_1 + \gamma' L_2)K_a = [(15.9)(2) + (19.33 - 9.81)(3)](0.307) = 18.53 \text{ kN/m}^2$
L_3	18.6	$\frac{\sigma_2'}{\gamma'(K_p - K_a)} = \frac{18.53}{(19.33 - 9.81)(3.25 - 0.307)} = 0.66 \text{ m}$
P	—	$\frac{1}{2}\sigma_1' L_1 + \sigma_1' L_2 + \frac{1}{2}(\sigma_2' - \sigma_1')L_2 + \frac{1}{2}\sigma_2' L_3$ $= \left(\frac{1}{2}\right)(9.763)(2) + (9.763)(3) + \left(\frac{1}{2}\right)(18.53 - 9.763)(3)$ $+ \left(\frac{1}{2}\right)(18.53)(0.66)$ $= 9.763 + 29.289 + 13.151 + 6.115 = 58.32 \text{ kN/m}$
$\bar{z}$	—	$\frac{\Sigma M_E}{P} = \frac{1}{58.32}\left[\begin{array}{l} 9.763(0.66 + 3 + \frac{2}{3}) + 29.289(0.66 + \frac{3}{2}) \\ + 13.151(0.66 + \frac{3}{3}) + 6.115(0.66 \times \frac{2}{3}) \end{array}\right] = 2.23 \text{ m}$
σ_5'	18.11	$(\gamma L_1 + \gamma' L_2)K_p + \gamma' L_3(K_p - K_a) = [(15.9)(2) + (19.33 - 9.81)(3)](3.25)$ $+ (19.33 - 9.81)(0.66)(3.25$ $- 0.307) = 214.66 \text{ kN/m}^2$
A_1	18.17	$\frac{\sigma_5'}{\gamma'(K_p - K_a)} = \frac{214.66}{(19.33 - 9.81)(3.25 - 0.307)} = 7.66 \text{ m}$
A_2	18.18	$\frac{8P}{\gamma'(K_p - K_a)} = \frac{(8)(58.32)}{(19.33 - 9.81)(3.25 - 0.307)} = 16.65 \text{ m}^2$
A_3	18.19	$\frac{6P[2\bar{z}\gamma'(K_p - K_a) + \sigma_5']}{\gamma'^2(K_p - K_a)^2}$ $= \frac{(6)(58.32)[(2)(2.23)(19.33 - 9.81)(3.25 - 0.307) + 214.66]}{(19.33 - 9.81)^2(3.25 - 0.307)^2}$ $= 151.93 \text{ m}^3$
A_4	18.20	$\frac{P(6\bar{z}\sigma_5' + 4P)}{\gamma'^2(K_p - K_a)^2} = \frac{58.32[(6)(2.23)(214.66) + (4)(58.32)]}{(19.33 - 9.81)^2(3.25 - 0.307)^2}$ $= 230.72 \text{ m}^4$
L_4	18.16	$L_4^4 + A_1 L_4^3 - A_2 L_4^2 - A_3 L_4 - A_4 = 0$ $L_4^4 + 7.66 L_4^3 - 16.65 L_4^2 - 151.93 L_4 - 230.72 = 0; L_4 \approx 4.8 \text{ m}$

Thus,

$$D_{\text{theory}} = L_3 + L_4 = 0.66 + 4.8 = \mathbf{5.46 \text{ m}}$$

Part b

The total length of the sheet piles is

$$L_1 + L_2 + 1.3(L_3 + L_4) = 2 + 3 + 1.3(5.46) = \mathbf{12.1 \text{ m}}$$

Part c

Finally, we have the following table.

Quantity required	Eq. no.	Equation and calculation
z'	18.21	$\sqrt{\dfrac{2P}{(K_p - K_a)\gamma'}} = \sqrt{\dfrac{(2)(58.32)}{(3.25 - 0.307)(19.33 - 9.81)}} = 2.04 \text{ m}$
M_{max}	18.22	$P(\bar{z} + z') - \left[\dfrac{1}{2}\gamma' z'^2 (K_p - K_a)\right]\dfrac{z'}{3} = (58.32)(2.23 + 2.04)$ $-\left[\left(\dfrac{1}{2}\right)(19.33 - 9.81)(2.04)^2(3.25 - 0.307)\right]\dfrac{2.04}{3}$ $= 209.39 \text{ kN} \cdot \text{m/m}$
S	18.29	$\dfrac{M_{max}}{\sigma_{all}} = \dfrac{209.39 \text{ kN} \cdot \text{m}}{172 \times 10^3 \text{ kN/m}^2} = \mathbf{1.217 \times 10^{-3} \text{ m}^3\text{/m of wall}}$

From Table 18.1, use PS-31.

18.5 Special Cases for Cantilever Walls Penetrating a Sandy Soil

SHEET-PILE WALL IN DRY SAND

In the absence of the water table, the net pressure diagram on the cantilever sheet-pile wall will be as shown in Figure 18.11, which is a modified version of Figure 18.9. In this case,

$$\sigma_2' = \gamma L K_a \tag{18.24}$$

$$\sigma_3' = L_4(K_p - K_a)\gamma \tag{18.25}$$

$$\sigma_4' = \sigma_5' + \gamma L_4(K_p - K_a) \tag{18.26}$$

$$\sigma_5' = \gamma L K_p + \gamma L_3(K_p - K_a) \tag{18.27}$$

$$L_3 = \frac{\sigma_2'}{\gamma(K_p - K_a)} = \frac{LK_a}{(K_p - K_a)} \tag{18.28}$$

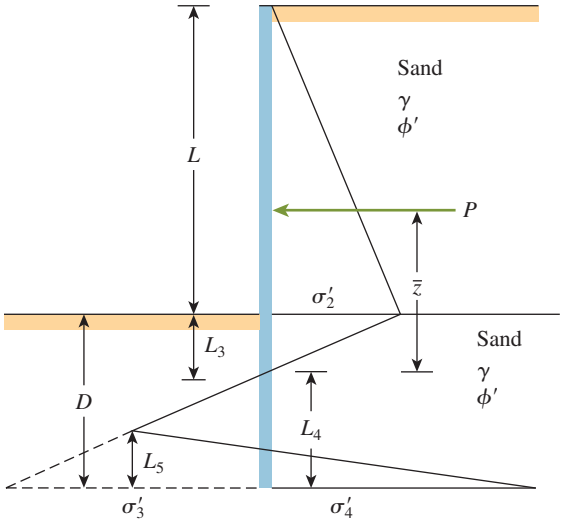


FIGURE 18.11 Sheet piling penetrating a sandy soil in the

$$P = \tfrac{1}{2}\sigma'_2 L + \tfrac{1}{2}\sigma'_2 L_3 \tag{18.29}$$

$$\bar{z} \approx L_3 + \frac{L}{3} = \frac{LK_a}{K_p - K_a} + \frac{L}{3} = \frac{L(2K_a + K_p)}{3(K_p - K_a)} \tag{18.30}$$

and Eq. (18.16) transforms to

$$L_4^4 + A'_1 L_4^3 - A'_2 L_4^2 - A'_3 L_4 - A'_4 = 0 \tag{18.31}$$

where

$$A'_1 = \frac{\sigma'_5}{\gamma(K_p - K_a)} \tag{18.32}$$

$$A'_2 = \frac{8P}{\gamma(K_p - K_a)} \tag{18.33}$$

$$A'_3 = \frac{6P[2\bar{z}\gamma(K_p - K_a) + \sigma'_5]}{\gamma^2(K_p - K_a)^2} \tag{18.34}$$

$$A'_4 = \frac{P(6\bar{z}\sigma'_5 + 4P)}{\gamma^2(K_p - K_a)^2} \tag{18.35}$$

It can be seen that Eqs. (18.16) and (18.31) are of the same form. Replacing the submerged unit weights in Eqs. (18.17) to (18.20) by the bulk unit weight gives Eqs. (18.32) to (18.35).

FREE CANTILEVER SHEET PILING

Figure 18.12 shows a free cantilever sheet-pile wall penetrating a sandy soil and subjected to a line load of P per unit length of the wall. For this case,

$$D^4 - \left[\frac{8P}{\gamma(K_p - K_a)}\right]D^2 - \left[\frac{12PL}{\gamma(K_p - K_a)}\right]D - \left[\frac{2P}{\gamma(K_p - K_a)}\right]^2 = 0 \tag{18.36}$$

$$L_5 = \frac{\gamma(K_p - K_a)D^2 - 2P}{2D(K_p - K_a)\gamma} \tag{18.37}$$

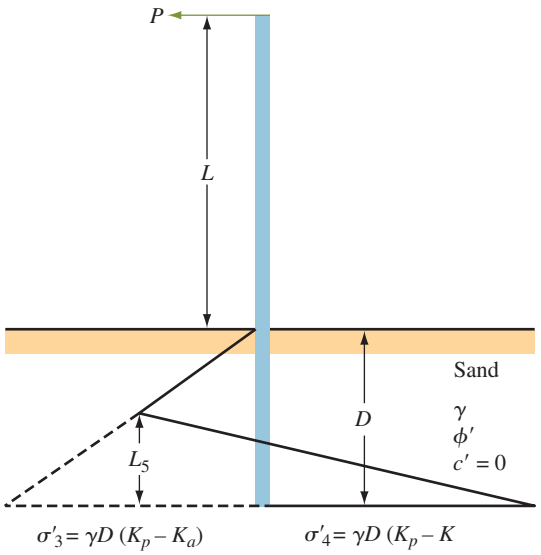


FIGURE 18.12 Free cantilever sheet piling penetrating a layer

$$M_{max} = P(L + z') - \frac{\gamma z'^3 (K_p - K_a)}{6} \tag{18.38}$$

and

$$z' = \sqrt{\frac{2P}{\gamma(K_p - K_a)}} \tag{18.39}$$

Equations (18.37) to (18.39) are also valid for the previous case, where dry sand is present to the entire height above the excavation level on the right side, shown in Figure 18.11.

EXAMPLE 18.2

Redo parts a and b of Example 18.1, assuming the absence of the water table. Use $\gamma = 15.9$ kN/m^3 and $\phi' = 32°$. *Note:* $L = 5$ m.

SOLUTION

Part a

Quantity required	Eq. no.	Equation and calculation
K_a	—	$\tan^2\left(45 - \frac{\phi'}{2}\right) = \tan^2\left(45 - \frac{32}{2}\right) = 0.307$
K_p	—	$\tan^2\left(45 + \frac{\phi'}{2}\right) = \tan^2\left(45 + \frac{32}{2}\right) = 3.25$
σ'_2	18.24	$\gamma L K_a = (15.9)(5)(0.307) = 24.41$ kN/m^2
L_3	18.28	$\frac{LK_a}{K_p - K_a} = \frac{(5)(0.307)}{3.25 - 0.307} = 0.521$ m
σ'_5	18.27	$\gamma L K_p + \gamma L_3 (K_p - K_a) = (15.9)(5)(3.25) + (15.9)(0.521)(3.25 - 0.307)$ $= 282.76$ kN/m^2
P	18.29	$\frac{1}{2}\sigma'_2 L + \frac{1}{2}\sigma'_2 L_3 = \frac{1}{2}\sigma'_2 (L + L_3) = (\frac{1}{2})(24.41)(5 + 0.521) = 67.38$ kN/m
$\bar{z}$	18.30	$\frac{L(2K_a - K_p)}{3(K_p - K_a)} = \frac{5[(2)(0.307) + 3.25]}{3(3.25 - 0.307)} = 2.188$ m
A'_1	18.32	$\frac{\sigma'_5}{\gamma(K_p - K_a)} = \frac{282.76}{(15.9)(3.25 - 0.307)} = 6.04$ m
A'_2	18.33	$\frac{8P}{\gamma(K_p - K_a)} = \frac{(8)(67.38)}{(15.9)(3.25 - 0.307)} = 11.52$ m^2
A'_3	18.34	$\frac{6P[2\bar{z}\gamma(K_p - K_a) + \sigma'_5]}{\gamma^2(K_p - K_a)^2}$ $= \frac{(6)(67.38)[(2)(2.188)(15.9)(3.25 - 0.307) + 282.76]}{(15.9)^2(3.25 - 0.307)^2} = 90.01$ m^3
A'_4	18.35	$\frac{P(6\bar{z}\sigma'_5 + 4P)}{\gamma^2(K_p - K_a)^2} = \frac{(67.38)[(6)(2.188)(282.76) + (4)(67.38)]}{(15.9)^2(3.25 - 0.307)^2} = 122.52$ m^4
L_4	18.31	$L_4^4 + A'_1 L_4^3 - A'_2 L_4^2 - A'_3 L_4 - A'_4 = 0$ $L_4^4 + 6.04 L_4^3 - 11.52 L_4^2 - 90.01 L_4 - 122.52 = 0$; $L_4 \approx 4.1$ m

$$D_{theory} = L_3 + L_4 = 0.521 + 4.1 \approx \mathbf{4.7\ m}$$

Part b

Total length, $L + 1.3(D_{theory}) = 5 + 1.3(4.7) = \mathbf{11.11\ m.}$

■

EXAMPLE 18.3

Refer to Figure 18.12. For $L = 5$ m, $\gamma = 17.3$ kN/m^3, $\phi' = 30°$, and $P = 30$ kN/m, determine:

a. The theoretical depth of penetration, D
b. The maximum moment, M_{max} kN · m/m

SOLUTION

$$K_p = \tan^2\left(45 + \frac{\phi'}{2}\right) = \tan^2\left(45 + \frac{30}{2}\right) = 3$$

$$K_a = \tan^2\left(45 - \frac{\phi'}{2}\right) = \tan^2\left(45 - \frac{30}{2}\right) = \frac{1}{3}$$

$$K_p - K_a = 3 - 0.333 = 2.667$$

Part a

From Eq. (18.36),

$$D^4 - \left[\frac{8P}{\gamma(K_p - K_a)}\right]D^2 - \left[\frac{12PL}{\gamma(K_p - K_a)}\right]D - \left[\frac{2P}{\gamma(K_p - K_a)}\right]^2 = 0$$

and

$$\frac{8P}{\gamma(K_p - K_a)} = \frac{(8)(30)}{(17.3)(2.667)} = 5.2$$

$$\frac{12PL}{\gamma(K_p - K_a)} = \frac{(12)(30)(5)}{(17.3)(2.667)} = 39.0$$

$$\frac{2P}{\gamma(K_p - K_a)} = \frac{(2)(30)}{(17.3)(2.667)} = 1.3$$

so

$$D^4 - 5.2D^2 - 39D - (1.3)^2 = 0$$

From the preceding equation, $D \approx 4$ m.

Part b

From Eq. (18.39),

$$z' = \sqrt{\frac{2P}{\gamma(K_p - K_a)}} = \sqrt{\frac{(2)(30)}{(17.3)(2.667)}} = 1.14 \text{ m}$$

From Eq. (18.38),

$$M_{max} = P(L + z') - \frac{\gamma z'^3(K_p - K_a)}{6}$$

$$= (30)(5 + 1.14) - \frac{(17.3)(1.14)^3(2.667)}{6}$$

$$= 184.2 - 11.39 \approx \mathbf{173\,kN \cdot m/m}$$

18.6 Cantilever Sheet Piling Penetrating Clay

At times, cantilever sheet piles must be driven into a clay layer possessing an undrained cohesion $c(\phi = 0)$. The net pressure diagram will be somewhat different from that shown in Figure 18.9a, which is for granular soil with $c' = 0$. Figure 18.13 shows a cantilever sheet-pile wall driven into clay with a backfill of granular soil

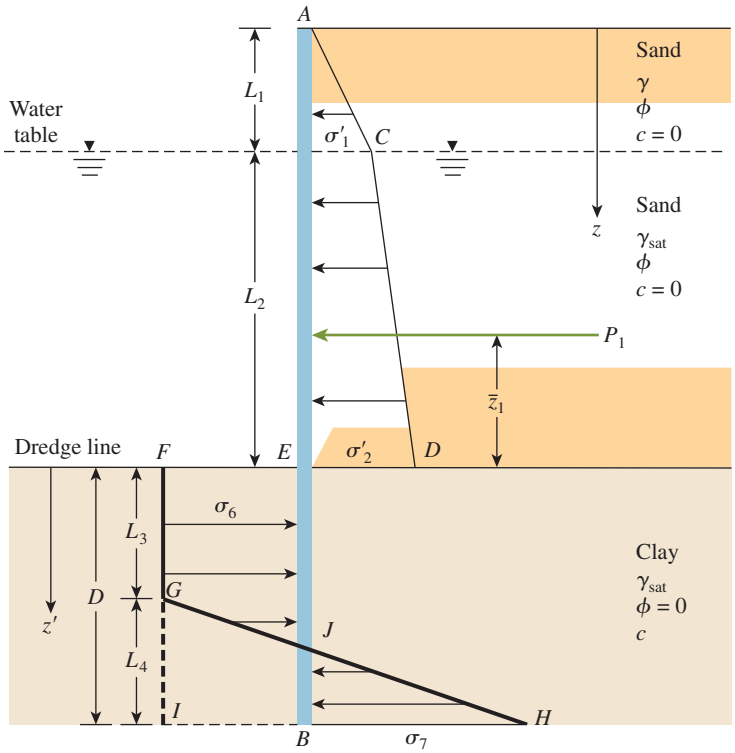


FIGURE 18.13 Cantilever sheet pile penetrating clay

above the level of the dredge line. The water table is at a depth L_1 below the top of the wall. As before, Eqs. (18.1) and (18.2) give the intensity of the net pressures σ'_1 and σ'_2, and the diagram for pressure distribution above the level of the dredge line can be drawn. The diagram for net pressure distribution below the dredge line can now be determined as follows.

At any depth greater than $L_1 + L_2$, for $\phi = 0$, the Rankine active earth-pressure coefficient $K_a = 1$. Similarly, for $\phi = 0$, the Rankine passive earth-pressure coefficient $K_p = 1$. Thus, above the point of rotation (point O in Figure 18.8a), the active pressure, from right to left, is

$$\sigma_a = [\gamma L_1 + \gamma' L_2 + \gamma_{sat}(z - L_1 - L_2)] - 2c \tag{18.40}$$

Similarly, the passive pressure from left to right may be expressed as

$$\sigma_p = \gamma_{sat}(z - L_1 - L_2) + 2c \tag{18.41}$$

Thus, the net pressure is

$$\begin{aligned}\sigma_6 = \sigma_p - \sigma_a &= [\gamma_{sat}(z - L_1 - L_2) + 2c] \\ &\quad - [\gamma L_1 + \gamma' L_2 + \gamma_{sat}(z - L_1 - L_2)] + 2c \\ &= 4c - (\gamma L_1 + \gamma' L_2)\end{aligned} \tag{18.42}$$

At the bottom of the sheet pile, the passive pressure from right to left is

$$\sigma_p = (\gamma L_1 + \gamma' L_2 + \gamma_{sat} D) + 2c \tag{18.43}$$

Similarly, the active pressure from left to right is

$$\sigma_a = \gamma_{sat} D - 2c \tag{18.44}$$

Hence, the net pressure is

$$\sigma_7 = \sigma_p - \sigma_a = 4c + (\gamma L_1 + \gamma' L_2) \tag{18.45}$$

As before, let's include the area *IBJG* on both sides of the pressure diagram to make the solution simpler. For equilibrium analysis, $\Sigma F_H = 0$; that is, the area of the pressure diagram *ACDE* minus the area of *EFIB* plus the area of *GIH* = 0, or

$$P_1 - [4c - (\gamma L_1 + \gamma' L_2)]D + \tfrac{1}{2}L_4[4c - (\gamma L_1 + \gamma' L_2) + 4c + (\gamma L_1 + \gamma' L_2)] = 0$$

where P_1 = area of the pressure diagram *ACDE*.

Simplifying the preceding equation produces

$$L_4 = \frac{D[4c - (\gamma L_1 + \gamma' L_2)] - P_1}{4c} \tag{18.46}$$

Now, taking the moment about point B ($\Sigma M_B = 0$) yields

$$P_1(D + \bar{z}_1) - [4c - (\gamma L_1 + \gamma' L_2)]\frac{D^2}{2} + \frac{1}{2}L_4(8c)\left(\frac{L_4}{3}\right) = 0 \tag{18.47}$$

where $\bar{z}_1$ = distance of the center of pressure of the pressure diagram *ACDE*, measured from the level of the dredge line.

Combining Eqs. (18.46) and (18.47) yields

$$D^2[4c - (\gamma L_1 + \gamma' L_2)] - 2DP_1 - \frac{P_1(P_1 + 12c\bar{z}_1)}{(\gamma L_1 + \gamma' L_2) + 2c} = 0 \tag{18.48}$$

Equation (18.48) may be solved to obtain D, the theoretical depth of penetration of the clay layer by the sheet pile.

STEP-BY-STEP PROCEDURE FOR OBTAINING THE PRESSURE DIAGRAM

Step 1. Calculate $K_a = \tan^2(45 - \phi'/2)$ for the granular soil (backfill).

Step 2. Obtain σ_1' and σ_2'. [See Eqs. (18.1) and (18.2).]

Step 3. Calculate P_1 and $\bar{z}_1$.

Step 4. Use Eq. (18.48) to obtain the theoretical value of D.

Step 5. Using Eq. (18.46), calculate L_4.

Step 6. Calculate σ_6 and σ_7. [See Eqs. (18.42) and (18.45).]

Step 7. Draw the pressure distribution diagram as shown in Figure 18.13.

Step 8. The actual depth of penetration is

$$D_{\text{actual}} = 1.4 \text{ to } 1.6(D_{\text{theoretical}})$$

MAXIMUM BENDING MOMENT

According to Figure 18.13, the maximum moment (zero shear) will be between $L_1 + L_2 < z < L_1 + L_2 + L_3$. Using a new coordinate system z' (with $z' = 0$ at the dredge line) for zero shear gives

$$P_1 - \sigma_6 z' = 0$$

or

$$z' = \frac{P_1}{\sigma_6} \tag{18.49}$$

The magnitude of the maximum moment may now be obtained:

$$M_{max} = P_1(z' + \bar{z}_1) - \frac{\sigma_6 z'^2}{2} \tag{18.50}$$

Knowing the maximum bending moment, we determine the section modulus of the sheet-pile section from Eq. (18.23).

EXAMPLE 18.4

In Figure 18.14, for the sheet-pile wall, determine

a. The theoretical and actual depth of penetration. Use $D_{actual} = 1.5D_{theory}$.
b. The minimum size of sheet-pile section necessary. Use $\sigma_{all} = 172.5$ MN/m^2.

SOLUTION

We will follow the step-by-step procedure given in Section 18.6.

Step 1.

$$K_a = \tan^2\left(45 - \frac{\phi'}{2}\right) = \tan^2\left(45 - \frac{32}{2}\right) = 0.307$$

Step 2.

$$\sigma_1' = \gamma L_1 K_a = (15.9)(2)(0.307) = 9.763 \text{ kN/m}^2$$
$$\sigma_2' = (\gamma L_1 + \gamma' L_2)K_a = [(15.9)(2) + (19.33 - 9.81)3]0.307$$
$$= 18.53 \text{ kN/m}^2$$

Step 3. From the net pressure distribution diagram given in Figure 18.13, we have

$$P_1 = \frac{1}{2}\sigma_1' L_1 + \sigma_1' L_2 + \frac{1}{2}(\sigma_2' - \sigma_1')L_2$$
$$= 9.763 + 29.289 + 13.151 = 52.2 \text{ kN/m}$$

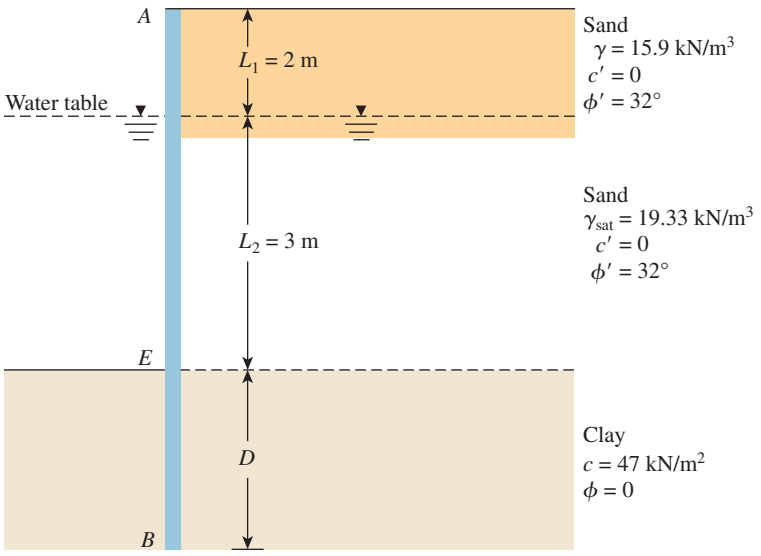


FIGURE 18.14 Cantilever sheet pile penetrating into saturated clay

and

$$\bar{z}_1 = \frac{1}{52.2}\left[9.763\left(3 + \frac{2}{3}\right) + 29.289\left(\frac{3}{2}\right) + 13.151\left(\frac{3}{3}\right)\right]$$
$$= 1.78 \text{ m}$$

Step 4. From Eq. (18.48),

$$D^2[4c - (\gamma L_1 + \gamma' L_2)] - 2DP_1 - \frac{P_1(P_1 + 12c\bar{z}_1)}{(\gamma L_1 + \gamma' L_2) + 2c} = 0$$

Substituting proper values yields

$$D^2\{(4)(47) - [(2)(15.9) + (19.33 - 9.81)3]\} - 2D(52.2)$$
$$- \frac{52.2[52.2 + (12)(47)(1.78)]}{[(15.9)(2) + (19.33 - 9.81)3] + (2)(47)} = 0$$

or

$$127.64D^2 - 104.4D - 357.15 = 0$$

Solving the preceding equation, we obtain $D = 2.13$ m.

Step 5. From Eq. (18.46),

$$L_4 = \frac{D[4c - (\gamma L_1 + \gamma' L_2)] - P_1}{4c}$$

and

$$4c - (\gamma L_1 + \gamma' L_2) = (4)(47) - [(15.9)(2) + (19.33 - 9.81)3]$$
$$= 127.64 \text{ kN/m}^2$$

So,

$$L_4 = \frac{2.13(127.64) - 52.2}{(4)(47)} = 1.17 \text{ m}$$

Step 6.

$$\sigma_6 = 4c - (\gamma L_1 + \gamma' L_2) = 127.64 \text{ kN/m}^2$$
$$\sigma_7 = 4c + (\gamma L_1 + \gamma' L_2) = 248.36 \text{ kN/m}^2$$

Step 7. The net pressure distribution diagram can now be drawn, as shown in Figure 18.13.

Step 8. $D_{\text{actual}} \approx 1.5\, D_{\text{theoretical}} = 1.5(2.13) \approx \mathbf{3.2\ m}$

Maximum Moment Calculation

From Eq. (18.49),

$$z' = \frac{P_1}{\sigma_6} = \frac{52.2}{127.64} \approx 0.41 \text{ m}$$

Again, from Eq. (18.49),

$$M_{\max} = P_1(z' + \bar{z}_1) - \frac{\sigma_6 z'^2}{2}$$

So

$$M_{\max} = 52.2(0.41 + 1.78) - \frac{127.64(0.41)^2}{2}$$
$$= 114.32 - 10.73 = 103.59 \text{ kN·m/m}$$

The minimum required section modulus (assuming that $\sigma_{all} = 172.5\ \text{MN/m}^2$) is

$$S = \frac{103.59\ \text{kN}\cdot\text{m/m}}{172.5 \times 10^3\ \text{kN/m}^2} = \mathbf{0.6 \times 10^{-3}\ m^3/m\ of\ the\ wall}$$

18.7 Special Cases for Cantilever Walls Penetrating Clay

SHEET-PILE WALL WITH DRY SAND BACKFILL

As in Section 18.5, relationships for special cases for cantilever walls penetrating clay may also be derived. Referring to Figure 18.15, we can write

$$\sigma_2' = \gamma L K_a \tag{18.51}$$

$$\sigma_6 = 4c - \gamma L \tag{18.52}$$

$$\sigma_7 = 4c + \gamma L \tag{18.53}$$

$$P_1 = \tfrac{1}{2} L \sigma_2' = \tfrac{1}{2}\gamma L^2 K_a \tag{18.54}$$

and

$$L_4 = \frac{D(4c - \gamma L) - \frac{1}{2}\gamma L^2 K_a}{4c} \tag{18.55}$$

The theoretical depth of penetration, D, can be calculated [in a manner similar to the calculation of Eq. (18.48)] as

$$D^2(4c - \gamma L) - 2DP_1 - \frac{P_1(P_1 + 12c\bar{z}_1)}{\gamma L + 2c} = 0 \tag{18.56}$$

It is possible to deduce Eq. (18.56) from Eq. (18.48). In Eq. (18.56),

$$\bar{z}_1 = \frac{L}{3} \tag{18.57}$$

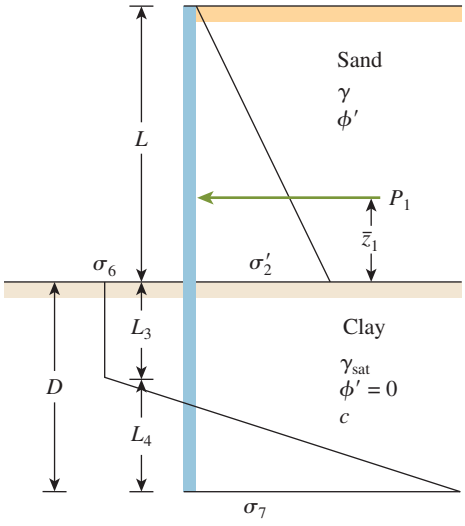


FIGURE 18.15 Sheet-pile wall penetrating clay

The magnitude of the maximum moment in the wall is

$$M_{\max} = P_1(z' + \bar{z}_1) - \frac{\sigma_6 z'^2}{2} \tag{18.58}$$

where $z' = \dfrac{P_1}{\sigma_6} = \dfrac{\frac{1}{2}\gamma L^2 K_a}{4c - \gamma L}$. (18.59)

FREE CANTILEVER SHEET-PILE WALL PENETRATING CLAY

Figure 18.16 shows a free cantilever sheet-pile wall penetrating a clay layer. The wall is being subjected to a line load of P per unit length. For this case,

$$\sigma_6 = \sigma_7 = 4c \tag{18.60}$$

The depth of penetration, D, may be obtained from the relation

$$4D^2c - 2PD - \frac{P(P + 12cL)}{2c} = 0 \tag{18.61}$$

Also note that for a construction of the pressure diagram,

$$L_4 = \frac{4cD - P}{4c} \tag{18.62}$$

The maximum moment in the wall is

$$M_{\max} = P(L + z') - \frac{4cz'^2}{2} \tag{18.63}$$

where

$$z' = \frac{P}{4c} \tag{18.64}$$

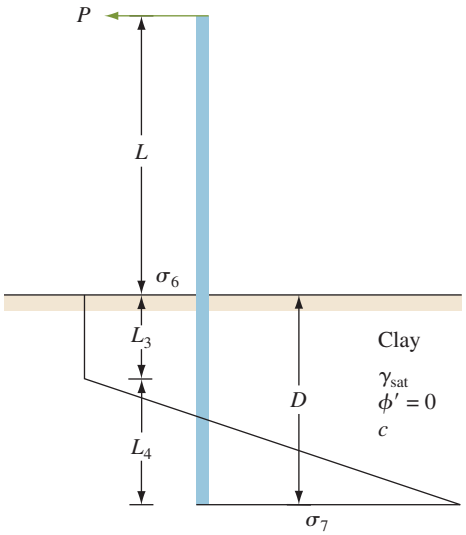


FIGURE 18.16 Free cantilever sheet piling penetrating clay

EXAMPLE 18.5

Refer to the free cantilever sheet-pile wall shown in Figure 18.16, for which $P = 32$ kN/m, $L = 3.5$ m, and $c = 12$ kN/m^2. Calculate the theoretical depth of penetration.

SOLUTION

From Eq. (18.61),

$$4D^2c - 2PD - \frac{P(P + 12cL)}{2c} = 0$$

$$(4)(D^2)(12) - (2)(32)(D) - \frac{32[32 + (12)(12)(3.5)]}{(2)(12)} = 0$$

$$48D^2 - 64D - 714.7 = 0$$

Hence $D \approx$ **4.6 m.**

EXAMPLE 18.6

Refer to Figure 18.15 for the sheet-pile wall penetrating clay. Given:

Sand: $L = 6$ m, $\gamma = 16$ kN/m^3, $\phi' = 30°$

Clay: $\gamma_{sat} = 18.9$ kN/m^3, $\phi' = 0$, $c = 95$ kN/m^2

Determine:

a. The theoretical depth of penetration D
b. The magnitude of the maximum moment in the wall

SOLUTION

Part a

From Eq. (18.54),

$$P_1 = \frac{1}{2}\gamma L^2 K_a$$

$$K_a = \tan^2\left(45 - \frac{\phi'}{2}\right) = \tan^2\left(45 - \frac{30}{2}\right) = \frac{1}{3}$$

$$P_1 = \left(\frac{1}{2}\right)(16)(6)^2\left(\frac{1}{3}\right) = 96 \text{ kN/m}$$

From Eq. (18.56),

$$D^2(4c - \gamma L) - 2DP_1 - \frac{P_1(P_1 + 12c\bar{z}_1)}{\gamma L + 2c} = 0$$

From Eq. (18.57),

$$\bar{z}_1 = \frac{L}{3} = \frac{6}{3} = 2 \text{ m}$$

Hence,

$$D^2[(4)(95) - (16)(6)] - (2)(D)(96) - \frac{96[96 + (12)(95)(2)]}{(16)(6) + (2)(95)} = 0$$

or

$$284\,D^2 - 192\,D - 797.5 = 0$$

$$D \approx \mathbf{2.1\,m}$$

Part b

From Eq. (18.58),

$$M_{\max} = P_1(z' + \bar{z}_1) - \frac{\sigma_6 z'^2}{2}$$

From Eq. (18.59),

$$z' = \frac{\frac{1}{2}\gamma L^2 K_a}{4c - \gamma L} = \frac{(0.5)(16)(6)^2\left(\frac{1}{3}\right)}{(4 \times 95) - (16 \times 6)} = 0.338\,\text{m}$$

From Eq. (18.52),

$$\sigma_6 = 4c - \gamma L = (4 \times 95) - (16 \times 6) = 284\,\text{kN/m}^2$$

$$M_{\max} = (96)(0.338 + 2) - \frac{(284)(0.338)^2}{2} = 224.45 - 16.22 = \mathbf{208.23\,kN \cdot m/m}$$

18.8 Cantilever Sheet Piles Penetrating Sandy Soil—A Simplified Approach

Consider a cantilever sheet pile in *dry granular soil* with a unit weight of γ and friction angle of ϕ'. The sheet pile is driven to a depth of $L + D$, and excavation is carried out to a depth of L. When the sheet-pile wall deflects toward left as a result of the excavation, it rotates about a point O near the tip (Figure 18.17a) that is at a depth of D_o below the excavation level. The top of the sheet pile moves from A to A', and the bottom tip moves from B to B'. Assuming that there is enough movement to mobilize active and passive resistance in the surrounding soil, it is possible to define these zones as shown in Figure 18.17b, based on the directions of wall movements. The lateral pressure distribution on both sides of the sheet pile is shown in Figure 18.17c.

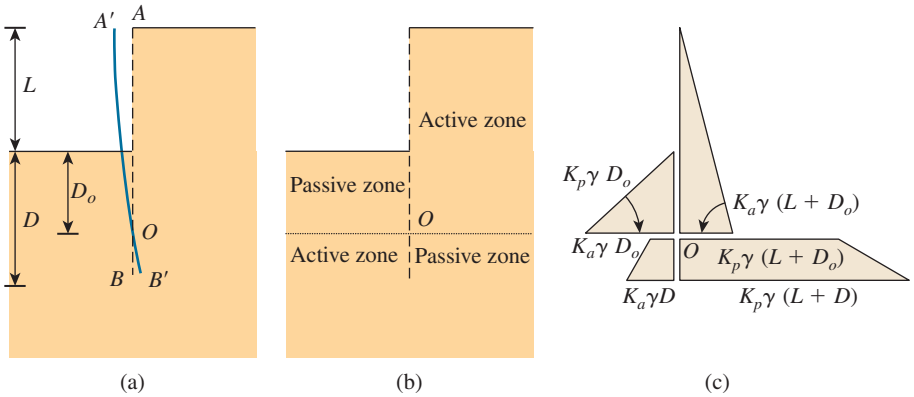


FIGURE 18.17 Analysis of cantilever sheet pile: (a) original and deflected positions; (b) active and passive zones; (c) lateral pressure distribution

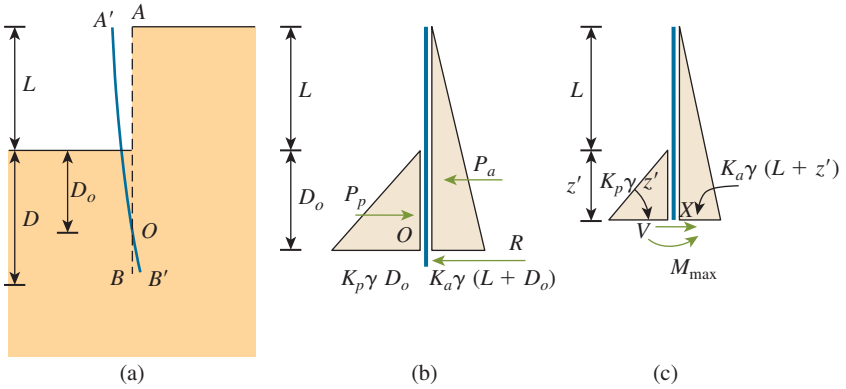


FIGURE 18.18 Simplified analysis: (a) original and deflected positions; (b) approximate lateral pressure distribution; and (c) maximum bending moment analysis

It can be assumed that the point of rotation O is close to the tip of the sheet pile B and that the lateral pressure distribution below O is replaced by a horizontal point load (R) acting at O. With this simplification, the lateral pressure distribution reduces to the one shown in Figure 18.18b, which is the basis for the design of cantilever sheet piles. Here, the sheet pile is in equilibrium under three forces: active thrust P_a, passive thrust P_p, and horizontal reaction R, where $P_a = \frac{1}{2}K_a\gamma(L + D_o)^2$ and $P_p = \frac{1}{2}K_p\gamma D_o^2$.

Taking the moment about O,

$$P_a\left(\frac{L + D_o}{3}\right) = P_p\frac{D_o}{3}$$

$$\frac{1}{2}K_a\gamma(L + D_o)^2\left(\frac{L + D_o}{3}\right) = \frac{1}{2}K_p\gamma D_o^2\frac{D_o}{3}$$

Therefore,

$$D_o = \frac{L}{\sqrt[3]{\frac{K_p}{K_a}} - 1} \tag{18.65}$$

From the friction angle of the granular soil and L, D_o can be determined. The maximum bending moment in the sheet pile occurs below the excavation line where the shear force is zero. This depth (z') below the excavation line can be determined from equilibrium consideration of the horizontal forces (Figure 18.18c). The shear force at depth z' is given by

$$V = \frac{1}{2}K_a\gamma(L + z')^2 - \frac{1}{2}K_p\gamma z'^2 = 0$$

Therefore,

$$z' = \frac{L}{\sqrt{\frac{K_p}{K_a}} - 1} \tag{18.66}$$

Taking the moment about X in Figure 18.18c, the maximum bending moment can be computed as

$$M_{max} = \frac{1}{6}\gamma[K_a(L + z')^3 - K_p z'^3] \tag{18.67}$$

From Eq. (18.23), the section modulus (S) required for the cross section of the sheet pile can be determined.

With all the approximations made, we have not yet incorporated any safety factor in the analysis. It can be done in two ways:

a. Increase the value of D_o computed by 20−40%, or
b. Provide a factor of safety (FS) of 1.5–2.0 on the passive resistance and use K_p/FS. Here we assume that a fraction of passive resistance is mobilized and hence do not rely on the full passive resistance for stability.

EXAMPLE 18.7

A 4 m deep excavation is to be carried out in dry sand where $\phi' = 34°$ and $\gamma = 18\ \text{kN/m}^3$. Determine the depth of penetration required for the sheet pile using (a) the net lateral pressure diagram and (b) the simplified approach.

SOLUTION

$$\phi' = 34° \rightarrow K_a = 0.283 \text{ and } K_p = 3.537$$

Part a: Using the net pressure diagram (see Figure 18.11),

$$\sigma'_2 = \gamma L K_a = 18 \times 4 \times 0.283 = 20.4\ \text{kN/m}^2$$

$$(K_p - K_a)(\gamma) = (3.537 - 0.283)(18) = 58.6\ \text{kN/m}^2$$

$$L_3 = \frac{K_a}{K_p - K_a} L = \frac{0.283}{3.537 - 0.283} \times 4 = 0.35\ \text{m}$$

$$P = 0.5 \times 20.4 + 0.5 \times 20.4 \times 0.35 = 40.8 + 3.57 = 44.37\ \text{kN/m}$$

$$\bar{z} = \frac{40.8 \times 1.683 + 3.57 \times 0.233}{44.37} = 1.57\ \text{m}$$

$\bar{z}$ can be approximated as [Eq. (18.30)]

$$\bar{z} = L_3 + \frac{L}{3} = 0.35 + \frac{4.0}{3} = 1.68\ \text{m}$$

$$\sigma'_5 = K_p \gamma L + (K_p - K_a)\gamma L_3$$
$$= 3.537 \times 18 \times 4 + (3.537 - 0.283) \times 18 \times 0.35 = 275.16\ \text{kN/m}^2$$

$$A'_1 = \frac{\sigma'_5}{\gamma(K_p - K_a)} = \frac{275.16}{18(3.537 - 0.283)} = 4.70\ \text{m}$$

$$A'_2 = \frac{8P}{\gamma(K_p - K_a)} = \frac{8 \times 44.37}{18(3.537 - 0.283)} = 6.06\ \text{m}^2$$

$$A'_3 = \frac{6P[2\bar{z}\gamma(K_p - K_a) + \sigma'_5]}{\gamma^2(K_p - K_a)^2}$$
$$= \frac{6 \times 44.37 \times [2 \times 1.57 \times 18(3.537 - 0.283) + 275.16]}{18^2 \times (3.537 - 0.283)^2} = 35.62\ \text{m}^3$$

$$A'_4 = \frac{P(6\bar{z}\sigma'_5 + 4P)}{\gamma^2(K_p - K_a)^2} = \frac{44.37(6 \times 1.57 \times 275.16 + 4 \times 44.37)}{18^2 \times (3.537 - 0.283)^2} = 35.82\ \text{m}^4$$

Therefore, Eq. (18.31) becomes

$$L_4^4 + 4.70L_4^3 - 6.06L_4^2 - 35.62L_4 - 35.82 = 0$$

By trial and error, $L_4 = 2.93$ m.

$$D = L_4 + L_3 = 2.93 + 0.35 = \mathbf{3.28\ m}$$

Part b: Using the simplified analysis and hence applying Eq. (18.65),

$$D = D_o = \frac{L}{\sqrt[3]{\frac{K_p}{K_a}} - 1} = \frac{4}{\sqrt[3]{\frac{3.537}{0.283}} - 1} = \mathbf{3.03\ m}$$

In the preceding equation, D, determined from both methods, has to be increased by 20–40%.

Note: When the water table or more than one soil layer is present, there will be breaks in the lateral pressure diagram, but the concepts remain the same. Example 18.8 illustrates the simplified approach for such a situation.

EXAMPLE 18.8

In a sandy soil ($\phi' = 33°$; $\gamma = 17.0$ kN/m^3, and $\gamma_{sat} = 19.0$ kN/m^3), the water table is located at a depth of 5 m below the ground level. How deep would you drive a sheet pile to carry out an excavation to a 4.0 m depth? Use the simplified approach discussed in Section 18.8, with a factor of safety of 1.5 on passive resistance (i.e., use $K_p/1.5$).

SOLUTION

$\phi' = 33° \rightarrow K_a = 0.295$, $K_p = 3.392$ and $K_p/\text{FS} = 3.392/1.5 = 2.261$. Also, $\gamma' = 19 - 9.81 = 9.19$ kN/m^3.

The right side of the sheet pile is in active state and the left is in passive state. The lateral earth pressure variation with depth is shown in the figure. There is also a horizontal reaction R at the bottom of the sheet pile (see Figure 18.18b) for equilibrium.

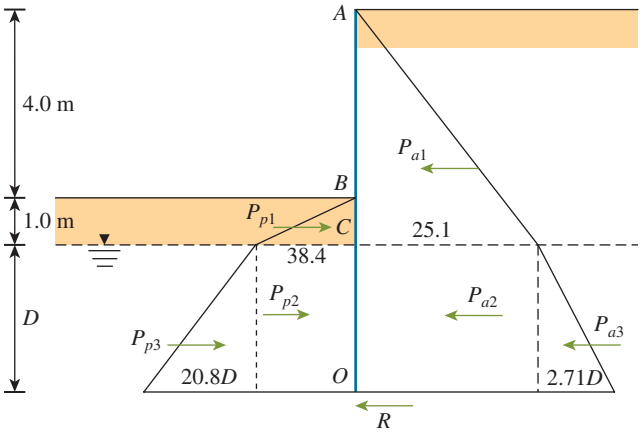
At C, the active earth pressure is $(0.295)(5 \times 17) = 25.1$ kN/m^2.

At C, the passive earth pressure is $(2.261)(1 \times 17) = 38.4$ kN/m^2.

At the bottom of the sheet pile O,

the active earth pressure is $(0.295)(5 \times 17 + 9.19D) = 25.1 + 2.71D$, and

the passive earth pressure is $(2.261)(1 \times 17 + 9.19D) = 38.4 + 20.8D$.



Note: All stresses are in kN/m^2

FIGURE 18.19 Solution by simplified approach

The lateral earth pressure diagram is shown Figure 18.19. Now, we divide the earth pressure loads into six separate components as shown.

Horizontal load (kN/m)	Height above O (m)	Moment about O (kN · m/m)
$P_{a1} = 0.5 \times 5 \times 25.1 = 62.75$	$D + 1.67$	$62.75D + 104.8$
$P_{a2} = D \times 25.1 = 25.1D$	$0.5D$	$12.55D^2$
$P_{a3} = 0.5 \times 2.71D \times D = 1.355D^2$	$0.33D$	$0.45D^3$
$P_{p1} = 0.5 \times 1 \times 38.4 = 19.2$	$D + 0.33$	$19.2D + 6.39$
$P_{p2} = D \times 38.4 = 38.4D$	$0.5D$	$19.2D^2$
$P_{p3} = 0.5 \times 20.8D \times D = 10.4D^2$	$0.33D$	$3.47D^3$

Taking the moment about O,

$$\Sigma M_o = (62.75D + 104.8) + (12.55D^2) + (0.45D^3) - (19.2D + 6.39) - (19.2D^2) - (3.47D^3) = 0$$

$$3.02D^3 + 6.70D^2 + 43.55D - 98.4 = 0$$

$$D = 3.75 \text{ m}$$

The sheet pile should be driven to a depth of 8.75 m.

18.9 Anchored Sheet-Pile Walls

When the excavations get deeper than about 6 m (≈20 ft), the loadings on the sheet piles increase significantly, resulting in larger bending moments and larger depths of embedment (D), making it necessary to go for thicker sections, which can become uneconomical. The depth of embedment and the section can be reduced significantly by anchoring the sheet pile as shown in Figure 18.20a. Such *anchored sheet piles* or *anchored bulkheads* are commonly used in waterfront structures. Here the tie rod is attached to the sheet pile and anchored at the other end using a *deadman*, batter piles, sheet piles, etc. A deadman is simply a concrete block that provides anchorage to a tie rod. It can also be in the form of a *continuous beam* to which all tie rods are connected. There are two different methods to design an anchored sheet pile: (a) the *free earth support* method and (b) the *fixed earth support* method.

The free earth support method assumes that the sheet pile is not deep enough to provide fixity at the bottom and allows rotation at the bottom tip of the sheet pile. The simplified approach discussed in Section 18.8 is used here to show the lateral earth

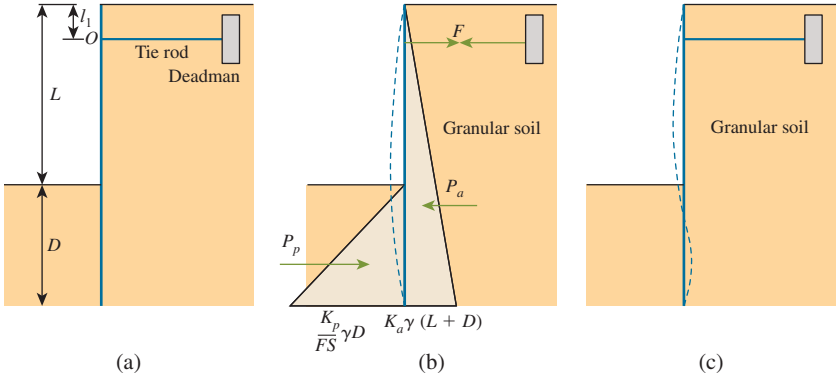


FIGURE 18.20 Anchored sheet pile: (a) anchored using a deadman; (b) free earth support; (c) fixed earth support

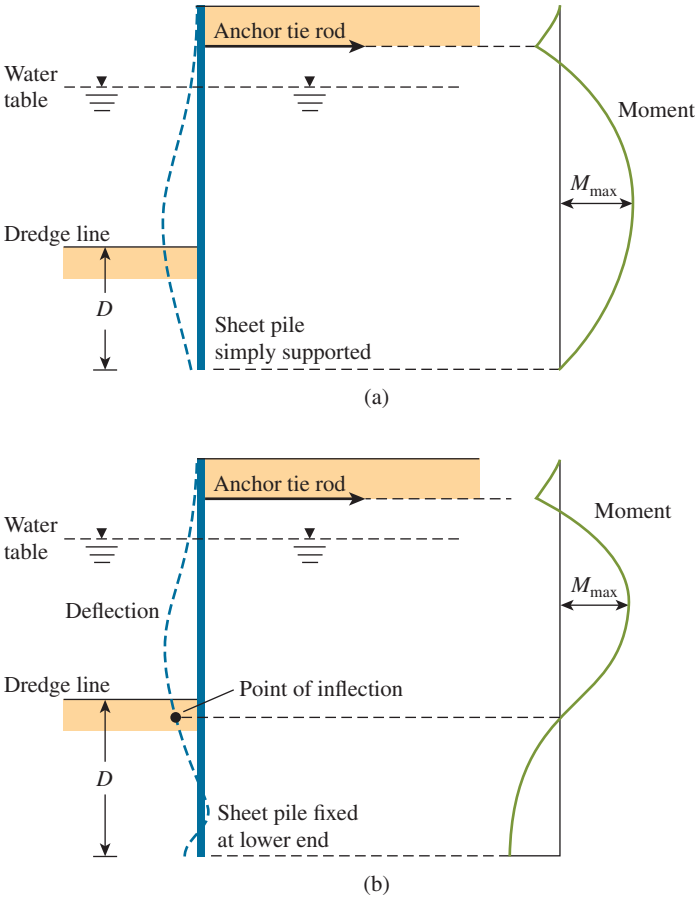


FIGURE 18.21 Nature of variation of deflection and moment for anchored sheet piles: (a) free earth support method; (b) fixed earth support method

pressure distributions for this method. The sheet pile acts as a simply supported beam in equilibrium under P_a, P_p, and F. The analysis is straightforward and is discussed below. The deflected shape of a sheet pile in the free earth support method is shown by a dashed line in Figure 18.20b.

The fixed earth support method assumes that the sheet pile is driven deep enough to provide some fixity at the bottom of the sheet pile, which introduces a reverse bend, as shown by the dashed line in Figure 18.20c. The analysis is more complex. The depth of penetration is greater for the fixed earth support method, but the maximum bending moment may be less, so the cross section of the sheet pile can be smaller. The bending moment diagrams for the two cases are shown in Figure 18.21.

Due to its simplicity, only the free earth support method is discussed in this chapter.

18.10 Free Earth Support Method for Penetration of Sandy Soil—A Simplified Approach

Let us consider a simple situation where the anchored sheet pile is in dry granular soil, where the lateral pressure distribution is as shown in Figure 18.20b. The active state is fully mobilized on the right side, and the passive state is only partially mobilized on the left. The resultant active and passive forces are $P_a = \frac{1}{2} K_a \gamma (L + D)^2$

and $P_p = \frac{1}{2}\frac{K_p}{\text{FS}}\gamma D^2$. Note that there is no horizontal reaction R that was present at the bottom of the sheet pile in the case of the cantilever sheet pile (Figure 18.18b).

Equating the horizontal forces to zero,

$$F = P_a - P_p \tag{18.68}$$

Taking the moment about O,

$$P_a\left[\frac{2}{3}(L + D) - l_1\right] - P_p\left(L - l_1 + \frac{2}{3}D\right) = 0 \tag{18.69}$$

D can be determined from Eq. (18.69). The force in the tie rod, F, can be obtained by substituting for D in Eq. (18.68). Note that F calculated from Eq. (18.68) is per unit length at right angle to the cross-section; hence, it has to be multiplied by the tie rod spacing for determining the tie rod load. The factor of safety (FS) on passive resistance is generally 1.5–2.0, as in the case of the cantilever sheet pile. As before, an alternate approach is not to use FS and simply increase D by 20–40%. It is also possible to use net pressure diagrams as before. This is discussed in the next few sections.

EXAMPLE 18.9

Find the depth of embedment D for the anchored sheet pile in sands ($\phi' = 32°$, $\gamma = 16.0$ kN/m^3, $\gamma_{sat} = 19.5$ kN/m^3) as shown Figure 18.22, with a factor of safety of 2.0 on passive resistance. Also find the force on the tie rods placed at 3 m horizontal intervals.

SOLUTION

$\phi' = 32°$ gives $K_a = 0.307$ and $K_p = 3.255$.

The horizontal pressures σ'_1, σ'_2, and σ'_3 are given by:

$$\sigma'_1 = 0.307(2 \times 16.0) = 9.82 \text{ kN/m}^2$$

$$\sigma'_2 = \left(\frac{3.255}{2}\right)(19.5 - 9.81)(D) = 15.77D$$

$$\sigma'_3 = 0.307[(2)(16) + (6 + D)(19.5 - 9.81)] = 2.98D + 27.67$$

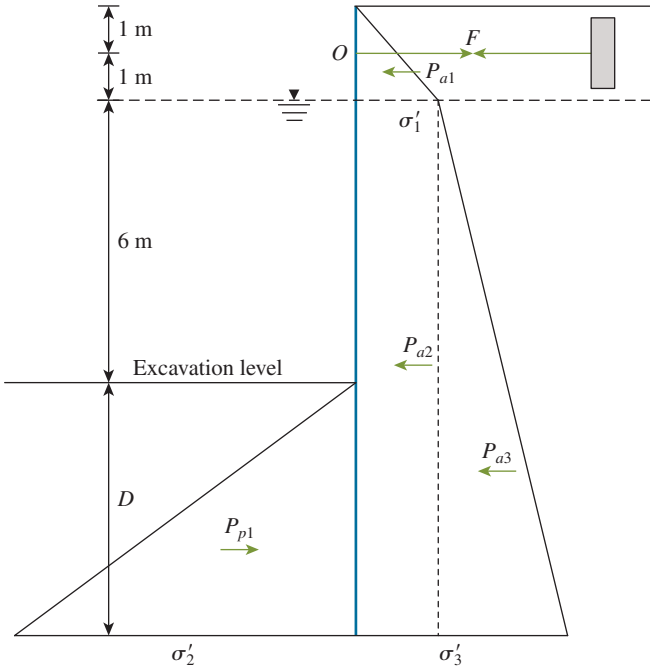


FIGURE 18.22 Solution by simplified approach

Now we divide the lateral earth pressure diagram into separate components, P_{a1}, P_{a2}, P_{a3}, and P_{p1}, as shown in the figure to obtain the moment about O.

Horizontal load (kN/m)	Distance below O (m)	Moment about O (kN · m/m)
$P_{a1} = (0.5)(2)(9.82) = 9.82$	0.33	3.24
$P_{a2} = (D + 6)(9.82) = 58.92 + 9.82D$	$4 + 0.5D$	$235.7 + 68.74D + 4.91D^2$
$P_{a3} = (0.5)(D + 6)(2.98D + 17.85)$ $= 1.49D^2 + 17.87D + 53.55$	$5 + 0.67D$	$D^3 + 19.42D^2 + 125.23D + 267.75$
$P_{p1} = (0.5)(15.77D)(D) = 7.89D^2$	$7 + 0.67D$	$55.23D^2 + 5.29D^3$

From the above table,

$$\Sigma M_o = 3.24 + (235.7 + 68.74D + 4.91D^2) + (D^3 + 19.42D^2 + 125.23D + 267.5) - 55.23D^2 - 5.29D^3 = 0$$

$$4.292D^3 + 30.9D^2 - 193.97D - 506.69 = 0$$

Solving the above equation by trial and error, $\boldsymbol{D = 5.3}$ **m**. For equilibrium,

$$F = P_{a1} + P_{a2} + P_{a3} - P_{p1} = 9.82 + (58.92 + 9.82D) + (1.49D^2 + 17.87D + 53.55) - (7.89D^2)$$

Substituting $D = 5.3$ m, $\boldsymbol{F = 89.3}$ **kN/m**. If the tie rods are spaced at 3 m intervals, the load per tie rod is $89.3 \times 3 =$ **267.9 kN**.

18.11 Free Earth Support Method for Penetration of Sandy Soil—Net Lateral Pressure Method

Figure 18.23 shows an anchor sheet-pile wall with a granular soil backfill; the wall has been driven into a granular soil. The tie rod connecting the sheet pile and the anchor is located at a depth l_1 below the top of the sheet-pile wall.

The diagram of the net pressure distribution above the dredge line is similar to that shown in Figure 18.9. At depth $z = L_1$, $\sigma_1' = \gamma L_1 K_a$, and at $z = L_1 + L_2$, $\sigma_2' = (\gamma L_1 + \gamma' L_2)K_a$. Below the dredge line, the net pressure will be zero at $z = L_1 + L_2 + L_3$. The relation for L_3 is given by Eq. (18.6), or

$$L_3 = \frac{\sigma_2'}{\gamma'(K_p - K_a)}$$

At $z = L_1 + L_2 + L_3 + L_4$, the net pressure is given by

$$\sigma_8' = \gamma'(K_p - K_a)L_4 \tag{18.70}$$

Note that the slope of the line DEF is 1 vertical to $\gamma'(K_p - K_a)$ horizontal.

For equilibrium of the sheet pile, Σ horizontal forces $= 0$, and Σ moment about $O' = 0$. (*Note:* Point O' is located at the level of the tie rod.)

Summing the forces in the horizontal direction (per unit length of the wall) gives

$$\text{Area of the pressure diagram } ACDE - \text{area of } EBF - F = 0$$

where F = tension in the tie rod/unit length of the wall, or

$$P - \tfrac{1}{2}\sigma_8' L_4 - F = 0$$

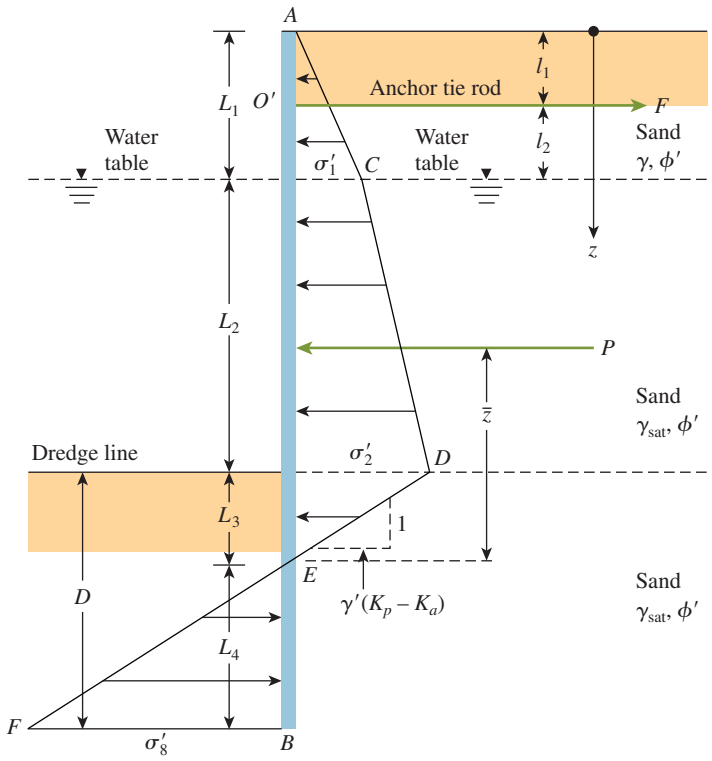


FIGURE 18.23 Anchored sheet-pile wall penetrating sand

or

$$F = P - \tfrac{1}{2}[\gamma'(K_p - K_a)]L_4^2 \tag{18.71}$$

where P = area of the pressure diagram $ACDE$. Now, taking the moment about point O' gives

$$-P[(L_1 + L_2 + L_3) - (\bar{z} + l_1)] + \tfrac{1}{2}[\gamma'(K_p - K_a)]L_4^2(l_2 + L_2 + L_3 + \tfrac{2}{3}L_4) = 0$$

or

$$L_4^3 + 1.5L_4^2(l_2 + L_2 + L_3) - \frac{3P[(L_1 + L_2 + L_3) - (\bar{z} + l_1)]}{\gamma'(K_p - K_a)} = 0 \tag{18.72}$$

Equation (18.72) may be solved by trial and error to determine the theoretical depth, L_4:

$$D_{\text{theoretical}} = L_3 + L_4$$

The theoretical depth is increased by about 30 to 40% for actual construction, or

$$D_{\text{actual}} = 1.3 \text{ to } 1.4D_{\text{theoretical}} \tag{18.73}$$

The step-by-step procedure in Section 18.4 indicated that a factor of safety can be applied to K_p at the beginning [i.e., $K_{p(\text{design})} = K_p/\text{FS}$]. If that is done, there is no need to increase the theoretical depth by 30 to 40%. This approach is often more conservative.

The maximum theoretical moment to which the sheet pile will be subjected occurs at a depth between $z = L_1$ and $z = L_1 + L_2$. The depth z for zero shear and hence maximum moment may be evaluated from

$$\tfrac{1}{2}\sigma_1' L_1 - F + \sigma_1'(z - L_1) + \tfrac{1}{2}K_a\gamma'(z - L_1)^2 = 0 \tag{18.74}$$

Once the value of z is determined, the magnitude of the maximum moment is easily obtained.

EXAMPLE 18.10

Let $L_1 = 3.05$ m, $L_2 = 6.1$ m, $l_1 = 1.53$ m, $l_2 = 1.52$ m, $c' = 0$, $\phi' = 30°$, $\gamma = 16$ kN/m^3, and $\gamma_{sat} = 19.5$ kN/m^3, as in Figure 18.23.

a. Determine the theoretical and actual depths of penetration. (*Note*: $D_{actual} = 1.3D_{theory}$.)
b. Find the anchor force per unit length of the wall.
c. Determine the maximum moment, M_{max}.

SOLUTION

Part a

We use the following table.

Quantity required	Eq. no.	Equation and calculation
K_a	—	$\tan^2\left(45 - \frac{\phi'}{2}\right) = \tan^2\left(45 - \frac{30}{2}\right) = \frac{1}{3}$
K_P	—	$\tan^2\left(45 + \frac{\phi'}{2}\right) = \tan^2\left(45 + \frac{30}{2}\right) = 3$
$K_p - K_a$	—	$3 - 0.333 = 2.667$
γ'	—	$\gamma_{sat} - \gamma_w = 19.5 - 9.81 = 9.69$ kN/m^3
σ_1'	18.1	$\gamma L_1 K_a = (16)(3.05)(\frac{1}{3}) = 16.27$ kN/m^2
σ_2'	18.2	$(\gamma L_1 + \gamma' L_2)K_a = [(16)(3.05) + (9.69)(6.1)]\frac{1}{3} = 35.97$ kN/m^2
L_3	18.6	$\frac{\sigma_2'}{\gamma'(K_p - K_a)} = \frac{35.97}{(9.69)(2.667)} = 1.39$ m
P	—	$\frac{1}{2}\sigma_1' L_1 + \sigma_2' L_2 + \frac{1}{2}(\sigma_2' - \sigma_1')L_2 + \frac{1}{2}\sigma_2' L_3 = (\frac{1}{2})(16.27)(3.05) + (16.27)(6.1) + (\frac{1}{2})(35.97 - 16.27)(6.1) + (\frac{1}{2})(35.97)(1.39) = 24.81 + 99.25 + 60.01 + 25.0 = 209.07$ kN/m
$\bar{z}$	—	$\frac{\Sigma M_E}{P} = \left[\begin{array}{l}(24.81)\left(1.39 + 6.1 + \frac{3.05}{3}\right) + (99.25)\left(1.39 + \frac{6.1}{2}\right) \\ + (60.01)\left(1.39 + \frac{6.1}{3}\right) + (25.0)\left(\frac{2 \times 1.39}{3}\right)\end{array}\right]\frac{1}{209.07}$ $= 4.21$ m
L_4	18.72	$L_4^3 + 1.5L_4^2(l_2 + L_2 + L_3) - \frac{3P[(L_1 + L_2 + L_3) - (\bar{z} + l_1)]}{\gamma'(K_p - K_a)} = 0$
		$L_4^3 + 1.5L_4^2(1.52 + 6.1 + 1.39) - \frac{(3)(209.07)[(3.05 + 6.1 + 1.39) - (4.21 + 1.53)]}{(9.69)(2.667)} = 0$
		$L_4 = 2.7$ m

(continued)

Quantity required	Eq. no.	Equation and calculation
D_{theory}	—	$L_3 + L_4 = 1.39 + 2.7 = 4.09 \approx$ **4.1 m**
D_{actual}	—	$1.3D_{theory} = (1.3)(4.1) =$ **5.33 m**

Part b

The anchor force per unit length of the wall is

$$F = P - \tfrac{1}{2}\gamma'(K_p - K_a)L_4^2$$
$$= 209.07 - \left(\tfrac{1}{2}\right)(9.69)(2.667)(2.7)^2 = 114.87 \text{ kN/m} \approx \textbf{115 kN/m}$$

Part c

From Eq. (18.74), for zero shear,

$$\tfrac{1}{2}\sigma_1' L_1 - F + \sigma_1'(z - L_1) + \tfrac{1}{2}K_a\gamma'(z - L_1)^2 = 0$$

Let $z - L_1 = x$, so that

$$\tfrac{1}{2}\sigma_1' L_1 - F + \sigma_1' x + \tfrac{1}{2}K_a\gamma' x^2 = 0$$

or

$$\left(\tfrac{1}{2}\right)(16.27)(3.05) - 115 + (16.27)(x) + \left(\tfrac{1}{2}\right)\left(\tfrac{1}{3}\right)(9.69)x^2 = 0$$

giving

$$x^2 + 10.07x - 55.84 = 0$$

Now, $x = 4$ m and $z = x + L_1 = 4 + 3.05 = 7.05$ m. Taking the moment about the point of zero shear, we obtain

$$M_{max} = -\frac{1}{2}\sigma_1' L_1\left(x + \frac{3.05}{3}\right) + F(x + 1.52) - \sigma_1'\frac{x^2}{2} - \frac{1}{2}K_a\gamma' x^2\left(\frac{x}{3}\right)$$

or

$$M_{max} = -\left(\frac{1}{2}\right)(16.27)(3.05)\left(4 + \frac{3.05}{3}\right) + (115)(4 + 1.52) - (16.27)\left(\frac{4^2}{2}\right)$$
$$-\left(\frac{1}{2}\right)\left(\frac{1}{3}\right)(9.69)(4)^2\left(\frac{4}{3}\right) = \textbf{344.9 kN·m/m}$$

18.12 Design Charts for Free Earth Support Method (Penetration into Sandy Soil)

Using the free earth support method, Hagerty and Nofal (1992) provided simplified design charts for quick estimation of the depth of penetration, D, anchor force, F, and maximum moment, M_{max}, for anchored sheet-pile walls penetrating into sandy soil, as shown in Figure 18.23. They made the following assumptions for their analysis.

a. The soil friction angle, ϕ', above and below the dredge line is the same.
b. The angle of friction between the sheet-pile wall and the soil is $\phi'/2$.
c. The passive earth pressure below the dredge line has a logarithmic spiral failure surface.
d. For active earth-pressure calculation, Coulomb's theory is valid.

The magnitudes of D, F, and M_{max} may be calculated from the following relationships:

$$\frac{D}{L_1 + L_2} = (GD)(CDL_1) \tag{18.75}$$

$$\frac{F}{\gamma_a(L_1 + L_2)^2} = (GF)(CFL_1) \tag{18.76}$$

$$\frac{M_{\max}}{\gamma_a(L_1 + L_2)^3} = (GM)(CML_1) \tag{18.77}$$

where

γ_a = average unit weight of soil

$$= \frac{\gamma L_1^2 + (\gamma_{\text{sat}} - \gamma_w)L_2^2 + 2\gamma L_1 L_2}{(L_1 + L_2)^2} \tag{18.78}$$

GD = generalized nondimensional embedment

$$= \frac{D}{L_1 + L_2} \qquad (\text{for } L_1 = 0 \text{ and } L_2 = L_1 + L_2)$$

GF = generalized nondimensional anchor force

$$= \frac{F}{\gamma_a(L_1 + L_2)^2} \qquad (\text{for } L_1 = 0 \text{ and } L_2 = L_1 + L_2)$$

GM = generalized nondimensional moment

$$= \frac{M_{\max}}{\gamma_a(L_1 + L_2)^3} \qquad (\text{for } L_1 = 0 \text{ and } L_2 = L_1 + L_2)$$

CDL_1, CFL_1, CML_1 = correction factors for $L_1 \neq 0$

The variations of GD, GF, GM, CDL_1, CFL_1, and CML_1 are shown in Figures 18.24, 18.25, 18.26, 18.27, 18.28, and 18.29, respectively.

Here the generalized nondimensional values GD, GF, and GM are developed for the special case where $L_1 = 0$. The correction factors are there to account for situations where $L_1 \neq 0$. For $L_1 = 0$, the three correction factors are unity.

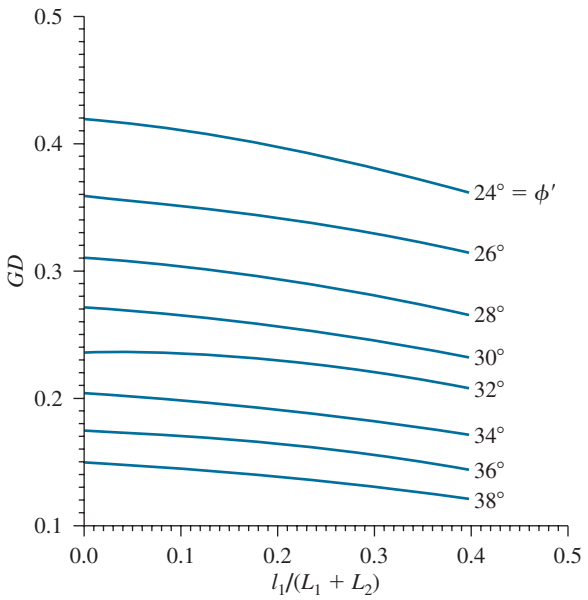


FIGURE 18.24 Variation of GD with $l_1/(L_1 + L_2)$ and ϕ' (Based on Hagerty, D. J. and Nofal, M. M. (1992). "Design Aids: Anchored Bulkheads in Sand," *Canadian Geotechnical Journal*, Vol. 29, No. 5, pp. 789–795.)

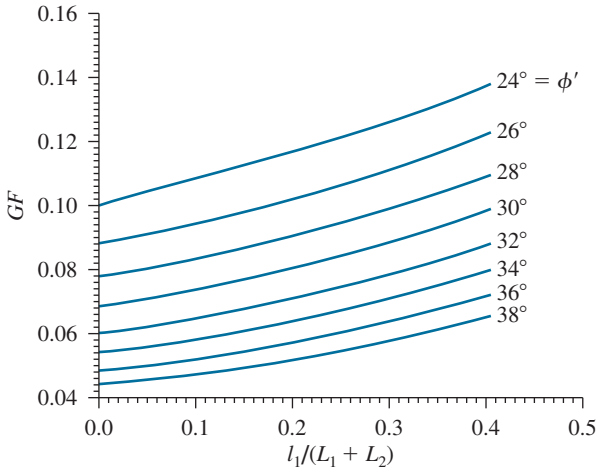


FIGURE 18.25 Variation of GF with $l_1/(L_1 + L_2)$ and ϕ' (Based on Hagerty, D. J. and Nofal, M. M. (1992). "Design Aids: Anchored Bulkheads in Sand," *Canadian Geotechnical Journal*, Vol. 29, No. 5, pp. 789–795.)

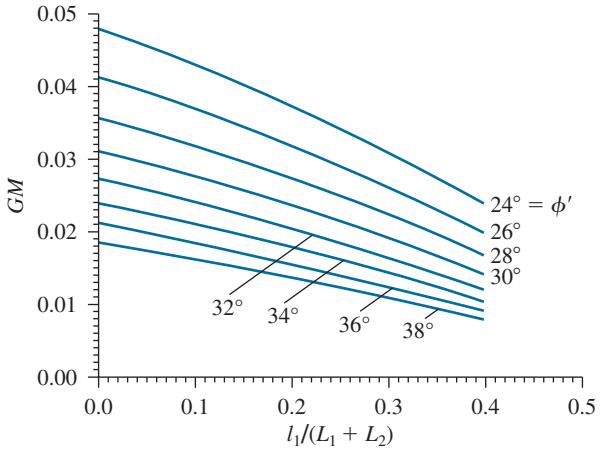


FIGURE 18.26 Variation of GM with $l_1/(L_1 + L_2)$ and ϕ' (Based on Hagerty, D. J. and Nofal, M. M. (1992), "Design Aids: Anchored Bulkheads in Sand," *Canadian Geotechnical Journal*, Vol. 29, No. 5, pp. 789–795.)

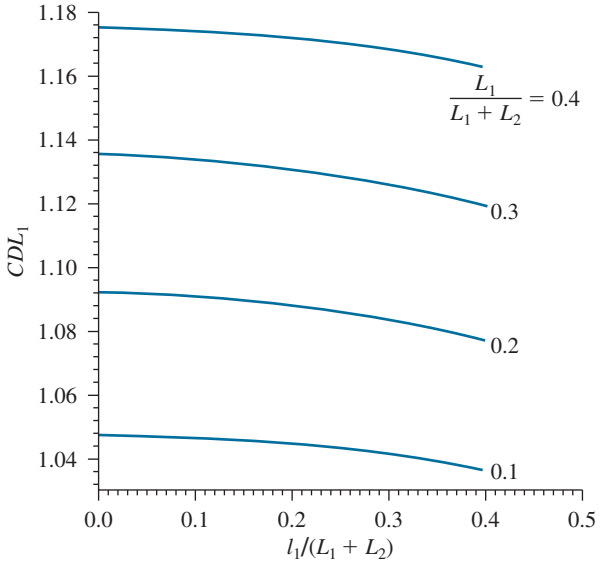


FIGURE 18.27 Variation of CDL_1 with $L_1/(L_1 + L_2)$ and $l_1/(L_1 + L_2)$ (Based on Hagerty, D. J. and Nofal, M. M. (1992). "Design Aids: Anchored Bulkheads in Sand," *Canadian Geotechnical Journal*, Vol. 29, No. 5, pp. 789–795.)

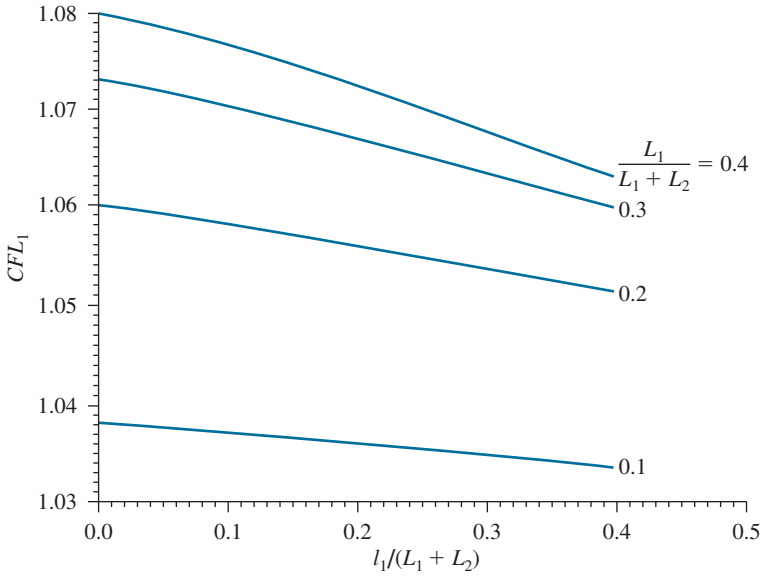


FIGURE 18.28 Variation of CFL_1 with $L_1/(L_1 + L_2)$ and $l_1/(L_1 + L_2)$ (Based on Hagerty, D. J. and Nofal, M. M. (1992). "Design Aids: Anchored Bulkheads in Sand," *Canadian Geotechnical Journal*, Vol. 29, No. 5, pp. 789–795.)

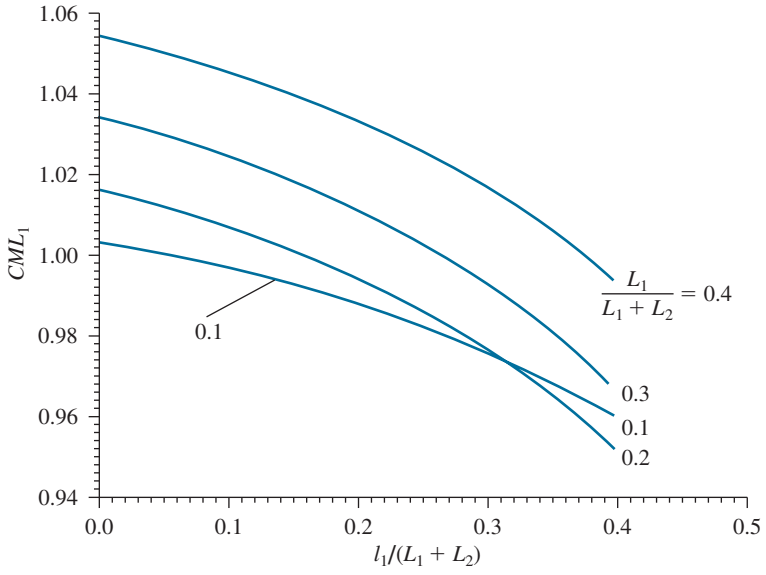


FIGURE 18.29 Variation of CML_1 with $L_1/(L_1 + L_2)$ and $l_1/(L_1 + L_2)$ (Based on Hagerty, D. J. and Nofal, M. M. (1992). "Design Aids: Anchored Bulkheads in Sand," *Canadian Geotechnical Journal*, Vol. 29, No. 5, pp. 789–795.)

EXAMPLE 18.11

Refer to Figure 18.23. Given: $L_1 = 2$ m, $L_2 = 3$ m, $l_1 = l_2 = 1$ m, $c = 0$, $\phi' = 32°$, $\gamma = 15.9$ kN/m^3, and $\gamma_{sat} = 19.33$ kN/m^3. Determine:

a. Theoretical and actual depth of penetration. *Note:* $D_{actual} = 1.4D_{theory}$.
b. Anchor force per unit length of wall
c. Maximum moment, M_{max}

Use the charts presented in Section 18.12.

SOLUTION

Part a

From Eq. (18.75),

$$\frac{D}{L_1 + L_2} = (GD)(CDL_1)$$

$$\frac{l_1}{L_1 + L_2} = \frac{1}{2 + 3} = 0.2$$

From Figure 18.24, for $l_1/(L_1 + L_2) = 0.2$ and $\phi' = 32°$, $GD = 0.22$. From Figure 18.27, for

$$\frac{L_1}{L_1 + L_2} = \frac{2}{2 + 3} = 0.4 \qquad \text{and} \qquad \frac{l_1}{L_1 + L_2} = 0.2$$

$CDL_1 \approx 1.172$. So

$$D_{\text{theory}} = (L_1 + L_2)(GD)(CDL_1) = (5)(0.22)(1.172) \approx 1.3$$

$$D_{\text{actual}} \approx (1.4)(1.3) = 1.82 \approx \mathbf{2\ m}$$

Part b

From Figure 18.25, for $l_1/(L_1 + L_2) = 0.2$ and $\phi' = 32°$, $GF \approx 0.074$. Also, from Figure 18.28, for

$$\frac{L_1}{L_1 + L_2} = \frac{2}{2 + 3} = 0.4, \quad \frac{l_1}{L_1 + L_2} = 0.2, \quad \text{and} \quad \phi' = 32°$$

$CFL_1 = 1.073$. From Eq. (18.73),

$$\gamma_a = \frac{\gamma L_1^2 + \gamma' L_2^2 + 2\gamma L_1 L_2}{(L_1 + L_2)^2}$$

$$= \frac{(15.9)(2)^2 + (19.33 - 9.81)(3)^2 + (2)(15.9)(2)(3)}{(2 + 3)^2} = 13.6\ \text{kN/m}^3$$

Using Eq. (18.76) yields

$$F = \gamma_a (L_1 + L_2)^2 (GF)(CFL_1) = (13.6)(5)^2(0.074)(1.073) \approx \mathbf{27\ kN/m}$$

Part c

From Figure 18.26, for $l_1/(L_1 + L_2) = 0.2$ and $\phi' = 32°$, $GM = 0.021$. Also, from Figure 18.29, for

$$\frac{L_1}{L_1 + L_2} = \frac{2}{2 + 3} = 0.4, \quad \frac{l_1}{L_1 + L_2} = 0.2, \quad \text{and} \quad \phi' = 32°$$

$CML_1 = 1.036$. Hence from Eq. (18.77),

$$M_{\text{max}} = \gamma_a (L_1 + L_2)^3 (GM)(CML_1) = (13.6)(5)^3(0.021)(1.036) = \mathbf{36.99\ kN \cdot m/m}$$

18.13 Moment Reduction for Anchored Sheet-Pile Walls Penetrating into Sand

Sheet piles are flexible, and hence sheet-pile walls yield (i.e., become displaced laterally), which redistributes the lateral earth pressure. This change tends to reduce the maximum bending moment, M_{max}, as calculated by the procedure outlined in Sections 18.10 and 18.11. For that reason, Rowe (1952, 1957) suggested a procedure for reducing the maximum design moment on the sheet-pile walls *obtained from the free earth support method.* This section discusses the procedure of moment reduction for sheet piles *penetrating into sand.*

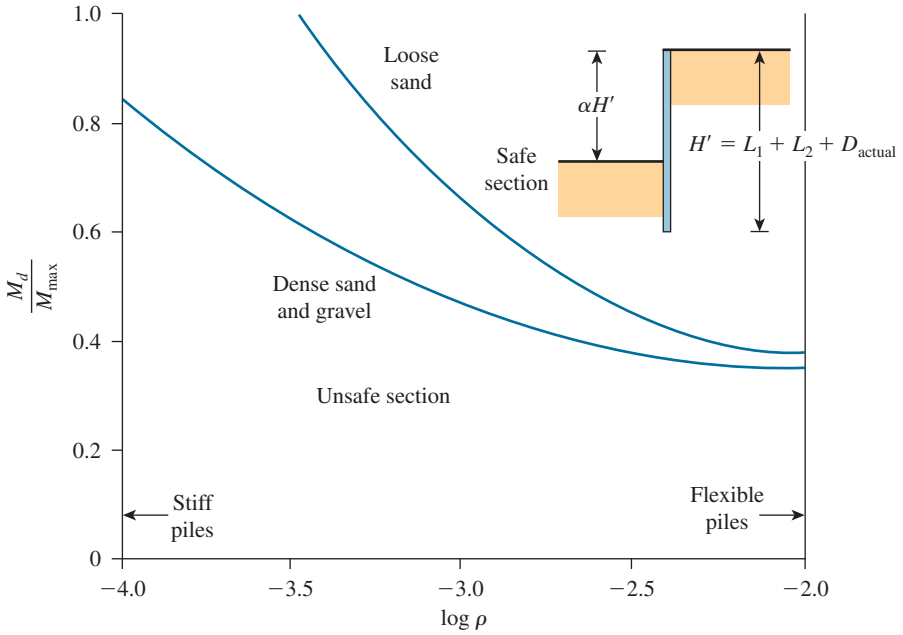


FIGURE 18.30 Plot of log ρ against M_d/M_{max} for sheet-pile walls penetrating sand (Based on Rowe, P. W. (1952). "Anchored Sheet-Pile Walls," *Proceedings, Institute of Civil Engineers*, Vol. 1, Part 1, pp. 27–70.)

In Figure 18.30, which is valid for the case of a sheet pile penetrating sand, the following notation is used:

1. H' = total height of pile driven (i.e., $L_1 + L_2 + D_{actual}$)
2. Relative flexibility of pile $= \rho = 10.91 \times 10^{-7}\left(\frac{H'^4}{EI}\right)$ (18.79a)

   where

   H' is in meters

   E = modulus of elasticity of the pile material (MN/m^2)

   I = moment of inertia of the pile section per meter of the wall (m^4/m of wall)
3. M_d = design moment
4. M_{max} = maximum theoretical moment

In English units, Eq. (18.79a) takes the form

$$\rho = \frac{H'^4}{EI} \tag{18.79b}$$

where H' is in ft, E is in lb/in^2, and I is in in^4/ft of the wall.

The procedure for the use of the moment reduction diagram (see Figure 18.30) is as follows:

Step 1. Choose a sheet-pile section (e.g., from among those given in Table 18.1).

Step 2. Find the modulus S of the selected section (Step 1) per unit length of the wall.

Step 3. Determine the moment of inertia of the section (Step 1) per unit length of the wall.

Step 4. Obtain H' and calculate ρ [see Eq. (18.79a) or Eq. (18.79b)].

Step 5. Find log ρ.

Step 6. Find the moment capacity of the pile section chosen in Step 1 as $M_d = \sigma_{all} S$.

Step 7. Determine M_d/M_{max}. Note that M_{max} is the maximum theoretical moment determined previously.

Step 8. Plot log ρ (Step 5) and M_d/M_{max} in Figure 18.30.

Step 9. Repeat Steps 1 through 8 for several sections. The points that fall above the curve (in loose sand or dense sand, as the case may be) are *safe sections.*

The points that fall below the curve are *unsafe sections.* The cheapest section may now be chosen from those points that fall above the proper curve. Note that the section chosen will have an $M_d < M_{max}$.

Figure 18.30 suggests that the maximum theoretical moment (M_{max}) computed in Sections 18.9 and 18.11 can be significantly greater than the moment carrying capacity (M_d) of the sheet-pile section.

EXAMPLE 18.12

Refer to Example 18.10. Use Rowe's moment reduction diagram (Figure 18.30) to find an appropriate sheet-pile section. For the sheet pile, use $E = 207 \times 10^3$ MN/m^2 and $\sigma_{all} = 172{,}500$ kN/m^2.

SOLUTION

$$H' = L_1 + L_2 + D_{actual} = 3.05 + 6.1 + 5.33 = 14.48 \text{ m}$$

$M_{max} = 344.9$ kN·m/m. Now the following table can be prepared.

Section	I (m^4/m)	H' (m)	$\rho = 10.91 \times 10^{-7}\left(\frac{H'^4}{EI}\right)$	log ρ	S (m^3/m)	$M_d = S\sigma_{all}$ (kN·m/m)	$\frac{M_d}{M_{max}}$
PZ-22	116.2×10^{-6}	14.48	19.94×10^{-4}	−2.7	98.92×10^{-5}	170.64	0.495
PZ-27	255.9×10^{-6}	14.48	9.05×10^{-4}	−3.04	166.66×10^{-5}	287.49	0.834

Figure 18.31 gives a plot of M_d/M_{max} versus log ρ. It can be seen that PZ-27 will be sufficient.

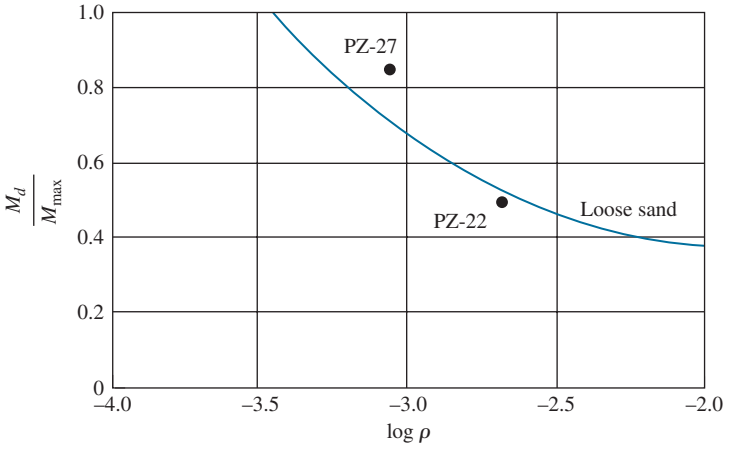


FIGURE 18.31 Plot of M_d/M_{max} versus log ρ

18.14 Computational Pressure Diagram Method for Penetration into Sandy Soil

The computational pressure diagram (CPD) method for anchored sheet piles penetrating a sandy soil is a simplified method of design and an alternative to the free earth method described in Sections 18.10, 18.11, and 18.13 (Nataraj and Hoadley, 1984). In this method, the net pressure diagram shown in Figure 18.23 is replaced by rectangular pressure diagrams, as in Figure 18.32. Note that $\overline{\sigma}'_a$ is the width of the net active pressure diagram above the dredge line and $\overline{\sigma}'_p$ is the width of the net passive pressure diagram below the dredge line. The magnitudes of $\overline{\sigma}'_a$ and $\overline{\sigma}'_p$ may respectively be expressed as

$$\overline{\sigma}'_a = CK_a\gamma'_{av}L \tag{18.80}$$

and

$$\overline{\sigma}'_p = RCK_a\gamma'_{av}L = R\overline{\sigma}'_a \tag{18.81}$$

where

γ'_{av} = average effective unit weight of sand

$$\approx \frac{\gamma L_1 + \gamma' L_2}{L_1 + L_2} \tag{18.82}$$

C = empirical soil pressure coefficient

$$R = \frac{\overline{\sigma}'_p}{\overline{\sigma}'_a} = \frac{L(L - 2l_1)}{D(2L + D - 2l_1)} = \text{coefficient} \tag{18.83}$$

The range of values for C and R is given in Table 18.2.

The depth of penetration, D, anchor force per unit length of the wall, F, and maximum moment in the wall, M_{max}, are obtained from the following relationships.

DEPTH OF PENETRATION

For the depth of penetration, we have

$$D^2 + 2DL\left[1 - \left(\frac{l_1}{L}\right)\right] - \left(\frac{L^2}{R}\right)\left[1 - 2\left(\frac{l_1}{L}\right)\right] = 0 \tag{18.84}$$

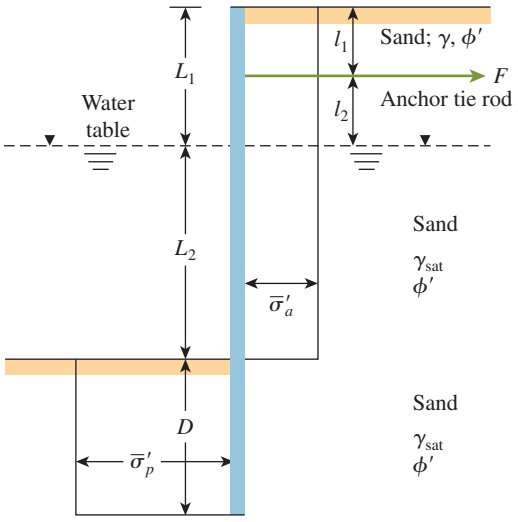


FIGURE 18.32 Computational pressure diagram method (*Note:* $L_1 + L_2 = L$)

TABLE 18.2 Range of Values for C and R [from Eqs. (18.80) and (18.81)]

Soil type	C^a	R
Loose sand	0.8–0.85	0.3–0.5
Medium sand	0.7–0.75	0.55–0.65
Dense sand	0.55–0.65	0.60–0.75

[a]Valid for the case in which there is no surcharge above the granular backfill (i.e., on the right side of the wall, as shown in Figure 18.32)

ANCHOR FORCE

The anchor force is

$$F = \bar{\sigma}'_a(L - RD) \tag{18.85}$$

MAXIMUM MOMENT

The maximum moment is calculated from

$$M_{\max} = 0.5\,\bar{\sigma}'_a L^2\left[\left(1 - \frac{RD}{L}\right)^2 - \left(\frac{2l_1}{L}\right)\left(1 - \frac{RD}{L}\right)\right] \tag{18.86}$$

Note the following qualifications:

1. The magnitude of D obtained from Eq. (18.84) is about 1.25 to 1.5 times the value of D_{theory} obtained by the conventional free earth support method (see Section 18.11), so

$$\begin{array}{ccc} D & \approx & D_{\text{actual}} \\ \uparrow & & \uparrow \\ \text{Eq. (18.84)} & & \text{Eq. (18.73)} \end{array}$$

2. The magnitude of F obtained by using Eq. (18.85) is about 1.2 to 1.6 times the value obtained by using Eq. (18.71). Thus, an additional factor of safety for the actual design of anchors need not be used.
3. The magnitude of $M_{\max}$ obtained from Eq. (18.86) is about 0.6 to 0.75 times the value of $M_{\max}$ obtained by the conventional free earth support method. Hence, the former value of $M_{\max}$ can be used as the actual design value, and Rowe's moment reduction need not be applied.

EXAMPLE 18.13

For the anchored sheet-pile wall shown in Figure 18.33, determine (a) D, (b) F, and (c) $M_{\max}$. Use the CPD method; assume that $C = 0.68$ and $R = 0.6$.

SOLUTION

Part a

$$\gamma' = \gamma_{\text{sat}} - \gamma_w = 19.24 - 9.81 = 9.43 \text{ kN/m}^3$$

From Eq. (18.82),

$$\gamma'_{\text{av}} = \frac{\gamma L_1 + \gamma' L_2}{L_1 + L_2} = \frac{(17.3)(3) + (9.43)(6)}{3 + 6} = 12.05 \text{ kN/m}^3$$

$$K_a = \tan^2\left(45 - \frac{\phi'}{2}\right) = \tan^2\left(45 - \frac{35}{2}\right) = 0.271$$

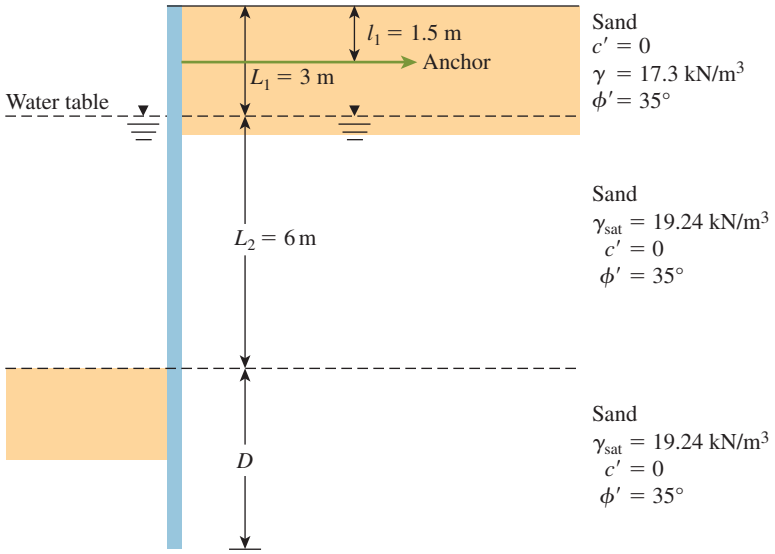


FIGURE 18.33

$$\overline{\sigma}'_a = CK_a\gamma'_{av}L = (0.68)(0.271)(12.05)(9) = 19.99 \text{ kN/m}^2$$

$$\overline{\sigma}'_p = R\overline{\sigma}'_a = (0.6)(19.99) = 11.99 \text{ kN/m}^2$$

From Eq. (18.84),

$$D^2 + 2DL\left[1 - \left(\frac{l_1}{L}\right)\right] - \frac{L^2}{R}\left[1 - 2\left(\frac{l_1}{L}\right)\right] = 0$$

or

$$D^2 + 2(D)(9)\left[1 - \left(\frac{1.5}{9}\right)\right] - \frac{(9)^2}{0.6}\left[1 - 2\left(\frac{1.5}{9}\right)\right] = D^2 + 50D - 1000 = 0$$

Hence $D \approx$ **4.6 m.**

Check for the assumption of R:

$$R = \frac{L(L - 2l_1)}{D(2L + D - 2l_1)} = \frac{9[9 - (2)(1.5)]}{4.6[(2)(9) + 4.6 - (2)(1.5)]} \approx \textbf{0.6—K}$$

Part b

From Eq. (18.85),

$$F = \overline{\sigma}'_a(L - RD) = 19.99[9 - (0.6)(4.6)] = \textbf{124.74 kN/m}$$

Part c

From Eq. (18.86),

$$M_{max} = 0.5\overline{\sigma}'_aL^2\left[\left(1 - \frac{RD}{L}\right)^2 - \left(\frac{2l_1}{L}\right)\left(1 - \frac{RD}{L}\right)\right]$$

$$1 - \frac{RD}{L} = 1 - \frac{(0.6)(4.6)}{9} = 0.693$$

So,

$$M_{max} = (0.5)(19.99)(9)^2\left[(0.693)^2 - \frac{(2)(1.5)(0.693)}{9}\right] = \textbf{201.6 kN} \cdot \textbf{m/m}$$

18.15 Field Observations for Anchor Sheet-Pile Walls

In the preceding sections, large factors of safety were used for the depth of penetration, D. In most cases, designers use smaller magnitudes of soil friction angle, ϕ', thereby ensuring a built-in factor of safety for the active earth pressure. This procedure is followed primarily because of the uncertainties involved in predicting the actual earth pressure to which a sheet-pile wall in the field will be subjected. In addition, Casagrande (1973) observed that if the soil behind the sheet-pile wall has grain sizes that are predominantly smaller than those of coarse sand, the active earth pressure after construction sometimes increases to an at-rest earth-pressure condition. Such an increase causes a large increase in the anchor force, F. The following two case histories are given by Casagrande (1973).

BULKHEAD OF PIER C—LONG BEACH HARBOR, CALIFORNIA (1949)

A typical cross section of the Pier C bulkhead of the Long Beach harbor is shown in Figure 18.34. Except for a rockfill dike constructed with 76 mm (3 in.) maximum-size quarry wastes, the backfill of the sheet-pile wall consisted of fine sand. Figure 18.35 shows the variation of the lateral earth pressure between May 24, 1949 (the day construction was completed) and August 6, 1949. On May 24, the lateral earth pressure reached an active state, as shown in Figure 18.35a, due to the wall yielding. Between May 24 and June 3, the anchor resisted further yielding and the lateral earth pressure increased to the at-rest state (Figure 18.35b). However, the flexibility of the sheet piles ultimately resulted in a gradual decrease in the lateral earth-pressure distribution on the sheet piles (see Figure 18.35c).

With time, the stress on the tie rods for the anchor increased, as shown in the following table.

Date	Stress on anchor tie rod (MN/m^2)
May 24, 1949	151.11
June 3, 1949	177.33
June 11, 1949	193.2
July 12, 1949	203.55
August 6, 1949	213.9

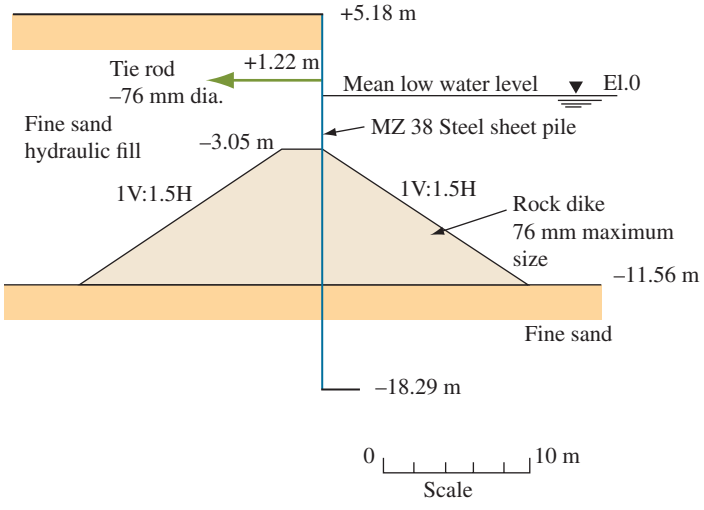


FIGURE 18.34 Pier C bulkhead—Long Beach harbor (Based on Casagrande, 1973)

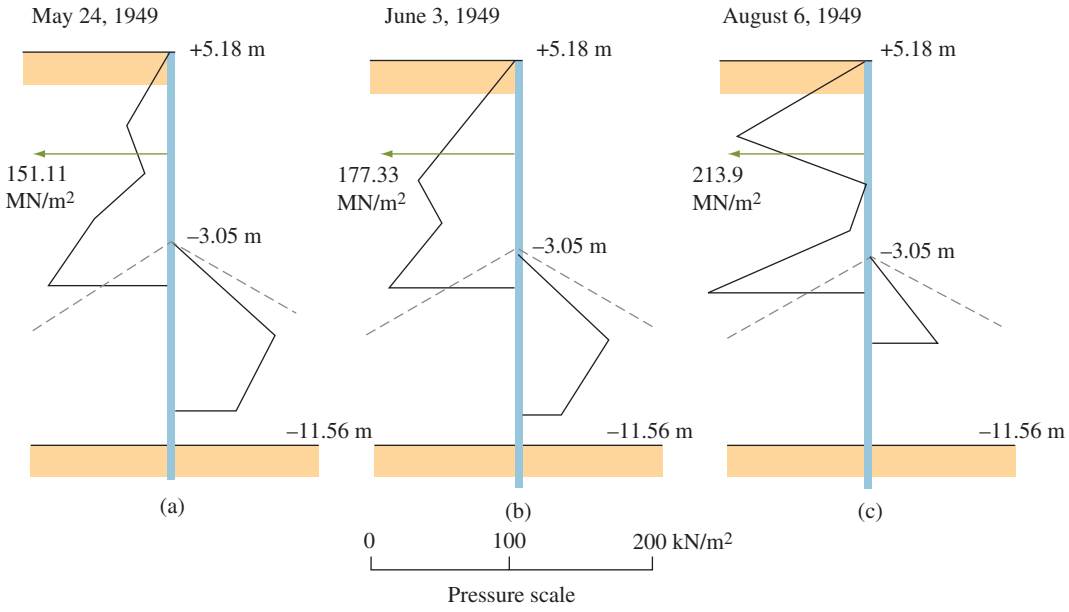


FIGURE 18.35 Measured stresses at Station 27 + 30—Pier C bulkhead, Long Beach (Based on Casagrande, 1973)

These observations show that the magnitude of the active earth pressure may vary with time and depend greatly on the flexibility of the sheet piles. Also, the actual variations in the lateral earth-pressure diagram may not be identical to those used for the design.

BULKHEAD—TOLEDO, OHIO (1961)

A typical cross section of a Toledo bulkhead completed in 1961 is shown in Figure 18.36. The foundation soil was primarily fine to medium sand, but the dredge line did cut into highly overconsolidated clay. Figure 18.36 also shows the actual measured values of bending moment along the sheet-pile wall. Casagrande (1973)

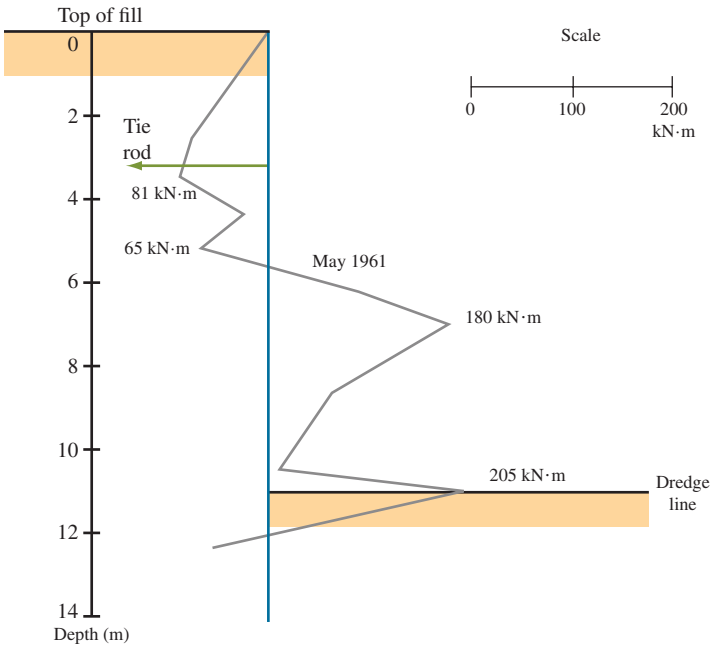


FIGURE 18.36 Bending moment from strain-gage measurements at test location 3, Toledo bulkhead (Based on Casagrande, 1973)

used the Rankine active earth-pressure distribution to calculate the maximum bending moment according to the free earth support method with and without Rowe's moment reduction.

Design method	Maximum predicted bending moment, M_{max}
Free earth support method	146.5 kN · m
Free earth support method with Rowe's moment reduction	78.6 kN · m

Comparisons of these magnitudes of M_{max} with those actually observed show that the field values are substantially larger. The reason probably is that the backfill was primarily fine sand and the measured active earth-pressure distribution was larger than that predicted theoretically.

18.16 Free Earth Support Method for Penetration of Clay

Figure 18.37 shows an anchored sheet-pile wall penetrating a clay soil and with a granular soil backfill. The diagram of pressure distribution above the dredge line is similar to that shown in Figure 18.13. From Eq. (18.42), the net pressure distribution below the dredge line (from $z = L_1 + L_2$ to $z = L_1 + L_2 + D$) is

$$\sigma_6 = 4c - (\gamma L_1 + \gamma' L_2)$$

For static equilibrium, the sum of the forces in the horizontal direction is

$$P_1 - \sigma_6 D = F \tag{18.87}$$

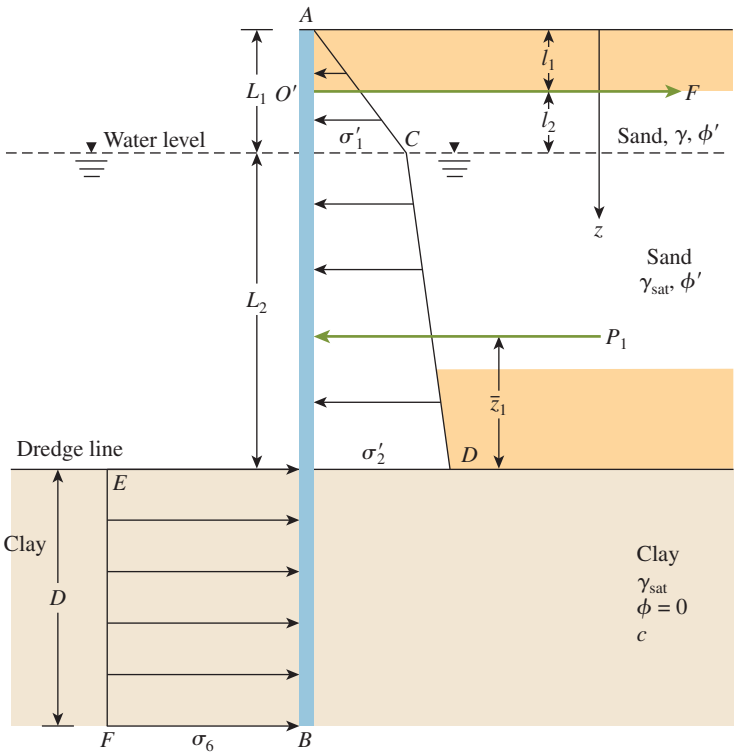


FIGURE 18.37 Anchored sheet-pile wall penetrating clay

where

P_1 = area of the pressure diagram ACD

F = anchor force per unit length of the sheet-pile wall

Again, taking the moment about O' produces

$$P_1(L_1 + L_2 - l_1 - \bar{z}_1) - \sigma_6 D\left(l_2 + L_2 + \frac{D}{2}\right) = 0$$

Simplification yields

$$\sigma_6 D^2 + 2\sigma_6 D(L_1 + L_2 - l_1) - 2P_1(L_1 + L_2 - l_1 - \bar{z}_1) = 0 \tag{18.88}$$

Equation (18.88) gives the theoretical depth of penetration, D.

As in Section 18.11, the maximum moment in this case occurs at a depth $L_1 < z < L_1 + L_2$. The depth of zero shear (and thus the maximum moment) may be determined from Eq. (18.74).

A moment reduction technique similar to that in Section 18.13 for anchored sheet piles penetrating into clay has also been developed by Rowe (1952, 1957). This technique is presented in Figure 18.38, in which the following notation is used:

1. The stability number is

$$S_n = 1.25\frac{c}{(\gamma L_1 + \gamma' L_2)} \tag{18.89}$$

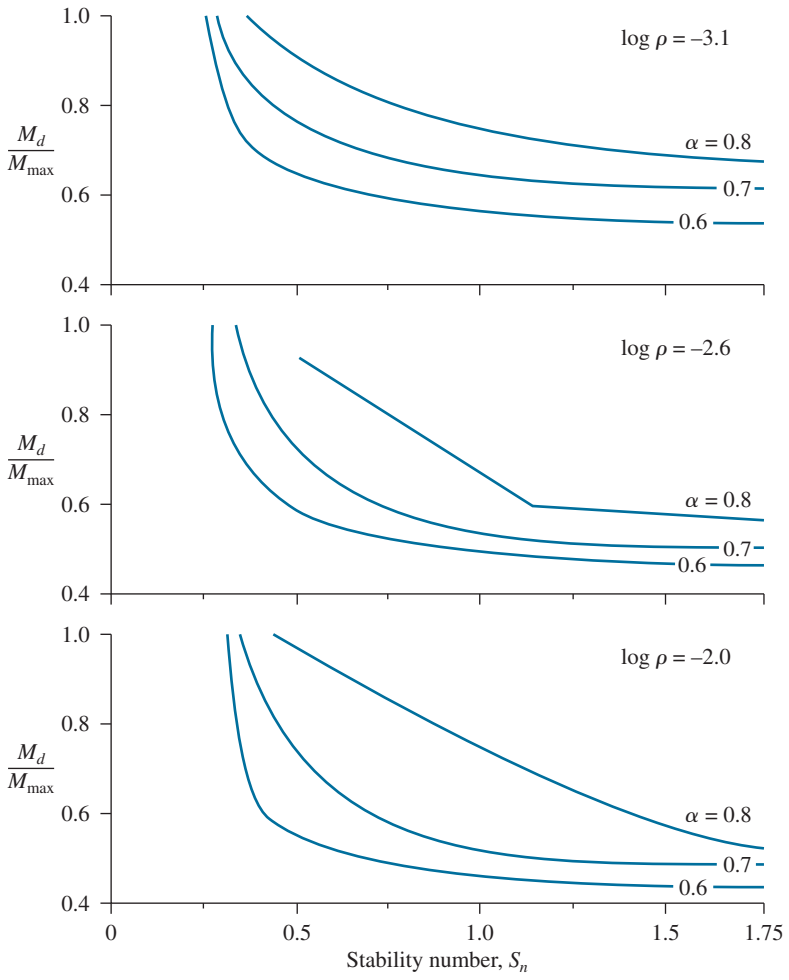


FIGURE 18.38 Plot of M_d/M_{max} against stability number for sheet-pile wall penetrating clay (Based on Rowe, P. W. (1957). "Sheet-Pile Walls in Clay," *Proceedings, Institute of Civil Engineers,* Vol. 7, pp. 654–692.)

where c = undrained cohesion ($\phi = 0$).

For the definitions of γ, γ', L_1, and L_2, see Figure 18.37.

2. The nondimensional wall height is

$$\alpha = \frac{L_1 + L_2}{L_1 + L_2 + D_{\text{actual}}} \tag{18.90}$$

3. The flexibility number is ρ [see Eq. (18.79a) or Eq. (18.79b)].
4. M_d = design moment
   $M_{\max}$ = maximum theoretical moment

The procedure for moment reduction, using Figure 18.38, is as follows:

Step 1. Obtain $H' = L_1 + L_2 + D_{\text{actual}}$.

Step 2. Determine $\alpha = (L_1 + L_2)/H'$.

Step 3. Determine S_n [from Eq. (18.89)].

Step 4. For the magnitudes of α and S_n obtained in Steps 2 and 3, determine $M_d/M_{\max}$ for various values of log ρ from Figure 18.38, and plot $M_d/M_{\max}$ against log ρ.

Step 5. Follow Steps 1 through 9 as outlined for the case of moment reduction of sheet-pile walls penetrating granular soil. (See Section 18.13.)

EXAMPLE 18.14

In Figure 18.37, let $L_1 = 3$ m, $L_2 = 6$ m, and $l_1 = 1.5$ m. Also, let $\gamma = 17$ kN/m^3, $\gamma_{\text{sat}} = 20$ kN/m^3, $\phi' = 35°$, and $c = 41$ kN/m^2.

a. Determine the theoretical depth of embedment of the sheet-pile wall.
b. Calculate the anchor force per unit length of the wall.

SOLUTION

Part a

We have

$$K_a = \tan^2\left(45 - \frac{\phi'}{2}\right) = \tan^2\left(45 - \frac{35}{2}\right) = 0.271$$

From the pressure diagram in Figure 18.39,

$$\sigma_1' = \gamma L_1 K_a = (17)(3)(0.271) = 13.82 \text{ kN/m}^2$$

$$\sigma_2' = (\gamma L_1 + \gamma' L_2)K_a = [(17)(3) + (20 - 9.81)(6)](0.271) = 30.39 \text{ kN/m}^2$$

$$P_1 = \text{areas } 1 + 2 + 3 = 1/2(3)(13.82) + (13.82)(6) + 1/2(30.39 - 13.82)(6)$$
$$= 20.73 + 82.92 + 49.71 = 153.36 \text{ kN/m}$$

and

$$\bar{z}_1 = \frac{(20.73)\left(6 + \frac{3}{3}\right) + (82.92)\left(\frac{6}{2}\right) + (49.71)\left(\frac{6}{3}\right)}{153.36} = 3.2 \text{ m}$$

From Eq. (18.88),

$$\sigma_6 D^2 + 2\sigma_6 D(L_1 + L_2 - l_1) - 2P_1(L_1 + L_2 - l_1 - \bar{z}_1) = 0$$

$$\sigma_6 = 4c - (\gamma L_1 + \gamma' L_2) = (4)(41) - [(17)(3)$$
$$+ (20 - 9.81)(6)] = 51.86 \text{ kN/m}^2$$

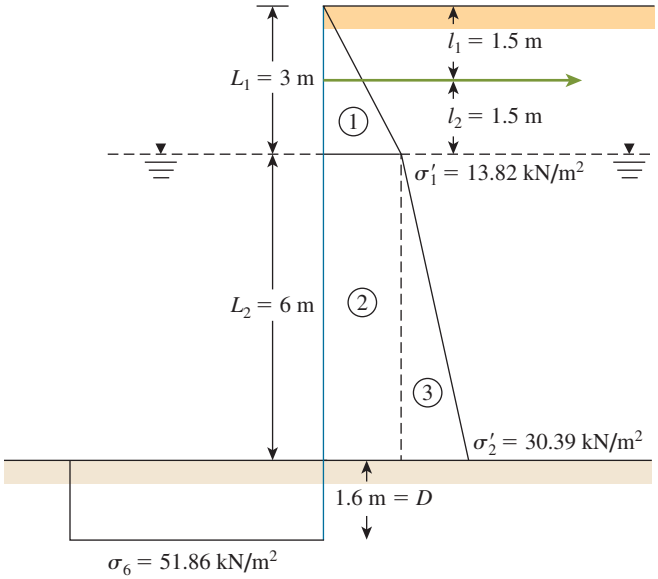


FIGURE 18.39 Free earth support method, with sheet pile penetrating into clay

So,

$$(51.86)D^2 + (2)(51.86)(D)(3 + 6 - 1.5) - (2)(153.36)(3 + 6 - 1.5 - 3.2) = 0$$

or

$$D^2 + 15D - 25.43 = 0$$

Hence,

$$D \approx \mathbf{1.6\ m}$$

Part b

From Eq. (18.87),

$$F = P_1 - \sigma_6 D = 153.36 - (51.86)(1.6) = \mathbf{70.38\ kN/m}$$

EXAMPLE 18.15

Refer to Example 18.14.

a. Increase the actual depth of penetration as $D_{actual} = 1.75D_{theory}$.
b. Determine M_{max}.
c. Use Rowe's moment reduction diagram (Figure 18.38) to find an appropriate sheet-pile section. For the sheet pile (Table 18.1), use $E = 207 \times 10^3$ MN/m^2 and $\sigma_{all} = 172{,}500$ kN/m^2.

SOLUTION

Part a

$$D_{actual} = 1.75D_{theory} = (1.75)(1.6) = \mathbf{2.8\,m}$$

Part b

From Eq. (18.87),

$$F = P_1 - \sigma_6 D_{theory} = 153.36 - (51.86)(1.6) = 70.38\,\text{kN/m}$$

From Eq. (18.74), for zero shear use

$$\frac{1}{2}\sigma_1' L_1 - F + \sigma_1'(z - L_1) + \frac{1}{2}K_a\gamma'(z - L_1)^2 = 0$$

Let $z - L_1 = x$. So,

$$\frac{1}{2}\sigma_1' L_1 - F + \sigma_1' x + \frac{1}{2}K_a\gamma' x^2 = 0$$

or

$$\left(\frac{1}{2}\right)(13.82)(3) - 70.38 + (13.82)(x) + \left(\frac{1}{2}\right)(0.271)(20 - 9.81)x^2 = 0$$

$$1.38x^2 + 13.82x - 49.65 = 0$$

From the above equation, $x \approx 3$ m. Taking the moment about the zero shear point,

$$M_{\max} = -\frac{1}{2}\sigma_1' L_1\left(x + \frac{L_1}{3}\right) + F(x + l_2) - \frac{\sigma_1' x^2}{2} - \frac{1}{2}K_a\gamma' x^2\left(\frac{x}{3}\right)$$

or

$$M_{\max} = -\left(\frac{1}{2}\right)(13.82)\left(3 + \frac{3}{3}\right) + 70.38(3 + 1.5) - \frac{(13.82)(3)^2}{2} - \left(\frac{1}{2}\right)(0.271)(3)^2\left(\frac{3}{3}\right)$$
$$= \mathbf{225.66\ kN \cdot m/m}$$

Part c

From Eq. (18.89),

$$s_n = 1.25\frac{c}{\gamma L_1 + \gamma' L_2} = 1.25\left[\frac{41}{(17 \times 3) + (20 - 9.81)(6)}\right] = 0.457$$

From Eq. (18.90),

$$\alpha = \frac{L_1 + L_2}{L_1 + L_2 + D_{\text{actual}}} = \frac{3 + 6}{3 + 6 + 2.8} = 0.763$$

Now, referring to Figure 18.38 for $S_n = 0.457$ and $\alpha = 0.763$, we have

$\log \rho$	$M_d/M_{\max}$
−3.1	≈ 0.9
−2.6	≈ 0.9
−2.0	≈ 0.9

Hence, for all log ρ values, $M_d/M_{\max} \approx 0.9$. The following table now can be prepared.

Section	I (m⁴/m)	H' (m)	$\rho = (10.91 \times 10^{-7}) \times (H'^4/EI)$	$\log \rho$	S (m³/m)	$M_d = S\sigma_{\text{all}}$	$M_d/M_{\max}$
PZC-12	192.06×10^{-6}	11.8	5.93×10^{-4}	−3.2	120.42×10^{-5}	207.72	0.92

Note: $H' = L_1 + L_2 + D_{\text{actual}} = 3 + 6 + 2.8 = 11.8$ m
$M_{\max} = 225.66\,\text{kN} \cdot \text{m/m}$

Figure 18.40 shows the plot of $M_d/M_{\max}$ versus log ρ. Section PZC-12 falls above the line of $M_d/M_{\max} = 0.9$. So,

PZC-12 will be sufficient.

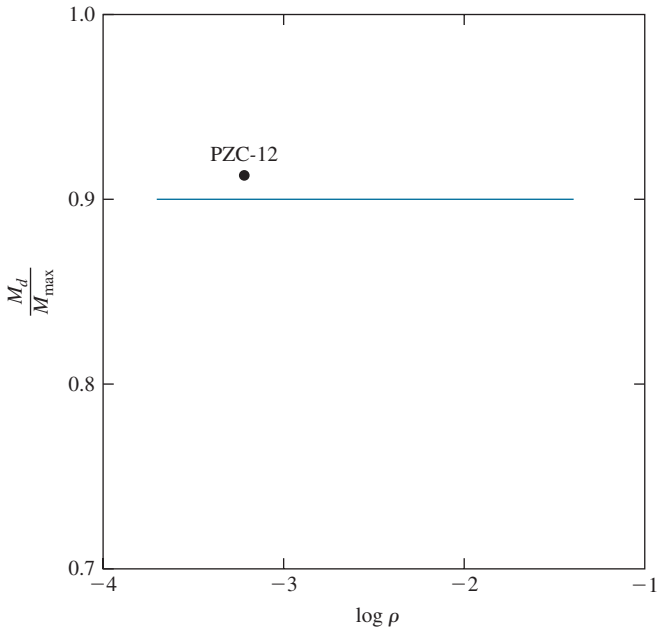


FIGURE 18.40 Plot of M_d/M_{max} versus log ρ (Example 18.15)

18.17 Anchors

Sections 18.10 through 18.16 gave an analysis of anchored sheet-pile walls and discussed how to obtain the force F per unit length of the sheet-pile wall that has to be sustained by the anchors. The current section covers in more detail the various types of anchors generally used and the procedures for evaluating their ultimate holding capacities.

The general types of anchors used in sheet-pile walls are as follows:

1. Anchor beams (deadman anchors)
2. Anchor plates
3. Tiebacks
4. Vertical anchor piles
5. Anchor beams supported by batter (compression and tension) piles

Anchor plates and beams are generally made of cast concrete blocks. (See Figure 18.41a.) The anchors are attached to the sheet pile by *tie rods*. A *wale* is placed at the front or back face of a sheet pile for the purpose of conveniently attaching the tie rod to the wall. To protect the tie rod from corrosion, it is generally coated with paint or asphaltic materials.

In the construction of *tiebacks*, bars or cables are placed in predrilled holes (see Figure 18.41b) with concrete grout (cables are commonly high-strength, prestressed steel tendons). Figures 18.41c and 18.41d show a vertical anchor pile and an anchor beam with batter piles.

PLACEMENT OF ANCHORS

The resistance offered by anchor plates and beams is derived primarily from the passive force of the soil located in front of them. Figure 18.41a, in which AB is the sheet-pile wall, shows the best location for maximum efficiency of an anchor plate. If the anchor is placed inside wedge ABC, which is the Rankine active zone, it would not

provide any resistance to failure. Alternatively, the anchor could be placed in zone *CFEH*. Note that line *DFG* is the slip line for the Rankine passive pressure. If part of the passive wedge is located inside the active wedge *ABC*, full passive resistance of the anchor cannot be realized upon failure of the sheet-pile wall. However, if the anchor is placed in zone *ICH*, the Rankine passive zone in front of the anchor slab or plate is located completely outside the Rankine active zone *ABC*. In this case, full passive resistance from the anchor can be realized.

Figures 18.41b, 18.41c, and 18.41d also show the proper locations for the placement of tiebacks, vertical anchor piles, and anchor beams supported by batter piles.

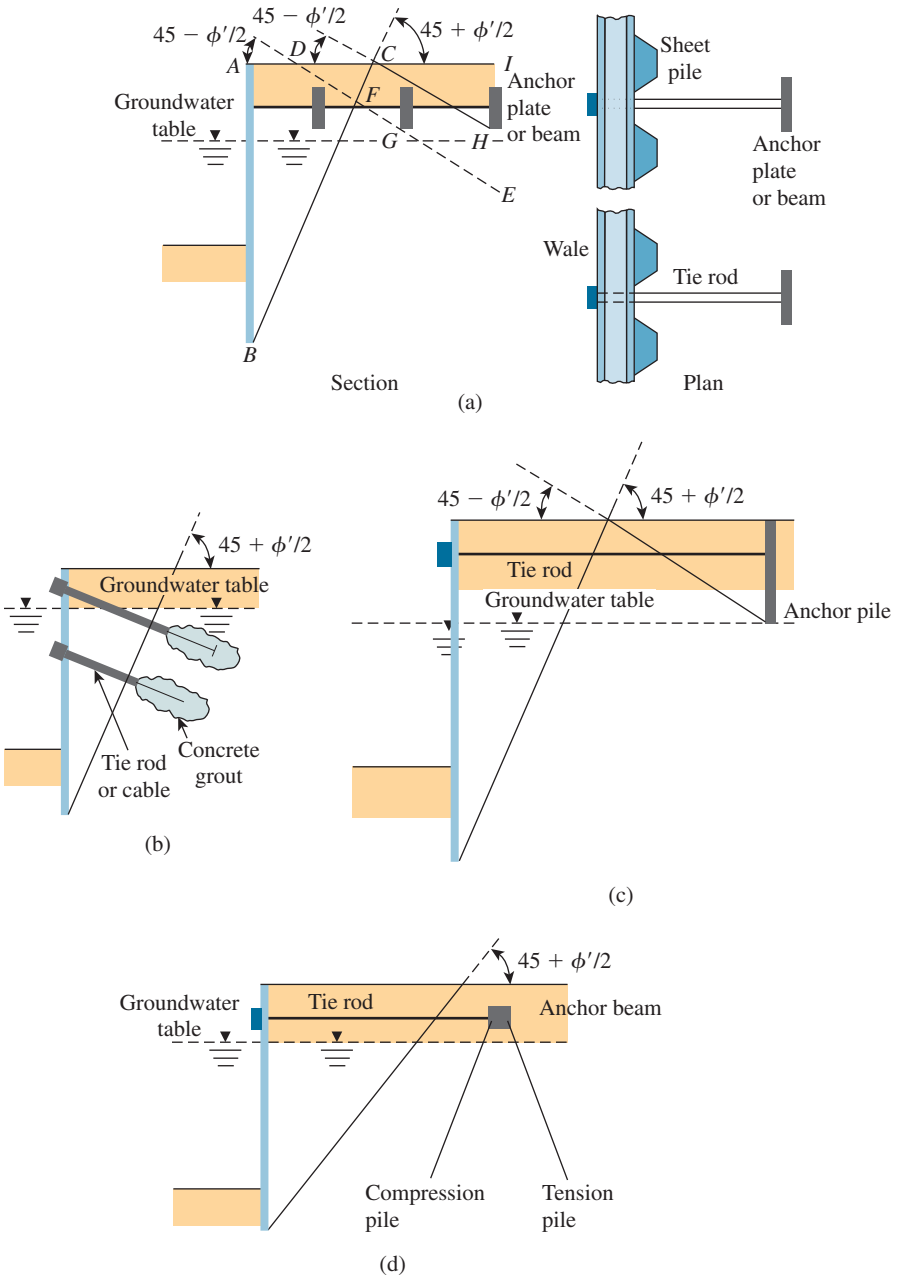


FIGURE 18.41 Various types of anchoring for sheet-pile walls: (a) anchor plate or beam; (b) tieback; (c) vertical anchor pile; (d) anchor beam with batter piles

18.18 Holding Capacity of Deadman Anchors

The deadman anchor should be located far away from the sheet pile, as shown in Figure 18.42a, where the minimum distance is governed by the two dashed lines defining the active and passive failure zones. This ensures that the passive wedge created by the anchor does not interfere with the active wedge behind the sheet pile.

The anchor is designed for a higher load, with a factor of safety (FS) of about 1.5–2.0. If the anchor is near the ground surface, with $h > 0.5H$, it can be assumed that the soil above the anchor and the anchor act together as a rigid block, with active pressure on the right and passive pressure on the left acting over the entire depth of the anchor H. In the case of a continuous beam deadman, from equilibrium considerations,

$$\text{FS} \times T = \left(\frac{1}{2}K_p\gamma H^2 - \frac{1}{2}K_a\gamma H^2\right)s = \frac{1}{2}(K_p - K_a)\gamma H^2 s \qquad (18.91)$$

where T is the tie rod force and s is the horizontal spacing of the tie rods. The depth of the anchor can be determined from Eq. (18.91).

18.19 Holding Capacity of Anchor Plates in Sand

SEMI-EMPIRICAL METHOD

Ovesen and Stromann (1972) proposed a semi-empirical method for determining the ultimate resistance of anchors in sand. Their calculations, made in three steps, are carried out as follows:

Step 1. **Basic Case.** Determine the depth of embedment, H. Assume that the anchor slab has height H and is continuous (i.e., B = length of anchor slab perpendicular to the cross section = ∞), as shown in Figure 18.43, in which the following notation is used:

P_p = passive force per unit length of anchor

P_a = active force per unit length of anchor

ϕ' = effective soil friction angle

δ' = friction angle between anchor slab and soil

P'_{ult} = ultimate resistance per unit length of anchor

W = effective weight per unit length of anchor slab

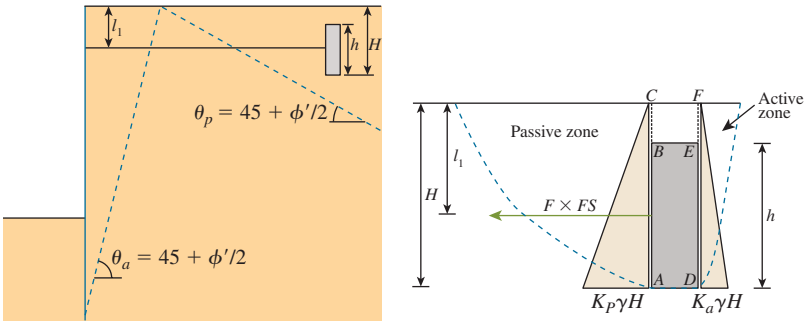


FIGURE 18.42 Deadman anchor: (a) location; (b) equilibrium

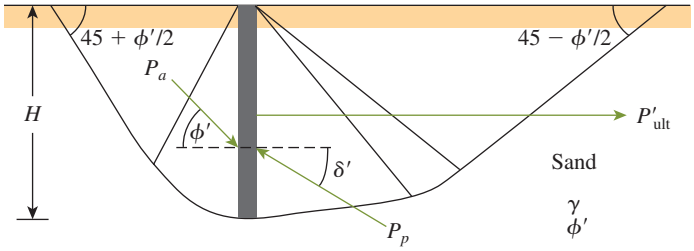


FIGURE 18.43 Basic case: continuous vertical anchor in granular soil

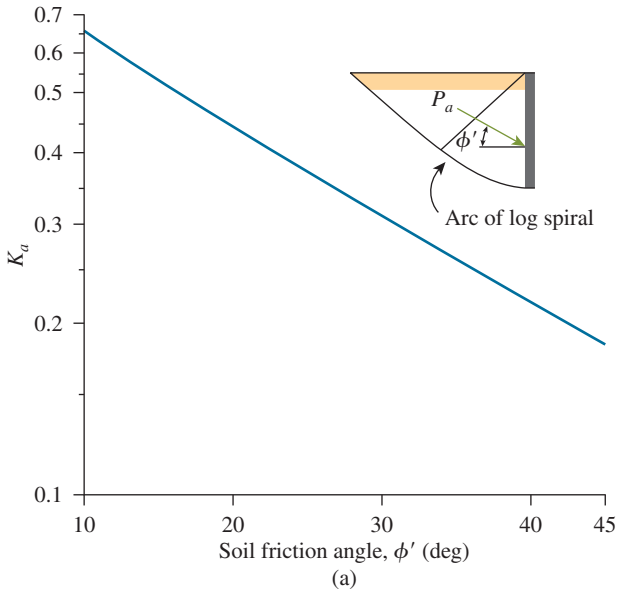
Also,

$$P'_{ult} = \tfrac{1}{2}\gamma H^2 K_p \cos\delta' - P_a \cos\phi' = \tfrac{1}{2}\gamma H^2 K_p \cos\delta' - \tfrac{1}{2}\gamma H^2 K_a \cos\phi'$$
$$= \tfrac{1}{2}\gamma H^2 (K_p \cos\delta' - K_a \cos\phi') \qquad (18.92)$$

where

K_a = active pressure coefficient with $\delta' = \phi'$(see Figure 18.44a)

K_p = passive pressure coefficient



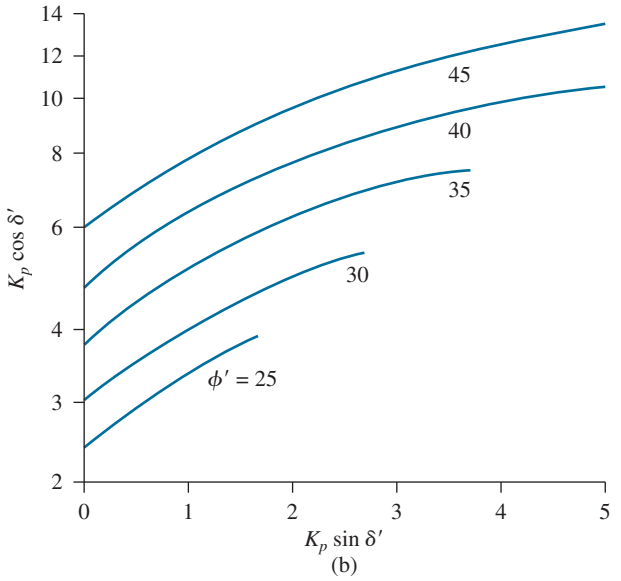


FIGURE 18.44 (a) Variation of K_a for $\delta' = \phi'$, (b) variation of $K_p \cos\delta'$ with $K_p \sin\delta'$ (Based on Ovesen and Stromann, 1972)

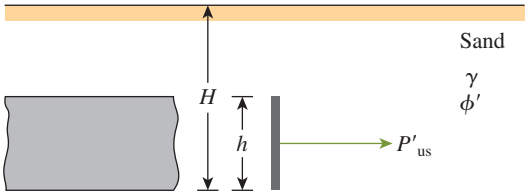


FIGURE 18.45 Strip case: vertical anchor

To obtain $K_p \cos \delta'$, first calculate

$$K_p \sin \delta' = \frac{W + P_a \sin \phi'}{\frac{1}{2}\gamma H^2} = \frac{W + \frac{1}{2}\gamma H^2 K_a \sin \phi'}{\frac{1}{2}\gamma H^2} \tag{18.93}$$

Then use the magnitude of $K_p \sin \delta'$ obtained from Eq. (18.93) to estimate the magnitude of $K_p \cos \delta'$ from the plots given in Figure 18.44b.

Step 2. **Strip Case** (Strip Anchor of Height $h < H$). Determine the actual height h of the anchor to be constructed. If a continuous anchor (i.e., an anchor for which $B = \infty$) of height h is placed in the soil so that its depth of embedment is H, as shown in Figure 18.45, the ultimate resistance per unit length is

$$P'_{us} = \left[\frac{C_{ov} + 1}{C_{ov} + \left(\frac{H}{h}\right)}\right] \underset{\text{Eq. (18.92)}}{\underset{\uparrow}{P'_{ult}}} \tag{18.94}$$

where

P'_{us} = ultimate resistance for the *strip case*

C_{ov} = 19 for dense sand and 14 for loose sand

Step 3. **Actual Plate Anchor.** In practice, the anchor plates are placed in a row with center-to-center spacing S', as shown in Figure 18.46a. The ultimate resistance of each anchor is

$$P_{ult} = P'_{us} B_e \tag{18.95}$$

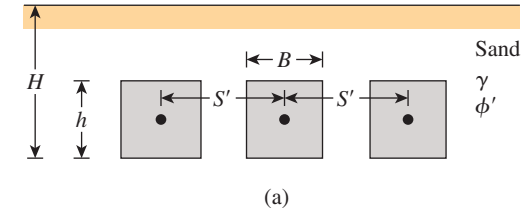
where B_e = equivalent length.

The equivalent length is a function of S', B, H, and h. Figure 18.46b shows a plot of $(B_e - B)/(H + h)$ against $(S' - B)/(H + h)$ for the cases of loose and dense sand. With known values of S', B, H, and h, the value of B_e can be calculated and used in Eq. (18.95) to obtain P_{ult}.

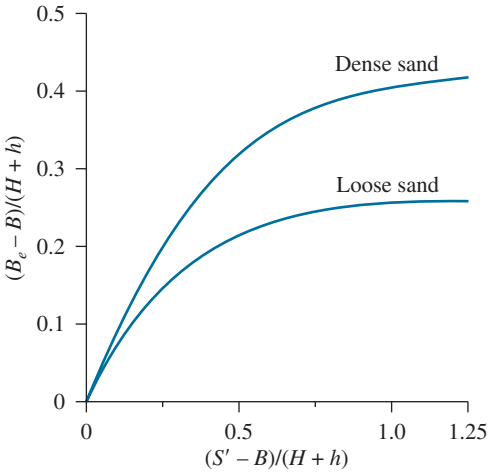
STRESS CHARACTERISTIC SOLUTION

Neely et al. (1973) proposed a stress characteristic solution for anchor pullout resistance using the *equivalent free surface* concept. Figure 18.47 shows the assumed failure surface for a strip anchor. In this figure, OX is the equivalent free surface. The shear stress (s_o) mobilized along OX can be given as

$$m = \frac{s_o}{\sigma'_o \tan \phi'} \tag{18.96}$$



(a)



(b)

FIGURE 18.46 (a) Actual case for row of anchors; (b) variation of $(B_e - B)/(H + h)$ with $(S' - B)/(H + h)$ (Based on Ovesen and Stromann, 1972)

where

m = shear stress mobilization factor

σ'_o = effective normal stress along OX

Using this analysis, the ultimate resistance (P_{ult}) of an anchor (length = B and height = h) can be given as

$$P_{ult} = M_{\gamma q}(\gamma h^2)BF_s \tag{18.97}$$

where

$M_{\gamma q}$ = force coefficient

F_s = shape factor

γ = effective unit weight of soil

The variations of $M_{\gamma q}$ for $m = 0$ and 1 are shown in Figure 18.48. For conservative design, $M_{\gamma q}$ with $m = 0$ may be used. The shape factor (F_s) determined experimentally is shown in Figure 18.49 as a function of B/h and H/h.

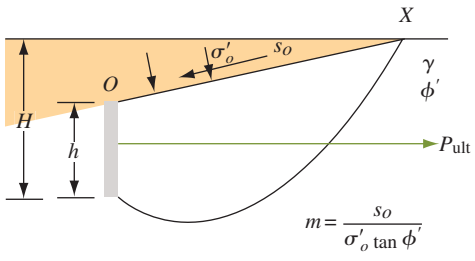


FIGURE 18.47 Assumed failure surface in soil for stress characteristic solution

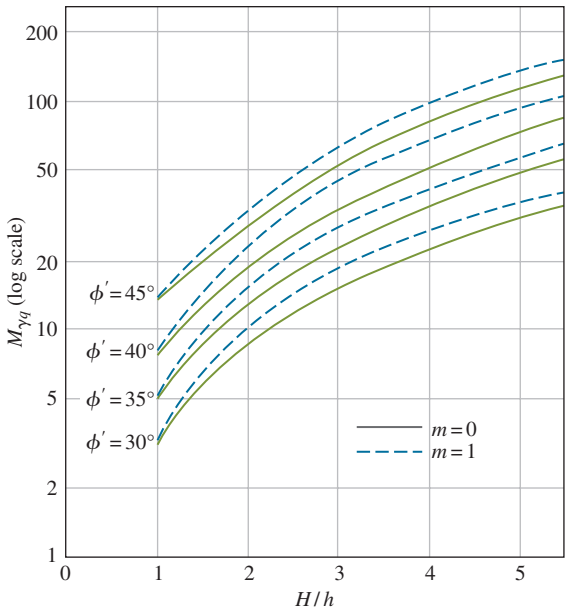


FIGURE 18.48 Variation of $M_{\gamma q}$ with H/h and ϕ' (Based on Neeley et al., 1973)

EMPIRICAL CORRELATION BASED ON MODEL TESTS

Ghaly (1997) used the results of 104 laboratory tests, 15 centrifugal model tests, and 9 field tests to propose an empirical correlation for the ultimate resistance of single anchors. The correlation can be written as

$$P_{ult} = \frac{5.4}{\tan \phi'}\left(\frac{H^2}{A}\right)^{0.28} \gamma AH \tag{18.98}$$

where A = area of the anchor = Bh.

Ghaly also used the model test results of Das and Seeley (1975) to develop a load-displacement relationship for single anchors. The relationship can be given as

$$\frac{P}{P_{ult}} = 2.2\left(\frac{u}{H}\right)^{0.3} \tag{18.99}$$

where u = horizontal displacement of the anchor at a load level P.

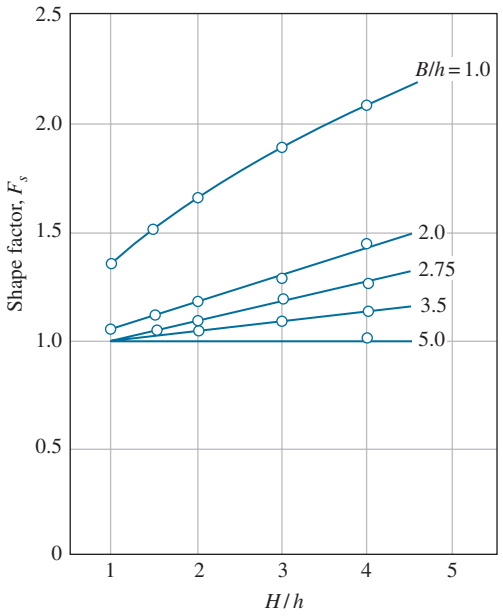


FIGURE 18.49 Variation of shape factor with H/h and B/h (Based on Neeley et al., 1973)

Equations (18.98) and (18.99) apply to single anchors (i.e., anchors for which $S'/B = \infty$). For all practical purposes, when $S'/B \geq 2$ the anchors behave as single anchors.

FACTOR OF SAFETY FOR ANCHOR PLATES

The allowable resistance per anchor plate may be given as

$$P_{all} = \frac{P_{ult}}{FS}$$

where FS = factor of safety.

Generally, a factor of safety of 2 is suggested when the method of Ovesen and Stromann is used. A factor of safety of 3 is suggested for P_{ult} calculated by Eq. (18.98).

SPACING OF ANCHOR PLATES

The center-to-center spacing of anchors, S', may be obtained from

$$S' = \frac{P_{all}}{F}$$

where F = force per unit length of the sheet pile.

EXAMPLE 18.16

Refer to Figure 18.46a. Given: $B = h = 0.4$ m, $S' = 1.2$ m, $H = 1$ m, $\gamma = 16.51$ kN/m^3, and $\phi' = 35°$. Determine the ultimate resistance for each anchor plate. The anchor plates are made of concrete and have thicknesses of 0.15 m.

SOLUTION

From Figure 18.44a, for $\phi' = 35°$, the magnitude of K_a is about 0.26.

$$W = Ht\gamma_{concrete} = (1 \text{ m})(0.15 \text{ m})(23.5 \text{ kN/m}^3)$$
$$= 3.525 \text{ kN/m}$$

From Eq. (18.93),

$$K_p \sin \delta' = \frac{W + \frac{1}{2}\gamma H^2 K_a \sin \phi'}{\frac{1}{2}\gamma H^2}$$

$$= \frac{3.525 + (0.5)(16.51)(1)^2(0.26)(\sin 35)}{(0.5)(16.51)(1)^2} = 0.576$$

From Figure 18.44b, with $\phi' = 35°$ and $K_p \sin \delta' = 0.576$, the value of $K_p \cos \delta'$ is about 4.5. Now, using Eq. (18.92),

$$P'_{ult} = \tfrac{1}{2}\gamma H^2(K_p \cos \delta' - K_a \cos \phi')$$
$$= \left(\tfrac{1}{2}\right)(16.51)(1)^2[4.5 - (0.26)(\cos 35)] = 35.39 \text{ kN/m}$$

In order to calculate P'_{us}, let us assume the sand to be loose. So, C_{ov} in Eq. (18.94) is equal to 14. Hence,

$$P'_{us} = \left[\frac{C_{ov} + 1}{C_{ov} + \left(\frac{H}{h}\right)}\right] P'_{ult} = \left[\frac{14 + 1}{14 + \left(\frac{1}{0.4}\right)}\right](35.39) = 32.17 \text{ kN/m}$$

$$\frac{S' - B}{H + h} = \frac{1.2 - 0.4}{1 + 0.4} = \frac{0.8}{1.4} = 0.571$$

For $(S' - B)/(H + h) = 0.571$ and loose sand, Figure 18.46b yields

$$\frac{B_e - B}{H + h} = 0.229$$

So

$$B_e = (0.229)(H + h) + B = (0.229)(1 + 0.4) + 0.4$$
$$= 0.72$$

Hence, from Eq. (18.95),

$$P_{ult} = P'_{us} B_e = (32.17)(0.72) = \mathbf{23.16\ kN}$$

EXAMPLE 18.17

Refer to the *single anchor* given in Example 18.16 using the stress characteristic solution. Estimate the ultimate anchor resistance. Use $m = 0$ in Figure 18.48.

SOLUTION

Given: $B = h = 0.4$ m and $H = 1$ m. Thus,

$$\frac{H}{h} = \frac{1\text{ m}}{0.4\text{ m}} = 2.5$$
$$\frac{B}{h} = \frac{0.4\text{ m}}{0.4\text{ m}} = 1$$

From Eq. (18.97),

$$P_{ult} = M_{\gamma q} \gamma h^2 B F_s$$

From Figure 18.48, with $\phi' = 35°$ and $H/h = 2.5$, $M_{\gamma q} \approx 18.2$. Also, from Figure 18.49, with $H/h = 2.5$ and $B/h = 1$, $F_s \approx 1.8$. Hence,

$$P_{ult} = (18.2)(16.51)(0.4)^2(0.4)(1.8) \approx \mathbf{34.62\ kN}$$

EXAMPLE 18.18

Solve Example 18.17 using Eq. (18.98).

SOLUTION

From Eq. (18.98),

$$P_{ult} = \frac{5.4}{\tan \phi'} \left(\frac{H^2}{A}\right)^{0.28} \gamma A H$$

$$H = 1\text{ m}$$

$$A = Bh = (0.4 \times 0.4) = 0.16\text{ m}^2$$

$$P_{ult} = \frac{5.4}{\tan 35} \left[\frac{(1)^2}{0.16}\right]^{0.28} (16.51)(0.16)(1) \approx \mathbf{34.03\ kN}$$

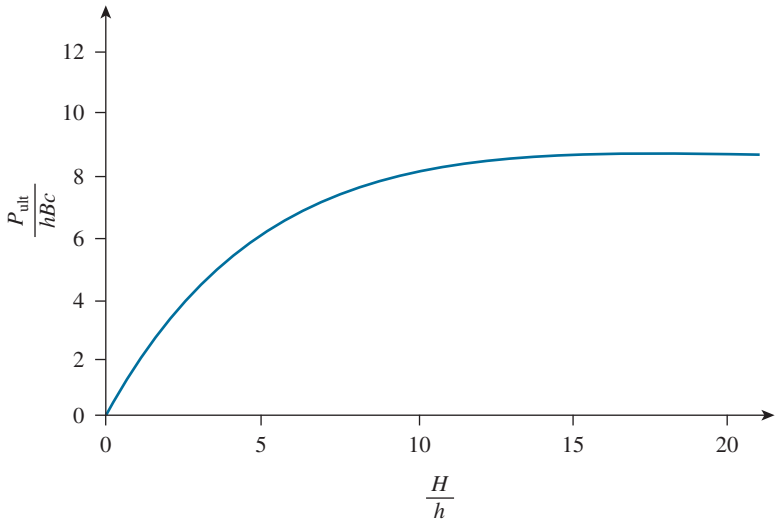


FIGURE 18.50 Experimental variation of $\frac{P_{ult}}{hBc}$ with H/h for plate anchors in clay (Based on Mackenzie (1955) and Tschebotarioff (1973))

18.20 Holding Capacity of Anchor Plates in Clay ($\phi = 0$ Condition)

Relatively few studies have been conducted on the ultimate resistance of anchor plates in clayey soil ($\phi = 0$). Mackenzie (1955) and Tschebotarioff (1973) identified the nature of variation of the ultimate resistance of strip anchors and beams as a function of H, h, and c (undrained cohesion based on $\phi = 0$) in a nondimensional form based on laboratory model test results. This is shown in the form of a nondimensional plot in Figure 18.50 (P_{ult}/hBc versus H/h) and can be used to estimate the ultimate resistance of anchor plates in saturated clay ($\phi = 0$).

18.21 Ultimate Resistance of Tiebacks

According to Figure 18.51, the ultimate resistance offered by a tieback in sand is

$$P_{ult} = \pi d l \bar{\sigma}'_o K \tan \phi' \tag{18.100}$$

where

ϕ' = effective angle of friction of soil

$\bar{\sigma}'_o$ = average effective vertical stress ($=\gamma z$ in dry sand)

K = earth pressure coefficient

The magnitude of K can be taken to be equal to the earth pressure coefficient at rest (K_o) if the concrete grout is placed under pressure (Littlejohn, 1970). The lower limit of K can be taken to be equal to the Rankine active earth pressure coefficient.

In clays, the ultimate resistance of tiebacks may be approximated as

$$P_{ult} = \pi d l c_a \tag{18.101}$$

where c_a = adhesion

The value of c_a may be approximated as $\frac{2}{3}c_u$ (where c_u = undrained cohesion). A factor of safety of 1.5 to 2 may be used over the ultimate resistance to obtain the allowable resistance offered by each tieback.

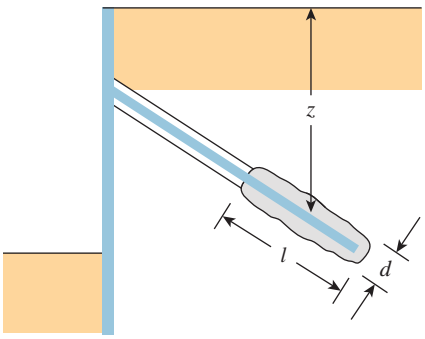


FIGURE 18.51 Parameters for defining the ultimate resistance of tiebacks

18.22 Summary

When the excavation area is very wide, it is not possible to use horizontal struts between the walls to ensure stability. In that case, sheet piles are driven into the ground prior to excavation, to a depth that provides sufficient embedment and, hence, fixity to support the wall during the excavation. Cantilever sheet-pile walls act like vertical cantilevers that are fixed at the bottom, with active and passive earth pressures on the two sides. They are effective for supporting the walls of excavations up to about 6 m (≈20 ft) in depth.

The first few sections of the chapter discussed cantilever sheet piles, and following sections covered anchored sheet piles and then anchors. In each case, the situations in sands and clays were treated separately. While the main focus was on theoretical developments, including the failure mechanisms under active and passive states within the soil, empirical design methods were also discussed.

PROBLEMS

18.1 Refer to Figure 18.9. A cantilever sheet pile is driven into a granular soil where the water table is 2 m (L_1) below the top of the sand. The properties of the sand are $\phi' = 40°$, $\gamma = 17.5$ kN/m^3, and $\gamma_{sat} = 19$ kN/m^3. It is proposed to excavate to a depth of 6 m (L) below the ground level. Determine the actual depth to which the sheet pile must be driven ($L + D$), using the net lateral pressure diagram. Note:

$$D_{actual} = 1.3(L_3 + L_4)_{theory}$$

18.2 In Problem 18.1, determine the maximum moment and its location. Assuming an allowable stress of 170 MN/m^2, select a sheet-pile section from Table 18.1.

18.3 A 5 m deep excavation is required in a dry sand where $\gamma = 17.5$ kN/m^3 and $\phi' = 32°$ (see Figure 18.11). Determine the actual depth to which the sheet pile has to be driven and the required section (from Table 18.1), assuming allowable stress of 190 MN/m^2. Use the net pressure diagram.

$$D_{actual} = 1.3D_{theory}$$

18.4 Refer to Figure 18.13. Given $L_1 = 1.5$ m, $L_2 = 3$ m; for the sand, $\phi' = 33°$, $\gamma = 16.5$ kN/m^3, $\gamma_{sat} = 19.0$ kN/m^3; and, for the clay, $c = 50$ kN/m^2, $\phi = 0$, and $\gamma_{sat} = 20$ kN/m^3. Determine the depth of sheet pile required, allowing for a 50% increase from the theoretical estimate.

18.5 In Problem 18.4, find the maximum bending moment in the sheet pile and determine the required section modulus, assuming an allowable stress of 190 MN/m^2.

18.6 In a sandy soil ($\phi' = 35°$; $\gamma = 18.0$ kN/m^3, and $\gamma_{sat} = 20.0$ kN/m^3), the water table is located at a depth of 5 m below the ground level. How deep would you drive a sheet pile to carry out an excavation to 4.0 m depth? Use the simplified approach discussed in Section 18.8, with a factor of safety of 1.5 on passive resistance (i.e., use $K_p/1.5$).

18.7 The water table at a site is at 5 m below the ground level, and it is required to excavate to this level. The soil profile consists of a thick bed of sand where the unit weight is 17.0 kN/m^3 above the water table and 20.0 kN/m^3 below the water table. The friction angle of the sand is 37°. The walls of the excavation will be supported by a cantilever sheet pile.

a. How deep would you drive the sheet piles? Use the simplified approach discussed in Section 18.8, with factor of safety of 1.5 on the passive resistance.

b. Determine the maximum bending moment in the sheet piles and the required section modulus for the sheet-pile section, assuming an allowable stress of 190 MN/m^2.

18.8 The water table lies at a depth of 3 m below the ground level at a site that consists entirely of sands. A 7 m deep excavation is to be made with the use of anchored sheet piles to support the excavation. The tie rod of the anchor will be placed 1 m below the ground, with horizontal spacing of the tie rods being 3 m. The unit weights of the sand above and below the water table are 17.0 kN/m^3 and 20.0 kN/m^3, respectively. The friction angle of the sand is 35°.

a. How deep would you drive the sheet pile, allowing a factor of safety of 1.5 on the passive resistance?

b. What is the load on the tie rods?

Use the simplified approach described in Section 18.10.

18.9 Refer to Figure 18.23. Given $L_1 = 3$ m, $L_2 = 6$ m, $l_1 = 1.5$ m, $\gamma = 16.5$ kN/m^3, $\gamma_{sat} = 19.0$ kN/m^3, and $\phi' = 35°$.

a. Find the required depth of the sheet pile, increasing the theoretical estimate by 30%.

b. Determine the force in the tie rods if they are spaced 3 m apart horizontally.

c. Find the maximum bending moment in the sheet pile.

18.10 Redo Problem 18.9 using the Hagerty and Nofal (1992) charts from Section 18.12.

18.11 In Problem 18.9, apply Rowe's moment reduction and select a sheet-pile section from Table 18.1, assuming $E = 210 \times 10^3$ MN/m^2 and $\sigma_{all} = 210 \times 10^3$ kN/m^2.

18.12 In Problem 18.9, use the computational pressure diagram method discussed in Section 18.14, and determine the depth of sheet pile, the anchor force, and the maximum bending moment. Assume $C = 0.72$ and $R = 0.6$.

18.13 Refer to Figure 18.37. Given: $L_1 = 4$ m, $L_2 = 6$ m, $l_1 = 2$ m; for the sand, $\gamma = 17.0$ kN/m^3, $\gamma_{sat} = 19.0$ kN/m^3, $\phi' = 34°$; and for the clay, $\gamma_{sat} = 20.0$ kN/m^3, $c = 40$ kN/m^2, $\phi = 0$.

Determine the theoretical depth of embedment (D) and the anchor force (F).

18.14 Refer to Problem 18.8. Using the results of Problem 18.8, design a continuous anchor (Section 18.18) and show a sketch with dimensions. Use FS = 1.5 for the tie rods.

18.15 The tie rods from anchored sheet piles will be connected using a row of anchors, as shown in Figure 18.46a. Here $H = 2.0$ m, $h = 1.25$ m, $B = 1.5$ m, $S' = 2.5$ m, $\phi' = 32°$, and $\gamma = 17.5$ kN/m^3. The anchor plates are made of 100 mm thick reinforced concrete with a unit weight of 24.0 kN/m^3. Determine the ultimate holding capacity of the anchor using Ovesen and Stromann's method.

18.16 Using Eq. (18.97) with $m = 0.5$, determine the ultimate holding capacity of the anchor in sand where $H = 1.2$ m, $h = 0.75$ m, $B = 0.9$ m, and $\phi' = 32°$.

18.17 Assuming that the spacing of the anchors S' is very large in Problem 18.16, determine the ultimate holding capacity using Eq. (18.98). What would be the anchor displacement when the load on the tie rod is 100 kN?

REFERENCES

Casagrande, L. (1973). "Comments on Conventional Design of Retaining Structures," *Journal of the Soil Mechanics and Foundations Division*, ASCE, Vol. 99, No. SM2, pp. 181–198.

Das, B. M. and Seeley, G. R. (1975). "Load–Displacement Relationships for Vertical Anchor Plates," *Journal of the Geotechnical Engineering Division*, American Society of Civil Engineers, Vol. 101, No, GT7, pp. 711–715.

Ghaly, A. M. (1997). "Load–Displacement Prediction for Horizontally Loaded Vertical Plates." *Journal of Geotechnical and Geoenvironmental Engineering*, ASCE, Vol. 123, No. 1, pp. 74–76.

Hagerty, D. J. and Nofal, M. M. (1992). "Design Aids: Anchored Bulkheads in Sand," *Canadian Geotechnical Journal*, Vol. 29, No. 5, pp. 789–795.

Littlejohn, G. S. (1970). "Soil Anchors," *Proceedings, Conference on Ground Engineering*, Institution of Civil Engineers, London, pp. 33–44.

Mackenzie, T. R. (1955). *Strength of Deadman Anchors in Clay*, M.S. Thesis, Princeton University, Princeton, NJ.

Nataraj, M. S. and Hoadley, P. G. (1984). "Design of Anchored Bulkheads in Sand," *Journal of Geotechnical Engineering*, American Society of Civil Engineers, Vol. 110, No. GT4, pp. 505–515.

Neeley, W. J., Stuart, J. G., and Graham, J. (1973). "Failure Loads of Vertical Anchor Plates in Sand," *Journal of the Soil Mechanics and Foundations Division*, American Society of Civil Engineers, Vol. 99, No. SM9, pp. 669–685.

Ovesen, N. K. and Stromann, H. (1972). "Design Methods for Vertical Anchor Slabs in Sand," *Proceedings, Specialty Conference on Performance of Earth and Earth-Supported Structures*. American Society of Civil Engineers, Vol. 2.1, pp. 1481–1500.

Rowe, P. W. (1952). "Anchored Sheet-Pile Walls," *Proceedings, Institution of Civil Engineers*, Vol. 1, Issue 1, pp. 27–70.

Rowe, P. W. (1957). "Sheet-Pile Walls in Clay," *Proceedings, Institution of Civil Engineers*, Vol. 7, Issue 3, pp. 654–692.

Tschebotarioff, G. P. (1973). *Foundations, Retaining and Earth Structures*, 2nd ed., McGraw-Hill, New York.

Tsinker, G. P. (1983). "Anchored Sheet Pile Bulkheads: Design Practice," *Journal of Geotechnical Engineering*, American Society of Civil Engineers, Vol. 109, No. GT8, pp. 1021–1038.

19

Braced Cuts



Aisyaqilumaranas/Shutterstock.com

19.1 Introduction 815
19.2 Braced-Cut Analysis Based on General Wedge Theory 817
19.3 Pressure Envelope for Braced-Cut Design 820
19.4 Pressure Envelope for Cuts in Layered Soil 822
19.5 Design of Various Components of a Braced Cut 823
19.6 Case Studies of Braced Cuts 831
19.7 Bottom Heave of a Cut in Clay 835
19.8 Stability of the Bottom of a Cut in Sand 839
19.9 Lateral Yielding of Sheet Piles and Ground Settlement 843
19.10 Summary 845
PROBLEMS 845
REFERENCES 846

19.1 Introduction

Sometimes construction work requires ground excavations with vertical or near-vertical faces—for example, basements of buildings in developed areas or underground transportation facilities at shallow depths below the ground surface (a cut-and-cover type of construction). The vertical faces of the cuts need to be protected by temporary bracing systems to avoid failure that may be accompanied by considerable settlement or by bearing capacity failure of nearby foundations.

Figure 19.1 shows two types of braced cut commonly used in construction work. One type uses the *soldier beam* (Figure 19.1a), which is a vertical steel or

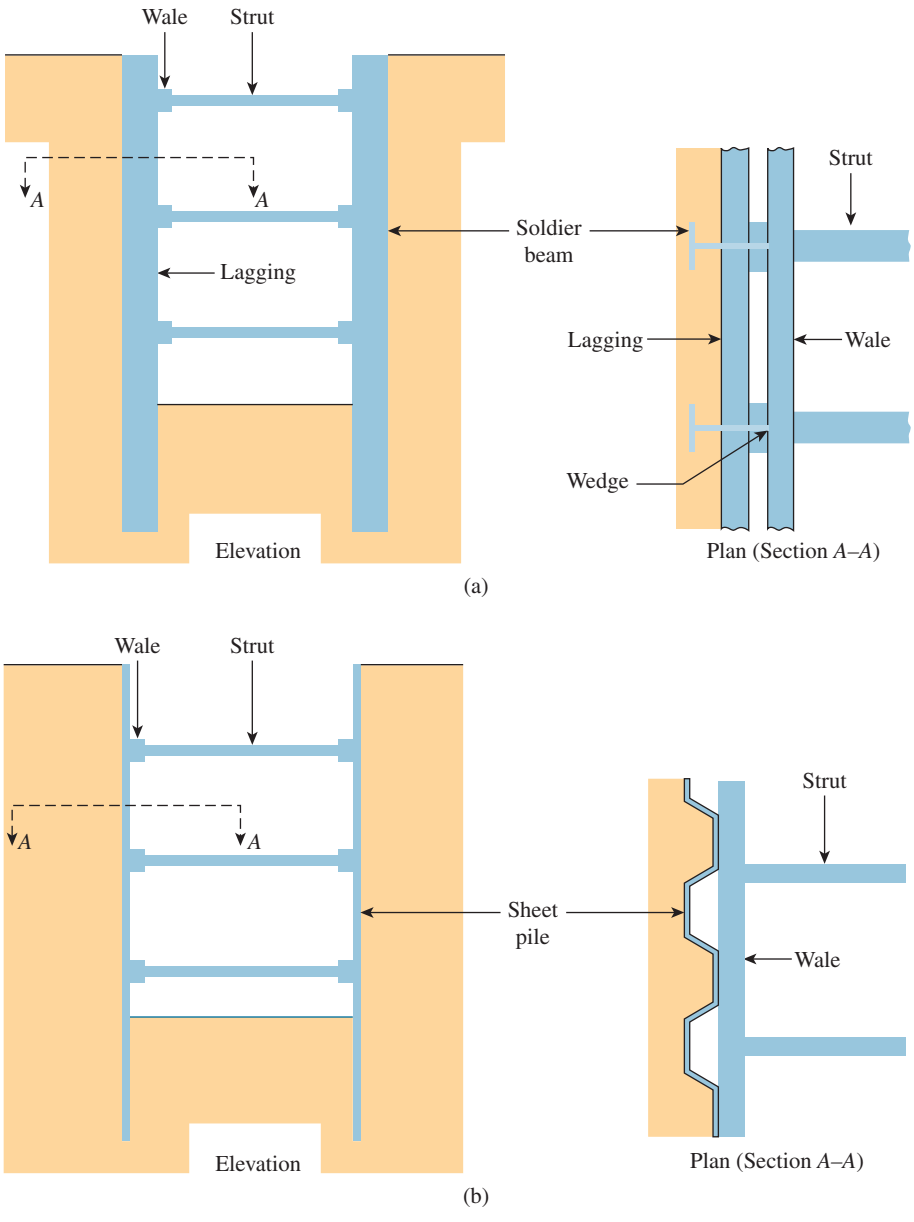


FIGURE 19.1 Types of braced cut: (a) use of soldier beams; (b) use of sheet piles

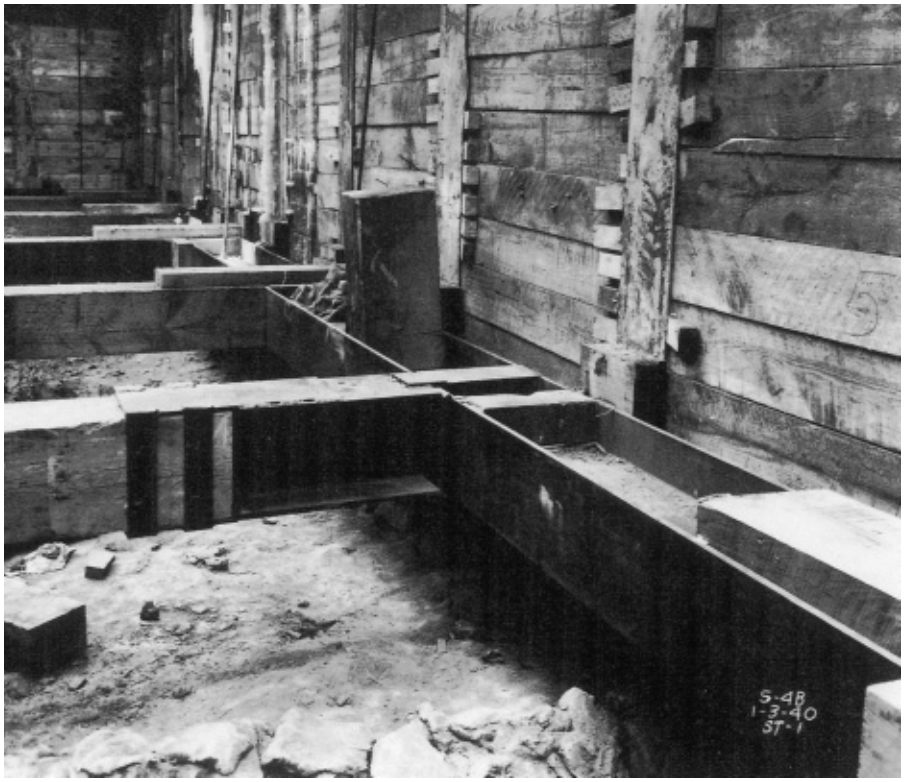


FIGURE 19.2 Braced cut in Chicago Subway construction, January 1940 (Courtesy of Ralph B. Peck)

timber beam driven into the ground before excavation. *Laggings*, which are horizontal timber planks, are placed between soldier beams as the excavation proceeds. When the excavation reaches the desired depth, *wales* and *struts* (horizontal steel beams) are installed. The struts are compression members. Figure 19.1b shows another type of braced excavation. In this case, interlocking *sheet piles* are driven into the soil before excavation. Wales and struts are inserted immediately after excavation reaches the appropriate depth.

Figure 19.2 shows the braced-cut construction used for the Chicago subway in 1940. Timber lagging, timber struts, and steel wales were used. Figure 19.3 shows a braced cut made during the construction of the Washington, DC, metro in 1974. In this cut, timber lagging, steel H-soldier piles, steel wales, and pipe struts were used.

To design braced excavations (i.e., to select wales, struts, sheet piles, and soldier beams), an engineer must estimate the lateral earth pressure to which the braced cuts will be subjected. The theoretical aspects of the lateral earth pressure on a braced cut are discussed in Section 19.2. The total active force per unit length of the wall (P_a) can be calculated by using the general wedge theory. However, that analysis will not provide the relationships required for estimating the variation of lateral pressure with depth, which is a function of several factors, such as the type of soil, the experience of the construction crew, the type of construction equipment used, and so forth. For that reason, empirical pressure envelopes developed from



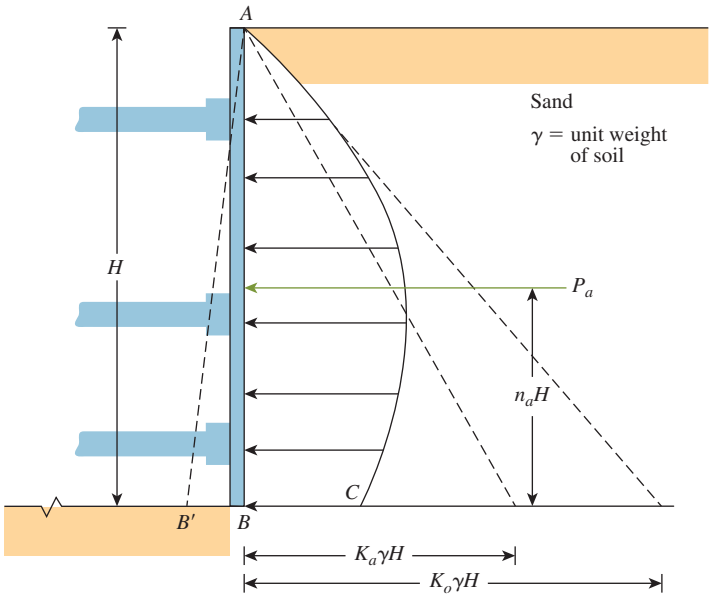
FIGURE 19.3 Braced cut in the construction of Washington, DC Metro, May 1974 (Courtesy of Ralph B. Peck)

field observations are used for the design of braced cuts. This procedure is discussed in the following sections.

19.2 Braced-Cut Analysis Based on General Wedge Theory

Figure 19.4 shows a braced cut of height H. Let us assume that AB is a *frictionless* wall retaining a granular soil. During the excavation process followed by the placement of struts, the upper portion of the soil mass next to the cut does not undergo sufficient lateral deformation. However, as the depth of excavation increases, the time lag between the excavation and placement of struts increases, also resulting in a gradual increase in the lateral deformation of wall AB. Ideally, at the end of excavation, wall AB will be deformed to the shape AB'. The lateral earth pressure distribution along wall AB will be of the nature shown in Figure 19.4. It is important to note the following:

- The wall AB rotates about A (i.e., rotation about the top).
- At A, the lateral earth pressure will be close to the at-rest earth pressure (practically no lateral deformation of the wall).



Note: K_o = earth pressure coefficient at-rest
K_a = Rankine active earth pressure coefficient

FIGURE 19.4 Earth pressure behind a frictionless wall retaining sand, with wall rotation about the top

- At B, the lateral earth pressure may be less than the Rankine active earth pressure. (The deformation of the wall is large, and the soil may be in a state well past the plastic equilibrium.)
- Hence, the lateral earth pressure diagram will approximate to the form ACB, as shown in Figure 19.4.

With this type of pressure distribution, the point of application of the resultant active thrust, P_a, will be at a height n_aH measured from the bottom of the wall. The magnitude of n_a will be greater than 1/3.

The magnitude of the active thrust, P_a, can be determined by considering several trial failure surfaces in soil, based on the general wedge theory (Terzaghi, 1943). Figure 19.5 shows a braced cut AB in $c'-\phi'$ soil. Bb_1 is assumed to be a failure surface in the soil behind the wall that is an arc of a logarithmic spiral with its center located at O_1. The equation for the logarithmic spiral can be given as

$$r = r_o e^{\theta \tan \phi'} \tag{19.1}$$

where

r = radius of the spiral

r_o = starting radius at $\theta = 0$

ϕ' = angle of friction of soil

θ = angle between r and r_o

An important property of the logarithmic spiral defined by Eq. (19.1) is that any radial line makes an angle ϕ' with the normal to the curve drawn at the point where the radial line and the spiral intersect.

The forces *per unit length of the cut* acting on the soil wedge are

- Weight of the wedge = W_1
- Resultant of the normal and shear forces (frictional) along Bb_1 = F_1

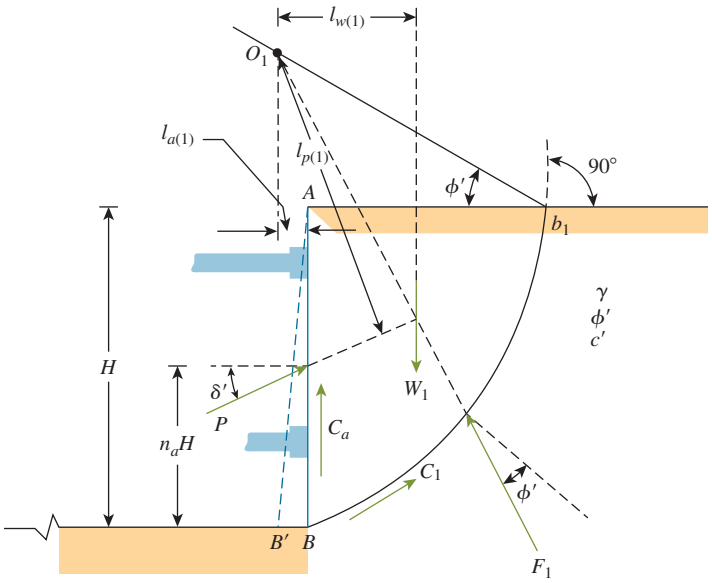


FIGURE 19.5 Determination of active force on bracing system of open cut in a $c'-\phi'$ soil—the general wedge theory

- Cohesive force along $Bb = C_1$
- Adhesive force along $AB = C_a = c'_aH$ (where c'_a = unit adhesion)
- Active force P inclined at an angle δ' to the normal drawn to the wall AB

Now, taking the moment of all the forces about O_1,

$$W_1 l_{w(1)} + F_1(0) - C_a l_{a(1)} - M_{C(1)} - P l_{p(1)} = 0 \tag{19.2}$$

where

$M_{C(1)}$ = moment of the cohesive force C_1

$$= \frac{c'}{2\tan\phi'}(r^2 - r_o^2) \tag{19.3}$$

$r_o = \overline{O_1 b_1}$

$r = \overline{O_1 B}$

c' = unit cohesion

Thus, from Eq. (19.2),

$$P = \frac{W_1 l_{w(1)} - C_a l_{a(1)} - M_{C(1)}}{l_{p(1)}} \tag{19.4}$$

If this procedure for determining P is repeated for several trial wedges, the maximum value of $P = P_a$ (active thrust) can be obtained.

Table 19.1 provides the variation of $P_a/(0.5\gamma H^2)$ with ϕ', δ'/ϕ', and n_a for granular soil ($c' = 0$) determined by using the general wedge theory described previously. The values of $P_a/(0.5\gamma H^2)$ may be, in general, 15 to 20% more than those obtained from Coulomb's theory for similar wall and soil parameters. However, the analysis does not provide the distribution of the lateral earth pressure with depth. Also, the magnitude of n_a will depend on several factors that may be soil and site specific.

TABLE 19.1 Active Pressure for Wall Rotation—General Wedge Theory (Granular Soil Backfill)

Soil friction angle, ϕ' (deg)	$P_a/0.5\,\gamma H^2$				
	δ'/ϕ'	$n_a = 0.3$	$n_a = 0.4$	$n_a = 0.5$	$n_a = 0.6$
25	0	0.371	0.405	0.447	0.499
	1/2	0.345	0.376	0.413	0.460
	2/3	0.342	0.373	0.410	0.457
	1	0.344	0.375	0.413	0.461
30	0	0.304	0.330	0.361	0.400
	1/2	0.282	0.306	0.334	0.386
	2/3	0.281	0.305	0.332	0.367
	1	0.289	0.313	0.341	0.377
35	0	0.247	0.267	0.290	0.318
	1/2	0.231	0.249	0.269	0.295
	2/3	0.232	0.249	0.270	0.296
	1	0.243	0.262	0.289	0.312
40	0	0.198	0.213	0.230	0.252
	1/2	0.187	0.200	0.216	0.235
	2/3	0.190	0.204	0.220	0.239
	1	0.197	0.211	0.228	0.248
45	0	0.205	0.220	0.237	0.259
	1/2	0.149	0.159	0.171	0.185
	2/3	0.153	0.164	0.176	0.196
	1	0.173	0.184	0.198	0.215

19.3 Pressure Envelope for Braced-Cut Design

As mentioned in Section 19.1, the lateral earth pressure in a braced cut is dependent on the type of soil, construction method, and type of equipment used. The lateral earth pressure changes from place to place. Each strut should also be designed for the maximum load to which it may be subjected. Therefore, the braced cuts should be designed using apparent-pressure diagrams that are envelopes of all the pressure diagrams determined from measured strut loads in the field. Figure 19.6 shows the method for obtaining the apparent-pressure diagram at a section from strut loads. In this figure, let $P_1, P_2, P_3, P_4, \ldots$ be the measured strut loads. The apparent horizontal pressure can then be calculated as

$$\sigma_1 = \frac{P_1}{(s)\left(d_1 + \frac{d_2}{2}\right)}$$

$$\sigma_2 = \frac{P_2}{(s)\left(\frac{d_2}{2} + \frac{d_3}{2}\right)}$$

$$\sigma_3 = \frac{P_3}{(s)\left(\frac{d_3}{2} + \frac{d_4}{2}\right)}$$

$$\sigma_4 = \frac{P_4}{(s)\left(\frac{d_4}{2} + \frac{d_5}{2}\right)}$$

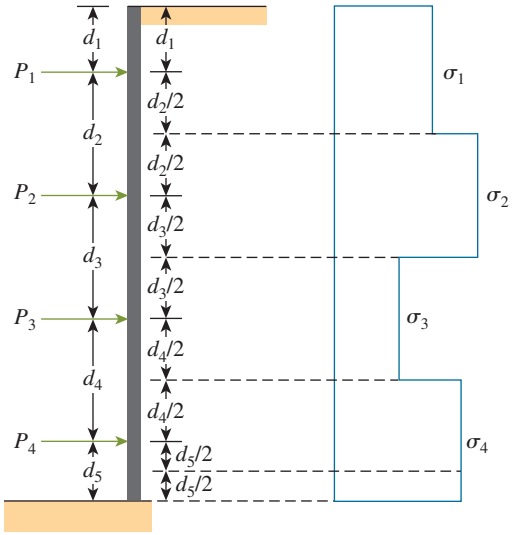


FIGURE 19.6 Procedure for calculating apparent-pressure diagram from measured strut loads

where

$\sigma_1, \sigma_2, \sigma_3, \sigma_4$ = apparent pressures

s = center-to-center horizontal spacing of the struts

Using the procedure just described for strut loads observed from the Berlin subway cut, Munich subway cut, and New York subway cut, Peck (1969) provided the envelope of apparent-lateral-pressure diagrams for design of cuts in *sand*. This envelope is illustrated in Figure 19.7, in which

$$\sigma_a = 0.65\gamma H K_a \tag{19.5}$$

where

γ = unit weight

H = height of the cut

K_a = Rankine active pressure coefficient = $\tan^2(45 - \phi'/2)$

ϕ' = effective friction angle of sand

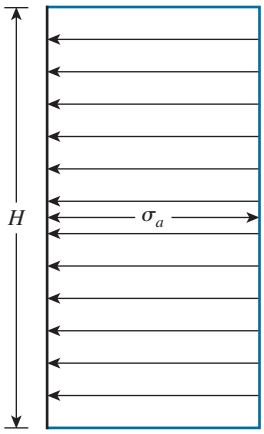


FIGURE 19.7 Peck's (1969) apparent-pressure envelope for cuts in sand

CUTS IN CLAY

In a similar manner, Peck (1969) also provided the envelopes of apparent-lateral-pressure diagrams for cuts in *soft to medium clay* and in *stiff clay*. The pressure envelope for soft to medium clay is shown in Figure 19.8 and is applicable to the condition

$$\frac{\gamma H}{c} > 4$$

where c = undrained cohesion ($\phi = 0$).

Here $\gamma H/c$ is a dimensionless number that is used to separate soft to medium clay from stiff clay.

The pressure, σ_a, is the larger of

$$\sigma_a = \gamma H\left[1 - \left(\frac{4c}{\gamma H}\right)\right] \quad \text{and} \quad \sigma_a = 0.3\gamma H \tag{19.6}$$

where γ = unit weight of clay.

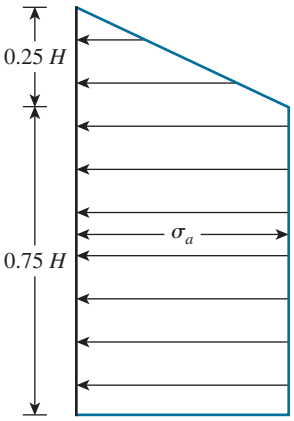


FIGURE 19.8 Peck's (1969) apparent-pressure envelope for cuts in soft to medium clay

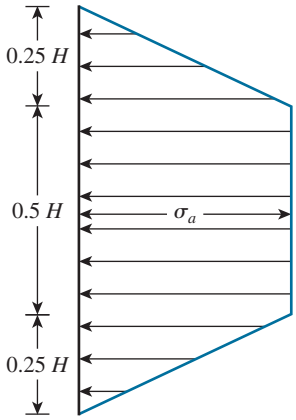


FIGURE 19.9 Peck's (1969) apparent-pressure envelope for cuts in stiff clay

The pressure envelope for cuts in stiff clay is shown in Figure 19.9, in which

$$\sigma_a = 0.2\gamma H \text{ to } 0.4\gamma H \qquad \text{(with an average of } 0.3\gamma H\text{)} \tag{19.7}$$

is applicable to the condition $\gamma H/c \leq 4$.

When using the pressure envelopes just described, keep the following points in mind:

1. They apply to excavations having depths greater than about 6 m (≈20 ft).
2. They are based on the assumption that the water table is below the bottom of the cut.
3. Sand is assumed to be drained with zero pore water pressure.
4. Clay is assumed to be undrained and pore water pressure is not considered.

19.4 Pressure Envelope for Cuts in Layered Soil

Sometimes, layers of both sand and clay are encountered when a braced cut is being constructed. In this case, Peck (1943) proposed that an equivalent value of cohesion ($\phi = 0$) should be determined according to the following formula (see Figure 19.10a):

$$c_{\text{av}} = \frac{1}{2H}\left[\gamma_s K_s H_s^2 \tan \phi_s' + (H - H_s) n' q_u\right] \tag{19.8}$$

where

H = total height of the cut

γ_s = unit weight of sand

H_s = height of the sand layer

K_s = a lateral earth pressure coefficient for the sand layer (≈1)

ϕ_s' = effective angle of friction of sand

q_u = unconfined compression strength of clay

n' = a coefficient of progressive failure (ranging from 0.5 to 1.0; average value 0.75)

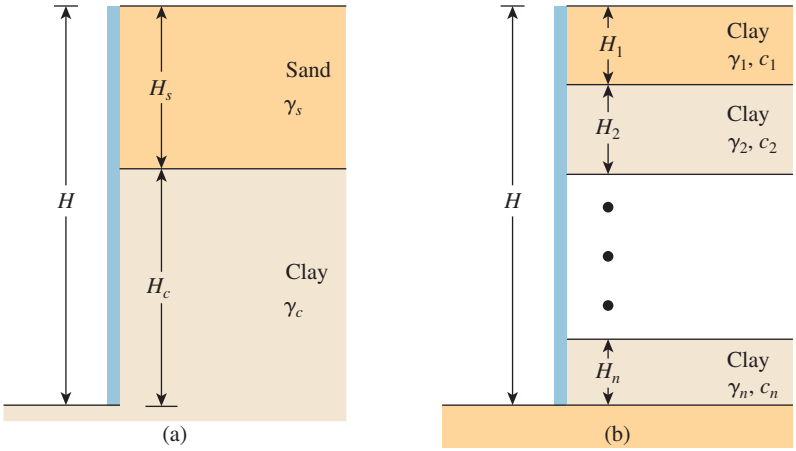


FIGURE 19.10 Layered soil in braced cuts

The average unit weight of the layers may be expressed as

$$\gamma_a = \frac{1}{H}[\gamma_s H_s + \gamma_c(H - H_s)] \tag{19.9}$$

where γ_c is the saturated unit weight of clay layer.

Once the average values of cohesion and unit weight are determined, the pressure envelopes in clay can be used to design the cuts.

Similarly, when several clay layers are encountered in the cut (Figure 19.10b), the average undrained cohesion becomes

$$c_{av} = \frac{1}{H}(c_1 H_1 + c_2 H_2 + \cdots + c_n H_n) \tag{19.10}$$

where

$c_1, c_2, \ldots, c_n$ = undrained cohesion in layers $1, 2, \ldots, n$

$H_1, H_2, \ldots, H_n$ = thickness of layers $1, 2, \ldots, n$

The average unit weight is now

$$\gamma_a = \frac{1}{H}(\gamma_1 H_1 + \gamma_2 H_2 + \gamma_3 H_3 + \cdots + \gamma_n H_n) \tag{19.11}$$

19.5 Design of Various Components of a Braced Cut

STRUTS

In construction work, struts should have a minimum vertical spacing of about 2.75 m (9 ft) or more. Struts are horizontal columns subject to bending. The load-carrying capacity of columns depends on their *slenderness ratio*, which can be reduced by providing vertical and horizontal supports at intermediate points. For wide cuts, splicing the struts may be necessary. For braced cuts in clayey soil, the depth of the first strut below the ground surface should be less than the depth of tensile crack, z_c. From Eq. (16.11),

$$\sigma'_a = \gamma z K_a - 2c'\sqrt{K_a}$$

where K_a = coefficient of Rankine active pressure.

For determining the depth of tensile crack,

$$\sigma'_a = 0 = \gamma z_c K_a - 2c'\sqrt{K_a}$$

or

$$z_c = \frac{2c'}{\sqrt{K_a}\gamma}$$

With $\phi = 0$, $K_a = \tan^2(45 - \phi/2) = 1$, so

$$z_c = \frac{2c}{\gamma}$$

A simplified conservative procedure may be used to determine the strut loads. Although this procedure will vary depending on the engineers involved in the project, the following is a step-by-step outline of the general methodology (see Figure 19.11):

Step 1. Depending on the soil, assume one of the three apparent-pressure envelopes shown in Figures 19.7, 19.8, and 19.9. Draw the pressure envelope next to the wall of the excavation. In Figure 19.11, the soil is assumed to be sand. The struts are labeled *A, B, C*, and *D*, carrying compressive forces P_A, P_B, P_C, and P_D. They are placed at horizontal spacing of s. The connection between the strut and the sheet pile (or soldier beam) is assumed to be a hinge (i.e., carrying no moment) at all

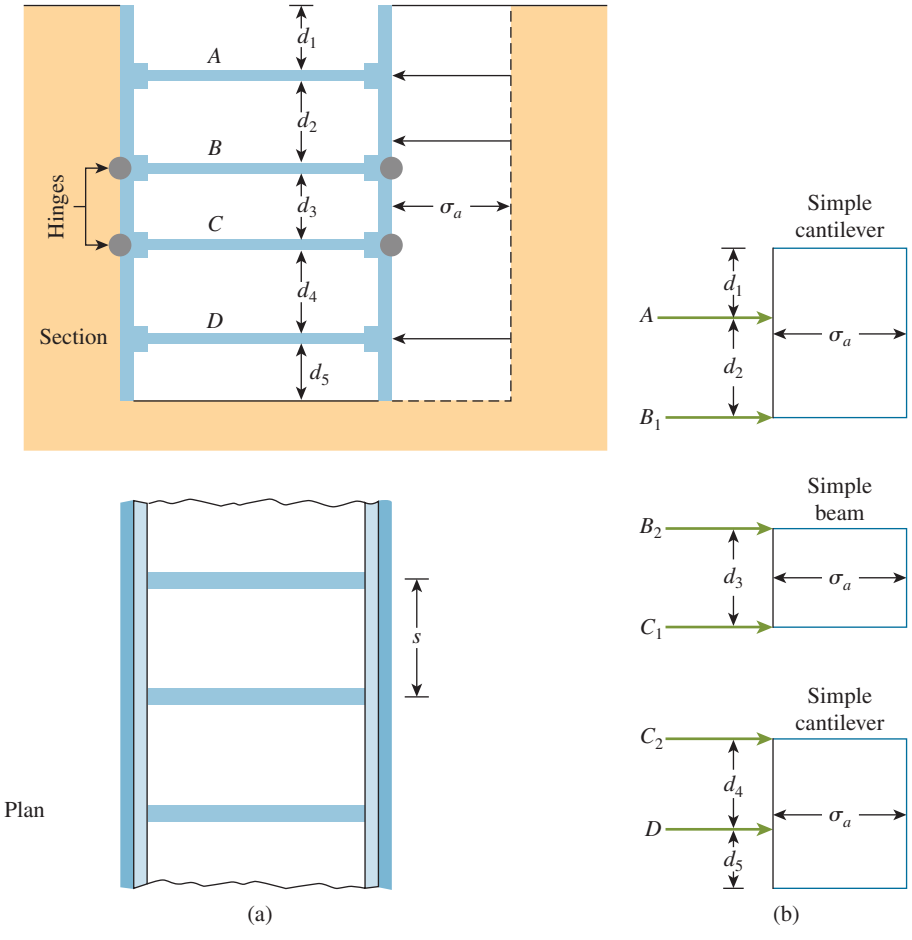


FIGURE 19.11 Determination of strut loads: (a) section and plan of the cut; (b) method for determining strut loads

strut levels, except for the top and the bottom ones. In Figure 19.11a, only the ends of struts B and C act as hinges. Some designers assume hinges at all levels except for the top.

Step 2. The assumption of hinges makes it possible to separate the pressure diagram into a series of cantilever (top and bottom) and simply supported (the middle ones) beams, as shown in Figure 19.11b. At the hinges, where the beams are separated, the strut load is split into two components (e.g., B_1 and B_2) acting on adjacent beams. Each beam has two unknown strut loads, which can be determined from equilibrium considerations. In Figure 19.11b, the strut loads per unit length of the excavation are A, $B = B_1 + B_2$, $C = C_1 + C_2$, and D.

Step 3. With center-to-center horizontal strut spacing of s (see plan in Figure 19.11a), the strut loads can be summarized as follows.

$$\left.\begin{aligned} P_A &= As \\ P_B &= Bs = (B_1 + B_2)s \\ P_C &= Cs = (C_1 + C_2)s \\ &\text{and} \\ P_D &= Ds \end{aligned}\right\} \tag{19.12}$$

Step 4. Knowing the strut loads at each level and the intermediate bracing conditions allows selection of the proper sections from the steel construction manual.

SHEET PILES

The following steps are involved in designing the sheet piles:

Step 1. For each of the sections shown in Figure 19.11b, determine the maximum bending moment.

Step 2. Determine the maximum value of the maximum bending moments (M_{max}) obtained in Step 1. Note that the unit of this moment will be, for example, kN · m/m (lb · ft/ft) length of the wall.

Step 3. Obtain the required section modulus of the sheet piles, namely,

$$S = \frac{M_{max}}{\sigma_{all}} \tag{19.13}$$

where σ_{all} = allowable flexural stress of the sheet-pile material.

Step 4. Choose a sheet pile having a section modulus greater than or equal to the required section modulus from a table such as Table 18.1.

WALES

Wales may be treated as continuous horizontal members if they are spliced properly. Conservatively, they may also be treated as though they are pinned at the struts. For the section shown in Figure 19.11a, the maximum moments for the wales (assuming that they are pinned at the struts), which occur at the mid-span, are

$$\text{At level } A, \quad M_{max} = \frac{(A)(s^2)}{8}$$

$$\text{At level } B, \quad M_{max} = \frac{(B_1 + B_2)s^2}{8}$$

$$\text{At level } C, \quad M_{max} = \frac{(C_1 + C_2)s^2}{8}$$

and

$$\text{At level } D, \quad M_{\max} = \frac{(D)(s^2)}{8}$$

where A, B_1, B_2, C_1, C_2, and D are the reactions under the struts per unit length of the wall (see Step 2 of strut design).

Now determine the section modulus of the wales:

$$S = \frac{M_{\max}}{\sigma_{\text{all}}}$$

The wales are sometimes fastened to the sheet piles at points that satisfy the lateral support requirements.

EXAMPLE 19.1

The cross section of a long braced cut is shown in Figure 19.12a.

a. Draw the earth pressure envelope.
b. Determine the strut loads at levels *A, B*, and *C*.
c. Determine the section modulus of the sheet-pile section required.
d. Determine a design section modulus for the wales at level *B*.

(*Note:* The struts are placed at 3 m, center to center, in the plan.) Use

$$\sigma_{\text{all}} = 170 \times 10^3 \text{ kN/m}^2$$

SOLUTION

Part a

We are given that $\gamma = 18$ kN/m^2, $c = 35$ kN/m^2, and $H = 7$ m. So,

$$\frac{\gamma H}{c} = \frac{(18)(7)}{35} = 3.6 < 4$$

Thus, the pressure envelope will be like the one in Figure 19.9. The envelope is plotted in Figure 19.12a with maximum pressure intensity, σ_a, equal to $0.3\gamma H = 0.3(18)(7) = \mathbf{37.8\ kN/m^2}$.

Part b

To calculate the strut loads, examine Figure 19.12b. Here, the strut–sheet-pile connection at B is assumed to be a hinge, so the pressure diagram is separated at B into two blocks. Taking the moment about B_1, we have $\Sigma M_{B_1} = 0$, and

$$A(2.5) - \left(\frac{1}{2}\right)(37.8)(1.75)\left(1.75 + \frac{1.75}{3}\right) - (1.75)(37.8)\left(\frac{1.75}{2}\right) = 0$$

or

$$A = 54.02 \text{ kN/m}$$

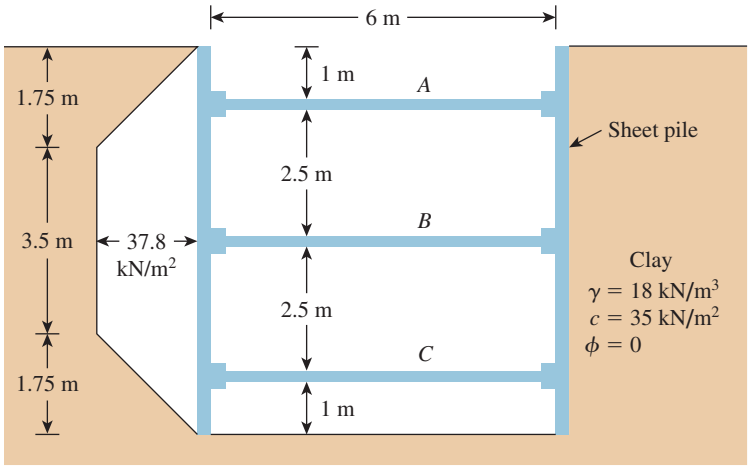
$$\tfrac{1}{2}(1.75)(37.8) + (37.8)(1.75) = A + B_1$$

or

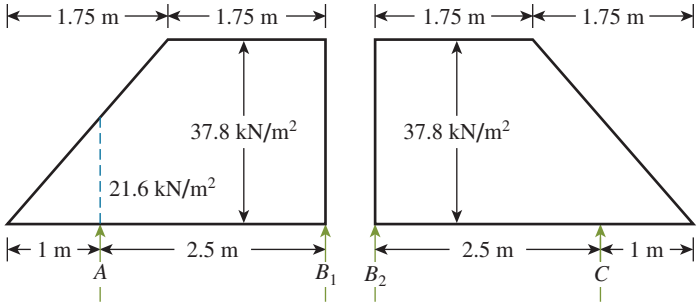
$$33.08 + 66.15 - A = B_1$$

So,

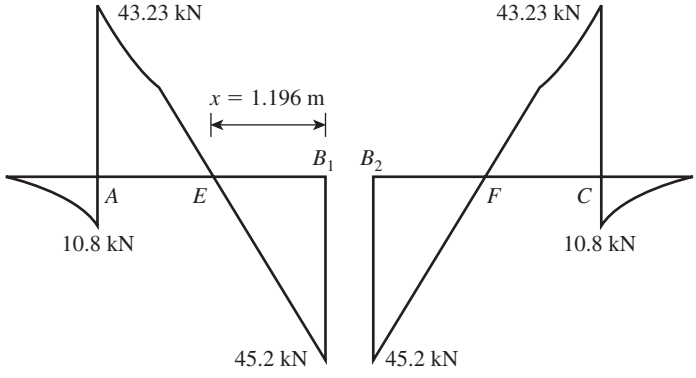
$$B_1 = 45.2 \text{ kN/m}$$



(a) Cross section



(b) Determination of reaction



(c) Shear force diagram

FIGURE 19.12 Analysis of a braced cut

Due to symmetry,

$$B_2 = 45.2 \text{ kN/m}$$

and

$$C = 54.02 \text{ kN/m}$$

Hence, the strut loads at the levels indicated by the subscripts are

$$P_A = 54.02 \times \text{horizontal spacing, } s = 54.02 \times 3 = \mathbf{162.06\ kN}$$
$$P_B = (B_1 + B_2)3 = (45.2 + 45.2)3 = \mathbf{271.2\ kN}$$

and

$$P_C = 54.02 \times 3 = \mathbf{162.06\ kN}$$

Part c

At the left side of Figure 19.12b, for the maximum moment, the shear force should be zero. The nature of the variation of the shear force is shown in Figure 19.12c. The location of point E, where the maximum moment occurs, can be given as

$$x = \frac{\text{reaction at } B_1}{37.8} = \frac{45.2}{37.8} = 1.196 \text{ m}$$

Also,

$$\text{Magnitude of moment at } A = \frac{1}{2}(1)\left(\frac{37.8}{1.75} \times 1\right)\left(\frac{1}{3}\right)$$
$$= 3.6 \text{ kN} \cdot \text{m/meter of wall}$$

and

$$\text{Magnitude of moment at } E = (45.2 \times 1.196) - (37.8 \times 1.196)\left(\frac{1.196}{2}\right)$$
$$= 54.06 - 27.03 = 27.03 \text{ kN} \cdot \text{m/meter of wall}$$

Because the loading on the left and right sections of Figure 19.12b is the same, the magnitudes of the moments at F and C (see Figure 19.12c) will be the same as those at E and A, respectively. Hence, the maximum moment is 27.03 kN · m/meter of wall.

The section modulus of the sheet piles is thus

$$S = \frac{M_{\text{max}}}{\sigma_{\text{all}}} = \frac{27.03 \text{ kN} \cdot \text{m}}{170 \times 10^3 \text{ kN/m}^2} = \mathbf{15.9 \times 10^{-5}\ m^3/meter\ of\ the\ wall}$$

From Table 18.1, PZ-22 is adequate.

Part d

The reaction at level B has been calculated in part b. Hence,

$$M_{\text{max}} = \frac{(B_1 + B_2)s^2}{8} = \frac{(45.2 + 45.2)3^2}{8} = 101.7 \text{ kN} \cdot \text{m}$$

and

$$\text{Section modulus, } S = \frac{101.7}{\sigma_{\text{all}}} = \frac{101.7}{(170 \times 1000)}$$
$$= \mathbf{0.598 \times 10^{-3}\ m^3}$$

EXAMPLE 19.2

Refer to the braced cut shown in Figure 19.13, for which $\gamma = 112$ lb/ft^3, $\phi' = 32°$, and $c' = 0$. The struts are located 12 ft on center in the plan. Draw the earth pressure envelope and determine the strut loads at levels A, B, and C.

SOLUTION

For this case, the earth pressure envelope shown in Figure 19.7 is applicable. Hence,

$$K_a = \tan^2\left(45 - \frac{\phi'}{2}\right) = \tan^2\left(45 - \frac{32}{2}\right) = 0.307$$

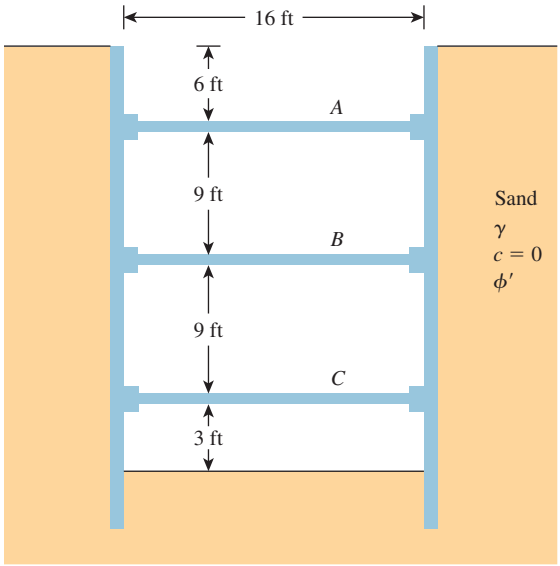


FIGURE 19.13

From Equation (19.5),

$$\sigma_a = 0.65\gamma HK_a = (0.65)(112)(27)(0.307) = 603.44 \text{ lb/ft}^2$$

Figure 19.14a shows the pressure envelope. The strut–sheet-pile connection at B is assumed to be a hinge. Refer to Figure 19.14b and calculate B_1:

$$\Sigma M_{B_1} = 0$$

$$A = \frac{(603.44)(15)\left(\frac{15}{2}\right)}{9} = 7543 \text{ lb/ft}$$

$$B_1 = (603.44)(15) - 7543 = 1508.6 \text{ lb/ft} \approx 1509 \text{ lb/ft}$$

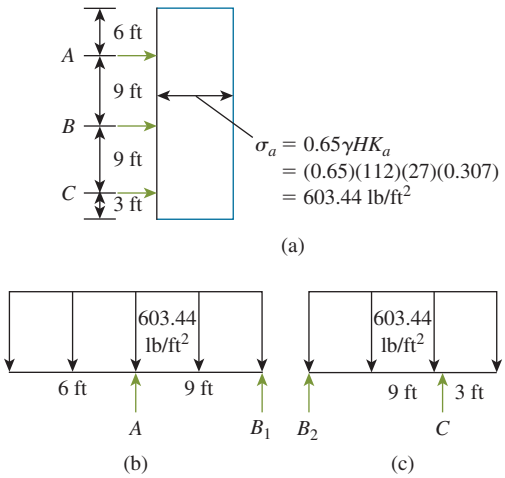


FIGURE 19.14 Load diagrams

Now, refer to Figure 19.14c and calculate B_2:

$$\Sigma M_{B_2} = 0$$

$$C = \frac{(603.44)(12)\left(\frac{12}{2}\right)}{9} = 4827.5 \text{ lb/ft} \approx 4827 \text{ lb/ft}$$

$$B_2 = (603.44)(12) - 4827.5 = 2413.7 \text{ lb/ft} = 2414 \text{ lb/ft}$$

The strut loads are

At A, (7.543)(spacing) = (7.543)(12) = **90.52 kip**
At B, ($B_1 + B_2$)(spacing) = (1.509 + 2.414)(12) = **47.07 kip**
At C, (4.827)(spacing) = (4.827)(12) = **57.93 kip**

EXAMPLE 19.3

For the braced cut described in Example 19.2, determine:

a. The sheet-pile section modulus
b. The required section modulus of the wales at level A; assume that $\sigma_{all} = 24 \text{ kip/in}^2$

SOLUTION

Part a

Refer to the load diagrams shown in Figures 19.14b and 19.14c. Figure 19.15 shows the shear force diagrams based on the load diagrams. First, determine x_1 and x_2:

$$x_1 = \frac{3.923}{0.603} = 6.5 \text{ ft}$$

$$x_2 = \frac{3.017}{0.603} = 5 \text{ ft}$$

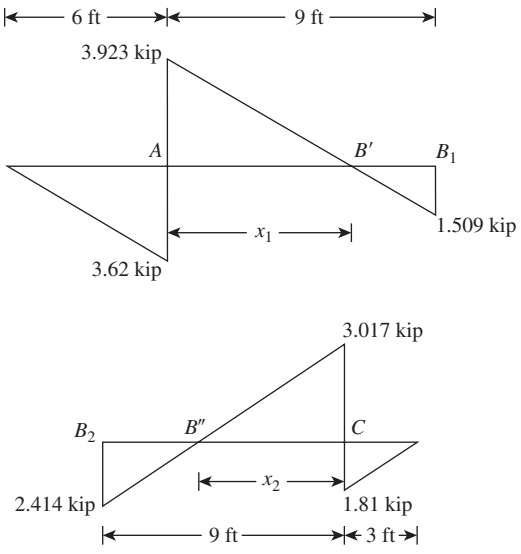


FIGURE 19.15 Shear force diagrams

Then the moments are

$$\text{At } A, \quad \frac{1}{2}(3.62)(6) = 10.86 \text{ kip} \cdot \text{ft/ft of wall}$$

$$\text{At } C, \quad \frac{1}{2}(1.81)(3) = 2.715 \text{ kip} \cdot \text{ft/ft of wall}$$

$$\text{At } B', \quad \frac{1}{2}(1.509)(2.5) = 1.89 \text{ kip} \cdot \text{ft/ft of wall}$$

$$\text{At } B'', \quad \frac{1}{2}(2.414)(4) = 4.828 \text{ kip} \cdot \text{ft/ft of wall}$$

M_A is maximum, so

$$S = \frac{M_{\max}}{\sigma_{\text{all}}} = \frac{(10.86 \text{ kip} \cdot \text{ft})(12)}{24 \text{ kip/in}^2} = \mathbf{5.43 \text{ in}^3\text{/ft}}$$

From Table 18.1, use PZ-22.

Part b

For the wale at level A,

$$M_{\max} = \frac{A(s^2)}{8}$$

$A = 7543$ lb/ft (from Example 19.2). So,

$$M_{\max} = \frac{(7.543)(12^2)}{8} = 135.77 \text{ kip} \cdot \text{ft/ft}$$

$$S = \frac{M_{\max}}{\sigma_{\text{all}}} = \frac{(135.77)(12)}{24 \text{ kip/in}^2} = \mathbf{67.9 \text{ in}^3}$$

19.6 Case Studies of Braced Cuts

The procedure for determining strut loads and the design of sheet piles and wales presented in the preceding sections appears to be fairly straightforward. It is, however, only possible if a proper pressure envelope is chosen for the design, which is difficult to do. This section describes some case studies of braced cuts and highlights the difficulties and degree of judgment needed for successful completion of various projects.

SUBWAY EXTENSION OF THE MASSACHUSETTS BAY TRANSPORTATION AUTHORITY (MBTA)

Lambe (1970) provided data on the performance of three excavations for the subway extension of the MBTA in Boston (test sections A, B, and D), all of which were well instrumented. Figure 19.16 gives the details of test section B, where the cut was 58 ft, including subsoil conditions. The subsoil consisted of gravel, sand, silt, and clay (fill) to a depth of about 26 ft, followed by a light gray, slightly organic silt to a depth of 46 ft. A layer of coarse sand and gravel with some clay was present from 46 ft to 54 ft below the ground surface. Rock was encountered below 54 ft. The horizontal spacing of the struts was 12 ft center to center.

Because the apparent pressure envelopes available (Section 19.3) are for *sand* and *clay* only, questions may arise about how to treat the fill, silt, and till. Figure 19.17

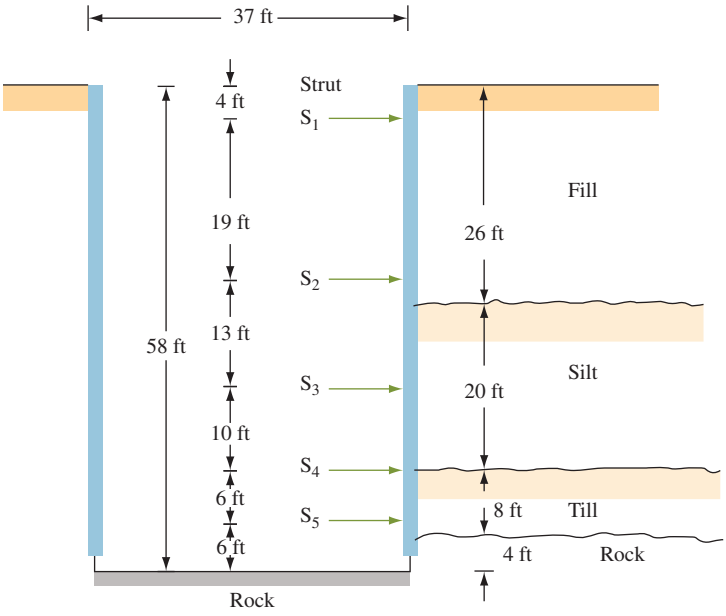


FIGURE 19.16 Schematic diagram of test section B for subway extension, MBTA

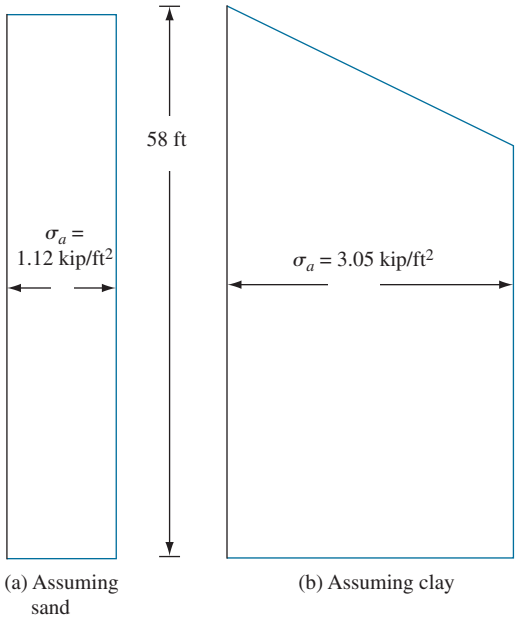


FIGURE 19.17 Pressure envelopes: (a) assuming sand; (b) assuming clay

shows the apparent pressure envelopes proposed by Peck (1969), considering the soil as *sand* and also as *clay*, to overcome that problem. For the average soil parameters of the profile, the following values of σ_a were used to develop the pressure envelopes shown in Figure 19.17.

SAND

$$\sigma_a = 0.65\gamma H K_a \tag{19.14}$$

For $\gamma = 114\,\text{lb/ft}^3$, $H = 58\,\text{ft}$, and $K_a = 0.26$,

$$\sigma_a = (0.65)(114)(58)(0.26) = 1117\,\text{lb/ft}^2 \approx 1.12\,\text{kip/ft}^2$$

CLAY

$$\sigma_a = \gamma H - 4c \tag{19.15}$$

For $c = 890\ \text{lb/ft}^2$,

$$\sigma_a = (114)(58)\left[1 - \frac{(4)(890)}{(114)(58)}\right] = 3052\ \text{lb/ft}^2 \approx 3.05\,\text{kip/ft}^2$$

Table 19.2 shows the variations of the strut load, based on the assumed pressure envelopes shown in Figure 19.17. Also shown in Table 19.2 are the measured strut loads in the field and the design strut loads. This comparison indicates that

1. In most cases the measured strut loads differed widely from those predicted. This result is due primarily to the uncertainties involved in the assumption of the soil parameters.
2. The actual design strut loads were substantially higher than those measured.
3. From Figure 19.17, it can be seen that the predicted strut loads would vary significantly, depending on whether the entire soil is assumed to be sand or clay.

TABLE 19.2 Computed and Measured Strut Loads at Test Section B

Strut number	Computed load (kip)		Measured strut load (kip)
	Envelope based on sand	Envelope based on clay	
S-1	182	230	70.4
S-2	215	580	215
S-3	154	420	304
S-4	108	292	230
S-5	75	219	274

CONSTRUCTION OF NATIONAL PLAZA (SOUTH HALF) IN CHICAGO

The construction of the south half of the National Plaza in Chicago required a braced cut 70 ft deep. Swatek et al. (1972) reported the case history for this construction. Figure 19.18 shows a schematic diagram for the braced cut and the subsoil profile. There were six levels of struts. Table 19.3 gives the actual maximum wale and strut loads.

Figure 19.19 presents a lateral earth pressure envelope based on the maximum wale loads measured. To compare the theoretical prediction to the actual observation requires making an approximate calculation. To do so, we convert the clayey soil layers from Elevation +1 ft to −56 ft to a single equivalent layer in Table 19.4 by using Eq. (19.10).

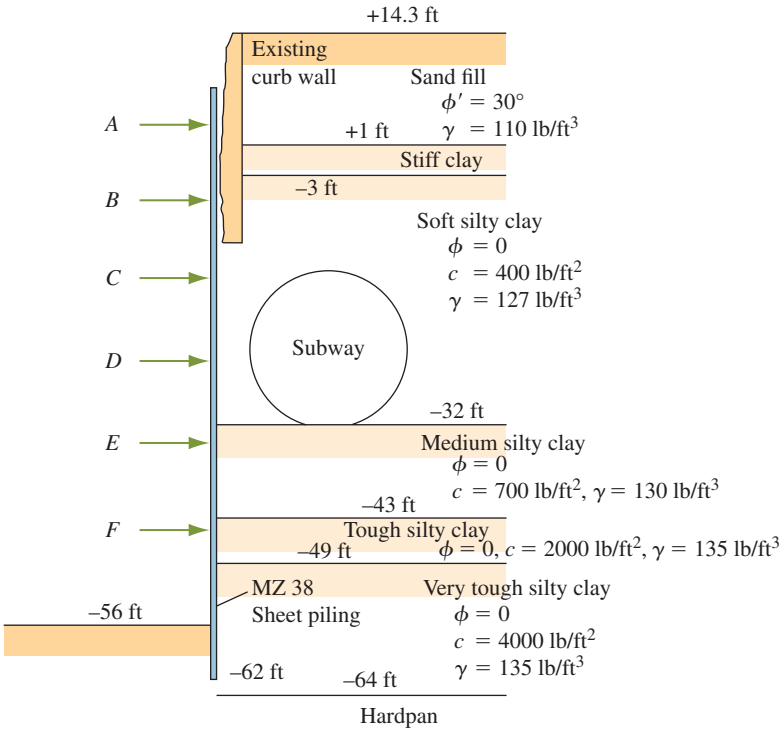


FIGURE 19.18 Schematic diagram of braced cut—National Plaza of Chicago

TABLE 19.3 National Plaza Wale and Strut Loads

Strut level	Elevation (ft)	Load measured (kip/ft)
A	+3	16.0
B	−6	26.5
C	−15	29.0
D	−24.5	29.0
E	−34	29.0
F	−44.5	30.7
		Σ160.2

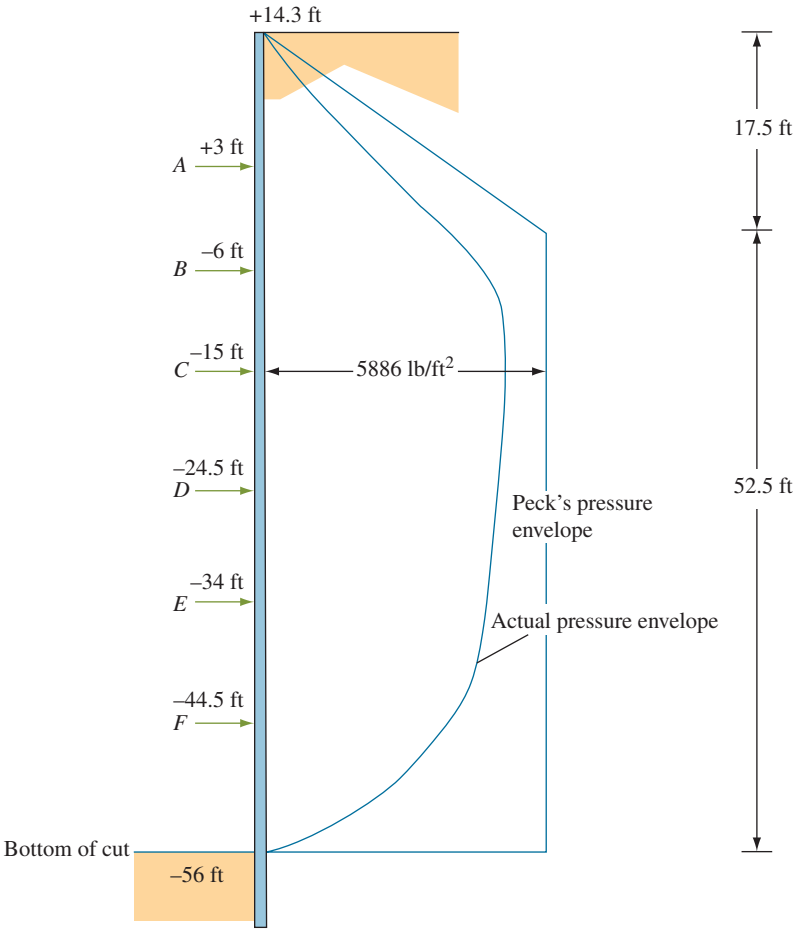


FIGURE 19.19 Comparison of actual and Peck's pressure envelopes

Now, using Eq. (19.8), we can convert the sand layer located between elevations +14 ft and +1 ft and the equivalent clay layer of 57 ft to one equivalent clay layer with a thickness of 70 ft:

$$c_{av} = \frac{1}{2H}[\gamma_s K_s H_s^2 \tan \phi_s' + (H - H_s)n' q_u]$$

$$= \left[\frac{1}{(2)(70)}\right][(110)(1)(13)^2 \tan 30 + (57)(0.75)(2 \times 1068)] \approx 730 \text{ lb/ft}^2$$

TABLE 19.4 Conversion of Soil Layers Using Eq. (19.10)

Elevation (ft)	Thickness, H (ft)	c (lb/ft^2)	Equivalent c (lb/ft^2)
+1 to −32 ft	33	400	$c_{av} = \frac{1}{57}[(33)(400) + (11)(700) + (6)(2000) + (7)(4000)]$ $= 1068\ \text{lb/ft}^2$
−32 ft to −43 ft	11	700	
−43 ft to −49 ft	6	2000	
−49 ft to −56 ft	7	4000	
	Σ57		

Equation (19.11) gives

$$\gamma_{av} = \frac{1}{H}(\gamma_1 H_1 + \gamma_2 H_2 + \cdots + \gamma_n H_n)$$
$$= \frac{1}{70}[(110)(13) + (127)(33) + (130)(11) + (135)(6) + (135)(7)]$$
$$= 125.8\ \text{lb/ft}^3$$

For the equivalent clay layer of 70 ft,

$$\frac{\gamma_{av} H}{c_{av}} = \frac{(125.8)(70)}{730} = 12.06 > 4$$

Hence the apparent-pressure envelope will be of the type shown in Figure 19.8. From Eq. (19.6),

$$\sigma_a = \gamma H\left[1 - \left(\frac{4c_{av}}{\gamma_{av} H}\right)\right] = (125.8)(70)\left[1 - \frac{(4)(730)}{(125.8)(70)}\right] = 5886\ \text{lb/ft}^2$$

The pressure envelope is shown in Figure 19.19. The area of this pressure diagram is 201 kip/ft. Thus Peck's pressure envelope gives a lateral earth pressure of about 1.8 times that actually observed in this case. This result is not surprising, because the pressure envelope provided by Figure 19.8 is an envelope developed by considering several cuts made at different locations. Under actual field conditions, past experience with the behavior of similar soil can help substantially to reduce overdesign.

19.7 Bottom Heave of a Cut in Clay

Braced cuts in clay may become unstable as a result of heaving of the bottom of the excavation. Terzaghi (1943) analyzed the factor of safety of long braced excavations against bottom heave. The failure surface for such a case in a homogeneous soil is shown in Figure 19.20. In the figure, the following notations are used: B = width of the cut, H = depth of the cut, T = thickness of the clay below the base of excavation, and q = uniform surcharge adjacent to the excavation.

The ultimate bearing capacity at the base of a soil block *fije* with a width of B' can be given as

$$q_{ult} = cN_c \tag{19.16}$$

where $N_c = 5.7$ (for a perfectly rough foundation).

The vertical load per unit area along *fi* is

$$q = \gamma H + q - \frac{cH}{B'} \tag{19.17}$$

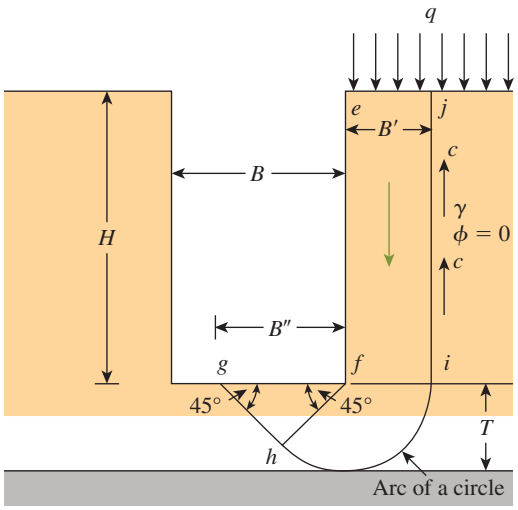


FIGURE 19.20 Heaving in braced cuts in clay ($\phi = 0$)

Hence, the factor of safety against bottom heave is

$$\text{FS} = \frac{q_{\text{ult}}}{q} = \frac{cN_c}{\gamma H + q - \dfrac{cH}{B'}} = \frac{cN_c}{\left(\gamma + \dfrac{q}{H} - \dfrac{c}{B'}\right)H} \tag{19.18}$$

For excavations of limited length L, the factor of safety can be modified to

$$\text{FS} = \frac{cN_c\left(1 + 0.2\,\dfrac{B'}{L}\right)}{\left(\gamma + \dfrac{q}{H} - \dfrac{c}{B'}\right)H} \tag{19.19}$$

where $B' = T$ or $B/\sqrt{2}$ (whichever is smaller).

In 2000, Chang suggested a revision of Eq. (19.19) with the following changes:

1. The shearing resistance along ij may be considered as an increase in resistance rather than a reduction in loading.
2. In Figure 19.20, fg with a width of B'' at the base of the excavation may be treated as a negatively loaded footing.
3. The value of the bearing capacity factor N_c should be 5.14 (not 5.7) for a perfectly smooth footing because of the restraint-free surface at the base of the excavation.

With the foregoing modifications, Eq. (19.19) takes the form

$$\text{FS} = \frac{5.14c\left(1 + \dfrac{0.2B''}{L}\right) + \dfrac{cH}{B'}}{\gamma H + q} \tag{19.20}$$

where

$B' = T$ if $T \le B/\sqrt{2}$

$B' = B/\sqrt{2}$ if $T > B/\sqrt{2}$

$B'' = \sqrt{2}B'$

Bjerrum and Eide (1956) compiled a number of case records for the bottom heave of cuts in clay. Chang (2000) used those records to calculate FS by means of

TABLE 19.5 Calculated Factors of Safety for Selected Case Records Compiled by Bjerrum and Eide (1956) and Calculated by Chang (2000)

Site	B (m)	B/L	H (m)	H/B	γ (kN/m^3)	c (kN/m^2)	q (kN/m^2)	FS [Eq. (19.20)]	Type of failure
Pumping station, Fornebu, Oslo	5.0	1.0	3.0	0.6	17.5	7.5	0	1.05	Total failure
Storehouse, Drammen	4.8	0	2.4	0.5	19.0	12	15	1.05	Total failure
Sewerage tank, Drammen	5.5	0.69	3.5	0.64	18.0	10	10	0.92	Total failure
Excavation, Grey Wedels Plass, Oslo	5.8	0.72	4.5	0.78	18.0	14	10	1.07	Total failure
Pumping station, Jernbanetorget, Oslo	8.5	0.70	6.3	0.74	19.0	22	0	1.26	Partial failure
Storehouse, Freia, Oslo	5.0	0	5.0	1.00	19.0	16	0	1.10	Partial failure
Subway, Chicago	16	0	11.3	0.70	19.0	35	0	1.00	Near failure

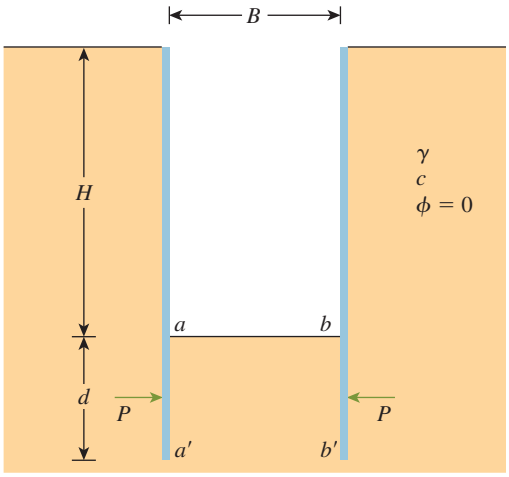


FIGURE 19.21 Force on the buried length of sheet pile

Eq. (19.20); his findings are summarized in Table 19.5. It can be seen from this table that the actual field observations agree well with the calculated factors of safety.

Equation (19.20) is recommended for use in this test. In most cases, a factor of safety of about 1.5 is recommended.

In homogeneous clay, if FS becomes less than 1.5, the sheet pile is driven deeper. (See Figure 19.21.) Usually, the depth d is kept less than or equal to $B/2$, in which case the force P per unit length of the buried sheet pile (aa' and bb') may be expressed as (U.S. Department of the Navy, 1971)

$$P = 0.7(\gamma HB - 1.4cH - \pi cB) \qquad \text{for } d > 0.47B \tag{19.21}$$

and

$$P = 1.5d\left(\gamma H - \frac{1.4cH}{B} - \pi c\right) \qquad \text{for } d < 0.47B \tag{19.22}$$

EXAMPLE 19.4

In Figure 19.22, for a braced cut in clay, $B = 4\,\text{m}$, $L = 15\,\text{m}$, $H = 6\,\text{m}$, $T = 1.5\,\text{m}$, $\gamma = 17\ \text{kN/m}^3$, $c = 40\ \text{kN/m}^2$, and $q = 0$. Calculate the factor of safety against heave. Use Eq. (19.20).

SOLUTION

From Eq. (19.20),

$$\text{FS} = \frac{5.14c\left(1 + \dfrac{0.2B''}{L}\right) + \dfrac{cH}{B'}}{\gamma H + q}$$

With $T = 2\,\text{m}$,

$$\frac{B}{\sqrt{2}} = \frac{4}{\sqrt{2}} = 2.83\,\text{m}$$

So

$$T \le \frac{B}{\sqrt{2}}$$

Hence, $B' = T = 2\,\text{m}$, and it follows that

$$B'' = \sqrt{2}B' = (\sqrt{2})(2) = 2.83\,\text{m}$$

and

$$\text{FS} = \frac{(5.14)(40)\left[1 + \dfrac{(0.2)(2.83)}{15}\right] + \dfrac{(40)(6)}{2}}{(17)(6)} = \mathbf{2.55}$$

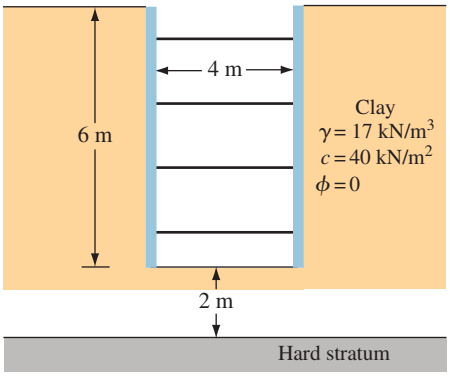


FIGURE 19.22 Factor of safety against heaving for a braced cut

19.8 Stability of the Bottom of a Cut in Sand

The bottom of a cut in sand is generally stable. When the water table is encountered, the bottom of the cut is stable as long as the water level inside the excavation is higher than the groundwater level. In case dewatering is needed (see Figure 19.23), the factor of safety against piping should be checked. [*Piping* is another term for failure by heave, as defined in Section 2.12; see Eq. (2.50).] Piping may occur when a high hydraulic gradient is created by water flowing into the excavation. To check the factor of safety, draw flow nets and determine the maximum exit gradient [$i_{\max(\text{exit})}$] that will occur at points A and B. Figure 19.24 shows such a flow net, for which the maximum exit gradient is

$$i_{\max(\text{exit})} = \frac{\frac{h}{N_d}}{a} = \frac{h}{N_d a} \tag{19.23}$$

where

a = length of the flow element at A (or B)

N_d = number of drops (*Note:* In Figure 19.24, $N_d = 8$; see also Section 2.11.)

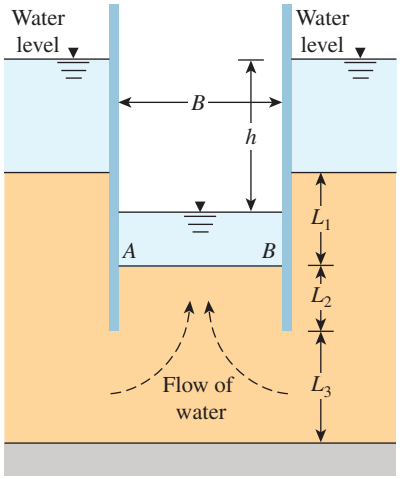


FIGURE 19.23 Stability of the bottom of a cut in sand

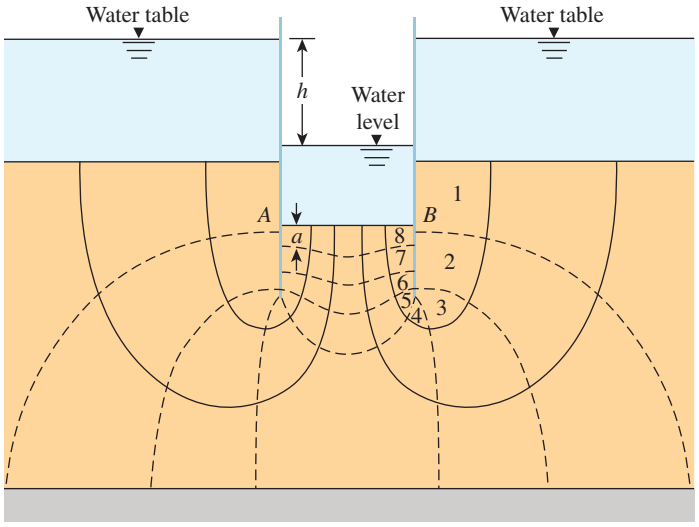


FIGURE 19.24 Determining the factor of safety against piping by drawing a flow net

The factor of safety against piping may be expressed as

$$\text{FS} = \frac{i_{cr}}{i_{max(exit)}} \tag{19.24}$$

where i_{cr} = critical hydraulic gradient.

The relation for i_{cr} can be given as

$$i_{cr} = \frac{G_s - 1}{e + 1}$$

The magnitude of i_{cr} varies between 0.9 and 1.1 in most soil, with an average of about 1. A factor of safety of about 1.5 is desirable.

The maximum exit gradient for sheeted excavations in sands with $L_3 = \infty$ can also be evaluated theoretically (Harr, 1962). (Only the results of these mathematical derivations will be presented here. For further details, see the original work.) To calculate the maximum exit gradient, examine Figures 19.25 and 19.26 and perform the following steps:

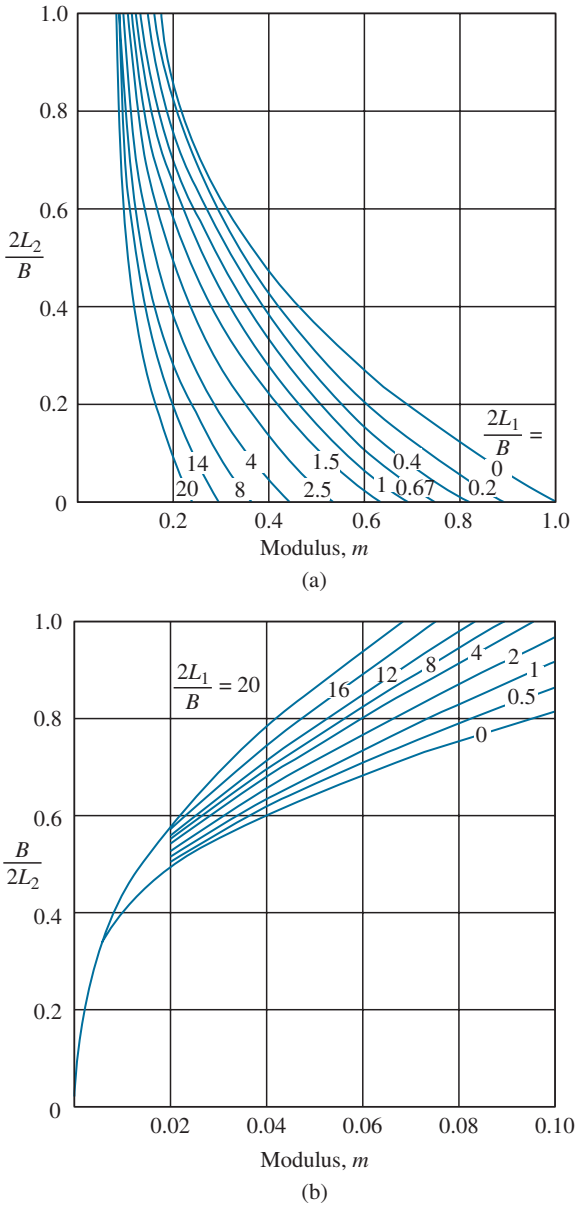


FIGURE 19.25 Variation of modulus (Based on *Groundwater and Seepage*, by M. E. Harr. McGraw-Hill, 1962)

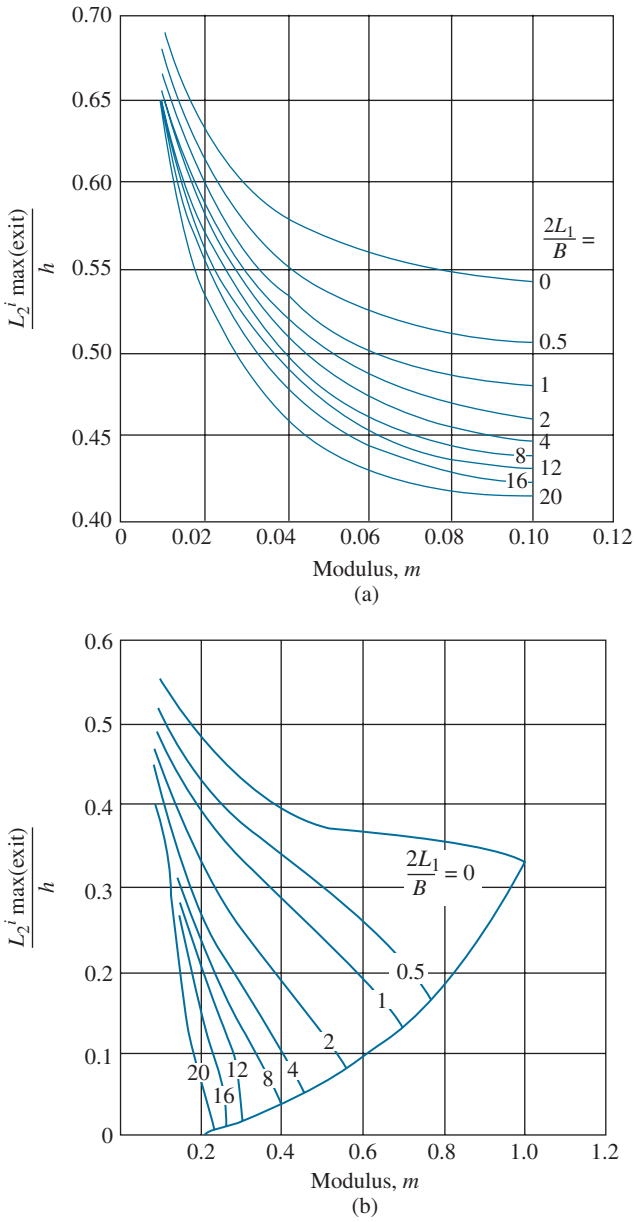


FIGURE 19.26 Variation of maximum exit gradient with modulus (Based on *Groundwater and Seepage*, by M. E. Harr. McGraw-Hill, 1962)

1. Determine the modulus, m, from Figure 19.25 by obtaining $2L_2/B$ (or $B/2L_2$) and $2L_1/B$.
2. With the known modulus and $2L_1/B$, examine Figure 19.26 and determine $L_2 i_{\max(\text{exit})}/h$. Because L_2 and h will be known, $i_{\max(\text{exit})}$ can be calculated.
3. The factor of safety against piping can be evaluated by using Eq. (19.24).

Marsland (1958) presented the results of model tests conducted to study the influence of seepage on the stability of sheeted excavations in sand. The results were summarized by the U.S. Department of the Navy (1971) in NAVFAC DM-7 and are given in Figures 19.27a, b, and c. Note that Figure 19.27b is for determining the sheet-pile penetration L_2 needed for the required factor of safety against piping when the sand layer extends to a great depth below the excavation. By contrast, Figure 19.27c represents the case in which an impervious layer lies at a limited depth below the bottom of the excavation.

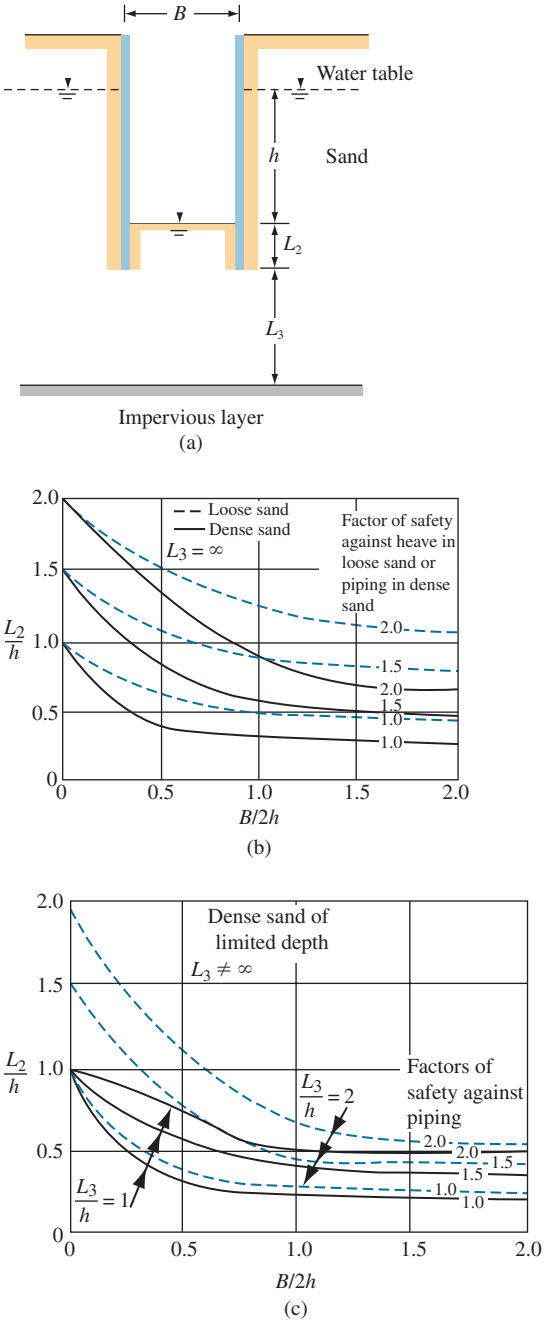


FIGURE 19.27 Influence of seepage on the stability of sheeted excavation (US Department of Navy, 1971)

EXAMPLE 19.5

In Figure 19.23, let $h = 4.5\,\text{m}$, $L_1 = 5\,\text{m}$, $L_2 = 4\,\text{m}$, $B = 5\,\text{m}$, and $L_3 = \infty$. Determine the factor of safety against piping. Use Figures 19.25 and 19.26.

SOLUTION

We have

$$\frac{2L_1}{B} = \frac{2(5)}{5} = 2$$

and

$$\frac{B}{2L_2} = \frac{5}{2(4)} = 0.625$$

According to Figure 19.25b, for $2L_1/B = 2$ and $B/2L_2 = 0.625$, $m \approx 0.033$. From Figure 19.26a, for $m = 0.033$ and $2L_1/B = 2$, $L_2 i_{\max(\text{exit})}/h = 0.54$

$$i_{\max(\text{exit})} = \frac{0.54(h)}{L_2} = 0.54(4.5)/4 = 0.608$$

and

$$\text{FS} = \frac{i_{\text{cr}}}{i_{\max(\text{exit})}} = \frac{1}{0.608} = \mathbf{1.645}$$

19.9 Lateral Yielding of Sheet Piles and Ground Settlement

In braced cuts, some lateral movement of sheet-pile walls may be expected. (See Figure 19.28.) The amount of lateral yield (δ_H) depends on several factors, the most important of which is the elapsed time between excavation and the placement of wales and struts. As discussed before, in several instances the sheet piles (or the soldier piles, as the case may be) are driven to a certain depth below the bottom of the excavation. The reason is to reduce the lateral yielding of the walls during the last stages of excavation. Lateral yielding of the walls will cause the ground surface surrounding the cut to settle. The degree of lateral yielding, however, depends mostly on the type of soil below the bottom of the cut. If clay below the cut extends to a great depth and $\gamma H/c$ is less than about 6, extension of the sheet piles or soldier piles below the bottom of the cut will help considerably in reducing the lateral yield of the walls.

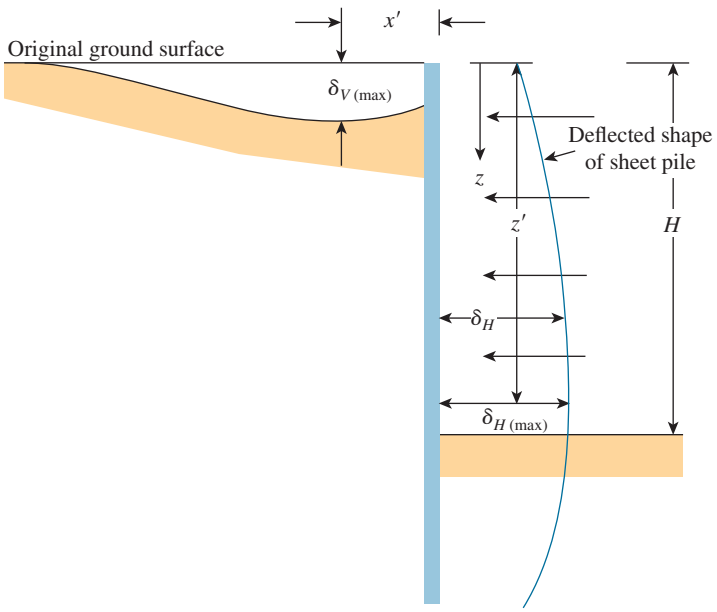


FIGURE 19.28 Lateral yielding of sheet pile and ground settlement

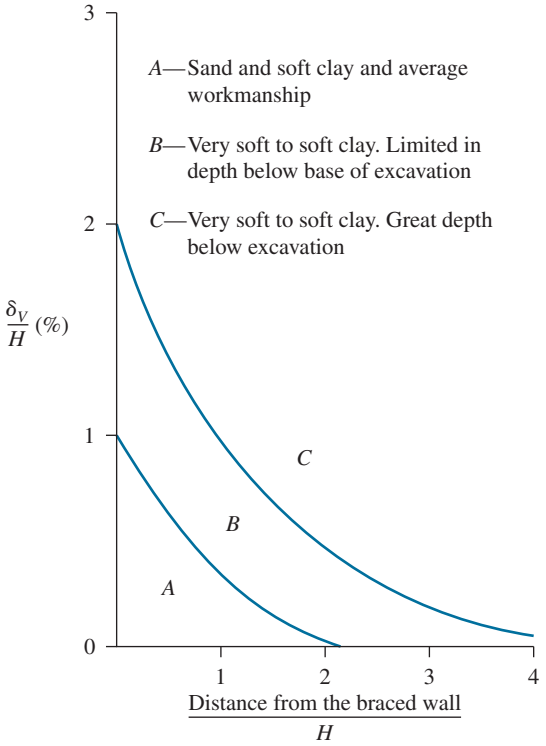


FIGURE 19.29 Variation of ground settlement with distance (Based on Peck, R. B. (1969). "Deep Excavation and Tunneling in Soft Ground," *Proceedings, Seventh International Conference on Soil Mechanics and Foundation Engineering*, Mexico City, State-of-the-Art Volume, pp. 225–290.)

However, under similar circumstances, if $\gamma H/c$ is about 8, the extension of sheet piles into the clay below the cut does not help greatly. In such circumstances, we may expect a great degree of wall yielding, which could result in the total collapse of the bracing systems. If a hard layer of soil lies below a clay layer at the bottom of the cut, the piles should be embedded in the stiffer layer. This action will greatly reduce lateral yield.

The lateral yielding of walls will generally induce ground settlement, δ_V, around a braced cut. Such settlement is generally referred to as *ground loss*. On the basis of several field observations, Peck (1969) provided curves for predicting ground settlement in various types of soil. (See Figure 19.29.) The magnitude of ground loss varies extensively; however, the figure may be used as a general guide.

Moormann (2004) analyzed about 153 case histories dealing mainly with the excavation in soft clay (that is, undrained shear strength, $c \leq 75$ kN/m^2). Following is a summary of his analysis relating to $\delta_{V(\max)}$, x', $\delta_{H(\max)}$, and z' (see Figure 19.28).

- Maximum Vertical Movement $[\delta_{V(\max)}]$
  $\delta_{V(\max)}/H \approx 0.1$ to 10.1% with an average of 1.07% (soft clay)
  $\delta_{V(\max)}/H \approx 0$ to 0.9% with an average of 0.18% (stiff clay)
  $\delta_{V(\max)}/H \approx 0$ to 2.43% with an average of 0.33% (noncohesive soil)
- Location of $\delta_{V(\max)}$, that is, x' (Figure 19.28)
  For 70% of all case histories considered, $x' \leq 0.5H$.
  However, in soft clays, x' may be as much as $2H$.
- Maximum Horizontal Deflection of Sheet Piles, $\delta_{H(\max)}$
  For 40% of excavation in soft clay, $0.5\% \leq \delta_{H(\max)}/H \leq 1\%$
  The average value of $\delta_{H(\max)}/H$ is about 0.87%.

In stiff clays, the average value of $\delta_{H(\max)}/H$ is about 0.25%.
In noncohesive soil, $\delta_{H(\max)}/H$ is about 0.27% of the average.

- Location of $\delta_{H(\max)}$, that is, z' (Figure 19.28)
  For deep excavation of soft and stiff cohesive soil, z'/H is about 0.5 to 1.0.

19.10 Summary

In designing braced cuts, it is necessary to know the lateral earth pressure distribution along the vertical walls. The lateral earth pressure distribution along the walls depends on several factors, including the soil type, the method of construction, and the type of equipment used. Due to the difficulties associated with determining the lateral earth pressure distribution, we use lateral earth pressure envelopes, which conservatively include all possible scenarios. Three pressure envelopes for sand, soft-medium clay, and stiff clay proposed by Peck (1969) are commonly used in the design of struts, wales, and the sheet-pile sections. While the struts resist compressive axial loads, the wales and the sheet piles undergo bending stresses.

In clay, the braced excavation may fail by bottom heave in spite of properly designed struts, wales, and sheet piles. This is more common in soft clay, where the clay from the sides is pushed into the excavation through the bottom. This was treated as a bearing capacity problem, and an expression for the factor of safety was suggested.

PROBLEMS

19.1 A 5 m wide braced excavation is made in a saturated clay, as shown in Figure P19.1, with the following properties: $c = 20$ kN/m^2, $\phi = 0$, and $\gamma = 18.5$ kN/m^3. The struts are spaced at 5 m center to center in plan.

a. Determine the strut forces.
b. Determine the section modulus of the sheet pile required, assuming $\sigma_{all} = 170$ MN/m^2.
c. Determine the maximum moment for the wales at levels B and C.

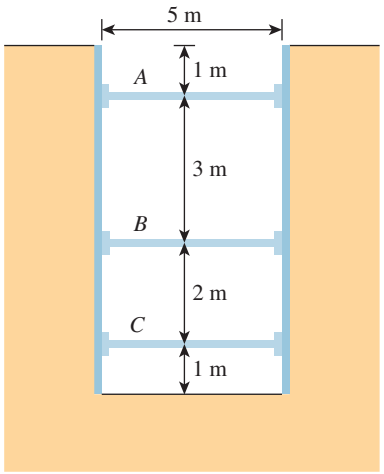


FIGURE P19.1

19.2 A 5 m wide and 12 m deep braced excavation is carried out in sand, as shown in Figure P19.2, where $\gamma = 18$ kN/m^3 and $\phi' = 37^\circ$. The struts are placed at horizontal spacing of 2.5 m.

a. Determine the strut loads.
b. Determine the required section modulus of the sheet-pile section, assuming $\sigma_{all} = 170$ MN/m^2.
c. Determine the maximum moment for the middle two wales.

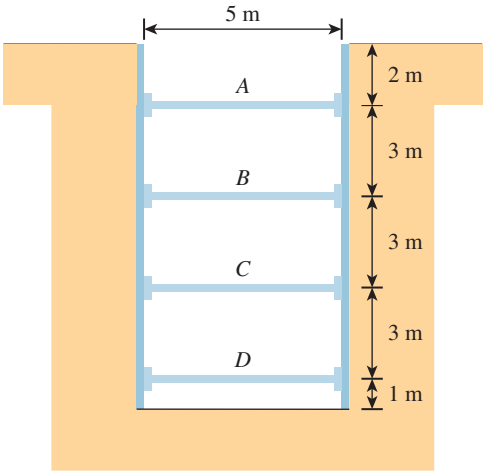


FIGURE P19.2

19.3 A braced cut shown in Figure P19.3 is to be made to a depth of 9.0 m in a saturated clay deposit where the unit weight is 17.65 kN/m^3 and the undrained shear strength is 30 kN/m^2. The struts are spaced horizontally at 3.0 m center to center. Find the strut loads.

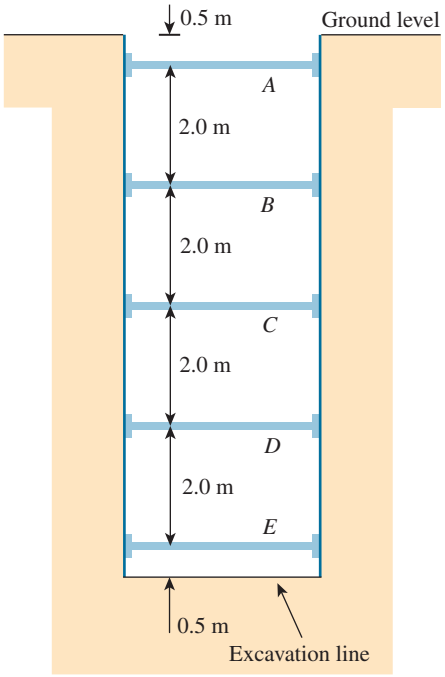


FIGURE P19.3

19.4 A braced cut is carried out to 10 m depth at a site where the soil consists of 4 m of sand ($\gamma = 17.0$ kN/m^3, $\phi' = 33°$) at the top underlain by 6 m of clay ($\gamma = 18.5$ kN/m^3, $c = 35$ kN/m^2).

a. What would be the average value of cohesion and the unit weight for the equivalent homogeneous soil profile?

b. Show the lateral earth pressure envelope you would use in determining the strut loads.

19.5 A construction site consists of layers of clays with different soil properties. For a 25 ft deep braced cut, the cohesion and unit weight values are as follows:

Layer	Thickness (ft)	Cohesion (lb/ft^2)	Unit weight (lb/ft^3)
Top	5	600	110
Middle	8	1200	120
Bottom	12	850	105

Determine the average cohesion and unit weight of the equivalent homogeneous clay soil that can be used in the lateral pressure envelope.

19.6 For Problem 19.1, determine the factor of safety against bottom heave. Use Eq. (19.20) suggested by Chang (2000), assuming a smooth base for the excavation. There is no stiff stratum or bedrock in the vicinity of the bottom of the excavation, which is very long.

19.7 Redo Problem 19.6, using Eq. (19.19) and assuming a smooth excavation base with $N_c = 5.14$.

19.8 In Problem 19.3, if the width of the excavation is 3.0 m, determine the factor of safety against bottom heave. Assume the excavation base to be rough, and use Eq. (19.19), where $q = 0$, $L = 25$ m, and T is very large.

REFERENCES

Bjerrum, L. and Eide, O. (1956). "Stability of Strutted Excavation in Clay," *Geotechnique*, Vol. 6, No. 1, pp. 32–47.

Chang, M. F. (2000). "Basal Stability Analysis of Braced Cuts in Clay," *Journal of Geotechnical and Geoenvironmental Engineering*, ASCE, Vol. 126, No. 3, pp. 276–279.

Harr, M. E. (1962). *Groundwater and Seepage*, McGraw-Hill, New York.

Lambe, T. W. (1970). "Braced Excavations." *Proceedings of the Specialty Conference on Lateral Stresses in the Ground and Design of Earth-Retaining Structures*, American Society of Civil Engineers, pp. 149–218.

Moormann, C. (2004). "Analysis of Wall and Ground Movements Due to Deep Excavations in Soft Soil Based on New Worldwide Data Base," *Soils and Foundations*, Vol. 44, No. 1, pp. 87–98.

Peck, R. B. (1943). "Earth Pressure Measurements in Open Cuts, Chicago (ILL.) Subway," *Transactions*, American Society of Civil Engineers, Vol. 108, pp. 1008–1058.

Peck, R. B. (1969). "Deep Excavation and Tunneling in Soft Ground," *Proceedings, Seventh International Conference on Soil Mechanics and Foundation Engineering*, Mexico City, State-of-the-Art Volume, pp. 225–290.

Swatek, E. P., Jr., Asrow, S. P., and Seitz, A. (1972). "Performance of Bracing for Deep Chicago Excavation," *Proceedings of the Specialty Conference on Performance of Earth and Earth Supported Structures*, American Society of Civil Engineers, Vol. 1, Part 2, pp. 1303–1322.

Terzaghi, K. (1943). *Theoretical Soil Mechanics*, John Wiley & Sons, New York.

U.S. Department of the Navy (1971). "Design Manual—Soil Mechanics, Foundations, and Earth Structures." NAVFAC DM-7, Washington, DC.

Answers to Problems

CHAPTER 2

2.1 0.054

2.3 $e = 0.729$

$\gamma = 18.25$ kN/m^3

2.5 60.6%

2.7

Soil	Symbol
A	GM
B	SW-SM
C	SP
D	CH

2.9 97.2 m^3/day

2.11 $e = 0.675$

$\gamma_{sat} = 19.8$ kN/m^3

$\sigma = 138.3$ kN/m^2

$u = 88.3$ kN/m^2

$\sigma' = 50$ kN/m^2

2.13 **a.** Overconsolidated; OCR = 1.37

b. 52.9 mm

2.15 **a.** 225.4 mm

b. 0.41

2.17 $c' = 5.4$ kN/m^2

$\phi' = 23.2°$

2.19 **a.** 83.8 kN/m^2

b. 0.73

2.21 $c' = 10$ kN/m^2; $\phi' = 24.7°$

2.23 **a.** 35.2°

b. 36.8°

CHAPTER 3

3.1 9.3%

3.3 $c_{u(\text{average})} = 106.78$ kN/m^2

Average OCR = 5.69

3.5

Depth (m)	$(N_1)_{60}$
1.5	12
3.0	11
4.5	10
6.0	8
7.5	12
9.0	12

3.7 33°

3.9 30.45°

3.11 44%

3.13

Eq. no.	D_r (%)
3.21	71.4
3.22	74.8
3.23	51
3.24	55
3.25	63.2

3.15 **a.** 26

b. 65.8

c. 42.7°

d. 520,000 lb/ft^2

3.17 4.04

3.19 3.52

3.23

Depth (m)	D_r (%)
2.0	42.2
3.5	42.8
5.0	43.1
6.5	54.1
8.0	59.0

3.25 $c_u = 40.4$ kN/m^2

$\sigma_c' = 184$ kN/m^2

OCR = 2.4

3.27 4121.6 kN/m^2

3.29 38.2°

3.31 $v_1 = 492$ m/s; $Z_1 = 2.6$ m

$v_2 = 1390$ m/s; $Z_2 = 7.24$ m

$v_3 = 3390$ m/s

CHAPTER 5

5.3 Standard Proctor:

$w_{opt} = 22.4\%$; $\gamma_{d(\max)} = 15.05$ kN/m^3

Modified Proctor:

$w_{opt} = 16.2\%$; $\gamma_{d(\max)} = 16.86$ kN/m^3

5.5 **a.** 10,530

b. 40,102.5 m^3

c. 193.3l

d. 19.7%

5.7

Soil	S_N	Rating	Soil type
A	62.2	Unsuitable	GM
B	12.0	Good	SW-SM
C	3.6	Excellent	SP

5.9 235.84 kN/m^2

5.11 **a.** 32.4%
b. 55.2%

5.13 45.6 mm

CHAPTER 6

6.1 **a.** 5195 lb/ft^2
b. 372.8 kN/m^2
c. 280 kN/m^2

6.3 **a.** 5675 lb/ft^2
b. 373.7 kN/m^2
c. 368.8 kN/m^2

6.5 156.8 kip

6.7 576.8 kN

6.9 5670 kN

6.11 707.3 kN

6.13 1504.4 kN/m

6.15 **a.** $\beta = 3.4°$; $e = 0$
b. $\beta = 0$; $e = 100$ mm
c. $\beta = 4.8°$; $e = -50$ mm (i.e., 50 mm to the left of the center line)

6.17 615 kN; Short-term stability critical

6.19 $B = 2.6$ mm

6.21 **a.** 941.4 kN/m
b. 1130.9 kN/m

CHAPTER 7

7.1 22.5 kip/ft^2

7.3 4185 kN/m^2

7.5 276.3 kN/m^2

7.7 203 kN/m

7.9 489 kN

7.11 **a.** 294.3 kN/m^2
b. 1049 kN/m^2

7.13 **a.** 147.3 kN/m^2
b.

b (m)	q_u (kN/m^2)
0	285.6
2	374
4	476
6	476

7.15 700.5 kN/m^2

7.17 26.0 MN/m^2

7.19 126.4 kN

CHAPTER 8

8.1 **a.** Below $O \rightarrow 0.49\dfrac{P}{b^2}$
Below $A \rightarrow 1.986\dfrac{P}{b^2}$
b. Below O: 9.8 kN/m^2
Below A: 39.7 kN/m^2

8.5

r (ft)	$\Delta\sigma$ (lb/ft^2)
0	1093.2
1	1082.4
2	1042.8
3	955.2
4	775.2
5	500.4

8.7 @ A—177.6 lb/ft^2
@ B—394.4 lb/ft^2
@ C—735.2 lb/ft^2

8.9 @ A—38.4 kN/m^2
@ B—14.6 kN/m^2
@ C—14.3 kN/m^2

8.11 **a.** 854 lb/ft^2
b. 874 lb/ft^2
c. 706 lb/ft^2

8.13

	$\Delta\sigma$	
Point	Boussinesq (ton/ft^2)	Westergaard (ton/ft^2)
A	0.66	0.56
B	0.12	0.08
C	0.01	0.01
D	0.17	0.15
E	0.09	0.07
F	0.03	0.02

CHAPTER 9

9.1 3.02 mm

9.3 0.87 in.

9.5 0.41 in.

9.7 12.4 mm

9.9 $S_e = 8.0$ mm
Settlement due to creep = 2.6 mm

9.11 57.2 mm

9.13 11.3 kip/ft^2

9.15 17.2 mm

9.27 900 kip

CHAPTER 10

10.1 4.5 ft

10.3 8200 lb/ft^2

10.5 0.94 in.

10.7 **a.** 120 kN/m^2
b. overconsolidated
c. 87.8 mm

10.9 101.7 lb/in^3

10.11 From Eq. (10.45)—10.7 MN/m^3
From Eq. (10.46)—16.0 MN/m^3

CHAPTER 11

11.1 3.5 m

11.3 3.4 m

CHAPTER 12

12.1 **a.**

Depth, z (m)	Q_z (kN)
0	1500
10	871.6
15	321.7

b. $z = 0$ to 10 m: $f_z = 44.6$ kN/m^2
$z = 10$ to 15 m: $f_z = 63.7$ kN/m^2

12.3 $Q_p = 496$ kN
$Q_s = 1028.8$ kN
$Q_{all} = 502$ kN

12.5 $Q_p = 498.7$ kN
$Q_s = 562.6$ kN
$Q_{all} = 353.8$ kN

12.7 **a.** 1655 kN
b. 1291 kN
c. 1473 kN
d. 769.4 kN
e. 560.51 kN

12.9 376 kN

12.11 111.25 kip

12.13 **a.** 237 kip
b. 301 kip
c. 212 kip

12.15 230.8 kip

12.17 1059.3 kN

12.19 **a.** 400 kN
b. $s_t = 39.6$ mm; $s_{net} = 35.5$ mm

12.21 24.9 kN

12.23 54.7 kN

12.25 340 kip

12.27 227 kip

12.29 $S = 1.724$ mm ($\approx$ 15 blows/25 mm)

12.31 5.51 kN

12.33 **a.** 68%
b. 74%

12.35 281 kip

12.37 217.7 mm

CHAPTER 13

13.1 $Q_{all} = 1628$ kip; Percent of load carried by shaft = 0.62%

13.3 **a.** 12,590 kN
b. 16,267 kN

13.5 1596.2 kN

13.7 58.7 kip

13.9 13.03 MN

13.11 9856 kN

CHAPTER 14

14.1
$$P_r = P_t\left(\frac{0.15K_r}{K_p - 0.7K_r}\right)$$
$$P_p = \frac{K_p - 0.85K_r}{K_p - 0.7K_r}$$
$$K_{pr} = \frac{K_p - 0.7K_r}{K_p - 0.72(K_r/K_p)}$$

14.3 $K_{pr} = 5697$ MN/m
$X = 0.24$

14.5 $P_1 = 657.9$ MN
Settlement = 116 mm

CHAPTER 15

15.3 287 mm

15.5 84 mm

15.7 **a.** 3.67 in.
b. 5.5 ft

15.9 5.2 m

CHAPTER 16

16.1 $P_o = 7348.5$ lb/ft; $\bar{z} = 5$ ft

16.3 @ $A \rightarrow 14.85$ kN/m^2
@ $B \rightarrow 86.68$ kN/m^2

16.5 $P_o = 94.1$ kN/m; $\bar{z} = 1.7$ m

16.7 $P_o = 108.15$ kN/m; $\bar{z} = 1.46$ m

16.11 **a.** 1.56 m

b.

z (m)	σ'_a (kN/m^2)
2	4,540
3	14,994
4	25,488
5	36,000
6	46,537

c. $P_a = 103.3$ kN/m acting at 1.48 m above the base

16.13 139.9 kN/m

16.15 $P = 31.5$ kN/m; $\bar{z} = 3.49$ m

16.17 $P_{ae} = 185.4$ kN/m; $\bar{z} = 2.46$ m

16.19 $P_p = 21{,}937.5$ lb/ft; $\bar{z} = 6.02$ ft

CHAPTER 17

17.1 $FS_{(overturning)} = 4.62$
$FS_{(sliding)} = 2.11$
$FS_{(bearing\ capacity)} = 7.4$

17.3 $FS_{(overturning)} = 4.37$
$FS_{(sliding)} = 1.58$
FS = 2.81

17.5 $FS_{(overturning)} = 3.74$
$FS_{(sliding)} = 1.44$
$q_{max} = 101.1$ kN/m^2
$q_{min} = 88.3$ kN/m^2

17.7 **a.** 5.44 mm
b. 14.79 m

17.9 $S_V = 0.336$ m; $L = 3.7$ m; $l_l = 1$ m

CHAPTER 18

18.1 12.25 m

18.3 10.89 m; PZC-13

18.5 $M_{max} = 69.43$ kN·m/m
$S = 0.365 \times 10^{-3}$ m^3/m

18.7 **a.** 10.6 m
b. $M_{max} = 230.7$ kN·m/m
$S = 121.4 \times 10^{-5}$ m^3/m

18.9 **a.** 13.0 m
b. 254.8 kN
c. 229.06 kN·m/m

18.11 PZ-22

18.13 $D = 2.573$ m; $F = 105.5$ kN/m

18.15 243.5 kN

18.17 $P_{ult} = 151.4$ kN; $u = 21.7$ mm

CHAPTER 19

19.1 **a.** $P_A = 413.4$ kN
$P_B = 545.7$ kN
$P_C = 556.9$ kN
b. 30.8×10^{-5} m^3/m of wall
c. @ Level *B*—341.06 kN·m
@ Level *C*—348.06 kN·m

19.3 $P_A = 82.7$ kN
$P_B = 257.1$ kN
$P_C = 286.2$ kN
$P_D = 277.3$ kN
$P_E = 223.6$ kN

19.5 $c_{av} = 912$ lb/ft^2; $\gamma_{av} = 110.8$ lb/ft^3

19.7 1.14

A

A parameter, Skempton:
  definition of, 55
  typical values, 56
AASHTO classification system, 20–22
Active earth pressure:
  Coulomb, 658–664
  earthquake condition, 668–671
  Rankine, 644–647, 649–652
Active zone, expansive soil, 614
Activity, 19–20
Adobe, 76
Aeolian deposit, 69, 75–76
Allowable bearing capacity, shallow foundation:
  correlation with standard penetration resistance, 361–362, 363–365
  general, 216
Allowable stress design:
  definition, 429
  factor of safety, typical values, 431-432
Alluvial deposit, 69, 71–73
Anchor:
  factor of safety, 809
  holding capacity, clay, 811
  holding capacity, sand, 804–809
  placement of, 802–803
  plate, 804
  spacing, 809
Anchored sheet pile wall:
  computational pressure diagram method, 792–793
  design charts, free earth support method, 785–788
  general, 779–780
  moment reduction, sand, 789–791
  penetrating clay, 797–799
  penetrating sand, 780–784
  relative flexibility, 790
Angle of friction, 51
Apparent cohesion, 51
Approximate flexible method, mat, 313–316
Area ratio, 84–85
At-rest earth pressure, 640–643
At-rest earth pressure coefficient, 641
Atterberg limits, 18–19
Average degree of consolidation, 43
Average vertical stress,
  circular load, 323
  rectangular load, 318–320

B

B parameter, Skempton, 55
Backswamp deposit, 73
Bearing capacity:
  allowable, 216
  closely spaced, 280–282
  drilled shaft, settlement, 561–565, 570–572
  drilled shaft, ultimate, 558–561, 568–569
  eccentric inclined loading, 251–252
  eccentric loading, 236–241, 242–247, 249–250
  effect of compressibility, 231–233
  effect of water table, 217–218
  factor, Terzaghi, 215
  factor of safety, 216
  failure, mode of, 208–211
  general equation, 218
  granular trench, 278–279
  layered soil, 266–268, 268–273, 275–276
  on a slope, 285–286
  on top of a slope, 262–263
  seismic, 286–288
  theory, Terzaghi, 212–216
  ultimate, local shear failure, 209
Boring depth, 78–79
Boring log, 120
Braced cuts:
  bottom heave, 835–837
  design of, 820–822
  general wedge theory, 817–819
  ground loss, 844
  ground settlement, 843–845
  lateral yielding, 843–845
  pressure envelope, clay, 820–822
  pressure envelope, layered soil, 822–823
  pressure envelope, sand, 821
Braided-stream deposit, 71–72

C

Caliche, 76
Cantilever footing, 399
Cantilever retaining wall, general, 696
Cantilever sheet pile wall:
  penetrating clay, 767–770
  penetrating sand, 758–762
Cement stabilization, 187–189
Chemical bonding, geotextile, 724
Chemical weathering, 68
Circular load, stress, 304–305
Clay mineral, 12
Coefficient:
  consolidation, 43
  gradation, 11
  subgrade reaction, 415–418
  uniformity, 11
  volume compressibility, 43

Cohesion, 51
Collapse potential, 607
Collapsible soil:
  chemical stabilization of, 611–612
  criteria for identification, 606–608
  densification of, 611
  foundation design in, 609–610
  settlement, 608–609
Combined footing, 397–400
Compaction:
  control for hydraulic barriers, 156–159
  curves, 148–149
  empirical relations for, 150–152
  maximum dry unit weight, 148
  optimum moisture content, 148
  Proctor test, 147–149
  relative, 149
  relative density of, 150
  specification for, 150
Compensated foundation, mat, 407
Compressibility, effect on bearing capacity, 231–233
Compression index:
  correlations for, 39
  definition of, 38
Concentrated load, stress, 303–304, 328–330
Concrete mix, drilled shaft, 555
Cone penetration test, 100–103
Consolidation:
  average degree of, 43
  definition of, 36–37
  maximum drainage path, 45
  settlement, group pile, 536–537
  settlement calculation, 380–384
  time rate of, 42–46
Construction joint, 714–715
Contact stress, dilatometer, 111
Continuous flight auger, 80
Contraction joint, 715
Conventional rigid method, mat, 411–413
Core barrel, 117
Coring, 117–120
Correction, vane shear strength, 98
Corrosion, reinforcement, 723
Coulomb's earth pressure:
  active, 658–664
  passive, 681–682
Counterfort retaining wall, 696
Critical hydraulic gradient, 35
Critical rigidity index, 232
Cross-hole seismic survey, 125–126
Curved failure surface, passive pressure, 683–687

D

Darcy's law, 27
Darcy's velocity, 80
Deep mixing, 199–211
Deflocculating agent, 11
Degree of saturation, 13
Depth factor, bearing capacity, 220–221
Depth of tensile crack, 646
Dilatometer modulus, 112
Dilatometer test, 111–114
Direct shear test, 51–52
Displacement pile, 452–453
Double-tube core barrel, 118
Drained friction angle:
  variation with plasticity index, 58
  variation with void ratio and pressure, 57–58
Dredge line, 756
Drilled shaft:
  bearing capacity, settlement, 561–565, 570–572
  bearing capacity, ultimate, 558–561, 568–569
  concrete mix, 555
  construction procedure, 548–554
  lateral load, 576–581
  load transfer, 555–556
  rock, 583–586
  settlement, working load, 575
  types of, 547–548
Drilling mud, 83
Drop, flow net, 33
Dry unit weight, 14
Dune sand, 75
Dynamic compaction:
  collapsible soil, 611
  design, 196–197
  general principles, 195–196
  significant depth of densification, 195–196

E

Earth pressure coefficient:
  at-rest, 641
  Coulomb, active, 659
  Coulomb, passive, 682
  Rankine active, horizontal backfill, 646
  Rankine active, inclined backfill, 653
  Rankine passive, horizontal backfill, 676
  Rankine passive, inclined backfill, 679
Earth pressure cell, 138
Eccentric load, bearing capacity, 235–236
Effective area, 237
Effective length, 237
Effective stress, 33–35
Effective width, 237
Elastic settlement:
  based on Pressuremeter test, 370–373
  flexible foundation, 339–340
  general, 337
  rigid, 339–340
  strain influence factor method, 354–356, 358–359
Elasticity modulus of clay, typical values for, 338
Electric friction-cone penetrometer, 101

Embankment loading, stress, 325–326
Equipotential line, 32
Expansion stress, dilatometer, 111
Expansive soil:
  classification of, 621
  construction on, 626–629
  criteria for identification, 622–623
  free swell ratio, 621
  general definition, 612–615
  swell, laboratory measurement, 615–616
  swell pressure test, 617–619

F
Factor of safety, shallow foundation, 216
Field load test, shallow foundation, 388–389
Field vane, dimensions of, 97
Filter design criteria, 715–716
Flexible foundation, elastic settlement, 339–340
Flow channel, 33
Flow line, 32
Flow net, 32
Fly ash stabilization, 189
Foundation design, collapsible soil, 609–610
Free swell, expansive soil, 615–617
Friction angle, cone penetration test, 105
Friction pile, 451
Friction ratio, 103
Function, geotextile, 725

G
General bearing capacity, shallow foundation:
  bearing capacity factors, 219
  depth factor, 220–221
  equation, 218
  inclination factor, 221
  shape factor, 220
General shear failure, bearing capacity, 208
Geogrid:
  biaxial, 726
  function, 727
  general, 725–726
  properties, 725–726
  uniaxial, 726
  with triangular aperture, 727
Geotechnical instrumentation:
  earth pressure cell, 138
  inclinometer, 139
  load cell, 138
  piezometer, 137–138
  settlement plate, 139
  strain gauge, 139
Geotextile, general, 723–725
Glacial deposit, 74
Glacial till, 74
Glacio-fluvial deposit, 74
Gradation coefficient, 11
Grain-size distribution, 8–11
Granular trench, bearing capacity, 278–279
Gravity retaining wall;
  definition, 695–696
Ground moraine, 74
Group index, 20–21
Group name:
  coarse-grained soil, 24
  fine-grained soil, 25
  organic soil, 26
Group pile:
  efficiency, 528–531
  ultimate capacity, 531–533
Guard cell, pressuremeter test, 108
Gumbo, 76

H
Hammer, pile driving, 453–457
Heave, 35
Helical auger, 80
Horizontal stress index, 112
Hydraulic conductivity:
  constant head test, 28
  definition of, 27–28
  falling head test, 28
  relationship with void ratio, 29
  typical values for, 28
Hydraulic gradient, 28
Hydrometer analysis, 11–12

I
Illite, 12
Inclination factor, bearing capacity, 221
Influence factor:
  embankment loading, 326
  rectangular loading, 313
Inclinometer, 139
Iowa borehole shear test, 114–116

J
Jet grouting, 198–199
Joints, retaining wall, 714–715

K
Kaolinite, 12
Knitted geotextile, 723–724

L
Laplace's equation, 32
Lateral earth pressure, surcharge, 665–667
Lateral load:
  drilled shaft, 576–581
  elastic solution for pile, 502–508
  ultimate load analysis, pile, 508–511
Laterite, 76
Layered soil, bearing capacity, 266–267, 268–273, 275–276

Lime stabilization, 184–187
Liquid limit, 18
Liquidity index, 19
Load cell, 138
Load resistance factor design:
  coefficient of variation, 430
  definition of, 430, 432
  load factor, 432, 234
  resistance factor, 432, 434
Load transfer mechanism, pile, 458–460
Loam, 76
Local shear failure, bearing capacity, 209
Loess, 75

M

Mat foundation:
  bearing capacity, 403–405
  compensated, 407
  differential settlement of, 406
  gross ultimate bearing capacity, 403
  net ultimate bearing capacity, 403–404
  types, 401–402
Material index, 112
Meandering belt of stream, 72
Mechanical bonding, geotextile, 724
Mechanical friction cone penetrometer, 100
Mechanical weathering, 68
Mesquite, 78
Modes of failure, 208–209
Mohr-Coulomb failure criteria, 51
Moist unit weight, 14
Moisture content, 14
Montmorillonite, 12
Moraine, 74
Muck, 76
Mud line, 756
Muskeg, 76

N

Natural levee, 73
Needle-punched nonwoven geotextile, 725
Negative skin friction, pile, 524–527
Nondisplacement pile, 452
Nonwoven geotextile, 724
Normally consolidated soil, 88

O

Optimum moisture content, 148
Overturning, retaining wall, 701–703
Organic soil, 76
Outwash plains, 74
Oxbow lake, 73

P

P-wave, 121
Passive pressure:
  Coulomb, 681–682
  curved failure surface, 683–687
  earthquake condition, 688–690
  Rankine, horizontal backfill, 676–678
  Rankine, inclined backfill, 679–681
Percent finer, 10
Percussion drilling, 83
Piezometer, 137–138
Pile capacity:
  Coyle and Castello's method, 469–470, 475–476
  flight auger pile, 450–451
  frictional resistance, 474–476
  Meyerhof's method, 463–464, 476
  rock, 487, 538
  Vesic's method, 466–469
Pile driving analyzer, 518
Pile driving formula, 514–516
Pile installation, 452–453
Pile load test, 493–496
Pile type:
  composite, 449–450
  concrete, 444–448
  continuous flight auger, 450–451
  steel, 441–444
  timber, 448–449
Piled raft foundation:
  creep piling, 595
  general, 593–594
  piled raft, interaction factor, 596
  piled raft stiffness, 596
  stiffness of pile group, 596
  stiffness of raft, 596, 597
Piston sampler, 93, 95
Plastic limit, 19
Plasticity chart, 22
Plasticity index, 19
Pneumatic rubber-tired roller, 154
Point bar deposit, 72
Point bearing pile, 451
Point load, stress, 303–304, 328–329
Pore water pressure parameter, 55
Porosity, 13
Post hole auger, 80
Pozzolanic reaction, 185
Precompression:
  general consideration, 165–166
  midplane degree of consolidation, 167
Preconsolidated soil, 38
Preconsolidation pressure, 38
Prefabricated vertical drain, 179–183
Pressuremeter modulus, 109
Pressuremeter test, 108–111
Proportioning, retaining wall, 697
Punching shear coefficient, 270
Punching shear failure, bearing capacity, 209

Q

Quick condition, 35

R

Radial shear zone, bearing capacity, 212
Rankine active earth pressure:
  horizontal backfill, 644–647
  inclined backfill, 649–653
Recompression curve, consolidation, 37–38
Recompression index, 40
Reconnaissance, 78
Recovery ratio, 118
Rectangular combined footing, 397–398
Rectangular load, stress, 312–316
Refraction survey, 121–123
Reinforced earth, 723
Relative compaction, 149
Relative density, 16–17
Residual friction angle, 59
Residual soil, 69–70
Residual strength envelope, 59
Resistivity, 126
Retaining wall:
  application of earth pressure theories, 698–699
  cantilever, 696
  counterfort, 696
  deep shear failure, 700
  drainage, backfill, 715–716
  geogrid reinforcement 725–727
  geotextile reinforcement, 723–725
  gravity, 695
  joint, 714–715
  proportioning, 697
  stability check, 699–701
  strip reinforcement, 723, 728–736
Rigidity index, 232
Rock quality designation, 119
Roller:
  pneumatic rubber-tired, 154
  sheepsfoot, 154
  vibratory, 154
Rotary drilling, 83

S

S-wave, 121, 125–126
Sand compaction pile, 194
Sand drain:
  average degree of consolidation, radial drainage, 171–175
  general, 170–171
  radius of effective zone of drainage, 170
  smear zone, 171
  theory of equal strain, 171–175
Sanitary landfill:
  general, 630–631
  settlement of, 631–632
Saprolite, 75
Saturated unit weight, 15
Saturation, degree of, 13
Seismic refraction survey, 121–123
Sensitivity, 61–62
Settlement, pile:
  elastic, 497–501
  group, 534–535
Settlement calculation, shallow foundation:
  consolidation, 380–384
  effect of water table, elastic, 378–379
  elastic, 337–338, 339–352
  secondary consolidation, 386–387
  stiffness variation with stress level, 366–369
  tolerable, 390–392
Settlement plate, 139
Shape factor, bearing capacity, 220
Sheepsfoot roller, 154
Sheet pile:
  precast concrete, 753
  steel, 754–756
  wall construction method, 756–757
  wooden, 753, 754
Shelby tube, 193
Shrinkage limit, 19
Sieve analysis, 10–11
Sieve size, 10
Single-tube core barrel, 118
Size limit, 12
Skempton-Bjerrum modification, consolidation settlement, 383
Skin, 728
Sliding, retaining wall, 703–706
Smear zone, sand drain, 171
Smooth wheel roller, 154
Soil classification systems, 20–26
Soil compressibility factor, bearing capacity, 232–133
Spacing, boring, 79
Specific gravity, 15, 16
Split-spoon sampler, 83–84
Spring core catcher, 85
Stability check, retaining wall:
  bearing capacity, 706–708
  overturning, 701–703
  sliding, 703–706
Stability number, 282
Stabilization:
  cement, 187–188
  fly ash, 189
  lime, 184–185
  pozzolanic reaction, 185
Standard penetration number:
  correlation, consistency of clay, 86
  correlation, friction angle, 90–91
  correlation, overconsolidation ratio, 87
  correlation, relative density, 89–90
Stepped-blade test, 116–117

Stone column:
equivalent triangular pattern, 191
general, 189–192
stress concentration coefficient, 191
ultimate bearing capacity, 192–193
Strain gauge, 139
Strain influence factor, 354–355, 358–359
Stress:
circular load, 304–305, 330–331
concentrated load, 303, 329
embankment load, 325–326
isobar, 317–318
line load, 305–306
rectangular load, 312–316, 331–332
strip load, 306–309, 310–311
Structural design, mat:
approximate flexible method, 413–415
conventional rigid method, 411–413
Subgrade reaction coefficient, 415–417
Suitability number, vibroflotation, 161
Swell pressure test, 617–619
Swell test, unrestrained, 516–517
Swelling index, 40

T

Tensile crack, 646
Terminal moraine, 74
Terra Rossa, 76
Thermal bonding, geotextile, 724
Tie failure, retaining wall, 733
Tie force, retaining wall, 732
Time factor, 43
Time rate of consolidation, 42–46
Tolerable settlement, shallow foundation, 390–392
Trapezoidal footing, 398–399
Triaxial test:
consolidated drained, 54
consolidated undrained, 54
unconsolidated undrained, 55

U

Ultimate bearing capacity, Terzaghi, 212–215
Unconfined compression strength, 57
Unconfined compression test, 56–57
Undrained cohesion, 55
Unified classification system, 22–27
Uniformity coefficient, 11
Unit weight:
dry, 14
moist, 14
saturated, 15
Unrestrained swell test, 615–616
Uplift capacity, shallow foundation, 293–297

V

Vane shear test, 96–99
Velocity, P-wave, 123
Vertical stress, average, 318–320, 323
Vibratory roller, 154
Vibroflotation:
backfill suitability number, 161
construction method, 160–161
effective range, backfill, 161
vibratory unit, 162
Virgin compression curve, 39
Void ratio, 12
maximum-minimum relationship, 17
Volume, coefficient of compressibility, 43

W

Waffle slab, 622–627
Wash boring, 82
Water table, effect on bearing capacity, 217–218
Water table observation, 95–96
Wave equation analysis, pile, 521–524
Wedge-shaped foundation, bearing capacity, 291–293
Weight-volume relationship, 12–16
Wenner method, resistivity survey, 126
Westergaard solution, stress:
circular load, 330–331
point load, 329–330
rectangular load, 331–332
Winker foundation, 414

Z

Zero-air-void unit weight, 149

CONVERSION FACTORS FROM ENGLISH TO SI UNITS

Length:	1 ft	= 0.3048 m
	1 ft	= 30.48 cm
	1 ft	= 304.8 mm
	1 in.	= 0.0254 m
	1 in.	= 2.54 cm
	1 in.	= 25.4 mm
Area:	1 ft^2	= 929.03 $\times$ 10^{-4} m^2
	1 ft^2	= 929.03 cm^2
	1 ft^2	= 929.03 $\times$ 10^2 mm^2
	1 in^2	= 6.452 $\times$ 10^{-4} m^2
	1 in^2	= 6.452 cm^2
	1 in^2	= 645.16 mm^2
Volume:	1 ft^3	= 28.317 $\times$ 10^{-3} m^3
	1 ft^3	= 28.317 $\times$ 10^3 cm^3
	1 in^3	= 16.387 $\times$ 10^{-6} m^3
	1 in^3	= 16.387 cm^3
Force:	1 lb	= 4.448 N
	1 lb	= 4.448 $\times$ 10^{-3} kN
	1 lb	= 0.4536 kgf
	1 kip	= 4.448 kN
	1 U.S. ton	= 8.896 kN
	1 lb	= 0.4536 $\times$ 10^{-3} metric ton
	1 lb/ft	= 14.593 N/m
Stress:	1 lb/ft^2	= 47.88 N/m^2
	1 lb/ft^2	= 0.04788 kN/m^2
	1 U.S. ton/ft^2	= 95.76 kN/m^2
	1 kip/ft^2	= 47.88 kN/m^2
	1 lb/in^2	= 6.895 kN/m^2
Unit weight:	1 lb/ft^3	= 0.1572 kN/m^3
	1 lb/in^3	= 271.43 kN/m^3
Moment:	1 lb-ft	= 1.3558 N·m
	1 lb-in.	= 0.11298 N·m
Energy:	1 ft-lb	= 1.3558 J
Moment of inertia:	1 in^4	= 0.4162 $\times$ 10^6 mm^4
	1 in^4	= 0.4162 $\times$ 10^{-6} m^4
Section modulus:	1 in^3	= 0.16387 $\times$ 10^5 mm^3
	1 in^3	= 0.16387 $\times$ 10^{-4} m^3
Hydraulic conductivity:	1 ft/min	= 0.3048 m/min
	1 ft/min	= 30.48 cm/min
	1 ft/min	= 304.8 mm/min
	1 ft/sec	= 0.3048 m/sec
	1 ft/sec	= 304.8 mm/sec
	1 in./min	= 0.0254 m/min
	1 in./sec	= 2.54 cm/sec
	1 in./sec	= 25.4 mm/sec
Coefficient of consolidation:	1 in^2/sec	= 6.452 cm^2/sec
	1 in^2/sec	= 20.346 $\times$ 10^3 m^2/yr
	1 ft^2/sec	= 929.03 cm^2/sec

CONVERSION FACTORS FROM SI TO ENGLISH UNITS

Length:	1 m	= 3.281 ft
	1 cm	= 3.281×10^{-2} ft
	1 mm	= 3.281×10^{-3} ft
	1 m	= 39.37 in.
	1 cm	= 0.3937 in.
	1 mm	= 0.03937 in.
Area:	1 m^2	= 10.764 ft^2
	1 cm^2	= 10.764×10^{-4} ft^2
	1 mm^2	= 10.764×10^{-6} ft^2
	1 m^2	= 1550 in^2
	1 cm^2	= 0.155 in^2
	1 mm^2	= 0.155×10^{-2} in^2
Volume:	1 m^3	= 35.32 ft^3
	1 cm^3	= 35.32×10^{-4} ft^3
	1 m^3	= 61,023.4 in^3
	1 cm^3	= 0.061023 in^3
Force:	1 N	= 0.2248 lb
	1 kN	= 224.8 lb
	1 kgf	= 2.2046 lb
	1 kN	= 0.2248 kip
	1 kN	= 0.1124 U.S. ton
	1 metric ton	= 2204.6 lb
	1 N/m	= 0.0685 lb/ft

Stress:	1 N/m^2	= 20.885×10^{-3} lb/ft^2
	1 kN/m^2	= 20.885 lb/ft^2
	1 kN/m^2	= 0.01044 U.S. ton/ft^2
	1 kN/m^2	= 20.885×10^{-3} kip/ft^2
	1 kN/m^2	= 0.145 lb/in^2
Unit weight:	1 kN/m^3	= 6.361 lb/ft^3
	1 kN/m^3	= 0.003682 lb/in^3
Moment:	1 N·m	= 0.7375 lb-ft
	1 N·m	= 8.851 lb-in.
Energy:	1 J	= 0.7375 ft-lb
Moment of inertia:	1 mm^4	= 2.402×10^{-6} in^4
	1 m^4	= 2.402×10^{6} in^4
Section modulus:	1 mm^3	= 6.102×10^{-5} in^3
	1 m^3	= 6.102×10^{4} in^3
Hydraulic conductivity:	1 m/min	= 3.281 ft/min
	1 cm/min	= 0.03281 ft/min
	1 mm/min	= 0.003281 ft/min
	1 m/sec	= 3.281 ft/sec
	1 mm/sec	= 0.03281 ft/sec
	1 m/min	= 39.37 in./min
	1 cm/sec	= 0.3937 in./sec
	1 mm/sec	= 0.03937 in./sec
Coefficient of consolidation:	1 cm^2/sec	= 0.155 in^2/sec
	1 m^2/yr	= 4.915×10^{-5} in^2/sec
	1 cm^2/sec	= 1.0764×10^{-3} ft^2/sec